

MOLECULAR
SPECTROSCOPY
OF OXIDE CATALYST
SURFACES

MOLECULAR SPECTROSCOPY OF OXIDE CATALYST SURFACES

Anatoli Davydov

University of Alberta, Edmonton, Canada

Syntroleum Corporation, Tulsa, Oklahoma, USA

Edited by N. T. Sheppard



WILEY

Copyright © 2003

John Wiley & Sons Ltd, The Atrium, Southern Gate, Chichester,
West Sussex PO19 8SQ, England

Telephone (+44) 1243 779777

Email (for orders and customer service enquiries): cs-books@wiley.co.uk

Visit our Home Page on www.wileyurope.com or www.wiley.com

All Rights Reserved. No part of this publication may be reproduced, stored in a retrieval system or transmitted in any form or by any means, electronic, mechanical, photocopying, recording, scanning or otherwise, except under the terms of the Copyright, Designs and Patents Act 1988 or under the terms of a licence issued by the Copyright Licensing Agency Ltd, 90 Tottenham Court Road, London W1T 4LP, UK, without the permission in writing of the Publisher. Requests to the Publisher should be addressed to the Permissions Department, John Wiley & Sons Ltd, The Atrium, Southern Gate, Chichester, West Sussex PO19 8SQ, England, or emailed to permreq@wiley.co.uk, or faxed to (+44) 1243 770620.

This publication is designed to provide accurate and authoritative information in regard to the subject matter covered. It is sold on the understanding that the Publisher is not engaged in rendering professional services. If professional advice or other expert assistance is required, the services of a competent professional should be sought.

Other Wiley Editorial Offices

John Wiley & Sons Inc., 111 River Street, Hoboken, NJ 07030, USA

Jossey-Bass, 989 Market Street, San Francisco, CA 94103-1741, USA

Wiley-VCH Verlag GmbH, Boschstr. 12, D-69469 Weinheim, Germany

John Wiley & Sons Australia Ltd, 33 Park Road, Milton, Queensland 4064, Australia

John Wiley & Sons (Asia) Pte Ltd, 2 Clementi Loop #02-01, Jin Xing Distripark, Singapore 129809

John Wiley & Sons Canada Ltd, 22 Worcester Road, Etobicoke, Ontario, Canada M9W 1L1

Wiley also publishes its books in a variety of electronic formats. Some content that appears in print may not be available in electronic books.

Library of Congress Cataloging-in-Publication Data

Davydov A. A. (Anatoli Aleksandrovich)

Molecular spectroscopy of oxide catalyst surfaces / Anatoli Davydov ; edited by N.T. Sheppard.
p. cm.

Includes bibliographical references and index.

ISBN 0-471-98731-X (cloth : alk.paper)

1. Metallic oxides – Surfaces – Analysis. 2. Molecular spectroscopy. I. Sheppard, N. T. II.

Title.

QD509.M46 .D38 2003

541.3'3 – dc21

2002191080

British Library Cataloguing in Publication Data

A catalogue record for this book is available from the British Library

ISBN 0-471-98731-X

Typeset in 9.5/11.5pt Times by Laserwords Private Limited, Chennai, India

Printed and bound in Great Britain by TJ International, Padstow, Cornwall

This book is printed on acid-free paper responsibly manufactured from sustainable forestry in which at least two trees are planted for each one used for paper production.

Dedicated to my wife Marina

CONTENTS

Preface	xi
Symbols and Abbreviations	xiii
Introduction	xv
1 Theoretical fundamentals and experimental considerations of the spectroscopic methods used in surface chemistry	1
1.1 Electronic spectroscopy	1
1.1.1 Transmission spectra	4
1.1.2 Diffuse reflection spectra	5
1.2 Vibrational spectroscopy	5
1.2.1 Infrared spectroscopy	11
1.2.2 Photoacoustic spectroscopy	18
1.2.3 Raman spectroscopy	19
1.3 Electron energy loss spectroscopy	21
1.4 Inelastic electron tunneling spectroscopy	22
1.5 Inelastic neutron scattering spectroscopy	23
1.6 Other vibrational spectroscopies	23
1.6.1 Infrared ellipsometric spectroscopy	23
1.6.2 Surface electromagnetic wave spectroscopy	23
1.7 <i>In situ</i> measurements	24
1.8 Quantitative measurements	25
2 The nature of oxide surface centers	27
2.1 Systems investigated	27
2.1.1 Solid structures	27
2.1.2 Surfaces	28
2.1.3 Active sites	29
2.2 Spectra of oxide surfaces	31
2.2.1 Vibrations of metal–oxygen bonds on oxide surfaces	32
2.2.2 Molecular forms of adsorbed oxygen	44
2.2.3 Surface hydroxyl groups	56
2.3 Determination of the nature of surface sites and their chemical properties using the adsorption of simple molecules	77
2.3.1 Adsorption of ammonia and pyridine	78
2.3.2 Adsorption of carbon monoxide	95
2.3.3 Adsorption of hydrogen and nitrogen	114

2.3.4 Adsorption of water	120
2.3.5 Adsorption of nitrogen oxide and nitrogen dioxide	123
2.3.6 Adsorption of carbon dioxide	133
2.3.7 Adsorption of hydrogen sulfide	139
2.3.8 Adsorption of sulfur dioxide	146
2.3.9 Surface isocyanate complexes	157
2.4 Determination of acidic surface properties	161
2.4.1 Protic acid sites	162
2.4.2 Lewis acid sites	166
2.5 Determination of basic surface properties	171
2.6 Surface defects	177

3 Study of cation states by DRES and FTIR spectroscopies of the probe molecules

3	181
3.1 Copper-containing systems	182
3.1.1 Zeolites	182
3.1.2 Oxides	200
3.2 Nickel-containing systems	207
3.2.1 Zeolites	207
3.2.2 Oxides	215
3.3 Co-containing systems	217
3.3.1 Zeolites	217
3.3.2 Oxides	218
3.4 Iron-containing systems	220
3.4.1 Zeolites	220
3.4.2 Oxides	222
3.5 Silver-containing systems	223
3.6 Palladium-containing systems	228
3.6.1 Zeolites	228
3.6.2 Oxides	235
3.7 Rhenium-, ruthenium-, and rhodium-containing systems	237
3.8 Platinum-containing systems	238
3.8.1 IR-Spectra of CO adsorbed on supported metals	238
3.8.2 Cationic states of platinum	248
3.9 Molybdenum-containing systems	252
3.9.1 Molybdenum–aluminum oxide compounds	252
3.9.2 Molybdenum–silicon oxide compounds	253
3.9.3 Molybdenum–titanium oxide compounds	255
3.10 Vanadium-containing systems	257
3.10.1 Vanadium–titanium oxide compounds	259
3.10.2 Vanadium–silicon oxide compounds	263
3.10.3 Vanadium–aluminum oxide compounds	266
3.11 Chromium-containing systems	269
3.12 Effects of the states of adsorption sites on the stretching frequencies of adsorbed carbon monoxide and nitrous oxide and the problem of detecting the states of cations in oxide catalyst surfaces	271
3.12.1 M^{2+} –CO, M^{n+} –CO ($n > 2$)	272
3.12.2 M^+ –CO and M^0 –CO	274

4 Interactions of inorganic compounds with oxide surface active sites	277
4.1 Organometallic complexes	281
4.2 Metal carbonyls and nitrosyls	282
4.3 Interactions with simple acids and bases	284
4.3.1 F ⁻ and Cl ⁻ -modified oxide systems	285
4.3.2 SO ₄ ²⁻ -modified oxide systems	286
4.3.3 BO ₃ ²⁻ -modified oxide systems	291
4.4 Heteropoly compound systems	294
4.4.1 Effects of the supports	295
4.4.2 Acidic properties of molybdenum heteropoly compounds	300
4.5 Thermal stabilities of molybdenum compounds, decomposition mechanisms and the role of modifiers	303
4.5.1 Bulk and supported heteropoly acids	303
4.5.2 Modified molybdates	305
4.6 Cationic modification	308
5 Formation of surface complexes of organic molecules	309
5.1 Complexation of alkenes	310
5.1.1 Complexation with OH groups	310
5.1.2 Carbenium ions and alkoxy compounds	313
5.1.3 Interaction with cations	327
5.1.4 Interaction with cation–anion pairs	342
5.1.5 The complexation of alkenes with surface oxygen	351
5.2 Complexation of aryls and aryl halides	355
5.2.1 Hydrogen-bonding	355
5.2.2 Alkylaromatic carbenium ions	358
5.2.3 π -complexes	366
5.2.4 Interaction with ionic pairs	373
5.2.5 Complexation with surface oxygen	376
5.2.6 Formation of aryl halide complexes	378
5.3 Complexation of alkynes	381
5.3.1 Silicon dioxide zeolites	381
5.3.2 Aluminum oxide	385
5.3.3 Zinc oxide	386
5.3.4 Titanium oxide	387
5.4 Complexation of alkanes	389
5.4.1 Interactions with OH groups, carbenium-like ions	389
5.4.2 Interaction with cations	392
5.4.3 The activation of C–H bonds in alkane molecules	395
5.5 Complexation of chlorofluorocarbons	407
5.6 Complexation of nitriles	411
5.6.1 Acetonitrile	411
5.6.2 Benzonitrile	415
5.7 Complexation of alcohols	416
5.7.1 Saturated alcohols	416
5.7.2 Phenol	427
5.8 Complexation of aldehydes and ketones	430
5.8.1 Formaldehyde and acetaldehyde	430

5.8.2 Acrolein	435
5.8.3 Benzaldehyde	439
5.8.4 Maleic anhydride	440
5.8.5 Acetone	442
5.9 Complexation of acids	445
5.9.1 Formic acid	445
5.9.2 Acetic acid	453
5.9.3 Acrylic acid	453
5.9.4 Benzoic acid	455
5.10 Deactivation catalysts due to carbonaceous depositions as a result of catalyst interactions with hydrocarbons and their derivatives	456
6 The mechanisms of heterogeneous catalytic reactions	459
6.1 Reactions involving carbon monoxide	461
6.1.1 The oxidation of carbon monoxide	461
6.1.2 The water-gas shift reaction	466
6.1.3 Carbonization and hydroformylation	473
6.1.4 The synthesis and decomposition of alcohols	475
6.2 Reactions with the participation of hydrocarbons	479
6.2.1 Complete oxidation of hydrocarbons and their derivatives	479
6.2.2 Selective transformations of alkenes	483
6.2.3 Partial oxidation	499
6.2.4 Ammoxidation of hydrocarbons and their derivatives	518
6.3 Transformations of aldehydes and ketones	526
6.3.1 Oxidation of acrolein	526
6.3.2 Oxidation of formaldehyde	531
6.3.3 Transformation of acetone	531
6.3.4 Hydrogenation of aldehydes and ketones	532
6.4 Transformations of alcohols	532
6.4.1 Dehydration of alcohols	532
6.4.2 Dehydrogenation of alcohols	536
6.4.3 Methanol oxidation to formaldehyde	538
6.5 Transformations of nitrogen-containing compounds	545
6.5.1 Decomposition of nitric oxide	545
6.5.2 The reduction of nitrogen oxides	552
6.5.3 Reactions of NO_x and NH_3 Mixtures	556
References	559
Index	643

PREFACE

Molecular spectroscopic methods, together with X-ray diffraction, have played key roles in establishing the concepts of coordination chemistry, as originally developed in the study of individual transition-metal complexes in aqueous solutions or the solid state. This present book is concerned with the even greater importance of molecular spectroscopic methods in developing similar understandings of the coordination chemistry of oxide surfaces where application of diffraction methods is much more difficult. The adsorption of molecules on the surfaces gives rise to ligands attached to free sites on the surface cations.

The book commences with an account of the basic theoretical principles and experimental techniques of the various molecular spectroscopic methods as applied to surfaces, namely the electronic (UV–Vis), vibrational (transmission IR, diffuse reflection, reflection–absorption IR and Raman), electron energy loss, inelastic electron tunneling, and inelastic neutron scattering spectroscopies. Special attention is devoted to *in situ* measurements where the oxide or catalyst sample is in contact with the adsorbate or reactant. The local approach has been chosen as the basis of the spectroscopic analysis of adsorption on the active sites of the oxide surfaces, while the collective properties of the solid adsorbents, based on analysis of their crystal structures, is used to describe the sites themselves. This approach is applied to pure oxides and also to oxide systems such as cation-substituted zeolites, heteropoly compounds of molybdenum, or supported catalysts prepared by ionic exchange or the interaction of the support with various complexes.

In some cases, the crystallographic positions of both cations and anions can be unambiguously determined by means of molecular spectroscopic (ESR, UV–Vis, Mössbauer, etc.) or diffraction (for zeolites, etc.) methods.

An attempt has been made to cover all of the spectroscopic literature on oxide adsorption studies, covering many different oxide–adsorbate systems in a comparative manner. Because the number of such publications is now very large (numbered in thousands), it is impossible to analyze all of them individually in one single book. A particular goal is to provide a critical analysis of the literature on the interpretation of the spectra of surface compounds on oxides going back to the earliest days of the 1950s. A comparative analysis of the changes in the IR spectra of adsorbed molecules, based on an improved knowledge of the bonding between the adsorbed molecule and the surface site, has allowed this present author to improve the reliability of interpretation of many of the spectra. Special emphasis is placed on the spectral characteristics of active sites on oxide surfaces—hydroxyl groups, or coordinatively unsaturated surface cations and oxygen anions. The concept of the decisive role played by surface sites in surface–molecule adsorption is used to systematize and classify the spectral data relating to the interaction of numerous organic and inorganic molecules, and their transformation products, with the types of surfaces referred to above. The structures of many surface species have been identified from the spectroscopic data.

A detailed account is presented of methods for spectroscopically characterizing the oxidation state and degree of coordination of surface cations and oxygen anions by the adsorption of probe molecules such as NH₃, pyridine (Py), CO, CO₂, H₂, N₂, H₂O, NO, NO₂, H₂S and SO₂ (Chapter 2). Special attention is paid to the critical investigation of protic and aprotic acidic and

basic surface centers, including specific correlations for comparing the strengths and concentrations of surface centers on different oxides, zeolites, supported oxides, etc. by using the UV–Vis, ESR and IR spectral characteristics of the adsorbed probe molecules, particularly CO and NO. This includes the testing of cation states during the process of stationary-state heterogeneous catalytic reactions. Systems containing Cu, Ni, Co, Fe, Ag, Pd, Re, Ru, Rh, Pt, Mo, V and Cr are examined in detail. The vibrational frequency ranges of the CO and NO probes characteristic of different surface states are presented.

Attention is also paid to the interactions of organometallic (allylic and other types) and inorganic compounds (such as metal carbonyls), simple acids and heteropoly compounds with various supports (Al_2O_3 , SiO_2 , TiO_2 and MgO), i.e. to the problems that occur during the preparation or modification of supported catalysts. The dependence of the structure and properties of the surface complexes formed and the properties of the catalytic systems are also shown.

The complexation of many organic molecules – alkenes, alkene halides, alkynes, aryls, aryl halides, alkanes, nitriles, alcohols, aldehydes, ketones and acids (saturated and unsaturated, aromatic and non-aromatic) – with different oxide systems are critically examined. The surface compounds formed are classified in relation to the nature and properties of the available surface centers (H^+ , OH^- , O^{2-} , M^{n+} , $\text{M}^{n+}\text{O}^{2-}$, etc.).

The final chapter is devoted to discussions of possible mechanisms of catalytic reactions as deduced from spectroscopic identification of the reaction intermediates. The latter identifications are based on the comparison of the rates of reaction with those of the transformations of surface compounds. The catalytic reactions discussed include carbon oxide oxidation, the water–gas shift (WGS) reaction, the synthesis and decomposition of alcohols, carbonization, hydroformylation, full and partial transformations of alkenes (including isomerization, hydrogenation, oligomerization, polymerization, cracking and metathesis), partial oxidation of alkanes, alkenes and aryls, ammoxidation of hydrocarbons, alcohols and aldehydes, conversion of alcohols, transformations of aldehydes and ketones, NO decomposition, $\text{NO} + \text{CO}$, $\text{NO}/\text{hydrocarbons}$, and reactions between NO and NH_3 .

Taking into account common understandings and the results of the analysis of detailed schemes, the mechanisms of heterogeneous catalytic reactions can be classified as stepwise (when sequential interactions of the reaction components occur) or associative (where the stages of product separation and interaction of the reaction mixture components with the catalyst occur in parallel) with the help of spectroscopic analyses.

This book is intended for specialists working in the fields of surface physical chemistry, surface science, adsorption phenomena and heterogeneous catalysts.

Special thanks are due to Professor N.T. Sheppard for his attention, interest, valuable corrections and useful advice, to Professor J.T. Yates Jr for important comments, and also to my wife, Dr M. Shepot'ko, and son, Davydov, A.A. Jr, for their help in the preparation and design of this book.

Anatoli Davydov
Tulsa, OK, USA

SYMBOLS AND ABBREVIATIONS

AES	Auger electron spectroscopy
AFS	atomic fluorescence spectroscopy
AO	atomic orbital
BAS	Brønsted acid site
BS	basic site
CTB	charge-transfer band
DRES	diffuse reflection electron (UV–Vis) spectroscopy
DRIRS	diffuse reflection infrared spectroscopy
EELS	electron energy loss spectroscopy
EHM	extended Hückel Method (quantum-chemical calculations)
EPR	electron proton resonance (spectroscopy)
ES	electron spectroscopy
ESR	electron spin resonance (spectroscopy)
FTIR	Fourier-transform infrared (spectroscopy)
GC	gas chromatography
HFB	high-frequency band
HM	Hückel Method (quantum-chemical calculations)
HOMO	highest-occupied molecular orbital
HPA	heteropoly acid
HPC	heteropoly compound
HREELS	high-resolution electron energy loss spectroscopy
IETS	inelastic electron tunneling spectroscopy
INSS	inelastic neutron scattering spectroscopy
IP	ionization potential
IRAS	infrared absorption spectroscopy
IRES	infrared ellipsometric spectroscopy
IRS	infrared spectroscopy
LAS	Lewis acid site
LFB	low-frequency band
LOMO	lowest-occupied molecular orbital
M	metal
$M_{\text{c}^{\text{to}}}^{n+}$	coordinatively unsaturated octahedral site (on a metal)
$M_{\text{c}^{\text{us}}}^{n+}$	coordinatively unsaturated site (on a metal)
$M_{\text{c}^{\text{t}}}^{n+}$	coordinatively unsaturated tetrahedral site (on a metal)
MO	molecular orbital
MS	mass spectrometry
MY-A	faujasite-type zeolite containing preferably strong associated cations
MY-I	faujasite-type zeolite containing preferably isolated cations
NMR	nuclear magnetic resonance (spectroscopy)

NRS	nuclear γ -resonance spectroscopy (Mössbauer spectroscopy)
PAS	photoacoustic spectroscopy
R	hydrocarbon fragment
RAIRS	reflection-absorption infrared spectroscopy
RS	Raman spectroscopy
SAPO	silicoaluminophosphate
SCR	selective catalytic reduction
SERS	surface-enhanced Raman spectroscopy
SEWS	surface electromagnetic wave spectroscopy
SIC	surface isocyanate complex
SIMS	selected-ion mass spectrometry
SMSI	strong metal-support interaction
TPD	temperature-programmed desorption
UEP	unshared electron pair
UHV	ultra-high vacuum
UV-Vis	spectroscopy in the ultraviolet and visible region
VAPO	vanadiumsilicophosphate
WGS	water-gas shift
XPS	X-ray photoelectron spectroscopy
XRD	X-ray diffraction
<i>A</i>	absorbance
<i>A</i> ₀	absorption coefficient
<i>e</i>	electron charge
<i>E</i>	activation energy
<i>g</i>	parameter of level split in ESR spectrum
<i>K</i>	reaction rate constant
<i>N</i>	number of active sites
<i>PA</i>	proton affinity
<i>q</i>	charge (on a dipole)
<i>Q</i>	heat of absorption
<i>r</i>	interatomic distance (Å)
δ	deformation vibration
ε	extinction coefficient (cm ² molecule ⁻¹)
θ	surface coverage
ν	vibration wavenumber (reciprocal wavelength, 1/ λ) (cm ⁻¹)
ϱ	out-of-plane deformation vibration

INTRODUCTION

Numerous technological processes are dependent on the nature of the molecular and chemical interactions which occur on contact of various media with solid surfaces. These include, for example, the separation of mixtures by adsorption, heterogeneous catalysis, the chromatographic separation of pure substances, the production of polymer and lubricant fillers, materials for microelectronics and the manufacture of controlled-property semiconductors, pigments and catalysts. It is therefore an important objective to gain a better understanding of the nature of the processes which occur at the surfaces of solids.

This book is concerned with the development of the principles of the coordination chemistry of oxide surfaces as brought about by the use of analyses of experimental data obtained by means of molecular spectroscopy methods which are the most widely used in chemistry [1–35a]. The concepts of coordination chemistry, originally established for transition-metal complexes in aqueous solutions [35b–e], can frequently be usefully extended to heterogeneous systems consisting of transition-metal ions dispersed on the surfaces (or incorporated within a solid matrix) of oxides despite the differences in behavior of transition-metal ions at gas–solid or liquid–solid interfaces [30, 35f–h]. The phenomena occurring at the latter interfaces can be described in terms of the coordination chemistry concept of coordination number of the transition-metal ion (the number of atoms donated by ligands) which can vary over a wide range. At the solid surface, a transition-metal ion has necessarily a lower coordination number than in the bulk of the solid and so it can complete its coordination sphere by bond formation through adsorption from the gas or liquid phase. The first coordination sphere predominantly determines the reactivity and properties of the central transition-metal ion in both homogeneous and heterogeneous systems, although the influence of the addition of ligands to the coordination spheres is much greater in heterogeneous systems. This can lead in the latter case to the existence of a number of transition-metal ion complexes and, moreover, this is the cause of the creation and stabilization of species with unusual oxidation states or coordination numbers at solid surfaces which are different from those in the bulk of the oxide. Compared with homogeneous coordination chemistry, such species show new types of reactivity. Thus, these peculiar features of heterogeneous coordination systems containing transition-metal ions open up new, special and unique potentialities in adsorption and catalysis [30, 35f–h].

The principles of coordination chemistry, established essentially by Grinberg, Jorgensen and Werner, were based on results obtained for solution complexes with the single transition-metal ion surrounded by ligands [35b–e]. The properties of these complexes were the main subjects of study, for example, reactivity, structure, the nature of the different chemical bonds involved, the presence of optical and/or geometric isomers, the number of isomers, optical and magnetic properties, chemical reactivities, etc. Different theoretical treatments, such as crystal field, molecular orbital, valence bond, etc., improved the understanding of the transition-metal complexes in solution or in the solid state.

Attempts to apply these theories to catalytic processes have been more successful for homogeneous than for heterogeneous systems. The main results are that (i) the properties of the partially filled d-orbitals of oxide surfaces can be studied at a molecular level by using probes with

characteristic optical properties, (ii) oxide surfaces may act as either s-donor or p-donor ligands and hence be classified within the spectrochemical series of ligands, (iii) an oxide support can play a role in reactivity similar to that of a solvent, and (iv) the distinctions and similarities between interfacial coordination chemistry and surface organometallic chemistry can be made in a similar fashion as for complexes in solution [30, 35f–h].

Molecular interactions at solid surfaces are very complicated because of a number of factors. The most important of these are the nature and properties of the adsorption centers, which determine the types of surface complexes formed. Hence, the main tasks in surface chemistry are the identification of these surface centers, the determination of their concentrations and characteristic chemical properties (for instance, via investigations of the interaction between a given center and adsorbed molecules with different chemical properties) and the establishment of the relationships between bulk crystal structures and the nature of the surface centers.

Morrison's term 'surface center' [35i] will be applied in this book to describe the microscopic group of atoms which exhibits a particular chemical activity on the surface. This term applies to a surface atom of the lattice with a free bond, the free bonding orbital with a low ionization potential, etc.; such centers can be situated on a uniform surface or can occur in nonhomogeneous areas, where their activity is often highest. It has been shown that surface heterogeneity has a great effect on the chemical properties of surfaces as it leads to a wide range of different types of adsorption centers. These centers may be related to defects, e.g. sites where a crystal defect meets the surface. It should be noted that the surface itself, in both the microscopic and the electronic senses, is a major defect of a three-dimensional crystal structure. Hence, any real surface is in principle nonhomogeneous. Additional nonhomogeneity is caused by a variety of possible microscopic defects (steps, cracks, dislocations, corners, etc.) or point defects (vacancies, interstitial atoms, substitution or insertion atom sites). Defect concentrations on real surfaces increase with diminishing crystal size. In highly dispersed systems, they may reach, or at times exceed, the concentrations of normal surface sites.

In addition, any real surface may have chemical nonhomogeneities formed during its preparation or from adsorption in the form of surface chemical compounds which modify the surface properties. It is therefore evident that all properties of a surface must be taken into account when considering its further interactions. Cause and effect can be difficult to distinguish here. Although the surface itself determines the nature of the adsorption of molecules from its surroundings, those adsorbed molecules often modify the surface properties.

Classifications of surface centers, plus a knowledge of the chemistry of surface complexes (the chemical properties governing the interaction of molecules with each type of center), make it possible to characterize the various possible types of surface compounds formed after adsorption. The facility for surface-compound formation is more diverse than, and qualitatively different from, that of individual molecular complexes since the surface may incorporate cationic states of various coordinations and valencies, sometimes unusual ones. Location on a surface can change the oxidative–reductive properties of a ligand site; adsorption is dependent on the collective properties of the solid and multi-centered adsorption can occur [30].

The study of the nature and properties of a surface entails great experimental difficulties. As the traditional methods of defect analysis (electro-physical methods and radioactive labeling) practically cannot be applied to polydispersed materials, it is clear that the development of concepts of the mechanisms of molecular processes on solids (which require information about the nature of bonds formed, surface structure, molecular mobility, etc.) is impossible without spectral analysis, which yields direct data on interactions at the molecular level. A particularly versatile role is played by vibrational spectroscopy. ESR (EPR) and NMR spectroscopies are limited to selected elements; the former requires paramagnetic ions or radical forms of adsorption, while the latter requires nuclei with a magnetic moment. In addition, changes resulting from adsorption

can be detected by UV or visible spectroscopy only for the limited proportion of species that give well-defined electronic absorption spectra. The vibrational spectroscopic methods (especially Fourier-transform infrared (FTIR), Raman and high-resolution electron energy loss spectroscopy (HREELS)) are by far the most versatile techniques for the analysis of surface layers on solids.

Vibrational spectroscopy provides data on the composition and structure of surface compounds, the nature of the bonds formed between adsorbed molecules and the surface, and the existence of different types of surface compounds and active surface centers. As the vibrational spectrum reflects both the properties of the molecule as a whole and the characteristic features of separate chemical bonds, this method offers the fullest possible information on the perturbation experienced by a molecule on contact with the solid surface, and often determines the structure and properties of adsorption complexes and of surface compounds.

Terenin [17, 35j] first pioneered the successful study of adsorption using molecular spectroscopy in the near-infrared region. Today, the literature contains much generalized experimental material on the character of interactions of various molecules with surfaces of silica gels, alumina gels, aluminosilica gels and zeolites as determined by infrared spectroscopy in the fundamental region. The principles of the study of surface compounds and adsorbed molecules by molecular spectroscopy have been described in several books [18–35a]. New experimental developments have been reviewed pertaining to studies (for example, by IR spectroscopy) of solids at high pressures and/or temperatures in various chemical media, to the determination of kinetic parameters for individual stages of surface reactions, and to the use of computers to process spectral data in order to improve the volume of information.

This book does not repeat a consideration of these problems but instead concentrates on the analysis of surface properties, the interaction of relevant simple molecules with the surface of the solid, and the reactions which occur on the surface of oxides of the transition-metals. This latter choice has been made for two reasons: first, transition-metal oxide systems were not extensively studied by molecular spectroscopy in the earlier days and the more recent results have not been subjected to detailed analysis and comparison, and secondly, such oxides and their surfaces are important because of their wide use as heterogeneous catalysts. The main objective of this work is to systemize scientific approaches to spectral studies in this area of surface chemistry. The entire volume of data obtained for each individual system cannot be examined in detail. Bearing in mind that catalysis is of central importance in a conceptual chemistry of the surface, and that it provides a means for achieving chemical transformations in the laboratory and in nature, this author considers it important to discuss the currently considered concepts by using catalytic systems and processes as examples.

As the main objects of early molecular spectroscopy studies were systems involving silica gels, alumino gels and aluminosilica gels, and as it proved fairly easy to obtain their spectra in the OH-stretching region, the greatest attention was at first focused on establishing the existence and significance of surface hydroxyl groups in adsorptive interactions. At that time, there were practically no methods accurate enough for the qualitative, let alone quantitative, differentiation of coordinatively unsaturated cations and anions on the surface of oxides. The difficulties involved in the analysis of the nature and surface properties of the latter oxides also proved a major obstacle to determining the character of the interactions between such centers and adsorbed molecules. In fact, until recently no data have become available on some aspects of the interaction between, say, alkenes and Lewis centers, even in such well-studied systems as alumina and crystalline or amorphous aluminosilicates, which are widely used as catalysts in hydrocarbon transformations.

The specificity of the material discussed here required novel approaches to the properties of the surface. It is known that in the important stage of initial complex formation, mechanisms of catalytic reactions involve interactions with transition-metal ions and/or oxygen on the surface of the catalyst. Evidently, both the nature and valency/coordination state of the cations, together

with the properties of the surface oxygen ions, exert a considerable influence on the character of activation and, possibly, on the directions of transformation of the adsorbed molecules. Hence, there is a need to find methods for the identification of such centers on the surface and to establish their concentrations and their differences in chemical properties.

The use of 'probe molecules', based on the analysis of their spectral changes as a result of donor or acceptor molecules interacting with their opposites on the surface, have been widely used for investigating these centers. This book contains a preliminary description of the author's approach to the analysis of surface properties, which includes the isolation of specific interactions of elementary simple molecules – so-called probe molecules – with every possible type of center on the solid.

This author's views on the main goals of molecular spectroscopy in surface chemistry can be described as the analysis of the important relationships between the nature of the surface centers on oxides, and the forms and directions of transformation of molecules adsorbed on them; these considerations account for the manner in which the material is presented. Information about the surface states of solids (particularly oxides), about their active sites, and also about the structures of surface compounds formed upon adsorption of the various types of molecules, is very important. Such information can be obtained by means of different physico-chemical methods, among which those of molecular spectroscopy [1–16] are the most widely used in chemical applications. In the past few decades, these have been very effectively used to investigate the surface chemistry of oxide systems [17–35].

Taking into account the large amount of literature covering these fields, the methods of IR and UV–Vis spectroscopies have been the principal means of investigating the surface chemistry of such solids. A short introduction to the development and analysis of the data obtained by means of these techniques, and the theory of such methods, is given in Chapter 1 of this book. For the EPR method, the strong reasons for its use as a tool for the investigation of transition-metal chemistry on oxide surface have been described in reference [35h], while the theoretical basis of such applications has been reviewed in various references [25, 31, 33]. Therefore, in this present book I will only use the results of this informative method.

The various molecular spectroscopic methods play even more of a key role in the development of the concepts of the surface coordination chemistry originally established for transition-metal complexes in aqueous solutions. The local approach has been chosen as the basis of the interpretation of the absorption bands which characterize the active sites on oxide surfaces and the interaction of these sites with adsorbing molecules. The collective properties of the solid adsorbents are also used, based on the analysis of the crystal structures of the oxides or of systems such as cation-substituted zeolites, heteropoly compounds of molybdenum, precisely prepared (for example, by ionic exchange or interactions of supports with complexes) supported systems in which the crystallographic positions of both cations and anions can be well and unambiguously determined by means of ESR, UV–Vis or Mössbauer spectroscopic methods. In the middle of the 1980s, a first attempt was made to develop the principles of surface coordination chemistry of transition-metal oxides based on the analysis of principally my own spectroscopic investigations of oxides surfaces and the compounds formed upon them through adsorption (of a limited number of molecules) [30]. In this present book, practically all of the international literature has been analyzed for the developing concepts and experimental data over a very wide range of molecular reactants and oxide systems. A correct comparative approach limits the number of published works that have to be considered individually, such as those which take into account results for only one molecule or another. The total number of such publications is so large (in thousands) that it is impossible to analyze all of them in detail in one single book.

A dramatic increase in the number of recent studies concerning applications of molecular spectroscopic methods to studies of the surface states, and to the structures of adsorbed species, has

led to the writing of this present book. More sensitive methods, such as FTIR, laser Raman spectroscopy and Surface-enhanced Raman Scattering (SERS), the sensitivities of which are order of magnitude greater than those of earlier vibrational spectroscopic methods, and especially the creation of new methods for obtaining vibrational spectra (diffuse reflection, high-resolution electron energy loss spectroscopy, electron tunneling spectroscopy and the spectroscopy of electromagnetic waves), as well as the wide use of computers to process the spectral information (for instance, to subtract spectra and to separate complex spectral contours into those of separate components), have stimulated progress in the study of the physico-chemical properties of heterogeneous systems and processes proceeding at the 'gas-solid', 'gas-liquid' and 'solid-liquid' interfaces, at the molecular level [17–66]. Due to these advances, it is now possible to obtain practically any spectra which reflect the interaction of a surface with molecules in the gaseous or liquid states. It is reasonable to affirm that these developments in spectral methods have caused a renaissance in interest in the surface chemistry and catalytic applications [67–108] of oxides and metals.

The appearance of more sensitive methods and new techniques has become a reason for a reassessment of a significant part of the spectral information obtained ten and more years ago, based on the use of more modern techniques. New spectral effects and characteristics, which could not be observed in earlier studies because of very low concentrations of the corresponding surface species, or because of low values of extinction coefficients, can now be detected. Unfortunately, authors of such new studies do not always cite the related previous work, although they use the main ideas and conclusions as a basis for interpretation. This is why, in this book, the data obtained in the 1970s and 1980s or earlier are reexamined, along with those from studies published during the past decade.

A significant contribution to the development of spectroscopic investigations of surface compounds has been made by the evolution of cryoscopic methods [109, 110], which allow the registration of the spectra of individual molecules, their fragments, ions and radicals, both in free states and in interaction with clusters of metal particles of different sizes (from monatomic upwards) or with cations (anions) frozen in a matrix. Since these interactions have similarities with such structures formed on solid surfaces, the use of this cryoscopic data helps in the interpretation of the spectra of reactive surface compounds.

The development of the catalytic systems based on the organometallic compounds supported on different supports (so-called precise catalysts) [111–115] became another way in catalytic chemistry that contributed a lot to the identification of the surface compounds.

It should be particularly pointed out that, in spite of the now relative ease of obtaining spectral information (including spectra registration), the interpretation of the spectra obtained and associated phenomena (which are investigated by means of spectral methods) is extremely difficult. In order to solve these problems, it is necessary to have knowledge in at least three areas: spectroscopy itself, the surface chemistry and heterogeneous catalysis. It cannot be assumed that the presence of an absorption band, close in position to that expected in the spectrum of a possible fragment, provides a sufficient reason to draw such a conclusion about the structure of the complex (and all the more about its subsequent participation in different interactions). Such a simplified approach to the use of spectral information to explain, for example, catalytic phenomena, has often led to wrong conclusions which in turn have caused further mistaken studies. As will be shown below, 'doubtful' surface compounds are often postulated as intermediates in certain reaction mechanistic schemes. This is why this author, who has devoted more than 30 years to the application of spectroscopic methods in surface chemistry, and particularly heterogeneous catalysis, has undertaken the difficult task of summarizing and analyzing the voluminous related literature and data on the investigation of surface centers and the interactions of these centers with a large number of molecules of both inorganic and organic types. Principal attention is paid to the spectral identification of surface compounds (especially to evidence for their formation)

formed upon the interaction of different molecules with solid surfaces. The development of spectral criteria to identify such compounds is the second subject of this book, since at present the main problem in using physical methods in surface chemistry is to obtain reliable proof that the suggested surface compounds are really present.

Chapter 1 summarizes the fundamentals of the different vibrational spectroscopy methods, and their main strengths and weaknesses with respect to each other, as well as their different fields of application in studies of surface chemical problems. Several substantial books and reviews devoted to such subjects, and analysis of the applications of different spectroscopic methods in adsorption and catalysis, have already been published [27, 43, 44, 52, 63–66]. Among them, the books devoted to particular spectroscopic methods [24, 25, 31, 32, 34, 34a] have been written by leading scientists in their fields. Readers who are interested in the possibilities of some particular spectral method can find the answers in the appropriate text. The main question of *in situ* studies, including kinetic and spectral measurements, have also been described in reasonable detail [35a, 63–65].

It should be pointed out that such numerous data have been obtained by different spectral methods during investigations of surface phenomena and that it is impossible to describe and analyze all such data in a single book. In general, studies can be divided into two groups, (i) those devoted to spectroscopic investigations, and (ii) works in which spectroscopic methods are used to check on the information obtained by nonspectroscopic methods. The second group is widely represented in the literature, and is used for the study of adsorption and catalysis. However, the spectral information obtained in a large number of such works is not sufficiently reliable and the formation of one or another type of a postulated surface compound is not always proven. For these reasons, the conclusions of such studies are not always discussed in detail in this book, although appropriate ones will be mentioned. Studies of the other group, which form the basis of this book, are as a rule carried out by highly qualified spectroscopists and are based on a detailed analysis of the spectral information obtained. These studies contain very important data about solids and the surface compounds formed during interaction with different molecules.

Chapter 2 is devoted to the examination of spectral images of both simple oxides and binary oxide surface systems in the various regions where they occur, and includes discussions of the following: (i) the fundamental frequencies of the lattices, (ii) surface cation–anion bonds, (iii) molecular states of adsorbed oxygen, and (iv) surface hydroxyl group vibrations. Particular attention is given to the study of electron-donating centers, oxygen ions, electron-accepting centers and coordinatively unsaturated cations. The principles of crystal structures of oxides are used to interpret the spectra, because it has been shown earlier that the homogeneity or otherwise of an oxide surface, as well as the properties of different surface centers, depends on the degree of dispersion and is related to the exposure of different crystal faces. The reactivity of surface centers to different adsorbed molecules is analyzed for numerous oxide systems. The different types of surface centers observed on oxide systems are classified, and the procedures used for their investigation by means of molecular spectroscopy are analyzed.

Probe molecules with spectral parameters sensitive to the state of different adsorption centers are described. Particular attention is paid to data on the identification of both Brønsted and Lewis acidic sites on the surfaces of different oxide systems through the IR spectra of adsorbed ammonia and pyridine. Practically all of the data in the literature on spectral patterns from ammonia bonded to coordinatively unsaturated surface cations are considered in this chapter. Correlations revealed between the changes in the frequencies of the symmetric deformational vibration of the ammonia molecule due to adsorption ammonia and the acceptor abilities of coordinatively unsaturated surface cations show the relative strengths of different cation acceptor centers on the oxide surfaces (the established influence of the nature of the cations on their acceptor ability). It is shown that ammonia adsorption opens the way to the identification of surface acid–base pairs

(both surface cations and anions) which lead to ammonia dissociation and the formation of NH_2 and OH species. For a number of systems involving acid-forming oxides, the presence of protic acid centers is demonstrated, in which a proton compensates for a charge on several surface anions through mobility.

Analysis of the different spectral methods of determination of both the acidic and basic properties of an oxide surface is represented in this chapter. Sections where these questions are examined contain (i) equations to calculate the strengths of both protic and aprotic surface centers in simple and complex oxide systems, (ii) quantitative data on the different nature of active surface centers, and (iii) extinction coefficients and values of integral intensities for a number of the most commonly used probes (NH_3 , Py and CO). In several cases an analysis of the correlations between the quantitative characteristics of different types of surface centers and the pre-treatment and/or preparative conditions of the surfaces is carried out. Spectral characteristics of both regular and defective surface centers are also examined in this chapter.

In Chapter 3, the states of different cations in zeolites, oxides, supported oxides and heteropoly acid systems, which depend on preparation methods and other experimental conditions are analyzed on the basis of detailed examinations of diffuse reflection electronic and ESR spectra. Special attention is paid to the cations of copper, nickel, cobalt, palladium, silver and platinum, and to their changes upon modification by supports or other active components. Spectral characteristics of metal particles are dependent on their sizes, types of support (including strong metal-support interaction (SMSIs)) and upon lateral interactions between adsorbed molecules. Analysis of the spectra of adsorbed species on a number of metals, as well as the spectral manifestations of the complexes formed at the 'active-component support' interface, are also considered.

The data covered in Chapter 3 illustrate the special roles of CO and NO molecules as probes. Use of these molecules, coupled with the direct study of cationic states (by diffuse reflectance electron spectroscopy (DRES), ESR, etc.), enables the establishment of correlations between νCO (NO) and both the charge and coordination states of the cations. A number of model examples of real oxide surfaces, created on the basis of oxide crystal structures, are examined. These models describe sufficiently the experimental data obtained about interactions of the probes with both active and inactive surface centers and surface structures. Sections are devoted to the detailed examination of the spectral data in this field available from the literature concerning the interactions of different types of oxide surfaces with other simple molecules such as H_2 , N_2 , NO, H_2S , SO_2 , NO_2 and CO_2 . Such data establish the direct interrelationships between the nature of the activation and properties of the surface sites and the activation of these molecules. For each molecule, the analysis of its electronic structure is carried out and changes observed upon complexation are explained in terms of the changes in the vibrational spectra. It is shown that the N_2 molecule is a good probe for investigating electron-acceptor centers, whereas the H_2 molecule is a unique one for describing the properties of acid-base pairs. This chapter concludes with data about the limits of spectral ranges characteristic for the complexes of CO (NO) with the variable valence and coordination states of different cations, and also with metal clusters of different sizes.

The potentialities of spectral methods to investigate the interactions of inorganic or organometallic compounds with oxide surfaces are briefly summarized in Chapter 4. Principal attention is given to data representing the analysis of spectral changes resulting from the interactions between molybdenum heteropoly acids (HPAs) and the surfaces of different supports, and also the changes in properties of such unsupported systems themselves. It is shown that the examined spectra enable us to determine whether or not such interactions occur, and can also detect the interactions of different types of organometallic systems such as metal-allylic and carbonyl compounds of different cations or metals. The results of the modification of oxide surfaces by anions, in particular SO_4^{2-} , occupy a significant part of the data discussed in this chapter.

Interactions between oxide surfaces and organic molecules of different types, such as alkanes, alkenes, alkynes, aryls (including their halide derivatives), nitriles, alcohols, aldehydes, ketones and acids, are presented in Chapter 5. Wherever possible, the complexation with each type of surface center is differentiated and analyzed separately. Spectral images of the complexes formed, their features and spectral parameters, which depend on the type and particularities of the surface center, are examined in detail.

Using the spectral data, general correlations are demonstrated between the character of the nature and reactivity of the complex being formed from a particular adsorbate and its dependence upon the nature of the surface center. The formation of new types of surface species (such as unsaturated compounds interacting with coordinatively unsaturated surface cations), first revealed by spectral features, is described for a number of systems. This chapter also contains numerous energy and spectral characteristics of the surface compounds, such as the π - and π -allylic complexes of unsaturated hydrocarbons, formed upon dissociative interactions of organic molecules with oxide surfaces.

Special attention is paid to the estimation of the character of C–H bond activation in alkanes. Analysis of recently obtained data on methane activation allows the representation of a scheme which establishes and provides a correlation between the active surface centers and the particular intermediate species formed upon them. The latter provide a possibility for understanding the pathway by which hydrocarbons are converted to other products on the different surfaces. As a result of the spectral classification of the different adsorption species, new types of surface compounds have been shown to be formed on oxide surfaces, which are otherwise absent or extremely unstable under normal conditions.

Finally, in Chapter 6 a discussion is given of the mechanisms of a number of catalytic reactions which have been investigated by means of vibrational spectroscopy.

1 THEORETICAL FUNDAMENTALS AND EXPERIMENTAL CONSIDERATIONS OF THE SPECTROSCOPIC METHODS USED IN SURFACE CHEMISTRY

Three principal types of problems may be distinguished in the application of molecular spectroscopic techniques in surface chemistry, namely (i) the characterization of the surface, (ii) the estimation of the type and structures of surface compounds, and (iii) the obtaining of information required to understand the mechanisms of the processes proceeding on the surface of a solid. The first problem requires the determination of the types and properties of surface centers, which are dependent on the structure and morphology of the solid. The second and third problems concern adsorption processes and involve the study of the following: (i) the structures and properties of the surface compounds forming at different surface centers, (ii) reaction intermediates, and (iii) the directions of their transformations to the products. During recent years, the situation in this area has greatly improved, and different spectroscopic methods are now available for these studies.

The general principles of all of the techniques is the interaction between the incident radiation or particle beam and the specimen and the following analysis of both the nature and energy of the beam after such interaction. The energy regions involved in the different spectral methods involving electromagnetic radiation are represented in Figure 1.1, while Table 1.1 summarizes some of the essential characteristics of the various techniques.

It is clear today that any progress in the field of surface chemistry is impossible without the application of such modern methods of molecular spectroscopy as UV–Vis spectroscopy, Fourier-transform infrared (FTIR) spectroscopy, Raman spectroscopy, electron energy loss spectroscopy, (EELS) including high-resolution electron energy loss spectroscopy (HREELS), and neutron spectroscopy.

The main feature of these methods is that they are nondestructive analytical methods, because the electromagnetic (radiation) or particle beams which are used, disturb the investigated system insignificantly. This is why such vibration techniques in different electromagnetic variants, such as transmission, reflectance and emission, or the low-energy electron loss spectroscopies, are very widely used nowadays.

1.1 Electronic spectroscopy

Electronic spectroscopy (ES) is normally concerned with the valence electronic transitions between molecular orbitals. The transmissions between the electronic levels (Figure 1.2) are

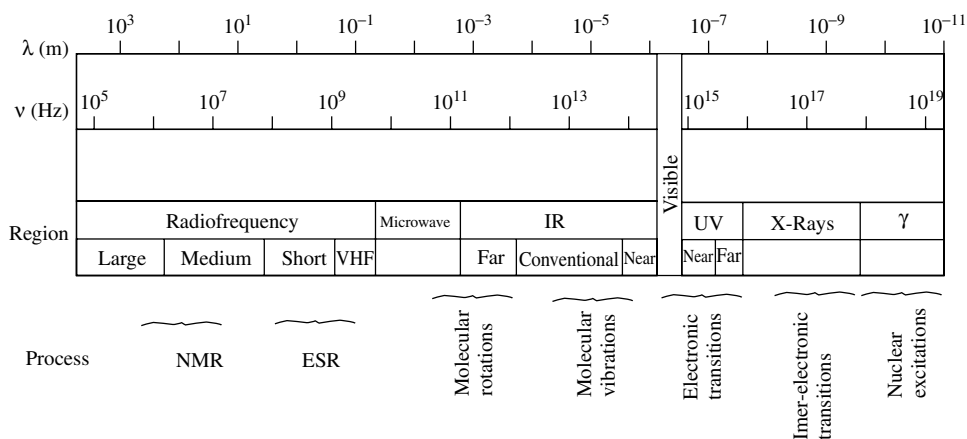


Figure 1.1. The regions of the electromagnetic spectrum, classified according to the experimental techniques employed and the molecular information that can be obtained.

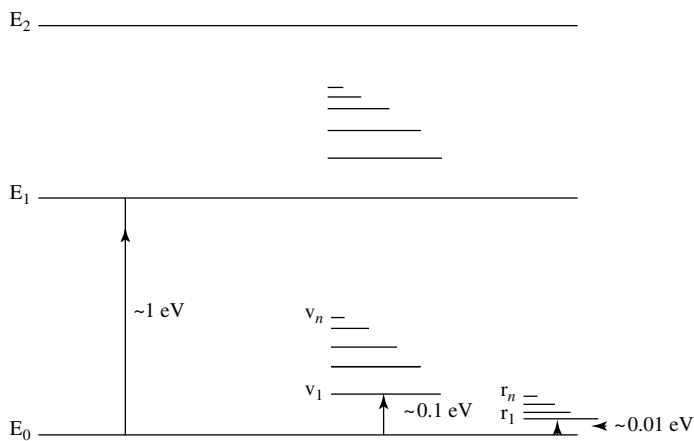


Figure 1.2. Scheme of energy levels: E, electronic; v, vibrational; r, rotational.

located in the range of the electromagnetic spectrum ($50\,000\text{--}3000\text{ cm}^{-1}$) – this is the basis of UV–Vis spectroscopy. The energies associated with the electronic ‘jumps’ are large enough to *provoke* vibrations of the molecule, and the transitions are thereby broadened [6, 8–10, 33, 116].

Light in the UV–Vis region of the electromagnetic spectrum can be used to study the electronic transitions of the substrates. According to the nature of the electronic jumps, the electronic transitions found in organic and inorganic chemistry can be classified into several groups: (i) $d \rightarrow d$ transitions (Figure 1.3(a)), (ii) charge transfers, (iii) $\pi \rightarrow \pi^*$ transitions (Figure 1.3(b)), and (iv) $n \rightarrow \pi^*$ (Figure 1.3(b)). In the far-UV range are found other transitions, e.g. ($n \rightarrow \sigma^*$) and ($\sigma \rightarrow \sigma^*$) (Figure 1.3(b)). Charge transfers occur due to electron transfers from an occupied orbital localized on a donor to an unoccupied orbital of an acceptor. In organic systems, these transitions are between electron acceptors and electron donors and produce the absorption bands in the UV and visible regions of the spectra with $\epsilon \sim 10^3\text{--}10^6$ (see below). In inorganic systems, the charge-transfer phenomena are of two types, involving an electron

Table 1.1. Comparative characteristics of the different spectral methods used in surface chemistry.

Characteristic	Technique										
	Molecular spectroscopy					Resonance spectroscopy				Surface studies	
	IR, PAS	Raman	UV-Vis	EPR	NMR	Mössbauer	Neutron spectroscopy	EELS	XPS	AFS	SIMS
Thickness analyzed	mm	mm	mm	mm	mm	100 μm	0.1 mm	μm	20–50 \AA	10–20 \AA	2–3 \AA
Area analyzed	cm^2	cm^2	cm^2	cm^2	cm^2	cm^2	mm^2	cm^2	cm^2	cm^2	cm^2
Sample degradation	No	Possible	No	No	No	No	Possible	Very small	Possible	Possible	No
Sample preparation	Easy	Easy	Easy	Easy	Easy	Easy	Difficult	Difficult	Easy	Easy	Easy
Quantitative measurements	Possible	difficult	Possible	Yes	Yes	Yes	Yes	–	Yes	Possible	Possible
Gaseous atmosphere	Yes	Yes	Yes	Yes	Yes	Yes	Yes	No	Difficult	Difficult	No
Temperature range ($^{\circ}\text{C}$)	–196 to 500	–196 to 500	–196 to 500	–269 to 1000	–196 to 200	–269 to 400	–269 to 800	Ambient	–180 to 600	–180 to 600	Ambient
Information obtained	Functional groups; adsorbing species	Functional groups; adsorbing species	Degree of oxidation; ion symmetry; adsorbing species	Paramagnetic species; degree of oxidation; symmetry	Functional groups	Degree of oxidation; symmetry of environment	Adsorbing species; atomic structure	Metal–ligand bonds	Degree of oxidation; surface composition	Surface composition	Surface composition

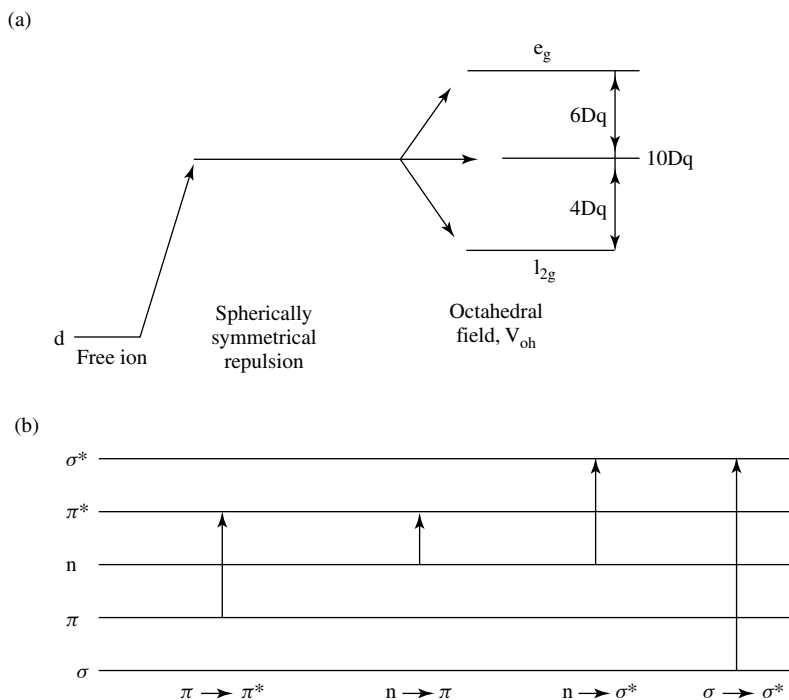


Figure 1.3. Schemes of electron transfers: (a) $d \rightarrow d$ electron transitions in an octahedral field; (b) relative energies of electronic transitions between different types of orbitals typical of organic molecules (σ , π and n).

transfer in different directions: (i) from an orbital mainly localized on the metal to that mainly localized on the ligand ($M \rightarrow L$), and (ii) in the opposite direction ($L \rightarrow M$). The energies of these transitions is higher than that for $d \rightarrow d$ transitions, and accordingly the absorption bands are in the UV region of the spectra ($\varepsilon \sim 10^3 - 10^6$). Optical spectra can be directly obtained by either internal or external reflection-absorption techniques (reflectance spectroscopy).

1.1.1 TRANSMISSION SPECTRA

The transmitted light of intensity I is related to the incident light intensity I_0 by the *transmittance*, T , given by I/I_0 ($0 < T < 1$). For thin samples, the transmittance can be related to the concentration of the absorber (c) and the thickness of the sample (l) by the Lambert-Beer law, as follows:

$$T(\nu) = \exp(-\varepsilon l c) \quad (1.1)$$

where ε is known as the *molar absorption coefficient* ($\text{cm}^2 \text{mol}^{-1}$). The *optical density* or *absorbance*, $A (= \log(I/I_0))$ is also used frequently. It is often preferable to use this parameter in the integral form (A), as follows:

$$A = \int_{\nu_1}^{\nu_2} A(\nu) d\nu = \int_{\nu_1}^{\nu_2} \ln[I_0(\nu)/I(\nu)] d\nu \quad (1.2)$$

UV–Vis spectroscopy is distinguished by a fairly high sensitivity. In particular, the intensity of the absorption for allowed one-electron $d \rightarrow d$ transitions is characterized by a molar absorption coefficient of the order of $\sim 1-100$. The ε value is significantly lower for complexes with a high symmetry and is much greater in the case of the bands characteristic of the charge transfer in the complex.

1.1.2 DIFFUSE REFLECTION SPECTRA

In surface chemistry, the UV–Vis spectroscopic method is usually used in its diffuse reflection modification. The radiation reflected from a powdered crystalline surface consists of two components, i.e. (i) that reflected from the surface without any transmission (mirror or specular reflection), and (ii) that absorbed into the material and which then reappears at the surface after multiple scattering. Modern spectrometers minimize the first component, and the term ‘reflectance’ is thus used for diffusely reflected radiation [25, 117].

Since only a part of the diffuse radiation is returned to the detector, measurement of the diffused intensity is difficult. For this purpose, a special integrative sphere (Table 1.2), coated inside with a highly reflecting layer, such as MgO or BaSO₄, is used. Such a sphere increases the part of the diffused intensity that reaches the detector (30–50 %). Spectra are recorded ‘in ratio’ with a sample which has similar diffusion characteristics to the sample under investigation, but without any absorption losses.

The evaluation of the intensities of diffuse reflectance spectra is based on the theory of Kubelka and Munk. The reflectance is given by $R = I/I_0$ ($0 < R < 1$). For a nontransparent thick layer, R is called R_∞ and the ratioed $R'_\infty = R_\infty(\text{sample})/R_\infty(\text{standard})$. The quantity $\log(1/R')$ is known as the *apparent absorbance* and is not strictly proportional to the concentration of the absorbing species [117]. To calculate the Kubelka–Munk function, the measurable reflectance R'_∞ can be used as follows:

$$F(R'_\infty) = (1 - R'_\infty)^2 / 2R'_\infty \quad (1.3)$$

This quantity, for a layer of infinite thickness, has been related to the parameters K and S ($F(R'_\infty) = K/S$), which are themselves linked to the absorption (K) and the reflection–diffusion (S is a scattering coefficient). The theoretical base, as well as the conditions of application of the Kubelka–Munk function, has been discussed in detail elsewhere [25, 117].

Electronic spectroscopy may be used to determine the local symmetry and oxidation state of a transition metal, and thus it is a sensitive probe for the type of site in which such an ion exists. The applicability of this method is not limited to transition-metal-containing systems. It can be also used to measure the electronic spectra of adsorbed molecules and to obtain direct information about the excited and ground states of such species.

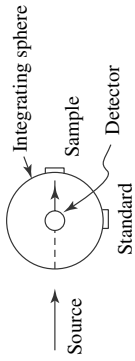
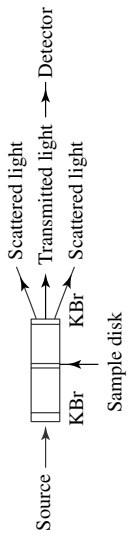
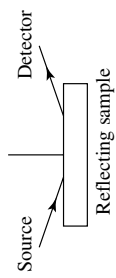
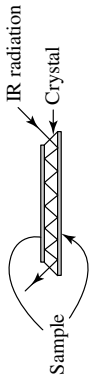
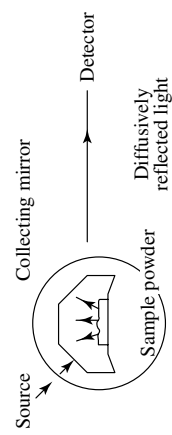
There are no problems in constructing a cell for electron spectroscopy since quartz is fully transparent to UV–Vis radiation. Some types of cells used to study the UV–Vis spectra of cations in oxide systems and adsorbed molecules are described in the literature [25, 117].

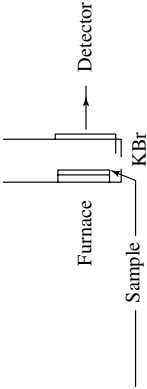
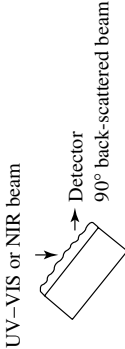
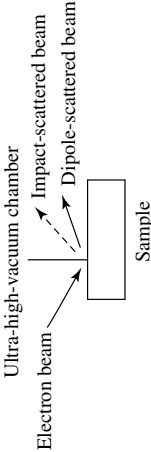
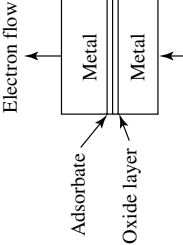
1.2 Vibrational spectroscopy

Vibrations in molecules are excited by absorption (infrared spectroscopy (IRS) or by scattering (Raman spectroscopy) of photons, electrons (electron energy loss spectroscopy (EELS)) or neutrons (inelastic neutron scattering (INS)).

Since the bands in the spectra are observed at specific frequencies, it follows that the rotational, vibrational and electronic motions leading to electrical dipole changes must occur at specific frequencies. A classical model gives considerable information concerning the existence of vibrational

Table 1.2. Basic experimental principles and applications of the different spectral methods used for surface chemistry analysis.

Method	Common scheme	Thickness analyzed	Quantitative measurements	Information obtained
UV-Vis		mm	Possible	Ion symmetry; adsorbing species; degree of oxidation
Transmission IR		mm	Possible	Adsorbed species; surface active sites; functional groups
Reflection IR (RAIRS)		mm	Possible	Adsorbed species; surface active sites; functional groups
ATR		mm	Possible	Adsorbed species; surface active sites; functional groups
Diffuse reflection (DRIRS)		mm	Possible	Adsorbed species; surface active sites; functional groups

Emission IR		Possible	Adsorbed species; surface active sites; functional groups
Raman		Possible, but with difficulties	Functional groups; adsorbed sites; surface structure; bulk structure; structure of adsorbed species
EELS		-	Metal-ligand bonds; phase transitions; chemical structure
IETS		Possible, but with difficulties	Vibrational spectra of minute quantities of materials

frequencies of atoms within the molecules, but allows us to explain the existence of rotational frequencies only if the electronic motions occur at the same frequencies.

The vibration of a diatomic molecule can be reduced to the motion of a single particle of reduced mass μ_m . In this model, the problems are simplified by considering that the diatomic molecule can be analogous to the harmonic oscillator (Figure 1.4), in which two masses (m_1 and m_2) are joined by a perfect spring of length r_0 . A restoring force f is directly proportional to the distance r , as follows:

$$f = -kr = \mu_m(d^2r/dt^2) \quad (1.4)$$

where k is known as the harmonic force constant, and is a function of the potential energy U in accordance with Hooke's law:

$$f = -dU/dr = -kr \quad (1.5)$$

Integration of this equation leads to the following parabolic relationship see (Figure 1.4(a)):

$$U = 1/2kr^2 \quad (1.6)$$

For diatomic molecules A–B, r represents the displacement of the atoms from the equilibrium separation r_0 . A small displacement of one of the masses relative to the other will cause the system to vibrate as a simple harmonic oscillator with a frequency given by the following:

$$\nu_0 = (1/2\pi)\sqrt{k/\mu_m} \quad (1.7)$$

where μ_m is the reduced mass of the system. At the assignment of the frequencies observed in the infrared spectra, this relationship is often used in conjunction with isotopic exchange, in particular deuterio exchange, as follows:

$$\nu_{X-H}/\nu_{X-D} = \sqrt{2} = 2m_x/(2 + m_x) \quad (1.8)$$

where m_x is the mass of the X atom. This ratio is 1.37 for OH–OD and NH–ND, and 1.36 for CH–CD (i.e. ca. $\sqrt{2}$).

According to quantum theory, the energy of the molecule is given in terms of a series of discrete energy levels, E_0 , E_1^v , E_2^v , etc. (see Figure 1.2), and each discrete molecule must exist at one or other of these levels. The frequency of absorption or emission of radiation for a transmission between the levels with energies E_0 and E_1 is given by the following:

$$\nu = (E_1 - E_0)/h \quad (1.9)$$

where h is the Planck constant.

From the Schrödinger wave equation, the total energy of vibration is as follows:

$$E_{\text{vib}} = h\nu(v + 1/2) \quad (1.10)$$

where ν is the frequency of vibration of the oscillator and v is the vibrational quantum number. For any transition between quantized levels in which $v' \pm v'' = 1$.

$$\Delta E = h\nu \quad (1.11)$$

The differences between two levels arise directly as a result of the quantum-mechanical derivation of Equation (1.10). For the simple quantum-mechanical model, the presence of combination bands and overtones in the spectrum is forbidden, because such bands involve jumps between

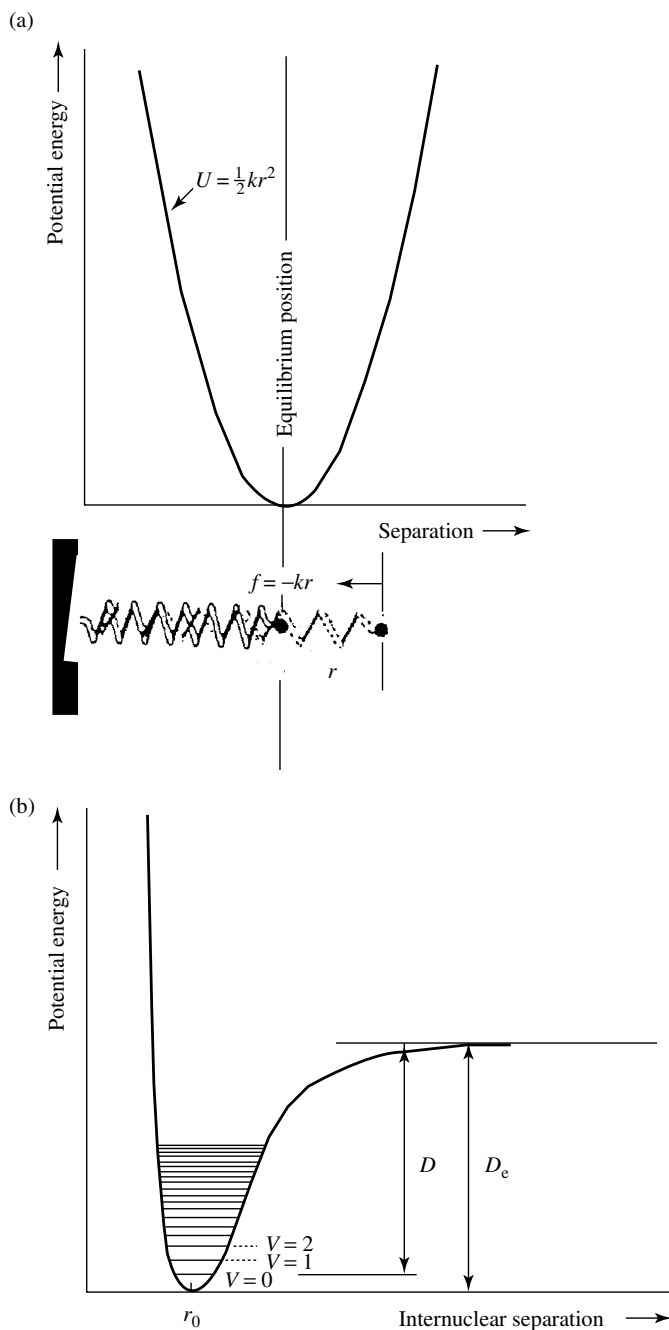


Figure 1.4. Potential-energy functions for (a) a mass and spring system obeying Hooke's law, and (b) a real diatomic molecule with a dissociation energy D_e and equilibrium bond length r_e (where r_0 represents the first energy level).

several different quantum levels. There are no such stringent rules in the case of an anharmonic oscillator, where overtone and combination bands can appear, often weakly in the spectra, according to the following:

$$E_{\text{vib}} = h\nu(v + 1/2) - x_e(v + 1/2)^2 \quad (1.12)$$

where x_e is the anharmonicity constant. Introduction of this parameter leads to the potential curve shown in Figure 1.4(b).

The movements of the atoms in a molecule during vibration can be approximately classified into two groups, i.e. (i) bond stretching, and (ii) angle deformations. For an N -atomic molecule, the number of fundamental vibrations is $3N - 6$ for a nonlinear and $3N - 5$ for a linear molecule. There are four types of vibrations, i.e. ν , δ , γ , and τ (Figure 1.5). Generally, the frequencies of these vibrations decrease in the order $\nu > \delta > \gamma > \tau$.

All molecules can be classified into a limited number of symmetry groups, which obey the rules of group theory. A knowledge of the symmetry group of a molecule allows the determination of the symmetry classes of the $3N - 6$ normal modes of vibration and their activities in IR and Raman spectroscopies.

Assignment of the bands in the spectrum to particular types of vibrations is an important stage and is based, as a rule, on *group-characteristic* (of limited dependence on the nearest molecular environment) modes. Calculations based on vibrational theory are used for more accurate assignment [4, 14–16]. These calculations show that there are no strictly characteristic vibrational modes; frequencies of many group vibrations are coupled and make certain contributions to each other. A vibration with a minimum contribution from other vibrations is known as a *group characteristic*. Usually, interpretations of the spectra of adsorbate–adsorbent systems are made by the

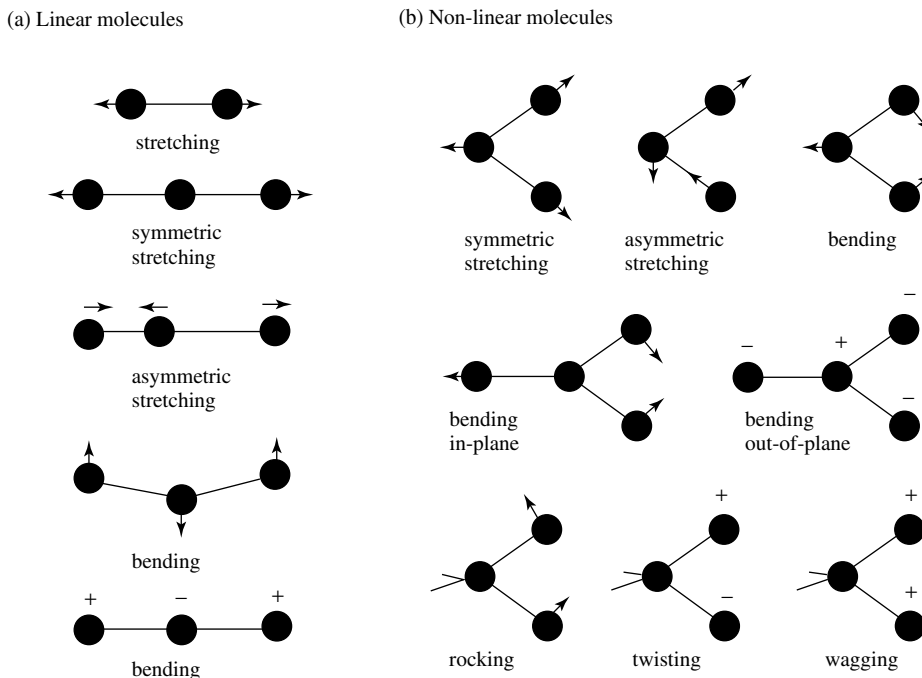


Figure 1.5. Fundamental modes of vibration of (a) linear, and (b) nonlinear molecules.

comparison with the spectra of bulk compounds or fragments isolated in a matrix. However, in this way only certain types of compound can be identified. Calculations of the vibrational spectra of individual surface species based on the modeling of the potential function of the molecule (vibrations in the force constants of the potential function) are useful for interpreting changes in vibrational frequencies and their reactions to changes in the force field of molecules subjected to the influence of a highly nonuniform field at an adsorbent surface [19, 118].

Several forms of vibrational spectroscopy are now in routine use, i.e. (i) transmission infrared, (ii) Raman, (iii) diffuse reflection, (iv) reflection-absorption infrared, and (v) electron energy loss, but in the study of surfaces none has found wider application than infrared spectroscopy.

1.2.1 INFRARED SPECTROSCOPY

The infrared (IR) region corresponds to the energies of the vibrations and rotations of molecules. If a molecule is subjected to IR radiation whose frequency is equal to that of one of its oscillators, this oscillator will resonate and absorb part of the radiation. The absorption (emission) intensity is given by the transition probability between the ground and excited states. Not all vibrations are observed—only those transitions corresponding to vibrations with variation of the dipole moment are active in IRS. The intensity of the infrared band is proportional to the square of the change in dipole moment. The principles of this method have been presented in numerous books and reviews [1–5, 11–16, 119–123] and are summarized in Table 1.2.

In the study of processes occurring on surfaces, transmission, reflectance, emission and diffuse reflection infrared spectroscopies are used.

Transmission spectroscopy

A common infrared transmission spectrum is obtained as a result of the direct transmission of an infrared beam through a sample when the following conditions apply: $\Delta\nu = +1 (\partial\mu/\partial Q)_0 \neq 0$, where μ is the dipole moment, and Q is a normal coordinate. As in UV-Vis spectroscopy, the spectrometer records the transmission, $T (= I/I_0 = \exp(-kl))$, the intensity of which can be found from the Lambert-Beer law (Equation (1.1)). The sensitivity of this method is determined by both the characteristics of the radiation detector and by the absorption coefficient of the medium. Approximately a 10-fold gain in sensitivity can be achieved by the use of the Fourier transform (FT) technique [1, 120].

To study the spectra of bulk oxides, dilution in either KBr (down to 400 cm^{-1}) or CsI (down to 200 cm^{-1}), or polyethylene disks are used. If the sample is stable in air and does not react with KBr or CsI, these are the methods most often used. However, if any interactions take place, then the techniques of attenuated total (internal) reflection (ATR) or emission spectroscopies have to be used.

For both cases, in order to obtain a typical transmission IR spectrum from oxides in the region of surface vibrations (in this case, the thickness of the corresponding sample is ten times more, as a minimum, than that of the corresponding samples prepared in an immersion media), the sample has to allow at least a partial transmission, preferably 10 % or more, of the IR beam. Scattering of the radiation by the particles can be another factor which leads to low transmission. The transparency is improved when the oxide particle sizes are small relative to the radiation wavelength. Scattering may be significantly reduced by the use of pressed disks or highly dispersed samples (particle size less than $1 \mu\text{m}$). The latter can be prepared in two different ways, i.e. (i) sedimentation of the dissolved sample from an inert solvent or from air onto a transparent window, or (ii) by using an electrical field [42]. When a material is pressed into a thin flat self-supported disk, the scattering, which takes place during the transmission of the IR radiation through the sample, can be substantially reduced. In general, such a disk should be from one to a few tenths of a millimeter in thickness and have a density between 10 and 100 mg cm^{-2}

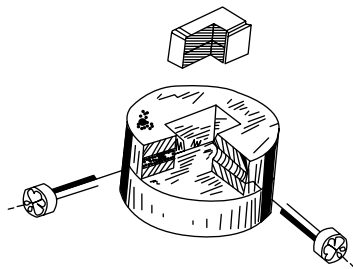


Figure 1.6. A typical mold used for compressing self-supported pellets of adsorbent in infrared studies.

in order to give good transmission in the infrared and also to have good mechanical properties. It is better to press the samples in a demountable mold (Figure 1.6) [19, 42], which then allows adjustment of the lateral pressure on the compressed sample by means of a number of screws and plates, in order to prevent cracking of the thin disk and to facilitate its removal from the mold. Preparation of such thin samples, especially from transition-metal oxides or zeolites, is truly ‘an art’. If the solids are not transparent or cannot be molded as disks and hence have to be handled as powders, the following methods can be useful: (i) the use of a grating; (ii) a (powder) technique in which the powder is finely pulverized, sifted, and then spread out on an IR-transparent disk (such as KBr, CaF_2 or a silicon single crystal) and, if this covering is stable, then covered by a second disk; (iii) dilution of the sample in a compound that is transparent and inert to the reaction being studied (e.g. SiO_2 and Al_2O_3); (iv) the use of special cells. The problem of sample preparation is minimized in the case of diffuse reflection spectroscopy [25, 61, 122–124].

To record the infrared spectra of adsorbed molecules, special vacuum cells are used – these are available in many different and widely variable types, depending on the system being studied [18–21, 23–26, 28–35, 42, 44–46, 63, 64]. Ideally, these cells should be designed so that the sample can be heated up to 1273 K, and cooled to liquid nitrogen temperature, to adsorb/desorb both gases and vapors at different temperatures, be able to maintain a high vacuum, and to record the spectra of adsorbed molecules without exposing the pellet (disk) to the air. The main problem here is achieving an hermetic sealing of the ‘windows’ (plates) which are transparent in the IR (Table 1.3 [42, 119, 125–127]). Frequently, such a sealing is made by the use of different cements and glues with low vapor pressures, or alternatively by using O-rings and flanges.

There are two types of cells used for recording infrared spectra under high vacuum over a wide temperature range: (i) a cell, large in length, which gives the possibility of separating a heater from the region of the sealed windows, i.e. where the recording of spectra and the heating of the sample are carried out in different parts of the cell or if a static sample is heated, a cooling of the windows is required (see, for example, a cell design resulting from the work of this present author (Figure 1.7) [42, 128]); (ii) a cell with a very short optical pass (<10 mm), and thus the absorption spectrum is not affected by the gaseous-phase molecules, even at high pressures (Figure 1.8(b)) [42]. As a rule, in the second type of cell (Figure 1.7(a); Figure 1.8(a)) a sample has to be moved to the heating zone, which is far from the site of hermetic sealing. The necessity to move the sample is a disadvantage of such cells because of the possibility of irreproducible measurements. It should be noted that in order to measure the temperature of a sample with a thermocouple, direct contact of the latter with the sample and contact of the sample with a furnace are needed. For this purpose, special samples holders, in which the samples are situated on the heated walls (Figure 1.9), are used. If heating of the sample is only by radiation, the measured temperatures of the sample in vacuum and in the presence of gas may be significantly different and thus can lead to errors. Several designs of cells used in adsorption studies have

Table 1.3. Various optical materials used for lenses and windows in infrared studies.

Material	Low-energy cutoff (cm^{-1})	Comments
Sapphire	>1600	High mechanical strength; inert; connected with metal; hard; expensive
Quartz	>2500	Good for high-temperature work and in the overtone region; insoluble; easy to work in fused form
LiF	>1200	Good dispersion in the near-IR region; easily scratches
MgF ₂	1400	Strong; chemically durable
CaF ₂	1200	Inert to most chemicals; tends to be costly; slightly soluble; good from 73–373 K
MgO	>1200	Hard and costly; can be sealed to a high-expansion glass
Silicon	1100	Inert; insoluble; connected with glass; not transparent at high temperatures
NaF	1000	Slightly hygroscopic
BaF ₂	900	Hard; expensive
ZnS	714	Good up to 1073 K; strong; chemically durable
NaCl	600	Slightly hygroscopic; cheap; easily worked
KCl	550	Slightly hygroscopic; cheap
AgCl	500	Photosensitive; can corrode metals
ZnSe	500	Good up to 573 K; soluble in acids
KBr	350	Hygroscopic; easily scratched; used as powder for pressed-disk technique
CsBr	250	Very hard; expensive
KRS-5	250	Very soluble; expensive; toxic; deforms under pressure
CsI	180	Very hard; expensive

been reviewed by Little [18], Kiselev and Lygin [19], Delgass *et al.* [25], Shchekochikhin and Davydov [42], Bell [119, 127], and Basu, Ballinger, Yates *et al.* [128a], as well as in numerous original studies.

The best materials for windows directly connected to glass are silicon, MgO and AgCl, while sapphire is the best material for connection to metals (see Table 1.3). Quartz cells, which are usually routinely used in the visible and UV regions of the spectrum, can also be employed in the infrared region, but only above 2000 cm^{-1} . A very convenient cell is one with silicon single crystal windows (Figure 1.8(a)) but, unfortunately, this cannot be used at temperature higher than 473 K because of the reduced transparency of the silicon single crystal as a result of internal electron transfer mechanisms.

There are several types of cells of minimized volume, used in order to record spectra under dynamic conditions (e.g. at high temperatures during catalytic transformations – so-called *in situ* conditions – see, for example, Figures 1.7(b) and 1.10). A simple flow-cell-reactor made from metal [42] or quartz [64, 65] practically without any ‘free volume’, has been proposed (Figures 1.7(b) and 1.11). The main part of such a cell is a reactor made from metal or quartz. Both the reactor and windows (CaF₂, BaF₂, ZnS or ZnSe) are polished and clamped to each

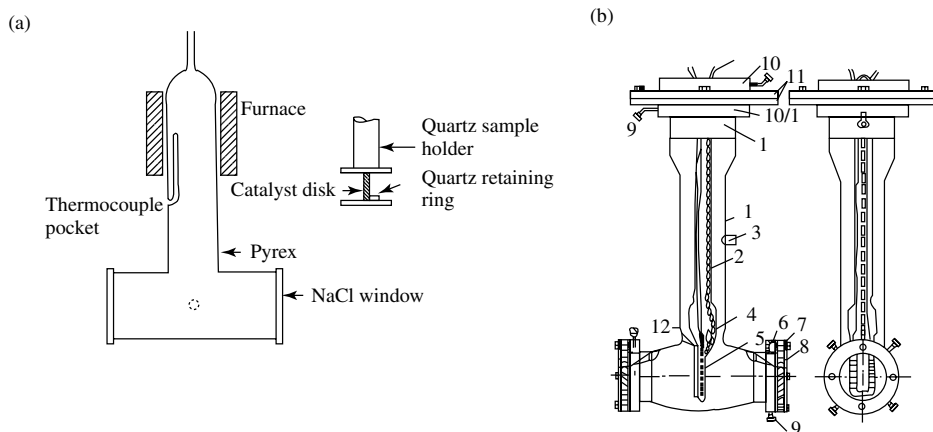


Figure 1.7. Schematics of cell-reactors used for studying the spectra of adsorbed molecules at (a) room, and (b) high temperatures: 1, cell body; 2, sample holder; 3, evacuation port; 4, case for thermocouple; 5, container for heater; 6, 10, cooling channels; 7, 11, flanged connectors; 8, windows; 9, connectors; 12, sample pocket.

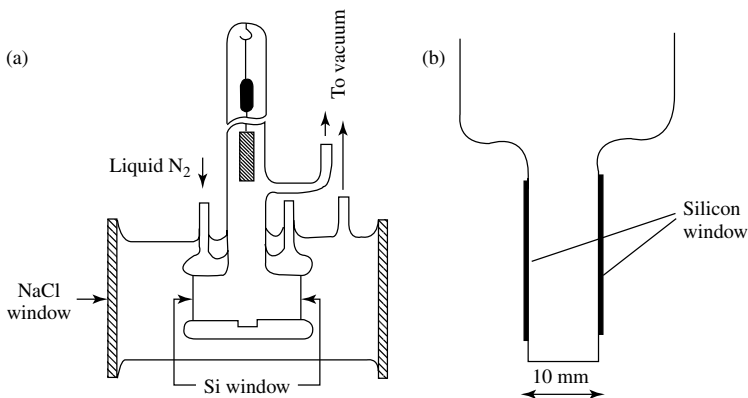


Figure 1.8. Schematics of vacuum cells with silicon windows: (a) for low-temperature investigations; (b) with a short optical path.

other [64, 65]. Connections between the cell body and the windows is achieved by using iridium or gold foils, or with Teflon [42]. The Graseby Specac company now produces standard *in situ* high-temperature cells for temperature ranges up to 773 K, as well as high temperature and pressure cells.

Emission spectroscopy

Methodological difficulties in the study of surface species caused by strong scattering or absorption of infrared light by the adsorbing sample can be eliminated if emission spectra are recorded [1, 25, 35]. This method, however, is less frequently used since the intensities of the emission bands are quite low, except at higher temperatures. Emission spectra are usually produced by heating the sample above 473 K (Figure 1.12) [129] and are the most appropriate in cases where

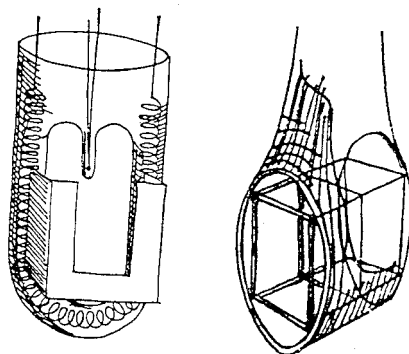


Figure 1.9. Schematics of types of sample holder.

reactions proceed on surfaces at high temperatures (see Table 1.2). The spectrum is obtained by measuring the ratio of the emitted radiation at any wavelength to that emitted by a perfect ‘black body’ at the same wavelength and temperature. According to the Kirchoff law, $\varepsilon_v = a_v$, where a_v is the absorbance (fractional absorption) of the substance. It follows from the Lambert–Beer law that emission of a thick nonopaque emitter will approach that of a black body, so the ideal sample to record an emission spectrum is a thin layer supported on a near perfect reflector such as a metal.

The basic equation for quantitative measurements is as follows

$$\varepsilon + r + t = 1 \quad (1.13)$$

where r and t are the reflectance and transmittance coefficients of the substance, respectively. It follows from this that for an opaque sample ($t \sim 0$), $c = 1 - r$, and thus selected peaks in the reflection spectra will be recorded as minima in the emission spectra.

In principle, emission spectra can be recorded by employing any one of the cells described above for use in transmission spectroscopy, including the cell-reactor design for recording spectra *in situ* (see Figure 1.11) in which the sample in the infrared beam is heated (see Table 1.2).

The high sensitivity of the FTIR technique has significantly increased the possibilities for emission spectroscopy, and this can now be used to study the structure of solid surfaces, molecules adsorbed on the surfaces of different substances, formation of oxide films, etc. More details of the application of this method are available in a number of references [1, 25, 31, 64].

Reflection spectroscopy

Numerous oxide systems exist as opaque powdered samples from which light is reflected and not transmitted. Reflected radiation, in this case, consists of two components: the specular component reflected from the surface without transmission (mirror or specular reflection), and the diffuse component which is absorbed into the sample and reappears at the surface after multiple scattering [2, 9, 130]. The various forms of reflection spectroscopy (see Table 1.2) are less frequently used than the transmission methods, although they do have some important specific uses. In principal, the best way of obtaining absorbance and reflectance mode information from flat samples is by reflection spectroscopy (which gives signals that depend on these two related variables), in which the data is then analyzed by use of the Kramer–Kronig equation.

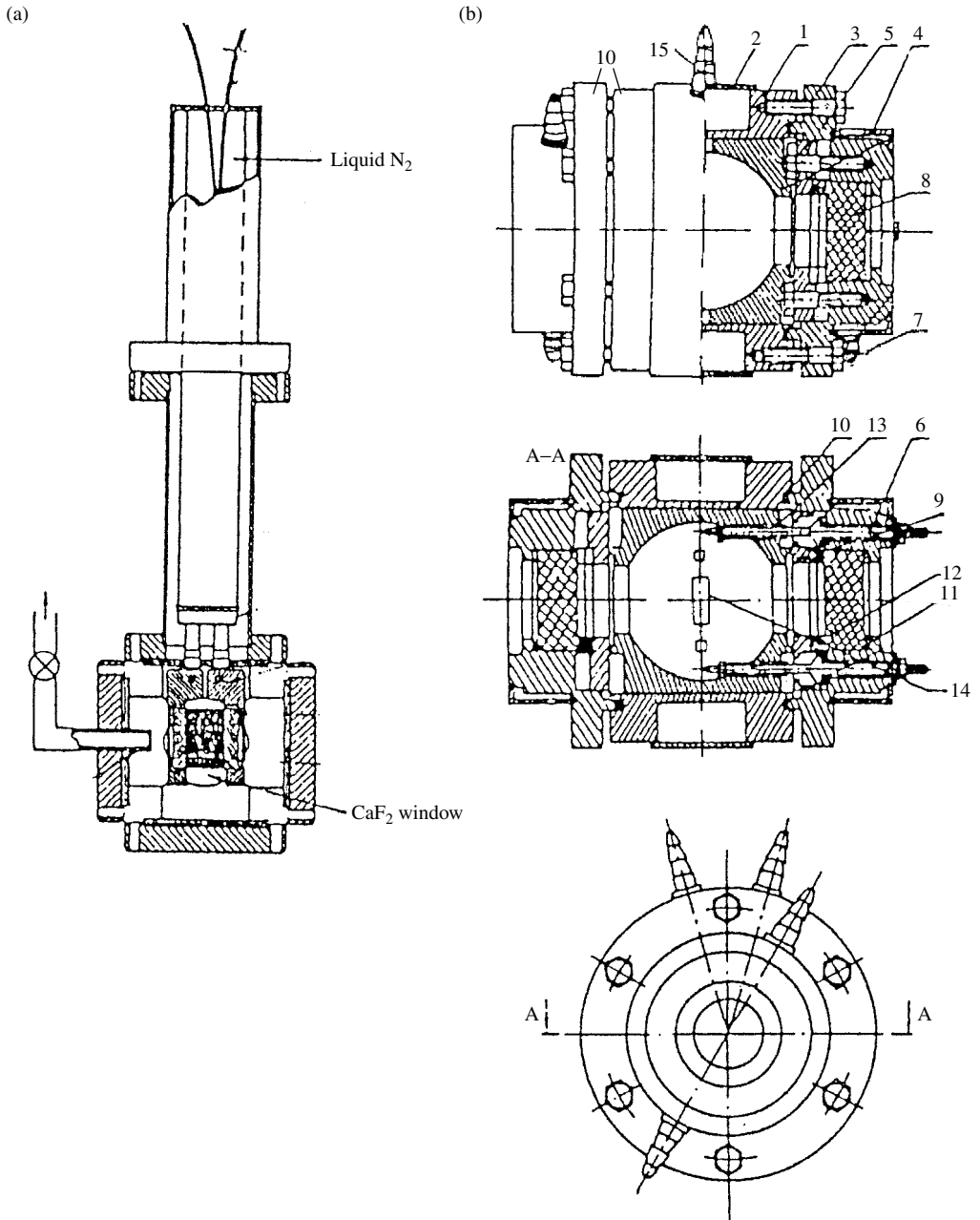


Figure 1.10. Schematics of cell-reactors used to study *in situ* spectra at (a) low temperatures [128c]. Reprinted with permission from Basu, P., Ballinger, T. H. and Yates, J. T., Jr, *Rev. Sci. Instrum.*, **59**, 1321–1327 (1988), American Institute of Physics, and (b) high temperatures and high pressures: 1, body of the cell; 2, 4, 6, cooling channels; 3, window holder; 5, 7, bolts; 15, water connectors; 8, window; 9, leads for heater and thermocouples, 10, flange seal between cell and window holder; 11, 12, O-ring seals; 13, insulating tube; 14, sample holder.

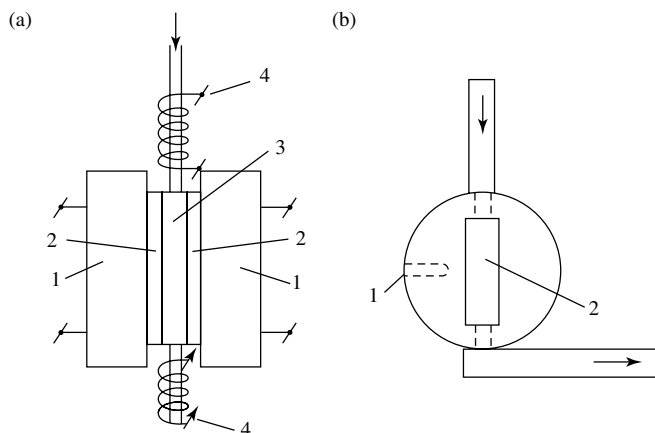


Figure 1.11. Schematics of a flow-cell-reactor of minimal volume: (a) 1, heater; 2, window; 3, reactor; 4, auxiliary heaters; (b): 1, thermocouple pocket; 2, sample position [64]. Reprinted from *Catal. Today*, **25**, Matushak, V. A. and Krylov, O. V., 'In situ IR spectroscopy of intermediates in heterogeneous oxidative catalysis', 1–88, copyright (1996), with permission from Elsevier Science.

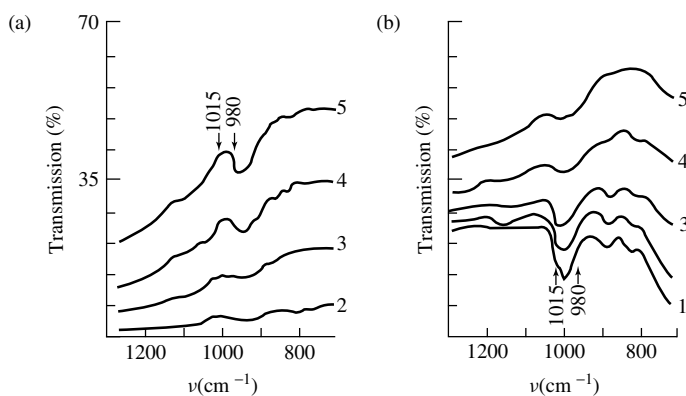


Figure 1.12. Infrared (a) emission, and (b) absorption spectra of oxygen adsorbed at 673 K on chromium oxide, recorded at (1) 345, (2) 373, (3) 473, (4) 573, and (5) 673 K.

Mirror reflection (reflection–absorption IR spectroscopy – RAIRS)

As was predicted by Greenler [131] and then experimentally verified later [132–135], a good metal reflector gives rise to maximum absorption from a monolayer near grazing incidence as a result of the phase shift between the incident and reflected waves which combine to form a standing wave mode approximately normal to the surface. The trade-off between the high incident electric fields at the surface and the number of reflections leads to an optimum value for the latter (see Table 1.2). It is often possible to use only one reflection without any loss of sensitivity if the optimal angle (88°) of the beam incidence is chosen [131].

Internal reflection spectroscopy (attenuated total reflection – ATR)

This technique is elementary to the more usual external reflection spectroscopy. In this case, the infrared radiation approaches the solid–gas interface via the solid phase [2, 9, 25, 136]. The

radiation is totally reflected back into the solid if the angle of incidence exceeds a critical angle when the absorbing molecules are absent. The incident and reflected waves superimpose and form a standing nonpropagating electric field (see Table 1.2). The sample, prepared as a very fine powder in order to maximize optical contact, is dispersed on one of the two faces of a KRS (TlBr + TlI) single crystal, which has a high refractive index. The IR beam enters via the input side of the crystal, leading to n reflections on the two faces. A small part of the light is adsorbed by the sample at each reflection [136]. This method can be used to obtain the spectra of adsorbed species [130–137].

Diffuse reflection infrared spectroscopy (DRIRS)

In this technique, diffuse scattered radiation is collected by the sphere or an ellipsoidal mirror and focused on the detector (see Table 1.2), with the infrared absorption spectrum being described by the Kubelka–Munk function (Equation (1.3) above) [19, 25, 35, 61, 122–124, 137]. The relationship between the intensity of the band due to an adsorbed substance and its concentration is as follows:

$$F(R) = I[1/(R - R_\infty)] = 2\epsilon c/S \quad (1.14)$$

This equation assumes that the scattering coefficient S is wavelength-independent (which is not the case line in regions of very low absorption).

Theoretical studies indicate that diffuse reflection spectroscopy is more sensitive than transmission spectroscopy if the effectively scattering components are investigated. However, reflection spectroscopy has not been used in the IR region until fairly recently because of the insufficient sensitivity of infrared detectors, and the great difficulty in constructing integration spheres for collecting diffuse radiation in this region. The sensitivity problem was overcome by the development of FTIR spectroscopy. In addition, this method allows the direct investigation of powdered materials contained in cells of small volume. Therefore, it has significantly simplified sample preparation, as well as pretreatment techniques and the obtaining of the spectra, particular at low temperatures.

In order to obtain diffuse reflectance spectra, various commercial attachments (for example, the Harrick or Spectra-Tech Collector, which is more convenient for adjustment) and *in situ* cell-reactors [1], including chambers for high-temperature, pressure or vacuum work, are now available. An interesting variation of this technique which uses an additional internal source of radiation has been proposed by Kazansky and coworkers [124]. For measurements in the near-infrared region, thin-walled quartz ampoules have been used as IR cells, while in the mid-infrared range, CaF₂ or BaF₂ windows are preferred.

1.2.2 PHOTOACOUSTIC SPECTROSCOPY

If radiation is absorbed by a sample in a closed cell, it is converted into heat and the temperature of the sample increases. This is so-called *photothermic effect*. If the sample is irradiated with a modulated IR beam, the photothermic effect in turn periodically heats a gas in contact with the sample in the boundary layer, $2\pi/a_g$, where $1/a_g$ is the thermal diffusion length of the gas. The energy is hence transferred to the gas phase as modulated pressure changes. The modulation of the gas pressure can be detected by a microphone and amplifier. Blank and Wakelfield [138] showed that for absorbing compounds the photoacoustic signal is proportional to the absorbance, and thus a photoacoustic spectrum is similar to an absorption spectrum, except that the thickness of the layer giving rise to the acoustical output increases with the wavelength of the incident radiation.

An advantage of this method is the possibility of investigating surface species without any special preparation of the sample being required. Photoacoustic spectroscopy (PAS) is well suited

to the study of turbid media, including liquids, solids and gases, and suitable equipment is now commercially available [25, 125].

1.2.3 RAMAN SPECTROSCOPY

The *Raman effect* is based on the inelastic scattering of electromagnetic radiation due to its interaction with molecular vibrations or rotations (see Table 1.2). Raman spectra are recorded as a function of the wavenumber of inelastically scattered light which results from the excitation of vibrations in molecular and crystalline materials. Because the shifts in the frequency of the scattered radiation are usually in discrete vibrational quanta, this technique provides the same kind of detailed molecular structural information that can be obtained from infrared absorption, except for the differing relative intensity relationships between the vibrational features. The excitation source is a single monochromatic line of a continuous gas laser in the visible or UV region. In Raman spectroscopy, the optics employed in optical microscopy can be used for measurement of samples down to a few μm in size [5, 12, 15, 139–146].

When the molecule recovers its energy after an elastic collision process, the emerging photon has its former energy ($h\nu_0$), but its direction or angular momentum can be changed. This is known as the *Rayleigh effect*. If the energy of the molecule is changed to E_n , corresponding to a new quantum state, the collision is inelastic, and the emitted photon has a different frequency, as follows:

$$h\nu = h\nu_0 - (E_n - E_0) = h\nu_0 - h\nu_n \quad (1.15)$$

where ν_n is the frequency of a vibrational or rotational energy of the E_n level. In the so-called Raman Stokes scattering, the molecules receive extra energy from the photons and the frequency of the latter is decreased (Figure 1.13). Sometimes the molecule may be in an excited state and during the collision process can lose energy and return to the ground state. The energy of the emitted photon in this case is then greater:

$$h\nu = h\nu_0 + h\nu_n \quad (1.16)$$

This is known as Raman anti-Stokes scattering (Figure 1.13). For a particular situation such a peak has much lower intensity than the Stokes one, because the proportion of vibrationally excited molecules is usually small according to the Boltzmann distribution. The difference between the energies of the incident ($h\nu_0$) and emitted ($h\nu_n$) photons depends only on the vibrational and rotational energy levels of the molecules and not on the wavelengths or frequencies of the exciting radiation.

As in infrared spectroscopy, some vibrations are also forbidden in Raman spectroscopy. Only vibrations which change the polarizability of a molecule are Raman-active. Usually, this requires that the molecule changes its shape. From quantum-mechanical theory, it is possible to conclude that for harmonic vibrations Raman scattering occurs only if the following conditions apply:

$$\Delta\nu = \pm 1 \quad (1.17)$$

$$(\partial\alpha/\partial Q)_0 \neq 0 \quad (1.18)$$

where α is the polarizability, and Q is a normal coordinate. According to the selection rules, Raman spectroscopy is complementary to infrared spectroscopy since the vibrations forbidden in an IR spectrum are often active in the corresponding Raman spectrum, and vice versa. This is strictly the case for the vibrations of centrosymmetric molecules.

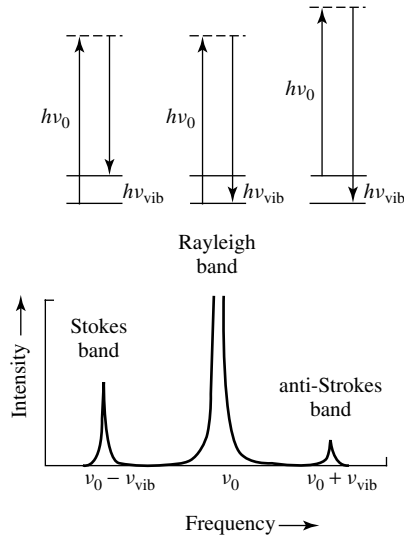


Figure 1.13. The energy-level transitions and spectral features in the Raman effect.

Raman spectroscopy is sensitive to molecular and crystal structure. Applications include chemical fingerprinting, examination of single grains in ceramics and rocks, single crystal measurements, aqueous solution investigations, identification of compounds in bubbles and fluid inclusions, and investigations of structure and strain states in polycrystalline ceramics, glasses, fibers, gels, and thin and thick films. It should be noted, however, that a significant disadvantage of the Raman technique is the small scattering cross-section, as the majority of the intensity is in the Rayleigh scattering mode which is much stronger than the Stokes bands.

The development of intense and monochromatic lasers has significantly increased the number of applications of Raman spectroscopy for the study of the surface chemistry of metal oxides [5, 25, 34, 35, 40, 41, 141–143, 145]. However, even so, a significant limitation for the application of Raman spectroscopy to the study of surfaces can be the superposed strongest fluorescence from the sample itself or from any impurities that might be present. The exciting and scattered frequencies are close together and are in the visible range. Thus, there is generally no problem of cell transparency whatever the material of the cell (silica, quartz, glass or Pyrex), or whichever diffused radiation is observed. There are no difficulties in the use of pressure cells and cells able to withstand very low or very high temperatures. In addition, there is no need for any special preparation of the samples. Powders, liquids, crystals, and even metallic surfaces, can all be studied. A strong point of its application in surface chemistry research is the fact that this technique is highly suitable for *in situ* studies. Even commercial flow-cell reactors have been constructed to study catalytic and adsorption phenomena *in situ*. More widely Raman spectroscopy is used to study the surface layers of supported oxides [104, 105] since the spectral lines of the oxides normally used as supports do not appear in the regions which are characteristic of the fundamental vibrations of the oxides themselves. Linkam Scientific Instruments Ltd and Wotton Scientific are two companies which now commercially produce simple and convenient *in situ* Raman cells. In the latter cell, the sample can be rotated, which thus reduces the heating of the sample by the laser beam radiation.

Despite some advantages (a wider spectral range than for infra red, easier sample preparation, etc.), there are several problems that limit the use of Raman spectroscopy [145], including the following:

1. The intensities of diffused Raman lines of adsorbed species are low and in some cases detection is not possible.
2. Fluorescence of ultra-low level traces of impurities can be so significant that the Raman scattered radiation can no longer be observed.
3. The local heating of the sample by the laser beam can be significant enough to modify or even destroy the sample.

Fortunately, technical progress over the last few years has overcome most of these difficulties. Thus, *resonance* Raman spectroscopy has solved the problem of the intensities of the Raman bands, pulsed lasers reduce fluorescence, cooling of the sample avoids heating and consequent desorption of the adsorbed species, while sample rotation allows different ‘parts’ of the sample to be examined, thus overcoming local heating problems.

Surface-enhanced Raman spectroscopy

This is a modification of the Raman technique which is used in surface chemistry to study molecules adsorbed on metal surfaces [24, 34, 147, 148]. A large number of mechanisms have been postulated in order to explain the very large enhancement process – of the order of up to 10^6 . These include electronic resonance phenomena similar to those observed in ‘standard’ Raman Spectroscopy (RS), based on the surface complexes and surface plasmons activated by the surface process resulting from electrochemical oxidation–reduction cycles [34], and cold deposition of the metal from the vapor state. Restrictions of this otherwise very attractive technique are the limited number of metal systems for which the surface-enhancement phenomena on is observed (silver, copper and gold) and the necessity for special pretreatment of the system under investigation.

Different aspects of the theory, experimental techniques and applications of the Raman effect are analyzed in detail elsewhere [25, 35, 141, 146].

1.3 Electron energy loss spectroscopy

In this method, a beam of mono-energetic, low-energy electrons (commonly with energies of 2–10 eV) falls on a surface and excites the lattice vibrations of the substrate, molecular vibrations of the adsorbed species and even electronic transitions [29, 122, 149–154]. The energy loss of the scattering electrons is described by the following:

$$E = E_0 - h\nu \quad (1.19)$$

where E is the energy of the scattered electron, E_0 is the energy of the incident electrons, h is the Planck constant, and ν is the frequency of the excited vibration.

A primary mechanism by which electrons lose some of their energy to the vibrational modes of an adsorbate is a long-range interaction between the electric field of the incoming electron and the dynamic dipole of the adsorbate [28, 29, 137, 151]. The inelastic collision electrons are mostly forward-scattered and appear close to the specular direction (see Table 1.2). Because of the dipole nature of this interaction, the same selection rule that applies to RAIRS is applicable, as follows:

$$(\partial\mu_{\perp}/\partial Q)_0 \neq 0 \quad (1.20)$$

i.e. only the vibrational modes of the adsorbate with a component of their associated dynamic dipole moment perpendicular to the surface are observable in electron energy loss spectroscopy (EELS). This limits the identification of modes in an EELS spectrum, but in the case when such

a mode can be identified, allows us to obtain information about the geometry and symmetry of the surface complex [137].

While the dipole mechanism of EELS is the most important, it is not the only mechanism of inelastic scattering. A second excitation mechanism, i.e. (impact scattering, involves a short-range interaction between the electron and the molecule which scatters the electrons over a wide range of angles (see Table 1.2). By this mechanism, all vibrations may be excited – not only the dipole-active ones. Similarly to Raman spectroscopy, the electron may take an amount of energy, $h\nu$, away from the excited molecules and leave the surface with an energy equal to $E_0 + h\nu$.

A strong point of EELS is that it detects losses in a very broad energy range from infrared to electronic transitions at several electronvolts. There are no difficulties with EELS in detecting vibrations in the range between 50 and 800 cm^{-1} , which are accessible only with difficulty in RAIRS studies.

There are three main requirements which EELS spectrometers have to satisfy: (i) the primary electrons should be mono-energetic, with as little spread in energy as possible, preferably by only a few meV; (ii) the energies of the scattered electrons should be measured with an accuracy of 1 meV or better; (iii) the low-energy electrons must effectively be shielded from magnetic fields [35]. A comparison of EELS with RAIRS on a number of points has been made by Niemantsverdriet [35]. Although, in principle, EELS can provide more information about the vibrational frequencies of modes involving atoms of the adsorbate or the surface of the adsorbent when compared with optical spectroscopies, its practical use is limited at present by the relatively poor resolution of EEL spectra (10–30 cm^{-1}) and the necessity for flat samples. It is principally used, as for RAIRS, to study monolayers on single crystal metal surfaces.

1.4 Inelastic electron tunneling spectroscopy

The inelastic electron tunneling spectroscopy (IETS) technique involves an electron tunneling between two metal electrodes separated by a thin oxide-based intermediate layer which constitutes the sample [155–159]. Inelastic electron tunneling (IET) junctions are prepared as follows: (i) a thin (ca. 1000 Å) metal film is evaporated onto a clean insulating substrate under vacuum (ca. 10^{-6} Torr); (ii) the film is oxidized by glow discharge anodization or by exposure to air or oxygen; (iii) the oxide is doped with the material of interest; (iv) the junctions are then completed by evaporating a counter-electrode through a second metal mask [158]. If adsorption is on the high-area oxide itself or on metal particles supported on the oxide, the loss processes in the tunneling electrons increase, corresponding to the vibrational quanta of the adsorbed species, and both IR- and Raman-active modes of vibration can be observed in this case.

Several different approaches have been presented in the literature concerning theoretical treatments of the IETS intensities, starting from the first published by Scalapino and Marcus and based on the modification of the tunneling potential barrier by a simple molecular dipole potential.

IETS is a very sensitive technique for obtaining the vibrational spectra of monolayer or sub-monolayer coverages of molecular layers at the oxide interface region of metal–insulator–metal tunneling junctions, has good resolution and a wide spectral range, is sensitive to all surface vibrations, and can be used on oxide and oxide-supported metal systems. IETS can also give information on the orientation of the molecules toward the surface. However, there are marked disadvantages, (i) i.e. the necessity to use a counter-electrode, (ii) spectra must be recorded at low (usually liquid helium) temperatures, and (iii) single crystal metal surfaces cannot be used. Nevertheless, IETS can be useful in catalytic and adsorption investigations on model oxide and supported metal systems.

1.5 Inelastic neutron scattering spectroscopy

This method is based on analysis of the energy distribution among neutrons, which are inelastically scattered by the chemical species under investigation. From a poly-energetic source, the energy dispersion of the scattering beam is limited by Bragg reflection from a single crystal operating as a diffraction monochromator located before the sample. In the case of a pulsed neutron beam, analysis of the energies is obtained by measuring the times of arrival at the detector by the scattered neutrons [155, 160–163]. There are no selection rules for inelastic neutron scattering spectroscopy (INSS), so all vibrational transitions are active in principle. However, their intensities depend on the INS cross-section and amplitudes of all of the atoms involved in the corresponding vibrational mode. Such cross-sections are characteristic of each element and do not depend on their chemical environments. However, there is a particularly high sensitivity to vibrations involving the moving of hydrogen atoms; The hydrogen (H) nucleon has a high cross-section, while the deuterium (D) nucleon has a low one. The INS technique can be used to determine the orientations and positions of the adsorbed molecules, as well as the strength and location of the forces bonding a particular molecule to a surface [161].

1.6 Other vibrational spectroscopies

1.6.1 INFRARED ELLIPSOMETRIC SPECTROSCOPY

Reflectance ellipsometry is concerned with the measurement of the polarizing properties of an interface, i.e. with measurement of $\tan \psi$ and Δ (ψ and Δ denoting the angles) or of the complex function R_p/R_s (values of the reflection coefficients, corresponding to the incident and reflected (complex) amplitudes for the p and s electric vectors, respectively) for the ‘clean’ and covered surface. From the following equation, defining the ellipsometric reflectance absorbance as:

$$A_e = \log_{10}(|R_p/R_s|^2/|R_p/R_s|^2) \quad (1.21)$$

it follows that:

$$A_e = A_p - A_s \quad (1.22)$$

This is the fundamental equation connecting ellipsometric reflection spectroscopy with photometric reflection spectroscopy. If the substrate is metallic, $A_e \approx A_p$, and so photometric and ellipsometric spectroscopies will yield the same absorption spectrum. Further details of the theory of this method can be found elsewhere [164, 165].

1.6.2 SURFACE ELECTROMAGNETIC WAVE SPECTROSCOPY

This technique has recently received considerable attention [166]. Surface electromagnetic waves (SEWs) are surface waves in the sense that the electric and magnetic fields decay exponentially as one moves away from the surface, either into the metal or into a vacuum (Figure 1.14).

SEW spectroscopy provides the possibility of researching the vibrational spectra of adsorbed molecules, the processes of surface reconstruction, corrosion processes, and determination of the optical constants for adsorbed layers and supported thin films, as well as for the metal surface

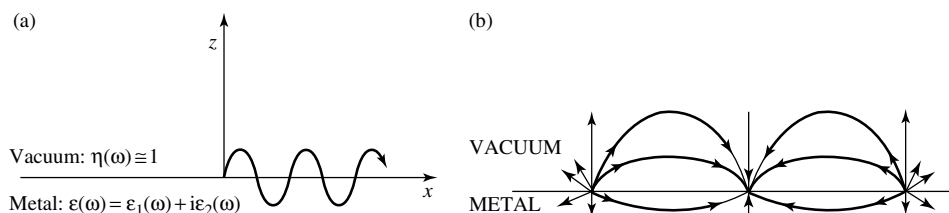


Figure 1.14. Schematic representations of (a) the coordinate systems for surface electromagnetic waves on a metal–vacuum interface, and (b) the electric field associated with a surface electromagnetic wave.

itself. The SEWS technique does not require ultra-high vacuum and can be carried out in the presence of reactant gases. It is a simpler method than ellipsometry for monolayer and sub-monolayer coverages. SEW spectroscopy has also been used to study oxide surfaces [167, 168].

1.7 *In situ* measurements

In studying the chemical transformations which take place during the interaction between a molecule and a solid surface it is very important to record the spectra under conditions (temperature, pressure, contact time, etc.) which are similar to those at which the process proceeds, in either steady-state or unsteady-state conditions in the case of catalytic reactions [21, 30, 129]. In parallel with the spectral registration, by using special cells it is possible to measure the catalytic

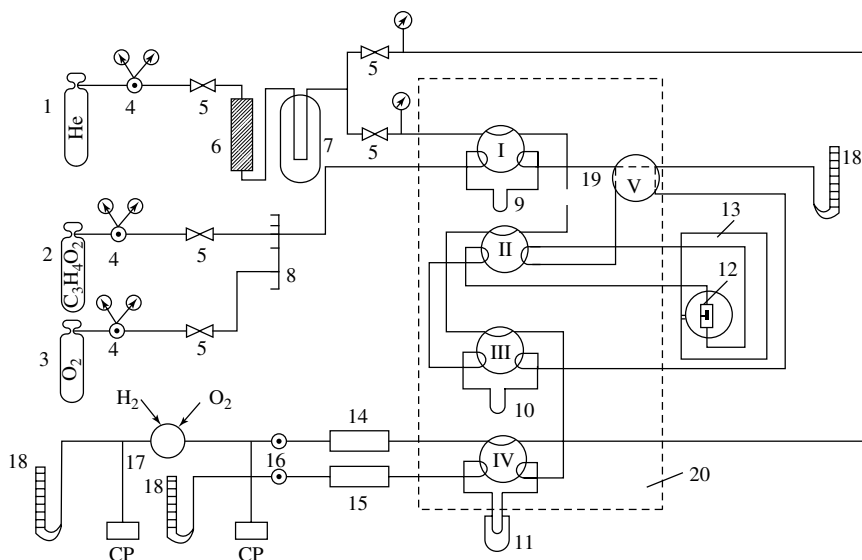


Figure 1.15. Schematic diagram of an experimental installation for studying the IR spectra of adsorbed molecules: 1, 2, 3, vessels with He, reaction mixture and O₂, respectively; 4, flow regulator; 5, stop valve; 6, 7, columns with molecular sieves to purify He from H₂O and O₂; 8, distribution 'comb' for gas mixtures; 9, dosing loop; 10, sampling loop to take samples for analysis from a flowing mixture; 11, freezing trap for reaction products; 12, cell-reactor; 13, cell compartment of IR spectrometer; 14, column with 'Porapak-Q'; 15, column with molecular sieves; 16, catharometers; 17, flame-ionization detector; 18, rheometers; 19, syringe sampler; 20, thermal case; I–IV, 6-port metal valves; V, 4-port valve; CP, control potentiometer.

activities of the samples. Several types of such apparatus have been described (see, for example, [169–171]). In catalytic measurements involving the simultaneous recording of infrared spectra, Davydov and coworkers [30, 129, 172], using a pulsed or flow catalytic cell-reactor combined with catalytic equipment (Figure 1.15), have determined the rates of transformation of a number of different surface species.

In principle, it is possible, by using infrared techniques, to study the kinetics of numerous different processes and transformations of surface complexes (so-called spectro-kinetic measurements). Unfortunately, the practical application of infrared spectroscopy to such studies was until recently very limited. This is because of a number of disadvantages of this approach, such as its certain method restrictions and the limited range of temperatures over which it is possible to take spectra. The ready, availability of FTIR techniques and of equipment for high-temperature IRS has now significantly increased the potential of this method for studying the kinetics of surface reactions (rates, rate constants and activation energies for separate stages).

Two different cases can be identified when the kinetics of surface reactions are being studied: (i) direct determination of the relationships between an absorbance for a characteristic band and the reaction times of complexes which are intermediates or products; (ii) indirect determination of the reaction rates on the basis of the interaction between the adsorbed molecule and surface center being reduced during the conversion of intermediates. In the second case, the adsorption rate should be much higher than that of the reaction rate. Such applications have been described in literature [172–175].

1.8 Quantitative measurements

The determination of the surface complexes concentrations is based on the use of the Beer–Lambert law for the separate bands. The extinction coefficient is determined in accordance with the Beer–Lambert law. For the adsorption of complexes, the following parameters are used: $\varepsilon = AS_{\text{pellet}}/C_s G$, where G is the sample weight(g), S_{pellet} is the sample area (cm^2) and C_s is the concentration of the adsorbed probe ($\mu\text{mol g}^{-1}$). Alternatively, in integral form, $A = 10^{-3} A_0 C_s \rho$, where $A = \int \log(T_0/T) d\nu$, is the integrated absorption coefficient of the band observed (cm^{-1}), A_0 is the integral absorption coefficient of the band when the adsorbate concentration is equal to $1 \mu\text{mol g}^{-1}$, and ρ is the amount of the catalyst per cm^2 of the light flux profile (in mg). In the latter case, potential mistakes in the determination of A_0 are reduced and there is no necessity to measure the geometrical thickness of the pellet.

Several factors influence the accuracy of such measurements: (i) the possibility of using the Lambert–Beer law for analyzing the infrared spectra of surface compounds; (ii) the influence of the changes in optical characteristics of the investigated systems during the interaction; (iii) the ranges over which absorptions change; (iv) conditions for the registration of kinetic curves. In the case when the Lambert–Beer law can be used, it is possible to obtain the relationships between the strength of a particular absorption band and both the time and pressure of the component in the gas phase. The relationship of the absorbance of the band of the surface compound to its concentration can be found by a comparison of infrared and adsorption (desorption) measurements. The values of the extinction coefficients of the most intense bands allow an estimation of the sensitivity of the method for particular surface compounds (for further details, see [20, 30]). By using the relationship between the change in concentrations of the surface compounds and the temperature it is possible to estimate the heat of adsorption [176].

The reliability of the spectral interpretations can be improved by a combination of the results obtained from molecular spectroscopy with those available from other physical techniques, in particular thermodesorption spectroscopy with analysis of the products (TDS), and ESR and NMR spectroscopies.

2 THE NATURE OF OXIDE SURFACE CENTERS

2.1 Systems investigated

The main adsorbents examined in this book are simple dispersed oxides, salts and zeolites. Using these as examples, the application of molecular spectroscopic methods for investigating the properties of oxide surfaces on the molecular level will be demonstrated. The chemical properties of oxides are determined by the electronic structure of the element forming the bond with oxygen and also by the geometry of the solid structures [67–75]. In fact, the degree of electron transfer from the metal to oxygen, which determines the degree of ionicity or covalence of the M–O bond, depends on the nature of the cation and on its coordination number, and this then determines properties of the oxide system. These parameters differ in the bulk and on the surface because the surface itself can be considered as a type of defect of the crystal lattice. There is no doubt that the chemical reactivity of the oxide surface is connected mainly with the presence of coordinatively unsaturated cations and anions on the surface. Overall, it is the surface properties that determine the chemical properties of oxides. As a rule, the macroscopic properties of such systems are well characterized, and there are many books containing such data [71–84]. However, the properties of these systems at the molecular level, and especially their chemical reactivity, which depend on their surface properties, are insufficiently studied as yet, although great progress has recently been made in this field [75–97].

As has been demonstrated [17–66], such information, which is the main subject of examination in this chapter, may be obtained by spectroscopic means only. For this, the high-sensitivity methods of molecular spectroscopy, such as FT-IR and laser Raman spectroscopies [1–3, 5], developed in recent years, play important roles.

2.1.1 SOLID STRUCTURES

This field is well investigated [71–84], at least for simple oxides (see, for example, [98–100]). The corresponding data are published and well known (one of the main types of structure, in which the oxide is crystalline, is represented in Figure 2.1). Although X-ray diffraction (XRD) methods are the main techniques used to identify crystal structures, the methods of molecular spectroscopy may also be successfully used, both to identify specific compounds and to investigate their structures [101–107]. It is well known that the vibration spectrum is the ‘fingerprint’ of a molecule. This extends to solids, including the oxides, for which there is much spectral information in the literature which allow the identification of specific oxides and their crystalline forms quite easily. The structural characterization of a crystalline solid can be made by means of the IRS and RS methods on the basis of factor-group analysis of the obtained fundamental vibrations (these are located in the low-frequency region of the vibrational spectra, $\nu < 1200 \text{ cm}^{-1}$) and also by

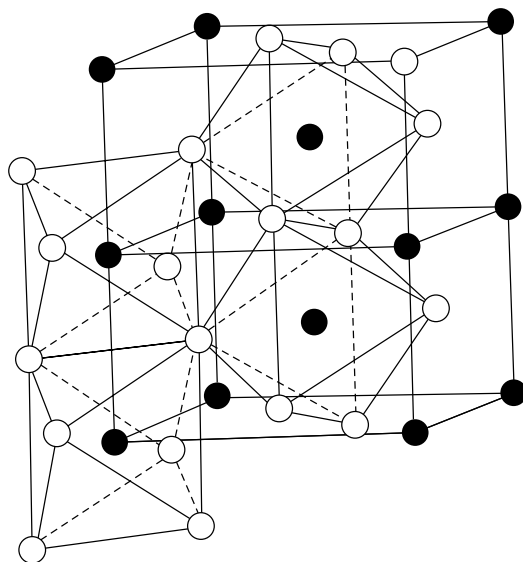


Figure 2.1. Structure of rutile: O, O^{2-} ; •, Ti^{4+} .

calculation of the vibrational spectra [4, 16]. These methods can also discern other structural features of the solid state including defects in the bulk structure [108] and the structure of matrix isolated species and supported complexes and compounds [109–113] (see also Chapter 4). Solid phases may be amorphous or microcrystalline, i.e. in forms which are not detectable by diffraction methods. In this case, Raman and infrared (vibrational) spectroscopy can be helpful in identifying crystalline and noncrystalline phases. The bulk of the reported oxide spectra, which can be useful in their identification, can be found in a number of specific sources [102–105].

In this present book, we do not have the possibility of examining the applications of molecular spectroscopic methods in the investigation of the structure of oxides in great detail. However, it should be borne in mind that the positions, intensities and contours of the lattice absorption also contain significant information about the surface properties. The region, where cutoff vibrations are observed, limits to some degree investigations of the surface modes, since the latter features overlap with the absorption from the bulk. The ‘volume/surface’ ratio is large, with specific areas varying from 10 to several hundred $m^2 g^{-1}$ in the case of highly dispersed samples. To examine oxide surfaces, we will generally use the structural information given in the above cited references.

2.1.2 SURFACES

As has been long established for metals [90], the coordination conditions of the surface atoms (the cations and anions in the case of oxides) and the surface chemical reactivity depend upon which crystal planes are exposed to the reactants. These surface arrangements can often be deduced from the orientation of the surface plane with respect to the three-dimensional surface lattice, although the influence of surface defects or even surface reconstruction have to be borne in mind. Most investigations of the surface reactivity of oxides have been made by using polydispersed samples where several crystal planes may be exposed simultaneously. This hinders the identification of active sites, although in some cases partial information can be indirectly deduced from the features of the spectra of adsorbates, e.g. whether linear (one surface atom) or bridging adsorption occurs. Unlike in the case of metals, where different surfaces can be chosen by cutting the crystal

appropriately, unfortunately there is a lack of spectroscopic data from adsorption on defined single crystal surfaces of oxides although the literature does contain high-resolution electron energy loss spectroscopy (HREELS) vibrational data only for several oxides (ZnO, MgO, TiO₂ [34a, 485 and references therein]). However, the single crystal approach, where feasible, significantly simplifies the interpretation of the spectra obtained from polycrystalline powders (see Chapter 3).

2.1.3 ACTIVE SITES

As we have seen above, the structures and chemical properties of the oxide surfaces are determined by the nature of the surface adsorption centers, i.e. by the types of sets of separate crystal planes that are exposed on the surface [30, 77, 78, 85, 90–97]. According to Morrison [85], the term ‘surface center’ describes the microscopic group of atoms which determines the specific chemical activity on the surface. This term applies to a surface atom of the lattice with a free valency, a free bonding orbital with an affinity for the electron, an occupied bonding orbital with a low ionization potential, etc. For all oxide systems, the following types of surface center for interaction can be distinguished: (i) electron-donating oxygen ions; (ii) electron-acceptor metal cations; and (iii) hydroxyl-hydrate cover. The polydispersity of oxide catalysts and the resulting emergence of various facets of the lattice, together with possible oxide defects, condition the nonhomogeneity of every type of active center and differences in their reactivity. This chapter examines the potential uses of molecular spectroscopy methods (including ESR) in the study of the above centers; the establishment of the character of their relationships with a number of elementary molecules; the determination of spectral features of each complex formed by elementary molecules with every type of center; and the dependence of spectral features of complexes on the properties of each type of center. Such centers can be situated on homogeneous surfaces or occupy nonhomogeneous areas, where their activity is often highest. It is known that surface nonhomogeneity can give rise to a wide range of different types of adsorption centers which can have significant effects on the chemical properties. These centers may also be due to sites where a defect occurs on the surface [108]. Any real single surface may be nonhomogeneous – this can be caused by a variety of possible defects, ranging from macroscopic defects (steps, cracks, dislocation corners, etc.) to point defects (vacancies, interstitial atoms, substitution or insertion atoms). The concentration of defects on real surfaces increases with diminishing crystal size. In highly dispersed systems, they may at times exceed the concentrations of normal surface sites.

There are many catalytically important materials, some of which are chemical combinations, such as silica–alumina. This catalyst, with a low alumina content, may consist of corner-sharing SiO₄ and AlO₄ tetrahedrons (similar to those found in zeolites), almost randomly distributed in the solid. At higher alumina contents, the structure is evidently more complicated. Charge neutrality requires the presence of cations at the surface, and silica–alumina materials have both Lewis and Brønsted acid sites, with some of the latter being very strong.

Zeolites [39, 73, 74, 76] have a special importance among the investigated systems because of their porous skeleton structure (Figure 2.2), in which the nature of the cages and channels depends on the ratio Si/Al. Molecular spectroscopy methods can be successfully applied for the identification of zeolite structures, since the different ratios of Si/Al are also reflected in their molecular spectra [107]. Practically all cations and anions in zeolites form surface sites and are accessible to interaction with various reagents. Another important property of zeolites is the fact that their active centers are located in defined crystallographic positions. This makes it easier to determine the character of the interactions proceeding within the zeolites (participation). Since catalysis occurs within their somewhat solvent-like environments, the zeolites provide a type of ‘transition state’, lying between solutions and gel-like organic solids (which have much of the character of solutions) and the more typical solids, which catalyze reactions on their surface [97].

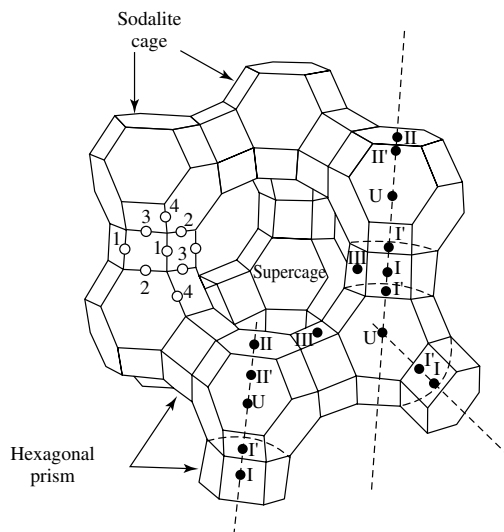


Figure 2.2. Structure of the zeolite faujasite: O, oxygen; ●, cations.

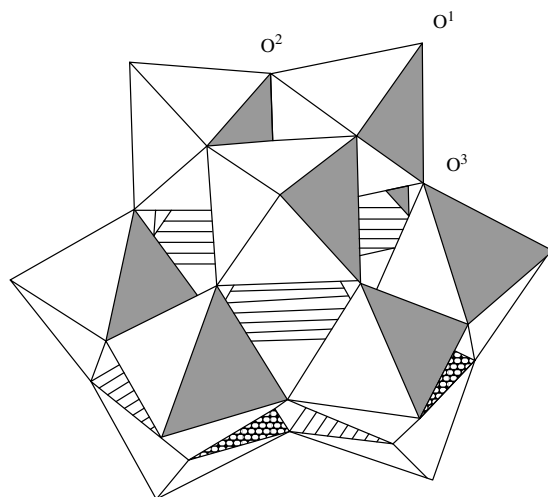


Figure 2.3. The 'Keggin' structure of the $\alpha\text{-XM}_{12}\text{O}_{40}^{\alpha-8}$ anion, showing terminal (O^1), edge-bridging (O^2) and corner-bridging (O^3) oxygen atoms; internal oxygen atoms are not shown.

A number of other mixed metal oxides also behave as strong acids, even 'superacids'. Some of the strongest solid superacids are formed by the adsorption of Lewis acids, such as SbF_6 , on solid Brønsted acids, such as silica–alumina, while others are formed by sulfating solids such as zirconia. Mixed oxides with reduction–oxidation (redox) properties are important catalysts, for example, in selective hydrocarbon oxidation [30].

Heteropoly compounds (HPCs) (spectral manifestations of such compounds are analyzed in detail in Chapter 4, along with their surface properties), which are also examined in this book, are very similar to zeolites in their properties. [75, 83, 84] (Figure 2.3). They are widely used in

heterogeneous catalysis and are effective catalysts of several important chemical processes. These compounds are also convenient as model catalytic systems due to their useful combination of acid–base and redox properties which allows the precise determination of both the composition and structure of the catalytically active center. Moreover, in the case of heteropoly compounds, it has become possible to control the variations of both the acidic and oxidation–reduction functions of the catalytic system, and in this sense they are superior to the zeolites. Supported heteropoly compound catalysts have several advantages, with the most important of which being their high mechanical strength and well-developed specific (surface) areas.

2.2 Spectra of oxide surfaces

As has been noted earlier [30], the surface of a solid may be regarded as a major lattice defect which disrupts its periodic three-dimensional nature. Atoms located at the surface have a smaller number of neighbors (coordinatively unsaturated) in comparison with atoms within the crystal. Of necessity, the forces applied to the atom in the surface layer are also different for both covalent and purely ionic lattices.

A number of studies summarized by Maradudin [177] have shown that the local symmetry, the related spectroscopic selection rules (as well as the dynamic properties of surface bonds, such as the mean square amplitude) the frequency and the force constant must deviate from the corresponding values that apply within the lattice. These factors condition the surface modes of vibration, which give additional bands in IR absorption and Raman spectra. Adsorption of atoms or molecules on the surface of the solid results in adsorbate-localized vibrations in cases where the mass of the adsorbed atom is less than one third to one quarter of that of the surface atom [30].

Dispersed oxide catalysts are suitable for the analysis of vibrational surface spectra of both the bulk lattice and surface impurities. Increasing the degree of dispersion of the solid changes the surface-to-volume ratio and increases the proportion of surface impurities such as chemically bonded OH groups, carbonates, etc. However, one of the essential limitations in the study of such systems is the absorption of IR irradiation by the bulk adsorbent which, of course, makes it difficult to obtain spectra of the surface impurities in the fundamental absorption spectral region of the bulk solid. For this reason, until FTIR spectroscopy became available, analysis was limited to the region above the so-called ‘cutoff’ frequency. To increase sensitivity, the sample transmissions are made wider by about one order of magnitude than would be used in the analysis of the spectra of the bulk adsorbents using potassium bromide or cesium iodide disks.

The IR spectra of routinely treated oxides above the fundamental absorption frequency of the crystal include a pattern characteristic for each oxide. Samples with specific areas $>1 \text{ m}^2 \text{ g}^{-1}$ (pellet of $10\text{--}100 \text{ mg cm}^{-2}$) can sometimes be studied. In the high-frequency region ($3500\text{--}3800 \text{ cm}^{-1}$), the spectra of oxides are easy to interpret, as the observed absorption bands characterize the bond-stretching vibrations of surface hydroxyl groups, which can be regarded as local vibrations of the adsorbed atom (H) on the surface. It has also been established that IR spectroscopy can give direct information on the vibrations of surface cation–oxygen bonds, e.g. metal–oxygen double bonds (having surface vibrations of an inherent nature) [30]. More generally, any real solid surface forms surface groupings (the surface impurities), by the reaction of coordinatively- or valence-unsaturated surface atoms of the bare surface with molecules of the atmosphere or other media. This is why in the spectra of the majority of oxides that have not been pre-treated in any way, intense absorption bands can be observed in the region $1200\text{--}3800 \text{ cm}^{-1}$, over the fundamental absorption limit of the (lattice) [30]. This indicates the importance of pre-treatment conditions in the analysis of the chemical properties of a surface. It should be pointed out, however, that the absence of any agreed standards of oxide pre-treatment hinders quantitative and qualitative analysis of comparisons of spectral data obtained by different authors from the surface impurities, and from subsequently adsorbed species from the same oxides.

Although variation of the treatment conditions represents a way of studying the surface properties, it should be remembered that the treatment temperature should not exceed any transition temperature corresponding to changes in the crystallographic phase within the system. Ultra-high vacuum conditions should also be avoided which can strongly change the stoichiometry of the oxide sample – it is better to monitor the state of the oxide after repeated successive treatments *in vacuo* (10^{-6} – 10^{-7} Pa). The samples should then be treated in oxygen at temperatures at which surface diffusion occurs (approximately equal 0.3 from the temperature of the oxide melting point–0.3 melting point) until the maximum possible amount of surface impurities have been removed, so as to provide an initial state of the oxide for subsequent experiments. To bring the oxide system into a state of equilibrium, the final treatment has to be carried out in an atmosphere of oxygen at similar temperatures to those used for the subsequent evacuation of oxygen (at 293–473 K). The final surface purity can then be monitored by IR spectroscopy in most cases. In general, surface impurities can play a significant role in changing the properties of the surface, including sometimes the production of different surface centers. Such impurities have caused numerous errors in the interpretation of surface phenomena and spectra. In a number of instances, it is not easy to remove such impurities from the surface and it is necessary to remember that these cannot always be observed in IR spectra.

2.2.1 VIBRATIONS OF METAL–OXYGEN BONDS ON OXIDE SURFACES

It has been shown during studies of the IR spectra of highly dispersed oxides after oxidation (pellet of 10 – 50 mg cm^{-2}), particularly for transition metal oxides, that individual oxides can yield characteristic modes in the region above the fundamental absorption frequency of the lattice [30] (see, for example, Table 2.1 for some of these oxides). On the basis of the analysis of the

Table 2.1. Absorption bands in the IR spectra of relevant oxide systems after high-temperature oxidation treatment.

Oxide	Fundamental frequency region (cm^{-1})	Region above the fundamental frequency (cm^{-1})
Cr_2O_3	625, 550, 435, 407	1015, 995, 980, 890, 820
MnO_2	615, 400	1170, 1140, 1120, 1065, 1040, 980
Fe_2O_3	560, 470	960, 925
NiO	650, 465	1050, 1140
CuO	610, 500, 410	1050, 830, 790
V_2O_5	1015, 860, 600	1035
Cu/Cr/O	620, 520	1010, 950, 900
Fe/Cr/O	560, 470	1005, 930
SnO_2	670, 610, 312	1060, 970
ZnCr_2O_4	670, 560	870, 980, 1010
$\text{ZnO}\cdot\text{ZnCr}_2\text{O}_4$	670, 560	960, 1015
$\text{ZnCr}_2\text{O}_4\cdot\text{K}$	670, 560	970
TiO_2 (anatase)	700–525, 347	950, 870, 770, 730
Co_3O_4	665, 560	800–1200
Mo/Sn/O	990, 660	1005–1010
$\text{V}_2\text{O}_5/\text{Al}_2\text{O}_3$	1015, 890, 600	1020–1035
SiO_2	1100, 775	908, 888
$\gamma\text{-Al}_2\text{O}_3$	800, 620	1050
ZnO	450	800–1200
Sn/V/O	670, 610	980, 1035
Sb_6O_{13}	740, 400	800–1200

numerous data presented in the literature, these bands have been assigned to the vibrations of 'surface cation–oxygen' bonds of greater strength [30] which occur as a result of the differences in coordination states of the surface cations. Some correlation have been possible between the coordination number of the cation, the order of the oxygen–metal bond and the absorption frequency [30, 178, 179]. It should be borne in mind that the combination vibrations of the fundamental absorption frequencies of the lattice may also appear in the same spectral region.

Chromium-containing oxide systems

These are the most frequently studied [178–186] from the point of view of spectral features from surface (M–O) bonds. The best investigated system in this respect is $\text{Cr}_2\text{O}_3\text{--O}_2$, which we shall use as an illustration of the spectral characterization of oxygen on the surface.

The IR spectra of Cr_2O_3 after high-temperature oxidation contain characteristic bands with a discrete absorption in the $700\text{--}1100\text{ cm}^{-1}$ region (Figure 2.4). These spectra are independent of the pre-treatment of the systems and precursors and are also unrelated to surface impurities, but are related to the crystal structure. Absorption bands in this region possess the following individual features, indicating that they characterize the vibrations of the metal–oxygen bond at the surface: (i) the band intensities can drop on thermal treatment *in vacuo* at temperatures below the phase transition point; (ii) the bands are restored by high-temperature oxidation treatment;

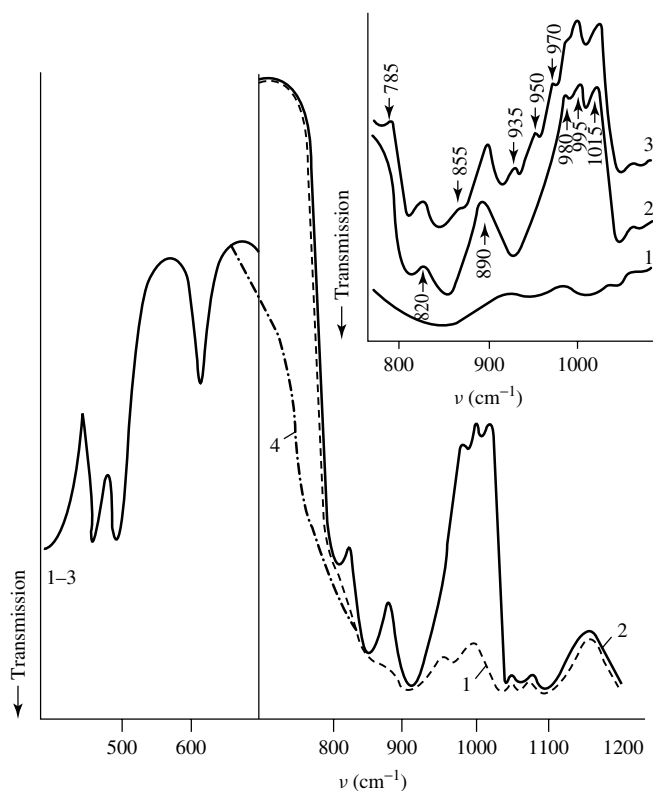


Figure 2.4. IR spectra of $\alpha\text{-Cr}_2\text{O}_3$: 1, after treatment *in vacuo* at 773 K; 2, following oxidation at 523 K; 3, following reaction with a mixture of $^{16}\text{O}_2$ and $^{18}\text{O}_2$ (40 % $^{18}\text{O}_2$) at 523 K; 4, following hydrogen reduction at 773 K.

(iii) the bands disappear or shift during the adsorption of other molecules; (iv) the frequencies of the absorption bands observed in the spectra coincide with, or are close to, the frequencies of a metal–oxygen bond with a bond order of between 1 and 2; (v) replacement of ^{16}O with ^{18}O atoms leads to an isotope-related band shift, which confirms their vibrational (stretching) nature; (vi) an increase in the degree of dispersion of the sample (i.e. alteration of the ratio between bulk and surface states) leads to an increase in absorption intensities in the $1100\text{--}700\text{ cm}^{-1}$ region, which parallel a decrease in the intensities of absorption characteristic of the bulk lattice; (vii) upon interaction with hydrogen or carbon monoxide these bands disappear, giving rise to the bands characteristic of surface hydroxyl or carbonate groups, respectively [30, 178, 179].

The formation of metal–oxygen groups of an ionic nature on oxide surfaces is equivalent to the appearance of O^{2-} oxygen ions adsorbed on metal cations. In the cases when the surface O^{2-} ion is bound to only one cation in the lattice, the bond between them is stronger than when it is between O^{2-} and metal ions within the lattice. Hence, the frequency of such a vibration is higher than that of the metal–oxygen bond inside the crystal. It is to the vibrations of such ions with respect to metal cations on the surface that the high-wavenumber absorption can be attributed. As the real surface of a polycrystalline sample has sets of different facets corresponding to various planes of the lattice, surface cations have correspondingly different coordinative saturation values (with respect to oxygen) [178]. The strength of oxygen bonds with such cations is also different. Hence, there are several absorption maxima corresponding to metal–oxygen bonds in the spectra [30, 178–186].

It is known that a decrease in coordination number of the metal atom at constant valence reduces the interatomic distance and increases the number of valence electrons per bond, i.e. increases the bond multiplicity. Both the strength and frequency of the bond should increase accordingly. Thus, it has been established [30, 178, 179] that a decrease in the coordination number of a cation leads to an increase in the vibration frequency generated by the cation–oxygen bond.

The state of oxygen on the (001) surface face of chromia has been examined by Zecchina *et al.* [181]. Cations with either one or two vacancies are to be expected on a partially dehydrated chromia surface. The former dominates at moderate dehydration temperature (573 K) and the latter at higher temperatures. The assignment of absorption bands appearing during the interaction of the oxide with oxygen was based on the concept of ligand and coordinate nonhomogeneity of the (001) face, such as can be represented by the scheme shown in Figure 2.5. This scheme provides

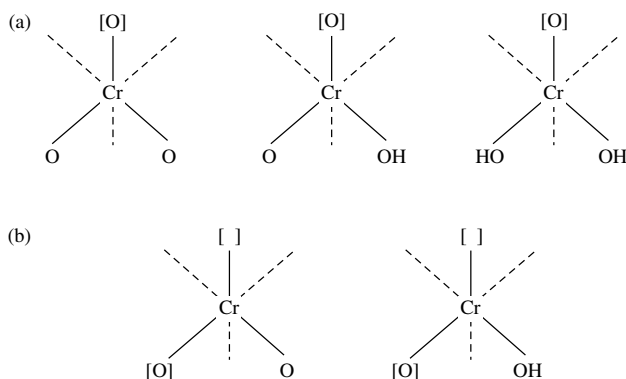


Figure 2.5. Possible Cr^{3+} states on the (001) face of $\alpha\text{-Cr}_2\text{O}_3$ [181]: (a) coordination number of 5, $\nu_{\text{Cr-O}} = 995\text{--}980\text{ cm}^{-1}$; (b) coordination number of 4, $\nu_{\text{Cr-O}} = 1040\text{--}1015\text{ cm}^{-1}$. Reprinted with permission from Zecchina, A., Coluccia, E., Guglielminotti, E. and Ghiotti, G., *J. Phys. Chem.*, **75**, 2783–2790 (1971). Copyright (1971) American Chemical Society.

an explanation only for the bands in the high-frequency region (980–1040 cm^{-1}). It is difficult to assign the remaining bands below 970 cm^{-1} with similar accuracy on the basis of Zecchina's model. These bands may arise from either the presence of more than one crystallographic face or sets of defects on the surface. The model does not explain why all three forms of adsorbed oxygen are observed on the fully dehydroxylated surface. Moreover, the (001) face cannot be the only face exposed to the surface as is confirmed by electron micrographs, which show that the chromia particles in most of the samples are shaped like polyhedrons. The adsorbed oxygen has to occupy the places of the oxygen vacancies, which are formed on the crystal surface by disruption of the lattice. This is why oxygen adsorbed on the (001) face of $\alpha\text{-Cr}_2\text{O}_3$ seems to be bound to two chromium ions, thus leading to a decrease in the vibration frequency of the newly formed structures. It is clear that in this case the order of the chromium–oxygen bond is close to one [185].

In order to determine the adsorption properties of oxides, and in particular, to build a model of oxygen states on the oxide surfaces, the structure of all planes which are characteristic of the crystal has been examined [185, 186]. For crystals of the corundum type, such as $\alpha\text{-Cr}_2\text{O}_3$, the surface planes (0001), (1120), (1010), (1121), (2241), (2243), (2021), (1011), (1012), (1014) and (14.14.28.3) are exposed on the surface [185, 187]. As a result, it has been established that the coordinatively unsaturated chromium ions have been divided into four- and five-coordinated types (Figure 2.6). Taking into consideration the low coverage of the Cr_2O_3 surface by oxygen (10 % of a monolayer), it has been suggested that the five-coordinated chromium ions are inactive towards most reagents. Even if oxygen is adsorbed on these ions, it is bound to two metal ions and, therefore, the $\text{M}=\text{O}$ double bond cannot be formed, i.e. the bands in the region 970–1120 cm^{-1} should not appear in the spectrum. It is more probably that the adsorbed oxygen is bound to four coordinated metal ions that are presented on side planes of the prismatic crystals. Similar considerations apply to the surfaces of TiO_2 [188] and MgO [56], which are discussed below.

It is known that the properties of metal ions with the same coordination number can strongly differ, depending on the coordination state of various ligands [30, 185]. More electron-positive central metal ions have the highest coordinative saturation by ligands (the smallest number of vacancies). This state can be written as $\text{Cr}^{n+}(\text{X}_1\text{-X}_2\dots\text{X})$. (The figures in parentheses indicate the coordination number of the chromium ion, with each figure itself characterizing the number of vacancies for corresponding ligands on that site.) The four-coordinated Cr^{3+} ion on a stoichiometric surface can therefore be depicted by the following:

- (1) $\text{Cr}^{3+}(2\text{-}0\text{-}0\text{-}0)$ on the (0001) plane
- (2) $\text{Cr}^{3+}(1\text{-}1\text{-}0\text{-}0)$
- (3) $\text{Cr}^{3+}(2\text{-}1\text{-}0\text{-}0)$ on side planes
- (4) $\text{Cr}^{3+}(2\text{-}1\text{-}1\text{-}0)$

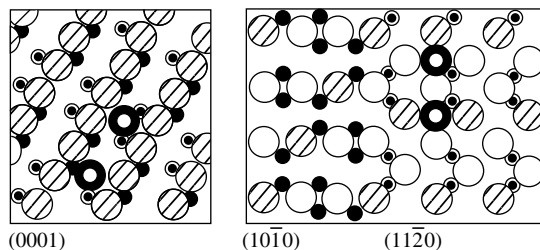


Figure 2.6. Schemes of two planes of stoichiometric Cr_2O_3 : ●, five-coordinated Cr^{3+} ; ⊙ four-coordinated Cr^{3+} ; ○ three-coordinated O^{2-} ; ⊗ two-coordinated O^{2-} ; ● oxygen to be adsorbed.

In cases (2)–(4), each chromium atom may be bound to one oxygen atom.

The vibration frequencies of metal-adsorbed oxygen atoms in the region $970\text{--}1020\text{ cm}^{-1}$ are much higher than those of the chromate ion (at $820\text{--}890\text{ cm}^{-1}$ [189]). This indicates the order of a Cr–O bond is higher (closer to 2). The vibration frequency of double-bonded Cr=O groups grows with the increase in electron positivity of the chromium ions. Therefore, absorption bands at 1015 , 995 and 980 cm^{-1} can be assigned to oxygen adsorbed on the four-coordinated chromium ions depicted above in (2), (3) and (4), respectively. It is clear that such an interaction increases the degree of oxidation of the chromium ions.

Non-stoichiometric oxygens (the bands at 890 and 820 cm^{-1} [185, 186]) probably correspond to sites on the (0001) plane. These structures have the order of the Cr–O bond as being not very different to that in the chromate. It is suggested that this plane is exposed to only a small degree because of evidence for the presence of only a small concentration of this type of oxygen ion (the low intensity of the corresponding absorption bands). Probably, this type of oxygen ion, together with those discussed earlier, represent those adsorbed on all four-coordinated chromium ions of $\alpha\text{-Cr}_2\text{O}_3$.

Investigation of surface vibrations in more complex, chromium-containing systems (such as chromate) have also been made, for example, for spinel-type oxides of magnesium, copper [190, 191], iron [192], and zinc [193]. Spectra in the regions of surface M–O bond vibrations of such structurally more complicated compounds are simpler than that of chromium oxide and are practically the same for all systems investigated (see Table 2.1). This shows that these vibrations depend on the structure of the compound since Cr_2O_3 is crystallized in the corundum form, while all of the others have spinel structures. Overall, the spectral manifestations of metal–oxygen bonds are similar to those observed for chromium oxide and have also been observed from the surfaces of all previously studied chromium-containing systems after high-temperature oxidation. Unlike $\alpha\text{-Cr}_2\text{O}_3$, on the surface of chromites oxygen forms only one type each of isolated Cr=O ($1005\text{--}1010\text{ cm}^{-1}$) and Cr–O ($800\text{--}900\text{ cm}^{-1}$) bonds, with the exact positions of the absorption bands being a little different from that observed in the case of $\alpha\text{-Cr}_2\text{O}_3$, probably because of the presence of a second cation.

Probably because of the presence of low-coordinated (four-coordinated) chromium cations on certain spinel planes, as well as on those of $\alpha\text{-Cr}_2\text{O}_3$, and also because of a low oxidation potential, i.e. $\text{Cr}^{3+} \rightarrow \text{Cr}^{6+}(\text{Cr}^{5+})$, the degree of oxidation of chromium ions on the surface is changed through additional coordination by oxygen, and then the $\text{Cr}^{6(5)+}=\text{O}$ units are formed on three places on chromium oxide, but on only one for spinels. The spectroscopic appearance of such groups is a unique characteristic of Cr-containing systems. Such states are easily reduced. The presence of isolated chromium ions with a high degree of oxidation on the surface of $\alpha\text{-Cr}_2\text{O}_3$ and spinel is confirmed by the nature of the interaction between ammonia and such surfaces (see Section 2.3.1).

As has already been mentioned, only a small amount (ca. 10 % of a monolayer) of oxygen is manifested in the IR spectra of chromium oxide as discrete maxima characteristic of M–O bonds on the surface. It is reasonable to suggest that these states correspond to the places on the surface with the greatest concentration of defects, differing strongly from the remainder of the surface oxygen. The latter should be close in their properties (for example, coordination number) to the bulk states and, therefore, they should be observed in the lower-frequency region. Study of chromium oxide spectra with oxygen reduction varying from 10 to 100 % of a monolayer showed that the increase in the degree of reduction leads to a general decrease in absorption at the edge of the fundamental absorption around $700\text{--}800\text{ cm}^{-1}$ (see Figure 2.4, spectrum 4). This indicates that considerable widening of these cutoff bands in polycrystalline samples can be related to both surface vibrations plus vibrations of groups in the immediate vicinity of the surface. It should be borne in mind that this band widening is also accounted for by vibrations in

at least the first five layers of the sub-surface volume which differ appreciably from those in the bulk. This is particularly apparent for oxide samples with low oxygen mobility, e.g. TiO_2 [194] and ZnO [195].

Zinc oxide

The above lines of reasoning are confirmed by studies of microcrystalline ZnO [195], for which it has been established that strong absorptions occur in the vicinity of $600\text{--}700\text{ cm}^{-1}$ (the cutoff region) and due to surface vibrations, whose sphere of influence extends several interatomic distances into the crystal [195]. A decrease in intensity or disappearance of separate absorption bands, or even this absorption in total, from the complex contour overlapping the cutoff vibrations of ZnO on the high-frequency side have also been observed after high-temperature interaction with H_2 [196], ammonia, nitriles, etc. [197]. It is not possible to assign the specific absorption bands in this spectral region to vibrations of the surface cation–oxygen bonds. It is also difficult to detect changes in intensity of absorption bands in the $800\text{--}1200\text{ cm}^{-1}$ region during reduction because the transmission of oxides in the whole spectral region from 800 to 4000 cm^{-1} is strongly reduced, even up to a complete disappearance. The decline of transmission of n-type semiconductors (ZnO is such a material) during reduction is caused, as will be shown below, by the appearance of free carriers (electrons in the conductivity zone) which absorb the infrared radiation.

Titanium dioxide

For titanium dioxide [30, 194], the surface-related vibrations do not manifest themselves as discrete spectra such as those observed for chromium-containing systems, but as high-frequency shoulders at 950 , 850 , 770 , and 730 cm^{-1} of the fundamental band. Absorptions in the $700\text{--}1000\text{ cm}^{-1}$ region for TiO_2 after reduction are caused by the removal of a certain proportion of surface oxygen. As the degree of reduction increases, more and more bonds are broken, manifested by a disappearance of the 950 and 850 cm^{-1} bands and by a reduction in the intensity of the bands at 770 and 730 cm^{-1} . When titanium dioxide is treated in such a way and then comes into contact with oxygen, the absorption bands in the $700\text{--}1000\text{ cm}^{-1}$ region are restored and the spectrum returns to that recorded before reduction.

The data obtained indicate directly the contributions of surface vibrations to the high-frequency shoulders on the lattice absorption band, and indicate that for titanium dioxide, in contrast to chromium oxide, the energy states of the surface oxygen bands differ much less from those within the lattice.

Ferric oxide

There are numerous data in the literature on investigations of the surface properties of iron oxide and the nature of its interaction with oxygen involving, IR spectroscopy [30, 178, 180, 198–209]. However, some questions in this field are not yet decided. First, there is the fact that the spectra in the region above the cutoff vibrations obtained by different authors are different, unlike those in the region of νOH surface vibrations which do not change. During the interaction of oxygen with iron oxide ($\alpha\text{-Fe}_2\text{O}_3$, according to XRD data), it has been shown that a characteristic spectrum is observed in the region at $790\text{--}960\text{ cm}^{-1}$ after high-temperature (623 K) treatment of the pure iron oxide (prepared from the nitrate [30, 207]) in oxygen, with the most intensive absorption band being at 930 cm^{-1} [30, 178]. Upon reduction, this band shifts to 905 cm^{-1} , and its intensity decreases (Figure 2.7(a)). The spectra obtained are caused, once again, by vibrations of the ‘surface cation–oxygen’ bands of various strengths, which change in bond order from single ($\text{Fe}\text{--}\text{O}$, the low-frequency component) to double ($\text{Fe}^{3+}\text{=O}$, $930\text{--}960\text{ cm}^{-1}$; $\text{Fe}^{2+}\text{=O}$, 905 cm^{-1}). This can be explained by the reduction of Fe^{3+} to Fe^{2+} and by a subsequent decrease in the frequency of the $\text{Fe}\text{--}\text{O}$ bond. Higher-frequency bands obtaining in the spectra of ferric oxide [178], except

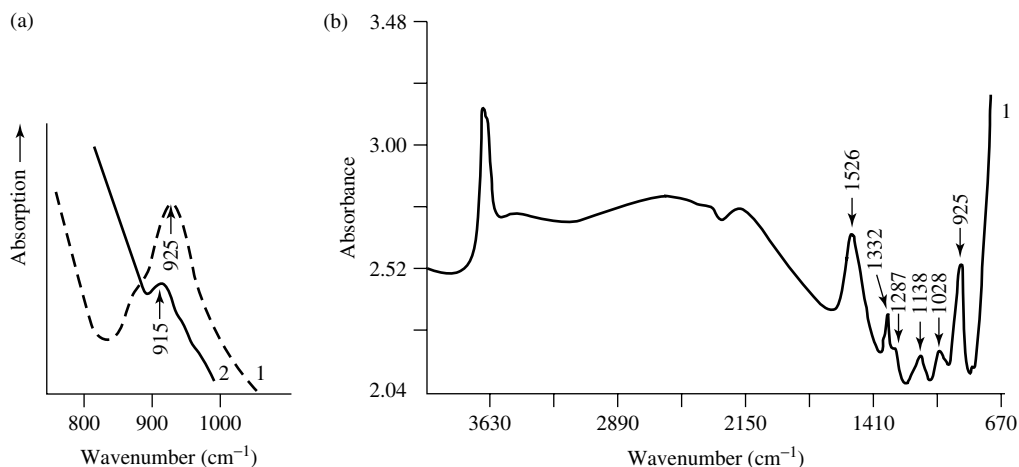


Figure 2.7. IR spectra of iron(III) oxide: 1, treated in O_2 at 773 K; 2, subsequent interaction with CO at 573 K.

a band at $1530\text{--}1550\text{ cm}^{-1}$ are characteristic of OH groups. The bands at $1530\text{--}1550\text{ cm}^{-1}$ have a nonfundamental vibrational nature, and characterize multiphonon vibrational absorptions [206, 207].

Griffiths *et al.* [198] have studied the adsorption of oxygen on Fe_2O_3 previously degassed at room temperature. Two absorption bands at 1350 and 1270 cm^{-1} were observed after the adsorption of oxygen at 623 K ; these have been assigned to adsorbed O_2 and O_2^- , respectively. In contrast, Davydov and co-workers [30, 199] suggested that these bands belong to species caused by impurities of a carbonate–carboxylate nature [199] or, more probably, sulfate [30, 206]. Certainly, as was established later, the bands characteristic of surface sulfates lie in the same area and the change in the spectra of Fe_2O_3 due to an increase of temperature and dehydration are similar to those of the sulfated samples. Al-Mashta *et al.* [203] have observed a number of bands and classified these into A-bands ($1350\text{--}1250\text{ cm}^{-1}$) and B-bands ($1100\text{--}900\text{ cm}^{-1}$), assigned to perturbed O_2^- and O_2^{2-} species, respectively, by comparisons with absorption frequencies of model dioxygen compounds. It should be noted, however, that though the frequencies of the A bands lie between those in superoxide and gas phase oxygen, the νOO in superoxides was never observed above 1200 cm^{-1} (Section 2.2.2). On the basis of subsequent experiments with isotopically labeled molecules, the B-bands have been reassigned by Sheppard to mononuclear oxygen groups of the type $Fe=O$ [39], similar to that reported above for chromium oxide systems [178]. Studies of iron oxide [202–206] have confirmed the presence of A- and B-bands in the spectra of this oxide as prepared by different methods, including conditions when the presence of sulfates is excluded.

In studies carried out by Davydov and co-workers [207–209] neither of these bands have been observed, nor those at 1270 and 1350 cm^{-1} . However, there was an intense band at $925\text{--}930\text{ cm}^{-1}$ (Figure 2.7(a)) and a number of weak bands at 1028 , 1138 , and 1325 cm^{-1} in these spectra (Figure 2.7(b)) [209]. The nature of the latter bands, as well as those of the A- and B-bands is not yet clear. It should be remembered that there was a discussion in the literature several years ago concerning the nature of several absorption bands (for example, 1460 cm^{-1} – in the same spectral region – observed in the spectra of several samples of aluminum oxides. In this case, the impurity nature of these bands was finally established.

In this connection, it should be noted that these special differences may be connected with the fact that such investigations have been made using samples prepared by different methods. Thus,

in references [30, 178, 199, 207–209] samples were prepared by high-temperature decomposition of the corresponding salts or hydroxides under an oxygen atmosphere, while in references [200, 201] α -Fe₂O₃ was prepared by the decomposition of α -FeOOH *in vacuo* at 453 K, followed by treatment with oxygen at 673 K. The samples obtained by this latter method or, at least their surfaces, may be in a nonequilibrium state and contain incompletely decomposed hydroxide. The treatment of such samples in oxygen even at 673 K, may not return the system to an equilibrium state as has been shown by work carried out by Davydov and co-workers [210, 211] for SnO₂. In addition, it is clear that the morphology of these samples differ, and this may directly influence the surface properties of the α -Fe₂O₃ samples.

Manganese dioxide

For MnO₂, as has been noted in references [30, 78], six absorption bands are observed in the spectral region 980–1170 cm⁻¹ when oxygen is adsorbed at 473 K. New information on the nature of the observed bands has not been obtained in recent years. However, it should be borne in mind that different phase transitions easily occur in the case of manganese oxides after high-temperature treatment, both *in vacuo* and under an oxygen atmosphere. Manganese hydroxides can be **produced** on the surface if a low-temperature treatment has been used. This last fact does not exclude the presence of molecular forms of adsorbed oxygen. New detailed studies are needed of manganese oxide samples with well characterized phase compositions.

Vanadium- and molybdenum-containing systems

As is known [98–100], there are short V⁵⁺=O and Mo⁶⁺=O bonds in the structure of vanadium (V₂O₅) and molybdenum (MoO₃) oxides. Stretching vibrations of these bonds appear in the IR spectra at 1015 and 990 cm⁻¹ [82, 189], respectively. Higher values of metal–oxygen bond frequencies on the surface of these systems, in comparison with the bulk, are also observed for highly dispersed V₂O₅ [212] at 1025 cm⁻¹ and also for supported vanadium- and molybdenum-containing systems: V₂O₅/Al₂O₃ [212–215], V₂O₅/SnO₂ [216], V₂O₅/TiO₂ [215, 217, 218] in the region 1025–1035 cm⁻¹, and MoO₃/SnO₂ [219, 220] and MoO₃/Al₂O₃ [221] in the region 1000–1010 cm⁻¹. For these systems, if the concentration of the active component is large (>10 atom %), and separate phases of molybdenum or vanadium oxide are present on the surface, the surface vibrations show up in the form of high-frequency shoulders on the absorption bands at 1015 cm⁻¹ (V⁵⁺=O) or 990 cm⁻¹ (Mo⁶⁺=O), characteristic of these oxides as has been established for such supports as Al₂O₃ and TiO₂ [215] (Figure 2.8). When two-dimensional layers (1–8 atom % active component) of active components on supports or isolated V and Mo cations are formed, only surface V=O (1020–1035 cm⁻¹) [212–218] or Mo=O (1000–1010 cm⁻¹) [219–221] bonds and M–O–M'(M) bonds (800–900 cm⁻¹), where M represents Mo or V cations, and M' the surface cations of the support, were observed. To obtain the true values of absorption frequencies from 'surface cation–oxygen' bonds, spectra should be registered after oxidation pre-treatment with pure O₂. Oxidation in air leads to impurities (H₂O and CO₂) adsorbed on the surface, and the absorptions of M–O and M=O bonds in samples with isolated cations, or if a two-dimensional phase is formed, are shifted to the lower-frequency regions. On reaction with reducing gases (Figure 2.8), the maxima corresponding to V⁵⁺=O and Mo⁶⁺=O bonds disappear, possibly due to cation reduction on the latter and a resulting shift of the corresponding absorption bands into the lower-frequency region, or alternatively from an increase in the cation coordination number as a result of extra coordination from the reductive agent acting as a ligand.

Silicon dioxide

Using IR spectroscopy, a set of surface vibrations of an inherent nature (Si–O vibrations) in highly dispersed silica have been identified [222]. These vibrations have been interpreted, on the

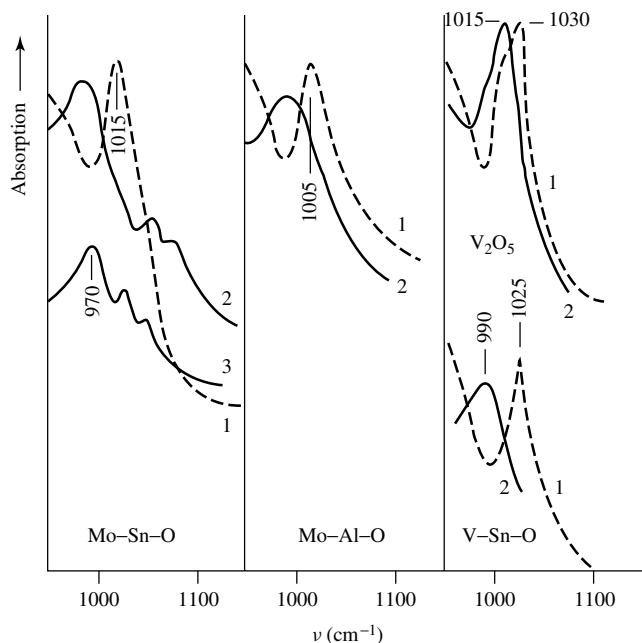


Figure 2.8. IR spectra of several Mo- and V-containing catalysts oxidized in O_2 at 723 K: 1, initial spectrum; 2, after adsorption of NH_3 ; 3, changes caused by hydrogen reduction at 473 K.

basis of analysis of their behavior during dehydration, as *deuteration* and *methoxylation* in terms of the concept of localized vibrations. Inherent surface vibrations are attributed to events on the surface. Boccuzzi *et al.* [222] regarded the surface as a set of extensive defects and explained these vibrations by differences between the strength and geometry of bonds on the surface and bonds in the bulk. Only the first steps have been taken towards the spectral analysis of such inherent surface vibrations and there are only a few reports of work in this area. Numerous questions pertaining to the behavior of surface vibrations on reactions of oxides with different molecular or atomic surface impurities remain with many oxide systems.

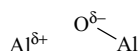
Boccuzzi *et al.* [222] and Morrow and Cody [223, 224] have made the important observation that when silica is subjected to outgassing *in vacuo* above 673 K, two new IR bands are observed at 908 and 888 cm^{-1} , with their intensities of reaching a maximum at 1473 K. These bands were assigned to strained asymmetrical surface siloxane bridges involving a silicon atom which is electron deficient and acts as a Lewis-acid site. Boccuzzi *et al.* [222] examined the IR spectrum of SiO_2 samples at various stages of dehydration. Besides a fairly detailed assignment of the silanol modes, including the Si-OH stretching features, two new bands were observed at 1000 and 830 cm^{-1} , which were assigned to coupled asymmetric and symmetric modes located on the outer (and thus more distorted) Si-O-Si bridges. On the basis of such data, these authors concluded that vibrational modes which are essentially localized at the surface can be observed by IR spectroscopy and hence that it is possible to obtain information on the surface structure from IR spectra.

Low [225] has suggested that the bands at 908 and 888 cm^{-1} are associated with a stishovite-like layer where the silicon atoms are not in tetrahedral coordination. This assumption gives a new contribution to the discussion about both the structures of the surface sites and the nature of SiO_2 surface reconstruction under dehydration conditions. According to a number of studies [223–226], the significant point to stress is that the force constants at the surface can be sufficiently altered

with respect to the bulk so as to allow the direct observation of the surface vibrations in spectral regions where the solid lattice does not contribute heavily.

Aluminum oxide

An examination of the data on observations of surface-localized vibrational modes has been carried out for the case of high-area transitions between different lattices of aluminas [27, 227, 228]. When a strong base such as pyridine is adsorbed on highly dehydrated transition aluminas, an appreciable increase of the IR transparency on the high-frequency side of the alumina cutoff is observed. This effect was interpreted on the basis of *in situ* experiments as due to the relaxation of some Al–O vibrations localized in the surface layer and absorbing in the spectral region around 1000 cm^{-1} [27, 227–229]. Differential absorbance spectra showed that a discrete weak and broad band centered at about 1050 cm^{-1} can be exposed in the spectra of dehydrated aluminas at increasingly higher temperatures. This band was ascribed to Al–O vibration modes localized in surface defective structures of the following type:



Scheme 2.1

The surface defect would be created during high-temperature surface dehydroxylation and readily destroyed during hydration of the alumina (the band at about 1050 cm^{-1} disappeared upon water adsorption [228]). Later, Marchese *et al.* [229] and Morterra *et al.* [230] confirmed the identification of a surface-localized Al–O vibration mode on both low- and high-temperature transition aluminas. They showed that no surface chemical changes (like, for instance, the rupture of a straightened Al–O bond) are actually needed to have the $\nu\text{Al–O}$ vibration shifted downwards to a lower value and that upon the reversible adsorption of a soft base, like CO, a complex band localized in the $1100\text{--}1000\text{ cm}^{-1}$ region is gradually and reversibly eliminated. Morterra *et al.* [230] inferred that on highly dehydrated aluminas, the adsorption of CO does not cause the rupture of bonds, but just polarization by weak σ -coordination onto unsaturated surface cations. The complex band at about $1050\text{--}1100\text{ cm}^{-1}$ has been interpreted as being due to spinel $\text{Al}^{\text{IV}}\text{--O}$ stretching modes localized at the surface. Such modes would be shifted upwards with respect to the regular bulk $\text{Al}^{\text{IV}}\text{--O}$ stretching mode(s), which absorb at ca. 850 cm^{-1} , and the shift caused by the surface increase of covalence, e.g. of the surface decrease of the Madelung energy, brought about by crystal truncation and surface dehydration [230]. Upon gas–solid adsorption, ligands are added to the coordination sphere of the surface cations, the overall coordination of surface ions increases, and the covalence of the surface then decreases. As a consequence, the surface-localized $\text{Al}^{\text{IV}}\text{--O}$ vibrational states shift downward toward the regular spectral positions of the bulk $\text{Al}^{\text{IV}}\text{--O}$ vibrations and outside of the spectral range observable in the *in situ* transmission mode. According to Knozinger *et al.* [227], similar effects have been observed on the interaction with pyridine and on the dissociative uptake of water.

Magnesium, calcium, barium and strontium oxides

The main improvements in investigations of the surface structures of alkaline earth oxides have been obtained by use of the methods of UV-absorption [231–233] and luminescence spectroscopy [234–237]. In the first case, surface states are manifested as additional maxima overlapping with the onset of bulk absorption (Figure 2.9). IR data do not yet give the possibility of separately observing surface vibrations, probably because of only small differences between the force constants of M–O bonds on the surface and in the bulk of MgO. High-surface-area oxides absorb

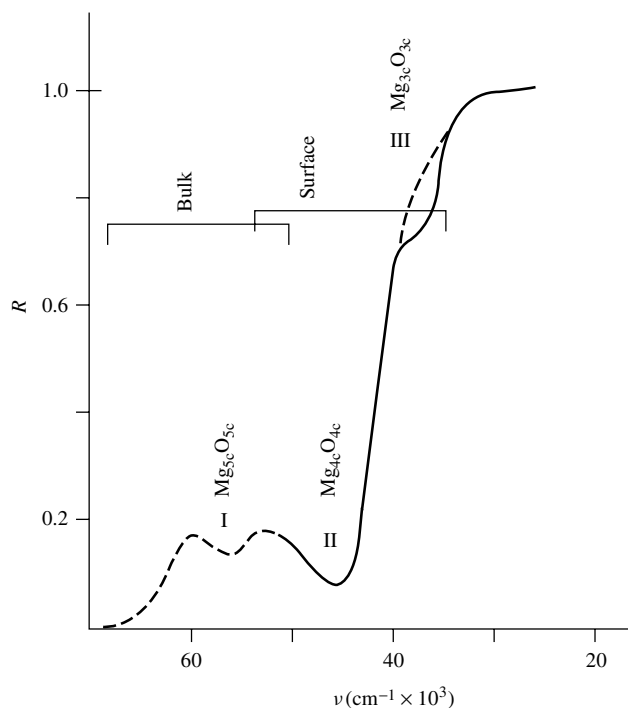
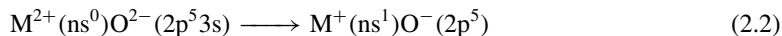
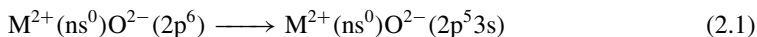


Figure 2.9. UV-Vis diffuse reflectance spectra of MgO activated at 973 K *in vacuo* before (—) and after (---) interaction with CH₄ at 573 K [56]. From Zecchina, A., Loohouse, A. and Stones, F.S., *J. Chem. Soc., Faraday Trans. 1*, **71**, 1467–1490 (1975). Reproduced by permission of The Royal Society of Chemistry.

UV light and emit luminescence, which is not observed from single crystals. Energy transfer may occur on the surface, so that excitons generated on anion–cation couples of high coordination on extended faces travel to those sites of lowest coordination at the corner positions, where the latter act as deep traps.

Exciton absorption in the high- ν region arises from the following processes:



where M^{2+} represents the alkaline cation and O^{2-} an anion in the bulk. For example, in the case of MgO, the absorption bands at 230 and 274 nm are of lower frequency than the band at 160 nm caused by bulk ion pairs. The bands at 230 and 274 nm are considered to be due to the surface O^{2-} ions of coordination numbers 4 and 3, respectively [231]. These long-wavelength components are reduced during the adsorption of contaminant molecules, while the degree of reduction depends on the molecular type (see Figure 2.9). Such observations confirm the surface nature of these bands.

The O^{2-} ion in the bulk of an oxide lattice is stabilized by interaction with neighboring ions. The stabilizing Madelung potential at the surface is weaker than in the bulk, and the coordination number is smaller at the surface. In the case of rock salt crystals, this decreases from 6 in the bulk to 5 at the (100), and 4 at the (110) and (111) crystal faces. Sites of diminished coordination

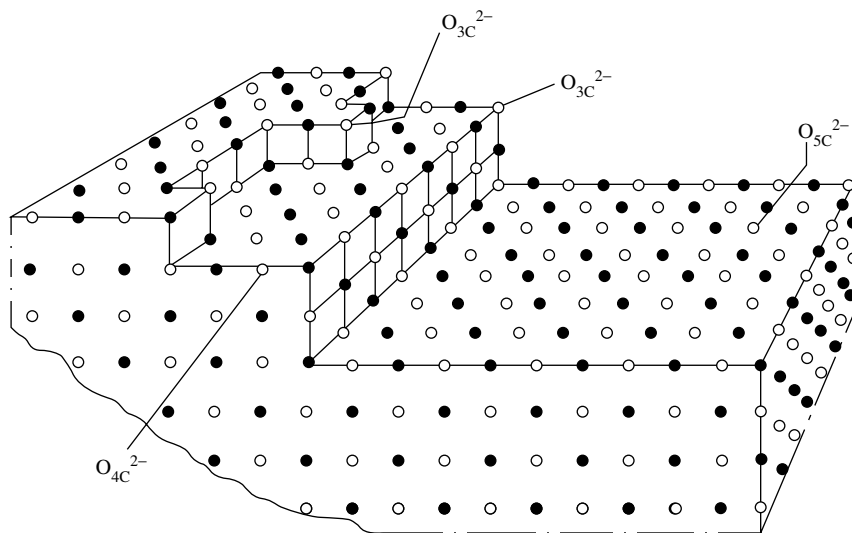


Figure 2.10. Representation of a surface (100) plane of MgO showing imperfections which provide sites for ions of low coordination [56]. Reprinted from Zecchina, A., Coluccia, S. and Morterra, C., *Appl. Spectrosc. Rev.*, **21**, 259–310 (1985), courtesy of Marcel Dekker, Inc.

exist also at the edges and corners of the crystals, while other sites can also be geometrically distinguished. According to electron microscopy, the surface of a real crystal is never ideally flat but contains steps, pits, etc. in which atoms of low coordination can exist (Figure 2.10). Che and Tench [238, 239] have symbolized low coordination oxide ions by O_{LC}^{2-} (e.g. O_{5C}^{2-} on an oxide ion in fivefold coordination).

Luminescence corresponds to the reverse process of UV absorption, and the shape of the luminescence spectrum varies with the excitation light frequency and with the adsorption of certain molecules. These migrate in surface ion pairs of low coordination numbers (see Figure 2.10). Changes in the spectra after adsorption indicate that ion pairs of lower coordination numbers have higher reactivities towards adsorption of even CH_4 (see Figure 2.9). As can be seen from Figure 2.10, several ion pairs of different combinations of coordination numbers exist on the surface. The existence of different sites was originally suggested due to the different activity of such sites towards CO and other molecules (see below). As has been pointed out by Gates [97], such models, although over-simplified, show the heterogeneity of the surface sites and provide a useful guide to the interpretation of the infrared spectra of adsorbed species. Analogous data on the effect of coordination of both cations and anions on the surface transitions and also on these ions towards different molecules have also been obtained for the reactivity of other oxides in this series [231–237]. The use of different systems enables the establishment of the effects of both surface impurities and modifiers on the surface states of the above oxides and on changes in surface properties [240, 241].

Other oxide systems

For other oxide systems, there has been little significant progress in this field of investigation. For a number of these systems, no reliable proof of surface cation–oxygen bond vibrations have been obtained, even though characteristic absorption bands were obtained in their IR spectra in regions above the fundamental frequencies of the oxides. For instance, no noticeable drop in

intensity could be observed for such absorptions on NiO and CuO [30] and Co_3O_4 [242, 243] in the regions above the fundamental absorptions of the crystals on high-temperature treatment *in vacuo*, or on interaction with reducing agents. The absence of such a decrease upon high-temperature treatment (surface diffusion temperature point) *in vacuo* for such oxides may be due to high rates of diffusion of oxygen anion from the lattice towards the surface. All of the above systems have the lowest energy of the oxygen bonds at the surface and in the bulk [82, 94]. It is much more difficult to explain the absence of effective decreases in the intensities of these absorption bands upon interaction with reducing gases at moderate temperatures. At high temperatures, the absorption of the bulk sample generally changes, which makes it impossible to draw any effective conclusions. However, in this spectral region some overtones of lattice modes can also be observed. Spectra in the region of the vibrations of 'surface cation-oxygen' bonds have been recorded for Sb_6O_{13} (e.g. in the region $800\text{--}1200\text{ cm}^{-1}$) [244], SnO_2 (e.g. 960 and 1060 cm^{-1}) [210, 211], Fe/Sb [245] and Ti/Sb [246] oxide system. However, these data have not yet been analyzed in any detail. They may be associated with states in the bulk rather than on the surface, such as disruptions of the crystalline lattice in the vicinity of vacant metal cations [180]. In this context, the assignment of absorption bands in the region above the fundamental absorption frequencies to surface vibrations requires more detailed investigations, analogous to those carried out for the $\text{Cr}_2\text{O}_3\text{--O}_2$ system, based primarily on the behavior of these absorption bands on chemical treatment at moderate temperatures.

Thus, two different states of oxygen with different nature of bonding can be identified on the oxide surfaces: First, an oxygen atom bound to a metal by strong $\sigma\text{--}\pi$ bonds, as in terminal $\text{Mo}=\text{O}_t$ on the (101) plane of MoO_3 ; in this case, the terminal oxygen is only weakly basic (electrophilic oxygen) since there is considerable transfer of electron density onto the metal orbitals [82]. Secondly, and in contrast, exposed bridging oxygen atoms which are more basic (nucleophilic oxygen); their lone pairs of electrons are able to cause a nucleophilic attack on an organic molecule. These two states can differ (in coordination number of cations and hence, in reactivity of active sites) with the exposure of different planes. Some cations in the low-oxidation state can be oxidized to the higher oxidation state (for example Cr^{3+} to Cr^{6+}) by forming terminal $\text{M}=\text{O}$ bonds.

Only the first steps have been taken towards spectral analysis of inherent surface states (including surface vibrations) of oxides. Numerous questions pertaining to the behavior of surface states during the reaction of oxides with different admixed molecules and atoms remain with many oxide systems. However, the author believes that this is an important direction for the investigation, allowing the state of oxide surfaces and their reactivity to be described with more detail, and methods of vibrational spectroscopy, UV-VIS, and especially photoluminescence spectroscopy [34a] promise to contribute a lot to the study of surfaces.

2.2.2 MOLECULAR FORMS OF ADSORBED OXYGEN

The main method for analyzing charged molecular forms of the adsorbed oxygen type O_2^- is ESR spectroscopy. The results have been surveyed in detail in several reviews [238, 239, 247]. The formation of O_2^- adsorbed species has been observed on more than 30 oxide systems, including supported and unsupported main-group and transition-metal oxides, as well as silica and some aluminosilicates – mainly zeolites. The molecular-orbital energy diagrams for the dioxygen molecule, and for dioxygen interaction with cation 3d orbitals in the case of both bent structures and side-on structures, are shown in Figure 2.11.

In the 1980s, it had been demonstrated that it is possible to use IR spectroscopy to detect molecular radical-ion forms of adsorption on the surfaces of oxide catalysts (see, for example, [30, 82, 238, 239, 248] and references therein). The IR method offers a number of complementary advantages to ESR, as it allows the observation of paramagnetic forms of adsorption on

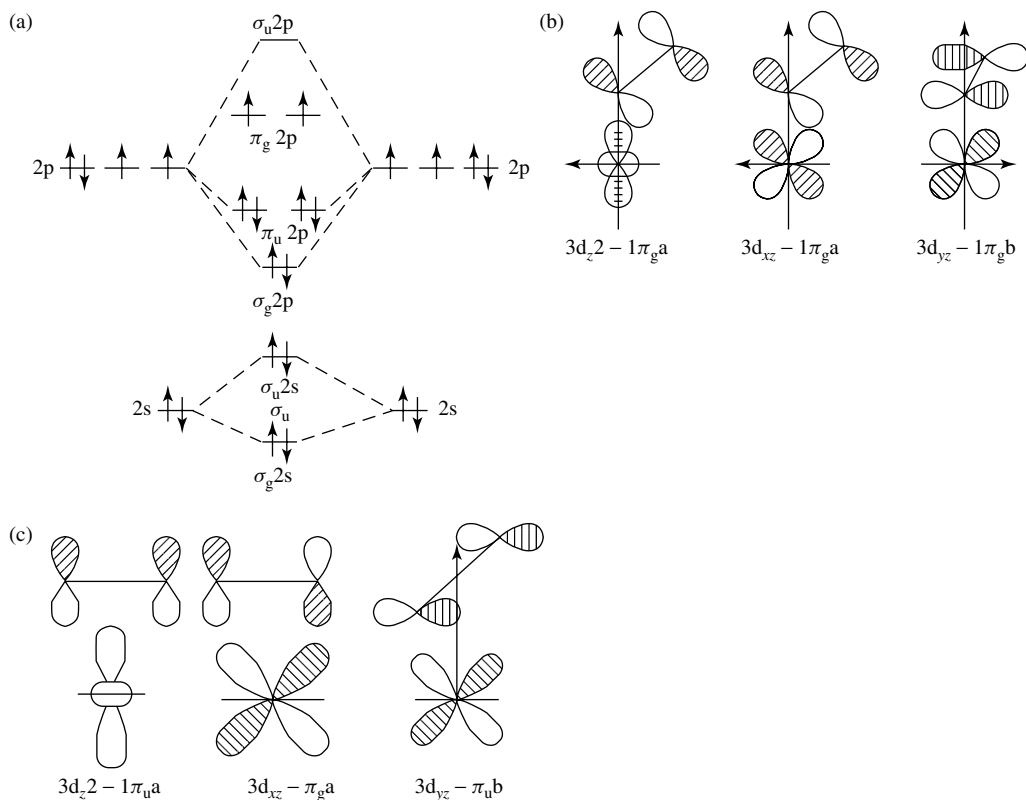


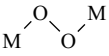
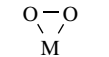
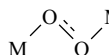
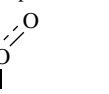
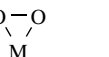
Figure 2.11. (a) The molecular orbital energy diagram for the dioxygen molecule, plus the main metal 3d–dioxygen interactions for (b) bent and (c) side-on structures.

paramagnetic oxides. It should be noted that IR spectroscopy can give information on coordinations of the oxygen molecules. The various vibration frequencies involving adsorbed oxygen, based mainly on the data of Davydov [30], together with those related to various other model systems (gas phase, solid state, and matrix-isolated species) [239] are listed in Table 2.2, while Figure 2.12 gives the frequency ranges of the oxygen species observed for the various systems. These data show that the frequencies of O–O vibrations lie in a wide range and overlap the vibration frequencies of M–O–M and M–O bonds. This last fact complicates the interpretation of spectral data for adsorbed species. In this connection, it has been indicated [30, 182] that in order to reliably identify such compounds by means of IR spectroscopy it is necessary to combine the IR data with the corresponding ESR results, and also with adsorption data from ¹⁶O/¹⁸O isotope mixtures. Unfortunately, there are few such studies in the literature at present. The spectral features of several oxygen-containing compounds with M–O and M=O bonds, as well as O₂ fragments in different states (gaseous, lattice-isolated, adsorbed, etc.) are depicted in Table 2.2.

Chromium oxide

One of the first studies was concerned with the detection of the O₂⁻ type of adsorbed molecular form of oxygen [182] on an evacuated chromium oxide (Cr₂O₃) surface. After oxygen adsorption at 293 K, the IR spectrum contained the absorption band at 985 cm⁻¹ (Figure 2.13, spectrum 2).

Table 2.2. Selected vibrational frequencies for species involving oxygen bonds.

Species	$\nu\text{O-O}$ (cm^{-1})	Reference
<i>Gas phase</i>		
$(^1\Delta_g)\text{O}_2$	1483.5	11
$(3\Sigma_g^-)\text{O}_2$	1555	11, 249
$(\text{O}_2)_2$	1586.1–1596.6	250
O_2^+	1876	11
<i>Oxygen carriers</i>		
 (peroxide-like)	780–884	251
 (peroxide-like)	800–932	251
 (Superoxide-like)	1075–1122	251
	1130–1195	251
<i>Solid State</i>		
Solid α -oxygen	1550–1590, 1616, 1636	252
O_2^{2-}	738–794	249, 253–255
M–O–M	800–900	15
M=O	900–1100	15
O_2^-	1137–1164	249, 254, 255
O_2^+	1825–1864	11, 256, 257
<i>Matrix-isolated species</i>		
	983	15, 258
O_2^- (peroxide-like) ^a	990–1115	259–263
<i>Adsorbed species</i>		
O_2^{2-}	640–970	264–267
M–O–M	750–900	30, 178–180, 268–270
M=O	900–1100	30, 178, 180, 183, 207, 270
O_2^-	970–1180	30, 179, 182, 184, 210, 211, 268, 271, 280, 284, 286
'Neutral' O_2	1460–1650	30, 267, 271, 281, 282, 286

^a Alkali and silver peroxides.

Assignment of the 985 cm^{-1} band to the molecular form of adsorbed oxygen has been proved by the adsorption of an isotopic mixture ($^{16}\text{O}_2$ and $^{18}\text{O}_2$), which results in a triplet caused by the three molecular forms, $^{16}\text{O}-^{16}\text{O}$, $^{16}\text{O}-^{18}\text{O}$ and $^{18}\text{O}-^{18}\text{O}$, the intensity ratio within which corresponds to the composition of the isotope mixture (spectrum 3). The charged state of adsorbed O_2 was

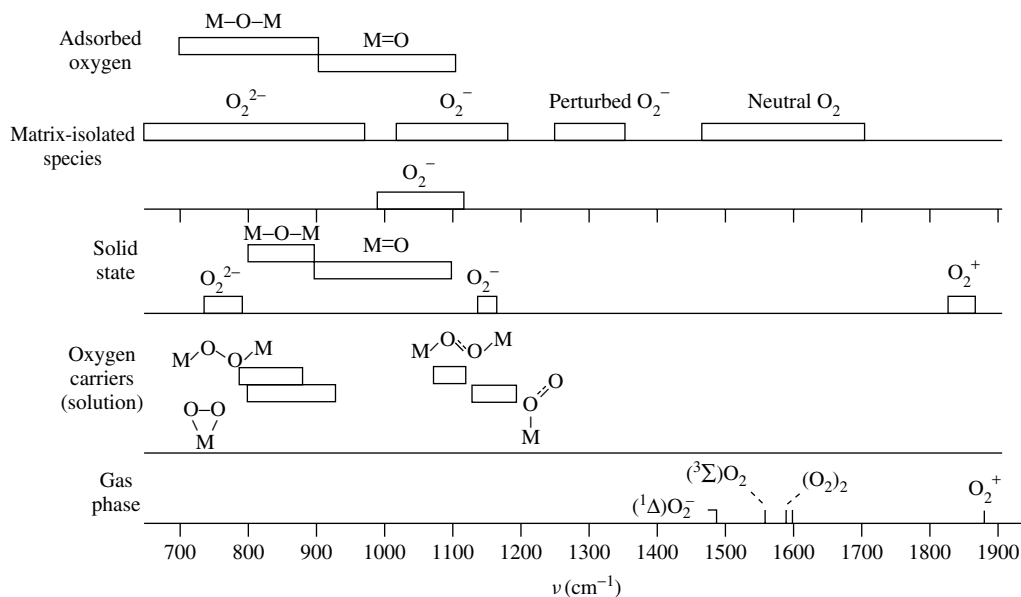


Figure 2.12. Infrared frequencies for species involving oxygen bonds [248]. Reprinted from *Rev. Chim. Minerale*, **21**, Che, M., Dyrek, K., Kermarec, M. and Tench, A. J., 'Characterization of oxygen species adsorbed on oxide surfaces by infrared spectroscopy', 669–691, Reproduced by permission of Editions scientifiques de médicaux Elsevier, © 1984.

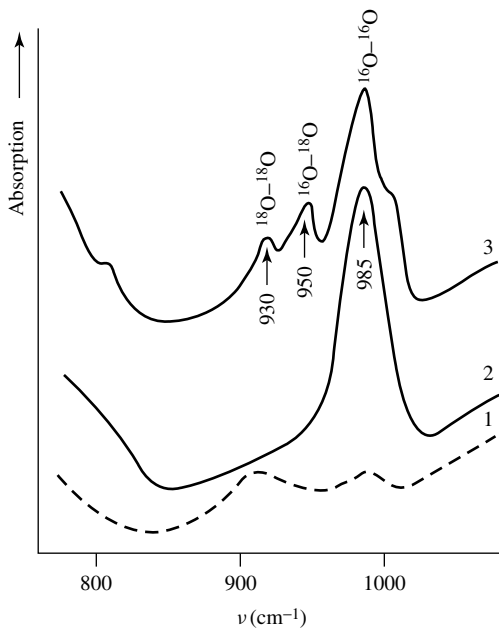


Figure 2.13. IR spectra of (1) $\alpha\text{-Cr}_2\text{O}_3$ following heat treatment at 773 K *in vacuo*, and subsequent addition at 293 K of (2) $^{16}\text{O}_2$ and (3) $^{16}\text{O}_2 + ^{18}\text{O}_2$ mixture.

inferred from a comparison of the frequency from radical-ion forms of O_2^- and also from the change in conductivity of the oxide during oxygen adsorption.

The later work of Carrot and Sheppard [183], in which the adsorption of oxygen on Cr_2O_3 has been studied by the use of isotopically substituted molecules, did not confirm these data. They showed that during the adsorption of oxygen on the surface of both amorphous and crystal α - Cr_2O_3 , already at room temperature a dissociative adsorption of oxygen is characterized by absorption bands in the same region (800–1050 cm^{-1}). For amorphous chromium oxide, adsorbed oxygen is exhibited as unresolved absorption bands with a maximum at 995 cm^{-1} , which in these experiments gives rise to only a single additional maximum when isotopically substituted molecules were adsorbed. This indicated that this band belonged to vibrations of the $M=O$ bond. When oxygen was adsorbed on crystalline chromium oxide, three absorption bands, undergoing an isotopic shift characteristic of $M-O$ bonds, were observed.

Special experiments carried out [184] to attempt understand the causes for disagreement between these two reports [182, 183] indicated that the reason was that the surfaces of the samples had been reduced to different degrees. The data obtained on the crystalline sample studied in the earlier work [182] showed that the single band at about 985 cm^{-1} was observed once again on this sample when treated *in vacuo* as after oxygen adsorption at 293 K. In the case when oxygen has been adsorbed at the same temperature, but on a sample treated at 673 K by CO and then *in vacuo*, there a triplet appeared in the region at 1000 cm^{-1} . This showed that dissociation of oxygen had taken place.

The use of CO molecules as probes to establish the degree of oxidation of chromium cations in samples before oxygen adsorption [184] indicated that in the case of samples treated *in vacuo* the state Cr^{3+} (the complex $Cr^{3+}-CO$ is characterized by an absorption band at 2195 cm^{-1}) is more probable, whereas reduction in CO at 673 K leads to the formation of Cr^{2+} ions (the complex $Cr^{2+}-CO$ being characterized by the 2170 cm^{-1} band). A detailed discussion of this problem is presented in Chapter 3. On the basis of this additional information, it was suggested [184] that the adsorption of oxygen at 293 K with the participation of Cr^{2+} ions occurs in a different way to that involving participation of the Cr^{3+} ions, realized under the conditions used in the earlier work [182]. With the participation of Cr_{cus}^{3+} ions, the $Cr^{4+}-O_2^-$ complexes are probably formed, while on Cr^{2+} ions a dissociative chemisorption of oxygen takes place.

Titanium dioxide

Davydov *et al.* [194] had revealed a correspondence of the form of adsorbed molecular oxygen observed by IR spectroscopy, which show a strong weakening of the oxygen–oxygen bond, to the O_2^- ion radicals observed in EPR spectra. In the case of TiO_2 (anatase) treated under reduction conditions, after adsorption of oxygen at 293 K, the O_2^- ion radicals are formed. These species are characterized by an IR band at 1180 cm^{-1} (Figure 2.14(a), spectrum 1); in the EPR spectra, a signal characteristic of an ion-radical molecular form of adsorbed oxygen appeared. Depending on the degree of reduction of the sample, different numbers of O_2^- ions (e.g. 1, 2, 3, 5, etc.), with differing degrees of loosening of the O–O bond can be observed. The frequencies of the O–O bond (ν_{O-O}) in the O_2^- ions appear in the 1060–1180 cm^{-1} interval (see Figure 2.14(a), spectrum 2) and have a different values of the g_z component in the ESR spectra. When the degree of reduction increases, the g_z value increases and the intensities of the ESR maxima decrease. This is probably connected with a decrease of the coordination saturation of the surface titanium ions.

It should be noted that the degree of reduction of TiO_2 in the above cases has not been specially monitored; it probably was high, and did not correspond to the degree of reduction reached by only evacuation of TiO_2 , as reported Davydov *et al.* [194]. The reduction of the sample used in this work [194], as it is now established, occurred due to the presence of carbon and, in particular, nitrogen-containing surface impurities on the TiO_2 sample. These had been incorporated in

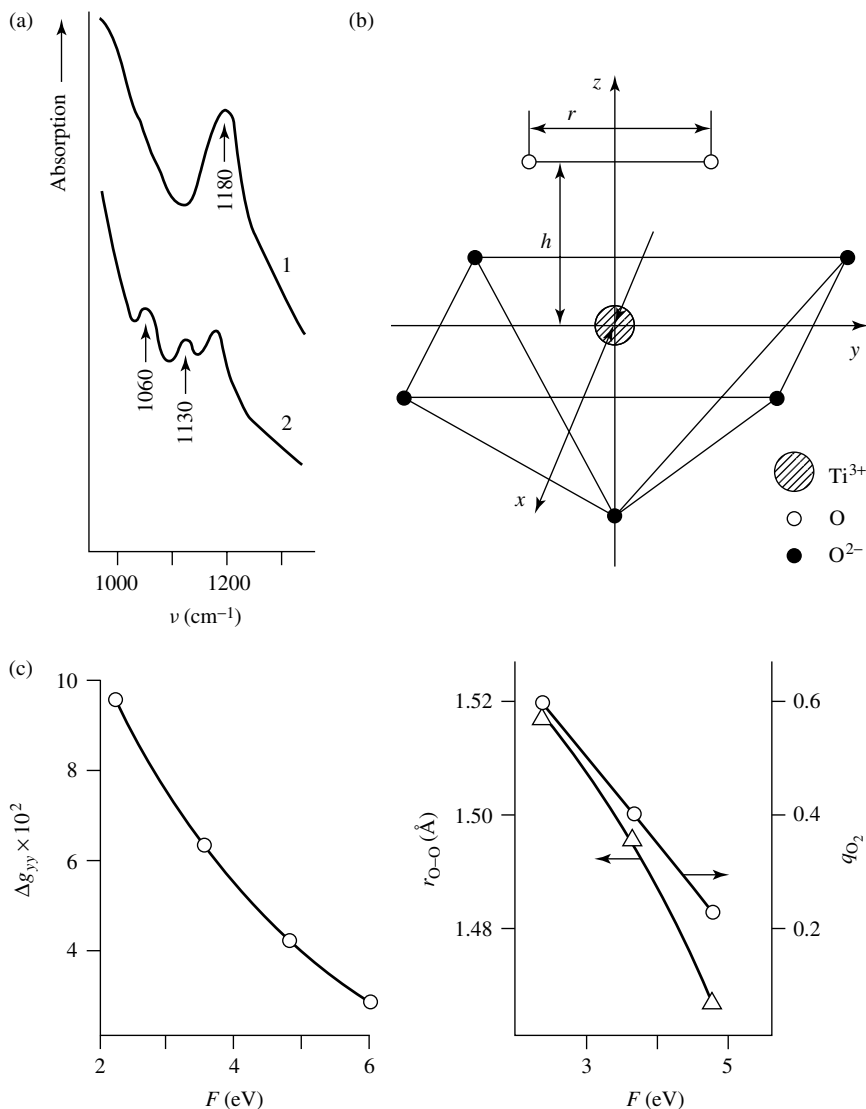


Figure 2.14. (a) IR spectra of oxygen adsorbed at 293 K on titanium dioxide (anatase) after various reduction treatments. (b) Model for oxygen adsorption on a coordinatively unsaturated titanium ion. (c) Dependence of $r_{\text{O-O}}$ and q_{O_2} on F .

the sample during the preparation of the pellets for investigation of the IR spectra. To prepare thin samples (the region 700–900 cm^{-1} is adjacent to the cutoff region of TiO_2), the so-called ‘foliated pie’ method was used, i.e. the TiO_2 was pressed in contact with $(\text{NH}_4)_2\text{CO}_3$, which was then decomposed by infrared heat. After this treatment, the sample obtained was immediately treated *in vacuo*. As shown from the spectra of such a sample, there was a significant amount of adsorbed NH_3 present, due to which strong reduction of the sample took place, unlike that obtained after evacuation of an initial TiO_2 sample. This factor had not been taken into account in the earlier studies [194].

The experimental data on the relationship between $\nu\text{O-O}$ and g_z in O_2^- , as obtained by Davydov *et al.* [194], have been interpreted by Lumnov *et al.* [272] by using a quantum chemistry approach. For this, the model of the paramagnetic center (see Figure 2.14(b)) has been examined. In order to obtain an energy minimum, the r and h values were varied between limits of 1.3–1.7 and 1.6–1.8 Å, respectively. As a result of these calculations, the following conclusions were obtained: (i) a correlation was established between the equilibrium distance O–O ($r_{\text{O-O}}$) and the energy of the interaction with the surface, F ; (ii) the electron charge on O_2 was dependent on F , in addition, the components of the g -tensor were investigated. The decrease in F leads to a more effective electron transfer into $\text{O}_{2(\text{ads})}$, an increase in Δg_{yy} , and a decrease in the frequency of the O–O vibrations (Figure 2.14(c)). Further details can be found in the texts by Davydov [30].

Tin dioxide

Molecular forms of adsorbed oxygen of the O_2^- type were also detected by IR spectroscopy on only on prerduced tin dioxide after oxygen adsorption at room temperature [210, 211]. In the case of SnO_2 containing defects (an SnO_2 sample obtained after drying for 10 h at 383 K and treatment *in vacuo* at 723 K contained reduced tin ions and has been termed a ‘defected’ sample) oxygen is adsorbed at low temperatures (293 K) in two forms of O_2^- ions, i.e. stabilized on Sn^{2+} ions ($\nu\text{O-O} = 1045 \text{ cm}^{-1}$) and Sn^{4+} ($\nu\text{O-O} = 1190 \text{ cm}^{-1}$) (Figure 2.15, spectrum 2), which agrees fairly well with the ESR data for the same samples [273]. For tin dioxide without defects the defect-free sample was prepared by heating the dried sample at 723 K in air; with this sample, reduced states of tin could be obtained only after heating in a reducing atmospheres at high temperatures, the spectral picture of adsorbed oxygen ranges is much more complex.

The appearance of high-frequency maxima at 1100, 1140, 1120, and 1090 cm^{-1} during the adsorption of oxygen at room temperature on nondefected SnO_2 reduced under vacuum (Figure 2.16, spectrum 1), which disappear from the spectrum after heating the sample in oxygen up to 473 K, may also be due to a number of low-temperature forms of adsorbed oxygen of the O_2^- type. Support for this comes from EPR studies [273]. It should be borne in mind that more complicated charged complexes, such as O_3^- and O_4^- may absorb in the same spectral region [210, 211], and it cannot be excluded that such species are responsible for the bands in the $1090\text{--}1160 \text{ cm}^{-1}$ region.

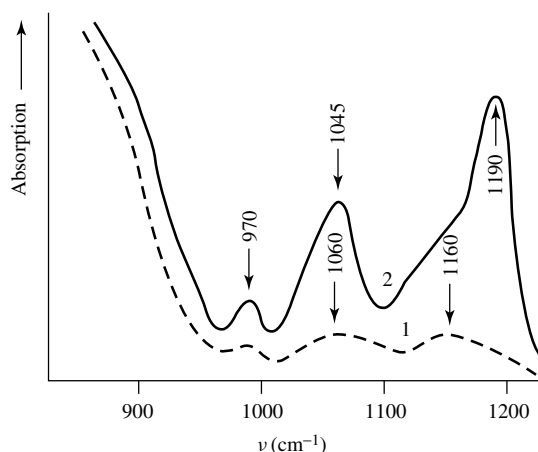


Figure 2.15. The IR spectrum of oxygen adsorbed at 293 K on the surface of defect-containing SnO_2 (2), trace (1) represents the background spectrum.

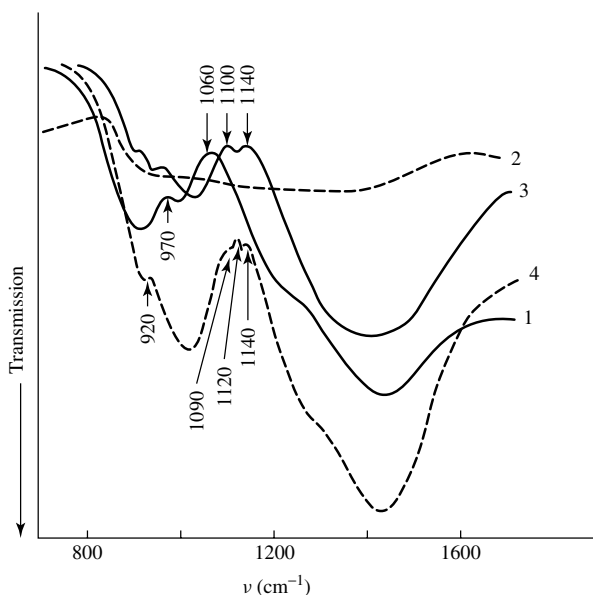


Figure 2.16. IR spectra of SnO₂-II. 1, initial spectrum of oxidized at 673 K sample; 2, reduction in CO and following evacuation at 673 K for 2 h; 3, following adsorption of oxygen, at 6.7 kPa and 293 K; 4, after 1 h in oxygen.

Significant differences in the spectra of oxygen adsorbed at moderate temperatures (up to 473 K) between defect-containing and defect-free samples (compare Figure 2.15 and 2.16), including the positions of the absorption bands from oxygen adsorption, have been noted in Gundrizer and Davydov [210]. Using a defect-free sample, Harrison and Thornton [269] obtained a spectrum with a set of absorption bands in the region 900–1200 cm⁻¹, which, in their opinion, had been attributed by Gundrizer and Davydov [210] to the absorption of ion-radical forms of the oxygen type O₂⁻. Their work showed that the bands in this region do not shift upon adsorption of ¹⁸O₂, so they concluded that these absorption bands cannot be attributed to certain oxygen states. In connection with this, it is necessary to examine the data of Harrison and Thornton [269] in more detail. The bands at 1160, 1060, and 970 cm⁻¹ which have been observed in the spectra of both defect-containing and defect-free SnO₂, before oxygen adsorption or after high-temperature heating at 673 K (Figures 2.15 and 2.16, spectra 1), were not attributed to O₂⁻ ions in [210]. This was, however, a misunderstanding, as the only suggestion made by Gundrizer and Davydov [210], as agreed in Che and Tench [239] and Davydov [211], was that these maxima are characteristic of Sn=O and Sn–O bonds, respectively. Use of isotopically substituted molecules for such wide and low intensity bands is, in any case, unreliable, since it is impossible under such conditions to detect these small band shifts of 10–20 cm⁻¹.

These forms of oxygen were observed by Gundrizer and Davydov [210] **only on reduced samples** of SnO₂ (in the case of defect-containing SnO₂, the method of preparation produced such defects; a defect-free SnO₂ sample has to be specially reduced). After the adsorption of oxygen on such samples, additional absorption bands, not observed in the work by Harrison and Thornton [269], appeared in the spectrum of prerduced sample (see Figures 2.15 and 2.16). The temperature, at which the oxygen complexes characterized by these bands were stable, was similar to that applicable to the complexes of O₂⁻ on Sn²⁺ and Sn⁴⁺, as detected by EPR spectroscopy on the same samples. The closeness of these frequencies to νO–O in isolated O₂⁻, the relationship

between $\nu\text{O}-\text{O}$ and the degree of oxidation of the center established earlier, and the temperature ranges over which these complexes exist on the surface, lead to the conclusion [210] that these absorption bands can also be assigned to $\nu\text{O}-\text{O}$ in O_2^- .

Ferric oxide

Unfortunately, the molecular forms of oxygen adsorbed on iron oxide (Fe_2O_3) have not been directly investigated, although their possible formation was discussed in several studies [198, 203–205]. The first study, by Griffiths *et al.* [198], noted that the absorption bands at 1270 and 1350 cm^{-1} observed in the IR spectra of oxidized iron oxide are probably connected with the molecular forms of adsorbed oxygen (but as shown in Table 2.2, these bands do not lie in the spectral region which is characteristic of $\text{O}-\text{O}$ bonds of ion radicals). Later investigations of this oxide [202–206] have not contributed significant improvements in the understanding of the nature of the above absorption bands. On similar basic principles, the authors of the reports listed above have assigned the absorption bands in the overall region of 800 to 1200 cm^{-1} to O_2^{2-} (900–1200 cm^{-1}) and to O_2^- (1200–1300 cm^{-1}).

The assignment made by Lorenzelli and co-workers [202–206] were predominantly based on the fact that these frequencies lie in the region between $\nu\text{O}-\text{O}$ in $\text{O}_{2\text{gas}}$ and in O_2^{2-} for peroxide systems. Some remarks about such the assignment of such bands have already been made (see Section 2.2.1 above). In addition, it should be noted that individual stable surface compounds such as O_2^{2-} and O_2^- are not characteristic for Fe_2O_3 , in contrast to those observed in the case of BaO_2 . So, the only way for such stable structures (O_2^- and O_2^{2-}) to exist involves metal peroxides. In fact, the formation of peroxide and superoxide structures is characteristic of the behavior of numerous **rare-earth and alkali-earth metal oxides** on interaction with oxygen [274, 275]. Such types of surface compounds are, as a rule, unstable – the highest stability (up to 523 K) was observed for O_2^- on TiO_2 – and they are formed only during oxygen adsorption on reduced surfaces. Thus, the O_2^- ion on Cr_2O_3 (σ type) was fully dissociated at 423 K, and likewise at room temperature on NiO (see below). In connection with this, the high stability under oxygen atmospheres (up to 673 K) of most of the bands, which various authors have assigned to O_2^- and O_2^{2-} on Fe_2O_3 , makes such assignments very doubtful.

CeO₂

Adsorption of dioxygen on well-outgassed and partially reduced cerium oxide has been studied by FTIR spectroscopy [276–278]. On CeO_2 dehydrated at 1000 K, bands at 2237 and 1126 cm^{-1} for $^{16}\text{O}_2$, or 2112 and 1063 cm^{-1} for $^{18}\text{O}_2$, are observed in the spectra and seem to be attributable to O_2^- species (the absorption bands in the region of frequencies above 2100 cm^{-1} are the first overtones of the fundamentals). The formation of such O_2^- ions depends on the treatment conditions, as follows:

Oxide treatment	Vibrational mode	$^{16}\text{O}_2$	$^{18}\text{O}_2$	$^{16}\text{O}_2/^{18}\text{O}_2$	Species
CeO_2 (1000 K)	ν_1	1126	1063	1.059	Superoxide, O_2^-
	$2\nu_1$	2237	2112	1.059	Superoxide, O_2^-
CeO_2 (673 K in H_2)	ν_2	883	835	1.057	Peroxide, O_2^{2-}
	ν_1	1128	1065	1.059	Superoxide, O_2^-
	$2\nu_2$	2239	2114	1.059	Superoxide, O_2^-

BaO₂

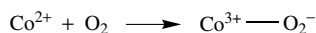
The formation of these structures is especially characteristic of barium oxide, when the high-temperature chemisorption of dioxygen species in both dia- and paramagnetic forms is so large

that it involves not only a surface, but also the bulk of the solid. In fact, Raman spectra of, for example, BaO_2 in the O–O stretching region, can be registered (with a main peak at 838 cm^{-1} , and at least two side-bands at 826 and 814 cm^{-1}) at different temperatures (up to 1100 K) under an oxygen atmosphere [279]. Although only one peroxide stretching band is expected according to the crystal symmetry, the three Raman bands observed at all temperatures were assigned to peroxide ions in different crystal environments caused by the relative locations of the oxide impurities. Similar results have also been obtained for BaO/MgO systems for which a Raman spectrum of barium peroxide has been observed at 373 K . However, no such situation occurs for $\alpha\text{-Fe}_2\text{O}_3$, where under similar conditions these structures are not thermally stable. The assignments given [202–206] are in agreement with this but there is no direct proof (such as isotopic data) in these papers for attributing the observed absorption bands to $\nu\text{O-O}$.

CoO–MgO

Giamello *et al.* [280] have observed five overlapping absorption bands in the IR spectra of oxygen adsorbed on diluted (5 mol%) CoO–MgO solid solutions after oxygen adsorption at 77 and 293 K . These bands could be slowly desorbed by evacuation at the same temperature at different rates in the following order: $1088 = 1095 > 1100 > 1124 = 1157\text{ cm}^{-1}$. It was therefore concluded that each component of the band corresponds to a different species. Using isotopic molecules, and by comparing the IR spectra with the corresponding ESR spectra, it was concluded that O_2 is adsorbed in the form of the superoxide ion O_2^- . In fact, the adsorption of $^{18}\text{O}_2$ molecules under the above-mentioned conditions gives rise to a set of IR bands shifted to lower frequencies by about 60 cm^{-1} , while the adsorption of a 1:1 $^{16}\text{O}\text{-}^{18}\text{O}$ mixture produced a spectrum which was nearly a superposition of the two previous ones. These results are typical for species having nearly pure O–O stretching modes. The signal obtained with a CoO–MgO solid solution and identified as corresponding to $\text{O}_2^-/\text{Co}^{3+}$ vanished *in vacuo* at room temperature, but the signal of $\text{O}_2^-/\text{Mg}^{2+}$ adsorbed on the same sample was stable until $400\text{--}500\text{ K}$ (Figure 2.17) [280].

It has been established that O_2^- ions are formed by the following reaction:



Scheme 2.2

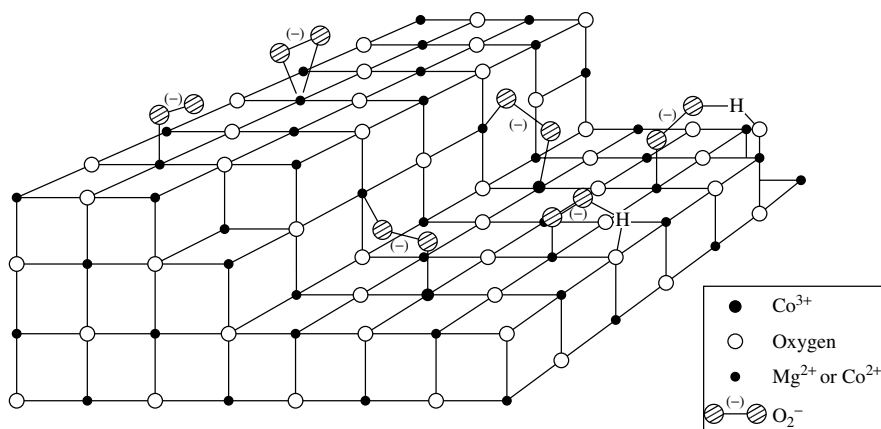


Figure 2.17. Different adsorbed oxygen species detected at the surface of a CoO–MgO solid solution [280]. Reprinted with permission from Giamello, E., Sojka, Z., Che, M. and Zecchina, A., *J. Phys. Chem.*, **90**, 6084–6091 (1986). Copyright (1986) American Chemical Society.

and that stabilization of the oxygen on the cobalt ions in a different coordination state takes place as follows:



Scheme 2.3

The evolution of adsorbed species on three- and five-coordinated cobalt ions localized on edges and corners has also been studied.

Nickel oxide

In this system, the O_2^- type of adsorbed oxygen has also been observed with a stretching frequency at 1070 cm^{-1} [271]. Radical-ion forms of molecularly adsorbed oxygen are only observed on reduced or irradiated oxide surfaces. Their formation is caused by the stabilization of oxygen molecules on coordinatively unsaturated cations when the oxidation degree is lower than on the defect-free surface or in the bulk. The adsorption is accompanied by an electron transfer from a center with excess electron density into the oxygen molecule. These forms are unstable at high temperatures, tending to decompose during heating with the re-oxidation of the catalyst surface.

Uncharged oxygen species on the surface

The presence of coordinatively unsaturated cations on the surface of oxide catalysts (in the oxidized state) should result in promotion of oxygen adsorption which is not accompanied by electron transfer into the oxygen molecule. The resulting uncharged forms of adsorbed molecular oxygen should differ slightly from unperturbed oxygen and hence give different $\nu\text{O}-\text{O}$ bands when it is IR-active and, therefore, can be detected [194, 271, 281–284]. In fact, in spite of the inactivity of the vibration of free O_2 molecules in IR spectra (D_{oh} symmetry), in low-symmetrical environments a vibrational dipole moment can be induced, e.g. under pressure in the gas phase, in the liquid and adsorbed states, in solid matrices or in molecular complexes (see Table 2.2).

Forster and Schuldt [282] have reported IR spectra where D_2 , N_2 and O_2 molecules gave quite strong absorptions in the region of the fundamental vibrations during the physical adsorption on NaA zeolites. For O_2 , in particular, absorption bands, with two maxima in the $1550\text{--}1570 \text{ cm}^{-1}$ region, has been observed.

The appearance of absorption bands in the $1500\text{--}1700 \text{ cm}^{-1}$ region (characteristic of $\nu\text{O}=\text{O}$ vibrations) after low-temperature adsorption of oxygen has been reported by Davydov [281, 284]. A comparison of the absorption bands observed in the spectra with the literature data (see Table 2.2) has led to the conclusion that the absorption bands in this region are characteristic of the $\nu\text{O}-\text{O}$ frequencies of molecular uncharged forms of adsorbed oxygen which are observable because of polarization by the solid surface. The main arguments in favor of these assignments of the maxima in the $1500\text{--}1700 \text{ cm}^{-1}$ region, following low-temperature adsorption of oxygen, have been summarized [281, 284]. Desorption of uncharged oxygen molecular observed by IR spectroscopy in the temperature range between 203 and 373 K, i.e. molecular forms of adsorbed oxygen, are unstable at high temperatures. The appearance of molecular forms characterized by absorption bands in the region of frequencies slightly above those for $\nu\text{O}-\text{O}$ in the gas phase is unusual. As can be seen from Table 2.2, it is also characteristic of liquid and solid oxygen. This is considered to be connected with suppression of the rotation of the molecules [284]. Similar increases have been observed on the adsorption of H_2 (see below). Unfortunately, it is difficult to

use isotopically substituted $^{18}\text{O}_2$ molecules to identify these adsorption forms of adsorbed species because of their low intensity and the significant half-widths of the bands. In addition, at low temperature, the spectral features of physically adsorbed oxygen will effectively mask those of the adsorbed species. An intense absorption has been observed at 1540 cm^{-1} for several samples of Fe_2O_3 [178, 198, 199, 204–209], but an increase of the sample temperature in the presence of oxygen as well as *in vacuo* leads to its disappearance. Its intensity is reduced on cooling. From the evidence it is possible to assign this absorption band to multi-phonon absorption [203, 207], in contrast to the conclusion drawn in the work by Busca and Lorenzelli [202] where it was assigned to $\text{O}_{2\text{ads}}$.

Low-temperature adsorption forms of oxygen has been observed by the temperature-programmed desorption (TPD) method on practically all metal oxides having coordinatively unsaturated surface cations (TiO_2 (anatase), Mn_2O_3 , Fe_2O_3 , Co_3O_4 , NiO , CuO , ZnO , CaO , ZrO_2 , Bi_2O_3 , La_2O_3 , SnO_2 , MgO , Sb_6O_{13} and $\gamma\text{-Al}_2\text{O}_3$). The desorption activation energy of such weakly adsorbed forms was $17.6\text{--}39.6\text{ kJ mol}^{-1}$ [283]. For ZrO_2 , using the differential isotope method, it has been established that the weakly bound form in this case is adsorbed molecular ('neutral') oxygen, i.e. uncharged molecular oxygen is confirmed by IR spectroscopy. It seems that all coordinatively unsaturated cations in the oxidized state can bind the oxygen molecule.

According to Sokolovskii *et al.* [285, 286], the uncharged molecular forms of adsorbed oxygen can act as intermediate forms in the low-temperature isotopic exchange of oxygen. Thus, it has been proved [285] that the removal of such a species from the surface of titanium dioxide at 223 K almost stops the isotopic exchange.

Table 2.2. provides data on the vibrational spectral characteristics of molecular forms of oxygen, both as individual species and as observed during adsorption on oxides.

O₃ adsorption

Trioxigen, (ozone) O_3 , thermodynamically unstable under normal conditions, is formed when an electric discharge passes through oxygen gas. The molecule of ozone, the allotropic modification of oxygen, isoelectronic with the NO_2^- ion, has an angular shape and has C_{2v} point group symmetry. The bond angle of $116^\circ 45'$ indicates sp^2 hybridization of the orbitals of the central oxygen atom. Recently, several studies have been published devoted to ozone adsorption on oxides surface [287]. The observed vibration frequencies (about 1145 and 990 cm^{-1}), as well as the isotopic shifts observed for ozone enriched by ^{18}O , reveal a strong distortion of the molecule in such a complex. No molecular adsorption of ozone has been detected on strong Lewis-acid sites, with the data obtained providing evidence for ozone dissociation on the surface. Ozone molecules form coordinative complexes bound via the terminal oxygen atom to weaker sites. The formation of small amounts of $(\text{O}_2)_2$ in the gas phase occurs only at low temperatures.

Spectral features of oxide conductivity

As has been observed for TiO_2 [194], the transmission of samples during reduction may decrease over a wide range, even up to complete transmission loss. This is characteristic of n-type semiconductors, and is associated with increasing concentrations of free carriers (electrons) [42, 288–290] and with the absorption of radiation by the latter. Changes in the spectra during reduction, similar to those seen for TiO_2 , have been observed for Fe_2O_3 [178, 207], Fe–Cr–O [192], Zn–Cr–O [193], ZnO [196, 197], SnO_2 [210, 211] and a series of other oxides. We will examine this phenomenon on the basis of the most widely investigated oxides.

In the case of zinc oxide, which can be taken as an example of an n-type semiconductor, slow desorption of oxygen localized in the surface layers begins *in vacuo* at 550 K [82, 290]. The zinc remains in the near-surface layer as interstitial excess atoms, thus forming

electron-donor centers. The processes can be represented by the following equations (expressed by using Kroger–Vink symbols):



The neutral interstitial zinc atoms $(\text{Zn}_i)_s$ can supply free electrons, e^- , thus increasing the electron conductivity of the surface layer, as follows:



In ZnO, the formation of such defects is enhanced by treatment of the oxide *in vacuo*. Other oxides, for example, CuO [30], NiO [30, 290] and Co_3O_4 [242, 243], which are semiconductors of the p-type (hole-type), improve their transmissions under reduction. A typical example is nickel oxide, which stoichiometrically chemisorbs oxygen with the formation of acceptor centers in the form of neutralized cationic vacancies V_{Ni} , as follows:



The neutral $(V_{\text{Ni}})_s$ center consists of a cationic vacancy, which formally bears two negative charges, together with two Ni^{3+} ions (positive holes represented by h); the free positive holes act as carriers of electric current. The presence of Ni^{3+} ions in the surface layer of NiO has been established by various analytical methods. It has also been qualitatively established that the black(non-stoichiometric) sample transforms in to a green form (stoichiometric NiO). X-ray photoelectron spectroscopy (XPS) data [290] have confirmed the presence of Ni^{3+} ions.

Although simple maxima are not observed in the spectra during the changes in conductivity, the changes in overall transmission enable the evaluation of the reduction–oxidation processes taking place on the surfaces of these systems and this is widely used to investigate various semiconductor and catalytic systems. This approach has been employed, for example, during investigations of the mechanism of the water-gas-shift (WES) reaction [192].

Investigations of the transmission spectra of ZnO samples activated by various metals, e.g. Cu [291], Pt [292], Ru [293, 294], and Pd [295], have shown that, *in vacuo*, electron transfer from donor centers in the ZnO to the metal particle takes place for all of these systems (see Figure 3.14). In the presence of H_2 , the IR absorption strongly increases, thus reflecting an increase in the concentration of donor centers on the ZnO surface due to proton ‘spillover’ from the metal particles [291, 296]. Such electronic effects associated with adsorbed species are relevant in gas sensor devices [296].

2.2.3 SURFACE HYDROXYL GROUPS

Actually, the broken bonds on the crystal surface become saturated as a result of dissociation of the H_2O molecules: hydrogen is bonded to an oxygen atom, whereas the hydroxyl groups bond the metal atoms. The appearance in the spectra of several bands characteristic of hydroxyl groups, as well as their different spectral characteristics and chemical properties (acidity, reactivity), are due to the exposure of several crystal faces and different kinds of defects on the oxide surface. Practically every study of surface properties and/or adsorption of molecules on oxides provides data about surface hydroxyl groups. Such data have been summarized in numerous books and reviews (see, for example, [18–31] and [297–348]). Among more recent studies, the texts by Fierro [31] are useful because most of the known data on hydroxyl groups on the surface of different oxides are examined in these volumes. Taking this into account, only the correlation

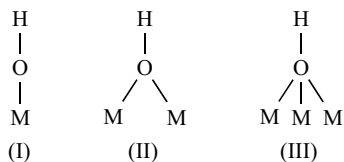
between the spectral features of surface OH groups and the structures of oxides will be the subject of examination in this present section.

As was noted above, after oxide dehydration at high temperature and following the removing of bound molecular water, the bands caused by OH vibrations (which can be regarded as localized vibrations of the adsorbed atom (H) on the surface) are observed at frequencies higher than those of the lattice cutoff absorption. For most oxides, the vibrations of bonds of isolated hydroxyl groups appear in the IR spectra as discrete absorption bands (Tables 2.3 and 2.4).

Oxides which had been heated at only moderate temperatures exhibit several other bands, the appearance of which depends on the preparative conditions and pre-treatment temperature. In general, the IR band due to the OH stretching vibration of an hydroxyl group appears at a lower wavenumber, is strengthened in integrated intensity and is broadened, if the group is involved in hydrogen-bonding interactions.

It is now clear that the spectral features of isolated surface hydroxyl groups depend on the chemical structures of the oxides, and their detailed interpretation conversely enables conclusions to be drawn about the structures of the oxide surfaces and about their active sites. The most generalized treatment of the influence of crystalline structure on the IR spectra of surface OH groups has been reported by Tsyganenko and Filimonov [310, 319].

A reason for the appearance of several bands due to free surface hydroxyl groups in the IR spectra is the capability of the oxygen atoms of the OH groups to be in contact with several immediate neighboring metal atoms. Hence, the number of the latter should exert a decisive influence on the vibrational frequency, νOH , which is observed. For isolated (free) hydroxyl groups, the oxygen can be bound to one, two, three, etc., metal atoms (types I, II, III, etc.).



Scheme 2.4

The formation of the coordination bond is found to diminish the frequency of the OH stretching vibration and hence the bands ascribed to the OH groups I, II and III will be positioned accordingly.

In order to establish a model for hydroxyl coverage, an analysis of the structure of specific crystal planes has been carried out [310, 319], with the expectation being that the planes appearing during crystal growth from the gas phase would be predominant. The oxygen of the OH group can form bonds with several metal atoms if this is allowed by their mutual arrangements. The oxygen atoms of the surface OH groups always occupy those positions where the O atoms would have been present in the infinite lattice. The number of metal atoms around the oxygen of an OH group is always smaller than the coordination number of oxygen in the lattice, i.e. the maximum number of OH groups for the oxide in question equals the oxygen coordination number minus one.

The stretching frequencies of nonassociated OH groups are thus determined mainly by their local surroundings, that is, by the number of bound metal atoms and their chemical nature, and to a lesser extent, by their coordination numbers. In accordance with data reported by Tsyganenko [320], the dependence of νOH for type 1 hydroxyls bound to atoms of different metallic

Table 2.3. Positions of absorption bands of isolated OH groups on alumina and their possible assignments.

Treatment	$\nu\text{OH}/\nu\text{OD}$ (cm^{-1})	Assignment ^a	q^b	Reference	
Al ₂ O ₃ dehydrated at 823 K Peri's model	3800 A 3775 D 3745 B 3730 E 3710 C 3690 C	O O ⊗ O O	–	239	
		O O • O	–		
		O • O	–		
		• O	–		
		•	–		
		•	–		
Al ₂ O ₃ dehydrated at 1073 K Knozinger's model	Ia 3770 Ib 3790 IIa 3730 IIb 3745 III 3700	Δ	–0.25	53	
		□	–0.50		
		Δ O □	0.25		
		□ O □	0.00		
		□ O □	0.50		
Al ₂ O ₃ dehydrated at 773 K Busca's model	3800 3775 3745 3730 3710 3690 3590	Al ^{IV} □–O–Al ^{IV} Al ^{IV} □–O–Al ^{IV}	– – – –	27	
		Bridged	–		
		Bridged	–		
		'Tri-bridged'	–		
Al ₂ O ₃ dehydrated at 873 K Tsyganenko- Mardilovich model	3800–3750/2800–2765 3750–3700/2765–2730 3700–3635/2730–2650	OH ^{VI}		–0.50	299
		OH ^V	Type I	–0.40	
		OH ^{IV}		–0.25	
		OH ^{III}		0.0	
		OH ^{VI,VI}	Type II	0.0	
		OH ^{VI,V}		0.10	
		OH ^{V,V}		0.20	
		OH ^{VI,IV}		0.25	
		OH ^{V,IV}		0.35	
		OH ^{IV,IV}		0.50	
		OH ^{VI,III}		0.50	
		OH ^{V,III}		0.60	
		OH ^{VI,VI,VI} ; OH ^{VI,VI,VI} ; OH ^{VI,V,V} ; OH ^{VI,VI,IV} ;		0.5; 0.6 0.7; 0.75	
		OH ^{VI,V,IV} ; OH ^{V,V,IV} ;	Type III	0.85; 0.95	
		OH ^{VI,VI,III} ; OH ^{VI,V,III}		1.0; 1.1	

^aO, O²⁻; •, OH; Δ, tetrahedrally coordinated Al; □ octahedrally coordinated Al.

^b q , net charge, according to [53]

Table 2.4. Positions of absorption bands of isolated OH groups for different oxides, plus the acidic properties of some of these systems.

Oxide	OH (cm ⁻¹)	OD (cm ⁻¹)	PA ^a (kJ mol ⁻¹)	Reference
TiO ₂ (anatase)	3725	–	1340	188
	3670	–	1380	–
	3728–3715	–	–	302, 304
	3715, 3676–3670, 3640	–	–	309, 310
TiO ₂ (rutile)	3735	–	1375	301
	3685, 3655, 3410	–	–	302
	3700, 3670, 3420	–	–	306
	3680, 3650, 3410	–	–	307
ZnO	3675	–	–	308
	3622	–	1600	308
	3680–3660	–	–	308
	3630–3610	–	–	310
NiO	3735, 3680, 3630	–	–	310
CoO	3680	–	–	310
MgO	3750–3730, 3630–3610	–	–	313, 319
	3740	–	1560	–
Cr ₂ O ₃	3720	2720, 2670	–	179
Ga ₂ O ₃	3670	–	–	301
Fe ₂ O ₃ – dehydrated at 723 K	–	2705, 2690, 2660	–	30●, 207
Fe ₂ O ₃ – haematite	3720, 3700	2745, 2730	1495	200, 315, 316
ZrO ₂	3770, 3670	–	1600	310, 311
Er ₂ O ₃ – dehydrated at 1073 K	3675	2705	–	318
ZnCr ₂ O ₄ – dehydrated at 723 K	3700, 3665	–	–	–
	3675	2705	–	193
	3655	2690	–	–
	3625	2670	–	–
ZnO·ZnCr ₂ O ₄ – dehydrated at 723 K	3520	2595	–	–
	3770	2730	–	193
	3700	2715	–	–
Fe ₂ O ₃ /Cr ₂ O ₃	3680	2670	–	–
	–	2705	–	192
CuCr ₂ O ₄	–	2650	–	–
	–	2755, 2690	–	190
		2565	–	–

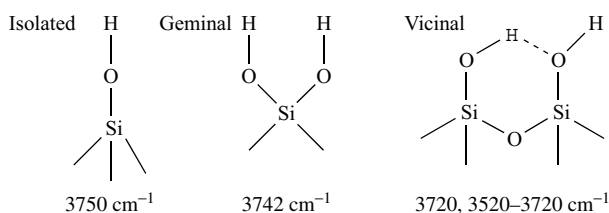
^aPA, proton affinity; values taken from Paukshtis [298].

elements is not a smooth function of these atoms' electronegativities or their positions in the Periodic Table. For elements in the Second Period, the maximum occurs for aluminum, while for types II and III hydroxyls, the maximum values shift towards the less acidic metals. The value of ν_{OH} increases in going from type III to type I hydroxyls. We will now examine a number of results as examples of this behavior.

SiO₂

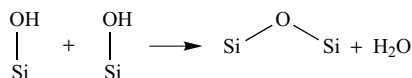
The bulk structure of silica is built up from SiO₄ tetrahedra covalently bound to each other through oxygen atoms [226]. Silicas can be classified into *pyrogenic silicas* (aerosols and cabosils) and *silica gels*. Pyrogenic silicas are usually nonporous (S_{sp} is about 200–400 m² g⁻¹), whereas the best known examples of silica gels – xerogel and aerogels obtained by polymerization of silicic acid – have a surface area above 500 m² g⁻¹ and pore diameters of about 2–10 nm.

The fully hydroxylated surface of a silica gel consists of a layer of silanol groups (SiOH) and physically adsorbed water. Most of the water is removed upon drying in air at 400–500 K. In the spectra of silica-containing systems several absorption bands are observed in the region 3800–3400 cm⁻¹. Silanol groups are left on the surface and exist in three different configurations:

**Scheme 2.5**

Isolated and vicinal groups may be hydrogen bonded to each other. The combination ($\nu\text{OH} + \delta\text{OH}$) band due to surface silanol lies at about 4550 cm⁻¹ and allows distinction between OH species and molecular water. The combination band ($\nu_2 + \nu_3$) for the latter has been observed between 5100 and 5300 cm⁻¹ (depending on the degree of hydration). The first overtone (ν_{02}) of the νOH mode at 3750 cm⁻¹ (ν_{01}) was found at 7285 cm⁻¹.

Silanol groups are progressively lost with increasing temperature with the formation of new surface siloxane groups:

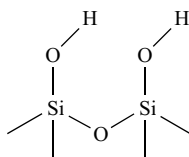
**Scheme 2.6**

These newly formed siloxane bond are very reactive since dehydration leaves the surface in a strained condition. At temperatures greater than 973 K, complete removal of the silanol groups is observed, hence resulting in a significant change in surface morphology.

In the case of nonporous SiO₂, for example, the following bands occur: 3747, 3725, 3700 cm⁻¹, with a very broad separate absorption at 3600–3200 cm⁻¹ [321].

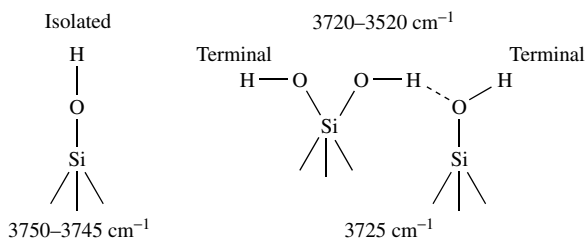
According to Zecchina *et al.* [321], bands in the region 3800–3650 cm⁻¹ correspond to stretching modes of OH groups which are not involved in (i.e. free of) hydrogen bonding. These groups include isolated OH (either external and internal to the lattice) and terminal hydroxyls of hydrogen-bonded sequences (either internal and external), whereas the bands in the 3650–3200 cm⁻¹ region characterize the stretching modes of hydrogen-bonded OH groups (internal and external). Based on a computer graphic simulation and high-resolution microscopy results indicating that the exposed faces are regular and flat, the below interpretation has been suggested.

Preferred exposures of the (010), (100), (001) and (101) faces on the nonporous SiO₂ cause the presence of the following types of SiOH groups [321, 330]:



Scheme 2.7

On the (100) faces, the silanols are isolated, with an OH density of 3.1 OH nm^{-2} and a minimum OH–OH distance of 0.36 nm, while on the 001 faces the hydroxyl density is about 5 OH nm^{-2} and the minimum OH–OH distance is 0.25 nm. On the (101) faces, the situation is similar to that found on the [001] faces: the OH density is 3.8 OH nm^{-2} , and the minimum OH–OH distance is 0.25 nm. In all these cases silanols are isolated. On the (001) face, the structures:



Scheme 2.8

are simultaneously present. The minimal OH...OH distances are 0.25 nm (second structure), i.e. sufficiently low to ensure hydrogen bonding.

The bending vibrations are also used to characterize the surface hydroxyls. Thus, the IR spectra of free silanol groups (3745 cm^{-1}) show combination bands with the in-plane δOH and out-of-plane (or rotational) γOH vibrations. In the spectra taken at low temperature the OH band is split into two maxima at 840 and 765 cm^{-1} because of interactions with different $\nu\text{Si–O}$ stretching vibrations on different sites. Such a large difference between the frequencies of the two bending modes is typical of the type I hydroxyls [322].

Comprehensive studies by means of various physical and chemical methods showed that the pyrogenic silica surface is built up of regions with the structure of the (111) face and, to a lesser extent, the (100) face, of χ -cristobalite with silanol and silane diol end-groups, separated by a distance of 0.7 nm [323, 324]. The bulk phase of such SiO_2 samples consists of approximately equal amounts of the quartz and cristobalite structures.

Results of the dehydration, dehydroxylation and rehydroxylation for amorphous silica surfaces have been examined by Zhuravlev *et al.* in a series of studies and reviewed in reference [325]. The data concerning surface hydroxyls of silica and siliceous materials can be found in references [18–20, 34a, 54, 321–327].

The number of silanol groups on silica gel has been estimated by using a variety of techniques. The concentration of silanol groups on silica gel treated at 1073 K was measured as ca. $3 \mu\text{mol m}^{-2}$ [79].

A model of the surface based on the examination of the crystal chemical structure of SiO_2 has been proposed by Chukin and Apretova [328]. The IR spectra of dispersed silicas during the processes of desorption and adsorption of water and other molecules have been investigated. The interpretation of the absorption bands of dispersed silicas is based on a crystal chemical model of dispersed SiO_2 . In this, primary globules of SiO_2 are spherical particles covered by SiO_2 chains

of different lengths (peripheral structures). The spatial macrostructure of SiO_2 is produced by the interaction between the peripheral structures of adjacent Si-O nuclei (see Figure 2.18).

In recent years, some progress in the understanding of surface processes has been achieved by computer experiments which have revealed some characteristics of the systems investigated which were not available from direct experimental measurements. For example, in the case of SiO_2 computation of the atoms on isolated silica surface OH groups revealed that the splitting of the bending vibration is characteristic of two coupled oscillators of geminal silanol groups [329].

All of the above models have analyzed the properties of OH groups characterized by the band at 3750 cm^{-1} and assigned this band to the OH^- ion, by comparison with the spectroscopic criteria for other OH-containing species such as acidic OH groups, OH^- ions, HOH molecules and H_3O^+ . In order to establish the structural chemistry features of the silica gel structure, spectra in the region of the skeleton Si-O vibrations have been investigated. A comparison of the silica gel spectrum with those of silicates which display such skeleton vibrations has shown that it is similar to the spectra of quartz and cristobalite, except that the band at ca. 1200 cm^{-1} in the spectrum of silica gel is characteristic of silicates with 'belt structures' (ksonotolite). On this basis, it was suggested that the silica gel structure consists of at least two irregularly interchanging regions: (i) crystallites which are close to the structure of cristobalite (three-dimensional polymeric skeleton), and (ii) a range between disordered crystals with silicon-oxygen two-dimensional layers and belts of the ksonotolite type. According to Chukin and Apretova [328], two types of hydroxyls, namely basic

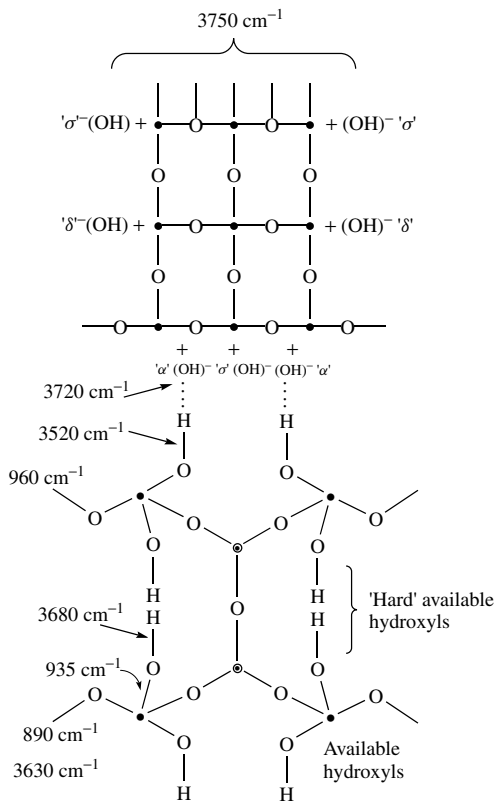
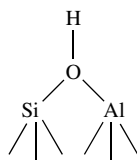


Figure 2.18. Model of the structure of dispersed silica according to Chukin and Apretova: O, oxygen atom; ●, silicon atom [328].

and acidic, correspond to these two types of structures; the OH^- ion (at 3750 cm^{-1}) can be assigned to the skeleton structure, and the weakly acidic OH group (at ca. 3630 cm^{-1}) to the belt structure. Because the 3720 and 3520 cm^{-1} bands have been interpreted as vibrations of the OH^- ion and a weakly acidic Si–O–H group, respectively perturbed by the mutual hydrogen bond, it has been suggested that the two components of the silica gel structure are interrelated. One of the possible variants of a two-component structure of amorphous silica, together with the possible interpretations of the absorption bands, is depicted in Figure 2.18. A molecular dynamics computer simulation was carried out to investigate the spectral features of the geminal hydroxyl groups on a silica surface. The density of proton vibrational states and the IR stretching vibrations were calculated [322]. Four intense peaks at 196 , 600 , 800 and 3736 cm^{-1} in the spectra obtained are ascribed to the ‘out-of-plane-like’ modes (196 cm^{-1}), the in-plane bending modes (600 and 800 cm^{-1}) and the stretching vibration (3736 cm^{-1}) of the general pair of OH groups. The in-plane spectral bending vibrations reveal a strong temperature dependence, unlike the bands of other vibrations.

Zeolites

These are a class of tectosilicates built from corner-sharing SiO_4^{4-} and AlO_4^{5-} tetrahedra, and can be described by the general formula $\text{M}^{n+}_{x/n}[(\text{AlO}_2)_x(\text{SiO}_2)_y]^{x-z}\text{H}_2\text{O}$ [73]. The number of constituent aluminum atoms determine the net negative charge on the framework as compensated by exchangeable M^{n+} , usually Na^+ , NH_4^+ , or H^+ from bridged OH group:



Scheme 2.9

The Si/Al ratio in many zeolites can be changed from 1 (zeolite X) through 1.6–3.0 (zeolite Y), and beyond 500 (high-silica zeolites) (Table 2.5).

In the case of zeolites, usually three types of OH groups can be identified by IR spectroscopy [22, 330–352]. Typical values of the OH stretching frequencies of the Brønsted acidic protons vary

Table 2.5. Positions of absorption bands of bridged OH groups in IR spectra of zeolites of different structure and their acidic properties.

Zeolite	$\text{SiO}_2/\text{Al}_2\text{O}_3$ ratio	Size of the oxygen ring ^a		
		12	8–10	6
HA	2	3672	–	–
HX	2.46	3660 (1250–1260) ^b	–	3570 (1250–1260) ^b
HY	4.8	3645 (1230–1240) ^b	–	3550 (~1200) ^b
H-shabazite	4.7	–	3630	–
H-erionite	6.1	–	3610	–
H-ferrierite	12	–	3612 (~1200) ^b	–
H-mordenite	14.7	–	3610	–
H-ZSM	>30	–	3610 (1180) ^b	–

^aNumber of oxygen atoms on which the OH group is localized.

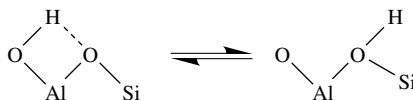
^bProton affinity (PA) values (kJ mol^{-1}) taken from Paukshtis [298].

between 3650 and 3550 cm^{-1} , and may be compared with the silanol frequency at 3745 cm^{-1} . The relatively small decrease in the stretching frequency corresponds to a slightly weakened OH force constant of the acidic protons. The in-plane bending modes of the Brønsted acidic protons have a frequency at about 1050 cm^{-1} [337], while the out-of-plane bending mode lies at about 400 cm^{-1} [338]. Indirect measurements of the bending modes are available from infrared combination bands [339] and direct measurements have also been made using inelastic neutron scattering spectroscopy [340].

Different types of OH groups with various properties can be observed if the Si/Al ratio in a crystalline zeolite is changed (see Table 2.5) [330, 341–345] or, if amorphous aluminosilicates are used [346, 347], or if different cations are added (see, for example, references [22, 346, 348]). Cation exchange can result in changes in the original OH groups of the zeolite but also be accompanied by the appearance of new hydroxyl absorptions ('exchanged cation-OHs').

For HZSM zeolites, the following bands can be resolved: (i) a weak peak at 3780–3775 cm^{-1} , which is usually connected with the presence of Al_2O_3 microparticles [334]; (ii) a band at 3750–3745 cm^{-1} , and a shoulder at 3725 cm^{-1} , which are similar to those observed for silica and correspond to isolated and terminal hydroxyls respectively [321, 330, 348–352]; (iii) a maximum at 3670–3665 cm^{-1} , which is usually assigned to hydroxyls attached to 'extraframework aluminum'; (iv) a band at 3625–3610 cm^{-1} , which is the well-known stretching mode of the acidic bridged hydroxyls $[\text{Al}(\text{OH})\text{Si}]$; (v) a broad band at ca. 3250 cm^{-1} , accompanied by a second broad one at 2550 cm^{-1} , which are typical of the protonated form of ZSM-5 [353, 354].

Zholobenko *et al.* [334], using the method of infrared diffuse scattering spectroscopy, revealed a band at 3300 cm^{-1} for the H-bonded OH groups, for the interpretation of which they proposed the following:



Scheme 2.10

However, Paukshtis [298] has shown that if the temperature increases, the intensities of both the 3300 and the 3610 cm^{-1} bands decrease. The last fact does not correspond to the Borovkov–Kazansky model. One of the possible ways of assigning the band at 3300 cm^{-1} could be to the OH groups bonding the separate microcrystals in large zeolite crystals. Zecchina *et al.* [330], however, believe that the band at 3300 cm^{-1} (with a shoulder at 2550 cm^{-1}), in accordance with Ugterhoeven *et al.* [345], belongs to H_3O^+ .

It should be noted that the appearance of the stretching vibration frequencies of hydroxyl groups in the spectral region at about 3200 cm^{-1} has also been observed in numerous oxide systems. For example, such vibrations have been observed in the diffuse reflectance IR spectra of rare-earth-metal oxides [318] and also in the spectra of numerous transition-metal oxides [355]. When the evacuation temperature increases, the intensity of this band, as well as that of the isolated hydroxyl groups, gradually decreases. This is why Ivlieva *et al.* [318] believe that the 'continuous' absorption namely belongs to surface structures with strong symmetrical hydrogen bonds, which are formed due to interactions between closely placed hydroxyl groups, as well as being due to the solvation of OH groups by adsorbed water molecules. Such absorption is typical for aqueous solutions of bases and has been attributed to asymmetric stretching vibrations of a proton in negatively charged fragments $[\text{O} \cdots \text{H} \cdots \text{O}]^-$ [356].

Not all hydroxyl groups, as observed in absorption spectra from highly dispersed solid oxides, are always located on the surface. For transition aluminas with a spinel structure, protons can

penetrate cation vacancies [357] to form structural OH groups which are not exchanged with deuterated water or ammonia at room temperature, or interact with adsorbed molecules, and have broad absorption bands at about $3500\text{--}3200\text{ cm}^{-1}$. Such protons trapped in bulk vacancies play a great role in the formation of the oxide structure and account for different properties of the aluminas. A stabilization of a zeolite crystal structure is due to the presence of both cationic acidic (3650 cm^{-1}) and anionic weakly basic (3750 cm^{-1}) hydroxyls. A study of the nature and properties of such centers in different zeolites has been carried out by Chukin *et al.* [349–352].

Al_2O_3

As is well known, the transition aluminas (γ - and η - Al_2O_3) have a spinel-type structure, whereas α - Al_2O_3 crystallizes in a corundum form. The conceptions which describe the surface properties of different aluminas are quite interesting. Peri [297] in 1965 first proposed a model of the surface of alumina which was founded on the hypothesis that the planes exposed preferentially are those of index (100), thus explaining the absorption bands observed in the Al_2O_3 spectra of five types of surface hydroxyl groups (see Table 2.3). Although this model does not adequately describe all of the surface properties, it is still of considerable interest. In 1978, Knozinger and Ratnasamy [53] proposed a very detailed OH model as an extension of the Peri model [297]. The basic assumption of this model is that a mixture of low-index crystal planes ((111), (110) and (100)) are exposed on the surface of the crystallites. The relative abundance of different faces is assumed to vary for different aluminas. Five types of OH groups were considered, corresponding to the coordination of the hydroxyl groups, either to tetrahedral or octahedral aluminum anions, a combination of each, or to both (Figure 2.19). Five absorption bands in the region $3800\text{--}3700\text{ cm}^{-1}$ have been assigned to these different types of OH groups. The very important concept to arise from this analysis is that surface OH groups has differing net charges as a function of their environments. For example, a type-III OH with a net positive charge of $+0.5$ is expected to be the most acidic one. According to this model, it is possible to foresee an increase in the acidity of the Al^{3+} sites, and in the basicity of the O^{2-} sites, with the temperature of activation of the alumina since the lability of the OH groups is a function of the basicity of the oxide (see Table 2.4).

Quantum chemical calculations are needed in order to analyze the nature of the anion hydroxyl groups. In the literature, there are different viewpoints concerning assignment of the highest frequency band at 3800 cm^{-1} . According to Morterra and Magnassa [27], this band belongs to an OH group bound to tetrahedral aluminum, whereas Knozinger and Ratnasamy [53] have attributed it to the most basic OH group bound to an octahedral aluminum atom. Calculations of both the charge on the hydrogen atom [358] and the νOH of hydroxyl groups bound with different numbers of aluminum atoms in different coordinations, as well as those for SiO_2 and zeolites, showed that the highest-frequency absorption band in the spectrum of aluminum oxides is due to the OH groups bound to four-coordinated aluminum. These results confirm the conclusion made by Knozinger and Ratnasamy [53] that the OH groups bound to octahedral aluminum have less acidity.

Qualitative quantum chemical models of the dependence of the acidity and frequency characteristics of surface OH groups on both the number and electronegativity of the metal atom connected with them has been examined by Pelmeshnikov *et al.* [359]. This model has been used to explain the lack of a smooth correlation between the νOH of mono-coordinated OH groups and the electronegativity of the metal atoms in numerous oxides. The dependence of νOH on the electronegativity of the metal atom (X_M) is found to be represented by a curve with a maximum reached when $q = 0$ in the point of change in the polarity of the OH bond.

According to the data of Baumgarten *et al.* [360] and Mardilovich and co-workers [299, 361], νOH_{\max} corresponds νOH_t in the spectra of Al_2O_3 . Because of the stronger coordination ability of the three-coordinated in comparison with the five-coordinated aluminum atom, $XAl_t > XAl_o$.

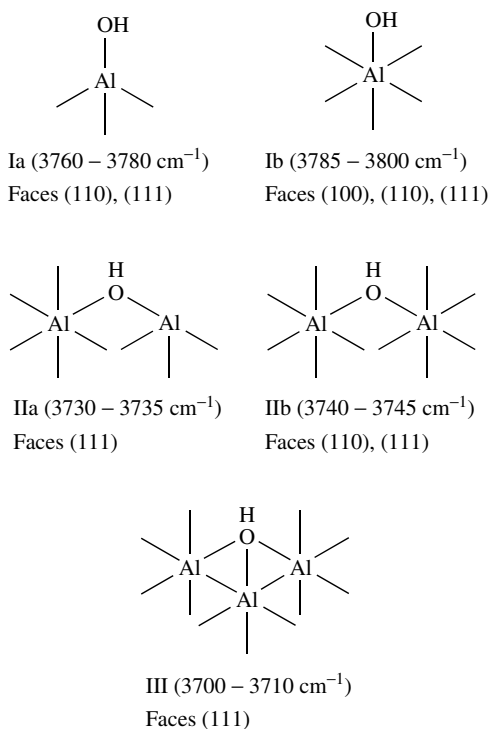


Figure 2.19. Different superficial OH groups on alumina according to the model of Knozinger and Ratnasamy [53]. Reprinted from Knozinger, H. and Ratnasamy, C., *Catal. Rev: Sci. Eng.*, **17**, 31–70 (1978), courtesy of Marcel Dekker, Inc.

On the basis of this, and also the assumption that the change in the number of aluminum atoms in the first coordination sphere of the OH group influences its properties much more significantly than that of the number in the second coordination sphere, the following dependence is derived from this model:

$$\nu\text{OH}_t > \nu\text{OH}_o > \nu\text{OH}_{oo} > \nu\text{OH}_{to} > \nu\text{OH}_{ooo} > \nu\text{OH}_{too}$$

Calculations for cluster models of OH groups on the basis of the MINDO/3 method have confirmed the above conclusion.

It is not possible to describe all of the properties of the active sites, in particular, for the OH groups, because of the use of various approximations in the supposed models. Certain simplifications of these models have been used. Thus, for alumina oxides, Busca *et al.* [362, 363] and Della Gatta *et al.* [364] have proposed models using the same general criteria, based on the presence of cation vacancies (Figure 2.20).

The investigation of transition aluminas [299, 354, 361, 365–367] showed that the IR spectra of Al_2O_3 are also more complex and contain at least nine quite clearly resolved absorption bands of hydroxyls which are not hydrogen-bonded. The question of the assignment of the bands to free or H-bound OH groups of alumina has been analyzed in detail by Chukin and co-workers [368, 369]. Trokhimets *et al.* [365–367] interpreted the observed bands on the assumption that the vibration frequency of the OH groups depends on the coordination number of both aluminum and oxygen. It was suggested that the aluminum coordination number on Al_2O_3 surfaces can be equal to five,

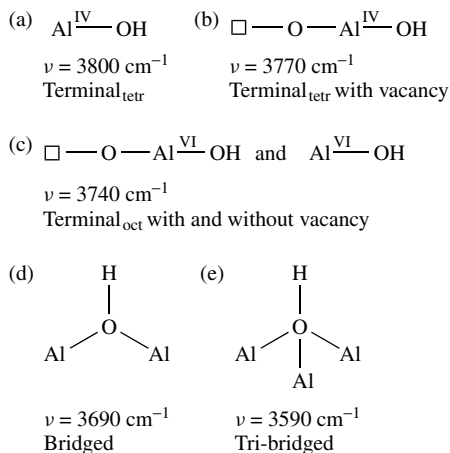


Figure 2.20. Possible OH structures, and corresponding νOH frequencies, at the surface of defect-containing spinel transition aluminas. (Symbols: \square , cation vacancy; ν , average value of νOH frequency).

as well as four and six. The different types of hydroxyl group absorptions, their effective charges and suggested assignments are listed in Table 2.3 above. As follows from this table, the values of the effective charges on OHs in groups I, II, and III form three almost nonoverlapping regions [299]. Detailed data on such spectral manifestations of hydroxyl groups on aluminas are reported elsewhere [27, 53, 299]. Chukin and co-workers [368, 369] have presented a model of the surface of $\gamma\text{-Al}_2\text{O}_3$, which easily explains both hydration and dehydration of the Al_2O_3 surface, as well as the reversibility of dehydroxylation and rehydroxylation. On the basis of an examination of the decomposition mechanisms on boemite–corundum faces, a model for the primary crystal lattice was developed, based on IR spectroscopic data and crystal structure analysis of the oxides and hydroxides of aluminum. A joining of dehydroxylated boemite ‘packets’ during heat treatment is assumed to be accompanied by the formation of Al–O–Al bonds and migration of a portion of the Al^{3+} cations into the freshly formed octahedral cationic vacancies. Three types of Lewis acid sites (LASs) and six types of OH groups have been identified on the fully hydroxylated $\gamma\text{-Al}_2\text{O}_3$. According to Chukin and Seleznev [369], the partially dehydroxylated surface of $\gamma\text{-Al}_2\text{O}_3$ consists of seven types of electron-accepting centers, three types of extra lattice Al^{3+} cations, two types of $\text{Al}_{\text{cus}}^{3+}$, and two types of electron-deficient O atoms.

The values of proton affinity (PA) for different surface hydroxyls of Al_2O_3 , calculated from the shifts of the OH frequencies due to formation of H-bonds with bases and represented in [298], can be used to compare the chemical properties of this oxide surface hydroxyls:

$\nu\text{OH} (\text{cm}^{-1})$	PA (kJ mol^{-1})
3790–3805	1440
3780–3785	1550–1590
3750–3765	1550–1590
3725–3745	1440
3710–3715	1410
3685–3695	1380
3670–3673	1380–1440

In order to determine the number of proton-containing sites, two approaches have been used. One of these is based on measurements of the number of OH groups directly from the intensities

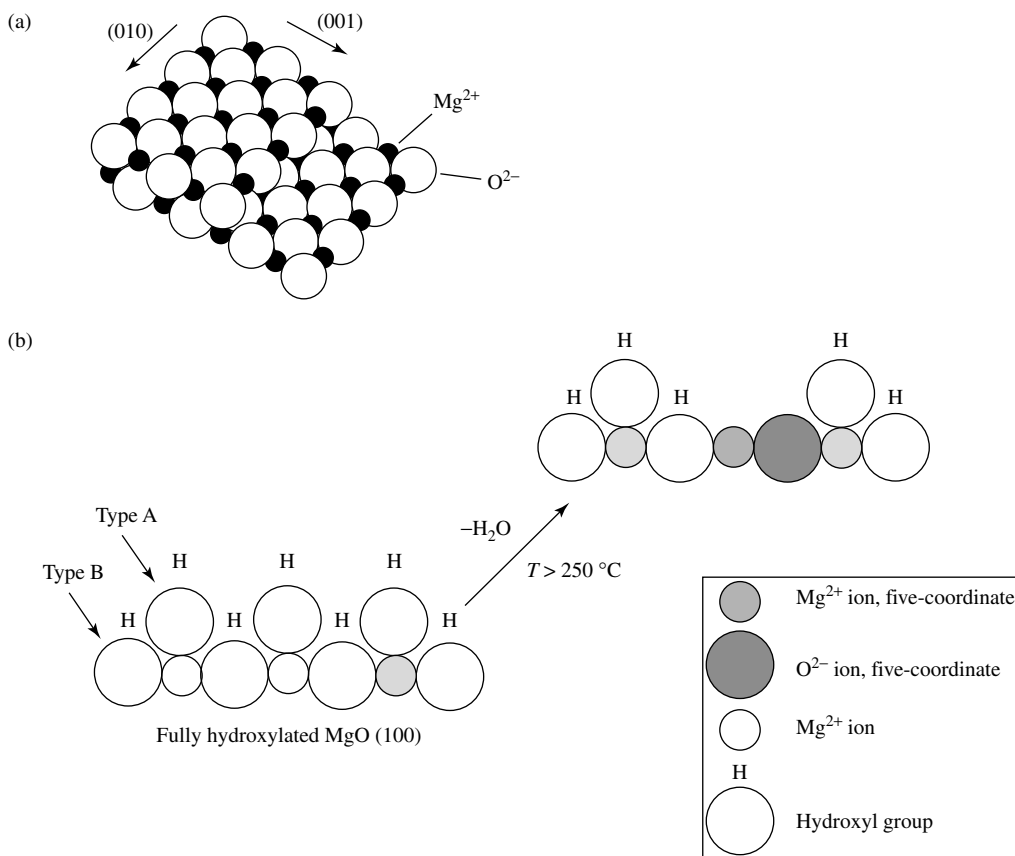


Figure 2.21. (a) Model of the MgO (100) plane, showing a unit atomic step in the [001] direction, and (b) a simplified representation of the dehydroxylation of MgO.

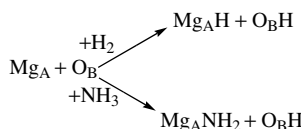
of the νOH bands; the second involves measurement of the number of protonated bases generated. If OH groups are not isolated, the concentration of protic centers is determined by the intensity of the bands in spectra of protonated probes (ammonia, pyridine, etc.), as, for example, has been done in the case of supported heteropoly acids (HPAs), sulfates, etc. Absorption coefficient (A_0) values for the OH groups of zeolites and in silica gels can be found in Paukshtis [298].

MgO

A more simple picture is observed for MgO, which has a rock salt structure with only one (100) face predominantly exposed on the surface (Figure 2.21a). A schematic cross-section of the surface of MgO is shown in Figure 2.21(b), where the process of dehydroxylation is illustrated. The opposite process – hydroxylation – is the reaction with water to give surface OH groups and protonated surface O^{2-} ions. In this simplified picture of the surface, there are two kinds of OH groups (at 3650 and 3740 cm^{-1} , corresponding to type V and type I, respectively, according to the classification of Tsyganenko and Filimonov [310]). One provides the sixth coordinating group to a coordinatively saturated Mg^{2+} ion, while the other results from protonation of an O^{2-} ion which terminates the bulk. The O^{2-} ions and OH groups on the surface of MgO are basic.

The desorption spectra discussed in Boehm and Knozinger [54] show a strong 3700 cm^{-1} band with two high-wavenumber shoulders at 3714 and 3738 cm^{-1} , and upon degassing at higher temperatures, both the 3714 and 3700 cm^{-1} peaks disappear. At 723 K , the highest-wavenumber peak is asymmetric, and at about 3750 cm^{-1} , and there is a very weak band near 3620 cm^{-1} . In Coluccia *et al.* [312], it was shown that the 3700 cm^{-1} band could be attributed to $\text{Mg}(\text{OH})_2$.

Anderson *et al.* [313] attributed the band at 3740 cm^{-1} to the A-layer OH groups and a broad band from 3650 to 3550 cm^{-1} to the B-layer OH groups which are highly perturbed (see Figure 2.21(b)). This model has been criticized by Coluccia *et al.* [312] who argued that the B-layer hydroxyls are eliminated preferentially before the A-layer hydroxyls. This seems improbable if the B-layer oxygen has five nearest neighbors while the A-layer oxygen has only one neighbor. They also showed that because both H_2 and NH_3 dissociate in the following way:



Scheme 2.11

only the B-type hydroxyls should be formed, whereas both O_BH and O_AH are formed in reality.

Coluccia *et al.* [312] developed a new model for the hydroxylated surface and showed that the hydroxyls on extended (100) faces should absorb at lower frequencies (3650 – 3450 cm^{-1}) due to interactions with three-, four-, and five-coordinated sites because of the increasing possibilities of perturbation by neighboring species. The A-layer OH groups extend above the surface, whereas the B-layer OH groups are slightly below the surface. Therefore, the A hydroxyls would be less perturbed by surface neighbors and might well have a frequency near 3700 cm^{-1} , whereas the B-type hydroxyls are more reasonably attributed to a broad absorption band near 3500 cm^{-1} .

Fe_2O_3

The surface hydroxyl groups, observed on Fe_2O_3 by different authors, have shown a variable number of bands and different frequencies, e.g. 3660 and 3486 cm^{-1} [207–209, 355], 3675 , 3630 and 3480 cm^{-1} [317], and 3660 and 3500 cm^{-1} [201]. Morterra *et al.* [370] ascribed this situation to differences in the more favorable terminations of high-surface-area [201, 371] and low-surface-area preparations [370], as well as to the lack of surface reconstruction phenomena at the low temperatures preceding the goethite–haematite phase transformation. Bulk hydroxyls of α - FeOOH broadly adsorb at 3140 – 3160 cm^{-1} .

The existence of surface hydroxyl groups and adsorbed water on haematite (α - Fe_2O_3) is well established [317, 372]. The chemisorption of water on haematite leads to the formation of surface hydroxyl groups. The number of hydroxyl groups per unit surface area have been evaluated and the proportion of hydroxyl groups with acidic or basic character have also been determined.

It has been shown by Rochester and Topham [200] and Busca and Rossi [315] that both the surface structure and morphology of α - Fe_2O_3 strongly depend upon the preparation procedure. Thus, Rochester and Topham [200] observed eleven absorption bands of surface hydroxyls of variable relative intensities in the 3750 – 3350 cm^{-1} spectral region from samples produced from ferrigels. On the other hand, on haematite produced from goethite, Busca and Lorenzelli [316] obtained only three components, none of which coincided with any of the bands reported by Rochester and Topham (see Table 2.4).

Infrared bands at 3700, 3675 and 3430 cm^{-1} are characteristic of haematite which has been heated to high temperatures (see Table 2.4). These OH groups are mainly removed from the surface by heat treatment in oxygen at temperatures up to 823 K. Hydroxyl groups responsible for the infrared band at 3675 cm^{-1} are more resistant than the others two types to removal from the surface by thermal activation. The maxima at 3700 and 3625 cm^{-1} were ascribed to two types of isolated hydroxyl groups, with each probably liganded to a single Fe^{3+} ion and unperturbed by lateral hydrogen-bonding interactions with adjacent hydroxyl groups [200]. The band at 3430 cm^{-1} was attributed to surface hydroxyl groups involved in hydrogen-bonding interactions with adjacent groups.

An attempt to explain the spectra of the free hydroxyl groups on haematite on the basis of its crystallographic structure was made by Rochester and Topham [200]. These authors did not attempt a complete analysis of the available spectroscopic results. However, consideration of the likely exposed crystal planes of haematite substantiates the infrared evidence that several different types of hydroxyl group exist on the oxide surface.

The unit cell of the haematite structure contains two Fe_2O_3 units and is a rhombohedral, the side of which has $a = 0.542 \pm 0.001$ nm, with a rhombohedral angle $\alpha = 55^\circ 17'$. Crystal faces such as {0001}, {0112} and {0118}, and also {1123} and {1121}, are exhibited on the haematite crystal surfaces.

A plan and a section of an {0001} crystal face of haematite are represented in Figure 2.22, on which are shown two layers of hexagonal close-packed oxygen atoms with iron atoms filling two thirds of the octahedral holes. All of the surface oxygen atoms laying above the underlying puckered layer of the iron atoms are equivalent and each is bound to two Fe^{3+} ions in the

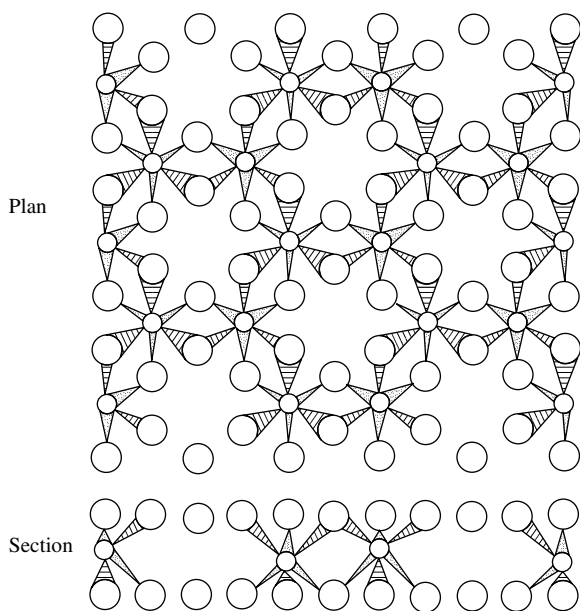


Figure 2.22. Array of iron (small circles) and oxygen (large circles) atoms in the {0001} faces of haematite. The oxygen atoms liganded to Fe^{3+} ions by 'shaded' bonds are above the plane containing the Fe^{3+} ions, whereas the oxygen atoms liganded by 'dotted' bonds are below the plane [200]. From Rochester, C. and Topham, S.A., *J. Chem. Soc., Faraday Trans. 1*, **75**, 1259–1267 (1979). Reproduced by permission of The Royal Society of Chemistry.

underlying layer. Rochester and Topham [200] concluded that only one type of surface hydroxyl groups exists on the {0001} faces of haematite. These groups are sufficiently close together for the formation of hydrogen-bonds between adjacent hydroxyl groups. The existence of these cyclic six-membered structures on such surfaces can be postulated and, in accordance with Rochester and Topham [200], each such cycle has three hydroxyl groups.

Two possible configurations of the ring structures are shown in Figure 2.23. The nomenclature used in this figure is identical to that used for the plane of the {0001} faces depicted in Figure 2.22. In the authors' opinion [200], it is unlikely that three hydrogen atoms in each ring are planar with the three oxygen atoms in the same ring. The cyclic structures either lie directly above the underlying iron atoms in the surface, or above vacant octahedral holes which do not contain iron atoms (see Figure 2.23). The desorption from pairs of surface hydroxyl groups as molecular water is unfavorable in either case because it could lead to considerable steric strain, or to excessive fluctuations in charge density in the surface plane. It was proposed that the hydroxyl groups on the {0001} faces of haematite are each hydrogen-bonded with two of their neighbors and are difficult to remove from the surface by thermal activation. The 3430 cm^{-1} band present in the spectrum of haematite, even after high temperature treatment, supports this view. This band has been assigned by the authors to the OH stretching vibrations of the hydroxyl groups on the (0001) exposed planes of haematite.

A section through the {0112} surface planes of haematite is also depicted in Figure 2.23. Four different types of oxygen atoms (marked as A, B, C and D) are exposed on the {0112} faces.

TiO_2

Three crystal modifications are known for TiO_2 , i.e. anatase, rutile and brookite. The surface properties of the first two of these have been investigated in detail (see, for example, [188, 302–310, 319, 320, 376–378]) and reviewed by Parfitt [306] and Zecchina *et al.* [56]. Differences in their crystal structures lead to different spectral manifestations of the hydroxyl groups (see Table 2.4).

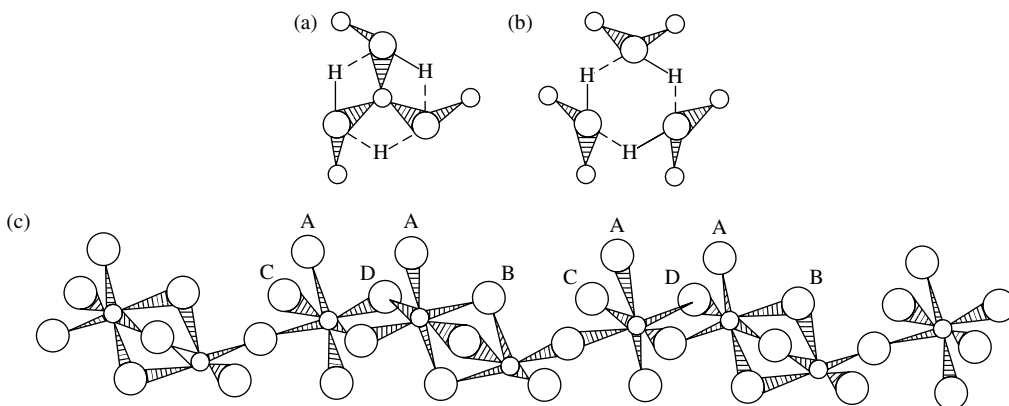


Figure 2.23. (a, b) Possible configurations of cyclic structures, consisting of triads of surface hydroxyl groups and each containing three hydrogen-bonds, on the {0001} exposed faces of haematite (a, b), and (c), section of the {0112} surface planes of haematite [200]. From Rochester, C. and Topham, S.A., *J. Chem. Soc., Faraday Trans. 1*, **75**, 1259–1267 (1979). Reproduced by permission of The Royal Society of Chemistry.

Anatase

Bands near 3715, 3670–3676 and 3640 cm^{-1} are due to surface TiOH species on different faces of anatase at sites with different coordinations [188, 302–304, 376, 378]. The surface layer of the hydrated oxide was found to be made up of hydroxyls (absorptions in the 3800–3300 cm^{-1} region) and of up to some 50 % of undissociated water as monitored by the strong characteristic ‘scissors’ deformation mode(s) of H_2O in the 1600–1650 cm^{-1} range. The latter species are quite strongly held in comparison with its adsorption on other oxides. As dehydration/rehydration patterns show, both the frequencies and the relative intensities of the various surface OH species, as well as the relative abundance of dissociative and undissociated forms of surface hydration, vary greatly with the crystal phase (rutile, anatase, etc.), with the preparative procedure, and with the resulting surface termination. In fact, some crystal faces are believed to carry only undissociated H_2O species, others only OH groups, and some others both types [378]. On the anatase surface, two types of isolated hydroxyl groups are observed [302–304]. Different models of the anatase surface have been proposed on the basis of IR spectra of TiO_2 . Primet *et al.* [302, 303] have considered the (001) face to be the main face exposed on the surface. According to these authors, both types of surface hydroxyls are localized on coordinatively unsaturated titanium cations. The 3715–3728 cm^{-1} band characterizes isolated hydroxyl groups, situated on neighboring titanium cations. Dehydroxylation of the surface leads to its reconstruction, which explains the undissociated water adsorption. The coordinatively unsaturated titanium cations which are formed by this are termed the β -sites, whereas the dehydroxylated titanium cations from unreconstructed centers are named the α -sites. This early model of the anatase surface was based on the point of view that only (001) faces exist on the surface. From studies of numerous titanium oxides of different morphology, it has been established [188] that the hydroxyl groups giving a 3665 cm^{-1} absorption band are bound to $\text{Ti}^{3+}(1-0-0-0)$ ions so as to form a $\text{Ti}^{4+}(1^{\text{OH}}-1-0-0-0)-\text{OH}$ complex, where ‘1^{OH}’ indicates the oxygen ion of the hydroxyl group. The position of another absorption band at 3715 cm^{-1} indicates that the OH bond is stronger and the bond with the surface consequently weaker. These hydroxyl groups are probably bound to $\text{Ti}^{3+}(1-1-0-0)$ sites forming a $\text{Ti}^{4+}(1^{\text{OH}}-1-1-0-0)-\text{OH}$ complex. More details of the TiO_2 surface model proposed by Hadjiivanov and co-workers [188] are presented below.

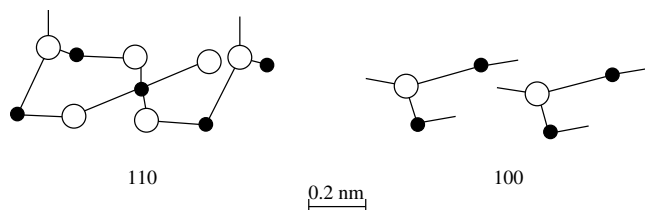
Rutile

Primet *et al.* [302, 303] observed bands at 3685, 3655 and 3410 cm^{-1} for TiOH species in the spectrum of rutile and suggested that the highest-wavenumber band is due to isolated species, whereas the others represent hydrogen-bonded species. On the other hand, Parfitt [306] assigned the bands at 3700, 3670 and 3420 cm^{-1} to a bridged hydroxyl, an isolated hydroxyl and a hydrogen-bonded hydroxyl, respectively. Jones and Hockey [307] attributed the bands at 3650 and 3410 cm^{-1} to TiOH species and the 3680 cm^{-1} band to adsorbed water. These authors developed a model of the rutile surface based on (110), (101) and (100) planes which they expected to be the predominantly exposed faces. Suda and co-workers [305] have shown that a fully hydroxylated rutile contains about eight OH groups per square nanometer (as water and OH) and that this decreases markedly to less than 1 nm^{-2} after evacuation at 523 K.

The most appropriate centers for dissociative adsorption of water molecules are situated on the (110) face for two reasons: (i) the (110) face contains the most acidic four-coordinated Ti^{4+} ions, and (ii) the cationic vacancies on this plane are bridged, i.e. two coordinatively unsaturated O^{2-} ions act together as a Lewis base [304]. This point of view implies a low concentration of the centers for dissociative adsorption, but is not supported by direct experimental evidence.

It is important to establish the reasons for the predominant molecular adsorption of alcohols and water on anatase and for their dissociative adsorption on rutile. The rutile cleavage planes

contain five-coordinated Ti^{4+} and two coordinated O^{2-} ions. The [110] and [100] rutile faces can be represented by the following:



Scheme 2.12

In contrast with the case of anatase, the coordinative vacancies of the Ti^{4+} and O^{2-} ions in rutile are either not parallel to each other or are situated in different layers. The same applies to the other faces of rutile. Thus, a two-center adsorption of water or alcohol is possible on anatase, whereas on rutile dissociation is necessary in order to ensure adsorption to two surface sites simultaneously.

The above model explains well the high heterogeneity of the anatase surface and the relative concentration of the different sites. It is also confirmed by the dependence of the concentration of the different sites on the sample morphology.

ZrO₂

Several infrared studies have been carried out [379–384] to investigate the surface hydroxyl groups of ZrO_2 . The spectra of samples activated at 473 to 723 K exhibit two sharp bands at 3775 and 3650 cm^{-1} . Structural attributions for these hydroxyls are not yet known, but the 3775 cm^{-1} band has been assigned to an OH group bound to a single Zr atom, whereas the other has been assigned to multiple Zr ions [384] (see Table 2.4).

Rare-earth metal oxides

Similar types of spectra have been observed for the surfaces of the rare-earth metal oxides Er_2O_3 , Y_2O_3 and Ho_2O_3 [318]. The stable crystalline modification for Y, Er and Ho oxides is a body-centered cubic lattice with six-coordinate metal cations surrounded by tetrahedrally coordinated oxygen anions, the so-called ‘C-form’. This form of the oxides is close in structure to the fluorite crystal lattice and is obtained from it by the removal of a quarter of the anions. In natural crystals of such compounds, as well as in crystals obtained by (chemical) crystallization, the preferred crystal face is (111). Compounds of this type also often form cubic crystals for which the surface face is (100). Crystals with exposed (110) faces are encountered less rarely. Figure 2.24 shows schematic representations of the (100), (110) and (111) faces, and the positions of the different types of OH groups on the hydrated (111), (100) and (110) planes.

The recording of the observed νOH bands can be accounted for on the assumption that the surfaces of polycrystalline oxides are represented by (100), (001) and (111) faces [318].

ZnO

Atherton *et al.* [308] have shown that there are infrared bands at 3670, 3640, 3620, 2550 and 3440 cm^{-1} in the spectrum of a ZnO sample calcinated at 673 K in an oxygen atmosphere. Analogous spectra have been observed by other workers [373, 374, 385, 386]. These OH bands

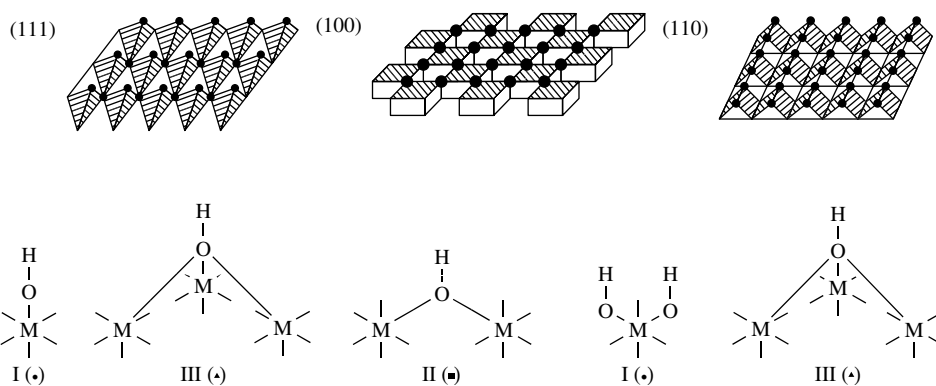


Figure 2.24. Schematic representations of various OH types on the (111), (100) and (110) cleavage surfaces of Y, Er, and Ho oxide single crystals, where the metal cations are arranged in planes of a section parallel to the anionic surface layers. The elementary cells of the anion lattice with cations in the center are shown as cross-hatched.

are not due to adsorbed water and have been attributed by various authors to free and hydrogen-bonded hydroxyl groups on different crystal faces (see Table 2.4).

The OH groups on the discussing oxides have been characterized in terms of the stretching vibrations of hydroxyl groups. The bending OH vibrations are much less easy to characterize experimentally, although information can be obtained from combination bands with the stretching mode. However, in the case of ZnO dissociative adsorption of hydrogen [387] gives bands at 840 and 810 cm^{-1} that are attributable to two bending modes of one and the same type-III OH groups, with the symmetry of the site slightly lowered because of a nonequivalence of the three adjacent Zn atoms on the (1010) crystal face.

Spinel

Investigations of Zn–Cr–O systems with various concentrations of ZnO show that the spectral manifestations of surface hydroxyls depend on the crystal structure of the system. For example, these are bands at 3520, 3625, 3655 and 3675 cm^{-1} (see Table 2.4), characteristic of the OH groups, in the spectrum of ZnCr_2O_4 [193]. The closeness of these bands to those corresponding to the surface hydroxyl groups of ZnO (νOH at 3450, 3622, 3650 and 3675 cm^{-1}) is significant. This suggests that in ZnCr_2O_4 , a normal spinel with zinc ions in tetrahedral positions (as in ZnO) is present, and the spectrum of the OH groups is contributed mainly by coordination to the zinc ions, and not appreciably by the chromium ions which presumably are in octahedral surroundings.

In ZnO– ZnCr_2O_4 , the spectrum of the OH vibrations is entirely different from that of ZnCr_2O_4 , and includes bands at 3700 and 3660 (shoulder), and 3770 cm^{-1} ; the corresponding OD bands are at 2715 and 2690 (shoulder), and 2730 cm^{-1} (see Table 2.4). This spectrum differs from the spectra for the OH groups on both ZnO and Cr_2O_3 , as well as on ZnCr_2O_4 , thus suggesting the formation of a new compound. This spectral behavior is not surprising, since it is known that compounds of the R-phase type [388], in which the zinc ions can occupy octahedral positions, are formed in these systems.

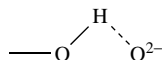
Bands at 3790, 3720 and 3670 cm^{-1} , characteristic of non-hydrogen-bonded hydroxyl groups, are observed in the infrared spectra of the noninverse NiAl_2O_4 spinel [362, 363]. After evacuation at 710 K, a much broader band is also detected at about 3580 cm^{-1} , due to hydrogen-bonded hydroxyl groups. These spectra are very similar to those obtained for $\delta\text{-Al}_2\text{O}_3$ and for other transition aluminas. The corresponding spectra of CoAl_2O_4 are significantly different: after evacuation

at 773 K, there is only one band, centered at 3740 cm^{-1} , with a shoulder at 3725 cm^{-1} ; after weaker evacuation treatment, another band at about 3695 cm^{-1} has been detected. The spectra observed in this case are similar to those for normal spinels such as magnesium and zinc aluminates, when main bands in the $3750\text{--}3680\text{ cm}^{-1}$ region are observed after strong outgassing of the samples.

Molybdenum- and vanadium-containing oxide systems

The IR spectra of oxides with transition-metal cations in the highest oxidation states [30, 212–216, 219–221, 389–397] contain no discrete absorption bands similar to those obtained for $\gamma\text{-Al}_2\text{O}_3$ and aluminosilicate systems in the νOH region (e.g. for $\text{V}_2\text{O}_5/\text{Al}_2\text{O}_3$, see Figure 2.25(a), spectrum 1), in spite of observations that for these systems NH_3 adsorption data revealed the presence of a considerable number of mobile protons ($>10^{17}$ centers m^{-2}) $-\text{NH}_4^+$ ions (spectrum 2) δNH_4^+ band at around 1440 cm^{-1} (see Section 2.2. for details). It is not possible to attribute the absence of discrete absorption bands in the region of νOH vibrations to the low sensitivity of the method, because of the large specific surface area (usually $>100\text{ m}^{-2}\text{g}$) of the investigated systems. Certainly, interaction of the surface with a molecular probe (especially like NH_3) may reveal Brønsted acid sites (BASs) in such systems (e.g. heterolytic dissociation of a probe molecule on the ionic pairs of the $\text{M}^{n+}\text{O}^{2-}$ surface with H^+ cation formation). However, this suggestion is disputed because BASs are also identified by pyridine (Figure 2.25(a), spectrum 7). Diffuse scattering spectroscopic studies of the νOH bands reveal additional effects of surface sites that do not appear in IR-transmission spectra [334, 338, 389, 398]. For instance, absorption in the νOH region appears in the IR diffuse scattering spectrum (e.g. for $\text{V}_2\text{O}_5/\text{Al}_2\text{O}_3$, see Figure 2.25(a), spectra 1,2). It should be emphasized that the observed band is broad and nonuniform because of its origin (the protic site forms hydrogen-bonds) and the possible energetic heterogeneity of these sites.

Such additional effect of surface hydroxyl groups was detected for zeolites by means of diffuse scattering spectroscopy [334, 338, 398], when investigating the broad, low-frequency absorption bands of νOH for zeolites with strong acidic properties, Borovkov *et al.* [398] have assumed single hydrogen-bonding of the OH group with a neighboring oxygen anion:



Scheme 2.13

It has been demonstrated that the same spectral features of surface hydroxyls are also observed for stoichiometric compounds, e.g. the molybdates [219, 220, 389–393], vanadates [216, 389], tungstates [389], antimonates [244–246] or heteropoly compounds, both supported or in the bulk [221, 395–397]. The excess cations of acid-forming oxides in the catalyst–surface zone leads to a sharp increase in the concentrations and the strengths of such sites.

One of the possible reasons for the presence of such broad spectral features of OH groups in oxide systems is that in systems with multiply charged cations, a proton can simultaneously serve as both a mobile cation and a surface anion (a so-called ‘delocalized proton’) [30, 219, 389]. This ‘multi-site’ proton stabilization may considerably broaden the νOH absorption band and shift it towards longer wavelengths. For example, in the $2000\text{ to }4000\text{ cm}^{-1}$ region, discrete, clearly discernible νOH adsorption bands in the IR-transmission spectra of the investigated systems can be observed.

Both the considerable heterogeneity of the surface protic sites and the presence of mobile protons in the surface zone may be responsible for the incomplete disappearance of the observed

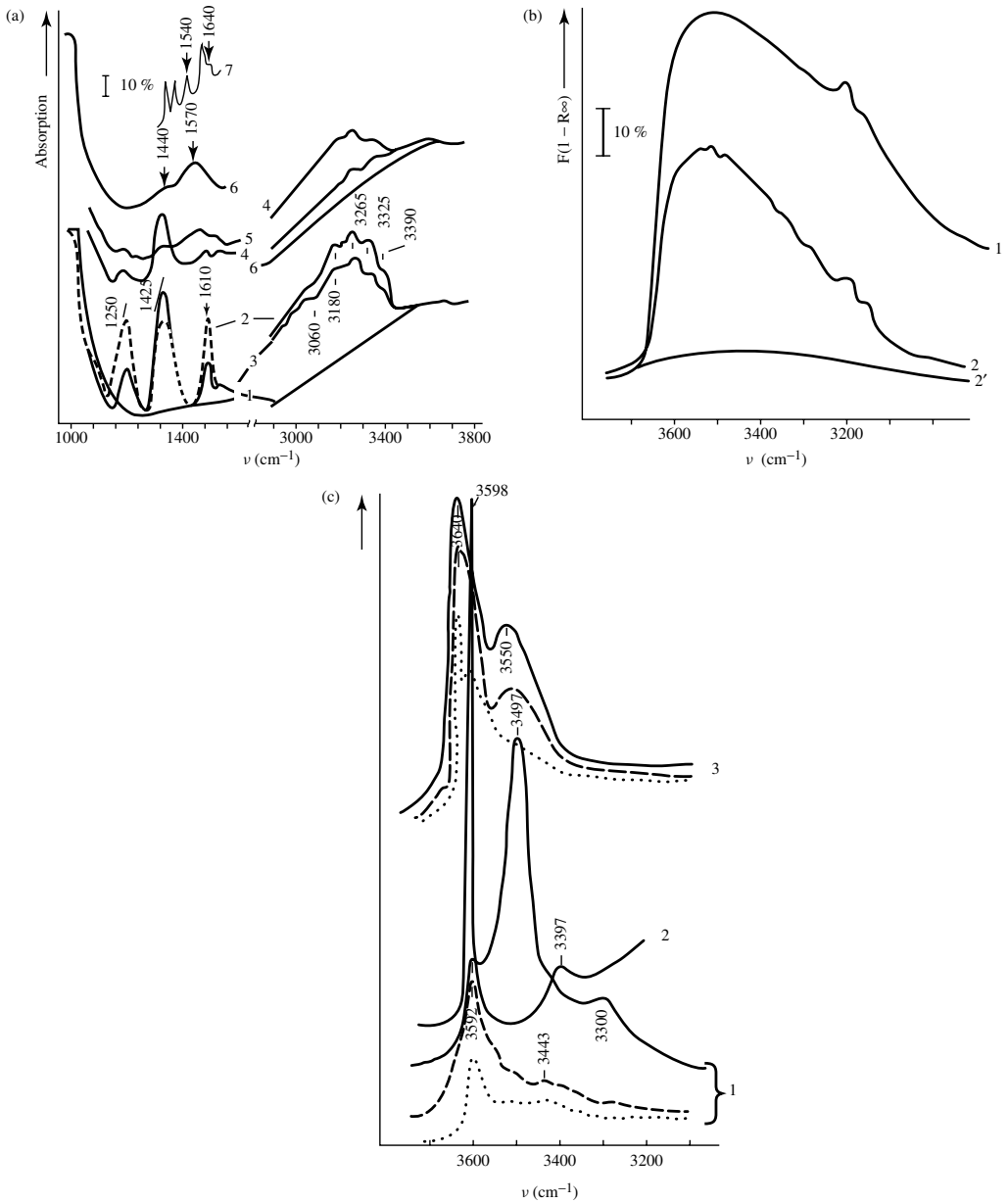


Figure 2.25. (a) IR-transmission spectra of NH_3 and pyridine adsorbed on an oxidized $\text{V}_2\text{O}_5/\text{Al}_2\text{O}_3$ catalyst (10 wt % V_2O_5) after treatment in O_2 at 723 K and following removal of O_2 at 573 K: (1) background; (2) 2 Torr NH_3 at 300 K; (3–6) subsequent desorption at 300, 373, and 573 K; and (7) 4 Torr Pyridine at 300 K and subsequent desorption at 373 K. (b) diffuse scattering IR spectra of $\text{V}_2\text{O}_5/\text{Al}_2\text{O}_3$ (10 wt% V_2O_5) in the OH vibration region: (1) after O_2 treatment of the sample at 723 K; (2) O_2 removal at 573 K; (2') after evacuation at 873 K. (c) Raman spectra of: (1) BaO_2 , (2) Sm_2O_3 , and (3), CeO_2 dehydroxylated at 373 (solid line), 473 (dashed lined), and 573 K (dotted line).

absorption bands upon strong dehydroxylation (Figure 2.25(a), spectra 2). Slow exchange at room temperature, which does not lead to the complete disappearance of protic acid sites, occurs upon attempted isotopic substitution of deuterium for hydrogen in the OH groups using D₂O. The above data also confirm the presence of mobile protons in the surface zone.

As can be seen from the above data, the main advances in the determination of oxide hydroxyl–hydrate coverage were achieved by using IR spectroscopy. For the investigation of oxide hydroxyl–hydrate coverage by using Raman spectroscopy, only the first steps have been carried out. Such studies are predominantly related to hydroxyl–hydrate coverage of SiO₂ [41]. However, Raman spectra in the range of the νOH bands can be easily obtained for numerous other oxides. As an example, changes in the Raman spectra of hydroxyl–hydrate coverage of several oxides upon dehydration (*in situ*) are represented in Figure 2.25(c).

2.3 Determination of the nature of surface sites and their chemical properties using the adsorption of simple molecules

The data discussed above show that investigations of the spectra of oxide catalysts in the region above the fundamental lattice frequencies can yield direct information on the presence of surface hydroxyl groups and the adsorbed states of oxygen. It should be noted, however, that criteria for a comparative investigation during direct examination of the state of oxygen and surface hydroxyl groups in oxides of various nature are still lacking. Despite the difficulties in describing the surfaces of polycrystalline oxides, the first IR studies of adsorption proved that data on the nature of the surface centers, including the cations, and on the chemical properties can be obtained by the analysis of IR spectra of the molecules that come into specific interaction with them. Certain absorption bands of the adsorbates are sensitive to the type of bonding with the surface centers, and can thereby provide information about their natures and concentrations (so-called method of adsorbed probe-molecules).

In connection with the use of probe-molecules for characterization of the surface sites, the theory of ‘soft’ and ‘hard’ acids and bases can be quite profitable to study the nature and properties of surface centers. According to this theory, all Lewis acids and bases are divided on two main classes, i.e. ‘soft’ and ‘hard’. The latter are characterized by a small size, high degree of oxidation and low electron polarizability. The former are larger, have lower degrees of oxidation and are readily polarizable. Highly polarizable molecules are soft bases, whereas at the other extreme very non-polarizable molecules are hard acids. The classification of Lewis acids, according to Basolo and Person [69], is represented in Table 2.6. Carbon monoxide, olefins

Table 2.6. A classification of Lewis acids. Reproduced by permission of the original authors, R. G. Pearson and F. Basolo, from *Mechanisms of Inorganic Reactions. A Study of Metal Complexes in Solution*, 2nd Edn, Wiley, New York, 1967.

Hard	Soft
H ⁺ , Li ⁺ , Na ⁺ , K ⁺ Be ²⁺ , Mg ²⁺ , Ca ²⁺ , Sr ²⁺ , Mn ²⁺	Cu ⁺ , Ag ⁺ , Au ⁺ , Tl ⁺ , Hg ⁺ Pd ²⁺ , Cd ²⁺ , Pt ²⁺ , Hg ²⁺ , CH ₃ Hg ⁺ , Co(CN) ₅ ²⁻ , Pt ⁴⁺ , Te ⁴⁺
Sc ³⁺ , Ga ³⁺ , In ³⁺ , La ³⁺ , Cr ³⁺ , Co ³⁺ , Fe ³⁺ , As ³⁺ , Ge ³⁺ , Si ⁴⁺ , Zr ⁴⁺ , Th ⁴⁺ , Ru ⁴⁺ UO ₂ ²⁺ , (CH ₃) ₂ Sn ²⁺ , VO ²⁺ , MoO ³⁺	M ⁰ (metal atoms) Bulk metals
RCO ⁺ , CO ₂ , NC ⁺	
<i>Boundary</i> Fe ²⁺ , Co ²⁺ , Ni ²⁺ , Cu ²⁺ , Zn ²⁺ , Pb ²⁺ , Sn ²⁺ , Sb ³⁺ , Bi ³⁺ , Rh ³⁺ , Ir ³⁺ , SO ₂ , NO ⁺ , Ru ²⁺ Os ²⁺ R ₃ C ⁺ , C ₆ H ₅ ⁺	

and aryl species were assigned as soft bases, with the nitrogen species as hard ones. According to this classification, soft acids easily form complexes with soft bases (CO, olefins and aryl hydrocarbons), whereas hard acids interact with hard bases such as ammonia and pyridine. It is clear that this classification of hard and soft acids and bases can be useful when it is necessary to choose a probe molecule. We will examine the data concerning spectral manifestations on the adsorption of simple molecules such as CO, NO and NH₃ to establish the possibility of using these molecules to identify the type of centers on oxide surfaces.

The following ideal requirements for probe molecules are: (i) adsorption of the probe should not lead to irreversible changes (reconstruction) of the surface itself, and (ii) the probe molecule has to interact with certain sites specifically, (iii) introduce little further perturbation of the systems during the process, and (iv) have a sufficient sensitivity of the spectral parameter to the changes in electron structure of the adsorbed site, as well as a guaranteed absence of surface modification via side-reaction. These criteria have been formulated still in [30]. More strict criteria for choosing the probe-molecule have been proposed by Knozinger [34a].

2.3.1 ADSORPTION OF AMMONIA AND PYRIDINE

The study of ammonia and pyridine adsorption on oxides by means of infrared spectroscopy is a classical method for identifying both Brønsted and Lewis acid sites. For this, the formation of NH₄⁺ (PyH⁺) ions is a criterion of the presence of Brønsted acid centers, while the presence of coordinated ammonia (pyridine) shows that there are Lewis acid centers on the surface. The spectral features of the coordinated ammonia (pyridine) molecule are significantly different from those of ammonia (pyridinium) ions (Table 2.7 and Figure 2.26). This allows the identification of the formation of such complexes by infrared spectroscopy. The greatest differences are observed in the spectral region of the NH deformation vibration frequencies.

Due to their strong basic properties and proton affinities, both ammonia and pyridine are good probe molecules for establishing the presence of even weak Lewis and Brønsted acid sites on the surface. However, the distinctions that can be made by these two probe molecules are not identical. The first difference between them is their relative sizes, i.e. NH₃ < pyridine. Another difference is their relative basicity. In an aqueous solution, ammonia is a stronger base than pyridine [413]. The p*K*_a value for ammonia is around 9, while that for pyridine is about 5 [414]. However, in the gas phase the basicity of pyridine is significantly greater than that of NH₃ [415]. It could be argued that for metal surfaces [416, 417], gas-phase basicity is a more appropriate measure of the basic strength of the adsorbate, as no solvation effects occur during adsorption. For metal oxides, the situation is more complicated. When the adsorption proceeds via coordination to the metal cation, the gas-phase basicity is probably the appropriate one to apply. However, when hydrogen-bonding or adsorption on a Brønsted acid site takes place, neighboring anions or hydroxyl groups may be involved in the interaction [413]. There are some similarities with the case of a solvated molecule.

Experimental results for the adsorption of ammonia or pyridine on alumina indicate the presence of NH₄⁺ ions but not PyH⁺ ions. Thus, in spite of the stronger gas-phase basicity of pyridine in comparison to that of ammonia, pyridine is not protonated on the surface of Al₂O₃. This fact shows that the p*K*_a value reflects the acid properties of the surface more correctly and indicates that solvation-type effects are significant and that it is difficult to use the approaches of gas-phase reaction chemistry to describe the acid properties of the surface. In the theory of acids and bases, the p*K*_a scale is widely used. Since in the case of heterogeneous catalysis, both reagents and reaction products interact with the surface from the gas phase, the proton affinity (*PA*) scale can also be useful, and Paukshtis and co-workers [298, 418] have tried to use this scale to characterize the strengths of surface sites. Clearly, the p*K*_a values depend significantly on the specificity of the medium in which both acids and bases are ionized. That is why a correlation between the

Table 2.7. Spectral characteristics of the NH₃ molecule^a.

Compound	$\nu_1(s)$ (cm ⁻¹)	$\nu_2(s)$ (cm ⁻¹)	$\nu_3(as)$ (cm ⁻¹)	$\nu_4(as)$ (cm ⁻¹)	Reference
NH ₃ (gas)	3337	950	3414	1628	12,399
NH ₃ (liquid)	–	1032 ^b	3382	1628	400
NH ₃ (CCl ₄)(solution)	3312	–	3414	1615	401
NH ₃ (solid)	3223	1060	3378	1646	402
F ₃ B:NH ₃	3285	–	3340	1596	403
H ₃ B:NH ₃	3285	–	3315	1597	404
(CH ₃) ₃ B:NH ₃	3280	–	3370	1595	405
[Pt(NH ₃) ₆] ⁴⁺	–	1385	–	–	15,406
Cr(NH ₃) ₆ X ₃	3280 ^b	1334	3330 ^b	1622	15
TiF ₄ :2NH ₃	–	1280, 1320	–	1660	407
Cu(NH ₃) ₄ Cl ₂	3270 ^b	1245	–	1596	15
NH ₄ ⁺ (gas)	3040 ^b	1680 ^b	3100–3332	1390–1484	15,360
NH ₄ ⁺	–	–	3030–3300	1390–1430	408
NH ₄ Cl	–	–	3126	1403	409
NH ₄ ClO ₄	–	–	–	1423	15
H ₂ NH...N–	3313	987	3440, 3404	–	411
H ₂ NH...Br	3283	–	3413, 3370	–	412
NH ₃ ...N–, O	3315–3290	1035–990	3440–3380	1630–1615	412
C–H...NH ₃	3309	1036	3408	1625	412
O–H...NH ₃	–	1105–1055	–	–	412
N–H...NH ₃	–	1105–1055	–	–	412

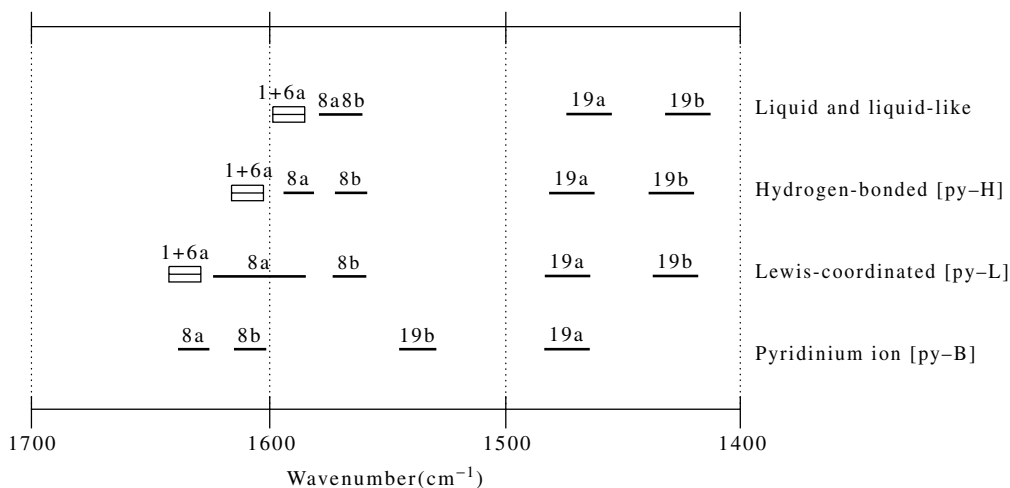
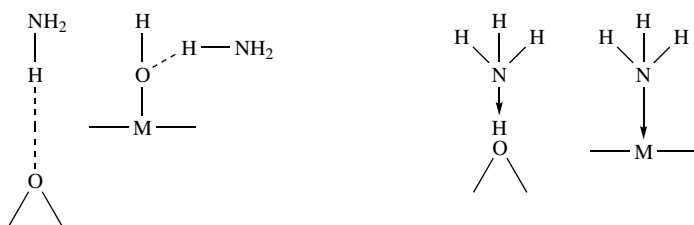
^as, symmetric; as, asymmetric.^bForbidden in IR spectrum.

Figure 2.26. Schematic representation of the spectral ranges of the 8a–8b and 19a–19b modes for some Py-containing systems by Morterra and Magnassa [27]. No reference is made to the intensity ratio of the bands, nor to their breadth; the bars show the ranges of occurrence for the various vibrational modes. The differences between the fundamental and combination modes is also indicated. Reprinted from *Catal. Today*, **25**, Morterra, C. and Magnassa, G., ‘A case study: surface chemistry and surface structure of catalytic aluminas, as studied by vibrational spectroscopy of adsorbed species’, 497–432, Copyright (1996), with permission from Elsevier Science.

values of pK_a and PA have only been established for compounds containing the same number of protons, i.e. the proportionality between pK_a and PA exists only for bases of the same type. In dilute water solutions, it is adequate to use only the values of pK_a in order to establish the degree of base protonation by the acid. Based on the values of PA^{acid} and PA^{base} in the gas phase, it is not possible to predict proton transfer because the minimum value of PA^{acid} is more than 250 kJ mol^{-1} larger than the highest value of PA^{base} . In the gas phase, the formation of noninteracting acid anions and the derived protonated bases is impossible, and the formation of the ion pair would seem to be more probable (see Section 2.4).

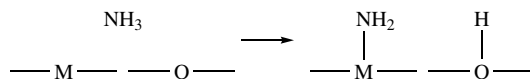
Ammonia

The ammonia molecule can be bound to the oxide surface by either (i) a hydrogen-bond, $\text{NH}\cdots\text{O}^{2-}$, with a surface oxygen atom anion or with the oxygen of a surface hydroxyl group, (ii) a hydrogen-bond between the nitrogen atom and a surface hydroxyl atom, or (iii) a coordination bond with a surface cation (Lewis acid site):



Scheme 2.14

Moreover, complete proton transfer can occur with the formation of an NH_4^+ ion or alternatively ammonia dissociative adsorption with the formation of surface NH_2 and OH groups can also take place:



Scheme 2.15

Each type of surface complex gives information about the types of surface centers through qualitative differences in its spectral manifestations and can also reflect types of qualitative differences in the properties of the same type of center (see Table 2.8).

The spectral manifestations of various species of adsorbed ammonia have been analyzed in detail by Filimonov and co-workers [412], Davydov [30] and Kung and Kung [57]. Analysis of these data shows that certain kinds of vibration frequencies reflect the presence of each of the above-mentioned structures. The mechanism of ammonia adsorption depends significantly on the state of the hydroxyl coverage of the oxide surface. In the case of strongly hydroxylated surfaces, the adsorption predominantly occurs on the surface hydroxyl groups via the formation of hydrogen-bonds between these OH groups and nitrogen atoms (the band $\delta_s\text{NH}_3$ in such a form of adsorption appears in the region $1150\text{--}1100 \text{ cm}^{-1}$). This form of adsorption is thermally unstable and is also destroyed by evacuation at room temperature of the clean oxide (Table 2.8). Increase of the evacuation temperature for the clean oxide leads

Table 2.8. Spectral characteristics of NH₃ molecules adsorbed on different oxides.

Oxide	Frequency (cm ⁻¹)	Structure	Reference
SiO ₂	3400, 3320	OH...NH ₃	18, 19
MgO	3300–3100, 1625, 1024	O...HNH ₂	419
	3330–2250, 1600, 1090–1056	Mg ²⁺ ...NH ₃	
	1515	Mg...NH ₂	
TiO ₂ (anatase)	3360	OH...NH ₃ or H ₂ NH...O	30, 188, 376, 412
Dehydroxylated at 773 K	3395, 3280, 3170, 1605, 1065	Ti ⁴⁺ ← NH ₂ H...O	412
TiO ₂ (rutile)	3310, 1620	OH...NH ₃ or H ₂ NH...O	
Dehydroxylated at 773 K	3400, 3350, 3250, 1605, 1180	Ti ⁴⁺ ← NH ₂ H...O	
	3400, 3350, 3160, 1605, 1230	Ti ⁴⁺ ← NH ₂ H...O	
TiO ₂ (anatase and rutile)	3250	OH...NH ₃	303, 412
Dehydroxylated at 673 K	3385, 3245, 1190	Ti ⁴⁺ ← NH ₂ H...O	
	3300, 3140, 1220	Ti ⁴⁺ ← NH ₂ H...O	
V ₂ O ₅	1425	NH ₄ ⁺	212–215, 427
Evacuated at 673 K	1620, 1260	V ⁵⁺ ← NH ₂ H...O	
ZnO	3420, 3380, 1630, 1220	Zn ²⁺ ← NH ₂ H...O	308
Evacuated at 773 K	3400, 3350, 1560	Zn ²⁺ –NH ₂ (H)...O	19, 412
	1515, 3320	NH ₂	
ZrO ₂	3410, 1140	OH...NH ₃	412
Evacuated at 723–773 K	3380, 3280, 1610, 1230, 1190	Zr ⁴⁺ ← NH ₂ H...O	
Ga–La–Sb oxide	3450, 3380, 3300, 3250, 1600, 1090	O...H–NH ₂	391
Oxidized	3630, 3460–3410, 3390–3320, 1560	NH ₂ ⁻	
	1430	NH ₄ ⁺	
Sn/Mo oxide	3500–2600, 1610, 1035	O...H–NH ₂	219, 220
Oxidized	3500–2600, 1610, 1255	Mo ⁶⁽⁵⁾⁺ ← NH ₃	
	3500–2600, 1445	NH ₄ ⁺	

to progressive dehydroxylation of the surface and to an increasing concentration of ammonia bound with surface oxygen via NH...O hydrogen-bonds ($\delta_s\text{NH}_3$ at 1070–1020 cm⁻¹). The number of coordinatively unsaturated surface cations capable of forming a coordinative bond with ammonia molecules ($\delta_s\text{NH}_3$ at 1280–1150 cm⁻¹) grows with the dehydroxylation of the oxide surface. The detailed position of the $\delta_s\text{NH}_3$ band is, in this case, sensitive to the electron-acceptor ability of the cation and increases when the cation electronegativity increases [30, 420]. The $\delta_s\text{NH}_3$ bands can be also observed at lower frequencies (<1150 cm⁻¹). In such cases, it is difficult to distinguish these bands from those of hydrogen-bonded ammonia. It is then necessary to use additional procedures to prove that the relevant species is formed and hence that sites of a corresponding nature are present on the surface. The frequencies of different ammonia complexes observed in the spectra of ammonia adsorbed on a series of simple and complex oxides are collected in Table 2.9. In the spectra of several oxides, especially those pre-evacuated at high temperatures, bands attributable to surface hydroxyl groups appear and grow in intensity upon the adsorption of ammonia. This shows that some of the ammonia molecules dissociate on the surface of these oxides, forming OH and NH₂ groups, thus revealing the presence of surface acid–base pairs such as Mⁿ⁺O⁻². It should be noted that spectral identification of NH₂ groups by using only the absorption bands of the νNH and δNH types, without taking into account the appearance of the surface hydroxyl groups, is not reliable.

Table 2.9. Spectral features of coordinated ammonia and ammonium ions on various oxide catalysts.

Adsorbent	$\delta_s^a \text{NH}_3$ (cm ⁻¹)	X^a	$\delta_{as}^a \text{NH}_3$ (cm ⁻¹)	Site	δNH_4^+ (cm ⁻¹)	Reference
TiO ₂ (anatase)	1180, 1220	1.58, 1.85	1605	Ti ⁴⁺	–	30, 188, 376
V ₂ O ₅	1270	2.19	1610	V ⁵⁺	1415(I) 1485(II)	
V ₂ O ₅ /SiO ₂	–	–	1610	V ⁵⁺	1420(I) 1450(II)	30, 212–215, 421–423
V ₂ O ₅ /SiO ₂ ^b	–	–	1610	V ³⁺	Undetected	
V ₂ O ₅ /Al ₂ O ₃	1250	2.05	1610	V ⁵⁺	1425	30, 213–215
V ₂ O ₅ /Al ₂ O ₃ ^b	1220	1.85	1620	V ³⁺	Undetected	
Cr ₂ O ₃	1220	1.85	–	Cr ³⁺	Undetected	179, 186, 421
Cr ₂ O ₃ ^b	1150	1.39	1610	Cr ²⁺	Undetected	
CrO ₃ /SiO ₂	–	–	1610	Cr ⁶⁺	1440	30
CrO ₃ /Al ₂ O ₃	1255	2.08	1620	Cr ⁶⁺	1430	30
MnO ₂	1230	1.92	1620	Mn ⁴⁺	Undetected	30
Fe ₂ O ₃	1220	1.85	1620	Fe ³⁺	Undetected	30, 208, 209
Fe ₂ O ₃ ^b	1190	1.65	1610	Fe ²⁺	Undetected	30, 208
NiO	1100	1.09	1610	Ni ²⁺	Undetected	30, 412
CuO	1175	1.55	1610	Cu ²⁺	Undetected	30
Cu ₂ O	1155	1.43	1610	Cu ⁺	Undetected	30
Al ₂ O ₃	1240–1315	1.98	1620	Al ³⁺	1395, 1473	426
CoO	1130	1.30	1620	Co ²⁺	Undetected	412
ZnO	1220	1.85	1610	Zn ²⁺	Undetected	197, 412, 425, 427
MoO ₃	1260	2.12	1610	Mo ⁶⁺	1420	428
MoO ₃ /SiO ₂	–	–	1610	Mo ⁶⁺	1410–1440	396
MoO ₃ /Al ₂ O ₃	1260–1280	2.12–2.26	1620	Mo ⁶⁺	1440–1460	221, 395
Sb ₆ O ₁₃	–	–	–	–	1405, 1425, 1465	244
SnO ₂	1240–1250	1.98–2.05	1620	Sn ⁴⁺	Undetected	30
ZnCr ₂ O ₄	1255	–	1625	–	–	193
ZnO.ZnCr ₂ O ₄	1215	–	1615	–	–	193
Cr–Mo–O	1260, 1270	1.98, 2.19	1610	–	1420	391
V–Mo–Si–O	–	–	–	–	1425	392
Sn–Mo–O	1240–1255	1.98–2.08	1610–1615	–	1440	30
(Sn/Mo = 9 ^b)	1190–1210, 1190	1.78–1.65	1605	–	–	219, 220
Cr–V–O	1240–1260	1.98–2.12	1610	–	1440	30
(5 % V ₂ O ₅)	–	–	–	–	–	–
Sn–V–O	1245–1255	2.02–2.08	1615	–	1460	30, 216
(5 % V ₂ O ₅)	–	–	–	–	–	–
Sb–V–O	1260	2.12	–	–	1440–1430	–
(10 % V ₂ O ₅)	–	–	–	–	–	–
Fe–Sb–O	–	–	1610	–	1405, 1430, 1460	246
Ti–Sb–O	–	–	1605	–	1400–1460	245
Sn–Sb–O	1150	1.39	1610	–	1450	–
Bi–Mo–O	1220–1260	1.85–2.05	1620–1630	–	1430–1440	–
WO ₃	–	–	1610	–	1420	30, 394
Cr–W–O	~1250	2.05	1620	–	1420	30
Sb–V–Bi	1235	1.96	1615	–	1445	–
Fe–Mo–O	–	–	–	–	1430	393
(Fe/Mo = 1.53)	–	–	–	–	–	–
MnO _x /Al ₂ O ₃	1220–1130	1.98, 1.30	1610	–	1459	–
ZnAl ₂ O ₄	1130–1220	1.98, 1.85	1610	–	–	425

^as, symmetric; as, asymmetric; X, electronegativity.^bReduced samples.

The δNH_2 and νNH_2 values for both metal amides $\text{M}(\text{NH}_2)_n$ and surface NH_2 groups occur over wide ranges of 1490–1630 and 3200–3580 cm^{-1} (Table 2.10). As shown, the position of δNH_2 of such groups is overlapped by the δ_{as} of coordinated NH_3 . This is why there are difficulties in assigning bands to the vibrations of NH_2 species adsorbed on oxides, and especially on those oxides with strong electron-acceptor sites, because both NH_2 groups and the molecules of coordinatively bound ammonia can be present on the surface simultaneously. The covalence of the $\text{M}-\text{N}$ bond increases with increasing metal electronegativity, as is shown by the spectra of the alkali-earth metals. This is accompanied by a simultaneous increase in all frequencies of the NH_2 vibrations (see Table 2.10).

The splitting of the ν_{as} and ν_{s} vibrations of surface NH_2 groups is well described by the Bellamy–Uilyams equation [13], as follows:

$$\nu_{\text{s}} = 0.876\nu_{\text{as}} + 345.5 \quad (2.7)$$

Table 2.10. Vibrational frequencies of NH_2 groups in molecular and surface compounds^a.

Structure	$\nu_1(\text{s})$ (cm^{-1})	$\nu_2(\text{NH}_2)$ (cm^{-1})	$\nu_3(\text{as})$ (cm^{-1})	Reference
<i>In individual (molecular) compounds</i>				
$[\text{Hg}(\text{NH}_2)_n]\text{Cl}_n$	–	1534	–	15
LiNH_2	3238	1564	3313	411, 430
NaNH_2	3206	1529	3256	417, 430
KNH_2	3206	1529	3256	417, 430
CH_3-NH_2	3361	1623	3427	14
Aryl- NH_2	–	1560–1640	3400	408
NH_2^+	–	1575–1600	–	408
NH_2-NH_2	3280	1628, 1587, 1493	3350, 3325	15
$\text{F}_3\text{B}-\text{N}_2\text{H}_4$	–	1620	–	405
$\text{H}_3\text{B}-\text{N}_2\text{H}_4$	3240	1602	3320	404
NH_2OH (solid)	3245, 2173	1564, 1515	3302	15, 431
NH_2OH (gas)	3297	1605	3350	431
$\text{Pt}-\text{NH}_2\text{OH}$	3205	1588	3245	431
$\text{Me}:\text{OH}-\text{NH}_2$	3302	1593	2249	431
$\text{Me}:\text{NH}_2\text{OH}$	3297	1608	3338	431
$\text{Mg}(\text{NH}_2)_2$ (1.23 ^b)	3270	1556	3323	419, 433
$\text{Ca}(\text{NH}_2)_2$ (1.04 ^b)	3243	1550	3306	419
$\text{Sr}(\text{NH}_2)_2$ (0.99 ^b)	322	1536	3279	419
$\text{Ba}(\text{NH}_2)_2$	3138	1532	3240	419
<i>In surface compounds</i>				
$\text{Si}-\text{NH}_2$	3450–3440	1550	3550–3520	19, 412
$\text{B}-\text{NH}_2$	3490–3470	–	3580–350	19
$\text{Ge}-\text{NH}_2$	3393	1535	3467	19
$\text{P}-\text{NH}_2$	3440	1570	3530	19
$\text{Al}-\text{NH}_2$	3335	1510	3386	19
$\text{Al}-\text{NH}_2$	3440	1560	3520	432
$\text{Zn}-\text{NH}_2$	3415	1565, 1515	3520	56, 197

^as, symmetric; as, asymmetric.

^bElectronegativity values (according to Oldrih) have been adopted from Gordymova and Davydov [432].

examination of the data obtained by Filimonov and Tsyganenko for the values of ν_{as} and ν_{s} of surface NH_2 groups shows that the frequencies of the NH_2 stretching vibrations in X-NH_2 spectra depend upon the electronegativity of the X atom. This dependence can be used to estimate the vibration frequencies of NH_2 groups on other oxide surfaces. However, such estimates should take into account the fact that the effective electronegativity of the metal ion also depends on its coordination number (see Table 2.10) [432].

Pyridine

There is practically no oxide system for which pyridine adsorption has not been investigated by means of IR spectroscopy. In fact, this molecule seems to be more useful for the detection of both Lewis and Brønsted acid sites on the same surface. Moreover, it is more stable towards oxidation than other nitrogen-containing bases such as amines and nitriles that have been used as a probe molecules. A dependence of the spectral parameters on the state of the adsorption center, i.e. a correlation between $\nu_{19\text{a}}$ and the strength of the Lewis acid site (namely between the cation acceptor ability (e/r) and the shift of $\nu_{19\text{a}}$) has been established [19], although the value of such a shift is only 5–15 cm^{-1} for the most characteristic band.

Pyridine can interact at the surfaces of oxide systems in three ways: (i) the nitrogen unshared pair can hydrogen-bond to weakly acidic surface OH groups, so yielding a very weak perturbation of the adsorbed molecule, (ii) if the Brønsted acidity of a surface OH group is sufficiently high, a proton can be extracted to yield a pyridinium ion species (PyH^+), on (iii) the nitrogen unshared pair can interact by σ -donation to surface coordinatively unsaturated cationic centers, acting as Lewis acid sites.

The large amount of data available in the literature concerning homogeneous and heterogeneous pyridine compounds and their complexes, allows the schematic representation of the spectral range 1700–1400 cm^{-1} and of the pyridine vibrational modes therein shown in Figure 2.26 above. The ring vibration modes 8a–8b and 19a–19b, are the most sensitive vibrations of pyridine with regard to the nature and strength of the adsorptive interaction [19, 27]. For this reason, inspection of the IR spectral region 1700–1400 cm^{-1} of adsorbed pyridine is routinely employed for assessment of the surface acidities of metal oxides.

Upon pyridine desorption on acidic catalysts at high temperatures, a band at 1462 cm^{-1} generally appears. Some authors have suggested that this is a signal for pyridine adsorbed on strong Lewis acid centers, since this band appears at a higher frequency than the usual Lewis acid–pyridine band (1450–1455 cm^{-1}) [436, 437]. According to Morterra *et al.* [436], pyridine in the complex, as characterized by the 1462 cm^{-1} band, interacts simultaneously with a tri-coordinated aluminum operating as a Lewis acid site and an OH group present in the same framework position, or which is formed during the desorption–diffusion process through the ‘jumping’ of pyridine as a ‘pyridinium ion’. Pyridine is hydrogen-bonded to the Brønsted acid sites at low temperatures (lower than room temperature) and forms a pyridinium ion at higher temperatures. The latter are mobile at elevated temperatures and jump from site to site [436]. Sometimes, a jump as a pyridinium ion carries the proton from an hydroxyl group to another oxygen of the zeolite framework. If pyridine finds a Lewis acid site during a series of such jumps, it may instead become adsorbed on this alternative site. The probability of pyridine adsorption on a Lewis acid site increases with the decreasing distance between the acid sites.

Other amines and nitriles have also been used to unambiguously indicate the chemical nature and the number of active sites on oxide surfaces. However, amines can quite readily undergo various surface reactions, especially at elevated temperatures. As for nitriles (e.g. benzonitrile and acetonitrile), it has been established that the value of $\Delta\nu_{\text{CN}}$ does not, in practice, depend on the strength of the adsorption center and is not specific for each cation, despite claims by Paukshtis and Yurchenko [418].

Lewis acid sites

The ammonia molecule is a strong base. The orbital that makes it an effective ligand is that occupied by the unshared electron pair on N. The three stable N–H molecular orbitals are too low in energy to react with the cation. On interaction of ammonia with an oxide surface, the orbital of a free electron pair is overlapped by the vacant orbitals of the surface coordinatively unsaturated cations, which means that there is an analogy between amino complexes and surface coordination compounds. Formation of a coordination bond between NH_3 and the cation complex-forming agent leads to great changes in the character of the vibrations of this molecule. Svatos *et al.* [420] established that the frequencies of the deformation vibrations of ammonia molecules are sensitive to the nature of the cation (to which it is bound). The frequencies of the in-plane rocking vibration (ρNH_3) and of the symmetric deformation (in-phase bending) vibration (ρ_s) are the most sensitive. The frequency of the asymmetric deformation vibration (δ_{as}) is the least sensitive to the nature, charge, composition and geometry of the coordination site. The formation of the coordination bond enhances the force constant and the frequency of the symmetric deformation vibration. Earlier, it had been reported [406, 425, 438, 439], and examined in detail [30], that the relative acceptor abilities of the surface cations may be correlated with the values of their electronegativities, calculated according to the following equation:

$$\delta_s^2 \times 10^{-5} = 3.66X + 8.12 \quad (2.8)$$

The values of the electronegativities, calculated from this equation, for all of the oxide surface cations for which the spectra of adsorbed ammonia have been investigated are represented in Table 2.9 together with the spectral characteristics of coordinated ammonia on different oxide catalysts. The presence of coordinatively unsaturated cations on the surface has been established for practically all of the metal oxides investigated, after impurities have been removed from their surfaces. Absorption bands characteristic of δ_s of coordinated ammonia usually have a complex structure which manifests itself in a gradual displacement of the band maximum on desorption of ammonia, with the high-frequency components usually being the last to disappear [30, 412]. This indicates a considerable distribution of Lewis acid centers on the surfaces of oxides. The value of the δ_s frequency maximum is a sufficiently sensitive characteristic here. This can be illustrated by using the example of the well-studied $\text{Al}_2\text{O}_3/\text{Cl}$, $\text{Al}_2\text{O}_3/\text{Na}-\text{NH}_3$ systems [30, 432] (see Chapter 4). There are many studies devoted to the modification of oxide surfaces where the IR spectra of both adsorbed ammonia and pyridine have been used to investigate the change of acidic properties of the surfaces. The estimated concentration of electron-accepting centers on Al_2O_3 dehydrated at 773 K, based on combined gravimetric and IR spectroscopic studies of ammonia adsorption, is 2×10^{13} centers per cm^2 [435]. The initial heat of adsorption of ammonia on Al_2O_3 is as high as 120 kJ mol^{-1} [19].

Table 2.9 shows that the acceptor power of cations on oxide surfaces, monitored by the interaction with ammonia molecules, varies substantially. A greater acceptor power is naturally exhibited by ions in the highest oxidation states and this declines with decreasing cation valence (V, Cr, Fe, Cu, etc.). The alteration of δ_s per unit cation valence change is considerable, and this makes it possible to use this molecule together with, e.g. CO and NO (see Chapter 3), to establish the predominant state of oxidation of ions on the oxide surfaces. In all cases (see Table 2.9), when there is a correlation between the state of oxidation of the ions that coordinate to ammonia and δ_s , additional data on the valence state of surface cations need to be obtained by independent methods such as ESR, UV–Vis or IR spectroscopy of adsorbed probe molecules. This can be illustrated by using copper oxides as examples.

CuO/Cu₂O

Adsorption of ammonia on CuO results in absorption bands at 1175 (δ_s) and 1600–1620 cm^{-1} ($\delta_{\text{as}} \text{NH}_3$) (see Table 2.9). Cations exist on the surface of this catalyst predominantly as Cu^{2+} ions, which can be established by NO adsorption, for which the spectra have a band at ca. 1860 cm^{-1} , characteristic of the Cu^{2+} –NO complex (Chapter 3). Adsorption of ammonia on the surface treated with NO leads to the disappearance of the band at ca. 1860 cm^{-1} , and produces the same maxima as for NH_3 adsorption alone, i.e. ammonia molecules displace NO molecules adsorbed on Cu^{2+} ions. In the case of Cu_2O , the δ_s frequency of coordinated ammonia appears at 1155 cm^{-1} . CO molecules were displaced from Cu^+ ions by ammonia, thus confirming the nature of the ammonia-stabilizing center.

It should be noted, however, that ammonia molecules can become oxidized on the surface of some transition-metal oxides. This makes an identification of the surface centers more difficult (part of the surface cations are reduced, and new types of surface hydroxyl groups appear). The possibility of oxidized ammonia complexes being formed upon its adsorption has been reported by Belokopytov *et al.* [421] for chromia near ambient temperatures, but for the majority of oxides this takes place only at higher temperatures.

The simultaneous presence of several types of Lewis acid centers has been observed for a number of individual oxide catalysts where the surface cations are in a single oxidation state. This fact may be explained by the presence of these surface cations with different coordinations (with various coordination numbers), which can appear, for example, as a result of the exposure of different planes of the crystalline lattice. Many combinations of binary oxides have been reported to generate acid sites on the surface. A mechanism for the generation of acid sites by mixing two oxides has been proposed by Tanabe [79] – this suggests that such acidity generation is caused by an excess of a negative or a positive charge within the model structure of the binary oxide, which is related to the coordination numbers of the positive and negative cations and anions.

The differences in acceptor power between cations of varying nature allow one to establish their presence on the surface of binary oxide catalysts (see Table 2.9), and to investigate their mutual influence (see, for example, Budneva and Davydov [391]). A presence of both Lewis and Brønsted acid sites on the surface of the above-mentioned systems investigated by ammonia adsorption has been supported by the pyridine adsorption data.

Al₂O₃

It is important to note that if different families of Lewis acid sites exist at the surface, as in the case of transition aluminas, they can be identified by pyridine adsorption studies [27, 53, 435–441]. Thus, Knozinger and co-workers [53, 435], on the basis of the frequencies of the 8a modes, separated three types of Lewis acid sites (1614, 1617 and 1624 cm^{-1}) and assigned them to Lewis acid centers constituted by single-oxide vacancies, formed in the earliest stages of surface dehydration. The strongest Lewis acid centers are formed by pair- or triplet-oxide vacancies, found under more severe conditions of surface dehydration. The presence of oxidation centers ('X-sites') on alumina surfaces, which lead to the oxidation of pyridine species (during pyridine adsorption) or of bicarbonate formation when CO_2 is adsorbed, has been established. These sites contain three or more exposed aluminum ions or a doublet vacancy with adjacent hydroxyl groups (probably adsorbing at 3775 cm^{-1}). The surface concentrations of these active X-sites has been evaluated to be in the order of 10^{13} cm^{-2} (0.1 sites per nm^2), corresponding to less than 1 % of the surface of alumina.

There is a point of view in the literature [27, 299, 436, 440, 441, 443] that pyridine allows a better differentiation of the Lewis acid sites (at least for aluminates) than ammonia. This results from studies of the changes in the analytical by sensitive mode 8a in pyridine adsorption–desorption

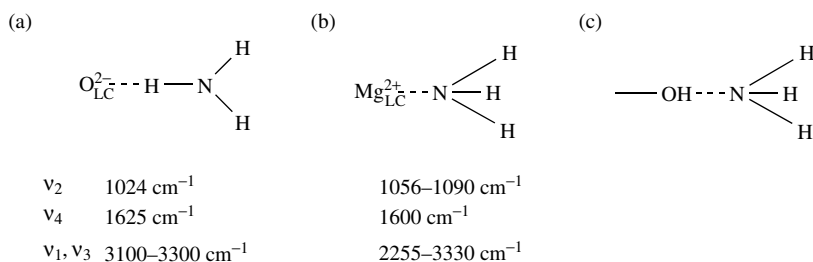
cycles as the temperature increases. The data obtained for pyridine adsorption on aluminates have been examined in detail in a recently published study [27].

The correlation between the Al coordination state ($\text{Al}_{\text{cus}}^{\text{VI}}$, $\text{Al}^{\text{VI}}\text{-Al}^{\text{IV}}$ and $\text{Al}_{\text{cus}}^{\text{IV}}$) and Py-L strength has been recognized by Morterra and Magnassa [27]. They suggested that the coordination of coordinatively unsaturated Al ions is preliminary responsible for the change of frequency exhibited by the analytical ring modes of the adsorbed pyridine, and especially of the most sensitive mode 8a. The bands have been assigned in the following manner: at 1598 cm^{-1} , to pyridine Lewis-acid coordinated to $\text{Al}_{\text{cus}}^{\text{VI}}$ ions $[\text{Py-L}]_{\text{o}}$; at $1610\text{--}1620\text{ cm}^{-1}$, to pyridine Lewis-acid coordinated to coordinative vacancies shared by an $\text{Al}^{\text{VI}}\text{-Al}^{\text{IV}}$ cation pair $[\text{Py-L}]_{\text{o,t}}$; at 1625 cm^{-1} , to pyridine Lewis-acid coordinated to $\text{Al}_{\text{cus}}^{\text{IV}}$ sites $[\text{Py-L}]_{\text{t}}$. The maximum concentrations were as follows: $[\text{Py-L}]_{\text{o}}$, 1 Py molecule per nm^2 ; $[\text{Py-L}]_{\text{t}}$, 0.6 Py molecules per nm^2 ; $[\text{Py-L}]_{\text{o,t}}$, 0.4 Py molecules per nm^2 . The most reactive X-sites represented approximately 0.2 to 0.1 Py molecules per nm^2 .

Tsyganenko *et al.* [299, 357] proposed for Al-containing systems a model involving an examination of three states of the cations, namely octa-, tetra- and pentahedrally coordinated ions. This allowed them to separate the several types of Lewis acid sites formed upon the dehydroxylation of different surface faces.

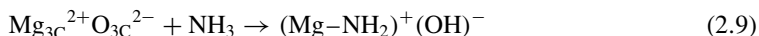
MgO

It should be noted that the strength of the acid acceptor sites on the surface of MgO, CaO, SrO and BaO is not strong, whereas the basicity of oxygen is very strong. A number of surface species are produced by ammonia adsorbed on these systems in molecular form [419] and via heterolytic dissociation (ionic pairs) [433]. When ammonia interacts with a surface cation or anion, or hydroxy groups, three different structure of adsorbed NH_3 are identified by IR spectroscopy:



Scheme 2.16

A small portion (<10 %) of ammonia undergoes heterolytic dissociation on ionic pairs, producing OH^- and NH_2^- groups as follows:

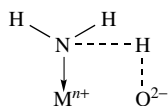


The NH_2 deformation mode falls in the $1600\text{--}1500\text{ cm}^{-1}$ region (Table 2.10). It is not possible to exclude the further dissociation of NH_2 groups; the resultant NH fragments would absorb in lower-wavenumber regions when compared to the NH_2 groups, but probably with lower extinction coefficients, and are thus not detected [433].

ZnO

The bands at 1220 , 1630 , 3370 and 3415 cm^{-1} in the IR spectrum of ammonia adsorbed at room temperature on ZnO [197] (in the case of ND_3 at 915 , 1195 , 2570 and $2660\text{--}2670\text{ cm}^{-1}$, respectively) characterize, in accordance with numerous literature data, the vibrations of coordinated

ammonia molecules, whereas the presence of bands at 1515 and 3320 cm^{-1} (1110 , 2525 and $2660\text{--}2670\text{ cm}^{-1}$ for ND_3) indicates the formation of NH_2 groups. Detailed investigations of ammonia adsorption on Al_2O_3 [432] and ZnO [197] show the presence of ammonia molecules bound to cation and anion centers in the pre-dissociation stage:

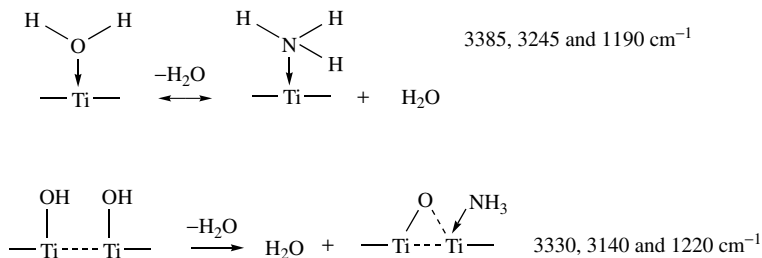


Scheme 2.17

as characterized by the bands at 1205 (δ_s) and 1560 (δ_{as}). The last of these shifts to 1145 cm^{-1} for ND_3 , thus confirming the interpretation suggested.

TiO_2

Primet *et al.* [302, 303] reported two types of surface sites created through evacuation of TiO_2 at high temperature, as indicated by NH_3 adsorption:



Scheme 2.18

This was later confirmed by Hadjiivanov and co-workers [188] (see Table 2.9). Taking into consideration the above data concerning the spectral features of both coordinated ammonia and NH_2 (see Tables 2.9 and 2.10), the assignment of the 1220 cm^{-1} band to δNH_2 , as well as the band at 3350 cm^{-1} to $\nu_{as}\text{NH}_2$ and the 3190 cm^{-1} band to $\nu_s\text{NH}_2$, as suggested by Hadjiivanov *et al.* in later publications [442], seems to be incorrect.

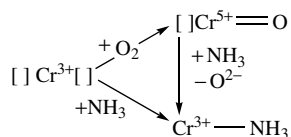
Lewis acidity can be created by dehydroxylation of the surface. The formation/destruction of these sites can be observed by monitoring the intensities of the bands belonging to the surface hydroxyl groups, as well as the bands of both NH_3 and pyridine later coordinated to such sites. Pyridine adsorption on rutile has been reported by Parfitt *et al.* [444] and Jones and Hockey [307], and on anatase by Primet *et al.* [302, 303] and Morterra *et al.* [376]. The main disagreement among the findings of these authors is the assignment of the bands of pyridine adsorbed on Lewis and/or Brønsted acid sites, to $\text{OH}\cdots\text{H}$ -bonded Py, and to physically adsorbed pyridine. These data, also reported by Morterra and co-workers [27, 436], indicate once again that the most sensitive region is that of the 8a and 8b modes ($1500\text{--}1700\text{ cm}^{-1}$).

Cr_2O_3

Starting from Burwell *et al.* [443], who established the presence of Lewis acid sites on Cr_2O_3 and were the first to propose a model of the surface on the basis of the examination of the (001) face of $\alpha\text{-Cr}_2\text{O}_3$, these sites have been intensively investigated by adsorption of ammonia,

pyridine, oxygen and carbon monoxide. Burwell *et al.* [443] showed that the anionic vacancies on the (001) face of α -Cr₂O₃ may easily chemisorb water molecules, leading to the formation of OH⁻ ions covering the whole surface, (OH_o)_s. The dehydroxylation of such a surface results in the exposure of cations. On the basis of IR spectra from adsorbed NH₃, Belokopytov *et al.* [421] reported that the surface of Cr₂O₃ has only one Lewis acid sites, while Davydov and coworkers [30, 179] revealed two types of LASs (see Table 2.8). Later [185, 186], it was shown that for high coverage of the chromia surface by ammonia, three absorption bands at 1150, 1180, and 1220 cm⁻¹ are observed for the δ_s of ammonia coordinated by chromium ions in sites of different degrees of coordination. Upon coverage, only the band at 1220 cm⁻¹ was observed. This is in agreement with the model of the chromia surface examined earlier and suggested a presence of several chromium ions in different coordination states on the surface (Section 2.2.1).

Another way for ammonia to interact with chromia having an oxidized surface (i.e. containing Cr=O groups), has been suggested by Klissurski *et al.* [186] on the basis of both the above model of the Cr₂O₃ surface and the fact that the CO adsorption shows no Lewis acid sites on the oxidized surface. The adsorption of ammonia is accompanied by a shift of the high-frequency absorption Cr=O bands (1015–980 cm⁻¹) to lower values, together with the appearance of bands of coordinated ammonia (δ_s NH₃ = 1220 cm⁻¹). This indicates that under such conditions the adsorption of ammonia occurs through the participation of Cr=O groups. First, the fact that the values of δ_s for ammonia coordinated by chromium ions in high degrees of oxidation are quite low has to be explained. As a rule, the acceptor ability of such ions, including Cr⁶⁺, is higher and δ_s of the coordinated ammonia in the case of such ions is observed in the higher-frequency region (>1260 cm⁻¹). The results can be explained by the following scheme:



Scheme 2.19

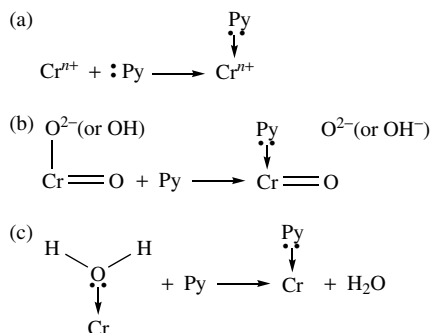
where [] denotes a coordination vacancy [186]. It is clear that the more electropositive ions are more active surface Lewis acid sites and form more stable complexes with ligands such as ammonia. This is why ammonia, when the coverage is low on the nonoxidized surface, predominantly interacts mainly with these types of coordinatively unsaturated chromium ions and does not interact with the two other types. The suggested identification of the location of the adsorbed oxygen on reoxidized chromia conforms with these experimental results. Thus, the three forms of coordinated ammonia probably relate to three centers of the oxygen adsorption. The band at 1220 cm⁻¹ can also be partly caused by ammonia adsorbed on four-coordinated Cr³⁺(2-0-0-0) ions on the (0001) face because the acidity of these centers is close to that for Cr³⁺(1-1-0-0).

The value calculated for the concentration of the strongest Lewis acid sites (the corresponding stretching vibration of the Cr=O bond lies at 1015 cm⁻¹) is 2.8 centers nm⁻², while the total concentration of Cr=O groups comprises about 5.0 centers nm⁻². The calculated oxygen coverage is about 25 % of a monolayer and is almost equal to one oxygen atom per one four-coordinated surface chromium ion [185, 186].

Infrared spectroscopic studies of pyridine and ammonia adsorbed on supported CrO₃ have made possible the distinction between Brønsted and Lewis acid sites for all samples, except those with low chromium concentrations, when only CrO₄²⁻ ions are present [30] (Table 2.9). For example, in the case of pyridine adsorbed on CrO_x/ZrO₂ evacuated at 773 K, there are peaks at 1443,

1488, 1497, 1554, 1580, 1595 and 1605 cm^{-1} in the infrared spectra. Many of these peaks, which decreased after evacuation at 523 K, can be assigned to hydrogen-bonded pyridine [445]. The bands at 1554 and 1497 cm^{-1} belong to pyridinium ions formed on Brønsted acid sites, whereas the maxima at 1443, 1482, 1580 and 1605 cm^{-1} are caused by pyridine coordinatively bound to Lewis acid sites [445].

Zecchina *et al.* [446] studied the adsorption of different molecules (O_2 , H_2 , CO and pyridine) on $\alpha\text{-Cr}_2\text{O}_3$ by means of IR spectroscopy, and showed that both hydroxyls and Cr^{3+} ions with different coordination numbers are present on this oxide surface. In the opinion of these authors, Cr^{3+} ions react with pyridine molecules according to the following scheme:



Scheme 2.20

On dehydroxylated and oxygen-free surfaces, strong absorption occurs on the Cr^{3+} ions through a coordination bond (Scheme 2.20(a)). The corresponding band observed in the IR spectra is typical for pyridine bound to Lewis acid sites. In the authors' opinion [446], the coordination sites are not fully occupied by dissociatively adsorbed oxygen in this case; however, the data on CO adsorption do not confirm this conclusion (see Section 2.3.2). This is why the Lewis acidity due to Cr^{3+} ions can be observed by the pyridine adsorption even if the surface is exposed to oxygen (Scheme 2.20(b)). On the hydrated surface, pyridine is strongly chemisorbed on Cr^{3+} ions (Scheme 2.20(c)), together with weak physical adsorption on surface hydroxyls or H_2O groups through hydrogen-bonding.

Fe_2O_3

It has again been reported that ammonia [30, 200, 207–209, 421] and pyridine [421, 447] coordinate to Fe^{3+} surface Lewis sites. Rochester and Topham [200] observed that both NH_3 and Py interact with Lewis sites only on haematite that has been dehydrated at temperatures above 513 K, whereas highly dehydrated specimens (973 K) only exhibited a weak H-bonding activity of the residual surface hydroxyls. Busca and Lorenzelli [447] reported that pyridine is strongly coordinated on $\alpha\text{-Fe}_2\text{O}_3$ and cannot be desorbed as such. These authors suggested that the (0001) face was dominant [206]. They noted that only coordinatively unsaturated octahedral Fe^{3+} ions are expected to act as Lewis acid sites. Using the model of a (0001) face of $\alpha\text{-Fe}_2\text{O}_3$ (Figure 2.27(a)) they also identified isolated OH groups either bound to a single tetrahedrally coordinated ferric ion (A), or bridged between two octahedral ferric ions (B). According to this study, two types of Lewis acid sites may also be identified in such a model, due to Fe^{3+} ions bound to three oxygens (D) that would act as a coordinatively unsaturated tetrahedral site, and to pairs of near-octahedral cations with one or two coordinative unsaturations (E). The last sites are

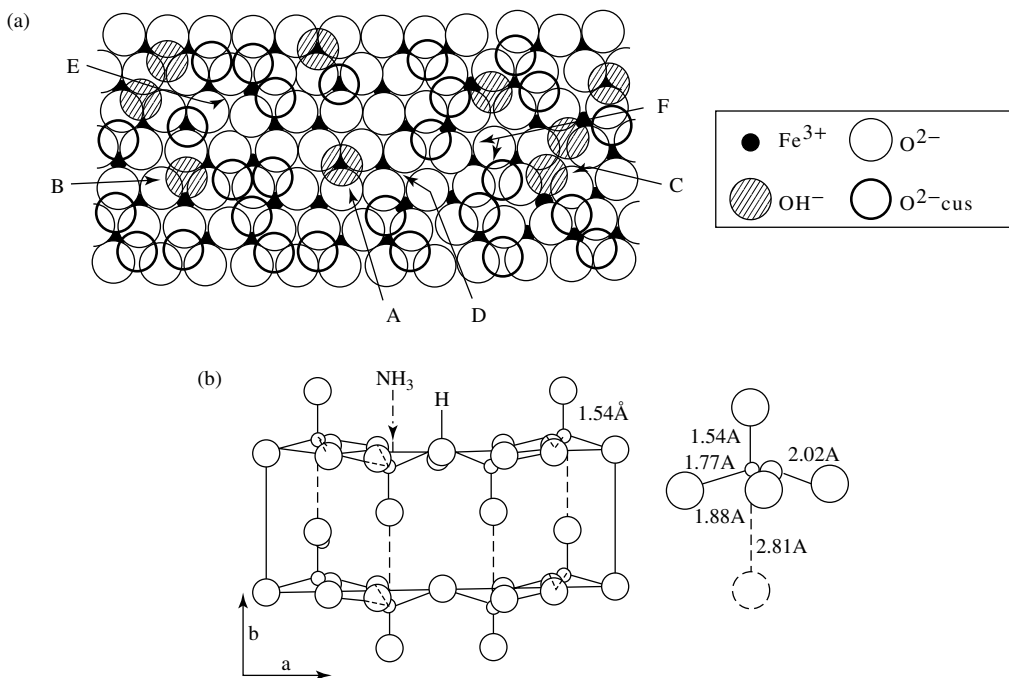


Figure 2.27. (a) Model for a disordered {0001} face of α - Fe_2O_3 [362]. Reprinted with permission from Busca, G., Lorenzelli, V., Ramis, G. and Willey, R.J., *Langmuir*, **9**, 1492–1499 (1993). Copyright (1993) American Chemical Society; (b) NH_3 coordination involving the vanadium cations on the fragment of the structure of V_2O_5 (001). Small circles denote vanadium atoms; large circles are oxygen atoms.

similar to those proposed by Morterra *et al.* [436] for weaker Lewis acid sites on η - Al_2O_3 . Similar sites, when placed near exposed oxide ions (as at an F site), would also act as acid–base dissociating sites.

V-, Mo-, Sb- and W-containing catalysts

Lewis acid sites has also been revealed by the adsorption of both ammonia and pyridine on the surface of acid-forming oxides like MoO_3 [219–221, 391–397, 448–458], V_2O_5 [212–216, 422, 423, 427–429, 459, 460], WO_3 [394] and Sb_6O_{13} [244–246] when supported on SiO_2 , Al_2O_3 , and TiO_2 . For example, bands at 1270 and 1610 cm^{-1} , which are observed in the spectrum from ammonia adsorbed on V_2O_5 , can be assigned to δ_s and δ_{as} vibrations of coordinatively bound ammonia (Lewis acid sites) (see Table 2.9). More probably, the V^{5+} ions are the Lewis acid sites of the oxidized sample of V_2O_5 [212–216]. In fact, it is possible to represent V_2O_5 as a polymer, with its structure being described as a distorted trigonal bipyramid. Ammonia can be coordinated in an equatorial plane towards a $\text{V}=\text{O}$ bond with the formation of a tetragonal pyramid (Figure 2.27(b)). Support for this comes from the shift of the $\nu(\text{V}=\text{O})^{3+}$ vibrations. On the Lewis acid sites, ammonia is adsorbed quite strongly; the characteristic adsorption bands disappear from the spectra only after desorption above 473 K. It should be noted that the NH_2 groups on V_2O_5 were not observed by infrared spectroscopy because of electron transfer from NH_2^- followed by oxidation, but such groups have been observed [212] on the reduced surface. Similar data have been obtained for Mo- W- and Sb-containing systems.

The incorporation of molybdenum into the surface of magnesia leads to an increase in the surface acidity, causing the development of Lewis acid sites, which coordinate pyridine stronger than on bare magnesia, on which pyridine is only physisorbed. Samples calcinated at 1100 K would be expected to behave differently, because of the formation of MgMoO_4 , as detected by XRD, although the spectra recorded are very similar to those obtained upon adsorption on magnesia [452, 453]. These results suggest that the formation of MgMoO_4 still leaves Mg^{2+} species exposed on the surface of the crystallites, on which strong adsorption of carboxylic acids also takes place. Thus, the reaction between molybdenum and magnesia seems to be different from that between molybdenum and other acidic supports.

Brønsted acid sites

Protic acid sites of oxides significantly influence the transformations of reacting molecules. This effect is clearly demonstrated for zeolite-containing systems [19, 454] and is discussed further in Chapters 4 and 5. Investigations [30, 212, 219–221, 244–246, 389–397, 455] revealed the presence of Brønsted acid sites on the surface of numerous transition-metal oxides with cations of V [212–216], Mo [106, 219–222, 389–397, 448–450], Sb [244–246], and W [394] in the highest degree of oxidation (≥ 4), and in the complex systems containing more the one of these cations [30, 389] (Table 2.9). Hence, it is possible to use such systems as bi-functional catalysts with both acid and redox functions [456]. These sites are revealed by IR spectroscopy of adsorbed molecular probes (NH_3 and Py), since they can protonate these probes forming NH_4^+ and PyH^+ ions. IR spectroscopic measurements of ammonia adsorbed on Brønsted acid sites are represented in Tables 2.8 and 2.9.

Brønsted acid sites are thought to be either hydroxyl groups with rather mobile protons (for example, bridged OH groups) or coordinated water molecules, or otherwise H_3O^+ , H_5O_2^+ or more complicated aggregates [30, 389]. Such compounds and fragments are clearly manifested in IR transmission spectra, e.g. in the νOH region, thus enabling us to elucidate the nature of the Brønsted acid sites. The probability of the presence of both H_2O molecules and H_3O^+ ions on the surface of oxides dehydrated at elevated temperatures (≥ 773 K) is rather low. Therefore, OH groups appear to be the main ‘carrier’ of protic acidity in these systems.

It has been described above how Brønsted acid sites on the surface of $\gamma\text{-Al}_2\text{O}_3$ and Al–Si–O are the OH groups of the bridge type, which have well-defined spectra in the region of νOH vibrations, whereas transition-metal oxides with cations in the highest oxidation state give rise to the so-called delocalized ‘multi-sited’ proton (a proton that spends equal times near different basic sites), manifested in the IR spectra by broad νOH absorption bands shifted to low frequencies. As it was shown by Davydov [30], the detailed spectral manifestations of ammonia can provide additional information about the symmetry of the NH_4^+ ion (type and numbers of H-bonds) and about the strength of the Brønsted acid sites (BASs) [432].

The absorptions of the ammonium ions in various systems suggests that the weakest hydrogen-bonding is found in NH_4^+ ions formed on V_2O_5 and MoO_3 (δ_{as} , 1415 and 1420 cm^{-1}), whereas the strongest H-bond is for ions formed on $\gamma\text{-Al}_2\text{O}_3$ (1473 cm^{-1}). The strength of the hydrogen bond from the NH_4^+ ion is determined by the degree of proton transfer to the NH_3 molecule and depends on the polarity of the O–H bond which characterizes its Brønsted acidity. Accordingly, $\gamma\text{-Al}_2\text{O}_3$ has the weakest proton-donating centers among all of the oxide catalysts [426].

The trend underlying the shift of the $\delta_{\text{as}}\text{NH}_4^+$ frequency towards higher frequencies is from 1420 cm^{-1} for MoO_3 to 1440 cm^{-1} for Sn/Mo (90:10), and to 1470 cm^{-1} for Sn/Mo (95:5) [219], which also points to the weakening of Brønsted acid centers in this series. Such an increase in deformation frequencies corresponds to stronger H-bonds due to a high probability of proton donation from NH_4^+ . Such a pattern of proton donation on the surface of molybdenum-containing

catalysts is also confirmed by the decomposition temperatures of the ammonium ions, which also reduce through this series [219].

Hydration over a wide temperature range (293–773 K) fails to locate mobile protons on the surface of oxides which have no Brønsted centers. Hence, the presence of molecules with pK_a values which change from 16 (H_2O) to 35 (NH_3) in the reaction medium does not yield Brønsted centers. Qualitative differences are observed after the hydration of oxides on the surfaces on which mobile protons are detected. The concentration of such protons increases sharply after treatment with water at both room and higher temperatures, as established in agreement with changes of the absorption bands from the ammonium ions [221, 392].

What is the reason for BAS appearance? The presence of protic sites (H^+) themselves stipulated by the nature of these systems or, as several authors suggested, the interaction of a surface with a molecular probe such as NH_3 ? The last may cause Brønsted acid site formation in these systems (e.g. by heterolytic dissociation of a probe molecule on the ionic pairs of the $M^{n+} O^{2-}$ surface with H^+ cation formation). In connection with the NH_3 molecules are already dissociated at room temperature, the formation of ammonium ions on V_2O_5/Al_2O_3 (Figure 2.25(a), spectra 2,3) can be explained by the interaction of further ammonia molecules with an OH proton formed as a result of the ammonia dissociation. The pyridine molecule has been used for the identification of the Brønsted acid centers, because the possibility of dissociation of the pyridine molecule via a C–H bond is much less than that of NH_3 molecules via a N–H bond. In the IR spectra of pyridine adsorbed on an oxidized surface of V_2O_5 , the absorption bands of the pyridinium ion occur at 1535 and 1635 cm^{-1} , together with bands of coordinated pyridine at 1488 and 1635 cm^{-1} [460] (Figure 2.25(a), spectrum 7).

The second important question is: what is the carrier for Bronsted acidity? Either hydroxyl groups with rather mobile protons or coordinated water molecules (or else H_3O^+ , $H_5O_2^+$, and more complicated aggregates), i.e. water remaining on the surface even after high temperature dehydration. In order to answer this question, the IR-measurements of Py adsorption on the surface pretreated by D_2O at different temperatures have been performed [389]. Experiments on the adsorption of pyridine at 673 K on the V_2O_5/Al_2O_3 system, followed by dehydration at

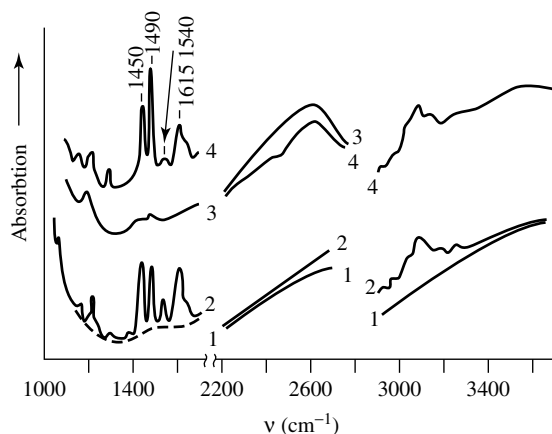


Figure 2.28. IR spectra of pyridine (Py) adsorbed on V_2O_5/Al_2O_3 (10 wt% V_2O_5): (1) treatment of the sample in D_2O at 623 K, then in O_2 at 773 K, with the last O_2 portion removed at 293 K; (2) subsequent Py adsorption at 293 K with further removal of the Py gaseous phase; (3) treatment of the initial sample in D_2O at 293 K, with further evacuation at 293 K; (4) Py adsorption on sample 3 with removal of the Py gaseous phase at 293 K.

the same temperature on a surface pre-treated by D_2O , showed that PyD^+ ions (identified by a band at $1488\text{ cm}^{-1} - \nu_{19b}$ [460]) are predominantly formed in this case. This indicates that the formation of PyH^+ ions is not a result of the dissociation of pyridine molecules. Upon Py interaction with Brønsted acid sites (on the catalyst surface pre-treated with D_2O), the formation of PyD^+ complexes was expected. The position of the $\nu_{19(s)}$ band (stretching vibration of the ring) for pyridine bound to the surface by coordination (1450 cm^{-1}) differs from that for the pyridinium ion (PyH^+) formed on the surface (1540 cm^{-1}) [461a]. Therefore, Davydov and co-workers [460] selected the former band to characterize the coordination complexes formed. The $\nu_{19(s)}$ band is shifted toward 1488 cm^{-1} in the case of PyD^+ . Figure 2.28 illustrates the results that were obtained [389, 461]. Spectrum 2 demonstrates that on these surfaces Py is adsorbed both on Lewis (1450 and 1615 cm^{-1}) and Brønsted (1540 cm^{-1}) acid sites. The absorption band at 1540 cm^{-1} attributed to PyH^+ indicates that either deuteration was not complete or that Py dissociation occurs with formation of H^+ sites. D_2O adsorption at 293 K and further evacuation at the same temperature leads to the emergence of the 1200 and 2600 cm^{-1} absorption bands in spectrum 3. These two bands represent the bending and stretching vibrations of D_2O , most likely adsorbed on the Lewis acid sites. When pyridine is adsorbed on an oxide surface with pre-adsorbed D_2O (spectrum 4), the PyH^+ concentration decreases (the 1540 cm^{-1} intensity decreases), and the concentration of PyD^+ ions grows (the relative intensity of the 1490 cm^{-1} absorption band increases). The relative intensities of the 1450 cm^{-1} absorption band in spectra 2 and 4 are almost the same. Hence, the amount of Py adsorbed on Lewis acid sites remains constant, that is, pyridine displaces water from the Lewis acid sites. Disappearance of the 1200 cm^{-1} absorption band and a considerable decrease in the 2600 cm^{-1} band intensity is also indicative of Py substitution for water.

Thus, despite incomplete deuteration, a considerable amount of pyridine is combined in the PyD^+ form, which unambiguously points to the presence of D^+ ions on the surface of the sample. The degree of deuteration can be raised by increasing the number of cycles of D_2O treatment of the sample at elevated temperatures. Such treatment increases the intensities of the PyD^+ form but decreases the intensities of the PyH^+ absorption bands, i.e. pyridine dissociates only insignificantly, if at all. These data indicate that the coordinated water is not a carrier of the protic acidity since all such water is replaced from the surface by the pyridine molecules. However, after pretreatment by water the number of protic centers has grown due to the dissociation of water and the formation of the additional H^+ (D^+) ions. Hence, the sample contains a large amount of H^+ ions, which, however, do not show up as a discrete maximum in the νOH spectral region, as has been explained earlier in Section 2.2.3.

It was confirmed that the protic acid sites causing ammonia and pyridine protonation contribute to this broad absorption band in the νOH region ($3500\text{--}3600\text{ cm}^{-1}$) obtaining only in DRIR spectra by the appreciable decrease in Brønsted acid sites, as tested by NH_3 adsorption, upon high-temperature (873 K) dehydration of the sample.

Both the considerable heterogeneity of the surface protic sites and the presence of mobile protons in the surface zone may be responsible for the incomplete disappearance of the observed absorption band in the OH region upon 'severe' dehydroxylation (Figure 2.25(b), spectra 2). Slow exchange, leading to incomplete disappearance of the protic acid sites, occurs upon isotopic substitution of the D_2O deuterium for hydrogen in the OH groups. The above data also confirm the presence of mobile protons in the surface zone.

Brønsted acid sites have also been revealed by the adsorption of both ammonia and pyridine on the surface of all acid-forming oxides, such as V_2O_5 , MoO_3 , Sb_6O_{13} and WO_3 themselves, these oxides supported on SiO_2 , Al_2O_3 , and TiO_2 [389], and also compositions including these oxides as components (see Table 2.9). Due to its high basicity and small molecular size, ammonia reveals most acidic sites. For example, NH_4^+ ions were detected by infrared spectra on all three

forms (oxidized, reduced or sulfided) of Mo/Al₂O₃ [390] and Mo/SnO₂ [457] catalysts, while no pyridinium ion was detected, except on the oxidized form. The absence of the pyridine protonation can be connected with a decrease in acidity of the protic centers after reduction and sulfidation.

Various authors [106, 221, 395–397] have shown showed that in the Mo–Si–O, Mo–Ti–O and Mo–Al–O systems the Brønsted acidity could be caused by the formation of poly- and heteromolybdates on the carrier surface (i.e. by the formation of compounds similar to strong acidic heteropoly acids). In the surface layer of the systems involving individual acid-forming oxides, the isopoly-compounds may be formed in the presence of water. These compounds are responsible for the protic acidity [106], which because of their decomposition vanishes upon high-temperature dehydration (>773 K). In other words, isopoly- or heteropoly-compounds on the surface may also be responsible for the protic acidity exhibited by individual acid-forming oxides.

2.3.2 ADSORPTION OF CARBON MONOXIDE

As has been discussed by Davydov [30], chemisorption of carbon monoxide on oxide surfaces occurs with the participation of surface oxygen atoms or ions, surface hydroxyl groups and coordinatively unsaturated surface cations. This molecule has been almost universally used to elucidate the nature of all surface sites. During the interaction of CO with different states of surface oxygen, carbonate compounds are often formed, the structures of which depend on the initial states of oxygen on the oxide surface, which are reflected in the spectral characteristics of the species formed. The interaction of CO with basic hydroxyls produces surface formate complexes, the spectral characteristics and properties of which also correlate with the initial state of the surface hydroxyls [30]. It should be taken into account that these reactions lead to the reduction of the surface, and correspondingly influences the properties of the surface cations. Spectral characteristics of these carbonate and formate compounds are presented and discussed in the literature [18–20, 30], and are also examined in Section 2.3.6, which is devoted to the adsorption of CO₂ itself.

Interaction with cations

Carbon monoxide has a special ability as a probe molecule, because of its small size and very simple ν CO spectrum. Using CO, it is possible to investigate the state of supported metals, as well as acid sites (see [27, 30, 31, 34a] and Chapter 3). Carbon monoxide can behave as either an acid or a base on metal oxide surfaces because both acidic and basic sites are present on them. To identify surface sites, it is better to adsorb the CO molecules at low temperatures since the corresponding surface complexes are unstable (heats of adsorption are 20 to 70 kJ mol⁻¹). Carbon monoxide molecules have been most often used to investigate the Lewis acid sites of coordinatively unsaturated surface cations, although identification of their type is combined with certain difficulties. This is why it is useful to vary the CO surface coverage widely when a new system is being investigated. The dependence of the spectra on the surface coverage, plus data based on isotopically substituted CO molecules, permit the elucidation of the resonance interactions between vibrating dipoles and the effects of induced heterogeneity, i.e. weakening of the electron-acceptor properties of the cations, by the occupation of adjacent sites by adsorbed molecules, as has been shown for Zn²⁺ ions [466]. It is known that the frequency of the stretching vibrations of the carbon–oxygen bond in the gaseous-phase CO molecule occurs at 2143 cm⁻¹. In accordance with traditional views on the structure of homogeneous metal carbonyls, the binding occurs via a σ -bond (donor–acceptor) between the filled CO σ -orbitals, normally the lone-pair orbital or the carbon atom and an unfilled metal d-orbital. In some cases, the bond is strengthened by back donation from the filled metal d-orbitals to the vacant CO π^* -orbital (Figure 2.29).

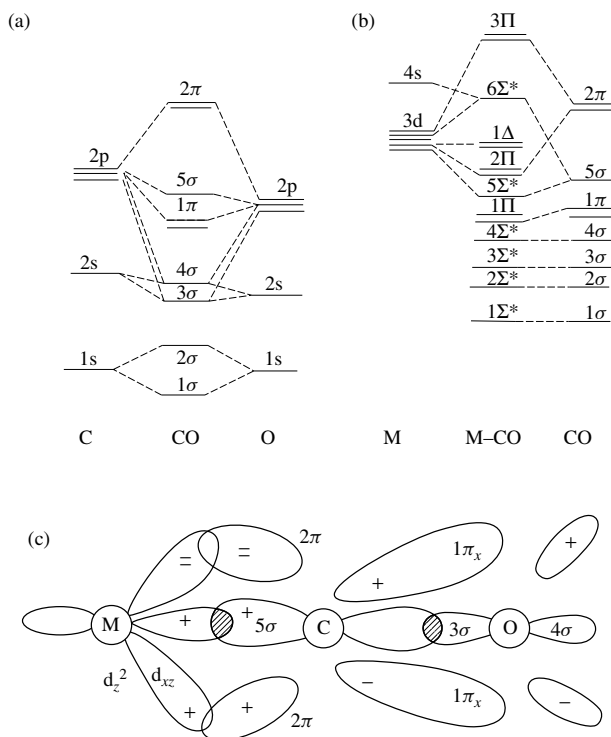


Figure 2.29. Scheme of CO molecular orbitals.

It was earlier established by IR spectroscopy that CO molecules interact with coordinatively unsaturated cations, including those in zeolites [18–20, 22, 23, 30, 31, 34a, 38, 49, 51, 55–57, and references therein]. Absorption bands in the region above the gas-phase ν_{CO} value high frequency (HF) band in the infrared spectra of carbon monoxide adsorbed on zeolites can show interaction with different cations. The dependence of the frequency of this absorption band on the cation indicates that the complex between the adsorbed CO molecules and the cations has a linear structure of the type M–CO. The frequency shift above the gas-phase value increases with increases in the ratio of charge to cation radius. A shift in the absorption band in this direction is seldom observed in physical adsorption. Although binding in such complexes most often involves the unshared electron pair at the C atom, in a few cases a low temperature adsorption via the lone pair at the oxygen atom has been observed, with band shifts in the opposite direction (LF band) (see sections 3.1 and 3.2 and [326, 461b, 461c, 461d and references therein]). A low-frequency band is observed in the region of 2100–2130 cm^{-1} . Several authors have pointed out that this LF band could be assigned to the C–O stretching mode of $\text{Me}^{n+} \dots \text{OC}$ adducts. The formation of such species would lead to a bathochromic shift of the CO stretching frequency. It has been shown [461d] that there is an isomerization equilibrium $\text{Z-Na} \dots \text{CO} = \text{Z-Na}^+ \dots \text{OC}$ with the enthalpy of 3.8 kJ/mol in the case of NaZSM zeolites.

Formation of the adsorbed CO σ -complexes (with absorption frequencies above those of gaseous CO) was first established directly by using ESR and IR spectroscopies [462]. Photoelectron spectroscopy has also provided direct experimental data establishing that the surface bonding between CO and the coordinatively unsaturated surface Zn ions of ZnO at room temperature occurs via the C atom. The bond is formed with participation of the CO 5 σ molecular orbital

[463–465]. As only one absorption band at 2190 cm^{-1} is observed in the IR spectra of ZnO after adsorption of CO at 293 K, this relates to the data obtained for the single CO surface complex studied by photoelectron spectroscopy. The high frequency of the adsorbed CO absorption band can be explained on the basis of the above-described electronic structure of homogeneous carbonyls provided that, in these cases, i.e. on cations, the donor–acceptor bond with surface cations is primarily ‘sigma’ in nature. In relation to the concern of some workers [88], who believe that the coordinative binding has need of the π -component for stabilization, it is noted that the complexes with high-frequency maxima are relatively unstable and as a rule are removed by degassing at room temperature. They are usually formed only under a CO atmosphere after high-temperature treatment of the oxide surface *in vacuo*. The latter is often necessary to uncover the coordinatively unsaturated ions on the surface by removing surface impurities. In the presence of some other ligands (e.g. water), their formation can be totally suppressed, as will be shown below.

When $d \rightarrow \pi^*$ donation takes place, the CO molecule is partially bound to adsorption sites by the use of occupied d-orbitals, and typical carbonyl complexes are formed, for which νCO is lowered compared to $\nu\text{CO}_{\text{gas}}$. Carbon monoxide absorptions in such complexes are usually detected below 2100 cm^{-1} . Examination of the nature of the binding in $M^{n+}\text{CO}$ complexes suggests that the frequency of adsorbed CO (νCO) should depend on the valence and coordination states of the cations, that is, on their abilities to accept σ -donation (increasing νCO) and to donate π -orbitals of the CO (decreasing νCO , as for carbonyl complexes). Carbonyls involving π -donation can have different structures – linear or bridged – and the number of metal atoms bonded to the CO molecule can also be different. The νCO in such surface complexes occur in different regions: linear at $2100\text{--}1900\text{ cm}^{-1}$, bridged below 1900 cm^{-1} , and three-coordinated bridged below 1800 cm^{-1} [18–31, 55]. Complexes involving cations can only be linear (terminal) because in an M–O–M situation the distance between cations is too great to form a bond between a CO molecule and two cation sites simultaneously. In the presence of two free coordination places, the dicarbonyl complexes are easily formed.

SiO₂, zeolites

At low temperatures, carbon monoxide undergoes H-bonding interactions with surface OH groups. Simultaneously, the CO stretching mode was observed at ca. $2150\text{--}2160\text{ cm}^{-1}$ (Figure 2.30, spectrum 2). The results indicate [34a] that the low frequency shift of νOH due to the interaction correlates with the sequence of acid strength of hydroxyls, thus allowing use of this molecule to measure the acidity of OH groups. Another important feature of the CO low temperature interaction is possibility to detect the presence of weak electron-acceptor centers on the surface (Figure 2.30 spectrum 2) which do not interact with CO at ambient temperature.

The hydroxyl groups of nonporous SiO₂ and Na- and Al-free silicalites (both isolated and terminal Si–OH) located in the microcavities are selectively perturbed by CO [320]. The original bands are progressively removed and new ones are generated at lower frequencies. For the silicalites, the hydroxyls in the terminal position at 3704 cm^{-1} are consumed first, giving a replacement peak at 3582 cm^{-1} (downward shift, $\Delta\nu = 120\text{ cm}^{-1}$), while the isolated hydroxyl groups at 3742 cm^{-1} are consumed at higher CO pressures, giving a peak at 3637 cm^{-1} ($\Delta\nu = 100\text{ cm}^{-1}$). The band from the hydrogen-bonded hydroxyls is not substantially eroded when CO is dosed but new hydrogen-bound adducts are formed on the terminal OH groups. The νCO band at 2156 cm^{-1} is associated with the formation of 1:1 adducts with isolated and terminal groups. The 2138 cm^{-1} peak corresponds to CO physically adsorbed on channel walls and is analogous to that observed in the spectra of liquid and/or solid CO. When probed with a weak Lewis base, such as CO, hydroxyl groups only form stable hydrogen-bound adducts at 77 K [321].

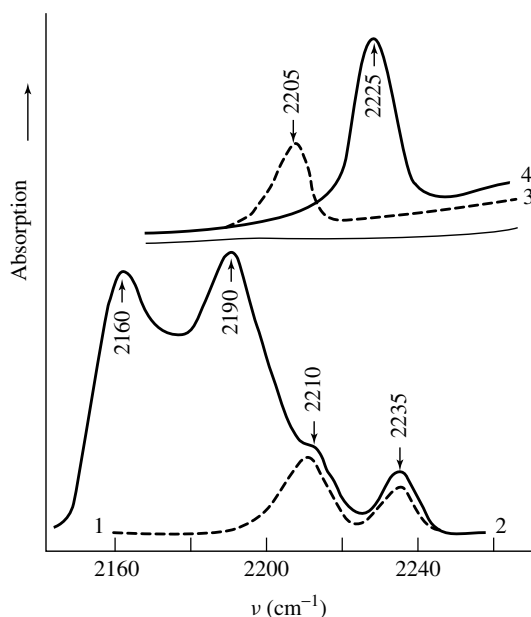
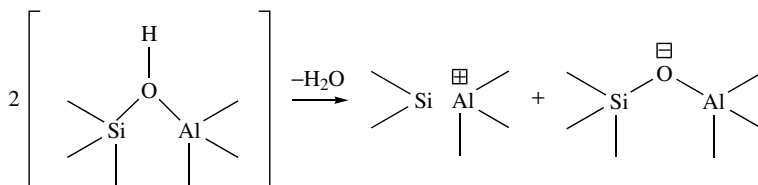


Figure 2.30. IR spectra of CO adsorbed at 293 K (1, 3, 4) and 173 K (2) after dehydration at 773 K: (1, 2) γ - Al_2O_3 ; (3) γ - $\text{Al}_2\text{O}_3/\text{NaOH}$; (4) HY zeolite.

The νOH bands at $3670\text{--}3665\text{ cm}^{-1}$ and $3625\text{--}3610\text{ cm}^{-1}$, assigned to acidic OH groups in zeolites, are changed by CO adsorption with the formation of two new bands at 3450 and 3275 cm^{-1} ($\Delta\nu = 220\text{--}215$ and $350\text{--}325\text{ cm}^{-1}$, respectively) [330].

Lewis acidity is generated when zeolites are dehydroxylated during thermal pre-treatment or activation. The mechanism of this process can be represented by the following scheme:



Scheme 2.21

'Nonframework' aluminum species are the source of Lewis acidity in zeolite Y. Support for this view comes from IR spectroscopic data (Figure 2.30): the band at 2222 cm^{-1} in the spectra is from CO adsorbed on three-coordinated aluminum ions [30, 468]. For H-ZSM-5, the situation is less clear because both dislodged aluminum and trigonal framework species (Al and Si^+) can be Lewis acidic sites [469–472]. Moreover, a band at 2178 cm^{-1} is associated, according to Zecchina and co-workers [487], with $\text{Na}^+ \cdots \text{CO}$ adducts formed by the interaction of CO with residual Na^+ ions (Table 2.11).

The νCO values in complexes of CO with cations occupying different positions in the zeolite lattice (see Figure 2.2) depend on the type of cation, its position in the zeolite and also on the degree of clustering. The νCO values in CO complexes with cations located in different positions

Table 2.11. Spectral features of CO adsorbed on the surfaces of various oxide systems.

System and Treatment conditions	ν CO	Center ^a	Reference
SiO ₂ Dehydrated at 773 K	2156	SiOH	330
HNaZSM-5	2138	Physisorbed	330
	2175–2168	Si(OH)Al	
HNaY	2225	Al _{cut} ³⁺	30
	2178	Na ⁺ –CO	
Al ₂ O ₃	2235, 2210	Al _{cus(cut and cuo)} ³⁺	30
Al ₂ O ₃	2160	OH· · CO	27
Dehydrated at 773 K	2178–2182	Al _{cuo} ³⁺	
CO adsorption at 190 K	2195–2215	Al _{cut} ³⁺	
	2235–2245	Al _{3+def, cut}	
Al ₂ O ₃ treated by NaOH	2205–2210	Al _{cuo} ³⁺	30, 473
TiO ₂ (anatase)	2188, 2208	Ti _{cus} ⁴⁺	188, 303, 304, 376, 378
	2115	Ti _{cus} ³⁺	
	2205	Ti _{5C} ⁴⁺	
	2190	Ti _{4C} ⁴⁺	
MgO	2200	Mg ²⁺	474–478
CuO, Cu ₂ O	2115	Cu ¹⁺ from Cu ²⁺ in planar form	479, 480
	2145	Cu ¹⁺ from Cu ²⁺ in pyramidal form	
Cu film (oxidized)	2135, 2113	Cu ¹⁺ –CO	37
CuCr ₂ O ₄	2120, 2160	–	190
	2190	Cr ³⁺ –CO	191
CuCr ₂ O ₄ /Al ₂ O ₃	2150	Cu ¹⁺ –CO	
	2200	Cr ³⁺ –CO	
CuO/Al ₂ O ₃	2130	Cu ¹⁺ –CO	479, 481
CuO/SiO ₂	2212–2190	Cu ²⁺ –CO	
	2140–2110	Cu ¹⁺ –CO	
	<2100	Cu ⁰ –CO	
Cu(II)/SnO ₂ oxidized at 638 K	2121	–	482
Ag ₂ O/Al ₂ O ₃	2170	Ag ¹⁺	30
ZnO	2191	Zn ²⁺	
ZnO	2148	–	466
CO adsorption at 77 K	2168	ZnOH· · CO	
	2192–2178	Zn ²⁺ –CO	
ZnCr ₂ O ₄ , Oxidized	2210	Cr ³⁺ CO	
Reduced	2170	Cr ²⁺ CO	193
ZnO.ZnCr ₂ O ₄ Oxidized	2210, 2150		
Reduced	2185, 2100–2110	Cr ²⁺ CO, Zn ⁺ CO	193
Co ₃ O ₄	2190, 2180	Co ²⁺ CO	242, 243

(continued overleaf)

Table 2.11. (continued)

System and Treatment conditions	νCO	Center ^a	Reference
Co/SiO ₂	2177	Co ²⁺ CO	483
NiO	2190	Ni ²⁺ -CO	30
NiO (nearly stoichiometric)	2125, 2075 1970 1910, 1880	Ni(CO) _x Ni(CO) ₂ or Ni(CO) ₃ Ni · · · CO Ni ₂ CO and/or NiCO	30, 92
Fe ₂ O ₃ evacuated at 723 K	2170	Fe ²⁺	207, 208
Fe/Al ₂ O ₃ evacuated at 723 K	2180	Fe ²⁺ CO	30, 207, 208
Fe(II)/SiO ₂	2172	Fe ²⁺ CO	467
BeO	2193, 2203	Be ²⁺	301
Ga ₂ O ₃	2167	Ga ³⁺	301
ZrO ₂	2183, 2203	Zr ⁴⁺	301
NiO-MgO-MoO ₃	2190	Ni ²⁺	30
CoO-MgO-MoO ₃	2190	Co ²⁺	30

^aCus, coordinatively unsaturated site; cut, coordinatively unsaturated tetrahedral site; CuO, coordinatively unsaturated octahedral site; def, defected.

of the zeolite lattice are different because of their different coordination states. In addition to linear carbonyl complexes with cations in different crystallographic positions in zeolites or on the oxide surface, CO can also form dicarbonyl or even polycarbonyl complexes (see Tables 2.11 and 3.10) due to additional vacancies in the coordination sphere of some cations. This is especially characteristic of reduced states of cations, the coordination sphere of which is pure in oxygen. The formation of dicarbonyls leads to both an increase in the extinction coefficient and to the appearance of two absorption bands instead of the single one observed for monocarbonyl complex. One of these bands is shifted to high, and the other to low frequencies compared with the band in a monocarbonyl compound. The interaction of CO with acidic hydroxyl groups in H-mordenite and with extraframework cations in alkali-metal-exchanged X-mordenite (X = Li, Na, K, Rb, Cs) has been studied by means of FTIR spectroscopy [487]. The dipolar CO molecule was found to interact specifically with extraframework metal ions located at two different sites, i.e. the main channels and the side pockets. For cations inside the main channels of the zeolites, the νCO values increase continuously from 2155 cm⁻¹ for Cs⁺ up to 2188 cm⁻¹ for Li⁺. Cations located at the bottom of the side pockets were found to induce smaller shifts. The observed frequency shifts have been used to evaluate the electrostatic field inside the main channel created by the extraframework cations. Values in the range of 2–8 V nm⁻¹ were obtained. Nonspecifically adsorbed (physisorbed) CO was also observed, giving rise to a complex IR absorption band at about 2138 cm⁻¹.

Oxides

The adsorption of CO on numerous oxides has been investigated in order to identify the Lewis acid sites. Some of the data obtained are presented in Table 2.11. It can be seen from this table that coordinatively unsaturated ions are observed on the surfaces for the majority of the systems investigated. In the case of a large number of systems, several types of Lewis acid sites are observed. To describe the detailed structure of the surface and active surface sites, examination of such systems has been made on the basis of both the crystallographic structure of the oxides

and data obtained for the number and properties of hydroxyl groups. In the first case, this has been carried out for Al_2O_3 .

Alumina

There are a number of studies in the literature of the interaction of CO with aluminas at different temperatures [27, 30, 298–301, 473]. There are no doubts that the strongest centers of the alumina surface indicated by the CO adsorption (the band at 2235 cm^{-1}) are due to $\text{Al}^{3+}_{\text{cus}}$ ions [27, 30, 53]. Detailed investigations showed that these centers are involved in the so-called ‘X-centers’, the concentrations of which are small (about 10^{16} centers m^{-2}). X-centers are acid–base pairs, e.g. $\text{Al}^{3+}_{\text{cut}}\text{O}^{2-}$. Support for this assignment comes from the absence of dissociative adsorption of both ammonia and propene [30, 473] upon their adsorption on Al_2O_3 samples treated with NaOH. The band at 2235 cm^{-1} , characteristic of the strongest centers of the alumina surface, is not obtained for the latter types of sample. Data on H_2 adsorption (Section 2.3.3) also confirm such an interpretation. Taking into consideration both the nature and concentration of these centers it becomes clear that they occur at defect sites. The nature of the complexes characterized by the absorption band at 2215 cm^{-1} which is also observed upon CO adsorption at room temperature, is not so clear. However, they are probably also due to the presence of $\text{Al}^{3+}_{\text{cut}}$ ions [27].

A comparison of the spectra of CO adsorbed on Al_2O_3 at different temperature is shown above in Figure 2.30. At room temperature, two bands at 2210 and 2235 cm^{-1} are identified [30], while as the CO pressure increases, the intense absorption of CO in the gas phase appears in the 2100 – 2200 cm^{-1} region so that it is difficult to identify the weakly bound complexes on the surface with the lower-frequency bands [473]. On saturation of the surface at low temperature, three new bands appear in the spectrum. One of these belongs to physically adsorbed CO because its position corresponds to that in the gas and liquid states of the molecule: $\nu\text{CO} = 2140$ – 2150 cm^{-1} . The 2160 cm^{-1} band corresponds to CO adsorbed on OH groups through hydrogen-bonding because there is a decrease in the intensity of the original OH groups with the simultaneous appearance of lower-frequency νOH bands. Similar results have been obtained by Zaki and Knozinger [455]. Bands in the region above 2180 cm^{-1} belong to the complexes of CO with Lewis acid sites [30, 298, 301, 455]. Thus, the bands in the 2195 – 2210 cm^{-1} (species $(\text{CO})_{\text{A}}$), 2215 – 2220 cm^{-1} (species $(\text{CO})_{\text{B}}$) and 2235 – 2240 cm^{-1} (species $(\text{CO})_{\text{C}}$) regions are assigned to the presence of coordinatively unsaturated tetrahedral Al^{3+} ions. The higher-frequency $(\text{CO})_{\text{C}}$ and $(\text{CO})_{\text{B}}$ bands have been assigned to two families of sites involving $\text{Al}^{3+}_{\text{cut}}$ ions located in crystallographically defective configurations, and the lower-frequency adsorbed species $(\text{CO})_{\text{A}}$ to sites involving particularly exposed $\text{Al}^{3+}_{\text{cut}}$ ions located in extended areas of regular low-index crystal planes [27].

It should be pointed out that Morterra and Magnassa [27] have suggested that $\text{Al}^{3+}_{\text{cuo}}$ ions located in octahedral positions cannot be coordinatively unsaturated and adsorb CO. The absence of absorption bands in the IR spectra of CO adsorbed on oxidized $\alpha\text{-Fe}_2\text{O}_3$ [207, 208] and $\alpha\text{-Al}_2\text{O}_3$ [485, 488, 489] provides evidence for this suggestion. However, according to calorimetric data [488], there is a form of adsorption of CO with a heat of adsorption of around 36 kJ mol^{-1} in the case of $\alpha\text{-Al}_2\text{O}_3$. Such a value corresponds to the absorption band at about 2170 – 2180 cm^{-1} which was not observed for these samples, probably due to their low specific areas ($S_{\text{sp}} = 2\text{ m}^2\text{ g}^{-1}$) and small number of such active centers.

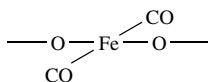
In several studies (see, for example, [298, 299]) the existence of a great number of Lewis acid sites, including three-, four- and five-coordinated Al^{3+} cations, as well as pairs of Lewis acid sites which form upon the removal of a bridge oxygen atom, has been analyzed. Borovkov *et al.* [490] observed two bands in the 2210 – 2215 cm^{-1} region and at 2245 cm^{-1} in the infrared spectra of CO adsorbed on different Al_2O_3 samples. The high-frequency band is attributed to CO molecules adsorbed on α - or X-centers, which include the Al^+O^- acid–base pairs.

The concentrations of the different surface centers are important characteristics, and many authors have tried to estimate these by different ways, including IR spectroscopy of adsorbed CO. The Lewis acid site concentration on transition aluminas is quite high, depending on the degree of dehydration, and amounts to 0.015–0.03 sites nm^{-2} . Knozinger and Ratnasamy [53] have given value of about 0.1 sites nm^{-2} . According to Morterra and Magnassa [27], the concentration of Lewis acid sites on $\gamma\text{-Al}_2\text{O}_3$ activated at 773 K equals 0.1 molecules nm^{-2} and 0.23 molecules nm^{-2} on alumina activated at 1023 K. The distribution among the different sites is 0.14 molecules nm^{-2} of strong acid Lewis sites on the crystal planes, about 0.06 molecules nm^{-2} for strong Lewis acid sites in crystal defects, and about 0.03 molecules nm^{-2} for the strongest and more defective sites. The maximum concentration of pyridine strongly adsorbed onto the $\text{Al}^{3+}_{\text{cut}}$ ions (derived from the band at 1625 cm^{-1}) is three to four times larger than the maximum overall CO uptake obtainable at 300 K.

Fe_2O_3

In the case of an oxidized Fe_2O_3 surface, only coordinatively unsaturated octahedral Fe^{3+} ions are expected to act as Lewis acid sites. Shepot'ko and Davydov [207, 208] have suggested that such ions do not coordinate CO at room temperature, in contrast to NH_3 and NO (the so-called 'structural flexibility' of the surface). Thus, the Fe^{3+} ions are coordinatively saturated when compared to adsorption of weak electron donors such as CO. The Fe^{2+} ions present on the surface of Fe_2O_3 after reduction, adsorb both CO (2200 cm^{-1}) and NH_3 .

Rebensdorf and Larsson [467] detected a band near 2171 cm^{-1} after adsorption of CO on silica-supported iron oxide at temperatures below 260 K. By varying the experimental conditions, these authors established that the ratio of adsorbed CO was close to two CO molecules per Fe^{2+} cation and suggested that the 2171 cm^{-1} band should be assigned to the following structure:



Scheme 2.22

A shoulder near 2165–2169 cm^{-1} , only observed upon low-temperature adsorption for an oxidized sample, has been attributed to CO adsorbed on coordinatively unsaturated Fe^{3+} species.

A set of data concerning the infrared spectra of CO, NO and NH_3 adsorbed over $\alpha\text{-Fe}_2\text{O}_3$, $\text{Fe}_2\text{O}_3/\text{Al}_2\text{O}_3$ and FeY zeolites [30, 207, 208, 491] established that both the isolated Fe^{2+} and Fe^{3+} ions, and also the paired-centers $\text{Fe}^{2+}\text{OFe}^{2+}$, $\text{Fe}^{2+}\text{OFe}^{3+}$, and $\text{Fe}^{3+}\text{OFe}^{3+}$, exist on the surface. The change in the value of the νCO in the $\text{Fe}^{2+}\text{-CO}$ complex depends on the environment and increases the number of $\text{Fe}^{2+}\text{OFe}^{2+}$ in paired centers. Carbon monoxide is not stabilized on Fe^{3+} ions, whereas isolated Fe^{2+} ions in the complexes are characterized by νCO at 2195–2205 cm^{-1} . The band $\nu\text{CO} \sim 2185\text{--}2175 \text{ cm}^{-1}$ is characteristic for the nonisolated Fe-O-Fe (clustered) ions, which have the highest reactivity and are easily reduced, thus forming sub-carbonyl complexes of the type $\text{Fe}_n^0(\text{CO})_m$ with $\nu\text{CO} \sim 2060, 2030$ and 1980 cm^{-1} [192].

In the case of the $\text{Fe}_2\text{O}_3/\text{ZrO}_2$ system [492], FTIR spectra of adsorbed CO were used as fingerprints of the degree of reduction of iron oxidation in the system. Carbon monoxide was not adsorbed on oxidized samples, but depletion of oxygen *in vacuo* from samples reduced at 500 K produced coordinatively unsaturated iron sites, hence resulting in reversible adsorption of CO. Reduction at 623–773 K produced a highly dispersed, oxygen-deficient FeO-like surface phase. The oxide-support interaction hindered further reduction of FeO to metal. Even at 773 K, small iron carbonyl clusters were formed, but very little Fe^0 . Oxidation at 300–473 K fully reversed the reduction process.

Cr_2O_3

There is no CO adsorption on oxidized samples of α - Cr_2O_3 [179, 184], in contrast to the cases of ammonia and pyridine. This fact indicates that the surface of Cr_2O_3 is coordinatively saturated in relation to CO adsorption. A weak band at 2220 cm^{-1} , observed for several oxidized samples of Cr_2O_3 , most probably characterizes coordinatively unsaturated Cr^{4+} ions. Coordinatively unsaturated Cr^{3+} ions (four-coordinated Cr^{3+} as well as five-coordinated Cr^{3+}), which are in principle able to adsorb CO, are oxidized by oxygen and do not adsorb CO. Upon reduction, an intense band of adsorbed CO, characteristic of νCO in the $Cr^{3+}_{cus}-CO$ complex, is observed at $2190-2200\text{ cm}^{-1}$, depending on the coverage. The appearance of this band seems to be stimulated by the reduction of the chromium ions in the highest oxidation states. A further increase of the degree of reduction leads to a lower-frequency band which appears at 2170 cm^{-1} . This band's intensity indicates that there is a stronger $d \rightarrow \pi^*$ interaction in the new $Cr-CO$ complex with respect to that of the $Cr^{3+}_{cus}-CO$ complex. This fact, together with the data for CO adsorption on a sample of Cr (0.1 %)/ SiO_2 for which the band at 2175 cm^{-1} was observed on a sample which had been fully reduced up to Cr^{2+} (established by ESR spectroscopy), allowed the attribution of the 2170 cm^{-1} band to the $Cr^{2+}_{cus}-CO$ complex [184].

Using IR spectroscopy, Zecchina *et al.* [493] studied the reversible interaction of CO with the surface of a 0.5 % Cr/SiO_2 catalyst at 293 K and found bands at 2181, 2186 and 2191 cm^{-1} , plus a very weak one at 2095 cm^{-1} . The triplet was assigned to the stretching mode of a 1:1 linear CO complex formed on paired centers of Cr^{3+} ; bands from isolated Cr^{3+} ions were not been observed. There are no doubts that the chromium ions form carbonyl and even dicarbonyl complexes (see Table 3.10); however, a reliable interpretation of the spectra of adsorbed CO seems to be impossible without data on both the degree of oxidation and cluster formation (two or more Cr ions containing oxygen which do not belong to the support) of the chromium ions. Such an interpretation will be presented in the next chapter.

There are literature reports of the formation of dicarbonyl complexes (see Table 3.10) upon CO adsorption in the case of chromium, as well as on vanadium, molybdenum and other cations (Re, Ru, Rh and W), on various supports. However, because of the different cluster formations of these cations, it is difficult to identify the spectra of adsorbed CO without analysis using other methods (see Chapter 3).

TiO_2

As has been shown by Davydov and co-workers [30, 188], by using the infrared spectra of adsorbed CO, one or two types of Ti^{4+}_{cus} ions occurring in different stoichiometric surrounding can be found on the TiO_2 surface depending on the morphology. These ions are characterized by absorption bands at 2189 and 2205 cm^{-1} . Tanaka and White [378] observed additional bands, indicating that the CO molecules are oxidized to form adsorbed carbonates. This finding is in disagreement with later data [188] where CO oxidation did not occur and only $Ti^{4+}-CO$ complexes were observed at 295 K (α and β Ti^{4+} sites).

In a study by Busca *et al.* [304], the Lewis acids centers were correlated with titanium ions with different coordination numbers and in different valence states (Ti^{3+} and Ti^{4+}). Identification of the behavior of the oxidized and reduced samples indicates that the observed acid centers should be correlated with coordinatively unsaturated Ti^{4+} ions. There are four to seven Ti^{4+} ions per nm^2 on the surface of anatase, which is larger than the number of centers which were found in later studies [188].

To establish the nature of the active centers, different investigators have examined the structures of several faces of anatase [188, 302, 304, 309, 310, 319] and rutile [307, 310, 319, 496]. The study [188], in which samples with different morphologies were investigated, is of particular interest because of certain predominantly exposed facets. According to Ormont [99], anatase

crystallizes in a tetragonal lattice. The coordination number of titanium in the bulk is equal to six, and that of oxygen is three. The faces (101) and (001) principally occur on the surface, although (100), (010), (111) and (113) can be exposed to a smaller degree [187]. While these same faces are characteristic of the surface of the microcrystal, the concentrations of ions located on the edges and corners will also be significant and can attain values of several % [185]. The surface atomic arrangements characteristic of anatase are shown in Figure 2.31.

In consideration of the second coordination sphere, the coordinatively unsaturated titanium ions on the clean surface of anatase can be divided into several types (Table 2.12). In this table,

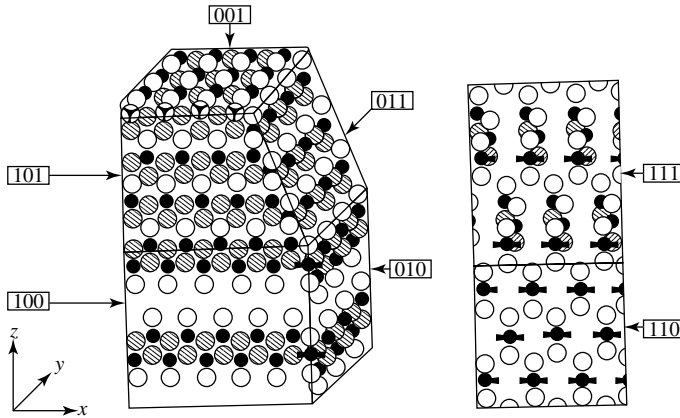


Figure 2.31. Scheme of an anatase crystal with different exposed faces: \odot – $\text{Ti}_{\text{cus}}^{3+}$ ions; \bullet – five-coordinated Ti^{4+} ; \bullet – four-coordinated Ti^{4+} ; \circ – two-coordinated O^{2-} ions; \otimes – three-coordinated O^{2-} ions.

Table 2.12. The basic surface forms characteristic of anatase.

State of Ti	Facets	Edges	Apices
$\text{Ti}^{4+}(1-1-1-0-0)$	–	(001) × (100)	–
	–	(001) × (010)	–
	–	(001) × (101)	–
	–	(001) × (011)	–
$\text{Ti}^{4+}(1-1-0-0-0)$	(001)	(101) × (011)	(101) × (011) × (101) × (011)
	(111)	–	–
	(112)	–	–
	(113)	–	–
$\text{Ti}^{4+}(1-0-0-0-0)$	(101), (011)	(100) × (101)	–
	$\nu\text{CO } 2190 \text{ cm}^{-1}$ (type I)	(100), (010)	(101) × (101)
$\text{Ti}^{4+}(1-1-0-0)$	(110)	(100) × (010)	(100) × (010) × (101) × (011)
	$\nu\text{CO } 2205 \text{ cm}^{-1}$ (type II)	(111)	(110) × (100)
	–	(110) × (010)	–
$\text{Ti}^{3+}(1-1-0-0)$	–	(110) × (111)	–
	–	(001) × (111)	(001)
	–	(001) × (112)	–
$\text{Ti}^{4+}(1^{\text{OH}}-1-1-0-0)$	–	(001) × (113)	–
	$\nu\text{OH } 3755 \text{ cm}^{-1}$	–	–
$\text{Ti}^{3+}(1-0-0-0)$	–	(001) × (100)	–
	–	(001) × (010)	–
$\text{Ti}^{4+}(1^{\text{OH}}-1-0-0-0)$	–	(001) × (101)	–
	$\nu\text{OH } 3665 \text{ cm}^{-1}$	–	–
–	–	(001) × (011)	–

the number of figures in parentheses indicates the number of ligands or the coordination number, while the figures themselves indicate the number of vacancies for each ligand.

Some of the coordinatively unsaturated titanium ions on the surface are apparently inactive with respect to adsorption of NH_3 and CO , are not bound to hydroxyl groups, and exhibit weak electrophilicity. There is a comparatively low concentration of $\text{Ti}^{4+}(1-1-1-0-0)$ on the sample, with $S_{\text{sp}} = 130 \text{ m}^2 \text{ g}^{-1}$, which are not only expected to be inactive: most of the inactive species are $\text{Ti}^{4+}(1-1-0-0-0)$ ions. The titanium ions bound to hydroxyl groups that are similar with respect to their electrophilicity will also be inactive. These latter ions are probably responsible for the other form of CO adsorption observed at 243 K in similar studies [301, 455]. Two other types of coordinatively unsaturated titanium ions are more electrophilic, and they can be bound with two types of Lewis acid centers: type I $\text{Ti}^{4+}(1-0-0-0-0)$, responsible for adsorption of CO with a 2190 cm^{-1} absorption band, and type II $\text{Ti}^{4+}(1-1-0-0-0)$ with νCO at 2205 cm^{-1} . This interpretation is in agreement with the morphology of the samples. A comparison of samples of different specific areas showed that the concentrations of acid–base pairs, and the corresponding type I centers, decrease due to an increase in the concentration of ions localized on the edges. The concentration of type II centers decreases, on the one hand due to the larger number of edges, and on the other hand, due to emergence of facets for which other states of titanium (for example, four-coordinated titanium or titanium from acid–base pairs) are characteristic. The presence of only type II centers on a surface corresponds to the presence of four-coordinated titanium.

Where both types of centers should be observed due to the morphology, an examination of samples indicates that type II Lewis acid centers can be blocked by chlorine ions which are not eliminated by simple washing, so that the cations become inactive to adsorption. The chlorine ions can be eliminated from the surface by prolonged washing with water.

If the extinction coefficient of adsorbed CO is equal to $1.4 \times 10^{19} \text{ cm}^2 \text{ mol}^{-1}$ [30], the number of Ti^{4+} centers is about one to two sites nm^{-2} . Increase of the equilibrium CO pressure or a decrease in temperature leads to a low-wavenumber shift of the corresponding bands [497]. Co-adsorption of ammonia and CO showed that coordinated ammonia does not affect the frequency of adsorbed CO and hence, by implication, the acidity of neighboring sites.

At present, practically all oxides of transition and nontransition metals have been investigated with respect to adsorption of CO (see Table 2.11). The adsorbed CO spectra give information about the presence of coordinatively unsaturated cations on the surface of such systems. In numerous cases, on the basis of these results, together with crystallographic data, detailed structures of the adsorption-active surface sites have been established.

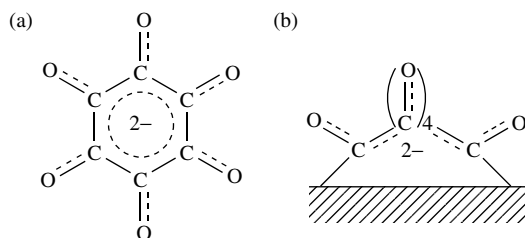
MgO, CaO, BaO and SrO

The interaction of these oxides with CO is very similar. That is why the interaction with MgO as an example is analyzed here.

Carbon monoxide adsorption on MgO at 77 K mainly produces adducts with Mg^{2+} ions exposed on extended plans (absorption bands at 2150 cm^{-1}), edges and corners ($2170\text{--}2200 \text{ cm}^{-1}$) of well formed cubic crystallites. As has previously been noted, the most basic oxides interact with CO to form carbonate species. Carbon monoxide molecules σ -bonded to (or polarized by) Mg^{2+} ions adjacent to anion sites of enhanced basicity (edges, steps and corners) can undergo nucleophilic attack, forming several complex surface species and correspondingly complex spectra are observed. Unambiguous interpretation of these spectra has still not yet been achieved. A typical example is magnesium oxide, which has been much investigated by IR spectroscopy [474–478, 484, 485, 498–503]. In contrast to the results of Smart *et al.* [498], who found only carbonate species after CO adsorption on MgO , Zecchina and co-workers [474–476, 485, 499] observed six adsorbed species by both IR [474, 475] and UV [475, 499] spectroscopy: CO monomer adsorbed on Mg^{2+} ions (species I), two different types

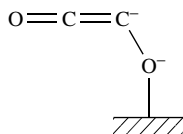
of dimer incorporating ketenic groups (species II and III), a hexamer with a negatively charged ring structure (species IV), a $(\text{CO})_2^{2-}$ dimer (species V), and various carbonate-like structures (species VI). Later [476], it was shown that the first product formed upon interaction of CO with a fully dehydroxylated surface of MgO is the CO_2^{2-} species, which is generated by nucleophilic attack of a surface O^{2-} on a CO molecule initially weakly σ -bonded to a Mg^{2+} cation in an adjacent position. The CO_2^{2-} species generates $\text{C}_3\text{O}_4^{2-}$ by the addition of two CO molecules. The type of species present depends on the temperature, e.g. at 347 K the trimeric species (and unreacted CO_2^{2-}) are the most abundant components.

The following types of structural attributions of surface compounds have been made for the IR spectra of CO adsorbed on MgO [476]. A group of four bands at 1066, 1197, 1275 and 1480 cm^{-1} was associated with anionic pink-colored oxygen-sensitive species, described [474] as either *conjugated cyclic* (Scheme 2.23(a)):



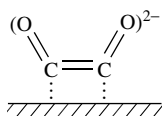
Scheme 2.23

or linear in nature (Scheme 2.23(b), $\text{C}_n\text{O}_n^{2-}$ polymers, where n is predominantly equal to six). Pairs of bands in the 2084–2108 and 1358–1392 cm^{-1} regions have been assigned to the asymmetric and symmetric modes of a ketenic-like dimeric $\text{C}_2\text{O}_2^{2-}$ species:



Scheme 2.24

Pairs of bands at 1160 cm^{-1} and in the 1548–1582 cm^{-1} region were ascribed to a second family of dimers ($\text{C}_2\text{O}_2^{2-}$):



Scheme 2.25

Residual bands were assigned by the authors to oxidation (carbonate-like or carboxylate-like) products. A weak and narrow peak at 2200 cm^{-1} was assigned to CO adsorbed by σ -bonding to Mg^{2+} cations, with the lowest coordination on the surface of the microcrystals (the corner positions).

However, Tsyganenko and co-workers [477, 478] also studied the same adsorption system by using isotopically labeled CO. They assigned the bands in the 2150–2140 cm^{-1} region to nonspecifically adsorbed CO molecules (compound I in Table 2.13). On the basis of the isotopic shifts $^{12}\text{C} \rightarrow ^{13}\text{C}$ and $^{16}\text{O} \rightarrow ^{18}\text{O}$, and calculations of the vibration spectra of the different surface compounds, together with a comparison of the spectra with those of the compound M_2CO_2 stabilized in a low-temperature matrix [504, 505], they deduced the formation of three types of CO_2^{2-} groups (compounds II and III in Table 2.13). The νCO stretching vibrations in such complexes with nonequivalent CO bonds lie in the 1495–1478 and 890–850 cm^{-1} regions. The

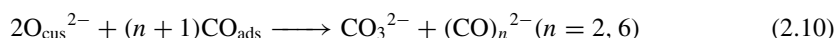
Table 2.13. Positions and isotopic shifts of the IR bands arising after CO adsorption on CaO (after several cycles of adsorption–desorption).

Compound	ν (cm^{-1})		$\Delta\nu$ (cm^{-1})			Proposed structure
	$^{12}\text{C}^{16}\text{O}$ on Ca^{16}O	$^{13}\text{C}^{16}\text{O}$ on Ca^{16}O	$^{12}\text{C}^{18}\text{O}$ on Ca^{16}O	$^{12}\text{C}^{16}\text{O}$ on Ca^{18}O	$^{12}\text{C}^{18}\text{O}$ on Ca^{18}O	
I	2163	48	52	0	–	
	2155	48	52	0	–	
	2145	48	52	0	–	
IIa	1485	32	32	0	–	
	890	20	10	–	–	
	743	3	11	22	–	
IIb	1480	32	32	0	–	
	850	17	0	9	–	
	717	8	4	–	–	
III	1227	32	5	16	–	
	865	15	8	–	–	
	733	5	–	–	–	
IV	1195	10, 29	12, 22	0	–	
	982	12, 22	0	7	7	
V	2038	4, 50, 56	26	0	–	
	1356	–	–	–	–	
	1339	15, 35	0	3	–	
	1300	10, 28, 37	10	2	–	
	1137	5, 20, 23	8	13	–	
	760	–	4	4	–	
VI	1403	38	9	0	9	
	1234	28	16	0	4, 19	
	1135	10, 27	0	0	6	

frequencies of the bands of these compound II are close to those expected for a CO_2^{2-} group with C_s symmetry. The spectral characteristics attributed to the different species discussed in this work [477, 478] are presented in Table 2.13. The experimental data discussed above allow a representation of the main chain of CO transformations on the surface of MgO, CaO, BaO and SrO by the following sequence: $\text{O}^{2-} \rightarrow \text{CO}_2^{2-} \rightarrow \text{C}_2\text{O}_3^{2-} \rightarrow (\text{CO})_n^{2-} + \text{CO}_3^{2-}$ [506]. Tashiro *et al.* [503] have further classified all the spectra from such adsorbed species into five groups, as shown in Table 2.14.

In spite of the different points of view expressed on the structural types of surface compound formed, and also on the natures of the surface centers responsible for their formation, the existence of anionic species at the surface is the main common feature deduced from the spectra of CO adsorbed on the basic oxides [58, 506]. Alternative models involving direct electron transfer from defect sites, the so-named F_s^+ centers, as a result of the interaction of CO with MgO [507], have been substantially rejected by Zecchina *et al.* [508].

It was originally suggested [499, 509], that anionic CO polymers might be produced on these oxides by the following mechanism:



where the carbon monoxide molecules which undergo a disproportionation reaction on coordinatively unsaturated $\text{O}_{\text{cus}}^{2-}$ ions exposed on the surface in corner and edge positions play a key role. Other authors [477, 478, 510] have described the formation of CO_2^{2-} species upon CO adsorption on basic oxides by a different mechanism, as follows:

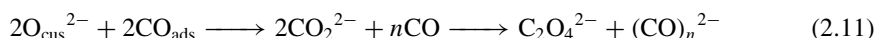


Table 2.14. Adsorbed CO species on MgO [503]. Reprinted with permission from Tashiro, T., Ito, J., Sim, R.-B., Mijazawa, K., Hamada, E., Toi, K., Kobayashi, H. and Ito, T., *J. Phys. Chem.*, **99**, 6115–6122 (1995). Copyright (1995) American Chemical Society.

Species	Desorption temperature (K)	IR band (cm^{-1})	Structure
$\text{K}_0(1)$	170 ^a –210	2147	Linear monomer on Mg^{2+}
$\text{K}_0(2)$	170 ^a –210	2161	
$\text{K}_0(3)$	170 ^a –210	2166	
$\text{K}_0(4)$	170 ^a –210	2184	
$\text{K}_0(5)$	210–230	2200	
K_1	230–240	1315, 1280	Chained ^d monomer on O^{2-}
K'_1	–	1475	Linear monomer on O^{2-}
K_{2A}	400	1615, 1594, 1571, 1473, 1263, 1180	Chained ^d tetramer on O^{2-}
K_{2X}	400	1615, 1594, 1571, 1468, 1263, 1186	
K_{3A}	520	2095, 1520, 1350, 1320, 1155	Linear trimer on O^{2-}
K_{3B}	550	2091, (1570–1540), ^b 1377, 1320, 1169	
K_{3C}	580	2106, (1570–1540), ^b 1365, 1320, 1169	
K_{3X}	550	2106, (1570–1540), ^b 1354, 1320, 1155	
K_{4A}	680	(1450, 1373, 1105) ^c	
K_{4B}	725	(1450, 1373, 1105) ^c	
K_{4C}	790	(1450, 1373, 1105) ^c	

^aDesorption began below 170 K.

^bAssignment of bands in this region to sub-species K_{3B} , K_{3C} and K_{3X} was difficult.

^cAssignment of these three bands to each K_4 sub-species was difficult.

^d'Chained' indicates that the adsorbed species has a chain-like structure with both ends bound to the surface.

Both mechanisms lead to oxidized (CO_3^{2-} , CO_2^{2-} , $\text{C}_2\text{O}_4^{2-}$, etc.) and reduced ($(\text{CO})_n^{2-}$) products and do not require direct electron transfer from the surface to the $(\text{CO})_n$ cluster to form anionic products.

Similar compounds have been observed in cases of the interaction of rare-earth metal oxides with CO, showing that these oxides are strongly basic in comparison with the alkali-earth metal oxides [511–513]. Unlike the above cases, the interactions of solid solutions of transition-metal cations in magnesium oxide with CO are through transition-metal cation clusters on the solid solution surface [479, 484, 514, 515], leading to the formation of monomeric, non-anionic structures with transition metal cations only and so, such systems are described in the sections devoted to corresponding transition metal cations.

ZnO

The spectra of Zn^{2+} -CO complexes in the 2178–2190 cm^{-1} range have been studied as a function of surface coverage [516, 517]. At 77 K, there is only an absorption band at 2148 cm^{-1} from the CO molecules hydrogen-bonded to OH groups, over ZnO. Higher pre-treatment temperatures leads to the appearance of bands at 2190 and 2178 cm^{-1} , and, after the admission of further doses of CO, additional weak bands at 2192 and 2189 cm^{-1} appear in the spectrum. When the surface coverage is large, these bands disappear and new bands are observed at lower frequencies. The data obtained from isotopically substituted molecules revealed the effects of resonance interactions of vibrating dipoles and induced heterogeneity, i.e. the weakening of the electron-accepting properties of the Zn^{2+} ions, as a result of the occupation of adjacent sites by adsorbed molecules. The fine structure in the bands of CO adsorbed on ZnO reflects the process of stepwise occupation of adjacent sites by adsorbed molecules. Both the static and dynamic band shifts appear to be successfully calculated by using equations given in Tsyganenko *et al.* [517]. These results are shown for ZnO and for some other oxides in Table 2.15. The dependence on static and dynamic effects has been shown previously for metals, where such effects were attributed to the resonance interaction of vibrating dipoles [518]. Usually, such vibrational dipolar interactions shift the observed frequencies to higher values. However, in some cases this shift is almost completely cancelled by the ‘chemical shift’ which decreases the CO frequency. These two competitive effects can be distinguished by means of experiments using isotopically substituted molecules. The dipolar resonance interaction in the case of oxides also increases the observed CO frequencies. Unlike with metals, this effect does not dominate the observed frequency shift, but partially compensates the static frequency decrease which occurs with increasing coverage.

Table 2.15. Maximum coverage (θ_{max}) and infrared spectral data (ν) for CO adsorbed at 77 K on various oxides [596].

Oxide	s ($\text{m}^2 \text{g}^{-1}$)	t (K)	θ_{max} (molecules nm^{-2})	ν^* (cm^{-1})			$\Delta\nu^*$ (cm^{-1})	
				ν_0	ν_s	ν_a	$\Delta\nu_{\text{ch}}$	$\Delta\nu_{\text{dyn}}$
ZnO	10	770	2.0	2192	2168	2162	30	6
				2189	2178	2174	15	4
TiO ₂ (anatase)	70	720	2.6	2212	2207	2207	5	0
				2195	2179	2176	19	3
				2180	2176	–	4	–
				–	2164	2161	–	3
BeO	110	870	2.4	–	2151	–	–	–
				2207	2187	–	20	–
				2200	2180	–	20	–

(continued overleaf)

Table 2.15. (continued)

Oxide	$s(\text{m}^2 \text{g}^{-1})$	$t \text{ (K)}$	θ_{max}	$\nu^* (\text{cm}^{-1})$			$\Delta\nu^* (\text{cm}^{-1})$	
				2188	2173	2173	15	0
$\eta\text{-Al}_2\text{O}_3$	70	1070	2.5	2235	—	—	—	—
				2202	2176	2171	31	5
SiO_2	300	870	—	2158	2158	2158	0	0

$\Delta\nu_{\text{st}}$ – the static (or chemical, $\Delta\nu_{\text{ch}}$) shift; $\Delta\nu_{\text{dyn}}$ – the dynamic shift; ν_0 – stretching vibration of isolated CO molecule; $\nu_0 = \nu_{\theta \rightarrow 0}$ (singleton); $\Delta\nu_{\text{dyn}} = \nu_s - \nu_a$; $\Delta\nu_{\text{st}} = \nu_a - \nu_0$; ν_a – the value obtained by the extrapolation of ^{12}CO in the $^{13}\text{CO} + ^{12}\text{CO}$ mixture; ν_s – the value for ^{12}CO adsorbed at the same coverage.

The CO molecule has been used as a probe in a number of infrared studies of CO adsorption on ionic microcrystalline systems [485, 519], and both dynamic and static adsorbate–adsorbate interactions have been studied in detail for ionic crystals such as NaCl, MgO, ZnO [495, 516, 519].

The interaction between adsorbed molecules causes a decrease in the heat of adsorption. The consequential stepwise frequency reduction can be either direct via dipolar resonance or mediated by the adsorbent [516, 517]. When it occurs through the crystal, the induced heterogeneity is due to the weakening of the electron-accepting properties of surface Zn^{2+} ions through CO adsorption on the adjacent sites. Such an interpretation has been confirmed by experiments with ZnO doped by electronegative additives such as Al, Ga and F, so leading to an increase in the coordinatively bound CO frequency (up to 2210 cm^{-1}); after complete occupation of the coordinatively unsaturated sites effected by doping, this band was displaced to $2170\text{--}2175 \text{ cm}^{-1}$. In contrast, Li, when employed as an additive decreases both the CO frequency and the region of frequencies.

Bands at 2178 and 2169 cm^{-1} have been previously assigned to CO coordinated on zinc ions exposed on the two different crystalline faces, (1011) and (1010), respectively [385]. These two bands are drastically reduced in intensity on copper–zinc samples.

ZnCr₂O₄ and ZnO.ZnCr₂O₄

The interaction of CO with oxidized surfaces of these catalysts produces carbonate and formate compounds characterized by absorption in the $1200\text{--}1600 \text{ cm}^{-1}$ region. When the interaction is with reduced surfaces at high temperatures, the formation of carbonates is suppressed, and formates and carbonyls as the predominant surface species are formed by participation of the coordinatively unsaturated cations [193]. The spectral manifestation of carbonyl-like compounds on reduced surfaces depends on the system and on the extent of reduction. Thus, the reduction of ZnCr_2O_4 in CO at only 573 K reduces the chromate ions. When this occurs, a band at 1010 cm^{-1} from $\text{Cr}=\text{O}$ groups disappears and, due to CO adsorption, a new band with ν_{CO} at 2210 cm^{-1} appears in the spectrum. As such bands characteristic of carbonyl complexes have been observed on Cr_2O_3 , it was concluded that these bands imply the reduction of the chromate ions.

The interaction of an oxidized $\text{ZnO.ZnCr}_2\text{O}_4$ catalyst with CO causes the reduction of cations even at room temperature, producing bands at 2210 and 2150 cm^{-1} , shifting to 2185 and 2100 cm^{-1} , respectively, as the temperature of the CO treatment increases. Since no absorption was found at 2100 cm^{-1} on reduced chromium-containing catalysts, and low-frequency vibrations at $2100\text{--}2110 \text{ cm}^{-1}$ are characteristic of the CO molecule stabilized as carbonyl complexes on metal atoms [30], this absorption seems to be due to the formation of $\text{Zn}^{\delta+}\text{CO}$ complexes. The band at 2150 cm^{-1} has been attributed to the Zn^+CO complex. The high-frequency band at 2210 cm^{-1} is associated with a carbonyl complex stabilized on Cr^{3+} ions, and its frequency decreases as the Cr^{3+} ions are reduced to Cr^{2+} with formation of the Cr^{2+}CO complex (absorption band at ca. 2185 cm^{-1}).

CuO

The reduction of CuO starts to occur at 100 K on interaction with CO due to the formation of carbonates [479, 480]. Such an interaction also leads to the formation of the Cu^{1+}CO complex (an absorption band at 2120 cm^{-1}) [520, 521]. When the temperature increases, the $2110\text{--}2120\text{ cm}^{-1}$ band (depending on the coverage) decreases in intensity and splits into two components ($2110\text{--}2115$ and 2145 cm^{-1}).

The CuO lattice has a layered structure – square-planar environment – for the copper ions (state I). As a consequence of the tendency for coordination of copper at the fifth site, it may be assumed that any violation of the periodicity of the CuO lattice, which is equivalent to the appearance of a defect, will result in the appearance of copper ions with square-pyramidal coordination (or a somewhat distorted equivalent), together with copper ions in a square-planar environment (state II). The effective charge on the copper ions in such an environment is obviously somewhat lower than that on the Cu^{2+} ions in pyramidal coordination (in the latter case, the d-electrons participate in bonding with the five oxygen atoms as opposed to the four in the case of the square-planar environment). This should be reflected in the spectroscopic characteristics of the CO and NO probe molecules which are observed.

In the case of $\text{CuO}/\text{Al}_2\text{O}_3$ (8 wt% CuO), when probed with CO, only a state of copper giving $\nu\text{CO} = 2130\text{ cm}^{-1}$ has been detected [480]. This is in agreement with the fact that in such a catalyst copper presents the five-coordinated state (nearly tetrahedral–pyramidal configuration) (state near II) because of its thermodynamically more advantageous configuration. The reduction of copper to the Cu^{1+} state occurs in configuration with the carbonates formation; however, in this case, the carbonates are stabilized on the support due to their higher bonding energy in such a situation. The increase in the value of the effective charge on the copper causes the rise of the νCO frequency which, in the case of the copper ions isolated in the Al_2O_3 matrix, is observed at 2160 cm^{-1} . A more detailed correlation of νCO with the valence and coordinative states of copper is examined in Chapter 3. The dependence of the frequencies of both the CO and NO stretching vibrations in $\text{M}^{n+}\text{--CO(NO)}$ complexes differ substantially depending on the type of compound that contains the cation (the degree of ionicity–covalence of the cation–oxygen bond and the coordination state of the cation). This allows one to consider the possible use of IR spectroscopy to establish the presence of different phases [30, 522]. This is of particular importance for supported systems with a low percentage of the active component, where the use of other conventional techniques for establishing the phase state is impossible or substantially restricted.

We will examine this by using the $\text{CuCr}_2\text{O}_4/\text{Al}_2\text{O}_3$ system and other examples [523]. CO adsorption on such a system at room temperature leads to two absorption bands at ca. 2150 and 2200 cm^{-1} appearing in the IR spectra which characterize the $\text{Cu}^{1+}\text{--CO}$ and $\text{Cr}^{3+}\text{--CO}$ complexes, respectively [523]. The complexes of the first type are evidently formed by the reduction of divalent copper ions from the copper chromite phase. Unlike the case of CuO, this is indicated by the presence of only one absorption band and by the high frequency of νCO in such a complex. This shows a stronger ionic character of the Cu–O bond comparing with CuO due to the presence of chromium ions, manifestations of which are similar to those of the copper ions in copper aluminate [520–522]. The appearance of Cu^{1+} ions due to reduction has also been indicated by the changes in the spectra at different exposure times in CO: the intensity of the band at ca. 2150 cm^{-1} is increased, and absorption bands in the $1200\text{--}1700\text{ cm}^{-1}$ region corresponding to carbonate species were observed. In such a catalyst, a significant portion of the chromium ions is evidently coordinated by oxygen. Only a weak absorption band is observed at about 2200 cm^{-1} .

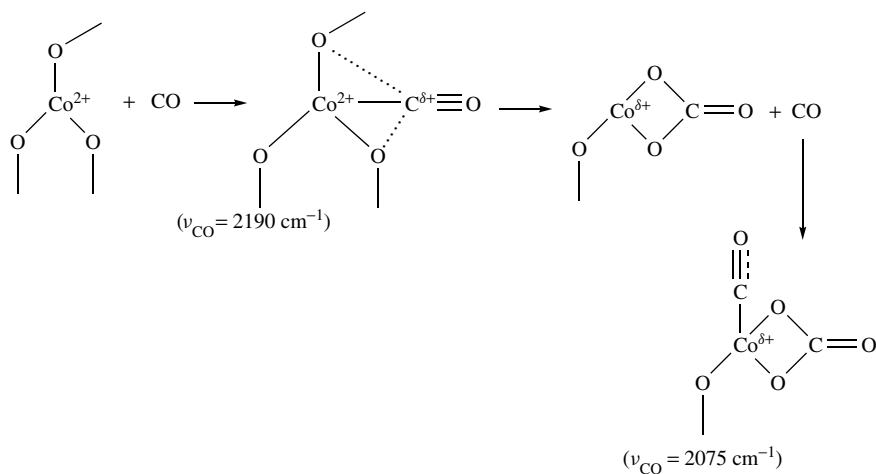
There are several attempts in the literature to represent the structure of surface centers (copper cations) in detail based on the infrared data (see, for example [524]). It should be noted, however, that except for the tendency to change the νCO frequency with the change in coordination number

or oxidation degree, noted above, there is no further spectroscopic evidence available for this purpose and hence any firm conclusions are unlikely to be reached.

In the case of a CuO–MgO solid solution, MgO decreases the effective charge of both Cu^{1+} ($2090\text{--}2110\text{ cm}^{-1}$) and of the metallic clusters ($2050\text{--}2070\text{ cm}^{-1}$) due to the influence of the basic oxide, as has been detected by the IR spectra of CO adsorbed on the copper ions [30, 479, 480], i.e. a new effect of the basic oxide carrier on the electron state (increase in electron density) of the cation has been revealed.

Co_3O_4

Figure 2.32 demonstrates that CO adsorption on non-stoichiometric cobalt oxide gives rise to a band corresponding to $\text{Co}^{2+}\text{--CO}$ at 2190 cm^{-1} in addition to the formation of carbonates, as the stoichiometric cobalt oxide interacts with CO to give maxima below 2100 cm^{-1} , together with carbonate bands. These low-frequency bands indicate that CO is stabilized on cations reduced to practically the metallic state. The formation of carbonates in both cases demonstrates that carbon monoxide reduces cobalt ions at temperatures as low as 293 K. These data can be accounted for on the assumption that the reduction of non-stoichiometric cobalt oxide containing Co^{3+} ions involves the $\text{Co}^{3+} \rightarrow \text{Co}^{2+}$ electron transition in the surface followed by CO stabilization on the Co^{2+} ions thus formed (absorption band at 2190 cm^{-1}) [243]:



Scheme 2.26

At the same time, the reduction of stoichiometric CoO appears to involve the $\text{Co}^{2+} \rightarrow \text{Co}^0$ transition (unlike Cu^{1+} , Cu^{1+} , the Co^{1+} state is unstable in oxide phases), and cobalt ion states with an effective charge close to zero are formed in the surface. The reduction proceeds through the formation of carbonates in the coordination sphere of Co^{2+} . Surface reduction is not compensated for by oxygen diffusion from the bulk, apparently owing to the temperature being too low for diffusion to occur (the band at 2075 cm^{-1}). The nonuniformity of these reduced ions, and also the presence of even furthermore reduced cobalt ions (with a lower charge), are obviously responsible for the presence of absorption bands at lower frequencies for the carbonyl complexes (2020 and 1940 cm^{-1}), as is confirmed by the increased intensity of these bands in the case of the adsorption of CO on a previously reduced sample (Figure 2.32, spectrum 8).

Strongly associated ions or clusters existing on the surface of CoO–MgO solid solutions (such ions differ from isolated ions in the MgO lattice by having oxygen ions as common ligands), as

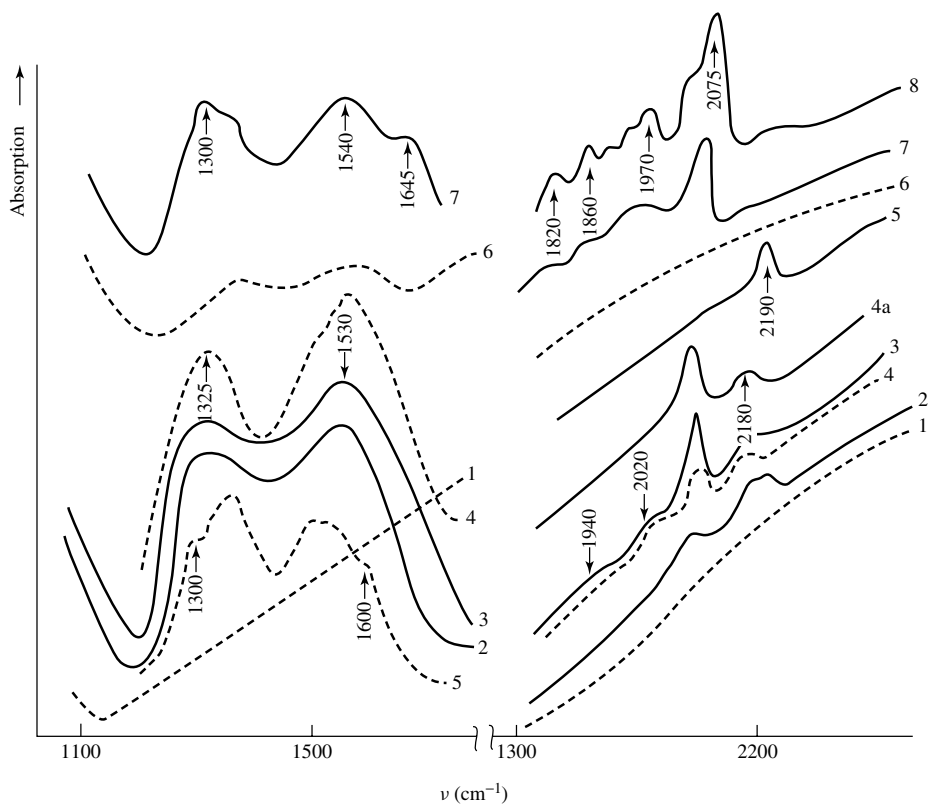


Figure 2.32. IR spectra of carbon monoxide adsorbed on Co_3O_4 : 1, spectrum of Co_3O_4 treated at 573 K; 2, adsorption of CO (3996 Pa) at 293 K; 3, after long (20 h) exposure to CO; 4, 5, after interaction with CO at 373 and 473 K, respectively; 6, after evacuation at 573 K for 1 h; 7, after further adsorption of CO (3996 Pa) at 293 K; 8, further exposure to CO (20 h); 4a, increase in exposure time at 373 K.

well as on NiO and NiO–MgO [30, 56, 525], are readily reduced by adsorption of CO up to $\text{Co}^{\delta+}$ and Co^0 . Because of this, the bands characteristic for $\text{Co}^0\text{--CO}$ and $\text{Co}^{\delta+}\text{--CO}$ complexes appear in the IR spectra of adsorbed CO [242, 243]. As for the optical properties (charge-transfer bands in the UV spectra), these clusters are similar to the ion states in the phase of the corresponding oxide [526]. Support for this comes from the data reported by Rao *et al.* [527].

ZrO₂

Upon FTIR spectroscopic investigation of the strong surface Lewis acidity of monoclinic ZrO_2 , two types of σ -coordinated CO species have been characterized by slightly different νCO values, by the heat of adsorption and by the concentration dependence on both the pressure and activation temperature [528, 529]. Spectral features of both CO species were influenced by the nature and surface concentration of the resulting charge-withdrawing species (including CO itself), as well as by the surface concentration of polar species such as OH groups.

At ambient temperature, CO adsorption occurs only on surface cationic Lewis acid sites located in crystallographically defective configurations [528]. Upon CO adsorption at low temperature (ca. 77 K), weaker adsorbed species are assigned to CO adsorptions on cationic Lewis acid sites

located in regular areas of the low-index crystal planes, and to CO hydrogen-bonded to surface hydroxyl groups.

V, Mo, W and Cr oxides

These oxide systems which contain cations in the highest degree of oxidation (+5; +6) do not adsorb the CO molecule because of full coordination. The frequency values obtained in the spectra of CO adsorbed on reduced samples are shown in Table 3.10. However, the assignments represented in this table are only hypothetical, since it is difficult to assign the observed bands to particular structures.

IR data on CO adsorption on other oxides, either in bulk or as supported on various supports, are available in the literature; however, not all of these have been considered above. This is connected with the fact that a large part of them, such as the systems containing Ni, Co and Cu, can change their oxidation degree upon interaction with CO. Moreover, different complexes can be formed on the surface of a support. This is why it is difficult to identify the spectra of adsorbed CO systems without a study of the states of the cations by other methods; such data (both ν CO and states of the cations) are examined in Chapter 3, using the results obtained from other analytical techniques.

Several oxides are reduced upon interaction with CO, even at low temperatures, leading to the appearance of reduced surface cations, which participate in the subsequent adsorption of CO. Such reduction is characteristic for oxides with the lowest energies of the surface M–O bond, such as CuO, Co₃O₄ and NiO. If this phenomenon is not taken into account, incorrect conclusions can be drawn, as has been noted either by Davydov [30].

2.3.3 ADSORPTION OF HYDROGEN AND NITROGEN

As has been shown from the data discussed in the previous section, the frequency of the stretching vibration for molecular adsorbed oxygen depends on the adsorption center, namely the cation, on which a stabilization of oxygen takes place (e.g. O_{2ads} on both the oxidized and reduced surfaces of TiO₂). The low extinction coefficients characteristic of O_{2ads} and O_{2ads}⁻ complexes (vibrations of such symmetrical diatomic species in the gas phase are not active in IR spectra) make their use difficult in characterizing such species. An application of low-temperature measurements, to give an increase in surface coverage by adsorbed oxygen, and other simple molecules such as hydrogen and nitrogen [235, 530–533], and also the use of DRIR spectroscopy [534–537], can increase the sensitivity of the IR method by at least a factor of ten [536], allowing the investigation of active sites on the oxides surfaces by means of such probe molecules. There are very few studies in the literature using oxygen as a probe molecule [282, 314], whereas both H₂ and N₂ molecules have been used widely [235, 471, 531–554] and very successfully. The most effective adsorption of H₂ occurs at 77 K [542]. Since the presence of acid–base pairs is needed to activate the H₂ molecule, especially interesting information may be obtained by a comparison of the adsorption data of H₂ with those of the CO molecule, which is adsorbed only on Lewis acid sites.

When such homonuclear diatomic molecules are adsorbed on dispersed adsorbents, the absorption forbidden in the gas-phase absorption spectra is observed at the positions of their vibrational frequencies. In early studies, such absorptions had been revealed after H₂ adsorption on porous glass [531], zeolites [282], alkali halides [538] and ZnO [532].

Hydrogen

On the surface of silica gel which contained only SiOH groups, the hydrogen adsorption at 77 K leads to the appearance of a single band at 4130 cm⁻¹, shifted to lower frequencies (by 30 cm⁻¹)

with respect to the frequency of the H–H vibrations in the spectrum of the gaseous hydrogen. The intensity of this band decreases if the pre-treatment temperature increases [536], and accordingly these authors assigned this band to H₂ molecules interacting with the SiOH groups.

In the case of Al₂O₃ and the amorphous silica–aluminas, the absorptions near 4110–4130 cm⁻¹ of H₂ adsorbed at 77 K similarly by decreased in intensity with dehydroxylation. This implied that hydrogen is perturbed by OH groups in a similar way. However, unlike the case of silica gel, dehydroxylation of these samples resulted in the appearance of additional low-frequency bands of adsorbed hydrogen at 3980 and at 4030 cm⁻¹ for Al₂O₃ and silica–aluminas, respectively. According to adsorption measurements, the concentration of Lewis acid sites for both samples is about 10¹⁷ sites m⁻².

In an IR spectrum of hydrogen adsorbed at 77 K on MgO, the electron-accepting properties of which are not so strong as for Al₂O₃ or silica–aluminas, there is only one band at 4080 cm⁻¹ which is most likely connected with H₂ molecules adsorbed on some of the cationic centers (e.g. Mg²⁺ cations).

After adsorption of H₂ on zeolite calcined at 763 K, bands in the 4010–4070 cm⁻¹ region were not observed, whereas those of adsorbed CO were present (see above). The reason for such differences between H₂ and CO adsorption is not yet clear. It is possible, however, that if H₂ characterizes the acid/base pairs of centers [534], then the deformation of the Al–O fragment which can be achieved by the high dehydration temperature is necessary to form a complex between H₂ and the Lewis acid sites. This means that H₂ can be used to identify the Lewis acid sites of the zeolites treated in *vacuo* at temperatures above 873 K.

The IR spectra of hydrogen adsorbed at 77 K on the Na-forms of zeolites A, X, and Y show absorptions in the 4075–4160 cm⁻¹ region, which can be assigned to H₂ molecules interacting with Na⁺ cations, with certain differences depending on the zeolite forms. In the case of NaY zeolite, maxima are observed at 4105, 4125 and 4155 cm⁻¹, corresponding to hydrogen molecules interacting with Na⁺ cations localized in S_I, S_I' and S_{II} positions of the framework. Lower-frequency bands at 4035 and 4060 cm⁻¹ were assigned to ν_{HH} in complexes formed with three-coordinated silicon ions and Al atoms, respectively. For decationized zeolites such as Y and HZSM, the band at 4105 cm⁻¹ corresponds to ν_{HH} in the complex with Al³⁺ cations which compensate the negative charge of the framework. The assignment of the bands at 4035 and 4010 cm⁻¹ in this case is analogous to that for the Na-form zeolites. The 4060 cm⁻¹ band has been assigned to aprotic extra lattice sites of the ⁺Al=O type, with the band at 4105 cm⁻¹ to H₂ molecules interacting with metal cations and OH groups.

The molecule H₂ has been explored most widely as a probe in the work of Maslov *et al.* [533]. These authors have studied a number of different oxides (Table 2.16). The spectra of SiO₂, BeO,

Table 2.16. Infrared spectral characteristics of H₂ adsorbed on various oxides [533]. Reprinted from Maslov, S. Yu, Denisenko, L. A., Tsyganenko, A. A. and Filimonov, V. N., 'Infrared spectroscopic studies of dihydrogen adsorbed on oxide surfaces', *React. Kinet. Catal. Lett.*, **20**, 273–276 (1982), with permission from Akademiai Kiado.

Adsorbent	H ₂	Adsorbent	H ₂	D ₂	H ₂	D ₂	H ₂ /D ₂		
SiO ₂	4140	ZnO	4160 ^a	4040	2985 ^a	2900	120	85	1.41
ZrO ₂	4115			4080		2930			
BeO	4110	TiO ₂	4270 ^a	4040	3070 ^a	2902	230	168	1.37
Sc ₂ O ₃	4080		4215 ^a	4084	3029 ^a	2935	131	94	1.39
Ga ₂ O ₃	4015	NaX	4225 ^a	4095		2942	130		
Al ₂ O ₃	4110	Silica–alumina		4135					
	4060			4040					

^aThe nature of these bands is not fully clear.

ZrO₂, Sc₂O₃ and La₂O₃ exhibit only one ν HH band. For SiO₂, the authors reported a related shift of the ν OH at 3750 to 3735 cm⁻¹, which confirmed that the silanol groups are the sites of H₂ adsorption. The absorption band at about 4135 cm⁻¹ for ν HH has also been observed for an alumina-silica. Using the method of competing adsorption, these authors showed that the bands at 4040 cm⁻¹ for the alumina-silica, 4110 and 4060 cm⁻¹ for Al₂O₃, 4080 and 4040 cm⁻¹ for ZnO, and 4084 and 4040 cm⁻¹ for TiO₂ characterize the H₂ adsorption on the different ion pairs which are involved.

The nature of the hydrogen uptake of monoclinic ZrO₂ consists of heterolytic dissociation of molecular hydrogen and the simultaneous formation of OH species and hydride species at adjacent O²⁻ and Zr³⁺ surface sites. Powders of polymorphic zirconia contain crystallites incorporating monoclinic and tetragonal domains. Thermal activation in high vacuum results in a insignificant amount of highly reactive radical surface centers (O⁻, Zr³⁺, etc.) mainly located in tetragonal surface sites [553]. Their exposure to molecular H₂ leads to heterolytic dissociation processes which are clearly shown by IR spectroscopy. These processes give rise to an irreversible formation of multiple-coordinated surface OH groups on tetragonal surface sites (3668 cm⁻¹) and to the reversible formation of linear ZrH (1565 cm⁻¹) and bridged hydrides, e.g. Zr₂H (1360 cm⁻¹). The linear hydrides are very reactive towards any kind of oxygen species such as O²⁻ and O₂⁻. Their reaction with physisorbed oxygen leads to the further irreversible formation of multiple-coordinated OH groups and O₂⁻ radical anions (ν O-O⁻ = 1118 cm⁻¹) as shown by ¹⁸O₂ isotopic experiments. The appearance of these OH groups necessarily implies surface mobility of the intermediately existing H atoms on both monoclinic and tetragonal surface domains. The interaction of H₂ with ZrO₂ at high temperatures (673–873 K) has been studied by using *in situ* IR spectroscopy [554]. Hydroxyl species are formed with ν OH at 3650 cm⁻¹ on the surface of monoclinic and at 3730 cm⁻¹ on the surface of tetragonal zirconia.

Kazanskii and co-workers [535] observed three absorption bands at 3975, 4020 and 4105 cm⁻¹ upon H₂ adsorption on η -Al₂O₃. They ascribed these bands to the interaction of H₂ molecules with aprotic sites. In addition, a band at 4160 cm⁻¹ was assigned to H₂ molecules weakly interacting with surface OH groups. The band at 3975 cm⁻¹ was found to correspond to very strong Lewis acid sites, i.e. 'X-sites' (involving nearby coordinatively unsaturated oxide ions) and to be completely inhibited by the room temperature pre-adsorption of CO in the form adsorbing at ca. 2245 cm⁻¹. At temperatures above 240 K, Kazanskii and co-workers have observed two bands (1860 and 1895 cm⁻¹) in the ν Al-H stretching region and, using D₂, several bands (2595, 2660, 2705, 2725 and 2785 cm⁻¹) in the ν O-D stretching region.

The relatively weak bands located on the higher-frequency sides of the above bands of adsorbed H₂ (see footnote for Table 2.16 [533]) have also been formed in the spectrum of H₂ adsorbed on NaX zeolite and on both ZnO and TiO₂. Forster and Schuldt [282] observed similar satellites near the absorption bands of D₂ adsorbed on a NaCaX zeolite and associated these with the interrupted rotation of the adsorbed molecules. Such features are known to be typical for the IR spectra of both liquid and solid hydrogen [547]. However, Maslov *et al.* [533] believe that the bands in the 4270–4160 cm⁻¹ region arise from the combination of ν H₂ with low-frequency vibrations of the H₂ molecule towards the surface. This is because the differences, $\Delta\nu$, between the possible satellites and the main bands of adsorbed hydrogen for D₂ is not half those found for H₂, as would be expected for the rotation structure. The observed value of $\Delta\nu$ H₂/ $\Delta\nu$ D₂ (at about 1.4) is more characteristic of vibration frequencies.

The adsorption and polarization of molecular hydrogen on cationic forms of A, X, Y, mordenite and ZSM-5 zeolites have been studied by diffuse reflectance IR spectroscopy [544]. The extent of the H-H bond polarization characterized by the stretching frequency was found to strongly depend on the cation nature (electrostatic field, presence of d-electrons, etc.) and on the lattice

basicity, with the sequence being as follows: ZSM-5 < mordenite < Y < X < A. This confirms a two-point mechanism of H₂ adsorption on acid-base pairs formed by a cation and a neighboring framework oxygen. Thus, the hydrogen molecule can be used a test for acid-base pairs, where the latter can also indicate the reason for the appearance of the ν HH vibration in the IR spectra of adsorbed hydrogen.

Chang *et al.* [532] studied the spectra of H₂ adsorbed on ZnO at 78 K. Following Eischens and Pliskin [45], they showed that the dissociation of H₂ proceeds on the ion pairs Zn²⁺O²⁻ with formation of OH (3502 cm⁻¹, or 2591 cm⁻¹ for OD) and Zn-H (1691 cm⁻¹, or 1219 cm⁻¹ for Zn-D) groups. Moreover, a certain proportion of hydrogen (5–10 % from the total surface coverage) is bound to the surface in the molecular form. The spectral characteristics of this form are listed in Table 2.17. The heat of adsorption of hydrogen in the molecular form is 9.2–10.5 kJ mol⁻¹. Dent and Kokes [550] have noted that the appearance of the absorption bands of H₂ molecules is caused by an induced surface dipole moment, although they did not examine the nature of the adsorption center. It has been shown [550] that a reversible form of dissociatively adsorbed hydrogen is formed on ZnO even at room temperature, appearing in the spectra as the Zn-H and OH-Zn groups (absorption bands with ν Zn-H = 1709 and ν OH = 3500 cm⁻¹).

Further work [533, 536] has shown that in addition to the molecular forms of adsorbed hydrogen usually observed in the low-temperature adsorption of H₂, other forms of adsorbed H₂ (dissociatively adsorbed) can also be found. According to Zecchina and co-workers [374], on ZnO the ν Zn-H (1708 cm⁻¹) band corresponding to ν OH (3498 cm⁻¹) (or ν Zn-D = 1233 cm⁻¹ and ν OD = 2585 cm⁻¹) is accompanied by the 1475 cm⁻¹ band, assigned to ν Zn-H-Zn and by the 3400 cm⁻¹ band assigned to ν OH...O (or ν Zn-D-Zn = 1075 cm⁻¹ and ν OD...O = 2500 cm⁻¹), i.e. to two-center forms of adsorbed hydrogen, more strongly bound to the surface. Hussain and Sheppard [550b] presented a review of data on the IRS identification of the nature of hydrogen species adsorbed over ZnO.

Interesting results were obtained upon the adsorption of H₂ on Cu-Zn-Cr and Zn-Cr systems [551]. In particular, it was shown that the position of the ν M-H vibration band depends on the composition of the system, and this feature was ascribed to the specific metal to which the H atom is coordinated. Davydov *et al.* [552] showed that the dissociation of hydrogen is accompanied by the formation of different metal hydrides: Zn-H(D) (1710 cm⁻¹, or 1255 cm⁻¹ for Zn-D) and M-D-M' (1115, 1060 and 960 cm⁻¹), where M and M' differ in their nature or state of oxidation for Zn-Cr catalysts.

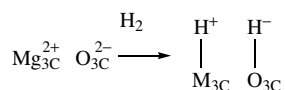
The centers responsible for the dissociative adsorption of hydrogen are shown to coincide with those for the low-temperature adsorption of molecular hydrogen. They seem to be the acid-base pairs M⁺-O⁻ which cause the heterolytic dissociation of hydrogen at higher temperatures [536]. The formation of three types of surface hydrides, for example, for Al₂O₃ (ν Al-H = 1860, 1895 and 1905 cm⁻¹, and for the corresponding OD groups at 2595, 2662 and 2706 cm⁻¹), proves that Al atoms could have different coordination numbers on the surface. The number of sites responsible for the low-temperature dissociative adsorption of hydrogen is very small, i.e. about 10¹⁶ sites g⁻¹.

The infrared spectra of hydrogen adsorbed at room temperature on MgO, CaO and SrO [56, 548, 549] show absorptions in two regions; i.e. 3800–3000 and 1350–60 cm⁻¹. Absorption in

Table 2.17. The spectral features of hydrogen adsorbed on ZnO.

Adsorbate	ν (gas)(cm ⁻¹)	ν (ads)(cm ⁻¹)	$\Delta\nu$ (cm ⁻¹)	$\Delta\nu/\nu \times 100$
H ₂	4161	4019	142	3.41
HD	3627	3507	142	3.41
D ₂	2990	2887	103	3.44

the first region has been attributed to νOH of the hydroxyls, whereas that in the second interval has been assigned to hydride groups produced by heterolytic dissociation of H_2 molecules over anion-cation pairs of the lowest coordination:



Scheme 2.27

The spectrum ‘inside’ the family of three-coordinated ions is heterogeneous. The majority of the band components are broad and have been assigned to bridged structures, whereas a few sharp bands (e.g. at 1326 and 3750 cm^{-1} in the case of MgO) were assigned to the stretching vibrations of ‘terminal’ surface hydrides and ‘free’ hydroxyls. In addition, O_2^- radicals were produced by electron transfer from the pre-formed negative ions (H^-) to the newly adsorbed oxygen species, as has already been observed with other molecules. The total number of active sites was ca. 6.0×10^{16} sites m^{-2} , corresponding to 0.6 % of the total number of ionic pairs [535]. Ito *et al.* [548, 549] identified eight different states of adsorbed hydrogen, in spite of a very low uptake. They obtained important information on the energy state, structure, and mobility of each adsorbed species, which confirmed the heterolytic mechanism. The δMgH mode was estimated to be at 555 cm^{-1} .

There are numerous data in the literature concerning the study of dissociative H_2 adsorption over certain faces of different metals by means of high-resolution electron energy loss spectroscopy (HREELS). Table 2.18 [555] summarizes the frequencies of the ν_s vibrational modes measured for hydrogen adsorbed on a variety of single-crystal metal surfaces in three different adsorption sites: the fourfold hollow, the threefold hollow and the twofold bridging sites. It can be seen that the ν_s frequency strongly depends on the nature of the adsorption site occupied by H_{ads} , namely it increases, for example, as the number of surface Pt atoms bound to the hydrogen atom (the hydrogen coordination number) decreases. Looking at Table 2.18, it can be seen that great progress has been achieved in this field.

As for supported metals, chemisorption of H_2 on a metal surface occurs in similar fashion to that of metal single- and poly-crystals at room temperature, mainly through dissociation of the

Table 2.18. The ν_s mode frequencies measured for hydrogen adsorbed on a variety of single-crystal metal surfaces in the 4- and 3-fold hollow and bridge states [555]. Reprinted from Zemlyanov, D. Yu., Smirnov, M. Yu. and Gorodetskii, V. V., *Catal. Lett.*, **43**, 181–187 (1997), with permission of Kluwer Academic.

4-Fold hollow			3-Fold hollow			Bridge		
Surface	$\nu_s(\text{cm}^{-1})$	Reference	Surface	$\nu_s(\text{cm}^{-1})$	Reference	Surface	$\nu_s(\text{cm}^{-1})$	Reference
Ni(110)	530–630	556	Ni(111)	1120	561	Rh(100)	1330	570
Ni(510)	470	557	Ru(001)	1140	560	Ni(510)	1110–1145	557
				685, 1140	562			
Rh(1000)	660	558	Rh(111)	1100	563	Fe(110)	1060	557
Pd(100)	510	559	Ir(111)	560	564	Cu(111)	1040	571
			Pd(111)	1000	565	W(100)	1050	560, 572
			Pt(111)	905, 550, 1255	566–568	W(100)	1260–1300	573
			Ag(111)	820–855	569	Mo(100)	1200–1220	573
						Mo(100)	1030, 1125	574, 575

molecule and the adsorption of the two hydrogen atoms so produced, onto surface metal terminal $-M-H$, bridge $M-H-M$ or multi-bonded $-M_3H$ forms. Unfortunately, due to absorption of supports, it is practically impossible to get any information about bridges and multi-bonded forms of supported metals. Terminal groups of adsorbed hydrogen on alumina-supported platinum at 2105 and 2055 cm^{-1} (for adsorbed H_2) and 1512 and 1480 cm^{-1} (for D_2) have been observed due to two $Pt-H$ vibration [45]. As for other supported metals (such as Ni, Co, etc.), for the most part they have no absorption bands in the region of terminal $M-H$ bonds, also the amount of hydrogen adsorbed was similar in quality to that adsorbed on alumina-supported platinum. This is likely due to the hydrogen atoms being associated with two, three or more surface metal atoms. In this case the Raman spectroscopy seems to be a very promising method since the supports do not have the spectra in the fundamental vibrations region where the multi-bonded hydrogen atoms are detected.

Nitrogen

Data concerning coordinatively unsaturated surface cations can be obtained by N_2 adsorption, as well as by the adsorption of CO. Thus, Zubkov *et al.* [576] have investigated the adsorption of N_2 on Al_2O_3 surfaces. There is a band at 2360 cm^{-1} in the IR spectra, which is 30 cm^{-1} higher than the ν_{NN} vibration of the free molecule. It has been shown by using adsorption isotherms that about a third of the $Al_{\text{cus}}O$ pairs that dissociatively adsorb H_2 interact at 300 K with N_2 . The heat of N_2 adsorption was 45 kJ mol^{-1} . More details of studies of N_2 adsorption on different oxides have been reported by Maslov *et al.* [533]. Increase in the vibration frequencies of the molecules on adsorption were observed in the spectra of all of the oxides investigated, with the exception of SiO_2 . Common features of the adsorption of N_2 and CO showed that the same coordinatively unsaturated metal cations are the centers for adsorption of N_2 on the oxides' surfaces.

The adsorption of N_2 has not been observed by IR spectroscopy on the surfaces of MgO and CaO which do not have strong Lewis acid centers, while for TiO_2 , BeO and Al/Si which have, according to CO adsorption, Lewis acid sites of different strengths, several bands of adsorbed N_2 species appeared in the IR spectra. It is interesting to compare the centers identified by the adsorption of H_2 and N_2 , because this allows the identification of Lewis acid sites by 'soft' bases. DRIFT and Raman spectroscopies have been used [540] to examine N_2 and O_2 adsorption on cation-exchanged (K, Na, Sr, Ca and Li) low-silica X (LSX) zeolites. IR and Raman bands were observed for the molecular vibrations of adsorbed N_2 and O_2 at room temperature and atmospheric pressure. The intensity (in Kubelka-Munk units) of the IR band increased with N_2 pressure and mirrored the adsorption isotherm for N_2 . Both N_2 and O_2 displayed a similar dependence of the molecular vibrational frequency on cation charge density, which suggests that both gases are interacting directly with the cations. The vibrational frequencies for adsorbed N_2 and O_2 were more sensitive to the cation charge density than to the framework Al content, as evidenced from an IR study of complexes ' N_2 -cations' within the sorption cavity of the zeolite. Thus, adsorbed N_2 can be used to probe the accessibility of specific cations within the zeolite framework. The spectroscopic data are consistent with the theory that the stronger interaction of N_2 when compared with O_2 is caused by the stronger influence of the electric field the larger quadrupole on accent of moment of N_2 .

The first study of N_2 adsorption on metals by IRS was made by Ravi *et al.* [577]. This involved the case of adsorption on oxides, and established a significant lowering in the ν_{NN} (2185 cm^{-1}) for the IrN_2 complex when compared with the gas phase. Further adsorption of nitrogen over metal catalysts was intensively studied by means of IRS in Russia the 1970s because of the particular interest in nitrogen fixation [578-582]. Already at room temperature, characteristic absorption bands in the region of vibrations of molecular nitrogen (forbidden in infrared spectra) at 2230-1800 cm^{-1} were observed due to the interaction between N_2 and

Table 2.19. Spectral Features of nitrogen adsorbed over some noble metals.

Complex	ν_{NN} (cm^{-1})	Complex	ν_{NN} (cm^{-1})
RuN ₂	2202	RuN ₂ H _n	2257
	2232		
RhN ₂	2237	RhN ₂ H _n	2275
	2231		2257
	2219		
IrN ₂	2185	IrN ₂ H _n	2193
NiN ₂	2202	NiN ₂ H _n	2252
			2266

Table 2.20. Adsorption bands in the IR spectra of nitrogen adsorbed over iron and nickel.

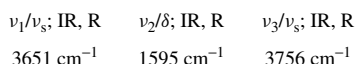
Metal	Adsorption temperature (K)					Desorption temperature (K)	Interpretation
	293	323	373	423	723		
Ni	2230					293	Adsorption on untightly packed faces
		2205				293	
			2170			293	Adsorption on close-packed (111) and (100) faces
Fe				2020	–	–	
					1830	293	Adsorption on tightly packed (100) faces

different metals. An exception was iron, in which case such a form of adsorption appears only at 673 K (Table 2.19) [578].

Infrared data on the molecular adsorption of N₂ on Ni, Rh and Ru ($\nu_{\text{N}} \equiv \text{N} = 2237 - 2202 \text{ cm}^{-1}$), including the adsorption of isotopically substituted molecules, have also been obtained [580–582] (Table 2.20). Complexes of molecular nitrogen with metals, when interacting with H₂ at low temperatures, reversibly form the M(N₂)H_n complexes in which the frequency of ν_{NN} is higher than that in the initial complex. Nitrogen on the metal surface is hydrogenated by surface hydrogen at higher temperature, forming NH-containing complexes.

2.3.4 ADSORPTION OF WATER

Water adsorption on oxide surfaces has been much investigated because of the problem of solid hydroxylation. The H₂O molecule has a nonlinear structure, and its chemical reactivity is determined by an unshared electron pair localized on the oxygen atom, i.e. the H₂O molecule is therefore a typical σ -donor. It should also be noted that there is a high tendency of the hydrogen atom in this molecule ($\text{p}K_{\text{a}} = 12.6$ [583, 584]) to form hydrogen-bonds. This increases with the growth of the strength of the coordination bond to a cation in M–OH₂. The vibrations frequencies and selection rules for a free H₂O molecules are as follows:

**Scheme 2.28**

The regions of high frequencies, i.e. 3550–3670 cm^{-1} for adsorbed H_2O and 2680–2726 cm^{-1} for D_2O , contain absorption bands that differ little from those of water molecules in the free state.

Water was one of the first molecules for which adsorption was investigated in detail by infrared spectroscopy on the surfaces of silica, alumina and zeolites. Numerous studies devoted to this have been summarized and examined [18–20, 31, 41, 73, 76, 79–81, 85–93, 95–97]. There is no necessity to analyze these results here; only the main agreed conclusions that were obtained need to be noted. Water molecules may be adsorbed via H-bonds with surface sites or between each other (polysorption) and also through interaction with Lewis acid sites (LASs). It is difficult to separately distinguish forms of this adsorption on the basis of the changes in the spectra of the H_2O molecules upon adsorption because there are perturbed hydroxyl groups present in both cases. The $\delta\text{H}_2\text{O}$ absorption near 1620 cm^{-1} provides the evidence for the presence of water molecules on oxide surfaces but these are not very strong, causing ambiguities at low coverage. The dissociative chemisorption of water molecules leads to the formation of hydroxylated oxide surfaces. The initial coordination of the H_2O molecule (Lewis base) to the surface cation (Lewis acid) can be immediately followed by nucleophilic attack from the adjacent surface base with the formation of OH groups.

The surface can be cleaned from adsorbed water by evacuation at progressively higher temperatures, with the last hydroxyl groups to disappear being those located at defect sites. Unless high-temperature treatment has been effected, and contact with the atmosphere avoided, the surface of active metal oxides is usually hydroxylated. Surface OH groups have Brønsted acid–base character, changing from weakly acidic for silica to strongly basic for magnesia. They can interact with molecules from the gas phase if the surface is not fully dehydroxylated, and act as hydrogen-bonding sites for suitable ligands. Basic OH groups interact only with acidic (A) molecules, leading to the formation of AOH species, whereas acidic OH groups interact with weakly basic (B) molecules to form hydrogen-bonded OH...B species, and with strong bases to give the protonated species $\text{O}^- \dots \text{BH}^+$. In the case of H_2O molecules it is $[\text{O}^-(\text{H}_3\text{O})^+]$ or even more complex aggregates. Below, several examples of the interaction between H_2O molecules and oxides surface are examined for the oxides the surface centers of which and, therefore, their surface properties are very different.

SiO₂

The fully dehydroxylated silica surface appears to be very unreactive. Normal Si–O–Si bridges do not easily undergo either nucleophilic or electrophilic attack, because of their homopolar character. Only when these bridges are strained, i.e. asymmetric and hence polar, $\text{Si}-\text{O}^{\delta-}-\text{Si}^{\delta+}$, as at the surface, can they react with bases like H_2O to form hydrogen-bonded silanol pairs. The hydroxyl groups of partially dehydroxylated silica surfaces are weakly acidic and can react with water in different ways with formation of H-bonds [18–20].

Zeolites

Interaction of water with the dried zeolite HZSM-5 first causes the adsorption of water molecules on Lewis acid sites, followed by the appearance of aluminum hexa-aquo complexes and then the formation of free hydroxonium ions [585]. Smith *et al.* [586] have reported direct structural information derived from neutron diffraction data to identify both hydrogen-bonded neutral water molecules and hydroxonium ions, as has been confirmed by *ab initio* quantum chemistry calculations [587]. The surface acidic properties of calcined and reduced CoAPO-18 catalysts were reported by Marchese *et al.* [588]. The bands at 3751 and 905 cm^{-1} observed in the FTIR spectrum of the reduced template-free catalyst have been assigned, respectively, to ν and in-plane

(δ) bending vibration of OH groups bridging Co(II) ions. It has been shown that Co(II) substitutes for Al in the lattice of the zeolite structure. Bridged hydroxyls are centers of Brønsted acidity, the strength of which has been tested by the adsorption of H₂O. Some bands produced by the interaction between bridged hydroxyls and water are sensitive to the acidic strength of the Brønsted centers. This strength is found to exceed that of the structurally similar HSAPO-34. Calcined CoAPO-18 has Co(III) centers and the Brønsted acidity disappears, and it is deduced that redox Co(II)/Co(III) couples are intimately associated with the presence of Brønsted acid sites (BASs). Adsorption of H₂O has revealed that LASs are also present on both calcined and reduced catalysts. Both the spectroscopic features and the acidities of OH and OD groups are sensitive to the presence of Co in the structure of aluminophosphate molecular sieves, and an analysis of the ν and δ OH (and OD) bands from SAPO-34 and CoPO-18 has been presented by Marchese *et al.* [588].

Al₂O₃

When H₂O interacts with a dehydroxylated alumina surface, reaction easily occurs, and the surface of the oxide becomes hydroxylated [589]. Surface Al³⁺ ions (Lewis acid sites) strongly coordinate H₂O via a lone electron pair at the oxygen atom, transforming the water molecule in protic center, while surface O²⁻ ions (Lewis base sites) simultaneously abstract a proton.

MgO

This is characterized by the high ionicity due to the charges localized at magnesium and oxygen atoms being nearly equal to 2. Surface Mg²⁺ and O²⁻ ions act as Lewis acid and Lewis base centers, respectively, as tested by such probes as CO, NO, H₂O and CO₂. Due to the significant basicity of O²⁻ ions on this oxide surface, adsorption of water does not stop at the first step; each adsorbed H₂O molecule undergoes heterolytic dissociation, and the oxide surface immediately becomes covered with a full layer of hydroxyl groups [312, 313, 590].

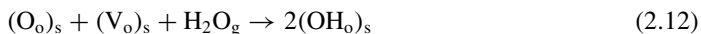
Fe₂O₃

The adsorption of water on α -Fe₂O₃ surfaces has been studied by FTIR spectroscopy and by heat flow microcalorimetry [315]. The spectrum of desorbed water shows broad components at about 3430 and 3050 cm⁻¹, due to strongly hydrogen-bonded water molecules. After desorption at 383 K, two rather broad absorptions appear at 3485 and 3430 cm⁻¹, and an intense triplet with maxima at 3665, 3648 and 3628 cm⁻¹ is observed with shoulders on both sides (at 3690 and 3590 cm⁻¹). When the evacuation temperature is increased to 773 K, the low-frequency absorption disappears, and a slight decrease in the relative intensities of the 3628 and 3590 cm⁻¹ components is detected.

In the hydrated form, both haematite and goethite possess variable amounts of undissociated water, coordinated to exposed surface cations, as characterized by the scissors deformation mode at 1635 cm⁻¹. These are easily desorbed at low temperatures [203, 370]. Physically adsorbed water molecules in the first adsorption layer are bound to the oxide through the H-bonding interactions involving single water molecules and pairs of adjacent surface hydroxyl groups [317, 372, 374]. Each water molecule in the second adsorption layer is involved on average in the formation of a single hydrogen bond [375].

Cr₂O₃

Burwell *et al.* [443] have shown that surfaces containing anionic vacancies, such as those in the (111) face of MgO and the (001) face of α -Cr₂O₃, may easily chemisorb water molecules, forming OH⁻ ions covering the whole surface:



where $(O_o)_s$ is a surface oxygen atom in an anionic position, $(V_o)_s$ is a surface anionic vacancy, and $(OH_o)_s$ is a surface hydroxyl group filling an anionic vacancy. The dehydroxylation of such a surface results in the exposition of cations and the formation of catalytically active centers for various reactions, e.g. hydrogenation or isomerization.

Two kinds of water adsorption were confirmed spectroscopically on Cr_2O_3 : (i) adsorption of H_2O molecules on localized OH groups, and (ii) adsorption of H_2O molecules on specific hydroxyls (3656 and 3408 cm^{-1}) strongly perturbed by H_2O adsorption, leading to two-dimensional condensation at the critical temperature at which shifts of the two OH stretching modes were observed [591]. After evacuation of the sample, three intense maxima are observed at 3656 , 3614 and 3408 cm^{-1} . There is also a broad peak at about 3290 cm^{-1} and weak ones at 3510 , 3514 and 3539 cm^{-1} (stretching modes of OH groups). During water adsorption, the bands due to hydroxyls at 3656 and 3408 cm^{-1} begin to decrease, and new peaks at 3618 and 3336 cm^{-1} appear instead. Maxima at 3714 , 3614 , 3539 and 3510 cm^{-1} do not change significantly at this stage. According to Kittaka *et al.* [591] such spectral changes show that the oxygen atoms of the 'ice structure' are anchored by surface OH groups. With an increase in the heating temperature, the broad peak at about 3290 cm^{-1} disappears at 473 K . A small initial peak begins to appear at 3726 cm^{-1} , instead of the 3714 cm^{-1} peak at 573 K . The intense peaks at 3656 , 3614 and 3408 cm^{-1} , as well as the smaller ones at 3539 and 3510 cm^{-1} , simultaneously disappear between 573 and 623 K . The peak at 3693 cm^{-1} was assumed to correspond to a localized strong adsorption of H_2O on the surface hydroxyls.

A chromium ion in highly hydrated Cr_2O_3 is coordinated octahedrally by six hydroxyls, with the top three of these being surface OH groups, and the bottom three solid-phase Madelung contributions. Water molecules are considered to be adsorbed on the top hydroxyls without any lateral interactions. The heat of interaction between H_2O and an hydroxyl groups is 51 kJ mol^{-1} [591] and is similar to the differential isosteric heat of adsorption, which is 55 kJ mol^{-1} . This type of adsorption seems to occur at the corners or edges of the Cr_2O_3 crystal.

The adsorption of water on various other oxides has also been investigated (see for example, [375, 377, 378, 592a]).

2.3.5 ADSORPTION OF NITROGEN OXIDE AND NITROGEN DIOXIDE

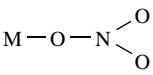
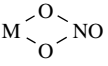
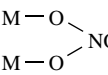
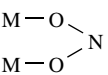
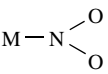
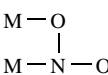
Nitrogen oxide

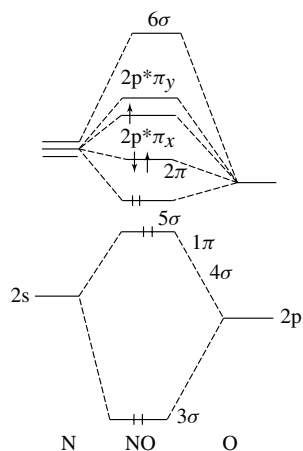
Nitric oxide (nitrogen oxide) reacts with the surface oxygen of oxides to yield nitrate and nitrite compounds [30, 593–596]. Their spectral identifications can be carried out by analogy with corresponding spectra of inorganic complexes (Table 2.21).

As seen earlier for carbonates, the differences in the structures of nitrate or nitrite surface compounds primarily reflect the differences in properties of the surface oxygen which participates in their formation, and interpretations of their complex spectra are largely schematic. Such spectra reflect the differences in the ionic-covalent properties of the metal-oxygen bonds on the surface.

Figure 2.33 shows that the distribution of electrons in the NO molecule is similar to that in the CO molecule. The main difference between CO and NO is that the additional electron in NO occupies the π^* -orbital. This causes a greater NO sensitivity to the electronic state of the cation during formation of the M-NO bond than for CO, since even slight alterations in electron density in this orbital noticeably change the frequency of the NO stretching vibration, ν_{NO} . In fact, when an electron is removed from the NO molecule and a nitrosonium ion, NO^+ , is formed, the frequencies of the NO stretching vibrations shift into the region of higher frequencies, at about 2300 cm^{-1} for the ionically bonded species (Table 2.22). The filling of the π^* -orbital with an additional electron yields the NO^- species, which has NO absorption bands in the region at

Table 2.21. Stretching vibration frequencies of NO_3^- and NO_2^- in inorganic coordination compounds.

Structure	ν_3 (cm^{-1})	ν_1 (cm^{-1})
NO_3^-	1380	1050 ^a
	1530–1480	1290–1250
	1565–1500	1300–1260
	1650–1600	1225–1170
Structure	ν_s (cm^{-1})	ν_{as} (cm^{-1})
NO_2^-	1260	1330
	1220–1205	
	1440–1335	1350–1315
$\text{M}-\text{O}-\text{N}=\text{O}$	1470–1450	1065–1050
	1520–1390	1260–1180

^aForbidden in the IR spectrum.**Figure 2.33** Scheme of NO molecular orbitals.

ca. 1350 cm^{-1} (Table 2.22). Clearly, in different compounds, even in those close to the purely ionic state, the frequencies of the NO^+ and NO^- vibrations vary within certain limits, which are related to various degrees of electron transfer into or from the π^* -orbital of the NO molecule.

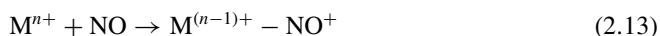
It is evident that even greater differences will be observed during NO-complex formation with variable-valence cations, for which other binding types are realizable as well as the ionic ones.

Table 2.22. Spectral features of NO stretching vibrations in various inorganic model compounds.

Compound	Frequency (cm ⁻¹)	Reference	Compound	Frequency (cm ⁻¹)	Reference
NO ⁺ HSO ₄ ⁻	2340	597	NO (gas)	1876	597
NO ⁺ ClO ₄ ⁻	2313	597	Li ⁺ NO ⁻	1352	598–600
NO ⁺ [Cu ⁺ Cl ₂] ⁻	2271	597	Na ⁺ NO ⁻	1358	598–600
[NO NO ₂] ⁺	2240	597	K ⁺ NO ⁻	1372	598–600
NO ⁺ AlCl ₄ ⁻	2236	597			

As with CO, the N atom in NO has an isolated electron pair (5σ), which is characterized by a higher energy than that on the O atom. Hence, coordination and adsorption are observed from the nitrogen atom. However, as might be expected, a more important role is played by the relative positions of the unpaired electrons of the π^* -orbitals and of the d-orbitals of the cation. The nature of the binding in NO–metal complexes (where the metal changes its valence) can be described as follows [601]:

- (i) NO donates an electron from the π^* -orbital and becomes NO⁺, and then a pair (5σ) of N atom electrons is donated to the metal ion, thus creating the coordination bond (NO donates three electrons in this case):



- (ii) NO accepts an electron from the metal ion and becomes NO⁻. Simultaneously, a pair (5σ) of electrons is donated to the metal ion, thus creating a coordination bond (NO donates one electron in this case):



- (iii) NO forms a bond only with participation of the 5σ -electrons of the N atom (coordination bond).
 (iv) Unpaired NO electrons and the metal ion form a new bond.

A classification of ν NO spectra in accordance with the prevailing type of NO binding (Table 2.23) has been given by Roev and Alekseev [597]. Despite its tentative nature, the proposed classification shows that the spectral ranges of ν NO in complex compounds are wide, with substantial overlaps, and that its limits are determined by the degree of interaction of the unpaired electrons and the d-orbitals of the cations.

Table 2.23. Classification of NO bonding and approximate spectral regions for adsorption on oxide surfaces.

Structure	Bond type	Frequency range (cm ⁻¹)
M–N=O	Covalent	1600–1800
M:NO	Coordination	1700–1870
M ⁻ NO ⁺ } M ⁺ NO ⁻ }	Ionic	2100–2400
		1500–1700
$\left. \begin{array}{l} M^- \cdot NO^+ \\ M^- - N^+ M^- \begin{array}{l} \vdots N \\ \vdots \\ \vdots \\ \vdots \\ \vdots O \end{array} \end{array} \right\}$	Ion-coordination	1900–2100

Table 2.24. Absorption bands in the IR spectra of NO adsorbed over various metals, oxides and salts [604]. Reprinted from *Spectrochim. Acta*, **15**, Terenin, A. and Roev, L., 'Infrared spectra of NO adsorbed on transition metals, their salts and oxides', 946–957, Copyright(1959), with permission from Elsevier Science.

Metal	ν (cm ⁻¹)	Oxide	ν (cm ⁻¹)	Salt ^a	ν (cm ⁻¹)
Cr	2010	Cr ₂ O ₃	2093	Cr ³⁺	2010
	1905		2028		1920
	1830				1830
Mn	–	–	–	Mn ²⁺	1730
					2005
					1900
					1830
Fe	1910	–	1925	Fe ²⁺	1850
	1820		1805		1740
Co	–	CoO	1840	Co ²⁺	1900
			1795		1810
					1740
Ni	2090	NiO	1805	Ni ²⁺	1850
	1860				1735
	1820				
Cu	1890	–	–	–	–
	1820				
	1750				

^aIn the form of sulfates.

Numerous studies have shown that nitric oxide molecules are coordinated to metal cations or metals on the surfaces of oxides and metals respectively (see, for example, [578, 593–600, 602–606], and references cited therein). The data obtained for the infrared spectra of NO adsorbed on oxides and salts of various transition metals, and also over several metals, obtained by Roev and co-workers [597, 604, 605], are presented in Table 2.24.

It is clear that the spectra of NO adsorbed on metals differ from those obtained on oxides, both in the number of absorption bands and their positions. This seems to be explained by the differences in the effective charges of NO adsorbed on these surfaces; NO dissociative adsorption occurs also on each metal. The dissociated oxygen atom oxidizes parts of the metal surface, and one form of NO adsorption occurs on such oxidized sites. Support for this comes from NO adsorption over oxides. Nevertheless, it has been shown [723] that upon NO adsorption over metals, in particular on Ru, NO is decomposed with the formation of oxidized centers. This should be taken into account in the interpretation of spectra of adsorbed NO since NO complexes with oxidized metals are formed. This concept was later developed in the work of Sokolova and co-workers in a large number of studies of NO adsorption on metals of the 7th Group of the Periodic Table (see, for example, [607, 608]). The adsorption of NO is accompanied by the appearance of absorption bands in the 1700–1900 cm⁻¹ region, characteristic for ν NO. According to Sokolova and co-workers, this evidences that NO interacts with the metal surface non-dissociatively. The authors concluded that at least two adsorption forms are formed on the surface. There are several models for NO adsorption on metal surfaces, which could explain the presence of more than one absorption band in the vibration spectrum, e.g. by the formation of the dimer and dinitrosyl adsorption as M(NO)₂, or by different states of adsorbed NO molecules (linear and bent forms of adsorbed NO). In the model based on single-molecule adsorption, the presence of the high-frequency band is explained by NO

Table 2.25. Some characteristics of NO adsorbed species on the surfaces of highly dispersed samples of rhenium and technetium metals.

Adsorption form	$\nu\text{NO}(\text{cm}^{-1})$		$\Delta\nu_{1/2}$		Decomposition temperature (K)	
	Re	Tc	Re	Tc	Re	Tc
I $\text{M}(\text{NO})_2$	1860–1850 1780–1760	1876	40	40	170	150
II $\text{M}-\text{NO}$	1760–1740	1795	50	50	250	300
III $\text{M}_n\text{NO}(n = 2?)$	1740–1720	1780–1760	60–80	60–70	450	350
IV $\text{M}_m\text{NO}(m = 3?)$	1700–1680	1740–1720	80–120	60–80	400	350
V $\text{M}_t\text{NO}(t = ?)$	–	1525	–	50	–	150

adsorption on oxidized centers, whereas a low-frequency band characterizes adsorption of NO on reduced sites. All such relationships are observed in the IR spectra. In the opinion of Sokolova and co-workers, the features observed in the IR spectra (Table 2.25) can be explained if the high-frequency bands are examined individually, including the dinitrosyl at 1860–1780 cm^{-1} , while absorptions in the low-frequency region are due to combinations of several overlapping band ranges belonging to different adsorption forms of NO, i.e. $\text{MNO} - 1760 \text{ cm}^{-1}$, $\text{M}_2\text{NO} - 1740 \text{ cm}^{-1}$, and $\text{M}_3\text{NO} - 1700\text{--}1680 \text{ cm}^{-1}$ (the quoted frequencies are those obtained on Re). However, such a scheme of interpretation does not seem to be altogether convincing. The data of [593b] are very useful for an interpretation of the spectra of adsorbed NO.

The data on the vibrational frequencies of the surface nitrosyl complexes are presented in Table 2.26 for different oxides and even more detailed in a recently published review [593c]. Such a complex absorbs in a wide (1700–1950 cm^{-1}) spectral range. In mononitrosyl complexes with ions in a high oxidation state, the νNO is higher than that of gaseous NO (preferable σ -bonding) while in the complexes with low-valent ions the νNO is observed below 1870 cm^{-1} due to a π -back donation. It is not observed for dinitrosyl complexes. Below we will examine the data on NO adsorption over oxides on which the unusual complexes of NO are formed.

An interpretation of the spectra of adsorbed NO in the cases of Fe_2O_3 and Cr_2O_3 [594, 595] has been made on the basis of the correlations presented in Table 2.21 above. The formation of the following surface compounds has been established: (i) bidentate nitrates (1570 cm^{-1}), (ii) bridged nitrates (1625 cm^{-1}), (iii) cyclic (bidentate) nitrites (1170 cm^{-1}), and (iv) bridged nitrites (1195 cm^{-1}). It has been shown that the band at 1305 cm^{-1} , attributed to a nitrate species, is complex, with two separate maxima, with the ν_s of the nitrates making a contribution to its intensity. On the basis of analysis of the bands near 1300 cm^{-1} and spectral data for NO^- available from the literature, Davydov *et al.* [594] have established that the second component of this band is characteristic of the NO^- ion forming on coordinatively unsaturated Cr^{2+} ions.

According to reported results, NO activation and decomposition occur on the same centers as those adsorbing oxygen [594]. In fact, the behavior of the NO molecule is similar in several respects to that of the oxygen molecule which is readily dissociated on $\alpha\text{-Cr}_2\text{O}_3$ surfaces, with one possible route for the dissociation of O_2 being its activation in the O_2^- molecular form (985 cm^{-1}), with likewise NO^- for NO. From the resemblance of the electronic structures of NO and O_2 , and the fact that their dissociations proceed on the same centers of an $\alpha\text{-Cr}_2\text{O}_3$ surface, it is natural to assume that the process of nitric oxide decomposition may occur via formation of an NO^- molecular structure (analogous to O_2^-), but absorbing at about 1300 cm^{-1} .

Other sets of absorption bands which are characteristic of mono- and dinitrosyl complexes of NO with chromium cations in different coordination or oxidation states (weak bands at 1730, 1780, 1810, 1855, 1880 and 1915 cm^{-1} , plus a shoulder at 1940 cm^{-1}) were observed upon NO

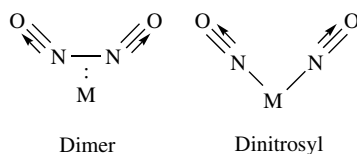
adsorption on chromia [594]. These absorption bands have been observed in numerous studies on supported Cr-containing systems and it has been established that they characterize complexes of NO with the chromium cations in different coordination and valence states. Peri [609] was the first to observe most of these bands in the spectra of NO adsorbed on α -Cr₂O₃ supported on Al₂O₃ (5 % Cr) and to assign them to different complexes of NO and N₂O₂ stabilized on single and pair centers of Cr²⁺ and Cr³⁺ (see Table 2.26). A detailed interpretation of the spectra of the NO complexes in terms of the states of the chromium ions is examined in Chapter 3.

In contrast to the case of Cr₂O₃, the adsorption of NO on reduced iron cations (Fe²⁺) does not lead to full electron transfer to the NO molecule with the formation of NO⁻ ions. Only the complexes with a weak loosening of the N–O bond (ν NO = 1810 cm⁻¹ for the complex Fe²⁺NO) are formed in this case because of the difference in donor ability of Cr²⁺ and Fe²⁺ cations. Unlike ammonia, NO molecules do not form complexes with Fe³⁺ cations.

Nitrogen oxide adsorption on an oxidized CuO sample at room temperature leads to the appearance of bands at 1220 and 1590 cm⁻¹, and also at 1855 and 1865 cm⁻¹ [479, 480]. The first two bands are accounted for as being from surface nitrites and nitrates. The two bands near 1860 cm⁻¹ are considered to characterize NO adsorbed on Cu²⁺ ions with different effective charges due to their different coordination states on the surface. The change in the coordination state of Cu²⁺ ions could be due to NO₂⁻ or NO₃⁻ formation at adjacent surface sites. Because of this, the effective charge of the cations would be expected to decrease since even an oxygen of the coordination sphere of the Cu²⁺ ions would be bound by nitrogen [520, 521].

The NO molecule is activated by protonation upon adsorption on heteropoly oxidic compounds, resulting in a weakening of the N–O bond. This NO activation, on rapid heating, results in N₂ production [610]. The infrared spectrum of H₃PW₁₂O₄₀ · 6H₂O has strong absorption bands at 980 cm⁻¹ (ν W=O_t), 1060 cm⁻¹ (ν _{as} of the central PO₄ tetrahedron), and at 1620 and 1710 cm⁻¹ from δ H₂O and δ H₅O₂⁺, respectively. Upon substitution of H₂O by NO, the H₂O bands were replaced by a single band at 2270 cm⁻¹, attributed to the nitrosonium ion (NO⁺). When NO is substituted by NH₃, the band at 1450 cm⁻¹ from NH₄⁺ replaced the 2270 cm⁻¹ band. Thus, these results indicate that NO is bound with a proton. After NO adsorption, additional bands at 1295 and 1390 cm⁻¹ appear in the spectrum [611]. Later [610], it was established that these two bands appear to be due to the interaction of the heteropoly compound with NO and KBr (from the KBr pellets which were used to obtain the spectra).

The interactions between the unpaired electrons of two NO molecules may support the stabilization of the dimer (ν _s = 1870–1860 cm⁻¹, ν _{as}NO = 1780–1760 cm⁻¹ in *cis*·(NO)₂ and ν _{as} NO ~ 1760 cm⁻¹ in *trans*-isomer) and could be the reason why two NO molecules are usually adsorbed on one site [57]. The pair of NO molecules may adsorb either as a dimer or as a dinitrosyl [612, 613]:



Scheme 2.29

The formation of both dimer and dinitrosyl leads to the appearance of LF (comparing with those of mononitrosyl) bands with ν NO lower than that for the gaseous NO. In the case of NO adsorbed on Mo/Al₂O₃ Kasuzaka and Howe [614] have proposed that two nitrosyl groups are adsorbed per Mo site to form the molybdenum–dinitrosyl complex which is stable even under

Table 2.26. Infrared spectral characteristics of NO adsorbed on various oxides as nitrosyl.

Oxide	νNO (cm^{-1})	Center	Structure	Reference
TiO ₂	1920, 1900–1910	Ti ⁴⁺	Ti ⁴⁺ –NO	602
SnO ₂	1910, 1830	–	Sn(NO) ₂	603
Cr ₂ O ₃	1950–1750, 1305	–	CrNO, Cr(NO) ₂ , NO [–]	594
	1875, 1745	–	Cr ³⁺ (NO) ₂	618
Cr/Al ₂ O ₃	1880	Cr ²⁺	NO	609
	1905	Cr ³⁺	NO	482, 609
	1755	Cr ²⁺ Cr ²⁺ or Cr ²⁺ Cr ³⁺ pairs	(NO) ₂ dimer	609
	1775	–	(NO) dimer	609
	1940	Cr ³⁺ Cr ³⁺ pairs	NONO	609
	1820	Cr ³⁺ in Al ₂ O ₃	Cr ³⁺	609
	1875	Cr ³⁺ in Al ₂ O ₃	NO	609
	2260	Cr ³⁺ in Al ₂ O ₃	NO ⁺	622–624
	Cr/SiO ₂	1887–1865, 1765–1745	–	Cr ⁿ⁺ (NO) ₂
1815–1800		–	Cr ⁿ⁺ –NO	622–624
CuO	1865, 1855	Cu ²⁺	–	479, 480
CuO/Al ₂ O ₃	1880	Cu ²⁺	–	481, 494
	1930–1900	Cu ²⁺ in Al ₂ O ₃	Cu ²⁺ –NO	520–522
CuCr ₂ O ₄	1920	–	Cu ²⁺ –NO	520–522
CuCl ₂	1875	–	Cu ²⁺ –NO	520–522
CuO–MgO	1850, 1845	–	Cu ²⁺ –NO	479, 480, 520–522
NiO	1820	–	Ni ²⁺ –NO	593
Ni ²⁺ /SnO ₂	1870	–	Ni ²⁺ –NO	482
CoO–MgO	1874, 1785	–	–	485, 613
Co ₃ O ₄	1875	–	Co ²⁺ –NO	613, 619
	1865, 1780	–	–	613, 619
CoAl ₂ O ₄	1860, 1780	–	Co ²⁺ (NO) ₂	613, 619
	1875	–	Co ²⁺ –NO	613, 619
Co/Al ₂ O ₃	1870–1860, 1795–1780	–	Co ²⁺ (NO) ₂	482, 613, 619
Co ²⁺ /SnO ₂	1840, 1765	–	Co(NO) ₂	482
	– oxidized 1874, 1785	–	Co ²⁺ (NO) ₂	482
Fe ₂ O ₃	1595	–	NO ^{δ–}	595
	1735	–	NO ^{δ–}	595
	1810	–	Fe ²⁺ –NO ^{δ–}	595
Fe ₂ O ₃ /SiO ₂	1910, 1810	–	Fe ²⁺ (NO) ₂	620
	– reduced 1830, 1750	–	Fe ²⁺ –NO	620
	1810	–	–	620, 621
	– oxidized 1750, 1700	–	Fe ³⁺ (NO) ₂	620
ZrO ₂	1820–1810	–	Fe ³⁺ –NO	620, 621
	1900	–	Zr ⁴⁺ –NO	593
MnO _x /Al ₂ O ₃	2260	–	NO ⁺	593
	1835	–	Mn ⁿ⁺ N=O ^{δ–}	482

high-temperature evacuation. Support for this structural assignment comes from the study of Rosen *et al.* [615] who calculated the angle between the two NO molecules to be 105° which is characteristic of a dinitrosyl species. According to these authors, an angle smaller than 90° should be representative of the presence of N–N interactions, which are nonexistent in the case of dinitrosyl species. Different authors therefore independently concluded that NO pairs adsorb and desorb as entities, that is, as dimers [616–624]. Since two NO molecules are adsorbed on each site, there are two absorption bands in the infrared spectrum: a higher-frequency one corresponding to ν_s , and a lower frequency one, ν_{as} of the *cis*-dimer. The existence of a *trans*-dimer (C_{2h}) is also possible depending on the environment and configuration of the adsorption site [613]. The relative intensities of the doublet peaks can be used to calculate the angle formed by two NO molecules [622, 623].

As for NO adsorption, there are many infrared data concerning NO adsorption on oxides (see Table 2.26, plus the data presented in Portela *et al.* [613]). However, a detailed interpretation of the absorption bands characterizing the $M^{n+}-(NO)_x$ complexes (see, for example, complexes Cr^{n+} in Table 2.26) is more complicated than in the case of CO because of the ability of NO to dimerize. Formed dimers in their spectral manifestations, are similar to dinitrosyls and, therefore, are hardly recognizable. Full interpretations are impossible without detailed information about the state of the cations on the oxide surfaces obtained by other methods (see, for example, Peri's data [609] in Table 2.26).

Nitrogen dioxide

It was shown in [625] that the NO_2 molecule is angular, with an O–N–O angle of 134° . Two variants of the NO_2 structure seem to be possible because of the fact that the angle lies between 120° and 180° which correspond to sp^2 and sp hybridization, respectively. According to Hückel approximations [625], the molecular orbitals in NO_2 are linear combinations of the wave functions of atomic p-orbitals, as represented in Figure 2.34.

With sp hybridization (Figure 2.34(a)) an unpaired electron occupies a nonbonding molecular orbital, and the lone electron pairs belong to the oxygen atoms. This means that the corresponding molecule should be linear. With sp^2 hybridization (Figure 2.34(b)), the unpaired electron occupies a nonbonding sp^2 hybrid orbital of nitrogen. The highest lone pairs belong to the oxygen atoms and are located on sp^2 hybrid orbitals. The molecule corresponding to this state should have an angular structure. In a real molecule, the electron levels are somewhat intermediate between these two extremes as represented in Figure 2.34(a,b).

It is clear that the electron structure of the NO_2 molecule determines its chemical properties. If the NO_2 interaction with a Lewis site ($NO_2 + M^{n+} \rightarrow NO_2^+ + M^{(n-1)+}$) is accompanied by the formation of the nitronium ion, NO_2^+ , the N–O bond becomes stronger. The nitronium ion, which is iso-electronic with CO_2 , should have a linear structure and be characterized by a high-frequency N–O vibration [626]. The frequency of the N–O stretching vibrations also increase during the proton transfer to the NO_2 molecule, accompanied by the formation of an O–H bond. For example, the highest frequency for the *trans*-HONO fragment is 1690 cm^{-1} , whereas for NO_2 it is only 1616 cm^{-1} [626] (see Table 2.27).

The dimerization of NO_2 takes place when the two odd electrons of the NO_2 molecules became paired. The electronic structure of the dimer formed (N_2O_4) is represented in Figure 2.34(c). The N_2O_4 dimer readily forms hydrogen-bonds with surface hydroxyl groups. This is because the lone electron pair is shifted to a higher energy level as a result of the dimerization and the dimeric molecule becomes more basic than monomeric NO_2 , i.e. acquires a high proton affinity (ca. 200 kcal mol^{-1} [627]). This allows the attribution of the band at 2140 cm^{-1} to the NO vibrations in the hydrogen-bonded complex (a), which approximates to the nitronium ion (b):

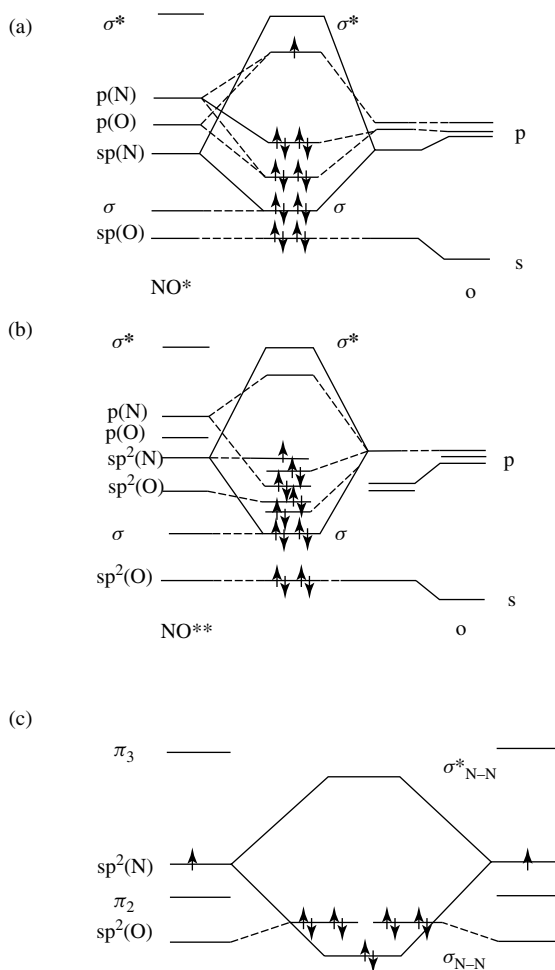
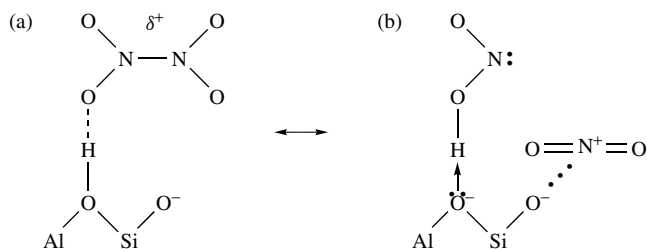


Figure 2.34. Electron structures of the upper molecular orbitals of NO_2 , corresponding to (a) sp , and (b) sp^2 hybridization; (c) molecular orbital structure of N_2O_4 .



Scheme 2.30

Thus, N_2O_4 interacting with OH groups, unlike NO_2 , can give rise to NO_2^+ , which seems to act as the nitrating agent in zeolites [628].

Table 2.27. Infrared absorbance bands of various nitro compounds and adsorbed $N_2O_4(NO_2)$ [628]. Reprinted from Malysheva, L. V., Paukshtis, E. A. and Ione, K. G., *Catal. Rev.: Sci. Eng.*, **37**, 179–226 (1995), courtesy of Marcel Dekker Inc.

Complexes, molecules	 $\nu_{as}N$ (cm^{-1})	 ν_sN (cm^{-1})
NO_2	1616	1319
N_2O_4	1710, 1758	1373, 1264
N_2O_3	1832	1630, 1305
HO– NO_2	1708	1331, 1324
HO–NO, <i>cis</i>	1640	1261
HO–NO, <i>trans</i>	1699	1265
NH_2NO_2	1613	1370
FNO_2	1791	1309
$ClNO_2$	1684	1286
NO_2^+	2360	1400
NO_2, N_2O_4 on SiO_2	1680	1380, 1625, 1600
NO_2, N_2O_4 on Al_2O_3	1580	1320
NO_2, N_2O_4 on H-Al–ZSM-5	2345, 2140	1320
	1580, 1640	–

The formation of free-radical species takes place due to the nonbonding orbital of the nitrogen atom involved in the interaction. The increasing ionization potential of the radical causes the growth of vibration frequencies [15, 626] because of the transfer of electron density from the nonbonding orbital. Support for this also comes from the fact that the vibration frequency grows upon the formation of the N_2O_4 dimer (see Table 2.27).

Adsorption of NO_2 has been studied on zeolites [629–632], as well as on oxide catalysts [633–639], because of the problem of removing nitrogen oxides from waste gases. The NO_2 adsorption species on SiO_2 have been studied with IR and ESR spectroscopies. The NO_2 molecule is found to interact with the OH groups of SiO_2 , thus forming hydrogen-bonded complexes with the oxygen atom of the N=O group. The NO_2 adsorbed on silica exists not only in a monomeric form but also as the N_2O_4 dimer. The band at around 1710 cm^{-1} observed in the IR spectra of NO_2 adsorbed on silica surfaces has been attributed to compounds such as HNO_3 . It should be noted that evidence from the IR and ESR methods is rather contradictory, and it is difficult to make clear-cut conclusions about the adsorbed species of NO_2 on this oxide.

The interactions of NO_2 with different types of zeolites has been studied by different authors [618, 629–635]. In the case of the HZSM-5 zeolite [628], NO_2 forms hydrogen-bonded complexes characterized by the 2850 and 2450 cm^{-1} νOH absorption bands. A simultaneous appearance of the bands at 1640 , 1320 , 2140 , 1760 , 1580 and 1870 cm^{-1} , plus the weak bands at 2345 and 1670 cm^{-1} , provide evidence, according to the data shown in Table 2.28 (see below) that the N_2O_4 dimer is formed. Adsorption of NO_2 on cationized zeolites leads to the formation of both nitrate and nitrite ionic compounds, as characterized by the absorption bands below 1600 cm^{-1} . The band at around 1400 cm^{-1} has been assigned to the stretching vibration of the NO_3^- ion [593]. When NO_2 reacts with Cr^{3+} -containing zeolites [618], strong absorption bands at 1630 , 1580 – 1560 , 1410 and 1370 cm^{-1} , characteristic of nitrates, and also at 2360 cm^{-1} , due to NO_2^+ complexes [15, 618] with Cr^{2+} , are generated. On the basis of ESR data, NO_2 was assumed to oxidize Cr^{3+} to Cr^{5+} . Moreover, in a number of studies the bands in the 2100 – 2140 and

2000–2050 cm^{-1} regions were observed. There is no common view-point concerning these bands in the available studies. Chao and Lunsford [632] assigned these bands to the NO_2^+ ion, while Naccache and Ben Taarif [618] have shown that this ion in the fully ionized state is characterized by the band at 2360 cm^{-1} . Malysheva *et al.* [628] believe that the bands above 2000 cm^{-1} should be assigned to the NO^+ fragments.

It was shown that NO_2 reacts with oxide surfaces to produce strongly adsorbed species [634–639] which, as most authors have reported, are from nitrates and molecular adsorbed NO_2 . The correlations shown in Table 2.21 above also seem to be useful in interpreting such spectra. In addition, NO_2 disproportionates on Lewis acid–base pairs giving NO_3^- and NO^+ , whereas only nitrates are formed on the surfaces after the interaction of NO_2 with hydroxyl groups [593, 639]. On interaction with cations, the dissociation of NO_2 , with the formation of nitrosyl complexes or NO^- and NO_2^+ may occur.

On $\alpha\text{-Cr}_2\text{O}_3$, NO_2 adsorption leads to the formation of bridged and bidentate nitrates, as well as various nitro species [637]. Under an atmosphere of NO_2 , the latter are oxidized to nitrates. When surface hydroxyls participate in the NO_2 adsorption, bridged nitrates and water are among the reaction products. Adsorption of NO_2 on reduced samples probably leads to NO adsorption and to oxidation of the surface with the formation of the same species as observed on oxidized surfaces, but in different concentrations. Pre-adsorbed water slightly affects NO_2 adsorption.

The adsorption of NO_2 has been studied on titania surfaces by various authors [634, 636, 638, 639, 641]. It was reported that $(\text{NO}_2)_{\text{ads}}$ appears to be the form of adsorption. Ramis and co-workers [634] observed mainly the formation of three surface species and interpreted these as two nitrates and/or molecularly adsorbed NO_2 . Dines *et al.* [636] observed different adsorption species and attributed these to bridged and bidentate nitrates. These authors showed that as the temperature increases, monodentate nitrates are formed. Besides the formation of different nitrates involving surface oxygen, NO_2 reacts with the surface hydroxyls of anatase to produce nitrates and water which is weakly bound to the latter. It has been reported [634, 636] that the surface compounds formed upon NO_2 adsorption on TiO_2 strongly affect the hydroxyl coverage on anatase.

On the Lewis acid–base pairs of the surface of oxides, a disproportionation of NO_2 to NO^+ and nitrates takes place, as was first established by Pozdnjakov and Filimonov [593] and confirmed later in [639]. The latter authors established that the first compounds that arise are $\text{Ti} \cdots \text{O}_2\text{NOH}$ groups, formed with the predominant participation of hydrogen-bonded hydroxyls. Larger amounts of added NO_2 leads to interaction with isolated hydroxyls with the formation of monodentate, bidentate and bridged nitrates, plus water. Adsorption on coordinatively unsaturated acid–base pairs ($\text{Ti}^{4+} - \text{O}^{2-}$) is the last process to occur and is accompanied by disproportionation and the formation of nitrates (on the titanium cations) and NO^+ (on oxygen anions). Saturation of the anatase surface with nitrogen dioxide leads to blocking of the Lewis acid sites and the generation of Brønsted acidity at the expense of the basic surface hydroxyl groups on the support.

Interesting data on NO_2 adsorption have also been obtained in the case of V_xO_y /support catalysts [635, 636, 641].

2.3.6 ADSORPTION OF CARBON DIOXIDE

Linear triatomic molecules of the type X_3 or YXY have four types of vibrations, of which the ν_2 vibration is doubly degenerated. In accordance with the selection rules, these vibrations which change the dipole moment appear in the infrared spectrum, while the vibrations that change the polarizability of the molecule occur in the Raman spectrum [15].

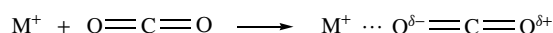
The CO_2 molecule may react like both an acid and a base, i.e. it is an amphoteric compound. It has been well established by IR spectroscopic investigations that the chemisorption of carbon

dioxide on oxide surfaces occurs with the participation of surface oxygen, surface hydroxyl groups and coordinatively unsaturated surface cations.

Interaction with cations

Even in the first studies using IR spectroscopy in adsorption and catalysis it was already established that CO₂ molecules can interact with cations, as, for instance, in zeolites (see, for example, [19, 642–644]). The infrared spectra of carbon dioxide adsorbed on the zeolites LiX, NaX and KX have been studied in detail [642]. These spectra have the adsorption band of the asymmetric linear vibration (ν_3) of adsorbed CO₂ molecules at 2368, 2355 and 2348 cm⁻¹ for LiX, NaX and KX, respectively. The dependence of the frequency of this absorption band on the type of exchanged cation indicates that there is an interaction between the latter and adsorbed CO₂ molecules and that the linear structure of the molecules is retained in the adsorbed state. The weak absorption band at 1380 cm⁻¹ observed in the spectrum is attributed to the symmetric vibration, ν_1 , which is inactive in the infrared spectrum of the free molecule.

As well as in the case of adsorption of CO molecules on cationated zeolites, the adsorption of CO₂ causes a shift towards higher frequencies of the absorption band ν_3 CO₂ with respect to the value in the free state [643, 644]. This shift increases with an increase in the ratio of charge to cation radius. A shift in the absorption band in this direction is seldom observed in molecular interactions. The direction of the shift in this band has been explained by the strong polarization of CO₂ molecules adsorbed on the zeolite, which interact with the ion-exchange cation according to the following:

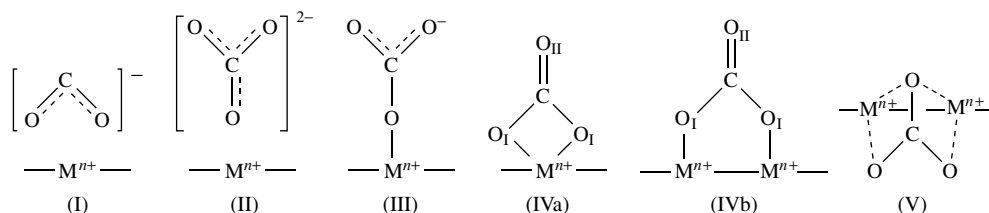


Scheme 2.31

The variation in the position of the absorption band of the asymmetric stretching vibration, ν_3 , of adsorbed CO₂ molecules has been studied as a function of the field strength. Different relationships were observed for zeolites of type X and Y which reflect the differences in the fields of these zeolites, and hence of the perturbations of CO₂ molecules adsorbed onto them [644]. The absorption bands of adsorbed CO₂ at 1380 and 1270 cm⁻¹ were attributed to a Fermi-resonance doublet between $2 \times \nu_1$ and ν_2 vibrations – these are usually only active in the Raman spectrum. It is difficult to explain the appearance of new bands on both sides of the absorption from ν_3 . It has been suggested that these bands may correspond to molecules which interact with the cations at different sites of attachment or to two CO₂ molecules adsorbed together in a state of mechanical resonance, or possibly to combinations of ν_3 of the CO₂ molecules with low frequencies involving the vibrations of the complete molecule with respect to the surface.

Interaction with surface oxygen atoms: spectral identification of surface carbonate–carboxylate compounds

Absorption bands in the region 1000 to 1700 cm⁻¹ characterize bond-stretching vibrations in surface carbonate–carboxylate compounds. In reports of studies of the interaction of CO with oxide surfaces, various schemes were presented for the interpretation of the spectral patterns generated by such compounds, based on analogies with the spectra of bulk compounds [15,



Scheme 2.32

18–20, 30, 650, 651]. The following types of carbonate–carboxylate groups are identified for both surface and bulk compounds:

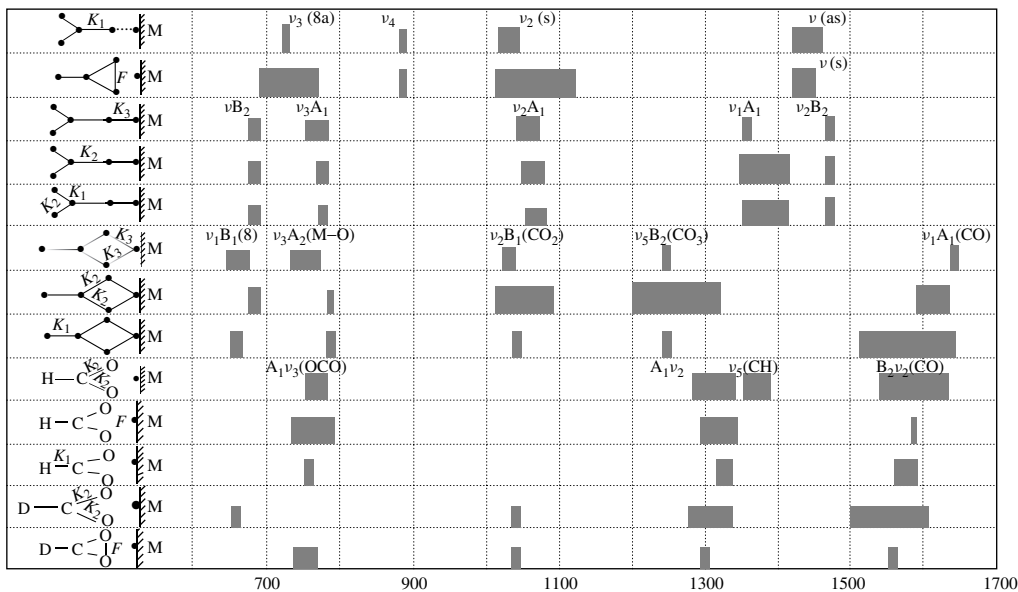
The attribution of the absorption bands of these structures of different symmetries has been presented by Davydov [30], and the scheme shown in Table 2.28 can be proposed for interpreting the spectra of surface carbonate–carboxylate compounds. This table contains the range of vibration frequencies for each structure in the region usually used to study the spectra of oxide-adsorbed molecules. The relative atomic displacements for the fundamental vibrational modes of the different types of carbonates can only be obtained by theoretical calculations. Calculations of the vibrational spectra of individual surface species based on the modeling of the potential function of the molecule (variation in the force constants of the potential function) were made for interpreting the changes in the vibrational frequencies and their reactions to changes in the force fields of molecules subjected to the influence of a highly nonuniform field at an adsorbent surface [118]. The correlation table based on these calculations (Table 2.29) shows the ranges for different kind of vibrations of different carbonates and formates and may be useful in interpretation of such spectra.

It should be pointed out that differences in the structure of the carbonate complexes III and IV (see Table 2.28) reflect the differences in the degree of participation of the surface oxygen atoms in their formation [20]. Taking this into account, the separation of various forms of carbonate compounds (such as III and IV) is only a useful approximation. Higher values of splitting between the first two CO bands testifies to a greater covalence of the M–O bonding to the surface. It is a very interesting fact that there can be several carbonates with different structures on the surface of one and the same oxide simultaneously. This fact was established by investigations of the spectra obtained during and after thermal desorption. Such data enable a conclusion to be reached about the different surface stabilities of the different carbonate structures. The latter reflects the different properties of the surface centers participating in the formation of carbonate-like compounds. The pairs $M^{n+}O^{2-}$ are examples of such centers because each carbonate is formed by the participation of a surface oxygen atom and the asymmetric field of the

Table 2.28. Correlation table for the assignment of absorption bands in IR spectra of surface carbonate–carboxylate compounds.

Type of compound		Spectral range of CO bond stretching vibrations (cm^{-1})				
Carboxylate, CO_2^-	I	1630–1560	$\nu_{\text{as}}\text{COO}^-$	1420–1350	$\nu_{\text{s}}\text{COO}^-$	
Noncoordinated carbonate	II	1450–1420	$\nu_{\text{as}}\text{CO}_3^{2-}$	1090–1020	$\nu_{\text{s}}\text{CO}_3^{2-}$	
Monodentate carbonate	III	1530–1470	$\nu_{\text{as}}\text{COO}^-$	1370–1300	$\nu_{\text{s}}\text{COO}^-$	1080–1040 $\nu\text{C}=\text{O}$
Bidentate carbonate	IVa	1620–1530	$\nu\text{C}=\text{O}$	1270–1250	$\nu_{\text{as}}\text{COO}^-$	1030–1020 $\nu_{\text{s}}\text{COO}^-$
	IVb	1670–1620	$\nu\text{C}=\text{O}$	1270–1250	$\nu_{\text{as}}\text{COO}^-$	1020–980 $\nu_{\text{s}}\text{COO}^-$
Organic-like carbonate	V	1850–1700	$\nu\text{C}=\text{O}$	~1260	$\nu_{\text{as}}\text{COO}^-$	1020–970 $\nu_{\text{s}}\text{COO}^-$
Acid carbonate, HOCO_2^-	VI	1700–1660	$\nu\text{C}=\text{O}$	1420–1390	$\nu_{\text{as}}\text{COO}^-$	1050–990 $\nu_{\text{s}}\text{COO}^-$

Table 2.29. Correlation table for interpretation of the IR spectra of surface carbonate – carboxylate structures drawing on the basis of calculations of these structures' vibrational spectra (modeling of potential functions as a function of changes in the force constants).



cation leads to the splitting of the νCO frequencies. The differences in spectral features of the surface carbonates hence depend particularly on the properties of the anions and their effective charges.

Bicarbonate structures are formed by the participation of surface hydroxyl groups which most probably have a basic nature. The main spectral manifestations of the bicarbonate structure in the region $1000\text{--}1800\text{ cm}^{-1}$ (see Table 2.28) are similar those observed for carbonates, but there is a higher value of νCO ($\sim 1700\text{ cm}^{-1}$) and, in addition, a low-frequency δOH absorption band at $\sim 1220\text{ cm}^{-1}$ and a band from νOH at $\sim 3600\text{ cm}^{-1}$. The identification of such compounds can be further authenticated by H–D exchange experiments.

There are many studies in the literature devoted to the interaction of both CO_2 and CO with surface oxygen and cations of different oxides and about the formation of surface carbonates as a result of such an interaction (see, for example, [625–630] and references therein). We have concerned ourselves only with the questions relating to the interpretation of the infrared spectra of the obtained surface compounds.

It should be borne in mind that the spectra of CO and CO_2 adsorbed on the same oxide, as a rule, vary in spectral images from the carbonate species (see, for example, [18, 30, 645–651]). However, because of the significant widths of the absorption bands and the formation of several types of carbonate species simultaneously, it is not easy to interpret these differences. A detailed analysis of the spectra as a function of coverage and temperature and thermostability of the surface species that are formed is needed. Moreover, it should be taken into account that the adsorption of CO_2 on reduced samples in some cases leads to the oxidation of the surface by direct reoxidation of the cations by dissociative adsorption of CO_2 and the formation of CO . The effective charge of the cations can also increase due to the production of carbonate species [479], whereas upon the adsorption of CO with the formation of carbonates the effective charge of the cation decreases.

Zeolites

Absorption bands in the region of 1200–1800 cm^{-1} , which are absent in the spectrum of gaseous CO_2 , also occur in the infrared spectra of carbon dioxide adsorbed on the zeolites LiX, NaX and KX [642]. These indicate that chemisorption has taken place. It has been established that the CO_2 molecules interact with the oxygen atoms of the zeolite framework, leading to a strong modification of zeolite properties which is reflected even in the cutoff region. Chemisorption proceeds in two stages and depends on the amount of CO_2 . Absorption bands at 1485 and 1425 cm^{-1} appear immediately after the adsorption of a small amount of CO_2 on the zeolites, in addition to the absorption band of adsorbed molecules at 2355 cm^{-1} . Absorption bands at 1715 and 1365 cm^{-1} appear in the spectrum more slowly. At high CO_2 pressures, the absorption bands at 1425 and 1485 cm^{-1} disappear completely, whereas the intensities of the absorption bands at 1715 cm^{-1} and 1365 cm^{-1} increase considerably. Desorption *in vacuo* with heating leads to reverse changes in the spectrum. The intensities of the absorption bands at 1365 and 1715 cm^{-1} decrease appreciably while those of the absorption bands at 1425 and 1485 cm^{-1} increase markedly. The absorption bands at 1365 and 1715 cm^{-1} disappear from the spectrum of a sample evacuated at temperatures below 373 K. The absorption bands at 1425 and 1485 cm^{-1} disappear after evacuation of the sample at 573 K.

The positions of the bands of the chemisorbed compounds are different for the LiX, NaX and KX zeolites. The absorption bands observed in the range 1250–1750 cm^{-1} lie in the region of the absorption bands seen in the spectrum of CO_2 adsorbed on oxides and are usually attributed to carbonate and carboxylate surface structures. However, the spectra of such structures on these zeolites differ from those of similar structures from the chemisorption of CO_2 on oxides. Hence, it is assumed that the formation of these structures is due to the formation of a bond between the carbon atom and a surface oxygen atom of the skeleton. It is assumed that the reaction proceeds in the immediate vicinity of the exchange cation, so that the carbonate ion formed is further stabilized by the positive charge of the ion-exchange cation. The adsorption of carbon dioxide and the formation of surface carbonate structures are facilitated by the pre-adsorption on zeolites of a small amount of water molecules. Habgood and co-workers [642, 643] concluded that during the adsorption of CO_2 , a change in the spectrum of H_2O previously adsorbed on the zeolites shows that the carbonate-like structures interact with the adsorbed water molecules by the formation of hydrogen bonds. Hence, it is assumed that the water molecules act only as catalysts of the reaction, and are not incorporated into the structures of the surface compounds that are formed.

No carbonate-like structures were observed during the adsorption of CO_2 on zeolites with divalent alkaline-earth exchange cations. Their absence was explained by the concept that the properties of cations differ at different sites of their attachment to the zeolite surface. The S_{III} sites are assumed to serve as centers for the formation of carbonate-like structures during the adsorption of CO_2 on LiX, NaX and KX zeolites. It is considered that the formation of such surface structures does not proceed in the case of the CaX, SrX and BaX zeolites, because the S_{III} sites are unoccupied by cations [644]. In recent years, the formation of carbonates has widely employed to modify the properties of zeolites.

Oxides

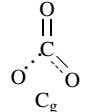
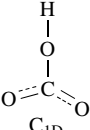
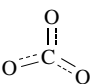
Because CO_2 molecules interact specifically with the cations, and their spectral characteristics depend on the cation properties, the spectra of adsorbed CO_2 molecules have been used to study the properties of aprotic sites on oxides. The spectrum of CO_2 molecules adsorbed on the highly dehydroxylated surface of alumina–silica gel [645] has an absorption band at about 2375 cm^{-1} , which gradually shifts toward higher frequencies as CO_2 molecules are removed by evacuation

at room temperature. It is assumed that the adsorbed CO_2 molecule preserves its linearity, and is adsorbed on centers through ion-quadruple interactions. In addition to the main intense absorption band at 2375 cm^{-1} , there are two absorption bands at 2405 and 2355 cm^{-1} in the spectra. Peri [645], when studying the CO_2 adsorption on Al_2O_3 , attributed these to rotation branches of the absorption bands of the adsorbed molecules. It is assumed, moreover, that the adsorption of CO_2 proceeds selectively on a small fraction of the aprotic Lewis centers, namely, on the so-called α -centers. According to Peri [645], the centers which selectively adsorb CO_2 molecules also selectively absorb the molecules of butene, acetylene and HCl . Molecules of H_2O and NH_3 are adsorbed fairly well on all aprotic centers, including the α -centers. There are many data in the literature concerning the use of CO_2 to test LASs. (see above)

The carbonate-carboxylate structures are again characterized by absorption bands in the region $1300\text{--}1900\text{ cm}^{-1}$ which originated on the surface, not only during the CO_2 adsorption, but also due to adsorption with decomposition of several other molecules [18, 19, 20, 30]. These compounds can be produced during the pre-treatment of the sample *in vacuo* at high temperatures due to the oxidation of organic contaminants which have appeared on the surface from the vapors from the greases and oil of vacuum pumps. Moreover, they are produced during the adsorption of the simple molecules CO_2 and CO [27, 30, 646]. Thus, the spectrum of CO_2 adsorbed on alumina has absorption bands at ca. 1750 , 1635 , 1500 and 1235 cm^{-1} , which were attributed to carbonate surface structures. The absorption band of molecularly adsorbed CO_2 was observed at ca. 2350 cm^{-1} , as seen for the adsorption on alumina-silica. Carbon dioxide is strongly chemisorbed by alumina at 298 K . In this case, the spectrum has absorption bands at ca. 1770 , 1640 , 1480 and 1320 cm^{-1} [646].

Peri [645] established the presence of at least three different types of compounds formed during the adsorption of CO_2 on an alumina surface evacuated at 873 K . The absorption bands in the $1800\text{--}1870\text{ cm}^{-1}$ region were assigned to molecularly adsorbed CO_2 . An interpretation of the spectra of CO_2 adsorbed on Al_2O_3 has also been made by Fink [647] (Table 2.30). Surface compounds of the types I–III are assumed to be in equilibrium. A type-II compound predominates on the surface at 233 K , while a type-III compound predominates at 298 K . A compound of type-III remains on the surface evacuated at temperatures of up to 473 K . Adsorption at temperatures above 473 K leads to the formation of a type-IV compound.

Table 2.30. Types of surface compounds formed during the chemisorption of carbon dioxide on the surface of $\gamma\text{-Al}_2\text{O}_3$.

Type of compound	Structure and symmetry	Frequency (cm^{-1}) and interpretation
I	CO_2 D_{3h}	2370 (ν_{as})
II		1200 (ν_s); 1785 (ν_{as})
III		1240 (β_{OH}); 1490 ($\nu_s(\text{COO}^-)$); 1645 ($\nu_{\text{as}}(\text{COO}^-)$); 3615 (ν_{OH})
IV		1500 (ν_a , very broad band)

The difference in the behavior of the absorption bands at 1480 and 1400 cm^{-1} in the course of the adsorption of CO_2 on alumina at temperatures ranging from 293 to 523 K indicates that monodentate carbonate structures are not formed on the surface. The absorption bands at 1650 and 1230 cm^{-1} were attributed to bidentate carbonate structures. There were also differences in the interaction of adsorbed CO_2 molecules with different types of surface hydroxyl groups of alumina. New data concerning CO_2 adsorption on the LASs of Al_2O_3 have recently been reported [27].

The interaction of CO_2 with the surface oxygens of different oxides, especially transition-metal oxides, produce spectra implying the formation of several different types of carbonates. The appearance of absorption bands in the region 1200–1800 cm^{-1} , which is typical for the stretching vibrations of CO bonds in individual carbonates, can be so interpreted. Frequently, the spectra of the surface compounds are identical to the spectra of bulk carbonates, thus implying the presence of free CO_3^{2-} ions. The results of the IR spectral analysis of carbonates can be used to establish the type (and sometimes the structure) of the carbonates formed on the oxide surfaces. Such data have been reported in detail [15, 18–20, 30].

Carbon dioxide adsorption on different oxide systems is still widely investigated (see, for example, [649–651]) because of its relevance to the basicity of various catalysts (see Section 2.5).

Detailed results resulting from IR spectroscopic investigations of CO_2 adsorption over different oxides have been presented by Busca and Lorinzelli [651]. It should be taken into consideration that there are differences in the spectral images (structures of surface carbonates) of CO_2 adsorption on oxidized and reduced samples of the transition-metal oxides [648]. In addition, CO_2 can be decomposed on reduced surfaces of transition-metal oxides [for example, 841], oxidizing the surface and producing carbon monoxide.

2.3.7 ADSORPTION OF HYDROGEN SULFIDE

The removal of H_2S is one of the most important processes in the chemical industry and hence adsorbents and catalysts which remove H_2S selectively have been intensively developed for a long time. In connection with these studies, data about the character of the H_2S interaction with such systems are very important.

In this section, the main attention is paid to the effect of surface centers on both the nature and properties of the adsorption forms of H_2S that are initially formed. It is well known that during high-temperature interactions, metal sulfides are formed [209].

The H_2S molecule is nonlinear with an angle of 92° and is similar to the H_2O molecule in its normal vibrational modes [12, 15] and in its electron structure. Due to the low energy of the highest-occupied molecular orbital (HOMO), H_2S has a low value of its ionization potential (IP) and tends to participate in donor–acceptor interactions. The nature of the H_2S interaction with oxide surfaces is determined by two factors. First of all, there is the high reactivity of H_2S as a very strong reducing agent (IP = 10.4 eV; for comparison, the IP values for CO, SO_2 and H_2O are 14.01, 12.34 and 12.6, respectively [583, 584]). Secondly, heterolytic rupture of the S–H bond occurs easily (i.e. the hydrogen of this molecule has a high mobility) ($\text{p}K_a = 7.04$) which increases upon formation of a donor–acceptor bond with the surface. Thus, it is apparent that the H_2S molecule should interact with all of the types of centers which are present on the oxide surface. The nature of the oxide, the type of the surface center and the conditions of the reaction strongly determine the character of the H_2S adsorption and of its transformations.

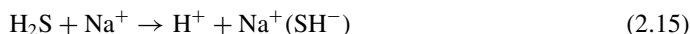
SiO₂ and Zeolites

On the surface of silica, according to the author's data, only H-bonding between the OH groups (3750 cm^{-1}) and H_2S takes place, similar to that on the proton centers of HZSM zeolites (νOH

$\sim 3610\text{ cm}^{-1}$). The perturbed νOH absorption is observed in the $3400\text{--}3500\text{ cm}^{-1}$ region in the case of SiO_2 and at 3200 cm^{-1} for zeolites (more strongly H-bonded). In the region of νSH , a doublet of bands at ca. 2570 and 2585 cm^{-1} is observed, which indicates that the HSH species is not dissociated.

The infrared data [652] indicate that H_2S is physically adsorbed on zeolites. The shifts of the H_2S frequencies are comparable to those observed upon the transition from the gas to the liquid phase. A strong hydrogen-bonding between the surface OH groups and H_2S is also possible. The H_2S molecule shows a rapid H–D exchange with the surface OH groups, with which it most strongly forms a hydrogen bond (3650 cm^{-1} for the HY zeolite).

Forster and Schuldt [653] studied the interaction of H_2S with NaA and CaA zeolites and showed that at low coverage, H_2S dissociates upon adsorption. They observed an infrared band at 2500 cm^{-1} and assigned this to SH^- groups bonded to cations. On the basis of an analysis of NMR spectra, Lechert and Henning [654] also suggested that at low coverage H_2S dissociates when adsorbing onto NaX zeolite. Systematic investigations of H_2S adsorption on NaX and NaY zeolites by means of combined infrared and UV–Vis spectroscopic methods were carried out by Karge *et al.* [655–657, 660, 661] and others [658, 659]. This work confirmed the dissociative adsorption of H_2S molecules and showed that both OH and SH stretching vibrations appear upon contact of H_2S with the NaX zeolite. Dissociative adsorption was assumed to occur according to the following equation:



with the protons generated via dissociation attacking the zeolite lattice and forming new (acidic) OH^- groups, as indicated by bands at around 3650 and 3580 cm^{-1} . Karge and Rasco [655] found that the amount of dissociatively adsorbed H_2S decreases with an increase of the Si/Al ratio in NaX zeolites. For NaY-type zeolites, with a Si/Al ratio of ca. 2.5 (or higher), H_2S dissociation did not occur. Moreover, there was strong evidence that the Na^+ cations on the so-called S_{III} sites at the walls of the ‘supercages’ were involved in the dissociative adsorption of H_2S . Thus, these data support an assignment of the 2560 cm^{-1} band to SH^- groups bound to cations.

The first molecules of H_2S adsorbed onto NaX suffer complete dissociation of hydrogen sulfide, as has been shown by the combination of IR and UV–Vis spectroscopic measurements [658–661]:



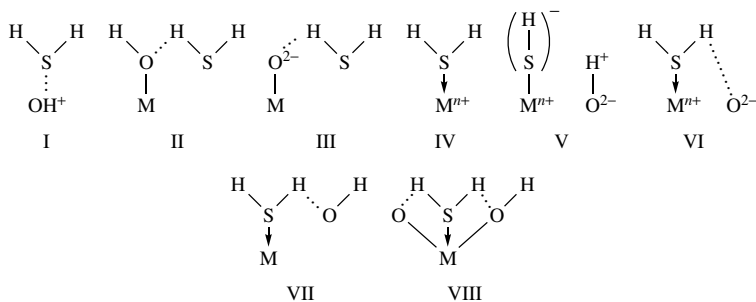
The adsorption of the first H_2S molecules ($<0.095\text{ mmol g}^{-1}$) does not give rise to the SH^- band in the IR spectra, while a very intense band at 235 nm is observed in the UV–Vis spectrum. An interpretation of this band was based on the comparison of data obtained from the UV spectra of hydrogen sulfide, sulfide and hydrosulfide ions in solution and sulfide ions in crystalline salts. The gradual increase in the amount of H_2S adsorbed ($>0.14\text{ mmol g}^{-1}$) led to the appearance of OH^- and SH^- (2560 cm^{-1}) stretching modes. At adsorbate concentrations higher than $0.33\text{ mmol (H}_2\text{S) g}^{-1}$, only physical adsorption or chemisorption on weak sites of the zeolite lattice (i.e. adsorption without any dissociation of H_2S molecules) took place. It was considered [662, 663] that the hydrogen atom of the SH group in the H_2S molecule, reversibly adsorbed on Na zeolites, acts as a Brønsted acid site and promotes, for example, a hydrocarbon conversion. Assignments of the bands to the species involved in the adsorption and interaction of H_2S on NaX zeolite and alumina are presented in Table 2.31. According to these data, new sulfur-containing species appear on the surface due to H_2S interaction. This was also suggested by the ESR data [664] because sulfur radicals were also observed upon H_2S interaction with zeolites.

Table 2.31. Assignment of bands to species supposedly involved in adsorption and interaction of H₂S and SO₂ on NaX zeolite and alumina [600]. Reprinted from *Zeolites* (now *Surf. Sci.*), 7, Karge, H. G., Ziolek, M. and Lanieski, M., ‘UV–Vis and infrared spectroscopic study of hydrogen sulfide adsorption on faujasite type zeolites’, 197–205, Copyright (1987), with permission from Elsevier Science.

NaX zeolite		Alumina		Species	Reference
UV–Vis (nm)	IR(cm ⁻¹)	UV–Vis (nm)	IR(cm ⁻¹)		
–	2560	–	2570	HS ⁻	647, 648, 653, 655, 664, 665
250	–	225–230	–	S ²⁻ , HS ⁻	655, 658, 666
–	2565	270	2570	H ₂ S, physisorbed	647, 648, 655, 664, 665
215	1240	215	1080	HSO ₃ ⁻	661, 664
250	–	230–250	–	S ₂ O ₅ ²⁻	650
280	1315	270	1330	SO ₂ , physisorbed	661, 664, 665
280	–	260–280	–	S ₈ and/or S ₈ , H ₂ S _n	647, 648
320	–	340	–	S ₈	647, 648
385	–	–	–	–	–

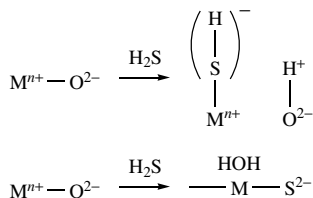
Oxides

There are many spectroscopic data about the interaction between H₂S and the surfaces of different oxides [176, 209, 457, 652, 656, 663–695]. Among these, the interaction with the surface of Al₂O₃ has been investigated in most detail. Based on these data, the following types of surface compounds appear to be formed:



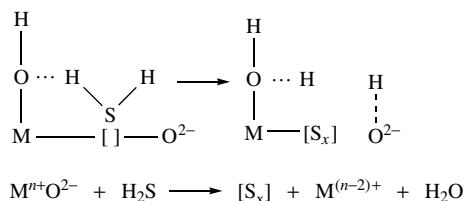
Scheme 2.33

and the following reactions occur:



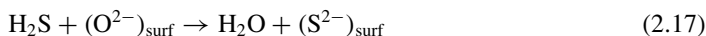
Scheme 2.34

On defective sites the interaction with H₂S is considered to occur in the following way:



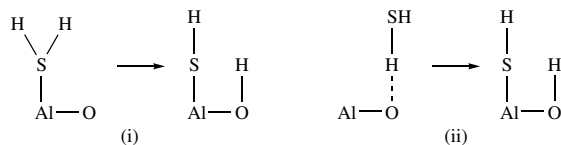
Scheme 2.35

Due to H₂S interaction with oxide surfaces (Figure 2.35), the bands of the molecularly adsorbed H₂O appear at 1600–1620 cm⁻¹, even for oxides where there is no formation of SH groups (see Ti/Sb). This shows that a direct exchange takes place between the sulfur atom from H₂S with the O²⁻ ion of the oxide surface, with the formation of both H₂O and sulfide ion, as follows:



The presence of the above-mentioned bands in the UV spectra of oxides (see Table 2.31), and the fact that the LASs on the surfaces of oxides are partially blocked after removal of the other forms of H₂S adsorption, both indicate the formation of S²⁻ groups on the oxide surfaces. The use of pre- and co-adsorption of H₂S with the probe molecules CO and NH₃ for LASs and/or CDCl₃ and CO₂ for basic sites (BSs) showed that H₂S is adsorbed on oxides with the participation of both LASs and BASs. In the case of alumina, more than 50 % of these centers are blocked directly after adsorption of H₂S at 293 K. Even after adsorbed H₂S was removed at 473 K, a certain portion (20–30 %) of such centers remained blocked [176, 666]. On the surface of Sn–Mo–O [457, 685, 687], V/TiO₂ [691] and V/Al₂O₃ [690], the H₂S interaction proceeds only via the rupture of both of the SH bonds.

The suggested schemes are supported by the infrared and UV–Vis spectroscopic data obtained for oxides with various types of surface sites, such as SiO₂, HZSM zeolite, Na/SiO₂, Sb₂O₄/TiO₂, MgO and CaO [665, 666], on the surfaces of which only one or two types of centers exist. Dissociative adsorption of H₂S on oxides [665–667] can proceed with the formation of compounds of the type S²⁻ (Mⁿ⁺S²⁻) and SH⁻ (Mⁿ⁺SH⁻). Such interactions takes place with the participation of the acid (LAS) and basic (BS) sites, or acid–base pairs, and depends on the properties of these centers as well as on the nature and properties of the oxide surface [665, 667]. The nature of the dissociative adsorption of H₂S, with the formation of SH⁻ groups, is identical for the oxides MgO, γ-Al₂O₃, CaO and TiO₂ [665, 688] and is characterized by the appearance of absorption bands in the spectral region at 2570–2590 cm⁻¹. The lower-frequency band at ca. 2535 cm⁻¹ is characteristic for TiO₂ (Table 2.32). The SH groups of different oxides have a different stability. For example, these groups are removed from the TiO₂ surface at 293 K, while on the surfaces of Al₂O₃, CaO and MgO they are present at temperatures up to 473 K. The poisoning effects of the bases suggest that the thiolate species can be formed on two different types of sites via two mechanisms, as follows:



Scheme 2.36

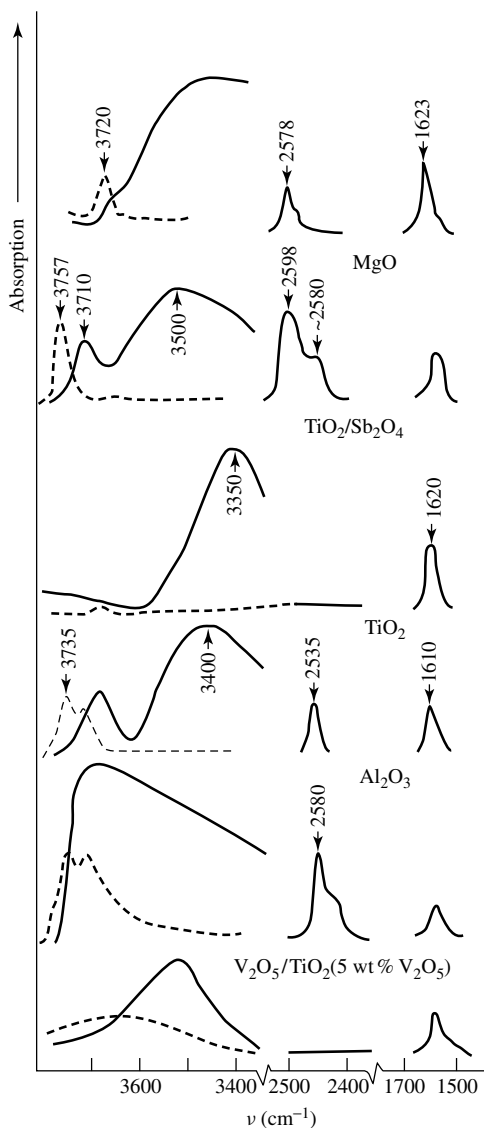


Figure 2.35. FTIR spectra of H₂S (10 torr) adsorbed at 293 K on different metal oxides after treatment at various temperatures: CaO, 973 K; MgO and TiO₂, 723 K; TiO₂/Sb₂O₄ and V₂O₅/TiO₂, 623 K; Al₂O₃, 773 K.

Lavalley *et al.* [672, 673] have reported the effect of CO₂ on the infrared spectra of species produced by H₂S, CH₃SH and (CH₃)SHSSH on Al₂O₃ (1600–1200 cm⁻¹ range). These authors consider that the intense bands at 1570 and 1340 cm⁻¹, observed by themselves, Deo *et al.* [652], Slager and Amberg [667] and Datta and Cavell [678], are the result of the interaction between H₂S and traces of CO₂ [672]. According to Lavalley *et al.* [673], these bands at 1570 and 1340 cm⁻¹ originate from the surface thiocarbonate species formed due to H₂S chemisorption on the acidic parts of the X-sites (i.e. on Al_{cus}³⁺) and CO₂ adsorption on the basic part (i.e. basic OH groups).

Table 2.32. Absorption forms of H₂S and their spectral manifestations on various oxide systems.

Oxide	λ BCT ^a M ⁿ⁺ → S ²⁻ (nm)	ν SH in SH ⁻ (cm ⁻¹)	Reversible – molecular form
10 % V ₂ O ₅ /TiO ₂	–	–	–
30 % Sb ₂ O ₄ /TiO ₂	230–250	–	–
TiO ₂	230–250	2532	–
CaO	230–250	2578	–
MgO	230–250	2580, 2598	–
γ -Al ₂ O ₃	230–250	2580, 2560	+
H-ZSM	235	2560	H ⁺ ← SH ₂ ^b
SiO ₂	–	–	OH ^{δ+} ← SH ₂ ^b

^aBCT, band of charge transfer.^bMost probable reaction.

Complexes of the types I–III (see Scheme 2.33) have similar spectral manifestations, and it is difficult to differentiate these by the use of IR spectroscopy. Such complexes represent the reversible adsorption of H₂S and are usually formed at a high coverage.

The most important bands appearing after the molecular adsorption of H₂S, for example, on alumina [652, 667], were observed at around 2560–2570 (stretching vibration) and 1335–1340 cm⁻¹ (deformation vibration). The high-frequency bands were attributed to the SH stretching modes (2611 and 2684 cm⁻¹ for the free molecule), while the 1335–1340 cm⁻¹ band of the adsorbate was ascribed to the scissors-like bending mode, ν_2 , of the SH₂ group. A broad infrared band at around 3400 cm⁻¹ reflects the formation of hydrogen-bonds between H₂S and the surface. It is difficult to observe molecularly adsorbed H₂S at a low coverage (the appearance of δ H₂S is the best indication of the presence of the molecular form on the surface) because all paired centers of the oxide surface lead to H₂S dissociation.

The heats of adsorption of H₂S have been measured for a series of oxide catalysts (Table 2.33 [176, 680]). It was possible to distinguish several types of reversible adsorption behavior on these oxides. The weakest-most probably hydrogen – bonded H₂S – has a heat of absorption of 18.8 kJ mol⁻¹ (q_{α_1}) for an amount of $\sim 2 \times 10^{-3}$ % of a monolayer on SiO₂. In the group of oxides,

Table 2.33. Heats of adsorption^a of SO₂ and H₂S on various metal oxides.

Sample	S_{sp} (m ² g ⁻¹)	$q_{SO_2}^0$ (kJ mol ⁻¹)			$q_{H_2S}^0$ (kJ mol ⁻¹)		
		α_1	α_2	β	α_1	α_2	β
SiO ₂	300	25	–	–	18.8	–	–
Fe ₂ O ₃	5.6	–	–	125	–	52	109
Bi ₂ O ₃	0.3	–	–	92	–	63	102
Bi ₂ S ₃	0.5	–	–	92	–	63	–
Al ₂ O ₃	230	–	–	127	–	–	130
MgO	92	–	–	113	–	–	130
Mn ₂ O ₃	4.5	–	–	109	–	–	117
TiO ₂	73	–	–	102	–	–	102
V ₂ O ₅ –Fe ₂ O ₃	6.4	–	65	–	–	42	100
V ₂ O ₅	3.2	–	50	–	–	–	84
CaO	3.3	25	–	117	–	–	–

^aThese were obtained by using the method of thermal desorption with slow programmed heating of the sample. The initial heats of desorption (heats of adsorption near to total coating) were calculated by using the Clausius–Clapeyron equations.

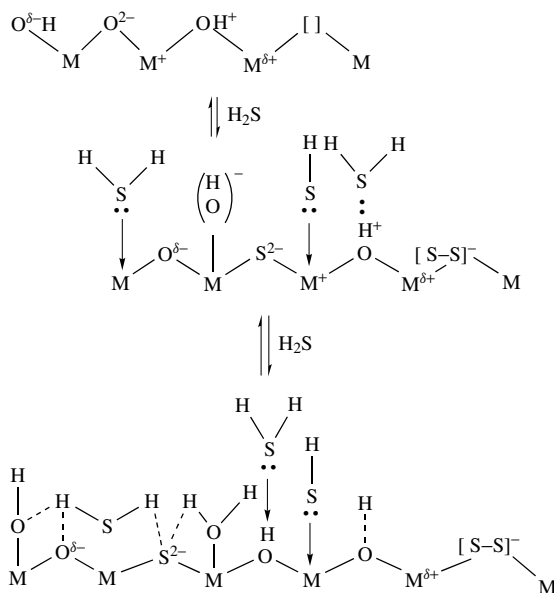
Bi_2O_3 , Fe_2O_3 and $\text{V}_2\text{O}_5\text{-Fe}_2\text{O}_3$ the heat of adsorption for H_2S in the α_1 form is 42–63 kJ mol^{-1} , which is close to the value of 54 kJ mol^{-1} observed on $\gamma\text{-Al}_2\text{O}_3$. The heat of adsorption for the strongest bound β -form of H_2S varies from 84 kJ mol^{-1} on vanadium pentoxide to $\sim 130 \text{ kJ mol}^{-1}$ on aluminum and magnesium oxides. For Al_2O_3 , these values were close to 142 kJ mol^{-1} , as found by Okamoto *et al.* [680]. Authors assigned the α_2 form to H_2S adsorbed with participation of cations. The sequences and temperature regions of the $\beta\text{-H}_2\text{S}$ desorption on TiO_2 , Al_2O_3 and MgO are in agreement with data on the thermal stability of SH groups. Upon dissociative adsorption of H_2S on the surface of these oxides, SH stretching vibrations (νSH at 2535, 2580 and 2580–2598 cm^{-1} , respectively) have been observed by IR spectroscopy (see Table 2.31).

The formation of SO_4^{2-} and SO_3^{2-} groups [457, 685, 687] is also observed on such samples after removal of the SH and H_2S compounds, followed by interaction with oxygen at higher temperatures. This also confirms the formation of S^{2-} species. The formation of sulfides has been directly indicated on Na/SiO_2 and $\text{Na/Al}_2\text{O}_3$ [652] during the interaction with H_2S (especially at high temperature) by X-ray diffraction and ESCA methods [685].

For oxides having cations of variable valency, the initial H_2S adsorption leads to the reduction of the surface cations and to the formation of elemental sulfur and to SO_x on the surface [209, 665, 685, 687–691]. According to ESR data [692–695], the interaction with transition-metal oxides also leads to the formation of the anion radicals S^- , S_2^- and S_3^- .

The fact that the properties of the oxide surfaces can be essentially changed upon interaction with H_2S is shown by the following observations: (i) the degree of formation of sulfides; (ii) a partial blocking of the LASs; (iii) the disappearance of the basic hydroxyl groups; (iv) the reduction of the cations and the oxidation of sulfur [689, 692, 694]. On the surfaces of oxides such as TiO_2 , Al_2O_3 and ZrO_2 a new BAS is formed and the basicity of the surface increases [685, 693]. The appearance of protonic acid centers is also possible due to the modification of the surface by the SO_x molecules [685, 693].

On the basis of the literature data presented above, the following schemes for the interaction of H_2S with different surface centers of oxide systems is proposed:



Scheme 2.37

2.3.8 ADSORPTION OF SULFUR DIOXIDE

The reaction of sulfur dioxide with zeolites and oxides often attracts the attention of investigators in connection with the problem of air pollution. First, zeolites and oxides are good catalysts for the modified Claus process ($\text{H}_2\text{S} + \text{SO}_2 \rightarrow \text{S}_x + \text{H}_2\text{O}$). On the other hand, zeolites (especially highly siliceous ones) are perspective adsorbents for the low-temperature recovery of SO_2 from waste gases. Although the number of papers devoted to the study of the interaction between SO_2 and oxides or zeolites is fairly large, the results of spectroscopic investigations are not always detailed. In a number of cases these data are contradictory because of the dual nature of SO_2 .

The SO_2 molecule is nonlinear with an angle of 119.5° and may appear either in the role of an electron donor due to the unshared electron pairs (UEPs) of the oxygen atoms or in the role of an electron acceptor due to a low-lying vacant molecular orbital which is localized mainly on the sulfur atom [696–700]. The vibrational spectra of the SO_2 molecule can be described as for a XY_2 nonlinear molecule with C_{2v} symmetry. As is known, there are two bond-stretching vibrational modes in the IR spectra of such a molecule (Table 2.34, top set of entries). The electronic structure of the SO_2 molecule, as well as those of two of its complexes are shown in Figure 2.36 [699].

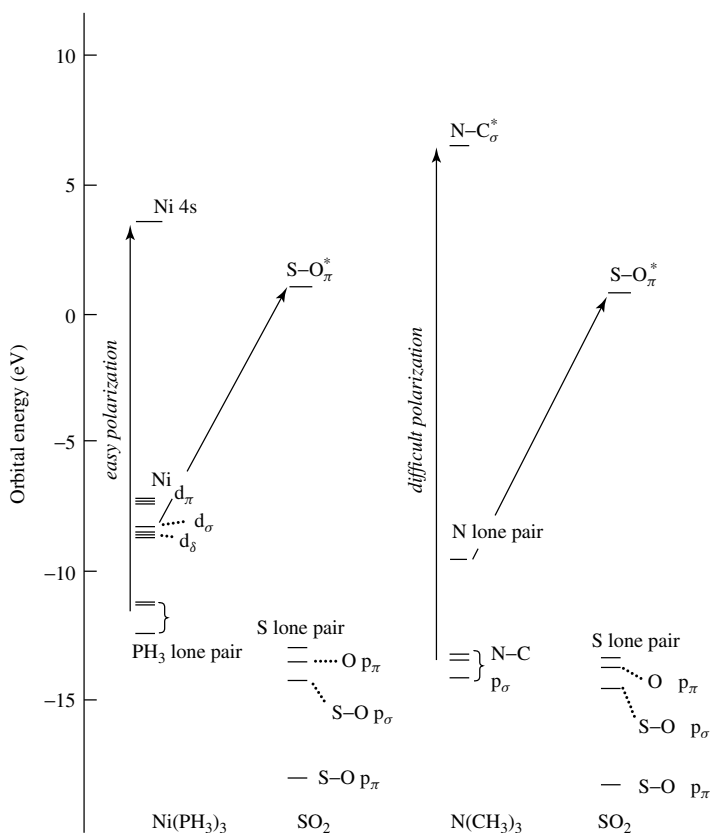
Table 2.34. Spectral manifestations of some sulfur-containing compounds.

Compound or ion	Structure	Symmetry	$\nu_1(\nu_s)(\text{cm}^{-1})$	$\nu_3(\nu_{as})(\text{cm}^{-1})$	Reference	
S=O	Linear	—	1123	1123	15	
SO_2 (gas)	Bent	C_{2v}	1151	1362	15	
SO_2^-	Bent	C_{2v}	984.8	1042	15	
$\text{IrCl}(\text{CO})\text{SO}_2(\text{PPh}_3)_3$, pyramidal	$\text{M}-\ddot{\text{S}}\begin{array}{l} \diagup \text{O} \\ \diagdown \end{array}$	I	C_s	1048	1198–1185	15,697
$[\text{Ru}(\text{NH}_3)_4\text{SO}_2\text{Cl}]\text{Cl}$, planar	$\text{M}-\text{S}\begin{array}{l} \diagup \text{O} \\ \diagdown \end{array}$	II	C_{2v}	1100	1301–1278	15,697
$\text{SbF}_5(\text{SO}_2)$	$\text{M}-\text{O}\begin{array}{l} \diagup \text{S}=\text{O} \\ \diagdown \end{array}$	III	C_s	1102	1327	15,697
$(\pi\text{-C}_p)\text{Fe}(\text{CO})_{22}\text{SO}_2$, bridging	$\begin{array}{c} \text{O} \\ \\ \text{M}-\text{S}-\text{M} \\ \\ \text{O} \end{array}$	IV	C_{2v}	993	1135	15,697
$\text{Ru}(\text{SO}_2)\text{NO}(\text{PPh}_3)_2$, chelate	$\begin{array}{c} \text{O} \\ // \\ \text{M}-\text{S} \\ \diagup \text{O} \\ \diagdown \end{array}$ (M)	V	C_s	940	1165	697
AlCl_3SO_2	$\begin{array}{c} \text{O} \\ // \\ \text{Al}-\text{S}=\text{O} \\ \diagup \end{array}$	VI	—	1085	1447	696
$(\text{C}_2\text{H}_5)_3\text{NSO}_2$	$\text{N}:\rightarrow\text{S}\begin{array}{l} \diagup \text{O} \\ \diagdown \end{array}$	VII	C_{2v}	1120	1263	696,698,700
SO_3^{2-} , pyramidal	—	C_{3v}	961	1010	15	
$\text{k}_6[\text{Pt}(\text{SO}_3)_4]\cdot 2\text{H}_2\text{O}$	$\text{M}-\text{S}\begin{array}{l} \diagup \text{O} \\ \diagdown \end{array}$	C_{3v}	964	1082–1057	15	
$\text{Co}[(\text{NH}_3)_5\text{SO}_3]\text{Cl}$, unidentate	—	C_{3v}	985	1110	15	

Table 2.34. (continued)

Compound or ion	Structure	Symmetry	$\nu_1(\nu_s)(\text{cm}^{-1})$	$\nu_3(\nu_{as})(\text{cm}^{-1})$	Reference
$\text{Tl}_2[\text{Cu}(\text{SO}_3)_2]$, unidentate		C_s	989	902–862	15
$\text{Na}[\text{Co}(\text{en})_2(\text{SO}_3)_2]$, bidentate		C_{2v} C_5	939	1068	15
$\text{Co}[(\text{en})_2(\text{SO}_3)]\text{Cl}$, bidentate bridging		C_s	984	1117–1075	15

The acceptor properties of sulfur dioxide have been investigated in a number of studies. The interactions of SO_2 with amines, ketones, nitriles and esters have been analyzed by spectroscopic methods [696–698], and the formation of complexes has been shown. The formation of such complexes causes a considerable change in the SO_2 spectrum. The positions of the ν_s and ν_{as} bands are displaced into the low-frequency region (Table 2.33, compound VII). Similar shifts of

**Figure 2.36.** Molecular orbitals of SO_2 and two of its complexes [699].

both absorption bands of SO_2 (ν_s and ν_{as}) into the low-frequency region have been observed in the spectra of other complexes, including complexes with transition metals in which SO_2 appears in the role of an electron acceptor. In conjunction with the results obtained from quantum-chemistry calculations of both the SO_2 molecule and of $\text{R}_3\text{N} \cdot \text{SO}_2$ complexes, the assembly of experimental data have made it possible to draw the conclusion that the accepting molecular orbital of sulfur dioxide is localized in the region of the sulfur atom and that it is located out of the plane of the SO_2 molecule.

Studies of Ir, Rh, Pt and Ni complexes containing the SO_2 molecule [697] have demonstrated a pyramidal coordination of the bonds to the sulfur atoms in these complex. Almost planar conformation of the $\text{M} \rightarrow \text{SO}_2$ fragment has been established for a number of complexes of both Ni and Co. Such an interaction involves donation of the lone pair of SO_2 (i.e. the $4a_1$ orbital) to the metal, forming a $\eta_1\text{-SO}_2$ species with either a pyramidal or planar structure. It has been suggested that SO_2 bonding to metals in a pyramidal form generally results from the strong $\text{M} \rightarrow \text{S}$ σ -donation into the $2b_1$ lowest-unoccupied molecular orbital (LUMO) orbital with rehybridization of the sulfur atom to sp^3 . In contrast, the planar configuration of SO_2 is favored if the metal fragment is capable of accepting an electron pair from the $4a_1$ orbital together with π back-bonding into the $2b_1$ orbital of sulfur. Since M^{n+} is potentially a very strong Lewis acid, the π -bonding is unlikely, and the main interaction with SO_2 is expected to arise from the strong polarization of the sulfur lone-pair orbital to form a relatively strong $\text{S} \rightarrow \text{M}$ σ -bond. This mode of bonding should, therefore, favor a planar configuration for SO_2 (see Figure 2.36).

Strong σ -bonding would have the effect of lowering the S–O stretching frequencies due to the weakening of the S–O bond, with the extent of lowering being dependent on the strength of the $\text{S} \rightarrow \text{M}$ bond. It has been observed [697, 699] that the vibrational frequencies of $\eta_1\text{-SO}_2$ in $[\text{MSO}_2]$ complexes depend primarily on the ancillary ligand of the metal fragment rather than on the geometry of SO_2 . Accordingly, the range of ν_s and ν_{as} values reported is relatively large (1045–1145 and 1190–1300 cm^{-1}) for a planar configuration. The 1189 and 1050 cm^{-1} bands have been tentatively assigned to ν_s and ν_{as} of SO_2 bound to, for example, the aluminum ion in planar form, respectively.

Charge transfer from the donor molecule to the lowest vacant orbital of the SO_2 molecule localized mainly on the sulfur atom should lead to a lengthening of the S=O bond and to a decrease in the O–S–O angle. The observed low-frequency shifts of ν_s and ν_{as} are directly connected with the lengthening of the S=O bonds. The results obtained are in good agreement with those of a quantum-chemical analysis of the SO_2 molecules as an electron acceptor, in which the SO_2 also appears in the role of an electron-donor due to its oxygen atom (compounds I–VI, Table 2.34).

The sulfonyl group of organic sulfones, R_2SO_2 , displays the properties of a bidentate donor upon reaction with strong acceptors (AlBr_3 , GaCl_3 , etc.) [697], that is, both oxygen atoms can give $\text{O} \rightarrow \text{M}$ donor–acceptor bonds. Consequently, the participation of one of the oxygen atoms of the SO_2 molecule in the formation of intermolecular $\text{O} \rightarrow \text{M}$ bonds leads to the shift of ν_s into the low-frequency region and of the ν_{as} band into the high-frequency region. Addition of the acceptor molecule leads to a reduction in symmetry of the molecule, which also causes shifts in ν_s and ν_{as} . The different sensitivities of ν_s and ν_{as} to a change in symmetry of the molecule during complex formation has been previously observed for sulfones and nitro compounds. For SO_2 , this effect is expressed more sharply, apparently because the symmetry of the original molecule is higher. Differences in the spectral manifestations of the SO_2 molecule during its complexation with both electron donors (compound VII, Table 2.34) and electron acceptors (compound VI, Table 2.34) can be used as a criterion for evaluating the state of SO_2 in such complexes.

Thus, sulfur dioxide may take one of the several structures (I–V), when it coordinates to a metal (see Table 2.34). Free SO₂ exhibit ν_{as} (SO₂) and ν_{s} (SO₂) at 1362 and 1151 cm⁻¹, respectively. The complex is O-bound if the $\Delta\nu$ ($\nu_{\text{as}} - \nu_{\text{s}}$) value is more than 190 cm⁻¹ and S-bound if it is smaller than this figure.

Zeolites

The different forms of SO₂ adsorption on zeolites have been detected by IR and UV spectroscopies [652, 653, 656, 660–663, 701]. Deo *et al.* [652] studied SO₂ adsorption on the NaY and HY zeolites. They showed that physical adsorption of SO₂ ($\nu_{\text{SO}_2} \sim 1330$ cm⁻¹) occurs on both catalysts. The addition of SO₂ and HY decreases the 3650 cm⁻¹ ν_{OH} band somewhat to give a broad hydrogen-bonded OH-group absorption.

Karge and co-workers [657, 661–663, 701], studying SO₂ adsorption on zeolites by means of UV–Vis and IR spectroscopies, concluded that SO₂ is physically adsorbed on NaY (bands at 1320 cm⁻¹ (IR) and 280 nm (UV–Vis)), whereas on NaX it is both chemisorbed (bands at 1240 cm⁻¹ (IR) and 215 nm (UV) at low coverage) and physisorbed (bands at 1320 cm⁻¹ and 280 nm, respectively, at higher coverage). The band at 1240 cm⁻¹ (or 215 nm in the UV) was ascribed to the HSO₃⁻ species (Table 2.31). The latter are formed by the reaction between SO₂ and water, as follows:



or between SO₂ and basic OH⁻ groups:



Another band observed at 250 nm (at higher coverage) was ascribed to S₂O₅²⁻, formed in the reaction:



X-ray and IR studies of faujasite-type zeolites after SO₂ adsorption show that in the case of both the Y- and X-types of these zeolites a partial destruction of the zeolite lattice occurs and this may be connected with the formation of sulfite-like compounds.

Adsorbed SO₂, having a desorption temperature close to that of the stable form and characterized by bands at 280 nm and 1320 cm⁻¹ in the UV and IR spectra, respectively, was reported by Karge *et al.* [663]. These authors believed that this is formed by ion–dipole interactions of SO₂ with Na⁺ or with O atoms of the framework directly bound to cations, and that the stable SO₂ form of adsorption is due to interaction with an oxygen atom of the framework of the Y zeolite. The weakly bound form ($T_{\text{des}} = 286\text{--}300$ K) brings the main contribution in the adsorption of SO₂ on highly siliceous Y-type zeolites. This species is formed via adsorbate–adsorbate interactions and is apparently delocalized within a large void. The measured desorption temperature, heat of adsorption and nature of the isotherms, imply that this can be assigned to physically adsorbed SO₂. The adsorption of SO₂ on NaY zeolites with different properties of cations has also been studied by IR spectroscopy. On the fully cationated sample, only one form of SO₂ adsorption was detected, characterized by a band at 1325 cm⁻¹ ($T_{\text{des}} = 373$ K).

There are two absorption bands at 1325 and 1335 cm⁻¹ in the case of HNaY zeolites. In addition, the intensity of the ν_{OH} mode decreases, and the absorption bands of perturbed OH⁻

groups appear. With a view to clarification of the nature of the SO_2 adsorption center, the co-adsorption of SO_2 with Py and CDCl_3 was investigated [665]. It was shown that the pre-adsorption of Py (by adsorption at 293 K, followed by desorption at 423 K) reduces the SO_2 adsorption by two to three times in comparison with the same amount of SO_2 admitted on the pure zeolites. Furthermore, pre-adsorption of CDCl_3 (the adsorption of CDCl_3 takes place due to the H-bonding with OH groups) completely suppresses the SO_2 adsorption, characterized by absorption at $1335\text{--}1338\text{ cm}^{-1}$. These data show that the SO_2 adsorption is characterized by the low-frequency band, occurring with the assistance of the exchanged Na^+ cations (or O^{2-} framework), while the interaction of SO_2 with the OH groups (H^+) of the zeolites is characterized by the bands in the higher-frequency $1335\text{--}1340\text{ cm}^{-1}$ region. The nature of such interactions is particularly determined by the formation of the OH bond.

ESR spectroscopy has also been used to study the paramagnetic species formed upon adsorption of SO_2 on zeolites [664, 657]. First, it was reported that SO_2 adsorbed on synthetic mordenite formed its anion radical. The SO_2^- radical has been identified by ESR spectroscopy in a number of investigations of SO_2 adsorption on Y-type zeolites [657, 664]. Karge *et al.* [657] suggested a correlation of the low-frequency band at about 1240 cm^{-1} on zeolites (1070 cm^{-1} on alumina) due to sulfite-like structures with the existence of the SO_2^- anion radical, but a later combined IR/ESR reinvestigation of alumina showed no correlation between the low-frequency band species of adsorbed SO_2 and SO_2^- [711, 712]. It should be noted that the g value of SO_2^- radicals studied in different experiments all fall in very narrow ranges ($g = 2.001\text{--}2.002$; $g = 2.008\text{--}2.010$). This indicates that the nature of the adsorption centers are considered to be very similar in all cases, and it is more probable that the electronegative aluminum sites are responsible for the charge transfer. In the case of SO_2^- radicals adsorbed on cation-exchanged Y zeolites, the cations are considered to be the adsorption centers for the SO_2^- radicals.

Oxides

On alumina, and calcium, magnesium and titanium oxides, the presence of at least two adsorption forms of SO_2 are indicated [702–711]. The strongly bound sulfite form is considered to be localized on the basic O^{2-} sites and are characterized by frequencies of SO stretching vibrations similar to those of bulk sulfites' absorptions (see Table 2.34): ν_1 for MgO, $954\text{--}960\text{ cm}^{-1}$, and for CaO, 930 cm^{-1} ; ν_3 for CaO, 990 cm^{-1} , and for MgO, Al_2O_3 and TiO_2 , $960\text{--}970$ and $1050\text{--}1090\text{ cm}^{-1}$.

Chang [706], Lavalley *et al.* [675], Karge and co-workers [656, 661] and Davydov and co-workers [665, 666] established the formation of sulfite-like structure characterized by the low-frequency band at $1060\text{--}1080\text{ cm}^{-1}$ on Al_2O_3 and showed that the basic sites are required for SO_2 chemisorption. Using UV–Vis spectroscopy, Karge and co-workers, and Davydov and co-workers observed the bands at 215–220, 230–250 and 280 nm and attributed them to HSO_3^- , $\text{S}_2\text{O}_5^{2-}$ and molecularly adsorbed SO_2 , respectively. In Lavalley *et al.* [675], the suggestion was made about the formation of bisulfite complexes on Al_2O_3 . The UV–Vis and IR spectroscopic investigations confirmed this and showed that this reaction occurs on zeolites [701] and Al_2O_3 [666]. Intensification of the HSO_3^- formation was, as expected, observed for hydroxylated surfaces of Al_2O_3 and TiO_2 [666, 689, 705] and $\alpha\text{-FeOOH}$ [704].

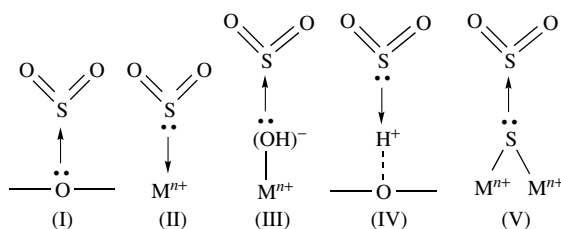
The adsorption of sulfur dioxide as SO_3^{2-} or HSO_3^- groups strongly modified the properties of the oxide surface. Surface acidity shows a considerable increase as a result of the induction effect arising from the withdrawal of the electron density from surface metal atoms by sulfite ions. The total concentration of LASs does not change, although stronger LAS and Brønsted centers appear [686, 702].

Multilayer coating with the formation of sulfite phases is possible for calcium oxide [176]. The changes in enthalpy in the following reaction:



was calculated by Marshneva *et al.* [176] for aluminum and magnesium oxides for which the heats of formation of sulfite phases are known. These were, respectively, 143 and 116 kJ mol⁻¹ at 298 K, i.e. they differed insignificantly from the heats of SO₂ adsorption on the corresponding oxides (127 and 113 kJ mol⁻¹). The data obtained show that SO₂ is chemisorbed on oxides in the form of surface sulfites with a relatively narrow range of heats of adsorption between 92 and 138 kJ mol⁻¹ (see Table 2.33).

The largest amounts of SO₂ chemisorbed on Al₂O₃ at 298 K was $\sim 2 \times 10^{18}$ molecules m⁻², and on TiO₂ $\sim 10^{17}$ molecules m⁻², i.e. only a fraction of the surface oxygen of these oxides interacts with SO₂ to form SO₃²⁻ ions. The strength and character of the SO₂ interaction with the oxide surfaces are determined by the basicity of the oxides. The basicity of the surface oxygen ions for the oxides increases in the following order: TiO₂, Al₂O₃, MgO and CaO (see Section 2.5), while the concentration of SO₃²⁻ forming on these oxides increases in the same order. The basicities of the surface oxygen ions decrease with increasing coordination. The less strong basic centers form the donor-acceptor complex I:



Scheme 2.38

Sulfur dioxide molecular adsorption (in the reversible form) is twice less stable when compared with the irreversible form; the frequencies of the SO₂ stretching vibrations of molecularly adsorbed SO₂ varied within the following limits for the different oxides: $\nu_1 = 1136\text{--}1150$ cm⁻¹ and $\nu_3 = 1320\text{--}1350$ cm⁻¹. Even on the surface of CaO, a small portion of such basic centers exists and they form complex (I). The ability of SO₂ to form molecular complexes with pyridine, trimethylamine and triethylamine, where it exhibits the properties of an electron-pair acceptor, has been reported [696–700]. In these complexes, the absorption bands corresponding to the vibrations of S=O bonds are shifted to the low-frequency region in comparison with those of the free SO₂ molecule (see Table 2.34). By using adsorbents (V₂O₅ and Ti–Sb–O, Figure 2.37) which have no Lewis acid sites, to coordinate weak and middle-strength bases it was shown [666] that: (a) the adsorption species (I) is formed on the oxide surface, and (b) ν_3 in complex (I) decreases with an increase of the oxide surface oxygen basicity (Figure 2.37) [666].

Datta *et al.* [707] have suggested the formation of five types of SO₂ complexes on the surface of Al₂O₃: A and B, physisorbed SO₂; C and D, chemisorbed SO₂ (with C being a planar complex on a single Al ion, and D a planar or pyramidal complex on Al clusters); (F), monodentate sulfite. Unfortunately, these results were based only on the different stabilities of the surface species and on a comparison of their frequencies with those for the bulk compounds. It was difficult to prove the presence of forms A–D because their symmetries and thermostabilities are very similar. The formation of each of these reversible complexes has been shown later by using systems

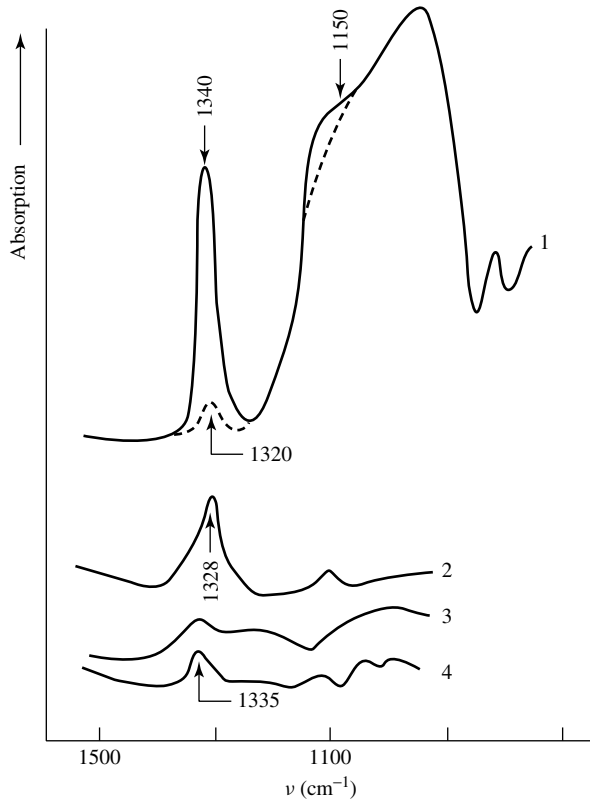


Figure 2.37. FTIR spectra of SO_2 adsorbed at 293 K (10 torr) on various oxides: 1, MgO, where the dashed line represents the spectrum obtained following desorption at 293 K; 2, $\text{Sb}_2\text{O}_4/\text{TiO}_2$; 3, V_2O_5 ; 4, $\text{V}_2\text{O}_5/\text{TiO}_2$.

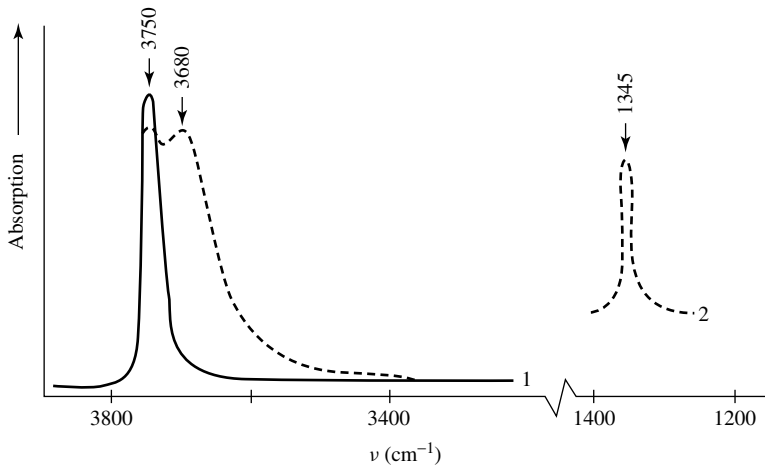


Figure 2.38. FTIR spectra of (1) SiO_2 (aerosil) which had been activated *in vacuo* and in oxygen (100 torr) at 823 K, and (2) after the addition of SO_2 (10 torr) at 293 K.

with preferably one type of adsorption center, or by blocking other centers by chemical reagents [666, 668].

The data about the perturbed surface hydroxyl groups for such oxides as SiO_2 (Figure 2.38 (there are only OH^- centers in this case)) [688, 702], MgO [702, 703] and Al_2O_3 [652, 675, 702] show direct evidence for the adsorption form (III, IV) of SO_2 (Scheme 2.38). Further viewpoints in the literature are that the changes of OH groups for MgO and Al_2O_3 are due to the SO_2 adsorption as a sulfite-like compound which perturbs the neighboring surface hydroxyl groups [702], or are due to sulfite or bisulfite formation.

Adsorption of SO_2 on the $\gamma\text{-Al}_2\text{O}_3$ surface leads to the appearance of the reversibly bound form of adsorbed SO_2 (the bands at ca. 1330 and 1140 cm^{-1} – see Table 2.35) [666, 683]. The authors of this work assume that the latter bands are due to $\nu_3\text{S-O}$ and $\nu_1\text{S-O}$ vibrations in the complexes of adsorbed SO_2 formed with basic centers of the O^{2-} type and that a 1065 cm^{-1} band arises from $\nu\text{S-O}$ in sulfite complexes (equation 2.21).

The bonding of the SO_2 molecule on one (I) or two LASs is another important possibility for the interaction of SO_2 with oxide surfaces. This type of interaction can give rise to dissociation of SO_2 molecules as was shown for Al_2O_3 [666, 710] (Figure 2.39). IR spectral manifestations of the complexes forming in this case were proposed for Al_2O_3 (Table 2.35) [666, 711, 712] and for TiO_2 (Table 2.36) [689].

The adsorbed species discussed above are formed with the participation of the regular surface. At the same time, SO_2^- anion radicals are formed on defect centers – in the present case, on anion vacancies. The number of such centers is an order of magnitude lower than the regular centers. If a catalyst has been reduced by H_2S , its oxidation proceeded faster than in the case of reduction by H_2 , because SO_2 interaction with $\text{S}^{2-\text{ads}}$ is possible (complex V, Scheme 2.38).

Reduced transition-metal oxides are oxidized by SO_2 molecules, as has been shown for TiO_2 [689], Sn-Mo oxide [687] and V/TiO_2 catalysts [691]. The mechanism of the first step of the SO_2 interaction with such catalysts seems to be identical to the mechanism proposed for Al_2O_3 (Figure 2.39) [666, 689, 691]. This is a two-center bonding, followed by dissociation with

Table 2.35. IR spectroscopic and thermally programmed desorption characteristics of adsorbed SO_2 species on alumina.

Type	Species	Frequency (cm^{-1})	T_{des} (K)	(molecules m^{-2})	(kJ mol^{-1})
1	$(\text{OH})^- \rightarrow \begin{array}{c} \text{O} \\ // \\ \text{S} \\ // \\ \text{O} \end{array}$	1330,1150	293	–	–
2	$\text{O}^{2-} \rightarrow \begin{array}{c} \text{O} \\ // \\ \text{S} \\ // \\ \text{O} \end{array}$	1320–1325, 1140	370	$\sim 2 \times 10^{18}$	40–80
3	$\text{Al}^{3+} \leftarrow \begin{array}{c} \text{O} \\ // \\ \text{S} \\ // \\ \text{O} \end{array}$	1300–1320, 1135	370	–	–
4	$\text{Al}^{3+} - \text{O} - \begin{array}{c} \text{O} \\ // \\ \text{S} \\ // \\ \text{O} \end{array}$	1360–1400	293	–	–
5	$\begin{array}{c} \text{Al} \\ \vdots \\ \text{S} = \text{O} \\ \\ \text{Al} - \text{O} \end{array}$	1190	470	$\sim 10^{17}$	–
6	SO_3^{2-}	970,1050–1060,	>570	$\sim 10^{18}$	>120
7	HSO_3^-	975,1135	>570	$\sim 10^{18}$	–

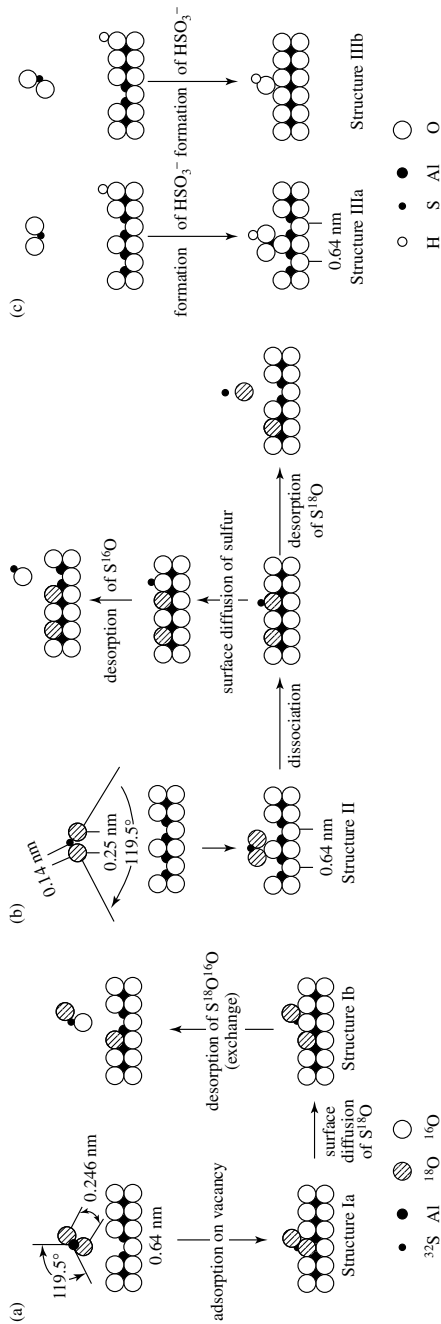
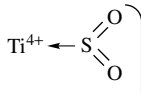
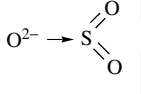
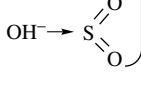
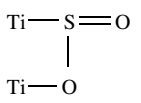


Figure 2.39. Simplified schemes for (a) oxygen exchange, (b) SO_2 dissociation, and (c) formation of HSO_3^- structures on an alumina surface: (a) adsorption of $S^{18}O_2$ and $^{18}O \leftrightarrow ^{16}O$ exchange with the surface of Al_2O_3 resulting in desorbed $S^{18}O^{16}O$; (b) adsorption of $S^{18}O_2$ and dissociation under formation of $S^{16}O$ and/or $S^{18}O$; (c) adsorption of SO_2 and formation of HSO_3^- structures [710]. Reprinted with permission from Dalla Lana, I.G., Karge, H.G. and George, Z.M., *J. Phys. Chem.*, **97**, 8005–8011 (1993). Copyright (1993) American Chemical Society.

Table 2.36. IR spectroscopic and thermally programmed desorption characteristics of adsorbed SO₂ species on anatase.

Type	Species	Frequency (cm ⁻¹)	T _{des} (k)	T _{max} (K)	θ (molecules m ⁻²)	q (kJ mol ⁻¹)
1		~1440, ~1330	293–370	320	~10 ¹⁸	40–60
2						
3						
4		1180	470	500–550	3 × 10 ¹⁷	–
5	SO ₃ ²⁻	1050–1060	570	550–615	~10 ¹⁷	>100
6	HSO ₃ ⁻	1070–1090 1140	570	–	~10 ¹⁷	–

oxidation of the surface cations. Such a mechanism is likely because the reduced cations of Ti³⁺, Mo⁵⁺ and V⁴⁺ in such catalysts are, as a rule, clustered. The oxidation of surface ions by SO₂ molecules is slower than by O₂, probably because the oxygen molecule has a stronger electron affinity than SO₂. Davydov *et al.* [666] have expressed the interesting idea that the band at about 1190 cm⁻¹ characterizes SO₂ adsorbed simultaneously on two surface centers (like complex 5 or complex 4 in Table 2.36).

The SO₂⁻ species identified by means of ESR spectroscopy appear to act as intermediates in the surface oxidation by SO₂ molecules, in a similar manner to O₂⁻ ions being intermediates in surface oxidation by oxygen. Moreover, the rate of the SO₂⁻ interaction with the surface of transition-metal oxides reduced by H₂S substantially increases [666, 664, 687, 691] because there are S²⁻ groups on the oxide surface. Clearly, S²⁻ groups decrease the barrier of the electron transfer to the adsorbed SO₂ group.

Thus, SO₂ molecules interact with various centers of the oxide surfaces due to their amphoteric properties. The types of surface compounds that can be formed on oxides are shown in Table 2.37. For example, the reversibly adsorbed form include five surface compounds. A definition of specific adsorption heats for the irreversible or reversible adsorption forms cannot be made because the measured experimental value characterizes the total process. Nonetheless, the values of the adsorption heat reflect, in a general way, the properties of specific oxide surfaces.

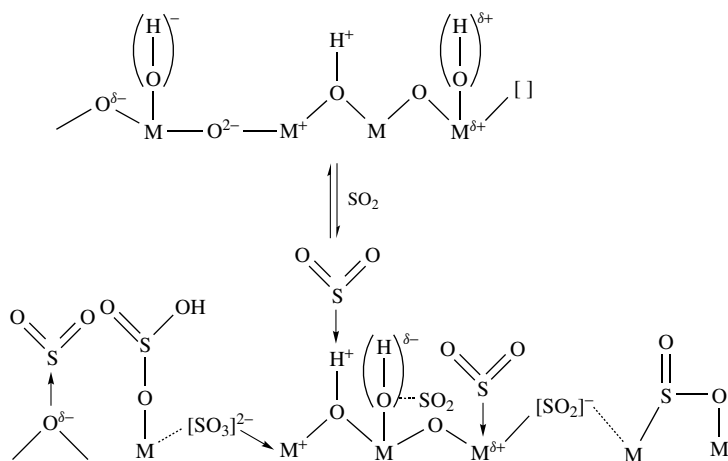
In the presence of oxygen in the gas phase, the interaction of SO₂ with oxides leads to the formation of sulfates with different structures, which are also formed on transition-metal oxides under analogous circumstance.

ESR spectroscopy has been widely used to study the paramagnetic species formed upon adsorption of SO₂ on oxides [656, 707, 711, 712]. For example, Schoonheydt and Lunsford [682] investigated the adsorption of SO₂ on partially reduced TiO₂ and over activated MgO by this technique. In both cases, SO₂⁻ radicals were observed. The adsorption sites for SO₂⁻ appear to be oxygen-ion vacancies. On Al₂O₃, two types of SO₂⁻ ion radicals were observed [656, 707, 712].

Table 2.37. Types of surface-adsorbed species of SO₂ on different metal oxides.

Centers of adsorption	Surface-adsorbed species										
	Al ₂ O ₃	SiO ₂	TiO ₂	MgO, CaO	V ₂ O ₅ , V ₂ O ₅ /TiO ₂	Sb ₂ O ₄ /TiO ₂	MoO ₃ /SnO ₂	NaY	NaX	HNaY	
M ⁿ⁺ O ²⁻	-	-	SO ₃ ²⁻	SO ₃ ²⁻	SO ₃ ²⁻	-	SO ₃ ²⁻	-	-	-	
O ²⁻	O ²⁻ → SO ₂	-	O ²⁻ → SO ₂	O ²⁻ → SO ₂	O ²⁻ → SO ₂	O ²⁻ → SO ₂	O ²⁻ → SO ₂	-	-	-	
M ⁿ⁺ OH ⁻	SO ₃ H ⁻	-	SO ₃ H ⁻	SO ₃ H ⁻	-	-	-	-	SO ₃ H ⁻	-	
OH ⁻	(OH) ⁻ SO ₂	-	(OH) ⁻ SO ₂	(OH) ⁻ SO ₂	-	-	-	-	-	-	
M ⁿ⁺	Al ³⁺ SO ₂	-	Ti ⁴⁺ SO ₂	-	-	-	-	-	Na ⁺ SO ₂	Na ⁺ SO ₂	
2M ⁿ⁺	2Al ³⁺ SO ₂	-	2 Ti ⁴⁺ SO ₂	-	-	-	-	-	-	-	
H ⁺	H ⁺ SO ₂	-	-	-	May be formed	May be formed	May be formed	-	-	H ⁺ SO ₂	

It is possible to propose the following scheme of the SO_2 interaction with oxides:



Scheme 2.39

The majority of the transition-metal oxides, e.g. MnO_2 , CuO , Cu_2O , NiO , CoO and Co_3O_4 , interact with SO_2 at high temperatures and form sulfite- or sulfate-like bulk compounds [665], as shown by means of X-ray diffraction data and IR spectroscopy. Such interactions start on the oxide surface, with the results being dependent on the nature of the oxide, the conditions of pre-treatment and the interaction temperature.

2.3.9 SURFACE ISOCYANATE COMPLEXES

In addition to diatomic and several threatomic (H_2S , H_2O , SO_2) molecules, there are many others (e.g. olefins – see Chapter 5), including triatomic species such as NCO and SCN , for which the spectral parameters are sensitive to the electron-acceptor abilities of the cations [15]. Ligands such as NCO and SCN have very strong electron-donor abilities and may be used to identify even very weak Lewis acid sites. Such fragments may be formed on the surface as a result of catalytic reactions, involving bonding through N or S atom-containing compounds, and can be used to investigate the surface properties.

When both NO and CO molecules are adsorbed on copper or iron oxides supported on Al_2O_3 [481, 713], absorption bands in the region $2100\text{--}2300\text{ cm}^{-1}$ have been observed in IR spectra only after high-temperature interaction (Figure 2.40, spectra 1 and 2). Using the isotopically substituted molecules ^{15}NO and ^{13}CO , it has been shown that the bands in this region belong to surface isocyanate complexes (SICs) (Table 2.38).

Table 2.38. Frequencies (cm^{-1}) observed in the IR spectra for the interaction of $\text{CuO}/\text{Al}_2\text{O}_3$ and $\text{Fe}_2\text{O}_3/\text{Al}_2\text{O}_3$ with isotopically substituted NO and CO molecules.

$^{14}\text{N}^{12}\text{C}$	$^{15}\text{N}^{12}\text{C}$	$^{14}\text{N}^{13}\text{C}$	$^{14}\text{N}^{15}\text{N}$	$^{12}\text{C}^{13}\text{C}$
2270	2250	2210	15	60
2240	2225	2185	15	60
2140	2125	2080	15	60

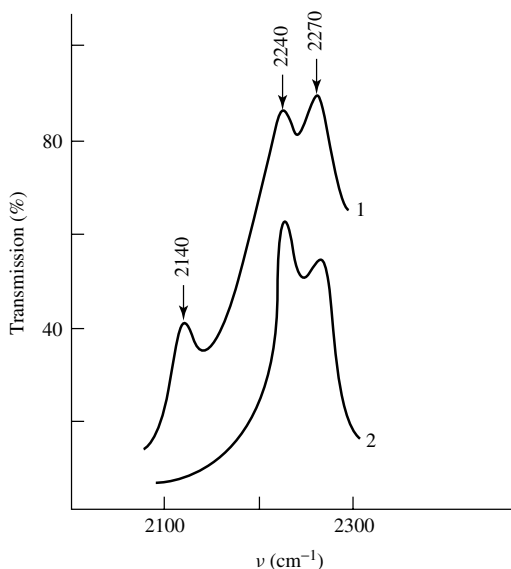


Figure 2.40. IR spectra of (1) CuO/Al₂O₃, and (2) Fe₂O₃/Al₂O₃, after interaction with a mixture of NO:CO (1:1) at 673 K.

Intense absorption bands of SICs have been observed in the spectra of Pt- [714, 715], Pd- [716] and Rh- [717] containing oxide systems supported on Al₂O₃ (Figure 2.41) and also of Pt supported on SiO₂ (Table 2.39) treated by NO–CO mixtures. It is clear that transition metals or their cations play a significant role in the formation of SICs, because none of the latter have been obtained upon the interaction of NO + CO mixtures of variable content on supports (SiO₂ Al₂O₃, MgO and HY zeolites oxide systems) which contain neither transition metals nor their cations.

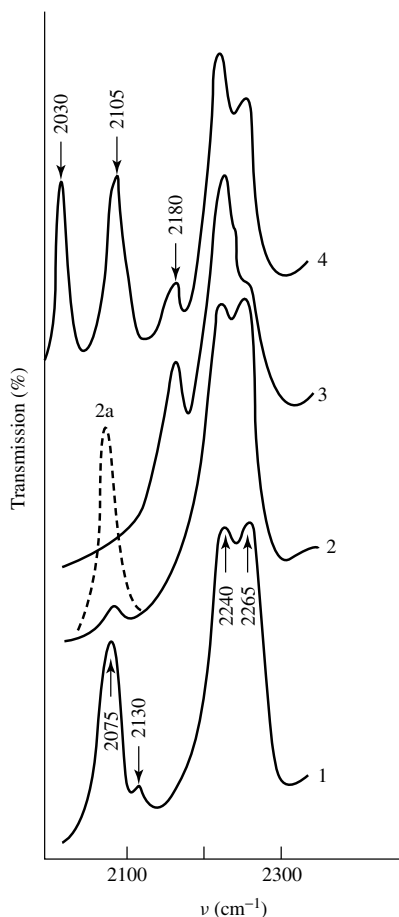
Various viewpoints exist on considering the possible sites for SIC stabilization. It has been suggested by various workers [718–721] that SICs are formed on an active site, but then migrate to the carrier and are localized there. Support for this comes from the fact that the number of SIC groups far exceeds the number of surface Pt atoms [719, 720], from the position of the absorption bands of HNCO adsorbed on supports [721, 724], and also from the strong influence of the support on the formation, stability and position of the absorption bands characterizing the SICs [721]. The same position of the absorption bands from SICs when formed on different metals supported on the same carrier also supports the above suggestion (Table 2.39). Another viewpoint suggests that the SICs are stabilized on the active adsorption site [64, 725–728].

It is very well known [15] that the ν NCO band may be found within rather wide limits (from 2100 to 2400 cm⁻¹) (see Table 2.39). An increase in covalence of the M–NCO bond leads to an increase in the ν NCO frequency.

To analyze the nature of the stabilization sites, we will divide the observed absorption bands characteristic of the SICs into two groups, namely bands in the region 2210–2350 cm⁻¹ (group 1) and bands in the region 2100–2200 cm⁻¹ (group 2) [713]. The first group of bands characterize SICs stabilized on the support. The following evidence supports this conclusion. First, an independence of the positions of the absorption bands from the SIC on the active component, both in the case of noble metals and their oxides when the same support is used. Secondly, CO adsorption (see Figure 2.41, spectrum 2a) on a Pd-containing system, with adsorbed SICs characterized by absorption bands at 2270 and 2240 cm⁻¹ (Figure 2.41, spectrum 2), causes the formation of a carbonyl complex, PdCO (2080 cm⁻¹) [716]. The intensity of the latter is comparable with that

Table 2.39. Absorption bands ($\nu(\text{cm}^{-1})$) of surface isocyanate complexes formed on catalysts in the reaction of $\text{NO} + \text{CO}$ mixtures and for the adsorption of HNCO on various carriers^a.

Carrier	Pt [713, 714, 719, 720]	Pd [713, 714, 717, 718, 721]	Rh [713, 717, 718, 726, 727]	Ru [718, 723, 730]	Ir [718]	Cu [713]	HNCO [721]	K^+NCO [722]
Al_2O_3	2270 2240 2140 (2138) 2175	2265 2240 2140 2175	2270 2240 2130 2180	2270 2240 2180	2270 2240 2126	2270 2240 2140	2272	2163
MgO	2228–2241 2213	2235 2217	2235 2210	2230 2215	2230		2223	
SiO_2	2318	2317	2315	2315	2310	2315	2313	

^aReferences shown in square brackets.**Figure 2.41.** IR spectra of: (1) $\text{NO}:\text{CO}$ (2:3) on $\text{Pt}/\text{Al}_2\text{O}_3$; (2) $\text{NO}:\text{CO}$ (0.9 %:1.3 %) on $\text{Pd}/\text{Al}_2\text{O}_3$; (2a) after subsequent adsorption of CO ; (3) $\text{NO}:\text{CO}:\text{O}_2$ (0.9 %:1 %:0.25 %) on $\text{Pd}/\text{Al}_2\text{O}_3$; (4) $\text{NO}:\text{CO}$ (1:1) on $\text{Rh}/\text{Al}_2\text{O}_3$. Studies were carried out at the following temperatures: (1) 523; (2) 473; (2a) 293; (3) 349; (4) 423 K.

observed on Pd/Al₂O₃ where SICs are absent, implying that the SICs are not occupying sites on Pd. Similarly, the adsorption of NO on Fe₂O₃/Al₂O₃ after the SICs were formed (2270 and 2240 cm⁻¹) and then the gas-phase materials were removed by evacuation, leads to the appearance of surface iron nitrosyls; the intensities of the bands characterizing the latter is not less than those on a freshly prepared Fe₂O₃/Al₂O₃ sample [713]. Thirdly, appearance of the SICs under discussion is accompanied by a disappearance of surface carbonates (nitrates), stabilized on the support, while finally, the temperature of SIC formation is the same for all systems containing noble metals and oxides (673 K).

There is also a definite relationship between spectral manifestations of the SICs and the structural peculiarities of the supports. Thus, in the case of γ -Al₂O₃, two types of SICs are formed. This is not surprising taking into consideration the fact that two types of coordinatively unsaturated Al³⁺ cations in tetrahedral and octahedral vacancies (Al³⁺_{cut} and Al³⁺_{cuo}, respectively) exist on the surface of γ -Al₂O₃ [30]. For Y-type zeolites, where aluminum is in only tetrahedral coordination only the band at 2280 cm⁻¹ characteristic of the SIC is observed [729]. Thus, as the electron-acceptor capacity of the cations increases from Al³⁺_{cuo} to Al³⁺_{cut}, an increase in the frequency of the SIC is observed.

When the degree of covalence of the M-NCO bond increases, the frequency of the ν NCO increases, reaching a maximum value in the case of SiO₂ (see Table 2.39). For MgO, an intermediate value of the frequency was recorded at about 2200 cm⁻¹ (Table 2.39). The dependence of the position of the bands characteristic of the SIC on the nature of the support is an important argument that the SIC is stabilized on the support. All of the above evidence supports the assignment of the absorption bands above 2200 cm⁻¹ (group 1) to surface isocyanate complexes stabilized on the support, in contrast to the viewpoint of various other workers [64, 725–728].

For group 2 absorption bands, the nature of the corresponding surface isocyanate complexes evidently differs from that discussed above. It has been suggested [718] that the absorption band at 2140 cm⁻¹, which has been observed for mixtures of NO:CO = 1:2 in the case of Pt/Al₂O₃ and Pd/Al₂O₃ (see Figure 2.41, spectrum 1), is also caused by isocyanate stabilized on the support but associated with adsorption sites with a different coordination environment from that characterizing the band at about 2270 cm⁻¹. However, it is evident from Table 2.39 that the differences in the positions of absorption bands caused by isocyanate stabilized on the same supports (Al₂O₃, MgO, etc.) at the participation of sites with various coordination for all noble metals is only 15–30 cm⁻¹. In the case of the 2140 cm⁻¹ band, the much greater $\Delta\nu$ (= 124–134 cm⁻¹) can be only explained by the fact that the band in this region characterizes an anionic form of isocyanate localized on an active component. This is also supported by the absence of such a band, for example, on Al₂O₃ when HNCO has been adsorbed [721, 724]. In fact, the behavior of these isocyanate absorptions also substantially differs from that observed in the case of isocyanate covalently bound to the support [715–717]. They are less stable with respect to the action of oxygen as well as to evacuation (373–473 K), and are broken down forming M-CN groups (M = Pd and Pt) [715–717]. The lower ν NCO in this case indicates that the electronic structures of such complexes are different and frequencies are close to those of anionic isocyanate.

The simplest molecular orbital (MO) analysis of the NCO structure shows that the highest-occupied molecular orbital (HOMO) is either nonbonding or antibonding. In principle, this may be an orbital of π or σ symmetry. However, the angle in the HNCO molecule is about 128°, i.e. it is more probable that this orbital has a π symmetry (the situation analogous to that for NO). In connection with this, the variable position of $\nu_{\text{as}}\text{NCO}$ may be related to changes in the electron density in the antibonding orbital; it is possible to assume that in this case either a transition metal cation in a low oxidation state or a metal are the sites of adsorption.

In the second group of bands characteristic of isocyanate, the band at ca. 2180 cm⁻¹ should be considered separately. This band is observed on all metal-containing systems, including Pt/SiO₂

[713]. However, the conditions of formation of this isocyanate are different for different systems. Thus, in the case of the Pt-containing systems [717] this band is observed only after treatment by a NO + CO mixture containing oxygen. The ‘lifetime’ of isocyanate complexes *in situ* in this case becomes much shorter as the reaction temperature is increased. On Pd/Al₂O₃ treated by a mixture of NO + CO, this band was also formed at low temperature (473 K) [716] in excess NO, while on Rh/Al₂O₃ it was formed from NO + CO mixtures with any ratio of the components [717]. Considering the conditions of the appearance of the 2180 cm⁻¹ band, it may be concluded that the isocyanate species are formed on an oxidized active site (M⁺NCO). Stabilization of these isocyanates on such an active site is supported by the fact that nearby absorption bands (2173–2180 cm⁻¹) were observed on films of Pt, Pd, Rh and Ir in the case of adsorption of HNCO [730, 731]. In addition, there is an inverse correlation of the intensity of the absorption bands characteristic of the MCO complexes and those discussed above [716]. Isocyanates stabilized on an active site are formed at low temperature, are not thermostable, and are removed by evacuation up to 473 K. The formation of different isocyanate species has been also established on series of supported metals with bands in the 2180 cm⁻¹ region [732–734].

Thus, ν NCO may serve as a good probe for the electronic states of stable adsorption sites. This confirms the expectation advanced by Davydov [30]. A distinguishing feature of this probe is its strong electron-donor properties (evidently comparable with, or even stronger than, those of the oxygen ions of the oxide). Therefore, in the case of SiO₂ and MgO, the electron-acceptor sites, which are not detected by the adsorption of one of the strongest donors, i.e. NH₃, are detected by NCO adsorption. Their relative electron-acceptor abilities in this specific case can be estimated by using ν NCO, with a position dependent on the properties and nature of the cation.

2.4 Determination of acidic surface properties

The derivation of an acidity scale for heterogeneous systems has not been achieved yet, in spite of the wide discussion between different authors [39, 79–81, 93, 413, 735–738]. In numerous studies [79–81, 413, 738], application of the Hammett method using acid–base indicators to characterize the strengths of both acidic and basic surface sites has been used. Thus, in the case of solids the indicator bases which change color, for example during protonation, are used to probe the Brønsted acid characteristics presented in Table 2.40. Unfortunately, interactions of the indicators with both Lewis and Brønsted centers cannot be separated on the basis of the analysis of UV–Vis spectra.

Using the analysis of diffuse reflectance spectra of the indicators adsorbed from the gas phase, the strength of acidic sites has been estimated on the basis of the minimum pK_a value of a protonating base, as follows:

$$H_0 = pK_{a\text{Ind}} - \log[\text{H}_{\text{Ind}}^+]/[\text{Ind}] \quad (2.22)$$

The second component of Equation (2.22) has often been neglected or it has been supposed that it is equal to one. However, this is not always correct. Thus, Tanabe [79–81] showed that the pK_a scale of the bases cannot be a basis for the measurement of surface acid properties. The main limitation in the use of the indicator method is the fact that equilibrium is not achieved on the surface:



and the $f_{\text{B}}/f_{\text{BH}^+}$ ratio is not a constant. This is why it is not quite correct to use the indicator method to determine the strength of acidic sites.

Another approach to study the strength of both Brønsted acids and bases on the surface has been proposed on the basis of a determination of the proton affinity values measured in the gas

Table 2.40. UV–Vis spectroscopic peak positions (nm) of a number of indicators studied on various solids [413]. Reprinted from Dixit, L. and Rao, P. T. S. R., *Appl. Spectrosc. Rev.*, **31**, 369–472 (1996), courtesy of Marcel Dekker Inc.

Solid	Indicator ^{a,b}					
	Ph ₃ COH (−3.3)	BzAP (−5.6)	TMBzOH (−8.7)	4NT (−11.3)	4NFB (−12.4)	2-4 DNT (−13.7)
Natural forms	215, 260	300	265	264	255	234
Acid forms	410, 430	415	470	377	360	339
Davisil-62	260, 410	315	–	285	274	265
M-46	410, 430	395	–	303	285	265
Nikki	410, 430	400	–	302	286	264
LZ-Y82	410, 430	420	470	330	302	267
LZ-210(12)	410, 430	415	470	317	299	266
HY(8.1)	410, 430	415	470	318	299	266
LZ-M8	410, 430	420	470, 375	318, 360	300	268
JRC-Z-HM(20)	410, 430	420	470, 375	318, 360	300	268
Beta	410, 430	415	470	318	299	266

^aPh₃COH, triphenylmethanol; BzAP, benzylacetophenone; TMBzOH, 2,2,4-trimethylbenzyl alcohol; 4NT, nitrotoluene; 4NFB, 4-nitrofluorobenzene; 2,4-DNT, 2,4-dinitrotoluene.

^bp*K*BH⁺ values shown in parentheses.

phase [298, 418]. The proton affinity (*PA*) values depend largely on the enthalpy of the reaction $AH \rightarrow A^- + H^+$ in the case of acids, or $HB^+ \rightarrow H^+ + B$ in the case of bases.

2.4.1 PROTIC ACID SITES

Determination of the dissociation energy of OH groups acting as Brønsted acid sites is carried out on the basis of their potential functions, assuming that the OH group is localized [739–741]. In this case, the hydroxy group may be treated as diatomic. In such a situation, it is much more appropriate to characterize the OH bond by its potential curve, i.e. by parameters such as the harmonic frequency ν_e , the anharmonicity constant $\nu_e x_e$ and the bond dissociation energy D_e , which are available from measurements of the fundamental and the first overtones. Observation of the overtones is the main problem. Dissociation energy measured from the equilibrium position r_e (internuclear separation at the equilibrium position) can be expressed by the following equation:

$$D_e = \nu_e^2 / 4\nu_e x_e \quad (2.24)$$

which can be obtained from the harmonic frequency ν_e and the anharmonicity constant $\nu_e x_e$ [739–741]. In order to be comparable to the experimental values, D_e must be changed to D_0 by the following:

$$D_0 = D_e - 1/2(\nu_e - 1/2\nu_e x_e) \quad (2.25)$$

To allow for zero-point energy, the last term is determined spectroscopically from the frequencies of the fundamental ν_{01} and the first overtone ν_{02} , according to the following:

$$\nu_e x_e = (2\nu_{01} - \nu_{02})/2 \quad (2.26)$$

According to Kazansky and co-workers [739, 740a], the dissociation energy of an isolated OH group cannot be used to characterize its acidity, and the shape of its potential curve appears to be only an approximate measure of the activation energy of proton transfer. This method is not

widely used in spite of the fact that determination of the overtones by using diffuse reflection or luminescence spectroscopy is not very difficult.

However, methods to characterize both the acidic and basic properties of the surface are extremely necessary, and also need to be fairly simple. It seems to be better to use energy units to characterize these surface properties. In order to compare the acidic properties of the surface, there are several approaches reported in the literature. Here, however, we will only examine molecular spectroscopic methods.

IRS is widely and successfully applied for the determination of the strength of protic acidic centers. For this, the molecules (bases with known pK_a values) disturbing the adsorption center (OH-group) are used. The properties of the center are characterized by this disturbing effect [742–749].

The strength of a protic acid site can be established by the method of hydrogen bonds based on the change in the stretching vibration frequency of the OH group. It was established that there is a certain relationship between the heat of formation of the H-complexes and $\Delta\nu_{OH}$ (see, for example, [19]). The correlations between the basicity (pK_a^{base}) or acidity (pK_a^{acid}) and frequency ($\Delta\nu_{OH}$) are described by the following equations: $\Delta\nu_{OH}/\nu^{baseOH} = a + bpK_a^{base}$; $\Delta\nu_{OH}/\nu^{acidOH} = a + bpK_a^{acid}$ [745b] at the variation of bases or acids respectively. Assuming the pK_a value for aerosol equal to +7, an equation for calculation of the acidic surface OH-group strength in the pK_a scale has been suggested [745c,d]. The strength of a protic acid site has been estimated on the basis of the value of pK_a for the H-bound base indicator that adsorbs on the surface [745c]:

$$\Delta\nu_{OH}/\nu_{OH} = 0.216 - 0.0096(\Delta pK_a) \quad (2.27)$$

where $\Delta pK_a = pK_a^{acid} - pK_a^{base}$. The pK_a is approximately 7 for the hydroxyl groups of aerosil (Table 2.41). This equation allows to estimate the strength of surface acidic hydroxyl groups in pK_a values with an accuracy of ± 2.5 .

However, Paukshtis and Yurchenko [418] prefer to estimate the strengths of acidic protic sites using the values of proton affinity (PA):

$$PA_{OH} = PA_{SiOH} - 442.5 \lg \Delta\nu_{OH}^B / \Delta\nu_{OH(SiO_2)}^B \quad (2.28)$$

To estimate the PA values of solid acids by using this equation it is necessary to know the $\Delta\nu_{OH}$ value when the base B acts on the OH of SiO_2 and on the acid being investigated. In the case of aerosil, $PA(SiOH)$ is 1390 kJ mol^{-1} [298, 418, 742–744]. This value agrees well with the point of view that silica gel as an acid is slightly stronger than phenol [79, 745].

Table 2.41. Comparison of the strengths of protic centers on a surface of several systems obtained by different methods.

Oxide	Method	Scale	Strength	Standard strength	Reference
SiO ₂	Indicator	H_0	+ (5–6)		81
SiO ₂	Titration	pK_a	+9.7	9.1 (phenol)	298
SiO ₂	H bond	pK_a	+7.1	9.1 (phenol)	20
SiO ₂	H bond	pK_a	+7.0	9.1 (phenol)	742
SiO ₂	H bond	pA^a	1390	–	418
HNaY	H bond	pK_a	–9	7.0 (SiO ₂)	418
HNaY	H bond	pA^a	1200	1390 (SiO ₂)	418
MgO	H bond	pA^a	1560 ± 40	1390 (SiO ₂)	418

^a – kJ mol^{-1}

A comparison of the strengths of protic centers (SiOH) on the silica gel surface as obtained by different methods is shown in Table 2.41. Using Equation (2.28), the value of PA for the hydroxyl groups of NaHY zeolite, several oxides, metal phosphates and sulfates [298] have been estimated (see Tables 2.3–2.5 above).

Acidity scales based on the IR shifts in positions of the hydroxyl groups in zeolites after perturbation with carbon monoxide (weak H bond) at low temperatures have also been adopted. The correlation between the energy characteristic of hydroxyl, the proton affinity and the shift ν_{OH} is as follows:

$$PA_{OH} = 2254 - 442.4 \log(\nu_{OH}) \quad (2.29)$$

Both the advantages and disadvantages of the above-mentioned methods have been examined in detail [298, 418]. Such methods are not ideal, particularly the first one.

The relative shift of the OH stretching frequency of an acid in complexes with base molecules is a measure of the acidity. Comparison of such data for molecules of known acidities has enabled the estimation of absolute acidity for surface hydroxyl groups. The frequency shift $\Delta\nu$ accompanied by hydrogen-bond formation can be calculated as follows:

$$\Delta\nu = 3qE/4\pi(2\mu)^{1/2}D^{1/2} \quad (2.30)$$

where q is the dipole charge, E is the field component along the O–H axis, μ is the reduced mass, and D is the bond dissociation energy. The frequency shift can be used to estimate the strength of the interaction between adsorbed basic molecules and XH groups and in the case of each OH group may characterize their acid properties [469]. The problem of estimating the strengths of protic acidic centers (OH groups) becomes more complicated if such groups are present on the surface at the same time.

If there are no analytical bands of free OH groups in an initial spectrum of the catalyst, the so-called ion-pair method can be used to estimate the surface acidity [744–746]. The following equation can be useful in this approach [389, 460, 747]:

$$\log \Delta\nu_{NH} = \log(1160) - 0.0024(PA_0 - 837) \quad (2.31)$$

Estimation of the strengths of protic acidic centers for the free and supported heteropoly acids, V_2O_5/Al_2O_3 [106, 460], MoO_3/Al_2O_3 [395, 397] and MoO_3/SiO_2 [397], are example of the use of Equation (2.31), because no absorption bands of isolated hydroxyl groups have been observed in the spectra of these oxides.

We will examine, as an example, the strength of the protic sites of V_2O_5/Al_2O_3 . This system has been studied by Budneva *et al.* [460] using an IR spectroscopic technique with the use of the dependence of the position of the pyridinium ion ν_{NH} absorption band on the proton-donor properties of the catalyst. The ν_{NH} band profile is very complex and therefore the ν_{NH} value is specified to be the center of gravity (cg) of the entire profile ($\nu^{cg}NH$) in the 2200 to 3400 cm^{-1} range. The $\nu^{cg}NH$ position was determined by numerically integrating according to Cook [389, 461a] and was also calculated by using the spectrum of adsorbed pyridine relative to that of the sample before adsorption (~ 2900 cm^{-1}). The strength of the protic sites, calculated from the following equation [460, 747]:

$$PA(kJ\ mol^{-1}) = \log(3400 - \nu^{cg}NH)/0.0023 - 51 \quad (2.32)$$

is ca. 1120 $kJ\ mol^{-1}$. This confirms that the protic sites of V_2O_5/Al_2O_3 are stronger than those in zeolites [460]. The experimental data of Davydov [389] show that the Mo^{6+} , V^{5+} and Sb^{5+} ions (ions in the highest state of oxidation) may produce the strongest Brønsted sites that are removed

by reduction. For example, in tin molybdenum oxide catalysts the number of strong Brønsted acid sites [748], capable of protonating propene and ethene with the formation of ether-like surface compounds, is $1.2 \times 10^{17} \text{ m}^{-2}$. These sites can also protonate the molecules of aromatic compounds with carbenium ions formation (see Chapter 5). Such sites on the surfaces of typical redox catalysts open up new prospects for the activation of molecules and for the development of unexpected methods of adsorbate conversion.

The concentration of acid sites on the $\text{V}_2\text{O}_5/\text{Al}_2\text{O}_3$ surface has been estimated from the IR spectra of adsorbed pyridine and ammonia molecules [460]. The PyH^+ concentration ($\mu\text{mol g}^{-1}$) was determined from the intensity of the $\nu\text{C}-\text{C}$ adsorption band at 1540 cm^{-1} as follows:

$$[\text{PyH}^+] = (D_\nu d\nu / A_0 \rho) \times 10^3 \quad (2.33)$$

where ρ is the thickness of a catalyst pellet (mg cm^{-2}) and $A_0 (= 3 \text{ cm mol}^{-1})$ is the integral absorptivity [749]. The concentration of pyridinium ions in an oxidized $\text{V}_2\text{O}_5/\text{Al}_2\text{O}_3$ catalyst was measured as $100 \mu\text{mol g}^{-1}$ (with an accuracy of around 15 %).

This catalyst adsorbs ammonia to produce two firmly bound forms, i.e. (i) coordination-bound ammonia on Lewis acid sites ($\delta_s\text{NH}_3 = 1250 \text{ cm}^{-1}$), and (ii) NH_4^+ ions on Brønsted acid sites (absorption band at 1425 cm^{-1}). It is possible to choose the conditions when only one adsorption form exists. Addition of water to adsorbed ammonia leads to the conversion of coordinatively bound ammonia into ammonium ions. By using a volume defined by a calibration loop, in order to incorporate small amounts of water into the cell, all of the coordinatively bound ammonia was converted into ammonium ions. A single form of adsorbed ammonia (NH_4^+) may also be obtained upon adsorption on a hydrated surface. Combined spectral and quantitative analytical measurements enabled us to determine the extinction coefficient (ε). The calibration curves to determine the values of ε of the absorption bands of NH_4^+ and coordinated ammonia are available in the literature [460]. The calculated ε ($\text{cm}^2 \text{ mol}^{-1}$) values are $\varepsilon_{1430} = 2.15 \times 10^5$ (ammonium ion), and $\varepsilon_{1250} = 5.3 \times 10^5$ and $\varepsilon_{1610} = 5.9 \times 10^5$ (coordinated ammonia).

The concentrations of coordinatively bound molecules and ions on the surface of an oxidized $\text{V}_2\text{O}_5/\text{Al}_2\text{O}_3$ catalyst have been estimated as $C_{\text{NH}_4^+} = 138 \mu\text{mol g}^{-1}$ and $C_{\text{NH}_3} = 427 \mu\text{mol g}^{-1}$, respectively. Water pre-adsorption on the oxidized surface of the catalyst increases the content of ammonium ions, and hence decreases the amount of coordinatively bound ammonia; the total amount of ammonia adsorbed on both types of sites is constant ($\sim 560 \mu\text{mol g}^{-1}$). The number of adsorbed water molecules determines the total number of protic sites. After complete coverage of the Lewis acid sites by water, the number of protic sites is $560 \mu\text{mol g}^{-1}$, and no Lewis acid sites are present. The total concentration of Brønsted and Lewis acid sites is constant and nearly equals the potential number of V^{5+} cations on the surface of the (110) plane [750].

To determine the amount of protic sites on the catalysts surface it is therefore possible to use two approaches. The first of these is connected with the direct measurement of the number of OH groups at the various νOH values, while the second is based on measurements of the number of protonated bases from spectral data. In a number of cases, each of these methods can be used.

In several cases, the concentration of protic sites can be directly determined by the intensity of the bands in the spectra of protonated probes such as ammonia, pyridine, etc. Supported heteropoly acids [397, 747] and sulfates [298] are examples of such catalysts. The values of ε and A_0 for pyridine measured for the 1540 cm^{-1} band is independent of the temperature or the nature of the protic acid. The A_0 value of this band in the case of surface ions is close to that obtained in the case of pyridinium salts. In contrast, for ammonia A_0 depends on both the temperature and strength of the acidic site [418, 460].

A standardized deconvolution procedure has been developed by Makarova *et al.* [751] for the reliable decomposition of the complex hydroxyl region in the infrared spectra of mordenites into high-frequency and low-frequency peaks. The peak extinction coefficients have been determined

which then allows the calculation of the overall number of Brønsted acid sites, their distribution between main channels and side pockets, and also the amount of extraframework aluminum. Results obtained by FTIR spectroscopy are in good agreement with those obtained by NMR spectroscopy [751].

A calculated value for the PA in the case of protic sites of the $H_3PMo_{12}O_{40}$ heteropoly acid is 1120–1130 kJ mol^{-1} [397, 747], showing that the energy of the proton breaking off from the heteropoly acid anion is 60–70 kJ mol^{-1} less than that from the acidic moiety of the alumina–silicate systems. This proves (qualitatively, as well as quantitatively) that the acidity of this heteropoly acid is stronger than for other acidic catalysts.

It has been shown [397, 747] that the concentration of the Brønsted acid sites of the heteropoly acid depends on the temperature of water removal, the content of Na ions in the sample and the nature of the support. When water is removed, the number of Brønsted acid sites decreases. Thus, at 723 K only 10–15 % of their initial amount are present in the sample. For Na-containing salts, the number of Brønsted sites is less than that for the heteropoly acid, and their strength (PA) decreases from 1120–1130 to 1160 kJ mol^{-1} . If Al_2O_3 is used instead of silica gel, the acidity of the heteropoly acid also decreases more significantly (ν_{NH} at 2600 cm^{-1}), down to 1220 kJ mol^{-1} . The acidities of both the free and supported heteropoly acid are practically the same.

The MoO_3/SiO_2 acidity in a hydrated state is close to that of the heteropolyacid [397], as deduced from the contour of ν_{OH} for PyH^+ on both of these samples. Such a coincidence is connected with the formation of Keggin units during the adsorption of MoO_3 on the surface of silica gel (see Chapter 4). Thus, the strong Brønsted acidities of the MoO_3/SiO_2 , MoO_3/TiO_2 [396, 397] and polymolybdate compounds in the case of MoO_3/Al_2O_3 [395, 397] is more probably caused by the formation of Keggin units. In the case of CrO_3 , MoO_3 and WO_3 supported systems, the Brønsted acidity is determined by the $M^{6+(5+)}-OH$ fragments.

As for phosphate samples, it is known that the terminal POH groups are protic sites, and the value of PA is 1220 kJ mol^{-1} according to quantum-chemical calculations [298]. The possibility of the formation of bridged AlOHP groups is not significant. Their concentration is 10^9 times less than that of terminal POH group, while their PA ($= 1165 \text{ kJ mol}^{-1}$) is also less. In the case of the similar aluminosilicate cluster, the value of PA is 1185 kJ mol^{-1} for the bridged AlOHSi. The experimental values of acidity on the pK_a scale is 5 for the phosphates of iron, zirconium and aluminum, while for zeolites it is 9 [298].

Other molecules like CO, N_2 and H_2 can be successfully used to estimate the properties of Brønsted acid sites. Thus, Sigl *et al.* [545] reported the adsorption of H_2 and D_2 as probe molecules on the series of [Al]-, [Ga]- and [Fe]-ZSM-5 and compared the results with those obtained with CO and N_2 probe molecules. A linear correlation between $(\Delta\nu_{OH})^{1/2}$, which is proportional to the heat of formation ΔH_B of the H-bound complex $O-H \cdots B$, and proton affinities has been found, as follows:

$$\Delta\nu_{OH}^{1/2} \sim aPA_B + b \quad (2.34)$$

where PA_B is the proton affinity. The $\Delta\nu_{OH}$ values for H_2 , N_2 and CO probe molecules correlate with their respective PA values (424, 477 and 598 kJ mol^{-1} , respectively).

2.4.2 LEWIS ACID SITES

The study of the complexing ability of cations on oxide surfaces has great value. The data cited above demonstrate the possibility of using ammonia molecules both to detect Lewis acid centers and to characterize the relative power of electron-acceptor centers on the surface of oxide catalysts, on the basis of the $\delta_s NH_3$ values (see Table 2.9). Extensive information on the interaction of ammonia, carbon monoxide and olefins with cations of oxide surfaces is now available. Our discussion will therefore be confined to these substances.

It is reasonable to quantify the complexing ability of the cations in terms of the energies of their interactions with adsorbate molecules [418, 488, 755–758]. However, if the interaction energy is determined from calorimetric data (the most widely used, convenient, and precise method), the interaction of the probe molecules should take place without dissociation and involve only surface cations. Unfortunately, this is observed only in a few systems under specially chosen conditions. As a result, the complexing power of the cations on oxide surfaces cannot be determined by this method without resorting to physical methods of measurement (such as IR spectroscopy) to establish the dominant type of interaction.

The estimation of the energies of complex formation from IR spectroscopic data is attractive [753]. However, in these measurements a correct evaluation of the interaction energy is possible only when the centers are uniform or very nonuniform. Furthermore, the methods need to be improved because errors in the direct spectral determination of the adsorption heats remain large at present [757].

The complexing ability of the cations is most satisfactorily evaluated through the adsorption of molecules which behave as typical σ -donors, namely ammonia, pyridine, water, alcohols, ketones and aldehydes. A sufficiently accurate spectral parameter related to the acceptor power of the cation is available only for ammonia, but even in this case it is difficult to construct a $\delta\text{NH}_3-Q_{\text{ads}}$ calibration plot because ammonia is adsorbed on different surface centers in different forms (bound by one to three strong hydrogen-bonds). This is also applicable to other molecules of this type. In spite of the above comments, the study of the isosteric heat of adsorption of NH_3 over Al_2O_3 has been done [418]. According to these data, a 1-cm^{-1} shift of the $\delta_s\text{NH}_3$ band in the IR spectra of adsorbed NH_3 corresponds to the change in Q_{NH_3} somewhere in the area of 1 kJ mol^{-1} .

For pyridine, the correlation between the heat of adsorption and the position of the $\nu\text{CC(N)}$ (1590 cm^{-1}) band has been evaluated [418] on Al_2O_3 and ZrO_2 , and also on Y-type zeolites. Unfortunately, such a correlation has to be described by a separate equation for each cation, for example:

$$Q_{\text{Py}}^{\text{Al}} = 6.6[\nu\text{CC(N)} - 1590] - 86; \quad Q_{\text{Py}}^{\text{Zr}} = 7.0[\nu\text{CC(N)} - 1590] - 26 \quad (2.35)$$

However, in general, for different cations it is impossible to use a comparison of the frequencies as a method to compare the strengths of the surface sites, and so this method is not universally used.

The more universal approach is to use the correlation, established by Davydov *et al.* [755], for nontransition- and transition-metal cations with the only σ -component of the M-CO bond:

$$\nu\text{CO} = 3.2Q_{\text{ads}} - 2050 \quad (2.36)$$

with a correlation coefficient of 0.96. In the case of nontransition-metal cations, the earlier suggested equation [418]:

$$Q = 10.5 + 0.5\Delta\nu\text{CO} \quad (2.37)$$

where $\Delta\nu\text{CO} = \nu\text{CO}_{\text{ads}} - 2143$, may also be useful.

There is also one important consideration which shows that the lateral interactions (Chapter 3) of the molecules adsorbed on oxides, in particularly CO molecules, appear to be significant. Such interactions are accompanied by changes of both frequency and adsorption energy. The change is different for different oxides and can distort the energy of the interaction between molecules and an adsorption center. Hence, unfortunately the above-mentioned estimation can only be correct for a particular system at a certain coverage by a particular probe.

Although the CO molecule is a quite useful probe, the molecules which are the components of the reaction mixture are the best probes if they have the spectral parameters dependent on the properties of the adsorption center. It is well known that olefin molecules are used in numerous

Table 2.42. Coefficients of absorption (ϵ) and of integral absorbance (A_0) for various absorption bands in the spectra of CO adsorbed on the Lewis acid sites of a number of oxide.

Oxide	Lewis acid center	ν (cm ⁻¹)	$A_0 \times 10^6$, (cm μ mol ⁻¹)	$\epsilon 10^{19}$, (cm ² mol ⁻¹)	Reference
Al ₂ O ₃	Al ³⁺	2203	1.0	—	753
		2190	0.6	—	
ZnO	Zn ²⁺	2212	3.9	—	752
		2200	2.4	—	
		2187	0.78	—	
		2190	0.5–0.7	0.6	
MgO	Mg ²⁺	2158	0.4	0.4	298
BeO	Be ²⁺	2193	1.2	—	298
		2203	1.0	—	
ZrO ₂	Zr ⁴⁺	2183	2.2	1.4	753
		2203	0.9	—	
TiO ₂	Ti ⁴⁺	2208	1.1	1.2	30
Ga ₂ O ₃	Ga ³⁺	2167	0.5	—	753
H-erionite	—	2228	1.2	—	753
NaY	Na ⁺	2173	0.3	0.6	753
NiY	Ni ²⁺	2190	1.3–1.7	1.4	30
		2191	0.6	—	
		2197	0.6	—	
		2217	1.2	1.4	
CoY	Co ²⁺	2190	0.5	2.0	298
		2206	0.8	—	
MnY	Mn ²⁺	2183	0.3	—	298
		2206	0.8	—	
CaY	Ca ²⁺	2197	0.5	—	298
CuY	Cu ⁺	2160	—	8.2	30
Cu metal	Cu ⁰	2100	3.7	—	754
AgO/Al ₂ O ₃	Ag ⁺	2170	11.5–15.5	6.0	30
Pt/SiO ₂	Pt ⁰	2100	26	—	30
		2095	11.7	20.5	
		2085	15.6	—	
		2140	3.1	—	
Cu ₂ O/SiO ₂	Cu ⁺	2136	16.5	—	752
		2135	15.6	—	
		2132	22.6	—	
		2140	10.6	12.2, 6.7	
Cu/Al ₂ O ₃	Cu ⁺	2140	10.6	12.2, 6.7	30,298
CuCr ₂ O ₄	Cu ⁺	2120	8.6	—	30,298
		2122	8.7	—	
NiO–MgO–MoO ₃	—	2190	1.8–2.2	2.0	30
CoO–MgO–MoO ₃	—	2190	1.5–1.0	1.7	30

catalytic reactions and have the spectral parameter ($\nu_{C=C}$) which depends on the nature of the surface bond. Although the $\nu_{C=C}$ value of olefins is not strongly characteristic [30] (see also Chapter 5), and the extinction coefficient of the $\nu_{C=C}$ band is less than that for CO, nevertheless sometimes these reagent molecules can provide unique information on the properties of surface cations. Furthermore, olefins can be used as a probe to determine the complexing ability of cations on oxide surfaces, irrespective of their nature [30], because the spectral changes of the C=C bond (a decrease in $\nu_{C=C}$, for example, in π -complexes) reflect both donor and acceptor interactions, and can be accurately correlated with the olefinic adsorption heats. In the case of the π -complexes

of deuterioethene and deuteropropene, $\nu\text{C}=\text{C}$ of which is more sensitive than that of the H-derivatives, a linear correlation between $\Delta\nu\text{C}=\text{C}$ and Q_{ads} has been established [30], as follows:

$$Q_{\text{ads}} = 0.15(\Delta\nu\text{C}=\text{C} + 49.0), \quad Q_{\text{ads}} = 0.13(\Delta\nu\text{C}=\text{C} + 52.0) \quad (2.38)$$

for ethene and propene, respectively.

Both the spectral and energy characteristics, as well as the number of centers, are shown in Table 2.43 for carbonyl-like complexes and for π -complexes of ethene and propene. The highest value of νCO is observed for Al_2O_3 , indicating that an acceptor capacity for Al^{3+} ions is higher than that for other cations. On the other hand, in the case of Cu^+ ions, which are able to undergo $d \rightarrow \pi^*$, as well as donor-acceptor interactions, the νCO frequency decreases, and the heat of adsorption increases. For olefins (for example, propylene) the change in $\nu\text{C}=\text{C}$ and in the adsorption heat for cations of different types have been evaluated. Therefore, the presence or absence of $d \rightarrow \pi^*$ interactions can be established by comparison of the spectral characteristics of the M^{n+} -olefin and M^{n+} -CO complexes.

The number of active centers (coordinatively unsaturated cations) is an important characteristic in surface chemistry. Table 2.43 shows the number of active centers for several oxides that are able to coordinate ethene, propene and CO. It can be seen that only part of the surface cations can interact with these molecules and, furthermore, that the numbers of coordinatively unsaturated cations able to interact with different molecular probes are different. These differences are connected not only with the σ - and π -components of the bonding since a different number of active centers is observed upon adsorption of various molecules, even in a case where there is no possibility of $d \rightarrow \pi^*$ interaction or it is very small.

The results shown in Table 2.43 for Ti^{4+} , Zn^{2+} , Ni^{2+} and Co^{2+} cations make it clear that this is a general property of cations in high states of oxidation. The difference in the number of active centers established by the adsorption of different molecules is determined by both the donor properties of these molecules and the properties of the surface cations. The number of active centers varies from 1 to 10 % of the total number of cations on the oxide surface [30]. In each system, this variation is due to different causes: (i) the main portion of the cations on the oxide surface is in a coordinatively saturated state, even after high-temperature treatment *in vacuo* (oxygen and OH ligands), and (ii) the acceptor power of the remaining portion of the cations is insufficient to form the bond because of the large coordinative saturation.

Molecules with a high donor capacity can interact with a greater number of cations than those molecules with a moderate donor ability. Thus, the V^{5+} , Mo^{6+} and Fe^{3+} ions on the surfaces of oxides and the Fe^{3+} ions in zeolites [30], which, in general, do not coordinate CO and NO

Table 2.43. Spectral manifestations (νCO in MCO (cm^{-1}), heats of adsorption (Q (kJ mol^{-1})) and the number of active sites ($n \times 10^{-19} \text{ g}^{-1}$) of some carbonyls and of adsorption π -complexes of ethylene and propylene on various oxide catalysts.

System	Center	CO			C_2H_4			C_3H_6		
		νCO	Q^a	n	νCC	Q^a	n	νCC	Q^a	n
ZnO	Zn^{2+}	2190	44	0.52	1600	51	0.80	1625	55	0.81
TiO_2	Ti^{4+}	2190	44	1.6	1615	50	3.0	1635	54	6.5
NiO-MgO-MoO_3	Ni^{2+}	2190	44	0.51	1613	48	2.0	1630	54	4.5
CoO-MgO-MoO_3	Co^{2+}	2190	44	0.66	1615	50	1.5	1635	54	3.3
$\text{Ag}_2\text{O/Al}_2\text{O}_3$	Ag^+	2170	53	2.0	1570	54	4.0	1595	59	9.6
$\text{Cu}_2\text{O/Al}_2\text{O}_3$	Cu^+	2130	71	9.3	1545	67	3.7	1550	69	6.6
Al_2O_3	Al^{3+}	2235	55	0.48	—	—	—	1600	60	0.12

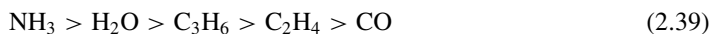
^aDifferential heats of adsorption are quoted for equilibrium coverage ($>15\text{--}20 \mu\text{mol g}^{-1}$).

molecules, can coordinate ammonia [30]. One of the most acceptable explanations for this effect was proposed by Pel'menshikov and Zhidomirov [756] and justified by allowing for the possible migration of the surface cations following adsorption (the so-called 'structural looseness' of the surface). It can be seen from Table 2.42 above that the increase in the number of centers correlates with an increase in the heat of adsorption, again confirming the dependence between the number of effective centers and the donor properties of the molecules.

In fact, the differences detected in a number of centers can be easily explained in terms of differences in the electron-donor ability of the adsorbates, since in the series $C_3H_6 > C_2H_4 > CO$ a good correlation is observed between the number of centers, the binding energies, and the ionization potentials ($IP(CO) = 14.1$ eV, $IP(C_2H_4) = 10.5$ eV, $IP(C_3H_6) = 9.73$ eV [583, 584]).

This dependence does not include the data obtained upon the adsorption of ammonia, even for such a typical σ -acceptor as Al_2O_3 . The concentration of electron acceptor centers on $\gamma-Al_2O_3$ dehydrated at 773 K, obtained on the basis of a combined gravimetric and IR spectroscopic study [435] of the ammonia adsorption, is $2 \times 10^{17} m^{-2}$. The initial heat of adsorption for ammonia on $\gamma-Al_2O_3$ is $120 kJ mol^{-1}$, i.e. it is much greater than the corresponding value for C_3H_6 . However, the ionization potential $IP(NH_3) (= 10.2$ eV) is greater than that of C_3H_6 . This is not incompatible with the above observation and merely points to the need to use molecules of the same type (for example, typical σ -donors or π -acceptors) to determine the complexing capacity of cations. A relationship between the IP s and the heats of adsorption is also observed for typical σ -donors such as ammonia, water and ketones.

In order to establish a common series of σ -donor activity of the ligands, experiments on the mutual displacement of molecules adsorbed on TiO_2 (a system for which $d \rightarrow \pi^*$ donation can be ignored, as for aluminum oxide) have been carried out [757, 759]. It was found that the strongest donor is ammonia which displaces molecularly adsorbed water and propene molecules adsorbed as π -complexes. The propene breaks down the π -complex of ethene, and both ethene and propene molecules break down the CO complexes. In this way, the experiments allow us to write the following single series of σ -donor activity for the ligands of interest [757]:



Similar series were also obtained for all cations of transition metals at the ends of periods in a state of oxidation of two, plus those for higher-valence cations (>2). The proposed series of ligands are confirmed by both the heats of adsorption of the molecules on the coordinatively unsaturated surface cations and the surface coverages which decrease according to the above sequence.

The electron-acceptor capacity of the molecules varies in the opposite sense to the σ -donor ability [757]:



i.e. in the case of cations which are able to undergo $d \rightarrow \pi^*$ interactions, the complex-formation energy is greater for CO than for C_2H_4 , and also greater for C_2H_4 than for C_3H_6 .

A single series of π -acceptor ability of the ligands was constructed by an analogous series of experiments in which TiO_2 was replaced by Cu_2O/Al_2O_3 , since the Cu^+ ions are typical π -donors. This produced the following [757]:



The results show that the so-called structural flexibility of the surface (the ability of the strong electron-donating molecules to alter the position of cations on the surface) is one of the important factors determining the interaction of the molecules with the surface cations. This factor introduces some complications into the concept of the number of active centers in the interactions with

Table 2.44. Properties of the Lewis acid sites on the surfaces of some simple oxides, based on the heats of adsorption of carbon monoxide.

Oxide	Dehydration temperature (K)	$\nu\text{CO}(\text{cm}^{-1})$	$Q_{\text{CO}}(\text{kJ mol}^{-1})$	Reference
BeO	673–723	2190	34	301, 753
		2203	40	753
MgO	723–873	2158–2165	22	301, 753
CaO	723–873	2155	16	301
ZnO	723–773	2190	44	30, 298
Al ₂ O ₃	450–1073	2178–2182	30	
		2186–2195	34	
		2203–2212	42	30
		2225–2235	54	
Cr ₂ O ₃	723	2196	40	30
Ga ₂ O ₃	723	2167	27	753
		2190	34	753
Y ₂ O ₃	723	2165	22	298
		2177	27	298
TiO ₂	673	2180–2190	–	301
		2207–2208	42	
ZrO ₂	723	2183	28	298
		2203	36	298
CeO ₂	673	2160	19	–

different molecules. The above series of σ -donor and the π -acceptor powers of the ligands can be used to calculate the predominant coverage of the active centers of the surface in reactions, and the correlation between the $\nu(\text{CO}, \text{C}=\text{C})$ frequencies and the heats of adsorption can be used to predict the energetics of the interaction directly from the spectral data.

In addition to chemical considerations, the structural factor – namely the coordination number of the cation – significantly influences the strengths of Lewis acid sites. Between the weakest and the strongest site of alumina, the difference in the heat of the CO adsorption is 24 kJ mol^{-1} , while the total change is about 40 kJ mol^{-1} between CaO and Al₂O₃. The heat of CO adsorption seems to be a more acceptable characteristic for comparing the acceptor ability of LASs [755, 757, 759]. It is clear that lateral interactions can change the value obtained in the case of some oxides.

The concentration of Lewis acid sites can be estimated from the intensities of the absorption bands in the IR spectra of probe molecules by using Equation (2.33) shown above for protic sites or represented in Section 1.8. For coordinated carbon monoxide, the data on the A_0 and ϵ values known at present are summarized in Table 2.42. As for change in the CO extinction coefficient due to adsorption, it has a complex dependence on the frequency and has been discussed in detail in [31, 752]. Characteristics of the Lewis acid sites of simple oxides obtained by the analysis of IR spectra of adsorbed CO are presented in Table 2.44.

2.5 Determination of basic surface properties

In addition to unsaturated cations and hydroxyl groups, there are oxygen ions on the surfaces of oxide systems. These anions (the basic surface centers) play the important role in initiating the reactions proceeding on the surface. That is why the characterization of such centers (qualitative and quantitative) is both interesting and important. Anions in different coordination environments which occupy the regular positions (O^{2-}) on the surface and have different effective charges (the

surface hydroxyl groups, and also paramagnetic sites of the type O^- , O_2^- and O_2^{2-}) may also play the role of such centers.

To estimate the proton-accepting (basic) properties of the surface, two groups of methods are used; i.e. titration with various reagents and spectral techniques. The titration method allows one to infer only the total content of surface basic centers and an averaged characteristic of their properties. However, there is no doubt that different types of basic centers with different properties are present on oxide surfaces. Thus, the main problem is to clarify the possibility of determining the concentration and relative strength of basic surface sites of both different or the same chemical natures, with different properties (for example, O^{2-} sites differently coordinated due to polydispersion of the samples). Evidently, the solution of this problem is impossible without the application of spectral methods because the titration methods give us only averaged information about the properties of the surface sites.

Precision physical methods of investigation (ESR, NMR, XPS, UV-Vis and IR spectroscopy, including the IR spectroscopy of adsorbed probe molecules) have been successful in understanding the nature and properties of surface centers in heterogeneous catalysts. The ESR method allows the monitoring of the properties of paramagnetic sites, and their inhomogeneity and reactivities with respect to different molecules. We will not analyze here all of the methods used because of the availability of several good reviews [52, 79, 413, 760-768]. We will only remark here on the most important of these, paying the main attention to the methods based on molecular spectroscopy.

The basicity of solids may be profitably characterized by X-ray photoelectron spectroscopy (XPS) [70, 413, 761-763]. The values of the binding energies of the elements depend, besides other factors, on the charge carried by the elements. Normally, this value decreases as a function of the negative charge carried by a particular element in a crude approximation of the Madelung potential. It follows that the binding energy value of the O1s peak is expected to decrease as the negative charge on the oxygen atom increases. Unfortunately, because of the charging effects on the sample due to the ejection of the electrons and the insulating properties, for example, of the zeolites, it is difficult to determine with sufficient accuracy and certainty the chemical shift of the O1s binding energy value and further work is obviously needed in this field. The method gives direct information about the effective charge of the anion, although it is also averaged because the information obtained in this way is from atoms in about one to two monolayers, while the number of active adsorption centers is low and may equal only a few %, or even less, of the total number of centers exposed on the surface.

Diffuse reflectance [231, 232] and photoluminescence [235-237] spectroscopies, together with electron microscopy, have been extensively used to define in more detail the nature of the active sites for intrinsic anions and cations in states of low coordination (O_{1C}^{2-} and M_{1C}^{2+}) on the surface of alkali-earth oxides. Different UV-Vis absorption and emission bands are related to three families of surface sites: five-coordinated ions (O_{5C}^{2-} and M_{5C}^{2+}) on extended (001) planes, four-coordinated ions (O_{4C}^{2-} and M_{4C}^{2+}) on edges, and three-coordinated ions (O_{3C}^{2-} and M_{3C}^{2+}) on corners. A characteristic of surface ions is that they have a reduced coordination number compared with ions in the bulk. Absorption caused by the formation of surface excitons will accordingly lie at lower energies (lower ν) since the Madelung potential decreases as the coordination number is reduced. However, not all oxides have well-structured spectra in this region and only in the case of the alkali-earth oxides have such spectra been obtained. This is a significant disadvantage of this method.

In order to study both the nature and properties of surface oxide sites, the methods used most widely are investigations based on establishing dependencies in the changes of spectral parameters of the probe molecules, interacting with surface sites in specific ways, on the properties of these sites. A few probe molecules have been proposed to establish the presence of basic sites on

the surfaces of heterogeneous catalysts and to determine their properties. By analogy with the methods employed to test the acidic properties, the method of hydrogen bonds between protic acids and bases is applied.

It should be recalled that a molecular probe must satisfy the following requirements: (i) have a specific interaction only with the surface site to be tested (ii) be spectrally sensitive to changes in the electronic state of the adsorption site and (iii) no surface modification should occur due to side-reactions. Let us consider, on the basis of this standpoint, the molecules which are now used [418, 764–769] as probes to study the basic properties of surfaces.

Applications of such probes as carboxylic acids and phenols is complicated, in our opinion, by a number of factors. First, such acids and phenols possess pronounced basic properties and are capable of producing stable complexes with aprotic centers (this can result, in particular, in a modification of the surface). Secondly, the adsorbents and catalysts used for investigation contain surface OH groups, and there is an overlapping of the corresponding absorption bands in the IR spectra with the OH bands of the acidic and phenolic probes, which are sensitive to the interaction with basic sites. Thirdly, the presence of strong surface protic centers can result in the formation of surface esters exhibiting spectral features close to those of the surface complexes of basic sites with acids or phenols.

To estimate the proton-acceptor properties of the surface, it is possible to use NH-acids, in particular, pyrrole [764–767], which is able to form the H-bond with basic surface centers. However, one may encounter some difficulties due to the high proton affinity of pyrrole and its strong interaction with OH groups. Dissociation of the N–H bond in the pyrrole molecule may also play a negative role in the investigation of the surface and it has also been noted that pyrrole can form dimers. Pyrrole is probably also able to undergo ‘double-center’ adsorption with the participation of both oxygen ions and cations, simultaneously. The latter, in particular, may be the explanation of the results, obtained by Scokart and Rouxhet [764], where these authors appear to have shown that the basicity of alumina is higher than that of MgO. However in the case of zeolites, this molecule is a good probe [739, 762, 763, 767], because in zeolites there are no strong ionic pairs.

Other authors [418, 768–771] have proposed the use of the chloroform molecule (in its deuterated form) as the most suitable probe capable of forming H-complexes with basic centers because it is a weak base and, on the opinion of Paukshtis and Yurchenko [418] virtually does not interact with other aprotic and protic surface acid sites. Moreover, there is no superposition of the CH (CD) bands with the bands attributed to the surface OH groups, and the complexes of the molecular probe with the basic centers can be easily identified in the spectra.

Correlations between $\Delta\nu\text{CD}$ and pK_a [418, 769] and between $\Delta\nu\text{CD}$ and PA (proton affinity) of the sites has been established:

$$\log \Delta\nu\text{CD} = 0.0057PA - 3.54 \quad (2.42)$$

These authors believe that this relationship may be used to estimate the absolute values of pK_a (PA) for basic centers. Deviations of the $\Delta\nu\text{CD}$ values from those calculated by using Equation (2.42) do not exceed 15 cm^{-1} . However, it has been shown more recently that (i) the basicity of the chlorine atom in chloroorganic compounds is sufficient to form complexes (Section 5.5) and (ii) as shown by Davydov and co-workers [768, 770], the chloroform molecule is not a perfect probe for testing surface basic sites because of its dissociation leading to the appearance of formates (oxidation) and modification of the surface with chlorine ions. In fact, the splitting-off of the chlorine from the chloroalkyl molecule and even from chloroaromatic compounds (see Chapter 5) is observed readily on a number of different oxide systems, even at low temperatures.

Although the possibility of using chloroform for the characterization of basic sites on the surfaces of several oxide systems has been shown later on the MgO surface [768] and for oxygen of various type of zeolites [771], there is no evidence, yet, on the possibility of using this molecule for suitable differentiation in the strength of such centers in the case of oxides was provided. In the case of MgO, chloroform reveals two types of basic centers: the sites of the first type, characterized by $\nu_{\text{CD}} = 2230 \text{ cm}^{-1}$ are complexes with surface hydroxyls (the absorption band at 3750 cm^{-1} is shifted), while the centers of the other type (absorption bands at $2190\text{--}2200 \text{ cm}^{-1}$) involve surface oxygen [646, 768, 772]. Although a broadening of the band at 2190 cm^{-1} attests to the nonuniformity of the corresponding centers, in our opinion it is not possible to distinguish centers of different types on the basis of a decomposition of this complex band into its overlapping components.

Uvarova *et al.* [771] showed that the molecule of chloroform is a suitable probe to test the strengths of basic centers of zeolites. In this case, no remarkable chemical transformations of chloroform occur after admission onto the zeolites under study (conversion of CHCl_3 takes place, however, in the presence of LASs on the zeolites). The low-frequency shift of the ν_{CH} band relative to the corresponding frequency in the gas phase ($\nu_{\text{gas}}\text{C-H} = 3034 \text{ cm}^{-1}$) is 17 cm^{-1} for Na-mordenite, 24 cm^{-1} for NaY, 34 cm^{-1} for NaX and 49 cm^{-1} for the Cs/NaX zeolites, which agrees fairly well with the stronger basic properties of X-zeolites when compared to Y- and MOR- (mordenite) zeolites and the Cs-forms compared to the Na-forms. Unexpectedly, in the case of trifluoromethane a high-frequency shift of the $\nu_{\text{C-H}}$ band has been observed. An increase in ν_{CH} implies a broken C-H bond and a repulsion interaction with the cation. Therefore, the value of such a shift may be used as a qualitative measure of the basicity of zeolite cationic forms. Acetylene and its derivatives form hydrogen-bonds of the surface type $\text{H-C}\equiv\text{C-H}\cdots\text{O}$. In the case of CHCl_3 adsorption on the alkaline forms of zeolites, a complex also involving a $\text{C-H}\cdots\text{O}$ fragment appears in the interaction.

The strengths of the protic sites on the *PA* scale can be used only in the case of the interactions of the Brønsted-type probe molecules. If Lewis acids, for example, CO_2 , NO_2 and SO_2 , are adsorbed on the surface, the use of this scale is a problem. It should be noted that the method of correlation used by Paukshtis and Yurchenko [418] to compare $\text{p}K_{\text{a}}$ with $\Delta\nu_{\text{CD}}$ has been criticized by Gordymova and Davydov [770]. However, if it is possible to employ this approach, then the use of the scale of *PA* for such a purpose has no physical sense in the case of fully ionic surfaces.

According to various authors [544, 773–776], paraffin molecules can in principal be considered the probes of widest usage for studying basic sites on oxide surfaces using hydrogen-bonding, because these molecules exhibit a poor ability for C-H bond dissociation. However, the use of these is still very limited, and investigations of the H-bonded paraffin complexes with oxides have encountered considerable difficulties because of the small concentrations of those centers that are able to perturb the C-H bond. Adsorption and polarization of molecular hydrogen and light paraffins on cationic forms of various zeolites has been studied by diffuse reflectance IR spectroscopy. The extent of polarization characterized by the stretching frequency is found to be strongly dependent on the nature of the cation (electrostatic field and the presence of d-electrons) and the zeolite framework (localization sites, basicity of oxygen, etc.) [544, 773–776].

In several recent reports, another method to investigate the basicity of oxide surfaces, which is based on the analysis of IR data on the formation of surface carbonates during the adsorption of CO_2 , has been proposed [646, 768, 772, 777, 778]. As has been shown above, the IR spectroscopic data on the formation of CO_2 complexes on oxide surfaces indicate the predominant interaction of CO_2 with the surface centers (O^{2-} and OH^-), yielding carbonate and bicarbonate species, respectively. Detailed analysis of the spectroscopic data allows us to distinguish different types of surface basic sites. According to Davydov and co-workers [646, 768, 772], at least four types of

basic centers exist on the surface of MgO and are involved in the formation of various carbonates (Table 2.45). Distinctions in the spectroscopic parameters of the observed carbonates, according to these authors [646, 768, 772], can be related to the different states of the surface oxygen. The structure within the intense bands in the 1700–1500 cm^{-1} region, which characterizes $\nu\text{C}=\text{O}$ vibrations in carbonates, indicates an energetic (structural) heterogeneity of oxygen participating in their formation. Several types of carbonates bound to the surface in different ways (the $\nu\text{C}=\text{O}$ absorption bands at 1650, 1630, 1585 and 1520 cm^{-1}) have been identified.

IR spectra from CO_2 adsorbed on Sm_2O_3 , La_2O_3 , CaO and $\gamma\text{-Al}_2\text{O}_3$ (see Table 2.44) exhibit a less complex pattern, from which it is concluded that the basic sites on the surfaces of these oxides are more uniform in comparison with MgO. No carbonate-forming basic centers were found on V_2O_5 within the accuracy of the spectral measurements.

Because of the structural nonuniformity of surfaces, there are differences in the effective negative charges on the oxygen ions, i.e. different basic properties. Variation of the effective

Table 2.45. Spectral features of carbonates formed at the surfaces of various oxides dehydrated at 973 K upon interaction with CO_2 (293 K) and the types of carbonate compounds formed.

Oxide	Spectral features			Carbonate complex formed (type and structure)
	$\nu(\text{cm}^{-1})$		$\Delta\nu(\text{cm}^{-1})$	
MgO	1710	1220		Bicarbonate (I), $\text{M}^{n+}(\text{HCO}_3)_n$
	1680	1280	360	Bidentate (II)
	1630	1315	315	
	1610	1370	240	
	1530	~1400	~130	Monodentate (III)
	1450	1450	–	Symmetric IV
CaO	1490	1410	80	Monodentate (III)
Sm_2O_3	1540	1410	130	Monodentate (III)
	1620	1330	290	Bidentate (II)
La_2O_3	1580	1350	230	Bidentate (II)
	1500	1400	100	Monodentate (III)
$\gamma\text{-Al}_2\text{O}_3$	1830, 1780	–	>500	Covalent-bonded carbonates similar to organic carbonates [V]
	1675, 1650	1490	–	Bicarbonate (I)

charge, in turn, influences the ionic-covalent character of the M–O bond which depends on the nature of the cation, its oxidation state and coordination number. It is known [20, 30] that the covalence of the M–O bond of the surface oxygen ions which become incorporated in the structure of monodentate carbonates (type II) is lower than that for bidentate carbonates (type III). This allows one to differentiate the strength of the basic centers. Furthermore, the value of the splitting ($\Delta\nu = \nu(\text{C}-\text{O}_I) - \nu(\text{C}-\text{O}_{II})$) for bidentate carbonates is found to be equal to approximately 300 cm^{-1} [15], and this value gradually increases with an increased covalent character of the M–O bond (decreasing basicity of oxygen). Obviously, such parameters as the angle formed by the C–O_I bonds, the electron-accepting properties of the M^{n+} cation, and the length of the M–O bond, also effect the $\Delta\nu$ value. As for the O_I–C–O_{II} angle and the M–O bond length, their influence on the $\Delta\nu$ value is far less pronounced, as the calculations of the vibrational spectra show [118]. Since the contribution of these parameters is small, the value of the splitting is determined principally by the oxygen basicity. For instance, for organic carbonates, i.e. compounds with a prevailing covalent character of the bonds, the value of the splitting is ca. 600 cm^{-1} [20, 30], i.e. it is increased by ca. 300 cm^{-1} compared with the surface species. Taking into account the fact that the $\Delta\nu$ value is even smaller (ca. 100 cm^{-1}) for monodentate carbonates formed with the participation of more basic oxygen ions than those involved in the bidentate carbonates [15, 20], authors of [646] used the value of the splitting ($\Delta\nu$) as a measure of the basicity of the oxygen participating in the carbonate formation. Bearing the above consideration in mind, it is also possible to assume that bidentate carbonates of three types are formed involving surface oxygen ions with different basic strengths. The other centers produce carbonates of other types. Therefore, the use of the CO₂ molecule as a probe for the surface basic sites allows one to reliably differentiate the centers, including those sites of the same type (for instance, O²⁻).

The results obtained by the analysis of IR spectra of adsorbed CO₂ on the formation of three types of carbonates over MgO are in good agreement with the data mentioned above [231–233], which showed that basic centers of at least three types are present on the MgO surface and represent oxygen anions in low-coordinated states (O_c²⁻): O_{5c}²⁻ ions localized on the (001) face, O_{4c}²⁻ ions on the edges, and O_{3c}²⁻ ions on the corners.

In the IR spectra of CO₂ adsorbed on CaO (see Table 2.45), only monodentate carbonates are observed on the surface of CaO, which is a more basic oxide when compared with MgO. Taking into account this fact and also the conclusions drawn during the study [20, 30] of the correlation between $\Delta\nu$ and ionicity (i.e. basicity) of the M–O bond, this spectral parameter ($\Delta\nu$) seems to be a measure of the relative strengths of surface basic sites: the smaller $\Delta\nu$ value corresponds to the stronger basic properties of the surface site involved in the interaction with CO₂. Based on this parameter, the following sequence for the strongest basic centers responsible for the formation of monodentate carbonates can be presented: MgO < Sm₂O₃ < La₂O₃ < CaO [646, 772]. The order obtained coincides with the oxides' basicities inferred from general theoretical considerations, as well as with those derived by other workers [69, 70].

The proposed approach allows us not only to differentiate basic sites of various types and their strengths but also to estimate the number of basic centers of a certain type if the values of the corresponding extinction coefficients (ϵ) are known. For example, for the centers involved in the formation of monodentate carbonates, the ϵ value equals $4.2 \times 10^{-19} \text{ cm}^2$ per molecule. According to the data obtained, the surfaces of oxides under study mainly differ in the absolute number of basic sites of this type (n) (Table 2.46). The total number of basic centers estimated by the concentration of surface carbonates changes in the following manner: V₂O₅ < γ -Al₂O₃ < MgO < Sm₂O₃ < La₂O₃ < CaO. This is in good agreement with other data on a number of such centers on the MgO surface [780].

Table 2.46. Number of active centers on various oxide surfaces based on data obtained from CO adsorption.

Parameter	Oxide											
	CaO		La ₂ O ₃		Sm ₂ O ₃		MgO		γ-Al ₂ O ₃		V ₂ O ₅	
T_{ads} (K)	293	573	293	573	293	573	293	573	293	573	293	573
$(n \times 10^{17}) \text{ m}^{-2}$	6.9	–	3.8	6.6	3.3	5.0	0.28	0.42	–	0.17	–	–

The method developed to estimate the basicity of surface centers on the basis of IR spectra of adsorbed CO₂ has been reported in detail [646, 772] and applied in the case of oxidative methane coupling catalysts [646, 772]. However, if the common scale of the basic centers for all types of carbonates on the different oxides reported by Davydov *et al.* [646, 768] is not yet widely supported, this is because it is very difficult to separate the effect of the influence of cations on the $\Delta\nu$ value. However, use of the $\Delta\nu$ parameter to compare the strengths of the basic centers in the case of catalysts of the same type, as has been suggested by Philipp *et al.* for the oxidative methane coupling catalysts on CaO and MgO supports [778], by Xu *et al.* [781] for SrO–La₂O₃/CaO catalysts, and also by Kaßner and Baerns [782] for CaO with additional components [783].

The results obtained allow the conclusion that the CO₂ molecule is a convenient probe which is suitable for testing the basic properties of oxide surfaces, differentiating centers of various types and strengths, and evaluation of their concentrations, even in spite of the formation of strongly bound complexes with the surface and the possibility of some surface sites being reconstructed. The spectral parameter $\Delta\nu$, chosen as a measure of the relative strengths of the basic centers, seems to be a reliable characteristic, which provides information on the properties of sites in both individual oxides and in series of oxides. A good correlation has been observed between the site strengths and the spectral features of the derived carbonates. The catalytic activities of oxide catalysts depend on the presence and concentration of the strongest basic sites on the oxide surface.

Estimations of the absolute or relative strengths of the basic centers are of particular interest [646, 772, 783]. In Sinev *et al.* [779], such an estimation was performed by using the heats of CO₂ adsorption. However, the given analysis of the spectral features of the CO₂ interaction with oxide surfaces shows that this approach is inadequate. Indeed, in all cases, interaction with CO₂ involves a pair-site, Mⁿ⁺O²⁻, i.e. the heat of CO₂ adsorption and the type of carbonate to be produced depend on the energy of CO₂ interaction with both Mⁿ⁺ and with O²⁻. The energies of such interactions are obviously different in the case of monodentate and bidentate complexes, as well as in the case of bidentate compounds of different types. At the same time, the basic properties of oxygen are apparently governed by only one component of this interaction, i.e. by the interaction in a CO₂–O²⁻ couple, which cannot be extracted from the average heats of adsorption. One also cannot rule out the possibility of surface rearrangement (movement of cations and anions at the surface) in the course of carbonate formation, which would have an impact on the energetics of the system. Therefore, the use of the heats of CO₂ adsorption as a measure of the strengths of basic sites in oxides is not an available approach.

2.6 Surface defects

There is a sense in which the surface itself with its coordinatively unsaturated atoms is the most numerous type of defect. The bulk of the experimental results, spectroscopic or otherwise, necessarily relate to adsorption on the more numerous and expected sites on oxide surface, such as coordinatively unsaturated cations or anions, hydroxyls, acid–base pairs, etc. We shall describe

these as regular sites. However the most active sites will be connected with defects in the normal surface [36, 108] which have unusual geometrical and/or local chemical compositional features. These may be present in concentrations that are one or two orders of magnitude less than those of the regular sites and their experimental detection can be correspondingly different.

In general, the majority of the experimental phenomena discussed above were connected with adsorption on the more numerous and expected sites on the oxide surface (coordinatively unsaturated cations, anions, hydroxyls, and their pairs). However, the appearance of the most active surface centers suggests a connection with defects in the solid [36]. The other factors influencing the properties of the 'real' oxide surfaces are: (i) the presence of different lattice defects in the surface layer, and (ii) their chemical composition, which in many cases, may differ from that in the bulk.

In spite of the fact that the concentration of the defect centers on the surface is one or even two orders of magnitude less than the concentration of regular active sites, their reactivities are very often higher. This is why such defect centers can participate in the reaction.

The presence of the so-called 'dangling bonds' (unsaturated valencies) at the surface creates electron energy states, usually named *intrinsic* states, which are present even in the case of a pure and strictly stoichiometric surface. Additional structural defects on the surface, which may be or may not be associated with adsorbed impurities, are said to create *extrinsic* surface states [82].

The role of intrinsic defects in the activation of adsorbed molecules has not yet been elucidated. The physics of such defects is also still in development. In contrast, the influence of extrinsic defects on chemisorption and catalysis has been the object of many investigations.

Crystals with perfect periodical arrangements of all of their structural elements cannot exist and real crystals show the presence of various imperfections described as defects [85]. They may be due to (i) the displacement of atoms from the lattice sites normally occupied by those atoms into other sites or interstitial positions, (ii) the presence of some vacant sites, or (iii) the displacement of part of a crystal with respect to another part along a crystal plane, etc. [784]. These defects are usually classified according to their dimensions into point defects (vacancies, interstitial or foreign atoms), linear defects (dislocations), flat or planar defects (shear planes and various internal and external grain boundaries) and spatial defects such as pores of foreign inclusions [82, 85]. For example, besides being a strong base, the highly dehydroxylated MgO surface is a good reducing agent. The reducing sites are apparently defects, possibly surface cation vacancies; the dissociative chemisorption of Brønsted acids blocks the reactivity of the reducing sites.

Investigation of small-surface-area bulk alkali earth-metal oxides, including MgO, e.g. as single crystals, shows that their photoluminescence is caused by defects in the crystalline lattice, namely by the F^+ and F^\bullet centers, i.e. the oxygen vacancies have captured one or two electrons, respectively [506, 785–787]. Such centers can be easily detected directly by EPR and/or by UV–Vis spectroscopic studies of the adsorption of molecules which easily form cation or anion radicals. Detailed analysis of such spectra obtained by using molecules with different but known values of ionization potential (*IP*) or electron affinity, allows us to obtain information about such an adsorption center, for example, on the basis of data on the transition to the radical state, and so to make a conclusion about its redox properties.

The problem of electron transfer and the formation of cation radicals on aluminosilicates and on alumina has been discussed for some 40 years [788]. The observed phenomenon of benzene ionization during its adsorption on the zeolite ZSM-5 has recently caused a rise in interest in this problem because of the high value of the benzene ionization potential. At present, it is well established from UV–Vis spectroscopy that both electron-donating and -accepting sites are observed on alumina and on Al–Si–O systems (see, for example, [789]) and also on other different oxide systems (see, for example, [790]), including zeolites. Such electron-donor properties

of oxides have become the object of increasing interest. Nitrobenzene and related compounds, such as di- and trinitrobenzene, along with some other materials such as tetracyanoethene, all of which exhibit a high electron affinity when adsorbed on an oxide surface and may acquire electrons and convert into negatively charged radicals, the presence of which can be detected by EPR measurements [791, 792].

The main method used to investigate such centers is electron paramagnetic resonance (EPR) spectroscopy. This is why they are not examined in detail in this present book. However, it should be remembered that the formation of radicals can proceed on the surface of practically all oxide systems, when easily ionizable adsorbates which are able to cause the formation of both main- and side-reaction products, are used.

In connection with the problem of defect sites, studies of mechanically activated oxide systems seems to be very interesting and useful. It is well known that mechanical activation (by grinding) effects an increase in the number of defects, including their exposition on the surface. This latter fact can facilitate an investigation of the defects formed upon mechanical activation.

Mechanical treatment is an effective method for creating defects in solids. Various mechanical activation effects are related to the formation of such defects and their subsequent chemical transformations. Some of these defects are free radicals, for example in the case of SiO_2 , i.e. $(=\text{Si}-\text{O}-)_3\text{Si}^\bullet$ and $(=\text{Si}-\text{O}-)_3\text{SiO}^\bullet$ [791, 792]. A new type of natural defect, namely silanone ($\text{Si}=\text{O}$) groups was identified on the surface of mechanically activated SiO_2 . A study was carried out by using their thermal stabilities, optical properties (a characteristic absorption band was found with a maximum at 5.3 eV) and reactivities, relative to simple molecules, such as CO_2 and N_2O , and radicals, such as H, D and CH_3 [792]. Studies of the IR and Raman spectra of the oxides MgO [793], Cr_2O_3 [794, 795], MoO_3 [796], Co_3O_4 and CuO [794, 797] in the regions of the cutoff vibrations allowed identification of sample amorphization during mechanical activation and also the decrease in the coordination number of both cations and anions as compared with nonactivated oxides. The latter leads to increases in the reactivities. According to IR spectra of adsorbed CO in the case of CuO and Co_3O_4 , the reduction of Cu^{2+} to Cu^+ and Co^{3+} to Co^{2+} cations was observed during mechanical activation.

In the diffuse reflectance electron spectroscopy (DRES) spectra of MoO_3 , the valence-to-conduction band transition exhibited a considerable blue shift with decreasing particle size. Excitonic absorptions observed in these spectra are also affected by the smaller particle size and by the altered crystallite surface. An increasing intensity of the bands was observed, and a linear dependence between the position of the band attributed to polaron conductance and the logarithm of the carrier concentration per Mo atom was obtained. Both of these fact revealed that a sub-stoichiometric MoO_{3-x} species was formed upon mechanical treatment. According to the ESR data, both milled and un-milled MoO_3 samples contained Mo^{5+} centers interacting with OH groups in close vicinity, but their concentration was much smaller in the case of un-milled MoO_3 . The main portion of these Mo^{5+} ions had C_{2v} or C_{4v} symmetry. These latter ions appear to result from the mechanical activation process and are suggested to be the precursors of a crystallographic shear structure. Exposure to O_2 reveals that all of these Mo^{5+} sites are located in the bulk and not necessarily on the surface, whereas free electrons are present at the surface. The high surface sensitivity of the IR technique when using adsorbed probe molecules revealed the formation of coordinatively unsaturated Mo^{4+} surface states in MoO_3 which was mechanically activated.

3 STUDY OF CATION STATES BY DRES AND FTIR SPECTROSCOPIES OF THE PROBE MOLECULES

The development of different methods of oxide system preparation, namely ionic exchange, interaction complexes with a support surface, etc., as well as the creation of new systems with fixed locations of active sites (zeolites and heteropoly compounds (HPCs)), including added cations, has enabled UV–Vis and EPR (in the case of paramagnetic ions) [25, 526, 798] spectroscopies to describe the electronic states of cations and even metal clusters in a new manner.

The so-called *coordinatively unsaturated ions* are considered as the active centers of the catalysts containing transition-metal ions in the majority of investigations. The interactions of adsorbed molecules on such ions with the formation of surface complexes can proceed with or without a change in the valence state of the coordinatively unsaturated ions. Complexes of the second type are formed as a rule when the molecules which are adsorbed are typical ligands in homogeneous complexes and have no oxidation–reduction properties. The complexes of the first type, involving a change in the oxidation degree of coordinatively unsaturated ions, are particularly characteristic of oxidant molecules such as O₂, N₂O, SO₂, etc. Electron transfer from the ion to the adsorbed molecule with the formation of radical anions, stabilized in the coordination sphere of the coordinatively unsaturated ions, takes place fairly frequently in such cases.

On the other hand, the use of different probe molecules is widely used at present to study the state of the adsorption centers on the oxide surfaces. Among the known probe molecules, CO and NO have some advantages: (i) it is possible to separate the interaction with only the cation on the basis of spectral information; (ii) the correlations between νCO (NO) in $M^{n+}\text{CO}$ (N) complexes and the electron density on the cation are already established; (iii) the extinction coefficient are large in these cases [30], thus allowing the detection of even a small amount of surface species.

The use of zeolites gives the widest possibility of applying these methods to the study of the cations state, since crystallographic positions, which can be determined by independent methods, determine the state of the cations and all such positions are available for the adsorption. Zeolites are in many ways ideal subjects for diffuse reflectance electron spectroscopy (DRES) measurements: they are white, showing neither near-infrared absorption (when completely dry) nor UV absorption at energies less than about 6 eV, and they scatter radiation strongly and with little wavelength-dependence. The scattering behavior, controlled by the framework, is virtually independent of the absorption behavior, which is a property of the exchanged ion or adsorbed species.

The author does not offer either a detailed description of each system analyzed below, or unambiguous characterization of the states, for example cations, in all these systems. Some systems such as, for example, ZSM-containing zeolite, are not analyzed at all in this chapter. The main goal of this chapter is to show the principles and methodology used by the author, and to illustrate the results that can be obtained by to the use of these principles.

3.1 Copper-containing systems

3.1.1 ZEOLITES

First, the known information about the electronic states of the Cu^{2+} ion in different crystal fields should be mentioned. The action of divalent copper results from a $3d^9$ electronic configuration. It is known from crystal field theory [7, 526, 798–800] that the fivefold degenerated 2D term is split in an octahedral ligand field: ${}^2D \rightarrow {}^2T_{2g} + {}^2E_g$ (Figure 3.1). The energy difference between the ${}^2T_{2g}$ and 2E_g levels (and hence the position of the absorption band maximum corresponding to the ${}^2E_g \rightarrow {}^2T_{2g}$ transition) is determined by the place of the ligands in the spectrochemical series [799]. However, the maximum symmetry configuration of this system with a twofold degenerate ground state is unstable and exhibits the Jahn–Teller effect. This causes a splitting of both the ground and excited states (Figure 3.1), as well as a corresponding splitting of the electronic absorption band. In the case of pure tetragonal symmetry, such splitting is more pronounced. The magnitude of the band splitting [800], $\Delta E = {}^2E_g - {}^2B_{2g}$ and the ratio ν_1/ν_2 ($\nu_1 = {}^2E_g - {}^2B_{1g}$; $\nu_2 = {}^2B_{2g} - {}^2B_{1g}$) characterize the extent of tetragonal distortion of the complex in the absence of rhombic distortions. At the same time, the condition of the ‘preserved center of gravity’ must be fulfilled [7, 799, 800]. Investigation of the structures of adducts formed

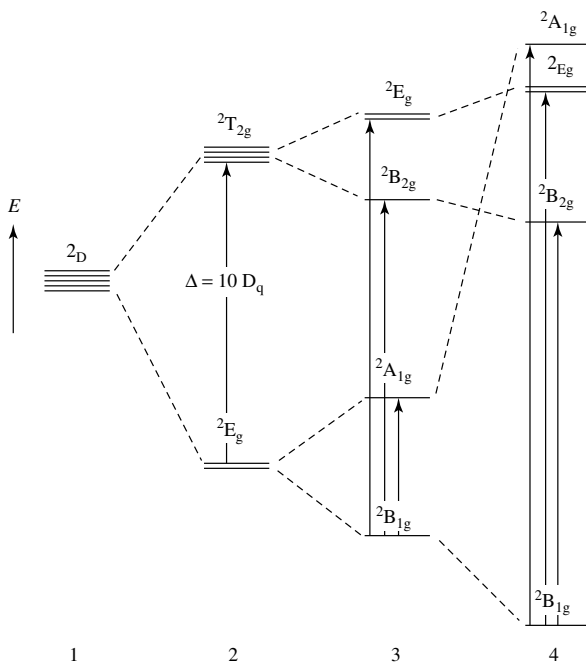


Figure 3.1. Splitting of the 2D term of Cu^{2+} ion in fields of ligands of different symmetry: 1, spherical field; 2, octahedral field (O_h); 3, axially extended octahedron; 4, square planar (D_{4h}).

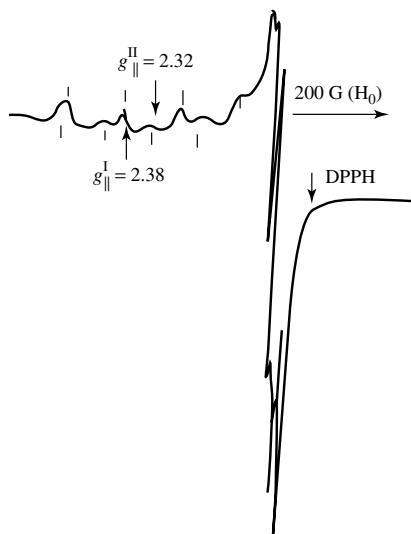


Figure 3.2. The ESR spectrum (at 77 K) of dehydrated Y-zeolite containing 0.8 % copper. Two types of Cu^{2+} ions can be observed.

by different copper complexes with bases [800] showed that the transition from a square planar environment to an octahedral one causes an increase in g_{\parallel} and a corresponding decrease in A_{\parallel} in the ESR spectra. For configurations approaching an octahedral form, the Jahn–Teller effect manifests itself, and the shape of the ESR spectrum depends on the measurement temperatures.

The ion-exchange conditions (pH, temperature, etc.) not only have an appreciable effect on the state and distribution of Cu^{2+} ions in the initial CuY-zeolites, but they also determine, to a large extent the state of copper cations during subsequent thermal treatment.

ESR spectra

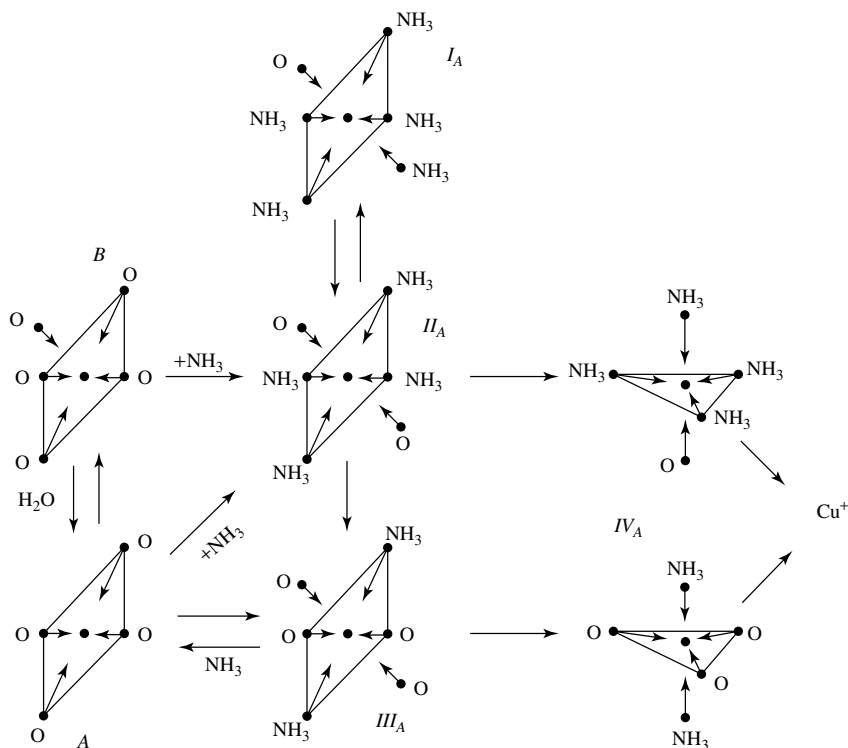
All of the results presented below of investigations of the ESR-spectra of CuY-zeolites relate to samples pre-heated under an oxygen atmosphere, so the main proportion of copper ions observed are isolated Cu^{2+} cations.

Figure 3.2 shows the ESR spectrum of a Y-zeolite sample low in copper, which was dehydrated by vacuum treatment. Two types of Cu^{2+} ions (I and II) are observed (Figure 2.2, Table 3.1). Analysis of these parameters for type I ions shows that these ions have a five-coordinated environment of oxygen anions while type II ions represent an environment approaching square planar, that is, the transition $\text{I} \leftrightarrow \text{II}$ is due to the additional coordination of the Cu^{2+} ion by water molecule along the fourfold axis.

After adsorption of ammonia onto the CuY-zeolite, at least four types (I_A , II_A , III_A and IV_A) of Cu^{2+} ions can be found [526] (Table 3.1). The ESR parameters show that type I_A ions correspond to penta-ammoniates, while the coordination spheres of type II_A and type III_A ions have four and two ammonia molecules, respectively, i.e., during the adsorption of ammonia on the hydrated samples there is complete replacement of the oxygen anions in the coordination sphere of the Cu^{2+} ion by the ammonia molecules. The ESR spectrum of type IV_A ions results from the Cu^{2+} ions having a d_{z^2} ground orbital of the unpaired electron. The mutual transitions and the coordination states of Cu^{2+} ions in the zeolites in terms of the above considerations are presented in Figure 3.3. The adsorption of pyridine, like that of ammonia, produces pyridinates. The adsorption of CO does not appreciably change the ESR parameters of the type I and II Cu^{2+} ions.

Table 3.1. ESR parameters of Cu^{2+} ions in the Y-zeolites.

Ion type	g_{\parallel}	g_{\perp}	A_{\parallel}	A_{\perp}
I	$2.38(2) \pm 0.004$	$2.07(5) \pm 0.004$	138	15
II	$2.32(6) \pm 0.004$	$2.05(5) \pm 0.004$	171	26
III	$2.39(3) \pm 0.005$	$2.07(8) \pm 0.004$	136	15^a
IV	$g_0 = 2.180 \pm 0.005^b$			
	$g_0 = 2.160 \pm 0.005$			
I_A	$2.25(0) \pm 0.004$	$2.04(0) \pm 0.004$	185	—
II_A	$2.34(4) \pm 0.004$	$2.04(3) \pm 0.004$	193	—
III_A	$2.27(5) \pm 0.004$	$2.05(0) \pm 0.004$	180	—
IV_A	2.00	2.20 ± 0.004	130	20

^aAt 77 K.^bAt 300 K.**Figure 3.3.** Scheme of the states and mutual transformations of Cu^{2+} ions in the Y-zeolites during the adsorption and desorption of ammonia.

For copper contents of more than 1.5 wt%, the increase in the ESR spectral intensity occurs in the symmetrical line, whereas the signal of the axial ions remains approximately constant. In this case, the symmetrical signal is due to dynamic rearrangements in the nearest environment of type II Cu^{2+} ions, since at lower temperatures axial Cu^{2+} ions have parameters approaching those of type I Cu^{2+} ions (see Table 3.1). The occurrence of the dynamic effect for type III ions, and its absence in this case of type I ions, indicates that type I ions are more strongly bound to the zeolite framework. The main reason for the appearance of type III ions may be as follows. Initially, sites

of the highest adsorption energy are occupied; these are sites produced after strong decationization. With further increases of the copper content, the Cu^+ ions occupy energetically less advantageous sites. This is possible due to both the initial stabilization of Cu^{2+} ions at S_I , and then at S_{II} , S_{III} sites and others (Figure 2.2), and the nonequivalency of the sites because of the nonuniform distribution of Al^{3+} ions in the zeolite lattice. In the latter case, regions with an increased local concentration of aluminum ions appear. For example, the Al^{3+} ions can occupy the nearest sites in a six-membered ring to form an oxygen vacancy (charge compensation is not required). If the Al^{3+} ions are separated by one cation, the charge in this site can be completely compensated for by the Cu^{2+} ion. Finally, the Al^{3+} ions stabilize at the opposite sites of the six-membered ring where the charge compensation by the Cu^{2+} ion is hindered because of the localization of the negative charge on the opposite ends of the oxygen ring. Thus, the Cu^{2+} ions in the Y-zeolites stabilize first in the sites, which ensure more complete compensation of the zeolite lattice charge.

If the local concentration of the introduced copper is higher than that required for the compensation of the negative lattice charge, the Cu^{2+} ions will tend to be reduced to Cu^+ . This is confirmed by a sharp decrease in the intensity of the ESR signal from Cu^{2+} ions. The stability of Cu^+ ions in the Y-zeolites is ensured by the presence of 'natural' sites in the zeolite lattice available for the charge compensation by single valence cations, whereas Cu^{2+} ions require additional coordinate groups. It is, therefore, not surprising that the Cu^{2+} ions in the Y-zeolites are rather easily reduced by hydrogen or ammonia.

The distribution and the nature of magnetic interactions of Cu^{2+} ions in the Y-zeolites

The ESR technique is a convenient means for studying the distribution of the paramagnetic ions, since the number of paramagnetic interactions between ions, which depends on the distance between the paramagnetic particles, determines to a large extent the shape of the ESR spectra. Accordingly, the states of the paramagnetic ions can be classified as follows: clusters or strong associates (A), representing groups of the paramagnetic cations, which share bridging anions and are separated by a distance of $\leq 4 \text{ \AA}$, weak associates, which represent groups of paramagnetic cations sharing no cations and separated by a distance of $\geq 5 \text{ \AA}$, and isolated (I) paramagnetic cations.

Clusters formed by paramagnetic ions are characterized by a broad ESR line due to considerable exchange interactions, and (the ESR spectra of the clusters) are generally not observed. In addition to dipole-dipole interactions, the weakly associated copper ions may exhibit exchange interactions, $J \leq g\beta H$. In this case, in the presence of paramagnetic ions with $S = \frac{1}{2}$ and a magnetically nonequivalent axis, the ESR spectrum represents a symmetrical line whose width decreases as the exchange interaction or the number of exchange-bound ions increases. In the hydrated Y-zeolites, there is a broadening of the ESR spectra with increases in the copper content. This broadening is mainly due to the dipole-dipole interaction (Figure 3.4). After dehydration, in addition to the spectrum of the isolated Cu^{2+} ions, a line approaching an asymmetrical shape is observed whose width reduces with the increase in copper content (Figure 3.5, spectrum (d)). This line is due to the Cu^{2+} ions which form weak associates in the Y-zeolites. The increased number of the exchange-bound Cu^{2+} ions in the associates leads to the narrowing of the ESR signal. In the hydrated samples, no exchange interactions take place. It can, therefore, be concluded that the exchange interactions in the dehydrated samples involve the zeolite lattice since, as has been shown earlier, during dehydration the Cu^{2+} ions are mostly 'strongly' bound to the zeolite framework. This conclusion is also confirmed by the fact that ammonia adsorption on the dehydrated CuY-zeolites decreases the exchange interactions between the Cu^{2+} ions. After the adsorption of ammonia on partially dehydrated samples, the anisotropic spectrum changes to a symmetrical line (Figure 3.5, spectra(a) and (b)), indicating the appearance of exchange interactions between the Cu^{2+} ions. These exchange interactions do not involve the zeolite lattice. This

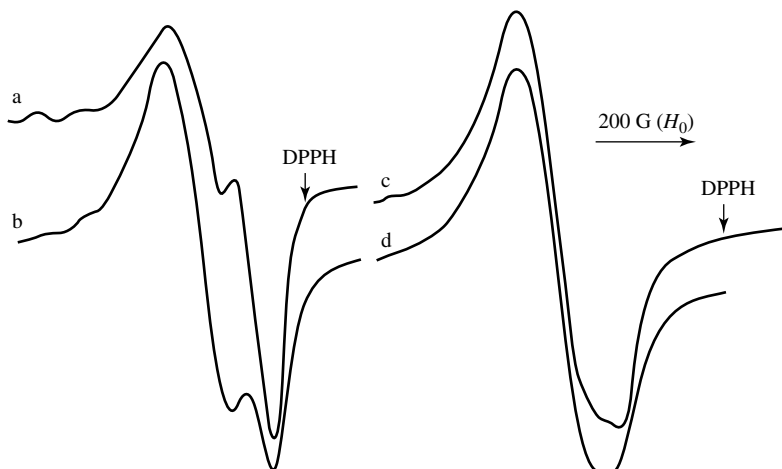


Figure 3.4. ESR spectra of hydrated Y-zeolites containing different copper contents: a, 1.5; b, 4.9; c, 7.2; d, 9 wt% copper. Superposition of the symmetrical and axial lines is observed.

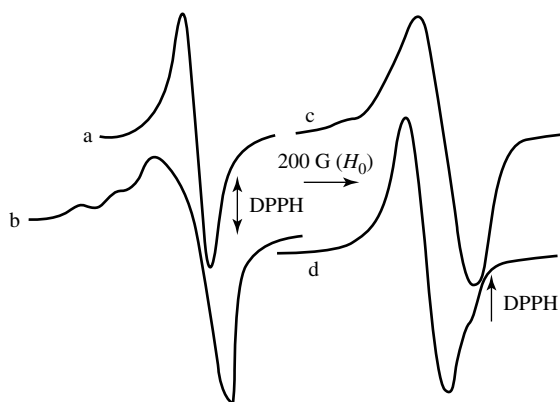
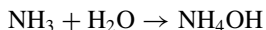


Figure 3.5. ESR spectra of Y-zeolites (measurement temperature, 77 K) containing 9 wt% Cu: a, after adsorption of ammonia on the sample (c); b, after adsorption of ammonia at 293 K on sample (d); c, preliminarily dehydrated at 373 K; d, preliminarily dehydrated at 673 K.

suggests that the ammonia and water in the zeolite form their own structures in which the anions of oxygen and nitrogen are chemically bound by protons according to the following scheme:



The adsorption of CO at low temperatures leads to partial broadening of the ESR signals of the weak associates, indicating the adsorption of CO molecules on the Cu^{2+} cations [801]. Thus, for the first time, the formation of complexes of Cu^{2+} cations with CO was observed. Interaction of copper ions with CO at high temperatures (above 573 K) leads to the reduction of Cu^{2+} to Cu^+ ions, and to a fall in the intensity of the ESR signal.

The above results was summarized as follows. The Cu^{2+} ions in the Y-zeolite stabilize as clusters or isolated ions depending on the exchange conditions. The adsorption of water or

ammonia gives rise to complexes of Cu^{2+} ions with adsorbed molecules. The most complete 'detachment' of the Cu^{2+} ions from the zeolite lattice occurs in the presence of additional cations capable of compensating for the negative charge of the anionic framework. It was shown that different sites are available for the compensation of the zeolite lattice charge by the Cu^{2+} ions. The latter occupy first the sites with the excess charge of the zeolite framework. The additional coordination of the Cu^{2+} ions during the adsorption of the coordinating molecules reduces the exchange interactions between the ions and the zeolite framework. Therefore, the Cu^{2+} ions will be more weakly bound to the zeolite lattice. An anomalous increase of the exchange interactions in an aqueous ammonia medium was also found.

Below, the samples containing copper ions as isolated ions or weak magnetic associates will be referred to as CuY-I zeolites, and those containing mainly strong associate clusters as CuY-A zeolites. The same is true for the NiY-zeolites (see below).

Spectra from d-d transitions

The electronic spectra of the hydrated CuY-I zeolites with low copper contents (0.2–1.5 wt%) show a broad absorption band with the maximum at 12 000 (ν_1) and a shoulder at 9000 (ν_2) cm^{-1} (Figure 3.6, spectrum 1). As the copper concentration in the zeolite increases, the absorption band and its low-frequency shoulder are shifted to shorter wavelengths. For samples with high copper contents (about 7 to 9 wt%), bands at 12 500 (ν_1) and 9800 (ν_2) cm^{-1} are observed (Figure 3.6, spectrum 3). It turns out that the intensity of the absorption band at 12 000 to 12 500 cm^{-1} , recalculated by using the Kubelka–Munk formula, is directly proportional to the copper content in the zeolite (Figure 3.7). This indicates that the extinction coefficients of type I and type III

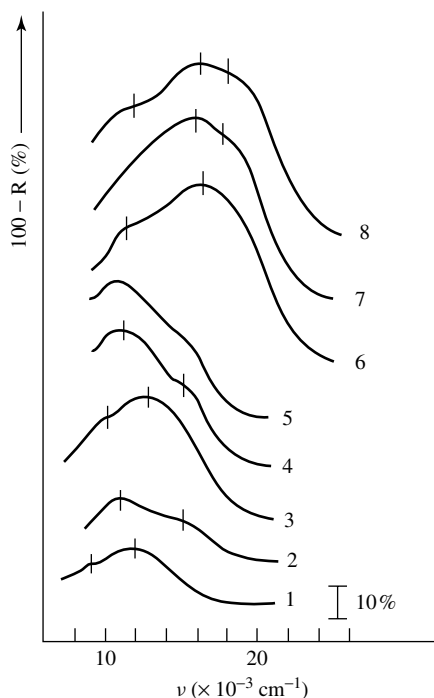


Figure 3.6. Electronic spectra of CuY-I zeolites containing 1.5 wt% copper (1, 2) and 7.2 wt% Cu (3–8); plus hydrated zeolites (2, 4) with subsequent adsorption of ammonia (7) and pyridine (8).

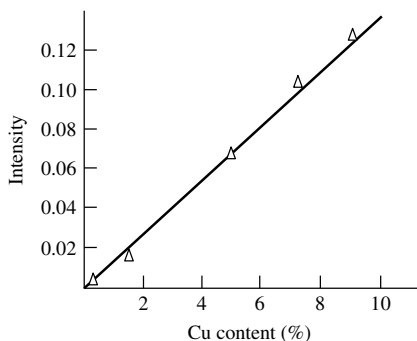


Figure 3.7. The intensity of the absorption band $\sim 12\,000\text{ cm}^{-1}$ in the spectra of the hydrated CuY-I zeolites as a function of the copper content.

ions observed by ESR spectroscopy are close to each other. This also indicates that the symmetry of the copper environment does not change with the variation of copper concentration. This conclusion is supported by the ESR data which shows that the extent of the ‘nonideal’ nature of the octahedral environment of type I and type III ions is small.

The spectra of the hydrated zeolites with high copper contents are identical to those of the hexaaqua complexes of copper [800]. The value of the splitting, ΔE , is equal to 2700 cm^{-1} , while the ratio $\nu_1/\nu_2 = 1.28$. This corresponds to the calculated and experimental values for a tetragonally distorted $\text{Cu}(\text{H}_2\text{O})_6^{2+}$ complex [800]. The condition of the preservation of the ‘gravity center’ of the levels permits us to calculate the value of the center of gravity, i.e. $11\,600\text{ cm}^{-1}$, which also corresponds to that observed for aqueous solutions of the salts of divalent copper [526, 799]. The $12\,500$ and 9800 cm^{-1} bands are due to the ${}^2\text{B}_{1g} \rightarrow {}^2\text{E}_g$ and ${}^2\text{B}_{1g} \rightarrow {}^2\text{B}_{2g}$ transitions, respectively. It can, therefore, be concluded that at higher degrees of ion exchange, the major part of the ions are stabilized as hexaaqua complexes $\text{Cu}(\text{H}_2\text{O})_6^{2+}$ located in the large cages of the zeolite (type III ions).

The spectra of the hydrated zeolites with low copper contents in which copper is present as isolated Cu^{2+} ions [526] differ from those of $\text{Cu}(\text{H}_2\text{O})_6^{2+}$ complexes, i.e. the absorption band and its long-wavelength shoulder are somewhat shifted toward lower frequencies. These spectra are characterized by a greater value of splitting, ΔE (3000 cm^{-1}), and by a greater ν_1/ν_2 ratio (1.34). This indicates that the tetragonal distortion of the octahedral coordination of type I ions is greater than that of the type III ions, which is also supported by the ESR data. The ‘gravity center’ of the electronic levels in such complexes with axial distortion lies at lower frequencies ($11\,000\text{ cm}^{-1}$) than in the $\text{Cu}(\text{H}_2\text{O})_6^{2+}$ complexes. An explanation of this fact may be found in the decreased splitting parameter, of 10 Dq . The simultaneous decrease of the splitting parameters with the increase of the axial distortion may be related to the formation of a complex in which the ligands are oxygen ions from the zeolite framework or structural hydroxyl groups, which coordinate the Cu^{2+} ion in an equatorial but not an axial position. This would create a nonuniform crystal field and restrict the mobility of the Cu^{2+} ions, thus causing the anisotropy of the g -factor. The assumption that type I ions in the zeolites have the framework oxygen or the hydroxyl groups in their coordination spheres is also supported by the similarity of the ESR parameters of these ions (see Table 3.1) to the parameters of type I ions in solution. The latter are observed in air-dried samples of a copper–magnesium oxide catalyst [802], whose copper ions are surrounded by ligands containing oxygen and hydroxyl groups creating a field with axial symmetry.

The electronic spectra of the dehydrated CuNaY zeolites show an absorption band with the maximum at $11\,000$ and the shoulder at $15\,000\text{ cm}^{-1}$ (see Figure 3.6), irrespective of the zeolite

composition. The change in the spectra after dehydration is due to the decomposition of hexaqua complexes and the stabilization of Cu^{2+} cations in the zeolite framework in the sites with strong tetragonal distortion. The bands at 11 000 and 15 000 cm^{-1} result from ${}^2\text{B}_{1g} \rightarrow {}^2\text{B}_{2g}$ and ${}^2\text{B}_{2g} \rightarrow {}^2\text{E}_g$ transitions, respectively (see Figure 3.1). Using the known formula [799], the observed energies of the electronic transitions can be compared with the g -factors of type II and type IV ions which are formed from type I and III ions during the zeolite dehydration. The calculations give $r_{\text{I}}^2 = \alpha^2 \times \beta^2 = 0.52$, and $r_{\text{II}}^2 = \alpha^2 \times \beta^2 = 0.54$ and, when estimated from the ESR spectra, the degree of covalence $\alpha^2 = 0.83$. It is characteristic that both the ESR spectra of the copper ions in the dehydrated zeolites are identical to those of type IV ions observed in the copper–magnesium oxide catalysts [802]. This indicates that on the surface of oxide catalysts the copper ions are stabilized in the same manner.

The electronic spectra of the hydrated samples show a difference between type I and type III ions, but it was impossible to establish the difference in the electronic spectra of dehydrated zeolite samples with high and low copper contents (see Figure 3.6, spectra 2 and 4). Type II and IV ions are similar to each other, both in their ESR and in their electronic spectra. Changes in the spectra during dehydration, due to the transition from type I to type II ions, support the conclusion that the Cu^{2+} cations are coordinated by the zeolite framework oxygen in an equatorial position. In fact, upon dehydration the absorption bands for these cations (9000 and 12 000 cm^{-1}) are shifted toward higher frequencies (11 000 and 15 000 cm^{-1} , respectively), the splitting, ΔE , increases to 4000 cm^{-1} , and the ν_1/ν_2 ratio increases to 1.37. These observations suggests that dehydration is accompanied by the removal of water molecules coordinated to type I ions in the axial position. This results in a stronger bonding of Cu^{2+} ions with the equatorial ligands and a simultaneous increase of the axial distortion of the complex.

The Cu^{2+} cations stabilized in the zeolite framework during dehydration are to a large extent coordinatively unsaturated and hence they are capable of coordinating the donor molecule. This is supported by the results obtained for the adsorption of water, ammonia and pyridine on the zeolites investigated. The adsorption of water onto the dehydrated samples gives rise to spectra characteristic of the hydrated zeolites, the spectra of the zeolites containing isolated Cu^{2+} ions have the absorption band at 12 000 cm^{-1} , and the spectra of the zeolites containing weak associates show the absorption band at 12 500 cm^{-1} .

It is known that in aqueous solutions, ammonia molecules very easily replace water molecules in the coordination sphere of Cu^{2+} cations to form ammoniates [800]. Such species are also formed during the adsorption of NH_3 on CuNaY -zeolites, but this adsorption leads to somewhat different results for the hydrated and dehydrated zeolites. In an ammonia atmosphere, the zeolites very rapidly become an intensive blue color. Their electronic spectra exhibit intense absorption bands with maxima at 16 000 cm^{-1} and shoulders at 11 000 cm^{-1} (see Figure 3.6, spectrum 6). The increase in the energy of the d – d transitions is due to the entry of ammonia into the coordination sphere of the copper ions in the CuNaY -zeolites. According to its position in the spectrochemical series [800], ammonia produces a stronger ligand field than water. The relative positions of the absorption bands in the electronic spectra are identical with those of $\text{Cu}(\text{NH}_3)_5^{2+}$ as to position, shape and intensity of the absorption band [800].

Since the ion exchange for the CuY -I zeolites was carried out in ammonia solutions, heating the samples at different stages of their preparation causes successive changes of the pentaammoniates to tetra-, tri- and diammoniates. It was of interest to study the electronic spectra of these transitions. After heating the CuNaY -zeolite samples with the adsorbed ammonia in air at 320 K, the maximum of the absorption band shifted to 16 500 cm^{-1} . This indicates that at least a portion of the pentaammoniates are converted to tetraammoniates [800, 803] since the low-frequency shoulder is still preserved. On raising the temperature to 350 K, the absorption band shifts to 15 700 cm^{-1} and the low-frequency shoulder disappears. Heating the zeolite at

393 K shifts the absorption band maximum to $15\,400\text{ cm}^{-1}$, and the shoulder at $17\,000\text{ cm}^{-1}$ appears. These spectral changes are related to the decomposition of pentaammoniates (bands at $11\,000$ and $16\,000\text{ cm}^{-1}$) and the formation of tetraammoniates (bands in the region from $16\,500$ to $17\,000\text{ cm}^{-1}$). The latter then change to $\text{Cu}(\text{NH}_3)_3^{2+}$ upon detachment of an NH_3 molecule (band at $15\,500\text{ cm}^{-1}$). As the temperature is increased further to 423 K, the absorption band shifts to $13\,000\text{ cm}^{-1}$, due to the formation of a complex with one ammonia molecule in the coordination sphere of the Cu^{2+} ion, i.e. $\text{Cu}(\text{H}_2\text{O})_5(\text{NH}_3)^{2+}$. This may be complex with a d_z^2 ground orbital [526].

The adsorption of ammonia on the dehydrated zeolites is also accompanied by a shift of the absorption bands of the d–d transition to higher frequencies. However, the maximum of the observed absorption band lies at longer wavelengths ($15\,200\text{ cm}^{-1}$) compared with the spectra of hydrated zeolites (see Figure 3.6, spectrum 7). It appears that in this case complexes with two to three ammonia molecules are mainly formed [800, 803]. The shoulder at $17\,000\text{ cm}^{-1}$ (see Figure 3.6, spectrum 7) suggests the formation of $(\text{Cu}(\text{NH}_3)_4)^{2+}$ [803]. The Cu^{2+} cations in those sites with tetragonal coordination are capable of coordinating such a strong ligand as ammonia to the fifth and sixth sites. This leads to a weakening of the bonding with less strong equatorial ligands and to the possibility of replacing some of them by ammonia molecules. However, the spectra obtained show dehydration produces complexes with a smaller number of ammonia molecules, unlike the hydrated zeolites. This follows from the ‘rigid’ stabilization of copper as exchanged cations in the zeolite framework.

The desorption of ammonia at 373 K causes a shift of the absorption band maximum to $14\,000\text{ cm}^{-1}$ and the disappearance of the high-frequency shoulder. It appears that under these conditions mono- and diammoniates are formed which can be detected by ESR spectroscopy. Evacuation of the zeolite at 573 K leads to a strong decrease in the intensity of the absorption band, which is shifted to $11\,000\text{ cm}^{-1}$ with a shoulder at $15\,000\text{ cm}^{-1}$. These spectra differ from those of the dehydrated zeolites by a considerably decreased intensity of the absorption band, which may be due to the reduction of some Cu^{2+} ion to Cu^+ ions during the desorption of ammonia. The adsorption of pyridine on the dehydrated zeolites is similar to the adsorption of ammonia as pyridine lies near ammonia in the spectrochemical series [800]. Therefore, the spectra of the corresponding ammoniates and pyridinates are similar [800]. After the adsorption of pyridine, the spectra of the zeolites containing copper have absorption band maxima at $15\,400\text{ cm}^{-1}$ and shoulders at $17\,200$ and $11\,200\text{ cm}^{-1}$ (see Figure 3.6, spectrum 8). These spectra indicate that, as in the case of ammonia, complexes are formed with two (band at $15\,400\text{ cm}^{-1}$) and four (band at $10\,200\text{ cm}^{-1}$) pyridine molecules in the coordination sphere of the Cu^{2+} cations. The absorption band at $11\,200\text{ cm}^{-1}$ may result either from the low-frequency d–d transitions in the pyridine copper complexes, or it may belong to the isolated Cu^{2+} cations, localized in small cages of the zeolite, which are not coordinated by pyridine molecules because of steric hindrance. The second explanation appears more likely. The desorption of pyridine leads to complete disappearance of the absorption in the near-infrared region as a result of the reduction of Cu^{2+} cations. After keeping the samples in air for several days, the absorption band at $12\,500\text{ cm}^{-1}$ reappears.

The adsorption of CO at room temperature produces no visible changes in the absorption spectra (see Figure 3.6, spectrum 5) or in the ESR spectra [801]. This is due to the very small electron-donating power of the CO molecule and to the specific ability of Cu^{2+} ions to coordinate weakly with axial ligands. Therefore, under these conditions complexes are not formed, but the copper ions in weak associates interact with CO at room temperature.

Charge-transfer bands

In addition to the absorption bands of the d–d transitions, the electronic spectra of the ‘I’ (isolated-cation) zeolites show intense absorption bands in the ultraviolet region. These bands are due to

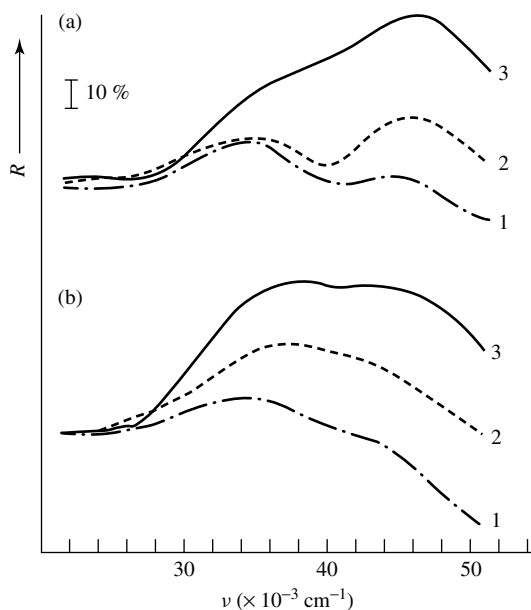


Figure 3.8. Charge-transfer spectra for (a) hydrated and (b) dehydrated CuY-I zeolites containing (1) 0.2, (2) 1.0 and (3) 3.0 wt% copper.

the charge transfer from the molecular orbital of the Cu^{2+} cation [800]. It is clear that the position of such absorption bands should be changed with replacement of the ligands. The low-frequency shift of the charge-transfer band (CTB) from the ligand to the metal is a characteristic indication of an increase in the degree of covalence of the ligand–metal bond, as well as of an increase in the oxidative nature of the metallic ion or in the reducing nature of the ligand.

In the spectra of the hydrated CuY-I zeolites, the CTBs have maxima at 35 000 and 45 500 cm^{-1} (Figure 3.8(a)). The intensity of the high-frequency absorption band increases as the copper content in the zeolite increases. This permits us to assign this band to the CTB of type III ions, the amount of which also increase. The position of this band is similar to the CTB in the spectrum of the hexaaqua complex $\text{Cu}(\text{H}_2\text{O})_6^{2+}$ (48 000 cm^{-1}). Therefore, there is no doubt that the nature of the complexes formed by type III ions is similar to that of $\text{Cu}(\text{H}_2\text{O})_6^{2+}$. This is shown by all of the experimental data obtained from the electronic spectra (d–d transitions and CTBs) and from the ESR spectra. The water molecule as a ligand lies at the very beginning of the nephelauxetic series [800]. This determines the ionic nature of the bonds which are formed between water and transition metal ions in the complexes. Therefore, the charge transfer energies are high.

The second absorption band (35 000 cm^{-1}) is due to the charge transfer in the complexes formed by type I ions. Low charge transfer energies indicate that these complexes are not equivalent to the $\text{Cu}(\text{H}_2\text{O})_6^{2+}$ ions. Therefore, Bersuker and Ablov [800] have proposed that the main equatorial ligands in type I copper ions are the oxygen anions of the zeolite framework, and the water molecule only coordinate the cations in the axial position, thus making the coordination octahedral. These are readily removed upon dehydration. Reflecting the charge in the nature of the ligands, the low-frequency CTB may be due to the more covalent nature of the bonds between the Cu^{2+} ion and O^{2-} as compared with H_2O .

During hydration of the zeolite, the ligands in the complexes formed by type I ions are not replaced. It is therefore expected that the positions of the corresponding CTBs in the complexes

formed by type III cations should undergo considerable low-frequency shifts during dehydration because of the change of the ligands (the water molecules are replaced by structural hydroxyl groups or oxygen anions from the zeolite lattice). In fact, the position of the low-frequency CTB at $25\,000\text{ cm}^{-1}$ remains unaffected during dehydration of the zeolites (see Figure 3.8(b), spectrum 1). An increase of the degree of tetragonal distortion of the corresponding complexes is detected from the d–d transitions (see Figure 3.6). During dehydration, a low-frequency shift of the second absorption band is observed (see Figure 3.8(b), spectra 2 and 3). This may be explained by the change of the ligands during the stabilization of the Cu^{2+} ions in the zeolite framework and by the increase of the degree of covalence of the metal–ligand bonds. The spectra of the d–d transitions (see Figure 3.6) and the CTBs (see Figure 3.8), plus the ESR spectral data (See Table 3.1) indicate the similarity of type II and IV ions in the dehydrated zeolites. Type IV ions, however, form weak magnetic associates, which are nonuniform [526] and differ both in the type and number of their Cu^{2+} cations. Therefore, the corresponding CTB is observed over a wide frequency range – $36\,000$ to $38\,000\text{ cm}^{-1}$. In spite of this, the tendency of the shift of the CTB toward lower frequencies during zeolite dehydration reflects the general regularity of the change of the ligand environment. Thus, the isolated Cu^{2+} ions, those weakly interacting and those coordinated by oxygen, can be detected from the CTB at $35\,000\text{ cm}^{-1}$. Different authors have observed a similar value of the energy of the charge transfer $\text{O}^{2-} \rightarrow \text{Cu}^{2+}_{\text{isol}}$ ($36\,000\text{ cm}^{-1}$) for the system CuO-MgO [526, 802]. This is additional evidence that the copper ions are stabilized in the same manner on the surfaces of oxide catalysts. These facts illustrate the ability of the CTB to identify the ligands surrounding the Cu^{2+} ions. It should be noted that sometimes the spectra of the dehydrated CuY-I zeolites show an absorption at $27\,000\text{ cm}^{-1}$ whose intensity is small (Figure 3.9). The nature of this absorption will be discussed later.

In addition to the isolated (Type II) and weakly associated (type IV) Cu^{2+} cations, the CuY-A zeolites contain strong magnetic associates. This causes some peculiar features in the electronic spectra of these zeolites. The spectra of the initial hydrated zeolites are characterized by the absorption band at $14\,000$ and by the shoulder at $12\,000\text{ cm}^{-1}$, as well as by the intense absorption in the near-ultraviolet ($33\,000$ to $34\,000\text{ cm}^{-1}$) (Figure 3.10, spectrum 2). These spectra approach the spectrum of copper hydroxide [526] but differ from it by lower frequencies of the d–d transitions and higher energies of the high-frequency CTBs. According to the results obtained, the coordination sphere of Cu^{2+} cations in such zeolites contains NH_3 molecules, but the intensity of the signal in the ESR spectra of these zeolites is at a minimum because of the broadening of this

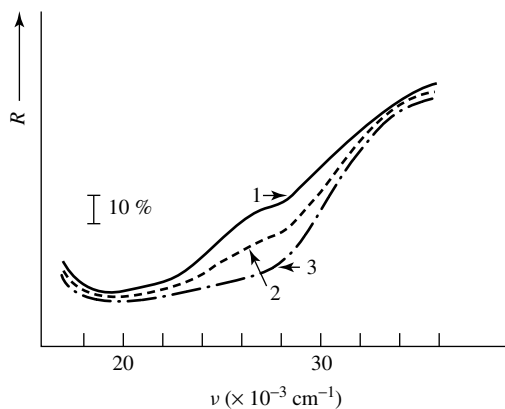


Figure 3.9. Changes in the charge-transfer spectra at $27\,000\text{ cm}^{-1}$ for CuY-I zeolites (5 wt% Cu) with the temperature of dehydration: 1, 473 K; 2, 673 K; 3, 873 K.

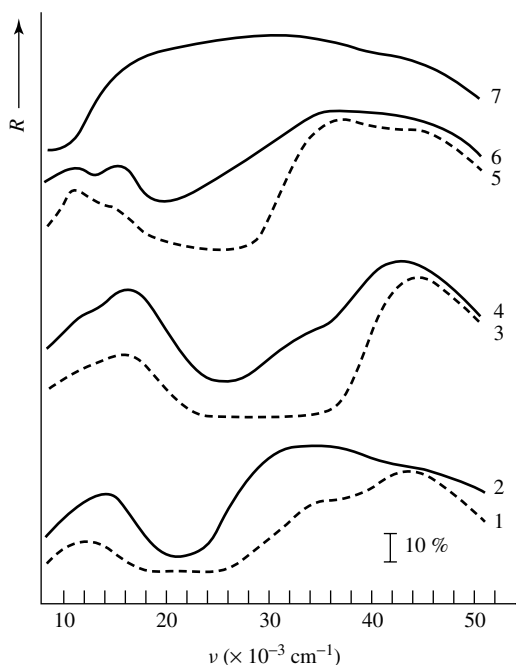


Figure 3.10. The electronic spectra of (1,2,3) CuY-I zeolites, and (2,4,6) CuY-A zeolites: (1,2), the spectra of initial hydrated zeolites, with (3,4) subsequent adsorption of ammonia, and (5,6) of dehydrated zeolites; (7), the spectrum of dehydrated zeolite containing a finely dispersed CuO phase (3.7 % Cu).

signal. It can be assumed that under these conditions of ion exchange the copper in the zeolites is present as hydroxoamino complexes, as a result of the hydrolysis of the initial salt, and that there are exchange interactions between the Cu^{2+} ions of these complexes. Such complexes are characterized by relatively low charge-transfer energies as compared with $\text{Cu}(\text{H}_2\text{O})_6^{2+}$, which are, however, higher than in pure $\text{Cu}(\text{OH})_2$ [526] because the formation of hydroxoamino complexes at this stage is a reversible process. The adsorption of ammonia on the initial hydrated CuY-A zeolites leads to an intense absorption band in the electronic spectra with a maximum at $16\,000\text{ cm}^{-1}$ and a shoulder at $11\,000\text{ cm}^{-1}$. At the same time, the CTB is shifted to shorter wavelengths, up to $43\,000\text{ cm}^{-1}$ (see Figure 3.10, spectrum 4). The adsorption of NH_3 on the hydrated CuY-I zeolites produces the same spectra (see Figure 3.10, spectrum 3). These are identical to the spectra of the pentaammoniates $\text{Cu}(\text{NH}_3)_5^{2+}$ [803]. It follows that the entry of ammonia into the coordination sphere of Cu^{2+} ions makes the CuY-A zeolites closely similar to the CuY-I zeolites, that is, this entry is accompanied by ‘disintegration’ of the hydroxoamino complexes, resulting eventually in the stabilization of copper as isolated ions.

The spectra of dehydrated CuY-A zeolites show absorption bands at $11\,000$ and $15\,800\text{ cm}^{-1}$, plus absorptions at $27\,000$ and $36\,000\text{ cm}^{-1}$ (see Figure 3.10, spectrum 6). The spectra of dehydrated CuY-I zeolites show no absorption band at $15\,800\text{ cm}^{-1}$ (see Figure 3.10, spectrum 5). Apart from this high-frequency band of the d-d transitions, the spectra of the dehydrated CuY-A zeolites differ from the spectra of the CuY-I zeolites by an intense absorption at $27\,000\text{ cm}^{-1}$. The second $15\,000\text{ cm}^{-1}$ band of these cations is distinct because of the more intense band at $15\,800\text{ cm}^{-1}$. The $15\,000\text{ cm}^{-1}$ band, as well as the absorption at $27\,000\text{ cm}^{-1}$, are probably due to strong associates not observable by ESR spectroscopy.

It has been proposed [526, 802] that strong associates in the zeolites exist as two-dimensional species involving $\text{Cu}^{2+}-\text{O}-\text{Cu}^{2+}$ bridges whose oxygen does not belong to the zeolite framework. It would be expected that the spectra of such strong associates would exhibit properties different from isolated ions. First, the high-frequency shift of the absorption band on passing from isolated ions to strong associates may be due to the polarizing action of the cation in the outer sphere. The isolated ions naturally have no such cations. The same is true for the hydrated zeolites. The second reason for the high-frequency shift of the d-d transitions is the formation of a strong covalent bond, Cu-O, in such associates. The covalence of the bonding in strong associates will be discussed below. The third, and main, reason for the high-frequency shift of the d-d transitions is the strong tetragonal distortion which occurs if the strong associates are built up from the planar squares of CuO_4 . The electronic spectra of the associates are characterized by the band at $15\,800\text{ cm}^{-1}$. However, the strong associates are detectable not only by the $15\,800\text{ cm}^{-1}$ band, but also by the absorption at $27\,000\text{ cm}^{-1}$. This absorption band is due to the charge transfer from the ligand to copper. The low energies of this process indicate a high covalence of the Cu-O bonds. This interpretation is based on an analysis of the available literature data on the Cu^{2+} complexes [526, 802]. A simultaneous study of the electronic and EPR spectra of the copper-magnesium oxide catalyst showed the formation of strong associates in this system which are characterized by the CTB at $27\,000\text{ cm}^{-1}$. This specific absorption band is observed in the spectra of copper dimers with a bridge structure. Such complexes show an anomaly in their magnetic properties because of the presence of exchange interactions between the copper ions. For a long time, there has been no unified opinion about the nature of the absorption at $27\,000\text{ cm}^{-1}$ in the spectra of such dimers. At present, it is believed that this absorption is due to the charge transfer from the nonbonding p_z -orbital of bridged oxygen to the free d-orbital of the Cu^{2+} cation. This interpretation is supported by the tendency of the absorption band to shift to the low-frequency region on passing from oxygen acting as a bridged ligand (at about $27\,000\text{ cm}^{-1}$) to the less electronegative chlorine ($19\,000\text{ cm}^{-1}$) [526].

Therefore, the nature of the strong associates in the zeolites closely resembles the nature of the associates in the copper-magnesium catalyst [802]. However, since exchange interactions in the associates have no effect on the splitting of the d-d orbitals, the position of the absorption bands of the d-d transitions is determined only by the coordination state of the Cu^{2+} cation. These states are different in the zeolites (a square planar CuO_4) and in the copper-magnesium catalyst (CuO_6 octahedron, regular or with some tetragonal distortion). It is noteworthy that the strong associates in the zeolites have discrete absorption bands ($15\,800$ and $27\,000\text{ cm}^{-1}$), whereas the dispersed copper (II) oxide on the same zeolites has continuous absorption over the whole spectral range under consideration, without any pronounced maxima (see Figure 3.10, spectra 7). One further consideration, important for the preparation of substituted zeolites, should be pointed out. It is usually believed [74] that it is very difficult to completely eliminate the hydrolysis of the ion-exchange salt under the conditions of ion exchange. As a result, the CuY-I zeolites must contain some strong associates which will cause catalytic oxidation. This point of view is confirmed by the work of Anufrienko *et al.* [526]. As was pointed out above, it is sometime possible to observe in the spectra of the dehydrated CuY-I zeolites the absorption band at $27\,000\text{ cm}^{-1}$, which is due to only the presence of Cu-O-Cu. However, since dehydration *in vacuo* has a reducing action, the high temperatures of such treatment may lead to complete reduction of the strong associates (see Figure 3.9) which are more reducible than isolated and weakly bound ions.

Thus, different states of copper were identified from the spectra of the d-d transitions in type-Y copper zeolites. By using the absorption bands of the charge transfer it was possible to show for the first time the difference between the electronic states of copper in the strong associates and the isolated and weakly associated ions. In completely hydrated CuY-I zeolites, two types of Cu^{2+} were found. Some ions are stabilized in the zeolite framework and have

a coordination approaching an octahedral form (type I). The electronic spectra of these ions show absorption bands at 9000, 12 000 and 35 000 cm^{-1} . Other ions (type III) are similar to the hexaaqua complexes of copper and are characterized by absorption bands at 9800, 12 500 and 45 500 cm^{-1} . During dehydration, the ligands in complexes formed by type-I ions are not replaced. The position of the CTB is unchanged and the increase in tetragonal distortion is detected from the shift of the absorption bands of the d-d transitions to 11 000 and 15 000 cm^{-1} (isolated ions). Type-IV ions (weakly associated ions) in the dehydrated zeolites are very similar to the isolated ions (the absorption bands at 11 000, 15 000 and 36 000 cm^{-1}). The isolated and weakly associated cations of the dehydrated zeolites in the sites with tetragonal symmetry are, to a large extent, coordinatively unsaturated and can form complexes with strongly coordinative ligands (ammonia, pyridine and water). During the ion exchange, the copper cations enter the CuY-A zeolites as complex hydroamino complexes producing strong associates of the Cu^{2+} cations during the dehydration of the zeolite. The Cu^{2+} cations in these associates have a square planar coordination and are bound to each other by bridged oxygen. The low charge-transfer energies of these associates, compared with those of isolated and weakly associated cations, indicate a high covalence of their Cu-O-Cu bonds, which makes the bridge oxygen very movable and facilitates the oxidation reaction involving this oxygen.

Infrared spectra

The infrared spectra of CO which was adsorbed over the temperature and pressure ranges from 196 to 293 K and from 20 to 100 torr, respectively, on the CuY-I zeolites with a copper content less than 1.5 % and in which the Cu^{2+} cations are present mainly as isolated ions, stabilized at S_1 sites (Figure 2.2) [798], do not differ from the spectra of CO adsorbed on the zeolite framework. This suggests that there is no specific interaction of CO with the Cu^{2+} ions stabilized at the S_1 sites. This is also supported by the ESR data [801] (see above).

An increase of the copper content to 6.3 % leads to the appearance of Cu^{2+} ions stabilized at the other sites of the framework. These ions may form weak magnetic associates [798]. After the adsorption of CO at 173 K, the amplitude of the ESR signal increases and the ESR signal of the associated ions broadens. Subsequent evacuation of the samples at the same temperature almost completely restores the amplitude of the ESR signal. The infrared spectra of CO adsorbed on the CuY-I zeolite (6.3 % Cu) at 193 K and 5 torr show adsorption bands at 2160 and 2190 (Figure 3.11a, Spectrum 1) due to the specific interaction of CO with the copper cations. The bands (2172 and 2130 cm^{-1}) which belong to CO physically adsorbed on the zeolite framework due to the interaction with $\text{Na}^+ - \text{CO}$ (2170 cm^{-1}) and $\text{Na}^+ \cdots \text{OC}$ (2130 cm^{-1}) are briefly removed by the evacuation.

The decrease in the amplitudes of the ESR signals of associated copper ions and their broadening which is observed after the adsorption of CO may indicate an additional coordination of such ions by the CO molecules due to the coordinative unsaturation of the ions. In the IR spectra, this complex corresponds to the absorption band at 2190 cm^{-1} . This follows from the fact that the complex, which is characterized by these frequencies and observed by ESR spectroscopy, has the same thermal stability and stability towards evacuation. The complex of CO with copper ions is unstable and is readily destroyed upon evacuation at low temperatures or upon heating to room temperature (Figure 3.11 spectrum 1a). The weak bond strength between CO and Cu^{2+} ions is explained by a specific property of the copper ions to form weak adducts with the bases (small enthalpies) coordinated to the fifth or sixth site.

The infrared spectra of CO adsorbed on CuY-A at 173 and 293 K differs from that of CO adsorbed on CuY-I and show the absorption band at 2160 cm^{-1} (except the bands due to physically adsorbed CO on the zeolite framework in the 2100–2200 cm^{-1} region) as well as bands at 1650 and 2370 cm^{-1} for zeolites with small and high copper contents. Under the same

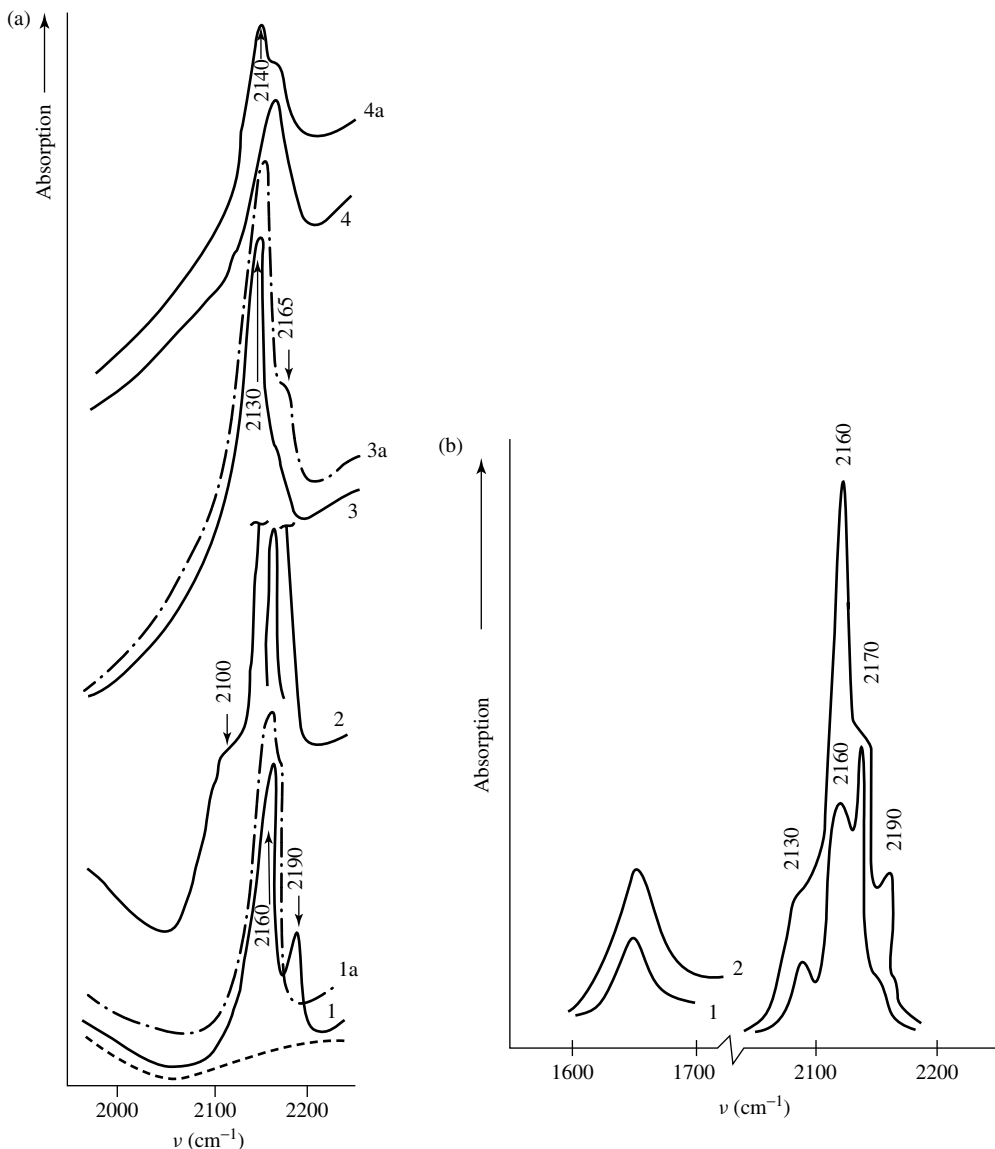


Figure 3.11. IR spectra of CO (a) adsorbed on (1,1a,2) the CuY-I zeolite, (3,3a) CuO/Al₂O₃, and (4,4a) CuCr₂O₄: (1), oxidized sample, CO adsorption at 173 K; (1a), after evacuation at 173 K; (2), sample reduced in CO at 673 K for 30 min.; (3), evacuation at 773 K; (3a) evacuation at 973 K; (4), oxidized sample; (4a), after heating in CO; (b) adsorbed at 193 K on CuY-A zeolite; (1), 0.9 wt-% Cu; (2), 5.8 wt-% Cu.

experimental conditions, the intensity of the band at 2160 cm⁻¹ is considerably greater for the CuY-A zeolite (Figure 3.11b) than for the CuY-I zeolite, even if the former zeolite has less copper. The absorption at 2370 cm⁻¹ is due to physically adsorbed CO₂, while the 1650 cm⁻¹ band belongs to a two-coordinate bidentate carbonate (Cu-O)₂CO. The presence of CO₂ and carbonates indicates the occurrence of a CO oxidation process, which is due to the presence

of reactive oxygen not belonging to the framework (strong magnetic associates). This oxygen participates in the strong exchange interaction between copper cations, due to which the strong associates are not observable by ESR. In fact, the concentration of copper in the CuY-A zeolites determined from the intensity of the ESR signal is only a small portion of the total amount of the introduced transition metal.

The intensity of the absorption band at 2160 cm^{-1} increases when adsorption of CO occurs on CuY-A zeolites treated under conditions producing only Cu^+ cations, and reduction of copper to the metallic state does not take place. According to various reports [801, 804], the absorption at 2160 cm^{-1} may be due to the stabilization of CO on Cu^+ ions only.

The fact that the absorption at 2160 cm^{-1} is observed even during treatment with CO at 193 K on CuY-A zeolites (Figure 3.11(b)) indicates that even under these conditions some Cu^{2+} cations are reduced to Cu^+ by carbon monoxide. In this case, only strong associated Cu^{2+} cations can be reduced, since oxygen of these associates participates in the oxidation of CO. It appears that the stabilization of CO on such reduced centers gives rise to the absorption band at 2160 cm^{-1} . The correctness of this assumption is supported by the fact that the intensity of the absorption band at 2160 cm^{-1} for the CuY-A zeolites is considerably higher than in this case of the CuY-I zeolites.

It is also known that in the samples prepared in the absence of the hydrolysis of the ion-exchanged salt, weakly associated Cu^{2+} ions can be reduced only upon high-temperature treatment of the sample under a CO atmosphere [801]. In the case of CuY-A zeolites, the formation of the reduced centers is observed even during interaction with CO at low temperatures. This fact is due to the high reactivity of the oxygen in the strong associates. It can be claimed that under these conditions the Cu^{2+} ions, which do not belong to the strong associates, are not reduced. This follows from the fact that the intensities of the ESR signals of weakly associated ions remain unchanged, even after treatment of the CuY-A zeolites with carbon monoxide at room temperature. On the basis of the differences in the reaction conditions, it is reasonable to assume that the reduced centers formed by strong associates should differ from the Cu^+ ions formed during the reduction of weakly associated ions. In fact, the interaction of CO with CuY-A zeolites which were reduced under more severe conditions, thereby also reducing weakly associated Cu^{2+} ions, produces a new maximum at 2140 cm^{-1} in addition to the band at 2160 cm^{-1} . The appearance of this maximum may also be related to the stabilization of CO on Cu^+ ions, which were formed during the reduction of weakly associated ions. The reduced centers resulting from the reduction of weak magnetic associates ($\text{Cu}^{2+} \cdots \text{Cu}^{2+}$) differ from those formed from strong associates (Cu–O–Cu). In the latter case, closely situated $\text{Cu}^+ \cdots \text{Cu}^+$ cations are formed. The fact that these centers can be reversibly reoxidized (for example under conditions of a catalytic process) indicate that this type of center is stable toward migration.

On the basis of the data obtained, the absorption at 2160 cm^{-1} should be assigned to the CO stabilized on the closely situated Cu^+ ions. The excitation of the CO molecule under the influence of the field of two ions, which leads to the increase of νCO , is larger than in the field of one ion, whereas the d-electrons are delocalized on the π^* orbital of CO from one Cu^+ cation. As a result, the νCO stabilized on the centers ($\text{Cu}^+ \cdots \text{Cu}^+$)–CO (2160 cm^{-1}) should be higher than in structures such as $\text{Cu}^+ \cdots \text{CO}$ (2140 cm^{-1}). The absorption band at 2160 cm^{-1} , observed during the adsorption of CO on the reduced CuY-zeolites [801, 804], appears to be due to the fact that the reduction was carried out for 36 h at 673 K. Under these conditions, the migration of copper cations becomes essential, so making possible the formation of clusters. The centers formed under these conditions may be similar to those formed during the reduction of strong associates.

Thus, the results of investigations of the states of copper cations in the CuY-zeolites by using infrared spectrometry agree with the conclusions made on the basis of ESR and electron spectroscopic data. New states of copper cations undetectable by ESR spectroscopy (strong associates and Cu^+ cations) were found.

It was shown (Chapter 2) that in inorganic and surface complexes, as well as in the complexes of NO with metals isolated in matrices, the range of variation of νNO is about 1000 cm^{-1} ($1300\text{--}2300\text{ cm}^{-1}$), whereas in complexes of CO this range is restricted to about 500 cm^{-1} ($1750\text{--}2250\text{ cm}^{-1}$), i.e. νNO should be more dependent on the state of the absorption center than νCO . It is, therefore, interesting to study the states of the cations in the zeolites using the NO molecule as a model.

Just as in the case of CO adsorbed on the CuY-I zeolites with low transition-metal content, no absorption bands attributable to the complexes of NO with the copper cation localized in the S_I sites were detected after the adsorption of NO (50 torr; 193–393 K) on CuY-I zeolites (1 % Cu). The interaction of NO with CuY-I zeolites containing 6.3 % Cu gives rise to absorption bands at 1920 and 1950 cm^{-1} (Table 3.2). It appears simultaneously with the disappearance of the ESR signal of Cu^{2+} ions [805]. Evacuation at room temperature leads to reappearance of the 1920 cm^{-1} absorption band. On this basis, the absorption at 1920 cm^{-1} was attributed to NO stabilized on Cu^{2+} . According to earlier studies [798], increased copper contents in CuY-I zeolites lead to the appearance of coordinatively unsaturated Cu^{2+} cations, which can form weak magnetic associates by exchange interaction. However, the possibility of the existence of isolated coordinatively unsaturated Cu^{2+} ions (i.e. not bound by exchange interaction), which can stabilize in the S_I , and S_{II} , sites, was not taken into consideration. (The exchange interaction occurs if the Cu^{2+} cations are separated by a distance not more than 30 \AA [801]; at a greater distance, the cations will be isolated.) At the same time, the appearance of two absorption bands in the infrared spectra of the adsorbed NO indicates that the CuY-I zeolites with high copper contents contain two slightly differing type of centers. These centers, in our opinion, are isolated, coordinatively unsaturated Cu^{2+} ions (1920 cm^{-1} , complex I) and weakly associated Cu^{2+} ions

Table 3.2. IR spectral features of CO and NO adsorbed on copper-containing systems.

Catalyst	Conditions of treatment	ν_{NO}	ν_{CO}	Adsorption site
CuY-I	Oxidized	1950	2190	$\text{Cu}^{2+}\text{O}^{2-}$ skeleton
CuY-A	Oxidized	1920	–	
CuY-A	Oxidized	1900	–	$\text{Cu}^{2+}\text{--O--Cu}^{2+}$
CuO	Oxidized	1865, 1875	–	Cu^{2+} on CuO surface
CuO/Al ₂ O ₃	Oxidized	1880	–	
CuO/Al ₂ O ₃	Heated in O ₂ at 500 °C for 10 h	1900–1930	–	Cu^{2+} in Al ₂ O ₃ lattice
CuCr ₂ O ₄	Oxidized	1920	–	Cu^{2+}
CuCl ₂	Evacuation at 150 °C	1875	–	Cu^{2+}
CuY-I, } CuY-A }	Reduction in H ₂ at 400 °C	1740	2160	Cu^+
CuY-I, } CuY-A }	Reduction in CO at 500 °C for 2 h	1820	2100–2110	Cu^0
CuY-A	Reduction in H ₂ at 400 °C	1790	2160	Cu^+
CuO	Vacuum treatment at 300 °C and above	1780	2115, 2140, 2130	Cu^+ on CuO surface
CuO/Al ₂ O ₃	Heated at 700 °C	–	2165	Cu^+ in Al ₂ O ₃ lattice
CuCr ₂ O ₄	<i>in vacuo</i>			
CuCr ₂ O ₄	Oxidized	–	2160	Cu^+ on CuCr ₂ O ₄ surface
CuCr ₂ O ₄	Heated in CO at 300 °C	–	2140	Cu^+ (products of CuCr ₂ O ₄ decomposition)

(1950 cm^{-1} , complex II), which differ only in the distance between the Cu^{2+} ions, e.g. in the latter case, the Cu^{2+} ions are divided by a distance less than 30 Å. It can be assumed that the additional stabilization of coordinatively unsaturated ions due to the exchange interaction will decrease the extent of interaction of the occupied d-orbitals of Cu^{2+} with the π^* -orbital of NO. As a result, νNO stabilized on the weak magnetic associates will be higher than in the case when isolated Cu^{2+} cations act as the adsorption centers. The absence of such differences between the states of the copper cations during the adsorption of CO is due to a greater sensitivity of νNO to the nature of the adsorption centers when compared with νCO . The intensity of the absorption bands at 1920 and 1950 cm^{-1} in the spectrum of NO adsorbed on CuY-I zeolites, which were subjected to reduction (I), is much lower than in the case of an oxidized sample. The reason for this is the reduction of a portion of Cu^{2+} cations to Cu^+ during treatment. In this case, the spectrum shows a weak absorption maximum at 1740 cm^{-1} . The appearance of this band may be related to the formation of a $\text{Cu}^+ \cdots \text{NO}$ complex (III). The presence of fewer electrons on the copper cation, as compared with Cu^{2+} , results in a more complete filling of the $d-\pi^*$ NO interaction, a weakening of the N–O bond, and a shift of the stretching frequency to longer wavelengths. This interpretation of the 1740 cm^{-1} absorption band is supported by the fact that this band is more intense in the spectra of NO adsorbed on more completely reduced samples. The $\text{Cu}^+ \cdots \text{NO}$ complex is unstable. On keeping the sample in an atmosphere of NO or on heating, the complex III decomposes to form N_2O (2240 cm^{-1}) and small amounts of NO_2 (1640 cm^{-1}), which is adsorbed on the zeolite framework. The disappearance of the 1740 cm^{-1} band is accompanied by an increase in the intensity of the absorption at 1920 cm^{-1} , i.e. the decomposition of NO is accompanied by a slow reoxidation of Cu^{2+} ions to Cu^+ . As a result, the number of the complexes III decreases while the concentration of complex I increases.

During the interaction of NO with CuY-A zeolites with low (0.9 %) and high (5.8 %) copper contents, an intensive absorption at 1900 cm^{-1} is observed in addition to the 1920 cm^{-1} and 1950 cm^{-1} bands (see Table 3.2 and Figure 3.12(a)). The stretching frequency of NO in this case (as in the case of CO adsorbed on NiY-A zeolites – see below) is shifted toward lower frequencies with respect to νNO in complexes I and II and corresponds to the nitric oxide stabilized on the Cu^{2+} cations of strong magnetic associates (complex IV). The lower value of νNO in this complex is due to a greater electronic density on the copper cations in strong associates, compared with isolated and weakly associated Cu^{2+} cations. The presence of high electron density follows from the fact that the ultraviolet spectra of the ions in strong associates exhibit a low-frequency charge-transfer band. The latter indicates a considerable covalence of the bond between the copper ion and oxygen, which does not belong to the zeolite framework. That is, there is a shift of the electron density to the copper cations of strong associates, compared with weakly associated Cu^{2+} ions in CuY-zeolites [526]. The absorption band at 1900 cm^{-1} is close to νNO adsorbed on the copper oxide phase (1880 cm^{-1}), but in the case of copper zeolites it is higher. As will be shown below, this is due to the different number of oxygen atoms not belonging to the zeolite framework, which coordinates the transition metal in the zeolite and the oxide phase. The increase of the temperature is accompanied by the appearance of the absorption bands of nitrates (1570, 1320 and 1640 cm^{-1}) in the infrared spectra of the CuY-A zeolites. At the same time, the intensity of the absorption band at 1950 cm^{-1} decreases. The formation of nitrates is due to the oxidation of NO by the oxygen of the strong associates. The stabilization of the oxidized complexes (NO_3) on the zeolite framework and on a portion of copper cations should disturb the exchange interactions between Cu^{2+} ions (as was the case during the adsorption of CO_2 on the surface of CuO–MgO solid solutions [802]). As a result, the Cu^{2+} ions which had become isolated to the concentration of complexes II, should decrease while those of complexes I should increase. In fact, in the infrared spectrum, which was recorded at 293 K, there is a very intense absorption band at 1920 cm^{-1} (NO adsorbed on isolated Cu^{2+}) and no absorption at

1950 cm^{-1} . These results may be considered as supporting the correctness of the assignment of the 1950 cm^{-1} band to NO bound to weakly associated ions.

As shown above, treatment of CuY-A zeolites in an atmosphere of H_2 (673 K; 0.5 h) leads to the reduction of some copper cations and the formation of only Cu^+ centers from coordinatively unsaturated Cu^{2+} ions. The strong magnetic associates should produce centers of the Cu^+Cu^+ type, which are adjacent to singly charged copper ions. Therefore, it should be expected that, unlike an oxidized zeolite sample, the adsorption of NO on such a CuY-A zeolite sample will lead to the formation of complexes of nitric oxide with reduced Cu^+ and Cu^+Cu^+ centers. In fact, the adsorption of nitric oxide is accompanied by the appearance of absorption bands at 1740, 1790 and 1835 cm^{-1} , in addition to the bands at 1900, 1920 and 1950 cm^{-1} (Table 3.2, Figure 3.12b, spectrum 1). The absorption at 1745 cm^{-1} is due to the above complex III ($\text{Cu}^+ \cdots \text{NO}$). The absorption bands at 1795 and 1835 cm^{-1} , which were not observed earlier, may be interpreted in terms of the following considerations. At low temperatures in the condensed phase, nitric oxide exist as a dimer with stretching frequencies of 1865 and 1768 cm^{-1} (ν_{as} and ν_{s} of the *cis*-dimer) [806]. However, in our case the temperatures used are not low enough for a condensed phase of NO to be formed. Moreover, the absence of absorption bands approaching the stretching frequencies of the *cis*-dimer in the spectra of the oxidized CuY-A zeolites indicates a specific interaction of nitric oxide with centers which are present only in a reduced form (Cu^+Cu^+). As the temperature is increased, complex III decomposes (the intensity of the band at 1745 cm^{-1} decreases), and the absorption bands at 1795 and 1835 cm^{-1} disappear. This is accompanied by the appearance of the absorption band of N_2O (2240 cm^{-1}) (see Figure 3.12, spectra 2 and 3). The simultaneous disappearance of the absorption bands at 1795 and 1835 cm^{-1} from the spectra, as well as the observed frequencies being close to the absorption bands of the *cis*-dimer, enable us to assign these absorption bands to the complex V. This complex is the *cis*-dimer $(\text{NO})_2$ stabilized on double centers (Cu^+Cu^+), which are formed during the reduction of strong associates.

The results obtained show that by using NO as a probe-molecule it is possible to obtain more detailed information about the state of transition-metal cations than in the case of CO molecules. However, one must take into consideration that the decomposition of NO may occur and the redox processes due to the decomposition of NO on reduced samples may change the state of cations. Due to the interaction with CO, a reduction of the Cu^{2+} cations takes place on the oxidized sample.

3.1.2 OXIDES

In order to identify the states of cations active for adsorption over the supported oxides (for bulk $\text{CuO}/\text{Cu}_2\text{O}$, see Chapter 2), we will examine the published data regarding the IR-spectroscopic study of the CO (NO) adsorption on Cu-containing catalysts, using the data analyzed above regarding spectral manifestations of CO and NO in complexes with cations, the states of which have been established independently.

Copper-containing systems were some of the first classes of materials where wide infrared spectroscopic studies of adsorbed CO and NO probes had been used to determine the state of the copper cations on the surfaces of catalysts [30, 479–482, 804–831]. At present, there are many studies in this field, because Cu-containing systems are widely used as catalysts for different processes, and especially because of the progressive investigations of the nature of the active component in alcohol-synthesis catalysts. In spite of the abundance of the data obtained, the conclusions of different studies concerning the spectral images of copper cations of different degrees of oxidation do differ. This especially concerns the papers in which the CO molecule is used as a probe because the majority of authors do not take into account the possibility of Cu^{2+} reduction by CO and/or presence of the remaining ions of Cu^{1+} on the surface of supported systems even after 'hard' reduction.

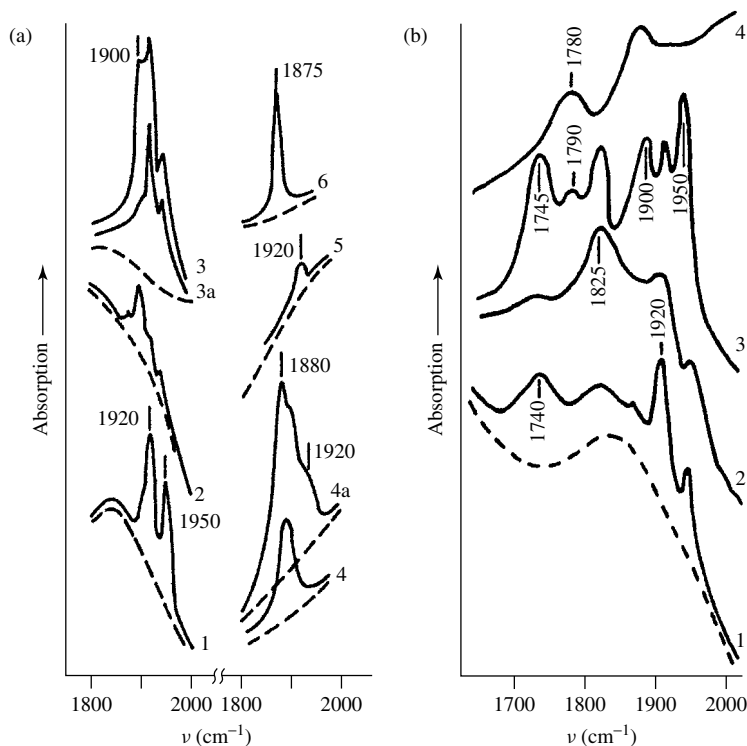


Figure 3.12. IR spectra of NO adsorbed at 293 K on oxidized (a) and reduced (b) copper-containing catalysts: (a) 1,2,3, CuY-I (6.3 % Cu), CuY-A (0.9 % Cu, CuY-A (5.8 % Cu), respectively; 3a, 373 K; 4, CuO/Al₂O₃; 4a, heated in O₂ at 773 K; 5, CuCr₂O₄; 6, CuCl₂; (b) 1, 2, CuY-I (773 K, 2 h in CO) and (773 K, 15 h in CO), respectively; 3, CuY-A (773 K, vacuum treatment); 4, CuO/Al₂O₃ (1 h of vacuum treatment at 973 K). Dashed lines represent background spectra.

There were no reason to suppose that ν_{CO} in Cu^{n+} -CO complexes has to be significantly different from that within the usual limits of spectral manifestations of M^{n+} -CO complexes observed in the case of cations of the end of the First Period (of the Periodic Table) [30, 807]: M^0 -CO ($\nu_{\text{CO}} \leq 2100 \text{ cm}^{-1}$), M^+ -CO ($\nu_{\text{CO}} 2120$ – 2160 cm^{-1}) and M^{2+} -CO ($\nu_{\text{CO}} \geq 2170 \text{ cm}^{-1}$). Most studies are in good agreement with such a scheme. Additional evidence for these scheme have also been obtained in recent studies. Thus, it has been confirmed that Cu^{2+} -CO species are only observed when using matrix-isolated techniques [832], and only monovalent copper forms of the ionic carbonyls type (Cu^+ -CO) are stable [832, 833]. The first species (Cu^{2+} -CO) are labeled as σ -complexes since the bond between the cation and CO has σ -character [30]. The low stabilities of the Cu^0 -CO carbonyls which have been analyzed in detail [30, 807] are considered to be due to the fact that both the σ - and π -components of the Cu-CO bond are weak [811, 833], whereas the high stabilities of the Cu^+ -CO species are stipulated by the simultaneous formation of σ - and π -bonds between the metal ion and CO and by the synergism [807] of both types of bonds. Both of these facts were supported in Huang [834].

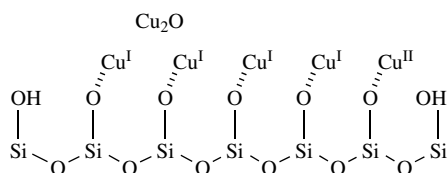
The published results have shown that the bands in the 2220–1980 cm^{-1} region appear in the infrared spectra of CO adsorbed on Cu-containing oxide surfaces [30, 479–482, 807–838]. Unstable Cu^{2+} -CO complexes with predominantly a σ -component of the M-CO bond are usually observed in the spectral region above 2160 cm^{-1} and are detected at low temperatures only.

CuO

In the case of copper in square planar coordination, stable carbonyls gives rise to the bands in the 2160–2110 cm^{-1} region. The assignment of these bands has been a subject of numerous discussions. There are two viewpoints concerning this question. There are many studies where such an absorption has been assigned to Cu^+-CO species. In contrast, some authors, on the basis of the fact that the copper oxidation state before CO adsorption was Cu^{2+} , have interpreted the adsorption in this spectral region as caused by $\text{Cu}^{2+}-\text{CO}$ species [808, 812, 827–830]. Analysis of the literature data concerning this problems gives many reasons in support of the assignment of the bands in the 2160–2110 cm^{-1} region to Cu^+-CO complexes. First, there is a sufficiently high stability of such complexes (both $\text{Cu}^{2+}-\text{CO}$ and Cu^0-CO complexes are unstable, as has been shown by Lohov and Davydov [807]). Moreover, it has been proved that the reduction of Cu^{2+} to Cu^+ takes place upon interaction with CO even at low temperature. This is accompanied by a decrease in the intensity of the band belonging to the $\text{Cu}^{2+}-\text{CO}$ species and by an increase in intensity of the absorption characteristic of Cu^+-CO .

CuO/SiO₂

Zecchina *et al.* [835] proposed for Cu/SiO₂ (17 atom% Cu) that the absorption bands at 2136 and 2163 cm^{-1} observed after the adsorption of CO characterize the CO complexes with Cu^+ ions on small clusters of Cu₂O (samples were evacuated at 1073 K), for example on reduced faces, edges, steps, etc. An absorption band at 2214 cm^{-1} characterizes the adsorption of CO on supported Cu^{2+} ions. Based on [809, 810], it can be suggested that Cu₂O is fixed on SiO₂ in a similar way:



Scheme 3.1

After reduction at 673 K, the Cu^{2+} ions practically disappear. Atoms located on the most exposed sites and, therefore, the more reactive areas are reduced even further. When CO is adsorbed on such a sample, a low-frequency ‘tail’ appears due to the CO adsorption on Cu^0 . Progressive reduction at 773, 873 and 923 K leads to the appearance of a new peak at 2112 cm^{-1} and to following growth in intensity of this band (CO adsorption on high-index faces of the single crystal Cu^0), together with a shoulder at 2080–2070 cm^{-1} as well as a band at 2099 cm^{-1} with a shoulder at 2070 cm^{-1} . The bands in the 2130–2140 cm^{-1} region change their intensities with increases in the reduction degree as observed in the IR spectra of adsorbed CO, up to reduction temperatures of 773 K. This indicates the presence traces of Cu^+ in the samples and are in good agreement with results obtained by Davydov and co-workers [817, 818]. In numerous studies, the absorption band characteristic of a linear $\text{Cu}-\text{CO}$ complex has been observed at 2105 cm^{-1} and below. However, several studies (see, for example, [839]) are in disagreement with this scheme because they did not take into account the fact that the copper cations can be easily reduced upon interaction with CO, even at low ($<0^\circ\text{C}$) temperatures. Thus, Hierl *et al.* [839] assigned the bands at 2138 and 2118 cm^{-1} observed upon CO adsorption on $\text{CuO}-\text{NiO}/\text{Al}_2\text{O}_3$ to νCO in $\text{Cu}^{2+}-\text{CO}$ complexes. The Cu^{2+} reduction to Cu^+ proceeds the most easily, with CO being

stabilized on the newly formed Cu^+ ions. It is clear that this fact must be considered when interpreting the spectra of CO adsorbed on Cu-containing systems [30, 807] and also on other related systems such as those containing Co or Ni.

In Jong *et al.* [808], the band at 2130 cm^{-1} has been connected with a $\text{Cu}^0\text{-CO}$ complex, although it has been shown by Davydov and co-workers [817, 818], that these bands more probably characterize the residual Cu^+ ions and are observed with a significant intensity in the case of strongly reduced samples because of the high value of the extinction coefficient in the $\text{Cu}^+\text{-CO}$ complex compared with that in the $\text{Cu}^0\text{-CO}$ complex [30, 807]. The adsorption of CO on metallic copper has been reviewed by Pritchard *et al.* [37]. Usually, CO is weakly bound to the metal and such an adsorption form gives rise to the band below 2110 cm^{-1} (see Table 3.2).

The properties of Cu^0 , are shown when using DRES by the onset of the metallic copper absorption edge at about 17000 cm^{-1} (Figure 3.13(a)) after reduction of Cu^{2+} by hydrogen over the range 425–625 K. Reduction at 480 K for 12 h induced, in addition to the 17000 cm^{-1} absorption edge, a series of eight intense narrow bands in the near-infrared region of the spectra (see Figure 3.13(b)). These bands appear to arise from optical transitions of atomically dispersed zero-valent copper. Their number corresponds to that of states originating from the excited configurations $(3d^9 4s^2)^2D_{1/2,3/2}$ and $(3d^{10} 4p)^2P_{3/2,1/2}$. The above application of the DRES method has demonstrated the wide set of chemical states present under these conditions, including metallic atomic copper [25].

Thus, the solutions to the main problems in the field of investigation of copper states on the surfaces of oxide systems seem to be clear. Only one still awaits a decision, namely an indication

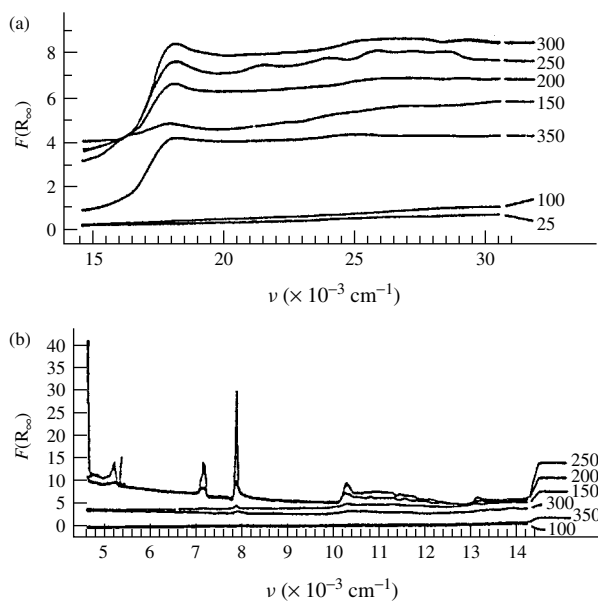


Figure 3.13. Absorption spectra of metallic copper in reduced Cu(I)-exchanged zeolite-Y. (a) Reduction under 1 atm pressure of hydrogen gas at increasingly high temperatures eventually produces metallic copper, identifiable from its absorption edge at ca. 17000 cm^{-1} . (b) In a narrow range of reduction temperatures, atomically dispersed zero-valent copper can be produced, as shown by the presence of the discrete narrow lines of Cu^0 [25]. Reprinted from Delgass, W.H., Haller, G.L., Kellerman, R. and Lusford, G.H., *Spectroscopy in Heterogeneous Catalysis*, Academic Press, New York (1979). Reprinted with permission from Academic Press.

of the copper states formed upon reductive treatment *in situ*, on alcohol-synthesis catalysts such as $\text{CuZn-Al}_2\text{O}_3$. In this case, the bands belonging to carbonyl complexes (at about 2090 cm^{-1}) lie in between the ranges characteristic for $\text{Cu}^0\text{-CO}$ and $\text{Cu}^+\text{-CO}$ complexes which causes uncertainty concerning the nature of the active component in such types of catalysts.

Such questions were examined in detail by Chiotti *et al.* [837] using the CO adsorption. Bands at 2178 and 2169 cm^{-1} in the spectra of CO adsorbed at 77 K could be attributed to CO molecules coordinated to Zn ions exposed on the $(10\bar{1}1)$ and $(10\bar{1}0)$ crystalline faces, respectively. These bands decrease for the copper-zinc oxide catalysts, and a quite intense band at about 2115 cm^{-1} appears, assigned to CO adsorbed on Cu^+ sites. Furthermore, for the copper-zinc oxide catalysts, quite intense bands are present in carbonate-like species regions, assigned to such species which are bi- or polycoordinated to Zn(II) ions and to Cu(II) ions dissolved in the ZnO matrix. Desorption up to 573 K is necessary to clean the binary-oxide surface. Carbon monoxide re-adsorption on such samples at 77 K showed some differences in comparison with the 'first-contact' experiments: no bands appeared in the region characteristic of carbonate-like species; in the $\nu\text{C}\equiv\text{O}$ stretching region the absorption due to the copper-related species shows clearly three components at 2136 , 2110 and 2098 cm^{-1} , irreversible for evacuation at 77 K , assigned to two different Cu^+ and to Cu^0 sites respectively; the band at 2178 cm^{-1} increases and a new band at 2172 cm^{-1} is present, assigned to the CO adsorption on Cu^{2+} ions dissolved in the ZnO phase [837]. Microgravimetric measurements of CO, both reversibly and irreversibly adsorbed on such treated samples, showed that about 60% of CO molecules are chemisorbed on Cu^0 or Cu^+ surface sites, and that the copper exposed on the surface represents $32\text{--}34\%$ of the total copper content, if a $\text{CO/Cu ratio} = 1$ is assumed.

Another situation is observed in the case of reduced samples. As far as pure ZnO is concerned, it completely loses any transparency in the region of frequencies lower than 2000 cm^{-1} , and a strong absorption at about 1400 cm^{-1} is assigned to IR photoionization of donor centers (single ionized oxygen vacancies) produced upon reduction treatment. Unlike pure ZnO, the reduced samples [291, 843] of Cu/ZnO exhibit good IR transparency, like oxidized ZnO and Cu/ZnO samples. This means that copper acts as a deep acceptor level in ZnO (Figure 3.14). Poor transparency of pure ZnO after reduction can be due to the presence of a strong and wide band caused by photoionization of V_o centers filled during the reduction treatment (Figure 3.14(a)). The absence of this band in the case of Cu/ZnO shows that copper modifies the properties of ZnO (Figure 3.14(b)).

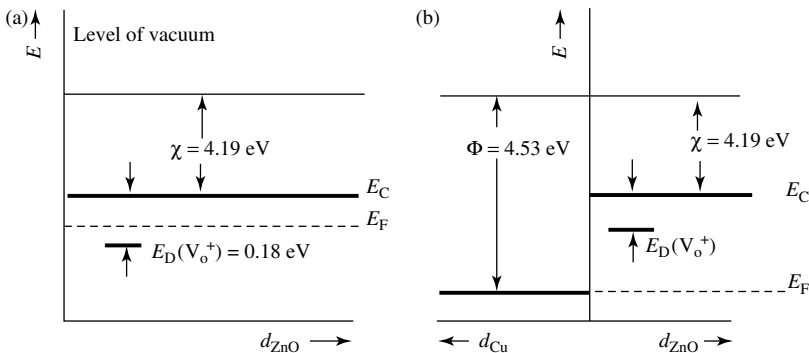


Figure 3.14. Schemes of energy levels for (a) ZnO, and (b) ZnO doped with copper ions [291]. Reprinted from *Surf. Sci.*, **183**, Bocuzzi, F., Chiorino, A., Chiotti, G., Francesco, P., Strukul, G. and Tessari, R., 'A metal-semiconductor interaction: effect of H_2 chemisorption on the IR transparency of Cu/ZnO', L285-L289, Copyright (1987), with permission from Elsevier Science.

In diffuse reflectance spectra of the oxidized Cu/ZnO samples, the following features are evident: the band at 6600 cm^{-1} is assigned to a d–d transition of Cu^{2+} ions in tetrahedral coordination, an absorption band at $11\,500\text{ cm}^{-1}$ to the CuO phase, and an absorption band at $27\,200\text{ cm}^{-1}$ to the ZnO phase. The spectrum of the reduced sample does not show the absorption edge of CuO and the d–d transition of Cu^{2+} in ZnO, but a very broad band with a maximum at $18\,000\text{ cm}^{-1}$ is present, superimposed on the spectrum of ZnO. The maximum is in the region of the excitation of the d-zone electrons into the conduction zone of metallic copper, and therefore, it can be ascribed to the formation of metallic particles [291]. Disappearance of the Cu^{2+} d–d transition and the broad band between 5500 and $18\,000\text{ cm}^{-1}$, according to Klier [840], can both be associated with the formation of a defective reduced Cu/ZnO phase. Carbon monoxide adsorption over such a reduced sample causes the appearance of the band at about 2100 cm^{-1} , which has been attributed [291] to CO adsorption on small Cu^0 clusters. On this basis, the author drew the conclusion that Cu^0 is an active component in such types of catalysts.

As well as in the above-cited studies, Cu–ZnO and Cu–ZnO– Al_2O_3 [841] with adsorbed CO exhibit only one absorption band with similar wavenumbers in the 2100 – 2115 cm^{-1} region (Figure 3.15), confirming the formation of a copper carbonyl complex [30, 479]. It can be concluded from this fact that first the copper ions are homogeneous in these samples, and secondly that the states of the copper ions on the surfaces of both catalysts are similar. The results obtained are in full agreement with an investigation of the state of copper in Cu/Zn/Al oxide-based solid solutions using the ESR method [479]. The data show the absence of the copper oxide phase (within the sensitivity limits of the method) in the investigated samples because, according to Davydov *et al.* [479], the surface copper ions in copper oxide exhibit the formation of two carbonyl-type complexes with νCO at 2115 and 2140 cm^{-1} .

The νCO value (2115 cm^{-1}) remained practically unchanged after CO adsorption on the sample evacuated at 573 K (see Figure 3.15, spectrum c) and after holding in O_2 at 573 K with following evacuation (see Figure 3.15, spectrum b). As was shown by Davydov [30], the νCO in carbonyl complexes depends on the charge and on the structure of the nearest environment of copper. A comparison of the νCO value observed with the characteristics of carbonyl complexes stabilized on copper in different states which are available in the literature, shows that the 2115 cm^{-1} νCO value is typical of carbonyl complexes on Cu^+ ions.

During CO adsorption on Cu–Zn and Cu–Zn–Al catalysts reduced in H_2 at 373 K and evacuated at the same temperature (see Figure 3.15, spectrum d) or held in the methanol synthesis reaction medium at 523 K with the gas phase removed at 523 K (see Figure 3.15, spectrum e), as well as in reports by other authors [291, 843], carbonyl complexes with νCO at 2100 cm^{-1} (such a value is usually found for CO adsorption on high-index faces of Cu^0 – see Table 3.2) were observed and assigned, in spite of the low νCO value, to νCO in the Cu^+ –CO complex. Such a lower νCO value can be caused by reduction of the effective charge on the copper ions due to the donor effect of both oxygen from the matrix and/or adsorbed water or OH–groups from the ligand sphere of a coordinating ion. The influence of water in lowering the νCO ($\Delta\nu \sim 15$ – 20 cm^{-1}) has been established for these carbonyl complexes [30, 311]. It appears to be suggested that in the above range of νCO it is impossible to make a single-valued conclusion about the cation oxidation degree on the basis of spectroscopic data alone. Donor properties of the matrices have an influence on both the ionic states of copper (Cu^+ and Cu^{2+}) and small metal clusters. An increase in the electron density in these cases leads to a decrease in the νCO value (2070 – 2050 cm^{-1}) [841]. Analogous spectral patterns have been observed in the cases of anionic-modified Cu-containing systems such as CuO–MgO [30, 479, 511], Cu/ZnO and Cu/ZnO– Al_2O_3 [841].

In addition, in the case of $\text{Cu}^{2+}/\text{TiO}_2$ [826], as well as in Cu^{2+}/Y and $\text{Cu}^{2+}/\text{SiO}_2$, Cu^{2+} ions are reduced to Cu^+ , and carboxylates are observed together with two kinds of Cu^+ –CO carbonyls.

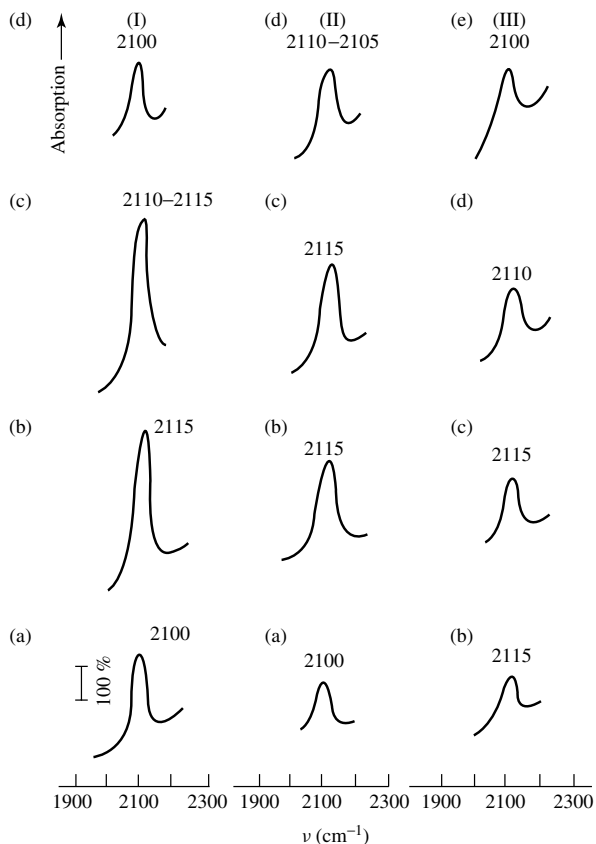


Figure 3.15. IR spectra of CO adsorbed on solid solutions based on anionically modified ZnO: I, 6 % Cu; II, 6 % Cu and 9 % Al; III, 23 % Cu and 20 % Al: (a) after pre-treating in oxygen with intermediate evacuation at 423 K; (b) as for (a) but at a temperature of 573 K; (c) reduced *in vacuo* at 573 K; (d) treated in H₂ (100 torr) at 273 K, evacuated at 373 K; (e) methanol synthesis reaction medium at 523 K, with evacuation at 523 K.

Using low-temperature CO adsorption, Cu²⁺-CO and Cu⁺-CO complexes have been detected [816].

Different techniques have been used [846] to characterize Cu/TiO₂ catalysts. Reduced samples produced infrared absorption bands in the 2070–2140 cm⁻¹ region with intensities and positions which are strongly dependent on the preparation method and also on the sample pre-treatment. The 2103 cm⁻¹ band was assigned to CO adsorption on Cu⁰ step and edge sites, the 2071 cm⁻¹ band to CO adsorbed on Cu(111) micro faces and on sites at the edges of small copper particles, and the 2126 cm⁻¹ band to CO adsorbed on isolated Cu atoms and/or two-dimensional small Cu clusters on the titania surface. These authors have shown that the wet impregnation method leads to samples in which three-dimensional copper particles are almost completely lacking.

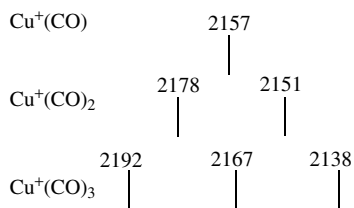
Copper catalysts based on rare-earth element oxides exhibit properties which are characteristic of each separate system [512]. The Cu²⁺-CO complex is reduced, and the Cu⁺-CO complex (2140–2110 cm⁻¹) is formed, whereas on the surface of the rare-earth oxide components the dimer structures (CO)₂²⁻ and (CO)₂⁻ can be obtained in high concentration, as found on the surfaces of pure rare-earth element oxides [274, 275].

Using infrared spectroscopy of adsorbed CO, the state of copper in a Ni–Cu–Cr oxide catalyst has been established [847]. It was shown that copper (when added) blocks the chromium ions in the Ni–Cr catalyst with contaminant stabilization as Cu^+ .

Complexes formed by the interaction of CO with CuO/ZrO_2 and CuO/ZnO/ZrO_2 aerogel catalysts are mainly of the carbonate type [848]. Carbon monoxide in such catalysts is irreversibly adsorbed on Cu^{2+} ions in the form of carbonyl-type species, which are then transformed into carboxylate- and, by oxidation, into carbonate type-species. The spillover from copper to zirconium ions of the species derived from the solid and the carbon monoxide has been investigated.

The (Cu/ZnO) copper-containing system was the first one where the formation of a species bound to both a zinc ion and a borderline Cu site simultaneously (absorption band at 1580 cm^{-1} , assigned to the νCO of an unusual four-electron donor carbonyl species [849]) has been revealed (see Section 3.10 for further details).

Concluding the examination of Cu-containing systems, the data on the CO adsorption on Cu–ZSM-5 zeolites should be noted. In this case, on testing the surface with CO, the existence of two types of sites has been revealed [844]: (i) associated Cu^+ cations, monitored by a CO band at 2137 cm^{-1} , and (ii) isolated Cu^+ sites formed from dicarbonyls at high CO equilibrium pressures (bands at 2177 and 2151 cm^{-1}). A decrease in the CO pressure leads to destruction of these species according to the reaction $\text{Cu}^+(\text{CO})_2 \rightarrow \text{Cu}^+ - \text{CO} + \text{CO}$ and after evacuation only monocarbonyls are detected by the band at 2158 cm^{-1} . Co-adsorption of water and CO on the isolated Cu^+ sites is accompanied by a ca. 30 cm^{-1} low-wavelength shift of this band. Such a shift is reversible and the original band position is restored after subsequent evacuation. Recently, it has been shown [845] that Cu^+ ions in HZSM zeolites can coordinate even three CO molecules:



Scheme 3.2

3.2 Nickel-containing systems

The ground state of the free Ni^{2+} ion is a ${}^3\text{F}$ term, while the excited state is a ${}^3\text{P}$ term. In an octahedral field, the ground ${}^3\text{F}$ state is split into the ${}^3\text{A}_{2g}$, ${}^1\text{T}_{2g}$ and ${}^3\text{T}_{1g}$ states with a decrease of the orbital degeneration, and the ${}^3\text{P}$ state remains unsplit as ${}^3\text{T}_{1g}$ [799]. The electronic transition from the ground ${}^3\text{A}_{2g}$ level to the excited triplets causes the appearance of three absorption bands in the spectra. In a tetrahedral field, the splitting components of each term remain unchanged, while the ground state will be ${}^3\text{T}_1$, then followed by ${}^3\text{T}_2$, ${}^3\text{A}_2$ and ${}^3\text{T}_1$ (P). For a tetrahedron, the value of the parameter 10 Dq will be lower than for an octahedron, and all terms will shift to lower energies.

3.2.1 ZEOLITES

Electronic spectra

The electronic spectra of the initial (after ion exchange) hydrated NiY-zeolites show absorption bands at 8700 , $13\,800$, $15\,200$ (shoulder) and $24\,800\text{ cm}^{-1}$ (Figure 3.16(a), spectrum 1) [526].

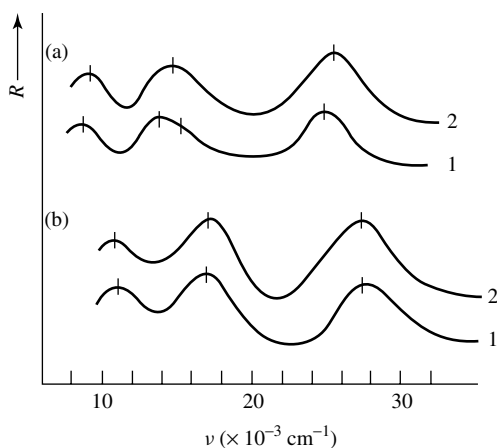


Figure 3.16. Electronic spectra of (a) the initial hydrated zeolites, and (b) after subsequent adsorption of ammonia: (1) zeolite NiY-I; (2) zeolite NiY-A.

These spectra are identical to those of aqueous solutions of the salts of divalent nickel [799, 800]. This fact indicates that with this ion-exchange method the Ni^{2+} ions in the zeolites are present as hexaaqua complexes, $\text{Ni}(\text{H}_2\text{O})_6^{2+}$. The observed bands are due to the electronic transitions from the ground ${}^3\text{A}_{2g}$ level of the Ni^{2+} ion to the excited ${}^3\text{T}_{2g}$, ${}^3\text{T}_{1g}$, ${}^3\text{E}_g$ (${}^1\text{D}$) and ${}^3\text{T}_{1g}$ (${}^3\text{P}$) levels, respectively. The relatively high intensity of the transition ${}^3\text{A}_{2g} \rightarrow {}^1\text{E}_g$ (${}^1\text{D}$) is explained by the small energy difference between the terms ${}^3\text{T}_{1g}$ (${}^3\text{F}$) and E_g (${}^1\text{D}$). As a result, the spin-orbital interaction mixes these two states and the rules of the selection of $\Delta S = 0$ are not observed.

In the spectra of NiY-A zeolites, the absorption bands corresponding to the three main transitions, ${}^3\text{A}_{2g} \rightarrow {}^3\text{T}_{2g}$, $\rightarrow {}^3\text{T}_{1g}$, and $\rightarrow {}^3\text{T}_{1g}$ (${}^3\text{P}$), are shifted toward higher frequencies and are observed at 9100, 14700 and 25500 cm^{-1} , respectively (see Figure 3.16(a), spectrum 2). In this case, the increase in the energy of the d-d transitions is explained by the polarizing action of the cation in the outer sphere, the presence of which is due to the formation of hydroxo complexes as a result of hydrolysis of the ion-exchanging salt under the given conditions of zeolite preparation. Mutual polarization of the Ni^{2+} cations bound by hydroxo complexes is accompanied by the additional stabilization of the ground state [526] and a corresponding increase in the energy of electronic transitions.

For the CuY-A zeolites, it was found that, during the adsorption of ammonia or during the treatment of these zeolites with aqueous ammonia solutions, the stabilization of Cu^{2+} as isolated ions is possible, which is accompanied by 'disintegration' of the clusters. This possibility was also investigated for NiY zeolites. For this purpose, the adsorption of ammonia from the gas phase on the initial NiY-I and NiY-A zeolites has been carried out. The spectra of the zeolite samples subjected to such treatment are identical and are characterized by three absorption bands at 10800, 17200 and 27500 cm^{-1} , irrespective of the preparation method for the initial zeolites (see Figure 3.16(b)). Analysis of the spectra (the positions of the bands and the relative increases in their intensities as compared with the spectra of the initial samples) allows us to conclude the formation of hexaammoniates [799, 800]; i.e. as in the case of CuY zeolites, the clusters of Ni^{2+} 'disintegrate' during the adsorption of ammonia due to the greater coordination power of ammonia molecules when compared with OH groups or water molecules.

One more characteristic feature of the NiY zeolites is that it is possible for the Ni^{2+} cations to be stabilized in the zeolite framework as isolated cations during treatment of the initial NaY zeolite with a solution of nickel ammoniate. However, the electronic spectra of the samples prepared by

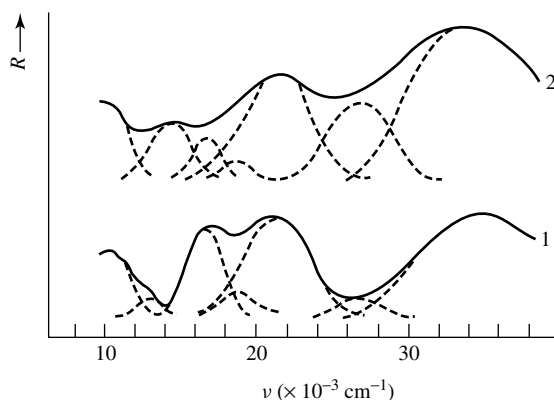


Figure 3.17. Electronic spectra of dehydrated (1) NiY-I, and (2) NiY-A zeolites.

this method, taken several days after the ion exchange had been carried out, completely coincide with the spectra of the NiY-A zeolites. It also turned out that the spectra of the NiY-I zeolites with pre-adsorbed ammonia became identical to the spectra of the initial NiY-A zeolites after the NiY-I zeolites had been kept for a short period of time in air. This can be understood by taking into consideration the ability of the nickel ammoniate to be decomposed by water. With copper/ammonia complexes, this trend is much less pronounced because of the lower instability constants. Thus, the state of nickel in the zeolite framework is strongly influenced not only by the conditions of the ion exchange, but also by the conditions under which the zeolites are stored.

The electronic spectra of the dehydrated zeolites represent a summation of partially superimposed bands. After separation of the spectra into their constituent Gaussian components, bands at 10 000, 18 500 and 21 300 cm^{-1} were obtained, which are common for zeolite types of materials (Figure 3.17). The spectra of the NiY-A zeolites are characterized by an intense absorption at 14 000 and 26 500 cm^{-1} . This absorption is little pronounced in the spectra of NiY-I zeolites. However, the latter do have an intense absorption band at 16 500 cm^{-1} . The observed spectra cannot be due to Ni^+ and Ni^{3+} ions [850], and result from different coordination states of the Ni^{2+} cations.

The spectra of the dehydrated nickel zeolites of the A, X and Y types have been described [851, 852], but were interpreted in terms of a uniform distribution of the Ni^{2+} ions in the zeolite framework and their stabilization in the sites characterized by octahedral [851] or trigonal [852] coordination. The spectra observed by Anufrienko *et al.* [526] have a number of common absorption bands but with different intensities. Therefore, they cannot be due to one single coordination state of the ions.

The absorption bands at 8500, 14 000 and 26 000 cm^{-1} are characteristic of compounds which contain Ni^{2+} in an octahedral coordination with respect to oxygen. The bands at 14 000 and 26 500 cm^{-1} observed in the spectra of type-A zeolites after dehydration can therefore be attributed to the octahedral complexes of divalent nickel. These bands are characterized by a comparatively high intensity, which is not typical of high-symmetry octahedral complexes. The high intensity of the bands may be related to the nonequivalency of the ligands in the complexes under consideration. The nonequivalency of the oxygen anions is due to their different nature: some of them are zeolite lattice anions, while the rest are bridged anions between two Ni^{2+} cations and do not belong to the zeolite framework. The presence of the nonlattice oxygen increases the coordination of these Ni^{2+} cations since the number of natural sites in the zeolites, characterized by a number of six, is restricted.

The absorptions at 13 000 and 26 000 cm^{-1} are also found for the NiY-I zeolites. The very weak intensities of these absorptions may be associated with the small number of nickel complexes of the type considered above, or it may be due to the high-symmetry environment. In the latter case, the Ni^{2+} cations should be assumed to be located inside a hexagonal prism (S_I sites). Regular octahedral coordination is ensured both with respect to the strength of the field produced by the ligands (all oxygen ions belong to the zeolite framework) and the symmetry of the ligand environment. However, in the case of CuY zeolites it was shown that the stabilization of multiply charged cations in the S_I site is possible only in the case of a strongly decationated zeolite, that is, if the zeolite containing the metal is prepared by using its ammonia form.

The absorptions at 10 000, 18 500 and 21 300 cm^{-1} may be assigned to Ni^{2+} ions whose environment corresponds to a trigonal bipyramid with a coordination symmetry D_{3h} [852]. This symmetry can be achieved if the Ni^{2+} cations are located in the S_{II} sites where the ions can be coordinated to three oxygen ions of the hexagonal window of the cubooctahedron (three coplanar ligands) and to two oxygen ions of H_2O or OH groups on the sides of large and small cages. The possibility of such coordination was found for Co^{2+} [853] and Mn^{2+} ions [854].

According to Boksha and Grum-Gruzimailo [850] the band at 16 500 cm^{-1} is characteristic of compounds containing Ni^{2+} cations with a tetrahedral coordination with respect to oxygen. In the zeolite structure, such coordination can be achieved in the case of localization of the exchange cations in the S_{IV} sites or in the S_{IV} and S_{II} sites where they interact with three oxygen ions of the hexagonal window of the cubooctahedron (Figure 2.2) and with the oxygen of an H_2O or OH group.

Thus, the spectra of the d-d transitions permit us to establish the existence of three states of Ni^{2+} cations which differ in the symmetry of the coordinated oxygen. Within these states, the likelihood of Ni^{2+} ions to undergo reduction is also different.

The Ni^{2+} ions with a tetrahedral coordination are isolated ions and are present mainly in the NiY-I zeolites. The Ni^{2+} ions with the coordination of a trigonal pyramid are detected from the spectra in both zeolite types. According to the data obtained for the CuY zeolites, these Ni^{2+} ions may be assumed to be weak magnetic associates which interact by forming hydrogen-bonds between the H_2O molecules, so coordinating these ions in axial positions. The Ni^{2+} ions with an octahedral coordination are observed mainly in the NiY-A zeolites, because they contain an additional 'coordinator', i.e. a bridged oxygen between two Ni^{2+} cations which does not belong to the zeolite framework. These ions form strong magnetic associates. However, they are detected not only from the increased coordination of the exchange cations, but also from the charge-transfer bands. As in the case of the copper-magnesium catalyst [802], a band of this nature has permitted us to detect the strong magnetic associates in the CuNa-Y zeolites. With the NiO-MgO system, Anufrienko *et al.* [526] succeeded in identifying the charge-transfer bands in the range from 39 000 to 36 000 cm^{-1} which are due to strong magnetic associates [855]. It turned out that in pure NiO enlargement of the associates is accompanied by a low-frequency shift of the CTBs up to 32 000 cm^{-1} .

In the spectra of NiY-I zeolite samples, the CTB from the ligand to the metal has a maximum at 35 000 cm^{-1} (see Figure 3.17, spectrum 1). This CTB may be related either to the charge transfer for isolated Ni^{2+} ions or to the charge transfer in the associates which are responsible for the bands of d-d transitions at 13 000 and 26 500 cm^{-1} . From the intensities of the bands of the d-d transitions it can be concluded that the concentration of these complexes is small, and the high energy of the CTB indicates that the complexes are still uncomplicated, and have two to three Ni^{2+} cations. The intensities of the d-d transitions in the spectra of NiY-A zeolites is significantly higher, the intensity of the CTB also sharply increases and the band shifts to lower frequencies, up to 33 600 cm^{-1} (see Figure 3.17, spectrum 2). The decrease in the energy of the

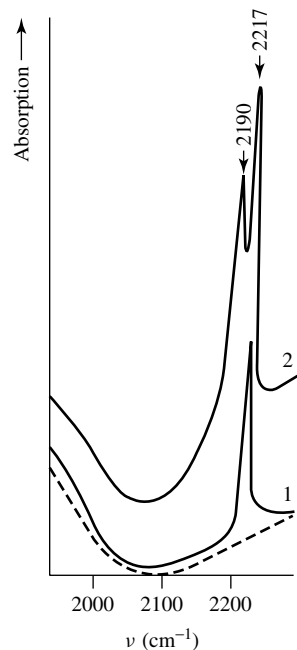


Figure 3.18. IR spectra of CO adsorbed at 293 K on (1) oxidized NiY-I, and (2) NiY/NiO zeolites (the dashed trace represents the background spectrum).

CTB indicates the growth of the associates. This state of the Ni²⁺ zeolites becomes predominant in this zeolite type and determines finally the catalytic properties of the material.

Infrared spectra

The absence of a specific interaction of CO with nickel cations in zeolites containing up to 3 % nickel may be explained by the fact that at low nickel concentrations the cations are located mainly in the S_I sites [855, 860]. In these sites, the oxygen atoms of the zeolite framework ensure an octahedral coordination of the cations. The adsorption of CO on NiY-I zeolites with a nickel content of more than 5 % is accompanied by the appearance of a band at 2217 cm⁻¹ (Figure 3.18, spectrum 2), which has been observed and assigned to CO bound to the cations mainly by σ -bonds [30]. The large shift of ν CO with respect to the gaseous molecule indicates a strong electron-accepting power of the Ni²⁺ cations in the zeolites. The fact that the band at 2217 cm⁻¹ was observed only in those zeolites with high nickel contents could be explained in two ways. It is known that in zeolites with high nickel contents, which were prepared by the procedure for MeY-I zeolites, a portion of the Ni²⁺ cations occupies the positions with a coordination lower than that of the S_I sites. These positions are the S_{IV} and S_{IV'} sites, where three oxygen atoms from the zeolite framework and one oxygen atom of the water molecule (or the hydroxyl group) provide only a tetrahedral coordination of the cations. Therefore, the appearance of a band above 2200 cm⁻¹ can be explained by the interaction of CO with these coordinatively unsaturated Ni²⁺ cations. The second explanation could be as follows. In zeolites analogous to the NiY-I types, the exchange interactions between the cations are observed at nickel contents above 5 %. The formation of such associates was observed earlier by ESR spectroscopy for the CuY zeolites containing more than 2 % copper. In this case, the presence of the 2217 cm⁻¹ band may be explained by the interaction of CO with weak magnetic associates of nickel cations.

The adsorption of CO on the NiY-A zeolites gives rise to bands at 2205 cm⁻¹ (2212 cm⁻¹ at low temperatures) and to maxima in the range from 1200 to 1800 cm⁻¹, which characterize

carbonate–carboxylate structures [855, 857, 860]. In addition to this, a band at 2370 cm^{-1} , which belongs to the CO_2 molecules, is observed. Thus, the interaction of CO with NiY-A zeolites is accompanied by the oxidation of CO to carbonate–carboxylate structures and CO_2 , even at 193 K. This indicates unambiguously that these zeolites contain oxygen of high reactivity. Such active oxygen cannot belong to the zeolite framework (since there are no oxidized complexes of CO on the NiY-I zeolites) and appears to be bound by the nickel cations, i.e. as Ni–O–Ni. The differences in the spectra of CO adsorbed on NiY-I zeolite samples in the range above 2200 cm^{-1} appear to be due also to the presence of reactive oxygen in these samples. The positions of the maxima of νCO at 2212 cm^{-1} and 2205 cm^{-1} indicate that the NiY-A zeolites contain Ni^{2+} centers of higher electronic density than the Ni^{2+} cations in the NiY-I zeolites (2217 cm^{-1}). One can assume that a higher electron density on the Ni cations in the NiY-A zeolites is due to the coordination of nickel by oxygen which does not belong to the framework and where the accepting power of which can be considerably lower than that of the framework oxygen. The band at 2212 cm^{-1} is observed only in the first few moments after the low-temperature adsorption. With time, the intensity of this absorption band decreases and the intensities of the absorption bands of the CO oxidation products increase. The nature of the changes in the spectra, as well as the positions of νCO , permit us to assign the band at 2212 cm^{-1} to the complex which is formed during the interaction of CO with the nickel cations bound to the reactive oxygen. The observed differences cannot be related to the presence of a separate oxide phase on the external surface of the NiY-A zeolite, since only one specific absorption band at ca. 2190 cm^{-1} was observed both on a highly dispersed NiO sample ($210\text{ m}^2\text{ g}^{-1}$) and on NiO/NiY (see Figure 3.18, spectrum 2). This absorption band, also observed for the adsorption of CO on NiO and NiO/SiO₂ [45, 857–859], is due to complex formation between CO and Ni^{2+} ions on the NiO surface. It should be noted that vacuum treatment leads to a faster decrease in the intensity of the absorption band at 2190 cm^{-1} compared with that at 2217 cm^{-1} , which points to a lower stability of the corresponding complex. The lower value of νCO stabilized on the nickel cations in the NiO phase, compared with the NiY-A zeolites, is due to the fact that in the NiO phase the nickel ions are bound to a greater number of active oxygen atoms, different from the zeolite framework oxygen. As a result, the electron density on the Ni^{2+} cations in the NiO phase increases to a greater extent than in the NiY-A zeolites. Thus, the active oxygen in the NiY-A samples can belong neither to the zeolite framework nor to the NiO phase, and is, in fact, a bridged oxygen between Ni^{2+} cations fixed in the zeolite framework (Ni–O–Ni).

The band at 2205 cm^{-1} appears simultaneously with the formation of the carbonate–carboxylate structures and CO_2 . The lowering of the νCO is probably due to the effect of CO_3^{2-} species on the carbonyls. The intensity of this band increases upon moderate heating of the zeolite (up to 373 K) in the presence of CO. More severe reduction of the NiY-A zeolites (CO at 483 K) decreases the intensity of the 2205 cm^{-1} band. After reduction at 673 K, the band disappears and the spectra show bands at 1940, 1970 and $2010\text{--}2070\text{ cm}^{-1}$, which characterize the interaction of CO with metallic nickel. These changes in the spectra, as well as the value of νCO (2205 cm^{-1}), indicate that this absorption band corresponds to CO stabilized on the nickel cations in a different coordination state than that of the initial Ni–O–Ni. Such a state is probably changed due to interaction with the first carbon monoxide molecule. This state of the nickel cations appears as a result of the interaction of CO with strong associates in the NiY-A zeolites at temperatures below 373 K.

Thus, studies of the UV-Vis and infrared spectra of CO adsorbed on NiY-zeolites have shown that the Ni^{2+} cations in the zeolites are stabilized in different states depending on the amount of the transition metal and the conditions of ion exchange. The NiY-I zeolites contain Ni^{2+} cations in the S_I sites, which do not interact with the CO molecules, and coordinatively unsaturated nickel ions coordinated by the zeolite framework oxygen in the S_V and S_{II} sites. In addition to this, the

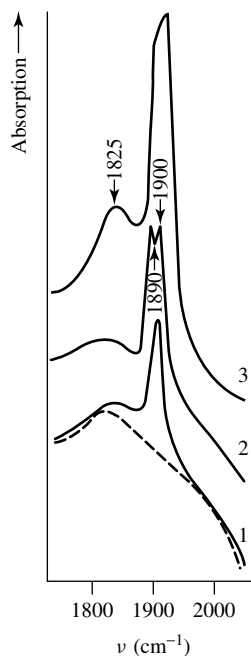


Figure 3.19. IR spectra of NO adsorbed at 293 K on oxidized NiY zeolites: (1) NiY-I; (2) NiY-A; (3) NiO/NiY (the dashed line represents the background spectrum).

NiY-A zeolites contain Ni^{2+} cations bound to oxygens not belonging to the zeolite framework. This oxygen appears to be due to the possibility of hydrolysis upon introduction of the transition metal into the zeolite.

Adsorption of NO on oxidized NiY-I zeolites gives rise to the absorption band at 1900 cm^{-1} (Figure 3.19, spectrum 1) associated with complexes between NO and Ni^{2+} ions. The complex is destroyed by long-term evacuation at 293 K.

In contrast to the results obtained for NiY-I zeolites, the spectra of NO adsorbed on NiY-A zeolites contain two absorption bands at 1900 and 1890 cm^{-1} (see Figure 3.19, spectrum 2). A new band at 1890 cm^{-1} characterizes a NO complex which is less stable than the complex corresponding to the 1900 cm^{-1} absorption band. By analogy with CuY zeolites, a decrease in νNO and the stability of the complex giving the 1890 cm^{-1} absorption may be due to increased covalence or, in other words, the 1890 cm^{-1} absorption band may be assigned to NO complexes with Ni^{2+} ions coordinated by oxygen ions, which do not belong to the zeolite skeleton (strongly associated Ni^{2+} ions). The presence of such ions is shown by UV spectroscopic data on NiY-A zeolites.

Adsorption of NO on NiY zeolites containing NiO crystals on the outer surface (as in bulk NiO) gives rise to an additional absorption band at 1825 cm^{-1} (see Figure 3.19, spectrum 3) which may be assigned to a complex between NO and Ni^{2+} ions formed on the surface of the NiO phase. A similar absorption band has been observed for adsorption on NiO [593]. A substantial decrease in νNO observed in this case (compared with complexes formed on NiY zeolites) may be due to two factors. First, as has been noted above, the covalence of the nickel–oxygen bond increases (or the number of metal–oxygen bonds increases) upon passing from the zeolite to the oxide phase. Secondly, the symmetry of the oxygen environment observed with NO may differ from that characteristic of NiY zeolites. The symmetry of the nearest environment characteristic of Ni^{2+} in dehydrated NiY zeolites is close to tetrahedral (three oxygen ions of the zeolite skeleton and a hydroxyl or a water molecule), as shown in investigations of NiY zeolites by

X-ray analysis [856]. With NiY-A zeolites, there is apparently an oxygen ion common to two Ni^{2+} ions instead of the hydroxyl or H_2O . The most reasonable symmetry for a coordinatively unsaturated Ni^{2+} ion on the NiO surface is that of square pyramidal, since the environment of the Ni^{2+} ions in the bulk of NiO is octahedral. An increase in the number of ligands, in this case, NiO, will substantially decrease the acceptability of the Ni^{2+} ion with respect to the π -electrons of NO and, on the other hand, stabilize the $d-\pi\text{NO}$ electron shift, which should lead to the decrease in νNO . As for $\text{Ni}^{2+}-\text{NO}$ complexes, νNO and the stabilities of the complexes both decrease on passing from the NiY zeolites to the NiO.

The spectrum of CO adsorbed on NiY zeolites reduced in H_2 [860, 861] contains a weak absorption band at 2217 cm^{-1} , indicating that some Ni^{2+} ions remain unreduced even after treatment in hydrogen. New absorption bands which appear at about 2110 and 2145 cm^{-1} are absent for oxidized samples (Figure 3.20). Since there is indirect evidence that metallic nickel is formed in the zeolite under these conditions of reduction [860], it is obvious that a low-frequency absorption band at 2110 cm^{-1} belongs to νCO in the Ni^0-CO complex. The νCO values characteristics of CO adsorbed on metallic nickel applied to non-zeolite carriers or to nickel films do not exceed $2080-2090\text{ cm}^{-1}$ [20]. A higher νCO observed in this case is due to the small size of the metallic nickel particles which are strongly influenced by stabilization sites [860]. The later are commonly considered to be electron accepting in nature and may represent Lewis acid sites (coordinatively unsaturated Al^{3+} ions) in zeolites [860]. The intermediate position of the absorption band at 2145 cm^{-1} between Ni^0-CO and $\text{Ni}^{2+}-\text{CO}$ may point to some intermediate degree of π -bonding between the adsorption site and CO. The Ni^+ ions were, indeed, found in reduced NiY zeolites by using ESR and UV spectroscopy [861, 862], while an absorption band at about 2140 cm^{-1} has also been observed in the IR spectra of such zeolites after CO adsorption.

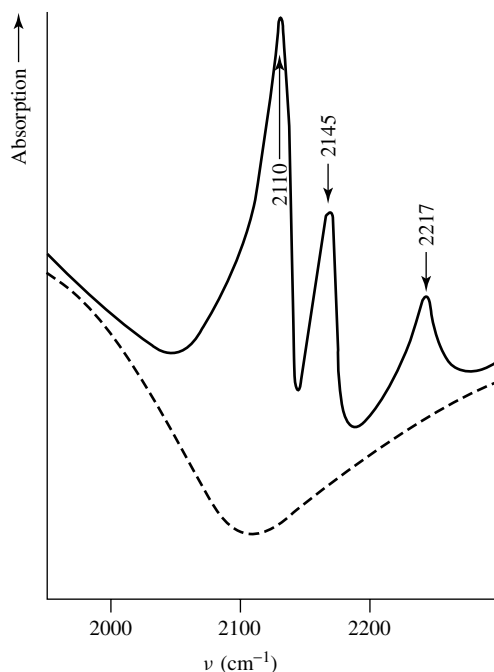


Figure 3.20. IR spectrum of CO adsorbed at 293 K on NiY zeolite, reduced with H_2 (the dashed line represents the background spectrum).

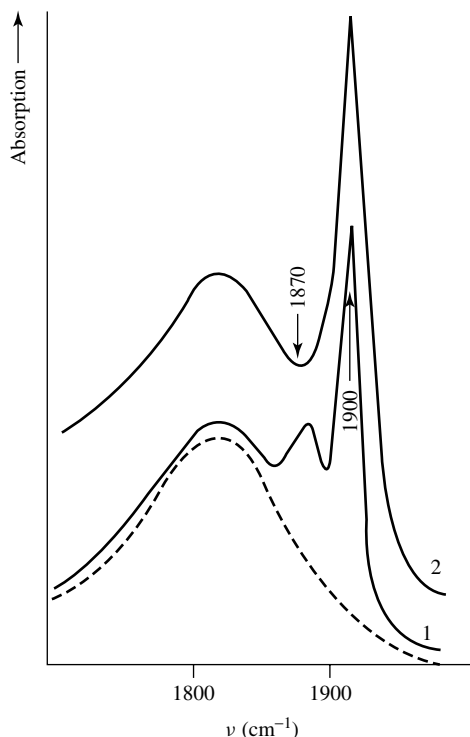


Figure 3.21. IR spectra of NO adsorbed on NiY zeolite reduced with H₂: (1) beginning of adsorption; (2) after 10 min (the dashed line represents the background spectrum).

As for Ni⁺-CO complexes, the absorption frequency of such complexes (2145 cm⁻¹), close to ν CO of the free molecule, appears to be due to the neutralization of the effects of σ - and π -bonding on ν CO.

In addition to an absorption band at 1900 cm⁻¹, adsorption of NO on reduced NiY zeolites gives rise to a weak band at about 1870 cm⁻¹ (Figure 3.21, spectrum 1). The latter band rapidly diminishes and disappears 5–10 min after introduction of NO. The nature of the NO adsorption sites providing the formation of such a complex has not yet been definitely established. The sites may either exist on crystals of metallic nickel or be Ni⁺ ions. In view of the fact that the decomposition of complexes with ν NO at 1870 cm⁻¹ increases the concentration of Ni²⁺-NO complexes (where Ni²⁺ are isolated ions), it is more reasonable to suggest that the absorption band at 1870 cm⁻¹ is associated with Ni⁺ ions, since in the case of metal oxidation in NO the NiO phase is more likely to be formed.

3.2.2 OXIDES

Nickel-containing systems have been studied by carbon monoxide adsorption for a long period of time [857, 858, 859, 863]. ‘Scientific intuition’ allowed Peri [859] to give a detailed interpretation of the IR spectra of Niⁿ⁺-CO complexes, in spite of the absence at that time of separate data on the states (oxidation degrees) of the cations. Based on the analyses of the CO frequencies in the complexes with Ni, the existence of nickel in different oxidation state has been proposed.

A great contributions to the investigation of Ni-containing systems, including UV-Vis NIR reflectance spectroscopy and ESR has been made by Che and co-workers [862]. Following earlier

Table 3.3. Assignment of bands of carbon monoxide stretching vibrations in species formed after the adsorption and desorption of carbon monoxide on partially reduced Ni/Al₂O₃, Ni/HY_{deal} and Ni/NaX [863]. Reprinted from *Appl. Catal. A: General*, **95**, Kubelkova, L., Novakova, J., Jaeger, N. I. and Schulz-Ekloff, G., 'Characterization of nickel species at Ni/γ-Al₂O₃ and Ni/faujasite catalysts by carbon monoxide adsorption', 87–101, Copyright (1987), with permission of Elsevier Science.

Species	ν (cm ⁻¹) ^a			
		Ni/γ-Al ₂ O ₃	Ni/HY _{deal}	Ni/NaX
<i>Adsorption</i>				
Ni _x ⁰ -CO	Linear	2050–2060 (w)	2050–2060 (w)	–
	Bridged	1940–1950 (w)	1950 (w)	–
Ni ^{δ+} -CO	Linear	2082 (m)	–	–
Ni ^{δ+} -(CO) ₂ bicarbonyl	–	–	2100, 2140 (m)	–
Na ⁺ , (Ni ⁺)-CO	–	–	–	2168 (w)
NiO, Ni ²⁺ -CO	–	2180 (w)	–	2180 (w)
Al(Lewis)-Ni ²⁺ -CO	–	–	2205, 2215 (w)	–
Ni(CO) ₄	–	2057 (s)	2053 (s)	1990 (s), 2022 (s), 2068 (sm), 2136 (w)
<i>Desorption</i>				
Ni _x ⁰ -CO	Linear	2060 (w)	2050 (w)	–
	Bridged	1942 (w)	1940 (w)	–
Ni ^{δ+} -CO from bicarbonyl	–	–	2118 (m)	–
Polynuclear carbonyls	–	–	–	1982, 2068 (w), 1812, 1835 (w), 1875 (w)

^as, strong; m, medium; w, weak.

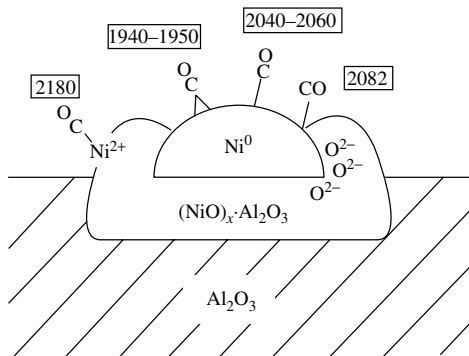


Figure 3.22. Schematic of carbon monoxide adsorption on NiO clusters on alumina, including wavenumbers (cm⁻¹) of vibrations of individual carbon monoxide complexes according to Kubelkova *et al.* [863]. Reprinted from *Appl. Catal. A: General*, **95**, Kubelkova, L., Novakova, J., Jaeger, N.I. and Schulz Eklof, G., 'Characterization of nickel species at Ni/γ-Al₂O₃ and Ni/faujasite catalysts by carbon monoxide adsorption', 87–101, Copyright (1987), with permission of Elsevier Science.

studies [857–861], the conditions of the Ni⁺ ions formation (unusual states in the case of Ni) on the surfaces of different heterogeneous systems has been detected [864] and the role of such nickel ions in oligomerization processes has been established. A scheme of the interpretation of the CO complexes with nickel in different oxidation state has been suggested by Kubelkova *et al.* [863] (Table 3.3 and Figure 3.22.). This scheme, based on infrared spectroscopic measurements, is similar to that presented earlier by Davydov and co-workers [30, 807, 855, 860].

Solid solutions of NiO–MgO as well as CuO–MgO are very interesting and have been very well investigated [30, 484]. As well as a NiO phase, they are easily reduced upon interaction with CO to a state close to the metal one, as follows from the similarity of the spectra of adsorbed CO on both reduced and oxidized samples. It was shown that two-dimensional clusters of NiO are under influence of the basic support reducing the effective charge of nickel. The data on CO interactions with both NiO–MgO and CuO–MgO solid solutions had been examined earlier [30]. Zecchina and co-workers [484], who also studied this system, obtained the following main results: (i) isolated Ni^{2+} ions emerging on the (100) face of the micro crystals do not react with CO at room temperature and form stable Ni^{2+} –CO adducts only at low temperatures; (ii) Ni^{2+} ions located on edges, steps and other defects are slowly reduced by CO at room temperature with the formation of carbonate species and a $[(\text{CO}_3)\text{Ni}(\text{CO})_2]^{2-}\text{Mg}^{2+}$ complex adsorbed on $\text{Mg}^{2+}\text{O}^{2-}$ pairs; (iii) clustered Ni^{2+} ions are more readily reduced than isolated ones and give rise to binuclear and polynuclear zero-valent carbonyls; (iv) the same binuclear and polynuclear species are generated by CO abstraction at room temperature from adsorbed $\text{Ni}(\text{CO})_4$ – the process is totally reversible and the mononuclear species are readily regenerated upon exposure to CO. Support for the above comes from studies of the reduced samples [30, 484], when the same complexes were observed. The data cited above show that the nickel ions are fully reduced upon interaction with CO, and even the formation of metallic clusters takes place. This fact shows the unsuitability of this molecule as a probe in the case of Ni-containing systems. It seems to be better to use the NO molecule instead of CO. In fact, the spectra of NO adsorbed on such systems are quiet characteristic. Thus, bands at 1760 and 1790 cm^{-1} are observed in the spectrum of NO adsorbed on NiO–MgO (10 wt% NiO), which indicate that two complexes of Ni^{2+} –NO are formed. Taking into consideration the presence of two types of Ni^{2+} ions (isolated and associated Ni–O–Ni), the bands observed can be connected with νNO in the complexes with such cations. Comparison of νNO observed in the case of NiO (1805 cm^{-1}) and NiY zeolite (1900–1890 cm^{-1}) with those of NiO–MgO shows a significant decrease of νNO in the latter system. This could be due to (i) an increase in the covalence of the M–O bond in the zeolite towards that in the oxide, or (ii) a change in symmetry of the oxygen surrounding the nickel ions, which is close to tetrahedral for zeolites and tetragonal pyramidal for both NiO and solid solutions.

Nickel supported on TiO_2 , unlike the other above examined systems, is not so easily reduced, and only the band at 2190 cm^{-1} is observed in its spectrum. This is probably due to the predominant presence in the samples of isolated Ni^{2+} ions and shows the absence of sites of the type Ni–O–Ni [826]. At the least, the electronic spectrum of Ni/ TiO_2 shows three absorption bands, with maxima at 25 640, 18 870 and 16 670 cm^{-1} (390, 530 and 600 nm). These bands are typical of hexa-co-ordinated Ni^{2+} ions and can be assigned to ${}^3\text{A}_2(\text{F}) \rightarrow {}^3\text{A}_2$ ${}^3\text{E}(\text{P})$, ${}^3\text{A}_2(\text{F}) \rightarrow {}^3\text{E}(\text{F})$ and ${}^3\text{A}_2(\text{F}) \rightarrow {}^3\text{A}_2(\text{F})$ transitions, respectively [826].

3.3 Co-containing systems

3.3.1 ZEOLITES

The properties of divalent cobalt ions exchanged into type-A zeolites have been intensively studied (see, for example, their description in Delgass *et al.* [25]). There are the bands at 9000, 21 000 cm^{-1} in the UV spectra of hydrated CoNa–A zeolites. These bands are similar to those obtained for hexaaqua complexes $[\text{Co}(\text{H}_2\text{O})_6]^{2+}$ with weakly distorted tetrahedral structures. A complete dehydration causes the corresponding changes in the spectra: new electronic bands centered at 7000, 16 000, and 25 000 cm^{-1} have replaced the bands at 9000 and 2100 cm^{-1} ($\text{Co}(\text{II})6\text{H}_2\text{O}$). Co^{2+} ion occupies the D_{3h} site or near that symmetry. In zeolite structures of the faujasite type, coordination on oxygen occurs in S_{II} , S_{IV} , S_{I} sites by three oxygen atoms of the hexagonal window of the cubooctahedron, and additionally by oxygens from the H_2O or OH group.

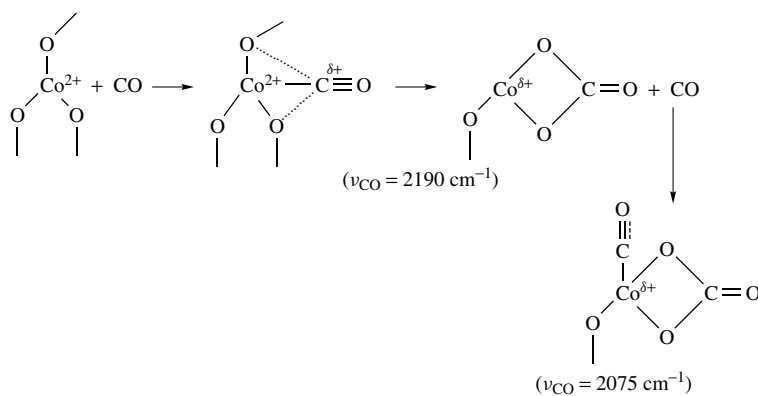
Angell [644] had earlier showed that CO molecules can be used as a probe to reveal bivalency in exchanged cations located in the large cavities of zeolite structures. After CO adsorption on CaCo-Y zeolites, two absorption bands were observed at 2193 cm^{-1} ($\text{Ca}^{2+}\text{-CO}$) and 2190 cm^{-1} ($\text{Co}^{2+}\text{-CO}$) and attributed to the interactions of CO with cations located in S_{II} positions. The existence of two bands in the 2200 cm^{-1} region upon CO adsorption on both CaNa-X and CoNa-X zeolites showed that Co and Ca cations located in different fixed places interact with CO. Since CO molecules cannot percolate into the small cavities of zeolites, this seems to suggest that the 2203 cm^{-1} band in CaNa-X and the 2200 cm^{-1} band in CoNa-X are due to the interactions of CO with Co and Ca cations located in the small zeolite cavities at six-membered oxygen 'windows'. Tetrahedral coordination is the most characteristic for Co, in comparison with all transition metals, and can be realized in a large cavity upon the fixation of cations, for example in S_{II} sites.

By using the spectra of adsorbed CO, it has been established that during dehydration of zeolites, the Co cations (when the exchange degree is $<33\%$) move from large cavities into sodalite units and hexagonal prisms of zeolite. The existence of two bands in the 2200 cm^{-1} region upon CO adsorption provides evidence that CO interacts with M^{2+} cations located in different positions.

When Co^{2+} is exposed to carbon monoxide, the 25000 cm^{-1} band disappears, while the 16000 cm^{-1} band shows enhanced splitting on the high-energy side and decreased splitting on the low-energy side. The observed phenomena can be explained by the change in environment of Co^{2+} , induced by an adsorbed CO molecule, from near D_{3h} to T_d , similar to that observed for the interaction of Co^{2+} with hydrocarbons molecules [25].

3.3.2 OXIDES

Cobalt ions bound by oxygen which does not belong to the carrier (two-dimensional oxide composition of cobalt), are easily reduced to the metallic state upon interaction with Co. In the case of solid solutions of CoO–MgO, the spectra of CO adsorbed on oxidized and reduced samples were identical, thus providing a demonstrative example. Zecchina and co-workers [484, 485], have observed both the main peak at 2015 cm^{-1} due to CO linearly bound (on top) to cobalt, and three low-frequency bands at 1660 , 1330 and 1015 cm^{-1} . Minor weak features at $2125\text{--}2075\text{ cm}^{-1}$ are likely to be associated with CO adsorbed on positively charged centers (unreduced Co^{2+} ions), the fraction of which, according to a comparison with the spectra of CO adsorbed on MgO–CoO solid solutions [484, 485], is very small. These data are in good agreement with the infrared features of CO adsorbed on other cobalt-containing oxide systems [242, 243], see, for example, Co_3O_4 , as follows:



Scheme 3.3

In contrast to the other above-examined systems, Co^{2+} supported on TiO_2 [826] is not easily reduced by CO similar to the case of Ni/TiO_2 , and there is only a band at 2190 cm^{-1} . This seems to be connected with the predominant existence of isolated Co^{2+} ions which occur (before dehydration) as octahedrally coordinated states. There are no Co–O–Co states according to these data. The spectrum of Co/TiO_2 also has three absorption bands, with their maxima being at $23\,700$, $18\,590$ and 1710 cm^{-1} (422 , 538 and 588 nm). Again, this spectrum is characteristic of hexa-coordinated tetragonal Co^{2+} complexes. The respective transitions are ${}^4\text{T}_1(\text{F}) \rightarrow {}^4\text{A}_2(\text{P})$, ${}^4\text{T}_1(\text{F}) \rightarrow {}^4\text{E}(\text{P})$ and ${}^4\text{A}_2(\text{F}) \rightarrow {}^4\text{B}_1(\text{F})$. Reduced states of both Co and Fe observed by CO adsorption under conditions leading to the formation of alloy-like compounds between these elements, and also for the compound with a support, have been examined by Davydov and Coville [864] by means of diffuse reflectance IR spectroscopy. It is well known that such samples strongly lose their transmission upon reduction, and there is not the possibility to study such systems by means of the transmission method. A mutual influence of the components was discovered, i.e. iron was found to promote reduction of cobalt. Similar results have been obtained during an IR spectroscopic study of the interaction between CO and the oxidized surface of mono-metallic and potassium-promoted Fe–Al–O and Co–Al–O systems. It has been shown that at 300 K cobalt oxide deposited on $\gamma\text{-Al}_2\text{O}_3$ is partially reduced by CO with the formation of quasi-isolated atoms of Co^0 . For samples of both oxides modified by potassium, reduction with the formation of surface metallic clusters under the same conditions occurs [865]. The influence of potassium on the reduction of Zn–Cr–O catalyst has also been pointed out [193]. In the case of cobalt aluminate, according to the data from CO adsorption, cobalt is more influenced by the support. A uniform distribution of cobalt cations in Al_2O_3 is achieved, and there are no clustered oxide species, such as a cobalt oxide–semioxide phase, at the surface. In effect, the latter are already readily reduced upon CO admission at room temperature, as shown by the appearance of low-frequency absorption bands at $\nu\text{CO} < 2100\text{ cm}^{-1}$ due to $\text{Co}^{\delta+}\text{-CO}$ carbonyl complexes with an oxidation extent of cobalt cations less than $+1$ [184, 185, 866]. Admission of CO on CoAl_2O_4 leads to the appearance of the absorption band at 2175 cm^{-1} in the spectrum, which can be assigned to the carbonyl complex stabilized on Co^{2+} [866–871] (Table 3.4). In this case, the appearance of metallic Co is observed only after strong reduction in hydrogen. As shown from this table, copper incorporation significantly decreases the temperature of the cobalt reduction as indicated by the IR spectra of adsorbed CO.

The IR spectra of CO adsorbed at 77 K on ZnO ‘ex-carbonate’ (and for comparison with ZnO Kadox) on CoO and on Co–ZnO solid solutions (containing 0.05 mole fraction of CoO) have been investigated [872a]. By diluting the cobalt ions within a ZnO matrix, a model solid has been designed where the Co^{2+} ions (which have a d^7 configuration and frontier orbitals with d character) emerge from the surface with the same ionicity and coordinative situation as Zn^{2+} (d^{10} configuration and frontier orbitals without any d character). Consequently, the observed differences in the CO stretching vibrations of the $\text{Zn}^{2+}\text{-CO}$ and $\text{Co}^{2+}\text{-CO}$ surface complexes has been ascribed to differences in the $d\text{-}\pi^*$ overlap contributions. The increased $d\text{-}\pi^*$ overlap effects are also responsible for the strong increase in the permanent ($\mu^{(00)}$, $\mu^{(11)}$) and transition ($\mu^{(01)}$) dipole moments of CO adsorbed on Co^{2+} in ZnO, in comparison with Co^{2+} in the MgO matrix or of CO adsorbed on ZnO and MgO. An interaction of the supported metal cobalt with CO molecules has also been analyzed by means of IRS (see, for example [872b–872n]).

In the case of Co-supported systems [916], the addition of Pd causes the oxidation of coordinatively unsaturated Co^{2+} ions to Co^{3+} . In the IR spectrum of adsorbed CO, a decrease in intensity of the band at 2160 cm^{-1} (Pd^{2+}) is accompanied by a simultaneous appearance of the 2185 cm^{-1} band due to $\text{Co}^{2+}\text{-CO}$. This fact shows that upon weak reduction of Pd–Co systems by CO, the binuclear complex $\text{Co}^{3+}\text{-O-Pd}^{2+}$ can be formed [916]. Addition of Ce, as well as Co, leads to a decrease of the Pd^+ ions loading in $\text{Pd/Al}_2\text{O}_3$. Upon reduction by CO, the luminescence bands

Table 3.4. Spectral features of carbon monoxide in carbonyl complexes formed upon CO adsorption on cobalt-containing catalysts with different degrees of reduction.

Treatment conditions	νCO (cm^{-1})	Nature of the center of CO adsorption
<i>CoAl₂O₄ system</i>		
Oxidized	2175	Co ²⁺
Reduced in H ₂ at 473–673 K	2175	Co ²⁺
Reduced in H ₂ at 723–773 K	2175	Co ²⁺
	2065, 2010–1990	Co ^{δ+} , Co ⁰
<i>Cu_{0.5}Co_{0.5}Al₂O₄ system</i>		
Oxidized	2120–2125	Cu ⁺
Reduced in H ₂ at 473 K	2100–2090	Cu ^{δ+}
	1950	Co ⁰ (small particles)
Reduced in H ₂ at 573 K	2090	Cu ^{δ+}
	1950	Co ⁰
Reduced in H ₂ at 773 K	2105	Cu ⁰
	2000–1955	Co ⁰ (large particles)

(27 780, 23 260 and 20 830 cm^{-1} (360, 430 and 480 nm)) and the absorption band (31 250 cm^{-1} (320 nm)) due to Ce³⁺ [916] appear. Alloy formation affects both the intensities and frequencies of the absorption bands of linear adsorbed CO [982], for instance, the presence of Cu in a Ni–Cu alloy significantly increases the reactivity of chemisorbed oxygen in reaction with CO.

3.4 Iron-containing systems

3.4.1 ZEOLITES

Nitric oxide

Nitric oxide adsorption on Fe³⁺-Y zeolites gives rise to a weak absorption band at ca. 1880 cm^{-1} with a shoulder at 1830 cm^{-1} (Figure 3.23(a), spectrum 1). The absorption band at 1830 cm^{-1} disappears at 373 K in the NO atmosphere, whereas that at 1880 cm^{-1} is removed only after treatment at 423 K. Nitrous oxide adsorption on Fe²⁺-Y zeolites gives rise to intense absorption bands at 1825 and 1880 cm^{-1} , a weak band at 1930 cm^{-1} and a shoulder at 1780 cm^{-1} (Figure 3.23(a), spectrum 2). An increase in either the temperature or time of the vacuum treatment at 293 K cause the absorption bands at 1930 and 1825 cm^{-1} to diminish, whereas that at 1780 cm^{-1} is enhanced (Figure 3.23(a), spectrum 3). The absorption bands at 1780 and 1880 cm^{-1} are removed by prolonged evacuation (1 h) at 293 K. Heating Fe²⁺-zeolites in NO decreases the intensity of all of the absorption bands [30, 874a].

Absorption bands due to NO adsorbed on Fe-Y zeolites are much more intense in the case of Fe²⁺-Y zeolites and belong to complexes between NO and Fe²⁺ ions. For NO adsorption on Fe²⁺-Y zeolites, their appearance may be due to partial reduction of Fe³⁺ ions. Adsorption of NO on Fe²⁺-Y zeolites has been studied by ESR and IR spectroscopies [873], with the IR spectroscopic data obtained being similar to those presented above. Based on this spectroscopic data, the absorption bands at 1880 and 1780 cm^{-1} have been ascribed to high- and low-spin Fe²⁺-NO complexes, respectively [873]. The position of νNO in the complexes under consideration does not contradict this assignment. Indeed, studies of nitrosyl complexes by γ (Mössbauer)-spectroscopy has revealed that low-spin ions tend to delocalize electrons strongly on the π -orbitals of ligands, which is not characteristic of high-spin ions [30, 873]. For the NO molecule, this is the π -orbital,

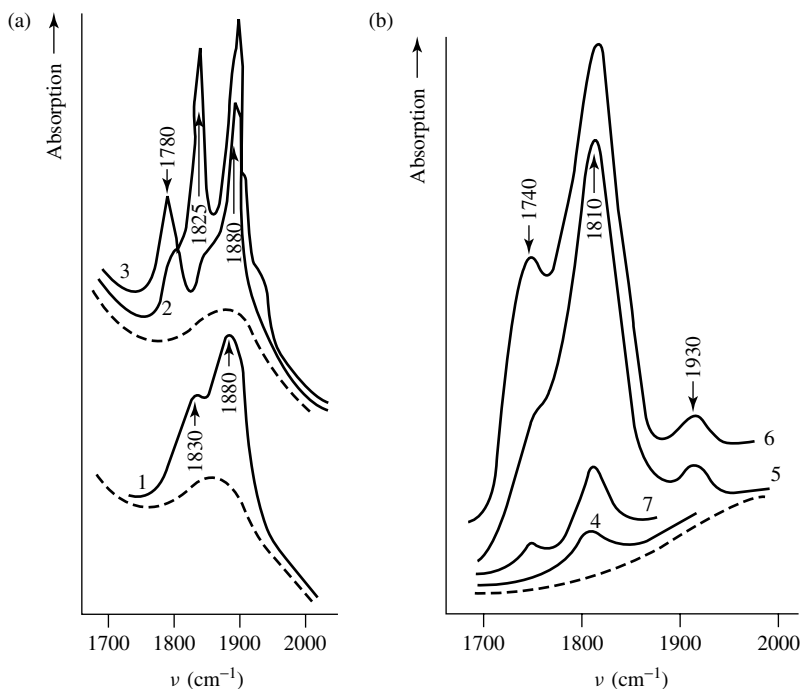


Figure 3.23. IR spectra of NO adsorbed on (a) Fe-Y zeolites, and (b) $\text{Fe}_2\text{O}_3/\text{Al}_2\text{O}_3$: (1, 4) adsorption at 293 K on oxidized samples; (2) adsorption at 293 K on reduced samples; (3) heating in NO at 373 K; (5) treatment *in vacuo*; (6) adsorption on samples reduced in CO at 523 K; (7) adsorption on samples reduced in H_2 at 773 K.

and an increase in the electron density in this orbital should decrease νNO for the complexes. In view of these findings, an interpretation of the absorption bands at 1780 and 1880 cm^{-1} proposed by Jermyn *et al.* [873] seems to be more reasonable. It is known from coordination chemistry that iron complexes exist in which the spin states of the central atoms can be reversibly changed depending on the ambient conditions (temperature and pressure). Here, however, this is not the case as no high-spin/low-spin interconversion has been shown to occur with the Fe^{2+} -NO complexes. The formation of complexes of the two types appears to be due to different states of the (iron) ions in the zeolite skeleton. Presumably, the high-spin complexes are formed with Fe^{2+} ions located in the large cavities of the zeolite (S_{II} and S_{III} sites) and low-spin complexes are formed in S_{I} and S_{II} sites.

No analogues have been found in ESR spectra corresponding to the IR absorption bands at 1820 and 1930 cm^{-1} . They can, however, be interpreted on the basis of γ -spectroscopic data [30, 491] which indicate that two states of ions exist in Fe-Y zeolites, referred to as the *ionic* and *covalent* states. The covalent ions have been interpreted in terms of structures such as Fe-O-Fe containing a bridge oxygen between the iron atoms which does not belong to the zeolite skeleton. Such states are identical with strongly associated ions considered in the case of Cu-Y and Ni-Y zeolites. The probability of the formation of strongly associated states in Fe-Y zeolites is very high, since the hydrolysis of the iron salt on introducing the iron into the zeolite is almost unavoidable in the pH range where the zeolite skeleton is not destroyed. The Fe^{2+} ions in such a state, and their complexes with NO, should not be detectable by ESR spectroscopy owing to strong exchange interactions through the bridge oxygen in Fe-O-Fe. Since the paramagnetic NO

complexes identified by Jermyn *et al.* [873] accounted for only ca. 20 % of the iron introduced, most of the Fe^{2+} ions may be present in the strongly associated form, and the absorption band at 1820 cm^{-1} can be assigned to NO complexes with these ions. Assuming the complexes of such a type to be high-spin, a lower νNO and stability observed in this case, compared with the high-spin complex with isolated ions (1880 cm^{-1}), may be accounted for in the same way as was done when considering the $\text{Cu}^{2+}-\text{NO}$ and $\text{Ni}^{2+}-\text{NO}$ complexes (an increase in the covalence of the bond with oxygen, resulting in a decrease in coordinative unsaturation, νNO and stability).

The position of the absorption band at 1930 cm^{-1} is too high to be assigned to complexes with Fe^{2+} ions. Absorption in this region is more characteristic of nitrosyl complexes of Fe^{3+} such as $[\text{Fe}(\text{CN})_5\text{NO}]^{2-}$, which have an absorption band at 1940 cm^{-1} in the νNO stretching region. However, if Fe^{3+} ions are the adsorption site, an intensity of the absorption band at 1930 cm^{-1} in the spectra of Fe^{3+} zeolites would be very high, which is not observed in experiments. It may be suggested that the absorption sites are associated, for example, as $\text{Fe}^{2+}-\text{O}-\text{Fe}^{3+}$. A low intensity of the absorption at 1930 cm^{-1} in the spectra of both $\text{Fe}^{3+}-\text{Y}$ and $\text{Fe}^{2+}-\text{Y}$ zeolites may be due to the domination of Fe^{3+} ions in the former and Fe^{2+} ions in the latter, with the probability of the formation of states such as $\text{Fe}^{2+}-\text{O}-\text{Fe}^{3+}$ being low in both cases. A similar absorption band is observed for NO adsorption on $\text{Fe}_2\text{O}_3/\text{Al}_2\text{O}_3$ where the formation of states [491] of a similar nature should be far more probable. The frequencies and interpretations of the absorption bands observed in the spectra of NO adsorbed on Fe-Y zeolites are summarized in Table 3.5.

CO adsorption on $\text{Fe}^{3+}-\text{Y}$ zeolites gives rise to weak absorption bands at 2200 , 1450 and 1545 cm^{-1} (Figure 3.24, spectrum 1). Heating in a CO atmosphere at 673 K increases their intensities and gives rise to an additional absorption band at $2350-2370\text{ cm}^{-1}$ (Figure 3.24, spectrum 2). The spectra of CO adsorbed on the $\text{Fe}^{2+}-\text{Y}$ zeolite contain an absorption band at 2200 cm^{-1} (Figure 3.24, spectrum 3) with an intensity much higher than that observed for $\text{Fe}^{3+}-\text{Y}$. Absorption bands at 1450 and 1545 cm^{-1} arising from the interaction between CO and $\text{Fe}^{3+}-\text{Y}$ zeolites (Figure 3.24, spectrum 2) belong to oxidized complexes of the carbonate or carboxylate type. Carbonates and CO_2 are not formed in the case of CO adsorption on the $\text{Fe}^{2+}-\text{Y}$ zeolite. Therefore, their formation upon the interaction between CO and $\text{Fe}^{3+}-\text{Y}$ zeolites indicates that CO oxidation occurs and is associated with the reduction of Fe^{3+} ions. An increase in the intensity of the absorption band at 2200 cm^{-1} observed under these conditions should naturally be attributed to CO complexation with Fe^{2+} ions formed by the reduction of Fe^{3+} . The existence of an intense absorption band at 2200 cm^{-1} in the case of $\text{Fe}^{2+}-\text{Y}$ zeolites confirms this conclusion. Data for CO adsorption demonstrate that Fe^{2+} ions in the zeolites are involved in the formation of only one complex, $\text{Fe}^{2+}-\text{CO}$, whereas NO is present in complexes of three types. There may be two factors responsible for this difference between CO and NO. First, when in the strongly associated state, iron ions may be unable to form complexes with CO because of the weaker electron-accepting properties compared with those of isolated Fe^{2+} ions. This apparently is why CO is not adsorbed on Fe^{3+} ions and the $\text{Fe}_2\text{O}_3/\text{Al}_2\text{O}_3$ surface, whereas NO does not form surface complexes. Secondly, CO molecules fail to penetrate into small cavities of the zeolites, which rules out the possibility of complexation with ions stabilized in these cavities [874a].

Table 3.5. Types of sites in iron-containing catalysts identified from spectral features of adsorbed NO.

νNO (cm^{-1})	Site type
1930	$\text{Fe}^{2+}-\text{O}-\text{Fe}^{3+}$
1875	Fe^{2+} in small cavities, high-spin complex
1825	$\text{Fe}^{2+}-\text{O}-\text{Fe}^{2+}$
1780	Fe^{2+} in large cavities, low-spin complex

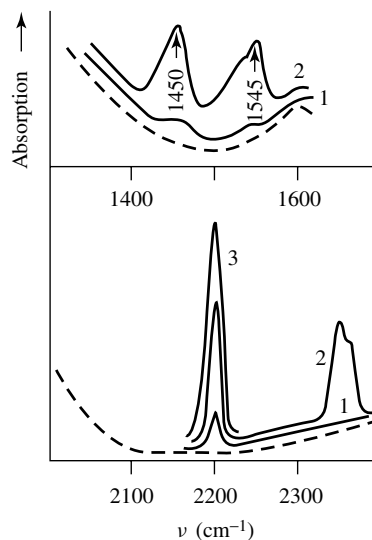


Figure 3.24. IR spectra of CO adsorbed on Fe-Y zeolites: (1) Fe³⁺-Y, CO adsorption at 293 K; (2) subsequent heating in CO at 673 K; (3) Fe²⁺-Y, CO adsorption at 293 K (the dashed lines represent the background spectra).

3.4.2 OXIDES

Only a weak absorption at 1830 cm⁻¹ is observed in the spectra of NO adsorbed on Fe₂O₃/Al₂O₃ treated in an oxidizing atmosphere (see Figure 3.23(b), spectrum 4). With a specimen treated *in vacuo*, or in CO, an intense absorption band at ca. 1810 cm⁻¹ and bands at 1930 and 1740 cm⁻¹ are observed after NO adsorption (see Figure 3.23(b), spectrum 5). All of the absorption bands are removed by vacuum treatment at 293 K, with the most stable being the complex with νNO at 1810 cm⁻¹. It is firmly argued that the absorption bands at 1740 and 1810 cm⁻¹ belong to NO complexes with Fe²⁺ ions and that the latter correspond to a complex with an absorption at 1825 cm⁻¹ for NO in zeolites [874a]. A similar complex have been observed after NO adsorption over Fe₂O₃ [595]. The interaction of supported metal iron with CO molecules has also been extensively analyzed by means of IRS (see, for example [874a–874h]).

3.5 Silver-containing systems

Electronic spectra

Electron spectroscopic studies of Ag-containing systems indicates that the DRES method is effective for the investigation of silver states in bulk and supported samples. A study of the electron spectra of silver in solutions and in inert gas media shows that the atoms, ions and clusters of silver have a number of characteristic absorption bands in the UV-Vis region. Thus, the bands at 52 630–43 480 cm⁻¹ (190–230 nm) were attributed to the 4d¹⁰ → 4d⁹5s¹ transition in Ag⁺ [875], and a set of bands in the 40 000–30 300 cm⁻¹ (250–330 nm) range has been ascribed to the 4d¹⁰5s¹ → 4d⁹5s¹5p¹, 4d¹⁰5s¹ → 4d⁹5s¹6p¹ or 5s¹ → 5p¹ transitions in Ag⁰ [876–878]. The possibility of using the pure spectra of metal silver which shows changes depending on its degree of clustering is a significant advantage of silver-containing systems. The clusters (*n* < 7) are considered as multi-atomic molecules with s → s* and n → s* transitions between the molecular orbitals corresponding to the bands at 30 300–27 800 cm⁻¹ (330–360 nm) and

Table 3.6. Interpretation of Absorption Bands in Electronic Spectra of Supported Silver.

Absorption bands, nm	Transition's nature	Assignment
190–230	$4d^{10} - 4d^5 5s^1$	Ag^+
250–330	$4d^{10} 5s^1 - 4d^9 5s^1 5p^1$; $4d^{10} 5s^1 - 4d^9 5s^1 6p^1$	Ag^0
330–360; 440–540	Multiatomic molecules with s-s* and n-s* transitions between the molecular orbitals	Ag_n clusters
350–380		Ag clusters ~ 1 nm
400–500 (> 10 nm)	Conduction of plasma resonance absorption	Large clusters
310–320	Intrinsic photo effect	Large particles and metallic films

22 700–18 500 cm^{-1} (440–540 nm), respectively [879–881]. Bands in the 28 600–2630 cm^{-1} 350–380 cm^{-1} region were attributed to silver clusters with sizes of around 1 nm [879]. In large silver clusters (>10 nm) and crystallites, there is light absorption by the collective electrons of conduction plasma resonance absorption at 25 000–20 000 cm^{-1} (400–500 nm) [882, 883]. Large particles and metallic films of silver have a band at 32 300–31 750 cm^{-1} (310–315 nm) associated with the intrinsic photoeffect. When studying supported Ag-containing systems by the DRES method, the above interpretation of the silver absorption bands are usually used. However, metal–support interaction is accompanied by charge transfer which influences the positions and intensities of the silver bands.

An analysis of the electron states of silver on different supports has been made [888–894], on the basis of the above data (Table 3.6). The character of the diffuse reflectance spectra depends on the distribution of Ag particles according to size, which is specified by the preparation method, the Ag content, and the specific surface of the support. In the case of samples in which the contribution of the Ag particles of size 1–7 nm is high, structureless absorption was observed. When particles with dimensions ranging from a few to several tens of nanometers predominate, the bands of the plasma resonance absorption of the Ag crystallites are observed in the 28 600–24 400 cm^{-1} (350–410 nm) range. In the case of samples containing coarsely dispersed silver with particles measuring more than 100 nm, an absorption band caused by the internal photoeffect of such particles is observed at 32 400–31 750 cm^{-1} (310–315 nm). The spectra of samples treated with nitric acid, in which the contribution of the tiny Ag particles is large, display absorption bands at 30 300 cm^{-1} (330 nm) and above, which have been assigned to silver clusters measuring about 1 nm on the basis of data from the small-angle scattering of X-rays [889, 893]. Silver particles in such a catalyst, characterized by the band at 31 250 cm^{-1} (320 nm), are isolated and predominantly <1 nm silver clusters, which are insoluble in HNO_3 but are oxidized in air.

The band at 31 750 cm^{-1} (315 nm) observed in all samples (Figure 3.25) has been attributed to large aggregates and a surface film of silver (electron inter-zonal transitions and intrinsic photoeffect). The support does not cause an effect in the electronic properties of large particles of the metal, so the position of this band in the same for all samples (including the bulk silver film). An intense band at 21 750 cm^{-1} (460 nm) is present in the spectrum of Ag/SiO_2 (see Figure 3.25, spectrum a) [894]. In accordance with Bogdanchikova *et al.* [891, 893], this signal may be attributed to plasma resonance absorption of large clusters and crystallites of silver (>10 nm). In some studies [895], the bands at 41 670–25 000 cm^{-1} (240–400 nm) are attributed to d–d electron transitions in Ag^{2+} and Ag^{3+} ions in a regular octahedral environment by oxygen ions in the support lattice. However, such an interpretation has been given without sufficient proof.

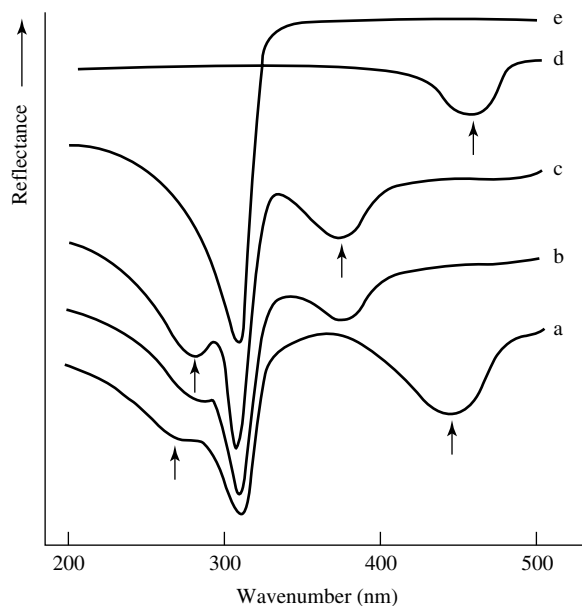


Figure 3.25. Diffuse reflectance electron spectra of different samples of silver-containing systems: (a) 10 wt% Ag/SiO₂; (b) 10 wt% Ag/Al₂O₃; (c) 10 wt% Ag/aluminosilicate; (d) 0.03 wt% Ag/CaO; (e) Ag film.

In the case of Ag/CaO, a band at $20\,850\text{ cm}^{-1}$ (480 nm) has been observed. In Kharlamov *et al.* [890] the ESR spectra indicated the presence of only Ag²⁺ ions isolated in the CaO lattice. That is why this band can be attributed to d–d electron transitions in Ag²⁺ ions in a regular octahedral environment by oxygen ions in the CaO lattice. Hence, the absorption ranges of the Ag²⁺ d–d transitions and the plasma resonance absorption of Ag particles partially overlap one another. However, highly charged Ag²⁺ and Ag³⁺ ions are not detected by the DRES method in Ag/support samples. Thus, there are no reasons to assign the bands in the $33\,300\text{--}20\,000\text{ cm}^{-1}$ (300–500 nm) region to silver ions with higher degrees of oxidation, as had been supposed [895]. As for Ag/Al₂O₃ and Ag/Al₂O₃:SiO₂, there are bands in the $35\,700\text{--}34\,500\text{ cm}^{-1}$ (280–290 nm) and $27\,000\text{--}25\,650\text{ cm}^{-1}$ (370–390 nm) regions which are usually attributed to $s \rightarrow s^*$ and $n \rightarrow s^*$ electron transitions in Ag_{*n*} clusters ($n = 2\text{--}7$).

It is necessary to note that the absorption bands at $41\,700\text{ cm}^{-1}$ (240 nm) correspond exactly to the isolated Ag⁺ ions, as in the spectra of bulk Ag₂O and AgNO₃ no bands at $45\,500\text{--}33\,300\text{ cm}^{-1}$ (220–300 nm) are observed.

IR spectra

From IR spectroscopic studies of adsorbed CO, it has been ascertained that the Ag⁺ state is very stable on supported silver catalysts and there exists a strong donor–acceptor interaction of the carriers and the supported Ag⁺ ions, accompanied by a change in the effective charge of Ag^{δ+} (Figure 3.26). The neighbors of silver in its sub-group, i.e. gold and copper, also show a stable oxidation state of 1+, but shift to high-charge Cu²⁺ and Au³⁺ states relatively easily.

As Figure 3.26 demonstrates, Ag⁺ cations supported on aluminosilicate have the highest νCO and, accordingly, the largest effective charge (Figure 3.26, spectrum b). This is explained by the minimal electron-donor influence of the surface oxygen ions O^{δ-} from the support crystal

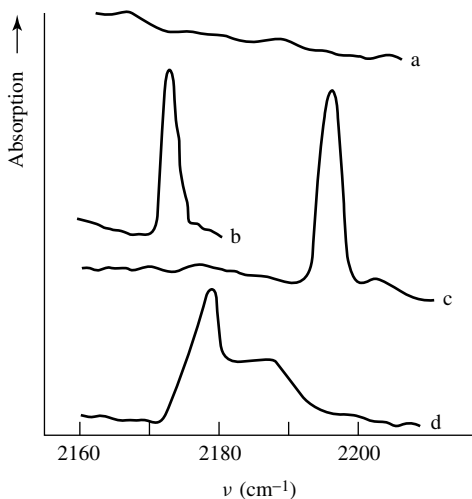


Figure 3.26. IR spectra of carbon monoxide adsorbed on samples oxidized in oxygen at 773 K: (a) Ag/MgO; (b) Ag/ γ -Al₂O₃; (c) Ag/aluminosilicate; (d) Ag/SiO₂.

lattice on Ag^{δ+} because these ions have a comparatively low effective charge in aluminosilicates. However, on highly polar MgO supports the electron-donor influence of oxygen is so strong that the Ag⁺ cations convert to a state close to metallic (under normal condition, carbon monoxide is not adsorbed on Ag⁰). Because of that, the CO adsorption on this sample was not observed (Figure 3.26(a)). On Al₂O₃ and SiO₂ supports, silver cations have an intermediate effective charge. In addition, on aluminosilicates Ag⁺ cations are characterized by a higher resistance to reduction in a carbon monoxide atmosphere. On MgO, silver is intensively reduced, even at 323 K. Of course, the silver particles in these samples had different sizes (from 1–3 to 50–100 nm) depending on the support type and silver content. Special investigations of silver catalysts with different average sizes of the metal particles showed that ν CO in Ag⁺–CO surface complexes is independent of the size of the silver clusters (at least up to 100 nm).

Spectral data have shown that Ag⁺ cations have a maximum effective charge compared with other noble metals. The spectroscopic data of electronic analogues of silver, i.e. the noble metals, whose configuration of the valence electronic shell is dⁿs¹ (Figure 3.27) [897, 898], show that for these metals the second ionization potential determines the stability of the valence d-electron shell and, accordingly, influences the M–CO bonding. A better way is to examine M⁺-Y zeolite samples, because in the zeolite the M⁺ cations can exist in an only isolated state (data for rhodium and ruthenium are inconclusive because these metals tend to form M⁺–(CO)_n multicarbonyl complexes absorbing at 2070–2140 cm⁻¹). As can be seen in Figure 3.27, in this series of metals silver cations have the most effective charge, and this correlates well with the peculiar catalytic properties of silver. The resistance of the d-shell of silver explains, in particular, its unusual weak capability to adsorb non-oxidizing adsorbates.

The influence of modifying additions with different compositions on the active states of silver is an important and interesting aspect in the formation of these active states. It has been shown that addition of zirconium and cerium oxides into the catalyst stabilizes the oxidation states of silver [898, 899]. On the other hand, addition of oxides of La, Rb or Cs hampers the oxidation of silver and reduces the effective charge of the Ag⁺ cations (low-frequency shift of ν CO (Figure 3.28). It was assumed that the positive influence of Zr and Ce oxides and the negative

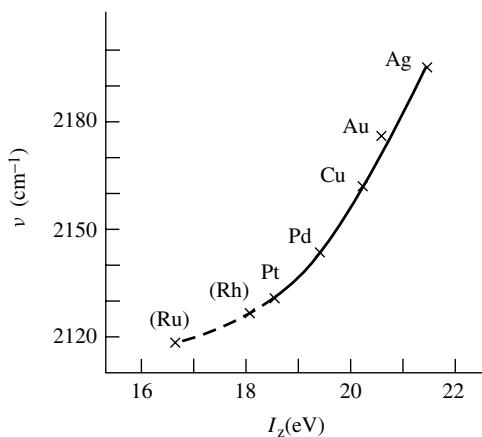


Figure 3.27. Variation in ν_{CO} of surface monocarbonyl complexes of M^+-CO in M^+-Y zeolites as a function of the second ionization potential of the metal.

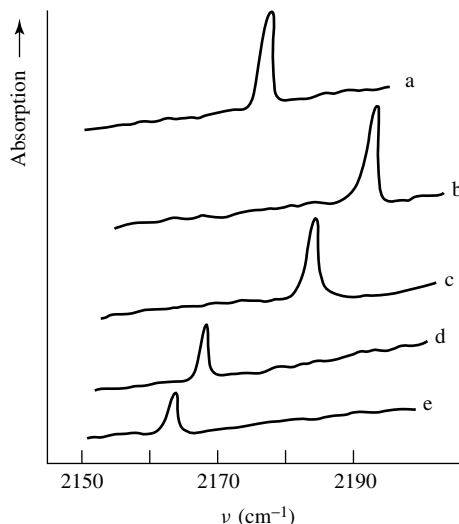


Figure 3.28. IR spectra of carbon monoxide adsorbed on oxidized samples: (a) $\text{Ag}/\text{Al}_2\text{O}_3$; (b) $\text{Ce}-\text{Ag}$; (c) $\text{Zr}-\text{Ag}$; (d) $\text{Rb}-\text{Ag}$; (e) $\text{Cs}-\text{Ag}$.

effect of La, Rb and Cs oxides are probably explained by their indirect influence on the electronic and redox properties of silver rather than on the intrinsic catalytic properties of the promoter or on other factors [899]. The fact that there is no dependence of the frequency shift from the coverage was seen as evidence for a small number of widely spaced sites being available for chemisorption so that coverage-dependent dynamic coupling and static chemical effects are not observed.

It was shown [900] that in the case of CO adsorption on Ag films and clusters the frequency of CO decreases with a decrease of desorption temperature. This can be explained by an increase in the back-donation from metal orbitals into the $2\pi^*$ antibonding orbitals of the CO molecule as the size of the Ag clusters decreases. For small Ag clusters, a greater density of states near

the Fermi level leads to a greater charge transfer into the CO antibonding orbital, thus resulting in a weaker CO bond.

Optical absorption spectra have been registered on samples of Au and Ag supported on amorphous SiO_2 with a great variation in the state of metal dispersion [901]. The degree of metal dispersion is evaluated from a packing factor determined by transmission electron microscopy. It was found that the spectral peak red-shifts with an increase of the packing factor (q) for either Au or Ag.

3.6 Palladium-containing systems

3.6.1 ZEOLITES

Adsorption of carbon monoxide

ESR studies of the states of the palladium cations in Pd-Y zeolites, coupled with IR data on CO adsorption [30, 904–909], have demonstrated that palladium cations in the catalyst may have different valencies depending on the conditions of treatment. The predominant species found in oxidized Pd-Y zeolites are Pd^{2+} cations. Therefore, intense absorption bands at 2215 and 2195 cm^{-1} observed immediately after introduction of CO (Figure 3.29, spectrum 2) may be assigned to νCO in Pd^{2+} -CO complexes [908, 909]. This assignment is confirmed by the lack of these maxima in the spectra of the reduced zeolites (Figure 3.30). The appearance of two absorption bands points to the existence of two types of Pd^{2+} ions which may be stabilized at different sites in the zeolite skeleton [908–910].

The intensities of the absorption bands at 2140 and 2125 cm^{-1} are low, both in the case of the reduced zeolites (see Figure 3.30, spectra 2 and 4) (that is, when palladium exists predominantly as the metal [904, 906]) and immediately after CO adsorption on oxidized samples (see Figure 3.29, spectrum 2) when the dominant species are Pd^{2+} . Hence, adsorption sites represent palladium cations with oxidation states between 0 and 2+, that is, Pd^+ [908]. Palladium ions in this state were detected by ESR spectroscopy in Pd-Y zeolites after reduction under mild conditions (H_2 , 293 K) [904–909]. The Pd^{2+} -Y zeolites can also be reduced with CO at 293 K to

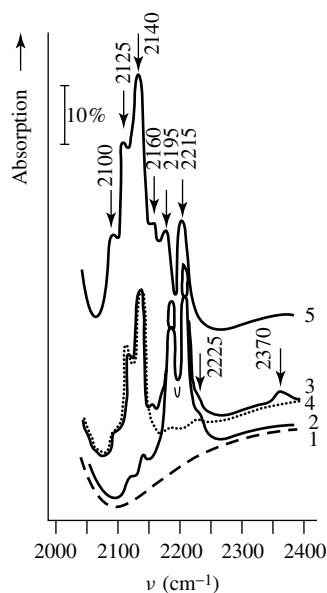


Figure 3.29. IR spectra of CO adsorbed on oxidized Pd-Y zeolites: (1) background; (2) CO adsorption; (3) 5 h after CO introduction; (4) after vacuum treatment at 293 K; (5) 35 h after CO introduction.

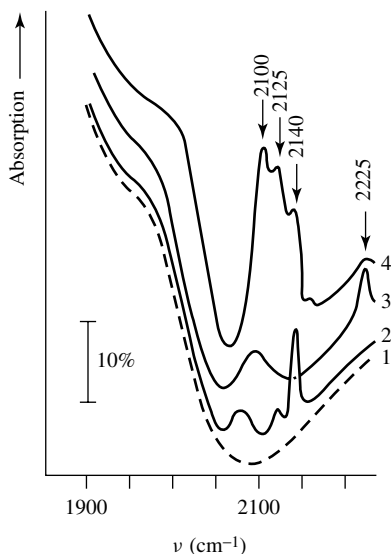


Figure 3.30. IR spectra of CO adsorbed on Pd-Y zeolites after reduction (H_2 , 573 K): (1) background; (2) CO adsorption; (3) subsequent vacuum treatment; (4) CO adsorption on samples heated *in vacuo* at 773 K.

give Pd^+ ions (complexes between CO and Pd^+), as follows from ESR studies on the interaction between CO and Pd-Y zeolites [907]. Correspondingly, in the IR spectra a decrease occurs in the intensities of the Pd^{2+} -CO complex absorption bands (2195 and 2215 cm^{-1}) while an increase in the bands at 2140 and 2125 cm^{-1} is observed on exposure of oxidized Pd-Y zeolites to carbon monoxide (see Figure 3.29, spectra 3 and 5). The appearance of the absorption band at 2370 cm^{-1} , associated with slightly perturbed CO_2 molecules (spectrum 3), proves that the reduction occurs. The Pd^+ -CO complexes have lower ν_{CO} values than the Pd^{2+} -CO complexes. This is due to a greater contribution of the d- and π -orbitals, thus decreasing ν_{CO} , and is an obvious consequence of an increasing electron-donor ability of cations with a reduction in the oxidation state. The ν_{CO} of Pd^+ -CO complexes is close to that observed for free molecules. This does not mean, however, that the CO perturbation is slight but rather results, as has been earlier pointed out, from the balance of opposite effects of σ - and π -bonding on ν_{CO} . From the above, it follows that CO should bind to Pd^+ more tightly than to Pd^{2+} . Indeed, Pd^{2+} -CO complexes are destroyed by vacuum treatment at 293 K (see Figure 3.29, spectrum 4), whereas the Pd^+ -CO structure is stable up to 373 K (see Figure 3.30, spectrum 4 and Figure 3.29, spectrum 3). ESR studies of complexes of CO and Pd^+ in Pd-Y zeolites have shown that these ions can be coordinated by one or two [904–909] CO molecules. The Pd^+ -CO complexes are formed from $\text{Pd}^+(\text{CO})_2$ complexes as a result of vacuum treatment at 293 K. The two intense absorption bands at 2140 and 2125 cm^{-1} correspond to the former complex in the IR spectra. These absorption bands, however, do not belong to ν_{s} and ν_{as} of a dicarbonyl complex as has been suggested by Naccache *et al.* [904]. First, the absorption bands undergo different changes after treatment (see Figure 3.29, spectrum 4). Secondly, such an assignment does not agree with experimental results on the adsorption of a 1:1 mixture of ^{12}CO and ^{13}CO . Adsorption of the isotopic mixture gives rise to two pairs of absorption bands at 2125 and 2140 and 2080 and 2095 cm^{-1} (Figure 3.31, spectrum 1). The latter pair corresponds to the former complex with an isotope shift characteristic of ^{13}CO . If the absorption bands at 2125 and 2140 cm^{-1} had belonged to two

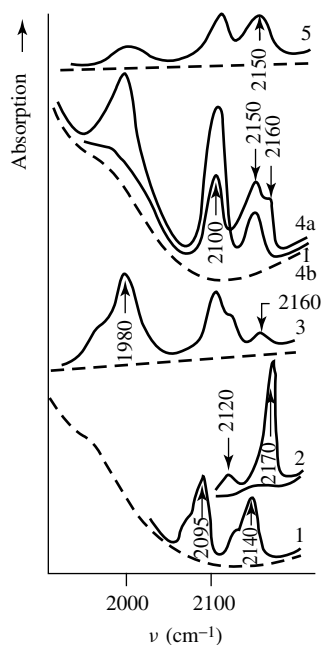


Figure 3.31. IR spectra of adsorbed CO: (1) Pd-Y, mixture of ^{12}CO and ^{13}CO (1:1) after contact of mixture for 10 h and evacuation at 293 K; (2) $\text{PdCl}_2/\text{Al}_2\text{O}_3$, evacuated at 330 K; (3) $\text{Pd}/\text{Al}_2\text{O}_3$, oxidized in O_2 at 293 K; (4) Pd/SiO_2 , oxidized at 673 K, (a) immediately after CO introduction, and (b) after 5 h; (5) $\text{Pd}/\text{Al}_2\text{O}_3$, oxidized at 673 K (the dashed traces represent background spectra).

CO molecules stabilized at the same site, there would have been a doublet in the spectrum of the isotope mixture between these bands, corresponding to the complex containing one molecule each of ^{12}CO and ^{13}CO . The absence of such an absorbance indicates that the absorption bands at 2140 and 2125 cm^{-1} are associated with two different CO complexes. Consequently, they should be considered as CO complexes with different Pd^+ cations. The $\text{Pd}^+(\text{CO})_2$ complex may produce the absorption bands at 2125 and 2160 cm^{-1} since these bands are changed simultaneously. Thus, upon vacuum treatment at 293 K the latter disappears and the former shifts to the low-frequency region and becomes slightly more intense, whereas CO re-adsorption (3 torr) causes the opposite changes in the spectral region. Such spectral changes suggest that the absorption bands at 2125 and 2160 cm^{-1} belong to the same $\text{Pd}^+(\text{CO})_2$ surface complex, with the removal of one CO molecule giving at Pd^+-CO complex with νCO at about 2120 cm^{-1} and a greater molar absorptivity. The removal of one ligand from the $\text{Pd}^+(\text{CO})_2$ complex should increase the strength of the bonding, particularly π -bonding, with the second CO molecule. This appears to account for a low-frequency shift of the absorption of the monocarbonyl complex relative to the dicarbonyl complex and a higher molar absorptivity of the former. Indeed, as has been found for $\text{M}-\text{CO}$ and $\text{M}-\text{NO}$ groups, the strengthening of the π -bonding is accompanied by an increase in integrated intensity. These complexes seem to be detected by ESR spectroscopy, as follows from the correlated behavior of the IR absorption bands and ESR signals [907]. Vacuum treatment at 293 K does not affect the absorption at 2140 cm^{-1} . This may mean that the corresponding complex contains one CO molecule or two molecules removed simultaneously when the complex is destroyed or that the removal of one molecule has no appreciable effect on the state of another. The first possibility is the most likely, although a lack of analogues for such complexes in the ESR spectra leaves matters uncertain. An absorption band at 2100 cm^{-1} is observed for samples reduced in H_2 (Figure 3.30) when Pd exists as the metal or after a long-term reduction of Pd^{2+} -Y zeolites in an atmosphere of CO (see spectrum 3.29, spectrum 5), which allows the assignment of this absorption band to CO adsorbed on Pd^0 sites. This assignment is consistent with the fact that

CO stabilized on transition metals absorbs below $2110\text{--}2100\text{ cm}^{-1}$ [30, 55]. The νCO decrease relative to $\nu\text{CO}_{(\text{gas})}$ observed in this case is due to the key role of π -bonding in CO stabilization.

It should be noted that the behavior of the absorption band at 2100 cm^{-1} depends on the conditions of the zeolite pre-treatment. The band that appears on exposing $\text{Pd}^{2+}\text{-Y}$ zeolites to CO (see Figure 3.29, spectrum 4) is not removed by vacuum treatment at 293 K, whereas that observed in the spectra of H_2 -reduced samples is removed by such treatment with the appearance of an absorption band at about 2075 cm^{-1} (see Figure 3.31, spectrum 4). This suggests that absorption at 2100 cm^{-1} corresponds to a different complex of chemisorbed CO. Effects similar to those observed with reduced zeolites have been described for CO chemisorbed on silica-supported metallic palladium (mean crystal size of 70 \AA) [908]. Therefore, the absorption band at 2100 cm^{-1} appearing in the spectra of H_2 -reduced samples should be assigned to CO adsorbed on crystals of metallic palladium of a larger size.

As for Pd/SiO_2 , the relatively high position of this absorption band in the spectrum is due to surface coverage effects (linear $\text{Pd}^0\text{-CO}$ complexes have νCO at about 2070 cm^{-1} at small coverage) [30, 908]. The presence of larger crystals is also shown by the presence of an absorption band in the $1900\text{--}1980\text{ cm}^{-1}$ region (observed also for Pd/SiO_2) associated with bridge surface structures of adsorbed CO [30, 908].

In contrast to the results obtained for reduced zeolites, the CO adsorption sites in the complex with νCO at 2100 cm^{-1} formed in nonreduced zeolites appear to involve small clusters or atomically distributed metal. This assignment is confirmed by the fact that the absorption band at 2100 cm^{-1} is not shifted on vacuum treatment, whereas with coarsely dispersed metals νCO decreases with decreasing coverage [30, 908]. Indeed, the effects of coverage are usually considered to be determined by the overall electronic properties of a metal. The absence of such effects points to the essentially local character of the interaction of CO with adsorption sites which is possible only with very small metal clusters or atoms. That palladium is formed in such a finely dispersed state is apparently due to the mild conditions of reduction (293 K in CO). The value of νCO in this case is higher than that characteristic of coarsely dispersed palladium (2070 cm^{-1} at small coverage). This is rationalized with the assumption that small clusters are stabilized on the electron-acceptor sites of the carrier, with the effect of these sites on the metal state being stronger than the size effects.

An absorption band at 2225 cm^{-1} (see Figures 3.29 and 3.30) belongs to the complex between CO and coordinatively unsaturated Al^{3+} ions. Complexes with similar νCO values are observed for CO adsorption on M-Y zeolites and Al_2O_3 [30] (see Section 2.3.2). The low intensity of this absorption band in the case of reduced zeolite (see Figure 3.30, spectrum 2) may be due to the blocking of Al^{3+} sites by the particles of metallic palladium stabilized on them, and an increase in the intensity observed on heating *in vacuo* at 773 K may result from metal sintering and the release of the Al^{3+} ions again (see Figure 3.31, spectrum 4). These results may be taken as indirect evidence for the stabilization of metallic particles at the electron-acceptor sites (Al^{3+} ions).

Thus, the studies of CO adsorption on Pd-Y zeolites have allowed the identification of CO complexes with Pd^{2+} (2195 and 2215 cm^{-1}), Pd^+ ($2120\text{--}2160\text{ cm}^{-1}$) and Pd^0 (2100 cm^{-1}).

Adsorption of nitric oxide

Absorption bands at 1810 , 1835 and 1870 cm^{-1} in the spectra of NO adsorbed on oxidized Pd-Y zeolites (Figure 3.32, spectrum 1) belong to the complexes between NO and Pd^{2+} ions since the state of palladium is predominant in oxidized samples [904–910]. The assignment of these absorption bands to νNO in complexes with relatively high charged ions is also confirmed by the fact that they remain unaffected by heating under an oxidizing atmosphere (NO or O_2). The same assignment of absorption bands at similar frequencies has also been reported [904, 906], although

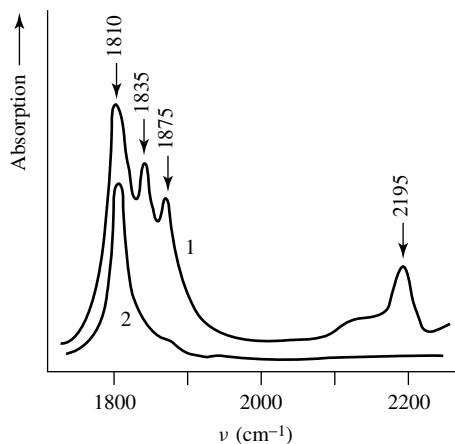


Figure 3.32. IR spectra of NO adsorbed on oxidized zeolites: (1) NO adsorption; (2) vacuum treatment at 573 K for 0.5 h.

other workers did not detect the presence of an absorption band at 1835 cm^{-1} . The NO complexes producing absorption bands at $1800\text{--}1870\text{ cm}^{-1}$ are stable to vacuum treatment at temperatures as high as $473\text{--}573\text{ K}$, with the most stable being the complex with νNO at 1800 cm^{-1} (see Figure 3.32, spectrum 3). The intensities of three absorption bands in the $1800\text{--}1870\text{ cm}^{-1}$ region undergo different changes depending on the conditions of zeolite pre-treatment, which suggest that they are associated with different complexes of chemisorbed NO.

An absorption band in the $2100\text{--}2200\text{ cm}^{-1}$ region (see Figure 3.32, spectrum 1) that appears after NO adsorption on oxidized Pd-Y zeolites is normally observed during the adsorption of NO_2 on zeolites and may be associated with the ν_{as} of structures such as NO_2^+ [910, 911]. In the case under consideration, such structures may be formed with the participation of oxygen atoms, which coordinate Pd^{2+} ions.

The presence of Pd^{3+} ions (1 % of the palladium introduced) in oxidized samples is shown from ESR data [904, 906]. Since palladium is introduced into the zeolite in the form of Pd^{2+} , it is necessary that oxygen not belonging to the zeolite skeleton be present in order that the Pd^{3+} ions can also be present. This oxygen might be involved in the formation of NO_2^+ , with electron transfer from the NO_2 molecule to Pd^{3+} being responsible for the disappearance of the ESR signal of Pd^{3+} [904]. A decrease in absorption intensity at $2100\text{--}2200\text{ cm}^{-1}$ and an increase in absorption at $1880\text{--}1870\text{ cm}^{-1}$ after the repeated introduction of NO confirms the assignment suggested above. The effects observed are due to the removal of nonskeletal oxygen in the form of NO_2 on Pd^{3+} reduction. Hence, the data on CO and NO adsorption lead to the conclusion that Pd^+ exists in Pd-Y zeolites in two and Pd^{2+} in three states, from which only two are involved in the complexation with CO.

To compare the data on the state of palladium cations obtained with CO and NO, sequential adsorption of these molecules has been studied. Pd^+ is oxidized to Pd^{2+} via interaction with NO, and Pd^{2+} forms more tightly bound complexes with NO than with CO. Therefore, one would expect all complexes of chemisorbed CO to decompose after introduction of NO on pre-adsorbed CO. Indeed, NO adsorption on CO pre-adsorbed on the Pd-Y zeolites removes the absorption bands at 2125 , 2140 and 2160 cm^{-1} and at 2195 and 2215 cm^{-1} (Figure 3.33, spectrum 1) belonging to CO complexes with Pd^+ and Pd^{2+} ions, respectively, whereas an absorption band at 2225 cm^{-1} ($\text{Al}^{3+}\text{--CO}$) becomes distinct. A maximum appears at 2150 cm^{-1} in the νCO region, whereas only an intense broad band at $1790\text{--}1810\text{ cm}^{-1}$ appears in the νNO region. Similar

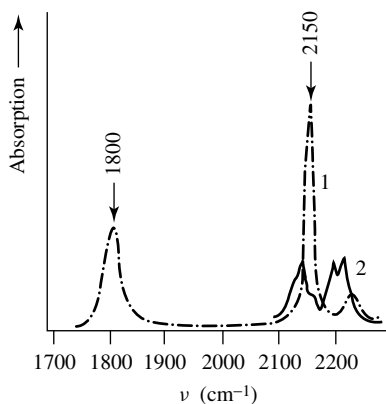


Figure 3.33. Effect of (1) NO adsorption on (2) the IR spectrum of CO adsorbed on Pd-Y zeolites.

changes are observed after introduction of CO on pre-adsorbed NO. High-frequency adsorption bands in the νNO region disappear, whereas an absorption band at 1800 cm^{-1} sharply increases. In the νCO region, an intense absorption band at 2150 cm^{-1} is observed and no absorption band associated with Pd^+-CO or $\text{Pd}^{2+}-\text{CO}$ complexes appears. Since the simultaneous NO and CO adsorption changes in the νNO region affect only those complexes producing the 1865 and 1835 cm^{-1} bands, one can conclude that the $\text{Pd}^{2+}-\text{CO}$ complexes (2215 and 2195 cm^{-1}) correspond to $\text{Pd}^{2+}-\text{NO}$ complexes characterized by high-frequency absorption bands at 1865 and 1835 cm^{-1} , whereas an absorption band at 1800 cm^{-1} belongs to NO bound to Pd^{2+} ions not involved in the complexation with CO.

The effect of CO on NO complexes (and vice versa, the effect of NO on $\text{Pd}^{2+}-\text{CO}$) will now be considered. The complexes formed in such a way and containing both NO and CO (as follows unambiguously from the reversibility of changes in the spectra and CO adsorption-desorption cycles) give rise to bands at about 1800 and 2150 cm^{-1} due to νNO and νCO , the intensities of which are less than those observed for separate adsorption. This can be explained on the assumption that CO coordinates Pd^{2+} ions in the direction perpendicular to that of NO coordination. In such a case, the same unoccupied d-orbital (or the hybrid $(4d + 5s)$ -orbital) of Pd^{2+} must accept the π -electron of NO and the 5σ electron pair of CO. As is reasonable, in the absence of CO, the electrons of NO are more shifted towards the cation in the $\text{Pd}^{2+}-\text{CO}$ complex, which accounts for higher νCO and νNO values in the $\text{Pd}^{2+}-\text{CO}$ and $\text{Pd}^{2+}-\text{NO}$ complexes compared with the $\text{Pd}^{2+}-(\text{CO})(\text{NO})$ complex. This might increase the electron shift to the π -orbitals of NO and CO, which would also decrease νNO and νCO . It should be taken into account, however, that CO bonding with $\text{Pd}^{2+}-\text{NO}$ is less strong than with Pd^{2+} (the absorption at 2150 cm^{-1} is removed by short-term evacuation at 293 K). This points to a low contribution of the π -bond in CO stabilization in the $\text{Pd}^{2+}-(\text{CO})(\text{NO})$ complex.

The appearance in zeolites of several types of metal cations with practically the same charge may be due to several factors. These include the following: (i) differences in the character of the ligands coordinating the metal cations, such as the presence of nonskeletal bridge oxygens (such states may be formed upon the hydrolysis of the ion-exchange salt when a metal is introduced into a zeolite) and the presence or absence of water in the coordination sphere of the cations; (ii) different sites of stabilization in the zeolite skeleton existing at several positions in the large and small cavities (except S_I sites where the coordination of metal ions by NO or CO molecules appears to be impossible); (iii) differences in the relative positions of the cations, such as the

presence of two or more cations located in close proximity to each other, as opposed to spatially isolated ions.

The available IR spectroscopic data do not allow a definite explanation of the existence of different states of palladium cations in the same oxidation state. Some possibilities can, however, be ruled out in order to select the most probable ones. Factor (i) can be neglected since the conditions for introducing palladium into the zeolite avoided hydrolysis of the salt, and if this had occurred to some extent the concentration of the corresponding states would be extremely low. The hypothesis involving different sites of cation stabilization in the zeolite skeleton seems the most likely explanation [911].

Adsorption of small amounts of benzene on vacuum-treated Pd-Y zeolite with pre-adsorbed CO leads to the disappearance of absorption bands at 2195 and 2215 cm^{-1} and the appearance of maxima at about 2130 and 2115 cm^{-1} . The absorption bands due to $\text{Pd}^+ - \text{CO}$ complexes (2142 cm^{-1}) and the band at 2225 cm^{-1} remain unchanged. The former become distinct after evacuation at 293 K, whereas absorption bands at 2115, 2130 and 2225 cm^{-1} are removed under these conditions. The latter again appear after introduction of CO, which points to the reversible formation of the corresponding species involving adsorbed CO. Similar effects are observed with benzene adsorption on pre-adsorbed NO. Absorptions at 1865 and 1835 cm^{-1} apparently shift to about 1800 cm^{-1} , while the initial spectrum in the νCO stretching region is restored on evacuation at 293 K.

Hence, it can be concluded that the $\text{Pd}^{2+} - \text{CO}$ and $\text{Pd}^{2+} - \text{NO}$ complexes with absorption bands at 2195 and 2215, and 1865 and 1835 cm^{-1} , respectively, are located in the large cavities of the zeolite. The complexes with νNO at 1800 cm^{-1} remain unchanged upon interaction with both CO and benzene, possibly because NO forms complexes with Pd^{2+} ions located in the small cavities of the zeolite skeleton, with these being inaccessible to CO and benzene molecules. As an alternative, one can consider that Pd^{2+} cations in such an extremely stable complex (up to 573 K *in vacuo*) are coordinatively saturated and cannot coordinate additional molecules. Information about the effect of CO and benzene on the $\text{Pd}^{2+} - \text{NO}$ complex (νNO at 1800 cm^{-1}) alone is insufficient to choose between these alternatives. However, in view of CO forming two, and NO three, types of complex with Pd^+ ions, the first hypothesis seems more likely. The following facts favor this conclusion. Nitrous oxide adsorption on Pd-Y zeolites reduced in H_2 at 773 K first results in the appearance and growth of absorption bands at 1865 and 1840 cm^{-1} , with the band at 1800 cm^{-1} almost absent [30, 908, 910]. The appearance of absorption bands associated with $\text{Pd}^{2+} - \text{NO}$ complexes upon interaction between NO and metallic palladium in the zeolite is indicative of palladium re-oxidation. It is reasonable to suggest that Pd^{2+} cations, resulting from the re-oxidation of metallic palladium located in the form of metal clusters in large cavities and in the external surface, will generally appear first before their appearance in small cavities. Therefore, the absence of the absorption band at 1800 cm^{-1} may indicate that the Pd^{2+} ions forming complexes (with νNO at 1800 cm^{-1}) are located in small cavities. The same assignment of this absorption band has been proposed by Che *et al.* [906].

A lower νNO for the nitrosyl complex located in small cavities compared with the νNO for the complex located in large cavities is attributed to the nonlinearity of the $\text{Pd}^{2+} - \text{NO}$ complex in the former case [906]. Such an explanation is not fully convincing because evidence is available showing that there is no interdependence between the geometry of nitrosyl complexes and νNO [912, 913]. A lower νNO in complexes with Pd^{2+} ions located in small cavities may be accounted for as follows. It is known that the majority of cations of oxidation degree 2+ are stabilized in small cavities (and hexagonal prisms), especially at low extents of exchange [22, 74]. This may be due to a number of factors, the most significant of which is that the exchange cations must neutralize the charge of the zeolite skeleton (AlO_4 tetrahedra). The distribution of the neutralizing cations must, obviously, reflect that of aluminum in the zeolite lattice. The preferential

stabilization of the exchange ions in small cavities appears to be due to the aluminum distribution being such that when in small cavities a doubly charged cation can neutralize, for instance, two AlO_4 tetrahedra at once. With large cavities, doubly charged cations may be unable to neutralize certain sites completely, which is apparently responsible for a weaker bond between the cations and the zeolite skeleton. Therefore, the ions located in large cavities would be expected to bear an excess positive charge in comparison with those in a small cavity and be more coordinatively unsaturated. In such a case, the νNO for complexes in a small cavity should be lower than that for ions in large cavities.

3.6.2 OXIDES

Taking into account the information obtained, let us now consider the CO adsorption on other palladium-containing catalysts. The CO adsorption on $\text{PdCl}_2/\text{Al}_2\text{O}_3$ gives rise to an absorption band at 2170 cm^{-1} (see Figure 3.31, spectrum 2) (not observed after evacuation at 293 K), which should be assigned to the $\text{Pd}^{2+}\text{-CO}$ complexes. In addition, there is a weak absorption band at 2120 cm^{-1} , which may be attributed to the $\text{Pd}^+\text{-CO}$ complex (see Figure 3.31, spectrum 2). With oxidized $\text{Pd}/\text{Al}_2\text{O}_3$ and Pd/SiO_2 samples, the spectra depend on the conditions of oxidation. Mild oxidation gives maxima at 2120 and 2160 cm^{-1} (see Figure 3.31, spectrum 3), together with an absorption band ascribed to CO adsorbed on the metal (2100 and 1980 cm^{-1}). Heating at 673 K in oxygen leads to the appearance of the absorption bands at 2160 and at 2100 cm^{-1} (see Figure 3.31, spectrum 4). The absorption band at $2120\text{--}2160\text{ cm}^{-1}$ becomes gradually weaker and then disappears, whereas the bands at 2100 and 1980 cm^{-1} increase, owing to the surface reduction. Complexes with a νCO at 2160 and 2150 cm^{-1} are less stable than those with a νCO at 2120 cm^{-1} and are apparently due to complexes involving Pd^{2+} . A low-frequency νCO shift relative to $\text{Pd}^{2+}\text{-CO}$ complexes formed in zeolites seems to be due to the lower Pd–O bond covalence in these systems [908].

A detailed investigation of the electron states in Pd-containing systems by using both UV–Vis and ESR spectroscopies has not only been made in the above studies of zeolites, but also in series of other papers (see, for example, [914–916] for supported systems with low palladium content). As shown in Table 3.7 [916], the state of the palladium ions in Pd catalysts depends significantly on the nature of the support. Thus, in the case of Pd/MgO catalysts the formation of Pd^+ , Pd^{2+} and Pd^{3+} has been revealed, whereas only Pd^{2+} ions are present in Pd/SiO_2 samples. These ions are different in their coordinations. On MgO , Pd^{2+} ions are present in the bulk and prohibit the adsorption of CO molecules, whereas on $\text{Pd}/\text{Al}_2\text{O}_3$ these ions easily coordinate CO, hence forming paramagnetic palladium carbonyls. Promotional additives such as Co cause a decrease of the concentration of Pd^+ ions in alumina–palladium catalysts. In both Co- and $\text{Pd-Co}/\text{Al}_2\text{O}_3$, the octahedrally and tetrahedrally coordinated ions of $\text{Co}^{2+}_{\text{oct}}$, $\text{Co}^{3+}_{\text{oct}}$ and $\text{Co}^{2+}_{\text{tet}}$, the Co_3O_4 phase (charge-transfer band in the $40\,000\text{--}28\,600\text{ cm}^{-1}$ (250–350 nm) region) has been observed by means of DRES, ESR and IRS methods. The spectral parameters of these ions are depicted in Table 3.7.

Electron paramagnetic resonance studies have been carried out on $\text{Pd}/\text{Y}_2\text{O}_3$ and $\text{Pd}/\text{La}_2\text{O}_3$ systems with low Pd loadings [917]. Oxidation of yttria-containing samples at 870 K leads to the formation of Pd^{3+} , which converts into Pd^+ when the samples are evacuated at 870 K. Both species are stabilized in the bulk. Mild reduction of doped yttria and lanthana in hydrogen gives another type of Pd^+ ion localized within the surface and sub-surface layers. Formation of O_2^- radical anions, coordinated with Y^{3+} or La^{3+} cations, occurs readily at 77 K upon oxygen admission. The decay and formation of adsorbed radical anions is sensitive to the electron-donating properties of the sample (i.e. the surface concentration of Pd^+).

In situ IR and ESR spectroscopy of Cu–Pd-exchanged Y zeolites [918] leads to the proposition of an active site consisting of a trinuclear Cu–O–Pd–O–Cu cationic complex giving use to a

Table 3.7. Spectroscopic characteristics of supported metals for low-content active components catalysts.

Catalyst	Ion ^d	ESR		Support ^b	Ion	DRES, λ (nm) ^c	Ion ^e	IRS (CO), ν (cm ⁻¹)
		$g_1(g_{\perp})$	$g_2(g_{\parallel})$					
Pd/MgO	Pd ⁺ _b	2.012	2.169	MgO _{am}	Pd ⁺	545, 650 (sh)		
	Pd ⁺ _b	2.060	2.090	MgO _{am}	Pd ²⁺	460		
	Pd ⁺ _s	—	2.250	MgO _{am}				
	Pd ³⁺ _s	2.009	1.985	MgO _{am}				
	Pd ⁺ _b	—	$g_{\text{iso}} = 2.121(21.53)$	MgO _{cr}				
	Pd ⁺ _b	2.007	2.112	Mg(OH) ₂				
	Pd ⁺ _b	2.135	2.221	Mg(OH) ₂				
	Pd ⁺ _b	2.101	2.326	(423)				
Pd/Al ₂ O ₃	Pd ⁺ _s	2.13	2.42	γ -Al ₂ O ₃	Pd ²⁺	480		2060–2080
	Pd ⁺ _s	2.13	2.92	γ -Al ₂ O ₃				2120
								2160
Pd/SiO ₂	—	—	—	SiO ₂	Pd ²⁺	480		
Co/Al ₂ O ₃	Co ²⁺ (O)	4.7	2.1	γ -Al ₂ O ₃	Co ²⁺ (O)	520, 1180		2185
Pd-Co/Al ₂ O ₃	Co ²⁺ _s	2.192(723)	2.032(553)	γ -Al ₂ O ₃	Co ²⁺ (T)	545, 575, 625(sh), 1230, 1360, 1550		2060–2080
Ce/Al ₂ O ₃	Co ⁰	$g_{\text{iso}} = 2.2-2.3$	—	γ -Al ₂ O ₃	Co ³⁺ (O)	450, 740		2120
	Pd ⁺ _s	2.13	2.42	γ -Al ₂ O ₃	Co ₃ O ₄	250–350		2160
Pd-Ce/Al ₂ O ₃	—	—	—	γ -Al ₂ O ₃	Ce ⁴⁺	300 ^d		2060–2080
	Pd ⁺ _s	2.13	2.42	γ -Al ₂ O ₃	Ce ³⁺	320		2120
					(Ce ³⁺)	($\lambda^e = 360,$ $\lambda^f = 430, 480(\text{sh})$)		2160

^a s, surface; b, bulk.^b am, amorphous; cr, crystalline.^c sh, shoulder.^d Charge-transfer band.^e Excitation.^f Radiation.

catalytic cycle for the Wacker oxidation, in which the re-oxidation of Cu^+ by dioxygen or Pd^0 by Cu^{2+} zeolite is rate-determining and content of the active component. In Pd/alumina catalysts with different metal loadings (0.1–1.0 %), two states ($25\,000\text{--}23\,810\text{ cm}^{-1}$ (400–420 nm) and $38\,500, 30\,000$ and $22\,990\text{ cm}^{-1}$ (260, 335 and 435 nm)) of palladium oxide have been found and compared with UV and X-ray diffraction results.

The state of Pd supported on TiO_2 , $\text{TiO}_2\text{--CaSO}_4$, $\text{TiO}_2\text{--Nb}_2\text{O}_5$, $\text{TiO}_2\text{--Nb}_2\text{O}_5\text{--CaSO}_4$ and $\text{TiO}_2\text{--Nb}_2\text{O}_5\text{--CaSO}_4\text{--R}_2\text{O}_3$ (where R is a rare-earth element) has been studied by IR spectroscopy using CO adsorption [919]. Reduction of palladium ions into $\text{Pd}^{\delta+}$ and Pd^0 occurs in oxidized samples at room temperature in the presence of CO. This process is most pronounced for the Pd/ $\text{TiO}_2\text{--Nb}_2\text{O}_5$ catalyst. In reduced samples containing no CaSO_4 and Re_2O_3 , a strong metal–support interaction has been found for Pd^0 species. The introduction of the above additives completely eliminates or partially reduces the effect of the strong metal–support interaction, and Pd–O species appear that are nonuniform in their properties and are capable of adsorbing CO with the formation of linear or several other types of bridging complexes.

The detailed analysis of the CO complexes with palladium metal clusters supported on different oxides, as well as their spectral manifestations, has been done by Palazov *et al.* (see, for example, [920]). In his papers, the comparison of spectral manifestations of CO adsorbed onto palladium dispersed over supports, and also on separate single crystal faces, has been done first.

3.7 Rhenium-, Ruthenium-, and Rhodium-containing systems

For the elements shown above, besides the CO adsorption on metals (the metal state dominates for these elements and IRS manifestations of the CO adsorption on different metals are similar and analyzed in Section 3.8.1), the complexes of CO with cations are always observed even on reduced catalysts, except for the adsorption of 1 molecule of CO involving one cation, the simultaneous adsorption of several CO molecules on one cation frequently occurs. As a rule, transition-metal cations (especially such as Pd, Ru, Ir, Rh, Re) with intermediate degrees of oxidation, which have several coordinatively unsaturated vacancies for the molecules to be adsorbed, are such centers¹. The same is fully characteristic of supported Pd (see above) Ru [921–923], Ir [924] and Rh [38, 725–737, 925–931]. Although for such di- and polycarbonyls the empiric rule for the spectral ranges of the CO complexes with cations in different valent states is valid, it should be taken into account that for the complexes of one cation with several CO molecules the $\text{LF}(\nu_s)$ components are observed in the region characteristic of metal carbonyls. This is due to the interaction of the vibrations (ν_s and ν_{as}). Thus, on Rh/ Al_2O_3 and Rh-Y zeolites, besides both linear and bridged complexes of CO with metal, those with cations, have been revealed. Their formation is accompanied by the appearance of absorption bands in the 2120–2110 and 2040–2020 cm^{-1} regions. According to various authors [38, 926, 928, 930, 932], Rh is present in dicarbonyl complexes as Rh^+ . Such complexes, $\text{Rh}^+(\text{CO})_2$, are observed even on samples reduced at 773 K in hydrogen with Rh/ Al_2O_3 [726, 727, 734, 927, 930, 932], Rh-Y [928, 931] and Rh/ SiO_2 [933], but are absent on Rh/MgO and Rh/ZnO [934]. It has been shown [933, 935], that the formation of Rh^+ on reduced Rh/ Al_2O_3 and Rh/ SiO_2 proceeds due to the oxidative action of the support caused by the participation of its OH groups. Monocarbonyl complexes forming with participation of metal are usually more stable than dicarbonyls [926, 936, 937]. However, such a conclusion is in disagreement with the data of Yates and co-workers [927, 929], from which it follows that the Rh–CO complex is more easily destroyed than $\text{Rh}^+(\text{CO})_2$. There are a numerous other data in the literature indicating the formation of dicarbonyl or even polycarbonyl complexes with ions of these metals (Rh^I , Ru^I , Ru^{II} , and even Ru^{III}) [939b–939z] due to the interaction of CO with supported ruthenium and rhodium.

¹ (see for example, for supported Pd above)

It is a well-established fact that the position of the νCO of the adsorbed CO molecule in this case depends on the coverage of the surface, dispersity of the supported metal, and the state of charge of the adsorption sites. As the coverage increases, the νCO shifts to higher frequencies. Such an effect has been observed upon adsorption of CO on metals by different researchers (see, for example, [55, 927]) and is caused by intermolecular interactions in the adsorption layer. An increase in νCO for linear carbonyls of $15\text{--}17\text{ cm}^{-1}$ has been observed as the size of particles increases [922, 938].

It was shown [726, 922] that the nitrosyl complexes formed in $\text{Rh}/\text{Al}_2\text{O}_3$ and Pt/SiO_2 systems and characterized by the absorption bands at 1910 and 1935 cm^{-1} are strongly bound (do not decompose upon evacuation until 673 K). The intensive bands at 1740 and 1830 cm^{-1} observed in the case of $\text{Rh}/\text{Al}_2\text{O}_3$ [726, 727] are assigned to the linear structures $\text{Rh}\text{--NO}^-$ and $\text{Rh}\text{--NO}$, respectively. Later, Heide *et al.* [734], based on an investigation of $\text{NO}/^{15}\text{NO}$ adsorption on Rh-Y zeolites, concluded that these absorption bands can belong to $\text{Rh}(\text{NO})_2$ dinitrosyl complexes. This has been confirmed by Liang and Wang [926, 939a].

3.8 Platinum-containing systems

3.8.1 IR-SPECTRA OF CO ON SUPPORTED METALS

The position of the νCO of the adsorbed CO molecules in this case depends on the coverage of the surface, dispersity of the supported metal, and the state of charge of the adsorption sites. As the coverage increases, the νCO shifts to higher frequencies. Such an effect has been observed upon adsorption of CO on metals by different researchers (see, for example, [55, 927]) and is caused by intermolecular (lateral) interactions in the adsorption layer. An increase in νCO for linear carbonyls of $15\text{--}17\text{ cm}^{-1}$ has been observed as the size of particles increases [922, 938].

It is already clear from the previous discussion that there is a great similarity in the formation of the bonds involving the CO group on metal surfaces and those in the metal carbonyls. So, the νCO in coordination metal compounds or metal clusters along with that in the matrix isolated compounds, plays the role of reference point in comparison with the spectra of CO adsorbed on different metal-containing systems. In the 1990s, De La Crus and Sheppard published a remarkable review [939aa] summarized such data. It made easier the interpretation of the spectra of CO adsorbed on metals. The authors presented the relationship between CO bond-stretching (νCO) and the less common types of CO/metal bonding patterns in transition-metal-carbonyl complexes and clusters. The linearly bonded MCO ($\sigma\text{-CO}$) groups and the twofold bridge-bonding M_2CO ($\mu_2\text{-CO}$) groups, with relatively wide wavenumber ranges were analyzed in terms of the effects of net charges or of electron-donating or electron-withdrawing CO ligands on the same metal atoms. They showed that, for example, for the platinum compounds, the approximate νCO wavenumber shifts, relative to the values for compounds with all-carbonyl ligands, a unit negative charge is -190 cm^{-1} , and unit positive charge is about $+90\text{ cm}^{-1}$. In the absence of such net charges or strongly perturbing ligands on the same metal atom, the average νCO values for the various types of CO ligands are estimated to be: MCO ($\sigma\text{-CO}$) $2070\text{--}2050$; M_2CO ($\mu_2\text{-CO}$) 1870 ; M_3CO ($\mu_3\text{-CO}$) 1800 ; keto-carbonyls M_2RCO (2K-CO) ca. 1700 for Pt; isocarbonyls $\text{MCO} \dots \text{M}'$, 1730 and $\text{M}_3\text{CO} \dots \text{M}'$, 1380 ; dihepto carbonyls MCO/M' , 1700 and $\text{M}_3\text{CO}/\text{M}'$, 1450 ; and $\text{MCO}/2\text{M}'$, i.e. CO σ -bonded to one metal atom and π -bonded to two others, 1380 cm^{-1} . The authors noted that these values correspond well to those observed at low coverage from MCO, M_2CO and M_3CO species on flat metal surfaces, and additional values are used to consider the structural origins of species which give low-wavenumber νCO values on metal surfaces usually involving steps and other defects. Moreover, a relationship was found between the related νCO and $r(\text{CO})$ values. (Typical pairs, $\text{\AA}/\text{cm}^{-1}$) are $1.15/2030$; $1.2/1730$; $1.25/1490$; $1.30/1320$; $1.35/1180$; $1.2/1730$; $1.25/1490$; $1.30/1320$; $1.35/1180$ with probable errors

of $\pm 0.025 \text{ \AA} / \pm 100 \text{ cm}^{-1}$. Usually, two types of the CO bond with metals, i.e. linear ($\text{M}-\text{C}\equiv\text{O}$) and bridged ($\text{M}_n-\text{C}\equiv\text{O}$), can be differentiated. The corresponding absorption bands lie in the $2000\text{--}2100 \text{ cm}^{-1}$ and $1800\text{--}2000 \text{ cm}^{-1}$ regions, respectively.

Influence of dispersion

As for Pt itself, already from the first infrared studies on adsorption of NO and CO on the Pt/Al₂O₃ surface [45, 938, 940] a substantial connection was discovered between the size of the metal particles and the stretching vibrations of the adsorbed molecule. In Primet *et al.* [940], it was noted that the greatest variation of $\nu(\text{NO}_{\text{ads}})$ is to be expected in the region of small metal particles. An investigation [938] has been carried out of the dependence of νCO in a Pt–CO complex on the particle size of the platinum supported on SiO₂ and Al₂O₃. To exclude effects of the preparation method, the samples were produced by the same approach [938]. In order to obtain ‘atomic’ distributions, platinum was deposited by interaction with the vapor of bis(π -methallyl)platinum. Before CO had been adsorbed, all impurities were removed from the sample [938].

The dependence of the dispersivity of deposited platinum, expressed as the fraction of surface platinum atoms (Pt_s/Pt_t), on the conditions of the heat treatment in a hydrogen atmosphere is shown in Table 3.8. It follows from these data that an increase of the heat-treatment temperature causes an agglomeration of platinum; this process occurs to a greater extent on silica gel when compared with alumina.

In the IR spectra of CO adsorbed on the samples, a single intense absorption band in the $2000\text{--}2100 \text{ cm}^{-1}$ region with a half-width of $20\text{--}60 \text{ cm}^{-1}$ from linear surface carbonyls (Pt–CO) is observed; its position depended on the conditions of the heat treatment of the sample (Figure 3.34 and Table 3.9). It follows from these data that νCO increases upon raising the heat-treatment temperature for both Pt/Al₂O₃ and Pt/SiO₂ samples. The dependence of νCO on the size of the platinum particles was calculated for SiO₂- and Al₂O₃-supported catalysts at full coverage of the surface, i.e. at $\theta(\text{CO}) = 1$. Since in this investigation the only variable parameter for the samples on each type of support was the size of the metal particles, the observed increase in νCO with the heat-treatment temperature can be linked to an increase in the size of the platinum particles. This result agrees with that obtained by Dalla Betta [922], where a higher value of νCO was found for particles of a larger size. It must be remarked that a considerable further increase of the platinum particle size (the absorption of CO was carried out on a Pt/Al₂O₃ sample with a platinum particle size of 140 \AA) leads to a further increase of the νCO value up to 2095 cm^{-1} . Direct confirmation of the established relationship between νCO and Pt particle size has been obtained for investigated samples (7% Pt/Al₂O₃) at the comparison of the dispersion (D) of supported platinum obtained by means of the ARD (atomic radial distribution) method and IR spectra of adsorbed CO:

$D(\text{Pt})$	ARD (\AA)	13	13	23	27	> 60	> 60
νCO	(cm^{-1})	2069	2070	2084	2083	2087	2088

Table 3.8. Dependence of the platinum dispersivity and of νCO on the heat-treatment conditions.

2.1 % Pt/Al ₂ O ₃			2.9 % Pt/SiO ₂		
T_{red} (K)	Pt_s/Pt_t	νCO (cm^{-1})	T_{red} (K)	Pt_s/Pt_t	νCO (cm^{-1})
673	0.94	2060	673	0.68	2063
773	0.91	2062	773	0.64	2077
873	0.88	2069	873	0.60	2079
973	0.85	2070	973	0.54	2080

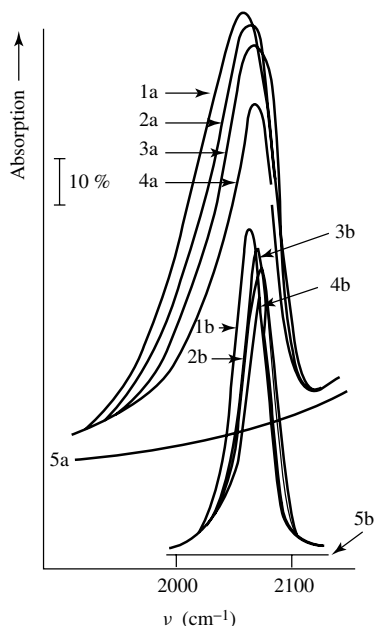


Figure 3.34. IR spectra of CO adsorbed on samples of (a) Pt/Al₂O₃, and (b) Pt/SiO₂, after treatment with H₂ at: (1), 673; (2), 773; (3), 873; (4), 973 K: (5), background spectra of the samples.

Table 3.9. Unusual CO bands in the IR spectra of platinum catalysts.

Catalyst	Pre-treatment of the reduced catalyst	$\nu(\text{cm}^{-1})$	Assignment
Pt/SiO ₂	–	2090	CO on Pt(111)
		2100	CO on terraces
6.2 % Pt/Al ₂ O ₃	CO oxidation by O ₂	2123	CO on PtO
		2090	CO on Pt ⁺
5 % Pt/Al ₂ O ₃	Heating under 100 torr O ₂ at 323 K for 1 h	2120	$\begin{array}{c} \text{O} \\ \\ \text{Pt} \\ \\ \text{CO} \end{array}$
		2090	
Pt–Cr/HZSM-5	No pre-treatment	2120	Pt ^{δ+} –CO
		2092	Pt–CO
0.5–5 % Pt/Mor	No pre-treatment	2123	–O–H···Pt ^{δ+} –CO
		2092	
1 % Pt/HZSM-5	No pre-treatment	2123	Pt ^{δ+} –(CO) ₂
		2092	
		2082	

Results obtained by Solomennikov and Davydov [938] permit us to conclude that the position of the absorption band of adsorbed CO depends on the metal particle size but only slightly depends on the conditions of the deposition and the platinum content in the sample. The shape of the νCO band in the 2100–2000 cm⁻¹ region can indicate the character of the distribution of

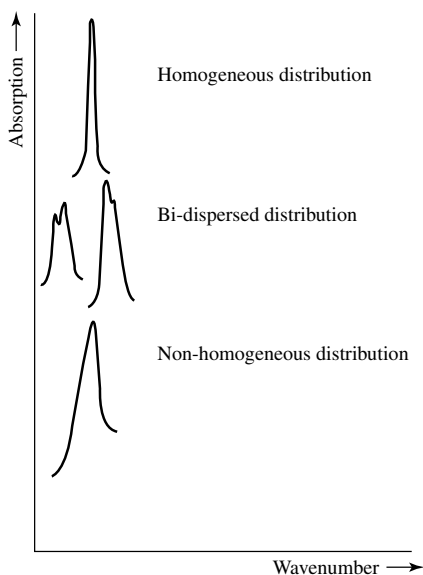


Figure 3.35. Illustration of the dependence of the IR spectra of adsorbed CO as a function of the type of metal distribution.

the particles over the surface, i.e. homogeneous, nonhomogeneous, or bi-dispersed distributions (Figure 3.35) [938].

Shifts in the CO band position are usually interpreted as evidence of changes in the electronic properties of supported metals [922–942]. The exact peak position depends on the surface coverage [943], size of the metal particles [938, 944], and on changes in the metal electron structure [945]. In view of this, the variation of ν_{CO} with variations in the dispersity of the deposited platinum indicates that the electronic states of the surface platinum atoms depends on their particle sizes. In fact, in theoretical articles devoted to calculations of the electronic structures of metal clusters, containing up to several tens of atoms [946], a substantial difference between the electronic properties of small clusters and those of the bulk metal has been noted (see Figure 3.37a). This fact has also been confirmed experimentally in a study of the dependence of the nickel emission spectra (with excitation by synchronous radiation) on the particle size of the supported nickel [947].

It is also well known that the spectral picture of adsorbed CO depends on the properties of the adsorption centers and on the character of interaction between the molecules adsorbed on the surface.

Lateral interactions

Spectral manifestations of the lateral interactions give the possibility of obtaining data about the coordinations of the surface sites and also about the influence of the surrounding atoms on the strength of these sites. This is why the frequency shifts caused by the interactions which take place on the surfaces of solids provide a good parameter for the study of the surfaces of catalysts.

The frequencies of the stretching vibrations of isolated molecules of adsorbed CO (singleton, ν_0) provide a sensitive test for metal electron density. However, the ν_{CO} observed after the adsorption of even small amounts of CO is shifted due to lateral interactions. When the adsorption is on the faces of a single crystal, these interactions are caused by the formation of small CO ‘islands’ on the surface [26, 36]. In the case of highly dispersed supported metals with inhomogeneous

distributions of the molecules over the surface, this occurs because of the difficulties for the migration of the CO molecules into the bulk of the catalyst.

In order to find the value of ν_0 , two methods are usually used. The first of these involves extrapolation of the obtained experimental correlation between ν_{CO} and the surface coverage to zero value. For this, it is first necessary to adsorb CO at a pressure which gives full coverage, and then to evacuate the sample at increasing temperatures with simultaneous recording of the spectra at each stage of desorption. A reduction in the coverage at higher temperatures is accomplished by decomposition of small CO islands and can cause a more homogeneous distribution of CO over the surface [950]. In the case of an inhomogeneous metal surface, the obtained value for ν_0 is characteristic of the centers with the largest electron densities.

The second method, suggested by Hammaker *et al.* [954] gives the possibility of separating the static (or chemical) shift ($\Delta\nu_{\text{st}}$), caused by the change in electron density on the metal atom due to CO adsorption on the neighboring atoms, from the dynamic shift ($\Delta\nu_{\text{dyn}}$) caused by the resonance interaction between vibrating dipoles. To obtain the value of the latter shift, a plot of the relationship between the position of the ^{12}C absorption band observed at full coverage of the surface against the concentration of the ^{12}C isotope has to be constructed and then extrapolated to zero. At the limit, the value obtained, ν_a , is different from that of pure ^{12}C adsorbed at the same coverage, ν_s , and $\Delta\nu_{\text{dyn}} = \nu_s - \nu_a$. The static shift is given by $\Delta\nu_{\text{st}} = \nu_a - \nu_0$. For instance, the shift on pure Pt became as small as that obtained on certain crystal faces [26, 943, 955], with a common dynamic ($\Delta\nu_{\text{dyn}}$) frequency shift. The geometric influences of the promoters are reflected in the value of ν_s and lead to a decrease of $\Delta\nu_{\text{dyn}}$. The reason for the change of the ν_a value points to the change of electron density on the strongest of the adsorption centers participating in the adsorption of CO. Since the value of $\Delta\nu_{\text{dyn}} = (\nu_s - \nu_a)$ is not found to change from low-dispersed to highly dispersed samples, it cannot be expected that the static shift obtained from Pt will be manifested in the spectra of highly dispersed samples. Hence, the value of $\nu_{\text{inhom}} = (\nu_a - \nu_0)$ in this case can be a measure of the inhomogeneity of the metal surface. With an increase in the degree of dispersion, the relative portions of the platinum atoms which interact with the support also increase. The latter is reflected in the increase of inhomogeneity.

Influence of promoters

The change of ν_0 on the addition of a second component gives information about the ligand action of the promoter. Both an inhomogeneity of the metal surface and lateral interactions in adsorbed layers affect the spectral picture of adsorbed CO with increase of coverage. The geometric influence of a promoter is to increase the distance between the neighboring metal atoms which are available for adsorption. Hence, both the interactions of adsorbed molecules and the frequency shifts decrease with the increase of coverage by the promoter. When ν_{CO} became independent of the coverage, in the case of a homogeneous metal surface, this is the sign that the sets of adsorptions have been isolated by the promoter.

To explain the action of promoters on bimetallic catalysts, the concepts of both ligand (electronic) and geometric (cluster) effects are usually used [978–981]. It is clear that the shift of the absorption band of CO linearly adsorbed over Pt at maximum coverage in promoted catalysts compared with that of the unpromoted sample characterizes a joint operation of both marked effects ($\Delta\nu_{\theta \rightarrow 1}$). The contribution of the ligand effect ($\Delta\nu_{\theta \rightarrow 1}$) can be estimated as the difference between the positions of absorption maxima of CO adsorbed on promoted and nonpromoted catalysts at the maximum surface coverage ($\theta = 0.1-0.05$). The geometric effect ($\Delta\nu_g$) can be calculated as follows: $\Delta\nu_g = \Delta\nu_{\theta \rightarrow 1} - \Delta\nu_{\theta \rightarrow 0}$.

The $\Delta\nu_{\text{dyn}} (= \nu_s - \nu_a)$ and $\Delta\nu_{\text{st}} (= \nu_a - \nu_0)$ values, characteristic of the properties of the surface metal clusters and their change upon promotion, can be estimated by using the values of ν_0

(singleton), ν_s (the frequency of pure ^{12}CO) and ν_a (the frequency of adsorption of CO molecules isolated among other molecules in an isotopic mixture) of monometallic and promoted samples.

The geometric effect of the metal promoter can be characterized by the change which took place on the addition of promoter, i.e. $\Delta\nu_g = \Delta\nu_{\text{dyn}}(\text{MM}_1) - \Delta\nu_{\text{dyn}}(\text{M})$, where MM_1 represents the promoted metal. The difference in the ν_0 frequencies of isolated molecules at low coverage for the promoted and nonpromoted states, $\Delta\nu_L = \nu_0(\text{MM}_1) - \nu_a(\text{M})$, can be a measure of the ligand effect of the promoter on the strongest centers. The ligand effect of the promoter on the most abundant centers can be estimated by the frequency change, $\Delta\nu_L = \nu_a(\text{MM}_1) - \nu_a(\text{M})$.

The change of the singleton value upon promotion measures the ligand effect of the promoter, i.e. the effect of the promoter on the strength of the Pt–CO ligand band. The geometric influence of the promoter results in an increase of the distance between neighboring platinum atoms available for adsorption. This is why the interaction between adsorbed molecules became weaker, and the shift of the band of adsorbed CO decreases with increasing coverage. If there is no dependency of νCO on the coverage, the case is realized of an energy-homogeneous platinum surface with Pt atoms isolated by the promoter.

All of these facts has been successfully used in the study of promoted metallic systems and alloys [955, 956, 982–988]. The ligand effect due to the resulting change in the electronic donor–acceptor properties of platinum adsorption sites has been observed for samples in which Mn or In are present (Table 3.10), whereas the geometric effect, which is probably due to the platinum dilution by the second component, reflected in the CO spectra, is exhibited on Pt catalysts (0.5–0.05 wt% Pt) promoted by In. Support for this conclusion comes from studies of infrared spectra of adsorbed ^{12}CO : ^{13}CO mixtures of variable content. The data obtained by these two separate methods are fully consistent.

Influence of support

The occurrence of a common frequency region for samples of Pt/ Al_2O_3 and Pt/ SiO_2 (2063–2070 cm^{-1}) shows that the electronic properties of surface platinum atoms can be the same for particles of different sizes on different supports (Figure 3.36). This fact can be understood from the suggestion that the nature of the support also affects the electronic properties of the surface platinum atoms. In this case, a variation in the electronic properties of the surface atoms,

Table 3.10. Influence of promoters on CO stretching vibrations in PT–CO complexes.

Sample (wt%)	Dispersity, $\text{Pt}_{\text{sur}}/\text{Pt}_{\text{tot}}$	νCO (cm^{-1})		Ligand factor, $\Delta\nu_{\theta \rightarrow 0}$ (cm^{-1})	Geometrical factor, $\Delta\nu_g$ (cm^{-1})
		$\theta_1 \rightarrow 1$	$\theta_2 \rightarrow 0$		
I 0.5 Pt	0.33	2085	2047	–	–
0.5 Pt–2.0 In	0.14	2060	2035	10	15
0.5 Pt–2.0 Ga	0.21	2082	2047	0	0
0.05 Pt	–	2075	2045	–	–
0.05 Pt–0.5 In	–	2060	2040	~5	10
II 0.5 Pt	0.77	2082	2045	–	–
0.5 Pt–1.0 Sn	0.35	2075	2045	0	~5
0.5 Pt–2.0 Sn	0.26	2080	2045	0	0
III 0.5 Pt	1.10	2083	2040	–	–
0.5 Pt–4.0 Mn	0.85	2075	–	–	–
		2050	2020	20	–

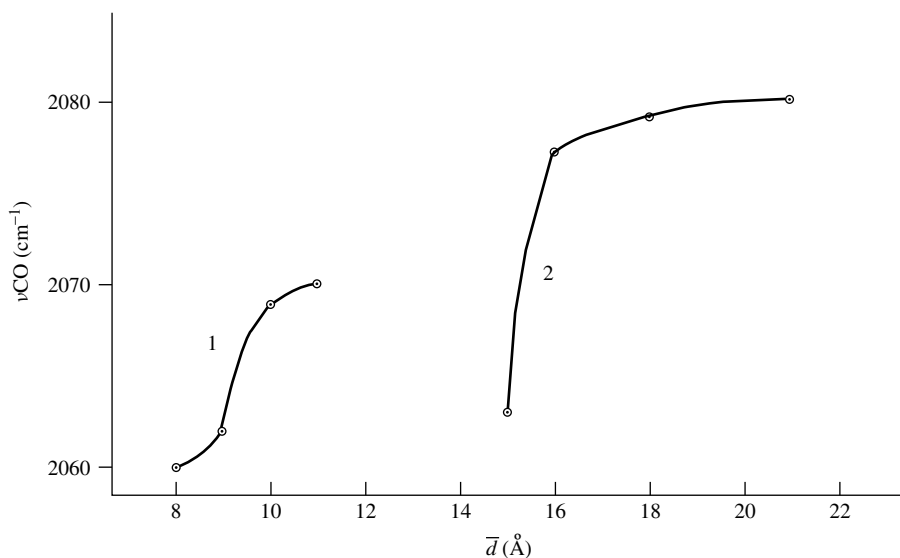


Figure 3.36. Dependence of the stretching vibrations of Pt-CO (at $\theta = 1$) on particle size for different supports: (1) Al_2O_3 ; (2) SiO_2 .

associated with a variation in the size of the metal particles, may be compensated for by a change of the electronic properties caused by different supports.

It is clear that to a certain degree the electronic properties of the surface atoms should depend on the particle size, if the different results obtained for the two extreme cases of bulk metal and separate atoms are borne in mind (Figure 3.37). Variations in the electronic properties of the surface metal atoms upon varying the particle size may be linked with the so-called 'geometric factor', i.e. with a change in the average number of neighboring metal atoms, i.e. a change of the coordination number of the surface atoms. In this case, as a model for a surface atom, i.e. a particle of any particular size, there is taken an atom with a coordination number equal to the average coordination number of a surface atom of a metal particle of such a size. This allows a linkage between the observed dependence of ν_{CO} on the metal particle size with the coordination number of the surface atom, as postulated by Blyholder [945]. According to this picture, a π -bond exists between the metal atom under consideration and its nearest surrounding neighbor, because of the partially filled d-orbitals of the metal. The metal atom which has the large coordination number is linked to the largest adjacent metal atoms. In this case, the adsorbed carbon monoxide molecule competes for d-electrons with the largest number of metal atoms. According to this molecular orbital (MO) theory, the degree of π -bonding of a carbon monoxide molecule to the metal atom is higher with a smaller number of metal atom neighbors. This in turn decreases the order of the carbon-oxygen bond in Pt-CO surface complexes and, therefore, ν_{CO} . Thus, it can be expected that an increase of the metal particle size should lead to an increase of the average stretching vibration frequency of linear carbonyl complexes (see Figure 3.37(a)).

However, there is another factor which may change the electronic properties of surface metal atoms, namely the effect on the metal particles of their interactions with the support at the stabilization center. It is assumed, as proposed by several authors [948], that the metal particle is stabilized on electron-acceptor centers of the support (protic or aprotic), so that a transfer of electron density from the atoms of the metal particle to the support is to be expected. Such a transfer would show up to a greater extent with a smaller number of atoms in the metal particle.

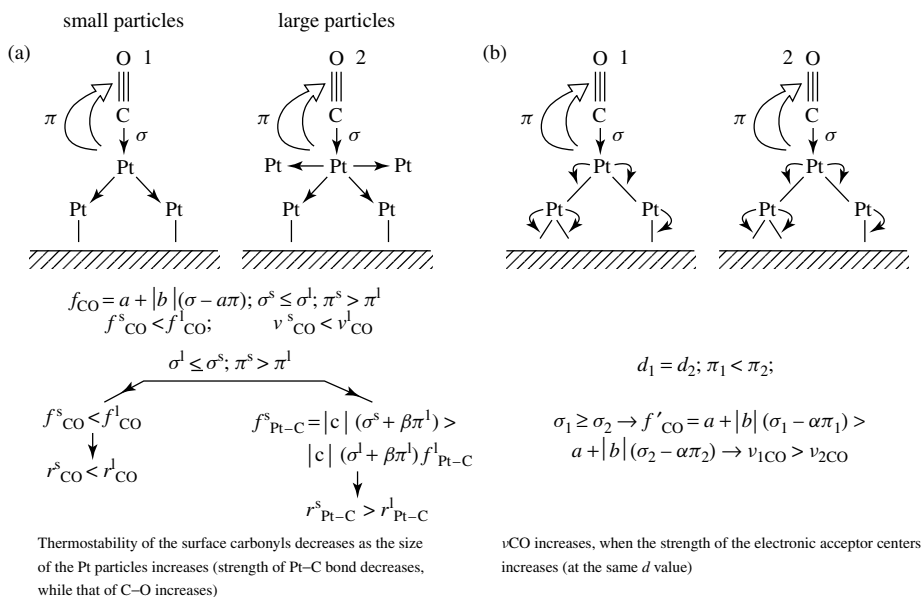


Figure 3.37. Influence of (a) the electronic states of the surface atoms depending on the size of cluster of platinum on their adsorption properties; (b) the stabilization centers of support on electronic properties of platinum. (a) r , bond order; c , β , constants; σ , π components of the M-CO bond; f , force constant; s , small particles; l , large particles; (b) d , size of platinum particles; σ , π , components of the M-CO bond.

This would lead to a lower capability of the surface metal atom to delocalize d-electrons into the π^* orbital of CO and to a lesser bonding of a surface metal atom to a carbon monoxide molecule. In other words, on reducing the size of the particles an increase of the ν_{CO} of the surface carbonyl groups should be observed (Figure 3.37(b)). Since in the experiments a lowering of ν_{CO} is observed upon a reduction in the metal particle size, it has to be concluded that of the two opposing effects the geometric factor (change of the number of neighbors of the surface metal atoms) prevails, when the size of the metal particles is varied for platinum deposited on SiO_2 or Al_2O_3 , in the range of dispersity investigated. The fact that the ν_{CO} values are very similar for Pt particles on SiO_2 and Al_2O_3 , although the latter has a greater electron-withdrawing power, implies that a compensation is provided by the larger average particle sizes on the SiO_2 -supported catalyst.

Thus, there are two effects acting in opposite ways on the position of the absorption band of the adsorbed carbon monoxide. The predominance of one effect, namely the geometric one, over the other can be explained in the following way. In the region where the greatest influence of the stabilization center on the electronic properties of the surface metal atoms would be expected, i.e. for particles of small size, there may take place a localization of the interactions associated with electron transfers within the metal particles, wherein the influence of the stabilization center extends only to the metal atoms which bring about the stabilization of the metal particles on the support and the immediate environment of those atoms. However, with larger metal particles sizes, i.e. under conditions where electron transfer in the particle is hindered (at sizes greater than 20–30 Å, according to the estimates of Anderson [949]), the transfer of electron density from atoms of the metal particles to the support (decreasing as the third power of the size) becomes insignificant. In view of this, the variation of ν_{CO} , depending on the metal particle sizes, can be linked with the change in the electronic properties of the surface metal atoms due to the change in the average coordination number (Figure 3.37(a)).

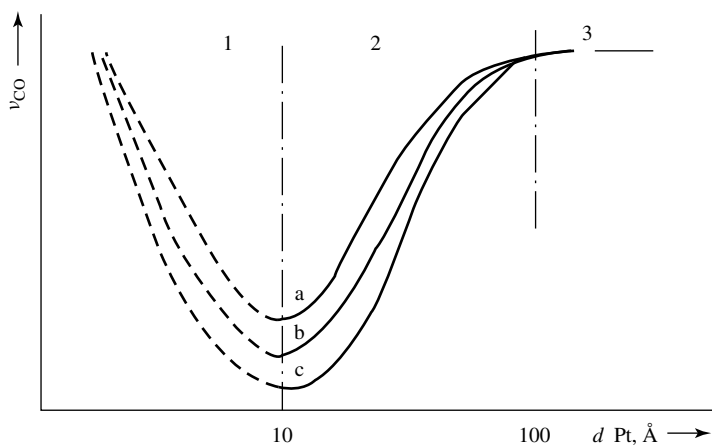


Figure 3.38. Influence of the degree of dispersion of platinum particles and the nature of the support on the electronic states of the surface atoms of the metal (curves a, b and c correspond to different supports).

A comparison of the results obtained in the case of CO adsorption on samples of dispersed platinum supported on different oxides leads to the conclusion that the nature of the center of stabilization of the metal particles influences the electronic properties of the surface platinum atoms. In terms of the mechanism expounded above, we can consider the existence of a frequency region in which the electronic properties of the surface platinum atoms, in particles of different sizes but over different supports, may be the same, i.e. they are characterized by the same values of ν_{CO} (Figure 3.38).

It is known that the strength of the electron-accepting centers on the SiO_2 surface is less than that on Al_2O_3 [19]. Thus, the transfer of electron density from atoms of a metal particle will be greater with stabilization on Al_2O_3 as compared to SiO_2 , and hence there will be a lesser degree of π -bonding of the carbon monoxide molecule to the surface atom of a metal particle stabilized on Al_2O_3 , relative to stabilization on SiO_2 . As has been shown previously, reduction in particle size leads to a greater degree of π -bonding of the carbon monoxide molecule to a surface atom of a metal particle. This results in a compensation effect of the support on the electron properties of the surface platinum atoms by the change in the metal particle size.

The CO stretching frequency has also been found to be very sensitive to the metal surface coverage by co-ligands [950]. Adsorption of unsaturated hydrocarbons (ethene and benzene [942, 951] or Lewis bases (ammonia and pyridine [952, 953]) on the metal surface 'pre-covered' by CO shifts the ν_{CO} band to lower wavenumbers.

It was noted earlier that the frequency of the stretching vibration of the isolated CO molecule (singleton, ν_0 , i.e. $\nu_{\text{M-CO}}$ at $\theta_{\text{CO}} \rightarrow 0$) is a sensitive measure of the electron density on metals, including Pt. However, the band observed after adsorption of even small amounts of CO at room temperature shifts because of lateral interactions. Primet [950], in order to determine the extent of the dipole-dipole coupling on the position of the CO frequency, used the isotopic dilution method [943, 954–956]. Mixtures of ^{12}CO – ^{13}CO with different isotopic concentrations were brought into contact with the sample of supported catalyst. By increasing the concentration of ^{13}CO in the mixture, the ^{12}CO molecules adsorbed on platinum were progressively substituted by ^{13}CO molecules; the interactions of the CO layer with the surface remain unchanged since the bonding of ^{12}CO and ^{13}CO molecules with the metal is identical. On the contrary, the dipole-dipole coupling between the ^{12}CO vibrations decreases with the amount of ^{13}CO molecules in the adsorbed layer since the ^{12}CO species are diluted by ^{13}CO molecules. In addition, ^{12}CO dipoles do not couple

with the ^{13}CO dipoles. By using various ^{12}CO – ^{13}CO mixtures and by extrapolating the $\nu^{12}\text{CO}$ frequency to zero coverage in adsorbed ^{12}CO , it is possible to find the $\nu^{12}\text{CO}$ frequency of singlet ^{12}CO , i.e. free of dipole–dipole coupling. For the Pt/ Al_2O_3 samples used by Primet [950] a νCO frequency close to 2052 cm^{-1} will be typical of adsorbed molecules free of dipole–dipole coupling or isolated CO molecules (singletons).

The higher frequencies observed in the spectra of CO adsorbed on Pt/supported systems can result from a heterogeneous distribution of the CO molecules over the platinum particles in the sense that all of the CO is adsorbed, at high local coverage, on the outer layers [943, 954–957]. Heating in a closed system results in redispersion of the CO molecules over the whole metallic phase. The frequency of the CO will be seen as a singleton, i.e. when there is no dipole–dipole coupling between adsorbed CO molecules after the redispersive treatment at 573 K and the CO molecules can be considered as isolated.

Hendricks *et al.* [957] compared the IR spectra of CO adsorbed on Pd/ SiO_2 and on flat single crystal planes. The IR spectra of CO adsorbed on Pd/ SiO_2 was monitored as a function of θ_{CO} and the isotopic composition x , where $x = ^{12}\text{CO}/(^{13}\text{CO} + ^{12}\text{CO})$. The results show that on rough curved surfaces of small Pd particles there is little tendency to clustering of CO, i.e. $\Delta\nu_{\text{dyn}}$ is small. Results do not support the idea of chemical (competition) effects. An alternative explanation of the large shifts ($\Delta\nu_{\text{max}}$) observed on flat single crystal planes is suggested: with increasing θ_{CO} , the CO molecules may also change their adsorption sites while the latter process is absent on small particles of Pd [957]. Recent evidence suggest that large νCO changes can occur with same adsorption sites, i.e. equal to 3-fold sites of CO or NO on (111) surfaces.

It should be noted that the problems under discussion are related directly to the question of what kind of information can be obtained by IR spectroscopy about adsorbed CO on supported metals. As stated above, the general characteristics of the metal are the singleton frequency (electronic state of the surface metal atoms) and the coverage-dependent νCO shift (the nature and extent of lateral interactions). Since both parameters are very similar for metals supported on inert oxides (SiO_2 and Al_2O_3) and for single crystals, it is clear that the supporting of metals did not notably affect their properties in CO adsorption. Furthermore, the singletons are not changed even for the oxides of transition and rare-earth elements, so it is obvious that the electronic states of the metal surfaces are not affected either. It can be so because, for the most part of the investigated systems, the size of the particles was greater than 50Å but this effect can be detected just for smaller particles [928]. As for the coverage-dependent shifts (or νCO at $\theta_{\text{CO}} = 1$) for the given metal, these values are somewhat different (ca. 10 – 15 cm^{-1}) for various supports but never exceed that for single crystals. It is clear that this is the result of a ‘geometric effect’, namely the difference in the sizes of the islands on metal surfaces accessible for CO adsorption, since the νCO shift-dependence could be observed when the sizes of these islands are related to the diameters of the metal particles. Indeed, for SiO_2 - and Al_2O_3 -supported catalysts it is known that the particle sizes affect the νCO at $\theta_{\text{CO}} = 1$, as has been shown above and by Solomennikov *et al.* [938].

Strong metal–support interaction

Under fixed conditions, a strong metal–support interaction (SMSI) is possible. This has been found in the case of transition-metal oxides, such as TiO_2 [969], and even for nontransition-metal oxides, such as Al_2O_3 [942, 970], SiO_2 [971, 972] and MgO [973]. The treatment of Pt/ SiO_2 with hydrogen at 773–923 K yields Pt/Si alloys at the lower temperatures and platinum silicides (Pt_3Si and Pt_2Si_5) at higher temperatures [974]. Such alloys are usually formed in the case of a ‘super-strong’ interaction of metal with a support and is usually characterized by a decrease in the sorption capacity of the metal. According to the CO chemisorption, an increase in the degree of alloying causes (i) the shift of νCO (for both linear and bridged carbonyls) to lower wavenumbers, (ii) decreases in the intensities of the νCO bands of linear carbonyls, and (iii) an

increase of the $\nu\text{CO}_{\text{bridged}}/\nu\text{CO}_{\text{linear}}$ intensity ratio. These authors interpreted the phenomena as a simultaneous effect of Pt surface dilution, enhanced back-donation from platinum to CO, and Pt d-band narrowing. In contrast, for the case of separated TiO_2 [975] (see Table 3.9), additional features in the spectra of adsorbed CO compared with other supports have been observed. However, it should be pointed out that these samples of Pt/TiO_2 have been prepared by ionic exchange. Many hypotheses have been proposed to explain SMSI. Initially, electronic effects were considered to be the cause, but now the following explanation is accepted. Titania from high-temperature reduction catalysts is partly reduced and a sub-oxide phase migrates onto the metal particles. This means that part of the metal surface, partially covered by TiO_x , is blocked. As a result, the chemisorption capacity of the metal strongly decreases and structure-sensitive reactions, which need a larger ensemble of metal atoms, are suppressed. The existence of admixtures, e.g. Na^+ , facilitates the migration of TiO_x moieties and an SMSI occurs at low temperatures of reduction. At high reduction temperatures, partial or complete encapsulation of the metal particles in the titania may occur. On reduction above 1073 K, intermetallic compounds and alloys are formed.

The structure and reactivity of Pt films supported on cubic ZrO_2 (100) surfaces were studied by using a combination of AES, TPD and HREELS [976]. Platinum films deposited from the vapor phase were found to grow in a layer-by-layer fashion on the ZrO_2 (100) surface at 300 K. Heating to temperatures of 700 K caused the Pt films to agglomerate into particles. Carbon monoxide was found to adsorb in both a linear configuration on the top and in a twofold bridging configuration on the two-dimensional supported Pt films.

Boundary species

Investigations using IR spectroscopy of the adsorption of CO on Rh-, Pd- and Pt-containing catalysts supported on TiO_2 and other transition-metal oxides or rare-earth oxides have clearly shown that additional broad bands appear from the carbonyl complexes below 1800 cm^{-1} , besides those observed with zeolites, silica or alumina as supports (Figure 3.39). Analogous absorption bands are obtained for all investigated systems involving Group Eight metals supported on transition-metal oxides. The spectral characteristics (for instance, the positions of the absorption bands) change significantly if the nature of the metal is varied while the nature of the transition-metal oxide remains the same. Two types of species localized along the boundary forming the intersection of the external surfaces of the support and the metallic particles have been verified on palladium by studying samples that differed in the size of the metal particles. Such compounds were proposed first for the Cu/ZnO system (νCO , 1580 cm^{-1}) [977].

3.8.2 CATIONIC STATES OF PLATINUM

In spite of the significant stability of platinum to oxidation, oxidation states can be more easily realized in the case of supports of the zeolite type which have stronger and more active centers than the oxides. The structure of these can be represented in the following way:

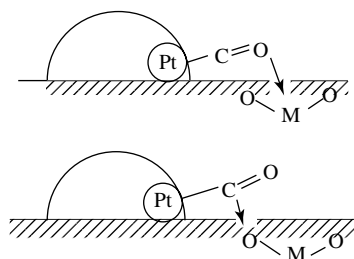


Figure 3.39. Schematic illustrations of two forms of boundary complexes.

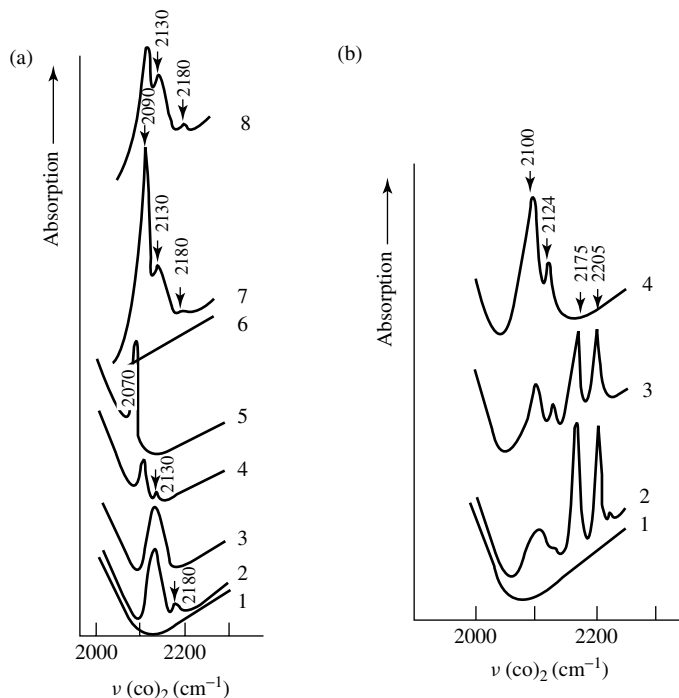


Figure 3.40. (a) Infrared spectra of CO adsorbed on Pt/Al₂O₃ and Pt/SiO₂ subjected to preliminary oxidative treatment: (1) background spectrum of Pt/SiO₂; (2) treatment of Pt/SiO₂ in NO₂; (3) subsequent vacuum treatment of Pt/SiO₂, at ca. 0.01 Pa for 0.5 h; (4) treatment of Pt/SiO₂ in NO; (5) reduction in H₂ at 673 K; (6) background spectrum of Pt/Al₂O₃; (7) treatment of Pt/Al₂O₃ in O₂ with vacuum treatment at 673 K; (8) treatment of Pt/Al₂O₃ in O₂ with vacuum treatment at 298 K. (b) Infrared spectra of CO adsorbed on Pt-HY: (1) background spectrum; (2) after adsorption of CO; (3) after vacuum treatment, at ca. 0.01 Pa for 0.5 h at 298 K; (4) after holding of the vacuum-treated sample for ca. 70 h.

The spectra of CO adsorbed on Pt-Y zeolites oxidized at 673 K show absorption bands at 2175 and 2205 (disappearing on prolonged evacuation at 293 K) and 2130 and 2100 cm⁻¹ (destroyed by vacuum treatment at 573 K) [941] – see Figure 3.40. These absorption bands can indicate the presence of platinum in oxidation states 2+, 1+ and 0. The conclusion that platinum can exist in zeolites in the form of singly charged ions lead to the expectation that these species can, in principle, be detected by ESR spectroscopy or ESCA. Similar complexes are formed on the surface of other supported on Al₂O₃ and SiO₂ platinum catalysts, too [941]. The presence of two absorption bands at 2175 and 2205 cm⁻¹ is an indication of the existence in zeolite of two types of Pt²⁺ ions, where the difference between which may be due to their stabilization at different sites in the zeolite skeleton. The influence of the sites within a zeolite on the electronic states of the surface atoms of platinum surpasses that for SiO₂ and Al₂O₃. A comparison of the frequencies shows that the dispersed platinum in zeolite is electronically deficient (in comparison with that of similar-sized particles on SiO₂ and Al₂O₃) but that the electronic states of the uncharged platinum atoms in the dispersed particles on the zeolite and in particles of larger size on the supports are similar (since the frequencies 2100 and 2095 cm⁻¹ are close). The surface atoms of metal particles with sufficiently large diameters on the SiO₂ and Al₂O₃ supports can serve as a model for the surface atoms of the solid metal, since the influence of the stabilization sites

of the metallic particles is small, and the mean coordination numbers of the surface atoms are very similar [945]. On this basis, it may be concluded that the electronic states of the surface atoms of the uncharged dispersed metal atoms on the zeolite and the solid metal are similar. In fact, when CO is adsorbed on a metallic foil (high coverage values), an absorption band is observed at 2101 cm^{-1} [958] for surface carbonyls. It should, however, be noted that the displacement of νCO from 2065 to 2101 cm^{-1} as a function of the coverage on the metal foil may be due to a dipole–dipole interaction or to energetic nonuniformity of the foil surface, i.e. the sites with the smallest coordination numbers (which produce the most tightly bound Pt–CO complexes and are characterized by the smallest values of νCO) will be filled first. The higher value, $\nu\text{CO} = 2101\text{ cm}^{-1}$, corresponds to the stabilization of CO on those sites with the highest coordination numbers, which are characteristic of the solid metal surface. The displacement of νCO relative to the frequency for gaseous CO is due to the transfer of electrons from the metal to the π^* -orbitals of CO. Thus, the adsorption of CO should cause a deficiency of electrons in the metal particles, which will be greater, the greater is the ratio of surface metal atoms to the bulk metal atoms. In the case of the metallic foil, the number of surface metal atoms is small in comparison with the bulk atoms, and the deficiency should also be small in comparison to the dispersed systems. Therefore, the influence of the so-called electronic factor on νCO for the metallic foil may be negligible.

Primet *et al.* [940], based on comparison of the spectral images of CO adsorbed on the metal foil, concluded that the electronic states of the surface atoms of dispersed platinum on the zeolite and the solid metal are practically identical and that the surface atoms of dispersed platinum supported on SiO_2 or Al_2O_3 have an electronic excess in comparison to the solid metal. All main conclusions made in this study have been confirmed in recently published work [959], the authors of which concluded that the vibrational spectra of CO adsorbed on dispersed metal catalysts give valuable information on (a) the dispersion and morphology of the particles, (b) the oxidation state of platinum, (c) the presence of co-adsorbed species, (d) the adsorbate–adsorbate interactions, and (e) metal–support interactions. The spectra of CO adsorbed on Pt/ Al_2O_3 samples indicate that two faces are dominant on the metal particles. Bands due to CO adsorbed on oxidized platinum sites are also observed on reduced samples. Comparison of spectra from samples with different Pt loadings indicate a metal–support interaction involving the most electron-deficient sites.

Carbon monoxide adsorption has also been studied on reduced Pt/NaY zeolites [960, 961]. These authors observed the 2070 and 1850 cm^{-1} bands attributed to linear and bridged species of CO adsorbed on Pt^0 , respectively. By using RAIRS measurements [960], two additional bands at 580 and 465 cm^{-1} have been detected and assigned to $\delta\text{Pt–CO}$ (or $\nu\text{Pt–O}$) and Pt–C stretching modes.

IR spectroscopy of adsorbed CO indicates that the electron density of supported platinum in Pt/LTL and Pt/ SiO_2 catalysts increases with increasing level of alkali on the support [962]. For both Pt/LTL and Pt/ SiO_2 samples, the bands of the linear, as well as the bridged coordinated CO, shift to low wavenumbers as the support alkalinity increases.

Adsorption of carbon monoxide on reduced Pt/ZSM-5 results in the appearance of two bands at 2123 and 2092 cm^{-1} [963]. An increase of the reduction temperature leads to the disappearance of both bands and the appearance of a narrow symmetric band between 2082 and 2060 cm^{-1} , corresponding to linearly adsorbed CO. The 2080 – 2060 cm^{-1} band shifts are due to elimination of dipole–dipole interactions with a decrease in surface coverage on the platinum particles. Upon thermodesorption, this band shifts toward lower frequencies and splits into two components, at about 2070 and 2050 cm^{-1} . The band at 2080 cm^{-1} has been attributed to small Pt particles inside the zeolite channels: the increase in the stretching vibration frequency of CO adsorbed on these particles results from the decrease of the electron density on the particles due to the interaction with strong Brønsted sites of the highly acidic HZSM-5 zeolite [963–965]. This band can also be

attributed to the particles on the outer zeolite surface. The electronic structures of these particles remain almost unaltered and the adsorbed CO exhibits the lower frequency, characteristic for Pt supported on a low-acidic support (see Table 3.9).

As for the 2123 and 2092 cm^{-1} bands observed in the spectra of CO adsorbed on Pt/ZSM-5, the intensities of these both change. Several alternative interpretations can be considered for these band assignments. Zholobenko *et al.* [966] have proposed in the case of Pt-mordenite that the 2123 cm^{-1} band be assigned to CO adsorbed on monatomic Pt^0 species. On the basis of chemisorption data, it has been shown that a CO/Pt ratio for samples with a high relative concentration of Pt in atomic dispersion is greater than 1. Bischoff *et al.* [967] therefore concluded that coordinatively unsaturated platinum atoms are able to coordinate two CO molecules, thus forming dicarbonyls. In this case, the 2091 cm^{-1} band should correspond to the asymmetric vibration, while the 2123 cm^{-1} band corresponds to the symmetric vibration of the dicarbonyl (see Table 3.9). The possible re-oxidation of Pt metal particles by protons from the zeolite, as observed in the case of Rh (see Section 3.7), should be borne in mind as a possible explanation for the observation of such an oxidized state of the metal atom.

An FTIR study of CO chemisorption on Pt metal clusters in KL zeolite showed the existence of two groups of platinum particles. The first group was localized on the outer surface of the KL microcrystals in the near-surface region; these had bands at 2060–2105 cm^{-1} , close to those of platinum on conventional supports. The particles of the second group were formed inside the KL channels, where their electronic structure was presumably strongly perturbed by the KL framework. Carbon monoxide adsorbed on the platinum particles of this group had coverage-dependent bands at 1960–1920 cm^{-1} . The marked downward shift of the νCO band was attributed to the increase of electron density on the second platinum species [968]. It was suggested that small platinum clusters inside the zeolite channels are transformed into $(\text{Zeol-O})_m\text{Pt}_x(\text{CO})_y$ species stabilized by basic oxygen atoms of the KL framework. The transformation was readily reversible upon CO adsorption–desorption at room temperature. These highly active clusters are related to an unusually high activity of this zeolite, for example, in the reaction of *n*-hexane aromatization. Platinum supported on fluorinated alumina contains well-dispersed Pt particles, in contrast to that on $\text{Pt}/\text{Al}_2\text{O}_3$. The high dispersion is a consequence of particle interactions with stronger electron-acceptor sites formed by the fluorination of alumina [968c].

To study the effect of promoters on the surface acidity of the oxide support, IR spectra of adsorbed pyridine were recorded [983]; spectra of adsorbed CO were used to characterize the state of platinum on the oxide support. Similar to the case of Pt-Fe- and Co-containing systems [989, 990], the additives can have the effect of either oxidation or reduction of platinum.

In certain cases, bi- and even multicomponent metallic systems can be formed. The surfaces of such systems, besides dilution and enrichment by one of the components, includes heterometallic groups of the type M_xM_y , detectable by infrared spectroscopy. Metal interaction appears to be indicated in the spectra that have been obtained [916, 991–993].

The IR spectrum of CO adsorbed on Pt/silicalite exhibits an intense band at 2050 cm^{-1} with a shoulder at 1990 cm^{-1} , and two weak bands at 1900 and 1800 cm^{-1} , whereas only the band at 2050 cm^{-1} with a shoulder at 1980 cm^{-1} and a weaker band at 1900 cm^{-1} are exhibited in the spectra of CO adsorbed on PtIn/silicalite [989]. It is known that the adsorption of CO on Pt particles gives rise to two vibration frequencies, one around 2050 cm^{-1} , assigned to Pt–CO linear species, and the other near 1850 cm^{-1} , due to bridged or multi-bound CO species, although the last are not formed on PtIn/silicalite. This is indirect evidence for the formation of PtIn bimetallic sites caused by a dilution of the Pt atoms with In. The wavenumber of the Pt–CO singleton is not very different for these two samples, although the value is low (lower than 2050 cm^{-1}) for high CO coverage. Such a behavior has been attributed by Meriauded *et al.* [988] to the formation of very small platinum particles.

The above results show that the study of cations and metal clusters on the surface of oxides, by examining the IR spectra of adsorbed simple molecules, is promising. It should be noted, however, that the approach proposed is complex and requires that the spectra of adsorbed test molecules be studied in detail for each particular system and in combination with other physical methods. In doing so, it is necessary to take into account, or rule out the possibility of the formation of reduced sites on interaction between CO and oxidized specimens, or their possible re-oxidation on interaction with NO.

3.9 Molybdenum-containing systems

3.9.1 MOLYBDENUM–ALUMINUM OXIDE COMPOUNDS

To prepare Al–Mo catalysts, several methods are available: the adsorption of $\text{MoO}_2(\text{OH})_2$ on Al_2O_3 from the gas phase [994], bonding metal-organic complexes to the Al_2O_3 surface [111], the adsorption of molybdate ions by the carrier from solution [995, 996], and co-precipitation from solutions of ammonium paramolybdate (APM) and $\text{Al}(\text{NO}_3)_3$. The simplest and most widely-used method relies on the impregnation of the Al_2O_3 carrier with solutions of ammonium paramolybdate followed by drying and then strong heating of the catalyst at given temperatures [994–999]. Depending on the concentration and pH of the APM solution, surface compounds of different composition can be obtained on the carrier [997–999]. This is primarily due to the presence of different associations in the APM solution, depending on the pH and on the concentration [1000]. Increasing the pH and lowering the concentration shifts the equilibrium towards the formation of molybdates containing molybdenum ions in a tetrahedral coordination (MoO_{2-4}). At low pH and high concentrations, the dominant species are the isopolymolybdates, in which the molybdenum ions have an octahedral coordination. Furthermore the $\gamma\text{-Al}_2\text{O}_3$ carrier itself has acid–base properties [1001–1004], and therefore an equilibrium, determined by the initial pH and concentration of solution and by the type of carrier (zeropoint potential, Figure 3.41(a)), is established at the interface with molybdenum solutions. By using a more acidic carrier (SiO_2) polymeric compounds can be stabilized at much lower molybdenum concentrations (down to 10 %) than on the more basic Al_2O_3 . On the strongly basic MgO, the formation of octahedral molybdenum polyanions was not detected at any concentration of APM [1002, 1004].

The surface OH groups of the carrier can interact with the molybdenum anions with the formation of surface compounds. A large decrease (or complete suppression) of the fluorescence background accompanying the Raman spectrum, which is attributed to the OH groups on the Al_2O_3 surface, has been noted [999] after the deposition of ammonium paramolybdate on the carrier, thus suggesting its reaction with the OH groups. A Raman study of Al–Mo catalysts prepared by the impregnation Al_2O_3 carriers with ammonium paramolybdate solution of pH between 6 and 11 led to the conclusion [998] that a low molybdenum concentrations (1–3 wt% MoO_3) only MoO_4^{2-} ions are formed on Al_2O_3 even at pH6, when the impregnating solution contains $(\text{Mo}_7\text{O}_{24})^{6-}$ ions. The dissociation of these ions is attributed [998] to an increase in the pH of the solution due to the increased concentration of OH^- ions in solution produced by the ion-exchange adsorption.

The presence has been established of tetrahedral molybdenum ions on the surfaces of Al–Mo catalysts prepared by adsorption of molybdate ions from dilute solutions of APM at a high pH (8.6) [995, 996]. Adsorption from concentrated solutions of APM or at low pH (4.0) results in the stabilization of octahedral Mo polyanions on the Al_2O_3 surface; these are retained when the sample is dried.

According to Giordano *et al.* [999], the Al–Mo catalysts (before being heated) contain tetrahedral ions weakly interacting with the OH groups of the Al_2O_3 . During the subsequent activation of the catalysts by oxidative high-temperature treatment, further interaction of the molybdenum compounds with the carrier surface takes place. Under these conditions, stable monomeric molybdate

complexes (MoO_{2-4}) are formed at low molybdenum concentrations. Experimental confirmation of the formation of a monolayer of tetrahedrally coordinated molybdenum ions was later obtained by different methods, including IR, Raman and UV spectroscopies, XPS and others [104–106, 221, 396, 397, 994, 997–999].

In general, the electronic spectra of molybdenum ions in the UV–Vis region are characteristic for molybdenum(VI) ions by the charge-transfer (CT) transition (related to charge transfer between molybdenum and terminal oxygen) falling in the 20 000–25 000 cm^{-1} region for octahedral coordination. For lower coordination, such as tetrahedral molybdenum(VI), the CT transition is expected at higher frequencies (30 000–35 000 cm^{-1} region). The CT transition for Mo(V) ions falls to higher frequencies (35 000–40 000 cm^{-1}), whereas the d–d transitions of octahedral Mo(V) ions fall in two regions: the $b_2(d_{x,y}) \rightarrow e(d_{xy}, d_{yz})$ near 13 000 cm^{-1} , and the $b_2(d_{xy}) \rightarrow b_1(d_{x^2-y^2})$ near 16 000 cm^{-1} . The d–d transition at higher frequencies ($b_2(d_{xy}) \rightarrow a_1(d_{x^2})$) is generally masked by CT transitions. The intensities of these d–d transitions are generally about ten times lower than those of the CT transitions.

According to most authors, at low concentration (5–10 wt% MoO_3) the whole of the molybdenum in the ‘roasted’ catalysts is present in a highly dispersed state, and mainly as tetrahedral ions (see, for example, [106, 999, 1005]. An increasing in the concentration of MoO_3 (to 16 wt%) increases the fraction of the molybdenum in the octahedral coordination and leads to polymolybdate structures after roasting. At even higher molybdenum concentrations, the MoO_3 and $\text{Al}_2(\text{MoO}_4)_3$ phases are formed [106, 998, 999, 1002–1008].

The degrees of crystallinities of the compounds formed in the MoO_3 – Al_2O_3 system depend on the concentration of molybdenum, while the extent of the reaction depends on the heat-treatment temperature. An X-ray study of amorphous molybdenum compounds, involving atomic radial distributions, and ESR spectroscopic methods have shown [999] that polymolybdates containing molybdenum in an octahedral coordination are formed, in addition to the MoO_3 and $\text{Al}_2(\text{MoO}_4)_3$ phases, during the interaction of APM with Al_2O_3 . An analysis of aqueous extracts from Al–Mo catalysts led to the same conclusion. According to these results, MoO_3 and $\text{Al}_2(\text{MoO}_4)_3$ are soluble in water, so that a large fraction of the supported molybdenum is transferred into solution when the Al–Mo catalysts are treated with water. The UV spectra of the aqueous extracts suggest the presence of molybdenum isopoly anions. It was therefore concluded that in addition to the MoO_3 and $\text{Al}_2(\text{MoO}_4)_3$ phases observed by XRD (which are insoluble and cannot pass into solution), the isopoly compounds are also formed on the surfaces of Al–Mo catalysts, especially at high molybdenum concentrations, as has been confirmed by the presence of water-soluble compounds on the support [106, 221, 396]. For a 25 wt% MoO_3 – Al_2O_3 sample, the bands in the 20 000–25 000 cm^{-1} and in the 11 000–18 000 cm^{-1} regions can be attributed to LCT transitions of octahedral molybdenum(VI) ions and to d–d transitions of octahedral Mo(V) ions, respectively. By combining these results with those obtained by XRD, ESR [999], Raman [998], UV and IR spectroscopies [999, 1003], with the help of specially formulated samples [106, 998, 1008] it is possible to conclude that these compounds are polymeric formations consisting of MoO_6 octahedral or heteropoly compounds of molybdenum and aluminum.

3.9.2 MOLYBDENUM–SILICON OXIDE COMPOUNDS

The chemical reactions in the Mo/SiO₂ system caused by the deposition of the active component are confined (at least, at low molybdenum concentrations) to the surface, and bulk phases are not formed (there are no reports of the formation of silicon molybdates or of solid solutions). The MoO_3 phase is usually observed only for high surface concentrations of molybdenum. The state of the molybdenum ions in the system was studied by various methods (mainly by optical, and ESR spectroscopies). Most of these studies were aimed at the local surroundings of the molybdenum ions (mainly because of the nature of the chosen methods).

The most important and complex problem seems to be to establish the relationship between the coordination state of the ion and the type of chemical compound formed on the carrier. XRD is the method traditionally used to solve this problem. However, as in the case of the Mo/SiO₂ system, it is applicable only at high concentrations of molybdenum, and therefore vibrational spectroscopy plays an important role [106] in analysis of the structures of the molybdenum compounds formed on the surfaces of SiO₂.

The coordination state of molybdenum at low concentrations was studied by ESR and UV spectroscopies [1005, 1010]. The formation of both tetrahedrally and octahedrally coordinated molybdenum ions was observed. The coordination state of molybdenum was identified from the ESR spectra of Mo⁵⁺ (used as a paramagnetic probe) on the basis of correspondence (well established in coordination chemistry) between the structure of the complex and the parameters of the ESR spectra [1110, 1011]. The ESR results agree well with those of diffuse reflectance spectroscopy [1005, 1012, 1013]. At low molybdenum concentrations, tetrahedral molybdenum ions are found on the SiO₂ surface irrespective of the method of preparing the catalyst. At higher concentrations, octahedral molybdenum ions are usually formed, as well as tetrahedral ions. However, there are also reports of molybdenum ions in the two coordination states in a 1:1 ratio at low enough surface concentration of molybdenum (0.1 Mo atom per nm²). Whereas the tetrahedrally coordinated molybdenum ions are present as isolated ions in structures of the dimolybdate and MoO₃ type, the nature of the compounds in which the molybdenum is octahedrally coordinated is still problematic. Castellan *et al.* [1113] studied the Si–Mo system over a wide range of molybdenum concentrations by using a combination of physico-chemical methods: XRD, optical spectroscopy, electron microscopy, acidometric titration, etc. From the results obtained they constructed the phase diagram of molybdenum as a function of the molybdenum content of the catalyst (Figure 3.41). This work led to the suggestion that molybdenum is present on the catalyst surface as isopoly and/or heteropoly acids, i.e. that it has a distorted octahedral coordination.

Mo–Si oxide systems containing between 1 and 20 wt% of Mo have been studied [106, 396, 1009, 1010, 1014] by ESR and IR spectroscopies. The results were used to correlate the octahedral

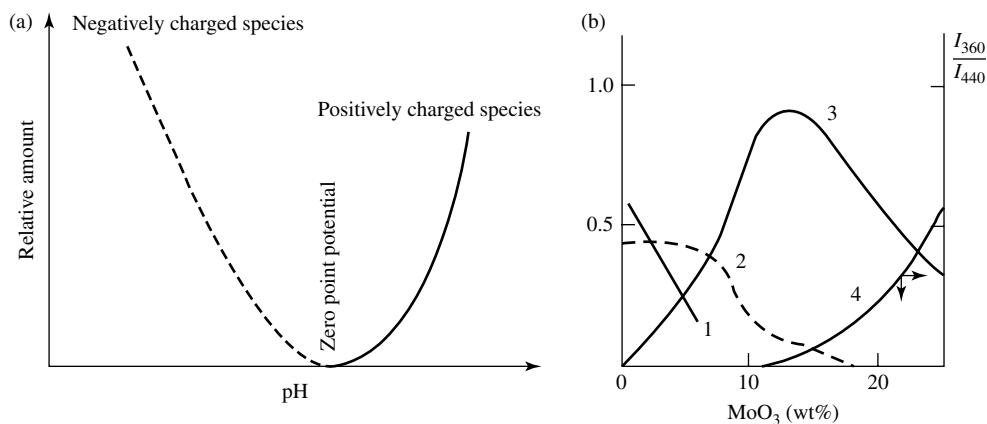


Figure 3.41. (a) Adsorption capacity of ionic species formed on a support as a function of pH (b) Distribution of the products in MoO₃/SiO₂ as a function of composition, established by titrations of (1) dimolybdate (DM), (2) molybdosilicic acid (MSA), (3) polymolybdate (PM), and (4) MoO₃. The proportions of MoO₃ (in relative units) was determined from the intensity ratios of the IR bands at 360 and 440 cm⁻¹ characteristic for MoO₃ and all molybdates, correspondingly.

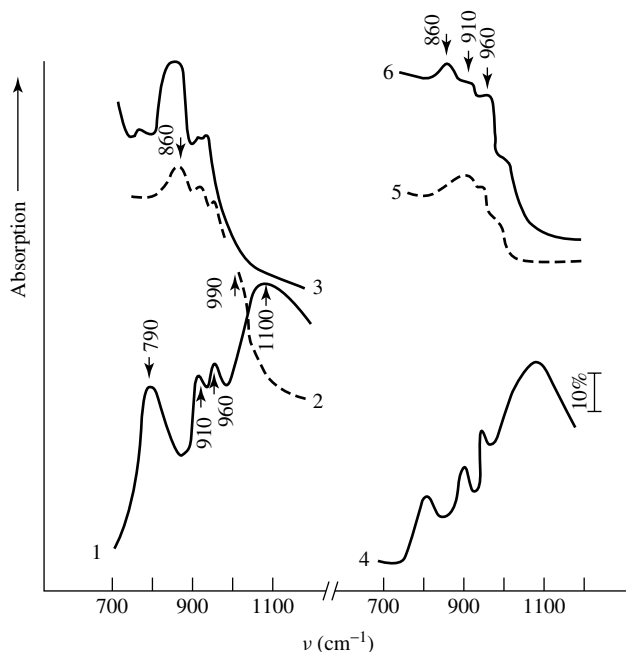


Figure 3.42. IR spectra of original HPA/SiO₂: (1) ordinary; (2) dehydrated at 673 K. IR spectra of: (3) ammonia paramolybdate; a Si-Mo catalyst, dried at (4) 383 K and dehydrated at (5) 673, 773 K and (6) 873 K. Spectra 2, 5, and 6 were obtained after subtraction of the spectra of SiO₂.

coordination of molybdenum with the formation of heteropoly compounds at high molybdenum contents. By comparing the results of the ESR studies of the state of the molybdenum as function of the formation temperature of the sample it was concluded [1010] that identical changes in the state of the molybdenum take place in the supported Si-Mo-HPA (Figure 3.42) and in the molybdenum oxide catalyst synthesized in the SiO₂ surface (the anisotropic signal denotes stabilization of the molybdenum in a distorted octahedral coordination of C_{4v} symmetry).

3.9.3 MOLYBDENUM-TITANIUM OXIDE COMPOUNDS

The physico-chemical and catalytic properties of Mo/TiO₂ catalysts are largely determined by the method of preparation [104, 106, 397, 1015–1019] as with the other systems listed above. Catalysts having different phase compositions can be prepared. Thus, in the synthesis of Ti-Mo catalysts by the co-precipitation of molybdenum and titanium oxides (series A), solid solutions based on titanium dioxide are formed [1016]. However, the situation is complicated by the formation of two modifications of TiO₂ under these conditions, namely anatase and rutile. A solid solution of molybdenum oxide in anatase is obtained when ammonium paramolybdate is added to titanium hydroxide paste [1017]. The stability of molybdenum is fairly high, i.e. up to 25–30 wt% of MoO₃. The formation of a solid solution is inferred from the abnormally high lattice parameters [1016] of the TiO₂ phase, due to the differences in size of Ti⁴⁺ ($r = 0.64 \text{ \AA}$), Mo⁶⁺ ($r = 0.66 \text{ \AA}$) and Mo⁵⁺ ($r = 0.65 \text{ \AA}$). When the Mo-Ti catalyst was prepared by the impregnation of anatase with molybdic acid at low concentrations of Mo, only the anatase phase was detected by X-ray diffraction (phases containing Mo could not be detected), while at high concentrations the MoO₃ phase was detected. In the synthesis of Mo-Ti catalysts from molybdenum tartarate complexes an X-ray amorphous form was obtained [1017].

The effect of the pH used to precipitate the titanium hydroxide on the phase composition of the resulting Mo–Ti catalyst has been studied [1016]. However, it was pointed out that the measurement in the region of $\text{pH} < 1.4$ cannot be correct since titanium hydroxide is deposited at $\text{pH} > 1.4$ [1018]. A detailed examination of the influence of the method of preparation of the catalyst on the phase composition and on the state of the molybdenum ions showed that the presence of added ions favors the low-temperature formation of rutile and the stabilization of the molybdenum on the lattice sites and in the interstitial positions within rutile. Molybdenum ions with an octahedral coordination, stretched along the tetragonal axis, are found in the lattice positions, whereas the interstitial ions are compressed along the same axis. In a catalyst prepared at a high pH, the phase composition was found to depend on the total concentration of added molybdenum [1016]. For molybdenum concentrations up to 25–30 wt% MoO_3 , a solid solution based on TiO_2 is observed by X-ray diffraction. At high molybdenum concentrations, MoO_3 is formed in addition to the solid solution. The XRD results were confirmed by IR spectroscopy [106, 219, 397, 1016]. It was found that the IR spectrum of the solid solution is almost indistinguishable from the spectrum of titanium dioxide in the region of its characteristic vibrations. It was reported [219] that the surface composition of Ti–Mo oxide catalyst differs markedly from the bulk composition by being richer in molybdenum. The IR spectrum of this surface layer also differs from the spectrum of the solid solution by the presence of bands characteristic of a compound containing molybdenum. It should be noted that a high proton acidity has been reported for the molybdenum compound formed on the surface of the TiO_2 support for concentrations of the active component greater than 5 wt% MoO_3 [219, 396]. This molybdenum compound is the active component (at least, in the oxidations of propene to acetone and methanol to formaldehyde). However, the compound itself has not yet been identified.

By using a combination of different methods (XRD, and ESR and IR spectroscopies), an attempt to establish the phase composition of the Ti–Mo oxide catalysts prepared by adding ammonium paramolybdate (APM) to a paste of titanium hydroxide and heating the product at 723 K (series A) or by impregnation of TiO_2 (anatase) with a solution of APM and heating of the product at 773 K (series C), was made [106, 396, 1019]. In the A-series catalysts, the lattice constants of the anatase increased with the molybdenum content, pointing to the formation of a solid solution. In this respect, the most interesting samples are those of the C-series containing up to 15 wt% Mo, in which the phases containing molybdenum are not detected by X-ray diffraction and there was no increase of the lattice parameters of anatase due to an increase of the molybdenum content.

A detailed study of the IR and ESR spectral parameters of various Ti–Mo oxide systems and of their changes in dehydration–rehydration processes at different temperatures, and also a comparison of these spectra with those of Ti–Mo–HPA supported on TiO_2 , showed [397, 1019] that Ti–Mo–HPA (stable up to 723 K) is formed on the surface during the synthesis of such Ti–Mo oxide catalysts.

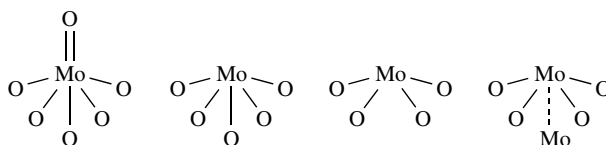
Thus, in the Ti–Mo oxide catalysts prepared by adding APM to a paste of titanium hydroxide (A-series), several phases are produced, depending on the molybdenum content, i.e. a solid solution of molybdenum in TiO_2 , Ti–Mo–HPA and MoO_3 . For molybdenum concentrations below 10 wt%, almost the whole of the added molybdenum dissolves in the anatase to give a solid solution. Increasing the concentrations of molybdenum in the catalysts results in the formation of new phases on the surfaces of the solid solutions, i.e. Ti–Mo–HPA and MoO_3 . As the concentration of molybdenum in the catalyst is increased still further, the concentrations of these phases increase.

In the Ti–Mo catalysts prepared by impregnating anatase with a solution of APM (C-series) and heating the sample at 723 K, Ti–Mo–HPA is formed for molybdenum concentrations lower than 15 wt%, although higher concentrations of MoO_3 are found as well as the HPA. The heteropoly

acid thus obtained has a high thermal stability (up to 723 K). Evacuation treatments at 700 K, under various conditions, strongly modify the electronic spectrum of the Mo/TiO₂. A strong increase in the 10 000–20 000 cm⁻¹ region is found, together with modifications of the absorption bands in the 20 000–28 000 cm⁻¹ region. According to the data [1005], octahedral Mo⁴⁺ ions show two absorption bands near 25 000 cm⁻¹.

Molybdenum oxide catalysts supported on TiO₂, Al₂O₃, ZrO₂, SiO₂ and Nb₂O₅ have also been recently investigated by Raman spectroscopy and Mo L3-Edge XANES (near edge X-ray absorption spectroscopy) and extended X-ray absorption fine structure (EXAFS) spectrometry [1020]. According to this study, under ambient conditions the structure of the hydrated surface molybdenum oxide species are the same as those observed in aqueous solutions: MoO₄²⁻, Mo₇O₂₄⁶⁻, and Mo₈O₂₆⁴⁻. Under dehydration conditions, the structures of the surface molybdenum oxide species depend on both the specific oxide support and the surface coverage. In the case of low surface coverage of MoO₃ on alumina and titania, the primary species is isolated and tetrahedrally coordinated. At high surface coverage of MoO₃ on TiO₂, the primary species is polymerized and octahedrally coordinated, whereas on Al₂O₃ there exists a mixture of tetrahedrally and octahedrally coordinated species. Monolayer coverage was achieved at the same surface density of MoO₃ on the different oxide supports, except for on SiO₂.

CO and NO can be selectively adsorbed as probe molecules for IR spectroscopy on the catalytically active coordinatively unsaturated sites of reduced Mo/Al₂O₃ [616, 1021, 1022–1026]. Carbon monoxide (when adsorbed on the reduced surface) gives rise to the band at 2183 cm⁻¹ assigned to coordinatively unsaturated Mo⁵⁺ [1023]. Support for this comes from reported ESR data [1022, 1024]. The Mo⁵⁺_{cus} cations most likely possess five coordination, denoted as Mo⁵⁺_{5C}, with only one open position exposed. In spite of this, the dinitrosyl (dimer) species is formed from NO at the Mo⁵⁺ ions. Other reduced molybdenum structures, the data for which have been obtained by means of spectroscopic methods [1023], can be represented as follows:



Scheme 3.4

The Mo⁴⁺_{4C} sites have two open positions and combinations of CO and NO can be adsorbed on such ions [1022, 1025, 1026]. Adsorption of CO on the Mo³⁺_{3C} site, which possesses three open positions, produces a tetrahedral complex. This complex then attaches two other NO molecules to form an octahedral complex. Without co-adsorbed CO, due to the higher electron density of the Mo³⁺_{3C} site, Mo³⁺_{3C}-(NO)₂ should exhibit a lower IR stretching frequency when compared to Mo⁴⁺_{4C}-(NO)₂ [1009, 1024]. The spectral characteristics of the CO complexes with molybdenum ions are represented in the lower section of Table 3.11.

3.10 Vanadium-containing systems

Different supported vanadium-containing oxide systems can be prepared by impregnation, ion exchange or via adsorption from the gas phase or organic solvents [215]. Depending on the conditions, different surface vanadium-containing species are formed [1027–1043]. For the majority of these cases, the surface hydroxyl groups of the support are assumed to be the active centers of the interaction.

Table 3.11. Spectral characteristics of CO adsorbed on various oxides.

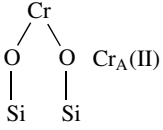
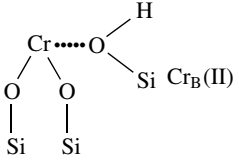
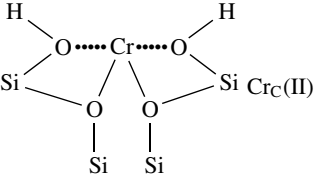
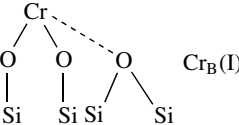
System	State of cation	$\nu\text{CO} (\text{cm}^{-1})$	Reference
Cr/SiO ₂	Cr ³⁺	2228, 2214, 2202	1027
Cr/SiO ₂	Cr ³⁺ -CO	2202	494
	Cr ²⁺ (CO) ₂	2189	
Cr/SiO ₂	 Cr _A (II)	2179	786, 1060
	 Cr _B (II)	2188	786, 1060
	 Cr _C (II)	Does not adsorb CO	786, 1060
Cr/SiO ₂	Cr ²⁺ -CO Monocarbonyl	2186, 2180	624 786
	 Cr _B (I)	2190	786
	Polycarbonylic (probably dicarbonylic) Cr _A (II)	2186, 2180	786
	Monocarbonylic Cr _A (II)	2182	786
Cr/SiO ₂ , Cr/Al ₂ O ₃	Oxochromium ions with 5-coordinated	2157, 2137	786
	CrO ₄ ²⁻ I ¹ A ₁ → ¹ T ₁ at 429-459		1059, 1967, 1068
	II ¹ A ₁ → ¹ T ₂ (1t ₁ → 2e) at 360-375 nm		
	III ¹ A ₁ → ¹ T ₂ (1t ₁ → 1t ₂) at 270-333 nm		
	IV ¹ A ₁ → ¹ T ₂ (6t ₂ → 2e) at 257-263 nm		
	Cr ₂ O ₃ > 600 nm		
	Cr ³⁺ and Cr ⁶⁺ 560 nm		

Table 3.11. (continued)

System	State of cation	$\nu\text{CO} (\text{cm}^{-1})$	Reference
Cr/TiO ₂	Cr ⁶⁺	Does not absorb	1066
	Cr ²⁺ _A -(CO) ₂	2120	1066
	Cr ²⁺ _C -(CO) ₂	2100, 2035	1066
	Cr ²⁺ _{A and C}	~2190	1066
		2185, 2180	
	Mono Cr _A (II)	7500 ^a , 1200 ^a	1066
	Di Cr _A (II)	28000 ^a	1066
Cr(III)	16600 ^a , 21600 ^a	1066	

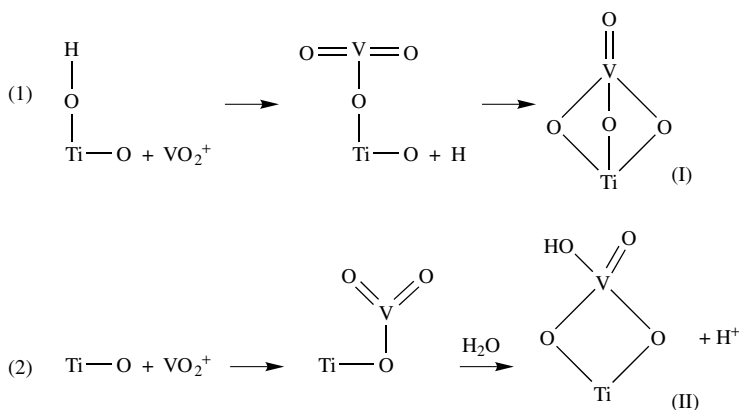
^aCharge-transfer band.

3.10.1 VANADIUM-TITANIUM OXIDE COMPOUNDS

It has been shown [215, 1029, 1030, 1034, 1044, 1045] that monolayer vanadium-oxide catalysts contain two types of surface compounds, i.e. isolated monovanadate groups, which strongly interact with the surface of titanium dioxide, and dimeric clusters of vanadium oxide, weakly bound to the support. The presence of a separate V₂O₅ phase [215, 1028, 1030, 1034, 1035] or polyvanadate ions [1043] is also observed, but only at high coverage. As it has already been noted for the molybdenum-containing systems, for the catalyst prepared by impregnation, the character of the interaction between a support and an active component is determined by the pH value of the solution. For most catalysts studied these days, the initial interaction proceeds predominantly between vanadate ion and basic hydroxyl groups of TiO₂. Support for this comes from the fact that the coordinatively unsaturated titanium cations exist at the surface of the catalysts even at a calculated monolayer coverage, or even at higher coverage of vanadium species.

Thus, the systems in which coordinatively unsaturated titanium ions are responsible for the interaction and bonding of vanadium oxide species are of considerable interest. Such systems have been comprehensively studied [1044, 1045].

Mononuclear VO²⁺ cations existing in aqueous solution of ammonium vanadate at pH 0.5 [1044, 1045] can interact with both OH groups and Ti⁴⁺. As follows from the changes in the IR spectra of TiO₂, the following reactions (1) and (2) occur, with structures I and II being the most probable species formed at the surface after calcination [1044, 1045]:

**Scheme 3.5**

Reaction (2) proceeds solely on strong Lewis acid sites (LASs) of anatase (α -centers characterized by $\nu\text{CO} = 2205\text{ cm}^{-1}$). According to the data obtained from diffuse reflectance UV–Vis spectroscopy, the above structures have an octahedral coordination in the hydrated state, as shown by the appearance of the absorption band at $23\,800\text{ cm}^{-1}$ (420 nm), while in the dehydrated state they are four- or five-coordinated $26\,700$ and $25\,000\text{ cm}^{-1}$ (375 and 400 nm, respectively) [215, 798, 1045]. It is known that electronic spectra of the V^{5+} ions in the $50\,000\text{--}8000\text{ cm}^{-1}$ region are characterized by the CT transition falling in the $20\,000\text{--}25\,000\text{ cm}^{-1}$ region for octahedral vanadium(V), whereas for lower coordinations such as tetrahedral vanadium(V), the CT transition is observed at higher frequencies ($30\,000\text{--}35\,000\text{ cm}^{-1}$) [1041]. In the case of V(IV) ions, the CT transition falls in the $35\,000\text{--}40\,000\text{ cm}^{-1}$ region, whereas the d–d transitions of octahedral VO^{2+} ions fall in the following regions: the $b_2(d_{xy}) \rightarrow e(d_{xy}, d_{yz})$ near $13\,000\text{ cm}^{-1}$ and the $b_2(d_{xy}) \rightarrow b_1(d_{x^2-y^2})$ near $16\,000\text{ cm}^{-1}$. The d–d transition at higher frequencies ($b_2(d_{xy}) \rightarrow a_1(d_{x_2})$) is generally masked by CT transitions, and are about ten times lower than those of the latter.

The appearance at the titanium dioxide surface of species containing vanadyl groups is confirmed directly by experimental data. Unlike with TiO_2 , in the IR spectra of the vanadium oxide catalyst which had been subjected to high-temperature oxidative treatment at 673 K, the absorption band at ca. 1028 cm^{-1} is observed; this is undoubtedly attributed to $\nu\text{V}^{5+}=\text{O}$ [30, 189]. A band at ca. 2060 cm^{-1} which is revealed in the spectrum may be ascribed to the first overtone frequency, and indicates the absence of polymeric vanadium structures on the surface of titanium dioxide, as well as the absence of a separate V_2O_5 phase [215, 1029, 1030, 1044–1046]. This is also supported by diffuse reflectance UV–Vis spectra, where no absorption characteristic for such entities (at $\sim 20\,000\text{ cm}^{-1}$ (500 nm) [1047]) is observed.

The fact that only one rather narrow absorption band of the $\text{V}=\text{O}$ group appears in the IR spectra allows one to exclude the possibility of the formation of structures of the $\text{O}=\text{V}=\text{O}$ type because two bands (ν_s and ν_{as}) separated by an interval of $10\text{--}20\text{ cm}^{-1}$ are expected in such a case [1041, 1046]. The presence of a band in the spectrum at $\sim 3680\text{ cm}^{-1}$, which is obviously assigned to $\text{V}\text{--OH}$ species (νOH bands for TiO_2 are revealed at 3700 and 3740 cm^{-1} [1044, 1045]), provides further argument in favor of the existence of type-II surface structures.

The character of the vanadium distribution discussed above is in good agreement with the IR spectra of adsorbed CO, NO and NH_3 [215]. Adsorption of CO on the oxidized sample of a V/TiO_2 catalyst leads to the appearance of a band at $\sim 2190\text{ cm}^{-1}$ (Figure 3.43, spectrum 2), which belongs to νCO in a $\text{Ti}^{4+}\text{--CO}$ complex involving β -centers of TiO_2 , whereas vanadium cations are not capable of interacting with CO. Upon adsorption of ammonia on this sample, absorption bands at ~ 1150 and 1600 cm^{-1} (Figure 3.43, spectrum 3) are revealed, attributed to δ_s and δ_{as} of ammonia bonded to the catalyst surface. Low-frequency components of the band at $\sim 1150\text{ cm}^{-1}$, the maximum of which is gradually shifted in the course of desorption, can be ascribed to δ_s in hydrogen-bonded (with surface oxygen and/or with surface hydroxyl groups) forms of adsorbed undissociated ammonia. The most strongly bonded adsorption form of ammonia most likely results from the formation of a hydrogen-bond with surface $\text{V}\text{--OH}$ groups, which are obviously more acidic than the $\text{Ti}\text{--OH}$ groups. The observed shift of the $\nu\text{V}^{5+}=\text{O}$ band (1030 cm^{-1}) toward lower frequencies may be accounted for by the influence of ammonia as a strong electron-donor ligand. This is then supported by the restoration of the band of $\nu\text{V}^{5+}=\text{O}$ after the complete removal of coordinated ammonia from the catalyst surface. These forms of ammonia may be responsible for the high-frequency components of the band at 1180 cm^{-1} , which appear at 1240 and, probably, at 1260 cm^{-1} (Figure 3.43, spectrum 5). This is shown by the spectra measured at the intermediate temperatures of NH_3 desorption from the samples. Thus, upon ammonia desorption at 523 K (Figure 3.43, spectrum 6), bands at about 1240 and 1610 cm^{-1} may be distinguished in the spectra which belongs to δ_s and δ_{as} of ammonia coordinated by vanadium cations, respectively. An interesting feature is the appearance of the

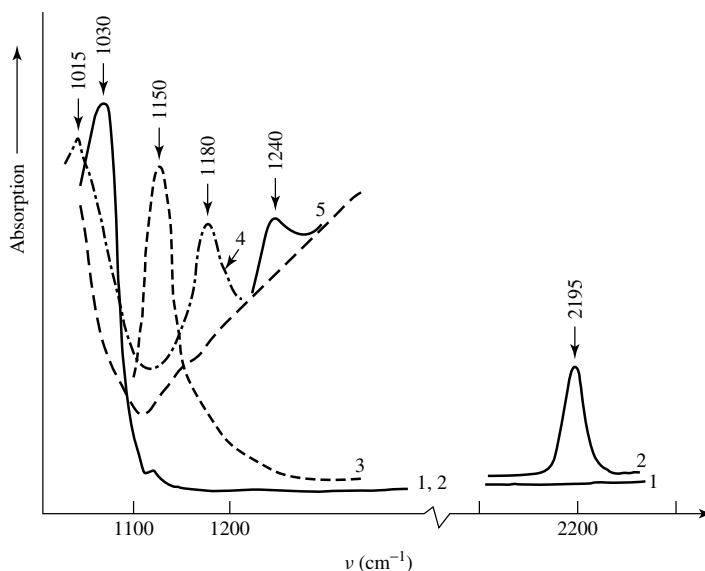
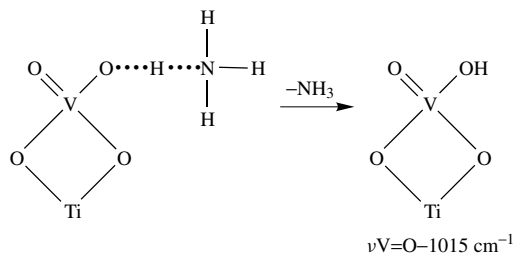


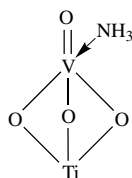
Figure 3.43. IR spectra of V/TiO₂: (1) after high-temperature oxidative treatment at 723 K; (2) further adsorption of CO (10 torr) on (1); (3) adsorption of NH₃ (4 torr) on (2); (4, 5) further desorption at 423, 523 K, respectively.

band at 1015 cm⁻¹ (Figure 3.43, spectrum 5) after the removal of H-bonded forms of adsorbed ammonia. These experimental data may indicate that the absorption band at 1030 cm⁻¹, assigned to ν V=O in structures of type I, overlaps with another ν V=O absorption band at 1015 cm⁻¹ in structures of type II, which is revealed after destroying the H-bonded complex with ammonia:



Scheme 3.6

The ammonia molecule bound to the vanadium ion in structure I:



Scheme 3.7

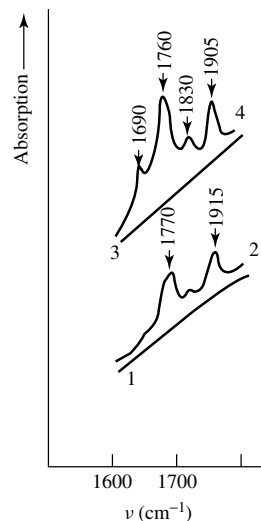


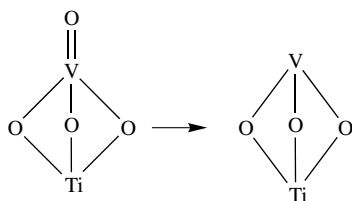
Figure 3.44. IR spectra of NO (4 torr) adsorbed at 293 K (2, 4) on the sample of V/TiO₂ reduced by ammonia desorption (adsorption of NH₃ at 293 K) at 623 K (1, 3).

is still held at the surface ($\delta_s\text{NH}_3$ absorption band at ca. 1240 cm^{-1}). The distinctive feature of this sample is characterized by the presence of predominantly isolated vanadium cations.

Using the samples reduced by ammonia to different degrees (Figure 3.44, spectrum 2), it has been shown that oxidized V^{5+} ions do not adsorb NO and CO, as reported by various authors [215, 1048, 1049].

According to Davydov *et al.* [1048] and Alekseev and Gerasimov [1049], assignment of the observed bands at ca. 1770 and ca. 1915 cm^{-1} in the spectra of adsorbed NO to ν_{as} and ν_{s} in a dinitrosyl complex, $\text{V}^{4+}-(\text{NO})_2$ is obvious. The bands at ca. 1700 and ca. 1830 cm^{-1} (Figure 3.44, spectrum 4) are attributed to ν_{as} and ν_{s} in the $\text{V}^{3+}-(\text{NO})_2$ dinitrosyl complex [30, 1048]. Hence, at such a degree of reduction, the formation of a certain amount of V^{3+} ions is observed.

Thus, the sample studied is characterized by the presence of isolated vanadium ions, most likely tetra-coordinated and penta-coordinated species, as in structures I and II, distributed over the support. Reduction of V^{5+} to V^{3+} in these structures proceeds according to the following scheme:



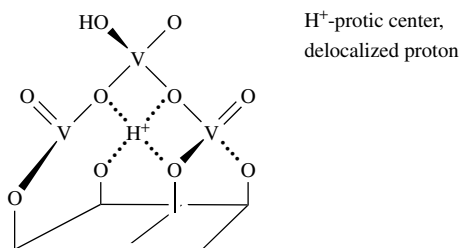
Scheme 3.8

Formation of V^{4+} takes place only on adsorption of ammonia or propene. Both $\text{V}=\text{O}$ and $\text{V}-\text{O}-\text{H}$ groups are present at the surfaces of the vanadium-containing catalysts that were studied and do not possess strong acidic properties (at least, they are not capable of ammonia protonation).

The samples with high concentrations of vanadium (even if being prepared by the interaction with VOCl_3 [1037, 1038]) contain both tetrahedrally and octahedrally coordinated vanadium cations (absorbance bands at 380 and 420 nm) which are manifested in the more complex contour of the 1020 cm^{-1} band and also in the presence of an absorbance band at 2050 cm^{-1} . As the data

on CO adsorption show, all of the α - and β -centers of the TiO_2 support in the sample under study are occupied. Easier reduction of the samples is yet another argument in favor of the presence of V–O–V bonds in the surface species. At 673 K, these samples can be greatly reduced in CO, as shown by a sharp decrease in the intensity of the bands of the V=O ($\sim 1030\text{ cm}^{-1}$) and V–O–V groups (950 cm^{-1}). From the spectrum of adsorbed CO, it follows that the reduction proceeds predominantly to V^{3+} (the 2185 cm^{-1} band is observed due to $\text{V}^{3+}\text{-CO}$) [1048]. These samples in the oxidized state are characterized by the presence of strong Brønsted acid sites (BASs), as revealed not only by ammonia adsorption and the appearance of ammonium ions, but also by the adsorption of such a weak base as propene.

Upon adsorption of NO on the reduced catalyst, both $\text{V}^{4+}\text{-(NO)}_2$ ($\nu_s = 1775$ and $\nu_{as} = 1910\text{ cm}^{-1}$) and $\text{V}^{3+}\text{-(NO)}_2$ species ($\nu_s = 1705$ and $\nu_{as} = 1840\text{ cm}^{-1}$), as well as $\text{V}^{3+}\text{-(NO)}$ (1760 cm^{-1}), are revealed. In the course of interaction with NO, re-oxidation of the V^{3+} cation by NO, with the formation of N_2O , takes place. This is a characteristic feature of the samples with associated vanadium ions. Vanadium is more probably distributed over the surface in the following manner:



Scheme 3.9

or growth of the second layer of vanadium-containing species may take place, which explains the presence of two somewhat different vanadyl bonds (at 1020 and 1030 cm^{-1}).

It is the appearance of the second layer (or associated vanadium cations) that is obviously responsible for the Brønsted acidity of the samples. According to various reports [30, 215], the BAS may be represented as a proton acting as a cation, which simultaneously compensates for the charge of several anions, or during the formation, a dispersed two-dimensional phase of V_2O_5 .

3.10.2 VANADIUM–SILICON OXIDE COMPOUNDS

It is beyond doubt that the character of the vanadium cation distribution is influenced content of vanadium. Hence, the V/SiO_2 sample ($\sim 1\%$ V), investigated in detail by ESR and UV spectroscopies [215], was prepared by the impregnation method and contained predominantly tetrahedrally coordinated vanadium cations [213–215]. Unfortunately, observation of $\nu\text{V=O}$ vibrations was not possible in this case due to the cutoff of SiO_2 . In the region of νOH , an observed adsorption band at $\sim 3680\text{ cm}^{-1}$ is attributed to the vibrations of V–OH groups. Protic acid sites in this system are not revealed by the NH_3 adsorption. Adsorption of NO and CO on the oxidized sample does not take place, i.e. in this case because the tetrahedrally coordinated vanadium cations are capable of interacting with strong ligands, such as NH_3 , which form the complex with V^{5+} , but they are unable to coordinate weak ligands, such as NO and CO [214].

Unlike the above case, for the sample reduced in H_2 at 773 K and then dehydroxylated at the same temperature, two absorption bands at 2178 and 2185 cm^{-1} are observed (Figure 3.45, spectrum 6) [1048] due to νCO in $\text{V}^{3+}\text{-CO}$ complexes. An increase in the vanadium content in the

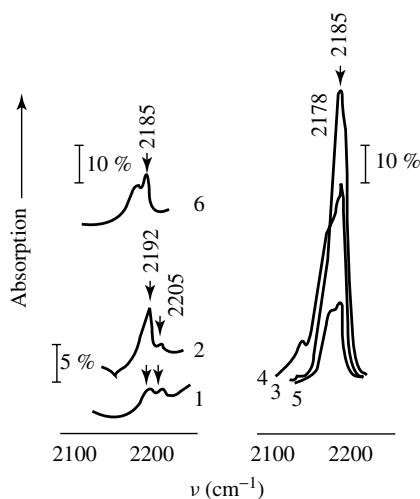
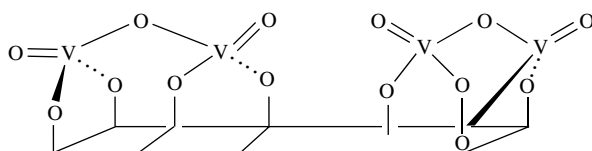


Figure 3.45. IR spectra of CO adsorbed on 2.29 % V_2O_5/SiO_2 with different degrees of reduction: (1) 25 torr of CO at 300 K on the sample reduced by desorption of ammonia at 773 K; (2) 10 torr of CO at 300 K on the sample reduced in C_3H_6 at 573 K; (3, 4) 10 torr of CO at 300 and 173 K on the sample reduced in H_2 at 773 K; (5) reduction of the CO pressure to 2×10^{-2} torr at 300 K; (6) 30 torr of CO on 1 % V_2O_5/SiO_2 reduced in H_2 at 773 K.

samples principally changes the distribution of vanadium on the support and, as a result, the character of the interactions with reacting molecules. In this case, samples of V/SiO_2 (2.25 wt% V_2O_5) were used. These samples mainly contained tetrahedrally coordinated vanadium cations, although octahedrally coordinated ions were also likely to be present [462]. The latter was indicated by the diffuse reflectance UV spectra of the samples, see below. Thus, in this case, tetrahedrally coordinated cations, connected via V–O–V bridges, are present at the surface of the SiO_2 , in addition to the isolated tetrahedrally coordinated cations, i.e. vanadium cations also exist in the associated state. Ammonia adsorption on this sample results in the formation of coordinatively bonded ammonia (bands at 1610, 3280 and 3380 cm^{-1}) and small amount of ammonium ions (bands at 1450, 3050 and 3180 cm^{-1}).

Thus, similar to V_2O_5 , BASs and LASs are revealed on the oxidized surface of the V_2O_5/SiO_2 sample only after formation of the associated vanadium ions [1047]. Most likely, the V^{5+} ions in a distorted tetrahedral coordination play the role of the LASs, and a vacancy is filled to some extent by the oxygen anion of another coordination polyhedral VO_4 , for example, according to the scheme:



Scheme 3.10

This is supported by a shift of the UV adsorption band to 20 000 cm^{-1} (500 nm) and by the ESR data [215]. Indeed, upon ammonia adsorption on the oxidized catalyst, V^{4+} ions with parameters

characteristic of $(V=O)^{2+}$ species (V^{4+} ions of type A: $g_{\parallel} = 1.928/1.951$; $g_{\perp} = 1.983/1.980$; $A_{\parallel} = 190/179$; $A_{\perp} = 69/66$ due to distorted tetragonal pyramid with $V=O$ bond at the vertex) already appear at low temperatures. The readily occurring reduction of this system points to the presence of bridging oxygens in the $V-O-V$ structures. The ESR spectrum of V^{4+} ions of this type is anisotropic and exhibits a correlated variation of the parameters of these ions. This may be accounted for by assuming a change in the coordination of vanadium from a penta-coordinated pyramid to an octahedron (additional coordination by the sixth place) [213]. A rather high coordination number of the V^{4+} ions is most likely determined by their additional coordination with NH_3 molecules. Therefore, on one hand, the appearance of V^{4+} ions upon interaction with NH_3 at 300 K points to the presence of surface oxygen atoms that are capable of oxidizing ammonia (only oxygen bound to vanadium ions may be responsible for this effect, i.e. these data support the hypothesis of the presence of vanadium ions connected via an oxygen bridge). On the other hand, they provide evidence for an enhanced (in comparison with tetrahedral coordination) coordinative saturation of vanadium cations. Even V^{4+} ions are, at least, penta-coordinated. This may be an indication of the formation of dimeric (polymeric) clusters of vanadium cations (V^{5+}) at the surface of SiO_2 .

An increase in the reduction temperature (for instance, in the case of reduction via ammonia desorption at 773 K, i.e. moderate reduction) leads to an enhancement of the ESR signal (ca. 2 % of the total V content). Moreover, the character of the signal and the parameters of the V^{4+} ions are substantially changed in that signals of type B appear. In accordance with other studies [213], these spectra may be characteristic of V^{4+} ions in a distorted tetrahedral coordination (Table 3.12). Changes in the ESR spectra of these ions after CO admission show that both types of ions are able to coordinate CO molecules [213]. The CO molecules most likely enter the coordination sphere of V^{4+} ions according to the scheme proposed by Mashenko *et al.* [462]. Such complexes are weak and can be easily destroyed by evacuation at 300 K. It should be noted that a substantial part of the V^{4+} ions (ca. 50 %) is not involved in complex formation with CO, even at 77 K. The presence of several types of V^{4+} ions, which are either capable or not capable of coordinating CO, is probably determined not only by steric hindrances but also by the extent of association (by the size of the vanadium oxide clusters) on the support.

Table 3.12. Spectral manifestations of V^{4+} ions and CO complexes with vanadium.

Sample	Treatment	g_{\parallel}	g_{\perp}	$A_{\parallel}G$	$A_{\perp}G$	Type	Coordination	ν_{CO} in $V^{n+}-CO$
V_2O_5/SiO_2 (2.25% V_2O_5)	Evacuation NH_3 , 773 K	1.89 – 1.88	≤ 1.97	150 – 160	≤ 60	B	Distorted tetrahedron	
	Reduced in H_2 , 773 K	1.90 – 1.89	≤ 1.97	150 – 165	≤ 60	B'	Distorted tetrahedron	
	CO adsorption on reduced sample	1.92(1 ± 2)	1.98(2 ± 1)	192 ± 2	73 ± 1	C	Tetragonal pyramid with $V=O$ bond	2192, 2205
		1.92(1 ± 2)	—	187 ± 2	—	C'		
		1.91(6 ± 5)	—	165	—	B_1	Distorted tetrahedron	
V_2O_5/Al_2O_3 (10% V_2O_5)	Oxidized sample	1.94(6 ± 2)	1.99(9 ± 1)	177 ± 2	76 ± 2	A_1	Distorted octahedron with $V=O$ bond in vertex	
	Reduced in H_2 , 773 K	1.92(4 ± 2)	1.98(3 ± 1)	185 ± 2	72 ± 2	A'	Tetragonal pyramid with $V=O$ bond	2200

The adsorption of CO on V_2O_5/SiO_2 samples with a moderate degree of reduction results in the appearance in the IR spectra of two weak absorption bands at 2192 and 2205 cm^{-1} (see Figure 3.45, spectrum 1), which may correspond to two $V^{4+}-CO$ complexes detected in the ESR spectra. It follows from the IR spectroscopic data that the complexes characterized by these absorption bands are easily destroyed at 300 K. The bands at 2192 and 2205 cm^{-1} are assigned to two different CO complexes, as shown by the IR spectra of CO adsorbed on V_2O_5/SiO_2 reduced under mild but different conditions. Taking into account the fact that, with the decreasing coordination number of a cation its effective charge increases, one may relate the appearance of the bands at 2192 and 2205 cm^{-1} to $V^{4+}-CO$ complexes with a somewhat different coordination (extent of the tetrahedron distortion), with the high-frequency component being ascribed to the V^{4+} ions with higher coordinative unsaturation (Table 3.12). The spectral characteristics of the $V^{3+}-CO$ complexes appearing in the spectrum of strongly reduced catalyst are also presented in Table 3.12.

Ammonia adsorption on samples with a moderate degree of reduction reveals the same adsorption forms as those present on the oxidized surface, i.e. NH_4^+ , coordinated ammonia (the band at 1440 cm^{-1} with a somewhat lower intensity) and NH_2 groups. As for strongly reduced samples, no NH_4^+ ions were revealed after ammonia adsorption. So, the protic centers exist only for vanadium ions in a high oxidation state.

3.10.3 VANADIUM-ALUMINUM OXIDE COMPOUNDS

As well as for V/TiO_2 or V/SiO_2 , in the case of V/Al_2O_3 the state of vanadium depends on the preparation conditions and vanadium content. However, in this case it is more difficult to prepare samples which contain only tetrahedrally coordinated cations. As a rule, the clustered ions are detected even in the samples with low vanadium content. That is why the V_2O_5/Al_2O_3 system with 10 wt% V_2O_5 is predominantly analyzed below. Thus, for samples with 10 % vanadium content, a monolayer coverage is reached.

Samples of V_2O_5/Al_2O_3 with a high V content (10 % V_2O_5) were prepared by impregnation of $\gamma-Al_2O_3$ by vanadium-containing structures, as shown by the absence in the IR spectra of these samples of the hydroxyl groups belonging to alumina and coordinatively unsaturated Al^{3+} cations (absorption bands were not observed in the IR spectra of adsorbed CO) [215]. In addition, adsorption of CO_2 was not observed, i.e., all active sites of the support are blocked by the vanadium-oxygen compound. In the IR spectrum of this catalyst, an adsorption band at 1020 cm^{-1} appears after oxidative treatment due to the $\nu(V=O)^{3+}$ vibrations. This spectral line, similar to the V_2O_5/TiO_2 system, is a superposition of several components, which indicates the inhomogeneity of the fragments containing $(V=O)^{3+}$ groups. The appearance of the band at ca. 815 cm^{-1} , in addition to the line at 1020 cm^{-1} , points to the presence of V-O-V bonds. All vanadyl groups are localized in the sites accessible to adsorbates because upon H_2O or NH_3 admission, almost complete disappearance of the band at 1020 cm^{-1} is observed. Its intensity also sharply decreases upon catalyst reduction. These data show that the clusters of vanadium oxide compounds which are formed are uniformly distributed over the surface of Al_2O_3 . All V^{5+} cations are accessible to adsorbates, and hence, the clusters are not bulk structures, but represent dimeric species with the possible formation of second and third layers, similar to V/TiO_2 and V/SiO_2 with a high vanadium content.

Additional information on this system may be derived from analysis of the IR spectra of adsorbed ammonia. The changes in the IR spectra during desorption of ammonia adsorbed at 293 K on the oxidized surface of V_2O_5/Al_2O_3 (Figure 3.46, spectra 3-6) in comparison with Al_2O_3 (Figure 3.46, spectrum 7) show that ammonia coordinated by V^{5+} ions (the δ_s band of NH_3 at 1250 cm^{-1}) is completely desorbed at $T < 573$ K (Figure 3.46, spectrum 6). Only a few oxidized complexes of ammonia (absorption bands at 1440 and 1570 cm^{-1}) are observed in this

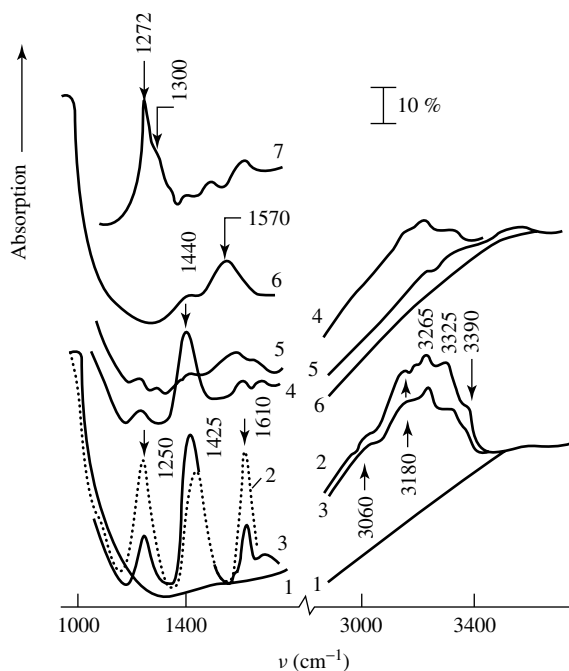


Figure 3.46. IR spectra of NH_3 adsorbed on the oxidized $\text{V}_2\text{O}_5/\text{Al}_2\text{O}_3$ catalyst: (1) background; (2) 20 torr of NH_3 at 300 K; (3–6) further desorption at 300, 373, 473 and 573 K, respectively; (7) adsorption of NH_3 at 293 K, followed by desorption at 523 K on Al_2O_3 calcined at 773 K.

case (Figure 3.46, spectrum 6). A comparison of the data obtained for Al_2O_3 and $\text{V}_2\text{O}_5/\text{Al}_2\text{O}_3$ also provides evidence for the complete coverage of the Al^{3+} cations at the surface of $\gamma\text{-Al}_2\text{O}_3$ by vanadium compounds because absorption bands at 1300 and 1275 cm^{-1} belonging to NH_3 coordinated by Al^{3+} ions in Al_2O_3 (Figure 3.46, spectrum 7) are not observed in the spectra. A considerable concentration of the BASs due to the presence of vanadium-containing compounds in the samples under investigation [30] is yet another distinctive feature of these systems. These BASs are strong, and similarly to the above case of V/TiO_2 with a high V content, they are capable of proton transfer for propylene and ethylene molecules with the formation of surface isopropylates and ethylates [1050]. Coordination of CO or NO to these oxidized vanadium ions was not observed. According to the ESR data (Table 3.12), even V^{4+} ions (type I), i.e. V^{4+} ions in an octahedral coordination involving covalently bonded oxygen, presumably in the $\text{V}-\text{O}-\text{V}$ bridging forms, are present in the initial oxidized catalysts [214].

Evacuation of the oxidized samples at 773 K leads to growth in the intensities of the ESR signals (by ca. 1.5–2 times), predominantly due to the appearance of V^{4+} ions (type II), which are characterized by the presence of the unoccupied sixth coordination place (Table 3.12), probably as a result of removing the covalently bonded ligand from the $\text{V}-\text{O}-\text{V}$ fragment. Carbon monoxide adsorption on the oxidized and evacuated samples has no appreciable effect on the ESR spectra. Heating the catalysts in the presence of CO at $T > 423$ K causes an enhancement in the intensity of the ESR signals assigned to V^{4+} ions of types I and II. This effect is mainly determined by the growth of the concentration of $(\text{V}=\text{O})^{2+}$ species (type II) having the coordination of the tetragonal pyramid, whereas the appearance of the broadened signal shows the formation of associates of the paramagnetic ions [213]. At 573 K, an essential contribution to the intensity

of the ESR signal is from V^{4+} ions, presumably due to either the formation of "clusters" of paramagnetic ions or a further reduction of V^{4+} .

Ammonia adsorption on the reduced catalysts leads to the appearance of an absorption band at 1220 cm^{-1} , which exhibits a high-frequency asymmetry, and to those at 1620 , 3270 and 3360 cm^{-1} (see Figure 3.46, spectrum 3). These are due to the bending and stretching frequencies of ammonia, most likely coordinated to V^{3+} ions. A decrease in δ_s of coordinated ammonia from 1250 cm^{-1} , for the oxidized sample, to 1220 cm^{-1} , for the reduced catalyst, may be related to the weakening of the acceptor ability of the vanadium cations upon reduction. This argument is supported by the variation of the electronegativity of the vanadium ions from V^{5+} (1.9) to V^{3+} (1.7). This assignment is also confirmed by a lower thermal stability of the coordinated ammonia molecules for the reduced sample.

Adsorption of ammonia on the reduced sample, as well as in the cases of reduced V/SiO_2 and V/TiO_2 , does not lead to the appearance of absorption bands of ammonia ions, i.e. the catalyst reduction eliminates Brønsted acidity. The data obtained show that in the course of reduction of catalysts, the bridging oxygen is removed from the $V\text{--}O\text{--}V$ fragments. In this case, polymeric vanadium oxide clusters are responsible for the presence of the BASs.

A study of the adsorption of NO and CO on 10 % V_2O_5/Al_2O_3 showed that either the oxidized samples or those reduced in CO at $T < 573\text{ K}$ were not capable of NO and CO coordination. Interaction with NO and CO was observed only for the reduced samples containing low-coordinated V^{4+} and V^{3+} ions. Figure 3.47 presents the evolution of the IR spectra of adsorbed CO and NO as a function of the extent of sample reduction. Two weak absorption bands at 1785 and 1910 cm^{-1} are observed for the partially reduced sample for NO (see Figure 3.47, spectrum 1) and only one band at 2200 cm^{-1} for CO.

With an increasing degree of reduction (heating in CO at 673 and 773 K), new bands at 1705 and ca. 1835 cm^{-1} appear in the spectrum of adsorbed NO and the intensities of the bands at 1775 and 1910 cm^{-1} increase (see Figure 3.47, spectra 2 and 3). Because the partially reduced sample contains low-coordinated V^{4+} ions, the appearance of the band at 2200 cm^{-1} in the spectrum of adsorbed CO and the bands at 1785 and 1910 cm^{-1} in the spectrum of adsorbed NO may be related

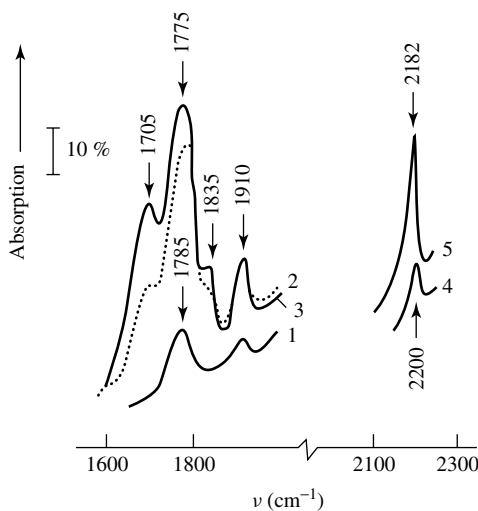


Figure 3.47. IR spectra of CO and NO adsorbed on V_2O_5/Al_2O_3 : (1) 10 torr of NO and (4) 10 torr CO on the sample reduced by desorption of toluene at 773 K ; (2) 4 torr of NO on the sample reduced in CO at 673 K ; (3) 4 torr of NO and (5) 10 torr CO on the sample reduced in CO at 773 K .

to the formation of monocarbonyl and dinitrosyl complexes of NO with V^{4+} ions, respectively [213, 215]. In the sample reduced by calcination in CO at 773 K, coordinatively unsaturated V^{3+} ions are present, which are capable of coordinating CO molecules ($\sim 2182\text{ cm}^{-1}$); therefore, the appearance of the additional bands at 1705 and 1835 cm^{-1} in the spectrum of NO adsorbed on this sample most likely results from the formation of dinitrosyl complexes with V^{3+} ions. The observed nitrosyl complexes can be partially destroyed by evacuation at room temperature, and their complete removal is achieved by prolonged evacuation at 373 K. The spectra of re-adsorbed CO and NO provide evidence of partial oxidation of the reduced centers upon NO adsorption. It is noteworthy that after NO desorption, re-oxidation of the surface by NO molecules occurs even for the sample containing only V^{4+} ions, as shown by the appearance of N_2O . This also confirms the presence of associated (clustered) forms of the vanadium oxide phase, i.e. the presence of vanadium ions at distances apart which ensure the formation of V–O–V bonds.

It is seen that the structures and properties of vanadium oxide species on supported surfaces can be studied successfully by using the methods of IR, DRE and ESR spectroscopies. These properties are determined by the nature of the carrier, vanadium content and preparation conditions (pH, the methods of vanadium introduction, etc.). The supported component is able to interact with the carrier via both surface hydroxyl groups and coordinatively unsaturated cations of the support. The structure of the neighboring surroundings of vanadium (coordination number) depends on the nature of the active sites at the surface of the support involved in the interaction with the active component and on the extent of the cluster formation for the cations.

The vanadium oxide moieties formed at the surface are found to exhibit substantially different chemical properties relative to simple molecules, such as NH_3 , CO and NO, which results in the differences of these systems in their catalytic behavior in the transformations of these molecules. It is shown that the use of molecular probes may provide detailed information on the state of the active component in the catalyst, which allows updating of the unique characteristics of their structures and properties. Data of this type can be used for the preparation of systems with properties necessary for the activation and transformation of molecules through a pathway favorable for the occurrence of this highly selective reaction.

3.11 Chromium-containing systems

Spectral data about supported Cr-containing systems and their dependence on the content of the active component, preparation method and type of support are so numerous that it could be a subject for a separate book. In this section only the application of different molecular spectroscopy methods for characterization of such systems is illustrated.

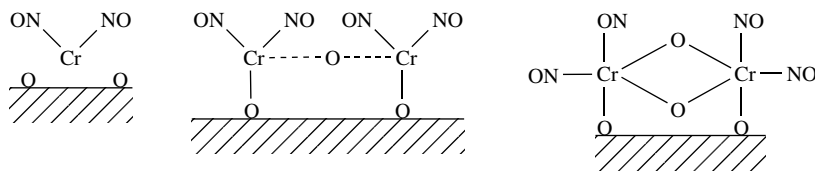
Interesting results have been obtained upon the addition of chromium ions to the surfaces of different supports [1051–1058]. As well as observed for V and Mo, different clustering degrees of chromium ions have been shown, i.e. the formation of isolated tetrahedrally coordinated chromium species and polymeric chromium oxide species possessing two terminal Cr=O bonds (according to Raman data [1051, 1055–1058]).

Different types of chromium ions have been established on various supports. Polymeric chromium oxide species preferentially exist on alumina, titania, zirconia and niobia supports, whereas isolated chromate species with two Cr=O bonds predominate on the SiO_2 support. As seems to be usual, significant differences are observed in the case of systems supported on MgO. Thus, non-stoichiometric compounds such as $Mg_x(CrO_4)_y$ were detected on the MgO support due to the strong acid–base interaction of CrO_4^{2-} with MgO.

Chromium-containing catalysts are widely investigated by UV–Vis spectroscopy [798, 1059, 1067, 1068]. The diffuse reflectance spectra of a number of metal chromates have been discussed by Szabo *et al.* [1059]. The chromate ion (CrO_4^{2-}) is characterized by four charge-transfer transitions: (i) $^1A_1 \rightarrow ^1T_1$ at $23\,300\text{--}21\,800\text{ cm}^{-1}$ (429–459 nm); (ii) $^1A_1 \rightarrow ^1T_2$ ($1t_1 \rightarrow 2e$)

at 27 780–26 670 cm^{-1} (360–375 nm); (iii) ${}^1A_1 \rightarrow {}^1T_2$ ($1t_1 \rightarrow 7t_2$) at 37 040–30 030 cm^{-1} (270–333 nm); (iv) ${}^1A_1 \rightarrow {}^1T_2$ ($6t_2 \rightarrow 2e$) at 38 910–38 020 cm^{-1} (257–263 nm) (see Table 3.11). Samples with low contents of Cr (0.5 wt% Cr) have been investigated, and in this case UV–Vis spectroscopy became essential for identifying chromium cations on the surface of this support. The authors did not find Cr^{3+} and interpreted the spectra as entirely ascribable to Cr^{2+} cations. No absorption due to α -chromia particles (17 000 and 22 000 cm^{-1}) was observed. Unfortunately, all known coordination states of Cr^{2+} yield two of the bands in the region 14 000–5000 cm^{-1} , including the (in this case, unrealistic) octahedral state so that no clear inferences about the coordination and symmetry states of Cr ions can be made by these means.

The acidic properties of chromium-containing systems have already been shown above (Table 2.8). It should also be noted that protonic acidic centers have been detected on chromium oxide containing chromium ions in high-oxidation states, in a similar way to the Mo- and V-containing systems. According to the infrared spectra of NO adsorbed on a chromia/silica–titania cogel reduced in carbon monoxide, a mono-nitrosyl surface complex gives a band at 1807 cm^{-1} [1062]. Four types of dinitrosyl complexes, identified by pairs of infrared bands at 1856/1742, 1868/1736, 1875/1755 and 1886/1766 cm^{-1} are ascribed to Cr^{2+} sites of different structural types:



Scheme 3.11

A Cr^{3+} site also gives infrared bands at 1875/1755 cm^{-1} due to the presence of a dinitrosyl complex on Cr/SiO_2 .

To obtain the particular coordination and oxidation states of ions, the photoreduction method appears to be very useful. Thus, in the case of Mo-, V- and Cr-containing systems supported on SiO_2 photoreduction in CO and H_2 has been used to prepare the systems predominantly containing Mo^{4+} , V^{3+} and Cr^{2+} ions (when reduction is carried out in CO) or Mo^{5+} , V^{4+} and Cr^{3+} (when reduction is carried out in H_2), respectively [1063]. Use of this method allows one to obtain spectral characteristics of both CO and NO with the above cations in different oxidation states.

The formation of surface nitrosyl complexes of d^2 ions (Mo^{4+} , V^{3+} and Cr^{4+}) has been studied by the ESR method. During NO adsorption, the transition of two d-electrons into the π^* -orbitals system of NO with the formation of the NO^{2-} paramagnetic species takes place in the coordination spheres of Mo^{4+} and Cr^{4+} ions. In the case of the V^{3+} ions, the NO^- diamagnetic species is formed as a result of a one-electron transition from NO.

There are three absorption bands attributed to the transitions, i.e. ${}^3A_2 \rightarrow {}^3T_2$, ${}^3A_2 \rightarrow {}^3T_1$ and ${}^3A_2 \rightarrow {}^3T_1$ (3P), inside the d-shells of tetrahedrally coordinated Mo^{4+} and V^{3+} ions in the UV–Vis spectra of both Mo/SiO_2 and V/SiO_2 photoreduced by CO. The Cr/SiO_2 samples photoreduced by CO exhibit only one absorption band in the d–d transitions region, with a maximum at 11 800 cm^{-1} , attributed to the $5T \rightarrow 5E$ transition of tetrahedrally coordinated Cr^{2+} ions.

Practically all Cr^{6+} ions can be thermally reduced to Cr^{2+} by CO. Only one band, at 12 400 cm^{-1} , corresponding to the $5T \rightarrow 5E$ transition of tetrahedrally coordinated Cr^{2+} ions, has been observed in the spectra. However, this band maximum has been shifted by 600 cm^{-1} to a lower wavelength, compared to that of the photoreduced samples. These spectral differences show that the photoreduced Cr^{2+} ions are more homogeneous in their crystal environment, and

that the strength of such a 'crystal surrounding' for the $5T \rightarrow 5E$ transition energy is a little less than that of photoreduced samples. This seems to be due to either a longer Cr–O bond in the CrO_4^{6-} tetrahedra or to a smaller number of ligands in the second coordination sphere.

The identified CO complexes with chromium cations in different oxidation states and with variable degrees of clustering are depicted in Table 3.10.

3.12 Effects of the states of adsorption sites on the stretching frequencies of adsorbed carbon monoxide and nitrous oxide and the problem of detecting the states of cations in oxide catalyst surfaces

The results obtained by studying cation-exchanged zeolites and other compounds of a number of metals (copper, nickel, palladium and iron) and by the analysis of IR spectroscopic data on CO adsorption available from the literature (Table 3.12) demonstrate that there is a distinct relationship between νCO in adsorption complexes and the state of charge at the adsorption site and on the character of its bonding (ionicity–covalence) with oxygen ligands. The general rule is that νCO is above 2170 cm^{-1} in $\text{M}^{n+}\text{-CO}$ ($n \geq 2$), between 2120 and 2160 cm^{-1} in $\text{M}^+\text{-CO}$ and below 2100 cm^{-1} in $\text{M}^0\text{-CO}$ complexes. The variation of νCO over this range depends on the nature of the metal and the character of the matrix containing the cations of the particular metal (the type of oxide compound). The revealed generality may be rationalized by considering the nature of the bonding with transition metals and their cations. As has already been pointed out, the nature of CO bonding with adsorption sites is at present commonly considered in terms of the σ – π bonding for the metal. According to this model, CO bonding with transition metals (cations) involves the delocalization of the CO 5σ -electron pair to unoccupied d (or hybrid d + s) orbitals of the adsorption sites (σ -bonding) and electron transfer from the occupied d-orbitals of the corresponding symmetry to the 2π (antibonding) orbitals of CO (the so-called reverse transfer, dative or π -bonding). The stretching vibration frequencies in complexes of adsorbed CO depends on the relative contributions of the σ - and π -bonding which, in turn, depend on the states of the adsorption sites (chemical nature, charge state, the character of the bonding with ligands, etc.). For highly charged transition-metal ions, the contribution of the π -bonding is relatively small, and CO adsorption involves mainly σ -bonding. This leads to stabilization of the 5σ -orbital which is weakly antibonding for CO and, correspondingly, to a νCO increase on going from the free molecule (2143 cm^{-1}) to higher frequencies to the $\text{M}^{n+}\text{-CO}$ complex. Since a σ -bond realized at such an interaction is practically electrostatic, an increase in νCO depends very weakly on the charge of the cation. With metals, a particularly significant role is played, apparently, by π -bonding, which increases the electron density on the antibonding orbitals of CO, thus resulting in a strong low-frequency νCO shift relative to $\nu\text{CO}_{(\text{gas})}$. For $\text{M}^+\text{-CO}$ complexes, the νCO value is close to that of the free molecule, which appears to be due to the balance of the opposing effects of σ - and π -bonding.

The scheme proposed is based on the above-cited experimental evidence obtained for cation-exchanged zeolites (see Table 3.13, upper part), the states of the ions in which have been established by independent methods (ESR, optical and Mössbauer spectroscopy) and described in the literature. Data on the adsorption of CO on those catalysts for which it is a difficult or even impossible to identify the states of the surface cations by the above techniques were interpreted by using the established relationship between νCO and the nature of the adsorption sites (see Table 3.13, middle part). In this table, the $\text{M}^+\text{-CO}$ column gives the νCO frequencies of complexes formed on the surface of supported metals subjected to oxidizing treatments and on the surface of oxides treated in a reducing atmosphere. The $\text{M}^{2+}\text{-CO}$ column gives the νCO frequencies for complexes of CO adsorbed on the surfaces of oxide and metallic catalysts after oxidizing treatment. This column also contains results obtained with the corresponding chlorides

Table 3.13. Frequencies (cm^{-1}) of CO stretching modes in surface complexes.

M^0 -CO	M^+ -CO	M^{2+} -CO
Cu 2100–2105	Cu-Y 2160	Cu-Y 2190
Ni 2050–2110	Ni-Y 2145	Ni-Y 2220
Pd 2070–2100	Pd-Y 2120, 2140	Pd-Y 2195, 2215
Fe 2000–2020		Fe-Y 2200
Pt 2060–2096	Pt-Y 2130	Pt-Y 2175, 2205
	CuO, Cu ₂ O 2115, 2140	CuO ^b –
	CuCl 2135	CuCl ₂ ^b –
	Cu ^a 2133	
	NiO/SiO ₂ 2135–2140	NiO/SiO ₂ 2198, 2210
		NiO/Ni 2193
		NiO/Ni-Y 2195
		NiCl ₂ 2200
	PdAl ₂ O ₃ ^a 2120	Pd/Al ₂ O ₃ ^a 2150, 2160
		Pd/SiO ₂ ^a 2150, 2160
		PdCl ₂ 2170
	Pt/Al ₂ O ₃ ^a 2130	Pt/Al ₂ O ₃ ^a 2180
	Pt/SiO ₂ ^a 2130	Pt/SiO ₂ ^a 2180
		Fe ₂ O ₃ /Al ₂ O ₃ ^b –
		Mn-Y 2208
		Co-Y 2208
		Zn-Y 2214
		Cd-Y 2209
		Fe-Y 2198
		Zn-O 2190–2210
		Ni-Y 2217
		Mg-Y 2213
		Ca-Y 2197
		Ba-Y 2187
		Sr-Y 2178

^aOxidized surface.^bNo carbonyl-like complexes at formed at 20 °C.

which substantiate the proposed scheme for the interpretation of the IR spectra of adsorbed CO. In the following sections, the properties of the complexes M^{2+} -CO, M^{n+} -CO, M^+ -CO and M^0 -CO are considered.

3.12.1 M^{2+} -CO, M^{N+} -CO ($n > 2$)

First, it should be noted that, as follows from the nature of the bond with CO, there should be no substantial differences between the cations of transition and nontransition metals in this case. This is indeed true for metals from the end of the first large period, as proved by data on CO adsorption on zeolites exchanged with Mg²⁺, Ca²⁺, Ba²⁺ and Sr²⁺ ions, given in the lower part of Table 3.13.

In general, complexes between CO and M^{2+} ions show low stabilities (they are readily destroyed by vacuum treatment at 293 K), which are due to the weak electron-donor ability of the CO molecule (5σ electron pair). It is natural to consider that the stability of a M^{2+} -CO complex is mainly determined by the ability of the cations to accept this electron pair. The ability of cations to accept electrons, and therefore the stabilities of the complexes, should decrease with increasing covalence of the metal–oxygen bond. Indeed, the complexes of CO with Ni²⁺, Pd²⁺

and Pt^{2+} ions in zeolites, where the metal–oxygen bonds are more ionic than in oxides, have been shown to be more stable than the corresponding complexes on the NiO surface or on oxidized palladium and platinum. In zeolites, the Fe^{2+} –CO complexes are formed at 293 K, whereas such complexes are not formed on $\text{Fe}_2\text{O}_3/\text{Al}_2\text{O}_3$ under these conditions, even though there are Fe^{2+} ions on the surface capable of coordinating NO molecules. Since the ability of a cation to accept the 5σ electron pair of CO determines the νCO , this can be expected to correspond to more stable complexes. In the general case, this correlation is difficult to follow since the stabilities of all complexes of this type are relatively low. However, when there are several complexes with M^{2+} ions in different states on the catalysts' surfaces, such a tendency does exist. For instance, the spectra of CO adsorbed on NiO/NiY show two absorption bands at 2195 and 2217 cm^{-1} , with the former disappearing much faster than the latter during the course of vacuum treatment.

Differing from other M^{2+} –CO complexes are the Pd^{2+} –CO and Pt^{2+} –CO species, which show a higher stability. The reason for this is that the outer orbitals of the 4d and 5d elements extend further (are more 'diffuse'), which can result in both a higher degree of overlapping with the CO 5σ -orbital compared with 3d ions and a greater contribution of π -bonding which it seems cannot be ignored even in the case of doubly charged ions. These are the factors which seem to be responsible for the increasing stabilities of CO complexes in the series Ni^{2+} (and other 3d ions), Pd^{2+} and Pt^{2+} , which nevertheless have close νCO values. The increase in the complex stability in the above series is in accordance with the well-known fact that 4d and 5d metals form stronger bonds with ligands than 3d ions.

To conclude the analysis of M^{2+} –CO complexes, let us consider the possibility of characterizing ions in higher oxidation states. The available IR spectroscopic evidence on CO adsorption on nontransition-metal oxides agrees with the proposed scheme. Thus, the data on CO adsorption on Al_2O_3 and HY zeolites may be accounted for in terms of the concept of two types of σ -complexes containing coordinatively unsaturated Al^{3+} ions. The frequencies of the CO stretching vibrations in complexes with Al^{3+} are higher than those usually observed with M^{2+} ions, with the stability of the complex with the higher νCO being much greater than that of M^{2+} –CO complexes (and Al^{3+} –CO complexes), pointing to a weaker electron-accepting ability of such Al^{3+} ions when compared with 'tetrahedral' complexes. This seems to be due to a high charge at the 'octahedral' Al^{3+} ion, stabilized by the greater number of oxygen anions. This example demonstrates that νCO depends not only on the charge on the adsorption site but also on the number of other ligands coordinating to it.

As for the transition metals themselves, species with higher oxidation states in oxide compounds are characteristic for many cations. The Fe^{3+} ions have been established to form no Fe^{3+} –CO (Fe^{3+} –NO) complexes in the case of Fe^{3+} -Y zeolites and oxidized $\text{Fe}_2\text{O}_3/\text{Al}_2\text{O}_3$ specimens. This may be due to a higher coordinative saturation (in the steric sense) of the Fe^{3+} ions. The same is apparently true for other ions at the end of periods (in the Periodic Table) (Ni^{3+} , Co^{3+} and Pd^{3+}). At the same time, metal ions from the beginnings of the periods may exist in coordinatively unsaturated situations with high oxidation states (Ti^{3+} , Ti^{4+} , V^{4+} , Mo^{5+} , Mo^{4+} , Cr^{4+} , Cr^{3+} , etc.) and adsorb molecules including CO. However, the interpretation of the IR spectra of adsorbed CO for the oxide compounds near the beginnings of periods (including Cr) requires a modification of the scheme of assignment of the absorption bands that are observed. Indeed, owing to their lower ionization potentials (greater d-electron energies) and larger radii (greater spatial extent of d-orbitals), metal ions from the beginnings of the periods possess weak electron-accepting abilities even in oxidation states 2+ and 3+ (Cr^{2+} and Ti^{3+}), while their electron-donor abilities grow when compared with ions near the ends of periods (Cu^{2+} and Ni^{2+}). These considerations suggest how the scheme of assignment should be modified as applied to νCO in M^{n+} –CO complexes where M is a metal from the beginning of a period. The νCO should be lower than in complexes with the corresponding metal ions near the end of the period when the latter can be formed.

On the other hand, at close frequencies and stabilities of $M_1^{n+}-CO$ (where M_1 is a metal from the beginning of a period) and $M_2^{m+}-CO$ (where M_2 is a metal from the end of the period) complexes, n must be greater than m and the difference should be the greater the closer M_1 is to the beginning of the period.

The data available substantiate this suggested modification of the scheme. Thus, CO adsorption on TiO_2 gives rise to absorption bands at $2180-2205\text{ cm}^{-1}$, corresponding to weakly bound CO and assigned to $Ti^{4+}-CO$ complexes. Similar surface complexes are formed by CO adsorption on reduced V_2O_5/SiO_2 specimens ($V^{4+}-CO$, νCO at 2200 cm^{-1}). Carbon monoxide adsorption on Cr_2O_3/SiO_2 and Cr_2O_3 gives rise to an absorption in the range $2190-2210\text{ cm}^{-1}$, which is not observed in the spectra after vacuum treatment at 293 K. This absorption may be assigned to $Cr^{3+}-CO$ complexes.

3.12.2 M^+-CO AND M^0-CO

These complexes are characterized by a much greater stability than $M^{2+}-CO$ and $M^{n+}-CO$ complexes. This is not surprising since individual coordination compounds with CO molecules as ligands are usually formed only with low-valency ions or metals (the metal carbonyls). This is due, apparently, to the ability of low-valency ions or sites such as M^0 to form a π -bond with CO, which increases the stabilities of the adsorption complexes and, in addition, increases the electron-donor ability to the 5σ π -accepting and σ -donor properties (the so-called synergistic effect) of the CO molecule. This effect appears to be particularly great with M^+-CO complexes, which makes them as stable as (and sometimes more stable than) M^0-CO complexes. This has been established conclusively for Pd-Y zeolites and for reduced CuO/Al_2O_3 specimens where both M^0-CO and M^+-CO complexes exist, with the former being destroyed faster on CO desorption. The low stabilities of CO complexes with metals from the ends of periods (compared with M^+-CO) may be accounted for on the assumption that no strong σ -bonds are formed on such complexation (that is, the 5σ -orbital is not involved in the formation of the M-C bond) and CO is stabilized mainly by π -bonding. This may be the case with nonlinear M^0-CO complexes (see below), which should be particularly characteristic of metals with completely occupied orbitals (Cu, Ag and Au).

The nonlinearity of complexes formed on CO adsorption on the exposed (110) plane of copper has been established in angle-resolved studies of photoemission spectra (an angle of ca. 35° between CO and the normal to the surface). The low stabilities of Cu^0-CO complexes may be accounted for also in terms of the molecular orbital method, even in the case of linear complexes. The 5σ -orbital of CO is part of the occupied 1σ (bonding) and 2σ (antibonding) orbitals of the complexes, that is, its involvement in CO bonding with Cu^0 does not contribute significantly to CO stabilization. At the same time, the 2π -orbital of CO contributes to the 1π (bonding) and 2π (antibonding) molecular orbitals of the complex, and the fact that there is only one electron in the latter provides a net gain in the formation of the Cu^0-CO complex which may be considered to result from weak π -bonding.

An important feature of M^+-CO (M^0-CO) complexes which is also due to π -bonding is their much higher molar absorptivities in the νCO stretching region as compared with those for $M^{n+}-CO$ complexes. This fact, together with higher stabilities of these complexes when compared with $M^{n+} CO$, allows the detection of M^+ and M^0 sites from the IR spectra of adsorbed CO even when their concentrations are substantially lower than that of M^{2+} complexes.

To conclude this discussion about CO complexes involving reduced sites, it should be emphasized that the assignment of absorption bands in the spectra of adsorbed CO giving M^+-CO complexes (where M is a transition metal) is possible only if complexes corresponding to these absorption bands are characterized by relatively high stabilities. This distinguishes these complexes from those involving "physically" adsorbed CO which, owing to a slight disturbance of the molecule, can also absorb in the region close to the νCO stretching region of the free molecule.

Differences in the energies of CO binding with cations in different valency states are obtained from direct calorimetric measurements (see Tables 2.42 and 2.43 above). The ϵ and Q values of the carbonyl complexes are nearly the same for cations at higher oxidation levels and increase substantially with a decrease in the oxidation level [30]. This is in full accord with the above considerations, confirmed by data available from the literature, and points to the key role of changes in polarity of the CO bond resulting from π -bonding. The molar absorptivities presented may be used to evaluate the amounts of coordinatively unsaturated cations in the surfaces of other oxide systems. Larger values of both ϵ and Q have been obtained in the case of CO adsorbed over metals.

For NO complexes, in contrast to the results for CO, no general relationship between ν NO and the stabilities of the corresponding complexes has been observed for adsorption sites of different chemical nature. This appears to be due to significant differences in the behavior of the metal to NO bond depending on the cation character. A monotonic dependence of ν NO on the charge of the absorption site of the same nature is also not observed (for example, Cu^{2+} -NO, Cu^+ -NO and Cu^0 -NO complexes on Cu zeolites show absorption bands at 1920, 1740 and 1820 cm^{-1} , respectively). In addition, many cations can be stabilized in the form of dinitrosyl complexes. All this substantially complicates interpretation of the IR spectra from adsorbed NO. At the same time, ν NO dependencies on the ionic/covalent character of the metal-oxygen bond and on the coordination numbers of the cations (copper-containing systems) can be observed, provided that the chemical nature and charge on the cation are constant. The examples presented show that the IR spectra of adsorbed NO provide more detailed information about the states of the cations on the surfaces of oxide systems than the spectra for CO are able to provide.

Intermolecular interaction

It should be taken into account that, as in the case of metals, for the situation of CO and NO adsorption on cations, intermolecular interactions take place at high coverage. These interactions lead to the changes of vibrational frequencies of adsorbed CO and NO molecules depending on coverage and to change in energy of their interaction with cations. For practically all of the investigated oxides, singletons can be obtained, including those coordinated by cations on separate faces and terraces by the use of isotope-containing mixtures analogous to that employed for CO-NaCl. A detailed examination of these data can be found in the review by Zecchina *et al.* [485] which is devoted to infrared studies of CO and NO adsorption on oxide single microcrystals such as MgO, NiO, NiO-MgO, CaO-MgO, ZnO, ZnO-CoO and α -Cr₂O₃, plus α -Al₂O₃, MgAl₂O₄ and other spinels, TiO₂, ZrO₂, and other oxides with a similar structure. In particular, the structures of the CO and NO adsorbed on the cationic sites of extended faces of these model solids have been presented and discussed with the aim of elucidating the natures of the M^{n+} -CO/NO bonds.

4 INTERACTIONS OF INORGANIC COMPOUNDS WITH OXIDE SURFACE ACTIVE SITES

The interaction of different inorganic and/or organometallic complexes with oxide surfaces is one of the new and wide-ranging directions in the synthesis of so-called 'precise' catalysts, i.e. the creation of catalytically active centers with particular properties. The interaction mechanisms already known from solution chemistry can often be applied to the new field of surface organometallic chemistry. Numerous studies have been devoted to these questions (see, for example, [111–113] and references therein).

These days, physical methods allow the detection of all steps in the interaction between inorganic (organometallic) or organic components and supports in the preparation of supported catalysts as well as stages of the formation of an active component. If the supported complex contains a fragment similar to the probe-molecule (for example, carbonyl or nitrosyl groups – see Section 4.2), very interesting and important information can be obtained.

The supported organometallic complexes can be catalysts themselves or produce the catalytically active species due to the decomposition under oxidative or reductive conditions. The adsorption and catalytic properties of supported complexes can be significantly different from those of the initial complexes, due to interaction with a support. The reaction media and temperature, in their turn, can influence a lot of the properties of supported complexes. The detailed study of changes in spectral manifestations of such complexes, as well as connected to these changes of adsorption and catalytic properties, is a one of the prospective directions of catalytic chemistry. It opens the way for creation of unusual (in classic chemistry) compounds on the surface of a support. It is illustrated in Sections 4.1 and 4.2.

More often the supported complexes are undergo destruction under different conditions. As a result, the metal or oxide species close to the usual complexes prepared by the impregnation are formed. The species formed in this way have some advantages as compared with those prepared by traditional methods: they are more homogeneously distributed on a support and are more dispersed.

Interaction between surface active sites and different reagents, including acids and alkalis, leads to modification of the surfaces. Such modification is an interesting field of investigation and has been widely studied. Thus, the spectral features of SiO_2 modified by different reagents were examined in detail even in the earliest reports devoted to the application of spectroscopic methods in adsorption [18–20]. It has been established that the modifier interacts with the surface centers in specific ways, leading to changes in the properties and related spectral features. In addition, intermediate species occur with new types of surface centers or the removal of existing ones with

corresponding changes to their properties. So, the modification of the surface allows creation of sorbents and catalysts with desired properties and gives a new way to manage catalytic reactions.

Supported (metal oxide) catalysts are synthesized by the deposition of the active metal oxide salt or other compound onto the surface of an oxide support (e.g. alumina, silica, titania, etc.). This can result in either isolated ions in different coordination (the latter is easily detected by both UV–Vis and ESR methods) in two-dimensional surface metal oxide overlayers or in three-dimensional metal oxide crystallites. Large three-dimensional crystallites can be detected by X-ray diffraction, in contrast to small three-dimensional crystallites (below 40 Å), two-dimensional metal oxide overlayers and, in particular, isolated ions. Thus, the absence of an XRD peak may be caused by small crystallite size, their low concentrations, or by the presence of a two-dimensional metal oxide overlayer. On the other hand, the presence of an XRD peak confirms only that large crystallites are present and does not provide information about the presence or absence of a two-dimensional metal oxide overlayer. That is where the methods of molecular spectroscopy have an advantage.

For supported catalysts, Raman spectroscopy has a great advantage when compared with IRS, since the spectrum of a support is usually very weak in the Raman spectrum, and only the spectrum of the catalytically active component is observed. Unlike XRD, the Raman signal is not dependent on long-range order and reveals only the vibrations of the M–O bonds. The different metal oxide structures that are present in the two-dimensional overlayers and in oxide crystallites produce different Raman and IR signals. This allows discrimination between these two structures.

Due to the numerous studies of Wachs and co-workers, summarized in reference [105], the Raman method is effectively used at present to investigate oxide structures and their defects in layers of different oxide catalysts such as CrO_3 , MoO_3 , V_2O_5 , etc. on various supports. It was found [995, 997–999, 1034, 1051, 1055, 1057, 1064, 1065, 1069] that the dehydrated surface metal oxide structures of alumina-supported rhenium(VII) oxide, molybdenum(VI) oxide, tungsten(VI) oxide, chromium(VI) oxide, vanadium(V) oxide and niobium(V) oxide are different from those under ambient condition where moisture is present on the surface (for example, for $\text{Mo}/\text{Al}_2\text{O}_3$ see Figure 4.1(a)). The presence of a highly distorted oxo species (containing M=O bond) was detected for supported molybdenum, tungsten, vanadium and niobium oxides at all loadings (see for $\text{MoO}_3/\text{Al}_2\text{O}_3$ Figure 4.1(b)). The lowest molybdenum oxide loading on the alumina support, when the MoO_3 crystallites are still detected by Raman spectroscopy (the band at 817 cm^{-1}), corresponds to 10 wt% of MoO_3 . Consequently, a monolayer coverage of the molybdenum oxide on alumina occurs slightly below this value (ca. 5 wt% MoO_3). The spectra of a series of oxidized $\text{MoO}_3/\text{Al}_2\text{O}_3$ catalysts in which the 998 cm^{-1} band arises from the two-dimensional molybdenum oxide over the layer and the 817 cm^{-1} band from MoO_3 crystallites are presented in Figure 4.1(b). At higher surface coverages, the M–O–M linkages indicative of polymeric structures are also observed on these systems. Above 10 % metal oxide loadings, monolayer coverage is exceeded, and crystalline MoO_3 , WO_3 , V_2O_5 and Nb_2O_5 characterized by the M=O bands particles are found on the alumina surface in addition to the dehydrated surface species. Oxides of different elements interact with the support in different ways, for instance, unlike molybdenum and vanadium, rhenium forms only oxide species. The structures of the surface rhenium oxide on various oxide supports (Al_2O_3 , ZrO_2 , TiO_2 and SiO_2) have been determined by means of Raman and IR spectroscopy [1069a]. The ReO_4 structure, forming at room temperature under dehydrated conditions, is present on the SiO_2 surface as one surface rhenium oxide species, whereas there are two such species on alumina, zirconia and titania supports. The latter structures are similar, and possess three terminal Re=O bonds and one bridging Re–O–support bond (C_{3v} symmetry). Only the strengths of their bonds to the support are different.

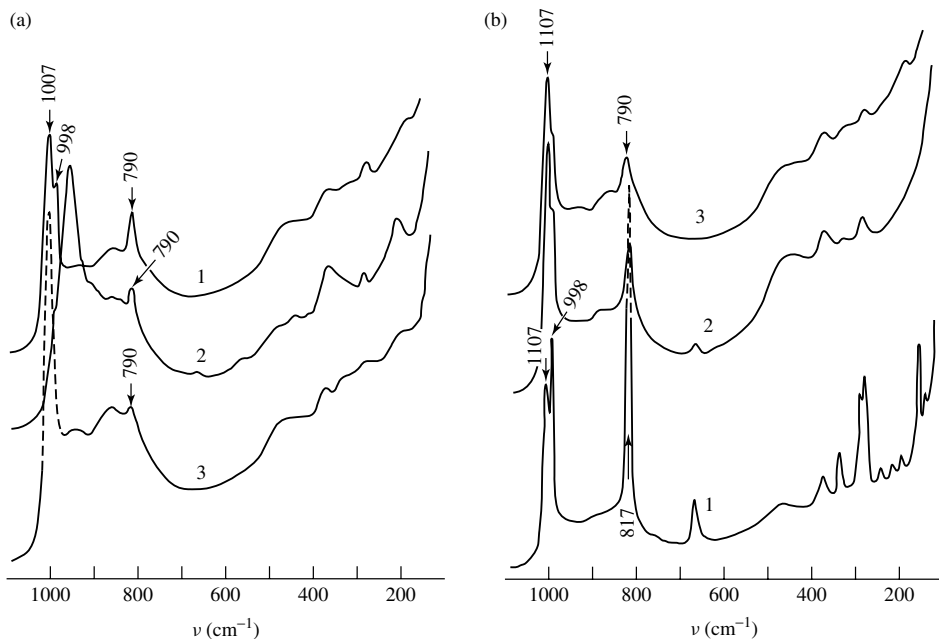


Figure 4.1. (a) Raman spectra of Mo/Al₂O₃ catalyst systems (8 wt% Mo): (1) sample oxidized at 823 K; (2) hydrated sample (24 h); (3) following dehydration at 773 K (2 h). (b) Raman spectra of Al₂O₃ catalyst systems with different molybdenum contents: (1) 10 wt% Mo; (2) 7 wt% Mo; (3) 3 wt% Mo.

Raman spectroscopy is not only effective in investigations of high-valence-cation oxides but also of other supported oxides. Raman spectra have been obtained for La₂O₃ dispersed on Al₂O₃ [1069b], but only after La₂O₃ coverages reached one theoretical monolayer or higher (20 % La₂O₃ and more). Sharp peaks at 104, 191 and 408 cm⁻¹ were observed in agreement with studies of bulk La₂O₃. Two additional bands were also observed at 322 and 935 cm⁻¹. The latter bands disappeared at 450 K or higher, but returned with the same intensity upon cooling to 300 K. These bands are present in low intensity in the Raman spectra of bulk La₂O₃ with a low surface/volume ratio. Raman spectra taken with different exciting laser lines showed that these bands can be attributed to a laser-excited luminescence. They provide evidence for the presence of oxygen anion vacancies.

Cobalt oxides prepared by the calcination of cobalt nitrate supported on Al₂O₃ have shown Raman (Figure 4.2(a)) and IR (Figure 4.2(b)) spectra of the samples with significant (>15 wt%) content of supported Co₃O₄ similar to those of Co₃O₄. This indicates that this is the predominant state of cobalt ions in supported oxidized samples. If the concentration of Co₃O₄ is less than 10 wt%, the additional bands appear in Raman spectra. Their appearance confirms the interaction between Co²⁺ ions and Al₂O₃. *In situ* Raman measurements (as well as IRS – see below) enable the study of reduction. The Co₃O₄ bands disappear upon reduction, giving new bands, probably characterizing amorphous phases of cobalt oxides (Figure 4.2(a)). No bands could be observed in the Raman spectra of metallic cobalt formed by the reduction. It is possible that the Co²⁺ ions, distorted due to interactions with the surrounding Al₂O₃, which occur are in an amorphous oxide form. This phase is also characterized by the Raman and IR bands, the positions of which are very close: ~560 cm⁻¹ in the Raman spectra (Figure 4.2(a)) and 520 cm⁻¹ in the IR spectra (Figure 4.2(c)). The position of this band in the Raman spectra is intermediate between the

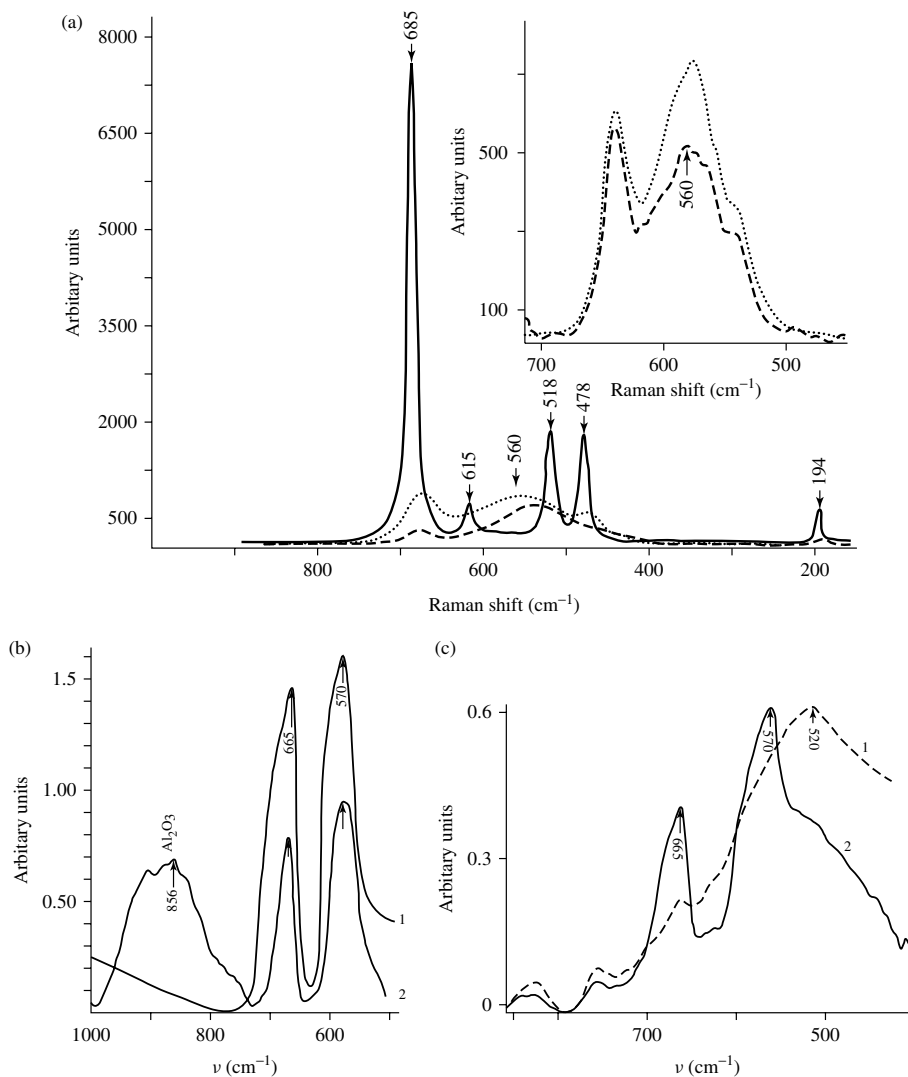


Figure 4.2. (a) Raman spectra of an $\text{Co}_3\text{O}_4/\text{Al}_2\text{O}_3$ catalyst system oxidized (solid line) and reduced in H_2 at 623 K (dotted line) and 673 K (dashed line). Spectra have been taken in air at room temperature after passivation of the samples. (b) DRIR spectra of (1) Co_3O_4 , and (2) $\text{Co}_3\text{O}_4/\text{Al}_2\text{O}_3$. (c) Changes in the DRIR spectra of (1) $\text{Co}_3\text{O}_4/\text{Al}_2\text{O}_3$, after (2) reduction in H_2 at 623 K.

positions characteristic of tetrahedral and octahedral Co^{2+} ions. These probably result from a two-dimensional phase of CoO .

An interesting application of Raman spectroscopy in the study of supported oxide systems has been described by Mar *et al.* [1069c]. These authors compared the Raman and XRD data obtained for thin films of RuO_2 on fused silica and alumina and showed that the bands characterizing RuO_2 are narrowed with an increasing of degree of crystallinity, as brought about by an increasing calcination temperature. That means that it is possible to (qualitatively) estimate the degree of crystallinity of an oxide by using the half-widths of the Raman bands. Moreover, Raman

spectroscopy enables the study of supported oxide layers down to monolayer coverage (possibly even lower), whereas XRD studies require five layers as a minimum.

Raman spectroscopy [1069d] and real-time surface-enhanced Raman spectroscopy (SERS) give quantitative information about thin films of oxides and their relative amounts, plus the extents of oxidation [1069e]. Raman scattering is also very useful in studying ultra-fine-grained materials. For example, it has been established that grain size effects can produce large shifts within, plus broadening of, the Raman spectrum [1069f].

IR and particularly FT IR spectroscopies can also be used successfully in a number of cases to evaluate the metal oxide structures, especially when the vibrations of an active component do not overlap with those of the support. In the latter cases, the method of support-spectrum compensation [1070a], involving computerized subtraction of the support spectrum from the total spectrum, enables the detection of the spectrum of the active component. In such a manner, the different heteropoly acids of molybdenum were identified [106] by means of IR spectroscopy.

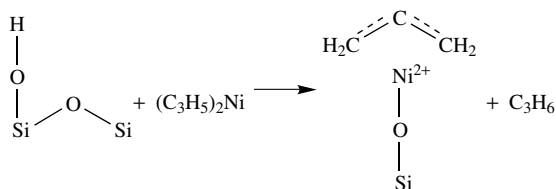
As can be seen from Figure 4.2(b), FTIR spectroscopy can also be used for identifying cobalt oxide phases supported on SiO_2 or Al_2O_3 . Such a possibility for silica-supported cobalt oxide has been shown by Banerjee and Chakrabarty [1070b]. Diffuse reflectance FTIR *in situ* measurements (Figure 4.2(c)) enable study of the changes in the spectra of cobalt oxides upon reduction and identification of the partially reduced cobalt oxides (see above).

4.1 Organometallic complexes

Interaction with organometallic compounds is mainly of the acid–base type. Coordinatively unsaturated cations and anions at the surface of the support provide, respectively, Lewis acceptor and donor centers. Corresponding adduct formations are similar to those observed under homogeneous conditions. The same applies to the interaction between organometallics and Brønsted sites (OH groups) of partially hydroxylated oxides and proton-exchanged zeolites.

On adsorption, supported complexes are subjected to the electrical potential of a large region of the solid and may involve interactions with more than one surface site. This is similar to the case of molecules trapped inside the pores and cages of zeolites, which are dependent on the molecular dimensions of these cavities.

Characterization of the surface complexes is a primary requirement for the understanding of the mechanism of the interaction between organometallic compounds and supports, and study of the reactivity of the surface adducts. Spectral methods have found wide application in this field through observations of changes in the states of ligands and the character of their interactions with support surfaces. For example, when a π -allylic compound of $\text{Ni}(\text{C}_3\text{H}_5)_2\text{X}_2$ ($\text{X} = \text{F}, \text{Cl}$ and Br) interacts with OH groups of SiO_2 , the C_3H_6 molecule is given off, leaving nickel allyl which is chemically bound over the SiO_2 surface [111, 1071]



Scheme 4.1

This leads to the formation of new surface centers. The process of complex formation and the changes in its properties have been identified by changes in IR spectra of both surface

hydroxyl groups and allylic complexes. The formation of such complexes on the surface allows the establishment of their roles in catalytic reactions [1071]. Studies of the interaction between dimeric complexes and the surface represent another example. Thus, $\text{Mo}(\text{OC}_2\text{H}_5)_5$ usually exists in dimeric form, but through interaction with SiO_2 this is decomposed and chemically interacts with the OH groups of SiO_2 , thus producing a separation of the alcohol [1072, 1073]. Supported complexes can be formed by interaction with Lewis acid sites, as well as with hydroxyl groups. In such cases, it may be necessary to use the method of competitive reactions with adsorbed NO, CO and NH_3 molecules to distinguish the different active sites. Such interactions have been examined by various workers [1074–1077], with interaction with carbonyls [60] as an example. Another way is to synthesize the organometallic complex directly on the surface of a support. Thus, special experiments on synthesis of allyl on $\gamma\text{-Al}_2\text{O}_3$ surface due to adsorption of C_3H_6 on the surface dehydrated at 773 K have been made [473]. The author then used such a catalyst in ethene oxide polymerization. The molecular mass of the polymer formed reached several hundred thousand. So, based on knowledge of the surface reactions and on spectral identification of the compound formed, a new prospective catalyst has been created.

4.2 Metal carbonyls and nitrosyls

Transition-metal carbonyls can interact with oxide surfaces in different ways, the majority of which have their analogies in homogeneous chemistry and have already been analyzed in detail in several reviews [60, 1072–1074]. The main interactions can be divided, according to Zecchina and Areat [60], into ligand-centered and metal-centered types. The first class includes (i) weak physisorption through van der Waals interactions, (ii) hydrogen-bonding to OH groups of partially hydroxylated oxides, and (iii) oxygen bonding to a surface Lewis acid site, whereas the second class comprises (i) decarbonylation and clustering at strong Lewis acid sites, (ii) nucleophilic attack by Lewis basic sites, (iii) nucleophilic attack by Brønsted basic sites, (iv) Lewis-base-assisted redox disproportionation, and (v) protonation.

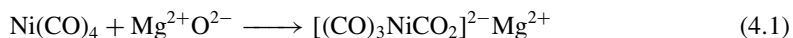
The primary interaction seems to be of the donor–acceptor type between CO ligands and Lewis acid sites at the support surface, forming an oxygen-bound surface adduct. Carbonyl ligands, both linear and bridging, surrounding the metal center have the oxygen atom pointing toward the exterior of the molecule, and form O-bound σ -adducts with Lewis acids. Formation of σ -adducts causes a perturbation of the CO vibrational spectrum. Low wavenumber shifts of 100–150 cm^{-1} and 200–400 cm^{-1} are typically observed for linear and bridging CO groups, respectively. Surface adducts formed at defective sites are more strongly held than those located on regular surface sites. Electron density withdrawal from the metal carbonyl is larger, and the perturbation of the CO vibrational spectrum is maximized in such cases. Electron withdrawal also facilitates transformation of bridging CO groups into linear ones.

As a rule, mononuclear carbonyls have high symmetry and correspondingly simple vibrational spectra. These spectra become more complicated after interaction of the complex with the surface, as new additional bands appear. IR spectroscopic studies of the $\text{Ni}(\text{CO})_4$ interaction with various types of supports (covalent, SiO_2 ; acid, $\gamma\text{-Al}_2\text{O}_3$; strongly acid, HY and HZSM-5 zeolites; basic, MgO) [1078] showed significant differences in the spectrum observed. Upon interaction with a surface, a tetrahedral molecule of $\text{Ni}(\text{CO})_4$, with T_d symmetry in the gas phase, is reduced in symmetry.

The IR spectrum of $\text{Ni}(\text{CO})_4$ on silicalite is very similar to that in hydrocarbon solution: only the band at ca. 2050 cm^{-1} is observed, and physical adsorption through the van der

Waals forces takes place. On highly dehydroxylated γ -Al₂O₃, Ni(CO)₄ forms oxygen-bound adducts. There are two low-frequency bands at about 1950 and 1850 cm⁻¹, corresponding to CO ligands σ -bound to surface Al³⁺ ions with different degrees of coordinative unsaturation. On some defective Lewis acid sites, the O-bound surface adducts are unstable and decompose with the elimination of CO ligands [60]. Sub-carbonyl species are then formed, as well as (Ni⁰)_n clusters. The Ni(CO)₄ interaction with HY and HZSM-5 zeolites leads to the formation of hydrogen-bonded adducts. Dehydroxylation of both HY and HZSM-5 by heating under vacuum leads to a progressive elimination of Brønsted acidity and simultaneous creation of Lewis acidity.

Upon the interaction of Ni(CO)₄ with fully dehydroxylated MgO, besides a number of bands in the 1800–2100 cm⁻¹ region, there are two absorption bands at about 1490 and 1050 cm⁻¹, corresponding to the asymmetric and symmetric stretching modes of the CO₂²⁻ group in a structure commonly observed when metal carbonyls are dosed on basic oxides:

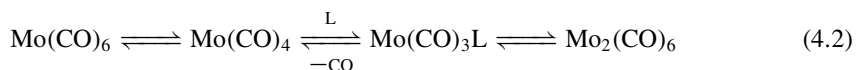


In this reaction the CO ligand interacts with an ionic pair.

The potential of UV–Vis and IR spectroscopies in the detailed study of the interaction of ruthenium carbonyl clusters has been reported [939v]. The change of the symmetry of the carbonyl complexes due to the interaction with the surface, as well as the decarbonylation, structure and reactivity of these complexes, including formation of the oxidized ruthenium complexes due to ruthenium oxidation by alumina, plus the ruthenium surface properties after full decarbonylation and reduction, have been analyzed.

In the case of the interaction between Ru₃(CO)₁₂ and Pd/SiO₂ [1079, 1080], in contrast to the interaction between Ru₃(CO)₁₂ and SiO₂ (for which, according to the IR spectra there is no chemical interaction), the IRS data suggest that the structure of the product of the Ru₃(CO)₁₂ interaction with metallic Pd is a Ru₃(CO)_x fragment coordinated on several neighboring Pd atoms (saturation concentration is 1 Ru atom per 3–5 surface atoms of Pd). The oxidation of Ru occurs due to hydroxyl groups. There were no absorption bands at 1970 and near 2090 cm⁻¹ characteristic of CO adsorbed on metallic palladium, and hence it has been proposed that the Ru ‘blocks’ the metallic palladium spectrum of CO adsorbed on the Ru–Pd catalyst. Since the spectrum sites on the Ru–Pd catalyst are not the superposition of the spectra that are characteristic of pure Ru and Pd, it is reasonable to suggest the formation of bimetallic particles.

UV–Vis spectroscopy has been applied to study the formation of the active catalyst component upon the interaction between Mo(CO)₆ and an alumina support [1081]. These data establish that the activation of the Mo(CO)₆/γ-Al₂O₃ catalyst is associated with the formation and rearrangement of sub-carbonyl structures on the surface. The formation of the Mo₂(CO)₆ active center may be represented as follows:



where L is the ligand (possibly a surface hydroxyl group). The formation of Mo₂(CO)₆ is associated with a decrease in energy.

All of the above examples demonstrate the effect of support surface centers on the initial complex, which is thereby changed to give an active component. Another situation is observed when the supported complex decomposes, and oxide or metallic active components are formed from it. The properties of the new active component depend on the initial structure of the complex

formed on the support, its transformation conditions, and also on the properties of the cluster formed on interaction with the support. As a rule, the use of such a system to prepare the catalyst allows the generation of a more dispersed and homogeneous distribution of the active component over the support in the cases of formation of oxide species in an oxidizing medium or metallic particles in a reductive atmosphere.

IR and UV-Vis spectroscopy have become very useful as a method of controlling catalyst preparation. With this help, excellent low-temperature catalysts for waste gas combustion have been prepared from iron penta- and hexacyanide complexes ($M[\text{Fe}(\text{CN})_5\text{NO}]$ and $M_2[\text{Fe}(\text{CN})_6]$, where $M = \text{Mn}, \text{Fe}, \text{Co}, \text{Ni}$ and Cu), synthesized on $\gamma\text{-Al}_2\text{O}_3$ supports [1082].

Phthalocyanine complexes attached to the support via a special incorporation of SO_3 groups into the complex have been investigated by means of both the IRS and UV-Vis methods [1083, 1084], which allowed a study of their interactions with different reagents (O_2 , CO , NO and NH_3).

In the case of the interaction between chromocene with both totally and partially dehydroxylated MgO , the reactivity of the adsorbed species towards CO have also been studied by IR spectroscopy [1085]. Cyclopentadienyl, $(\text{Cp})_2\text{Cr}$, is weakly adsorbed on residual surface MgOH groups, forming hydrogen-bound species, and on the extended (100) faces, forming clustered $(\text{CpCr})_n$ species. As with the other cases considered above, a stronger interaction was observed with the highly unsaturated ions located on the edges and corners of the MgO micro-crystals.

4.3 Interactions with simple acids and bases

One of the most widely used methods of modifying oxide surfaces is by interaction with acids or alkalis. Thus, the addition of Na^+ ions on alumina causes a decrease of the surface hydroxyl group liable for protic acidity, probably due to an exchange of H^+ of the hydroxyl group with Na^+ (LFB at around 3660 cm^{-1} disappears at this) [1086–1088]. Support for this comes from the IR spectrum of NH_3 adsorbed on such a catalyst: there are no bands of NH_4^+ ions in this case [1086, 1088]. IR data on the CO adsorption show that both the strongest Lewis acid sites (the band at 2235 cm^{-1}), as well as the Brønsted acid sites, are fully depressed after incorporation of sodium, whereas the acceptor abilities of the weaker Lewis acid sites (the band at 2210 cm^{-1} which shifts to 2205 cm^{-1}) decreases [1087]. In contrast, the treatment of alumina by HCl leads to the disappearance of two high-frequency bands of the OH groups due to the substitution of OH^- groups by Cl^- ions, accompanied by an increase in the strengths of both the protic sites and the LASs, probably because of the inductivity effect.

A comparison of ammonia centers on Al_2O_3 , $\text{Al}_2\text{O}_3/\text{Na}^+$ and $\text{Al}_2\text{O}_3/\text{Cl}^-$, treated identically, has indicated the differences in the distribution of Lewis acid centers [426]. For Al_2O_3 , the maximum of the δ_s band has been observed at 1240 cm^{-1} , for Na-modified Al_2O_3 at 1230 cm^{-1} , and for Cl^- treated aluminum oxide at 1260 cm^{-1} (Figure 4.3). The δ_s band for each system is wide and complex (Figure 4.3, spectra 2) because of the overlapping δ_s characterizing the H-bonded and coordinated molecules of NH_3 . However, even in this case a significant difference in δ_s value is observed. The increase in δ_s on transition from aluminum oxide to Cl^- -modified aluminum oxide indicates an increase in the proportion of stronger electron-accepting centers. After removal of the NH_3 hydrogen-bonded complexes (spectrum 2), the difference in acceptor ability of the Al^{3+} surface cations can be seen directly for the coordinated NH_3 molecules. Consequently, $\delta_s\text{NH}_3$ is sensitive to the ligands surrounding the adsorption center. Carbon monoxide adsorption on the sample treated with Cl^- leads to the 2245 cm^{-1} band appearing in the spectrum, instead of

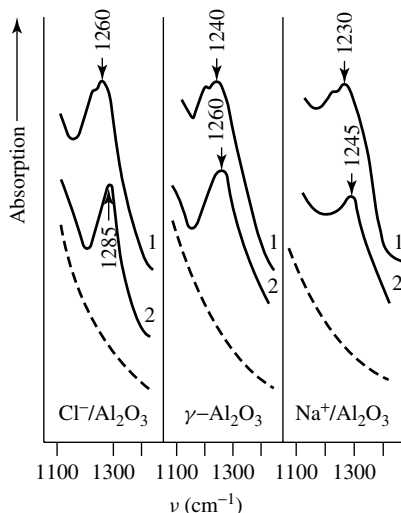


Figure 4.3. IR spectra of ammonia in the region of symmetric deformation vibration (γ - Al_2O_3 dehydrated at 773 K): (1) NH_3 adsorption at 293 K with subsequent desorption at 293 K; (2) desorption at 423 K the dashed lines represent the background spectra).

the 2235 cm^{-1} band, while the 2210 cm^{-1} band shifts to 2215 cm^{-1} . This confirms an increase in the acceptor ability of the Lewis acid sites.

IR experiments involving the adsorption of carbon monoxide or pyridine as probe molecules also showed that the introduction of even very small amounts of sodium decreased the number and the strength of the strongest Lewis acid sites [677]. It was found that the number of affected sites is one order of magnitude more than the quantity of Na^+ cations introduced.

4.3.1 F^- - AND Cl^- -MODIFIED OXIDE SYSTEMS

The IR spectra of pyridine adsorbed on alumina with 4.5 % F showed no evidence of the $1540\text{--}1550\text{ cm}^{-1}$ band assignable to the pyridinium ion formed by interaction between pyridine and Brønsted acid sites. This band appeared for those catalysts with 6.5 % F [1089]. On fluoriding alumina, the concentration of dual acid–base sites is diminished as the surface hydroxyls (the precursors of the dual sites) are substituted by stable F^- ions. This process is accompanied by an increase in the intrinsic acid strength of the remaining hydroxyls.

An introduction of either Cl^- or F^- is accompanied by strong increases of further new protic sites on the other oxide surfaces (Figure 4.4). As is shown from the spectra, after modification of Cr_2O_3 by HCl the strong protic sites (δNH_4^+ at 1410 cm^{-1}) appear on the surface [426].

Fluorination of aluminosilicates is also accompanied by the growth of the strength of both LASs and BASs but at the same time it was shown that the aluminosilicate structure has been destroyed, and free Al_2O_3 is formed. The analysis of the spectra of adsorbed pyridine shows that in proportion to the removal of Al from an amorphous Al/Si oxide the Lewis acidity decreases, as demonstrated by the decrease in intensity of the coordinated-pyridine band at 1450 cm^{-1} . Simultaneously, the number of Brønsted acid sites in samples with relatively low

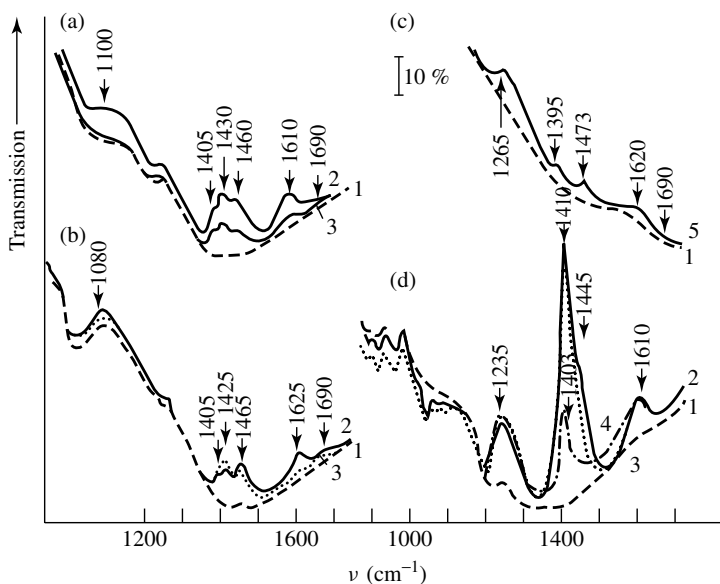


Figure 4.4. IR spectra of NH_3 adsorbed on (a) Fe-Sb-O, (b) Sb_6O_{13} , (c) $\gamma\text{-Al}_2\text{O}_3$ rehydroxylated at 573 K, and (d) $\text{Cr}_2\text{O}_3 + \text{HCl}$: (1) background; (2) 1 torr NH_3 ; (3, 4, 5) evacuated at 300, 373 and 473 K, respectively.

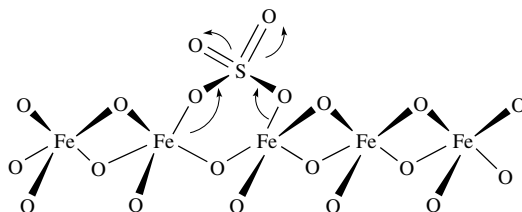
concentrations of Al_2O_3 (around 40 wt%) remains practically the same, as shown by the absence of any changes in the intensity of the PyH^+ ions absorption band at 1545 cm^{-1} . A small increase in Brønsted acidity takes place upon dealumination of high-alumina catalysts. A decrease in the Lewis acid sites concentration is due to free Al_2O_3 being dissolved, and when Al^{3+} cations occupy ionic-exchanged positions additional hydrogen ions are formed. Such a substitution provides a compensating negative charge of the Si/Al-O lattice and leads to an increase in the number of BASs [1090]. During fluorination of non-calcined Al/Si, fluorine is attached only to aluminum atoms, thus forming aluminum fluoride (absorptions at 553 and 678 cm^{-1}), whereas in the case of a calcined aluminosilicate sample, interaction with Si atoms also takes place (the bands at 490 and 750 cm^{-1}). The XRD data confirm the formation of the fluorine-containing compound.

4.3.2 SO_4^{2-} -MODIFIED OXIDE SYSTEMS

The protic-acidity effect has been observed for many transition-metal oxides containing cations in their highest oxidation states [30, 426] and for not normally acidic oxides upon their modification with inorganic acids (HCl , H_2SO_4 and H_3PO_4) or appropriate oxides (SO_3 and P_2O_5) and ions (Cl^- , SO_4^{2-} and PO_4^{3-}) (see, for example, [1091–1096]). Let us now examine in more detail the investigation of TiO_2/SO_4 presented by Hadjiivanov and Davydov [1091]. In this case, upon the introduction of the acid-forming oxide (SO_3) to the system (TiO_2), it exhibits protic acidity. Spectral manifestations of the protic acid sites are similar to those considered above (delocalized protons) [426, 1096]. It is very important that the infrared study of the adsorption of NH_3 , CO and Py allows the detection of both the cationic activity and the effect of the modifier, added or from impurities, as was demonstrated in [304, 1091].

The modification of oxide surfaces by such anions as SO_4^{2-} significantly changes the properties of the surface hydroxyls. This is reflected in their spectral patterns (see, for example, [79–81, 1091–1104]). The exchange of OH groups, their direct substitution and also the appearance of new hydroxyls are detected by these means. Many experimental studies have been made in this area. Unfortunately, it is not possible to examine all of these results here. As an example, an SO_4^{2-} -modified oxide system will be considered; it is known that several oxide systems (Fe_2O_3 , TiO_2 and ZrO_2) become super-acids after such modification [79].

$\text{Fe}_2\text{O}_3/\text{SO}_4$ [79] was one of the first systems with super-acid properties to be established; this was attributed to the presence of surface covalently bound sulfates observed by infrared spectroscopy ($\nu\text{S}=\text{O}$ at 1380 cm^{-1}). Tanabe [79] proposed the following model for a super-acidity site:



Scheme 4.2

Parfitt and co-workers [1098] found that sulfates, phosphates, selenates and oxalates are formed at the surfaces of goethites due to specific reactions with two single-coordinated hydroxyls (the band at 3486 cm^{-1}), yielding binuclear bridging complexes. The adsorption mechanism was interpreted in terms of the (100) face that may well be the predominant form of high-surface-area goethites.

Additional bands in TiO_2/SO_4 occur at 1045 , 1140 and 1205 cm^{-1} in the IR spectrum of the modified sample (pellet with KBr) [1091]. According to Nakamoto [15], these bands were assigned to the ν_3 frequency of the bidentately bound sulfate ion, which is split into three components due to a decrease in its symmetry from T_d to C_{2v} . The relatively high intensities of these bands show that they cannot be due to surface compounds alone. These sulfates are probably either in the layers near the surface or form a separate phase.

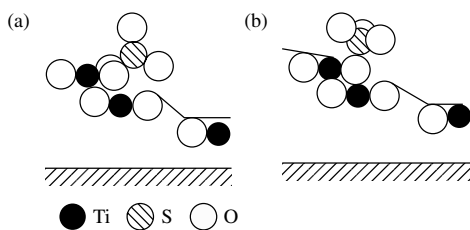
Absorption bands which are absent in the spectra of pure anatase were present in the $1200\text{--}1400\text{ cm}^{-1}$ region in all spectra of the modified samples after vacuum-heat treatment. An intense and asymmetric band with a maximum at 1400 cm^{-1} and a shoulder at 1250 cm^{-1} , and also an intense absorption in the $2800\text{--}3800\text{ cm}^{-1}$ region, were observed in the spectrum of the TiO_2/SO_4 (773 K) sample. Absorption bands at 1380 and 1320 cm^{-1} were observed in the spectrum of TiO_2/SO_4 (833 K), and the bands characterizing surface hydroxyl groups appeared in the $3600\text{--}3800\text{ cm}^{-1}$ region. The reversible change of the bands in the $1200\text{--}1400\text{ cm}^{-1}$ region upon hydration–dehydration at room temperature indicated that these bands belong to vibrations which characterize surface compounds. For assignment, they were compared with the frequencies of the vibrations of other sulfur-containing compounds (Table 4.1). This showed that in the spectrum of TiO_2/SO_4 (833 K), the observed absorption bands are close to the frequencies of vibrations of the $\text{S}=\text{O}$ bond in the spectra of gaseous SO_2 , organic sulfates and sulfonyl chlorides. These compounds have C_s or C_{2v} symmetry like bidentately bound sulfate, but the $\text{S}=\text{O}$ bond is close to a double bond, i.e. in the surface sulfates, the SO_2 group should apparently be considered as ‘quasi-isolated’, in contrast to the classic sulfates where the cation coordinates a still tetrahedral SO_4 group. The appearance of an absorption band at 1320 cm^{-1} in the spectrum

Table 4.1. Spectral manifestations of some sulfur-containing compounds and ions.

Compound or ion	Symmetry	ν_1 (cm^{-1})	ν_3 (cm^{-1})
SO ₂ (gas)	C _{2v}	1151	1302
SO	D _{3h}	1069	1330
SO ₃ ²⁻ (solid)	C _{3v}	1010	961
SO ₄ ²⁻ (free ion)	T _d	983	1105
SO ₄ ²⁻ (monodentate complex)	C _{3v}	970	1032–1044, 1117–1143
SO ₄ ²⁻ (bidentate complex)	C _{2v}	995	1050–1060, 1170, 1105
ROSO ₂ OR ₁ (R)	C _s (C _{3v})	1187–1200	
R–SO ₂ Cl	C _s	1168–1185	1390–1414, 1300–1390

of TiO₂/SO₄ shows that in this case, the S=O bond has close to double-bond character, but the symmetry is different: point group C_{3v} or D_{3h}. This shows that in this case the sulfate ion is bound with the surface metal cation through one oxygen atom, while in the case of TiO₂/SO₄ (833 K), it can formally be considered to be bidentately bound, but with an isolated SO₂ group.

The reaction of the coordinatively unsaturated titanium ion on the surface with the SO₄ group can be represented as a substitution of surface oxygen or OH groups by the SO₄²⁻ ion:

**Scheme 4.3**

The surfaces of modified oxides are characterized by the presence of protic acid sites, which, as has been suggested [1091] for TiO₂/SO₄, are related to the presence of the covalently bound SO₄ groups, during hydration of which the SO₃OH fragments are formed. Such an OH group is characterized by the broad absorption band at 3600–3400 cm⁻¹ (Figure 4.5). Upon modification of the oxides' surfaces by SO₄²⁻ ions, a specific manifestation of the original surface hydroxyl groups is observed. Surface sulfates (1380 cm⁻¹) and isolated hydroxyl groups are observed on the surface of TiO₂/SO₄ dehydrated at 833K (Figure 4.5, spectrum 3), and the position and relative intensities of the absorption bands are altered slightly in comparison to the unmodified sample of TiO₂. However, the spectral surface phenomena for TiO₂/SO₄ dehydrated at 773 K are the most interesting (Figure 4.5, spectrum 2). First, note the presence of an intense absorption in the region of perturbed hydroxyl groups (in the absence of $\delta\text{H}_2\text{O}$ at 1620 cm⁻¹), which indicates the presence of strong hydrogen-bonds that persist up to high temperatures (773 K). The study of NH₃ adsorption indicates the presence of a significant number of mobile protons in TiO₂/SO₄ (773 K), while these protons were not found for TiO₂/SO₄ (883 K). As a consequence, the presence of strong hydrogen-bonds for the samples of TiO₂/SO₄ (773 K) can be correlated with the presence of these mobile protons. Such mobile protons are not found for pure anatase, too. The spectrum of the SO₄²⁻ ion (Figure 4.5, spectrum 2) changes strongly if the mobile proton are present: the absorption band is broadened, split and shifted in comparison to spectrum 3.

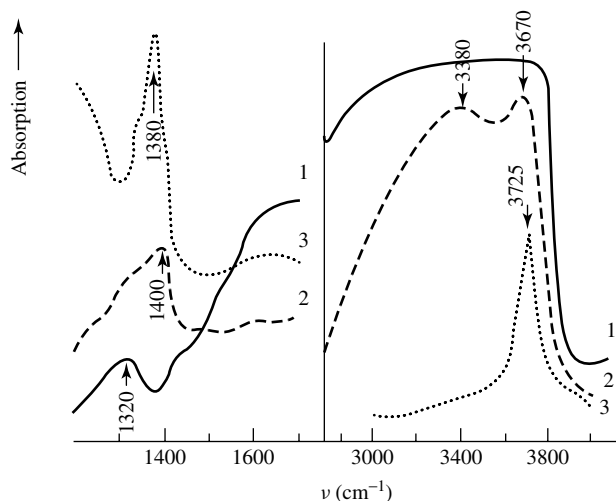
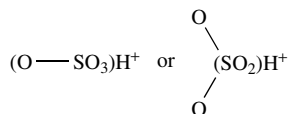


Figure 4.5. IR spectra of the modified sample TiO_2/SO_4 dehydrated at (1) 293 K, (2) 773 K, and (3) 833 K.

Similar absorption bands were observed [1092] in the reaction of SO_x groups with a proton, and for this reason, it is considered that:



Scheme 4.4

fragments can exist in the case of the TiO_2/SO_4 (773 K) sample. These perturb the isolated TiO_2 hydroxyls, and are manifested by the appearance of hydrogen-bonding absorptions (Figure 4.5, spectrum 2). In the case of TiO_2/SO_4 (773 K), the hydroxyl groups are directly bound to the cation which coordinates the SO_4 group, with the protons compensating the negative charges of the oxygen atoms in the sulfur-containing groups. On dehydration above 773 K, the spectrum of the SO_4 group is restored (a proton is eliminated, and the perturbation is removed from the SO_x group), and changes also qualitatively occur in the region of OH absorptions. Analysis of the IR spectra does not permit the determination of which of the two states is realized on the surface. The data obtained are well argued with those obtained for modified SO_4 ions on silica [1093], TiO_2 [1094] and alumina [304, 1094, 1098]. It has been reported that the structure $(\text{SiO})_2\text{SO}_2$, with two terminal $\text{S}=\text{O}$ bonds, is formed in the case of SiO_2 , whereas on sulfated Al_2O_3 and TiO_2 the $(\text{MO})_3\text{S}=\text{O}$ ($\text{M} = \text{Al}$ or Ti) species occurs. In the presence of water or excess surface OH groups, such a structure is converted to an $(\text{MO})_2\text{SOOH}$ group, thus accounting for the increased Brønsted acidity. It is not easy to establish the differences between these species on the basis of spectral data. It should be noted, however, that one important difference of super-acid systems, when compared to conventional ones, is that the super-acid sites are present on the surface until quite high dehydration temperatures (873 K for TiO_2/SO_4 [1091]), while on both SiO_2 and Al_2O_3 they are not observed at temperatures above 573 K. The character of the surface modification depends on the type of the modifying ligand. Thus, in the case of PO_4^{3-} anions, in contrast to

sulfates the band at 3680 cm^{-1} , characteristic for P–OH groups [1096] is not observed on the surface of dehydrated TiO_2/PO_4 .

As for bulk sulfates, hydroxyl groups are not observed [298] in the spectra, but in the case of phosphates it is known that the terminal P–OH groups (νOH at about 3680 cm^{-1}) are observed [1104–1106]. The surface properties of calcium phosphates were examined in detail by Kibby and Hall [1107].

Already in the first studies it was established that the strength of Lewis acid sites increases, for example, upon the modification of the TiO_2 surface by SO_4^{2-} ions [1091]. In this case, the band of adsorbed CO is observed at 2215 cm^{-1} , instead of the band at 2205 cm^{-1} observed for CO adsorbed on TiO_2 itself. Support for these results has been obtained by Lange *et al.* [1108], where the acidic properties of a TiO_2 sample containing approximately 1 wt% S have been investigated by IR spectroscopy using CO adsorption and the co-adsorption of both CO and NH_3 . Due to the almost negligible OH content of the sample, Brønsted acidity could not be observed, whereas Lewis acid sites with enhanced acid strength as compared to sulfate-free titania could clearly be detected. It is inferred that these sites (namely $\text{Ti}_{\text{cus}}^{4+}$ sites) are located in close proximity to sulfate groups and that CO (and NH_3) coordinated to the Ti^{4+} sites interacts with the sulfate groups, presumably via electronic inductive effects. On the other hand, PO_4^{3-} ions blocked these sites [1096]. More recently, the crystalline aluminophosphates have also been intensively investigated. The protic acidity is determined by the terminal POH groups (νOH at 3675 cm^{-1}) [1109]. A broad band at $3400\text{--}3500\text{ cm}^{-1}$ is related to hydrogen-bonded P–OH groups. The data cited above show that phosphate and silicate systems differ significantly in their properties. There are no bridged P(OH)M groups in the case of the first systems, and their acidity depends on terminal P–OH groups. This is why that in such cases the dependence of the Brønsted-site strength with the nature of metal is absent. For phosphates of Al, Fe, Zr and Mg, the value of PA is about 1300 kJ mol^{-1} , whereas for corresponding silicates this value is 100 kJ mol^{-1} lower [298]. The similarity of these systems is shown only in the geometry of the distribution of the Brønsted sites on the surfaces. In both cases, there are protic and aprotic centers available for ammonia, while these are prohibitive for pyridine and CO.

Infrared studies of TiO_2 , HfO_2 , ZrO_2 and Fe_2O_3 modified by SO_4^{2-} ions showed that such a modification leads to an increase in their common acidity, and in the case of $\text{ZrO}_2/\text{SO}_4^{2-}$ and $\text{HfO}_2/\text{SO}_4^{2-}$ also to the formation of Brønsted acid sites (bands at 3635 and 3655 cm^{-1}). An increase in common acidity was connected with the formation of additional acidic sites due to an increase in the effective positive charges on the metal atoms [1090]. According to infrared data, the acceptor ability of ZrO_2 ($\nu\text{Zr}^{4+}\text{--CO} = 2190\text{ cm}^{-1}$) increases due to such modification, and two types of LASs are observed (the bands at 2195 and 2205 cm^{-1}).

ZrO_2/SO_4 is one of the most widely used and studied super-acid catalysts [1090, 1095, 1099, 1100, 1110–1118]. Two structures have been proposed for the sulfated zirconia acid site. Yamagichi and co-workers [1119–1122] have proposed a bidentate sulfate species containing a $\text{O}=\text{S}=\text{O}$ moiety, whereas Bensitel *et al.* [384] have proposed a tridentate SO_4 species containing a single $\text{S}=\text{O}$ moiety. White and co-workers [1110] suggested that structures similar to those presented in Figure 4.6 seem to be responsible for the acid properties. Each sulfur atom in such structures is surrounded by five different oxygens.

The type and relative concentrations of surface acidic sites (both Brønsted and Lewis) turn out to depend primarily on the type and relative concentrations of the surface sulfates, which in turn depend on the temperature of calcination of the non-sulfated ZrO_2 precursor, the overall surface concentration of the sulfates, and the temperature of the vacuum-thermal activation of the sulfated ZrO_2 systems [1123, 1124].

Quantitative measurements of acidity for anhydrous sulfates of aluminum, zirconium, gallium and magnesium have been made [298] by means of FTIR spectroscopy. It is impossible to detect

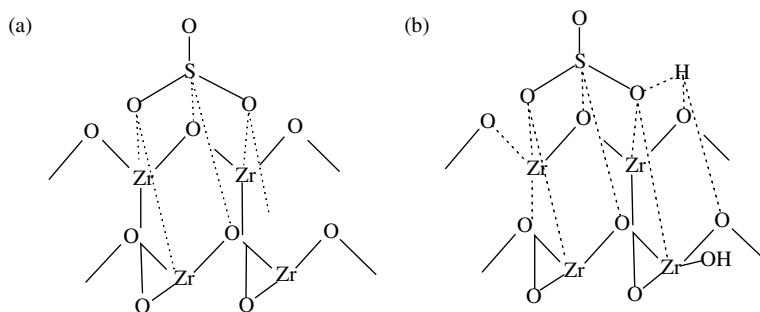


Figure 4.6. Possible sulfated zirconia acid site structures: (a) Lewis; (b) Brønsted.

the acidic OH groups (like isolated OH groups) on the surface of sulfates as well as on the oxide treated by sulfuric acid. According to Paukshtis [298], there is only intense absorption in the region $3600\text{--}2000\text{ cm}^{-1}$, characteristic for H-bonded acidic OH groups. The acidity of such groups on alumina completely covered by sulfate has been estimated from $\Delta\nu\text{NH}$ of PyH^+ . The $PA =$ value is $1170\text{--}1180\text{ kJ mol}^{-1}$, which is close to that of the aluminosilicate systems. The change of protic acidity in the series of metal sulfates does not coincide with the order of protic acidity of silicate or phosphate systems. In the latter case, the nature of the metal practically has no influence on proton donor ability, while for silicates such a dependence does exist and has a maximum ($\Delta PA = 45\text{ kJ mol}^{-1}$) at the transfer from Al to Mg. For sulfates, $\Delta PA = 15\text{ kJ mol}^{-1}$ in a series of Zr, Al, Ga and Mg sulfates.

The Brønsted acidity of dehydrated and rehydrated (inactive) super-acid sulfate-doped ZrO_2 systems has also been investigated via IR spectroscopy of adsorbed pyridine. The Brønsted acid sites on the surface were derived from acid protons, either in surface ZrOH groups with nearby sulfate groups, or more likely, in the coordination sphere of some surface sulfate groups [1123]. At higher surface hydration, acidic protons are involved in a diffuse system of multiple H-bondings. At medium to high hydration, at least some of the protic acidic centers are in an isolated hydrated form, whereas at medium to low hydration all of the available acidic centers are present in an anhydrous form, and variable fractions of the acidic centers are available for interacting with strong bases. At high dehydration, the majority of acidic protons are reversibly eliminated through OH condensation mechanisms. Very few protic centers are therefore still available at the surface for interaction with strong bases, although their presence is never completely eliminated before the surface sulfate groups start to decompose thermally.

The modification of zirconium dioxide by sulfate anions enhances the strength of both Brønsted acid sites (terminal or bridging ZrOH groups) and Lewis acid sites (low-coordinated Zr ions) [1123]. However, Brønsted acid sites with enhanced strength appear to be weaker than the bridging OH groups in zeolites. Modification also produces protons with a new environment. These protons are assumed to form nonlocalized bonds with the oxygen atoms of SO_4^{2-} anions or with neighboring basic oxygens and to possess acidic properties comparable to those of protons in zeolites.

4.3.3 BO_3^{2-} -MODIFIED OXIDE SYSTEMS

Boron as a modifier has been known for a long time, and data on spectral-monitored changes in surface properties are available in the literature (see, for example, [1125–1131]). Information about the structure of the borate species for different boron-containing systems can be obtained from their IR spectra. Interpretation of the spectral manifestations of different boron

compounds can be found in various publications [15, 1132–1135]. The bands in the region 1500–1200 cm^{-1} are due to the asymmetric B–O stretching modes of planar BO_3^{3-} groups [15, 1132–1135] of rare-earth orthoborates having calcite-like and aragonite-like structures ($\nu_{\text{as}}\text{BO}_3$ in the 1300–1200 cm^{-1} region [1132]). Such species can also be responsible for a symmetric stretching frequency near 940 cm^{-1} . Unfortunately, the latter usually cannot be observed in the spectra, because of its weakness and its overlap with fundamental frequencies of the support. In the case of ‘condensed’ planar borate structures such as in B_2O_3 , the absorption due to the asymmetric B–O stretching vibration is observed at 1260 cm^{-1} (maximum) to 1450 cm^{-1} (shoulder) [15, 1133]. The presence of the latter band gives the possibility of identifying this compound easily. Tetrahedral borate species are characterized by complex absorptions due to asymmetric and symmetric BO_4 stretching vibrations in the 1100–900 cm^{-1} region [1134, 1135].

In non-pretreated impregnated samples of ZSM-5 zeolite, boron exists as H_3BO_3 [1125]. Pretreatment at 673 K brings about the condensation of H_3BO_3 with the host zeolite Brønsted sites into an $=\text{Si}-\text{O}-\text{B}(\text{OH})_2$ species. Excess boron is present as amorphous B_2O_3 . There are absorption bands at 1386, 1212, 1100, 916, 820, 559 and 449 cm^{-1} in the spectra of zeolites modified by boron. The peak at 1386 cm^{-1} was assigned to trigonal boron sites, and the band at 916 cm^{-1} to tetrahedral boron sites.

For alumina, the analysis of different boron-containing compounds showed that the trigonal planar borates, responsible for the pair of bands at 1420 and 1300 cm^{-1} , definitely predominate over tetrahedral borates, which could be responsible for the shoulder near 1050 and 900 cm^{-1} . However, neither B_2O_3 nor its hydration products are present as separate phases. Adsorption of pyridine on such a sample allowed detection of the presence of both Lewis and Brønsted acidic centers. A small number of weak Brønsted sites are generated by boron addition to alumina. Boron itself does not act as a Lewis site. This is probably due to the fact that trigonal borate species are definitely predominant: in such species, the empty orbital on B is involved in π -type bonding with lone pairs of oxygen, and is consequently relatively unavailable for coordination. Tetrahedral B, as in BPO_4 , can act as a very strong Lewis site. The presence of B does not favor the stabilization of tetrahedral aluminum cations in amorphous alumina. Consequently, on amorphous alumina–boria, as on amorphous pure alumina, Al^{3+} cation remain predominantly octahedral and, when exposed on the surface, act as rather weak Lewis acid sites. Brønsted acidity, generated by B addition to amorphous alumina, is also very weak, in accord with the weakness of boric acid [1126, 1130].

Both FTIR transmission and DRIFT spectroscopic methods have been used by authors to study TiO_2 modified with boron. The transmission spectrum of TiO_2 samples with supported H_3BO_3 (2 % B) is shown on Figure 4.7. In the region below 1200 cm^{-1} , only the band at 1150 cm^{-1} is observed. The diffusion reflectance spectrum of the sample is shown in Figure 4.8. A comparison of Figures 4.7 and 4.8 shows that these spectra are similar. These data reveal that the DRIFT method can be used more effectively to investigate such boron–oxygen surface compounds. It is shown that the boron-free sample does not have any absorption bands in this region, but with incorporation of boron the appearance and gradual increase of a doublet band with maxima near 1250 and 1380 cm^{-1} is observed. These bands are likely to be due to the asymmetric B–O stretching modes of borates on the alumina surface [1126]. The band at 1380 cm^{-1} is very close to the band at 1385 cm^{-1} assigned to a trigonal B–O stretch on the boron-impregnated ZSM-5 catalyst [1125]. By increasing the boron content, the intensities of both bands (1380 and 1250 cm^{-1}) increase up to a boron content of 2 wt%, suggesting that up to this level the boron is deposited close to a monolayer form. Above such a boron loading, the band intensity increases more rapidly, and some B_2O_3 species seem to be formed.

The spectra of samples containing up to 1 wt% B show that in these materials the trigonal planar borates responsible for the pair of bands at 1380 and 1305–1330 cm^{-1} are predominant.

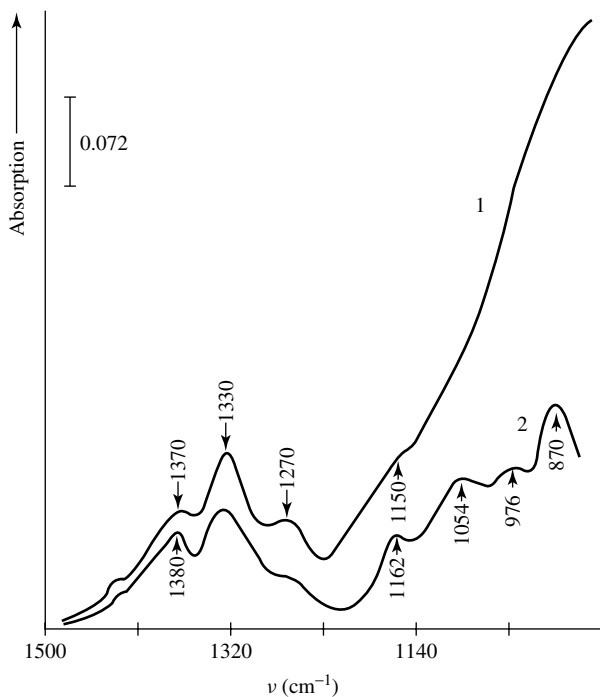


Figure 4.7. IR transmission spectra of (1) B/TiO₂ (2 wt% B) after subtraction of the TiO₂ spectrum, and (2) Co-Ti-B (2 wt% B) after subtraction of the Ti-B spectrum.

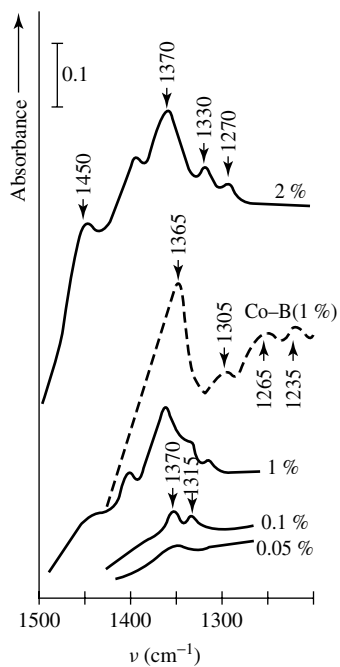
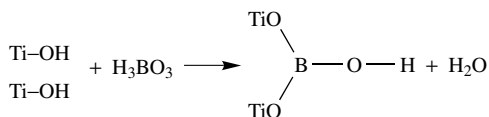


Figure 4.8. DRIFT spectra of B-TiO₂ samples with different boron loadings (the spectrum of TiO₂ is subtracted in all cases).

The results indicate that the boron is deposited as a monolayer on the surface of the titania up to a loading of 1 wt% B. Taking into account the data characterizing the complete absence after dehydration at 673 K of the hydroxyl groups for TiO_2 , it is possible to suppose that the interaction between TiO_2 and H_3BO_3 proceeds by the following scheme:



Scheme 4.5

with a predominant formation of the planar BO_3 groups. The appearance of the B–OH vibrations at 3668 cm^{-1} supports such a structure formation. All of the investigated samples of the Ti–B–oxide catalyst dehydrated at 673 K have no protic acid centers, as established by the IR spectra of adsorbed ammonia.

The addition of cobalt ions to a boron–titania catalyst changes the spectrum of the boron–oxygen surface compounds (see Figure 4.8). This was connected with a direct interaction between the cobalt ions and the boron–oxygen compounds. Cobalt probably substitutes weakly acid protons in the B–OH groups. After calcination at 773 K, cobalt oxide-like compounds are formed. The appearance of the absorption band in the $800\text{--}1000\text{ cm}^{-1}$ region confirms this [1131]. The incorporation of boron on the support leads to significant changes in distribution of the cobalt oxy-species.

4.4 Heteropoly compound systems

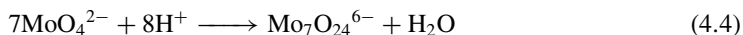
As has already been shown in Chapter 3, the supported cations of chromium, vanadium, and especially of molybdenum, in high oxidation states and concentrations more than 10 wt%, can form, under certain conditions, the complex oxide species similar to poly- and even heteropoly anions involving the surface cations of a support. Since the influence of the type and acid-basic properties of a support on character and distribution of the active component at low concentration (up to monolayer coverage of the support) was clearly shown above, we will try to describe such influences for more complex oxide compounds similar to HPA and the potential of spectral methods for studying such interactions. Heteropoly compounds (HPCs), heteropoly acids (HPAs) and their salts are now widely used in heterogeneous catalysis. They are effective catalysts of important chemical processes [83, 84] and are also convenient as model catalytic systems, offering a useful combination of acid and oxidation–reduction properties which allows strict determination of the compositions and structures of the catalytically active centers. HPCs are used in various phases, as homogeneous liquids, in two-phase liquids, and in liquid–solid and in gas–solid combinations. Furthermore, HPCs allow control of the variations of both the acidic and oxidation–reduction function of the catalytic system. In this sense, they are superior to the zeolites.

The acid strength and acid-site density can be controlled quite well in both solution and the solid state, but redox properties in the solid state are not well understood because of the lack of sufficient thermal stability of the mixed-metal heteropolyanions. The acid strengths of some solid heteropolyacids have been suggested to reach the range of those of super-acids, but they form weaker acids than sulfated zirconia.

Heteropolyanions are polymeric oxoanions formed by the condensation of more than two different mononuclear oxoanions, as follows:



Heteropolyanions formed from other kinds of polyanion are called isopolyanions:



Acidic elements such as Mo, W, V, Nb and Ta, which are present as oxoanions in aqueous solution, tend to polymerize by dehydration at low pH, forming polyanions and water [83]. In solution, heteropolyanions are present as the unit of the primary structure, being coordinated with solvent molecules and/or protonated. Most heteropolyanions tend to hydrolyze readily at high pH values. Protonation and hydrolysis of the primary structures are the main (structural) concerns in solution catalysis. In the solid state, heteropoly compounds form ionic crystals (sometimes amorphous) consisting of large polyanions, cations, water of crystallization and other molecules. This three-dimensional arrangement is called the 'secondary structure'. It is important to distinguish both the primary and the secondary structures (see Figure 2.3). The oxidative activity of cations can also be controlled since it correlates with the electronegativities of both the counterions (H^+ , Na^+ , Mg^{2+} , Ca^{2+} , etc.) and the heteroatoms (P^{5+} , As^{5+} and Si^{4+}) [1136]. Supported catalysts offer several advantages, among which a high mechanical strength and a developed specific surface are probably the most important for HPCs [1137]. Furthermore, a great cost saving over the expensive molybdenum compounds can be achieved by using supported catalysts.

In the investigation of such systems, FTIR spectroscopy can be a leading method [106]. The spectral manifestations of bulk HPCs have been studied in detail. They adequately characterize such compounds as belonging to different structural types. The IR spectra of bulk HPCs containing 6 and 12 Mo atoms (Mo_6 -HPC and Mo_{12} -HPC) are illustrated in Figure 4.9. In the spectra of Mo_6 -HPCs (spectra 4–6) in the region of $400\text{--}700\text{ cm}^{-1}$ we find strong absorption bands near 650 cm^{-1} (ν_{as}) and 450 cm^{-1} (ν_{s}), assigned to the vibrations of Mo–O–Mo bridging bonds [1138, 1139]. Furthermore, the vibrations of the Mo=O multiple bonds can be seen at $880\text{--}950\text{ cm}^{-1}$. The differences between the spectra of Mo_6 -HPCs in which the central atoms are triply charged (Fe^{3+} or Al^{3+} – Figure 4.9, spectra 5 and 6) or doubly charged (Cu^{2+} , Co^{2+} – Figure 4.9, spectrum 4) ions should be stressed. In the latter case, absorption bands are not found in the region of $400\text{--}700\text{ cm}^{-1}$. According to generally accepted suggestions [106], the IR absorption spectra of such Mo_{12} -HPCs in the $900\text{--}1000\text{ cm}^{-1}$ region correspond to the vibrations of the Mo=O terminal bonds (for example, the 965 cm^{-1} band in the spectra of PMo-HPCs – Figure 4.9, spectrum 2), whereas at $700\text{--}900\text{ cm}^{-1}$ are observed the stretching vibrations of the Mo–O–Mo bonds (absorption band at 780 cm^{-1} in the spectrum of SiMo-HPCs – Figure 4.9, spectrum 1). It has been noted that replacement of one molybdenum cation in the $\text{SiMo}_{12}\text{O}_{40}$ heteropolyanion by a different transition-metal ion (mixed HPCs – Figure 4.9, spectrum 3) shifts the absorption bands between $900\text{--}1000\text{ cm}^{-1}$ towards lower frequencies by $20\text{--}30\text{ cm}^{-1}$. Absorption at $720\text{--}730\text{ cm}^{-1}$, which is not seen in the spectra of the SiMo-HPCs [1137–1139] is also observed in this case. Thus, the IR spectra of Mo_6 -HPCs in the region $400\text{--}700\text{ cm}^{-1}$ differ markedly from those of Mo_{12} -HPCs, whereas the IR spectra of mixed HPCs at $700\text{--}1000\text{ cm}^{-1}$ differ from those of SiMo_{12} -HPCs. Such differences in the IR spectra of HPCs belonging to different types enable the behaviors of the HPCs supported on oxide carriers to be studied by IR spectroscopy.

4.4.1 EFFECTS OF THE SUPPORTS

The IR spectra of catalysts prepared by supporting the HPCs $(\text{NH}_4)_{6-n}\text{M}^{n+}\text{Mo}_6$ ($\text{M} = \text{Cu}^{2+}$, Co^{2+} and Fe^{3+}) on SiO_2 are almost identical (Figure 4.10, spectra 3–5) with the spectra of the

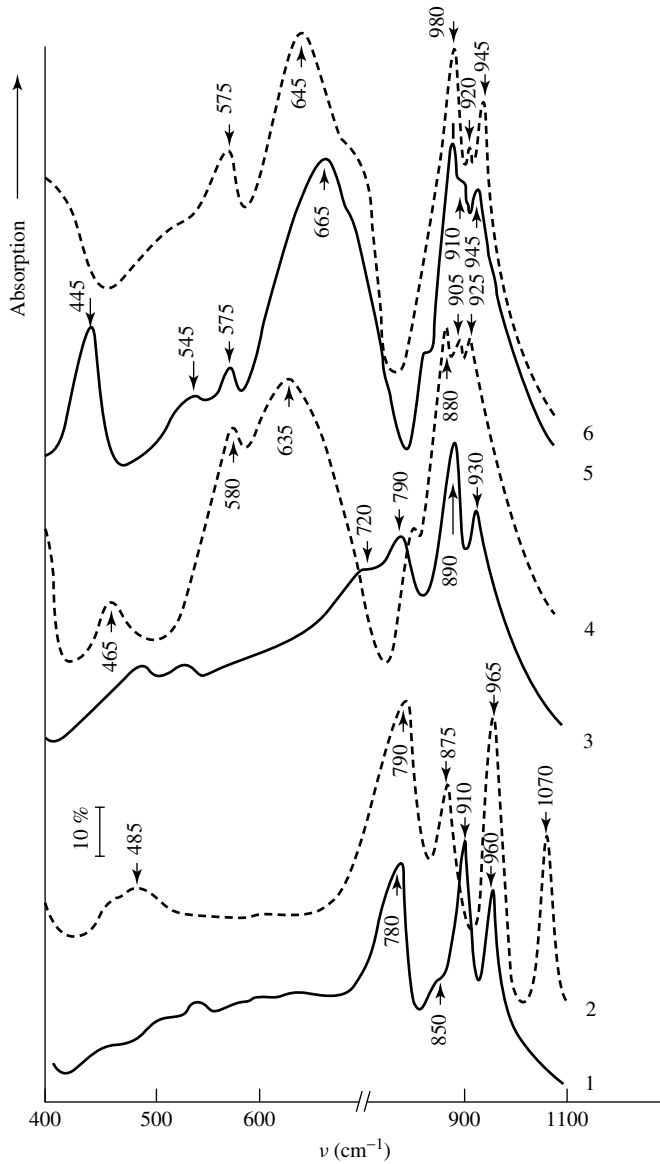


Figure 4.9. IR spectra of bulk HPCs dried at 373 K: (1) $\text{Cu}_2\text{SiMo}_{12}$; (2) $\text{Cu}_{2/3}\text{PMo}_{12}$; (3) $(\text{NH}_4)_6\text{SiMo}_{11}\text{Co}$; (4) $(\text{NH}_4)_4\text{CoMo}_6$; (5) $(\text{NH}_4)_3\text{AlMo}_6$; (6) $(\text{NH}_4)_3\text{AlFeMo}_6$.

Mo_{12} materials. For example, the spectrum of Mo_{11}Co -HPC is analogous to the IR spectrum of the mixed $\text{SiMo}_{11}\text{Co}$ -HPC (Figure 4.9, spectrum 3) [106, 1137]. This suggests that when the Mo_6 -HPCs of copper, cobalt, and iron are supported on SiO_2 , they become rearranged into mixed Si-Mo-M -HPCs, i.e. molybdenum ions are replaced by transition-metal cations. The IR spectra of samples prepared by supporting $(\text{NH}_4)_4\text{CuMo}_6$ (Figure 4.10, spectrum 7) and $(\text{NH}_4)_4\text{CoMo}_6$ (Figure 4.10, spectrum 8) on Al_2O_3 are almost identical, and significantly differ from the spectrum of unsupported $(\text{NH}_4)_4\text{CoMo}_6$ (Figure 4.9, spectrum 4). For example, their $\nu_{\text{Mo}=\text{O}}$ and

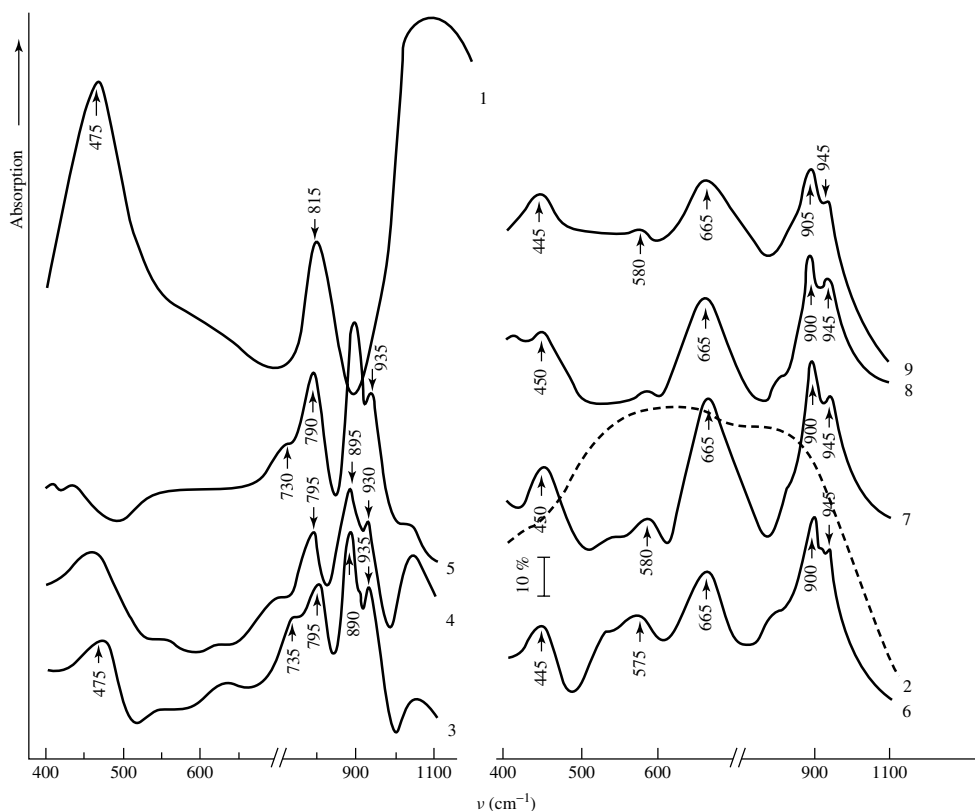
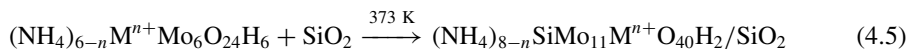


Figure 4.10. IR spectra of the carriers (1) SiO_2 and (2) Al_2O_3 and of the samples prepared by supporting an Mo_6 -HPC on these carriers: (3) $(\text{NH}_4)_4\text{CoMo}_6/\text{SiO}_2$ (16.5 % Mo); (4) $(\text{NH}_4)_4\text{CuMo}_6/\text{SiO}_2$ (16 % Mo); (5) $(\text{NH}_4)_4\text{FeMo}_6/\text{SiO}_2$ (15 % Mo); (6) $(\text{NH}_4)_3\text{CoMo}_6/\text{Al}_2\text{O}_3$ (16.1 % Mo); (7) $(\text{NH}_4)_4\text{CuMo}_6/\text{Al}_2\text{O}_3$ (17.6 % Mo); (8) $(\text{NH}_4)_4\text{CoMo}_6/\text{Al}_2\text{O}_3$ (16 % Mo); (9) $(\text{NH}_4)_4\text{FeMo}_6/\text{Al}_2\text{O}_3$ (16 % Mo).

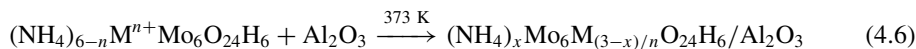
$\nu\text{Mo-O-Mo}$ frequencies are shifted (by 20 and 30 cm^{-1} , respectively) towards longer wavelengths as compared with the absorption bands at 925 and 635 cm^{-1} observed for the bulk compounds. These shifts in the positions of the IR absorption bands can be used to distinguish the Mo_6 -HPCs of doubly charged cations from the HPCs of triply charged cations. Comparison of the spectra of these catalysts (Figure 4.10, spectra 7 and 8) with that of the NH_4 salt of the AlMo -HPA supported on Al_2O_3 (Figure 4.10, spectrum 6) shows marked similarities, with coincident maxima for the most characteristic absorption bands. This suggests that the deposition of the molybdenum heteropoly compounds of Cu and Co on Al_2O_3 causes the formation of Al compounds, involving the Al surface atoms of the support. Under these conditions, the copper and cobalt cations usually continue to be the salt formers. The changes in color of the samples (from blue to green for the copper HPCs and from light brown to lilac for the cobalt HPCs) confirms a change in the state of the Mo_6 -HPCs of copper and cobalt when supported on Al_2O_3 .

An analysis of the IR results for samples prepared by supporting $(\text{NH}_4)_3\text{FeMo}_6$ on Al_2O_3 shows that in this case $\text{FeMo}_6\text{O}_{24}\text{H}_6^{3-}$ is converted to $\text{AlMo}_6\text{O}_{24}\text{H}_6^{3-}$. In the IR spectra of these catalysts in the $\nu\text{Mo-O-Mo}$ region (Figure 4.10, spectrum 9), the characteristic absorption of the Fe-Mo -HPCs at 645 cm^{-1} (Figure 4.9, spectrum 6) is replaced by an absorption band at 665 cm^{-1} , appropriate to the spectrum of the AlMo -HPC (Figure 4.9, spectrum 5); furthermore,

an absorption at 445 cm^{-1} , observed in the spectrum of the Al–Mo–HPC (Figure 4.9, spectrum 5), is also seen. However, at $880\text{--}950\text{ cm}^{-1}$ the behavior of these two compounds is similar. Thus, the M–Mo₆-HPCs (where M = Cu, Co and Fe) are unstable. When supported, they react with the oxide carrier and decompose even in the drying stage. On an SiO₂ surface, the silicon ions of the carrier form mixed SiMo–M-HPCs in which transition-metal cations replace molybdenum ions:



When supported on Al₂O₃, the MMo₆-HPCs (M = Cu, Co and Fe) are converted into AlMo₆-HPCs with the participation of Al atoms from the carrier surface:



These processes are interesting from the standpoint of the chemistry of HPCs, but have not yet been widely discussed in published work. Results so far available suggest that the tendency of surface atoms to form complexes with molybdenum depends on their nature, and in particular that this is more clearly developed for Si and Al atoms than for Cu²⁺, Co²⁺ and Fe³⁺. As a result, the aluminum and silicon atoms on the surface support can displace copper, cobalt and iron from the central ion position in the mixed HPC.

The IR spectra of Si–Mo₁₂- and P–Mo₁₂-HPCs supported on SiO₂ or Al₂O₃ are identical to the spectra of their copper and cobalt salts on the same supports. The form of the spectra is not dependent on the content of the HPC on the support (5–25 wt% Mo). Absorption bands at 970, 875 and 965 cm⁻¹ are also seen in the spectra of bulk P–Mo-HPCs (Figure 4.11, spectrum 2), and in the spectra of P–Mo-HPCs on SiO₂ and Al₂O₃. This indicates that the absorption band at 1065 cm⁻¹ seen in the spectra of bulk P–Mo-HPCs cannot be reliably resolved in the IR spectra of these compounds supported on SiO₂ because of the strong absorption of the support in this region (Figure 4.10, spectrum 1). In the spectra of Si–Mo-HPCs supported on SiO₂ and TiO₂, absorption bands can be seen at 780, 865, 910 and 960 cm⁻¹: these are characteristic of the heteropolyanion (HPA_n)SiMo₁₂O₄₀⁴⁻ (Figure 4.9, spectrum 1).

On the whole, the good agreement between the IR spectra of bulk P–Mo₁₂- and Si–Mo₁₂-HPAs (and their salts) with those of the samples supported on SiO₂ and TiO₂ suggests that the structure of the Mo₁₂-HPA anion is preserved when the material is supported on these carriers [106, 221, 396].

The IR spectra of the samples prepared by deposition of Cu and Co salts of Si–Mo-HPAs on Al₂O₃ (~15 % Mo) are similar. However, the changes have been found for Mo₁₂-HPC supported on Al₂O₃. Figure 4.11 (spectrum 2) shows as an example of the spectrum of Co₂Si–Mo₁₂/Al₂O₃, which markedly differs from the characteristic spectrum of the SiMo₁₂O₄₀⁴⁻ species, and is practically identical to that of the ammonium salt of Al–Mo–HPA supported on Al₂O₃ (Figure 4.10, spectrum 6). These results indicate the decomposition of SiMo₁₂O₄₀⁴⁻ when Cu and Co salts of Si–Mo-HPAs are supported on Al₂O₃ in concentrations of ca. 15 % Mo. Under these conditions, AlMo₆-HPCs are formed on the support. Unlike its salts, the SiMo-HPA itself is preserved when supported on Al₂O₃: the IR spectrum of the SiMo₁₂HPA/Al₂O₃ sample (16.8 % Mo) (Figure 4.11, spectrum 1) is similar to that of the bulk heteropoly acid (Figure 4.9, spectrum 1).

The IR spectra of the catalysts prepared by supporting P–Mo-HPA and its Cu and Co salts on Al₂O₃ (concentration of HPC ~15 % Mo) are similar (Figure 4.11, spectra 3 and 4), and almost indistinguishable from the spectrum of (NH₄)₃AlMo₆/Al₂O₃ (Figure 4.10, spectrum 6). Absorption bands characteristic of the P–Mo₁₂-HPC are not observed in the spectra of these samples.

An investigation of the interactions between a series of HPCs and different supports [106, 1137] convincingly demonstrates that Mo₁₂-HPCs (such as Si–Mo₁₂-HPA), when supported on

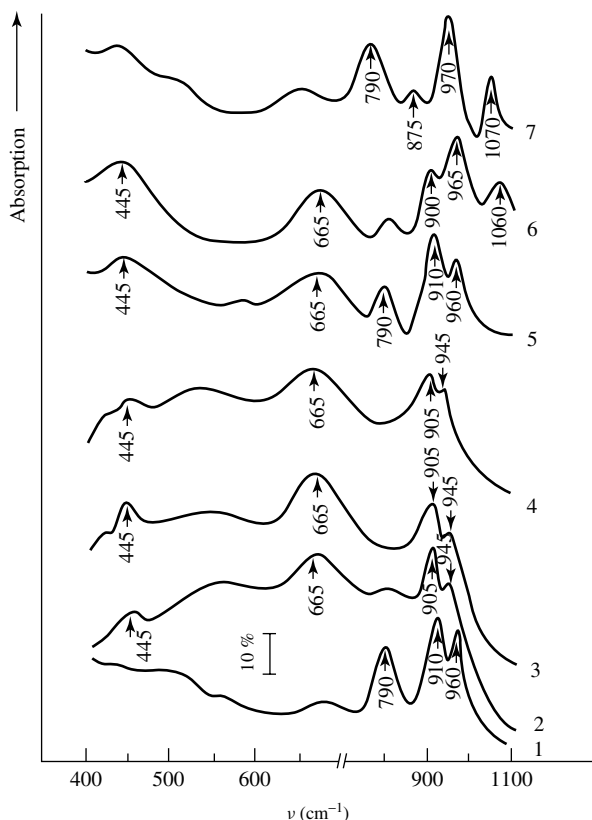


Figure 4.11. IR spectra of samples prepared by supporting an Mo₁₂-HPC on Al₂O₃ and drying at 373 K: (1) H₄SiMo₁₂ (16.8 % Mo); (2) Co₂SiMo₁₂ (15.5 % Mo); (3) Cu_{3/2}SiMo₁₂ (14.6 % Mo); (4) H₃PMo₁₂ (13.3 % Mo); (5) Co₂SiMo₁₂ (27.3 % Mo); (6) Co_{3/2}PMo₁₂ (21.5 % Mo); (7) H₃PMo₁₂ (23.4 % Mo).

alumina, show the conversion to Al–Mo₆-HPC (up to 15 % Mo), through reaction with the aluminum atoms of the Al₂O₃ surface, whereas copper and cobalt cations tend to form salts:



Figure 4.11 also shows the IR spectra of catalysts with large concentrations of Mo₁₂-HPCs on Al₂O₃ (23–27 wt% Mo, spectra 5–7). It can be seen that the increase in the concentration of the P–Mo₁₂-HPA and its salts (or Si–Mo₁₂-HPA salts) on the support produces, in addition to the weak band at 665 cm⁻¹, characteristic of AlMo₆-HPCs, absorption bands at 780, 860, 910 and 960 cm⁻¹, typical of Si–Mo₁₂O₄₀ (Figure 4.11, spectra 6 and 7). This suggests that the main part of the Mo₁₂-HPC is retained unchanged on the Al₂O₃ surface, if the concentration is high. Thus, the Mo₁₂-HPCs are preserved (irrespective of their concentrations on the surfaces) when deposited on SiO₂ or TiO₂, whereas on the surfaces of Al₂O₃ the P–Mo₁₂-HPAs decompose at low concentrations with the formation of Al–Mo₆-HPCs. These results have been explained [1137] in terms of the acid-based properties of the substrates and of the pH stability range of the supported HPC. As reported [999], the substrates can be arranged in the following order of decreasing acidity: SiO₂ > TiO₂ > Al₂O₃. It is known that P–Mo-HPAs are stable over a very narrow range of pH (0.8–1.5), whereas for Si–Mo-HPAs the range is much wider (from 1 to

4) [1140, 1141]. Solutions of the Cu and Co salts of Si–Mo- and P–Mo-HPAs are also acidic: pH \sim 2 for $M_{3/2}PMo_{12}$ and pH \sim for M_2SiMo_{12} [1140]. The Mo_6 -HPCs are stable at higher pH values (2–5.5), and, in particular, the $AlMo_6O_{24}H_{3-6}$ anions are preserved up to pH 5.5.

The stability of the Mo_6 -HPC structures, when supported on SiO_2 and TiO_2 , even at low concentrations of Mo, is probably due to the relatively high acidity of these supports. With a more basic support (such as Al_2O_3) and at low concentrations of the Mo_{12} -HPC on the support, the heteropoly compound decomposes, thereby lowering the acidity of the medium. As has been shown [221], under these conditions the formation of Al– Mo_6 -HPCs, whose anions are stable in less acidic media, is observed. At higher concentrations of the HPC on the Al_2O_3 (up to 20–25 wt% of Mo), the structure of the supported material is retained, probably as a result of the increased acidity of the medium.

The Si–Mo-HPA (unlike the P–Mo analogue – see above) does not decompose when supported on Al_2O_3 , even at low concentrations on the carrier. This is probably due to the wider stability range of this Si–Mo-HPA when compared to the P–Mo-HPA. On the other hand, the salts of Si–Mo-HPAs decompose under these conditions, probably because of the lower acidities of their solutions.

It could therefore have been expected that the creation of a strongly acid medium on the surfaces of those samples with low concentrations of HPCs on the Al_2O_3 would regenerate the Mo_{12} -HPC after this compound had been decomposed with the formation of an Al– Mo_6 -HPC. To test this hypothesis, the samples prepared by supporting P–Mo- and Si–Mo-HPCs on Al_2O_3 (\sim 15 % Mo) were treated with a solution of hydrochloric acid (1:1). In the IR spectra of these samples (Figure 4.12, spectra 2, 4 and 6), the absorption bands at 790, 875, 965 and 1065 cm^{-1} , characteristic of the P– Mo_{12} -HPA (spectra 2 and 4) and 790, 910 and 960 cm^{-1} , characteristic of the Si– Mo_{12} -HPA (spectrum 6), were found in contrast to the spectra of the initial catalysts (spectra 1, 3 and 5), i.e. the increased acidity of the medium induces the reverse conversion of the Al– Mo_6 -HPC into Si– Mo_{12} - and P– Mo_{12} -HPCs.

Thus, a study of the interactions of Mo_6 - and Mo_{12} -HPCs with oxide supports leads to the following conclusions. The M– Mo_6 heteropoly compounds containing copper, cobalt or iron as the central metal atom are unstable. When supported, they interact with the carrier, and mixed Si–Mo–M heteropoly compounds are formed on the SiO_2 surface as a result. On a γ - Al_2O_3 surface the Mo_6 -HPCs of the transition metals decompose with the formation of the Al– Mo_6 -HPA salts. The phase compositions of catalysts prepared by depositing Mo_{12} -HPCs on various supports depend on the acid–base properties of the support and on the pH stability range of the supported HPC, whereas the structures of the P– Mo_{12} - and Si– Mo_{12} -HPCs are retained when the compounds are supported on SiO_2 and TiO_2 , irrespective of their concentrations on the carrier. Deposition on Al_2O_3 causes a decomposition of the compounds (when present at low concentrations) and the formation of Al– Mo_6 -HPCs. Thus, the compositions of the compounds on the surfaces of basic carriers can be controlled either by variation in the concentrations of the supported heteropoly compounds or by treating the support with solutions of mineral acids.

4.4.2 ACIDIC PROPERTIES OF MOLYBDENUM HETEROPOLY COMPOUNDS

The number of publications dealing with the acidic properties of supported HPCs is not large. The acidic properties of P–Mo-HPAs supported on various oxide carriers (SiO_2 , TiO_2 and Al_2O_3), and also of Si–Mo-HPAs and the salts of P–Mo-HPAs on SiO_2 have been described [106, 747]. The adsorption of the basic-molecules (pyridine or ammonia) on these HPAs was studied by IR spectroscopy. It was found that the IR spectra of pyridine adsorbed on any of the HPCs in the 1300–1650 cm^{-1} region are similar. The presence of the absorption band at 1540 cm^{-1} , assigned to vibrations of the pyridinium ion, was interpreted as evidence for the presence of Brønsted acid centers (BACs) protonating the pyridine molecule in all of the catalysts under discussion. The

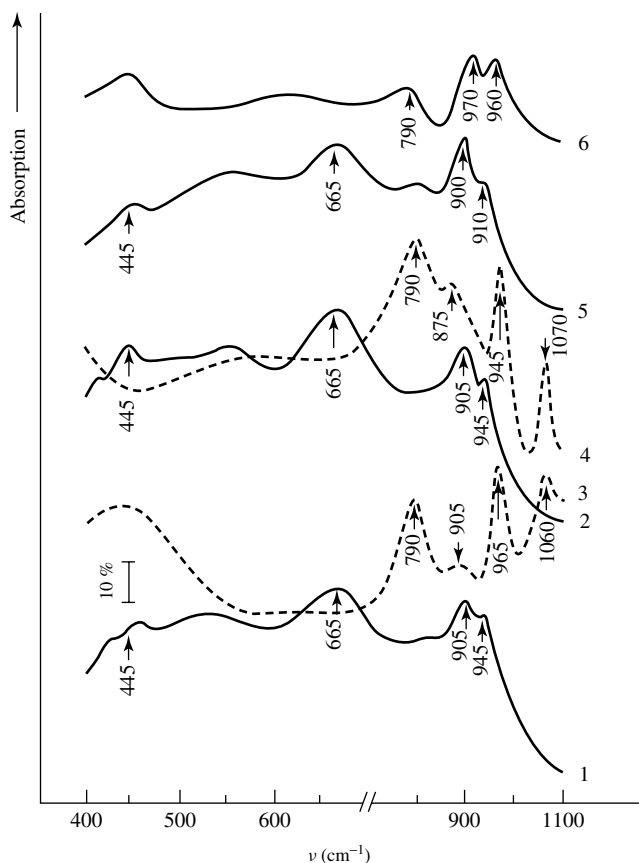


Figure 4.12. IR spectra of samples prepared by supporting Mo_{12} -HPCs on Al_2O_3 : (1, 2) $\text{H}_3\text{PMo}_{12}$ (13.3 % Mo); (3, 4) $\text{Co}_{3/2}\text{PMo}_{12}$ (14.1 % Mo); (5, 6) $\text{Cu}_2\text{SiMo}_{12}$ (16.6 % Mo). Spectra 2, 4, and 6 were recorded after treating the samples with a solution of HCl.

absorption band found at 1450 cm^{-1} denotes the formation of pyridine complexes with aprotic centers of the catalyst.

The dependence of the concentration of proton centers (in $\mu\text{mol PyH}^+ \text{ m}^{-2}$) on the content of P-Mo- and Si-Mo-HPAs on SiO_2 and of P-Mo-HPAs on Al_2O_3 has also been studied. All of these dependences are of the same type, suggesting that in the region of low HPA concentrations on the carriers (7–15 wt% of Mo) the amount of BACs increases as a proportion of the HPA concentration. At still higher concentrations of P-Mo- and Si-Mo-HPAs on the support (up to 20–28 wt% Mo), the concentration of mobile protons (in $\mu\text{mol PyH}^+ \text{ m}^{-2}$) stays unchanged, but the specific surface decreases.

Effect of concentration

The increase in the concentration of BACs with increasing HPA content (in the region of 7–15 wt% Mo) was attributed to the increased coverage of the carrier surface by the HPA molecules. A further increase in the content of HPAs causes agglomeration of the molecules, which lowers the specific surface area of the samples, while the concentration of the proton centers per m^2 stays constant.

Since, according to Okuhara *et al.* [1142], the acidities measured for bulk HPAs are the bulk values, the results of Goncharova *et al.* [106, 747] indicate that in the case of supported HPAs the properties of the surfaces play the main role. The strengths of the proton centres (expressed as proton affinity (*PA*)) [418] are characterized by the frequency of the stretching vibrations band of the pyridinium ion, which depends on the basic properties of the acidic residue. The strengths of the proton acid centers were unaffected by varying the contents of P–Mo and Si–Mo-HPAs on SiO₂ or of P–Mo-HPA on Al₂O₃: the parameter νNH_{cg} (defined as the position of the center of gravity of the νNH band) is 2900 cm⁻¹ for all of the samples of P–Mo- and Si–Mo-HPAs on SiO₂, and 2600 cm⁻¹ for the HPAs supported on Al₂O₃.

The acidic properties of the different HPCs were compared at high concentrations of these compounds on the carrier. When comparing the acidic properties of the HPAs with P and Si central atoms supported on SiO₂ it was shown that the concentrations of the BACs is 1.4 times greater in the case of H₃PMo₁₂/SiO₂ than in H₄SiMo₁₂/SiO₂ over the whole range of concentrations of the HPAs on the carrier. The strength of the proton centres (as defined by Paukshtis and Yurchenko [418]) is the same for P–Mo- and Si–Mo-HPAs supported on SiO₂: $\nu\text{NH}_{\text{cg}} = 2900 \text{ cm}^{-1}$.

Effect of the type of support

It was reported [1140] that the concentrations of mobile protons in P–Mo-HPAs supported on SiO₂ are much higher than in the same compounds on Al₂O₃ over a wide range of concentrations of the HPAs. The concentrations of the BACs in P–Mo-HPAs supported on TiO₂ (13.7 % Mo) is 0.4 μmol^{-2} , i.e. three or four times lower than the concentrations of BACs in P–Mo-HPAs on SiO₂ (13.6 % Mo), for which this quantity is 1.5 μmol^{-2} (for samples conditioned at the same temperature of 423 K). By comparing the νNH_{c} values obtained for P–Mo-HPA samples on different carriers, it was shown that the νNH_{cg} bands for HPA/TiO₂ and HPA/Al₂O₃ are strongly shifted towards lower frequencies. The calculated νNH_{cg} values were about 2600 cm⁻¹, as compared with 2900 cm⁻¹ for HPA/SiO₂. Therefore, supporting the P–Mo-HPAs on TiO₂ and on Al₂O₃ lowers the strengths of the proton centres.

Qualitative results on the change in the number of BACs caused by an increase in the conditioning temperatures of Si–Mo-HPAs and P–Mo-HPAs (and its salts) supported on SiO₂ were obtained by studying the adsorption of pyridine on these samples. The concentration of mobile protons on all of the samples decreases when the pre-treatment temperature increases. This effect becomes most marked following the increase in temperature from 523 to 723 K. The strengths of the proton centres (the shift in νNH_{cg}) was unaffected by increasing the conditioning temperature of the HPC/SiO₂.

Effect of replacing protons in the HPA by metal cations

This effect was studied [106, 747] for P–Mo-HPAs and their sodium and copper salts supported on SiO₂. Replacing some of the protons in P–Mo-HPA/SiO₂ by Na⁺ produces a large change in the proton-donor capacities of the acid centres (as shown by changes in the contour of νNH_{cg}). Upon the introduction of sodium cations, the νNH_{cg} band is shifted towards lower frequencies (the calculated νNH_{cg} is 2800 cm⁻¹ for the salts and 2900 cm⁻¹ for the acids). Similar effects were pointed out in the study of the decrease in the desorption temperature of pyridine from the Na⁺ salts of P–W-HPAs [1142] as compared with its desorption from the acid itself. For the Cu⁺ salts of P–Mo-HPAs this decrease in the strength of the proton centres is not observed: νNH_{cg} was the same for H₃PMo₁₂/SiO₂ and Cu_{3/2}PMo₁₂/SiO₂.

The change in the concentrations of mobile protons caused by the replacement of H⁺ by metal cations in P–Mo-HPAs showed [106, 747] that for conditioning temperatures between 423 and

723K the number of BACs (in $\mu\text{mol PyH}^+ \text{m}^{-2}$) decreases monotonically as the concentration of sodium or copper in the HPC is increased. However, even in the fully substituted salts, $\text{Na}_3\text{PMo}_{12}/\text{SiO}_2$ and $\text{Cu}_{3/2}\text{PMo}_{12}/\text{SiO}_2$, a small number of mobile protons is still detectable.

Lewis acid centres

As reported by Misono *et al.* [1143], bulk HPAs and their salts can be classified as protic acids. The concentration of Lewis acid centres (LACs) in these systems is negligibly small (the amplitude of the absorption band due to coordinated pyridine is small in comparison with the absorption band of PyH^+).

4.5 Thermal stabilities of molybdenum compounds, decomposition mechanisms and the role of modifiers

We shall now dwell on two problems directly related to the problems discussed above: (i) the changes induced in the HPCs by changes in temperature, and (ii) the influence of the reaction medium on these changes.

4.5.1 BULK AND SUPPORTED HETEROPOLY ACIDS

We shall discuss these aspects in terms of the most widely known HPAs, i.e. molybdophosphoric and molybdosilicic. As has been stated above, the IR spectra of Mo_{12} -HPA (the Keggin structure) are typical (Table 4.2), and those of P-Mo-HPAs between 700 and 1100 cm^{-1} are characterized by strong absorption bands at 805, 875, 965 and 1065 cm^{-1} (Figure 4.13). Heating of the HPA for 2 h in a stream of air at 673 K does not change the contour of the spectrum, showing that the structure of the Keggin anions is retained. After thermal conditioning of the HPA at 723 K, the intensities of the characteristic absorption bands of the HPA rapidly decreases and the spectrum is changed: absorption bands appear at 445 cm^{-1} and in the 700–900 cm^{-1} range, with the maximum at 870 cm^{-1} . Subsequent treatment of the sample with water regenerates the HPA (Figure 4.13) [106].

According to XRD results, the sample heated at 723 K is a mixture of two phases: MoO_3 and a phase with a structure similar to that of Mo_4O_{11} . The MoO_3 phase persists after the treatment with water, with changes in the relative intensities of the main diffraction lines. The phase with the Mo_4O_{11} structure disappears after the treatment with water [106, 1144]. According to ESR results, the state of the molybdenum ions is not markedly affected by heating the sample at 723 K: the molybdenum ions have a distorted octahedral surrounding of oxygen atoms, similar to their surroundings in the HPA. In Mo_4O_{11} , the majority of the molybdenum ions also have octahedral

Table 4.2. Absorption bands ($\nu(\text{cm}^{-1})$) in the IR spectra (700–1100 cm^{-1}) of Mo_{12} -HPCs (the Keggin structure).

Si-Mo-HPA	P-Mo-HPA	Ti-Mo-HPA (NH_4 salt)
999	1074	1072
960	968	970
909	911	908
859	869	868
782	795	790

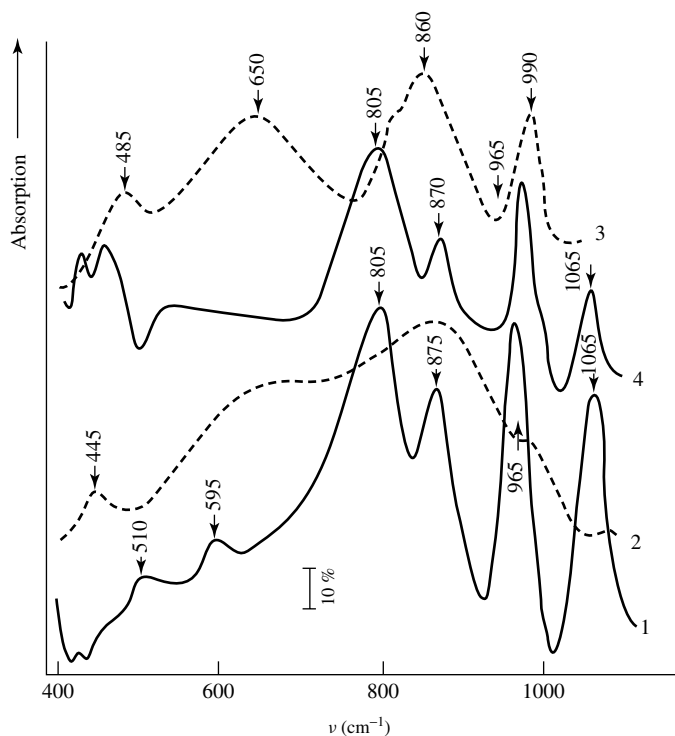


Figure 4.13. IR spectra of a P-Mo-HPA heated at different temperatures: (1) 673; (2) 723; (3) 773 K (spectrum 4 relates to a hydrated P-Mo-HPA heated at 723 K).

surroundings. In the IR spectrum of the sample heated at 773 K the absorption bands at 820, 865 and 1000 cm^{-1} , characteristic of MoO_3 , were found. After treating the sample with water the phase of P-Mo-HPA is formed, and the MoO_3 phase cannot be detected by IR spectroscopy (it can only be identified by XRD). By comparing the XRD and IR spectroscopic results, the following conclusions can be reached. After heat treatment of the P-Mo-HPA at temperatures below 623 K, the structure of the Keggin anion is retained, whereas heating at 773 K and above causes breakdown of the anion structure and the formation of oxides. In the intermediate temperature region, the rearrangement of the Keggin anion is observed with the formation of a heteropoly molybdate (poly-oxide) with a structure similar to that of Mo_4O_{11} . It should be stressed that the similarity between Mo_4O_{11} and the poly-oxide (which has been called a P-Mo-anhydride) is due to their very close structural types, while their chemical natures are quite different. During the hydrolysis, the heteropoly molybdate is rearranged into an anion with the Keggin structure, i.e. the process is reversed. According to these results, the process induced by heat treatment of the P-Mo-HPA can be described by the following scheme:



It follows from these results that in the region of 723 K the treatment with water produces a reversible rearrangement of the heteropoly anion into a phosphorus-molybdenum anhydride with a structure of the Mo_4O_{11} type. At 773 K, this P-Mo-anhydride (poly-oxide) decomposes with the formation of MoO_3 . The dissociation of the heteropoly anion, via an intermediate compound having an Mo_4O_{11} structure, has been reported [1145] for several HPAs and their salts. It is

interesting to note that the addition of water to the anhydride produces the HPA, and hence it follows that the poly-oxide is a dehydration product of the HPA, and also that the coordination of the molybdenum ion is not significantly changed in the transition from the heteropoly anion to the poly-oxide: the distorted octahedral coordination is retained. As a result, the reducibility of the molybdenum ions is the same in the HPA and in the poly-oxide.

The reduction temperatures of the Mo^{6+} ions to Mo^{5+} by hydrogen (with the corresponding temperatures for the reduction by atomic hydrogen shown in square brackets) are listed below for some HPAs, for the phosphorus–molybdenum polyoxide and (for comparison) for MoO_3 :

System	T (K)
Si–Mo-HPA/ SiO_2	373 [300]
Si–Mo-HPA	373 [300]
P–Mo-HPA	373–423
MoO_3	623

As can be seen, the poly-compounds are reduced at the same temperatures, which are much lower than the reduction temperature of MoO_3 .

Similar results have also been reported for supported systems [1144]. A study by IR spectroscopy and XRD of the change in the phase composition as a function of the heating temperature of the P–Mo-HPA supported on SiO_2 showed that after being conditioned at 673 K the sample consists of a mixture of phases: the HPA (the principal phase) and the anhydride. Increasing the heating temperature to 723 K increases the content of heteropolymolybdate in the sample, and also produces a phase of molybdenum oxide, MoO_3 . Therefore, the rearrangement of the Keggin anion continues at 723 K. As in the case of the bulk HPA, the heteropolymolybdate phase disappears during the subsequent hydrolysis, and the MoO_3 phase undergoes changes probably due to its ‘re-structuralization’ by the action of the water. After heat treatment at 773 K, the structure of the anion is completely broken down (according to the XRD results) and molybdenum oxide is formed: in other words (on the whole), the same stages in the thermal dehydration of the P–Mo-HPA supported on SiO_2 occur as in the dehydration of the HPA.

An analysis of the changes in the spectra of the supported Si–Mo-HPA during the heat treatment shows that above 673 K (or 573 K for the HPA) the compound dissociates with the formation of MoO_3 , as indicated by the appearance of the new absorption bands at 860 cm^{-1} ($\nu\text{Mo–O–Mo}$) and 990 cm^{-1} ($\nu\text{Mo=O}$) which are the most characteristic lines in the MoO_3 spectrum, whereas the appearance of absorption bands in the region of 1100 cm^{-1} denotes the presence of SiO_2 (see Figure 3.42 earlier) [396]. The complete decomposition of the supported Si–Mo-HPA with formation of MoO_3 and SiO_2 is observed at 773 K: in this case, the IR spectrum is a superposition of the spectra of the individual MoO_3 and SiO_2 . Thus, in spite of the fact that the deposition of the Si–Mo-HPA increases its thermal stability in comparison with the bulk HPA, the nature of the transformations during the thermal conditioning is unchanged.

It should be noted that it has not yet been possible in this case to identify the intermediate compound (anhydride) from the IR spectra (the difficulty being even greater for the Si–Mo oxide catalysts) because of the low intensities of the characteristic absorption bands [396]. However, as in the case discussed above for the P–Mo-HPA, the spectral changes caused by hydration are reversible up to a dehydration temperature of 773 K in the case of Si–Mo oxide systems.

4.5.2 MODIFIED MOLYBDATES

As has already been pointed out, modifiers are often added to complex catalysts containing molybdenum: for example, phosphorus (in the form of orthophosphoric acid [1146]). The modifier

alters the catalytic properties of the system. However, the role of the phosphorus is still unclear in most cases. There are reports of the formation of surface phases containing phosphorus and molybdenum during the modification by phosphorus additions which can be attributed to chemical changes in the formation of the P–Mo-HPA and its salts, since the addition of orthophosphoric acid provides an element capable of acting as a hetero atom as well as a lowering the pH of the medium.

The possibility of the formation of the P–Mo-HPA due to the modification of calcium molybdate with orthophosphoric acid has been investigated [1144]. The absorption bands at 960 and 1065 cm^{-1} , characteristic of the Mo=O vibrations and of the vibrations of the central PO_4 tetrahedron in the HPA anion, respectively, are clearly seen in the spectrum of CaMoO_4 modified by orthophosphoric acid (Figure 4.14, spectrum 4). The spectrum of the supported HPA (with compensation for the absorption of the carrier) is indistinguishable from that of the bulk HPA (Figure 4.14, spectra 1 and 2), i.e. these results show that the P–Mo-HPA on the surface of CaMoO_4 modified by orthophosphoric acid can be reliably identified from the IR spectra.

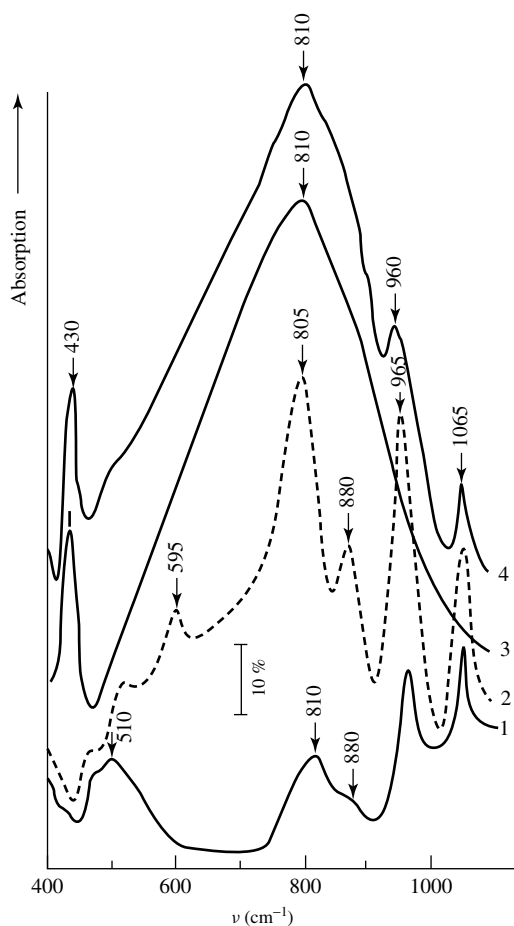


Figure 4.14. IR spectra of (1) a P–Mo-HPA supported on CaMoO_4 , (2) bulk P–Mo-HPA, (3) CaMoO_4 , and (4) CaMoO_4 modified by H_3PO_4 . Spectrum (1) has been taken against the CoMoO_4 absorption.

The introduction of a ‘super-stoichiometric’ amount of molybdenum into CaMoO_4 by treating it with a solution of ammonium paramolybdate and heating the product at 773 K leads to the formation of an MoO_3 phase (Figure 4.15). In this case, in addition to an absorption band at 430 cm^{-1} and a strong absorption in the $600\text{--}860\text{ cm}^{-1}$ region that are characteristic of the molybdate, absorption bands at 475 , 610 , 820 , 860 and 995 cm^{-1} , characterizing the molybdenum oxide (Figure 4.15, spectrum 2), are observed. By using the compensation procedure, a spectrum of CaMoO_4 which is exactly similar to the initial spectrum has been generated, thus confirming that the symmetry of the molybdenum in CaMoO_4 is not affected by the addition of a super-stoichiometric amount of MoO_3 , i.e. indicating the formation of an individual phase of MoO_3 . A similar effect has been observed in the case of magnesium molybdate containing super-stoichiometric MoO_3 [1147].

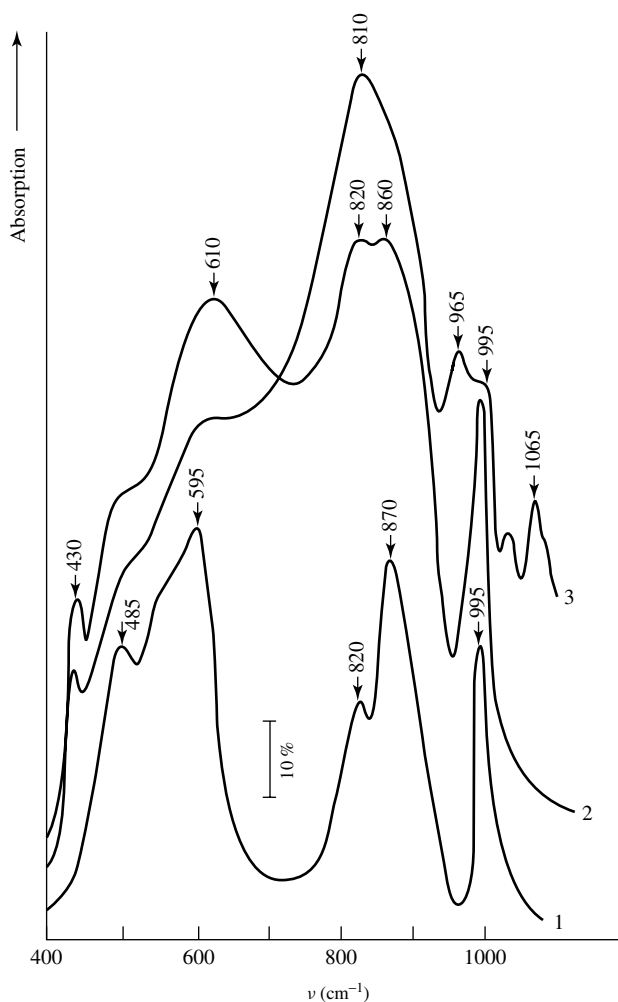


Figure 4.15. IR spectra of (1) MoO_3 , and (2) CaMoO_4 modified by 10 wt% of molybdenum; (3) represents the spectrum of the latter system after the addition of phosphorus.

Treating a $\text{CaMoO}_4\text{-MoO}_3$ catalyst with a solution of orthophosphoric acid produces substantial changes in the IR spectrum. The MoO_3 absorption band becomes weaker, and new absorption bands appear at 965 and 1065 cm^{-1} (Figure 4.15, spectrum 3). As was pointed out above, these bands are characteristic of the P-Mo-HPA supported on molybdate. Heating the catalyst at 623 K does not change the shape of the spectrum, thus confirming that the HPA is stable at this temperature. The absorption bands of the HPA are completely suppressed (i.e. the anion structure is broken down) only after heat treatment of the catalysts at 673 K.

Thus, the modification of calcium molybdate with a super-stoichiometric molybdenum content by treatment with phosphoric acid produces a P-Mo heteropolyacid stable up to 623 K.

4.6 Cationic modification

Cationic modification of supports is a widely used method of preparation of heterogeneous systems with fixed properties. Supported cations of Cu, Ni, Fe, Co, Pd etc., zeolite systems with different cations added to these systems in different ways are widely discussed in the literature and in this book (Chapter 3). The Mo-, V- and Cr-containing systems are the most interesting because of the wide variety in their coordination and valence states. The cations of these metals at a significant concentration of active component, are inclined to form complex oxide species similar to poly- and heteropoly anions analyzed above. So, it would be very reasonable to describe these species here. However, since the properties of such systems are predominantly determined by an active component (the nature of the supported cation, plus the structures and properties of the simple compounds that are formed), these questions have been addressed in Chapter 3, where supported oxide compounds of several elements and their properties are discussed and analyzed.

5 FORMATION OF SURFACE COMPLEXES OF ORGANIC MOLECULES

The elucidation of the type of interaction between molecules and oxide surfaces is an important step in studying the mechanism of catalytic transformations of the former. The widely used adsorption and thermal desorption techniques give information only on a limited scale. Their major disadvantage is that they provide only averaged data on adsorption rates, surface coverage and heats of adsorption, whereas adsorption of molecules on the oxide surfaces is known to involve the formation of several species.

As was shown by Davydov [30], in the first spectral studies of adsorption the identification of the surface compounds was performed unreliably, even for the simplest organic molecules like alkenes. The reliable assignment of absorption bands to surface compounds or complex molecules adsorbed on the oxide surface is difficult because the adsorption of the majority of organic molecules on numerous oxide systems results in the formation of a variety of structures with complex spectra. In such cases, the spectra of surface compounds cannot be interpreted by direct comparison with those of individual compounds, as is routinely done in the spectroscopy of physically adsorbed molecules. The appropriate analogies may be unavailable and, more importantly, the spectra of different complexes may overlap. To make the identification of surface compounds more reliable, different procedures have been used, including stepwise desorption which allows the separation of absorption bands in accordance with their behavior (the bands belonging to a single structure are assumed to undergo the same changes), the adsorption and spectroscopy of substances forming surface compounds similar to those likely to be formed on adsorption of the molecules, and the separation of surface compounds according to the strength of their bonding to the surface. As far as the last procedure is concerned, the combination of spectroscopy with thermal desorption has proved to be the most convenient (see, for example, for hydrocarbons [30, 1148–1150]), since if there are several states of adsorption with significantly different binding energies, one can substantially simplify the spectra and, in the ideal case, resolve the spectra of individual surface species by studying them during the course of desorption. Extremely promising is the combination of thermal desorption and chromatography or mass spectrometry of desorption products, which makes possible the resolution of bands due to reversibly adsorbed complex molecules (for example, for hydrocarbons, without C–C bond cleavage) and those due to irreversibly adsorbed species (with or without C–C bond cleavage).

The application of molecular spectroscopy to the analysis of surface compounds and complex mixtures is similar since the main problem in the former case is to identify the type of compound formed and to reveal changes in certain parts of the molecule. Thus, molecular spectroscopy

is used as an analytical (identification method only) rather than a structural method and indicates the presence of a surface compound of a certain type. This is primarily due to limitations imposed by the use of vibrational spectroscopy in surface chemistry, namely the lack of a full spectrum of a surface compound due to the overlapping of adsorbent and adsorbate spectra, to low concentrations of surface compounds, the presence of several absorption bands and the overlapping of the bands associated with different structures with the possibility of multi-site binding, etc.

The above discussion shows that there is a need for criteria for the spectral identification of surface compounds in order to gain reliable information about the type of compounds formed on adsorption. Owing to the lack of such criteria, no unified interpretation of the spectra of adsorbed molecules has become available so far [30, 89]. Each case has to be considered on its merits.

The main factors governing molecule chemisorption and determining the types of surface compounds formed, as was shown in Chapters 2 and 3, are the nature and properties of the surface sites. Although the interaction of different molecules (for example, alkenes) and oxides has been intensively studied by molecular spectroscopy, such studies have been mainly aimed at revealing the nature of the forms of adsorption, whereas the problem of complex molecule stabilization sites and their effect on the type of adsorption remains unresolved in many cases. It is obvious, however, that information about the nature of surface sites which provide the formation of different complexes is almost as important as information about the modes of adsorption. On the one hand, data on the nature of stabilization sites of surface compounds can improve the reliability of interpretation of spectra; in such cases, spectral changes may be correlated with the nature of the bond between a molecule fragment and a surface site. On the other hand, an understanding of the nature of the sites responsible for complex molecules activation, and of their transformation during adsorption, opens up the possibility of intentionally changing the chemical properties of these sites and also the properties of adsorbed fragments.

The diversity of surface compounds formed during adsorption is due to the presence of several types of active sites on the surface, their inhomogeneity, etc. However, each surface compound must have individual spectral features, which could permit its characterization. The identification of these features is the main objective of this chapter, together with associated vibrational modes in organic molecules and their fragments, and with their changes during adsorption.

Of paramount importance for the investigation of the spectral features of individual types of surface compounds, and the elaboration of criteria for the identification of these, is the choice of experimental conditions so that adsorption of one, or at most two, types can take place, that a limited number of reactions can proceed on the surface, and that the nature of the surface sites is known. Therefore, when analyzing the spectral properties of adsorption complexes we shall consider cases in which the reversible or irreversible adsorption of molecules has been observed by the thermal desorption and chromatographic methods.

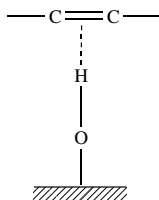
5.1 Complexation of alkenes

The adsorption of alkenes on oxide surfaces has been widely studied by means of spectroscopic methods beginning from the very first applications [18, 19]. However, most of those results published before 1980 are not fully correct. The situation has substantially changed during the last 20 years when many articles about such problems have been published with more success. We shall examine these results by using some previously formulated spectral criteria for identifying olefinic surface complexes [30, 1151].

5.1.1 COMPLEXATION WITH OH GROUPS

The interaction between alkenes, which are weak bases, and oxide surfaces depends considerably on the acid–base properties of the surface hydroxyls. Low-temperature adsorption experiments of

ethylene and other olefins over surfaces with Brønsted sites (active OH groups) provide evidence for the hydrogen-bonding interaction of these hydroxy groups with the π -electron cloud of the olefins. This is shown by the perturbation of the OH stretching vibrations of such surface groups, which are shifted down in frequency and strongly broadened upon olefin adsorption. Such an interaction has been established by many different studies. The compounds mentioned above are usually weakly bound, and spectral changes in the absorbates themselves are small. The availability of acidic hydroxyls on oxide surfaces (as tested, for instance, with ammonia) can nevertheless give rise to stable hydrogen-bonded complexes with the involvement of the alkene double bond [30, 1151–1156]:



Scheme 5.1

In this instance, the downward shifts of the OH group frequencies are 50–400 cm^{-1} . The magnitude of the shift of the OH stretching vibration depends on the acidity of the OH group. Such interactions occur with active hydroxyl groups, such as those of amorphous silica and HY zeolite [30, 1155–1157]. The C=C stretching mode of ethene, for example, is easily detectable as a sharp but weak band, made ‘infrared-active’ due to the loss of symmetry of the ethene molecule; this shifts down from 1625 cm^{-1} (the Raman gas-phase value) to 1618 cm^{-1} on silica and to 1612 cm^{-1} on HY zeolite. By using those catalysts which mostly have one type of surface center [30, 1151, 1153–1156, 1158], many data on H-bonded ethene complexes have been obtained. The interaction is able to shift the OH absorption from not less than 390 cm^{-1} on HY zeolite (strong Brønsted acidic surface) down to ca. 60 cm^{-1} for weak Brønsted acidic hydroxyl groups. Some relevant band shifts are given in Table 5.1. During the FTIR spectroscopic study of the hydrogen-bonded precursor of ‘growing’ oligomers, formed as a result of the ethene or propene interaction with HY, HM and H-ZSM-5 zeolites (see Section 5.2.2), ethene–hydroxyl and propene–hydroxyl π -complexes were evaluated from the downward shifts of both the νOH and $\nu\text{C}=\text{C}$ frequencies. For both alkenes, hydrogen-bonded precursor protonation was the rate-determining step [30, 1151].

A substantial modification of the electronic state of the alkene molecule upon interaction with Brønsted OH groups can also be deduced from the analysis of the out-of-plane (opl) and in-plane (inpl) olefinic bending modes and from integrated intensities of the C=C stretching (str) modes (Table 5.2) [1156, 1159–1161]. The ratio of the parameters ($A_{\text{inpl}}/A_{\text{str}}$) shows that they vary in a parallel way, and tends to increase upon adsorption. This indicates that the H-bonding interaction with Brønsted sites enhances strongly the charge on hydrogen due to the electron withdrawal from the molecule to the proton center.

To identify diagnostic features for distinguishing H-bond (‘physisorbed’, according to Busca’s opinion [1156]) and chemisorbed hydrocarbon species, the adsorption of propylene has been monitored on hydroxylated silica, alumina and silica–alumina. The lowering of the C=C stretching mode of the order of 10 cm^{-1} , depending on the Brønsted acidity of the adsorbent (from 1650 cm^{-1} in the gas to 1641 cm^{-1} on SiO_2 and 1637 cm^{-1} on $\text{SiO}_2\text{-Al}_2\text{O}_3$) and a strong lowering of the intensities of all C–H stretching absorptions (3100–2800 cm^{-1}) seem to

Table 5.1. Observed wavenumbers (cm^{-1}) and assignments for ethylene adsorbed on metal oxides [1156]. Reprinted from *J. Mol. Struct.*, **267**, Busca, G., Lorenzelli, V., Ramis, G., Saussey, J. and Lavalley, J. C., 'FTIR spectra of ethylene molecularly adsorbed on metal oxides', 315–329, Copyright (1992), with permission from Elsevier Science.

Vibration modes		Gas ^a		Solids ^{a,b}								
		IR	R	IR (75 K)	R (79 K)	Adsorbed on						
						SiO ₂ ^c	HY ^c	MgO	CaO	NiO	Fe ₂ O ₃	ZnO
ν_9	$\nu_{\text{as}}\text{CH}_2$	3105	–	3093, 3088	–	3097	3093	3095	3095	3090	3080	3057
ν_5	$\nu_{\text{as}}\text{CH}_2$	–	3083	–	3068, 3066	3069	3073	3063	3068	3065	3065	–
$\nu_2 + \nu_{12}$ combined		3067	–	3066, 3049								
ν_1	$\nu_{\text{s}}\text{CH}_2$	–	3021	–	3006, 2995	3010	3005	2992	2990	3000	2997	2984
ν_{11}	$\nu_{\text{s}}\text{CH}_2$	2989	–	2973, 2966	–	2978	2974	2978	2978	2972	2975	2060
$\nu_2 + \nu_{12}$ $2\nu\text{CH}_2$		1888	–	1897	–	1922	1940	1898	1898	1908	1960	1960
ν_2	$\nu\text{C}=\text{C}$	–	1625	–	1622, 1615	1618	1612	–	–	–	1618	1599
ν_{12}	δCH_2	1443	–	1440, 1436	–	1441	1442	1439	1442	1448	1439	1440
ν_3	δCH_2	–	1343	–	1348, 1328	1340	1338	1338	1342	1338	1340	1340
ν_7	ωCH_2	949	–	951, 942	–							
ν_8	ωCH_2	–	943	–	951, 942	m	m	956	960	968	990	1002
ν_{10}	ρCH_2	826	–	822, 820	–	m	m	–	–	–	–	–

^aIR, infrared; R, Raman.

^bSplittings are due to solid-state effects.

^cm, masked.

Table 5.2. Comparison of the total intensities of the CH modes for gaseous and chemisorbed ethene [1156]. Reprinted from *J. Mol. Struct.*, **267**, Busca, G., Lorenzelli, V., Ramis, G., Saussey, J. and Lavalley, J. C., 'FTIR spectra of ethylene molecularly adsorbed on metal oxides', 315–329, Copyright (1992), with permission from Elsevier Science.

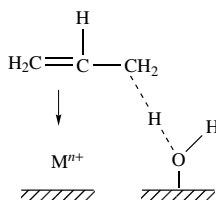
Vibration modes ^a	Gas	Adsorbed on							
		SiO ₂	HY	CaO	NiO	Fe ₂ O ₃	ZnO	TiO ₂	ZrO ₂
CH_{str}	1	1	1	1	1	1	1	1	1
CH_{inpl}	0.26	0.72	0.98	0.25	0.53	0.79	0.29	1.3	2.0
CH_{opl}	2.10	–	–	1.42	3.51	6.47	6.07	–	11.0
CH_{def}	2.36	–	–	1.67	4.04	7.26	6.36	–	13.0
$A_{\text{def}}/A_{\text{str}}$	2.36	–	–	1.67	4.04	7.26	6.36	–	13.0
$A_{\text{inpl}}/A_{\text{opl}}$	0.12	–	–	0.18	0.15	0.12	0.05	–	0.18
$A_{\text{inpl}}/A_{\text{str}}$	0.26	0.72	0.98	0.25	0.53	0.79	0.29	1.3	2.0

^astr, stretching; inpl, in-plane bending; opl, out-of-plane bending; def, total deformation modes.

be characteristic of propene interacting with surface OHs through π -electrons, while retaining approximate molecular planarity. As has been reported [1087, 1151], no physisorbed form has been detected on Al_2O_3 . The magnitude of the shift increases with the basicity of the alkene adsorbed. The $\nu\text{C}=\text{C}$ shift correlates with the parallel shift in νOH . The energy of the H-bond formed may be estimated by using equations suggested in Kiselev and Lygin [19].

When butadiene forms a H-bond on SiO_2 and $\text{SiO}_2\text{-Al}_2\text{O}_3$, a strong IR activation of all of the vibrational frequencies in the available spectral range is observed [19], half of which are only Raman-active in the gaseous centrosymmetric *s-trans* conformation (C_{2h} symmetry [1162]). Such types of interaction are the first stages in the formation of carbenium ions in the case of zeolites and alumina-silica systems (see below), or surface alkoxides in the case of transition metals containing the cations in high oxidation states (V^{5+} , Mo^{6+} , Cr^{6+} and W^{6+}) (see Sections 5.1.2 and 5.1.3 for further details). In some cases, the high acidity of such hydroxyls can provide the complete transfer of a proton to the alkene, and thus large changes in the spectra are expected.

Hydroxyls can be differentiated according to their type of interaction with alkenes. Basic hydroxyls [30, 1087] do not form stable complexes at room temperature (spectrometer beam temperature), which allows their binding energies to be estimated as ca. 40 kJ mol^{-1} . The availability of more energetically favorable sites on the oxide surface, such as coordinatively unsaturated cations, can also stabilize alkenes in the form of π -complexes. This may lead to some bonding of the allylic CH bonds of the alkene with hydroxyls [30, 1087, 1151, 1163]:



Scheme 5.2

The resulting shifts of the surface hydroxyl absorption bands are small ($80\text{--}150 \text{ cm}^{-1}$), which may also be taken as evidence for the low energy of such a bond [30]. It should be noted that the mobility of the H atoms from the CH_3 groups, as in propylene, increases on π -complex formation.

5.1.2 CARBENIUM IONS AND ALKOXY COMPOUNDS

Carbenium ion mechanisms are very well known in homogeneous catalysis for transformations of different organic compounds [735]. The Nobel Prize for Chemistry in 1994 was the recognition of merit for those scientists working in this field. However, the details about heterogeneous catalytic reactions using the carbenium ion mechanism are not yet decided. This is caused by significant difficulties in identifying the carbenium ions, especially the initial ones, on the surfaces of heterogeneous systems, as shown by the first studies in this field [18, 19, 46, 454].

Zeolites

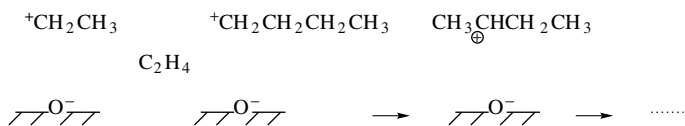
Proton transfer to olefin molecules upon their interaction with H-form zeolites proceeds easily and is well established. During the adsorption of hex-1-ene on decationated zeolites [1164], and other olefin molecules on the H-forms of zeolites [1152–1155] or aluminosilicates [46], the absorption band at 3090 cm^{-1} of the valence vibrations of the olefin groups, $=\text{CH}$ and $\text{C}=\text{C}$ ($1600\text{--}1650 \text{ cm}^{-1}$), disappears. Furthermore, the spectra of such structures in the regions of the

C–C stretching vibrations and C–H deformational vibrations display such absorption bands as characteristic of the saturated structures. Cyclization with the formation of aromatic structures has been observed at higher temperatures [1155, 1165]. The spectrum of hex-1-ene molecules adsorbed at 366 K shows the absence of the stretching vibration of C=C. Another absorption band at about 1600 cm^{-1} appears at 522 K and indicates the formation of olefin groups in polyene-type structures. This band shifts to 1580 cm^{-1} at higher temperature and characterizes the formation of aromatic structures [1155, 1164, 1165].

Many studies have been carried out by means of both IR and UV–Vis spectroscopy to investigate the nature of the compounds formed as a result of proton transfers to olefin molecules and the formation of saturated oligomeric structures. The main difficulties in identifying the surface compounds formed are connected with the absence of a correlation between the IR and UV–Vis data [46]. According to infrared spectroscopic studies, the saturated oligomer structures have been formed, while the UV–Vis method showed the formation of unsaturated carbenium ions. It was later established that such a type of carbenium ion formation is the result of secondary processes. The identification of carbenium ions in zeolites is complicated by olefin conversions at different centers.

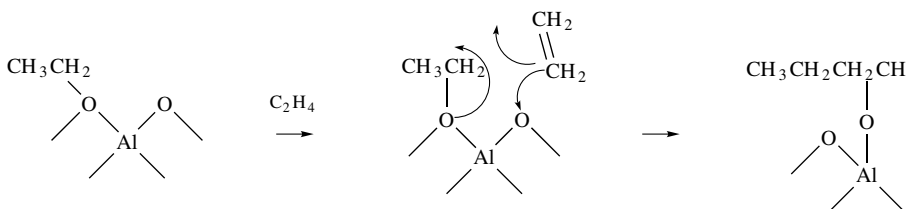
Olefin oligomerization proceeds on both **Lewis** (with **branched oligomer** formation) and **Brønsted** (with **linear oligomer** formation) acid centers [536, 543, 1166]. In the opinion of Kazansky and co-workers [543], two different mechanisms can take place when this process proceeds on Brønsted centers:

Carboionic



Scheme 5.3a

or alkoxy



Scheme 5.3b

Kazansky and co-workers [543] prefer the alkoxy mechanism of oligomerization with polyene structures formation, because the carbenium ions (in their opinion) have to be isomerized immediately. However, more recent results suggest that the carbenium ion mechanism is more probable for the following reasons:

- (i) There are numerous data about the formation of carbenium ions as a result of the secondary processes. The presence of allylic fragments is spectrally well recognized by both IR and

UV-Vis methods and has allowed the observation of the whole order of transformations via the carbenium ionic mechanism. It is logical to suggest that the initial saturated oligomer structures, which have no characteristic spectral images in either the IR or UV-Vis region, also have a carbenium ionic nature.

- (ii) To demonstrate that the process proceeds via carbenium mechanism, direct experiments on the interaction of butadiene with protic centers, where the carbenium ions with allyl fragment are synthesized, have been carried out. As will be described below, in the case of butadiene, the carbenium ions are already formed upon the initial interaction.
- (iii) It has been demonstrated that at least the 'strongly polarized covalent structures' [536, 1166], the so-called 'alkoxides', forming upon the interaction between olefins and the Brønsted acid centers of oxides (for example, V_2O_5/Al_2O_3 and MoO_3/Al_2O_3) are not the oligomerization centers [30, 748, 1050, 1167, 1168]. We will examine below the data evidence listed above in more detail.

Secondary olefin transformations with Brønsted acid sites have long been successfully investigated independently by UV-Vis or IR spectroscopic methods. First of all, the data from diffuse reflection spectra indicate that the reaction of olefins with zeolites leads to the formation of allyl carbocations [1169–1183]. It was proposed, on the basis of the UV-Vis data [1170–1173] that the interaction of olefins with H-ZSM-5, HY and HM zeolites at 298–473 K leads to the formation of allyl cations characterized by an absorption band at ca. $33\,300\text{ cm}^{-1}$ (300 nm). According to the IR spectra of the strongly acidic homogeneous systems, the formation of allyl carbenium ions should be accompanied by the appearance of the absorption band at 1530 cm^{-1} [1174]. In fact, when the temperature increases during the interaction of olefins with H-ZSM-5 and HY zeolites, an absorption band at around 1500 cm^{-1} appears in the spectrum [46, 1176–1183]. However, there have been different interpretations of this band. Some associate it with the formation of aromatic structures [536, 1176], some with COO^- groups [1179], and others with complexes with the transfer of a proton to the olefin to form a 'nonclassical carbenium ion' [1180].

Comparison of the data obtained by the IR and UV-Vis methods upon the investigation of the propene interaction with H-ZSM-5 zeolites, [1177, 1181, 1182] taking into account the data of Sorensen [1184], firmly indicates that the absorption bands in the $1500\text{--}1540\text{ cm}^{-1}$ region belong to the allyl or polyenyl carbenium ions ($\nu_{as}\text{ CCC}$). The formation of alkenyl carbenium ions is also supported by the UV-Vis, $33\,300\text{--}25\,000\text{ cm}^{-1}$ (300–400 nm) technique. Similar results were also obtained in both IR and UV-Vis studies of the interaction of propene or cyclopropane with HM zeolites [1172, 1173]. The adsorption of propene on H-ZSM-5 zeolite at 298 K with subsequent outgassing leads to the formation of surface compounds that are characterized in the IR spectra by a number of absorption bands in the δ and ν regions of saturated C–H bonds (Figure 5.1(a), spectrum 1). In this case, strong changes occur in the absorption of acidic hydroxyl groups, namely, a sharp decrease of the 3610 cm^{-1} absorption band intensity and the appearance of a low-intensity band at $3450\text{--}3550\text{ cm}^{-1}$. The bands in the absorption region of C–H bonds indicate the formation of saturated hydrocarbon surface structures, namely, oligomers [46, 1150, 1154, 1176, 1181–1183]. Heating leads to the formation of compounds of a new type. A simultaneous increase in intensities of the 1510 cm^{-1} (Figure 5.1(a), spectra 2–4 and Figure 5.1(b), 4) and 290–310 nm (Figure 5.1(b), spectra 1–3) absorption bands allows them to be attributed to the same surface compound. When the outgassing temperature of the sample increases up to 573 K, the complete removal of this compound occurs (Figure 5.1(a, b), spectra 6) and a restoration of the intensity of the 3610 cm^{-1} absorption band is observed.

With the use of deuterated reagents (C_3D_6 and D-ZSM), the 1510 cm^{-1} absorption band shifts upon the H–D exchange by 30 cm^{-1} . Both the location and the isotopic shift are not typical for $\delta\text{C-H}$ bond vibrations [1181–1183]. As has been noted, the appearance of the 1510 cm^{-1} absorption band cannot be attributed to aromatic complexes, since a comparison band at 1600 cm^{-1} is

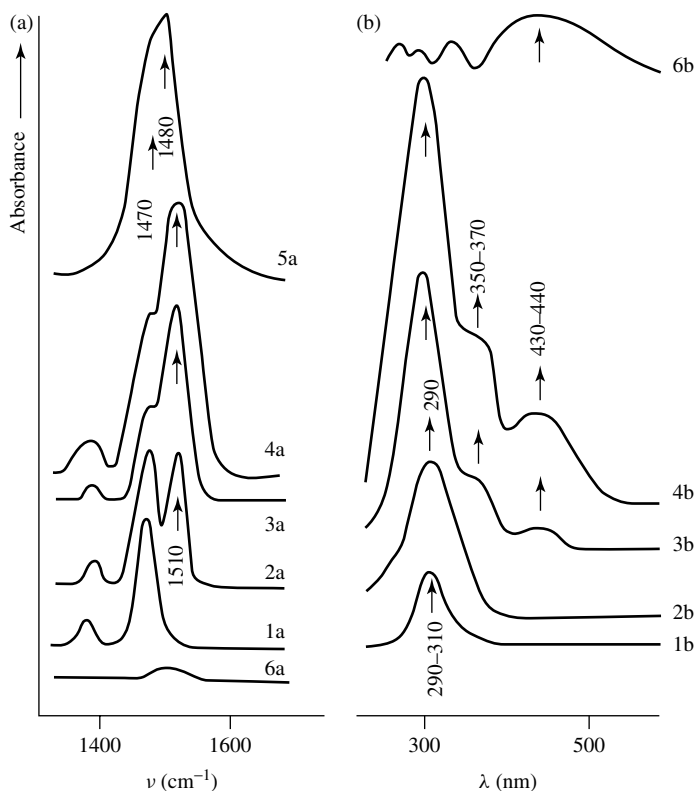


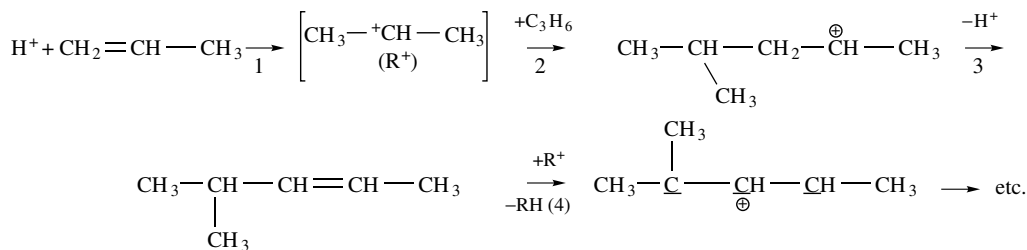
Figure 5.1. IR (a) and UV-Vis (b) spectra of H(D)-ZSM-5 zeolite (with $M = 30$) treated with propene: H-ZSM-5 zeolite treated with propene at 298 K (1 torr) and evacuated at (1a and 1b) 298 K, (2a and 2b) 373 K, and (3a and 3b) 473 K; H-ZSM-5 (D-ZSM-5) zeolite treated with (4a and 4b) C_3H_6 (0.2 torr) or (5a) C_3D_6 (0.6 torr) at 473 K for 2 h and then evacuated at 473 K; (6a and 6b) samples 4a and 4b after evacuation at 573 K.

not observed (along with the 1500 cm^{-1} band, this band is typical of the majority of aromatic compounds). The appearance of an absorption band in the region of $1550\text{--}1600\text{ cm}^{-1}$ does not occur if deuterated reagents are used. In addition, UV spectroscopy has not revealed the presence of aromatic hydrocarbons in the decomposition products of surface compounds. In the $180\text{--}240\text{ nm}$ region, bands typical of olefin and diene hydrocarbons are observed [1185]. One can hardly attribute the 1510 cm^{-1} absorption band to the COO^- group vibrations, since the thermostability of such groups (obtained during the study of $HCOOH$, CH_3COOH and CO_2 adsorption on the H-ZSM-5 zeolites) is very high and absorption bands above 240 nm are absent in the UV-Vis spectra of carboxylate. The assignment of the absorption band at $1510\text{--}1520\text{ cm}^{-1}$, observed after treatment at $373\text{--}473\text{ K}$, to a complex formed by proton addition to the olefin $C=C$ bond ('nonclassical ion') [1180] seems not to be reasonable, as shown by Demidov *et al.* [1182]. The activation process for the formation of such a carbenium complex is not clear, and the relatively high stability of the species in *vacuo* (up to 573 K), and the spectrum in the $33\,300\text{ cm}^{-1}$ (300 nm) region in the UV-Vis spectra seem not to be consistent with the presence of such species.

After a detailed investigation, the absorption bands at 1510 cm^{-1} and $33\,300\text{ cm}^{-1}$ (300 nm) have been attributed to allyl carbenium ions formed according to Scheme 5.4 (see below) [1171, 1173, 1177, 1181–1183]. Such attribution is based, first of all, on the fact that the absorption

band in the $33\,300\text{ cm}^{-1}$ (300 nm) region in olefin strong acid systems corresponds to allyl carbenium ion formation and a $1530\text{--}1540\text{ cm}^{-1}$ absorption band has previously been attributed to the allyl cation in homogeneous strong acidic media [1174, 1184]. The low-frequency ($\nu_{\text{as}}\text{ CCC}$) location of the allyl structure with respect to the location of the $\text{C}=\text{C}$ band in the spectra for olefins may be explained by charge delocalization between three hydrocarbon atoms, i.e. by the hybridized structure formation. The alternative assignment of the $33\,300\text{ cm}^{-1}$ (300 nm) band to polyene hydrocarbons (triene and tetraene [1185]) is not confirmed by the IR spectral data, since an absorption band for $\nu\text{C}=\text{C}$ near 1600 cm^{-1} should be observed for such compounds [13, 14]. It should be pointed out that the formation of a saturated structure in addition to the allyl carbenium ions is caused by the presence of acidic hydroxyl groups. Such surface structures do not occur on a partly dehydroxylated sample of a H-ZSM-5 zeolite with a low degree of crystallization which has nonacid hydroxyl groups characterized by 3750 and 3680 cm^{-1} absorption bands [1177, 1181, 1182].

It has been supposed [1181, 1182] that the existence of oligomer structures as precursors of allyl carbenium ions indicates an ionic character of the oligomer interaction with the surface (the formation of 'alkyl carbenium ion' is assumed). By describing the oligomer surface structure as an 'alkyl carbenium ion', it is not meant that it is bound via a pure ionic bond; there is obviously some contribution from a covalent component. We only emphasize its difference from pure covalent compounds, namely surface alkoxides (e.g. on $\gamma\text{-Al}_2\text{O}_3$ and other oxides, see below), for which olefin insertion into a $\text{R}-\text{C}-\text{O}-\text{M}^{n+}$ bond does not occur [30]. The following scheme of alkenyl cation formation from propene has been adopted in the literature [1170, 1173, 1177, 1181, 1182]:



Scheme 5.4

According to this scheme, the further course of these complex reactions is expected to be followed by polyenyl (di-, tri and tetraenyl) carbenium ion formation [1172, 1181, 1182]. Indeed, treatment of the H-ZSM-5 zeolite with propene at 473 K is accompanied by the appearance of 350–370 and 430–440 nm bands in the UV–Vis spectrum, additional to those from allyl carbenium ion formation (Figure 5.1(b), spectrum 4). The location of the bands observed is typical for dienyl and trienyl carbenium ion absorption, respectively (mainly for cyclic carbenium ions); these ions are obtained in acidic homogeneous media [1174, 1184]. In the IR spectra of D-ZSM-5 zeolites treated with C_3D_6 at 473 K, a 1470 cm^{-1} band is observed, as a shoulder on the 1480 cm^{-1} band (Figure 5.1(a), spectrum 5). These authors [1177, 1181–1183] supposed that, together with allyl cations, similar nonaromatic compounds containing $\text{C}\equiv\text{C}$ bonds are also formed. The 1470 cm^{-1} band may be attributed to polyenyl cations or, as is expected for HM zeolites, to dienyl cations [1172]. The thermostability of polyenyl cations, like that of allyl cations, does not exceed 573 K *in vacuo*. Such thermostability may be explained by the conjugation of the 'approximate' $\text{C}=\text{C}$ bonds in the alkenyl carbenium ions as well as by their cyclic (not aromatic [1183]) structure. These factors lead to an increase in the number of negatively charged

O^{2-} ions in the solvating cation shell and thus to stabilization of the cations on H-ZSM-5. The value of the isotopic shifting of $\nu^{as}CCC$ may be connected with the cyclic structure of such compounds.

The schemes proposed by various authors [1170, 1173, 1181, 1182] can be tested, for example, by the adsorption of diene hydrocarbons on zeolites because in this case the formation of allyl and polyenyl cations should proceed directly. Butadiene adsorption on H-ZSM-5 zeolite at 298 K is accompanied by the appearance of bands at 310, 350–380, 440 and 520–570 nm (Figure 5.2(b), spectra 1–3). The distribution of absorption maxima over these wavelengths is close to that reported by Sorensen for alkenyl carbenium ions in acidic homogeneous media [1184]. Similar results have been obtained for alkene adsorption on HM zeolites [1173]. By monitoring the butadiene dosage, it is possible to detect the predominant formation of methyl allyl carbenium ions ($CH_3-CH=CH=CH_2^+$) using UV–Vis spectroscopy (Figure 5.2(b), spectrum 1). The amount of dienyl and trienyl carbenium ions increases with increasing amounts of adsorbed butadiene (Figure 5.2(b), spectra 2 and 3). Using IR spectroscopy, the appearance of 1500 and 1480 cm^{-1}

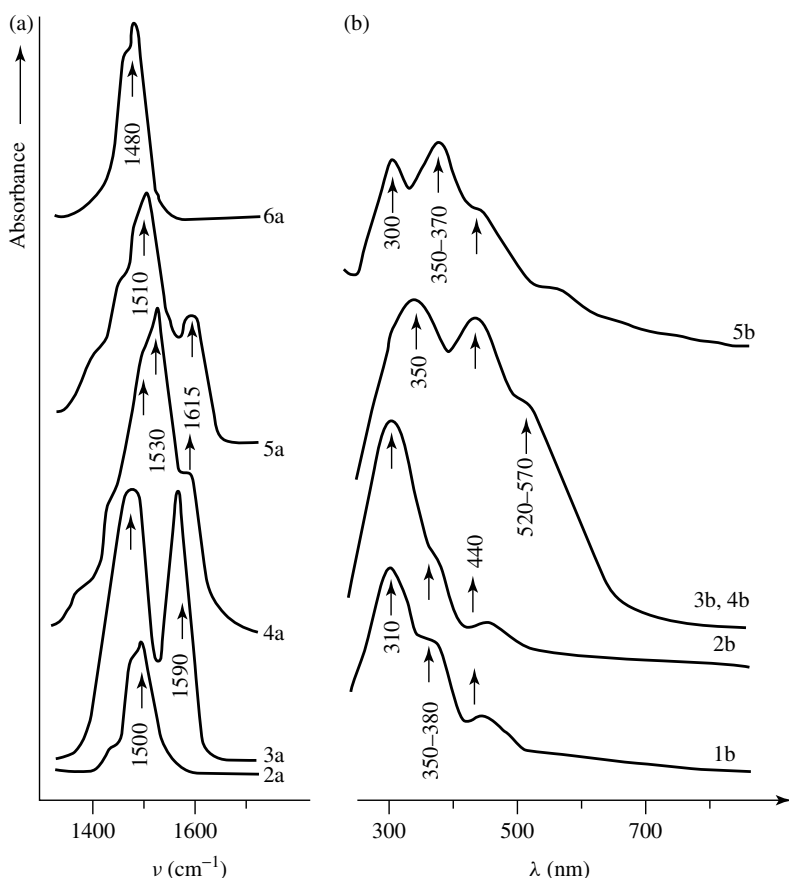
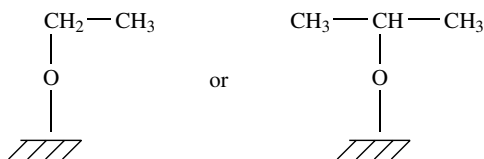


Figure 5.2. IR (a) and UV–Vis (b) spectra of H(D)-ZSM-5 zeolite (with $M = 30$) treated with butadiene and methanol: D-ZSM-5 zeolite treated at 298 K with C_4D_6 at 10^{-2} torr (1b), at 0.1 torr (2a and 2b), and at 1 torr (3a and 3b); H-ZSM-5 zeolite treated with C_4H_6 (0.05 torr) and evacuated at 473 K (4a and 4b); H-ZSM-5 zeolite treated at 495 K with CH_3OH (0.5 torr for 4 h) and evacuated at 473 K (5a and 5b); D-ZSM-5 zeolite ($M = 90$) treated with CD_3OD at 573 K (0.5 torr for 2 h) and evacuated at 473 K (6a).

absorption bands (the isotope shift upon H–D exchange is 30 cm^{-1}) has been shown (more clearly for deuterated reagents) (Figure 5.2(a), spectra 2–4). By analogy with the data obtained for propene and the results of the HM zeolite investigation [1173, 1177, 1181, 1182], the bands observed were attributed to allyl and polyenyl carbenium ions. Thus, the study of butadiene and H-ZSM-5 zeolite interaction confirms the conclusion about the formation of alkenyl carbenium ions from propene. The thermostability of alkenyl cations formed from butadiene and propene is the same. The formation of alkenyl carbenium ions in the case of butadiene is probably accompanied by their cyclization, as observed for homogeneous systems [1174, 1184].

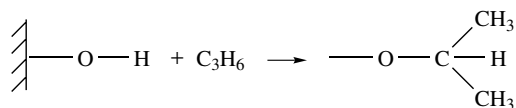
Oxides

Proton interactions with C_2H_4 and C_3H_6 on transition-metal oxides in the highest oxidation states (V^{5+} , Mo^{6+} , W^{6+} , Cr^{6+} , etc.) give rise to compounds with a covalent C–O bond as follows:



Scheme 5.5

which is typical for alkoxides [30]. The first such interactions were revealed by Davydov and co-workers [30, 215, 216, 219–221, 748, 1050, 1151, 1167, 1168, 1186]. Later, the formation of such complexes has been supported in other reports [1187–1189]. The IR spectra of these compounds (in the case of ethene and propene) are fully identical to those of alkoxides formed by the adsorption of ethyl or isopropyl alcohol (see, for example, for Sn–Mo–O catalysts [748, 1168, 1190]). Spectroscopically, such compounds are characterized by the lack of alkane fragment absorbance and the presence of characteristic $\nu\text{C–O}$ and $\nu\text{C–H}$ absorption bands typical of saturated compounds (Figure 5.3a, spectrum 2). The H–D isotopic shifts for δ and νCH vibrations are typical of hydrocarbon groups. The $\nu\text{C–O}$ vibration case is not completely characteristic, and this is why the $\Delta\nu\text{C–O}$ value is ca. $30\text{--}50\text{ cm}^{-1}$, which is close to the shifts observed for metal alcoholates and alcohols [30]. It has been found [30, 219, 748] that Brønsted acid sites are involved only in the adsorption of propene, for example, on the hydrated surface of the Sn–Mo–oxide catalyst, according to the following:



Scheme 5.6

In this instance, only 2-propylate surface species are formed, which allows the energy parameters of the process to be assessed. To elucidate the role of the Brønsted centers, Davydov *et al.* [748, 1168] have studied the infrared spectra of propylene on a catalyst characterized by the absence of such centers (mobile protons). To remove the latter, the catalyst was treated with a 0.1 N NaOH solution with subsequent rinsing of the residual Na^+ ions by water. For this sample, the spectra

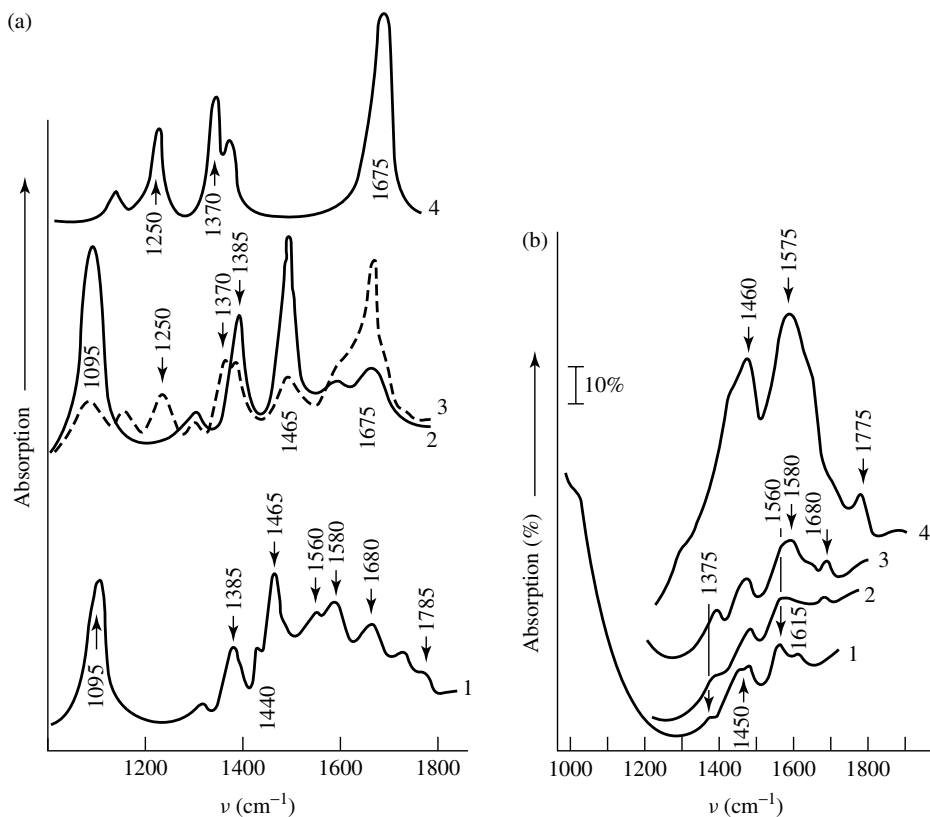


Figure 5.3. Changes of IR spectra of V_2O_5/Al_2O_3 (a) 1, after C_3H_6 adsorption on oxidized and dehydroxylated surface, 20 Torr C_3H_6 at 300 K; 2, 20 Torr C_3H_6 at 300 K on the sample hydrated in H_2O at 300 K; 3, following heating at 423 K; 4, 10 Torr acetone on the sample hydrated in H_2O at 300 K; (b): upon interaction of a reduced catalyst with: 1, 30 Torr C_3H_6 673 K; 2,3,4, $C_3H_6 + O_2$ mixture 297, 373, 573 K, respectively.

of adsorbed ammonia exhibit no bands in the region of 1440 cm^{-1} , which are typical for the δNH_4^+ ion. In this case, the Lewis acid centers remain practically unchanged. The adsorption of propene on this catalyst leads to the formation of weakly bound π -complexes on Sn^{4+} ions only [748, 1168].

As assessed from the adsorption isotherm, the concentration of Brønsted acid sites of the Sn–Mo–oxide catalyst (9:1) is 2.9×10^{19} sites g^{-1} (the maximum propene adsorption at 293 K is $48\ \mu\text{mol g}^{-1}$). The differential heats of propene adsorption on the Sn–Mo catalyst are shown in Figure 5.4. It follows that the Brønsted acid sites are nonuniform in the strength of their energy of interaction with propene, with the interaction of the weakest sites with C_3H_6 leading to an energy release of only 100 kJ mol^{-1} [748]. The range of energies of formation of 2-propylate complexes between propene and the Sn–Mo catalyst is $158\text{--}100\text{ kJ mol}^{-1}$. The same range is characteristic of other oxide systems capable of donating protons to alkenes. A similar value is also observed for the interaction with ethene. Note that this value is 2–3 times higher than the energy of formation of alkene π - and π -allylic complexes with cations (see Section 5.1.3), which allows one to establish the type of alkene interaction with the surface on the sole basis of energy

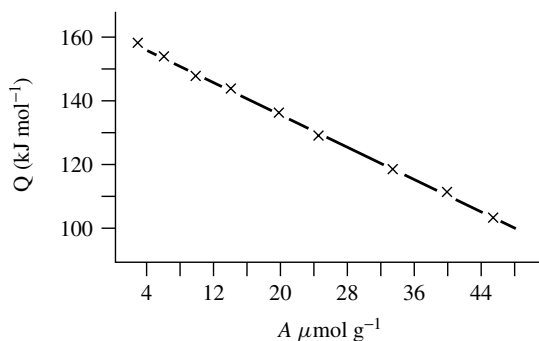


Figure 5.4. Differential heats of adsorption of propene on the hydrated surfaces of the Sn–Mo catalysts as a function of surface coverage.

parameters. As has been established [30, 748, 1050], the character of interaction of olefins with hydrated oxidized V-containing catalysts is determined by the presence of mobile protons; similar to the above Mo-containing catalysts, the initial stage of this interaction is the transfer of a proton to the double bond (isopropylate in the case of propene – Figure 5.3(a), spectrum 2). This follows from the presence in IR spectra of all absorption bands characteristic for such surface species. With increase in temperature, the surface isopropylate is converted to acetone (Figure 5.3(a), compare spectrum 3 with spectrum 4) and then to anhydrates and carboxylate [30, 215, 216, 219–221, 748, 1050, 1151, 1167, 1168, 1186]. The latter transformation depends on the type of support and the content of the active component. It should be pointed out that partial destruction of the reaction products is observed on the surface of such a catalyst even at room temperature on the catalysts dehydrated at high temperature (Figure 5.3(a), spectrum 1). In contrast, on reduced V-containing catalysts at room temperature, olefins are absorbed like π -complexes [30, 748, 1050]. Such π -complexes, in the presence of oxygen in the gas phase and high temperatures, are converted to aldehyde-, carboxylate-, and anhydrate-like compounds (Figure 5.3(b), spectra 1–4). In the case of interaction of iso- C_4H_8 with $\text{V}_2\text{O}_5/\text{TiO}_2$ (9.6 wt% V_2O_5) the tert-butoxy species are formed. For low vanadia contents (0.1 wt% V_2O_5), the absence of surface Brønsted acid sites leads to dimerization with the formation of 2,4,4-trimethylpentene on surface Lewis acid sites [1194–1196]. On the V–Ti–O catalyst, ethene is adsorbed only as such, without reaction at low temperature. Reactive adsorption is found to start from 373 K, producing surface ethoxides. If the reaction proceeds at temperatures below 373 K, the spectral features of slightly perturbed ethylene are observed (3092, 2975, νCH ; 1898; 1442, $\delta + \nu\text{CH}$; 1620 and 1342, $\nu\text{C}=\text{C}$ and δCH in the π -complex on cationic sites). At low temperatures (down to 200 K), C_3H_6 adsorbs as such through π -bonding and reacts later to give an adsorbed species identified tentatively as an allyl radical. This reacts with the surface OH group to give an isopropoxy species. Two main surface pathways for propene transformation are active, leading to surface species functionalized at the C_2 (isopropoxy species to acetone – Figure 5.3, spectrum 2) and C_1 atoms (acrolein and acrylates), as well as products arising from coupling of the allyl radical. The latter has been identified by absorption bands 1468, 1373 and 1165 cm^{-1} by comparison with the bands in the spectra of a π -bound allyl compound in both the $\text{C}_3\text{H}_5\text{PdCl}_2$ complex and an allyl radical isolated in a cryogenic matrix. However, the spectral identification of surface allyl radicals, in our opinion, is doubtful, since all absorption bands shown above are also observed in the spectrum of isopropylate. At a temperature of 423 K, the isopropyl compound transforms to adsorbed acetone as a product ($1680, 1420$ and 1250 cm^{-1}). After heating at 473 K, the appearance of new bands at 1870 and

1790 cm^{-1} was observed, strongly suggesting their assignment to a cyclic anhydride (ν_s and ν_{as} ($\text{C}=\text{O}$) in the system $\text{O}=\text{C}-\text{O}-\text{C}=\text{O}$, such as in maleic anhydride).

The interaction of a V-TiO₂ catalyst with 1-butene, cis-2-butene, trans-2-butene and iso-butene has been investigated by FTIR spectroscopy in the temperature range 150–673 K [1188, 1189, 1195, 1196]. At room temperature, the three normal butenes produce the 2-butoxide species which at higher temperatures undergoes oxidative dehydrogenation to methyl ethyl ketone and, following oxidative C–C bond cleavage, to acetate species. These species follow a different oxidative pathway with the formation of butadiene, furan and finally, maleic anhydride. Starting at ca. 200 K, iso-butene is oligomerized, giving the dimer 2,4,4-trimethylpent-1-ene and higher oligomers. At room temperature, hydration to tert-butoxide species is also observed. Further heating causes oxidative decomposition to acetone, carboxylate species, and, from the oligomers, to cyclic anhydrides. It should be noted, however, that in the absence of the transition metal cation in the catalyst, the character of the interaction between olefins and protic centers is changed and oligomeric species are predominantly formed similar to that observed with zeolites.

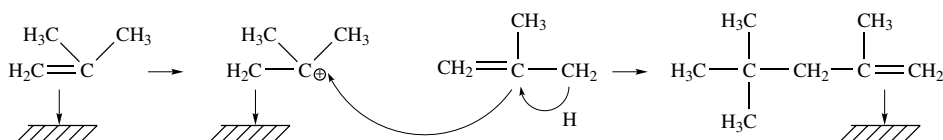
The IR spectra of iso-butene adsorbed at 170–300 K on pure silica, alumina, magnesia and titania oxides, as well as on phosphated samples prepared by impregnation of these pure oxides and of Al/Si with phosphoric acid, have been investigated [1117]. At low temperatures (170–220 K), the molecular adsorbed species are observed on the pure oxides with a spectrum similar to that of liquid iso-butene, although with specific perturbations of the modes primarily involving the vinylidene moiety. Iso-butene is transformed only on titania (even at low temperatures) into a new compound, identified as its dimer, 2,3,4-trimethylpent-1-ene. On phosphated samples, it has been established that the oligomerization occurs at 293 K, producing species identified as containing 5–10 monomeric units.

Busca *et al.* [1195] concluded that the dimerization (oligomerization) of iso-butene readily occurs on TiO₂ at room temperature. At the same time, it was noted [1196] that for TiO₂ only π -complexes of butenes are formed reversibly. However, it is impossible to exclude the proposal of Al-Mashta *et al.* [1197] that the oligomerization took place on impurity centers, as was established for the TiO₂ samples upon the adsorption of propene [1198]. In fact, it was shown that propene is oligomerized on the TiO₂ surface [1197], whereas Davydov [30] established the formation of the π -complexes only in the absence of impurities. However, Sheppard and co-workers [1199] later established the presence of sulfate ions in the samples of TiO₂ studied in the earlier work [1197]. It is suggested that these ions are responsible for the oligomerization activity. At least, the presence of strong protic centers formed during the modification of titania surface by sulfates can lead to the formation of oligomers via the mechanism similar to that proposed for their formation on zeolites.

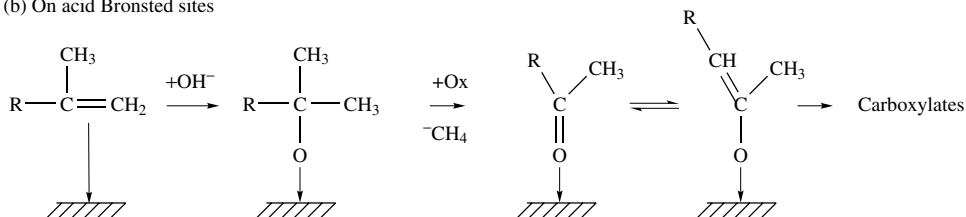
In the reaction of iso-butene with the surface of a V-Ti oxide system, containing about 9.6 wt% V₂O₅, tert-butoxy species were also formed [1194] which were then oxidized to ketone and to carboxylate species as the temperature was increased. Iso-butene oligomers and tert-butoxy species are formed on surface Lewis or Brønsted acid sites through the intermediate formation of a carbonium ion which, in the author's opinion, acting as an electrophilic agent, reacts with the C=C bond in the alkene molecule (oligomer formation) or with surface oxygen atoms (tert-butoxy formation).

On the V-Ti-O-system, iso-butene cation dimerization (or even oligomerization) is catalyzed even at room temperature due to the coordination of the olefin molecule to the vanadium cation through a π -bond, thus forming a carbocation able to react with another iso-butene moiety, so leaving a free cation [1194]. This process is easily detected on a catalyst containing 0.1 wt% V₂O₅/TiO₂. For higher vanadia content, an oxidative dehydrogenation of iso-butene takes place, leading mainly to the formation of carbonyl species that undergo further oxidation to carboxylate. A reaction scheme for both processes is depicted as follows:

(a) On Lewis acid sites

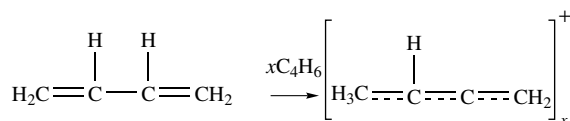


(b) On acid Bronsted sites



Scheme 5.7

When more complicate olefins (butadiene, etc.) are adsorbed on such types of catalyst the typical carbenium ion is formed by the participation of proton acid centers (see, for example, V_2O_5/Al_2O_3 [1192]). The spectra for 1,3-butadiene adsorbed on oxidized V_2O_5/Al_2O_3 (Figure 5.5, spectra 2) qualitatively differ from those observed for the $\gamma-Al_2O_3$ -1,3-butadiene systems (Figure 5.6, spectra 2), for propene adsorbed on V_2O_5/Al_2O_3 [1050] or 1,3-butadiene adsorbed on reduced V_2O_5/Al_2O_3 (Figure 5.6, spectra 5). In the latter cases, the formation of only π -complexes has been observed. In the spectra of C_4H_6 adsorbed on oxidized V_2O_5/Al_2O_3 (Figure 5.5), in contrast with reduced samples (Figure 5.6, spectra 5), an intense absorption band can be distinguished at ca. 1500 cm^{-1} with an asymmetric shape (spectra 2), which is absent in the case of C_3H_6 adsorption (Figure 5.3). In the light of the work mentioned above, without doubt, this denotes carbenium ions formation. That is, the ‘complication’ of the organic part of the molecule leads to stabilization by the distribution of the charge over the C–C bonds. This most probably prevents covalent C–O bond formation because of the effect of solvation by means of the surface. The intensity of the absorption band at about 1500 cm^{-1} increases with increasing contact time and the pressure of the butadiene adsorbed, while the frequency position of this maximum decreases (Figure 5.5, spectra 3). With the lowering of the concentration of strongly protic centers which is observed during hydration of the surface of this type of catalyst (as was observed, for example, for MoO_3/Al_2O_3 [221]) there is a substantial decrease in the intensity of the absorption band at 1515 cm^{-1} (Figure 5.5, spectra 3 and 6 obtained under identical conditions on a hydrated and dehydroxylated catalyst surface). This indicates the contribution of the strongly protic acid centers [30], and also confirms the hypothesis about the involvement of these centers in the formation of the carbenium ion. Taking into account the data presented above, it can be assumed that the 1515 cm^{-1} absorption band is caused by the surface compound having an allyl fragment and which is formed by the reaction:



Scheme 5.8

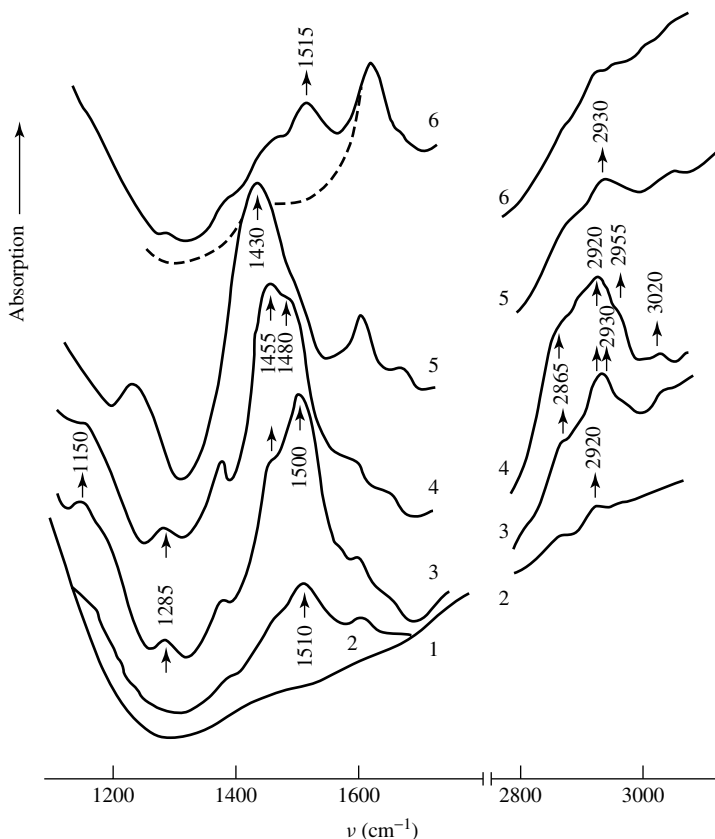


Figure 5.5. IR spectra of 1,3-butadiene adsorbed on V_2O_5/Al_2O_3 oxidized in O_2 at 800 K: (1) V_2O_5/Al_2O_3 ; (2) $6 \mu\text{mol g}^{-1}$ 1,3-butadiene; (3) 2 torr C_4H_6 for 1 min, followed by outgassing at 300 K; (4) 6 torr C_4H_6 for 20 h, followed by outgassing at 300 K; (5) followed by admission of 1 torr NH_3 ; (6) 2 torr C_4H_6 for 1 min, followed by outgassing at 300 K on hydrated surface (the dashed line represents the spectrum of the hydrated sample at 300 K with 4 torr H_2O , followed by desorption of water at 300 K).

A compound of this type (a simple alkenyl carbenium ion) is unstable and, in the course of time or in the presence of excess 1,3-butadiene, enters into reaction with the latter (cationic polymerization reaction) to form poly-alkenyl carbenium ions. This explains the increase in intensity of the band at 1500 cm^{-1} and its displacement to a lower frequency: from 1515 to 1500 cm^{-1} (Figure 5.5, spectra 2 and 3). Such a lowering of the ν_{as} CCC was observed [1181, 1182] in the conversion of alkenyl and polyenyl carbonium ions on H-ZSM zeolites and could point to an analogy between the processes occurring on zeolites and on V_2O_5/Al_2O_3 . Changes in the spectra in the region of CH vibrations (Figure 5.5, spectra 3 and 4) with increasing contact time and pressure of 1,3-butadiene also point to the formation of a complex polymeric structure. It should be noted that, in contrast to the interactions between propylene and ethylene (Figure 5.3) with the given catalyst [30], the intense absorption band at ca. 1100 cm^{-1} , characteristic of ν_{C-O} in alcoholates formed on V_2O_5/Al_2O_3 during adsorption of mono-olefins, is not observed in the spectra of adsorbed 1,3-butadiene. The weak absorption band at 1150 cm^{-1} which appears in the latter spectrum at higher pressures and longer contact times (Figure 5.5, spectra 3 and 4) can, most probably, be attributed to ν_s CCC in the allyl group. These absorption bands at 1150

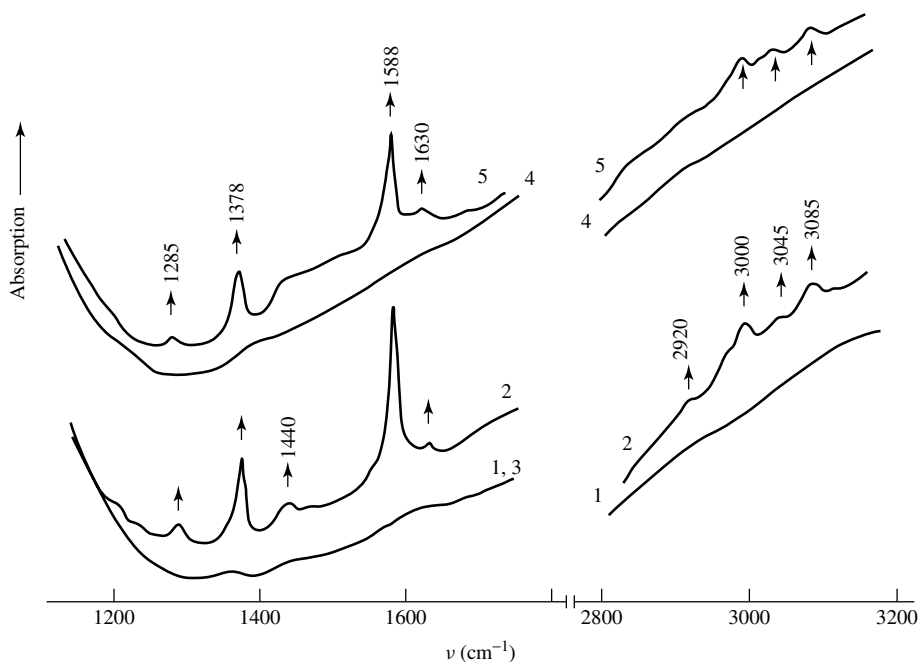


Figure 5.6. IR spectra of 1,3-butadiene adsorbed at 300 K (5 torr) on γ - Al_2O_3 dehydrated at 800 K (1–3), and reduced $\text{V}_2\text{O}_5/\text{Al}_2\text{O}_3$ (4, 5): (1) γ - Al_2O_3 ; (2, 5) 1,3-butadiene adsorption; (3) 1,3-butadiene desorption at 300 K; (4) reduced $\text{V}_2\text{O}_5/\text{Al}_2\text{O}_3$.

and 1515 cm^{-1} belong to the same structure, as shown by their simultaneous generation during adsorption processes (Figure 5.5, spectra 3 and 4) and exclusion by ammonia (Figure 5.5, spectrum 5). Therefore, the assumption that this absorption band could belong to νCO is unlikely to be true since the formation of a covalent C–O bond should have destroyed the conjugated system. Instead of an absorption band at ca. 1500 cm^{-1} , one would then expect to see an absorption band in the $1600\text{--}1650\text{ cm}^{-1}$ range characteristic of a terminal C=C bond. Among other things, it is possible to note that the carbenium ions do not form hydrocarbon-to-surface covalent bonds since such a bond would destroy the conjugated system which is responsible for the stability and characteristic spectra of these ions.

A significant argument in support of the formation of ionic structures from 1,3-butadiene is their almost complete displacement from the surface by ammonia (Figure 5.5, spectra 3 and 5) during which all absorption bands in the region $1200\text{--}1800\text{ cm}^{-1}$ disappear simultaneously and absorption bands characteristic of adsorbed ammonia appear. These are primarily vibrations characteristic of ammonium ions (absorption band at 1430 cm^{-1}) and coordinated ammonia (absorption bands at 1240 and 1620 cm^{-1}). Considering that ammonia has a greater affinity for protons than 1,3-butadiene, the system appears to follow the expected behavior. Chromatographic analysis of the products displaced from the $\text{V}_2\text{O}_5/\text{Al}_2\text{O}_3$ surface by ammonia shows that they do not contain 1,3-butadiene, but confirms the formation of polyenyl carbenium ions on the surface. For reasonable retention times in a GC column, the elution of other kinds of products of higher molecular mass (formation of polyenes), or the occurrence of ammoniation of carbenium ions with the formation of amines that would be strongly held by the surface, has not been observed. It should be noted that in the IR spectra, after displacement of the carbenium ions by ammonia, absorption bands of unknown origin were observed in the νCH region.

The adsorption form of 1,3-butadiene characterized by absorption bands at about 1500 cm^{-1} is fairly stable to heat and the decomposition (conversion) of the corresponding complex occurs *in vacuo* above 473 K. Absorption bands which show the presence of oligomers on the surface are then observed in the spectrum. The oligomer formed possibly has an aromatic nature (the occurrence of the absorption band at around 1600 cm^{-1}). By means of dosed 1,3-butadiene adsorption, it has been established that the maximum coverage of the surface by carbonium ions corresponds to ca. 10 % of the proton acid centers as determined by ammonia adsorption. Thus, these investigations have demonstrated the possibility of stabilization of alkenyl carbenium ions on the surface of the catalyst. However, the data obtained are inadequate to confirm whether the alkenyl carbenium ion formed in the initial stages of the interaction is a simple mono-enyl ion and not, for example, a dienyl one, etc. It only follows from the evidence that the system is easily transformed into a more stable state, i.e. polyenyl carbenium ions, with the possible inclusion of a cyclic structure [1192, 1193].

For this purpose, the IR spectra of adsorbed hexa- and pentamethylpentadienes on the oxidized surface of $\text{V}_2\text{O}_5/\text{Al}_2\text{O}_3$ were studied. In the IR spectra of adsorbed pentadienes an intense absorption band at ca. 1530 cm^{-1} (which was absent in the spectra of both the original molecules and of the molecules adsorbed in the form of π -bonded structures on $\gamma\text{-Al}_2\text{O}_3$ – see Figure 5.7,

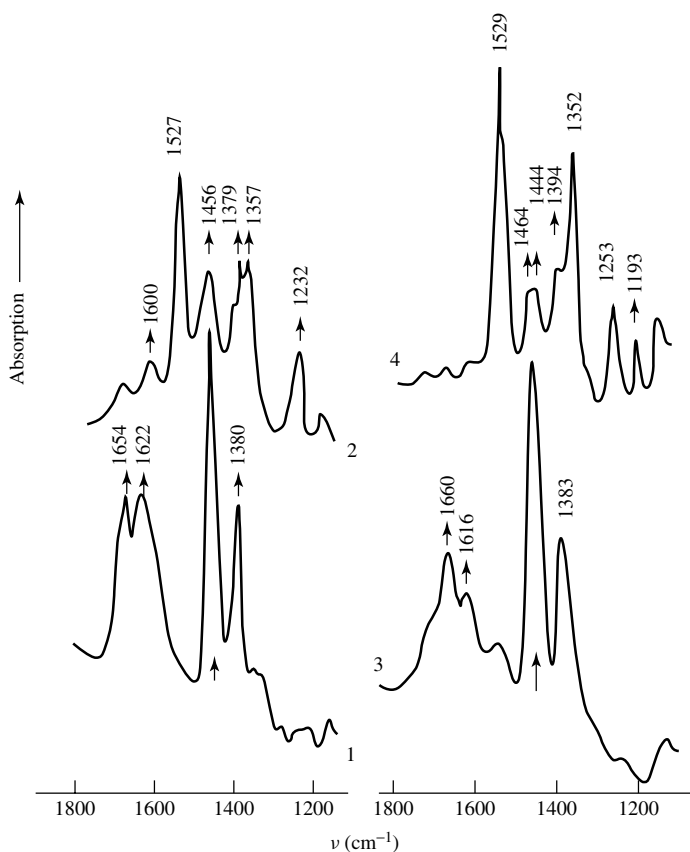


Figure 5.7. IR spectra of pentamethylpentadiene (1, 2) and hexamethylpentadiene (3, 4) adsorbed at 300 K on $\gamma\text{-Al}_2\text{O}_3$ dehydrated at 800 K (1, 3) and $\text{V}_2\text{O}_5/\text{Al}_2\text{O}_3$ oxidized in O_2 at 800 K (2, 4).

spectra 1 and 3) was observed in the region characteristic for the one and half CCC bonds (Figure 5.7, spectra 2 and 4). Its appearance in the spectra of pentadiene complexes could be due solely to the formation of carbonium ions in which case an alignment of the CCC bonds would also be realized. The complex characterized by this absorption band could be displaced from the surface by an NH_3 molecule having a greater proton affinity than pentadiene, analogous to the cases of aromatic carbenium ions [1193]. This fact confirms the carbenium-ionic nature of the complex formed in this case. The spectral data obtained from this study does not contradict the assumption expressed earlier concerning a cyclic structure for carbenium ions formed during 1,3-butadiene adsorption. It is obvious that the increase in energy of interaction in the case of a cyclic carbenium ion, formed by butadiene adsorption, makes its presence as an ion (not a covalently bonded alkoxide) more probable.

Thus, an analysis of the data in the literature shows that the use of physical methods, especially IR spectroscopy, together with UV–Vis spectroscopy, allows one to solve the problem of carbenium ion identification on zeolites and some oxides. At the same time, it is obvious that a more profound investigation of the spectral manifestations of such compounds is still necessary (including using the molecules with isotopic substitution, molecules with different chemical natures, investigating the nature of surface sites involved in the formation of surface compounds, etc.).

5.1.3 INTERACTION WITH CATIONS

The presence of coordinatively unsaturated electron-accepting cations on the surface of most catalysts coupled with the electron-donor properties of alkenes leads to the expectation that the adsorption of alkenes on oxide surfaces will result in the formation of the alkene π -complexes. Consideration of the nature of the bond between an alkene (or the C_3H_5 fragment – see below) and a cation in terms of the Dewar–Chatt model (Figure 5.8) leads to the conclusion that the spectral characteristics of these complexes are determined by the nature and valence state of the cation. It has been established for homogeneous π - and π -allylic complexes that the position of the most characteristic band in the $\nu\text{C}=\text{C}$ stretching region is largely determined by the properties of the central atom [30, 1200] and varies over a wide range (the $\nu\text{C}=\text{C}$ position for π -complexes is 15 cm^{-1} lower with Na^+ [1201], $60\text{--}80\text{ cm}^{-1}$ with Ag^+ , $115\text{--}130\text{ cm}^{-1}$ with Au^+ , and $100\text{--}150\text{ cm}^{-1}$ with Pt^0 [1200] as ligands). The spectral range of $\nu\text{C}=\text{C}$ for π - and π -allyl complexes is wide owing to its dependence on the electron-donor and electron-acceptor properties of the central atom, which precludes the possibility of using compounds with other cations or ligands as spectral analogs. This means that the conventional approach to the interpretation of

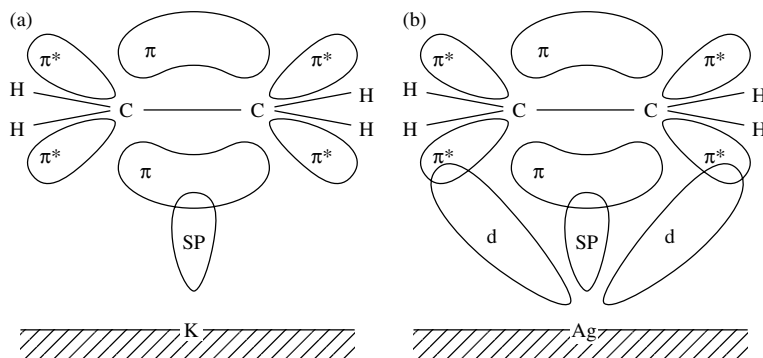


Figure 5.8. Configuration of orbitals involved in ethene bonding with (a) nontransition and (b) transition-metal cations.

the spectra of surface compounds [18, 19] is unacceptable here. Therefore, the question arises of how the valence and coordination states of the surface cation can be efficiently characterized.

In the majority of studies mentioned below, the nature of alkene adsorption sites has been established by using the methods of competing reactions. Simple molecules (e.g. CO, NO, NH₃ and CO₂), the spectral manifestations of which have been used to identify the state of cation (Chapter 3), stabilized on surface sites of different kinds, were replaced with alkenes if the former had a lower affinity to the surface or, in contrast, used to block surface sites in order to reveal their involvement in complexation.

π -complexes with cations

It is impossible to observe the formation of olefin π -complexes by UV-Vis spectra, because the $n \rightarrow \pi$ transitions for these complexes take place in the vacuum ultraviolet region (under 200 nm). This is why this method has not been effectively used, and to identify such complexes the IR spectroscopy method is mainly employed. If several years ago the question about olefins π -complexes formation on the oxides surface was uncertain, today their formation is reliably established. Together with the recognition of new systems in which the π -complexes are formed on the surface and identified, researchers have investigated both the properties and role of π -complexes in reactions proceeding on the surface. The criteria for the identification of these complexes had been formulated earlier [30, 1151, 1201–1203], because the spectral manifestations of π and other types of complexes formed are observed in the same spectral regions.

Zeolites

The formation of π -complexes from olefins, as in the majority of the cases, was first established on zeolites. It has been shown that in the case of zeolites with exchanged cations that molecules of ethylene are adsorbed, giving complexes with different strengths of bonding to the surface which depend on the type of cation – see, for example, [19, 1201].

During the adsorption of molecules with π -electron bonds, the spectrum has distinct properties related to the high polarizability of strongly delocalized π -electrons in the electrostatic field of the cations in zeolites. In this case, the polarization of the adsorbed molecule is stronger than in the case of olefin π -complexes formed by H-bonds with Brønsted acid sites. A modified CNDO method, whose Hamiltonian includes the terms describing the interaction of the electrons with the electrostatic field of the zeolite crystal, has been employed to study the influence of the faujasite electrostatic field on the physical characteristics of C₂H₄ [1204]. Beran thereby established that the ethylene molecule is polarized by the electrostatic field and its total CNDO/2 energy is decreased in comparison with that of the isolated molecule [1204]. This is particularly valid if the molecule is situated close to the S_{II} cationic position (Figure 5.9).

The dependence of the position of $\nu_{\text{C}=\text{C}}$ (ν_2) on the type of cation (Figure 5.10) indicates that mainly cations influence the π -system. The presence of ethylene molecules adsorbed on zeolites has been reported [19, 1201]. The strong polarization of adsorbed molecules is indicated by the appearance of the absorption bands of the stretching vibrations of C=C ν_2 and ν_3 in the spectrum of ethylene adsorbed on the zeolites AgX, CdX, LiX, KX, NaX, BaX and CaX. These bands are forbidden by the alternative exclusion principle for centrosymmetric molecules in the gaseous state but also in the solid. The frequencies of these bands and their shifts with reference to the gaseous phase are listed in Table 5.3.

The appearance of these absorption bands results from the distorted symmetry of the electronic structure of ethylene in the electrostatic field of the zeolite. The symmetry of the ethylene molecule is thus decreased from D_{2h} to C_{2v}. A strong distortion of the symmetry of the ethylene molecules is expected from the large contribution of the energy associated with this interaction to the

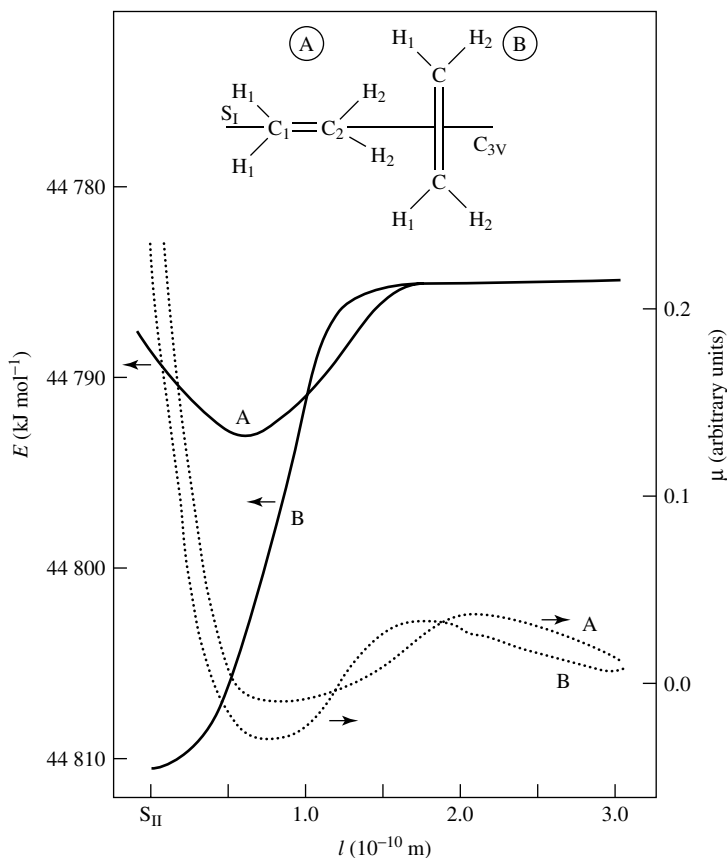


Figure 5.9. Depiction of changes in the total CNDO/2 energy (full lines) and dipole moment (dotted lines) of the ethene molecules as a function of the distance of its center from the S_{II} cationic position for orientations A and B [1204]. Reprinted from Beran, S., 'Quantum chemical study of the influence of the zeolite electrostatic field on the physical characteristics of ethylene', *React. Kinet. Catal. Lett.*, **24**, 385–390 (1984). Reprinted with permission from Akademiai Kiado.

total heat of adsorption of ethylene; on the zeolites LiX and CaX, this contribution is 4.5 and 5.0 kcal mole⁻¹, respectively. A strong distortion of the electronic structure of adsorbed ethylene and other unsaturated molecules is also confirmed by the changes in intensity of the CH stretching vibration.

In the spectrum of ethylene adsorbed on all zeolites except for AgX, the half-width of the absorption band ν_{12} (antisymmetric deformation vibration of CH₂ at 1455 cm⁻¹) is much larger than that of the induced absorption bands ν_2 and ν_3 (at 1584 and 1331 cm⁻¹). For example, in the case of ethylene adsorbed on the CdX zeolite, the band half-width is 40 cm⁻¹ for the vibration ν_{12} , and 4 cm⁻¹ for the vibrations ν_2 and ν_3 . The ratio between the half-widths of these absorption bands indicates a change in the vibrational dipole in the direction parallel to the surface, as a result of the rotation of the adsorbed molecule.

On exchanged cations of the AgX zeolite, the half-widths of the absorption bands ν_{12} , ν_2 and ν_3 for ethene molecules adsorbed on this zeolite are equal to 12.5 and 4 cm⁻¹, respectively (Figure 5.11), indicating the absence of rotation of the molecules in this case. The presence of

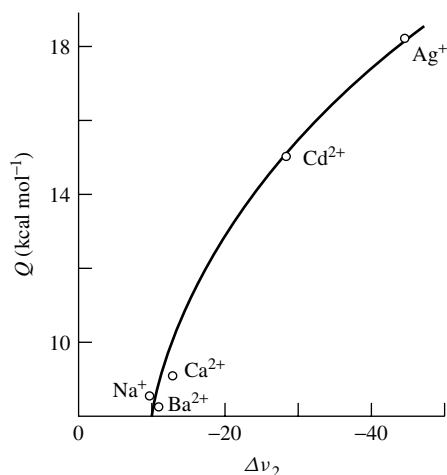


Figure 5.10. Relationship between the heat of adsorption of ethene and the shift in the frequency $\Delta\nu_2$ of the absorption band of the symmetric stretching vibration along the C=C bond for zeolites with different exchange cations [1201]. Reprinted with permission from Carter, J. L., Yates, D. J. C., Lucchesi, P. J., Elliott, J. J. and Kevorkian, V., *J. Phys. Chem.*, **70**, 1126–1132 (1966). Copyright (1966) American Chemical Society.

Table 5.3. Frequencies of the absorption bands of vibrations of ethylene molecules adsorbed on faujasite-type zeolites and their shifts with respect to the spectrum of the gas [1201]. Reprinted with permission from Carter, J. L., Yates, D. J. C., Lucchesi, P. J., Elliott, J. J. and Kevorkian, V., *J. Phys. Chem.*, **70**, 1126–1132 (1966). Copyright (1966) American Chemical Society.

Exchange cation	ν_2	$\Delta\nu_2$	ν_3	$\Delta\nu_3$
Ag $^+$	1578	-45	1320	-22
Cd $^{2+}$	1594	-29	1310	-32
Li $^+$	1614	-9	1340	-2
Na $^+$	1613	-10	1339	-3
K $^+$	1615	-8	1340	-2
Ba $^{2+}$	1612	-11	1339	-3
Ca $^{2+}$	1610	-13	1339	-3

two absorption bands of the vibration ν_3 at 1318 and 1310 cm^{-1} indicates that there are two forms of bonding between the molecules and the zeolite.

The differences in the strength of the bond between the adsorbed ethylene molecules and the Ag $^+$ cations is probably due to steric hindrances for the attainment of the most favorable arrangement for chemisorption. There is a correlation between the heat of adsorption and the shift in the adsorption band of the stretching vibration of the double bond (see Figure 5.10). The increase in the heat of adsorption of the series of zeolites with exchange cations Ba $^{2+}$, Na $^+$, Ca $^{2+}$, Cd $^{2+}$ and Ag $^+$ is accompanied by an increase in the shift of the ν_2 frequency. This shift and the heat of adsorption are especially high in the case of ethene adsorption on the CdX and AgX zeolites. According to Carter *et al.* [1201], the shift in the absorption band ν_2 of ethylene adsorbed on the AgX zeolite (52 cm^{-1}) is larger than the corresponding shift in the complex of ethylene

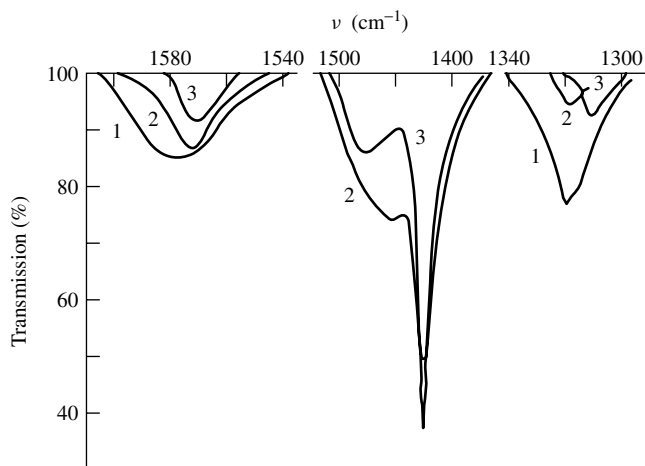


Figure 5.11. Spectrum of ethene adsorbed on the AgX zeolite: (1) pressure of ethene in cell, 109 torr; (2) after evacuation for 5 min at 298 K; (3) after further evacuation at 373 K for 15 min [1201]. Reprinted with permission from Carter, J. L., Yates, D. J. C., Lucchesi, P. J., Elliott, J. J. and Kevorkian, V., *J. Phys. Chem.*, **70**, 1126–1132 (1966). Copyright (1966) American Chemical Society.

with silver fluoroborate (38 cm^{-1}), indicating the greater stability of the complex adsorbed on zeolite. The high heats of adsorption of olefins and their decreases with an increasing radius of the cation, show that the principal interaction is that between the π -bond and the cations.

The π -complexes of both ethene and propene with copper and silver cations, which are well known in the homogeneous phase, were investigated in more detail in the case of the zeolites Cu(I)Y and Ag(I)Y [759, 1205]. Both ethene and propene are stronger adsorbed on Cu(I)Y when compared with Cu(II)Y.

Forster and co-workers [1206–1208] observed two different C=C absorptions for π -complexes when adsorbing 1-butene on A-type zeolites depending on the site of adsorption of the olefin. Propene adsorption energies on different sites of the zeolite has been obtained by Kirichi *et al.* [1209].

Oxides

In the 1980s, due to the use of the more sensitive Fourier-transform IR method, more reliable data about olefin complexation (π -complexes) on oxide surfaces appeared in the literature. The first reliable results were reported by Davydov [30], where it was established that upon the interaction of the majority of oxide systems with olefins several surface compounds characterized by absorption in similar regions are simultaneously formed. These compounds are formed at different surface centers. It is impossible to observe the whole spectrum of such surface complexes, because of the overlap with the spectrum of the adsorbent. This prevents the obtaining of information about the structure of the surface complexes in some cases. However, this author has developed criteria (both needed and sufficient) for reliably identifying the complexes formed on the oxide surfaces, on the basis of the main role of the nature and properties of the surface centers, in the case of π -complex formation in numerous systems. We will examine the typical case of the formation of the olefin complexes on oxide surfaces when only one type of the complex predominates.

Davydov and Efremov have examined the interaction of ethene with the oxidized surface of titanium dioxide (anatase) as a typical example of ethene π -complex formation. Such an interaction at 293 K is mediated by Ti^{4+} ions [1210, 1211]. The spectrum can be analyzed to a

Table 5.4. Infrared absorption band frequencies for gaseous ethene and ethene adsorbed on TiO₂.

$\nu(\text{cm}^{-1})$		Assignment	$\nu(\text{cm}^{-1})$		Assignment
C ₂ H ₄ (gas)	C ₂ H ₄ (adsorbed)		C ₂ H ₄ (gas)	C ₂ H ₄ (adsorbed)	
3105	3110	ν_{CH}	1623 ^a	1615	$\nu_{\text{C}=\text{C}}$
	3020		1444	1440	δ_{asCH_2}
2990	2980		1342 ^a	1340	δ_{sCH_2}

^aActive in Raman spectrum.

good approximation with regard to the MC₂H₄ fragment which has a lower local C_{2v} symmetry than that of free ethene (D_{3h}). For this reason, vibrations forbidden for the free ligand ($\nu_{\text{C}=\text{C}}$ and δ_{sCH_2}) become active for the MC₂H₄ fragment (Table 5.4). Adsorption of propene gives rise to a π -complex ($\nu_{\text{C}=\text{C}}$ at 1635 cm⁻¹ for C₃H₆ and 1575 cm⁻¹ for C₃D₆) with the participation of Ti⁴⁺ ions. The loosening of the C=C bonds (small $\nu_{\text{C}=\text{C}}$ decrease) of ethene and propene adsorption complexes and their low stabilities (decomposition on desorption at room temperature) points to a weak donor–acceptor interaction between the titanium ions and alkenes. For TiO₂, the use of the FTIR technique [1212] allowed the differentiation of two types of propene π -complexes with surface Ti⁴⁺ ions.

Spectral characteristics of ethene and propene in their adsorption π -complexes with Na⁺, Ca²⁺, Ni²⁺, Co²⁺, Ag⁺ and Cu⁺ ions are presented in Tables 5.5 and 5.6, respectively. It is shown that the stretching and deformation C–H vibrations of all types are present in the spectra of these complexes, with their positions being slightly different from those of the corresponding vibrations of gaseous alkenes (the maximum difference is 10–30 cm⁻¹). The greatest shifts (to low values) during adsorption are observed for bands associated with the $\nu_{\text{C}=\text{C}}$ stretching vibrations, which indicates once again the involvement of alkene π -orbitals in bonding with the cation. The π -complexes of ethene and propene with the ions under consideration differ in both the $\nu_{\text{C}=\text{C}}$ and binding energy values [30, 759, 1211], i.e. a greater $\nu_{\text{C}=\text{C}}$ decrease corresponds to a stronger bond when compared with free alkenes (Table 5.7). This means that the binding energy and the $\pi_{\text{C}=\text{C}}$ decreases in alkene adsorption π -complexes are determined by the nature of the stabilization site.

The same is shown by the $\nu_{\text{C}=\text{C}}$ values for ethene and propene π -complexes (both adsorption and matrix-isolated types) with metals of different valence states and nature, as shown in Tables 5.8 and 5.9. For transition metals, $\nu_{\text{C}=\text{C}}$ increases with the decreasing oxidation state of the stabilization site. The binding energies (heats of adsorption) of adsorbed π -complexes increase in the same sequence (Table 5.7) [30, 759, 1211]. The possibility of the isolation of alkene complexes with metals and low-valence ions in the form of individual coordination compounds also indicates their high stabilities. With nontransition-metal ions, ethene and propene π -complexes show only slight shifts in $\nu_{\text{C}=\text{C}}$ and low binding energies. The effects observed can be rationalized by considering the nature of an alkene bond with an adsorption site in terms of the scheme shown in Figure 5.8. According to this scheme, alkene bonding with transition metals or their cations involves electron delocalization from the alkene π -bonding orbital to vacant orbitals of the stabilization site (donor–acceptor interaction σ -bond) and filled d-orbitals of the latter to the alkene π^* -orbital (dative interaction or π -bond). The $\nu_{\text{C}=\text{C}}$ decrease for π -complexes is determined by the sum of the contributions from σ - and π -bonding, which depends on the electron acceptor and donor properties of the adsorption site, respectively, and in particular, on the charge on the metal (the metal's ability to form a π -bond obviously decreases with increasing oxidation state). In this instance, the contributions of the π -bonding can almost be neglected for

Table 5.5. Frequencies (in cm^{-1}) observed in the IR spectra of gaseous molecules and adsorption π -complexes of C_2H_4 .

Vibration mode	C_2H_4	Na^+ (C_2H_4)	Ca^{2+} (C_2H_4)	Ni^{2+} (C_2H_4)	Ag^+ (C_2H_4)	Cu^+ (C_2H_4)
$\nu_{\text{as}}=\text{CH}_2$	3105	3100	3095	3115	3090	3090
$\nu_{\text{s}}=\text{CH}_2$	3026 ^a	–	3020	3005	3020	3030
$\nu_{\text{s}}=\text{CH}_2$	2988	2990	2990	2985	2990	2990
$\nu\text{C}=\text{C}$	1623 ^a	1613	1610	1613	1570	1545
$\delta_{\text{as}}=\text{CH}_2$	1444	–	–	1440	1430	1430
$\delta_{\text{s}}=\text{CH}_2$	1342 ^a	1339	1339	1340	1331	–

^aActive in Raman.**Table 5.6.** Frequencies (in cm^{-1}) observed in the IR spectra of gaseous molecules and adsorption π -complexes of C_3H_6 and C_3D_6 .

Vibration mode	C_3H_6	Cu^+ (C_3H_6)	Ni^{2+} (C_3H_6)	Co^{2+} (C_3H_6)	C_3D_6	Cu^+ (C_3D_6)	Ni^{2+} (C_3D_6)	Co^{2+} (C_3D_6)
$\nu_{\text{as}}=\text{CH}_2$	3090	3080	3080	3080	2331	2330	2330	–
$\nu=\text{CH}$	3013	3010	3010	3005	2240	2245	2245	2245
$\nu_{\text{s}}=\text{CH}_2$	2991	2990	2975	2985	2224	2230	2220	2220
$\nu_{\text{as}}\text{CH}_3$	2954	2970	2960	2960	2204	–	2205	2205
$\nu_{\text{s}}\text{CH}_3$	2932	2930	2930	2930	2130	2130	2130	2130
$\nu_{\text{s}}\text{CH}_3$	2871	–	2860	2860	2090	2080	2070	–
$\nu\text{C}=\text{C}$	1650	1550	1630	1635	1590	1460	1570	1575
$\delta_{\text{as}}=\text{CH}_3$	1470	1460	1460	1460	1061	–	1055	1055
$\delta_{\text{as}}=\text{CH}_3$	1440	1440	1440	1440	–	–	–	–
$\delta=\text{CH}_2$	1420	1410	1420	1420	–	–	–	–
$\delta_{\text{s}}=\text{CH}_2$	1378	1380	1380	1380	–	–	–	–

Table 5.7. Positions of $\text{C}=\text{C}$ stretching frequencies (cm^{-1}) and binding energies (kJ mol^{-1}) in adsorption π -complexes of propene and ethene.

Adsorbent	Adsorption site	$\text{C}=\text{C}$ in C_3H_6	Q_{ads}^a in C_3H_6	$\text{C}=\text{C}$ in C_2H_4	Q_{ads}^a in C_2H_4	Number of active sites per g
TiO_2	Ti^{4+}	1635	54	1615	50	6.56×10^{19}
$\text{CoO}-\text{MgO}-\text{MoO}_3$	Co^{2+}	1635	54	–	50	3.30×10^{19}
$\text{NiO}-\text{MgO}-\text{MoO}_3$	Ni^{2+}	1630	54	1613	48	4.56×10^{19}
ZnO	Zn^{2+}	1625	55	1600	51	8.10×10^{18}
$\text{Ag}_2\text{O}/\text{Al}_2\text{O}_3^b$	Ag^+	1595	59	1570	54	9.60×10^{19}
$\text{Cu}_2\text{O}/\text{Al}_2\text{O}_3$	Cu^+	1550	69	1545	67	6.66×10^{19}

^aDifferential heats of adsorption at coverages larger than $10\text{--}16 \mu\text{mol g}^{-1}$ with Q being constant.^bIndividual coordination complexes of Ag^+ with C_2H_4 and C_3H_6 have been isolated, with their spectral parameters being the same as those for the $\text{Ag}_2\text{O}/\text{Al}_2\text{O}_3$ system. Therefore, we consider Ag^+ ions as sites of ethene and propene adsorption in this system.

transition-metal ions of high charge such as M^{2+} (Tables 5.8 and 5.9), while alkenes stabilized on M^{2+} , M^{3+} , etc. may be considered to be σ -bonded. In fact, regarding the loosening of the $\text{C}=\text{C}$ bonds, and the binding energies, such complexes are similar to those of nontransition metals where σ -bonding alone is responsible for the alkene binding.

With low-valence transition metal ions, such as M^+ , the contribution of π -bonding becomes significant, as shown by calculations (EHM) of ethene π -complexes with Ag^+ [1213]. This should also enhance the σ -donating properties of alkenes [800], which is reflected in a greater weakening

Table 5.8. Positions of the C=C stretching frequencies (cm^{-1}) in ethene π -complexes with metals and their cations.

M		M ⁺		M ²⁺	
Cu	1475	Cu	1545	Cu	No stabilization
Ag	1476	Ag	1570	Zn	1600
Au	1476			Cd	1594
Ni	1497			Ni	1613
Pt	1498			Nontransition metals	
Rh	1499	Li	1614	Ca	1610
Pd	1502	Na	1613	Ba	1612
		K	1615		

Table 5.9. Positions of the C=C stretching frequencies (cm^{-1}) in propene π -complexes with cations.

	M ⁺		M ²⁺		M ³⁺ , M ⁴⁺
Cu	1550	Cu	No stabilization	Al ³⁺	^a 1635
Ag	1595	Co	1635	Al ³⁺	^b 1600
		Ni	1630	Ti ⁴⁺	1635
		Zn	1625	V ³⁺	1615

^aOctahedral.^bTetrahedral.

of the C=C bond (greater than the $\nu\text{C}=\text{C}$ decrease) and in a strengthening of the M^+ -alkene bond. With metals (M^0), π -bonding is predominant for the formation of the M^0 -alkene bond, as shown by calculations (EHM) of ethene π -complexes with Cu^0 [1214] and Ni^0 (X_α) [1215], which account for the greatest $\nu\text{C}=\text{C}$, decrease and the highest complex stability. Thus, π -bonding is essential for stabilization of alkene complexes and weakening of the C=C bond. The significance of the π -bonding for stabilization of alkene π -complexes can be seen by comparing the properties of ethene complexes with Li^+ , Na^+ , K^+ and Cu^+ . With the first three ions, which provide no π -bonding, the complex is weak (binding energy, ca. 35 kJ mol^{-1}) and the $\nu\text{C}=\text{C}$ shift is small ($\Delta\nu$ is about 10 cm^{-1}). In contrast, for Cu^+ ions, which provide π -bonding, the complex is strong (binding energy, ca. 67 kJ mol^{-1}) and the $\nu\text{C}=\text{C}$ shift is ca. 78 cm^{-1} .

Hence, the above considerations indicate that the properties of alkene π -complexes ($\nu\text{C}=\text{C}$ position and binding energy) depend on the nature of the adsorption site in the sense that the lower its oxidation state, then the greater are the $\nu\text{C}=\text{C}$ shifts and the binding energies for transition-metal complexes. The following estimates have been obtained for the position of the $\nu\text{C}=\text{C}$ stretching vibration for adsorbed π -complexes of alkenes with metals and cations (M^{n+}): $>1600 \text{ cm}^{-1}$ for $n > 2$, $<1500 \text{ cm}^{-1}$ for $n = 0$ and $1500\text{--}1600 \text{ cm}^{-1}$ for $n = 1$.

It appears that a diagnostic feature for the characterization of adsorbed π -complexes is the absorbance associated with the C=C stretching vibrations. This imposes a stringent requirement for the reliability of the assignment of the absorption bands assigned to $\nu\text{C}=\text{C}$, especially if there are several close bands in the IR spectrum (e.g. δCH vibrations or bands due to complexes of other types formed on the surface). The main criterion for the assignment of the bands of adsorbed alkenes to a particular type of vibration is the value of the $\text{CH} \rightarrow \text{CD}$ isotopic shift. The isotopic shift is 300–400 cm^{-1} for the deformation CH vibrations whose frequencies are close to $\nu\text{C}=\text{C}$ [14]; δCD for adsorbed C_2D_4 and C_3D_6 should not be higher than 1150 cm^{-1} .

The $\nu\text{C}=\text{C}$ stretching vibrations in C_3H_6 and C_2H_4 occur at 1650 and 1623 cm^{-1} , respectively, and shift to 1590 cm^{-1} for C_2D_4 (for C_3D_6 , $\Delta\nu\text{C}=\text{C} = 60 \text{ cm}^{-1}$) and to 1517 cm^{-1} (for C_2D_4 , $\Delta\nu\text{C}=\text{C} = 106 \text{ cm}^{-1}$) [14, 30]. Therefore, the isotopic shift values permit unambiguous differentiation between the vibrations associated with δCH and $\nu\text{C}=\text{C}$. An analysis of the $\nu\text{C}=\text{C}$ isotopic shifts in ethene and propene π -complexes indicates their dependence on the initial $\nu\text{C}=\text{C}$ position. For π -complexes with slight weakening of the $\text{C}=\text{C}$ bond (a slight decrease in $\nu\text{C}=\text{C}$), the $\nu\text{C}=\text{C}$ value remains close to that characteristic of gaseous alkenes. The shift increases with an increasing degree of weakening of the $\text{C}=\text{C}$ bond [30]. The increased isotopic shift for $\nu\text{C}=\text{C}$ in π -complexes, in comparison with that of the free olefin, can possibly be explained by consideration of the nature of the normal mode associated mostly with $\nu\text{C}=\text{C}$. As an example, let us consider the ethene molecule.

An analysis of the frequencies and forms of the normal vibrations of C_2H_4 [4, 14] suggests that the predominantly $\nu\text{C}=\text{C}$ normal mode includes contributions from the δCH and νCH vibrations, with the former being much greater than the latter. As a zero approximation (ignoring the interaction with δCH and νCH), $\nu\text{C}=\text{C}$ in ethene is calculated to be equal to 1550 cm^{-1} . The $\nu\text{C}=\text{C}$ interaction with νCH (occurring at about 3000 cm^{-1}) decreases the value to 1520 cm^{-1} , while interaction with δCH (at about 1400 cm^{-1}) increases this to the observed 1623 cm^{-1} [4]. Therefore, the predominantly $\nu\text{C}=\text{C}$ normal mode in the C_2H_4 molecule is mixed to a large extent with δCH . With C_2D_4 [14], the contribution of δCD (acting to increase $\nu\text{C}=\text{C}$) substantially decreases and that of νCD (acting to decrease the $\nu\text{C}=\text{C}$) increases, which forces the observed $\nu\text{C}=\text{C}$ in C_2D_4 to shift to 1517 cm^{-1} .

It is known [4] in the general case that the normal modes of a given group in a molecule are more group-characteristic in frequency (that is, mixed to a smaller extent with other vibrations) and the smaller is the difference between the intrinsic frequencies of this group taken in isolation and those of the remainder of the molecule. Therefore, as the frequencies of the $\text{C}=\text{C}$ stretching vibrations decrease upon complexation of C_2H_4 and C_2D_4 with metals and their cations due to donor-acceptor interactions (we denote this as the electronic factor), the contributions of δCH and νCH (δCD and νCD) to the observed $\nu\text{C}=\text{C}$ change in such a way that the contributions of δCH or δCD grow and reduce the decrease in $\nu\text{C}=\text{C}$ caused by the electronic factor. However, the sum of the δCH and νCH contributions for C_2H_4 is much greater than the sum of the contributions of δCD and νCD to C_2D_4 [14] and, therefore, a decrease in the observed $\nu\text{C}=\text{C}$ for alkene adsorption complexes should always be greater with deuterioalkenes than with the parent alkenes, with the difference being approximately equal to the δCH contribution to the observed $\nu\text{C}=\text{C}$.

The existence of a $\nu\text{C}=\text{C}$ isotopic shift for gaseous propene, indicating that this mode is also noncharacteristic, demonstrates that the same considerations hold for propene π -complexes (and also, apparently, for any alkene on replacement of H with D). It should be noted, however, that the frequency of this mode is more ' $\nu\text{C}=\text{C}$ -characteristic' for propene than for ethene (that is, mixed to a smaller extent with δCH and νCH), as shown by a smaller $\nu\text{C}=\text{C}$ isotopic shift for the parent molecule and the complexes. In summary, the $\nu\text{C}=\text{C}$ isotopic shifts for alkene π -complexes are sensitive to the nature of the adsorption sites and are greater than in the case of gaseous alkenes.

From the above discussion, the following criteria can be formulated for the identification of surface alkene π -complexes. First, the presence of absorption bands characteristics of the νCH and δCH vibrations of the adsorbed parent alkene (indicating a largely preserved molecular structure), with the largest possible changes observed in the bands attributed to $\nu\text{C}=\text{C}$, as assigned by using $\text{H} \rightarrow \text{D}$ isotopic shifts. Secondly, the existence of an interdependence between the $\nu\text{C}=\text{C}$ position, the $\nu\text{C}=\text{C}$ isotopic shift and the nature and stability of the adsorption site. If the νCH range is indistinguishable owing to poor transmittance, the $\nu\text{C}=\text{C}$ data are adequate to judge whether alkene π -complexes are present on the surface.

It should be noted that propene molecules stabilized on Zn^{2+} [1163], Ni^{2+} or Co^{2+} [1216] ions (propene π -complexes) also form hydrogen-bonds with those surface OH groups whose frequencies become perturbed. No such perturbations occur in the case of ethene which can be accounted for by the smaller size of ethene when compared with propene, and the presence of an allylic CH_3 group in the latter whose hydrogen is much more mobile than that of an ethene CH_2 group. Since in the case of ZnO [1163] (a more basic OH group, whose oxygen atom also acts as a proton acceptor, is involved in hydrogen-bonding) and for $NiO-MgO-MoO_3$ and $CoO-MgO-MoO_3$ [1216], substantial perturbations of the rocking vibrations of the CH_3 group are observed, and hydrogen-bonds seem to be formed between the hydroxyl and/or surface oxygen and hydrogen of the π -complex CH_3 group during propene adsorption. Coordination of propene by a metal ion appears to facilitate hydrogen-bonding (via the increasing mobility of the CH_3 -group proton), since no hydrogen-bonding (e.g. on ZnO) is observed after the blocking of metal ions with CO_2 [1163].

Since $\nu_{C=C}$ in deuterioalkenes is more group-characteristic than in alkenes, a $\nu_{C=C}$ decrease in the π -complexes of the former will reflect the strength of interaction (heat of adsorption) more accurately (i.e. the $\nu_{C=C}$ decrease due to the electronic factor), especially with ions capable of appreciable dative interactions.

The experimental data shown in Table 5.7 indicate the existence of a linear relationship between the $\nu_{C=C}$ decrease for adsorbed π -complexes of deuterioalkenes (ethene and propene) and their binding energy (heat of adsorption) (Figure 5.12), with a $\nu_{C=C}$ shift of 100 cm^{-1} corresponding to ca. 2 kJ mol^{-1} . The $\nu_{C=C}$ decrease for adsorbed π -complexes is a maximum for M^0 and reaches about 200 cm^{-1} for C_2D_4 [1217], when the binding energy is about 80 kJ mol^{-1} [759].

Hence, the data obtained indicate that the spectral parameters in the $\nu_{C=C}$ stretching region can be used successfully to determine the complex-forming ability of cations on oxide surfaces, i.e. the relative strength of the Lewis acid sites on the surfaces of catalysts. It should be taking into consideration, however, that the extinction coefficient of the $C=C$ bond is less than that of the CO bond so that sometimes the $\nu_{C=C}$ is difficult to observe [30].

An important parameter for catalysts is the number of active sites on the surface capable of activating molecules. The number of ions on the surface capable of coordinating alkenes oxide surfaces can be calculated from the adsorption data given in Table 5.7. An analysis shows that only 10 % of the cations on the surface are capable of coordinating alkenes. This is in a good agreement with data on carbon monoxide adsorption.

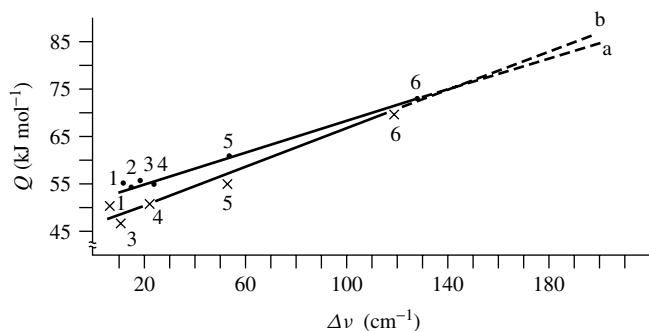


Figure 5.12. The relationship between the $\nu_{C=C}$ decrease ($\Delta\nu$) and the binding energy (Q) for surface π -complexes of (a) deuterioethene and (b) deuteriopropene with (1) Ti^{4+} ; (2) Co^{2+} , (3) Ni^{2+} , (4) Zn^{2+} , (5) Ag^+ , (6) Cu^+ ions.

From the beginning of 1984, the systematic investigation of the complexation of unsaturated hydrocarbons on oxide surfaces were carried out by the Italian scientists G. Busca and V. Lorenzelli and their co-workers [1156, 1194–1196, 1218, 1219]. In general, the concepts of these authors about the character and spectral manifestations of the olefin adsorption on oxides are close to those developing in the studies of Davydov *et al.* [30, 759, 1163, 1210, 1211, 1216]. Additionally, they tried to analyze with more detail the changes of the C–H bonds due to adsorption. It has already been examined above that the hydrogen-bonding interactions between unsaturated hydrocarbons (see above) and surfaces having active hydroxy groups, like amorphous silica, zeolites, and Al/Si, are observed, but for some transition-metal-oxide surfaces (TiO₂, ZrO₂, Fe₂O₃ and ZnO), the interaction is thought to occur with the coordinatively unsaturated cationic centers (Tables 5.10 and 5.11). It should be noted that the spectral regions of the bond vibrations in these complexes are overlapped (Table 5.10), and in the case of the simultaneous presence on the surface of these complexes, their differentiation is problematic.

Particularly stable ethene complexes are easily detectable, even at room temperature in the latter cases. Bands that are only Raman-active in the gas-phase molecule become activated (namely CH stretching and C=C stretching for ethene) and are shifted towards lower frequencies as was observed earlier by many other authors for such systems.

The CH₂ out-of-plane bending absorption shifts upwards by a large amount and is also much strengthened in intensity (see Table 5.1). It has been shown that there is a clear parallelism between the shift upwards of the modes ν_7/ν_8 , the shift downwards of ν_2 ($\nu_{C=C}$), and the increase of both the $A_{\text{def}}/A_{\text{str}}$ and $A_{\text{impl}}/A_{\text{str}}$ ratios for ethylene complexes on the surface OH groups (SiO₂ and HY) and on the cation centers of transition metals (see Table 5.2). This indicates that in all cases an interaction occurs that withdraws electron from the ethene molecule without a substantial loss of its planarity, due to the still relatively small overall spectral modification. After numerous studies by Davydov with co-workers [30], Busca, Lorenzelli and their co-workers established that the features of the surface complexes of ethene or propene on these transition-metal oxides are definitely different from those of π -bonded species detected on metal surfaces [1220–1224], as well as those of ethene–metal complexes well known in homogeneous complexes such as the so-called Zeise's salt [15] (see Table 5.10).

In all cases of the formation of π -complexes, the symmetry of the ethene molecule is thought to be lowered, due not only to the presence of the coordinated metal atom, but also to the bending of the C–H bonds only from the plane of the ethylene molecule, possibly partially due to the interaction with surface oxygen. This results in a strong shift downwards for ν_2 (C=C stretching) and of the coupled ν_3 (CH₂ in-plane bending) [1156].

Intensive consideration of the ethene complexes at the surface of the Cu(I)/TiO₂ catalyst (Table 5.10) provided evidence that in this case the proton charge on the hydrogens is much smaller than in the case of ethene adsorbed on other transition-metal oxides, implying the importance of electron flow from the metal center to the ethene molecule. This back-bonding interaction is nonexistent in the case of adsorption on TiO₂, ZrO₂ and ZnO (as expected because Ti⁴⁺ and Zr⁴⁺ are d⁰ cations and Zn²⁺ is d¹⁰ and does not back-bonds with adsorbed CO either and is negligible also on Fe₂O₃, as has been established for $\nu_{C=C}$ [30]. As for the 1265 cm⁻¹ band, its assignment to the $\nu_{C=C}$ in the complex of ethene with Cu⁺ ions (Table 5.10) given in [1156] seems to be incorrect. In light of the examined above studies, the band at 1534 cm⁻¹ (assigned by Busca and co-authors to the $\delta(\text{CH}_2)$) can be referred more probably to the $\nu_{C=C}$.

The formation of two types of both ethene and propene π -complexes on Fe₂O₃ (Tables 5.10 and 5.11) has been proposed by Busca *et al.* [1156, 1218, 1219]. Propene adsorbed on iron oxide (Figure 5.13) shows two sharp bands connected with C=C stretching vibration at 1638 and 1604 cm⁻¹, while the C–H deformation vibrations, (1500–1350 cm⁻¹) are very similar to those of the gas phase and the C–H stretching vibrations are very weak, practically undetectable. The

Table 5.10. Observed frequencies (cm^{-1}) and assignments of adsorbed ethene.

Vibration	Assignment	Symmetry		Gas		Adsorbed on ^d						ErCuCl
		IR	R	SiO ₂ H	TiO ₂ C	C	ZrO ₂ H	Fe ₂ O ₃ C	Cu(II)TiO ₂ C			
ν_9	$\nu_4\text{CH}_2$	3105	—	3097	3101	3104	3098	3080	—	3076 (R)		
ν_5	$\nu_5\text{CH}_2$	—	3083	—	—	—	—	—	—	3036 (R)		
$\nu_2 + \nu_{12}$	$\nu\text{C}=\text{C} + \delta\text{CH}_2$	3067 ^b	—	3069	3060	3079	3070	3065	3065	3059 (R)		
ν_1	$\nu_5\text{CH}_2$	—	3021	3010	3010	3008	3010	2997	2976	2976 (R)		
ν_{11}	$\nu_8\text{CH}_2$	2989	—	2978	2960	2978	2977	2975	2928	2924 (R)		
$\nu_7 + \nu_8$	2wCH ₂	1888	—	1922	1960	1975	1905	1960	1880	—		
ν_2	$\nu\text{C}=\text{C}$	—	1625	1618	1612	1610	1620	1618	1265 ^b	1275 ^b		
ν_{12}	δCH_2	1443	—	1441	1446	1445	—	1439	1423	1411		
ν_3	δCH_2	—	1343	1340	1341	1341	—	1340	1534 ^c	1533 ^c		
ν_4	tCH ₂	(1023) ^d	—	—	—	1048	—	—	1059	811		
ν_7	wCH ₂	949	—	—	—	1008	975	990	—	940		
ν_8	wCH ₂	—	943	—	—	—	—	975	—	960		
ν_{10}	rCH ₂	826	—	—	—	—	—	—	—	—		

^aC, coordinated; H, hydrogen-bonded.^bSolid.^cStrongly coupled modes.^dInactive.

Table 5.11. Observed frequencies (cm^{-1}) and assignments of adsorbed propene.

Vibration	Assignment	Symmetry ^a	Gas	Adsorbed on					$\text{C}_3\text{H}_6\text{PtCl}_3$
				SiO_2	Fe_2O_3	TiO_2	ZrO_2	Cu(I)TiO_2	
ν_1	$\nu_s\text{CH}_2$	a'	3091	3083	3080	3080	3078	3065	3068
Combined				3067	–	3058	3050	3030	3034
ν_2	νCH	a'	3017 ^b	3008	3000	3008	3005	–	3010
ν_3	$\nu_s\text{CH}_2$	a'	2991	2979	2977	2976	2975	2965	2971
ν_4	$\nu_s\text{CH}_3$	a'	2973	2972	2977	2976	2975	–	2965
ν_{15}	$\nu_s\text{CH}_3$	a''	2953	2950	2950	2953	2955	2949	2965
ν_5	$\nu_s\text{CH}_3$	a'	2932	2925	2918	2925	2923	2920	2911
$2\nu_7$	$2\delta_s\text{CH}_2$	–	2892	2894	–	2893	2870	2886	–
$2\nu_{16}$	$2\delta_s\text{CH}_2$	–	2868	2859	–	2853	–	2854	–
$2\nu_{19}$	$2w\text{CH}_2$	–	1829	1832	–	1885	1885	–	–
ν_6	$\nu\text{C}=\text{C}$	a'	1653	1640	1628	1629	1630	1539 ^d	1504 ^d
						1615	1621		
ν_7	$\delta_s\text{CH}_3$	a'	1458	1455	1455	1454	1451	1455	1449
ν_{16}	$\delta_s\text{CH}_3$	a''	1442	1439	1430	1442	1432	1437	1429
						1432			
ν_8	δCH_2	a'	1414 ^c	1416	1415	1416	1412	1302	1392
ν_9	$\delta_s\text{CH}_3$	a'	1378	1378	1377	1373	1372	1374	1365
ν_{10}	$\delta=\text{CH}$	a'	1298	–	–	1303	1302	1256 ^d	1252 ^d
ν_{11}	$r\text{CH}_2$	a'	1170	–	1178	1175	1172	1160	1175
ν_{17}	$r\text{CH}_3$	a''	1045	–	1042	–	1050	1040	1049
ν_{18}	$t\text{CH}_2$	a''	990	–	1002	–	1010	–	1010
ν_{19}	$w\text{CH}_2$	a''	912	–	940	–	950	–	995

^a a' , symmetric; a'' , asymmetric.^bTheoretical value.^cLiquid.^dStrongly coupled modes.

band at 1638 cm^{-1} readily disappears by short evacuation at room temperature. The more strongly held species interact with a cationic site via a π -bond ($\nu\text{C}=\text{C}$, 1604 cm^{-1}). Analysis of both of the C–H stretching deformation vibrations, according to the author's opinion, indicates that the olefin molecule essentially retains its planarity, as has already been observed for chemisorbed ethene [1218], without the out-of-plane bending mode usual in metal–olefin organometallic complexes. The lowering of $\nu\text{C}=\text{C}$ in the less strongly adsorbed species (12 cm^{-1}) may be associated with a second chemisorbed species, possibly interacting with a more oxidized center, where back-bonding is smaller or even absent. In their opinion, the $\nu\text{C}=\text{C}$ band (1638 cm^{-1}) is, more probably, from a complex which is H-bonded with surface oxygen (from CH_3 to O or from OH).

On TiO_2 , similar to the reported by Efremov and Davydov [1210], a single chemisorbed species of propene was observed and characterized by a rather strong $\nu\text{C}=\text{C}$ band at 1619 cm^{-1} (Figure 5.13). However, the strong intensity of the $\nu\text{C}–\text{H}$ bands from the methyl group, as well as a remarkable enhancement of the corresponding deformation frequencies, in the author's opinion, is connected with an out-of-plane bending of the bonds attached to the double bonds, and an enhanced polarization of the CH_3 group (Table 5.11).

The low-temperature interaction of ethene has also been investigated for metal oxides (MgO , CaO and NiO [1156]) with a rock-salt structure whose surface chemistry appears to be dominated by their behavior as bases, with a very small role attributed to surface cationic centers. The latter are, however, still able to interact with electron-donor molecules like carbon or

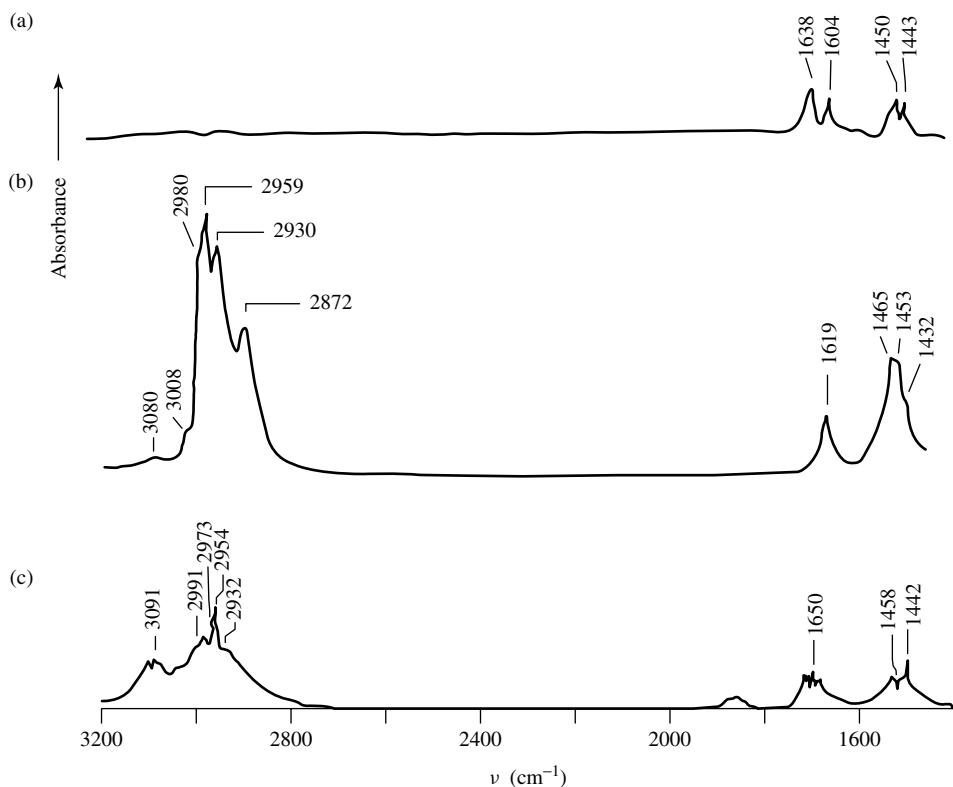


Figure 5.13. FTIR spectra of propene adsorbed on (a) α -Fe₂O₃, and (b) TiO₂ at room temperature, and (c) propene gas (Background spectra of the adsorbents were automatically subtracted) [1156]. Reproduced with permission from Busca, G., Marchetti, L., Zerlia, T., Girelli, A., Sorlino, M. and Lorenzelli, V., *Proceedings of the 8th International Congress on Catalysis*, Berlin (1984), Vol. 3, III299–III310, by permission of DECHEMA.

nitrogen monoxides. Interaction of these surfaces with ethene is indeed extremely weak and is only detectable at temperatures around 150 K. These adsorbed species are characterized by well-detectable IR spectra (see Table 5.1) where, together with the modes that are IR-active in the gas phase, some Raman modes are also weakly activated. In particular, ν_1 (CH_{str}) and ν_3 (CH₂ in-plane deformation) bands are weakly observed, while the ν_2 (C=C_{str}) band cannot be observed at all. Small but definite shifts of the vibrational modes can also be seen (Table 5.1), with the most evident being that of the CH₂ out-of-plane bending mode that shifts upwards by 20 cm⁻¹ on the NiO surface, where such perturbations are the greatest. These shifts seem to be sufficient to determine that these species are true adsorbed forms, excluding the alternative of a condensed ethene phase. In these cases, the region of the ν_7 and ν_8 out-of-plane vibration modes is sufficiently transparent that the intensity ratio between the total stretching and total bending modes becomes available. This ratio does not change very much in the cases of ethene adsorbed on rock-salt-type metal oxides compared to the gas, indicating that the positive charge on hydrogen is not significantly enhanced by adsorption on such oxides, and hence that electron withdrawal from the molecule to the surface is very small. The nature of these complexes is not yet fully established. It may be that both weakly bound π -complexes with surface cations and complexes with H-bonding with the surface OH groups are present.

Although the data for both ethene and propene adsorbed over oxides have been presented by Busca *et al.* [1219], these authors have examined only their own results, in spite of the fact, that most of these are repeat (analogous) data from other researchers, and draw conclusions which essentially coincide with those already published. Thus, the conclusions concerning the formation of weakly bound π -complexes of olefins with only a σ -type electron donor bond with cations in the highest degree of oxidation (Ti^{4+} and Zr^{4+}) (these have no analogies in organometallic chemistry), as well as the formation of surface alcoholates upon hydrogenation of the C=C bond by H^+ ions, had been published earlier by Davydov and co-workers [30, 456, 473, 748, 759, 1050, 1087, 1151, 1163, 1167, 1168, 1186, 1202, 1203, 1210].

Upon adsorption of ethene on oxidized samples of Cu/ZnO, the formation of non-dissociatively adsorbed species weakly bound to the surface Zn(II) cations (and, possibly, Cu(II)), which are reversible to evacuation at room temperature (bands at 1000, 1440, 1605, 2980 and 3060 cm^{-1}) [1225] are mainly observed. On reduced samples, the π -complexes are also formed, in these authors' opinion, onto copper metal particles (bands at 920, 1290 and 1550 cm^{-1}) and also on Zn(II) ions (bands at 1000, 1440, 1605, 2980 and 3060 cm^{-1}) but in lower concentrations than in the case of oxidized samples. However, according to the data mentioned above, the bands at 920, 1290 and 1550 cm^{-1} characterize more probably a π -complex stabilized on Cu(I).

The more complex alkenes form the same complexes. However, the energy of their bonding to the surface is different because of their higher reactivity. Moreover, the data obtained for the complex molecules are not as definite as those of ethane or propene.

1-butene may also form π -complexes upon adsorption on oxide surfaces. Their infrared spectra have been characterized by Burfield [1226] and Rozhkova *et al.* [1227] and show the formation of carboxylates on the catalysts that favored total oxidation, and π -complexes on the catalysts of partial oxidation (bands in the region $1600\text{--}1650\text{ cm}^{-1}$).

Interaction of olefins with V-P-O systems, which are the typical catalysts of the partial transformation of butane to maleic anhydride (through the formation of olefinic-like intermediates), have also been studied in detail [1228–1232]. Upon the interaction of butadiene (one of the key intermediates in this transformation) with SiO_2 , the symmetry of the molecule decreases, as follows from spectral data, due to physisorption giving rise to a *s-trans* \rightarrow *s-cis* conformational change. Moreover, the symmetry of the molecule is not significantly perturbed, as deduced from the strong IR detection of all (and only) the frequencies that are IR-active in the gas. Some forbidden bands are weakly activated as in the case of C=C stretching of physisorbed C_2H_4 . The spectrum of 1,3-butadiene adsorbed on hydroxylated $\gamma\text{-Al}_2\text{O}_3$ is also similar to that of the gas (like *s-trans* butadiene). However, the data obtained and conclusions drawn for the interaction of the V-P-O catalysts with olefins are still limited. Thus, Wenig and Schrader [1229] believe that 1,3-butadiene seems to be adsorbed on the V-P-O catalysts at 423 K in two different states: (i) both C=C double bonds form a π -complex with the surface, and (ii) a 1,4-addition complex via σ -bonds. It is more probable, according to these data, that the second species corresponds to a compound resembling the reaction product, i.e. that it contains the C=O bond (the band at 1680 cm^{-1}). The role of the surface protic acidic centers for such catalysts in the activation of olefins has not yet been explained. As was shown above for the 1,3-butadiene interaction with $\text{V}_2\text{O}_5/\text{Al}_2\text{O}_3$, protic centers can lead to the formation of carbenium ions.

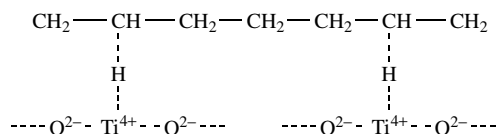
It was found that 1-butene adsorbed at 373 K on the V-P-O catalyst forms two different π -complexes but the formation of carboxylates can be neglected. However, the nature of these complexes are not clear. Some authors have called them ' π -like-complexes', although there were no $\nu=\text{CH}$ bands observable in the spectrum.

Ethylidene complexes

In recent studies of ethene adsorption on oxides (for example, ZrO_2 , [1233]), the formation of complexes similar to those formed upon the adsorption of ethene over metals, the so-named

'ethylidene complexes' ($\text{CH}_3\text{-CH}=\text{M}$), have been supposed. The weak band at 2750 cm^{-1} revealed in the spectrum, together with the absorption bands characteristic of H-bonded and π -complexes, has been assigned to σ - π -bound C_2H_4 , as identified by a band at 1338 cm^{-1} , bound by the H-bond with the metal cation of the surface (di- σ -bound ethene has not been observed). Although in the case of oxide catalysts, the formation of such bonds with surface oxygen is usual, there are data supporting the formation of σ - π -bound C_2H_4 . Zecchina and co-workers [1234] were the first to report an infrared spectroscopic study of ethylene polymerization over a chromia/silica catalyst, which included the observation of a weak and broad adsorption centered near 2750 cm^{-1} . This band was assigned to the νCH vibration of a $=\text{CH}$ end-group of the polymer located at the surface of the catalyst with the structural formula $\text{Cr}^{n+}=\text{CH}-[\text{CH}_2]_n-\text{CH}_3$.

Sheppard and co-workers [1199], studying by infrared spectroscopy a spontaneous polymerization of ethene on sulfate-containing TiO_2 (anatase) also showed that there is some evidence for an alkylidene surface end-group of the polymer and for substantial perturbation of the CH_2 groups of the polymer chain by interaction with the oxide surface:



Scheme 5.9

They proposed an alternative assignment for this band which was based on such a hydrogen-bond-type perturbation of CH groups along the polymer chain through interaction with the electron-deficient Ti^{4+} ions on the surface of anatase. This is schematically represented in Scheme 5.9. An additional band at 2900 cm^{-1} may be assigned, on the authors' opinion, to the free-CH of the hydrogen-bound CH_2 group in the above scheme. In the case of ZrO_2 , a polymerization mechanism due to H^+ , similar to that examined for TiO_2/SO_4 , also cannot be denied because the presence of SO_4^{2-} ions in ZrO_2 is explained by the presence of BACs [1235].

5.1.4 INTERACTION WITH CATION-ANION PAIRS

Allylic complexes

The interaction of alkenes with solid surfaces may lead to partial or complete dissociation of the C-H bond. Two alternative mechanisms of this interaction are possible, involving either a homolytic or a heterolytic activation with the formation of a carbocation (carbenium ion) or a carbanion. As expected [30, 82, 1236-1240], heterolytic dissociation with protonation by the action of the nucleophilic center is more probable with catalysts that contain positive and negative ions (ion pairs such as $\text{M}^{n+}\text{O}^{2-}$). The resulting ion can be stabilized by the π -electrons of the double bond (π -allylic complexes), by a C-M^{n+} σ -bond (σ -allylic complexes), or by both types of bonding (dynamic allyl or μ -allyl). It is almost impossible to evaluate the contribution of each particular bonding type owing to the lack of information about the spectral properties of such complexes on the surface. Therefore, following Davydov [30], we use the term ' π -allylic complex' for the bond formed mainly by the π -electrons of the double bond (involving a significant degree of weakening of the $\text{C}=\text{C}$ bond and a large $\nu\text{C}=\text{C}$ decrease) and the term ' σ -allylic complex' for the bond formed mainly by the σ -electrons at the carbon atom.

The formation of allylic species (that is, $\text{M}(\text{CH}_2\text{=CH}\equiv\text{CH}_2)$) has been proposed in numerous studies, see for example [30, 1148-1151, 1241-1254], and these structures have been suggested

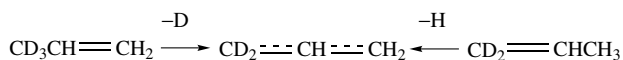
as intermediates in the partial oxidation reactions of olefins. However, its occurrence has not been proved for any hydrocarbons containing a triple bond [18]. Thus, complexes of this type have not been considered here. It can be mentioned that the individual σ -allylic compounds show absorbances in the δCH and νCH regions which are close to those observed for π -allylic compounds [30, 1148–1150], except that $\nu\text{C}=\text{C}$ for σ -allyl species occurs at 1600–1630 cm^{-1} , substantially higher than for π -allyls. The degree of weakening of the $\text{C}=\text{C}$ bond depends only slightly on the substrate (cations of different nature or, more particularly, variation of the anion). The formation of an allylic structure on the surface should lead to the simultaneous appearance of absorbance in the $\nu\text{C}=\text{C}$ region, a lack of CH_3 -group vibrations and with the appearance or growth of the bands attributed to surface hydroxyls. It is necessary to obtain data on the involvement of the metal cation in complexation with alkenes (e.g. by replacing it with a more weakly bound probe molecule), as complexes with similar absorbances in the $\nu\text{C}=\text{C}$ stretching region can also be formed with oxygen on the oxide surface. Unfortunately, no spectra of individual deuterated metal σ -complexes are available in the literature, to permit the $\Delta\nu\text{C}=\text{C}^{\text{H-D}}$ values to be estimated for σ -allylic metal complexes, although one can expect them to be close to the isotopic shifts for alkenes.

Much fewer spectral data are available for π -allylic adsorption complexes compared with those for π -complexes, because the formation of the former requires the presence of optimum ion pairs (in respect to both energy and geometry) [473, 1253] capable of $\text{C}-\text{H}$ bond cleavage in the alkene CH_3 group. In addition, alkenes, as has been noted, undergo more complete destruction on the majority of oxide systems, so not allowing unequivocal spectral identification of the intermediate allylic complexes. Therefore, studies of adsorption of alkenes resulting in major decompositions (nor those involving allyl formation) at room temperature are not considered here.

Although reliable identification of π -allylic complexes has been made only for ZnO [386, 1150, 1163, 1250], Al_2O_3 [473, 1087], MgO [1251, 1252, 1262], and Cu^{2+} -containing systems [1149, 1241, 1253], some additional conclusions concerning the spectral properties of such compounds can also be made.

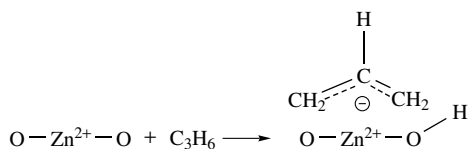
ZnO

Absorption bands at 1545 and 1202 cm^{-1} in the spectra of adsorbed propene characterize a complex stable at temperatures as high as 373 K which results from stronger, dissociative adsorption of propene in the form of a π -allylic complex [386, 1150, 1163, 1250, 1254–1257]. Absorption in the range of surface OH groups (3595 cm^{-1}) appearing after propene adsorption indicates that dissociative adsorption has occurred. The assignment of the adsorption bands at 1545 and 1202 cm^{-1} to $\nu_{\text{as}}\text{CCC}$ and $\nu_{\text{s}}\text{CCC}$ in the π -allylic complexes has been confirmed via the use of completely deuterated propene. With C_3D_6 , the bands at 1545 and 1202 cm^{-1} are shifted to 1473 and 1171 cm^{-1} , respectively, while in the range of OD vibrations a band at 2653 cm^{-1} replaces that at 3595 cm^{-1} for adsorbed C_3H_6 . The existence of a symmetrical π -allyl complex on the ZnO surface in the case of propene adsorption has been elegantly proved by Dent and Kokes [386] using partially deuterated propene. So, the adsorption of $\text{CD}_3\text{CH}=\text{CH}_2$ and $\text{CD}_2=\text{CHCH}_3$ give the same spectra of the allylic species, while a surface OD group appears in the former and an OH group in the latter case. This means that absorption leads to the formation of a symmetrical π -allylic complex in both cases:



Scheme 5.10

The π -allylic complex is stabilized on Zn^{2+} ions [1163]:



Scheme 5.11

The oxidation state of the cation remains unchanged, indicating that the π -allylic complex formed on ZnO has anionic character [1163, 1254–1257].

As propene forms two complexes with ZnO which differ considerably in stability (π - and π -allylic complexes), one can evaluate the heats of adsorption and surface coverage for particular adsorbed alkene species [1150, 1163]. Calorimetric determinations of the heats of adsorption for propene-derived π -allylic complexes were carried out as follows. Propene adsorbed in the form of π -complexes was removed by freezing these out in liquid nitrogen with a parallel determination of the thermal effects and the amount of desorbed propene. The differences in thermal effects and in the amounts of adsorbed and desorbed propene were used to evaluate the differential heat of adsorption of propene in the form of π - and π -allylic complexes. Half of the ZnO adsorption sites adsorb propene dissociatively, which gives a value of 8.10×10^{18} sites g^{-1} or 4×10^{17} sites m^{-2} .

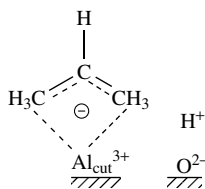
Butenes adsorbed on ZnO [1258, 1259] were also found to be stabilized as two complexes, including a weakly bound π -allylic complex. The appearance of new bands due to surface OH groups confirms that dissociative adsorption of butene occurs. Table 5.12 presents the $\nu\text{C}=\text{C}$ values for π - and π -allylic complexes resulting from butene adsorption on ZnO. The data presented show that, as for propene π -complexes, those of butene show a small $\nu\text{C}=\text{C}$ decrease (ca. 35 cm^{-1}) compared with gaseous alkenes, whereas for the π -allylic complexes the decrease is about 100 cm^{-1} .

Table 5.12. Positions of the C=C stretching frequencies (cm^{-1}) for π - and π -allylic complexes of butenes on ZnO.

Molecule	$\nu\text{C}=\text{C}$ (gas)	$\nu\text{C}=\text{C}$ in (π -complex)	$\nu\text{C}=\text{C}$ (π -allyl)
<i>trans</i> -But-2-ene	1676	1640	1582
<i>cis</i> -But-2-ene	1660	1625	1572
But-1-ene	1645	1610	1572

Al_2O_3

Davydov and co-workers [30, 473, 1087] have investigated the nature of $\gamma\text{-Al}_2\text{O}_3$ surface sites and their effect on the forms of adsorbed propene. Increases in the intensities of absorption bands associated with OH groups during C_3H_6 adsorption and the formation of OD groups upon the interaction with C_3D_6 indicate the dissociation of a certain proportion of propene molecules on alumina, even at room temperature, with the formation of allylic complexes:

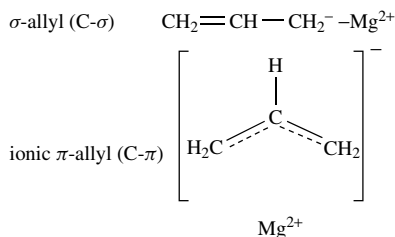


Scheme 5.12

Dissociation proceeds on the $\text{Al}^{3+}\text{O}^{2-}$ ionic pairs where coordinatively unsaturated Al^{3+} ions occupy tetrahedral vacancies. The allylic complex is characterized by an absorption band at 1575 cm^{-1} (1520 cm^{-1} for C_3D_6) in the $\nu\text{C}=\text{C}$ stretching region. The presence of a band at about 260 nm in the UV spectrum also points to the formation of allylic species, and the lack of any ESR signal shows a heterolytic cleavage of the CH bond in the CH_3 group of the alkene with the formation of the allyl anion. The observed increase in energy of electronic $n-\pi^*$ and the vibrational transitions (the absorption band at 1535 cm^{-1} for the unsubstituted anion) relative to purely ionic compounds is due to the increase of the covalent character of the bonding to Al^{3+} . At high temperatures, the above-mentioned complexes undergo a series of transformations leading to the formation of condensation products containing aromatic structures [1155]. Since the weak Brønsted acid sites of $\gamma\text{-Al}_2\text{O}_3$ are not converted, alumina seems to be suitable to establish the nature of condensation products adsorbed at Lewis acid sites. Anionic oligomerization with the formation of anion-dimers or anion-trimers at increasing temperatures has been established [1155]. Further increase of temperature leads to the formation of aromatic compounds. This probably occurs due to dehydrogenation of the complex anions, with a splitting-off of H^- or/and H_2 .

MgO

The UV spectra of propene adsorbed on MgO have been reported, together with those of but-1-ene. In both cases, there is loss of the 35000 cm^{-1} shoulder and also erosion of part of the 45000 cm^{-1} band of MgO. This is taken as evidence for dissociative chemisorption, and supports such a conclusion from the IR spectrum of adsorbed propene. However, in addition to the above effects, the adsorption of propene or but-1-ene is accompanied by the production of new bands at 26000 cm^{-1} and 34000 cm^{-1} [1251]. The authors consider that the new bands in this case are to be correlated with development of the two different forms of allyl species (or methylallyl in the case of but-1-ene), revealed by the IR results in Figure 5.14, namely σ -allyl and ionic π -allyl. Garrone and co-workers [1251, 1252] and Davydov and co-workers [1262] assigned the bands at 1625 and 950 cm^{-1} to $\nu\text{C}=\text{C}$ and $\nu\text{C}-\text{C}$ of σ -allyl species ($\text{C}-\sigma$ bands on Figure 5.14), respectively, and the bands at 1555 , 1250 , 1020 and 1055 cm^{-1} to ionic π -allyls ($\text{C}-\pi$ bands on Figure 5.14):



Scheme 5.13

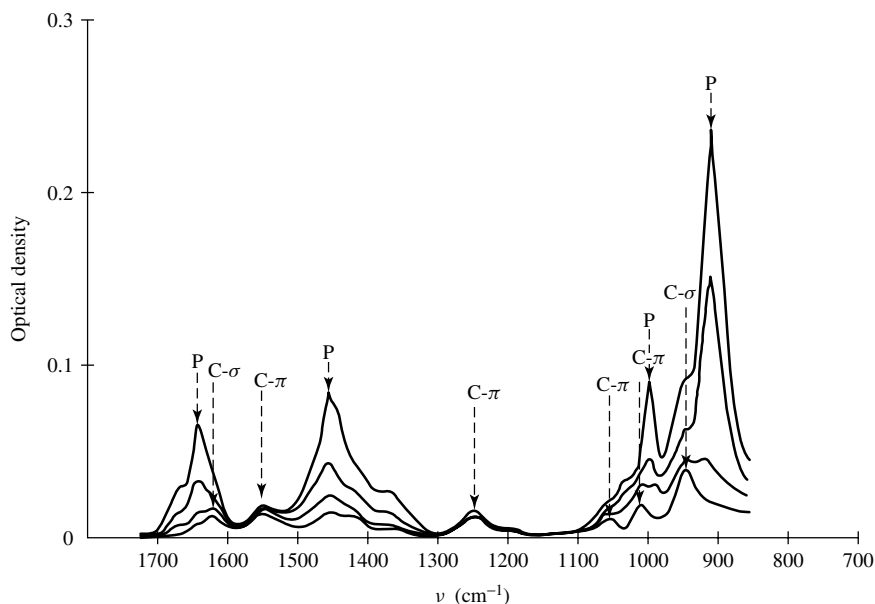


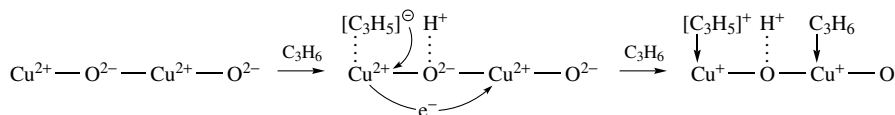
Figure 5.14. IR spectra of propene adsorbed on MgO at increasing propene pressures of 0.54, 1.0, 2.7 and 8.0 kPa [1251, 1252]. Reprinted from Zecchina, A., *J. Catal.*, **62**, 396–401 (1980). Reprinted with permission from Academic Press.

The bands marked 'P' identify undissociated propene (more probably, a π -complex) which only weakly interacts with the surface, since the band positions are not significantly different from those of gaseous propene.

The electronic excited state is likely to involve a very similar π^* -orbital in the case of both allyls: however, the ground state is a nonbinding orbital for σ -allyl and a lower-lying π -orbital for the ionic π -allyl. The UV band at $26\,000\text{ cm}^{-1}$ corresponds to an $n\text{-}\pi^*$ transition in σ -allyl, and that at $34\,000\text{ cm}^{-1}$ to a $\pi\text{-}\pi^*$ transition in the anionic π -allyl. The dissociative nature of adsorption, proved in this way, is good support for the anionic mechanism assumed for the catalytic isomerization of 1-alkenes on alkaline-earth oxides [1260, 1263, 1264].

Copper-containing systems

The formation of allylic compounds has been established on different Cu^{2+} -containing systems such as $\text{CuO}/\text{Cu}_2\text{O}$, $\text{CuO}\text{-MgO}$, Cu^{2+} zeolites and $\text{CuO}/\text{Al}_2\text{O}_3$ [30, 1148, 1149, 1241, 1253, 1256]. With $\text{CuO}/\text{Al}_2\text{O}_3$, an allylic complex of a carbenium-ion nature, whose adsorption gives rise to the band corresponding to surface hydroxyl groups, has been identified (with absorption bands at 1440 cm^{-1} for C_3H_6 and 1340 cm^{-1} for C_3D_6 in the $\nu\text{C}=\text{C}$ stretching region). At room temperature, no irreversibly adsorbed propene has been found by IR spectroscopy or by thermal desorption. The allyl species is stabilized on Cu^{2+} ions according to the following scheme:



Scheme 5.14

The Cu^+ ions, which appear on the surface as a result of such interactions, absorb propene molecules from the gaseous phase, yielding π -complexes.

The energy of interaction of propene with $\text{CuO}/\text{Al}_2\text{O}_3$, on the surface of which π -allylic compounds of a 'carbenium-ion' nature are formed, has been estimated [1253]. The differential heats of adsorption of C_3H_5 on $\text{CuO}/\text{Al}_2\text{O}_3$ are presented in Figure 5.15 as a function of coverage. At a coverage above $14 \mu\text{mol g}^{-1}$, the heats of adsorption are seen to remain unchanged at 77 kJ mol^{-1} . By using Scheme 5.14 and taking the heat of adsorption of C_3H_6 in the form of π -complexes ($\text{Cu}^+ \leftarrow \text{C}_3\text{H}_6$) to be equal to 69 kJ mol^{-1} [759], the heat of adsorption of propene on $\text{CuO}/\text{Al}_2\text{O}_3$ in the form of π -allylic compounds is ca. 86 kJ mol^{-1} . Estimations of the molar absorptivities for allylic compounds indicate that the sensitivity of the method to allylic compounds is similar to that in the case of π -complexes.

According to the above studies, the allyl complexes formed on ZnO , Al_2O_3 and copper-containing systems has low-intensity absorbances in the $\nu=\text{CH}$ region. The bands are usually shifted towards the low-frequency region with respect to the corresponding vibrations of π -complexes, presumably due to an expected higher degree of weakening of the $\text{C}=\text{C}$ bond [1265–1267]. The absorbance in the region of CH deformation vibrations is also of low intensity so that it is difficult to identify the surface π -allylic structures on the basis of stretching or deformation CH vibrations.

The most distinctive criterion for the formation of allylic species is the presence in the IR spectra of absorption bands belonging to $\nu_s\text{CCC}$ and $\nu_{\text{as}}\text{CCC}$ bonds together with those resulting from $\text{C}-\text{H}$ bond dissociation i.e. the lack of frequencies characteristic of CH_3 group vibrations and the appearance of absorption bands from surface hydroxyls. Manifestations of $\nu_{\text{as}}\text{CCC}$ will be discussed in more detail. Dissociative propene adsorption on oxide systems with stabilization of hydrogen and C_3H_5 fragments on oxygen and metal ions, respectively, is most likely to proceed heterolytically with the formation of C_3H_5^- fragments. Since neither significant nor partial transfer of electron density from C_3H_5^- fragments to the ZnO catalyst is observed from the lack of ESR spectra [1163, 1255], it is suggested that in this case that such compounds have a carbanionic character [1150, 1254–1257]. Indeed, the spectral characteristics of the π -allylic structures in this case are in good agreement with those of homogeneous allylic anions [1264]. The same allylic anions appear to be formed on Al_2O_3 and ZnO .

For copper-containing systems, ESR data [1253] indicate that the transfer of electron density from allylic fragments to the catalyst takes place, giving rise to the 'carbenium-ion' form of π -allylic complexes with ν_{as} around 1460 cm^{-1} . As was reported by Rybinskaya [1268], the spectral characteristics of allylic cations are very similar to those of anions and of radicals, following the energy levels for π -allylic systems (see Figure 5.15). However, this treatment neglects to account for the nature and donor-acceptor properties of the cation stabilizing the allyl. Hence, the lower $\nu\text{C}=\text{C}$ bands in olefin π -allylic complexes may vary over a wide spectral range but cannot exceed 1570 cm^{-1} ($\nu_{\text{as}}\text{CCC}$ for C_3H_5^-) [1264] and depend on the nature of the stabilization site and its ability to change valence during the interaction.

The assignment of an absorption band to $\nu_{\text{as}}\text{CCC}$ must necessarily be substantiated by IR spectra of the adsorbed deuterioalkenes because the ν_{as} vibration region overlaps with the $\nu\text{C}=\text{O}$ and δCH vibrations for complexes of other types. The $\nu_{\text{as}}\text{CCC}$ isotopic shifts for π -allylic complexes range from 70 to 90 cm^{-1} , that is, they are always greater than those for individual alkenes, like the $\nu\text{C}=\text{C}$ bands for π -complexes. This is because $\text{C}=\text{C}$ vibrations become less characteristic on passing from individual alkenes to the above complexes, and $\Delta\nu^{\text{H-D}} \text{C}=\text{C}$ seems to increase with decreasing $\nu_{\text{as}}\text{CCC}$. An increase in the $\nu_{\text{as}}\text{CCC}$ isotopic shifts for π -allylic compounds follows from calculations of frequencies and forms of normal vibrations in, e.g. π -allyl palladium chloride $(\text{C}_3\text{H}_5\text{PdCl})_2$ [1265–1267]. Thus, replacement of H by D results in a $\nu_{\text{as}}\text{CCC}$ shift of 96 cm^{-1} that points to a significant contribution of CH group vibrations to the observed

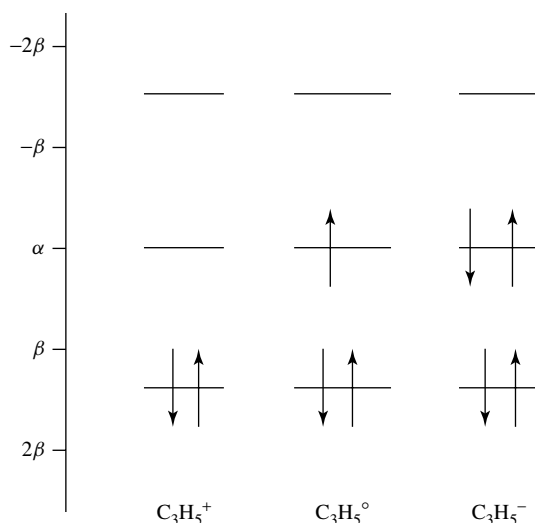


Figure 5.15. Energy diagram for the allyl π -system.

ν_{as} CCC [1266]. Calculations for completely deuterated allyl systems [1267] have demonstrated that the positions of the vibration frequencies agree well with the $(C_3H_5PdCl)_2$ H \rightarrow D spectra reported earlier [1267], where the value of the $\nu_{as}CCC$ isotopic shift was 143 cm^{-1} .

MgO and ZnO as Brønsted bases

MgO

The fact that MgO behaves as a Brønsted base has been established by spectroscopic studies of dissociative chemisorption for relatively weakly acidic molecules such as NH_3 , H_2S , H_2O , CH_3OH and alkenes [1252]. As was shown above, the propene molecule is easily dissociated with the formation of both σ - and π -structures. According to Garrone and Stone [1252], even the spectrum of adsorbed C_2H_4 also shows evidence of an initial formation of a dissociated species in that at low coverage the bands of the vinyl group at 995 and 950 cm^{-1} are reversed in intensity with respect to gaseous (and physisorbed) ethene. The spectra of benzene and toluene adsorbed on MgO, on the other hand, are not noticeably different from those of the pure liquids. The formation of O_2^- as detected by ESR, is a sensitive means of probing for the dissociative chemisorption of XH molecules. The O_2^- is formed by electron transfer from X^-_{ads} , according to the following: $X^- + O_2(g) \rightarrow O_2^-(ads) + X^*$, followed by $X^* + X^* \rightarrow X-X$ or $X^* + O_2 \rightarrow X-O-O^* \rightarrow$ further products. This accounts for the production of O_2^- , following pre-adsorption on MgO of propene, butene, acetylene, NH_3 , H_2 or ethene. Benzene and toluene also lead to O_2^- formation from O_2 on MgO, but pre-contact with CH_4 at room temperature has no effect [1252] (Table 5.13).

As has already been pointed out above, magnesium oxide outgassed at 1073 K exhibits three kinds of surface sites. There are five-coordinate sites ($Mg^{2+}_{5C}O^{2-}_{5C}$) at the (100) faces, four-coordinate sites ($Mg^{2+}_{4C}O^{2-}_{4C}$) at steps and edges, and three-coordinate sites $Mg^{2+}_{3C}O^{2-}_{3C}$) at kinks and corners. The electronic transitions associated with O^{2-} anions in low coordination at the surface can be observed in UV diffuse reflectance spectra [232]. This occurs above $50\,000\text{ cm}^{-1}$ for O^{2-}_{5C} , the band due to the excitation of O^{2-}_{4C} is in a more accessible region at $45\,000\text{ cm}^{-1}$, and the corresponding excitation of O^{2-}_{3C} ions is seen as a shoulder at ca. $35\,000\text{ cm}^{-1}$.

Table 5.13. Correlation of the solution pK_a of X-H molecules with their propensity for dissociative chemisorption on MgO at room temperature [1377].

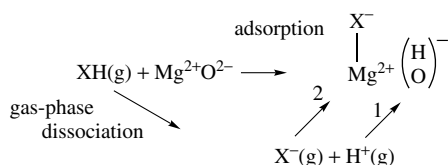
Molecule X-H	pK_a	Conclusion regarding dissociation		
		UV	IR	ESR (O_2^-)
Methane	40	–	No	No
Benzene	37	–	No	Yes
Ethylene	36	No	Yes	Yes
Ammonia	36	Yes	Yes	Yes
Toluene	35	–	No	Yes
Hydrogen	–	Yes	Yes	Yes
Propene	35	Yes	Yes	Yes
Acetylene	25	Yes	Yes	Yes
Methanol	16	–	Yes	No
Water	15.7	Yes	Yes	No

The partial erosion of the $45\,000\text{ cm}^{-1}$ band of MgO by alkenes indicates that these molecules are acidic enough to dissociate not only at the $Mg^{2+}_3C O^{2-}_3C$ sites but also at the less basic (and more abundant) $Mg^{2+}_4C O^{2-}_4C$ sites [232]. Acetylene also erodes the four-coordinate band of MgO, and does so to a greater extent than the 1-alkenes [1269]. The room-temperature adsorption of hydrogen is very small in extent (less than 1 % coverage), but it is dissociative and the UV diffuse reflectance spectra [233] show that only the three-coordinate ions of the surface are involved. With ethylene, evidence for a very small dissociative adsorption comes from IR work and ESR observations of O_2^- . As for benzene and toluene, it is necessary to go to the high sensitivity of the ESR test with O_2 to show that dissociative adsorption does occur [1252]. These authors assumed that in these last three cases only strongly basic three-coordinate sites of MgO are involved. Methane shows no response in the ESR experiment with O_2 , so is presumed to be of very low reactivity towards dissociative adsorption on MgO.

The collected data enable the ranking of the molecules to which we have referred in the following order of decreasing propensity towards dissociation on MgO [1252]: $H_2O, CH_3OH > C_2H_2 > C_3H_6, C_4H_8 > H_2, NH_3 > C_2H_4 > C_6H_6, C_7H_8 > CH_4$.

These authors have established a correlation of the dissociative adsorption with the pK_a values because the order of the acidity in solution given by Cram [1263] – $H_2O > CH_3OH > C_2H_2 > C_3H_6 > C_7H_8 > NH_3, C_2H_4 > C_6H_6 > CH_4$ – is more similar to the one obtained in the case of MgO, than the order of the gas-phase acidity [1270], i.e. $C_2H_2 > C_3H_6 > H_2O > C_6H_6 > H_2 > NH_3 > C_2H_4 > CH_4$.

The reason for the better agreement with the solution acidity scale is presumably that the MgO surface has an effect comparable to that of a solvent cage in stabilizing the anion produced during the dissociation (so-called solvation by the surface). Consider the following scheme [1252]:

**Scheme 5.15**

This regards the adsorption as being equivalent to the gas-phase dissociation followed by the formation of the hydroxyl (step 1) and the interaction of the X^- anion with the surface (step 2). The data obtained confirm the point of view expressed above that the properties of the molecules in the liquid phase reflect the transformations of the molecules on the surface better than those in the gas phase.

Garrone and Stone [1252] also revealed the interesting fact that carbon monoxide reacts with the chemisorbed allyl anions produced from propene. These reactions, identified by IR spectroscopy, are suggestive of mechanisms of carbonylation. In their opinion, CO is also capable of promoting the dissociation and the onward reaction of molecularly adsorbed ammonia.

ZnO

In a series of publications, Kokes and co-workers reported experimental evidence indicating that zinc oxide can act as a base in catalytic reactions with unsaturated hydrocarbons. From studies of the interaction of molecular nitrogen [1271] and molecular hydrogen [532] [1272] with dissociated hydrogen [550] on zinc oxide, they concluded that the limited number of active zinc and oxide sites are paired. This preliminary information suggested that zinc oxide can dissociate acids with pK_a values less than 36 and cannot dissociate those with pK_a values greater than 36.

IR data indicated that the ethene did not lose its vinyl hydrogen upon adsorption, such as ethene chemisorption on zinc oxide was nonassociative. In contrast, IR data obtained with deuterium-labeled propene [1163, 1273] showed that propene adsorption is dissociative on zinc oxide and involves the rupture of the methyl carbon-hydrogen bond. These studies also provided evidence that the dissociated hydrogen was attached to an oxide ion, whereas the hydrocarbon moiety was bound to the zinc ion of the active pair site. Inasmuch as the zinc and oxide ions of the pair are Lewis acids and bases, respectively, it is reasonable to expect that the allyl species will have anionic character and the abstracted hydrogen will have proton character.

In later reports, Chang and Kokes [1274] showed that the dissociative adsorption of $CH_3-C\equiv CD$ on zinc oxide produced propargyl ions ($^-CH_2\equiv C\equiv CD$) by the loss of hydrogen from the methyl group. The cleavage of the methyl carbon-hydrogen bond rather than the acetylene hydrogen-carbon bond suggested that the methyl hydrogen attained, at least, some allylic nature which they attributed to a change of the alkynic character of methyl acetylene to olefinic character when it is chemisorbed. Presumably, the adsorbed species are formed by the opening of one of the π -bonds. A similar phenomenon was reported by Little *et al.* [1275] in their adsorption studies of acetylenes on metals.

The chemisorption behavior of butenes was similar to that observed for propylene and acetylenes on zinc oxide: such materials chemisorbed zinc oxide without dissociation at low temperature [1259], but rapidly underwent dissociation and then isomerization at room temperature [1276].

The toluene is adsorbed on zinc oxide like a π -complex (the most characteristic region in the IR spectrum for the chemisorption of toluene is that of the vibration of the aromatic ring at 1600 and 1500 cm^{-1}) – bands at 1593 and 1487 cm^{-1} – and underwent dissociation. The formation of a new O-H band at 3575 cm^{-1} was accompanied by the growth of two new bands at 1585 and 1482 cm^{-1} . Additional adsorption studies with alpha-toluene- D_3 ($C_6H_5CD_3$) indicated that the dissociation of toluene occurred via the rupture of the methyl carbon-hydrogen bond. Chang and Kokes believe that *in situ* IR studies strongly support the view that zinc oxide acts as a basic catalyst and that its effective ‘basicity’ is comparable to that of the allylic carbanion, but weaker than that of the vinyl carbanion [1277].

5.1.5 THE COMPLEXATION OF ALKENES WITH SURFACE OXYGEN

Formation of hydrogen bonds from alkanes to oxygen (O^{2-})

The complexation of alkenes with surface oxygen is difficult to identify because the corresponding spectral changes are small, as in the cases of the formation of hydrogen-bonded complexes with hydroxyls or weakly bound π -complexes. In addition, the bands belonging to the $H \cdots O$ bond are usually weaker and broadened and are superimposed on the background spectrum.

Only a few cases have been registered where the hydrogen-bound complex is formed with the sole participation of surface oxygen [244–246, 1278]. Such a complex is formed during propene adsorption on Sb_6O_{13} since here there are nucleophilic centers of preference. In this instance, the heat of adsorption of propene is about 40 kJ mol^{-1} , which is lower than that for the formation of propene π -complexes with high-valence cations. The spectral parameters of the complexes are only slightly different from those of gaseous propene ($\nu C=C$ is observed at 1645 cm^{-1} , and is not changed relative to the gaseous molecule) [244].

Analogous weakly bound complex formation with the same spectral parameters was established for the numerous two components of propene partial oxidation to acrolein catalysts (Fe–Sb–oxide [246], Ti–Sb–oxide [245] and Bi–Mo–oxide [1278]). In the case of the latter two studies, the formation of a hydrogen-bond with the surface oxygen was directly confirmed due to the high sensitivity of the methods (FTIRS and DRIRS) used. Indeed, the IR spectra measured after C_3H_6 admission (Figure 5.16) exhibit absorption bands at ca. 2750 cm^{-1} , which may be assigned to the stretching vibrations of the loosened C–H bond (see also [774, 775]). An alternative assignment of this band to the loosened C–H bond due to the interactions with cationic centers [1279] is less probable because of the practical absence of such centers on the surface of Fe/Sb, Ti/Sb and Sb_6O_{13} systems. Comparing the spectra in the region of νCH , one should bear in mind that the intensity ratios for absorption bands in the diffuse reflectance and transmittance IR spectra is not the same. Thus, on the oxide surfaces, due to the interaction with surface oxygen, olefins may give weakly bound complexes such as:

Formation of surface alkenoxides

The adsorption of allyl halides on oxide catalysts, and the adsorption of propene on catalysts which have been partially oxidized [1148, 1149, 1280, 1281] leads to the formation of σ -allylic

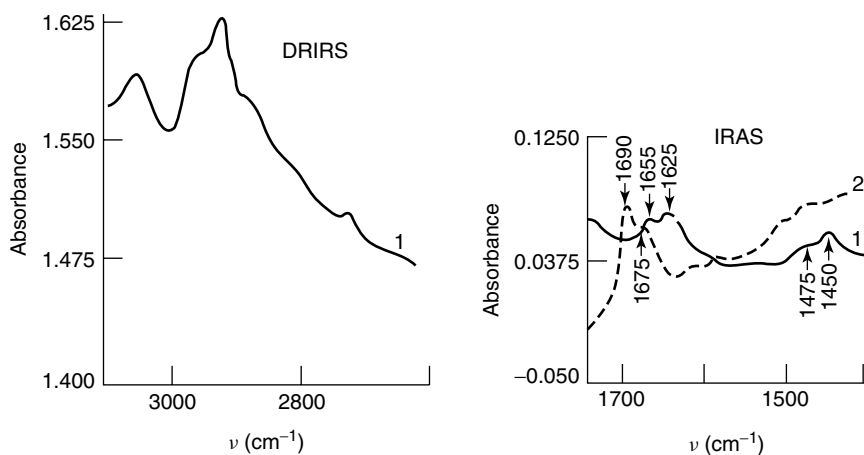
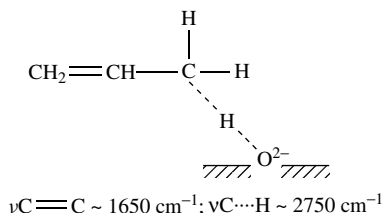


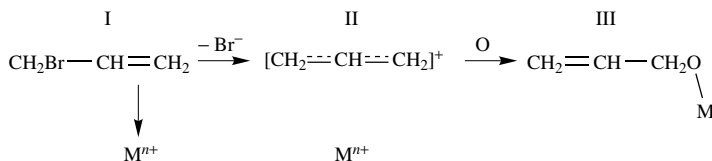
Figure 5.16. IR spectra of propylene adsorbed on the Bi–Mo oxide catalyst at (1) 293 and (2) 593 K.



Scheme 5.16

surface compounds in the form of surface ethers, such as $^-\text{OCH}_2\text{CH}=\text{CH}_2$. Such complexes can be identified by the presence of absorption bands in their spectra which are characteristic of both $\nu\text{C}=\text{C}$ and $\nu\text{C}-\text{O}$ bonds. Since propene $\text{C}=\text{C}$ fragments are not directly involved in the formation of the bond with the surface, the $\Delta\nu^{\text{H}-\text{D}}\text{C}=\text{C}$ decrease in such complexes is $30\text{--}50 \text{ cm}^{-1}$, that is, smaller than that observed for the adsorbed alkenes. This may result from changes in vibrational interactions in the C_3H_5 fragment owing to its addition to the surface oxygen [30].

The $\nu\text{C}-\text{O}$ stretching vibrations frequencies in such σ -allylic complexes occur near 1100 cm^{-1} (not to be confused with $\text{C}-\text{O}$ in structures such as alkoxides which are saturated and lack $\text{C}=\text{C}$ bond vibrations). The formation of $\text{C}-\text{O}$ bonds is interesting and important in itself, as it points to the formation of a chemical compound between the surface oxygen and the molecule adsorbed. The formation of σ -allylic complexes during allyl halide adsorption is natural in view of their tendency towards heterolytic dissociation to give a halide anion and C_3H_5^+ . The C_3H_5^+ fragments can be stabilized on oxygen anions with the formation of σ -allylic compounds. More probably, the formation of the C_3H_5^+ fragments occurs via rapid dissociation of the carbon-halogen ($\text{C}-\text{Hal}$) bond of the surface allyl halide π -complexes on surface cations [1280, 1281]. Probably, a stabilization of the C_3H_5^+ fragment on the cation (after dissociation of the $\text{C}-\text{Hal}$ bond in the π -complex) can be realized according to Scheme 5.14, or by the following way:



Scheme 5.17

This mechanism is probably also realized if the allyl halide is adsorbed over ZnO [1150]. In this case, the formation of the allyl cation by the participation of Zn^{2+} ions has been proposed based on the IR spectroscopy data ($\nu_{\text{as}}\text{CCC} -1460 \text{ cm}^{-1}$ [1150] has been observed upon the $\text{C}_3\text{H}_5\text{Br}$ adsorption instead of the band at 1545 cm^{-1} observed for the allyl anion upon adsorption of C_3H_6). The formation of C_3H_5^+ compounds during propene adsorption can be interpreted in terms of a change in the state of oxidation of oxide surface sites upon allyl stabilization, as has been demonstrated experimentally [1150, 1253] on Cu -containing catalysts (see also Section 6.2.3).

The $\nu\text{C}-\text{O}$ frequency in compounds (III), reflecting the strength of the bond between the molecular fragment adsorbed and the surface, depends on the type of cation to which oxygen is

bound and on its coordination and valence state [30, 1282]. Activation energies for alcoholate desorption vary over a wide range (60–120 kJ mol⁻¹) [30].

Formation of carboxylate-like compounds

The formation of carboxylate-like structures on oxide surfaces during interaction with hydrocarbons has long been pointed out from the data obtained by IR studies. According to this data, the prevalent forms of olefinic adsorption at room temperature on the oxidized surfaces of Cr₂O₃, MnO₂, Co₃O₄, NiO, Fe₂O₃, CuO, CuO–MgO, CoO–MgO and NiO–MgO are formate and other carboxylate fragments [30, 1148–1151, 1241, 1280, 1281, 1283, 1284, 1569, 1572–1574]. The most favorable temperatures for the formation of such compounds is 423–473 K (Figure 5.17). Oxidized fragments of the RCOO⁻ type, including those oxidized destructively at a C=C bond, are formed on transition-metal oxides and can be easily identified by the characteristic absorption bands of the COO groups in the ν_s (1340–1480 cm⁻¹) and ν_{as} (1550–1600 cm⁻¹) regions [30, 1148, 1149, 1283, 1284]. The spectral region in which the bands occur can be compared with those for individual salts or adsorbed acids. Deuterated derivatives show insignificant ν_s and ν_{as} COO⁻ isotopic shifts (10–30 cm⁻¹) except for HCOO⁻ where the ν_s COO⁻ band shifts by as much as 50 cm⁻¹ because of a considerable contribution from δ CH to this vibration (1390 cm⁻¹). The differences between formate and carboxylate groups are obvious; the absorbance at 1340–1390 cm⁻¹ in the ν_s COO⁻ region is characteristic of formates, whereas with other carboxylates the corresponding absorption band appears in the 1400–1480 cm⁻¹ range.

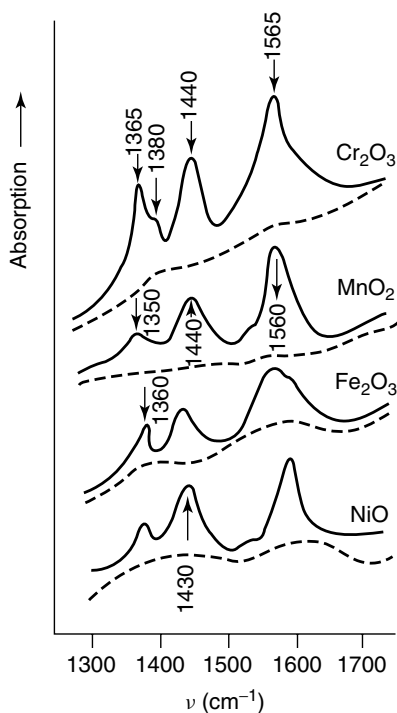


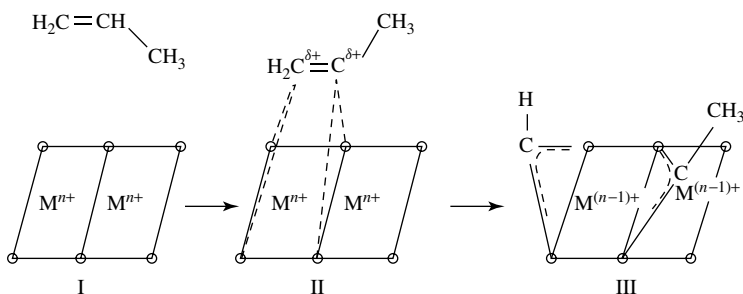
Figure 5.17. IR spectra obtained for propene adsorbed on the oxidized surfaces of various transition-metal oxides at 373 K (the dashed lines represent the background spectra).

For surface acrylate compounds of the type $\text{H}_2\text{C}=\text{CHCOO}^-$, in addition to COO^- vibrations similar to those for RCOO^- (where R is a saturated fragment), an additional band is observed at $1630\text{--}1640\text{ cm}^{-1}$ in the $\nu\text{C}=\text{C}$ stretching region, with an isotopic shift of $50\text{--}60\text{ cm}^{-1}$ similar to that of alkenes.

The isotherm for C_2H_4 adsorption on Cr_2O_3 at 393 K indicates that the maximum adsorption of ethene as formate species is ca. $14\text{ }\mu\text{mol g}^{-1}$. Taking into consideration that one C_2H_4 molecule gives rise to two formate molecules, the number of oxygen ions binding to ethene at 393 K, i.e. available to the amount of reactive oxygen on the surface of the Cr_2O_3 can be evaluated and constitutes 8 % of a monolayer. The least reactive oxygen of chromium oxide reacts with a heat of adsorption of 200 kJ mol^{-1} at 293 K [30, 1285]. The extinction coefficient of, e.g. $\nu_{\text{as}}\text{COO}^-$, in the formate structure is higher than that for $\nu\text{C}=\text{C}$ in π -complexes and corresponds to $5 \times 10^{-19}\text{ cm}^2$ per COO^- group.

The fact that the molar absorptivities for $\text{C}=\text{O}$ bonds are considerably higher than those for $\text{C}=\text{C}$ and $\text{C}\equiv\text{C}$, and the prevalent formation of oxidized compounds in these systems, makes it almost impossible to identify π and especially allylic compounds. In the latter case, ν_{as} falls inside the spectral range of ν_{s} and ν_{as} for COO^- groups. In view of this fact, the currently available IR spectroscopic data on the adsorption of alkenes over powdered catalysts does not allow an unequivocal conclusion about complexation with cations, although thermal desorption data unambiguously indicate that reversible adsorption over these catalysts is also possible [1283]. However, as has been remarked upon above, at low adsorption temperatures the π -complexes of olefins can be observed even over transition-metal oxides (see Table 5.1).

The character of alkene fragmentation on oxide surfaces (formates and acetates with propene, and formates with ethene) indicates that these oxidized compounds arise from destruction of the alkene double bond. All of the oxide surfaces on which formate and carboxylate compounds are formed were found to contain coordinatively unsaturated cations capable of coordinating the molecules of mild bases, including alkenes. This is likely to be the primary step in the formation of oxidized compounds. When the primary complex with the catalyst is formed, the electron density is transferred from the $\text{C}=\text{C}$ bond towards the cation ($\text{I} \rightarrow \text{II}$ transition):



Scheme 5.18

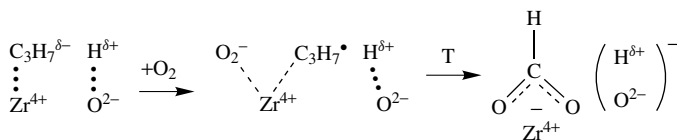
In the presence of weakly bound surface oxygen, the double bond is cleaved and surface formate and carboxylate species are formed ($\text{II} \rightarrow \text{III}$ transition). This mechanism of alkene fragmentation has been confirmed directly [1148] and by blocking coordinatively unsaturated surface cations with ammonia molecules, which decreased the rate of formation of the carboxylic compounds [1284].

The removal of reactive oxygen from the surfaces of the above catalysts by treatment under reductive conditions, or by the introduction of cations which increase the strength of oxygen

bonding, provides information about the character of the primary interaction between surface cations and alkenes. It was shown [30] that no propene destruction occurs during adsorption at room temperature on the surface of Cr/Mo and Cr/Al catalysts, although weakly bound alkene complexes (π -complexes) with chromium ions are formed. Upon adsorption of propene on NiO–MgO–MoO₃ [1216], only π -complexes with Ni²⁺ ions were formed. The reductive treatment of catalysts leads to the removal of reactive oxygen, and decreases the intensities of the bands associated with carboxylic compounds, thus allowing the detection of reversible states of alkene adsorption on these catalysts. It should be borne in mind, however, that the reductive treatment also alters the acceptor ability of surface cations, which affects the spectrum and energy characteristics of adsorption complexes.

As a rule, the increase in temperature of the interaction between olefins and oxides leads to a growth of the concentration of oxidized complexes. For other oxides with more strongly bound surface oxygens, the formation of oxidized compounds is observed only at high temperatures. For example, the study of the high-temperature interaction of propene or ethene with the oxidized titanium dioxide surface has demonstrated that the π -complexes undergo destruction above 573 K with the formation of formate and carboxylate compounds. No evidence for the dissociative adsorption of the olefins was observed up to 573 K, i.e. titanium dioxide is a less basic oxide than MgO, ZnO or Al₂O₃. The formation of formate- and carboxylate-like structures from the interactions of olefins with Al₂O₃ was observed at higher temperatures, and was not observed on SiO₂ or Al/Si catalysts at all.

An alternative mechanism for the production of surface formates and carboxylates from hydrocarbons with the participation of gas-phase oxygen has been suggested [1286]:



Scheme 5.19

5.2 Complexation of aryls and aryl halides

The spectra of adsorbed aromatic compounds have been less investigated than those for the olefins, although their interpretation is simpler because of the readily identified ring vibrations. However, data about the character of the interactions with different types of surface centers are not yet very extensive.

5.2.1 HYDROGEN-BONDING

In early spectroscopic reports it was noted that the molecules of cumene and cyclohexene were appreciably perturbed during adsorption on zeolite HY [19, 1287]. These molecules interact with the hydroxyl groups of this zeolite and participate in the H–D exchange reaction. The perturbations of the structures of hydroxyl groups are significantly less on the adsorption of benzene or cyclohexane molecules.

The data in the literature show that the H-bonds are formed between aromatic molecules and acid hydroxyl groups [18, 19, 342, 1157, 1181, 1249, 1277, 1288–1294] on both zeolites and oxides, as in the case of olefins. Together with perturbations of the OH group absorptions, changes in the spectrum of the initial molecule, namely small decreases of absorption bands characteristic of the ring vibrations, are observed (Figure 5.18). The formation of complexes

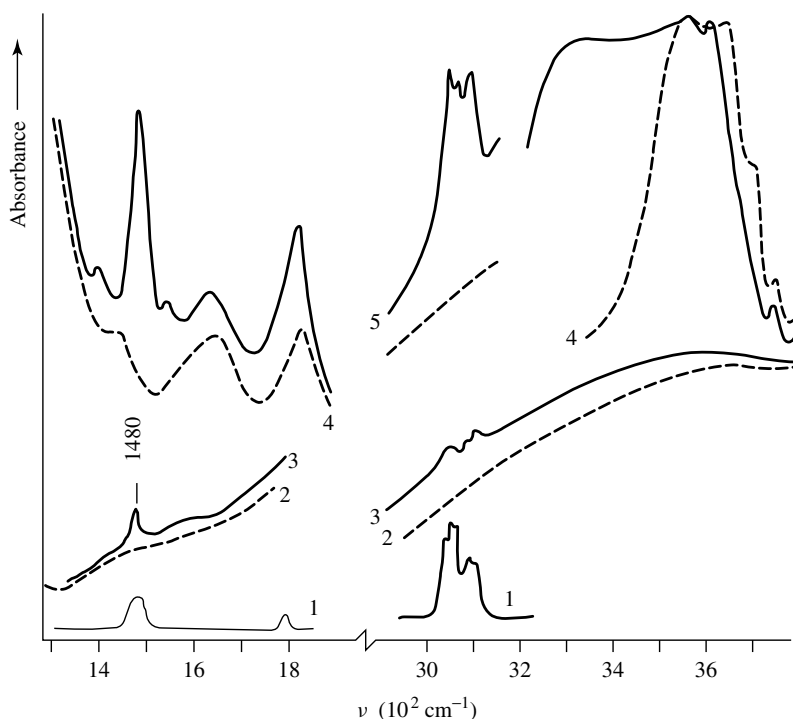


Figure 5.18. IR spectra of (1) the benzene gas phase, (2) V_2O_5/Al_2O_3 , (3) benzene adsorbed (15 torr) on V_2O_5/Al_2O_3 , (4) HY (0.55 wt% Na), and (5) the adsorption on (4) of 10 torr of benzene.

is observed even in the case of such weakly acid OH groups as on SiO_2 ($\Delta\nu = 120\text{ cm}^{-1}$ [19, 1157]; $Q = 53\text{ kJ mol}^{-1}$) [1288]. This value of the $\Delta\nu_{OH}$ shift increases with its increasing proton mobility. The shift value depends of the basicity of the hydrocarbon, and decreases when the basicity increases. The changes in the hydrocarbon spectra are similar to the case of π -complexes with cations (see below), but smaller in value. The character of the interaction between aromatic molecules and SiO_2 have been analyzed in detail by various authors [19, 1157, 1290] and is rather weak; the spectrum of adsorbed benzene was very similar to that of liquid benzene.

The investigation of the adsorption of benzene, toluene, iso-propylbenzene and 1,3-dimethylnaphthalene on H-ZSM-5 zeolite by means of UV-Vis and IR spectroscopy has established [1157, 1177, 1181, 1305] that the OH groups of the zeolite are perturbed with adsorption, although the positions of the absorption bands differ little from those of the individual hydrocarbons: as an example, the adsorption spectra of toluene are shown in Figure 5.19 (spectra 2a and 2b'). The complexes formed desorbed under vacuum at 373–473 K and, most probably, are the π -complexes of aromatic hydrocarbons with hydroxyl groups.

As a rule, the presence of H-bonded forms, plus π -complexes with cations, can be revealed by step-by-step evacuation of the gas phase at low temperatures. The intensities of the absorption bands of adsorbed aryl and hydrogen-bonded OH groups significantly decrease while more strongly bound π -complexes with cations remain on the surface. These are characterized by the same modes but with lower frequencies. For example, in the case of toluene adsorbed on Al_2O_3 , upon evacuation of the gas phase at 300 K, the intensities of the bands of adsorbed toluene and from hydrogen-bonded OH groups significantly decrease (Figure 5.20, spectrum 4) [1249]. The

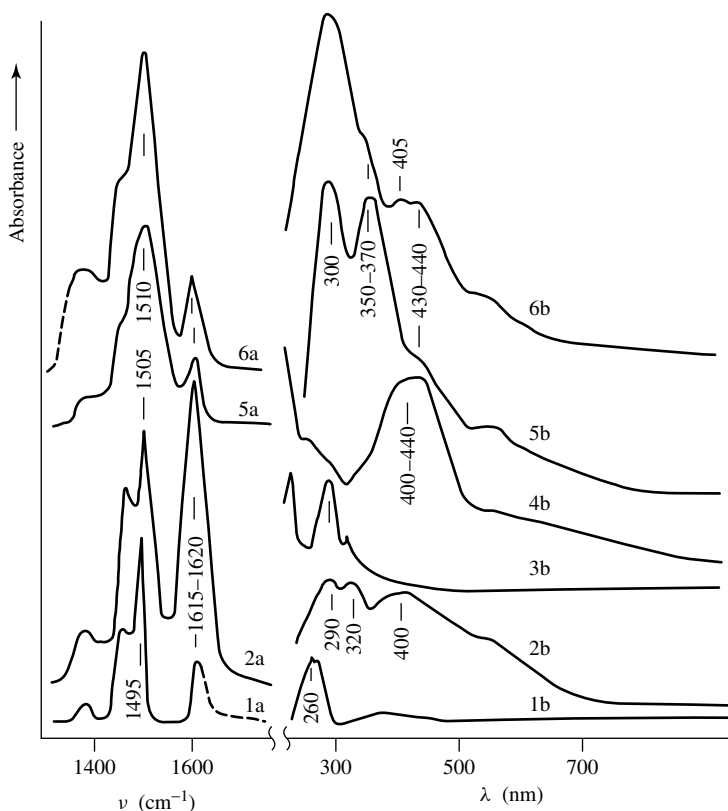
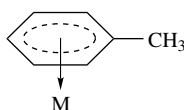


Figure 5.19. IR (a) and UV-Vis (b) spectra of: (1a, 1b) H(D)-ZSM-5 zeolite (with $M = 30$) treated at 298 K with toluene and then (2a, 2b) at 473 K with propene (0.1 torr, for 1 h) and evacuated at 473 K; (3b) at 298 K with $C_{12}H_{10}$; (4b) with $C_9H_{15}OH$; (5a, 5b) at 473 K with C_3H_6 (0.2 torr, for 2 h) and then evacuated at 473 K with further treatment at 473 K with CH_3OH (10^{-2} torr, for 2 h) and evacuated at 473 K; (6a, 6b) at 473 K with C_3H_6 (10^{-2} torr) plus H_2O (3×10^{-3} torr) and evacuated at 473 K.

3730 cm^{-1} band of surface OH groups restores its intensity, but this is not, so far the 3770 cm^{-1} band. An increase of the desorption temperature to 373 K further decreases the intensity of the absorption bands of adsorbed toluene and shifts the ring vibrations to lower frequencies, i.e. 1603 to 1593 cm^{-1} and 1497 to ca. 1492 cm^{-1} (Figure 5.20, spectrum 5). Restoration of the initial spectrum of $\gamma\text{-Al}_2\text{O}_3$ is observed at 473 K. Hence, it can be concluded that the OH groups are the adsorption centers of toluene, with the complexes formed with the participation of the hydroxyls with $\nu_{OH}=3770\text{ cm}^{-1}$ being particularly weakly bound. Hence, the basic hydroxyl groups of oxides do not themselves form stable complexes with aromatic compounds. However, under favorable geometrical conditions the π -complexes with cations:



Scheme 5.20

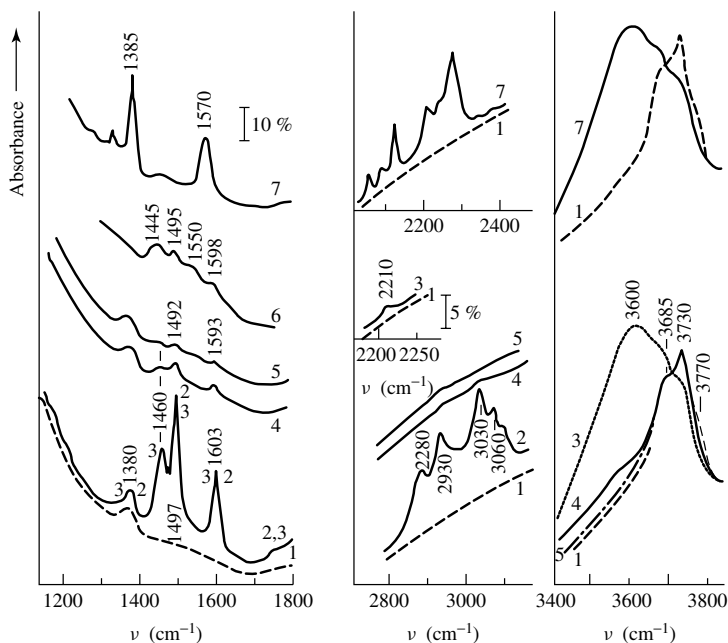


Figure 5.20. IR spectra of toluene and deuterotoluene adsorbed on γ - Al_2O_3 : (1) background spectrum; (2) adsorption of C_7H_8 (2 torr, at 300 K); (3) admission of 46 torr of CO to toluene; (4) desorption at 300 K; (5) desorption at 373 K; (6) adsorption of C_7H_8 at 723 K and subsequent evacuation at 300 K; (7) adsorption of C_7D_8 (4 torr, at 300 K).

can be additionally H-bonded with the basic OH groups (as for C_3H_6^- see above). The resulting shifts of the absorption bands of such hydroxyl groups are small (ca. 100 cm^{-1}), as in the case of the complexes with olefins.

In some cases, however (see below), complete transfer of a proton to aromatic molecules to form aromatic carbenium ions is observed, as for zeolites and for other oxides with strong Brønsted acid centers.

5.2.2 ALKYLAROMATIC CARBENIUM IONS

The formation of aromatic carbenium ions on the surfaces of heterogeneous systems having strong Brønsted acid centers is well shown by means of IR and UV-Vis spectroscopic methods. More reliably than for olefins, the formation of aromatic carbenium ions was revealed in the first combined spectroscopic studies, in particular, on aluminosilicates, with the adsorption of complex molecules such as 1,1-diphenylethene and triphenylmethane. These data have been examined in detail by Leftin and Hobson [46]. It should be noted that the range of the $\text{C}-\text{C}^+(\text{C})-\text{C}$ fragment vibrations ($1200\text{--}1300\text{ cm}^{-1}$) in the carbenium ion is very important for the identification of these ions. In the case of zeolites, this range is overlapped with the oxide cutoff vibrations and the identification of the carbenium ions in such cases becomes more difficult.

The formation of aromatic carbenium ions on transition metal oxide systems having strong acid centers was noted for the first time by Davydov [1157]. It was observed that the adsorption of toluene on the oxidized surface of $\text{V}_2\text{O}_5/\text{Al}_2\text{O}_3$ gave rise to a series of intense absorption bands at $1100\text{--}1600\text{ cm}^{-1}$ and also weak bands in the νCH region (Figure 5.21, spectrum 2). Evacuation

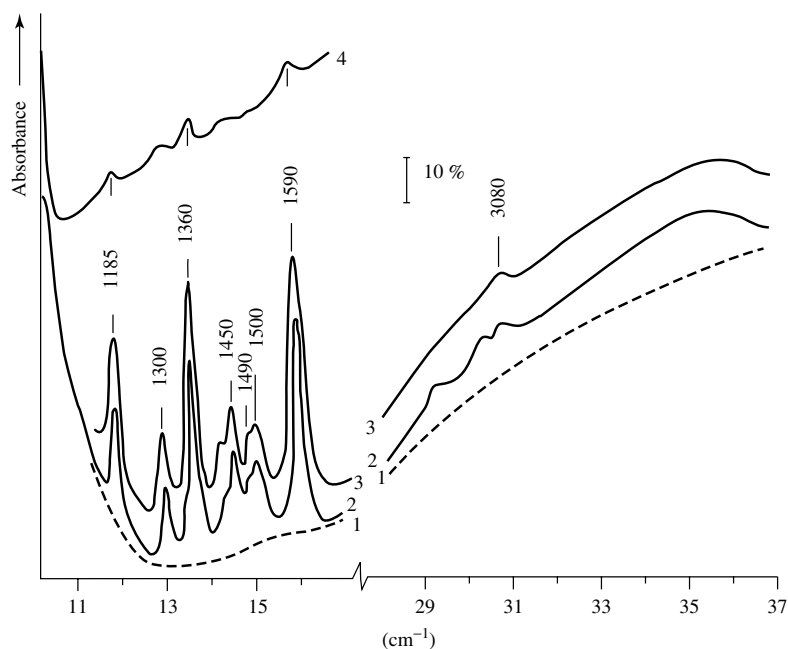
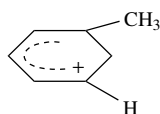


Figure 5.21. IR spectra of toluene adsorbed on V_2O_5/Al_2O_3 and on V_2O_5 : (1) background spectra of oxidized V_2O_5/Al_2O_3 ; (2) toluene adsorption (6 torr) at 300 K; (3) subsequent desorption at 300 K; (4) toluene adsorption (5 torr) on V_2O_5 .

at 300 K had little effect on the IR spectrum of the toluene-derived species (Figure 5.21, spectrum 3); in other words, the complex characterized by these bands is strongly bound. It can be seen that the spectrum of toluene adsorbed on the vanadium catalyst is qualitatively different from the spectra of toluene adsorbed as a π -complex or as a benzoate ion. For example, an absorption band of the benzene ring at 1590 (1608) cm^{-1} in (the frequency in brackets represents that of liquid toluene) has an abnormally high relative intensity as compared to the spectrum of the free toluene molecule and another absorption band of the benzene ring is observed. Spectrum 3 in Figure 5.21 characterizes the type of surface compound, since a concerted change in all of the absorption bands is observed during the adsorption–desorption cycles. This complex is not decomposed (transformed) even at 323 K in vacuum.

It has been shown earlier that the Brønsted acid sites are capable of protonating propylene with the formation on the surface of V_2O_5/Al_2O_3 of surface alkene oxides in high concentrations. Evaluation of the strength of the protic acid sites of this catalyst by the hydrogen-bonding method has allowed Budneva *et al.* [460] to show that these sites are stronger than those on HY or even ZSM zeolites. Taking into account the presence of mobile protons on the catalyst studied, leading to the possibility of proton transfer of the molecules of propylene [30, 219–221, 748, 1151], one may suppose that spectrum 3 belongs to a surface compound of the following type:



Scheme 5.21

Table 5.14. IR spectral data^a obtained for toluene adsorbed on various oxide catalysts at 300 K.

C ₆ H ₅ CH ₃	TiO ₂ π-complex	CuO benzoate	CuO/Al ₂ O ₃ π-complex on Cu ⁺	V ₂ O ₅ /Al ₂ O ₃ carbenium ion	V ³⁺ /Al ₂ O ₃ π-complex	Aluminum benzoate	C ₇ H ₉ ⁺
1184 (vw)	1180 (vw)			1185 (i)			1183 (i)
1218 (vw)	1215 (vw)			1240 (i)			1214 (i)
							1239
1330 (vw)				1295 (i)			1307 (i)
1380	1380		1385	1360 (i)	1385 (w)		1346 (i)
		1420	1430	1430		1430	
1460	1460		1460	1450	1460	1450	
1500	1497	1500	1497	1490–1497	1497	1495	1486
		1540	1555			1560	
1608	1603	1600	1602	1590	1602	1600	1600

^aIntensities: w, weak; vw, very weak; intense.

The formation of similar complexes was also observed during toluene adsorption on bulk V₂O₅ (spectrum 4), the surface of which also has Brønsted acid sites, as was reported earlier [212].

An IR spectrum of such ion (C₇H₉⁺) in the toluene–GaCl₃–HCl system is available in the literature [1295] (Table 5.14). By comparison of the spectrum observed [460, 1157] during toluene adsorption with that reported by Perkampus and co-workers [1295], Davydov [1157] showed that these spectra are similar, but not fully identical. A comparison of the data from Table 5.14 makes possible the elucidation of the general differences between the spectra of carbenium ions and those of π-complexes observed during toluene adsorption on oxides, i.e. the presence of intense bands at ~1200, 1300, 1360 and 1183 cm⁻¹. These bands do not appear either in the spectra of toluene and its π-complexes, or in the spectra of dissociation products via C–H bonds (e.g. C₆H₅CH₂⁻ or benzoate ions).

Benzene, which has a weaker affinity for protons, is not protonated on V₂O₅/Al₂O₃. The spectrum of benzene on this catalyst indicates the formation of only a weakly bound complex whose spectral characteristics are close to those of benzene and of hydrogen-bonded benzene on a HNaY zeolite with acid hydroxyl groups (νOH, 3300 cm⁻¹, Figure 5.18).

It has been proposed [1157] that toluene adsorption on V₂O₅/Al₂O₃ may lead to the formation of a methylbenzenium ion due to proton transfer from the surface to the toluene molecule, since the Brønsted acid sites of V₂O₅/Al₂O₃ are the strongest of all sites known for heterogeneous systems, as was shown by Budneva *et al.* [460]. It is also known that aromatic molecules characterized by a stronger proton affinity than toluene produce a quite characteristic IR spectrum of carbenium ions in solutions [1295–1297]. In Davydov *et al.* [1193], an attempt was made to use these molecules for elucidation of the possibilities of the formation of benzenium and triphenylcarbenium ions in heterogeneous systems. The IR spectra for individual toluene, mesitylene, hexamethylbenzene, ‘triene’ (4-methylene-1,1,2,3,5,6-hexamethylcyclohexa-2,5-diene) and triphenylcarbinol, plus their carbenium ions in solutions, as well as those for molecules adsorbed on γ-Al₂O₃ and V₂O₅/Al₂O₃, are shown in Figure 5.22.

It can be seen that the spectra of toluene, mesitylene and ‘triene’ adsorbed on Al₂O₃ (spectra 2) differ only slightly from the spectra of the individual substances (spectra 1). For adsorbed compounds in the spectral region under consideration all of their intense absorption bands are observed with only small changes in relative intensities. All of the absorption bands observed for toluene and mesitylene disappear upon outgassing at room temperature, i.e. they characterize, probably, a weakly bound complex. These and earlier data for adsorbed toluene suggest that these molecules form only π-complexes on Al₂O₃ and TiO₂ [1157, 1249].

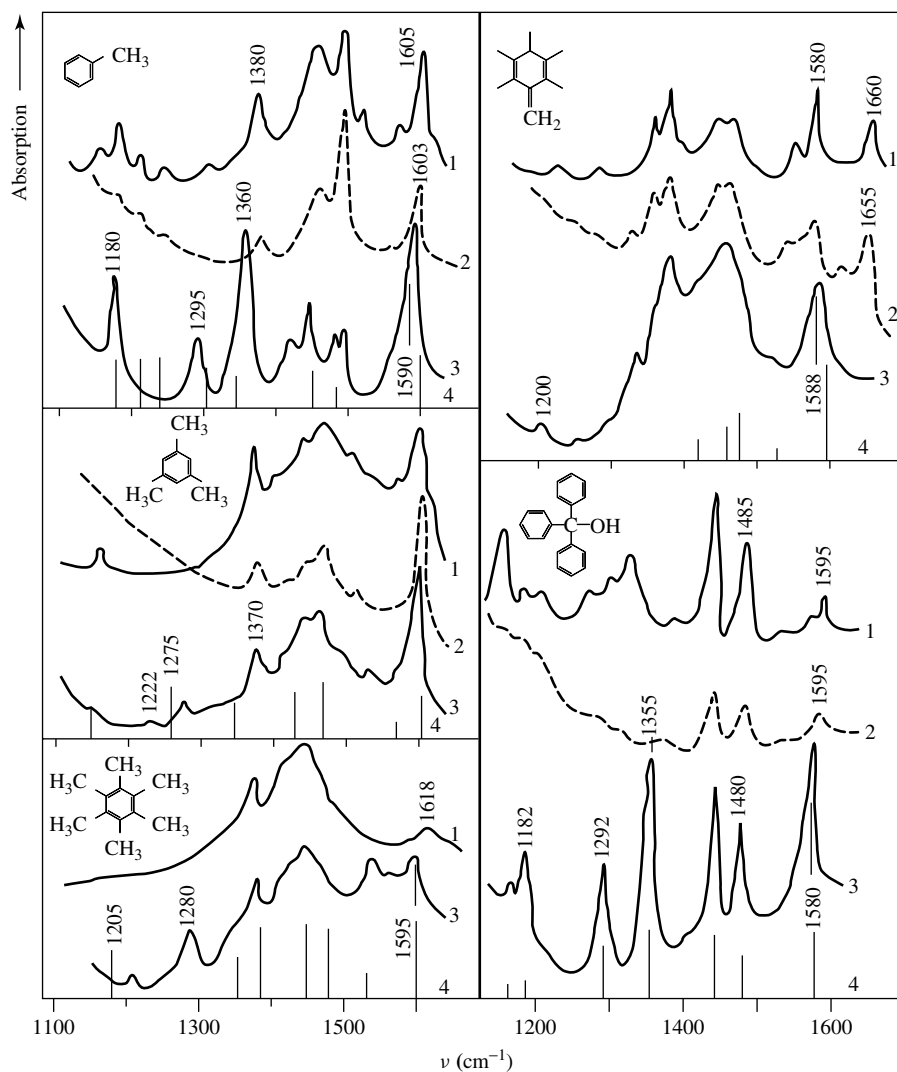
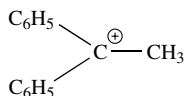


Figure 5.22. IR spectra of individual parent substances as (1) liquids, (2) adsorbed on Al_2O_3 , and (3) on $\text{V}_2\text{O}_5/\text{Al}_2\text{O}_3$. The vertical lines (4) correspond to the most intense absorption bands in the IR spectra of the corresponding carbenium ions (toluene, mesitylene, hexamethylbenzene, 'triene' and triphenylcarbinol).

Unlike Al_2O_3 , adsorption on $\text{V}_2\text{O}_5/\text{Al}_2\text{O}_3$ shows that all of the molecules under study form strong complexes which do not decompose during evacuation at room temperature. These spectra differ from the spectra of both parent and Al_2O_3 -adsorbed molecules and are similar to the spectra ascribed to carbenium ions in solution (spectra 3 and 4). A characteristic feature of the spectra of these strong complexes, in comparison with those of π -complexes, is the presence of absorption bands at $1200\text{--}1360\text{ cm}^{-1}$. A detailed analysis of the literature data on the spectra of carbenium ions in solution has been made by Koptuyg [1297] and has shown that it is this region, which is characterized by stretching vibrations of the CCC_2^+ fragment of carbenium ions, that make it possible to identify them. More specifically it was shown [19, 1298, 1299] that the spectrum of

triphenylmethyl carbenium ion is characterized by two bands at 1360 and 1300 cm^{-1} , which are more intense than the bands in the corresponding region for triphenylmethane. The 1360 cm^{-1} band is due, probably, to a C–C ring-stretching mode of the aromatic ring, which according to Whiffen [1300], absorbs at about 1323 cm^{-1} in the spectra of mono-halogen substituted benzenes and rises slightly as the electronegativity of the halogen increases. The band at 1300 cm^{-1} in the carbenium ion spectrum is probably due to a hydrogen in-plane deformation vibration of the aromatic ring, which Whiffen found to occur at 1261 cm^{-1} for iodobenzene and at 1290 cm^{-1} for fluorobenzene. These bands are apparently shifted to higher frequencies and intensified in the spectrum of the carbenium ion.

It was suggested [18] that the 1290 cm^{-1} band can represent the hydrogen in-plane deformation vibrations of the aromatic rings in the following carbenium ion:



Scheme 5.22

Buckles *et al.* [1301] have associated the intensity increases for the absorption bands at 1585, 1302, 1250, 1215 and 1116 cm^{-1} with the formation of carbenium ions. They also observed an intense band in the spectrum at 1366 cm^{-1} , which was regarded as characteristic for an aromatic carbenium ion. This band was also observed after the adsorption of triphenylmethanol on a silica–alumina catalyst, and was attributed to the triphenylmethyl carbenium ion.

The data [1193] obtained for triphenylcarbinol adsorbed on $\text{V}_2\text{O}_5/\text{Al}_2\text{O}_3$ (compare with Al_2O_3 , see Figure 5.22) also indicate the presence of this absorption band in the spectrum, and is similar to the spectrum ascribed to the triphenylcarbenium ion in solution [1298]. The same conclusion has been made in the study of triphenylcarbinol adsorbed on zeolites [1289]. On the contrary, in the case of Al_2O_3 a surface aryloxide seems to form (as shown by the appearance of an absorption band at 1170 cm^{-1}) due to an esterification reaction involving the surface hydroxyl groups.

The choice of the 4-methylene-1,1,2,3,5,6-hexamethylcyclohexa-2,5-diene as an adsorbate is due to the fact that the carbenium ion formation in solution [1297] leads to the disappearance of the 1650 cm^{-1} adsorption band, which is typical for $\nu\text{C}=\text{C}$ in trienes and associated with the CH_2 group. This serves as a test for ion formation. In fact, we have not observed this band upon triene adsorption on $\text{V}_2\text{O}_5/\text{Al}_2\text{O}_3$, in contrast to adsorption on Al_2O_3 , where this band is present and the formation of the carbenium ion is impossible (see Figure 5.22). Thus, the spectral data presented here strongly support the formation of the carbenium ions during triene adsorption on $\text{V}_2\text{O}_5/\text{Al}_2\text{O}_3$.

Spectral features of strongly bound complexes in the case of toluene and hexamethylbenzene [1193] also indicate the possibility of benzenium ion formation. In fact, the spectra observed differ significantly from those of the toluene π -complexes, benzyl anions, and benzoate structures. The spectra are similar to the spectra of the carbenium ion formed in case of the toluene- GaCl_3 HCl system (Figure 5.22), with absorption bands at 1200–1300 cm^{-1} being characteristic (Tables 5.14 and 5.15). These bands are generally characteristic of such carbenium ions, as has been mentioned above. The analysis of the numerous literature data concludes that the skeletal stretching vibrations are manifested at unusually high frequencies (ca. 1300 cm^{-1}) in the case of such arylcarbenium ions. This special feature of the spectra probably reflects the increasing of the force constants for C–C bonds (and consequent decreasing force constants of the C–H bonds) as a result of the involvement of the alkylsubstituent in hyper-conjugative interaction with the

Table 5.15. Frequency characteristics (cm^{-1})^a of C_7H_9^+ carbonium ions and C_7H_8^+ , including adsorbed as C_7H_9^+ on the surfaces of oxides.

C_7H_8 (liquid)	C_7H_9^+	$\text{V}_2\text{O}_5/\text{TiO}_2$	$\text{V}_2\text{O}_5/\gamma\text{-Al}_2\text{O}_3$	25 % $\text{MoO}_3/\gamma\text{-Al}_2\text{O}_3$		$\text{V-Sb-Bi-O}/\gamma\text{-Al}_2\text{O}_3$ (oxidized)		Assignment of bands
				Adsorption (20 °C)	'Pump-down' (20 °C)	Adsorption (20 °C)	'Pump-down' (20 °C)	
1184 (m)	1183 (i)	1187 (i)	1185 (i)	1180 (i)	1180 (i)	1187 (i)	1187 (i)	βCCH
1218 (w)	1214	—	—	—	—	—	—	$\nu\text{Ar-C}$
—	1239	—	—	—	—	—	—	—
—	1307 (i)	1298 (i)	1300 (i)	1300 (i)	1300 (i)	1297 (i)	1297 (i)	βCCH
1330 (vw)	1346 (i)	1362 (i)	1360 (i)	1360 (i)	1360 (i)	1363 (i)	1363 (i)	—
1380 (i)	—	—	—	1380	—	1380 (w)	—	$\delta_s\text{CH}_3$
—	1439 (w)	1428 (w)	1430 (w)	—	—	1430 (vw)	1430 (vw)	βCCH
1462 (i)	1452	1452	1450	1460	1460↓	1457	1457↓	$\nu\text{C-C}$
1500 (vi)	1486 (m)	1485, 1497	1490, 1500	1500	1500↓	1500	1500↓	$\nu\text{C-C}$
1581 (w)	1600 (vi)	1586,	1590 (i)	1605	1585	1597	1597	$\nu\text{C-C}$
1608 (vi)	—	1592	—	—	—	—	—	—

^a Intensities of bands: vw, very weak; w, weak; m, medium; i, intense; vi, very intense.

carbenium center. In particular, in the case of triphenylmethyl cation, the 1359 cm^{-1} frequency, which is insignificantly higher in value than in the case of triphenylmethane (1280 cm^{-1}), corresponds to the C–C bonds' stretching vibrations of C_3C^+ fragments of the cation. The presence of the 1280 cm^{-1} band in the spectrum of adsorbed, completely deuterated toluene confirms the above assignment. The other bands undergo the isotopic shifts characteristic of C–H and C=C vibrations.

To obtain additional support for ion formation, Davydov *et al.* [1193] have performed experiments on the replacement of the adsorbed molecules by ammonia. One could expect the disappearance of the characteristic hydrocarbon spectra and an evolution of the initial species into the gas phase only for the ions that are present. Indeed, admission of ammonia resulted in the formation of NH_4^+ ions and the appearance of gas-phase bands corresponding to weakly adsorbed toluene, 'triene' and triphenylcarbinol (the evolution of toluene into the gas phase has been established from the identity between the UV spectra of the gas phase and the toluene spectrum).

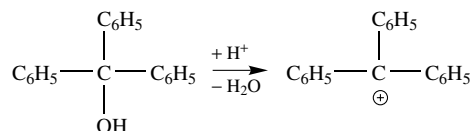
An analysis of the region of CH stretching vibrations also confirms the ionic conclusion. For example, a study of the spectrum for toluene adsorbed on $\text{V}_2\text{O}_5/\text{Al}_2\text{O}_3$ by means of IR spectroscopy allowed the registration of an absorption band at 2840 cm^{-1} which was absent in the toluene spectrum and which can be ascribed to a $>\text{CH}_2$ fragment. A similar band at 2800 cm^{-1} has been observed for individual $\text{CH}_3\text{C}_6\text{H}_5^+$ ions in solution [1297].

It should be noted that in the series, toluene ($\text{PA} = 208\text{ kcal mol}^{-1}$), mesitylene ($\text{PA} = 202\text{ kcal mol}^{-1}$), and hexamethylbenzene ($\text{PA} = 208\text{ kcal mol}^{-1}$), there is no monotonic dependence of protonation on the adsorbate basicity. The IR spectra of toluene and hexamethylbenzene on $\text{V}_2\text{O}_5/\text{Al}_2\text{O}_3$ are very similar to the spectra of the ions, while the spectrum of mesitylene resembles a superposition of the spectra of a protonated and nonprotonated compound. This nonmonotonic dependence can be explained by assuming that, as with a protonated pyridine, the benzenium ions are 'solvated' by the surface through the p-orbitals and are oriented parallel to the surface. In this instance, methyl groups can give rise to steric difficulties for such 'solvatus'. For this reason, the formation energy for protonated toluene appears to be higher than that of protonated mesitylene.

The formation of aryl carbenium ions after toluene adsorption was also identified on oxidized surfaces of both the V–Sb–Bi oxide catalyst (Table 5.15) [1303] and $\text{MoO}_3\text{-}\gamma\text{-Al}_2\text{O}_3$ [221]. Later, the aryl carbenium ions were observed upon adsorption of both toluene and *O*-xylene on the oxidized surfaces of $\text{V}_2\text{O}_5/\text{SiO}_2$, $\text{V}_2\text{O}_5/\text{TiO}_2$ and $\text{V}_2\text{O}_5/\text{Al}_2\text{O}_3$ catalysts [1304]. Unfortunately, the method of UV–Vis spectroscopy cannot be effectively used to identify the carbenium ions in all cases. It is well known [1295, 1296] that for aromatic hydrocarbon strong-acid homogeneous systems, the formation of benzene and benzyl carbenium ions is observed, which are sufficiently characterized by absorbency in the 400 nm region. However, as has been established [1181, 1305], the aromatic carbenium ions are not formed on zeolites in cases of the simple aromatic compounds. In such cases, the formation of carbenium ions does not occur, since no absorption above 330 nm is observed. Even in the case of quite complex aromatic molecules, their interactions with zeolite surfaces leads to carbenium ion formation in only some cases. For example, the adsorption of 1,3-dimethylnaphthalene at 298 K gives rise to a 290 nm absorption band in the UV–Vis spectrum and a low-intensity band at 325 nm (see Figure 5.19, spectrum 3b). The observed band is typical of alkyl-substituted naphthalenes and originates from a π -complex. Thus, the adsorption of aromatic compounds with two condensed rings also does not lead to the formation of stable carbenium ions. According to the IR spectra, the concentration of adsorbed dimethylnaphthalene is very low, and considering its molecular size, it is more probable that the adsorption occurs on the external surface of a crystalline H-ZSM-5 zeolite. This conclusion comes from the absence of perturbation of the acidic hydroxyl groups, most of which are located in the channels of these

zeolites [342]. Thus, the use of molecules of different sizes allows the testing of both internal and external surfaces.

The formation of the carbenium ion has been quite reliably shown in the adsorption of triphenylcarbinol on H-ZSM-5 zeolites, which is accompanied by the appearance of an absorption band with a 400–440 nm maximum, and an increase in absorbency at 260 and below 240 (see Figure 5.19, spectrum 4b). The sample color is yellow after adsorption. The appearance of a 400–440 nm absorption band may indicate triphenylmethyl cation formation [46, 1289], as the corresponding spectrum of the cations, obtained in acidic homogeneous media, has two bands of similar intensity at 404 and 431–434 nm in the visible region [1295, 1296]. Obviously, the reaction on H-ZSM-5 zeolites occurs as follows:



Scheme 5.23

The increase in absorbance at 1635 cm^{-1} , along with hydroxyl group perturbation, indicates the appearance of water during this reaction. The presence of adsorbed aromatics is not observed in this case by IR spectroscopy. Evidently, the formation of carbenium ions from such a large molecule takes place only on the external surfaces of crystallites. Decomposition of the carbenium ions occurs at 473 K under vacuum.

The protonation of the unsaturated side-chains (which has a proton affinity larger than those for the aromatic ring) of the alkyl aromatic compounds proceeds on the zeolites quite easily. Thus, the adsorption of styrene on H-ZSM-5 zeolites is followed by the appearance of bands at 320 and 400 nm and an increase in their intensities (Figure 5.23, spectra 1b–3b) accompanied by a gradual rise in the amount of adsorbed molecules. In the IR spectra of these samples, the appearance and intensity increases of the 1415 , 1455 , 1495 and 1615 cm^{-1} bands and the absorption bands of $\nu\text{C-H}$ in the $2800\text{--}3100\text{ cm}^{-1}$ region are observed (Figure 5.23, spectra 1a–3a). A simultaneous increase in the intensity of the 320 and 400 nm bands in the UV–Vis spectra, and of the more intense 1495 and 1615 cm^{-1} bands of the ν_{CCC} aromatic ring in the IR spectra, suggest that these bands can be attributed to the same types of aromatic surface compounds. The appearance of the maximum at a long wavelength in the UV–Vis spectrum is not due to formation of condensed (conjugated rings) compounds, since their formation is not likely at room temperature. The styrene molecule has its greatest wavelength maximum at 280–290 nm. The 320 and 400 nm absorption bands can be attributed to alkylaromatic carbenium ions, since in homogeneous systems the formation of similar structures corresponds to the appearance of the 310–340 and 380–450 nm bands [1295, 1296]. IR spectroscopy data also indicate the disappearance of unsaturated $\text{C}=\text{C}$ bonds conjugated with the ring during styrene adsorption, since in the 1600 cm^{-1} region the doublet typical of styrene molecules is not observed and absorption bands for C-H saturated vibrations appear at 1455 and $2800\text{--}3000\text{ cm}^{-1}$, respectively. The $\text{C}=\text{C}$ bond disappearance may be associated with its protonated form of carbenium ions. No significant differences are observed in the IR spectra at 1600 and 1500 cm^{-1} between charged and neutral aromatic rings [1289]; in some cases, this fact complicates the identification of alkylaromatic carbenium ions from the IR spectra. The identification of the 320 and 400 nm bands and ν_{CCC} at 1495 and 1615 cm^{-1} as arising from the same types of surface compounds, i.e. alkylaromatic carbenium ions, is also confirmed by the simultaneous disappearance of the latter bands after outgassing at 573 K (a

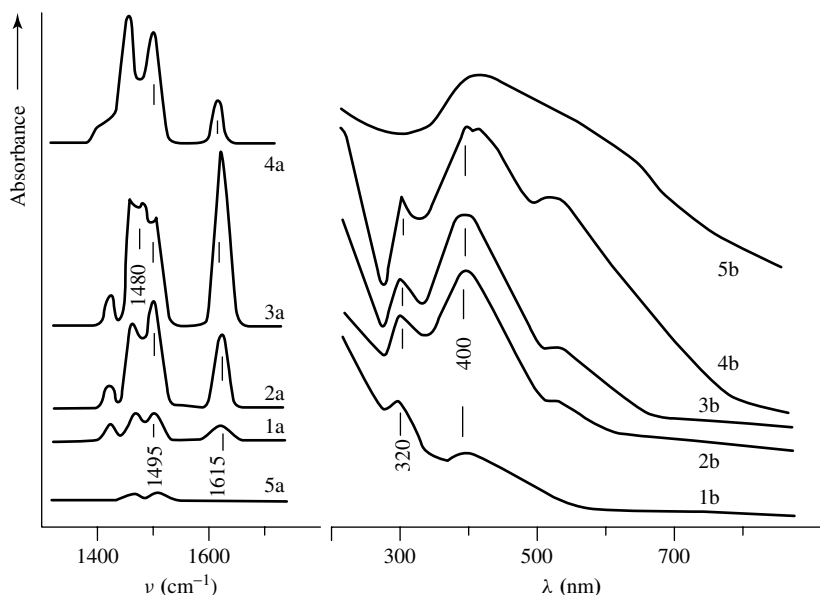


Figure 5.23. IR (a) and UV-Vis (b) spectra of H-ZSM-5 zeolite ($M = 30$) treated at 298 K with styrene: (1a, 1b) 10^{-3} torr; (2a, 2b) 2×10^{-3} torr; (3a, 3b) 3×10^{-3} torr; (4a, 4b) evacuated at 473 K; (5a, 5b) evacuated at 573 K.

strong decrease in intensity is also observed in the UV-Vis spectra) (see Figure 5.23, spectra 4a, 5a, 4b and 5b).

From the data obtained it follows that for large amounts of styrene adsorption is accompanied by secondary processes, as shown by the intensity increase of the 1615 cm^{-1} band and the appearance of a new absorption band at 1480 cm^{-1} (see Figure 5.23, spectrum 3a), due to $\nu_{\text{as}} \text{CCC}$ for alkenaromatic carbenium ions.

Thus, the formation of aromatic cations on H-ZSM-5 zeolites does not occur in the case of adsorption of aromatic hydrocarbons or condensed hydrocarbons such as dimethylnaphthalene. On this surface, alkylaromatic carbenium ions, are formed, either during protonation of an unsaturated substitute of the aromatic ring (for styrene) or during, for example, triphenylcarbinol dehydroxylation. It is evident that the presence of carbenium ions on H-ZSM-5 zeolites is due to conjugation of the ring(s) with the carbenium ions being formed via the reactions mentioned above. The lower stabilities of the triphenylmethyl carbenium ions from styrene, in comparison with alkylaromatic carbenium ions, is due to the arrangement of the latter in the zeolite pore volume, which provides a three-dimensional arrangement of the solvating (oxygen) ions.

5.2.3 π -COMPLEXES

Zeolites

The first results from the application of molecular spectroscopy to the study of the interaction between aromatic molecules and zeolites were easily analyzed by Kiselev and Lygin [19] and later by Primet *et al.* [1294]. They showed that the UV spectra reflect the type of electron system of the adsorbed molecules, the degree of perturbation of the ground and excited levels, and the exchange cations of the transition-metal elements in the zeolite which participate in the interaction. In the case of interaction with charge transfer, the UV spectra can be used to analyze the nature

of the ions formed, and hence to determine the nature of the acid centers of the zeolites. The spectrum of molecules adsorbed on zeolites with alkali exchange cations has absorption bands corresponding to molecular adsorption only. The small shift in the absorption bands (1–2 nm), corresponding to the $\pi \rightarrow \pi^*$ transition in the molecules of benzene, its aliphatic substitute, or aromatic compounds with condensed rings, can be explained in terms of the macroscopic effect of the environment on the molecules. There is a stronger change in the spectra during the adsorption of molecules of amine derivatives of benzene (for example, for aniline the shift is 5–8 nm) because of the change in the level of $n \rightarrow \pi^*$ transition which takes place due to participation of the substituent free electron pair in the interaction. According to Kiselev and Lygin [19], the red shift in the absorption band for adsorbed nitrobenzene is 15 nm and for *p*-nitroaniline, 90 nm. This seems to be explained by a perturbation of the excited electronic level that is greater than that of the ground level and which is related to an increase in the dipole moment of the molecules in the excited state. An increase in the electrostatic potential of an exchange cation, e/r , where e and r denote the charge and radius of the cation, respectively, leads to an increase in the shift in the absorption band. The differences in this wavelength dependence for molecules of *p*-phenylenediamine, aniline and pyridine, is due mainly to the different properties of the free electron pairs on the nitrogen atoms.

Strong perturbations of aromatic molecules were already observed in the first IR experiments on these molecules interacting with zeolites. For example, during the adsorption of benzene on zeolites, as in the adsorption of ethylene discussed above, a change is observed in the spectrum of the initial molecule, which indicates a strong polarization of the π -electron system [19]. Thus, after adsorption, in the spectrum of adsorbed benzene the intensity of the absorption band of the stretching vibration ν_{12} of the CH group of benzene is much lower than the intensity of the absorption band of the ring vibration ν_{13} , although the relative intensities of these bands are approximately the same in the liquid state. Similar smaller changes occur on the absorption of benzene on aerosil. Such a change in the intensity as a result of the decrease in the polarity of the CH bond of benzene is known for the condensed state. An increase in intensity of the ring vibration ν_{13} was also observed during the adsorption of a series of aromatic molecules on crystals of halides.

The appearance of the 260 nm transition in place of the fine structure of the UV band is proof of a loss of symmetry since this absorption is assumed to be a $0 \rightarrow 0$ transition which is forbidden for the free molecule [19]. The catalyst surface introduces asymmetry with respect to the ring plane. The observed blue shift may also be related to the lowering of symmetry if this causes an appropriate change in the permanent electric dipole moment or electric polarizability of the ground state relative to the excited state. The presence of the 262 nm band from various adsorbents has been explained by a benzene adsorption process involving the π -electron system of the aromatic ring. This may cause an overlap between the p'_x orbitals of the carbon atoms and the nonbonding p orbitals of the surface oxygen atoms. In this way, the electronic density of the aromatic ring is decreased and as a consequence, the bond order of the C–C bands of the ring and the force constant associated with this vibration mode must decrease. From a comparison of the IR spectra of benzene adsorbed on zeolites with that of the free molecule, it can be deduced that some frequencies are strongly displaced whereas others remain unaltered, and in addition the relative intensities of the bands are strongly modified. All of the bands with unchanged frequencies are due to fundamental vibrations which occur in the plane of the benzene ring, whereas the bands shifted to higher frequencies by adsorption are due to combinations (1964 and 1807 cm^{-1}) or fundamental (671 cm^{-1}) out-of-plane vibrations [19]. It has been assumed that the π -electrons of the aromatic ring are invalid in the adsorption process. However, the presence of lattice oxygen atoms near the adsorption sites produces steric hindrance, which limits vibrational hydrogen atom displacements below the plane of the ring. Moreover, when cations are present in the zeolite, the

out-of-plane vibrations exhibit two frequencies. For example, for calcium-exchanged Y zeolites the ν_{11} vibration mode was observed at 695 and 730 cm^{-1} , instead of 672 cm^{-1} for the free molecule or 695 cm^{-1} for the HY zeolite. The higher frequency vibration (730 cm^{-1}) correlated to a species that is more strongly held (π -complex with a cation), while the band at 695 cm^{-1} may belong to π -complexes involving hydroxyl groups. Adsorption measurements using CO as a test molecule have shown that benzene molecules adsorbed on Ca^{2+} ions are responsible for the strong perturbation of the out-of-plane vibration modes.

The spectra of benzene adsorbed on zeolites MgY, NiY, ZnY, AgY, CeY and CoY have also been investigated [1306]. The greatest changes also occur in the extra out-of-plane vibrations of the CH bonds of the aromatic ring. These authors proposed the formation of π -complexes because of the dependency of the frequencies of certain vibrations on the nature of the cations. Infrared analysis of benzene out-of-plane overtone bands (1960 ($\nu_5 + \nu_{17}$) and 1815 cm^{-1} ($\nu_{10} + \nu_{17}$) for the liquid phase) has also been used to study the interaction between benzene and alkaline cations in X and Y exchanged zeolites [1306–1319].

The formation of π -complexes with cations and with formation of the complexes with hydroxyl groups are the predominant processes [1314]. The shift of these bands to higher wavenumbers (around 20–30 cm^{-1} for the adsorption of benzene on cations, and around 50–60 cm^{-1} if the aromatic molecule interacts simultaneously with the cation acting as a Lewis acid, and with a basic oxygen-atom site) has been successfully used to investigate benzene adsorption. In addition, the changes with benzene loading of the intensities of the bands mentioned above give information about molecules adsorbed on each type of site.

In a recent paper, infrared spectra of adsorbed benzene were used to study the basicity of faujasites exchanged with various cations. The more basic zeolites give a strong interaction with the CH group of the aromatic molecule while the less basic LiY and NaY display a weak interaction [1309]. Additional recent Raman work has shown that highly polarizable molecules such as benzene can also be used to probe the properties of zeolites. Freeman and Unland [1320] studied the adsorption of benzene on a series of alkali-exchanged X and Y zeolites and used the measured shift of the ν_1 ring breathing mode (992 cm^{-1} for liquid benzene) as a diagnostic measure of the interaction with the exchange cations. In all cases, the ν_1 band shifted to lower frequencies relative to liquid benzene, with the shift being greatest for a larger ionic radius, which the authors interpreted as being evidence for an interaction between the π -electrons of benzene and the exchange cation.

The formation of π -complexes on zeolites are observed for practically all aromatic molecules, including those having several aromatic rings. Su and Barthomeuf [1316] established, by means of UV–Vis, diffuse-reflectance and photoluminescent spectroscopies, that donor/acceptor complexes of naphthalene and naphthylamine molecules are formed for alkali and alkali-earth cations with zeolites of type Y. Brønsted and Lewis acid sites of the zeolite framework could be considered to be the electron-accepting sites. The luminescent spectra of naphthalene supported the presence of such complexes with alkali and alkali-earth cations, together with physically adsorbed complexes in the X zeolites. On the surface of amorphous aerosil, naphthalene formed photostable dimer associates [1317].

Oxides

Investigations of the adsorption of individual aromatic compounds (benzene, toluene, cumene, *o*-xylene, biphenyl, naphthalene and anthracene) on $\gamma\text{-Al}_2\text{O}_3$ and MgO by means of UV–Vis and diffuse reflection spectra [1321] showed two types of adsorption of aromatic hydrocarbon molecules: (i) physical adsorption, which is characterized by a spectrum in which the vibrational structure of the bands remains present, even though the resolution may be poorer, and the bands themselves are slightly shifted towards the red region of the spectrum, and (ii) an

adsorption which is characterized by a spectrum in which the absorption bands of the vibrational structure is lost. The last type corresponds to a donor–acceptor π -complex and is characteristic for chemisorption of aromatic hydrocarbons. The comparatively small bathochromic shift of the $A_1 \rightarrow B_{2u}$ absorption band that has been observed by Asmolov and Krylov [1321] (for benzene, cumene and *o*-xylene of about 5–10 nm, which in the 260–270 nm region amounts to less than 1400 cm^{-1}) is explained on the basis that this transition is forbidden, and for weak transitions the dipole moment is little changed. Since aromatic hydrocarbons are highly symmetric, their dipole moment in the ground state A_1 and also the excited state B_{2u} is almost zero. Hence a Lewis acceptor center should give approximately equal stabilization of both states, and the authors observed only a small shift in the absorption bands.

The formation of π -complexes of aromatic compounds has been established for several oxide systems containing Lewis acid centers on the surface. The first IR spectra of toluene surface compounds were reported by Kokes and co-workers [1277]. These authors found that the toluene is chemisorbed on zinc oxide like a π -complex. The most characteristic absorption bands for such types of compounds lie in the region of the vibrations of the aromatic ring at 1605 (1610), 1494 (1500) and 1460 cm^{-1} (liquid and vapor phases). Due to the weak bonding, the first two of these absorption bands are shifted to 1593 and 1487 cm^{-1} . This is similar to the formation of the toluene–copper(II) montmorillonite complex. In this case, bands at 1593 and 1487 cm^{-1} have also been observed.

Among oxide systems, Al_2O_3 is really a typical Lewis acid. However, it should be noted that the H-bonded aryl can also give a complex with essentially the same spectral manifestations. The formation of the latter complex is more possible because there is a small concentration of acid hydroxyl groups on the surface of Al_2O_3 . Hence, in the case of this oxide direct proof is necessary that the coordinately unsaturated cations participate in complex formation, as it was done for olefins (see above). To elucidate the participation of coordinately unsaturated surface Al^{3+} ions in the stabilization of toluene molecules, Gordymova *et al.* [1249] studied the successive adsorption of CO and $\text{CH}_3\text{C}_6\text{H}_5$. After the addition of CO into the cell with toluene, the IR spectrum exhibits a weak band at ca. 2210 cm^{-1} , characterizing the $\text{Al(VI)}_{\text{cus}}\text{-CO}^*$ complex, which slightly increased in intensity after contact a long period of time (see Figure 5.20, spectrum 3). The intensity of the bands of adsorbed toluene slightly decreased, probably indicating the removal of a portion of the toluene molecules from the coordinately unsaturated Al^{3+} ions in the octahedral cavities by the CO molecules. The absence of the band of the $\text{Al(IV)}_{\text{cus}}\text{-CO}$ complex indicated the participation of coordinately unsaturated Al^{3+} ions occupying tetrahedral positions in complex formation with toluene. The π -complexes on $\text{Al(IV)}_{\text{cus}}$ ions are more stable than on the $\text{Al(VI)}_{\text{cus}}$ ions. Hence, not only the surface OH groups but also Al^{3+} ions of two types take part in the stabilization of toluene molecules.

The admission of toluene vapors to pre-adsorbed CO ($\nu\text{CO } 2210\text{ and } 2235\text{ cm}^{-1}$) does not lead to any perturbation of the OH groups or to the appearance of any toluene bands. Hence, with blocked Lewis acid centers, the surface OH groups are not the adsorption centers of toluene. Although, with the above sequence in the admission of reagents, a CO reaction (to be discussed elsewhere) takes place on the surface initially, the subsequent formation of by-products permits the molecular adsorption of toluene. With an increasing time of contact of the sample with the reaction medium at 300 K, the spectrum exhibits low-intensity bands of adsorbed toluene and absorption in the region of hydrogen-bonded OH groups. This is accompanied by a decreasing concentration of $\text{Al(VI)}_{\text{cus}}\text{-CO}$ complexes (the band at 2210 cm^{-1} decreases and shifts to 2208 cm^{-1}) and the practically complete removal of CO molecules from $\text{Al(IV)}_{\text{cus}}$ ions, which is shown by the vanishing of the maximum at 2235 cm^{-1} .

The results of this example a detailed analysis of the IR spectra in the case of adsorbed toluene [1249] confirm the existence of two-centered adsorption of toluene on coordinately

unsaturated aluminum ions and hydroxyl groups. The difference in the bond strengths of π -complexes with aluminum ions, according to the successive adsorption of CO and toluene (removed by CO from $\text{Al(VI)}_{\text{cus}}$ but not removed from $\text{Al(IV)}_{\text{cus}}$), permits the assumption that the weak complexes removed by desorption at 300 K are stabilized on $\text{Al(VI)}_{\text{cus}}$, and those retained up to 473 K and characterized by low-frequency ring vibrations (1492 and 1593 cm^{-1}) are bound with $\text{Al(IV)}_{\text{cus}}$ (TPD data likewise indicate the existence of two adsorption forms of benzene, I and II, whose adsorption activation energies are 92 and 165 kJ mol^{-1} , respectively [1322]. Analogous data were obtained for adsorbed ethylbenzene [1323].

Benzene on Al_2O_3 produces, according to the results of Busca *et al.* [1290], a reversible adsorption form which leads to perturbation of the surface hydroxyl groups. The formation of an irreversible adsorption form on the Al_2O_3 surface suggested in [1290] is connected with CO_2 impurities in the benzene as it was noted by Gordymova *et al.* [1249], but not with the presence of oxidizing centers of Al_2O_3 , and hence the heat of adsorption data for benzene molecules on Al_2O_3 reported by Rossi and Busca [1292] can be incorrect. It is more probable that the reversible form of adsorbed benzene is a π -complex with Lewis acid centers, as in the case of other aromatic molecules, which disturbs at the same time the OH group of Al_2O_3 . However, there are no direct data available in [1290] about Lewis acid centers participating in the formation of these complexes. The participation of TiO_2 Lewis acid centers in the formation of complexes with toluene was proved by Davydov [1157] by means of both FTIR (coadsorption with CO) and UV-Vis spectroscopies.

On the Fe_2O_3 surface, the presence of adsorbed species of benzene, toluene, ethylbenzene and styrene was observed by means of FTIR spectroscopy [1290, 1291] on the basis of the analysis of the IR spectra of both the free and adsorbed molecules. These authors have suggested that π -complexes are formed (Tables 5.16 and 5.17). For example, for benzene adsorbed on Fe_2O_3 , the authors observed the appearance of new bands at 1979 , 1839 , 1481 , 1403 and 1178 cm^{-1} , the assignments of which are given in Table 5.16. This species (benzene I) shows a significant enhancement of the $\nu_5 + \nu_{17}$, $\nu_{10} + \nu_{17}$, and $\nu_5 + \nu_{16}$ combination vibrations, all from out-of-plane deformation vibrations, which indicates that there is an interaction with an electron-withdrawing center nearly perpendicular to the ring. The extent of the enhancements on $\alpha\text{-Fe}_2\text{O}_3$ [1290] is more pronounced than those observed after contact with a stronger H-bonding donor such as silica [19] but is smaller than that measured on the Lewis acid centers on Na- and Ca-exchanged Y-zeolites [19], where interaction with surface cations appears to be well founded. This suggests that such a form is bonded with surface OH groups by H-bonds. These considerations, together with experimental observation of the perturbation of the bands in the $1350\text{--}1250\text{ cm}^{-1}$ region, indicates the formation of benzene species on rather strong Lewis acid centers. Support for this comes from the fact that no benzene adsorption was detected on a wet surface, where water 'poisons' the Lewis acid sites.

The most relevant spectral features of benzene II, in the authors' opinion, are the lowering of the in-plane vibration frequencies ν_{19} and ν_{20} , and the activation of ν_3 . These perturbations are similar (although smaller in extent) to those observed when benzene coordinates on a reduced metal center, as on dibenzene-chromium and analogs and on species adsorbed on metals [951, 1324]. Moreover, the measured shifts on adsorbed C_6D_6 , although small, cannot be consistent, in the authors' opinion, with a simple H-bonding interaction. It seems that benzene II is also adsorbed on a cation center, possibly reduced or sterically hindered. According to Busca, the d character of the cationic centers on Fe_2O_3 would justify the formation of π -bonded forms which are not observed on the more acidic Al_2O_3 [1324]. In our opinion, the d- π interaction cannot contribute enough to hydrocarbon stabilization on oxidized cations. Support for this comes from the analyses of CO/NO adsorption data obtained for these systems. Also, it was suggested [1290], but not confirmed that the perturbation of the surface OH groups would be due to the

Table 5.16. Vibrational frequencies (cm^{-1}) of benzene adsorbed on hematite [1290].

Benzene adsorbed on $\alpha\text{-Fe}_2\text{O}_3$		Liquid	Assignment	Notes
I	II			
3093	3089	3091	ν_{20}	Fermi resonance
3071	3069	3072	$\nu_{18} + \nu_{19}$	
3039	3038	3036	$\nu_1 + \nu_6 + \nu_{19}$	
2328	2327	2328	$\nu_{10} + \nu_{19}$	
2211	2210	2214	$\nu_9 + \nu_{18}$	
1979	1964	1960	$\nu_5 + \nu_{17}$	
1839	1821	1815	$\nu_{10} + \nu_{17}$	
	1755	1755	$\nu_6 + \nu_{15}$	
1481	1479	1479	ν_{19}	
1403	1395	1393	$\nu_5 + \nu_{16}$	
	1346	(1346)	ν_3	Inactive in D_{6h} symmetry
1178	1178	(1178)	ν_9	Raman-active in D_{6h} symmetry
1036	1036	1036	ν_{18}	

Table 5.17. Absorption frequencies (cm^{-1}) of some alkyl aromatics adsorbed on $\alpha\text{-Fe}_2\text{O}_3$ [1291].

Toluene		Ethylbenzene		Styrene		Assignments	
Adsorbed	Liquid	Adsorbed	Liquid	Adsorbed	Liquid	Ring	Chain
3089	3088	3083	3087	3090	3089	ν_{7a}	
—	—	—	—	3081	3082		νCH (vinyl)
3056	3064	3066	3066	3060	3060	ν_2	
3028	3029	3029	3029	3028	3027	ν_{20b}	
—	—	—	—	3010	3009		$\nu_s\text{CH}_2$ (vinyl)
—	2979	2970	2968	—	—		$\nu_a\text{CH}_3$
2921	2922	2940	2933	—	—		$\nu_s\text{CH}_3$
2874	2874	2881	2875	—	—		$\nu_{19a} + \delta_s\text{CH}_3$
—	1963	1975	1965	—	1960	$2\nu_5$	
1965	1941	1962	1943	1965	1945		$\nu_5 + \nu_{17a}$
1880	1855	1885	1866	1890	1885		$\nu_{10b} + \nu_{17a}$
1822	1803	1825	1801	1828	1820		$\nu_{10a} + \nu_{17a}$
1755	1740	1760	1742	1760	1740		$\nu_{10a} + \nu_{10b}$
—	—	—	—	1627	1630		$\nu\text{C}=\text{C}$
				1611			
1596	1605	1601	1605	1599	1602	ν_{8a}	
—	—	—	—	1576	1574	ν_{8b}	
1493	1496	1496	1496	1494	1494	ν_{19a}	
		1460	1460	1449	1448	ν_{19b}	
1456	1462	1453	1453	—	—		$\delta\text{CH}_2, \delta\text{CH}_3$
—	—	—	—	1417	1412		δCH_2 (vinyl)
1384	1379	1376	1376	—	—		δCH_3
—	—	—	—	1319	1317		δCH (vinyl)
1180	1175	1179	1185	1150	1155	ν_{9a}	

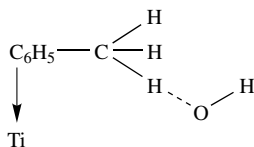
interaction of some of the hydrogens of the benzene with the nonbonding orbital of the hydroxyl oxygen, so justifying the small isotopic effect previously observed. Toluene and benzene form, more probably, just one type of molecular complex (Table 5.17).

In the case of styrene [1290, 1291], the presence of a rather weak component at 1611 cm^{-1} (Table 5.17), on the lower-frequency side of the $\nu\text{C}=\text{C}$ band, may be due to the presence of an adsorbed species where the vinyl double bond also interacts with electron-withdrawing centers. In the case of toluene, an increase in the time of contact leads to an anomalous increase of the band near 1460 cm^{-1} and to a new band at 2969 cm^{-1} . It was suggested that a new species has been formed which is more strongly bonded to the surface and is characterized by bands at 2961, 2940, 2878, 1498, 1469, 1393 and 1369 cm^{-1} . However, an identification of the nature of this species is rather difficult. On the basis of a comparison with ZnO, the authors suggest that these bands result from a chemisorbed benzyl species. However, there is insufficient data available to allow this complex which is formed to be identified.

At higher temperatures, the interaction with Fe_2O_3 exhibits oxidative properties. Starting from about 473 K, all three aromatic molecules are transformed on the iron oxide surface, and benzoate ions are clearly observed. In the case of styrene and ethylbenzene, at least one other type of carboxylate species is also present (probably an acetate), while a transient species, which further transforms to a benzoate, is also detected. This species, which adds to the bands which are characteristic of the phenyl group, shows two rather intense absorption bands at ca. 1540 and 1378 cm^{-1} . A tentative assignment of these bands has proposed them to be the $\nu\text{C}=\text{C}$ and δCH_2 of an η^2 surface complex of styrene, such as is known in homogeneous organometallic complexes. The nature of such oxidized complexes in the case of benzene has not yet been established, although the position and number of absorption bands observed in the IR spectra of adsorbed C_6H_6 (C_6D_6) indicate an aromatic character.

The data obtained for styrene adsorption [1290, 1291] also show that the styrene is very weakly adsorbed through the aromatic ring, presumably via a π -type bonding interaction. Adsorption of styrene onto the Fe_2O_3 surface at 298 K (Table 5.17) has only a minimal effect on the positions and relative intensities of the gas-phase features of the vinyl group. The $\text{C}=\text{C}$ stretching band frequency decreases from 1645 to ca. 1630 cm^{-1} , while the in-plane $\text{C}-\text{H}$ bands of $=\text{CH}_2$ and $-\text{CH}=\text{C}$ increase. The bending modes at 910 and 990 cm^{-1} are unaffected by the adsorption. Thus, the vinyl group of styrene is only moderately perturbed by adsorption onto the unpromoted Fe_2O_3 surface. However, the out-of-plane skeletal mode at 700 cm^{-1} is completely absent from the vibrations arising from the aromatic ring, hence suggesting that the ring is constrained in its movement due to surface interactions. The skeletal $\text{C}-\text{C}$ stretching bands between 1600 and 1000 cm^{-1} , and the $\text{C}-\text{H}$ out-of-plane band at 775 cm^{-1} , are largely unaffected by the adsorption, exhibiting only slight shifts to lower frequencies in the bands at around 1510 and 1600 cm^{-1} . Possibly, this species is a π -complex involving the ring.

In conclusion, it should be noted, that, through favorably geometric parameters, the π -complexes of aromatic compounds similar to that of olefins are able to form addition H-bonds with basic hydroxyl groups [1157, 1249]:



Scheme 5.24

The energy of interaction between CH and OH⁻ is not very high and is close to those in propylene complexes.

5.2.4 INTERACTION WITH IONIC PAIRS

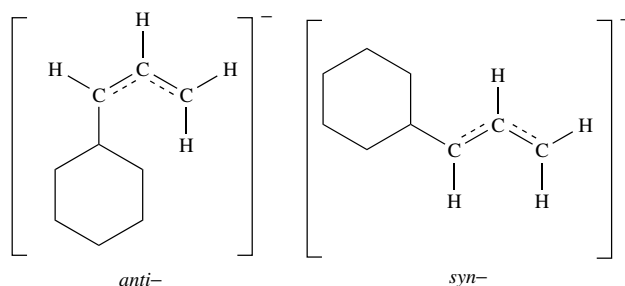
Adsorbed toluene on zinc oxide, according to Chang and Kokes [1277], underwent dissociation as was shown by the growth of a new OH band at 3575 cm⁻¹ and two new bands at 1585 and 1482 cm⁻¹ due to stronger chemisorption of the dissociated benzyl species. Prolonged evacuation at room temperature removed nearly all of the π -complex surface species, but little of the dissociated species. However, desorption of the dissociated species occurred when the sample was heated to 248 K.

It was found [1157, 1249] that on γ -Al₂O₃ and TiO₂, unlike on ZnO [1277], toluene dissociation to produce benzyl forms and OH groups does not occur; in other words, there is no splitting of the C–H bond of the methyl group at moderate temperatures. Based on a study of the adsorption of a series of H-containing weak acids on zinc oxide, the conclusion was drawn [1277] that the extent of dissociative adsorption depends mainly on the value of the pK_a of the adsorbate. Such a process takes place at pK_a < 36 but does not occur above that value (see Section 5.1). By comparisons with ZnO interactions with N₂ or H₂, they concluded that a limited number of paired zinc and oxygen sites are active.

According to the analysis of the data obtained for C₃H₆ and C₇H₈ adsorption over ZnO and Al₂O₃ and taking into account the close values of pK_a for toluene and propylene (pK_a = 35), it may be concluded that the dissociative adsorption of substances on paired ion sites, Mⁿ⁺O²⁻, is controlled not only by the pK_a of an H-containing adsorbate, but also by an optimal distance between the electron- and proton-donor sites in the adsorbate, that is, by the geometric correspondence between the surface ion pairs and the functional groups of the adsorbed molecules reacting with this pair. Support for this conclusion comes from structural data.

Toluene adsorbed on zinc oxide as a π -complex has bands at 1593 and 1487 cm⁻¹ and hence underwent dissociation. The formation of a new O–H band at 3575 cm⁻¹ was accompanied by the growth of two new bands at 1585 and 1482 cm⁻¹. Additional adsorption studies with alpha-D₃-toluene (C₆H₅CD₃) indicated that the dissociation of toluene occurred via the rupture of the methyl carbon–hydrogen bond. Chang and Kokes conclude that ‘in situ’ IR studies strongly support the view that zinc oxide acts as a basic catalyst and that its effective ‘basicity’ is comparable to that of the allylic carbanion, but weaker than that of the vinyl carbanion [1277].

Infrared spectra from allylbenzene (3-phenyl-1-propene, C₆H₅CH₂CH=CH₂) adsorbed on zinc oxide were recorded in the region 3800–1000 cm⁻¹ by Nguyen and Sheppard [1325]. In spite of the absence of a reported assignment of the vibrational spectrum of allylbenzene itself in the literature (Table 5.18), these authors have given quite a detailed interpretation of the spectrum observed. Together with a weakly bound adsorption form of allylbenzene, which was easily removed by evacuation and has spectral manifestations as for the free molecule, an additional band occurred at 1640 cm⁻¹ (which is probably, due to a π -complex). By analogy with the case of adsorbed propylene [1273], almost certainly denotes the formation of a dominant phenylallyl anionic species of the formula [C₆H₅CH₂CH=CH₂]⁻ from adsorbed allylbenzene. These results are in good agreement with previous observations for phenylpropynes [1326], ethynylbenzene [1327] and toluene [1277] adsorbed on zinc oxide. The difference between the wavenumbers of the ν CCC bands and those of the ν C=C of the parent hydrocarbons (–78 cm⁻¹ for allylbenzene compared with –107 cm⁻¹ for propylene) is probably caused by partial delocalization of the negative charge in the aromatic compounds away from the side-chain, leading possibly to weaker adsorption interactions with Zn²⁺ ions. Chang and Kokes [1277] remark that the anionic species depicted above could have two conformations, i.e. *syn*- and *anti*-:



Scheme 5.25

Table 5.18. Infrared frequencies (cm^{-1})^a of allylbenzene and adsorbed species from allylbenzene on zinc oxide alone and on the same oxide containing pre-adsorbed hydrogen.

(In CCl_4 solution)	Adsorbed on ZnO alone (after evacuation)	Adsorbed on ZnO containing preadsorbed hydrogen
1032 (st)	1025 (m)	1020 (m)
1074 (m)	1075 (mw)	1074 (mw)
1110 (w)	1110 (vw)	1107 (vw)
1158 (vw)	1150 (m)	1143 (m)
1180 (m)	1170 (sh,m)	1172 (w)
1192 (sh)	1210 (w)	1210 (w)
1285 (m)	1260 (sh,m)	1250 (w)
1297 (m)	1290 (st)	1287 (m)
1330 (w)		1300 (sh)
1340 (sh)	1325 (w)	1325 (w)
1358 (vw)	1340 (w)	1340 (w)
1382 (w)	1385 (w)	1375 (w)
1413 (m)	1420 (sh,w)	1420 (w)
1432 (vst)	1450 (m)	1448 (m)
1440 (sh)	1500 (vst)	1490 (st)
1453 (vst)		1515 (sh,m)
1470 (sh)		1560 (sh,m)
1494 (vst)	1560 (vst) $\nu_{\text{as}}\text{CCC}$	1570 (st)
1585 (sh)	1580 (st)	1584 (vst)
1600 (vst)	1600 (sh)	
1638 (vst)		1640 (w)
1802 (m)	1670 (vw)	1660 (w)
1830 (m)	2740 (vw)	
1940 (m)	2862 (w)	2857 (w)
1957 (w)		2900 (w)
2835 (m)	2925 (st)	2920 (m)
2902 (vst)	2942 (st)	2940 (w)
	2968 (st)	2958 (st)
	2995 (vw)	~2995 (vw)
2980 (vst)	3030 (vst)	3025 (st)
3006 (w)		3050 (m)
3030 (vst)	3065 (st)	3062 (st)
3065 (vst)	3082 (sh,w)	3082 (w,sh)
3087 (vst)	3105 (sh,vw)	
3100 (sh)	3520 (m)	3515 (m)
	3594 (m)	3590 (m)

^aw, weak; vw, very weak; m, medium; st, strong; vst, very strong; sh, shoulder.

Based on the study of Chang *et al.* [1259], about adsorption of *cis*- and *trans*-2-butene they favor the attribution of the prevailing ν C=C absorption to the more stable *anti*-form.

Another intense band at 1290 cm^{-1} , in the authors' opinion, probably originates from a CH in-plane deformation mode of the anionic group. A band at this position in the spectrum of allylbenzene itself is much weaker. The presence of a single δ CH₂ absorption near 1420 cm^{-1} is also consistent with removal of the hydrogen atom from the CH₂ group of allylbenzene. This fact is very interesting, because the 1420 cm^{-1} band can also be used to identify the benzyl anionic structures. The other types of vibrations for adsorbed phenylallyl are close to those of the parent molecule. Bands at ca. 1600, 1580, 1500, 1450 and 1025 cm^{-1} probably correspond to the analogous aromatic ring skeletal modes of the parent hydrocarbons.

The benzyl species were also observed on the adsorption of toluene on V-Sb-Bi-oxide catalysts (Table 5.19), the surface of which was pre-treated by ammonia [1303]. The presence of the 1430 cm^{-1} (δ CH₂) absorption band was significant for the identification of benzyl compounds and occurred together with other bands characteristic for benzene ring vibrations.

The adsorption of benzene, toluene and *m*-xylene on V₂O₅/ZrO₂ and V₂O₅/TiO₂ (1.2–3.0 wt%. V₂O₅) has also been investigated by means of FTIR spectroscopy [1328] indicating an important role for coordinatively unsaturated vanadium ions in forming surface π -complexes. Surface vanadyl species, acting as bases, abstract hydrogens from the methyl groups of the hydrocarbon π complexes to give benzyl species, which are oxidized to benzaldehyde at 373 K and to benzoate species at 473 K. The observed frequencies of the intermediate species formed upon room temperature adsorption are summarized in Table 5.20 and indicate that this compound retains an intact aromatic ring. The authors assigned the bands at 1428 and 1362 cm^{-1} to the scissoring and wagging modes of perturbed methylene groups in the surface benzyl species. The reason for assignment of the latter band is not clear as no supporting analogous results were indicated. The 1428 cm^{-1} band is close to the band observed by Azimov *et al.* [1303], on the basis of which the benzyl structure was identified.

Table 5.19. Frequency characteristics (cm^{-1})^a of toluene adsorbed as benzyl on V-Sb-Bi-O/ γ -Al₂O₃ catalyst systems, treated at 673 K with a (NH₃ + O₂) mixture, in comparison with IR spectroscopic data on benzyl halides.

Adsorption (20 °C)	Toluene		C ₆ H ₅ CH ₂ Cl	C ₆ H ₅ CH ₂ Br	Assignment of C ₆ H ₅ CH ₂ Hal bands
	Heating (100 °C)				
	2 min	10 min			
1187 (w)	1187 (↑)	–	1183 (w)	1181 (w)	β CCH
–	–	–	1209 (m)	–	ν Ar–C
–	–	–	1264 (m)	1226 (m)	ω CH ₂
1297	1297 (↑)	–	1323 (w)	1323 (w)	
1363	1363 (↑)	–	1333 (w)	–	–
1390	1390	1390	1387 (w)	–	–
1430	1430 (↑)	1430	1445 (m)	1441 (m)	δ_s CH ₂
1457 (I)	1457	1457	1456 (I)	1456 (I)	ν C=C, 19b
1502 (I)	1502	1502	1497 (I)	1497 (I)	ν C=C, 19a
1605	1600–1605	1605	1585, 1604	1590 (w), 1610 (w)	ν C=C, 8a, 8b

^aIntensities of bands: w, weak; m, medium; I, intense; ↑, shows an increase in intensity of the band.

Table 5.20. Absorption frequencies (cm^{-1}) of the intermediate product of toluene adsorption and comparison with metal–benzyl (Bz) species.

Toluene adsorption on V-Ti-O	$\text{C}_6\text{H}_5\text{CH}_2\text{-SnCl}_3$	$\text{C}_6\text{H}_5\text{CH}_2\text{-HgCl}$	Assignment
3075		3082 } 3062 } 3028 }	νCH (phenyl)
2980		2982 } 2940 }	νCH (methylene)
2930			
1592, 1586	1602, 1585	1597, 1581	8a, 8b
1497, 1485	1498	1493	19a
1452	1454	1454	19b
1428	1411	1416	δCH_2
1362		1117	ωCH_2
1298	1210	1212	$\nu\text{Ar-C}$
1187	1185	1182	9a

5.2.5 COMPLEXATION WITH SURFACE OXYGEN

Hydrogen-bonds with surface oxygen

As in the case of olefins, aromatic compounds can form weak complexes due to the formation of H-bonds with nucleophilic centers (O^{2-}). For strong nucleophilic centers such a bond is characterized by a low-frequency absorption band at 2750 cm^{-1} [774, 775] and can be easily observed. As a rule, such complexes are destroyed by evacuation at room temperature. However, reliable spectral manifestations of such complexes are still absent from the literature because of overlapping spectra from other surface compounds. It is necessary to choose special systems to observe such complexes, for example, as has been done for propylene.

The formation of such bonds can lead to the opening of the benzene ring due to nucleophilic attack on the C–H bond, for example, in a π -complex. As a result, oxidized complexes of benzene can be formed.

Formation of oxidized complexes

The adsorption of toluene at 300 K on an oxidized surface of CuO leads to the appearance of weak absorption bands at 1420, 1540 and 1600 cm^{-1} (Figure 5.24, spectra 2), the intensity of which increase with increasing contact time or on raising the temperature of adsorption (spectrum 3). These bands may be attributed to a benzoate surface structure ($1420, \nu_s\text{COO}$; $1540, \nu_{as}\text{COO}$ and νCCC) as they agree with the IR spectra of such species obtained from initially adsorbed benzaldehyde or benzoic acid. These 1420 and 1540 cm^{-1} absorption bands do not change their positions in the spectrum of adsorbed perdeuterotoluene. This appearance of benzoate complexes on the surface of CuO at 300 K is also evidence for the dissociation of the toluene molecules via the C–H bond in the CH_3 group. Based on analogy with data on propylene adsorption over copper-containing systems, it can be assumed that heterolytic dissociation occurs with the formation of benzyl structures. Unfortunately, it was impossible to confirm the formation of these structures themselves because of the high rate of their transformation to benzoate compounds. The concentration of benzoate complexes on CuO has a tendency to increase with increasing reaction temperature up to 473 K (spectra 4).

The formation of benzoate complexes occurs practically on all oxides, although the temperature of their formation depends on the strength of the ‘metal–oxygen’ bond and decreases as these decrease. In our opinion, the formation of the benzoate structures is also possible from the

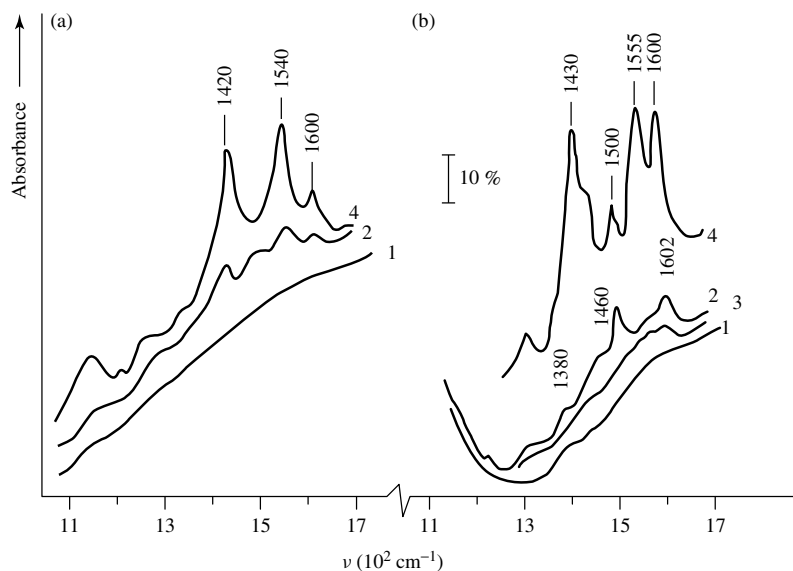


Figure 5.24. IR spectra of toluene adsorbed on (a) CuO and (b) CuO/Al₂O₃: (1) background spectra of the oxidized sample; (2) toluene adsorption (10 torr) at 300 K; (3) subsequent desorption at 300 K; (4) after heating in toluene at 473 K.

transformation of the carbenium ion, C₇H₉⁺, as has also been shown in the case of V₂O₅/Al₂O₃ for C₂H₄ and C₃H₆ [1050].

Upon increasing the interaction temperature to 723 K for γ -Al₂O₃ with toluene and ethylbenzene, the spectra exhibit two new maxima at around 1445 and 1550 cm⁻¹ (practically unshifted in CD₃C₆D₅ adsorption) besides the bands of ring vibrations [1249]. All of the maxima observed in the spectra under these conditions belong to the same species, as shown by their identical behavior in adsorption and desorption cycles. Taking into account that their position is close to the bands of aluminum benzoate [1249, 1329] and the spectra of adsorbed benzoic acid and benzaldehyde [1330], it can be postulated that at high temperatures toluene is adsorbed on Al₂O₃ as the benzoate, which is in agreement with Deflin *et al.* [1331]. Benzoate species formed on Al₂O₃ are stable, and their desorption (most likely with decomposition) occurs only at temperatures above 723 K.

It should be noted that, unlike Gordymova *et al.* [1249], Deflin *et al.* [1331] observed benzoate species in the adsorption of toluene on Al₂O₃ at more moderate temperatures (ca. 473 K). The formation of benzoates at low temperatures can be attributed either to the presence of different oxidation centers (transition-metal ions) on the alumina samples [1331], or to the insufficient purity of the toluene (e.g. with admixed benzaldehyde or benzoic acid).

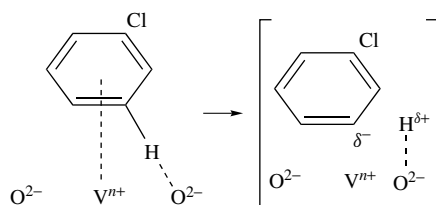
It was expected that the initial step of toluene adsorption could be confirmed by using copper oxide supported on alumina characterized by a lower oxidizability, e.g. with respect to propylene [1253], than pure CuO. The adsorption of toluene, on the oxidized surface of CuO/Al₂O₃ leads to the formation of complexes of the benzoate type (adsorption bands at 1430 (ν^s COO), 1560 (ν_{as} COO) and 1600 (ν CCC) cm⁻¹ (Figure 5.24, spectrum 4) and the formation of an additional weakly bound complex is observed (compare spectra 2 and 3). This complex has bands at 1380, 1500 and 1602 cm⁻¹, which are removed by outgassing at 300 K. In its spectral parameters and stability, this complex is similar to the π -complex formed on cations on alumina is converted to benzoate at high temperature (spectrum 4).

5.2.6 FORMATION OF ARYL HALIDE COMPLEXES

As for olefinic halides, it should be taken into account that the halide atom has (weak) electron-donor properties, so that donor-acceptor complexes (DACs) can be formed with $RCl: \rightarrow M^{n+}$ bonds. Such compounds are prone to dissociation of the C–Cl (or C–Hal) bonds with the participation of ionic pairs. In the case of transition-metal cations, which incompletely occupy d-orbitals, the tendency to form π -complexes increases, because of the contribution of the $d \rightarrow \pi$ interaction. The effect of solvation is also significant for π -complexes, since these, unlike those of the DAC-type, are adsorbed in a more ‘flat’ manner.

Interaction with cations and ionic pairs

The number of systems investigated is limited. The formation of aryl halide complexes on V_2O_5 has been studied in more detail. It is possible to believe that the initial interaction with V_2O_5 [1332] at low temperatures proceeds without a rupture of the C–Cl bond due to the ability of the π -system to promote π -complexes. IR spectra obtained after the adsorption of chlorobenzenes (chlorobenzene, *o*-, *p*- and *m*-dichlorobenzenes) at 293 K on the V_2O_5/Al_2O_3 catalyst surface contain intense absorption bands which differ little from those in the spectra of the parent compounds [14]. Intense absorption bands characterizing vibrations mainly involving the rings (absorption bands at 1485 cm^{-1} for benzene, at 1490 and 1585 cm^{-1} for chlorobenzene, and at 1470 and 1580 cm^{-1} for *o*-dichlorobenzene) and the deformation vibrations of the C–H and C–Cl bonds [14] appear in the experimentally accessible spectral range. These bands indicate the retention of the molecular structures of the adsorbates. All of the absorption bands observed (for the same hydrocarbons) behave similarly in the adsorption–desorption cycles. Such complexes are weakly bound to the surface and undergoes virtually complete removal as a result of desorption at 293 K. It is most likely that the observed complexes bond with the catalyst surface via their π -electron systems [1332, 1333]. There are absorption bands at 1085 cm^{-1} (chlorobenzene) and 1125 cm^{-1} (*o*-dichlorobenzene) which correspond, according to Sverdlov *et al.* [14], to the CCl bond vibrations, in the IR spectra of the adsorbed chlorobenzenes. However, after decomposition of such complexes by desorption at 373 K, the bands of the stronger adsorbed species were observed in the spectra (Figure 5.25, spectra 2–4). This indicates that the aromatic ring is retained in the strongly adsorbed compounds. The compounds characterized by these absorption bands represent, in our view, σ -bond complexes of hydrocarbons retaining the benzene ring. However, the spectral data do not allow the unambiguous identification of the σ -complex. Davydov and co-workers [1332, 1334], on the basis of the combined analysis of both IR and thermodesorption data, have suggested that the anion complex:



Scheme 5.26

can be formed. In the case of vanadium catalysts, phenoxide complexes have never been observed after adsorption of chlorobenzenes (Figure 5.25 spectra 4 and 5). This supports the argument that the initial splitting of hydrocarbons occur at C–H, and not C–Cl, bonds. The anionic hydrocarbon

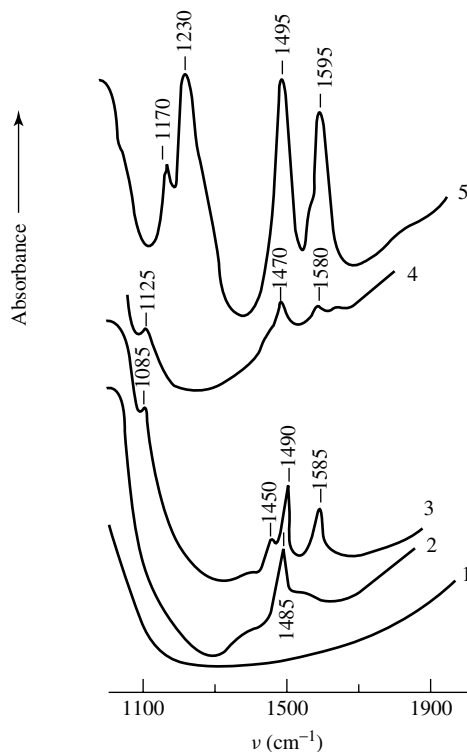


Figure 5.25. IR spectra of hydrocarbons adsorbed at 293 K on a $V_2O_5/\gamma\text{-Al}_2O_3$ after following desorption at 373 K: (1) background spectrum; (2) benzene; (3) chlorobenzene; (4) *o*-dichlorobenzene; (5) phenol.

fragment formed can rapidly give up electrons to the cationic center, especially when this center is oxidized (clearly the $V^{5+} \rightarrow V^{4+}$ oxidation–reduction potential is smaller than the $V^{4+} \rightarrow V^{3+}$ potential, etc.) or the reaction medium contains molecular oxygen which has a higher electron affinity. Thus, the hydrocarbon fragment will tend to become ‘cationic’ in nature as a result of electron transfer and will subsequently naturally undergo nucleophilic attack with the formation of a partial oxidation product (or intermediate). That means that in the equilibrium between σ -complexes and their reaction products the equilibrium is shifted towards the products so that the complex concentration cannot be large.

Together with the formation of adsorbed compounds retaining the aromatic ring (σ -complexes), the interactions with the vanadium catalyst at 473 K also involve the formation of surface compounds characterized by absorption bands at 1460 and 1560 cm^{-1} . There is no doubt that these absorption bands characterize the ν_s and ν_{as} vibrations of the COO^- groups in compounds of the type R-COO^- , i.e. they characterize the structure formed as a result of ring opening and interaction with the oxygen of the catalyst surface by the schemes suggested by Davydenko *et al.* [1332].

Interaction with oxygen

In contrast to the case analyzed above, another type of interaction between chlorobenzene and oxide is realized for CuO. The IR spectra of chlorobenzene adsorbed on CuO [1335] shows intense absorption bands at 1170, ca. 1260, 1485 and 1590 cm^{-1} (Figure 5.26, spectrum 2).

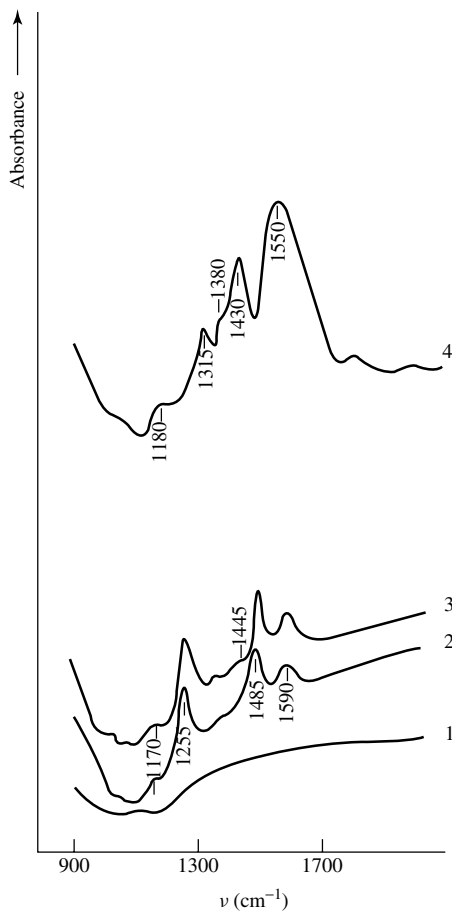


Figure 5.26. IR spectra of (1) the oxidized CuO sample, and after chlorobenzene adsorption at (2) 293, (3) 373, and (4) 473 K.

Interaction at 373 K (spectrum 3) changes the spectral pattern very little, whereas temperature elevation to 473 K (spectrum 4) gives rise to two new bands at 1430 and 1550 cm^{-1} and causes weak absorption at 1660 cm^{-1} . Variations in the spectra recorded during adsorption and desorption have been analyzed to show that the complexes, observed initially at low adsorption temperatures, vary in a similar way and can thus be assigned to surface compounds of the same type. The assignment of the narrow and rather intense absorption bands at 1485 and 1590 cm^{-1} to the ring vibrations is unambiguous. A comparison of this spectrum with that of chlorobenzene adsorbed on $\text{V}_2\text{O}_5/\text{Al}_2\text{O}_3$ (see Figure 5.25) points to significant differences in the character of chlorobenzene adsorption on CuO, as compared to $\text{V}_2\text{O}_5/\text{Al}_2\text{O}_3$. For example, the spectrum of chlorobenzene adsorbed on CuO shows no absorption band at about 1080 cm^{-1} , which is typical of chlorobenzene and its π -complexes and is assigned to the C–Cl bond vibrations (Figure 5.25, spectrum 3). Instead, it shows an intense band ca. 1260 cm^{-1} , which is missing in the spectra of chlorobenzene [14]. The absence of the band at ca. 1080 cm^{-1} (spectrum 2) indicates that, on chlorobenzene adsorption, either dissociation or substantial weakening of the C–Cl bond occurs. In the case of CuO, monitoring of this region is not a problem because CuO

itself exhibits no intrinsic absorption, in contrast to the majority of the other oxides, including V_2O_5 . An analysis of the position of the absorption band developed at 1260 cm^{-1} allows (using tables of characteristic vibrations [13, 14]) us to assign this band to $\nu\text{C-O}$, indicating the formation of a phenolate complex of the $\text{M-O-C-C}_6\text{H}_5$ type (Figure 5.25, spectrum 5). Here, the band at 1260 cm^{-1} characterizes νCO , the bands at 1485 and 1590 cm^{-1} belong to νCCC of the ring, and the band at 1445 cm^{-1} is assigned to δCH of this surface compound. Since the spectrum obtained is similar to that of surface copper phenolate (Table 5.27), this supposition was verified by a study of the IR spectra of phenol adsorbed on CuO [1336]. To summarize, this evidence indicates that, at low temperatures, chlorobenzene is adsorbed on CuO by a heterolytic dissociating mechanism with cleavage of the C-Cl bonds and the formation of the surface phenolate. Evidently, Cl^- is abstracted, and the carbon fragment retains a positive charge, which induces its interaction with the surface oxygen (O^{2-}), thus yielding phenolate.

Interaction at 473 K causes oxidation of a certain part of the surface phenolates. This is shown by the disappearance of the ring vibration bands and band of $\nu\text{C-O}$ (Figure 5.26, spectrum 4). The occurrence of the oxidation reaction is also corroborated by intense bands at ca. 1430 and 1550 cm^{-1} , assigned to $\nu_s\text{COO}^-$ and $\nu_{as}\text{COO}^-$ in the R-COO^- -type structure that have been reported in numerous IR spectroscopic studies [30, 1336]. Ring opening must be considered for the formation of such a structure from phenolate. Presumably, an increase in the oxygen mobility and reactivity in cupric oxide is caused by the elevation of the interaction temperature to 473 K . As a result, further oxidation of the phenolates with the ring opening becomes feasible.

5.3 Complexation of alkynes

Spectroscopic investigations of the adsorption of alkynes on oxide surfaces were started in early studies on the application of these methods in adsorption and catalysis (see, for example, [18, 19]).

The species so formed are of considerable interest, and various configurations for the adsorbed species have been proposed. These include both associative and dissociative reactions, as well as 'end-on' and 'parallel' adsorbed species. As observed for olefins (e.g. ethene), the spectral manifestations of the adsorbed acetylene on the oxide surfaces are determined by the strong polarization of the π -bonds on adsorption. As a result, the interaction of symmetrical substituted alkynes leads to a redistribution of the electron density of the π -bonds, thus eliminating the center of symmetry and producing new absorption band(s)

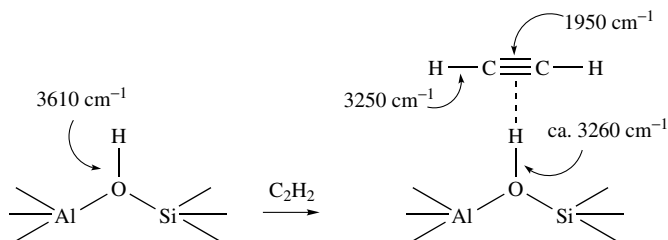
5.3.1 SILICON DIOXIDE ZEOLITES

H-bond silicon dioxide zeolites

The formation of a H-bond between the acetylene molecule and the OH groups of SiO_2 leads to an appearance of the $\nu=\text{CH}$ absorption band at 3250 cm^{-1} , which is usually active in the Raman spectrum only [531]. For gaseous acetylene, bands at 3374 and 1974 cm^{-1} are of the same symmetry and are from normal modes involving coupled νCH and $\nu\text{C=C}$ group motions, whereas that at 3289 cm^{-1} is a pure $\nu=\text{CH}$ mode [18].

Acetylene, methyl acetylene and ethyl acetylene interact with the Brønsted acid sites of H-ZSM-5 zeolites forming hydrogen-bound (precursor) species characterized by well-defined IR features [1337]. These authors assign the sharp band at 1950 cm^{-1} to the $\text{C}\equiv\text{C}$ stretching mode of the bound C_2H_2 molecules. Hydrogen bonding renders the Raman mode of free acetylene (at

1974 cm^{-1}) IR-active, and causes a low-wavenumber shift of 24 cm^{-1} (because electronic charge is removed from the π -orbitals). The corresponding C–H stretching, as expected, appears at 3250 cm^{-1} , superimposed on a broader composite spectrum due to hydroxyl groups perturbed by the hydrogen-bonding. The unperturbed hydroxyl groups which are involved absorb at 3670 cm^{-1} (Al–OH extra-framework species) and at 3610 cm^{-1} (bridged-framework hydroxyl groups with Brønsted character) [1337]. Silanol absorptions (the bands at 3750–3740 cm^{-1}) are unaffected by C_2H_2 adsorption at room temperature. The shifts caused by hydrogen-bonding are $\Delta\nu = 290$ and 350 cm^{-1} for the bridge and extra-lattice OH groups, respectively [1337]. These authors proposed the following scheme for the interaction with acid hydroxy groups:

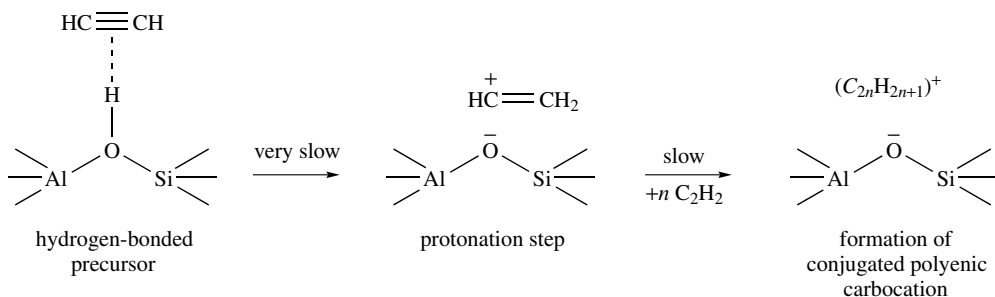


Scheme 5.27

Carbenium ions

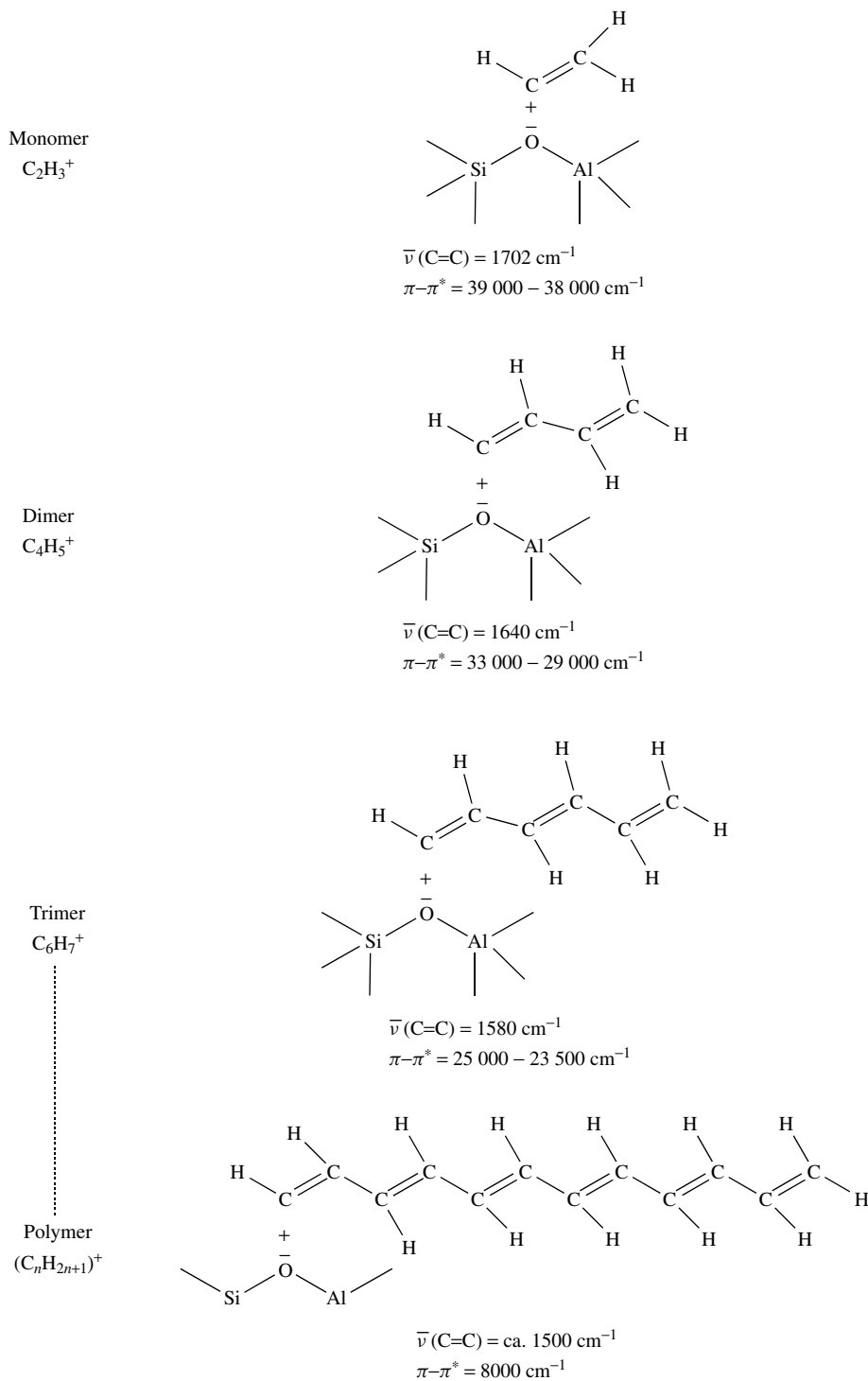
H-ZSM-5 is a highly acidic zeolite which can protonate acetylene similar to propene (see above) and initiate a carbocation polymer chain [1337–1341]. Pereira *et al.* [1339] have recently reported polymerization of acetylene in an H-ZSM-5 sample with Si : Al = 35 : 1. They found a negligible reaction rate at temperatures lower than 425 K. Polymerization of methyl acetylene in several H-zeolites has been reported by Cox and Stucky [1341], while CoY and NiY zeolites have also been used for acetylene polymerization [1342].

Bordiga *et al.* [1337], using both IR and UV–Vis spectroscopies have obtained data analogous to those for olefin transformations in zeolites. They showed that the following scheme of transformations is realized:



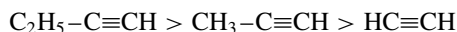
Scheme 5.28

On the base of spectral data, the following chain of transformations for carbocationic complexes has been established:



Scheme 5.29

In this case, as for carbenium ions of olefins, the authors observed a regular shifting of the $\nu\text{C}=\text{C}$ and $\pi-\pi^*$ transition bands when the length of the carbenium ion increased. Analogous transformations were also observed in the case of methyl acetylene and ethyl acetylene. Spectral identification of the species formed in these cases is shown in Table 5.21. The speed of protonation changes in the following order:



The positive charge in the carbocationic species can be captured by bases (NH_3 and Py) and subtracted to give π -delocalization. This is accompanied by the disappearance of the spectroscopic manifestations associated with the positive charge and by the appearance of new absorptions associated with neutral oligomeric chains.

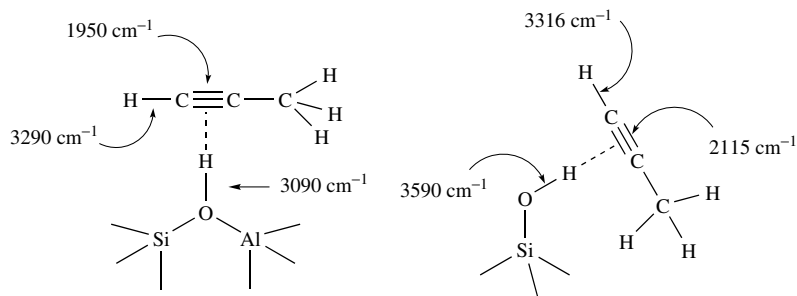
For methyl acetylene, the H-bound complexes are characterized by the frequencies represented in the following:

Table 5.21. Summary of IR and UV-Vis bands of some acetylenes [1337].

Carbocationic species	ν (C=C) (cm^{-1})	$(\pi-\pi^*)$ (cm^{-1})	Neutralized species	ν (C=C) (cm^{-1})	$(\pi-\pi^*)$ (cm^{-1}) ^a
Acetylene					
C_2H_3^+	1702	39 000–38 000	$\text{C}_2\text{H}_3 \cdot \text{ND}_3^+$	1645	(60 000–50 000)
C_4H_5^+	1640	33 000–29 000	$\text{C}_4\text{H}_5 \cdot \text{ND}_3^+$	1650–1570	45 500–42 000
C_6H_7^+	1580	25 000–23 500	$\text{C}_6\text{H}_7 \cdot \text{ND}_3^+$	1650–1570	39 000–36 000
				1510–1430	
C_8H_9^+	1565	20 500–19 500	$\text{C}_8\text{H}_9 \cdot \text{ND}_3^+$	1650–1570	36 000–32 000
				1510–1430	
$\text{C}_{10}\text{H}_{11}^+$	ca. 1550	18 500	$\text{C}_{10}\text{H}_{11} \cdot \text{ND}_3^+$	1650–1570	33 000–29 000
				1510–1430	
$\text{C}_{2n}\text{H}_{2n+1}^+$ ($n \rightarrow \infty$)	ca. 1500	8000	$\text{C}_{2n}\text{H}_{2n+1} \cdot \text{ND}_3^+$	1510–1430	15 000–14 000 ^b
				1650–1570	
Methyl acetylene					
$\text{CH}_3\text{C}_2\text{H}_2^+$	1680	38 500–25 000	$\text{CH}_3\text{C}_2\text{H}_2 \cdot \text{ND}_3^+$	1655	(50 000–40 000)
$(\text{CH}_3)_2\text{C}_4\text{H}_3^+$	1626	30 000–27 500	$(\text{CH}_3)_2\text{C}_4\text{H}_3 \cdot \text{ND}_3^+$	1660–1590	42 000–38 000
$(\text{CH}_3)_3\text{C}_6\text{H}_4^+$	1515	24 700–21 300	$(\text{CH}_3)_3\text{C}_6\text{H}_4 \cdot \text{ND}_3^+$	1660–1590	35 000–33 000
				1510–1450	(sh)
$(\text{CH}_3)_4\text{C}_8\text{H}_5^+$	1480–1440	19 300	$(\text{CH}_3)_4\text{C}_8\text{H}_5 \cdot \text{ND}_3^+$	1660–1590	28 000 (sh)
				1510–1450	
$(\text{CH}_3)_5\text{C}_{10}\text{H}_6^+$	1480–1440	16 500	$(\text{CH}_3)_5\text{C}_{10}\text{H}_6 \cdot \text{ND}_3^+$	1660–1590	22 000
				1510–1450	
Ethyl acetylene					
$\text{C}_2\text{H}_5\text{C}_2\text{H}_2^+$	1675	37 000–33 000	$\text{C}_2\text{H}_5\text{C}_2\text{H}_2 \cdot \text{ND}_3^+$	1636	(50 000–40 000)
$(\text{C}_2\text{H}_5)_2\text{C}_4\text{H}_3^+$	1620–1610	28 000–25 000	$(\text{C}_2\text{H}_5)_2\text{C}_4\text{H}_3 \cdot \text{ND}_3^+$	1650–1590	43 000–38 000
$(\text{C}_2\text{H}_5)_3\text{C}_6\text{H}_4^+$	1520–1510	23 000	$(\text{C}_2\text{H}_5)_3\text{C}_6\text{H}_4 \cdot \text{ND}_3^+$	1650–1590	36 000–35 000
					(sh)
$(\text{C}_2\text{H}_5)_4\text{C}_8\text{H}_5^+$	1520–1510	19 000	$(\text{C}_2\text{H}_5)_4\text{C}_8\text{H}_5 \cdot \text{ND}_3^+$	1650–1590	27 500

^ash, shoulder.

^bEdge.



Scheme 5.30

It should be noted that in this case the authors also separated the complexes of methyl acetylene with silanols.

π -complexes

In earlier studies, Tam *et al.* [1343] investigated the adsorption of acetylene, dimethyl acetylene and pyrazine on a series of alkali and alkaline-earth exchanged X zeolites, and of acetylene on A-type zeolites. For acetylene adsorbed on exchanged A and X zeolites, these authors found that the diagnostic C≡C stretching mode (1974 cm^{-1} for gaseous C_2H_2) shifted downwards upon adsorption, with the magnitude of the shift being proportional to the polarizing power of the cation, i.e. a larger shift for a larger cation radius, as was found by Freeman and Unland [1320] for benzene complexation. Later Heaviside *et al.* [1344] concluded that acetylene is physisorbed via its π -electron system in a ‘side-on’ orientation, perhaps to surface OH groups or to traces of retained water.

Uvarova *et al.* [771] have shown that acetylene and its derivatives can be suitable probe molecules for the basic centers of zeolites. The IR spectra of acetylene adsorbed on NaX, Cs/NaX and NaY zeolites display the formation of two types of complexes, namely π -complexes with metal cations (ν_{CC} at $3300\text{--}3310\text{ cm}^{-1}$) and H-bonded complexes with basic oxygen atoms of the framework (broad band below 3200 cm^{-1}). The decrease in the frequency of the stretching vibration in such complexes, as compared with the gas phase, may be accounted for by the weakening of the C–H bond by H–bonding. The ν_{CH} frequency decreases from 3216 cm^{-1} for NaM to 3205 cm^{-1} for NaY zeolites, and to 3175 and 3185 cm^{-1} for NaX and Cs/NaX zeolites, respectively. Other acetylenes, i.e. $\text{RC}=\text{CH}$ (where $\text{R}=\text{CH}_3$, C_6H_5 , $(\text{EtO})_2\text{CH}$ or EtOCH_2) showed the same trends as those considered for acetylene. Moreover, in the case of the latter acetylenes other type of interactions with cations becomes quite possible.

The IR spectra of methyl acetylene adsorbed on zeolites obtained by the same authors, were similar to those of acetylene. Adsorption bands at about 3250 cm^{-1} (with a shoulder at about 3150 cm^{-1}) were assigned to the $\text{C}-\text{H}\cdots\text{O}$ complexes and were characterized by frequencies which agree with the corresponding frequency shifts found for the acetylene adsorption.

5.3.2 ALUMINUM OXIDE

The IR spectrum of acetylene adsorbed on Al_2O_3 indicates the existence of two types of surface compounds [1346]. One of them (a H-bonded complex) is characterized by absorption bands at 3220 and 1950 cm^{-1} , corresponding to the stretching vibrations ν_3 and ν_2 of the C–H and C≡C groups, respectively, and is completely removed from the surface by evacuation at room temperature. The absorption band of the ν_3 of the C–H groups is strongly shifted (by 67 cm^{-1})

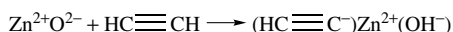
with reference to the corresponding absorption band of acetylene molecules in the gaseous phase (at 3287 cm^{-1}). This may indicate, in the authors' opinion, an interaction between the adsorbed molecules and the surface via the hydrogen atoms and the perpendicular orientations of the molecules with reference to the surface [1346].

Strongly adsorbed acetylene molecules remain on the surface on evacuation up to 573 K , and are characterized by absorption bands of the stretching vibrations C-H at 3300 cm^{-1} and $-\text{C}\equiv\text{C}$ at 2007 cm^{-1} . Most probably, this structure corresponds to strongly bound acetylide.

Nakajima *et al.* [1345], as well as Yates and Lucchesi [1346], postulated the adsorption of acetylene and methyl acetylene on $\eta\text{-Al}_2\text{O}_3$ to give in each case a strongly adsorbed species, considered to be adsorbed perpendicular to the surface, and a weakly adsorbed undissociated species which is adsorbed parallel to the surface. Yates and Lucchesi concluded that 'the (strongly) adsorbed species may consist of an undissociated acetylene molecule with the lower hydrogen strongly interacting with a surface atom (S), $\text{H-C}\equiv\text{C-H-S}$, or be of the type $\text{H-C}\equiv\text{C-}$ or $\text{H-C}\equiv\text{C-S}'$, but they did not decide firmly between these alternatives. Based on similar IR spectra obtained for acetylene and methyl acetylene on $\gamma\text{-Al}_2\text{O}_3$, it is possible to express a preference for the $\text{H-C}\equiv\text{C-Al}$ ($(\text{H-C}\equiv\text{C-})\text{Al}^{3+}$) interpretation in ionic terms. Saussey *et al.* [1347–1349] drew the same conclusions from investigations of but-1-yne adsorbed on alumina.

5.3.3 ZINC OXIDE

On the basis of IR spectroscopic investigations of the adsorption of acetylene and methyl acetylene and some of their deuterium-containing analogues, Chang and Kokes [1274] proposed the following scheme for acetylene adsorption:



Scheme 5.31

The main surface species in this case was characterized by νOH at 3550 cm^{-1} , $\nu\equiv\text{CH}$ at 3280 cm^{-1} and $\nu\text{C}\equiv\text{C}$ at 1975 cm^{-1} , while a second, more weakly adsorbed, species gave a $\nu\equiv\text{CH}$ at 3220 cm^{-1} .

As for methyl acetylene, these authors [1274] identified the formation of the propargylic anion $(\text{CH}_2\equiv\text{C}\equiv\text{CH})^-$ ($\nu_{\text{as}} = 1865\text{ cm}^{-1}$) and surface OH^- groups ($\nu\text{OH} = 3515\text{ cm}^{-1}$), and also undissociated $\text{CH}_3\text{C}\equiv\text{CH}$ surface species (the band at 2120 cm^{-1}). This latter band was reinterpreted [1349–1351] as an acetylene species, $\text{CH}_3\text{C}\equiv\text{C}^-$, analogous to the case for acetylene adsorption. Support for this comes from adsorption of tert-butyl acetylene [1348] and phenyl acetylene [1325, 1326], which are examples of molecules without $\alpha\text{-CH}$ bonds. Later, Nakajima *et al.* [1345], following investigations of alkynes adsorbed on ZnO , once again expressed a preference for a nondissociative interpretation of the bands at 3250 and 2120 cm^{-1} in terms of a π -bound nondissociative complex.

Infrared spectra of both C_2H_2 and C_2D_2 adsorbed on ZnO have been obtained by Husain and Sheppard [1350] between 4000 and 600 cm^{-1} . They interpreted the spectra in terms of the presence of (i) dissociatively adsorbed surface complexes of acetylide of the following two types: $(\text{H-C}\equiv\text{C-})\text{Zn}^{2+}(\text{OH}^-)$ (the bands at 3287 cm^{-1} – (strong) νCH , 1983 cm^{-1} weak $\nu\text{C}\equiv\text{C}$ and $645(\text{s})\text{ cm}^{-1}$ (strong) $\delta\text{H-C}\equiv\text{C}$, for species I; 3225 (medium), 1915 (weak) and 715 (medium) cm^{-1} for species I', together with 3430 and 885 (species I) and 3545 and 840 cm^{-1} (species I') for the νOH and δOH modes, respectively), and (ii) non-dissociatively chemisorbed complexes (the $3012/2983\text{ cm}^{-1}$ pair of absorption bands – νCH , and 1552 cm^{-1} – $\nu\text{C}=\text{C}$ of the type of a substituted ethene bound to surface zinc ions, possibly $(\text{Z})\text{-ZnHC}\equiv\text{CHZn}$.

5.3.4 TITANIUM OXIDE

Deuteroacetylene is adsorbed on anatase, predominantly with preservation of its molecular structure. Support for this comes from the appearance of band for $\nu\text{C}\equiv\text{C}$ at around 1740 cm^{-1} , and for $\nu\equiv\text{CD}$ at ca. 2400 cm^{-1} of weakly bound complexes in the spectrum (Figure 5.27, spectrum 2) [1212], corresponding to C_2D_2 (gas) ($\nu\text{C}\equiv\text{C}$, 1762 cm^{-1} ; νCD , 2427 cm^{-1}). There is practically no perturbation of the OH groups in this case. The appearance in the infrared spectrum of absorption bands from $\text{C}\equiv\text{C}$ bonds, which are normally inactive in the infrared region, is doubtless due to the breaking of the molecular symmetry, for example, via formation of additional bonds with surface oxygen centers. Support for this comes from a comparison of the spectral characteristics of the deuteroacetylene π -complexes on Al_2O_3 ($\nu\text{C}\equiv\text{C}$, 1735 cm^{-1} ; $\nu\equiv\text{CD}$, 2410 cm^{-1}) with those on TiO_2 ($\nu\text{C}\equiv\text{C}$, 1745 cm^{-1} ; $\nu\equiv\text{CD}$, 2400 cm^{-1}).

Molecules of C_2D_2 also participate in H–D exchange with OH groups. As a result, weak bands at 1850 ($\nu\text{C}\equiv\text{C}$), 3265 – 3280 ($\nu\equiv\text{CH}$) and 2540 and 2570 ($\nu\equiv\text{CD}$) cm^{-1} appear in the spectra, which can characterize the vibrations of C_2HD (C_2HD)_{gas}, i.e. $\nu\text{C}\equiv\text{C}$ – 1853 cm^{-1} , $\nu\equiv\text{CH}$ – 3335 cm^{-1} ; $\nu\equiv\text{CD}$ – 2584 cm^{-1} [14], and νOD – 2770 cm^{-1} (Figure 5.27, spectrum 2).

After a period of time, C_2D_2 is destructively oxidized, and the bands at 1335 ($\nu_s\text{COO}$) and 1570 ($\nu_{as}\text{COO}$) cm^{-1} increase, which is characteristic of the production of formates (DCOO) (spectrum 3).

The adsorption of methyl acetylene (MA) also leads to the formation of weakly bound molecular complexes with loosened $\text{C}\equiv\text{C}$ bonds: $\nu\text{C}\equiv\text{C}$, 2110 cm^{-1} ; $\nu\equiv\text{CH}$, 3240 cm^{-1} , for $(\text{CH}_3\text{C}_2\text{H})_{\text{gas}}$ ($\nu\text{C}\equiv\text{C}$, 2142 cm^{-1} ; $\nu\equiv\text{CH}$, 3334 cm^{-1}). These occur together with νCH bands in the region 2865 – 2985 cm^{-1} and δCH at 1380 – 1450 cm^{-1} for CH_3 groups (Figure 5.27,

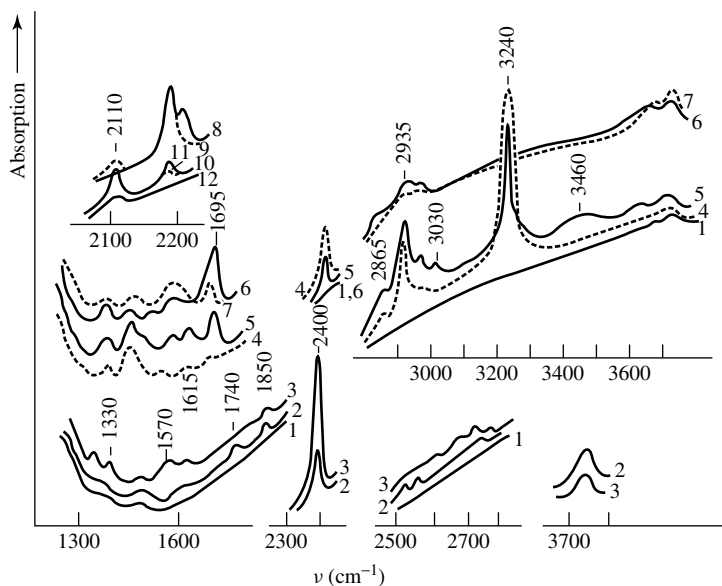
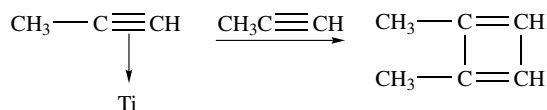


Figure 5.27. IR spectra of (2, 3) deuteroacetylene and (4–7) methyl acetylene adsorbed on (1) TiO_2 (anatase): (2) adsorption of C_2D_2 ; (3) after 36 h in C_2D_2 ; (4) adsorption of methyl acetylene at 533 Pa; (5) after 36 h in methyl acetylene; (6, 7) following evacuation at 295 K for 45 min and at 425 K for 20 min, respectively; (8) adsorption of CO; (9) followed by adsorption of methyl acetylene; (10–12) after 1 min, 10 min, and 1 h in methyl acetylene, respectively.

spectra 4). As shown by experiments on the displacement of pre-adsorbed CO by MA (Figure 5.27, spectra 9–12) the $\nu\text{C}\equiv\text{C}$ band is complex, with maxima at 2105 and 2111 cm^{-1} . These characterize the vibrations of the $\text{C}\equiv\text{C}$ bond in two types of π -complexes stabilized on different titania ions. It is shown from Figure 5.27 (spectra 8–10) that injection of MA onto the sample leads to the band at 2208 cm^{-1} (νCO in Ti^{4+}CO complex) disappearing and the band at 2105 cm^{-1} ($\nu\text{C}\equiv\text{C}$) bond appearing in the spectrum. After a period of time, the molecules of hydrocarbon also displace CO from the less strong acceptor center (νCO , 2189 cm^{-1}).

The decrease in intensity of νCO (2189 cm^{-1}) is accompanied by a shift to 2181 cm^{-1} , while further increases in MA absorption shifts this band to 2111 cm^{-1} . The molecules showing a less loosening of the $\text{C}\equiv\text{C}$ bond are bound more weakly to the surface and their disappearance shifts the maximum of the $\nu\text{C}\equiv\text{C}$ to low frequencies.

Other complexes with $\text{C}=\text{C}$ bonds ($\nu\text{C}=\text{C}$, 1610–1580 cm^{-1} ; $\nu=\text{CH}$, 3030 cm^{-1}) are also observed on the surface. The lower position of the $\nu\text{C}=\text{C}$ in such olefin complexes formed from acetylene adsorption, in comparison with those observed in the case of the adsorption of olefins, may be accounted for by the conjugation of adjacent double bonds. The absence of the bands from the end $=\text{CH}_2$ groups in the spectrum also indicates this. These data show the possibility of methyl acetylene oligomerization via the following scheme:



Scheme 5.32

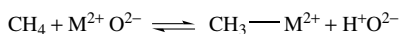
A small degree of oxidative transformations of acetylenes is also ruled out [1212]. As was shown by means of Raman spectroscopy [1351], *trans*-polyacetylene was obtained by the polymerization of acetylene at room temperature on a highly dehydroxylated surface of rutile. The Raman spectrum showed the formation of a range of different-length polymers, with the intensities of the skeletal bands being enhanced by the *resonance Raman effect*. However, it cannot be ruled out, taking into account the data mentioned above for anatase, that the oligomerization processes observed in this latter study could be due to the effects of laser radiation.

Infrared and Raman spectroscopic studies of some aromatic acetylenic compounds adsorbed on oxides have been carried out. For example, the infrared and Raman spectra of 3-phenyl-1-propyne and 1-phenyl-1-propyne adsorbed on zinc oxide were reported by Nguyen and co-workers [1325, 1326]. It has been established that the isomerization of these adsorbates occurs via the formation of phenylallene – the third isomeric possibility. Both adsorbates have a common behavior over zinc oxide in that each gives rise to two types of dissociative chemisorption to yield acetylide and propargylic species. The latter species are considered to be intermediates in the isomerization reactions, and their two possible structures are characterized by intense infrared absorptions, identically positioned at 1862 cm^{-1} , which are assignable to the $\nu\text{C}-\text{C}\equiv\text{C}$ modes.

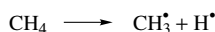
The acetylide species are characterized by the $\nu\text{C}\equiv\text{C}$ bands in the region 2080 to 2110 cm^{-1} in both the infrared and Raman spectra. Infrared spectra from $\text{C}_6\text{H}_5\text{CD}_2\text{C}\equiv\text{CD}$ adsorbed on ZnO, pre-treated with D_2O , were also recorded to help assignment of the infrared bands of the propargylic species from adsorbed nondeuterated compounds. These provide evidence for the two types of propargylic species, $(\text{C}_6\text{H}_5\text{CD}\equiv\text{C}\equiv\text{CD})^-$ and $(\text{C}_6\text{H}_5\text{C}\equiv\text{C}\equiv\text{CD}_2)^-$, in the form of absorption bands at 1830 and 1857 cm^{-1} , respectively.

5.4 Complexation of alkanes

Studies of the interactions of alkanes with oxide surfaces entails significant difficulties because the adsorption coefficients of such molecules is, as a rule, less than those of unsaturated molecules. The main problem is that the number of centers able to activate the strong C–H bonds of alkanes is very small. There are several points of view [1236–1240] concerning the character of activation of the C–H bond. Some authors believe that homolytic rupture of the C–H bond takes place [1237, 1352], whereas others consider that the rupture of the C–H bonds is heterolytic [1238–1240]. Based on the heterolytic mechanism of methane activation, the scheme for the interaction of methane with the surfaces of basic catalysts involving the ionic pairs can be represented by the following:



or for homolytic activation with participation of surface monoelectronic centers:



Scheme 5.33

The character of the C–H bond activation is still an open question and arguments in support of both mechanisms exist. Lunsford and co-workers [1352] have demonstrated that the C–H bond in methane can be activated on both distinguishable kinds of surface sites.

In addition, one type of mechanism could be hydride transfer, which was discussed by Gallo and Lazzeri [1353]. The activation of alkanes by hydride transfer is different to that involving super-acids. Let us now examine the dependence of alkane transformations on the nature of the oxides. We will use the example of methane to illustrate this.

5.4.1 INTERACTIONS WITH OH GROUPS, CARBENIUM-LIKE IONS

A study [531], devoted to the infrared investigation of methane interaction with porous glass surfaces was one of the first experiments to be carried out on alkane adsorption by means of physical methods. The data obtained are compared with those found for free methane molecules in Table 5.22. A band at around 2899 cm^{-1} , which is absent in the spectra of both gaseous and liquid methane, appears in the spectrum of adsorbed methane. It is clear that this band corresponds to the forbidden νCH frequency of the molecule which appears at 2914 cm^{-1} in the Raman spectrum. Since there is no change in the dipole connected with this vibration, the latter is forbidden in the infrared spectrum of gaseous methane. However, during adsorption, surface forces can distort one ‘side’ of the methane molecule more than the other. Any such distortion

Table 5.22. Spectral characteristics of methane and their changes upon adsorption of methane on porous glass [531]. From Sheppard, N. and Yates, D. J., *Proc. R. Soc. London, A*, **238**, 69–89 (1956). Reproduced by permission of the Royal Society.

Mode	Gas (cm^{-1}) ^a	Liquid	Adsorption (cm^{-1}) ^a	$\nu_{\text{gas}} - \nu_{\text{ads}}$ (cm^{-1}) ^a
ν_3	3018.8 (s)	3018 (s)	3006 (s)	12.8
ν_1	2916.5 (R)	–	2899 (m)	17.5
$\nu_2 + \nu_4$	2823 (w)	2820 (w)	2819 (w)	4.0

^as, strong; m, medium; w, weak; R, Raman-active.

causes the mode to be active in the infrared spectrum. For example, if the molecules are adsorbed with either a threefold or twofold axis perpendicular to a planar surface, the symmetry of the adsorbed molecule become C_{3v} or C_{2v} (see [11, 12] for symmetry symbols), respectively, and not T_d as in the gaseous phase. In both of these cases, the symmetry of the otherwise forbidden frequency (A_1) could be infrared-active. If the symmetry of the adsorbed molecule is C_{3v} , the triply degenerate infrared-active ν_{CH} of the gaseous methane, ν_3 , can split during adsorption into two components with an intensity ratio 2:1 (E and A_1 symmetry, respectively), whereas in the case of C_{2v} symmetry this frequency should split into three components of similar intensity (A_1 , B_1 and B_2) [531]. In practice, only a single broad and sufficiently symmetric band appears in the spectrum, even when studied under high resolution. This means that either the separate components are not resolvable or that the observed absorption band is caused by superimposed contributions from methane molecules in various configurations relative to the surface.

To interpret the data reported by Sheppard and Yates [531], Chen *et al.* [1354] used the FTIR spectroscopic method. The time correlation function obtained from this analysis of the ν_3 band counter has been compared with that calculated from two models, i.e. (i) a free rotating molecule, and (ii) a molecule which rotates only around the axis perpendicular to the surface. The results confirmed the conclusion made by Sheppard and Yates [531] about the rotation of methane adsorbed on SiO_2 . From the perturbation of surface OH groups upon adsorption, the authors believe that these groups participate in complex formation.

The physical adsorption of alkanes on the OH groups of HNaY zeolites was studied Datka [1355], where it has been shown that interaction occurs with the most acid OH groups (the band at 3640 cm^{-1}). The shift of the ν_{OH} band depends on the structure of the alkane and on the sodium concentration in the sample (the basicity of the OH group) (Table 5.23). Unfortunately, there was no the analysis of the CH vibrations in this work.

In general, the interaction of alkanes with OH groups is similar to that with cations, as follows from both the energetic and spectral characteristics obtained, for example, for zeolites. After interaction of methane with SiO_2 at 173 K, two bands at 3008 and 2900 cm^{-1} , characteristic of adsorbed methane, appear – similar bands to those observed by Sheppard and Yates [531] were obtained and hence given analogous interpretations [1356, 1357]. Relative to the gas-phase values, ν_3 and ν_1 were found to shift by -11 and -17 cm^{-1} , respectively.

Only in a few papers [1358–1360] has the role of Brønsted acid sites in methane activation been discussed. As follows from the low-temperature experiments, methane adsorption over HZSM-5 zeolite occurs mainly via the formation of weak hydrogen-bonds with surface hydroxyl groups.

Table 5.23. Effects of the adsorption of various alkanes on the high-frequency band of the OH groups in NaHY zeolites [1355]. From Datka, J., *J. Chem. Soc., Faraday Trans. 1*, **76**, 705–710 (1988). Reproduced by permission of The Royal Society of Chemistry.

Adsorbate	Polarization (\AA)	$\Delta\nu$ (cm^{-1})		A/A_0			q_2/q_1 after alkane adsorption		
		21^a	40^a	21^a	40^a	77^a	21^a	40^a	77^a
<i>n</i> -butane	8.14 ^b	100 ± 4	100 ± 3	–	2.0 ± 0.02	2.2 ± 0.02	–	1.44	1.51
<i>n</i> -hexane	11.82	102 ± 3	110 ± 3	1.0 ± 0.03	1.9 ± 0.02	2.3 ± 0.04	1.01	1.40	1.54
2,2,3-Trimethylpentane	15.37	120 ± 3	126 ± 2	2.3 ± 0.02	2.3 ± 0.02	3.1 ± 0.04	1.54	1.54	1.79
<i>n</i> -dodecane	23.40	125 ± 2	130 ± 4	–	2.3 ± 0.03	3.7 ± 0.04	–	1.54	1.96

^aDegree of exchange.

^bMean value obtained by interpolation.

Such a complex nevertheless participates in H–D exchange. Since no band attributable to O–D vibrations was observed during the interaction between CD_4 and NaZSM-5 (which contains almost no Brønsted acid protons), even at 873 K [1361], it can be concluded that the protons in HZSM-5 zeolites play the main role in the C–H bond rupture.

Further data [1362] show that, after the formation of the strong H-bond (νCH , lower than 2800 cm^{-1} – Figure 5.28, spectrum 3) between isobutane (2-methyl propane) and the acidic surface hydroxyl group of HZSM-5 (3610 cm^{-1}), on heating of the sample to 323–473 K, the formation of alkene carbocations is observed, as follows from the appearance of bands in the $1500\text{--}1515\text{ cm}^{-1}$ region in the infrared spectra and also maxima at 270 and 420 nm in the DRES spectrum. These data seem to provide evidence that the proton transfer from the zeolite to the alkane molecules, probably due to the mechanism of formation of $\text{C}_4\text{H}_{11}^+$ cations similar to CH_5^+ [1363], takes place. As the temperature increases, such a cation possibly transforms to mono- and dialkenyl carbenium ions [1362].

The formation of H-bonds between alkanes (including methane) and the OH groups of the HZSM-5 zeolite surfaces is a well-established fact [1364]. According to these studies, the methane activation occurs heterolytically via the participation of acid–base sites. At low temperatures, the activation of methane on both super-acid catalysts [1363] and Hg-based organometallic complexes [1365] occurs via heterolytic cleavage of the C–H bond. Thus, in the case of HZSM-5 zeolites, methane seems to be activated by interactions with protons, yielding CH_5^+ cations as intermediates, which then either decompose to CH_3^+ with the evolution of hydrogen or the reaction reverses back to methane [1363]. Data obtained upon the interaction of *n*-butane with sulfated zirconia [1366] confirm the occurrence of the above processes. The interaction of super-acid catalysts, for instance, ZrO_2/SO_4 , with alkane molecules is generally considered to involve carbocation intermediates [1363] which can be generated by the attack of the alkane molecule

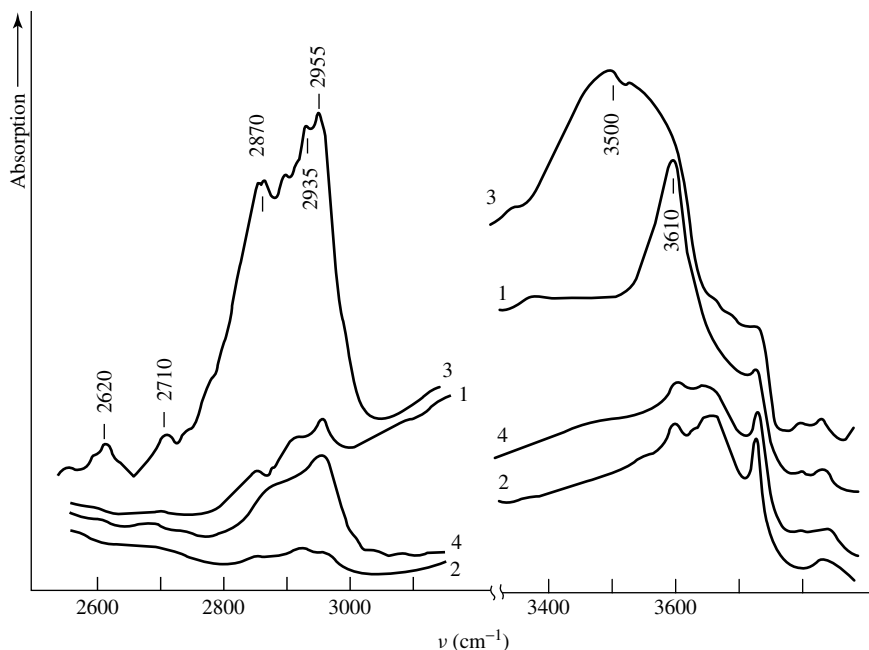


Figure 5.28. Diffuse reflection IR spectra of (3, 4) isobutane adsorbed at 293 K on (1) ZSM-5 type zeolite, and (2) the ‘destructured’ zeolite without strong Brønsted acid centers treated at 773 K.

via three different routes, i.e. (i) hydride abstraction by LASs, (ii) the attack of a C–H bond by the proton of a BAS, or (iii) the attack of the C–C bond by a BAS (protolysis). *In situ* Raman and UV–Vis diffuse reflectance spectroscopy, coupled with ESR spectroscopy, show that the formation of allylic and polyenylic cations and polycyclic aromatic compounds take place, the formation of which is largely prevented in the presence of H₂ [1366].

A controlled atmosphere ¹³C MAS (magic angle spinning) NMR spectroscopic study of the initial stages of propane activation over HZSM zeolites used propane (2-¹³C) as the labeled reactant. Rearrangement of the ¹³C label in the early stages of propane conversion suggested a cyclic transition state, such as a protonated cyclopropane, or pointed to a carbenium or carbonium pathway, respectively. The study of the role of protonic and aprotic acid sites and their strengths, and the effects of catalyst pre-treatment and co-adsorption of probe molecules (H₂O, CO and H₂) on the initial stages of propane activation, indicated a monofunctional mechanism involving propane protonation on the strong BASs and the formation of carbonium-ion-type transition states. The addition of small amounts of propylene or benzene led to a classical bimolecular initiation via hydride transfer with carbenium-ion-type intermediates. The mechanisms of the main reaction pathways leading to ¹³C rearrangement in propane, cracking to ethane and the formation of butanes was also observed [1367].

Infrared investigations on the interaction of methane with silica, aluminas (η , γ and δ) and HZSM-5 zeolites have been carried out [1361]. At low temperatures (173 K), methane adsorption was observed on these oxides and the HZSM-5 zeolites. The infrared-inactive ν_1 band at 2917 cm⁻¹ of a gaseous methane molecule became active and shifted to lower frequencies (2900 and 2890 cm⁻¹) when it adsorbed on the surfaces of these adsorbents. The results again demonstrated that the hydroxyl groups played a very important role in methane adsorption over the acidic oxides and the HZSM-5 zeolites. The band shift of the hydroxyl groups varied with different oxides, with the strength of the interaction decreasing according to the following sequence, Si–OH–Al > Al–OH > SiOH, which is in accordance with the order of their acidities. At higher temperatures, methane interacted quite differently with the various oxides and the HZSM-5 zeolite. It has been observed that the hydroxyl groups of silica, γ -alumina and HZSM-5 zeolite could exchange with CD₄ at temperatures higher than 773 K, while those on η -alumina could exchange at a temperature as low as 573 K. Another interesting observation was the formation of formate species over Al₂O₃ (both η and γ) at temperatures higher than 423 K. The formate species decomposes to CO₂, or produces carbonate species at much higher temperatures than 473 K. The formation of formate species was not observed over silica or HZSM-5 under similar conditions, while α -Al₂O₃ did not adsorb or react with methane in any case.

Chen *et al.* [1361, 1364] concluded that those hydroxyl groups with a larger number of near-neighbor negative oxygen ions interact easily with methane. The fact that methane interaction with Al–OH groups is fairly strong is confirmed by the large shift of the band at 3760 cm⁻¹ to 3707 cm⁻¹ ($\Delta\nu = 53$ cm⁻¹). The presence of a 3650 cm⁻¹ band can be due to either the interaction of methane with other types of hydroxyl groups on alumina or the formation of a new kind of hydroxyl group upon interaction of methane with the surface oxygen anions. According to data obtained by Chen *et al.* [1361, 1364], the amount of adsorbed methane on η -Al₂O₃ is about twice as large as on γ -alumina, whereas well crystallized α -aluminas do not adsorb methane at all.

5.4.2 INTERACTION WITH CATIONS

Infrared spectra of methane adsorbed on NaA, CaA and NaX zeolites evacuated at 673 K has been studied by Cohen de Lara and Deleval [1368]. A number of intense absorption bands appear in the spectrum (Table 5.24). The intensity of these bands decreased from sample to sample in the following sequence: NaX > CaA > NaA. It was shown from comparison of the diameters

Table 5.24. Changes in the IR spectra (ν (cm⁻¹)) of methane adsorbed on various zeolites with participation of cations.

Band	Gaseous CH ₄	CH ₄ adsorbed on		
		NaA	CaA	NaX
ν_4 (F)	1306 (IR)	1312	1303	1306
ν_1 (A ₁)	2914 (Raman)	2893	2893	2888
ν_3 (F)	3020 (IR)	3000	3006	3000

of the methane molecules (around 4.6 Å) and the zeolite cavities (8 Å for NaX, and 5 Å for CaA and NaA) that the variations in intensities of the absorption bands of adsorbed methane can be due to steric obstacles to CH₄ penetration into the zeolite cavities. The appearance of the forbidden ν_1 band is caused by a dipole moment induced in the molecule by the internal field of the zeolite cavity. The band intensity has to be proportional to the square of the field and will be highest at the wall of the cavity and lowest at this cavity's center ($E = 0$). In the spectra obtained, the intensity of the ν_1 band is similar to that of ν_3 , which shows that the CH₄ molecule is located near to the wall. The wide profiles of the ν_3 and ν_4 bands, together with the presence of a high-frequency shoulder on ν_3 , indicate that the adsorbed methane molecule has a certain rotational degree of freedom, as possessed by methane molecules in both the liquid state and adsorbed on porous glass [531]. The appearance of two ν_1 bands in the spectra of methane adsorbed on a CaNaA zeolite is probably due the formation of two types of complexes stabilized on Ca²⁺ and Na⁺ ions (Table 5.25) [1369].

Upon investigations of methane adsorption on NaA zeolites as a function of the temperature, using IRS and neutron scattering, and also from theoretical calculations of the interaction [1370], interesting data have been obtained. At low temperatures (210–260 K) the ν_1 and ν_3 bands shift to the low frequencies observed in the liquid and solid states. When the temperature decreases, the ν_1 band shift increases due to the stronger interaction with the surface, whereas the ν_3 position does not change. The decrease in the intensity of the ν_1 band of adsorbed methane is accompanied by a decrease in its bandwidth ($\Delta\nu_{1/2}$), which, in the authors' opinion, depends only on the life time of the vibration (τ_v):

$$\tau_v = 1/\pi c \Delta\nu_{1/2} \quad (5.1)$$

where τ_v varies from 5×10^{-13} s at 273 K to 13×10^{-13} s at 210 K.

Since the ν_1 band exists in the spectra only when the CH₄ molecules are close to the surface, it has been suggested that τ_v is equal to the time that the molecule is present on the

Table 5.25. Spectral manifestations (ν (cm⁻¹)) of individual and adsorbed methane.

CH ₄	ν_1 (A ₁) ^a	$\Delta\nu_1$	ν_3 (F) ^a	$\Delta\nu_3$	ν_4 (F) ^a	$\Delta\nu_4$
Gas	2914 R		3020 (IR, R)		1306 (IR, R)	
Liquid	^b		3010			
Solid	^b		3010			
Solution in CCl ₄			3008	-12		
Adsorbed on: porous glass	2899	-15	3006	-14		
NaA	2855	-29	3000	-20	1312	+6
NaCaA	2892	-22	3004	-16	1310	+4
		-12				
NaX	2888	-26	3004	-16	1306	+2

^aIR, infrared; R, Raman.

^bdo not observed.

adsorption center. In order to leave the surface, the molecule have to overcome the potential barrier ($\Delta\Phi$):

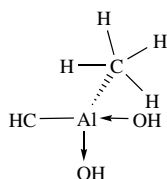
$$\tau A = \tau_0 \exp(\Delta\Phi/KT) \quad (5.2)$$

From this equation, it follows that the $\Delta\Phi$ value is about 6 kJ mol^{-1} at 700 K and, as follows from the experiments on neutron scattering, this characterizes the activation energy of the transition of CH_4 molecules from the walls of the 'supercages' to the center.

The ratio of the ν_3 and ν_1 band intensities has been measured by Yamazaki *et al.* [1371] at 190–273 K. Since in the supercages the force field changes from one point to an other, the intensities of the forbidden absorption bands (ν_1) from molecules located in different adsorption locations should be different. According to the quasi-elastic neutron scattering data, CH_4 molecules are delocalized in a supercage at 300 K but are close to the surface at 200 K. This conforms with the increase in intensity of the forbidden band at the decrease in the temperature. The finding that the intensity of the ν_3 band does not depend on either the position of the molecule in the supercage or the temperature leads to the conclusion that changes in the ratio of intensities of the ν_3 and ν_1 bands as a function of temperature characterize the mobility of CH_4 molecules in the zeolite supercages. The data obtained from both infrared spectroscopic and neutron scattering investigations are in good agreement.

In the NMR spectra of methane adsorbed on HZSM-5 zeolites, the ^{13}C line is fairly strongly shifted to the weak-field direction in comparison with that of gaseous methane [1372]. Simultaneously, the J -constant of the spin-spin interaction between the ^1H and ^{13}C nuclei of methane changes, which, in the authors' opinion, indicates that a complex of methane with the zeolite adsorption centers is formed. In the case of HY zeolites, such an interaction is not observed. The authors consider that the CH_4 molecules interact with isolated or weakly associated 'extra-network' aluminum atoms located in places where the channels cross. Such atoms provide strong Lewis acid sites.

Calculations of possible models for CH_4 interactions with such surface centers of zeolites, which have been made by the full equalization of the orbital electronegativity method, have confirmed this suggestion and show that the most probable adsorption model is the following:



Scheme 5.34

According to the calculations, the change of the chemical shift during such complex formation can reach approximately 60 parts per million (m.d), close to the values obtained from the experiment. The bond in such a complex is mostly due to the van der Waals interaction, and the bond energy is 50 kJ mol^{-1} .

Both adsorption isotherms and infrared spectra of adsorbed methane have also been obtained on silicalite and NaZSM-5 zeolites with different $\text{SiO}_2/\text{Al}_2\text{O}_3$ ratios [1373]. The differences in methane adsorption on the surfaces of silicalite and on the zeolites revealed in this study are (i) in the case of silicalite, the isosteric heat of adsorption is much more than that for NaZSM-5 zeolites, and (ii) the intensity of the absorption band $\nu_1\text{CH}_4$ (ca. 2885 cm^{-1}) in the IR spectrum of methane adsorbed on silicalite is very small, whereas it is fairly high in the spectrum of methane adsorbed on NaZSM-5 zeolites. It seems possible to explain such differences as being

due to the presence of strong cationic centers in the NaZSM-5 zeolites. Support for this comes from the proportionality between the ν_{OH} frequency in HZSM-5 zeolites and ν_1 , i.e. methane is adsorbed on such OH sites. Moreover, at low coverage methane molecules tend to adopt a tripod orientation toward adsorption sites, and both the values of the electrostatic field in the zeolite pair ($1.0\text{--}2.5 \times 10^5$ esu) and the lifetime of the adsorbed molecule ($6\text{--}9 \times 10^{-13}$ s) are practically independent of the $\text{SiO}_2/\text{Al}_2\text{O}_3$ ratio [1373].

Upon methane adsorption on cationic forms of the ZSM-5 zeolites containing H^+ , Li^+ , Na^+ , K^+ , Rb^+ or Cs^+ , two adsorption forms have been identified by FTIR spectroscopy [1374]. One of these forms is similar to that formed upon methane adsorption on silicalite and is characterized by the ν_3 band at around 3000 cm^{-1} . The second adsorption form has a higher adsorption energy (ca. 21 kJ mol^{-1}). This form exists on the cations and is detected in the spectrum by the ν_1 band at $2895\text{--}2880\text{ cm}^{-1}$. The spectral characteristics of this form of adsorption change in the following sequence, $\text{Li}^+ > \text{Na}^+ > \text{K}^+ > \text{Rb}^+ \geq \text{Cs}^+$. The data obtained allow the conclusion that electrostatic interaction is the main factor determining methane adsorption on the cations.

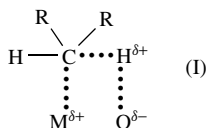
Methane adsorption on NaY and CsY zeolites using FTIR spectroscopy has also been studied [1373]. The results obtained indicate an adsorption-induced symmetry reduction of the CH_4 from T_d to C_{3v} . A splitting of the ν_1 mode in NaY can be attributed to the interaction of CH_4 with Na^+ ions in the different zeolite sites. The location of Cs^+ ions in different crystallographic positions cannot be spectroscopically resolved. In addition to CH_4 complexes with alkali cations, an interaction with weakly basic framework oxygen could also be detected in NaY. In the Cs^+ -containing Y zeolite, the ν_1 mode seems to be that of the $\text{Cs}^+ \cdots \text{H}\text{--}\text{CH}_3$ complex. The vibrational behavior of the adsorbed methane correlated with the electric field strength of the cationic sites in the zeolite matrix. IR spectra of CH_4 adsorbed on ion-exchanged ZSM-5 zeolites were also reported by Khodakov *et al.* [1375].

5.4.3 THE ACTIVATION OF C–H BONDS IN ALKANE MOLECULES

Molecular hydrogen-bonded forms with a strong loosening of the C–H bond

As has been pointed out above, during adsorption of alkanes hydrogen-bonded complexes are formed on the surface. However, only recently, due to the development of high-precision spectral methods such as FTIR and DRES, has it become possible to establish, together with the weak interactions mentioned above, that alkane H-bonded complexes can be formed with a strong loosening of the C–H bond, or even via dissociation, with fragmentation. The number of the centers on which these processes occur is small, and are the most defective ones. Such phenomena are of great interest.

One of the first studies in which the formation of H-bound alkanes complexes has been observed by infrared spectroscopy was the investigation of propane adsorption over a La–Ga–Sb–O system [1376]. The authors observed the stable molecular form of propane adsorption on the surface of the La–Ga–Sb oxide catalyst after interaction at room temperature. Later, the adsorption of cyclohexane on the surface of a Ti–Sb oxide catalyst [1377] and of $\text{C}_1\text{--}\text{C}_4$ alkanes on $\eta\text{-Al}_2\text{O}_3$ was studied [773–776]. Adsorption of alkanes is characterized by a significant loosening of the C–H bond [773–776, 1279, 1377, 1378] and by a decrease in the value of corresponding absorption band of $50\text{--}200\text{ cm}^{-1}$. The formation of such molecular complexes occurs on a limited number of centers, the nature of which has been unclear for a long time. Some authors [774, 776] believe that such centers are ion pairs including cationic and anionic centers ($\text{M}^{n+} \text{O}^{2-}$), and that the interaction of alkanes with the oxide surface is due to the formation of the following complex:



Scheme 5.35

whereas others consider that only cationic ($M^{n+} \dots H^{\delta-} \dots RCR-H$) (II) [1279] or anionic ($-O^{2-} \dots H^{\delta-} \dots R'C^{\delta-}R'-H$) (III) [1379] centers participate in the complex formation.

In the case of ethane adsorption over ZrO_2 at 113–253 K, two forms of the adsorbed ethane were identified [1279]: a strong adsorption form ('end-on'), bonded to the surface by one methyl group ($\nu_{CH} = 2798 \text{ cm}^{-1}$), which is stable at room temperature, and a weak adsorption form ('side-on'), which is stable only below 193 K. The spectral features of the latter are close to those of the molecule in the gas phase, where both methyl groups are equivalent. For interpretation, the authors used as analogues the spectra of surface compounds formed upon alkane adsorption on metals. However, this approach does not take into account such obvious differences in the chemical properties of the surfaces of oxides and metals, with the presence of strong nucleophilic oxygen anions and acid–base pairs participating in activation on the oxides.

In order to establish the proposed adsorption schemes (I)–(III), it is reasonable to study the influence of the properties of the surface on the activation of alkanes. For instance, it is possible to vary both the acceptor properties of cations [30] and the basic properties of anions [774] by using different oxides. The basicity of the surface oxygen has been shown to be the decisive factor that governs the extent of C–H bond loosening. It is enough to consider the experimental data on the adsorption of a specified hydrocarbon, for example, isobutane on oxides of zirconium and calcium [774]. Calcium oxide is known to possess strong basic sites [231], whereas the acceptor properties of surface cations for this oxide are much weaker than for the zirconium cations at the surface of ZrO_2 [30]. The experimental data show the stronger loosening of the C–H bond and a decrease in the ν_{CH} frequency for CaO (2730 cm^{-1} , Figure 5.29), as compared with ZrO_2 (2780 cm^{-1} , Figure 5.30), which is indicative of the increasing basicity of oxygen. The latter is not the only factor that influences the extent of the C–H bond loosening. Indeed, in the case of $\eta\text{-Al}_2\text{O}_3$, which is characterized by the presence of the strongest acceptor centers (coordinatively unsaturated Al^{3+} cations), the absorption band assigned to the perturbed C–H bonds is observed at 2735 cm^{-1} (Figure 5.29, spectrum 2), even though the basicity of the surface oxygens in CaO is obviously stronger than that in $\eta\text{-Al}_2\text{O}_3$.

The results obtained provide evidence in favor of a two-point adsorption of alkanes on ionic pairs, $M^{n+}O^{2-}$. Moreover, these data show that such centers, differing in their properties from the majority of surface sites, exist on the surface in low concentrations. The centers responsible for the strong loosening of the C–H bond are the strongest acid–base pairs; therefore, the intensity and position of the absorption bands attributed to the perturbed C–H bonds are likely to be determined by the extent of this bond polarization (the extent of the interaction with the pair site) and by the concentration of these centers. In the case of CaO, the interaction with strong basic sites alone, in spite of the sufficiently high concentration of these centers ($S_{sp} = 40 \text{ m}^2 \text{ g}^{-1}$), leads only to the appearance of a weak absorption band assigned to the perturbed C–H bonds (Figure 5.31, spectrum 1) because acceptor sites are practically not observed for CaO. Such sites are virtually absent in MgO (Figure 5.29, spectrum 3), which is characterized by a broad distribution of basic sites but by a small fraction of the strong basic centers [231–233, 771, 774].

The concentration of the centers of this type in $\eta\text{-Al}_2\text{O}_3$ is low (in the case of methane, it is equal to $0.6 \times 10^{17} \text{ m}^{-2}$ [775, 776]). However, the absorption band attributed to perturbed C–H bonds is visible (Figure 5.31, spectrum 1), probably because of a considerable polarization of this

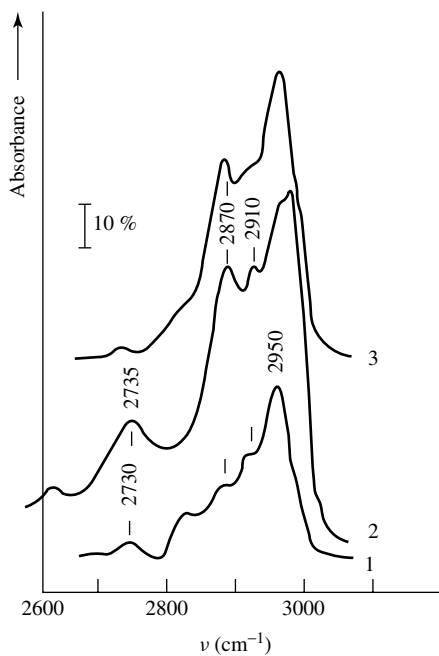


Figure 5.29. DRIR spectra of isobutane adsorbed at 293 K on (1) CaO, (2) η -Al₂O₃ and (3) MgO.

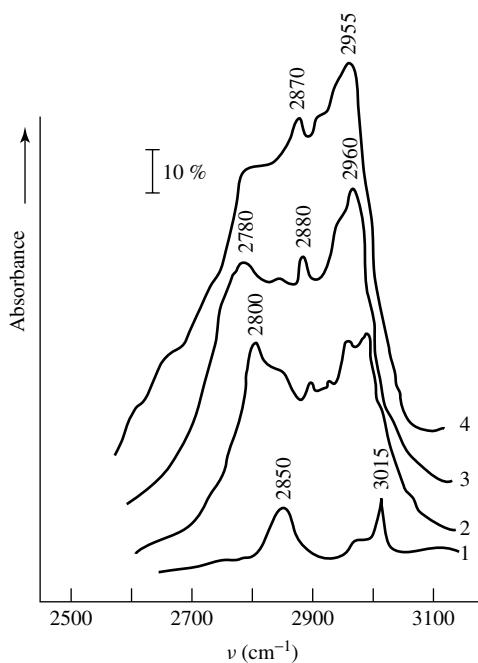


Figure 5.30. DRIR spectra of various hydrocarbons adsorbed on ZrO₂ at 293 K: (1) 60 torr of CH₄; (2) 45 torr of C₂H₆; (3) 10 torr of C₃H₈; (4) 30 torr of isobutane.

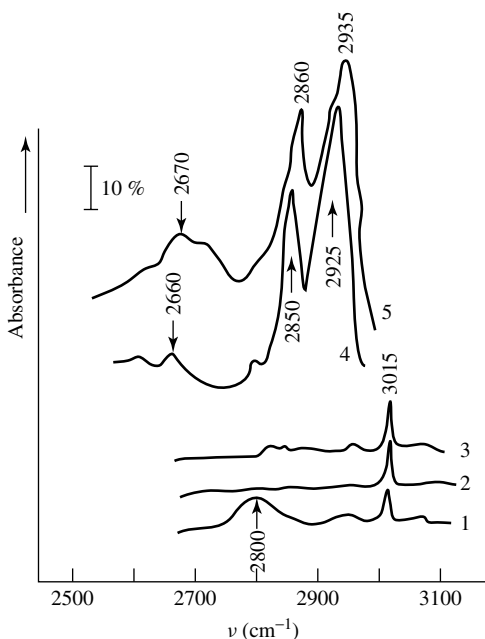


Figure 5.31. DRIR spectra of methane adsorbed at 293 K on (1) η - Al_2O_3 , (2) MgO and (3) CaO, and cyclohexane adsorbed on (4) MgO and (5) η - Al_2O_3 .

bond on the sufficiently strong Lewis acid site and basic site. At the same time, for MgO, which is characterized by a relatively higher concentration of strong basic centers, the absorption band of the perturbed C–H bonds is not revealed at all (Figure 5.31, spectrum 2), while in the case of CaO, only a weak absorption band is observed (Figure 5.31, spectrum 3). These results indicate a significant influence of the bond polarization by the ion-pair site on the intensity of the absorption bands. Broad absorption bands are not observed upon methane adsorption on samples previously treated by hydrogen or carbon monoxide at room temperature. This indicates that such molecules are preferentially coordinated to X-centers of η - Al_2O_3 . Broad absorption bands of the perturbed C–H bonds with maxima in the 2755–2680 cm^{-1} region have been observed in the spectra of saturated hydrocarbons with variable lengths of chains such as ethane, propane, iso-butane, and cyclohexane.

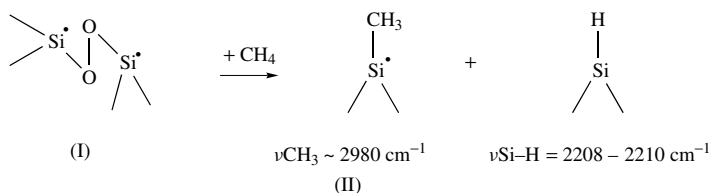
It should be noted that on magnesium oxide, as well as on other oxides, hydrogen-bonded forms of adsorbed alkanes such as cyclohexane, which are characterized by the strong loosening of the C–H bond, are present (Figure 5.31, spectrum 4). The intensity of these absorption bands is substantially lower on MgO than on η - Al_2O_3 (Figure 5.31, spectra 4 and 5), which is consistent with the absence of this band in the case of methane adsorption, due to its negligible intensity. Thus, the above-discussed data show that alkane adsorption on the surfaces of all oxides being studied occurs (at room temperature) on acid–base pairs, via interaction with C–H bonds, with the extent of perturbation being dependent on the properties both of the hydrocarbon and of the acid–base pair involved in the formation of such a complex. The extent of perturbation increase results in a decreased strength of the C–H bond which participates in the complex formation, and an enhanced acceptor ability of the cation and in the donor ability of the anion. The number of sites responsible for the interaction is low; therefore, it is not always possible to observe such complexes by IR spectroscopy at room temperature, especially when the transmittance technique

is used. One may expect that such H-bonded complexes are the precursors of dissociative forms of alkane adsorption.

The formation of complexes with strongly disturbed OH bonds has also been observed at room temperature upon the adsorption of cyclohexane on Ti–Sb oxide catalysts [1377]. It should be noted, however, that in the absence of strong Lewis acid centers in the surface ion pair there is no alkane dissociation. This indicates that for dissociation both strong basic and strong Lewis acid centers have to be present in this pair. It should be pointed out, however, that there is another point of view considering the assignment of the low-frequency absorption band (ν_{CH}). Thus, upon cyclohexane adsorption over Ag a 2788 cm^{-1} band, broadened and shifted to low frequency due to electronic interactions between certain hydrogen atoms in the molecule and the metal surface ($\text{C}\equiv\text{H}\equiv\text{M}$), has been observed [900]. More specifically, this has been described as ‘a two-way charge transfer from bonding $\sigma\text{-CH}$ orbitals to orbitals in the metal and from filled metal orbitals into the antibonding $\sigma^*\text{-CH}$ orbitals’. The latter process dominates. It is clear that in this case, the dependence of ν_{CH} on the acceptor strength of the cation should be observed. However, this is a subject of further investigation.

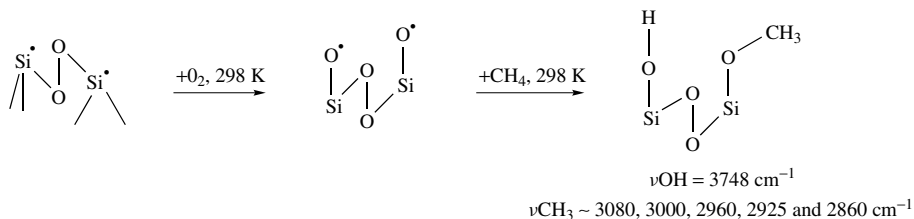
Dissociative forms of alkane adsorption

As has been established by means of infrared spectroscopy [50], the adsorption of methane proceeds on the SiO_2 surface when treated at high temperature ($>1123\text{ K}$) in the presence of methanol (i.e. after undergoing pyrolysis). The surface treated in this way has centers of type I, which already interact with methane at 293 K (the greatest interaction takes place at 573 K) with the formation of structures of type II:



Scheme 5.36

The surface concentration number of such centers is 0.17 centers per 100 \AA^2 . If, before methane adsorption, the sample has been treated by oxygen at 298 K , the character of the interaction, the properties of the adsorption center and the spectral manifestation of the adsorbed fragments change significantly:



Scheme 5.37

It has been pointed out [1379] that the formation of the reduced centers responsible for the partial oxidation of methane to formaldehyde is possible on an SiO_2 surface, and this has been

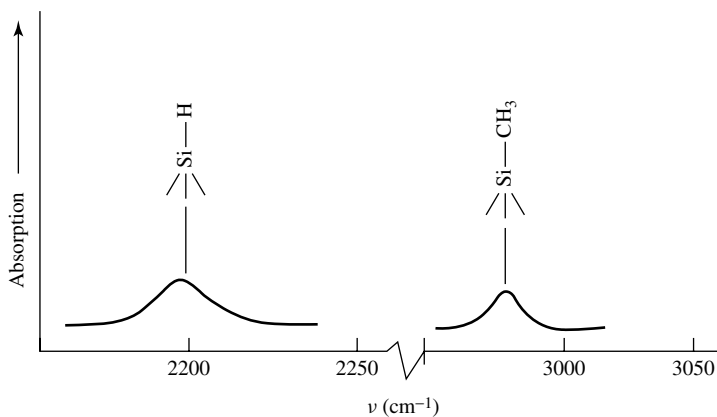


Figure 5.32. DRIR-spectrum of CH_4 after interaction with SiO_2 at 473 K. SiO_2 was pretreated with the ($\text{CH}_4/\text{O}_2 = 0.2/0.1 + \text{He}$) reaction mixture at 973 K.

studied by means of the DRIR method [1380]. The SiO_2 was activated by a methane–oxygen mixture (20 % CH_4 and 10 % O_2) at 873–973 K and then evacuated at the same temperature *in vacuo*. If the reaction products were not removed (by freezing-out) due to the pretreatment, it was possible to observe methane dissociation only at temperatures of 473 K and higher (Figure 5.32). Such interactions have not been observed in the case of samples treated only by heating up to 1023 K; the intensity of the absorption bands are extremely low, even when the DRIR method was being used, and are not observed at all when using FTIR spectroscopy. It is not yet clear how such centers appear; i.e. whether this is due to the opening of the siloxane bridge upon interaction with methane, or by means of chemical interactions with the reaction mixture, including the products of oxidation. The latter have properties similar to those of the compounds that are used to modify the SiO_2 surface in order to prepare reactive silica (by thermolysis) [50] or by other techniques.

In connection with the study of this system, it should be pointed out that, in our opinion, a disappearance of the 830 cm^{-1} absorption band (Si–O–Si bridges) after high-temperature interaction of SiO_2 with the $\text{CH}_4 + \text{O}_2$ mixture, observed by Viculov *et al.* [1381], may not necessarily provide evidence that CH_4 directly interacts with the siloxane bridge, as it has been suggested by these authors since the products of methane oxidation, including water, are formed upon high-temperature interaction. Water, as is well known [19], readily interacts with a siloxane bridge and opens it. Thus, the absence of spectral manifestations of adsorbed methane in the spectra of SiO_2 pretreated only at high temperature *in vacuo* [1381] is no surprise. Methane, perhaps, does not interact with such surface of SiO_2 and disappearance of the adsorption bands can be connected with the adsorption of the methane combustion products.

The heterolytic rupture of the C–H bond has been revealed on the surface of several oxide systems. The formation of alcoholate-like or metal–alkyl species, which are usually transformed on the surface of oxide catalysts into more oxidized species – carboxylate (formate) or carbonate types – has been observed, for example, in the IR spectroscopic method used by Davydova *et al.* [1382] for the study of paraffin activation on the surfaces of several simple metal oxides, such as chromia, iron oxide and vanadia. In the reaction of CH_4 with chromium oxide in the 373–673 K temperature region, absorption bands appear and increase in the spectrum at 1350 and 1550 cm^{-1} . Similar absorption bands are also observed in the high-temperature reaction of CD_4 , at 1335 and 1550 cm^{-1} , showing that these bands are due to formate species. In the case of the reaction of CH_4 with Fe_2O_3 , the formation of formate complexes in significant concentrations was also established at 423 K. However, in contrast to the reaction of CH_4 with Cr_2O_3 , in the

case of Fe_2O_3 the data obtained suggest that the surface methylates are also relatively stable on this oxide at the temperatures of pre-catalysis. The appearance in the IR spectra of absorption bands at 1040, 2870, 2940 and 2970 cm^{-1} in the reaction of methane with Fe_2O_3 at $T < 473$ K is evidence for this. The absorption band at 1040 cm^{-1} can be assigned to the stretching vibrations of the C–O bond in the methoxide, while the absorption bands at 2870, 2940 and 2970 cm^{-1} lie in the region characteristic of νCH_3 in this type of group. The reaction of methane with V_2O_5 has a very different character. In this case, based on the IR data, no formation of surface compounds has been observed below 573 K. Similar results were obtained for $\text{V}_2\text{O}_5/\text{SiO}_2$ (30 wt% V_2O_5) at 773 K.

According to the IR data [1376], on the surface of a La–Ga–Sb oxide catalyst an interaction with propane leads to $\text{C}_3\text{H}_7^{\delta-}$ fragments, and OH groups are formed due to the presence of centers of the type NH_2^- and/or NH^{2-} , which appear on the surface after pretreatment of the catalyst with the reaction mixture (Figure 5.33). Such centers are more basic than O^{2-} and seem to be responsible for providing heterolytic dissociation similar to that observed [775] on $\text{Al}^{3+}\text{O}^{2-}$ paired centers ($\sim 10^{15}$ centers m^{-2}) upon the interaction of methane with the $\eta\text{-Al}_2\text{O}_3$ surface. Both aluminum methyls and OH groups were formed during this interaction.

It is unlikely in the case of ethane interaction with Cr–Mo catalysts [1376] that surface ethoxides were formed. Probably, in the case of heterolytic dissociation followed by stabilization of the anionic species on the cations, electron transfer seems to be possible from this fragment to the cation, especially if the latter has a high value of electron affinity. The following interaction of the resulting fragment, charge-modified in this way, with an oxygen atom of the surface may be an explanation for the formation of alkoxide species. In fact, the use of $\text{C}_2\text{H}_5\text{Br}$ as an adsorbent, with a tendency to dissociation into C_2H_5^+ and Br^- , showed that alcoholates are predominantly formed [1377].

In contrast to alumina, silica does not react with $\text{C}_2\text{H}_5\text{Cl}$ [1383] at temperatures below 573 K. However, according to the infrared data, alumina reacts with ethyl chloride to give surface-bound ethoxy groups. The infrared data, with the suggestion that hydroxyl groups participate in the reaction, are in good agreement with the following reaction mechanism:

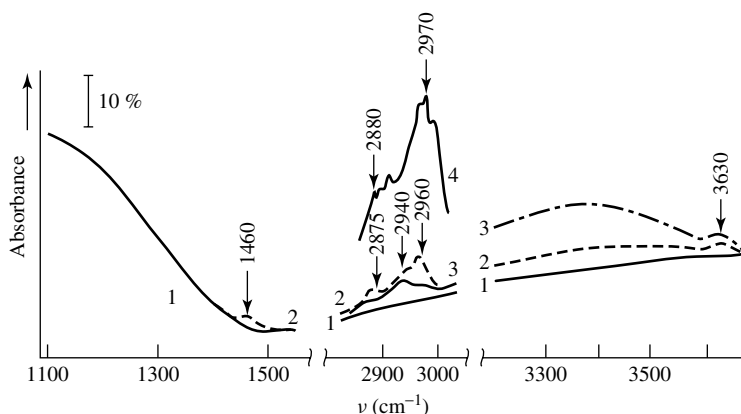


Figure 5.33. IR spectra of (4) gaseous propane adsorbed on (1) a Ga–Sb–oxide catalyst treated with the reaction mixture $\text{C}_3\text{H}_8 + \text{O}_2 + \text{NH}_3$; (2, 3) adsorption of C_3H_8 at 298 and 673 K, respectively.

Ballinger and Yates [1384] used transmission infrared spectroscopy to study the catalytic decomposition of 1,1,1-trichloroethane on alumina. At 300 K, CH_3CCl_3 is reversibly adsorbed on the isolated surface hydroxyl groups of Al_2O_3 via hydrogen-bonding. At temperature higher than 400 K, an α,β -HCl elimination occurs, forming $\text{CH}_2=\text{CCl}_2(\text{g})$. A small amount of surface carboxylate was also formed by means of a minor reaction pathway. It was found that LASs (Al^{3+}) participated in the primary reaction. The reaction of CH_3Cl with alumina surface hydroxyl groups produces CH_3O (at $T > 380$ K) [1385]. This reaction is entirely different from that reported for CH_3CCl_3 . An *in situ* FTIR spectroscopic study of the reaction of several halomethane compounds with an alumina surface [1386] indicated that halomethanes 'dissociatively chemisorb on heat-treated γ -alumina' and hexafluoropropane on TiO_2 [1387].

The formation of alkoxy groups upon the interaction of light hydrocarbons (methane, ethane and propane) with the oxidized surface of the spinel MgCr_2O_4 (an active hydrocarbon combustion catalyst) has been investigated by FTIR spectroscopy in the 300–773 K temperature range [1388]. During this interaction the catalyst is reduced, and oxygen-containing adsorbed species are formed. Every hydrocarbon reacts at its weakest C–H bond. On $\text{Cr}^{n+}=\text{O}$ ($n = 5$ or 6) surface sites, this arises from hydrogen abstraction, with C–O bond formation to alkoxy groups. These species are further oxidized to carbonyl compounds and/or carboxylate anions and, finally, to CO_2 or CO . The earlier intermediates (alkoxides and carbonyl compounds) are detectable only with the most reactive hydrocarbons (propane, *n*-butane and isobutane). With the least reactive hydrocarbons (methane and benzene), because of their very high activation temperatures, only the final surface products are detectable (carbonates and carboxylates).

It is very difficult to reveal the dissociative forms of alkane adsorption by using IR spectroscopy, which stems from the fact that the concentrations of such species is much lower than those of H-bonded complexes, especially at low temperatures of interaction. For instance, the concentration of centers responsible for the dissociative adsorption of methane on alumina at room temperature was shown [536] to be 10^{15} m^{-2} , which is two orders of magnitude lower than the concentration of centers responsible for methane adsorption in the molecular form. Furthermore, the presence in the νCH spectrum of absorption bands due to CH vibrations for some starting samples does not allow the observation of the IR spectrum of the dissociated forms. The use of deuterated alkanes (i.e. the shift to the νCD region) is not always efficient, since the extinction coefficients for the C–D bonds are lower than for the repeating C–H bonds.

Methane adsorption on $\eta\text{-Al}_2\text{O}_3$ at room temperature and further removal of the H-bound complex by evacuation leads to the appearance of only weak absorption bands in the spectra (Figure 5.34, spectrum 1). Taking into consideration the results reported by Kazanskii and co-workers in [775, 776], it may be assumed that, at room temperature, methane is adsorbed on the surface of alumina in the dissociative form, thus yielding Al-CH_3 and O-H species.

The data obtained allowed the deduction that isotopic exchange between hydrocarbons is accompanied by heterolytic rupture of the C–H bond. However, at room temperature this process occurs not on the X-centers but on centers of another nature, the number of which is two orders less ($\sim 10^{15} \text{ m}^{-2}$). The slow dissociation of saturated hydrocarbons takes place on X-centers (these are the multiple-anion vacancies, which include a three-coordinated aluminum atom exhibiting the properties of a strong Lewis acid; their number is about $2 \times 10^{17} \text{ m}^{-2}$) (Figure 5.34, spectrum 2) but only at 420 K. This is shown by a gradual decrease in both the intensities of the broad low-frequency bands corresponding to strongly perturbed CH vibrations and the formation of surface hydrocarbon fragments, stable to desorption up to 423 K. Since no formation of aluminum hydrides is observed upon dissociation of alkanes, this more probably results in the formation of aluminum alkyls and hydroxyl groups. At temperatures above 523 K, chemisorbed structures undergo conversion. It was revealed [776] for the Al_2O_3 samples on which propane or heavier alkanes have been adsorbed, that the aluminum hydrides are formed and reliably detected by the

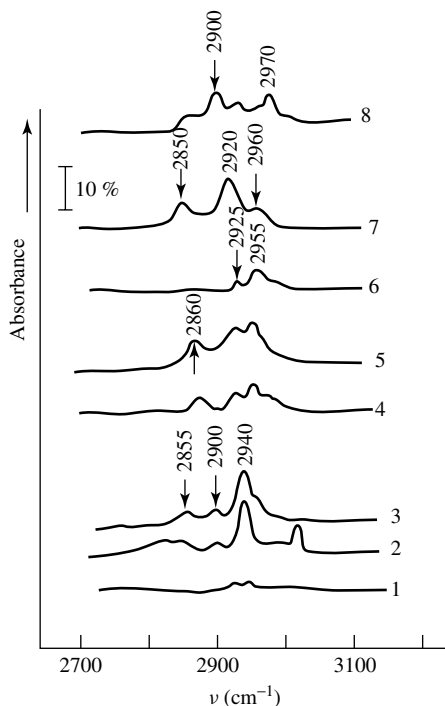


Figure 5.34. DRIR spectra of hydrocarbons adsorbed on (1–5) η - Al_2O_3 , (6, 7) MgO and (8) ZrO_2 : (1) adsorption of methane at 293 K and evacuation at 293 K; (2) after heating at 673 K in the presence of methane; (3) further evacuation at 293 K; (4) adsorption of isobutane at 293 K and evacuation at 423 K; (5) adsorption of cyclohexane at 293 K and evacuation at 423 K; (6) adsorption of methane at 623 K and evacuation at 293 K; (7) adsorption of cyclohexane at 293 K and evacuation at 293 K; (8) adsorption of ethane at 673 K and evacuation at 293 K.

$\nu\text{Al-H}$ absorption band at 1900 cm^{-1} . At the same time, in the UV spectra the intensive bands at 280 and 350 nm, corresponding to charged allyl and dienyl structures, respectively, are observed. Probably, under these conditions dehydrogenation of saturated hydrocarbons takes place with the participation of X-centers, and olefins formed at these are not desorbed to the gas phase. In the presence of H_2 at higher temperatures, the reverse process to the hydrogenation of olefins takes place.

Davydov and Budneva [774] argue that dissociation of methane at room temperature proceeds on ionic pairs that include highly uncoordinated aluminum atoms, localized in the vicinity of the cationic vacancies. The number of such centers is extremely low. An increase of the temperature of methane adsorption on the surface of η - Al_2O_3 to 423–573 K makes it possible to reliably detect absorption bands in the spectra which belong to the strongly adsorbed methane molecules (Figure 5.34, spectra 2 and 3). These adsorbed species are formed at elevated temperatures on the X-centers of aluminum oxide on which the complexes of hydrocarbons with strongly loosened C–H bond are formed at room temperature and remain in the spectra after evacuation of the sample at 473 K. Thus, the concentration of dissociatively adsorbed methane increases significantly with an increasing temperature of methane interaction with η - Al_2O_3 because its dissociation occurs on X-centers, which are present in a high enough concentration. It is noteworthy that the dissociative adsorption of alkanes with a higher molecular weight, for instance isobutane and cyclohexane, on

the surface of $\eta\text{-Al}_2\text{O}_3$ can be reliably established even at room temperature (Figure 5.34, spectra 4 and 5) as a result of the decrease in the energy of the secondary or tertiary C–H bonds in these hydrocarbons. Thus, aluminum–alkyl surface compounds, including aluminum–methyl species, formed upon alkane dissociation, were detected on the surface of $\eta\text{-Al}_2\text{O}_3$.

Analysis of diffuse reflectance IR spectra of methane adsorbed on magnesium oxide shows that the dissociative adsorption of methane proceeds to an appreciable extent only at temperatures of 573 K or higher (Figure 5.34, spectrum 6). Magnesium methylate is formed [1389]. This complex is stable and cannot be destroyed by evacuation at room temperature. The formation of the type of complex is governed to a considerable extent by the conditions of pre-treatment of magnesium oxide. In the case of the high-temperature oxidative treatment of the oxide, virtually no dissociative adsorption occurs. This confirms the hypothesis that the dissociative adsorption of methane proceeds on coordinatively unsaturated defect sites [1390], which can be eliminated by calcination in oxygen at high temperatures. The observed dissociative adsorption of methane evidently proceeds not only on the most coordinatively unsaturated centers, such as $\text{Mg}_{3\text{C}}\text{O}_{3\text{C}}$, but also on sites with a higher coordination number, probably $\text{Mg}_{4\text{C}}\text{O}_{4\text{C}}$. The latter are most likely responsible for the formation of the H-bonded methane complexes at room temperature, which are characterized by a weakening of the C–H bond.

The formation of dissociatively adsorbed species is facilitated if the molecular weight of the alkane is higher than that of methane and/or if a greater part of the centers is involved in the formation of these species. In the case of cyclohexane (Figure 5.34, spectrum 7), a considerable concentration of the strongly bonded complex is already attained after admission of the hydrocarbon at room temperature.

Ion pairs in zirconium dioxide, as can be deduced from the above-discussed data, are the weakest among the oxide systems that have been mentioned. Indeed, the frequency shift of the band assigned to the perturbed C–H bonds for a specified hydrocarbon adsorbed on ZrO_2 was the smallest among the oxides under consideration. Obviously, this explains the difficulties in detecting the dissociatively adsorbed alkane molecules on this oxide. In the case of methane, no spectral features indicating dissociative adsorption in the range of temperatures up to 573 K have been observed, but for higher alkanes, such as ethane, experimental data on dissociative adsorption were obtained (Figure 5.34, spectrum 8). However, the concentration of the dissociatively adsorbed species on ZrO_2 is low, and they appear at higher temperatures, as compared with other oxides. The decreasing acceptor ability of a cation and especially the basicity of oxygen cause a lower perturbation of the C–H bond in the course of low-temperature interactions and a decrease in the probability of dissociation of this bond in the course of high-temperature interactions.

Surface electromagnetic wave spectroscopy (SEWS) has been used to study methane adsorption on the surfaces of oxide films (Al_2O_3 , CaO and BaO) [1391]. A CO_2 laser is the source of radiation, in conjugation with a monochromator. The range of emission lines available was 157 cm^{-1} (from 1088 to 931 cm^{-1}). The interaction of methane with oxides (interaction temperature of ca. 600 K for Al_2O_3 and CaO , and ca. 500 K for BaO) leads to the appearance of absorption bands in the $1050\text{--}1100\text{ cm}^{-1}$ region, assigned to the symmetric stretching vibration of the C–O bond in the methoxy group (O-CH_3). Methane interaction with isotopically substituted ($^{18}\text{O}_2$) oxide films showed that these bands are really due to the vibrations of the C–O bond in which lattice oxygen is involved (a shift of ca. 30 cm^{-1} has been observed). It should be pointed out, however, that these are the only characteristic bands of the surface species which are measurable by SEWS. Such experiments only allow the assignment of the observed bands to the vibrations of the C–O bond, but such bond is observed for instance, in carbonates ($\nu_s\text{CO}_3$), too. This fact reduces the general significance of information obtained by this spectroscopic approach.

The interaction of methane with such a basic oxide as MgO is interesting. From the results of a later IR study [1389], it follows that the spectrum of an MgO sample treated at 973 and

1123 K essentially does not change after interaction with methane at 293 K: together with the 3750 cm^{-1} band characteristic for MgO, bands belonging to gaseous methane are observed. However, when the interaction temperature increases up to 573 K, the intensity of the 3650 cm^{-1} band increases, but then decreases with further elevation of the interaction temperature up to 773 K, then disappearing at 973 K. The appearance of bands belonging to surface hydroxyl groups upon heating the sample in methane up to temperatures at which no methane destructive oxidation is observed, at least to 573 K, indicates that at this temperature methane dissociation takes place. Bands are observed at 2940 and 2980 cm^{-1} and in the $1420\text{--}1450\text{ cm}^{-1}$ region (νCH and δCH of dissociatively chemisorbed species – Figure 5.35, spectrum 2) in the infrared spectrum of methane adsorbed under these conditions. These bands are changed in parallel with the appearance of the band at 3650 cm^{-1} , characteristic of surface hydroxyl groups. At the same temperature (573 K), according to Utaïama *et al.* [1392], the isotopic exchange also starts.

The analysis of the spectra of C–H vibrations, a comparison of the absorption bands obtained with those of methyl groups [1393, 1394], and also a comparison of the spectra of adsorbed methane with that of both individual $\text{Sn}(\text{CH}_3)_2\text{Cl}_2$ and adsorbed on MgO and also with that of oxymethyl groups formed upon methanol adsorption over MgO, give reason to propose that these absorption bands, observed by Davydov and co-workers [1389, 1395], belong to CH_3 groups stabilized on surface cations. At the interaction temperature of 573 K, a 3085 cm^{-1} band, which can belong to $\nu=\text{CH}$ [88], appears in the spectrum 2 and could be due to the formation of ethene molecules. The above conclusions are confirmed by the spectra of CD_4 adsorbed on MgO.

Comparison of the data obtained in the case of MgO with those of $\eta\text{-Al}_2\text{O}_3$, where methane dissociation is already observed at room temperature, also shows that over MgO activated methane dissociation takes place only at 573 K. According to FTIR data, H-bonded methane complexes with strongly loosened C–H bonds due to interaction with oxide surface oxygens (i.e. complexes similar to those obtained in the case of $\eta\text{-Al}_2\text{O}_3$) can also be formed on the MgO surface. For example, in the case of methane (CD_4) adsorbed on MgO there is a band at about 2000 cm^{-1} which, when compared with that obtained on $\eta\text{-Al}_2\text{O}_3$, characterizes the perturbed νCD frequency

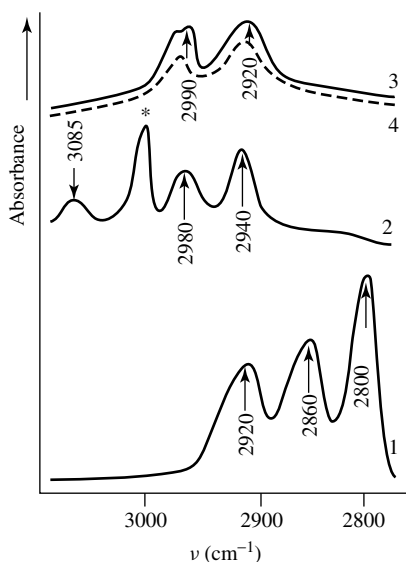
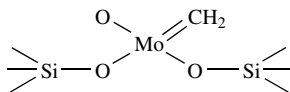


Figure 5.35. FTIR spectra of adsorbed on MgO (1) CH_3OH , (2) CH_4 , (3) $(\text{CH}_3)_2\text{SnCl}_2$, and individual (4) $(\text{CH}_3)_2\text{SnCl}_2$ in KBr. (* represent the band corresponding to gaseous CH_4).

in the methane D-bonded complex. The increasing strengths of basic sites on MgO that were observed due to introduction into MgO or CaO of the ions Li, Sm and La strongly increases the activity and selectivity of these types of catalysts in methane dimerization.

The formation of the carbene complex:



Scheme 5.38

which is stable *in vacuo* up to 673–723 K, has been observed by IR and UV–Vis spectroscopies upon cyclopropane adsorption over MoO₃/SiO₂, in which the Mo⁶⁺ ions have been photochemically reduced to Mo⁴⁺ [1396]. After cyclopropane adsorption at room temperature (at a final pressure of 1 torr), a rather complex IR spectrum was obtained in the C–H stretching region, showing absorption bands at 3100, 2985, 2930 and 2870 cm⁻¹ and shoulders at 3080 and 3020 cm⁻¹. The absorptions at 3100 and 3020 cm⁻¹ were assigned to C–H vibrations of the physically adsorbed molecules, with the bands at 3060, 2985 and 2870 cm⁻¹, and at 590 nm, being assigned to π -complexes of C₂H₄ and C₃H₆ (π -complexes with Mo⁴⁺). The bands at 3080 and 2945 cm⁻¹, together with the band at 450 nm, was attributed to the Mo=CH₂ species. Such carbene species are found to be thermally stable *in vacuo* up to 650–700 K [1396].

In situ FTIR studies illustrated the generation of a peroxide species (an absorption band at 895 cm⁻¹, which shifted to 849 cm⁻¹ when ¹⁶O₂ was replaced by ¹⁸O₂, and three absorption bands observed at 895, 870 and 849 cm⁻¹ from an adsorbed mixture of ¹⁶O₂–¹⁸O₂) on contact of an H₂–O₂ gas mixture, or of N₂O, with Fe–Al–P–O catalysts at $T \geq 573$ K [1397]. It was revealed that this species reacts with CH₄. The results showed that the intensity of the band at 890 cm⁻¹ decreased significantly when the temperature was raised to 473 K and bands at 3668, 2936, 2870 and 1050 cm⁻¹ appeared. The adsorption at 3668 cm⁻¹ has been assigned to the newly formed OH group due to the reaction of CH₄ with the iron peroxide species. The bands at 2936 and 2870 cm⁻¹ were therefore assigned to the ν_{as} and ν_s modes of CH₃ groups, and the band at 1050 cm⁻¹ to the ν C–O of the methoxyl species [1398].

Two important conversion reactions of the paraffins are dehydrogenation or oxidative dehydrogenation. Dehydrogenation of, for example, propane takes place on the same La–Ga–Sb oxide catalysts, probably via the mechanism of heterolytic rupture of the C–H bond with the formation of (C₃H₇ ^{δ^-}) anionic species, which can convert to propene due to hydrogen abstraction. The V–Mg–O system is a good catalyst for propane dehydrogenation, and its reaction mechanism has been investigated. From a study of the active surface under reaction conditions, with *in situ* techniques such as DRIFT and XPS analysis, a unique active site was assumed to include surface V⁵⁺ ions, lattice oxygen ions and anionic vacancies.

A very interesting way for the formation of acrylic acid by the direct catalytic oxidation of propane up to 693 K has recently been found [1399]. It was confirmed by IR studies that the catalysts for this reaction are reduced heteropolymolybdophosphoric acids and it has also been demonstrated that both the acidic character and the highly reduced state of the H₃PMo₁₂O₄₀ catalyst played substantial roles in the course of the propane oxidation with molecular oxygen. The authors propose the cooperation of both protons and electrons in the reduced acidic HPA catalyst in the activation of molecular oxygen and the subsequent activation of propane: molecular dioxygen first reacts with two protons and two electrons to form one molecule of water.

The most successful oxidation of a lower alkane is the selective oxidation of *n*-butane to maleic anhydride, which has been successfully demonstrated and commercialized by using crystalline

V–P–O catalysts [1400]. It should be pointed out, however, that in spite of this reaction having been investigated for a fairly long time, the character of the initial activation has not yet been established. Just after injection of the reaction mixture, the appearance of new bands at 1710 and 1780 cm^{-1} indicate the formation of a compound with an aldehyde bond [1401]. Probably, the formation of an olefin from butane proceeds directly after contact of the catalyst with the reaction mixture. It has been established that the oxidative dehydrogenation of butane to butene can take place on catalysts which contain heteropolyoxoanions. These systems, as is well known, are stable and selective heterogeneous catalysts for such processes [1402, 1403a].

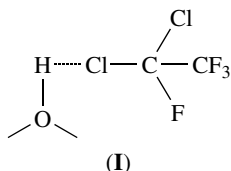
5.5 Complexation of chlorofluorocarbons

The reactions of chlorofluorocarbons (CFCs), the compounds which decrease the stratospheric ozone concentrations, over different types of catalysts have received much attention recently because of the necessity of converting these compounds to chemically inert species.

Metal oxides catalyze the oxidative destruction, exchange reactions, disproportionation and isomerization reactions of CFCs and hydrofluorocarbons (HFCs). In earlier parts of this chapter we have already paid attention to the IR spectroscopic studies of the interactions of halogenated hydrocarbons with oxide surfaces (see Sections 5.1.4, 5.2.6 and 5.4.3). In summary, the analysis of the IR data shows that, because of the high donor ability of halogen atoms, the first interaction step is a binding of the halogenated hydrocarbon to the surface hydroxyl groups with the formation of hydrogen-bonds. This may be followed by substitution of these hydroxyl groups by the Cl^- ions. If acceptor centers (coordinatively unsaturated cations) are present on the surface, formation of donor–acceptor complexes, again involving halogen ions, is also possible. The cation (R^+) formed is often attached to the surface oxygen, hence giving the alcoholate surface species. The transformation of these occurs by different pathways, depending on their properties, in particular on the strength of the bond with the surface. Oxidation with the formation of carboxylates is one of the possible transformation routes.

As an example, let us examine the interaction between CF_3CFCl_2 and an oxide surface. In general, as was shown by spectroscopic studies [1403b–1403d], the character of the CF_3CFCl_2 interaction with oxide surfaces is similar to that described above since the donor–acceptor bond is formed mainly through the Cl atom which has a larger donor ability than the F atom [1403e].

The importance of the nature of the surface sites in the interactions between CF_3CFCl_2 and oxides has also been determined. Thus, the CF_3CFCl_2 molecules are bonded with the surface hydroxyl groups of SiO_2 (3750 cm^{-1}) by the hydrogen-bond ($\sim 3450 \text{ cm}^{-1}$) through the chlorine atom to form the following complex:



Such a complex is weakly bonded to the surface and can be removed under vacuum at room temperature. Vibrations characteristic for this complex are similar to those observed in the spectrum of the gaseous molecule and have shown that the CFC molecule is only weakly perturbed (Table 5.26). After removing the complex (I), the surface hydroxyl groups remain perturbed due

Table 5.26. The fundamental vibration frequencies (cm^{-1})^a for individual molecule of CF_3CFCl_2 and when reversibly adsorbed on the surfaces of various oxides.

Infared		Raman ^a	Symmetry of species ^c	Assignment ^d	Adsorbed on			
Gas	Liquid				SiO ₂	TiO ₂	Al ₂ O ₃	
735 (vs)	734 (s)	734 (vs)	A'	CCl (str)	735	} Overlap with fundamental vibrations of oxides		
897 (vs)	891 (vs)	891 (vw)	A''	CCl (str)	Overlap with SiO ₂			
943 (vs)	938 (vs)	939 (vw)	A'	CC (str)	920			
1110 (vs)	1103 (vs)	1103 (w)	A'	CF (str)	Overlap with SiO ₂	1125	1190	
1232 (vs)	1217 (vs)	1218 (vw)	A''	CF ₃ (str)	Overlap with SiO ₂	1218	1215	
1232 (vs)	–	1247 (vw)	A'	CF ₃ (str)	Overlap with SiO ₂	1240	1245	
1295 (vs)	1292 (vs)	1292 (w)	A'	CF ₃ (str)	1290	1295	–	

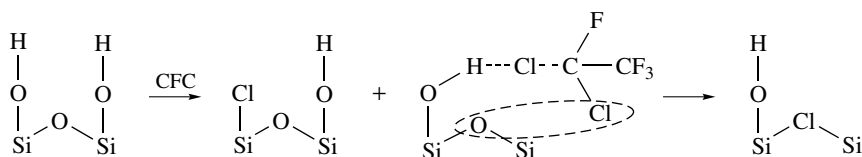
^avs, very weak; w, weak; vw, very weak.

^bLiquid.

^cA' and A'', symmetric and asymmetric, correspondingly.

^dstr, stretching.

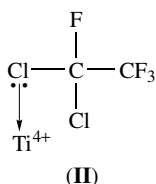
to the following interactions:



Absorption bands at 920 and 873 cm^{-1} appear in the spectrum of SiO₂ during high-temperature interaction with CF_3CFCl_2 . These bands are similar to the vibrations of the Si–F bond [15].

The same interaction occurs with the basic hydroxyl groups of TiO₂ and Al₂O₃, and in their subsequent transformations, probably due to halogen substitution in the CF_3CFCl_2 molecules through an exchange reaction between OH and Cl, whereas the acidic hydroxyl groups of HZSM-5 zeolites form only hydrogen-bonded complexes of CFC.

It has been shown that the primary interactions of CF_3CFCl_2 with the surfaces of TiO₂, Al₂O₃ and NaZSM-5 containing electron-acceptor centers (Lewis acid sites) involve lone electron pairs of the halogen atoms because the halogen derivatives displace pre-adsorbed CO from the Ti⁴⁺ cations. For example, in the case of TiO₂:

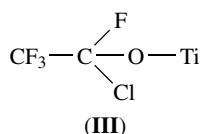


At elevated temperatures, a partial substitution of the halogen atoms for oxygen occurs, followed by the complete degradation of the adsorbed CFC molecules. Interaction between CF_3CFCl_2 and TiO₂ at 373 K proceeds more 'deeply' and, in addition to the weakly bonded complex (I), a chemisorbed complex (III) is also formed (Table 5.27). A new band at ca. 1030 cm^{-1} in the spectrum of this complex (III) is characteristic of the νCO mode in alcoholates [30], and together with the presence of absorptions characteristic of CF₃ and CF, suggest the formation of

Table 5.27. Species of CF_3CFCl_2 chemisorbed on various oxides and their spectral characteristics (ν).

Vibration	Adsorbed on					
	Al_2O_3		TiO_2		Cr_2O_3	
	ν (cm^{-1}) Compound		ν (cm^{-1}) Compound		ν (cm^{-1}) Compound	
νCO	—	—	1030	III	—	—
$\nu_{\text{as}}\text{CF}_3$	1190	III, IV	1190	III, IV	1190	IV
$\nu_{\text{as}}\text{CF}_3$	1215	III, IV	1220	III, IV	1220	IV
$\nu_{\text{s}}\text{CF}_3$	1240	III, IV	1250	III, IV	1250	IV
$\nu_{\text{s}}\text{COO}$	1500	IV	1480	IV	1480	IV
$\nu_{\text{as}}\text{COO}$	1670	IV	1640	IV	1645	IV

the following surface complex:



On the surface of Al_2O_3 at 300 K, CF_3CFCl_2 is (i) reversibly adsorbed through hydrogen-bonding with isolated OH groups, and (ii) coordinatively bonded to $\text{Al}^{3+}_{\text{cus}}$ via the lone pair of the chlorine atom. At higher temperatures, the Al^{3+} sites are needed for the dechlorination reaction, whereas the hydroxyl groups are not involved in this process.

The IR absorption bands of CF_3CFCl_2 adsorbed at 300–473 K on Al_2O_3 , and dehydroxylated at 773 K, suggest the formation of a trifluoroacetate species (complex **(IV)** in Table 5.27). Carboxylate surface species have also been reported for the adsorption of halogenated methanes on γ -alumina surfaces [1403f] and for hexafluoropropene on TiO_2 [1403g]. Trifluoroacetate complexes on alumina surfaces are extremely stable and only decompose at a significant rate above 593 K, releasing CO and CO_2 into the gas phase as the only products.

The results of an investigation into the interaction of CF_3CFCl_2 with Al_2O_3 at 300 °C in a catalytic flow reactor revealed a transient period followed by steady-state behavior. During the steady-state period, a catalytic halogen-exchange reaction involving the CF_3CFCl_2 occurred, leading to CF_3CCl_3 and $\text{CF}_3\text{CF}_2\text{Cl}$ products in a 1:1 molar ratio. A similar product distribution has been obtained for the conversion of CF_3CFCl_2 over AlF_3 . During the transient period, Al_2O_3 reacted with CF_3CFCl_2 stoichiometrically, resulting in the formation of CF_3CCl_3 as the only organic product. The formation of carbon oxides was also observed, as is required by mass balance, but these products were not quantified. At the same time, transformation of the Al_2O_3 to aluminum oxifluoride (AlF_xO_y) took place. Changes have been revealed in the concentrations and strengths of the acid sites due to fluorination of Al_2O_3 (an increase of νCO is known to be due to an increase in the acceptor ability of Al^{3+} ions after fluorination). Such fluorination is indicated by the appearance of Al–F vibrations in the Raman spectra of Al_2O_3 .

Because Cr_2O_3 is an active catalyst for hydrocarbon oxidation, the CFC on a chromia surface oxidized easily via the surface oxygens, leading to the formation of adsorbed fluorine-containing carboxylate and carbonate species, with their subsequent oxidation to carbon oxides.

Based on IR spectroscopic evidence, heterolytic C–X (X=F and Cl) bond cleavage occurs during destructive conversion of adsorbed CF_3CFCl_2 , with stabilization of the halogen ions on electron-acceptor centers, while the rest of the CFC molecule forms complexes with the surface oxygen atoms.

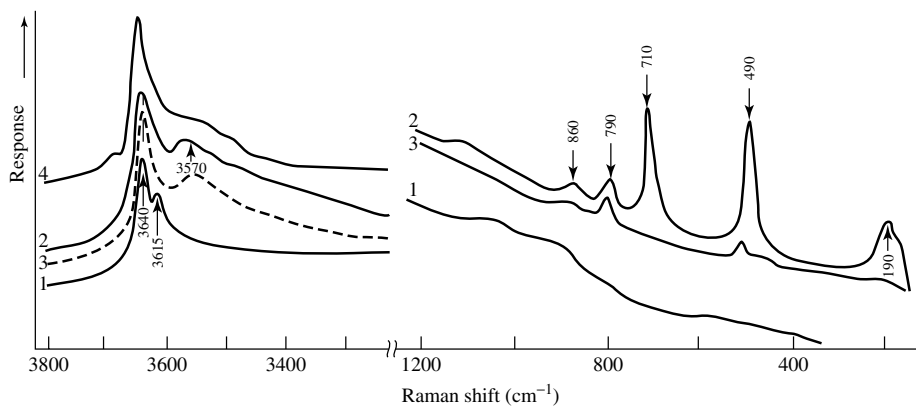
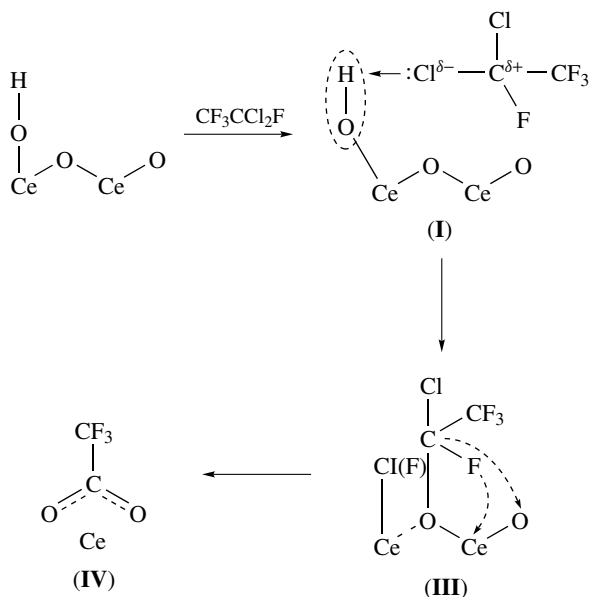


Figure 5.36. Raman spectra of SiO_2 (1) dehydrated at 773 K, (2) after adsorption of CF_3CFCl_2 at 293 K, and following desorption at (3) 293 K and (4) 473 K.

Raman spectroscopy is also a very useful (and ‘perspective’) technique for studying CF_3CFCl_2 adsorption. Raman data for the adsorption on several oxides, including SiO_2 (Figure 5.36), confirmed the results obtained by IR spectroscopy regarding the presence on the surface of only the H-bonded species, and also provided information about fluorination of SiO_2 . Support for the latter came from bands at about 790 and 860 cm^{-1} , which are close to the bands characteristic of the Si-F bond [15]. These were revealed after the removal of the CFC.

More detailed information about the character of the interaction has been obtained for CeO_2 . Practically all stages of this interaction have been revealed. Based on these data the following mechanism can be suggested:



The data obtained show that the reversibly adsorbed species of CF_3CFCl_2 (I) is probably bound to the surface through the hydroxyl group of the CeO_2 surface (Figure 5.37, spectrum 2). The

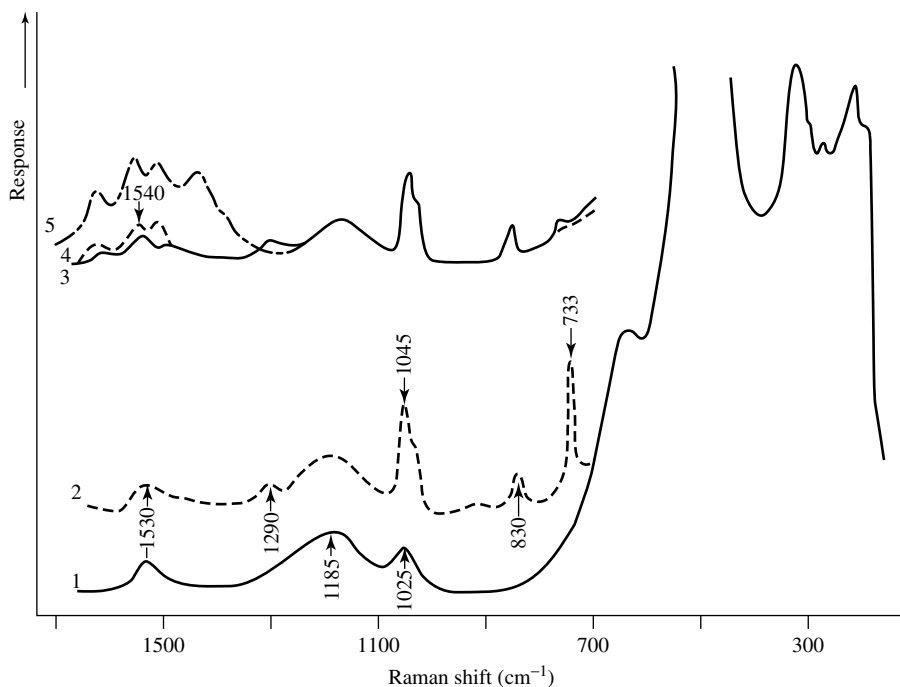


Figure 5.37. Raman spectra of CeO_2 (1) dehydrated at 673 K for 1 h in a N_2 flow, after CFC adsorption at (2) 293 K and (5) 473 K, and following desorption at (3) 373 K and (4) 473 K.

shift of the characteristic C–Cl bond, compared to that of the gas-phase CFC species, is much less in this case than that for SiO_2 – 5 and 30 cm^{-1} , respectively. Since CeO_2 is a more basic oxide than SiO_2 , this difference is not surprising. The more acidic hydroxyl group of SiO_2 move strongly accepts an (unpaired) electron pair of the chlorine atom than the basic hydroxyl group of CeO_2 . This provides additional support for the CFC interaction with surface hydroxyl groups involving the chlorine atom of the CFC molecule.

A band at about 1290 cm^{-1} appeared in the spectrum after CFC interaction with the CeO_2 surface at 293 K but disappeared at 473 K with a simultaneous increase of the bands characteristic of surface carboxylates (spectrum 5). This band is probably from the νCO in the surface ether-like compound (fluorine-containing alcoholate) of type (III). An increase of the interaction temperature to 473 K leads to a decrease in the concentration of compound (III) and an increase in the concentrations of the carboxylates (IV) (Figure 5.37). The formation of the latter (in small concentrations) is also observed upon CFC desorption from CeO_2 at 373 K (Figure 5.37).

5.6 Complexation of nitriles

5.6.1 ACETONITRILE

When the molecule of acetonitrile is free, the $\nu\text{C}\equiv\text{N}$ vibrations of CH_3CN are observed at 2251 cm^{-1} but are affected by a Fermi resonance with the $\nu\text{C}-\text{C} + \delta\text{CH}_3$ combination, lying at 2287 cm^{-1} [1404]. Exchange of the CH_3 fragment by CD_3 removes the effect of the Fermi resonance due to the strong decrease of the frequency of the combination vibration. This Fermi resonance complicates determination of the $\nu\text{C}\equiv\text{N}$ shift in complexes [1405]. Therefore the use of CD_3CN is preferred for surface acidity measurements [1406–1408] since in this molecule, the

$\nu\text{C}\equiv\text{N}$ vibration, observed at 2265 cm^{-1} , is little perturbed, although it is difficult to completely exclude couplings with the νCD_3 vibrations. However, as was reported for $\delta\text{-Al}_2\text{O}_3$ [1409], CD_3CN adsorption on dehydroxylated metal oxides can lead to $\text{H} \rightarrow \text{D}$ exchanges with surface hydroxy groups with a concomitant formation of partially deuterated or even nondeuterated acetonitrile.

Hydrogen-bonding

The molecules of acetonitrile easily form H-bonded complexes on oxide surfaces. Their interaction with SiO_2 is a typical example. The molecules are adsorbed on the silica surface by forming a hydrogen-bond between the silanol group and the nitrogen lone-pair electrons (Figure 5.38) [18, 19, 1410]. The broad feature near 3400 cm^{-1} arises from hydrogen-bonded silanols. At the same time, distinct peaks are observed in the CN stretching region, namely at 2298 and 2265 cm^{-1} (and also at 2256 cm^{-1} under high pressures of CH_3CN). By comparison with the IR spectrum of CH_3CN in CCl_4 , the peak at 2256 cm^{-1} was attributed to CH_3CN condensed on the silica surface. In the solution spectrum, a corresponding peak appeared at 2253 cm^{-1} . The 2256 and 2298 cm^{-1} bands can be assigned, respectively, to the CN stretching vibration and a combination mode of CH_3 deformation and C–C stretching vibrations of the CH_3CN bound to silanol groups. These peaks are shifted to higher values by 12 and 5 cm^{-1} , respectively, from the corresponding peaks at 2253 and 2293 cm^{-1} in the solution spectrum. Except for the CN stretching band, the peak positions of all of the other acetonitrile vibrational bands were observed to change by 5 cm^{-1} at most upon adsorption on silica. These data indicate that acetonitrile is adsorbed on the silica surface by forming a hydrogen-bond between the silanol group and the nitrogen long-pair electrons.

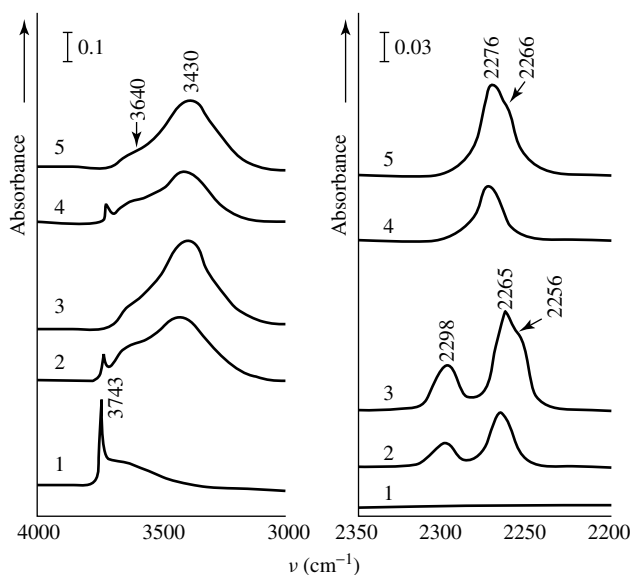


Figure 5.38. IR spectra of silica in the OH stretch and CN triple-bond stretch regions: (1) bare silica; in the presence of CH_3CN at (2) 0.9 and (3) 35 torr; in the presence of CD_3CN at (4) 0.9 and (5) 35 torr [1410]. From Yim, S.-G. Son, D. H. and Kim, K., *J. Chem. S.C., Faraday Trans. 1*, **89**, 837–843 (1993). Reproduced by permission of The Royal Society of Chemistry.

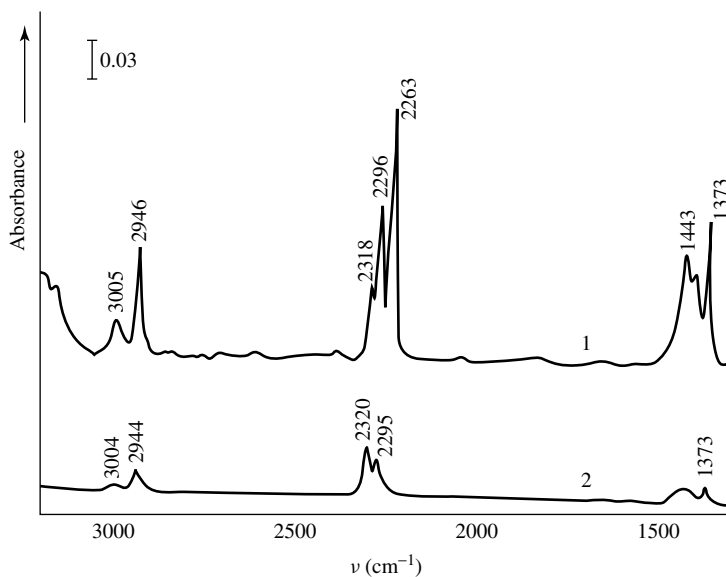


Figure 5.39. IR spectra of CH_3CN adsorbed on a silica-supported nickel surface (1) in the presence of 15 torr of CH_3CN and (2) after evacuation for 20 min [1410]. From Yim, S.-G. Son, D. H. and Kim, K., *J. Chem. S.C., Faraday Trans. 1*, **89**, 837–843 (1993). Reproduced by permission of The Royal Society of Chemistry.

The H-bonding between acetonitrile and the silanol group was, however, conjectured to be very weak since the adsorbed acetonitrile was desorbed immediately upon evacuation at 300 K, and a spectrum like that shown in Figure 5.38 (spectrum 1) was restored [1410]. This can be understood from the calorimetric data on the heats of formation of the hydrogen-bonds [1411]. In the case of aerosilgel, the heat of adsorption of acetonitrile molecules (21 kJ mol^{-1}) on the silanol groups is definitely higher than that of ordinary hydrocarbons (4.6 kJ mol^{-1}), but is substantially lower than that of other nitrogen-containing bases such as pyridine (29 kJ mol^{-1}) and trimethylamine (41 kJ mol^{-1}).

Complexes with cations

It has generally been accepted from studies of the metal-nitrile complexes and nitriles adsorbed on metal surfaces, using different spectral techniques [1412–1417], that linear coordination (σ -bonding) through the nitrogen lone-pair electrons results in an increase in the CN stretching frequency from that of the free molecule. On the other hand, coordination through the $\text{C}\equiv\text{N}$ π -systems is known to result in a decrease in the CN stretching frequency. The higher frequency shift of the ν_{CN} peak in the spectrum (Figure 5.39, Table 5.28) compared with that in the solution spectrum indicates that the acetonitrile is adsorbed on cations via its nitrogen lone-pair electrons.

The acetonitrile molecule has been often used as a probe to estimate the strength of aprotic (Lewis) acid centers of both zeolites and oxides [1418–1423]. The shift of the ν_{CN} ($\Delta\nu_{\text{CN}}$) bands during coordination is considered to be a measure of the strength of these centers. In fact acetonitrile easily forms complexes with cations, for example, Ca, Co, Ni, Cr and Na in Y-zeolites [1424, 1425]. The value of ν_{CN} depends on the nature of the cation. However, as has been estimated [1424], there is no clear functional relationship between $\Delta\nu$ and the heat of adsorption of acetonitrile on metal cations in Y-type zeolites. It has also been shown that when the coverage is

Table 5.28. Infrared frequencies (cm^{-1}) of acetonitrile adsorbed on silica-supported nickel and nickel oxide in the $3000\text{--}1300\text{ cm}^{-1}$ region [1410]. From Yim, S.-G., Son, D. H. and Kim, K., *J. Chem. Soc., Faraday Trans. 1*, **89**, 837–843 (1993). Reproduced by permission of The Royal Society of Chemistry.

CCl ₄ (3 vol%)		On Ni/SiO ₂ ^a		On NiO/SiO ₂ ^a		Vibrational assignment ^b
CH ₃ CN	CD ₃ CN	CH ₃ CN	CD ₃ CN	CH ₃ CN	CD ₃ CN	
3002		3004				asym CH ₃ str
2944		2944				sym CH ₃ str
2293		2295				sym CH ₃ def + CC str
2253		2320				C≡N str
1443						asym CH ₃ def
1376		1373				sym CH ₃ def
	2264		2306			C≡N str
	2116		2116			sym CD ₃ str
				2927		sym CH ₂ str
				1669		H ₂ O def
				1560		C=N str
				1455		C=C str
				1375		CH ₂ bend
					2755	OD str (silanol)
					2716	OD str (NiO)
					2111	CD ₂ str
					1539	C=N str
					1456	HDO def
					1405	C=C str

^aThe bands listed correspond to the spectra obtained after evacuating the weakly adsorbed species.

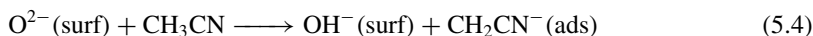
^bThe vibrational assignments are made by assuming the adsorbed species to possess the CH₂CN(CD₂CN) moiety: asym, asymmetric; sym, symmetric; str, stretch; def, deformation.

increased, the heat of adsorption decreased from $120\text{--}170\text{ kJ mol}^{-1}$ to $45\text{--}80\text{ kJ mol}^{-1}$, whereas it might be expected to remain constant for each type of cation. Moreover, the Fermi resonance can contribute to this phenomena. Thus, the νCN cannot be used as a probe for the estimation of the strength of aprotic centers.

Complexes with ion pairs

In such cases, acetonitrile is adsorbed on the oxide as a $[\text{CH}_2\text{CN}]^-$ surface species. Thus, on the nickel oxide surface, acetonitrile was adsorbed by forming a σ -bond via the nitrogen lone-pair electrons [1410]. By forming 'di- σ -bonds' with carbon and nitrogen atoms, the CC and CN bonds of the adsorbed species are thought to possess double-bond characters. Bands at 1560 and 1455 cm^{-1} have been assigned to the C=N and C=C stretching vibrations of adsorbed CH₂CN.

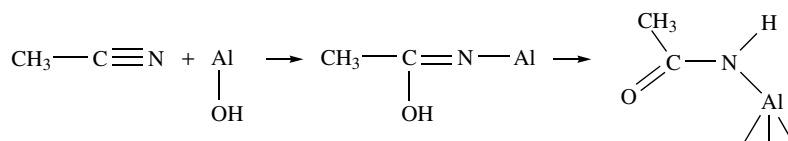
Hydrogen atoms of α -CH groups to the C=N bond, such as those of the methyl group of acetonitrile, present a proton donor character, in such a way that the formation of the CH₂CN⁻ carbanion can be observed from the rupture of a C–H bond. When the cation is Na⁺ or Li⁺, the $\nu\text{C}=\text{N}$ of the carbanion is near 2050 cm^{-1} [1426]. On metal oxides, the following reaction occurs:



The couple CH₃CN/CH₂CN⁻ and the acid–base character pair OH⁻/O²⁻ are involved in the reaction, but the participation of a cationic adsorption site is required to stabilize the CH₂CN⁻

carbanion. The $\nu\text{C}=\text{N}$ of the carbanion depends on the oxidation degree of the cation, for example, at 2098 cm^{-1} for Ce^{4+} but at 2026 cm^{-1} for Ce^{3+} [1427].

It should be noted that polymerization can also occur, leading in particular to the formation of the acetonitrile dimer monoanion [1428, 1429], so complicating the analysis of the spectrum. Moreover, acetonitrile can also react with surface hydroxy groups to give acetic acid and ammonia [1429]. On the surfaces of metal oxides like alumina, the reaction can be limited to the formation of the acetamide species [1430]:



Scheme 5.39

Such a reaction supposes a polarization of the $\text{C}=\text{N}$ bond by the Al^{3+} cations, before the nucleophilic attack of the OH^- groups. The presence of the acetamide monoanion species, CH_3CONH^- , has been considered in the case of MgO [1431], ZnO [1432] and Fe_2O_3 [1433]. However, its spectroscopic characterization was unclear in these papers. Aboulayt *et al.* [1434] have proposed such a characterization for ZrO_2 . These authors used *in situ* FTIR spectroscopy and proposed the presence of two acetamide monoanions (CH_3CONH^-), α and β , the formation of which has been associated with the main bands, respectively, at 1169, 1432, 1590 and 3320 cm^{-1} , and at 1196, 1471, 1557 and 3340 cm^{-1} . The use of ^{18}O - or D-labeled compounds gave poor results as far as the vibrational mode description was concerned, except for the δNH mode. However, the $\text{H} \rightarrow \text{D}$ substitution was very useful for determining the mechanisms. The authors proposed that the β -type acetamide species results from H_2O displacement from the surface and CH_3CN adsorption in Lewis acidic sites, followed by a hydroxylation of this latter species by H_2O re-adsorption. The formation of the α -type acetamide species was thought to be due to a direct interaction of acetonitrile with basic OH groups. At higher temperatures, the acetamide species were hydrolyzed into acetate species.

The interaction of other nitriles with oxide surfaces has also been investigated by means of IR spectroscopy and it has been proposed that the same types of species are formed. For example, it has been shown for adipodinitrile that the adsorption of this compound on a Ti-Sb-O catalyst at room temperature was accompanied by the appearance of all of the bands which are typical for the liquid nitrile [1435] with a shift of νCN (5 cm^{-1}) to low frequencies. Besides the hydrogen-bonded nitrile, a structure such as $\text{R}-\text{C}(\text{O})\text{N}$ was considered to be formed upon nitrile group oxidation by the oxide oxygen (the bands at 1570 and 1465 cm^{-1} for $\nu_{\text{as}}\text{CON}$ and $\nu_{\text{s}}\text{CON}$, respectively) and also a structure with a $\text{C}=\text{N}$ bond ($\nu\text{C}=\text{N}$, 1660 cm^{-1}) have been proposed.

Allylcyanide, crotononitrile and methacrylonitrile on a strongly basic (Na/NaY) surface produced anionic intermediates [1436, 1437], which were considered to be isomers of these unsaturated C_4 nitriles.

5.6.2 BENZONITRILE

In comparison with acetonitrile, benzonitrile is a better compound for investigating Lewis acidic centers because the intensities for νCN in the case of an aromatic nitrile are higher than those

for saturated nitriles, and there is no Fermi resonance in this case. An investigation of the spectra of benzonitrile adsorbed on numerous oxide catalysts allowed Paukshtis *et al.* [1420] to propose that it is possible to not only effectively identify the Lewis acid sites on the surface but also the nature of the coordinatively saturated cations. It has been shown that νCN is little changed upon variation of the anionic parts of the systems [1420]. Such variations from the oxide itself to silicate-, phosphate- and molybdate-containing systems, or even to zeolites, change the νCN by less than 10 cm^{-1} . On the basis of the correlation between νCN and the properties of the cation, the possibility of estimating the nature of the cation on the catalyst surface has been suggested. However, the changes of νCN obtained by these authors are too small. Moreover, the more accurate investigation made later did not confirm this [1438].

On the adsorption of benzonitrile on V–Sb–Bi–O supported on alumina it has been shown that both H-bonded (νCN , 2240 cm^{-1}) and coordinatively bonded (νCN , 2280 cm^{-1}) benzonitriles are formed [1303]. Surface conversion of the benzonitrile also takes place. Interpretation of the spectra observed supported the formation of the benzamide ions $\text{C}_6\text{H}_5\text{CONH}^-$ and $\text{C}_6\text{H}_5\text{CON}^{2-}$ ($\nu_{\text{as}}\text{CON}(\text{H})$, 1555 cm^{-1} ; $\nu_{\text{s}}\text{CON}(\text{H})$, 1430 cm^{-1}), and also a benzylimine structure ($\nu\text{C}=\text{N}=\text{}$, 1660 cm^{-1}) via electron transfer from the surface to benzonitrile. The formation of a benzylimine structure from benzonitrile was also proposed in the interaction of benzonitrile with the protic acid centers of zeolites.

5.7 Complexation of alcohols

5.7.1 SATURATED ALCOHOLS

Many studies of alcohol conversions (dehydrogenation, dehydration and oxidative dehydrogenation) have been carried out which involve the use of IR spectroscopy, and many very important questions, for example, about the mechanisms of alcohols transformations, have been decided by means of spectroscopic methods.

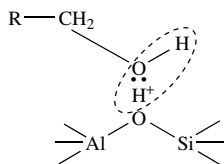
It is clear that in an alcohol molecule the COH fragment has a weakly basic OH group so that the lone electron pair on the oxygen atom is an active center for the interaction of saturated alcohols with acid–base centers of the oxide surface. The presence of different reactive centers in these molecules causes the alcohol molecule to bind with several surface centers simultaneously. Surface alcoholates and both coordinatively and H-bonded compounds are formed. Such forms can be produced by different mechanisms involving the participation of surface centers of all types.

Zeolites

It is clear that carbenium-ion mechanisms [454] play the main role in alcohols transformations on the H-forms of zeolites. These mechanisms form the basis of new and simple processes for the conversion of methanol and other oxygen-containing compounds to hydrocarbons. For this, an initial interaction between the weakly basic hydroxyl group of the alcohol with an acid hydroxyl group of the zeolite is very important. It should be noted that the spectra of alcohols after the formation of H-bonds are closely similar to those for free molecules, except in the region of νOH .

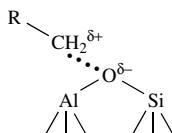
There are different viewpoints [1439, 1440] concerning the initial complexation of alcohol molecules with acidic hydroxyl groups:

(i) the formation of an **hydroxonium** ion:



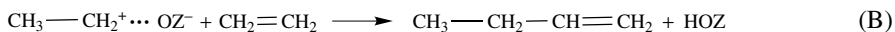
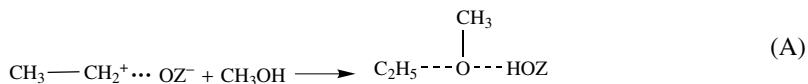
Scheme 5.40

(ii) the formation of an ionically bound **alkoxy**:

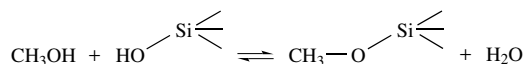


Scheme 5.41

However, in any case these compounds differ significantly from covalent-bound alkoxy groups (for example, by a lower bonding strength) formed on the interaction of alcohols with oxides. The ionic alkoxy easily interacts with other alcohol molecules which are formed and transforms to the alkene at 473–573 K. The number of schemes of ethene transformation to oligomers with the participation of Brønsted acid sites have already been demonstrated in the case of olefins (Section 5.1). The carbenium ion formed due to alcohols interaction with protic sites can react in two major ways [1440], one to form higher ethers (process A) by reaction with methanol, and the second to yield linear polyolefins by the addition of another ethene (or olefin) molecule (process B):



The IR spectra of hydroxyl groups characterizing both HY and HZSM-5 types of zeolites before the interaction with methanol, as well as those of the methyl groups which remain on the zeolites after methanol desorption at temperatures up to 473 K, have been reported [1441, 1442] and are depicted in Figure 5.40. The spectra indicate the presence of (i) skeletal methoxy groups, $\text{CH}_3\text{---O}_{\text{zeol}}$, formed by the interaction of methanol with skeletal hydroxyls according to the following scheme:



Scheme 5.42

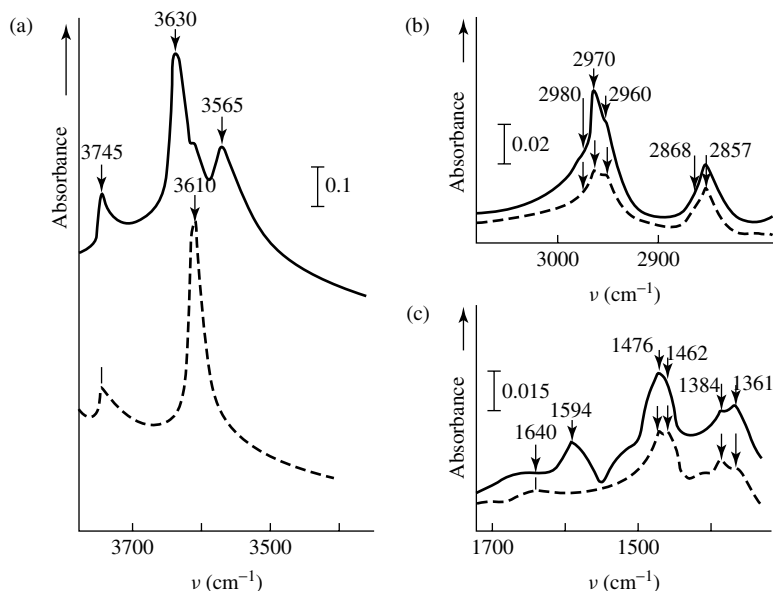
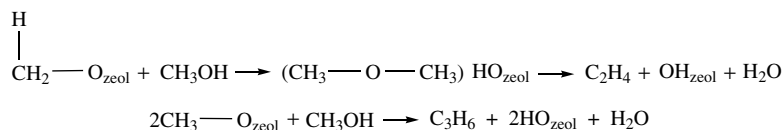


Figure 5.40. IR spectra of (—) dealuminated H and (- - -) HZSM-5 Zeolites: (a) OH groups before methanol adsorption; (b) methoxy groups after methanol desorption up to 473 K; (c) methoxy groups, formates and carbonates after methanol desorption up to 573 K. In (b) and (c), 4 mmol g⁻¹ of methanol have been pre-adsorbed [1441]. Reprinted from Novakova, J. and Kubelkova, L. and Dolejssek, J., *J. Catal.*, **108**, 208–215 (1987). Reprinted with permission from Academic Press.

(ii) methoxyls bonded to the Al electron-accepting sites, CH₃O–Al, and (iii) CH₃O–Si methoxyls formed by the reaction of methanol with silanol groups (band at 3745 cm⁻¹). With some remaining physisorbed methanol. The characteristic bands of these three compounds are at 2980, 2970 and 2960 cm⁻¹, respectively [1442]. Their thermal stabilities increase according to the sequence: CH₃OH < CH₃O–Al < CH₃–O_{zeol} = CH₃–O–Si. The decomposition of CH₃–O_{zeol} leads to the re-formation of framework hydroxyls.

After desorption above 473 K, bands at 1365–1386, 1460–1490, near 1590, and at 1650 cm⁻¹ are clearly visible in the spectrum. The bands at 1460–1490 cm⁻¹ can be assigned to the deformation vibrations of methyl groups, whereas the other bands, in these authors' opinion, are connected with the formation of formates and carbonate-like species, which are very stable and are observable even after evacuation at 673 K. Their amounts are far higher on HY than on HZSM-5 zeolites. The experiments carried out supported the assumption that gaseous methanol participates in the formation of primary C–C bonds:



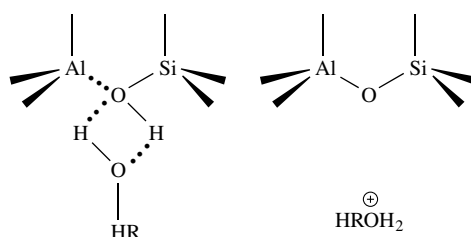
Scheme 5.43

Similar reactions can be written for the interaction of methoxyls with dimethyl ether, whose conversion over zeolites yields the same products as that of methanol, although it is also impossible to exclude the fact that these reactions may proceed with dimethyl ether which was previously formed from methanol. The reaction of dimethyl ether with methoxyls to yield propene was postulated by Ceckiewicz [1443], and the reaction of methanol or dimethyl ether with carbenium ions formed from methoxyls was also assumed to occur [1444]. In addition, these authors reported the spectral features of alcohols adsorbed on HZSM-5 zeolites. On the basis of a complex infrared examination of the adsorption of methanol, ethanol, 1-propanol, 1-butanol, 2-propanol and 2-methyl-2-propanol on HZSM zeolites, Ono and Mori [1444] made the following conclusions:

- (1) All ROH/HZSM-5 adsorption complexes are formed from metastable states and have stoichiometries of one alcohol per aluminum in the zeolite framework.
- (2) The IR spectroscopy of this 1:1 complex for methyl, ethyl, 1-propyl and 2-propyl alcohols is characterized by the appearance of C–H(D) stretching and bending modes at frequencies similar to those of the free alcohols, while the bands associated with the hydroxyl functionalities are significantly different from those of the gas-phase molecules. These species appear due to interactions of the alcohol hydroxy groups with the acidic zeolite hydroxy groups, as shown by the disappearance of the sharp ZOH(D) stretch at 3600–3650 cm^{-1} .
- (3) For 2-methyl-2-propanol chemisorbed at 295 K, both of the C–H(D) and O–H(D) frequencies in the complex are significantly different from those of the free alcohol. The observed spectrum is in reasonable agreement with an assignment for the *t*-butyl carbenium ion in $\text{FSO}_3\text{H}-\text{SbF}_3-\text{SO}_2$ solution [1445].

IR and UV–Vis data about this interaction of CH_3OH with H-ZSM zeolites at 500 K are shown in Figure 5.2. They are practically identical to those of propene adsorbed on the same zeolites, indicating the formation of carbenium ions and thus, confirming Scheme 5.43. These spectra also confirm the carboionic mechanism of alcohol transformations over zeolites.

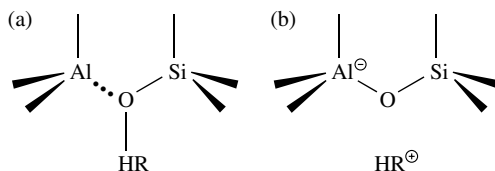
There are no doubts that the initial complex of alcohols with acidic hydroxy groups is the most interesting. In the case of oxonium ions, the data obtained demonstrated that the adsorbed alcohol molecule is ‘intact’. The C–H modes are relatively unperturbed, but the OH functionalities of the alcohol and zeolite interact strongly. One might consider two limiting descriptions of the hydroxyl interaction (Scheme 5.44). At one extreme, the alcohol molecule is hydrogen-bonded to the framework but the proton remains associated primarily with the zeolite. At the other extreme, the proton is fully transferred and the structure is best described as an ion pair. In effect, this question involves the description of the potential surface for proton transfer between two conjugate bases, i.e. ZO^- and $[\text{ROH}_2]^+$.



Scheme 5.44

The chemisorption energies for these alcohols on HZSM-5 lie in the range 63–126 kJ mol^{-1} . If the bulk of this energy is associated with hydroxy-group interactions, then the ion-pair structure

should probably be preferred. Two limiting structures have been suggested for the dehydrated complex:

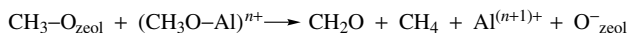


Scheme 5.45

In structure (a), the zeolite framework is acting like a nucleophilic medium and interacting with the adsorbed cation via specific bond formation, whereas in structure (b) the zeolite is 'non-nucleophilic' and is interacting nonspecifically. The relative stabilities of these structures are likely to be a function of R. The H/D exchange results obtained by Aronson *et al.* [1445] show that olefins are accessible from the carbenium-ion-like intermediates at low temperatures in the presence of additional H₂O. Based on the absence of AlOH and olefinic features in the IR spectra, the authors have argued that these olefins are not mobilized until desorption temperatures are reached.

Support for the formation of carbenium ions in the case of interactions between alcohols and zeolites comes from the IR data which have revealed the presence of a $\sim 1500\text{ cm}^{-1}$ band which characterizes a loosening C=C bond in a carbocation structure, as was established for the interactions between alcohols and zeolites (see Section 5.1, Figure 5.2).

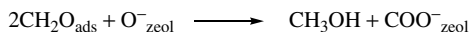
It was noted [1442] that if no gaseous methanol is present over HZSM-5, the methoxyls in this reaction quite probably formed methane and formaldehyde via disproportionation:



Scheme 5.46

Participation of the CH₃O-Al methoxyls in this reaction seems quite probable, since the incorporation of zeolitic oxygen into the product could hardly occur at 573 K. Moreover, the above reaction of methanol to methane and formaldehyde is known to take place over alumina.

Kubelkova *et al.* [1442] assumed that this reaction (Scheme 5.45) also takes place on HY zeolites, in this case, however, without the release of formaldehyde. This may be due to a 'Cannizzaro-like' type of reaction:

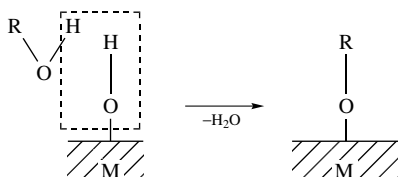


Scheme 5.47

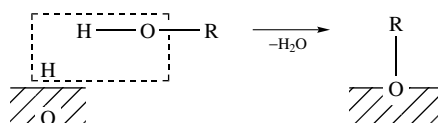
Such a reaction would yield the methanol needed for the formation of olefins and also surface formates or carbonate-like species.

Oxides

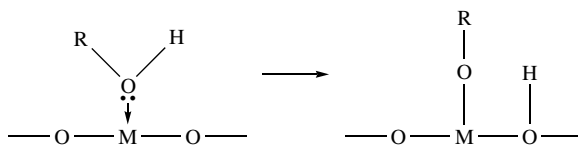
In the interaction of alcohols with oxides the main process is the formation of surface alkoxides. Such surface alcoholates can form according to the different mechanisms involving the participation of either basic hydroxyl groups [30]:

**Scheme 5.48**

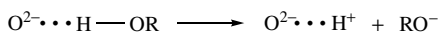
acidic hydroxyl groups:

**Scheme 5.49**

coordinatively unsaturated surface cations:

**Scheme 5.50**

coordinatively unsaturated surface anions O^{2-}

**Scheme 5.51**

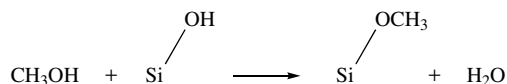
or double and triple combinations of these centers.

Surface alcoholates can be readily identified by comparison of their spectra with those of individual metal alcoholates (e.g. $\nu C-O$, which increases in comparison with $\nu C-O$ for alcohols in the gas phase). These alcoholates are the stable surface compounds.

Alcohols were one of the first classes of molecules for which adsorption on an oxide surface was investigated by means of infrared spectroscopy [18, 19, 30, 1446–1450]. Many studies have since been carried out in this area (see, for example, [1451–1485]), and it is impossible to

consider all of these papers here. We will mention only those studies which give rise to the formation of the main types of complexes on oxides with different surface properties.

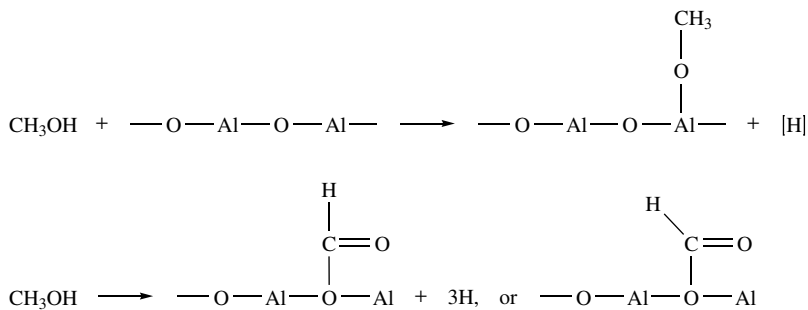
The reaction between methanol vapor and surface hydroxyl groups on porous silica glass was studied using infrared spectroscopy by Sidorov [1446]. It was found that besides formation of H-bonded alcohols, which are observed at significant coverages of the surface, the surface hydroxyl groups on silica can be replaced by alcoholates. For example, in the case of methanol the formation of methoxyl groups proceeds by the following reaction:



Scheme 5.52

The spectra showed a partial disappearance of the hydroxyl stretching band at 3750 cm^{-1} , and a corresponding growth in the methyl CH asymmetric and symmetric stretching vibrational bands in the region $2970\text{--}2850\text{ cm}^{-1}$. Reactions between adsorbed molecules and surface hydroxyl groups lead to drastic changes in the adsorption characteristics of the surface and were already discussed in some detail in earlier monographs [18, 19].

Greenler [1447] found that methanol (or ethanol) were adsorbed on the surface of alumina in the following manner:



Scheme 5.53

The spectrum of methanol adsorbed on Al_2O_3 at temperatures above 473 K gives absorption bands at 1597 and 1377 cm^{-1} , which belong to the ν_{as} and ν_{s} bands, respectively, in surface formates.

On the surface of Al_2O_3 , three types of alkoxy groups were formed ($\nu\text{C--O}$ of the methoxy groups at 1030 , 1100 and 1190 cm^{-1} , and $\nu\text{C--O}$ for ethoxy groups at 1080 , 1130 and 1170 cm^{-1}). To explore the mechanism of formation of these different surface groups, the spectra of surface compounds formed by the interaction of ethanol with an alumina surface preliminary exchanged with H_2^{18}O were studied [1282, 1450]. The spectra of the surface compounds had this time two absorption bands at 1120 and 1080 cm^{-1} . The results were interpreted as a proof of the formation of surface alkoxy groups by esterification of the surface hydroxyl groups of alumina with the participation of hydroxyl groups of the alcohols to give H_2^{16}O . The absorption bands at 1080 and 1120 cm^{-1} were attributed to the stretching vibrations of the C--O bonds in two different surface ethoxy groups, combined with surface aluminum atoms in octahedral and tetrahedral

coordinations. In a number of studies, it has been supposed that coordinatively bound alcohol is also formed on Al_2O_3 surfaces however, there has been no direct proofs of this. The $\nu\text{C}-\text{O}$ vibrational mode, which is the most characteristic for such a type of compound, should show a decrease relative to $\nu\text{C}-\text{O}$ for alcohols in the gas phase [30]. This absorption is difficult to identify owing to the superposition of the band ascribed to vibrations of the bulk adsorbent. As will be shown below, such identification has been later made for methanol adsorbed on Al_2O_3 by means of the δCOH vibration [1456].

The formation of this type of compound has been established on the basis of adsorption of methanol [1461] and ethanol [1472] on TiO_2 through the displacement of CO molecules by methanol from coordinatively unsaturated Ti^{4+} ions. As a rule, alcohol molecules bound to the surface via coordination have similar spectra to those bound via hydrogen-bonds. Another way to form surface alkoxy groups on TiO_2 is through interactions with two different types of hydroxyl groups. The spectral characteristics of methanol adsorbed on TiO_2 are presented in Table 5.29.

Isopropoxy species characterized by absorption bands at 2975, 2935, 2920, 2900 and 2870 cm^{-1} (νCH), 1468 and 1455 cm^{-1} ($\delta_{\text{as}}\text{CH}_3$), 1385 and 1370 cm^{-1} ($\nu_s\text{CH}_3$), 1330 cm^{-1} (βCH out-of-plane bending), 1168, 1140 and 1125 cm^{-1} (coupled $\nu\text{C}-\text{C}$, $\nu\text{C}-\text{O}$ and CH_3 rocking), and undissociatively adsorbed isopropyl alcohol, characterized by a typical δOH band near 1290 cm^{-1} , have been observed on TiO_2 [1477]. At a temperature of 423 K, the isopropyl compounds transformed to the product, i.e. adsorbed acetone (1680, 1420 and 1450 cm^{-1}).

Coordinatively bound alcohols could not be observed for adsorption of the alcohols C_1-C_3 on Cr_2O_3 . That may be connected with their fast transformation to surface alkoxides by heterolytic dissociation, with the participation of surface O^{2-} ions [1453]. The formation of surface alkoxides characterized, for example, for methanol, with $\nu\text{C}-\text{O}$ at 1090 cm^{-1} , $\delta\text{C}-\text{H}$ at 1470 cm^{-1} , and νCH at 2840–2940 cm^{-1} , together with alcohol H-bonded to surface oxygens through the alcohol hydroxyl group ($\nu\text{C}-\text{O}$ at 1045 cm^{-1} , and νOH at 3250 and 3450 cm^{-1}), has been shown after the adsorption of methanol on Cr_2O_3 [1453]. Most probably, the majority of the alkoxides are formed with the participation of the ion pairs $\text{Cr}^{3+}\text{O}^{2-}$, although on Cr_2O_3 it has been shown that the formation of methoxyls is possible only with the participation of the O^{2-} anions. The latter has been revealed by displacement of the strong electron donor, ammonia (which is stronger than alcohols), from the chromium ions on the subsequent adsorption of methanol on Cr_2O_3 . Such displacement reactions are accompanied by the production of alcoholates, which can occur only as a result of the formation of a stronger than ammonia electron donor, for example, RO^- (Scheme 5.51). Such a strong electron donor can be formed only as a result of the heterolytic dissociation of alcohols on the surface O^{2-} centers. The virtual absence of water ($\delta\text{H}_2\text{O}$ at 1620 cm^{-1}) upon the reaction of alcohols with Cr_2O_3 at room temperature allowed the authors [1453] to exclude the possibility of the formation of alkoxy species in large concentrations as a result of the dehydration reactions of the alcohols with surface hydroxyl groups. The spectral characteristics of the surface compound of methanol adsorbed on Cr_2O_3 are presented in Table 5.29. A comparison adsorption study for the C_1-C_3 alcohols showed that the strength of the $\text{O}-\text{Cr}$ bond in the surface alcoholates increases in the following sequence: $\text{iso-C}_3\text{H}_7\text{OH} \geq \text{C}_2\text{H}_5\text{OH} > \text{CH}_3\text{OH}$. The νCO of the alcoholates has been attributed to the increasing strength of the CO bond in the alcoholate series, thus leading to a corresponding weakening of the bond with the surface.

It should be noted that in the case of Cr_2O_3 , as well as for the majority of the other oxides, the CH_3 group of the surface alcoholates forms a $\text{O}_s \cdots \text{H}-\text{CH}_2-\text{OM}$ bond with a surface oxygen of the catalyst. This has been established by direct observation of perturbed OH groups (νOH at 3200–3400 cm^{-1}) in the case when only methoxy groups were present on the surface. Recently, by means of the DRIFT method it has been shown that a weak absorption band at about 2800 cm^{-1} , which characterizes the νCH in $\text{MO}-\text{H}_2\text{C} \cdots \text{H} \cdots \text{O}_s^{2-}$ (νCH at about 2800 cm^{-1} ,

Table 5.29. Spectral and energy characteristics of adsorbed forms of methanol on various transition-metal oxides and the compositions of the corresponding desorption products.

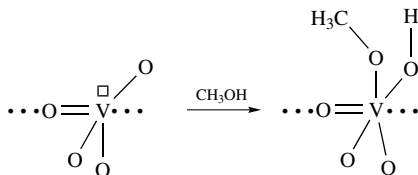
Oxide	Form of adsorption	Infrared absorption bands (cm ⁻¹)	Decomposition temperature (°C)	E_{des} (kJ mol ⁻¹)	Products
TiO ₂	(1) Coordinated methanol	3550 (ν_{OH}) ^a 1160 (ν_{OCH})	150	40 ± 4	CH ₃ OH, CH ₂ O
		$\begin{array}{c} \text{H}_2\text{C} - \text{OH} \\ \quad \quad \quad \downarrow \\ \text{H} \quad \quad \quad \text{O}^{\delta-} \quad \text{M}^{\delta+} \end{array}$			
	(2) Methoxy	2950 (ν_{asCH_3}) ^a 1050 ($\nu_{\text{C-O}}$) ^a	250	100 ± 15	CH ₂ O
	(3) Methoxy	1140 ($\nu_{\text{C-O}}$) ^a	350	160 ± 20	CO, CO ₂ , H ₂ O
	$\begin{array}{c} \text{M} \\ \diagdown \quad \diagup \\ \quad \text{O} - \text{CH}_3 \\ \diagup \quad \diagdown \\ \text{M} \end{array}$				
	(4) Formate	1560 (ν_{asCOO}) 1390–1370 ($\nu_{\text{sCOO}+\delta_{\text{CH}}}$)	350	160 ± 20	CO, CO ₂ , H ₂ O
MoO ₃	(1) Methanol bound via H-bond or coordination	1030 ($\nu_{\text{C-O}}$) ^a	150	42 ± 2	CH ₃ OH, CH ₂ O
	(2) Methoxy	1050 ($\nu_{\text{C-O}}$) ^a	250	117 ± 8	CH ₂ O, H ₂ O
	(3) Structure of aldehyde type	1670 ($\nu_{\text{C-O}}$) 1700	–	–	CH ₂ O
Fe ₂ O ₃	(1) Methanol bound via H-bond or coordination	3550 (ν_{OH})	100	32 ± 2	CH ₃ OH, CH ₂ O (trace)
	(2) Methoxy	1090 ($\nu_{\text{C-O}}$) ^a	250	–	CO, CO ₂ , CH ₄ (trace)
	(3) Formate	1580 (ν_{asCOO}) 1390–1370 (ν_{sCOO})	300	150 ± 10	CO, CO ₂ , CH ₄
Cr ₂ O ₃	(1) Methanol bound via H bond or coordination	3550 (ν_{OH}) ^a	150	40 ± 4	CH ₃ OH, CH ₂ O (trace)
	(2) Methoxy	1090 ($\nu_{\text{C-O}}$) ^a	200–250	112 ± 10	CO, CO ₂ , CH ₄ (trace)
	(3) Formate	1570 (ν_{asCOO}) 1390–1370 (ν_{sCOO})	350	160 ± 20	CO ₂ , H ₂ O

^aAbsorption bands at 2950(ν_{asCH_3}), 2840–2850 (ν_{sCH_3}), 1470 and 1450 cm⁻¹(δ_{CH_3}), which are characteristic of each of the given structural types, are also visible in the spectra. However, any assignment to separate compounds is impossible.

and νOH at $3200\text{--}2400\text{ cm}^{-1}$ in the case of methanol), is also observed in the spectra of surface alkoxy species.

For binary oxide systems such as Sn–Mo–O [1451], Fe_2MoO_4 and $\text{Fe}_2\text{MoO}_4 \cdot \text{MoO}_3$ [1470], Cr_2MoO_4 [1462, 1482], $\text{MoO}_3/\text{Al}_2\text{O}_3$ [221], MoO_3 [1463, 1464] and V–Sn–O [1483], the surfaces of which are characterized by the presence of the transition-metal cations in the highest oxidation state, together with Brønsted acid sites, the formation of the surface alkoxy groups occurs by the participation of protic acid centers by way of etherification. This has been shown by the adsorption of isopropanol on Sn–Mo–O catalysts poisoned by NaOH [1451], in the case of which, besides H-bonded alcohol (νCO at 1100 cm^{-1}), the formation of coordinatively bound (νCO at 1130 cm^{-1} , βOCH_3 at 1165 cm^{-1} , δCOH at 1290 cm^{-1} , δCH_3 at 1385 and 1465 cm^{-1} and νCH_3 at 2885 , 2940 and 2980 cm^{-1}) isopropyl alcohol has been observed. When isopropanol was adsorbed on unpoisoned oxide catalysts, the formation of H-bonded (νCO at 1100 cm^{-1} and δCOH at 1290 cm^{-1}) alcohol, isopropylate species (νCO at 1105 cm^{-1} , βOCH at 1165 cm^{-1} , δCOH at 1335 cm^{-1} , δCH at 1385 and 1465 cm^{-1} , and νCH at 2950 and 2990 cm^{-1}) and water ($\delta\text{H}_2\text{O}$ at 1620 cm^{-1}) was observed. The latter appears due to the alcohol dehydration. This was not observed for the catalyst poisoned by NaOH. Such an alcoholate structure is transformed to acetone (νCO at 1665 cm^{-1} , and $\nu\text{C-C}$ at 1250 cm^{-1}) at room temperature, unlike coordinatively bound alcohol on the poisoned catalyst. By the same mechanism, these highly selective catalysts cause the partial conversion of methanol to formaldehyde [1462, 1470].

In contrast to this, for pure V_2O_5 , $\text{V}_2\text{O}_5/\text{SiO}_2$ [1467] and $\text{V}_2\text{O}_5/\text{TiO}_2$ [1478], which, as already mentioned above, also have surface protic acid centers, the Rossi *et al.* [1477] have proposed that the methoxy species are formed by the participation of coordinatively unsaturated vanadium ions:



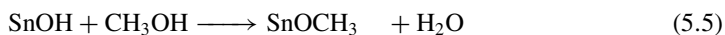
Scheme 5.54

However, these authors provide no direct proof for this mechanism [1477]. The problem of the participation of proton centers in the formation of alkoxy groups is very important because the presence of the surface protic centers was observed for all highly selective catalysts for methanol conversion to formaldehyde.

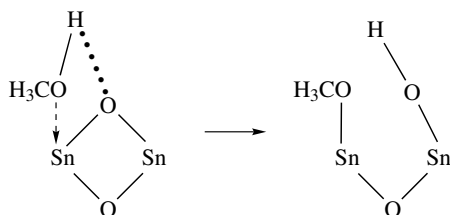
The formation of alkoxy species (νCO at 1070 cm^{-1} in the case of adsorption of methanol) was easily observed on the interaction of alcohols with CuO [30, 1469, 1473, 1474, 1475]. Only a small amount of H-bonded alcohol is observed on this oxide surface. Coordinated alcohol was not observed on the surface of CuO, probably due to its complete dissociation, with the formation of alkoxy species that blocked the surface cations. The formation of alkoxy species via the mechanism of the interaction with ion pairs is preferable in the case of interaction of alcohols with ZnO [1468, 1479] or with basic sites in the case of MgO [1480].

The two most likely mechanisms of the formation of methoxy groups from methanol on SnO_2 are [1483]:

(i) esterification



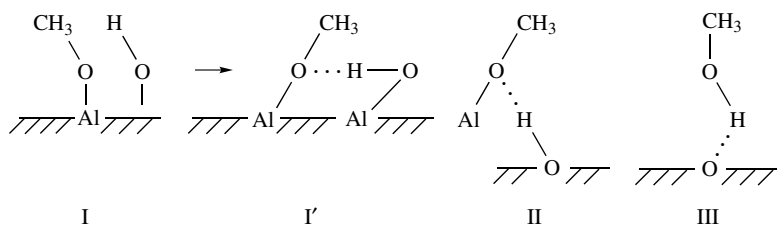
(ii) dissociation on the ion pairs



Scheme 5.55

Except for the species mentioned above, on the surface of all oxides the transformation of alkoxy groups to carboxylate species via nucleophilic attack of the surface oxygen is observed. In the case of isopropoxide species, the transformation of alkoxy groups to formate and acetate groups occurs through the formation of enolate species [1473, 1474]. The spectral characteristics for such carboxylate, formate and acetate species are clear and the same as those obtained on the adsorption of the corresponding acids and aldehydes (see Sections 5.8 and 5.9).

The forms of the molecular adsorption of methanol, which are very important for the following transformations, have been studied in detail recently on alumina, by Busca *et al.* [1456]. This work showed that at very low coverages the alcohols coordinate the strongest Lewis acid sites and easily transform into bridged methoxide species. With increasing coverage, another form, irreversibly adsorbed at room temperature but desorbed by evacuation at 373–473 K, becomes predominant. These authors identified this as undissociated methanol, strongly hydrogen-bonded on a cation–anion couple with a strong basic character. Finally, at high coverages, a reversible form of hydrogen-bonding to basic sites was detected. The spectral manifestations of the molecular surface compounds which form upon the adsorption of methanol are presented in Table 5.30. The identification of such species is made difficult due to the partial superpositions of their ranges of existence. For instance, the reversibly adsorbed species III is detected before the saturation of both species I and II. The spectrum of structure III also shows that it is characteristic of a nondissociative adsorption form of methanol. The high frequency of the δOH mode and the low frequency of νOH (Table 5.30) both indicate the formation of a relatively strong hydrogen-bond in which the OH in CH_3OH act as a proton donor. The following structures have been proposed for such compounds:



Scheme 5.56

A similar compound to species (III) has already been proposed for the high-coverage adsorbed species of methanol on TiO_2 [1461] and Fe_2O_3 [1481, 1485], as well as for reversibly adsorbed

Table 5.30. Infrared absorption characteristics (ν cm^{-1}) and assignments for free and adsorbed CH_3OH and CD_3OH [1456]. Reprinted with permission from Busca, G., Rossi, P. F., Lorenzelli, V., Banaissa, M., Travert, J. and Lavalley, J.-C., *J. Phys. Chem.*, **89**, 5433–5439 (1985). Copyright (1985) American Chemical Society.

Assignment	CH_3OH monomer, CCl_4 solution	Adsorbed on $\delta\text{-Al}_2\text{O}_3$				Assignment	CD_3OH monomer, CCl_4 solution	Adsorbed on $\delta\text{-Al}_2\text{O}_3$			
		I	I'	II	III			I	I'	II	III
$\nu(\text{OH})$	3645	3150	–	3150	3200	$\nu(\text{OH})$	3645	{ 3180 ^a	–	{ 3180 ^a	{ 3200 ^a
$\nu_{\text{as}}(\text{CH}_3)(\text{a}')$	2977	– ^b	2970	– ^b	2980	$2\delta(\text{OH})$	2565	{ 2780 ^a	–	{ 2780 ^a	{ 2780 ^a
$\nu_{\text{s}}(\text{CH}_3)^{\text{a}}$	{ 2938	2960	2955	2944	2940	$\nu_{\text{as}}(\text{CD}_3)(\text{a}')$	2230	2240	2225	2200	2230
	{ 2830	2850	2844	2825	2825	$\nu_{\text{s}}(\text{CD}_3)(\text{a}'')$	2210				2210
$\delta_{\text{as}}(\text{CH}_3)(\text{a}', \text{a}'')$	1460	– ^b	1472	– ^b	1465	Combination	2134	2140	2140	2140	2135
$\delta_{\text{s}}(\text{CH}_3)$	1440	– ^b	1458	– ^b	1445	$\nu_{\text{s}}(\text{CD}_3)$	2070	2090	2080	2060	2072
$\delta(\text{OH})$	1330	1420	–	{ 1480	1440	$\delta(\text{OH})$	1293	1420	–	1420	1425
				{ 1430							
$r(\text{CH}_3)$	1068	1190	1200	~1200	1090	$\delta_{\text{s}}(\text{CD}_3)$	1119	1110	1125	1130	1120
$\nu(\text{CO})$	1029	– ^b	1095	~1095	1035	$\delta_{\text{as}}(\text{CD}_3)$	1064	– ^b	– ^b	– ^b	1060
						$\nu(\text{CO})$	978	– ^b	~1060	1060	(980)

^aThese bands are perturbed by Fermi resonances, so their description is approximate.

^bNot observed.

halogenated alcohols on TiO_2 [1477]. Compound (II) is irreversibly adsorbed and desorbed at 373–473 K. The typical spectral manifestations for such compounds are (i) the broad band characteristic of δOH , (ii) the relatively low values of νCH , and (iii) the relatively high values of $\nu\text{C-O}$ (Table 5.30). Structure (II), as spectral data have shown, is nondissociated and more strongly bound to the surface (heat of adsorption is 110–100 kJ mol^{-1}) than structure (III) (heat of adsorption is 70 kJ mol^{-1}). The most stable surface species resists evacuation at 473 K and is characterized by a breaking of the CO-H bond, as deduced from the absence of the δOH vibrational mode. This species corresponds well to that already identified by Greenler [1447] as a methoxy group. High values for νCH and νCD suggest a relatively weak interaction of the CH bonds with the oxygen lone-pairs of the methoxides (and not the surfaces). This has been explained by considering a strong coordination bond between the methoxy groups and more than one Lewis acid site, hence leading to a bridging methoxyl (structure I).

Thus, the formation of alkoxy groups occurs through coordinatively bound alcohol or by etherification of the surface hydroxy groups. In accordance with this, alkoxy groups having different numbers of cations in the oxygen coordination sphere are formed on the surface (Table 5.29).

On the interaction of methanol with Fe_2O_3 , besides H-bonded methanol ($\nu\text{OH}\cdots\text{O}$; 3400 cm^{-1} , $\delta\text{OH}\cdots\text{O}$, 1420 cm^{-1} –) a complete methoxylation of the surface has been revealed [1481, 1485]. Methoxy groups are formed via the interaction of methanol with oxide OH groups [30, 1481]. Similar ethoxy or isopropoxy groups have been detected after the contact of hematite with ethanol or isopropanol [1481–1485]. The authors suggested the presence of free molecules of methanol on the surface under the same conditions as has been identified through the bands at 3690 and 1350 cm^{-1} (vapor phase of methanol, νOH at 3687 cm^{-1} , and δOH at 1346 cm^{-1}). If the methoxylated surface was heated at 323 K in helium, new species appeared, absorbing at 2880, 1555, 1370 and 1340 cm^{-1} , from surface formates.

5.7.2 PHENOL

Infrared spectroscopic manifestations of phenols adsorbed on oxide surfaces, especially on SiO_2 , TiO_2 and Al_2O_3 , were investigated in some of the early studies [18, 19]. In addition, the influence

of the nature of the oxide surface centers on the character of the adsorption of phenols has been investigated by IR spectroscopy and the spectral characteristics of the various forms of the adsorbed phenol have been established [1465] (Table 5.31).

As for simple alcohols, the adsorption of phenol is accompanied by the formation of H-bonds between the molecules of phenol and the oxide surface. Upon the adsorption of phenol on γ - Al_2O_3 [1465] two types of phenolate structures (νCO at 1285 and 1256 cm^{-1}), strongly bound to the surface, are formed. It seems that these are formed with the participation of Lewis acid centers. In fact, as was confirmed later, the adsorption of phenol on γ - Al_2O_3 leads to the appearance in the spectrum of several absorption bands (1495, 1595, 3045 and 3075 cm^{-1}) which characterize a strongly adsorbed species of phenol with the preservation of the phenol ring which is retained up to 723 K. Comparison of the spectrum observed with that for sodium phenolate (see Table 5.31) leads to the conclusion that the adsorption of phenol proceeds with the formation of surface phenolates. This is indicated by both the absence in the spectra of the intense absorption band at 1360–1370 cm^{-1} , belonging to δCOH , and the shift of the νCO frequency from 1235 cm^{-1} , usually characteristic of phenolates, to 1245–1295 cm^{-1} . These data show that the Lewis acid sites are the adsorption centers of phenol in this case. In fact, during the adsorption of phenol the surface hydroxyl groups are little perturbed; during esterification, they disappear almost completely. It is clear that phenol does not react as a base with the surface hydroxyl groups of Al_2O_3 . The observed perturbation of the surface hydroxyl groups occurs due to their interactions with the phenolates formed upon adsorption. The authors explained the observation of two absorption bands in the νCO region from the surface phenolates by the presence of two types of phenolate structures formed with the participation of two types of Al^{3+} ions. On the surface of the oxide sample treated by NaOH, on which one type of Lewis acid site was blocked, only one type of phenolate was formed and the surface hydroxyl groups did not react with the phenolate [1465].

In the case of completely dehydroxylated zinc oxide, as well as for γ - Al_2O_3 , two types of surface phenolates (νCO at 1260 and 1290 cm^{-1} , respectively) were observed. These are formed by the interaction of phenol with coordinatively unsaturated zinc cations, as has been established by CO adsorption.

Magnesium oxide, on the surface of which there are basic hydroxyl groups (3750 cm^{-1}), interacts with phenol to produce phenolates (νCO at 1300 cm^{-1}), formed due to the dissociation of phenol at the OH bond. The surface hydroxyl groups participate in the interaction through the formation of hydrogen-bonds with surface phenolates [1465].

The surface of Sb_6O_{13} is characterized by both the absence of Lewis acid sites and the presence of nucleophilic oxygen and acidic hydroxyl groups [244]. The formation of surface phenolates was not observed on this oxide, and the spectrum of adsorbed phenol is similar to that of liquid phenol. The presence of the intense δCO band at 1220 cm^{-1} , the position of which is practically the same as in the spectrum of free phenol, along with the presence of νOH at 3430 cm^{-1} and δCOH at 1350 cm^{-1} , indicate that phenol is nondissociatively adsorbed on Sb_6O_{13} as a hydrogen-bonded molecule [1465]. The formation of only one adsorbed species of phenol indicates that this surface is unable to adsorb phenol dissociatively and shows that the presence of Lewis acid centers is necessary for adsorption to occur.

On most oxides, phenolates are already formed at room temperature. With an increase in temperature, the phenolates are oxidized destructively by weakly bound reactive oxygens to form carboxylates, characterized by new absorption bands at 1440 and 1560 cm^{-1} ($\nu_s \text{COO}^-$ and $\nu_{as} \text{COO}^-$, respectively) of the acetate (Table 5.31).

Surface phenolate is the predominant form of adsorption of phenol on a reduced surface of Cr_2O_3 . Practically all of the absorption bands characteristic of the free molecules of phenol,

Table 5.31. Absorption frequencies (cm^{-1}) of phenol, sodium phenolate and phenol absorbed on oxides in the 1100–3500 cm^{-1} region and their assignments.

Solid phenol	Sodium phenolate	Assignment	SiO ₂ : H-bound phenol	Al ₂ O ₃ : aluminum phenolates	CuO: copper phenolate, carboxylate	Cr ₂ O ₃ : chromium phenolate, carboxylate	Sb ₆ O ₁₃ : H-bound phenol	MgO: magnesium phenolate
1150	1155	δ_{CCH}	Not observed	—	—	—	—	—
1170	1170	δ_{CCH}	because of superposition on the SiO ₂ absorption	1165	1170	1170	1170	1170
1235	1305	ν_{CO}		1245, 1295	1265	1260	1220	1305
1370	—	δ_{COH}		—	—	—	1350	—
1500	1485	ν_{sCC}		1495	1496	1490	1485	1490
3080	3080	ν_{CH}		3045, 3075	(1440, ν_{s} in RCOO ⁻)	(1440, ν_{s} in RCOO ⁻)	3075	3075, 3045
1600	1595	ν_{asCC}		1595	1590	1595	1590	1590
3235	—	ν_{OH}	3450–3200	3400–3600	—	(1560, ν_{as} in RCOO ⁻)	3200–3450	3400–3650

except the band at 1360 cm^{-1} (δCOH), are observed in the IR spectrum of phenol adsorbed on Cr_2O_3 . The absence of the band at 1360 cm^{-1} obviously indicates that the phenol is adsorbed with dissociation to form surface phenolate (Table 5.31). In contrast to this, on the oxidized surface of Cr_2O_3 , besides the formation of phenolates, carboxylates are already observed at room temperature. The latter indicates destructive adsorption of the phenol ring.

The data obtained show that the phenolates are formed through the participation of acid–base pairs. It should be noted that a definite correlation has been observed between the position of the νCO absorption bands in surface phenolates and the degree of covalence of the M–O bond. Upon a decrease in covalency, the value of νCO band increases. Thus, in the case of $\gamma\text{-Al}_2\text{O}_3$, the νCO bands lie at 1260 and 1295 cm^{-1} , for MgO at 1300 cm^{-1} , and for sodium phenolate at 1305 cm^{-1} .

5.8 Complexation of aldehydes and ketones

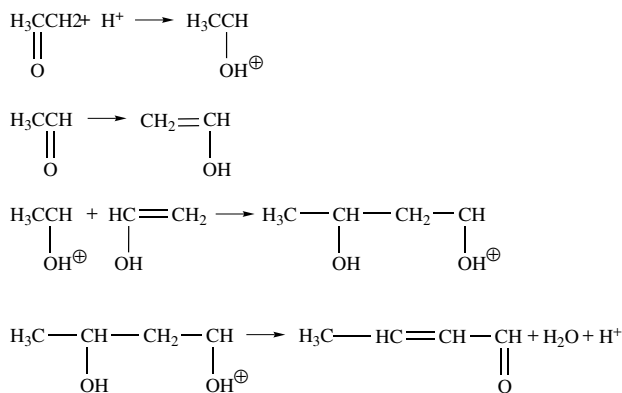
An examination of the electronic structure of aldehydes and ketones shows that the highest-occupied molecular orbital (HOMO) is the main characteristic of the unshared electron pair on the antibonding $n(\sigma)$ orbital localized on the oxygen atom of the carbonyl group. In terms of the Dewar–Chatt–Duncanson model (see, for example for acrolein, Figure 5.41), the nature of the bond between the C=O group and a transition-metal cation (Lewis acid site) is a donor–acceptor type, caused by interaction of the $n(\sigma)$ orbital of the aldehyde (ketone) and vacant orbitals of the cation (end-on complexes). Obviously, the spectral characteristics of adsorbed molecule will hence be determined by the nature and electronic state of the adsorption center. In the case of unsaturated aldehydes, similar considerations facilitate the formation of π -complexes via the $\pi\text{C=C}$ orbital and via $\pi^*\text{C–O}$ orbital in the case of strongly reduced cations and metals (side-on complexes). Through participation of ion pairs during the nucleophilic attack of the C–H bond by surface oxygen, surface carboxylate-like species incorporating surface oxygens are formed.

5.8.1 FORMALDEHYDE AND ACETALDEHYDE

Zeolites

The participation of CO groups of an aldehyde in a specific interaction with zeolite cations is indicated by the dependence of the shift in the absorption band of the CO group on the size of the cations. Thus, during the adsorption of aldehydes on LiX zeolites, the shift in the stretching vibration of CO relative to the gas is 36 cm^{-1} , and for CsX it is 47 cm^{-1} [19]. The shift of the frequency ($\nu\text{C=O}$) depends on the acceptor ability of the cation (Lewis acid site) and may be used to establish such an ability.

Diaz *et al.* [1486] studied the adsorption of acetaldehyde on HZSM-5 zeolites. They established that the primary interaction between acetaldehyde and the zeolite surface was by proton transfer (the band at 3600 cm^{-1} vanishes and the carbonyl vibration shifts to lower frequencies. Crotonaldehyde was identified as a product of aldol condensation, or as an intermediate in additional condensation reactions (almost identical spectra for adsorbed crotonaldehyde on its own to the spectrum from adsorbed acetaldehyde were observed at low adsorption pressures). Relatively high adsorption pressures induce polymerization (broad bands appear in the bending region). A scheme for the transformation of acetaldehyde with participation of zeolites can be represented as follows:



Scheme 5.57

Oxides

The adsorption of formaldehyde on oxides was investigated many years ago by spectroscopic methods, and important results have been obtained [30, 202, 1452, 1487–1495]. On different oxides (silica, pure and fluorided alumina, magnesia, titania, thoria, zirconia and iron oxide), the adsorption of formaldehyde has been investigated by FTIR spectroscopy in the temperature range 170–570 K [1487]. The following adsorbed species have been identified and characterized spectroscopically, namely (i) physisorbed HCHO, (ii) coordinated HCHO, (iii) dioxymethylene, (iv) polyoxymethylene, (v) formate ions, and (vi) methoxy groups. On silica at 170 K, formaldehyde is physisorbed on surface OH groups (Table 5.32) and, by warming, is then polymerized to produce linear polyoxymethylene (Table 5.33). On ionic oxides at about 250 K, dioxymethylene is always observed, generally together with variable amounts of the linear polymer (Table 5.34), as has been isolated on magnesia at 170 K.

Acetaldehyde H-bonded to Aerosil is characterized by the absorption bands at 1718 ($\nu\text{C}=\text{O}$) and 1383 cm^{-1} (δCH). At temperatures above 473 K, esterification of acetaldehyde with silanols takes place, producing the silylacetate (the bands at 1740, 1434 and 1381 cm^{-1}) [1488]. These authors note that the process of oligomerization of acetaldehyde also takes place in this case.

FTIR data, together with thermodynamic calculations for H-bonded complexes of formaldehyde, acetaldehyde, acetone, cyclopentanone cyclohexanone, and 2-cyclohexen-1-one on Aerosil have been reported [1489]. The stretching mode of the H-bonded hydroxyls showed in all cases an unusually complex shape (changing when physisorption took place), because of the coupling between the OH stretch and the anharmonic intermolecular modes. From the intensity of the νOH mode of the free hydroxyls as a function of pressure, the equilibrium constant for H-bond formation was calculated. Several correlations were drawn, i.e. $\Delta\nu\text{CO}$ with $(\Delta\nu\text{OH})^{1/2}$, proton affinity and ionization energy and ΔG and ΔS with the number of carbon atoms. An estimate for ΔH was made from $\Delta\nu\text{OH}$, so that a fairly complete thermodynamic characterization of the H-bonding process was achieved. It was shown that the isolated molecule is simply chemisorbed by Lewis acid sites, producing the band at 1700–1680 cm^{-1} (νCO), together with another band at about 1480 cm^{-1} (δCH_2).

For all ionic oxides, the thermal behavior has shown a strong parallelism, both on surfaces having a predominantly basic character (as on magnesia, zirconia and thoria) or an acidic character (as on alumina, titania and iron oxide).

Table 5.32. Absorption frequencies (cm^{-1}) of formaldehyde molecular species [1487]. Reprinted with permission from Busca, G., Lamotte, J., Lavalley, J.-C. and Lorenzelli, V., *J. Am. Chem. Soc.*, **109**, 5197–5202 (1987). Copyright (1987) American Chemical Society.

Vibration modes	Gas	O_2 matrix	HBr (complex)	Absorbed on		
				SiO_2 (180 K)	Al_2O_3 (170 K)	
$2\nu_2$	–	3471.3	3460.3	–	3430	3430
$2\nu_3$	–	2999.5	–	–	–	–
$\nu_2 + \nu_6$	–	3000.1	3000.6	–	2995	2988
ν_5	$\nu_{(\text{as})} \text{CH}_2$	2843.3	2873.6	2886.3	2894	2885
ν_1	$\nu_{(\text{s})} \text{CH}_2$	2782.5	2810.1	2819.4	2830	2818
$\nu_3 + \nu_6$	–	2719.2	2728.4	–	2732	2725
ν_2	νCO	1746.1	1740.0	1727.9	1725, 1717	1718
ν_3	δCH_2	1500.1	1505.3	1495.7	1501	1498, 1485
ν_6	$w\delta \text{CH}_2$	1249.3	1250.2	1247.2	–	1252
ν_4	$r\delta \text{CH}_2$	1167.1	1171.3	1172.9	–	–

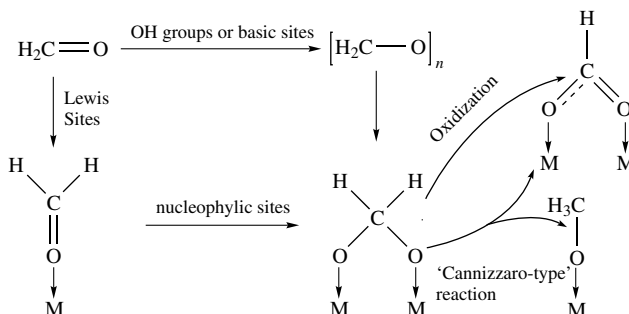
Table 5.33. Absorption frequencies (cm^{-1}) of polyoxymethylene (POM).

Assignment	Hexagonal POM	HCHO on		
		MgO (230 K)	SiO_2 (RT)	Al_2O_3 (170 K)
νCH_2	2984	2980	2980	2980
	2920	2918	2915	2910
δCH_2	1471	1485	1480	–
	$w\text{CH}_2$	1434	1430	1425
$t\text{CH}_2$	1384	1395	1385	–
	1290	1325, 1290	–	–
$R\text{CH}_2$	1238	1235	–	1230, 1210
	1098	1115, 1105	–	1110
νCO	936	940	–	–
	897	910	–	–

Table 5.34. Absorption frequencies (cm^{-1}) of dioxymethylene species.

Assignment	$\text{H}_2\text{C}-(\text{OCD}_3)_2$	Dioxolane- d_4	CH_2O on		
			TiO_2	ZrO_2	ThO_2
$\nu_{\text{as}} \text{CH}_2$	2945	2955	2950	2970	2960
$2\delta \text{CH}_2$	2932	3013	–	–	–
$\nu_{\text{s}} \text{CH}_2$	2882	2845	2868	2870	2840
$2w\text{CH}_2$	2770	2738	2763	2765	2750
δCH_2	1473	1510	1482, 1464	1490, 1470	1495
$w\text{CH}_2$	1401	1383	1418–1408	1410	1405
$t\text{CH}_2$	1302	–	1300	1315	1280
	1186	–	1251	1255	–
$r\text{CH}_2$	1138	–	1172, 1156	1180, 1157	1180, 1150
	1114	–	1113	1117	1112
$\nu \text{C}=\text{O}$	1086	–	1070	1070	1070
	–	–	–	965	948
	858	–	–	890	920

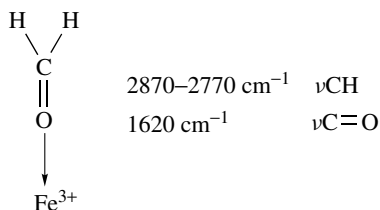
The most prominent species arising from the adsorption of HCHO on ionic oxides at room temperature are formate ions [30, 202, 1452, 1487, 1490–1495]. As noted by Busca *et al.* [1487], the spectroscopic features of such species, characterized mainly by a very strong absorption at 1600–1550 cm^{-1} ($\nu_{\text{as}}\text{COO}^-$) and another, usually split or multiple and slightly weaker, at 1410–1350 cm^{-1} (δCH plus $\nu_{\text{s}}\text{COO}^-$), have been discussed and summarized [1495]. The following scheme of formaldehyde transformation on an oxide surface has been presented by Busca *et al.* [1487] as follows:



Scheme 5.58

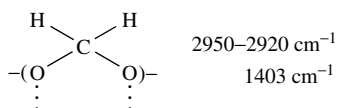
The species have been identified on the surface from the following analysis of the spectra:

- (a) Chemisorbed molecules, via the coordination bond on the Lewis acid sites, whose C=O stretching vibrations are at 1620 cm^{-1} , and with corresponding CH stretching vibrations measured at 2870 and 2770 cm^{-1} , which are similar to those of gaseous formaldehyde:



- (b) Formate ions, identified through their bands at 1555, 1375 and 1345 cm^{-1} ;
 (c) Species responsible for the bands at 2950–2920 and 1403 cm^{-1} , which can be tentatively identified as polymers of formaldehyde on the surface.

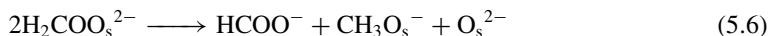
The types of species (a) and (b) are also observed in the case of adsorption of acetaldehyde on the surface of Fe_2O_3 [1496], while the species of type (c) corresponds to linear or cyclic polymeric compounds:



Scheme 5.59

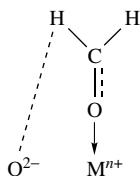
Similar assignments had already been proposed by Young and Sheppard [1497] for the bands of non-carbonyl-containing compounds measured after the adsorption of various aliphatic aldehydes on Cab-O-Sil.

Formaldehyde adsorbed on CeO_2 (1000 K) produce bands due to formate species at 2935, 2843, 1595, 1556, 1371 and 1359 cm^{-1} , and in addition, several bands at 1109, 1067 and 916 cm^{-1} . The latter bands may be attributed to dioxymethylene or polyoxymethylene species formed on the oxides by adsorption of HCOH but are often different from those reported in the literature [1487], since the two species give nearly the same bands below 1200 cm^{-1} . Here the three bands produced from the adsorption of HCHO on CeO_2 were tentatively assigned to dioxymethylene adsorbed species. It is interesting to note that formate species from the oxidation of methoxy did not occur below 473 K, whereas these were readily formed from the oxidation of dioxymethylene, even at room temperature. This indicates that on CeO_2 the direct oxidation of dioxymethylene to formate is more facile than the oxidation of methoxy to formate species. If the methoxy is progressively oxidized to formate via a dioxymethylene intermediate, the first step from methoxy to dioxymethylene will be a rate-controlling step. The formation of methoxy was accompanied by a decrease in the dioxymethylene species. This implies that a 'Cannizzaro-type' reaction occurs [1487] so that the methoxy and part of the formate are produced via disproportionation of dioxymethylene:



The contribution of the 'Cannizzaro-type' reaction to the production of formate species is notable.

The adsorption of formaldehyde on typical catalysts used for the full (Cr_2O_3 and TiO_2) or partial (Cr_2MoO_4 and MoO_3) oxidation of methanol to formaldehyde has been investigated [30, 1452, 1499], where it was established that on Cr_2O_3 and TiO_2 the formaldehyde is adsorbed predominantly as formates, while on the Mo-containing catalysts the molecular form of formaldehyde adsorption was observed. A weakly bound form of aldehyde is characterized by the following absorption bands: 2870 cm^{-1} , $\nu_s\text{CH}$; 1390 and 1470 cm^{-1} , δCH_2 ; 1700 cm^{-1} , νCO . The position of the νCO band in the spectrum of the adsorbed aldehyde suggests coordination bonding or the formation of a hydrogen-bond with the protic acid centers through the $\text{C}=\text{O}$ group. The formation of surface formates in very small amounts during the adsorption of formaldehyde on Cr–Mo catalysts is also suggested. The formation of aldehyde-like surface compounds, characterized by an absorption band at 1280 cm^{-1} ($\nu\text{C}=\text{O}$) has been suggested on MoO_3 and Cr_2O_3 :

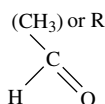


Scheme 5.60

The FTIR spectra of the surface species arising from the adsorption of formaldehyde on pure vanadia and vanadia–silica have been discussed by Busca [1498]. Formaldehyde was adsorbed at low temperatures in the form of dioxymethylene and polyoxymethylene species, which were weakly bound and desorbed near room temperature, leaving a clean surface. Formaldehyde does not produce stable surface-formate groups by oxidation, as in the case of Mo-containing catalysts. There are bands at 2989 and 2920 cm^{-1} ($\nu_s\text{CH}$) with a broad weak band near 2800 cm^{-1} , as well

as bands at 1238 and 1225 cm^{-1} , and at 1120 and 1105 cm^{-1} , in the spectrum of species formed due to the adsorption of formaldehyde on vanadia at 170 K. These bands correspond to those of the linear polymer of formaldehyde, i.e. polyoxymethylene [1498]. The authors assigned the weaker bands at 1470, 1430 and 1380 cm^{-1} to the same species, which is almost stable on evacuation at 270 K. Other bands, such as those at 1485 and 1410 (both weak), 1285 (medium–strong), and 1177 and 1162 cm^{-1} (very strong), and probably also near 1120 and 1080 cm^{-1} (superimposed on the strongest band of the polymer), disappear instead under evacuation at this temperature. All of these bands correspond well with those of the dioxymethylene species, as has been discussed in detail by Busca and co-workers [1494, 1498]. The decomposition of both dioxymethylene and polyoxymethylene does not leave any species on the surface, but near 290 K restores the clean vanadia surface. A very weak band with maxima near 1715 and 1680 cm^{-1} was observed only at 170 K, which is very probably due to νCO of the formaldehyde species adsorbed in molecular form.

Acetaldehyde, and other saturated aldehydes with longer chains, produce structures close to those found for formaldehyde adsorption, with the only difference being that the initial unit of the structure is as follows:



Scheme 5.61

and instead of the formates, for example, carboxylates are formed. The IR spectra of adsorbed acetaldehyde have been analyzed in detail [1500–1502]. The spectral manifestations of surface compounds of crotonaldehyde on VPO [1503] and $\text{V}_2\text{O}_5/\text{TiO}_2$ [1504] have also been studied.

5.8.2 ACROLEIN

Surface compounds of acrolein on oxide catalysts have been analyzed by Popova *et al.* in review [1505]. It has been established that acrolein forms different types of complexes with the participation of various surface centers of oxides. Figure 5.41 presents data on the energies

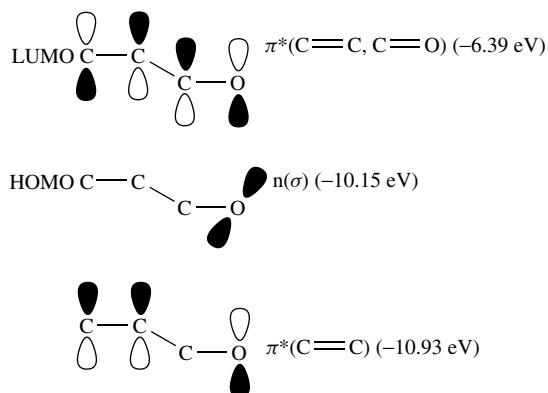


Figure 5.41. Boundary molecular orbitals of acrolein.

of the boundary molecular orbitals of acrolein obtained by XPS, and shows that the highest-occupied molecular orbital (HOMO) is the main characteristic of the unshared electron pair on the antibonding $n(\sigma)$ orbital localized on the oxygen atom of the carbonyl group. It should be noted that the π -orbital, which characterizes the C=C bond in acrolein, is close in energy to the HOMO. Acrolein exhibits the properties of a weak base due to the presence of the unshared electron pair of the carbonyl group; therefore, the character of its interaction with the surface depends to a considerable extent on the surface acid–base properties.

The formation of complexes with OH groups

The formation of such complexes depends on their acid–base properties. Hydrogen-bonded surface species may be formed with the participation of the surface OH groups, as evidenced by changes in the catalyst spectrum in the region of free and perturbed hydroxyl groups. These species are, as a rule, weakly bound to the surface, and only minor spectral changes are detected for the adsorbed molecule itself (see, for example, data for SiO_2 – Table 5.35).

When Brønsted acid sites are present on the surfaces of oxide catalysts (as revealed, for instance, by the adsorption of ammonia), rather stable hydrogen-bonded complexes may be formed via the C=O bond of acrolein. According to data on the adsorption of aldehydes and ketones on oxides [30, 1499], the frequency of the stretching vibrations of the C=O bond may decrease by 0.7–2.0 %, as compared with the $\nu\text{C=O}$ of the adsorbate in the gas phase. In this case, the shifts of the absorption bands attributed to surface OH groups are equal to 200–250 cm^{-1} . Such complexes have been observed upon acrolein adsorption on SiO_2 [1505, 1506], V–Mo–Si–O [1505, 1507, 1515] and Bi–Mo–Si–O [1508], and over practically all other catalysts [1505–1520] (Tables 5.35 and 5.36).

The formation of complexes with metal cations

As described above, the nature of the bond between acrolein and a transition-metal cation (Lewis acid) site, in terms of the Dewar–Chatt–Duncanson model, the donor–acceptor interaction, may be realized through either the $n(\sigma)$ or π -orbital of acrolein and a vacant orbitals of the cation, whereas the π -dative transfer of the electron density occurs from the HOMO of the center to the π^* -orbital of acrolein. The presence of coordinatively unsaturated cations on the surfaces of most oxide catalysts and the electron-donor properties of acrolein may involve the $n(\sigma)$ orbital or a π -complex of acrolein via the $\pi(\text{C=C})$ orbital. Taking into account the available experimental data [30], which showed that the ability of olefins to form π -complexes on the surface of various oxide catalysts diminishes with the increasing degree of oxidation of the metal, one may assume that acrolein adsorption on polyvalent cations of transition metals occurs exclusively through σ -complexes. It follows from this that the observed decrease in the $\nu\text{C=O}$ frequency in the IR spectra not only lends support to the formation of a coordinatively bound σ -complex of acrolein, but also provides evidence for the existence of coordinatively unsaturated polyvalent cations on the surface [1515]. The formation of π -complexes of acrolein and the appearance of absorption bands characterizing C=C stretching vibrations [1515] seems to be indicative of the presence of low-valence transition-metal ions at the surface. Such a correspondence between the type of coordination and the degree of oxidation of a transition-metal ion was observed for complexes of transition metals with dibenzylideneacetone (DBA) [1509]. Such complexes are formed on all oxide systems on the surfaces of which coordinatively unsaturated cations are present (see Tables 5.35 and 5.36) [1505, 1507, 1512, 1513, 1516, 1517–1520]. The value of $\nu\text{C=O}$ decreases by 2 % with respect to that of the gas phase. The value of $\nu\text{C=O}$ decreases as the acceptor-ability of the cation decreases ($\nu\text{C=O}$ in the complexes changes from 1690 up to 1640 cm^{-1}). This fact reflects the general properties of the C=O group in ketones and aldehydes

Table 5.35. Assignment of absorption bands (ν (cm^{-1})) in the infrared spectra of adsorbed acrolein ($T_{\text{ads}} = 298 \text{ K}$).

Sample	$\nu\text{C}-\text{C}$	$\delta\text{C}-\text{H}$	$\delta\text{CH}(\text{CHO})$	δCH	νCOO^-		$\nu\text{C}=\text{C}$	$\nu\text{C}=\text{O}$	$\delta\text{CH}(\text{CHO})$	δCH	δCH_2	$\nu\text{O}-\text{H}$
					Symmetric	Asymmetric						
SiO_2				1420			1625	1690	2720	2860	3020	3500
MgO	1150	1240	1370		1440	1580	1640	1740	2840	2940		
CuO	980 1080	1280	1370		1440	1560	1640	1710	2890			
$\text{MoO}_3/\text{SiO}_2$			1370	1420			1620	1690				3500
$\text{V}_2\text{O}_5/\text{SiO}_2$			1370	1420			1660	1705				3500
$\text{V}_2\text{O}_4/\text{SiO}_2$			1370	1420			1620	1680				3500
Sb_6O_{13}			1370	1420			1620	1690				
$\text{V}-\text{Sb}$			1370	1420			1620	1680				
$\text{K}_3\text{PMo}_{12}\text{O}_{40}$							1620	1715				
$\text{CH}_2=\text{CH}-\text{C} \begin{array}{l} \text{O} \\ \parallel \\ \text{H} \end{array}$	1159	1276	1360	1422			1620	1712	2800	3000	3102	
$\text{CH}_2=\text{CH}-\text{C} \begin{array}{l} \text{O} \\ \parallel \\ \text{OH} \end{array}$	1240			1432			1617	1725				3200 3500
$\text{CH}_2=\text{CH}-\text{C} \begin{array}{l} \text{O} \\ \parallel \\ \text{ONa} \end{array}$	1285		1368		1430-1450	1540-1570	1640			3012	3085	
Ester								1730				
Polymer				1428					2715	2880		

Table 5.36. Surface complexes (SCs) formed upon adsorption of acrolein on V–Mo–Si–O catalysts.

T_{ads} ($^{\circ}\text{C}$)	SC structure	SC	Absorption band frequency (cm^{-1})	T at which IR spectrum was recorded ($^{\circ}\text{C}$)
25		SC-I	$\delta\text{C-H}$, 1370 $\nu\text{C-C}$, 1625 $\nu\text{C=O}$, 1690 $\nu\text{O=H}$, 3500	50
25–100		SC-II	$\delta\text{C-H}$, 1370 $\nu\text{C=C}$, 1625 $\nu\text{C=O}$, 1660	50–130
25–100		SC-III	$\nu\text{C=C}$, 1625 $\nu\text{C=O}$, 1725	50
100–200		SC-IV	$\nu\text{C=C}$, 1630, 1640 ν_s COO, 1460, 1445 ν_{as} COO, 1560, 1520	50–250
150–285	–	SC-V	$\delta\text{C-H}$, 1420 $\nu\text{C=C}$, 1620 $\nu\text{C=O}$, 1750	150–300

which relate the values of the shift and half-width of the C=O band group to the strength of an aprotic site. This relationship may be used as a characteristic of the acid site distribution of strengths of the acid centers [30].

The formation of complexes with surface oxygen

It is known that adsorbed oxygen can act as a strong nucleophile in the interaction with Brønsted acids (carboxylic acids and alcohols), as well as with aldehydes and ethers. Oxygen may attack the carbon atom of a carbonyl group, resulting in the formation of surface carboxylates [1510].

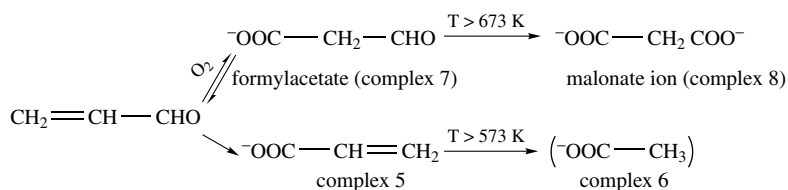
In accordance with the electronic structure of the reactants, the formation of an acrolein complex with surface oxygen may be considered as a nucleophilic attack of a surface oxygen atom at the carbon atom of the carbonyl group. Such adsorption character has been comprehensively studied in the case of the interaction of acrolein with the Keggin unit of a P–Mo heteropoly acid [1511]. The HOMO of the Keggin unit characterizes the linear electron pair on the bridging oxygen atom (O_{B}), with the lowest-unoccupied molecular orbital (LUMO) being the 4d Mo orbital. Both of these orbitals are, however, inaccessible for acrolein, since the surface is covered by oxygen atoms. The nucleophilic attack of a surface oxygen atom at the carbon atom of the carbonyl group occurs via two intermediate structures [1505], with the formation of asymmetric surface acrylate species.

The interaction of acrolein with surface oxygens possessing nucleophilic properties is similar to the reactions of nucleophilic substitutions in solution, for example, to the hydrolysis of esters

in a basic medium to yield a carboxylate ion and an alcohol molecule [1510]. Earlier [1507], detailed consideration was given to the spectral identification of this complex, which is termed in the literature as ‘carbonyl-bonded’, ‘ester-like’ [1505, 1521], or ‘asymmetric acrylate’ [1511], and is bound simultaneously with two centers M_1 and M_2 (Table 5.36) [1505]. The formation of acrylates during acrolein adsorption at room temperature has also been observed on Cr_2O_3 , ZnO and Al_2O_3 (two types of acrylates) and has been proved by IR studies of acrylic acid itself adsorbed on a number of oxides [1522] (see below).

Acrolein adsorption on the majority of oxide systems results in the formation of oxidized fragments even at room temperature (Table 5.35). This is indicated by the presence of absorption bands at 1440 and 1580 cm^{-1} in the spectra, which are characteristic for the ν_s and ν_{as} of the COO^- groups, along with a 1640 cm^{-1} band characteristic of $\nu C=C$. In the case of MgO and CuO, surface acrylates are converted to acetate and formate ions. Comparison of the absorption bands in the region of 800–1800 cm^{-1} with the absorption bands of the acrylate ion (Table 5.35) allows the assignment of these bands (except for that at 1740 cm^{-1}) to the corresponding vibrations of magnesium acrylate. On MgO, a formylacetate complex (absorption bands at 2989 and 1725 cm^{-1}) has been identified. This complex has been converted at high temperature into the malonate ion (absorption bands at 1390, 1450, 1585, 2850 and 2925 cm^{-1}), which is bound to the surface of MgO via both carbonyl groups.

The whole pattern of acrolein surface complex transformations on MgO may be presented in the following way [1516]:



Scheme 5.62

Due to the predominant formation of formylacetate and malonate ions it is likely that the main products of acrolein oxidation on MgO are the products of destructive oxidation (Table 5.35). The 2-formylacetate complex ($\nu C=O$ of 1728 and $\nu C-H$ of 2931 cm^{-1}) is also formed on Al_2O_3 [1505]. Acrolein admission to these catalyst leads to the formation of hydrogen-bonded and coordinatively bound complexes (for the assignment of the bands, see Table 5.35).

5.8.3 BENZALDEHYDE

According to the author's data, in the spectra of benzaldehyde adsorbed on transition metal oxides (Cr_2O_3 , NiO and Co_3O_4), two new absorption bands at 1570–1550 and 1420–1430 cm^{-1} were observed, together with absorption bands characteristic of the aromatic ring. These two bands were attributed to the symmetrical and asymmetrical vibration of COO^- groups in the benzoate ion, taking into account the spectra of adsorbed benzoic acid mentioned above. At high coverages of the surface, the molecular modes of adsorbed benzaldehyde are observed. Their spectral characteristics differ only little from those of free benzaldehyde, except for the values of $\nu C=O$, which are observed in the range from 1620 to 1720 cm^{-1} . On the basis of the spectral data from adsorbed aldehydes shown above, these vibrations characterize the $\nu C=O$ mode in coordinatively and H-bonded complexes of benzaldehyde. On several V- and Mo-containing catalysts

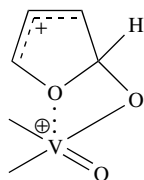
(V_2O_5/TiO_2 , V_2O_5/SnO_2 and MoO_3/Al_2O_3), only molecular adsorbed species of benzaldehyde were observed when the benzaldehyde was adsorbed at room temperature.

5.8.4 MALEIC ANHYDRIDE

Maleic anhydride is a product of the well-known transformation reaction of butane on V–P–O catalysts. It also forms as an intermediate in the production of furan from butane. For these reasons, the adsorption of maleic anhydride has been intensively investigated by infrared spectroscopy in recent years.

Maleic anhydride adsorbed at 373–573 K onto $V_2O_5-P_2O_5$ supported on alumina gives three surface species. The bands at 1856, 1800 (shoulder), 1780, 1760 (shoulder) and 1280 cm^{-1} have been attributed to physisorbed maleic anhydride [1231]. The bands at 1856 and 1780 cm^{-1} resulted from the symmetric and asymmetric C=O bonds vibrations, while the 1280 cm^{-1} band arises from a C–O–C bridge in the molecule. The C=C bond of maleic anhydride absorbs at $1590-1595\text{ cm}^{-1}$. These bands appear in nearly the same positions as for the free anhydride (Table 5.37). The strong absorption bands at 1580 and 1460 cm^{-1} belong to symmetric and asymmetric vibrations of a carboxylate ion, which is formed through the interaction between maleic anhydride and surface oxygen. Support for this comes from the similarities of the spectra of maleates formed from the adsorption of maleic acid, of maleate hydrates or acid maleate hydrates. The bands at 1730, 1680 and 1635 cm^{-1} characterize most probably, in the authors' opinion, adsorbed maleic acid and/or acid maleate. Maleic acid is an intermediate in the oxidative degradation of maleic anhydride.

The adsorption of furan has been studied by Jovel and Shimanskaya [1523], Rivasseau *et al.* [1524] and Ramstetter and Baerns [1231]. Rivasseau and co-workers could not identify any structures adsorbed on Mo–V oxide from the infrared spectra, while Jovel and Shimanskaya have found that furan is oxidized on V_2O_5 to form a succinate structure. According to Ramstetter and Baerns, furan is both oxidized (the bands at 1700 to 1850 cm^{-1}) and adsorbed by forming an addition complex via the 2-position of the ring:



Scheme 5.63

as indicated by bands at 1595, 1565 (ring vibrations), 1550, 1490 (ring vibrations), 1455 (ν_{CCC} in allyl) and 1395 cm^{-1} .

The influence of the properties of the oxide surfaces on the character of the maleic anhydride adsorption has been examined by Davydov [1525]. The IR spectral manifestations of the adsorption and transformations of maleic anhydride on such catalysts for complete or partial oxidation were studied. It was found that structures containing COO^- groups were predominantly formed on CuO, whereas on V_2O_5/Al_2O_3 maleic anhydride retained its molecular structure, and the adsorption occurred via the formation of donor–acceptor bonds with C=O groups. The nondissociative form of maleic anhydride is weakly bound to the surface; its concentration decreases at 293 K, and it is completely desorbed upon heating at 373 K. It has been proposed, from a consideration of the thermal stability and the spectral features of this form, that it is likely that

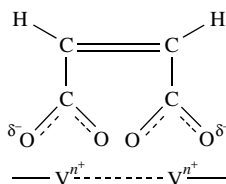
Table 5.37. Absorption frequencies (cm^{-1}) of the main reactants in the oxidation of 1-butene to maleic anhydride^{a,b} [1231]. Reprinted from Ramstetter, A. and Baerns, M., *J. Catal.*, **109**, 303–313 (1988). Reprinted with permission from Academic Press.

Butadiene	2-Butenaldehyde	2-Butenoic acid	Furan	2,5 H-Furanone	Maleic anhydride
			3167 (w)		3180 (w)
			3161 (m)		
			3140 (w)		
			3129 (m)		3123 (w)
				3100 (w)	
2980 (s)	2956 (m)				
		2940 (m)		2940 (w)	
2928 (sh)	2933 (m)				
	2892 (m)			2880 (w)	
2797 (w)	2793 (s)				
	2712 (s)				
		2650 (w)			
1821 (s)					1855 (m)
1767 (w)				1775 (s)	1780 (s)
				1745 (s)	
	1687 (vs)	1698 (vs)			
	1637 (s)	1655 (s)			
1592 (vs)				1605 (m)	1592 (m)
			1556 (s)		
1497 (w)			1491 (s)		
1437 (w)	1441 (s)	1446 (s)		1450 (m)	
		1420 (m)			
	1390 (s)				
1377 (m)	1374 (s)	1375 (m)	1384 (s)		
	1303 (m)	1310 (s)			
1292 (w)		1285 (sh)			
1280 (vw)			1267 (w)		1266 (s)
					1240 (s)
		1225 (s)			

^aData given correspond to gaseous 1,3-butadiene, to solid maleic anhydride, and to the liquid state of all other compounds.

^bvs, very strong; s, strong; m, medium; w, weak; vw, very weak; sh, shoulder.

maleic anhydride is bound via the acid proton sites of the $\text{V}_2\text{O}_5/\text{Al}_2\text{O}_3$ presented on the surface of this system. An alternative form of adsorbed maleic anhydride is as follows:



Scheme 5.64

This structure (maleate) is characterized by absorption bands at ca. 1280, 1330, 1380, 1450 and 1570 (broad) cm^{-1} . The strong absorption bands at 1450 and 1570 cm^{-1} , the intensities of which grow with an increase in the interaction temperature, belong to symmetric and asymmetric vibrations of the carboxylate group. The absorption band corresponding to $\nu\text{C}=\text{C}$ was identified in the 1580 cm^{-1} region.

It has been established that in the case of CuO only surface maleates are formed at 293 K, i.e. all maleic anhydride molecules are oxidized on the CuO surface. It was noted [1525] that the spectral features of the COO^- groups in maleates formed with the participation of copper and vanadium cations differ somewhat (1430 and 1555 cm^{-1} for CuO, and 1460 and 1570 cm^{-1} for $\text{V}_2\text{O}_5/\text{Al}_2\text{O}_3$).

Dichloromaleic anhydride adsorption was investigated in the same study [1525]. It was shown that this anhydride, molecularly adsorbed on $\text{V}_2\text{O}_5/\text{Al}_2\text{O}_3$, together with the formation of such complexes with conservation of the C–Cl bonds (predominantly at low temperatures), forms complexes containing COO^- groups. This latter form is in equilibrium with molecularly adsorbed maleic anhydride.

5.8.5 ACETONE

We will examine acetone as a typical example of a ketones because all of the other saturated ketones give surface compounds with close spectral characteristics. The adsorption of acetone, as well as of aldehydes, which have unshared electron pairs in an antibonding $n(\sigma)$ orbital localized on the oxygen atom of the carbonyl group, easily occurs with the participation of the surface cations and protic acid centers.

Zeolites

The formation of H-bonded complexes of acetone with protic acid centers of zeolites (H-forms), as well as the OH groups of SiO_2 , is accompanied by decreases in both νCO and νOH . The values of the shifts of these vibrations depends on proton mobility and increases when the proton acidity increases. The formation of donor–acceptor complexes has little influence on the other vibrations of the acetone molecule.

The adsorption of acetone molecules on zeolites with different exchanged cations was the subject of an early study [19]. The spectrum of the stretching vibration of the CO bond of acetone adsorbed on zeolites with monovalent (NaX) or divalent (CaX) exchanged cations gives overlapping bands with a joint maximum at 1710 cm^{-1} in the first case, and at 1702 cm^{-1} in the second case. The presence of several overlapping bands in the spectrum is characteristic of acetone adsorbed on zeolites with different monovalent cations. This can be explained by different perturbations of the CO groups due to differences in the energies of interaction of the acetone molecules with cations that are attached to different sites of the lattice skeleton of the zeolites.

As was noted in the first studies [19], the gradual desorption of acetone from channels of NaX zeolites does not affect the position of the absorption bands. However, during the desorption of acetone from CaX zeolites, the high-frequency band of the less-perturbed CO groups disappears very rapidly, and only the low-frequency band of the more perturbed groups remains in the spectrum. The position of the CO-stretching absorption band of the carbonyl groups in acetone is sensitive to the type of exchanged cation and can be a measure of the acceptor's ability.

Oxides

On the surfaces of most oxide catalysts at room temperature, acetone is adsorbed, producing the weakly bound complex, which then decomposes by desorption under vacuum up to 373 K,

and is H-bonded to the surface hydroxyl groups of the oxides. The vibration frequencies for such complexes differ little from those of the free acetone molecule, except for $\nu\text{C}=\text{O}$, which essentially decreases. As in the case of zeolites, $\Delta\nu\text{C}=\text{O}$ depends on the acidity of the OH groups, and varies by $<2\%$ in comparison with the free acetone molecule. Significantly larger $\Delta\nu\text{C}=\text{O}$ values are observed in the case of formation of the donor-acceptor bond between the surface cations. Thus, even in the first spectral studies of the interaction of acetone with Al_2O_3 it was already established that three absorption bands of the carbonyl groups occur – the first, at 1692 cm^{-1} , was attributed to the stretching vibrations of the CO group of the acetone molecule which was hydrogen-bonded to surface hydroxyl groups, while the others, at 1625 and 1600 cm^{-1} , were attributed to molecules which form coordination bonds with two different types of aprotic centers of the alumina surface [19]. The change in the absorption bands of the carbonyl groups of carbonyl-containing molecules of organic bases (e.g. 4-bromoacetophenone and benzylacetophenone) adsorbed on alumina has been interpreted as an indication of their interactions with aprotic acid centers. In more recent studies involving IR investigations of the interactions between acetone and Al_2O_3 , this has been interpreted as the dissociation of the CH bond in a small fraction of the acetone molecules, with the formation of enolate anions, i.e. $^-\text{O}-\text{C}=\text{C}/\text{O}=\text{C}-\text{C}^-$. The latter are formed with the participation of acid-base pairs due to nucleophilic attack of the oxygen ion on the CH bond in the CH_3 group of the coordinated acetone molecule.

Molecules of substituted ketones (for example, hexachloroacetone) may also be used as indicators of Lewis acid centers. The infrared spectrum of such an indicator adsorbed on the surface of an aluminosilicate catalyst showed that H-bonded hexachloroacetone (the band at 1691 cm^{-1}) is present on the surface, together with hexachloroacetone molecules chemisorbed on Lewis acid centers (absorption bands at 1625 , 1636 and 1650 cm^{-1}). The lower frequency of an absorption band corresponds to a stronger Lewis acid center.

In another early paper concerning the IR spectroscopic studies of acetone adsorption on MgO and NiO [1526], authors, using H- and D-substituted acetones, showed that the coordinatively bound species (1700 cm^{-1} for $(\text{CH}_3)_2\text{CO}$ and 1688 cm^{-1} for $(\text{CD}_3)_2\text{CO}$ on MgO; 1608 and 1580 cm^{-1} , respectively, for NiO) are formed, together with decomposition of the acetone to formates and acetates. The last process was firmly established and proceeded on these oxides at low temperatures. The authors proposed an 'enolate-type' complex formation, and noted that the bands at 1540 and 1324 cm^{-1} may be attributed to this complex. They did not, however, discuss the reasons for these assignments.

The surface hydroxyl groups of rutile forms H-bonds with the adsorbed acetone and this is also coordinatively adsorbed onto exposed Ti^{4+} ions [1527]. The band at 1680 cm^{-1} , is attributed to the $\nu\text{C}=\text{O}$ mode of the acetone molecule coordinated by Lewis acidic sites at low coverage; absorptions at 2970 , 2930 and 2875 cm^{-1} (νCH) also characterize this form of adsorbed acetone [79]. Moreover, the formation of enolate complexes (1545 and 1430 cm^{-1} or 1510 and 1425 cm^{-1} for D-substituted acetone) and of mesityl oxide (1655 and 1595 cm^{-1} , for $\nu\text{C}=\text{O}$ and $\nu\text{C}=\text{C}$, respectively) was also revealed. The latter bands correspond to mesityl oxide molecules coordinatively liganded to Lewis acidic Ti^{4+} ions. In the case of D-substituted acetone, the bands lie at 1643 and 1580 cm^{-1} , accordingly. The reaction:



proceeds slowly on Lewis titania ionic sites. Such a reaction has also been observed by Raman spectroscopy in the case of Al_2O_3 [1528]. The formation of mesityl oxide apparently involves the initial formation of an enolate, which is an intermediate for the condensation reaction. On the adsorption of mesityl oxide, the reverse reaction, namely enolate formation, takes place. When the temperature of interaction increases, surface acetates (for D-substituted acetone, the bands

at 1480 and 1430 cm^{-1} , for ν_{as} and $\nu_{\text{s}}\text{COO}^-$, respectively,) are formed, as has been established by other workers [1474, 1529, 1527]. At room temperature, it is difficult to establish whether surface acetates are formed.

An infrared study of the adsorption of hexafluoroacetone on rutile [1527] has provided information about the relative reactivities of various types of surface hydroxyl groups and changes in Lewis acid sites under different treatments, including oxidation and reduction. These authors showed that acetone is more strongly bound to rutile than hexafluoroacetone. However, acetone should be less susceptible to nucleophilic attack by surface OH or oxide ions, which for hexafluoroacetone led to the formation of adsorbed salts of hexafluoropropane-2,2-diol and trifluoroacetate ions.

An IR spectroscopic investigation of the interaction of $(\text{CH}_3)_2\text{CO}$ and $(\text{CD}_3)_2\text{CO}$ with both oxidized and reduced surfaces of Sn/Mo oxide catalysts established that the H-bonded acetone (the band at 1715 cm^{-1} ($\nu\text{C}=\text{O}$) for the H-substituted acetone, and at 1695 cm^{-1} for the D-substituted form) and isopropylate structures (the band at 1090 cm^{-1} ($\nu\text{C}-\text{O}$) are only formed on the oxidized surface [1529]. The latter probably involved the participation of the acid hydroxyl groups, apparently via the stage of isopropyl alcohol formation due to the direct transfer of the surface proton to the CO group of the acetone molecule. The formation of coordinatively bound acetone has been observed on the oxidized ($\nu\text{C}=\text{O}$ at 1665 cm^{-1}) and reduced ($\nu\text{C}=\text{O}$ at 1685 cm^{-1}) surfaces of the catalyst, together with the formation of enolate complexes (the bands at 1445 (1430) and 1565 (1555) cm^{-1}) (Table 5.38). The data obtained are in good agreement with changes in the surface properties of the catalyst after reduction. The absence of H-bonded acetone on the reduced surface is probably connected with the disappearance of the protic acid centers. The acceptor ability of surface cations decreases on reduction as is manifested in the shift of $\nu\text{C}=\text{O}$ in the coordinatively bound acetone. On CuO, acetone was adsorbed without the formation of a coordinatively bonded complex. As for the 'enolate-like' complex, its spectral characteristics were close to those found for Sn/Mo catalysts. Last complex is easily transformed to both acetates and formates after a period of time and at low temperatures [1474]. The dissociation of acetone probably proceeds by the participation of ion pairs, analogous to those discussed in the case of TiO_2 . It seems that the new absorption bands (1565 and 1445 cm^{-1} , and 1555 and 1430 cm^{-1} , for H- and D-substituted samples, respectively), which were observed in the spectra of adsorbed acetone (and which differ little from H- and D-substituted acetone) at room temperature on the surfaces of both oxidized and reduced samples, characterize the $\nu\text{C}-\text{O}$ and $\nu\text{C}-\text{C}$ modes in the enolate complex. Such an

Table 5.38. Absorption frequencies (cm^{-1}) of acetone and deuterioacetone in the free state and upon adsorption on an Sn–Mo catalyst.

Vibration	$(\text{CH}_3)_2\text{CO}$	Adsorbed $(\text{CH}_3)_2\text{CO}$	$(\text{CD}_3)_2\text{CO}$	Adsorbed $(\text{CD}_3)_2\text{CO}$
$\nu^{\text{as}}-\text{CH}_3$	3018	2290	2264	– ^a
$\nu^{\text{as}}-\text{CH}_3$	2972	2290	2227	– ^a
$\nu^{\text{s}}\text{CH}_3$	2937	2935	2123	– ^a
$\nu\text{C}=\text{O}$	1742	1715, 1665	1732	1695, 1660
$\delta^{\text{as}}-\text{CH}_3$	1435	1415	1050	– ^a
$\delta^{\text{s}}-\text{CH}_3$	1364	1370	1080	– ^a
$\nu\text{C}-\text{C}$	1218	1250	1242	1280
$\beta-\text{CCH}$	1096	1090	887	–
$\nu\text{C}=\text{O}$ in enolate	–	1565	–	1555
$\nu\text{C}=\text{C}$ in enolate	–	1445	–	1430

^aNot observed due to low intensity.

assignment is completely confirmed by the data of Griffiths and Rochester [1527] for adsorption on TiO_2 but differ from the results published in [1528]. When the temperature of interaction increases, 'formate-carboxylate-type' structures are formed, apparently due to the destruction of the 'enolate-type' complexes.

The adsorption of acetone on TiO_2 , K/TiO_2 (1–3 wt%) and Li/TiO_2 (ca. 1 wt% Li) at room temperature, and also on these samples with supported MoO_3 (1–3 wt% MoO_3), proceeds without any reactions [1528]. In this case, the vibrations characteristic of molecularly adsorbed acetone ($\nu\text{C}=\text{O}$ at 1690–1720 cm^{-1}) were observed, resolved into two components in this range. These values are ca. 20–44 cm^{-1} lower than those for gaseous acetone. The author believes that this shift is caused by electron release from the oxygen atom of the carbonyl group to fairly weak surface Lewis acid sites. The splitting of the $\nu\text{C}=\text{O}$ band in the undoped sample indicates the presence of acetone species coordinated to Lewis acid sites of different acid strength – probably differently coordinatively unsaturated Ti^{4+} cations. It has been established that the doped samples have lower Lewis acidity properties. Support for this also comes from the shifting of the $\nu_{\text{as}}\text{CCC}$ mode from 1215 cm^{-1} for gaseous acetone to 1240–1228 cm^{-1} . Other bands (1423 and 1370 cm^{-1}) are due to the bending mode of the methyl groups. Unlike the doped samples, for pure TiO_2 it was proposed that acetone dissociation proceeds and 'enolate-type' structure are formed. On the basis of previous IR studies of acetone adsorption on oxide surfaces [1526, 1527] this author attributed the weak bands at 1380 and 1570 cm^{-1} to the ν_{s} and ν_{as} modes of enolate anions.

Infrared spectroscopy of Me_2CO adsorbed on $\alpha\text{-Fe}_2\text{O}_3$ [1530] showed that acetone can be chemisorbed on Lewis acid sites and gives, at least partially, enolate anions which, produce a chemisorbed form of mesityl oxide via aldol condensation with molecules from the gas phase. At 523 K, acetate ions are formed. There were two different forms of trichloroacetate ions on the surface after the adsorption of hexachloroacetone and trichloroacetic acid.

The spectra of acetone adsorbed on V_2O_5 shows that at room temperature it is adsorbed without any reaction. In fact, all of the bands detected can be assigned to acetone adsorbed 'as such', e.g. $\nu\text{C}=\text{O}$ is observed at 1682 cm^{-1} , i.e. at a frequency significantly lower than that of the gas-phase molecule (1734 cm^{-1}). This suggests that it interacts with surface Lewis acid sites through coordination of one oxygen lone-pair. The other bands were assigned as follows: 2970 and 2925 cm^{-1} to νCH , 1421 and 1368 cm^{-1} to δCH_3 , ca. 1248 cm^{-1} to $\nu_{\text{as}}\text{CCC}$, and 1090 cm^{-1} to ρCH_3 .

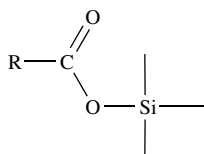
5.9 Complexation of acids

5.9.1 FORMIC ACID

Investigations of formic acid adsorption on oxides by means of IR spectroscopic methods started long ago and is still active [452, 514, 1495, 1531–1554]. It has been shown that formic acid is easily dissociated to form the surface formate species, together with both H-bonded and coordinated complexes.

Formic acid was found to be undissociated on the surface of silica and to be hydrogen-bonded with the surface hydroxyls. Some evidence has been reported, however, that a dehydration of formic acid can occur on silica. Hirota *et al.* [1531] have confirmed earlier studies, which showed that the adsorption of undissociated acid molecules took place on silica. No formate bands appear on the silica during heating.

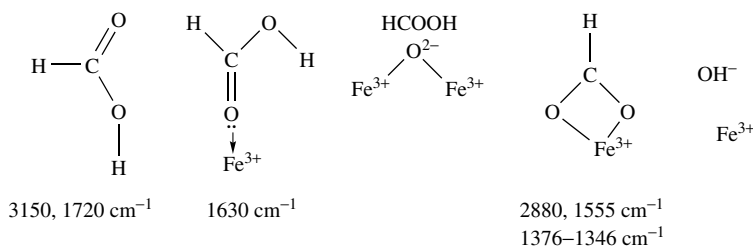
The increase on $\nu\text{C}=\text{O}$ in the case of the adsorption of carboxylic acids on SiO_2 has been shown by Eischens and co-workers [1521, 1532]. The absorption band at 1730 cm^{-1} is associated with the $\nu\text{C}=\text{O}$ vibrations in a surface complex of the following type:



Scheme 5.65

On alumina, the infrared spectrum revealed the presence of the formate ion, characterized by absorption bands at 1620 and 1344 cm^{-1} due to ν_s and ν_{as} of the COO^- group, respectively, and a band at 1402 cm^{-1} arising from the δCH deformation vibration in the plane of the formate group. At higher coverages of the surface, a second layer of undissociated formic acid molecules was observed. At 493 K , evidence for physical adsorption disappeared, but the formate bands were unaffected by prolonged heating at this temperature.

The decomposition of formic acid produced zinc formate on the surface of zinc oxide at room temperature [1531] and also showed the formation of formates on other oxides [1533, 1534]. Surface formates were also detected after the adsorption of formic acid on Fe_2O_3 by Takezawa [1538] and Busca *et al.* [202]. The following surface compounds are formed in the case of Fe_2O_3 :



Scheme 5.66

Bands due to labile species at 3150 and 1720 cm^{-1} can be assigned to formic acid molecules physisorbed through hydrogen-bonding where formic acid hydroxyls act as hydrogen donors, with their stretching frequencies being very strongly lowered (3150 cm^{-1}) with respect to the free molecule value, while the surface free OH absorption maximum at 3640 cm^{-1} is practically unaffected. The band at 1630 cm^{-1} can be assigned to the species coordinatively bound through the carbonyl oxygen to Lewis acid sites.

A large cycle of *in situ* IR spectroscopic studies of surface formates which were produced in the reaction between $\text{OH}_s^- + \text{CO}$ has been reported by Tamaru and co-workers [21, 1534, 1535] on the surfaces of MgO and ZnO, and by Davydov and co-workers [30, 311, 514, 1536, 1537] on the surfaces of copper- and chromium-containing catalysts. These studies, together with data about the mechanism of formic acid decomposition, are examined in detail in Chapter 6.

In most of Davydov and co-workers' IR spectroscopic studies of the interaction of alcohols, aldehydes, ketones and hydrocarbons with oxides (see above), the IR spectra of adsorbed acids (in particular, formic and acetic) have been used to identify formate-carboxylate surface compounds which are easily formed by the oxidation of the molecules on the oxide surfaces.

To elucidate the specific spectral features of surface formates, and to establish criteria for their identification, the spectra of formic acid adsorbed on the surfaces of different oxides have been measured [1539]. Formic acid is known to dissociate readily on the surface of most oxides to yield

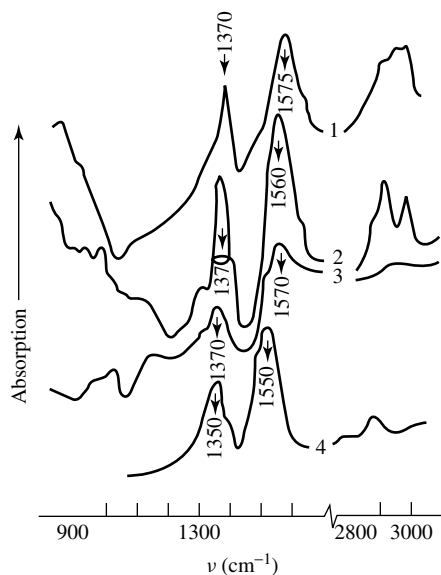


Figure 5.42. IR spectra of formic acid adsorbed on (1) CuO, (2) Cr₂O₃, (3) SbVO₄, and (4) Fe₂O₃ at 293 K and low coverages.

formate ions, which can be easily identified by spectroscopic techniques. Figure 5.42 shows the spectra of surface formate ions that are formed upon the adsorption of formic acid on some oxide catalysts at coverages of <10 % of a monolayer. In this case, the only formates are observed on the oxide surfaces and the molecular species are absent. These ions are also seen to exhibit intense absorption bands in the 1600 to 1200 cm⁻¹ region and maxima at 2700–3000 cm⁻¹. The surface formate ions can be identified by comparing the spectra with those of the formic acid salts [1540]. It is clear from these data that the observed absorption bands may be assigned to $\nu_{\text{as}}\text{COO}^-$ of 1550–1600 cm⁻¹ and $\nu_{\text{s}}\text{COO}^-$ of 1350–1390 cm⁻¹, whereas the shoulder in the 1400 cm⁻¹ region can be attributed to δCH vibrations. It should be noted that a more complicated spectrum resulting from Fermi resonance is observed in the region of the νCH stretching vibrations [1539, 1541, 1543]. In the case of formate on chromium oxide, the bands in the νCH range may be assigned to $\nu_{\text{as}}\text{COO}^-$ plus δCH (2975 cm⁻¹), νCH (2900 cm⁻¹) and $\nu_{\text{s}}\text{COO}^-$ plus δCH (2845 cm⁻¹) absorption bands.

It was found that bulk formates (carboxylates) can be monodentate, bidentate and bidentate-bridged. It has been shown that the frequency separation between $\nu_{\text{as}}\text{OCO}$ and $\nu_{\text{s}}\text{OCO}$ of the formate ion takes the following order: monodentate formate > free formate ion > bidentate formate. It can be supposed that in the case of surface formates, different types of species are observed. For example, on the surface of CuO–MgO the bidentate-bridged formates (formed by the participation of copper ions or both copper and magnesium ions) were separated, together with ionic species on magnesium [514, 1539]. For monodentately coordinated bulk formates, the larger the value of $\Delta\nu = \nu_{\text{as}} - \nu_{\text{s}}$, then the stronger is the ‘formate anion–surface cation’ bond which is formed [15]. The data of Figure 5.42 show that there is no such correlation in the case of surface formates on transition-metal oxides because the observed formates have similar values for $\Delta\nu$ while the temperatures of their complete decomposition is 673, 473 and 620 K for Cr₂O₃, SbVO₄ and Fe₂O₃, respectively. Evidently, this is attributable to differences in the types of coordination bonding with the cations. However, the above-discussed correlation between the

Table 5.39. Absorption frequencies (cm^{-1}) and thermal stability data for surface formates and carboxylate complexes formed upon the adsorption of different hydrocarbons on CuO.

Gas	H-COO ⁻		R-COO ⁻		T_{des} (K) ^a
	$\nu^{\text{s}}\text{COO}^-$	$\nu^{\text{as}}\text{COO}^-$	$\nu^{\text{s}}\text{COO}^-$	$\nu^{\text{as}}\text{COO}^-$	
CH ₄	1370	1570	–	–	673
C ₂ H ₆	1370	1570	1570	1570	673
C ₂ H ₄	1370	1560	1560	1560	573
C ₃ H ₆	1370	1560	1560	1560	573
C ₂ H ₂	1380	1550	–	–	523
C ₃ H ₄	1380	1550	1550	1550	523
C ₅ H ₈	1380	1550	1550	1550	523

^aTemperature of formate desorption.

$\Delta\nu$ value and thermal stability is applicable for a particular oxide. An IR spectroscopic study of adsorbed alkanes, alkenes and alkynes (Table 5.39) showed that they are chemisorbed at 473 K on such oxides, forming both formates and acetates (except for methane and acetylene, which are adsorbed as formates only) [1539]. The IR spectroscopic data indicate that the thermal stabilities of formates produced by alkane adsorption are higher than those of the surface formate–carboxylate compounds from the adsorption of alkenes and alkanes at elevated temperatures (for similar coverage). For instance, surface compounds formed upon the adsorption of alkenes and alkanes disappear from the catalyst surfaces at 673 and 573 K, respectively. For hydrocarbons with C≡C bonds, the thermal stabilities of surface compounds of the formate–carboxylate type decrease even more (down to 523 K). Furthermore, the transition from alkanes to alkenes and alkynes is accompanied by a natural shift of $\nu_{\text{as}}\text{COO}^-$, characteristic of surface complexes, to lower frequencies, e.g. from 1580 to 1570 to 1550 cm^{-1} , respectively. The frequencies of the asymmetric stretching vibrations of the COO⁻ group for metal acetates were shown [15] to be the most sensitive to the nature of the metal atom. For example, the frequency decreases with the structure of monodentately coordinated acetates as the M–O bond strength increases. Thus, lowering of the $\nu_{\text{as}}\text{COO}^-$ frequency of the surface complex can also characterize a decrease in the strength of bonding of these complexes with the surfaces, as confirmed by direct desorption measurements.

However, even within one system this relationship does not hold, when the formates are formed via essentially different mechanisms. For example, a formate complex formed upon adsorption of formic acid (Figure 5.42) is close in its spectral properties to the formate produced upon adsorption of CO on an hydroxylated chromium oxide surface at 523 K (Figure 5.43, spectrum 1) via the reaction $\text{OH}_{\text{ads}} + \text{CO} \rightarrow \text{H-COO}_{\text{ads}}^-$. The starting temperatures of decomposition for complexes of this kind, however, are about 473 K, whereas the formates produced by formic acid adsorption decompose even at 323 K. The activation energies for decomposition of these formates also differ considerably, e.g. they are 36 and 126 kJ mol^{-1} for the formates formed from formic acid and those formed by the interaction of CO with surface hydroxyl groups, respectively [1537]. Different formate coordinations or variation in covalence of the M–OOCH bond could be the causes for such differences.

There are some data available which indicate that the above-discussed correlation is also observed when the surface compounds are formed within different oxide systems but via the same mechanism. Thus, the IR spectra of formate compounds produced by the reaction of CO with OH groups, under steady-state conditions, on the surfaces of some catalysts for the water-gas shift reaction are shown on Figure 5.43. The relevant spectral and thermochemical data for

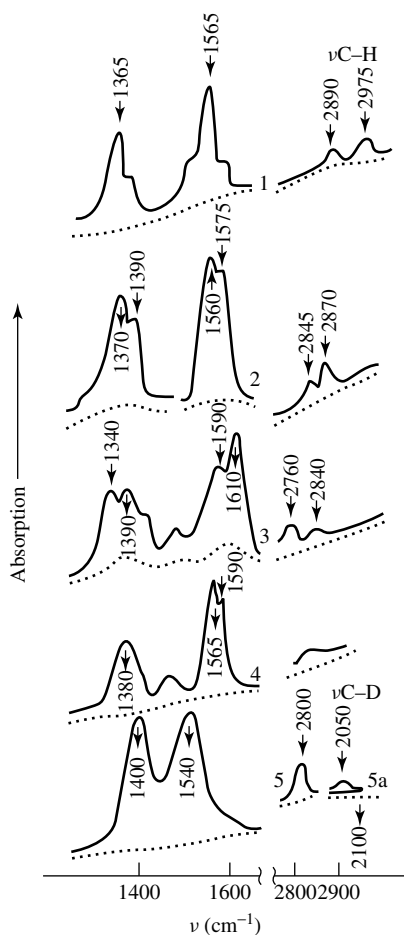


Figure 5.43. IR spectra of formate compounds formed on the surfaces of different oxide catalysts upon interaction with CO at 473 K: (1) Cr_2O_3 , (2) $\text{CuO-Fe}_2\text{O}_3$; (3) MgO ; (4) CuCr_2O_3 ; (5) CuO-MgO ; (5a) catalyst treated with $\text{CO} + \text{D}_2\text{O}$ at 293 K.

the various formate structures are compared in Table 5.40. Clearly, the properties and spectral characteristics of formate compounds differ between different systems, as well as for one system under different conditions of pre-treatment (see types I and II in Table 5.40). A comparison of the $\Delta\nu$ values and the thermal-stability sequence for the surface formates shows that they exhibit a good correlation with the series obtained for the bulk formate compounds, that is, the lower value of the splitting $\Delta\nu = \nu_{\text{as}} - \nu_{\text{s}}$, then the less thermally stable is the surface compound.

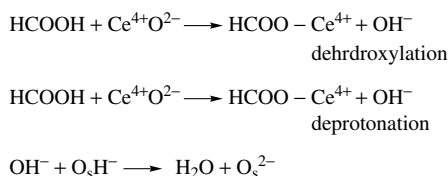
Recently, much attention has been concentrated on establishing the structure and properties of formic acid surface species, including the types of coordination [1545]. For example, the IR spectra of HCOOH adsorbed on CeO_2 dehydrated at 1273 K have been studied [1546]. After treatment *in vacuo*, the bands at 1734 and 1684 cm^{-1} obviously decreased in intensity, and they are accordingly ascribed to molecularly adsorbed dimers and HCOOH interacting via hydrogen-bonding with the surface oxygen anions of the cerium oxide. Broad bands ranging from 3600 to 2800 cm^{-1} are clearly due to strongly perturbed hydrogen-bonding. Other bands

Table 5.40. Absorption frequencies (cm^{-1}) and thermal stability data of surface formate compounds formed in the $\text{CO} + \text{OH}_{\text{ads}}$ reaction.

Type	$\nu_{\text{s}}\text{COO}^-$	$\nu_{\text{as}}\text{COO}^-$	$\Delta\nu$	$T_{\text{des}} (\text{K})^a$
<i>MgO</i>				
I	1340	1610	270	573
II	1390	1590	200	523
<i>Cr₂O₃</i>				
I	1365	1565	200	523
II	1390	1600	210	523
<i>CuCr₂O₃</i>				
I	1380	1565	185	423
<i>CuO–MgO</i>				
I	1350	1600	250	523
II	1400	1540	160	373

^aTemperature at which the concentration change (intensity of absorption) becomes observable within 30 min.

include νCH (2845 cm^{-1}), $\nu_{\text{as}}\text{OCO}$ (1599 , 1553 and 1542 cm^{-1}), δCH (1371 cm^{-1}), $\nu_{\text{s}}\text{OCO}$ (1362 and 1248 cm^{-1}) and δOCO (777 cm^{-1}). A band at 2933 cm^{-1} is attributed to a combination band of δCH and $\nu_{\text{as}}\text{OCO}$. A pair of bands at 1599 and 1248 cm^{-1} developed together with an increase in temperature from 300 to 373 K , indicating that they arise from the same species. The bands at 1599 and 1248 cm^{-1} can be attributed to monodentate formate species since the frequency separation of 351 cm^{-1} is much larger than that of the free formate ion (about 250 cm^{-1}). The remaining bands in the region 1600 – 1300 cm^{-1} are attributed to bidentate formate species because the frequency separation is smaller than 250 cm^{-1} . The $\nu_{\text{as}}\text{OCO}$ vibrations at 1533 and 1542 cm^{-1} indicate that two kinds of bidentate formate species were formed. The following dissociative routes are proposed in the formation of monodentate and bidentate species:

**Scheme 5.67**

Only bidentate formates are formed by the participation of CO with OH^- on CeO_2 [1546]. The same results were obtained for ZrO_2 , Al_2O_3 , MgO , CuO–MgO , CuCr_2O_4 [311, 514] and Cr_2O_3 [311].

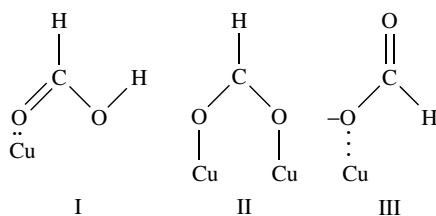
Adsorption of HCOOH on copper-containing catalysts has been a subject of detailed investigation because many researchers believe that the adsorbed formate species play a significant role in both methanol synthesis and in the water-gas shift reactions. Formic acid adsorbed on Cu/SiO_2 gives maxima at 1728 and 2954 cm^{-1} (Table 5.41), which are also present in the spectra of formic acid on silica alone and have been ascribed to physisorbed molecules on the support,

Table 5.41. Summary of main IR band (cm^{-1}) assignments for formic acid adsorbed on reduced and oxidized Cu/SiO₂, K/SiO₂, K/Cu/SiO₂, and SiO₂ alone.

SiO ₂	Reduced Cu/SiO ₂ ^a	Oxidized Cu/SiO ₂ ^a	Assignment ^b	K/SiO ₂	Reduced K/Cu/SiO ₂	Oxidized K/Cu/SiO ₂	Assignment
2945	2954 (sh)	2945	Physisorbed HCO ₂ H on SiO ₂	2923	2924	2918	Physisorbed HCOOH
1728	1728	1722		1718	1718		
1388	1388	1388 (sh)					
1358	1365 (sh) ^c		Ligated HCO ₂ H on Cu(I)				HCHO(g)
	2869						
	1674		Bidentate formate on Cu (II)				Physisorbed HCHO
	2937	2939					
	2857	2859					
	ca. 1550	1558 (sh)	Monodentate formate on Cu(III)	2776			(HCHO) _h
	1358	1359					
		2978	Monodentate formate on Cu(III)	2692			HCOO ⁻ K ⁺
		2904		1597	1597	1598	
		1583		1376	1380	1377	
				1355	1354	1352	
					2937		Bidentate formate on Cu
					2850		
					1358	1581 (?)	Monodentate/formate on Cu

^ash, shoulder.^bSee text (Scheme 5.69) for further details.^cBand obscured by overlapping bands.

while the bands at 1674 and 2869 cm^{-1} , in the opinion of Rochester and co-workers' [1545], result from formic acid physisorption on copper in the form of structure I:



Scheme 5.68

Maxima at 1354 and 1388 cm^{-1} , and also the broad band at 1550 cm^{-1} , are attributed to bidentate formate (structure II).

Hayden *et al.* [1542] discussed the presence of a combination band ($\nu_{\text{as}}\text{COO}^- + \delta\text{CH}$) at 2950 cm^{-1} in the spectra of adsorbed formate on copper. The band at 2957 cm^{-1} for formic acid on Cu/SiO_2 may be attributed to the CH stretching vibration of bidentate formate, because of its difference from the corresponding band at 2841 cm^{-1} for HCO_2Na [1543]. In the case of a reduced surface, the intense band at 1578–1583 cm^{-1} , and other bands at 2904 and 2978 cm^{-1} have been ascribed to monodentate formate on Cu (structure III). This is consistent with the analysis by Busca and Lorenzelli [651] of the expected band positions for adsorbed formate complexes. The expected weaker band due to the $\nu\text{C}-\text{O}$ vibration of the monodentate formate may contribute, on the low-wavenumber side, to the absorption maximum at 1359 cm^{-1} .

In the case of potassium-promoted Cu/SiO_2 , the formation of ionic (bi- and monodentate) formates of potassium on copper (Table 5.41) has been established.

Fourier-transform infrared spectra of formic acid on ZnO/SiO_2 , reduced $\text{Cu}/\text{ZnO}/\text{SiO}_2$ and deoxidized $\text{Cu}/\text{ZnO}/\text{SiO}_2$ catalysts have been reported by Millar *et al.* [1547, 1548]. It was shown that formic acid adsorption on ZnO/SiO_2 produces mainly bidentate zinc formate species with a smaller quantity of monodentate zinc formate. Formic acid on reduced $\text{Cu}/\text{ZnO}/\text{SiO}_2$ catalyst results not only in the formation of bridging copper formate structures, but also in an enhanced amount of formate relative to that for ZnO/SiO_2 catalysts. On oxidized $\text{Cu}/\text{ZnO}/\text{SiO}_2$, formic acid gives monodentate formate species on copper in addition to zinc formate.

FTIR spectra of the surface species arising from the adsorption of formic acid on pure vanadia and vanadia–silica were obtained and discussed by Busca *et al.* [1498]. The spectrum obtained in the case of vanadia corresponds to that expected for formate ions [1498]: the strongest bands were observed at 1568 cm^{-1} (asymmetric towards higher frequencies – $\nu_{\text{as}}\text{COO}^-$), 1390 cm^{-1} (δCH) and 1377 cm^{-1} (asymmetric towards lower frequencies – $\nu_{\text{s}}\text{COO}^-$). Weaker bands at 1690 and 1220 cm^{-1} arise from small amounts of adsorbed undissociated formic acid and decrease rapidly upon evacuation at room temperature. The adsorbed formate species are stable upon evacuation up to 470 K, at which temperature they begin to disappear. On vanadia–silica, the adsorption of formic acid produces similar bands (1569, 1385 and 1372 cm^{-1}) although with some relevant differences in the intensity ratios. It was noted that a strong band also appears at 1730 cm^{-1} , probably due to formate species bound to silicon in a covalent form. Formate ions on this catalyst disappear upon evacuation at 470 K.

5.9.2 ACETIC ACID

In the literature, there is a rather large number of investigations of forms of acetic acid adsorption involving IR spectroscopy-, see, for example, [200, 1555–1558]. The adsorption modes of acetic acid are of the same types as those found for formic acid. Acetic and other saturated carboxylic acids form H-bonded compounds and easily dissociate to give acetates–carboxylates, the spectra of which are practically the same in the spectral region 1800–1300 cm^{-1} . The spectrum of acetic acid adsorbed on alumina has intense absorption bands at 1335, 1423 and 1585 cm^{-1} , plus those of the acetate ion [1554, 1555]. Evacuation of the sample at 423 K only removed the absorption bands of the molecularly adsorbed acid.

Hasegawa and Low [1556] have studied the infrared spectra of acetic and deuterioacetic acids adsorbed on alumina from solutions in CCl_4 . The bands of the acetic ions in the region 1590–1465 and 1560–1420 cm^{-1} were observed at low concentrations. The surface states of acetic acid on MgO, CaO, MnO and ZnO were investigated by Imanaka *et al.* [1557], while the interaction of acetic acid vapors with a CuO surface was studied by Tompkins and Allara [1558]. It was established [1554] that on TiO_2 (rutile) CD_3COOD is adsorbed on Ti^{4+} sites with the formation of D_2O , OD^- and CD_3COO^- ions. All of the researchers observed the carboxylate structures possessing absorption bands in the region of 1100–1800 cm^{-1} in the spectra of the adsorbed acids. The adsorption of acetic acid over hematite leads to the formation of surface acetates [200]. In more recent studies, there has been an attempt to establish the structure of the acetate species in detail, as was also done in the case of formic acid.

Other, more complicated, saturated acids upon adsorption give spectra which do not differ essentially from the spectra of adsorbed acetic acid. The simultaneous presence of ν_{as} and ν_{s} of RCOO^- in the IR spectra is the main distinguishing characteristic of such carboxylates. Long-chain fatty acids have been adsorbed onto oxides from CCl_4 solutions. Only physical adsorption occurred on silica. Stearic acid is predominantly adsorbed as the monomer at low concentration, whereas its adsorbed dimers were also formed at higher concentrations. The predominant reaction of stearic acid with Al_2O_3 was the formation of a layer of stearate and the production of adsorbed water. The main reaction between magnesia and decanoic acid solution was the formation of a surface decanoate layer. Analogous data were obtained for stearic acid adsorbed on ZnO.

Neagle and Rochester [1560a] showed that the carboxylic acids are commonly involved in surface interactions as H-bonded donors or acceptors (Lewis bases or Brønsted acids) on BaSO_4 . It has been shown that the dissociative adsorption of water on BaSO_4 leads to the formation of surface hydroxyl groups which are not Brønsted acid sites, as assessed by both NH_3 and Py; the adsorption of HCl is accompanied by the transformation of sulfates to HSO_4^- anions and Brønsted acid centers are also manifested on the surface.

5.9.3 ACRYLIC ACID

On the addition of another reactive group such as $\text{C}=\text{C}$, which has weaker donor properties when compared to the $\text{C}=\text{O}$ group, to an acid molecule, the character of interaction between the acid and oxides is little changed. To study the forms of adsorption of acrylic acid, and to determine the possible pathways of conversion to surface acrylate compounds, IR spectroscopy and thermodesorption with chromatographic analysis of the desorption products, were used by Davydov *et al.* [1522]. The types of surface compounds formed on the surface of oxides and their spectral characteristics are shown in Table 5.42. The frequencies from complex carboxylic

Table 5.42. IR spectral characteristics of acrylic acid, sodium acrylate and tightly bound acrylic acid on oxide catalysts (at a adsorption temperature of 298 K).

Catalyst	Compound	M ^{m+}	Infrared absorption bands (cm ⁻¹)						T _{des} (°C)	Desorption products				
			$\nu\text{C}-\text{C}$	$\delta\text{C}-\text{H}$	$\nu_{\text{s}}\text{COO}$	$\nu_{\text{as}}\text{COO}$	$\nu\text{C}=\text{C}$	$\nu\text{C}=\text{O}$			$\nu\text{C}-\text{H}$	$\nu_{\text{s}}\text{CH}_2$	$\nu_{\text{as}}\text{CH}_2$	
	$\text{CH}_2=\text{CHCOOH}$		1240 1430	1385	-	-	-	1617 1720	-	-	-	-	-	
SiO_2	$\text{CH}_2=\text{CHCOOSi}$			1420	-	-	-	1640 1730	-	-	-	400	$\text{C}_3\text{H}_4\text{O}_2$	
$\text{V}^{2+}\text{Mo}-\text{O}$	} $\text{CH}_2=\text{CHCOO}^-$	V^{4+}		1370	1440	1540	1640	1640	-	-	-	300	$\text{C}_2\text{H}_4\text{O}_2$, CO_2 (trace)	
$\text{MoO}_3/\text{SiO}_2$		Mo^{6+}		1370	1430	1525	1640	1640	-	-	-	250	$\text{C}_2\text{H}_4\text{O}_2$, CO_2 (trace)	
CuO		Cu^{2+}		1280	1370	1440	1580	1640	1640	-	-	250	CO , CO_2	
MgO		Mg^{2+}		1280	1370	1460	1580	1640	2880 1640	2880	3050	3102	500	CO , CO_2 , $\text{C}_2\text{H}_4\text{O}$, $\text{C}_2\text{H}_4\text{O}_2$
	$\text{CH}_2=\text{CHCOONa}$		1285	1368	1430-1450	1540-1580	1640	1640	2940 2960	2915	3043	3085	-	-

acids are sensitive to changes in the nature of the cations (for example, electronegativity values) [15]; for acetate structures with the same 'dentate pattern' it has been established that with increasing strength of the metal–oxygen bond the frequency difference, $\Delta\nu$ ($= \nu_{as} - \nu_s$), of COO^- increases.

In order to determine the nature of the conversion to surface acrylate structures, the thermodesorption of acrylic acid has been studied. Virtually the only product of its desorption from the surfaces of molybdenum-containing catalysts is acrylic acid, which is entirely desorbed at ca. 573 K, in good agreement with conclusions drawn from the IR spectra.

The acrylate formed on MgO is tightly bound to the surface. Raising the temperature of desorption to 673 K leads to only a slight decrease in the intensities of the absorption bands. Further raising the temperature leads to partial desorption, accompanied by breaking of the C=C double bond (in the IR spectra, the absorption band of $\nu\text{C}=\text{C}$ at 1640 cm^{-1} disappears, while the intensities of the absorption bands ν_{as} and $\nu_s\text{COO}^-$, at 1580 and 1460 cm^{-1} , respectively, are preserved). The products of desorption of acrylic acid from MgO are acetic acid, acetaldehyde, formaldehyde and oxides of carbon. At temperatures higher than 673 K, the surface acrylates on MgO are destroyed with the formation of acetate (possibly also formate) surface compounds, desorbed in the form of products of extreme oxidation.

In contrast to MgO, on copper oxide, a typical catalyst for extreme oxidation, when the temperature is raised to ca. 273 K, an intensive oxidation of the surface acrylate compounds with the formation of acetates is already observed in the IR spectra. This is indicated by the decreases in intensities of the absorption bands characterizing surface acrylates ($\nu\text{C}=\text{C}$ (1640 cm^{-1}), $\nu_{as}\text{COO}^-$ (1580 cm^{-1}) and $\nu_s\text{COO}^-$ (1440 cm^{-1})) and the appearance of new absorption bands ($\nu_{as}\text{COO}^-$ (1560 cm^{-1}) and $\nu_s\text{COO}^-$ (1410 cm^{-1})), which are close in position to the absorption bands characteristic of copper acetate [15]. The low temperature of final oxidation, in our opinion, is due to the presence of loosely bound oxygen in CuO. Chromatographic analysis of the products of desorption of acrylic acid from the surface of CuO shows only oxides of carbon.

On all of the catalysts studied, the adsorption of acrylic acid is of a dissociative nature and is accompanied by the formation of surface acrylate compounds of types (I) and (II). Acrylates of type (II) differ in the strength of the bonding to the surface. Loosely bound acrylates decompose, liberating acrylic acid into the gas phase; tightly bound acrylates undergo final oxidation to surface acetates or formates, followed by desorption in the form of products of full and destructive oxidation.

At 373 K, the IR spectrum of acrylic acid adsorbed on Sb_6O_{13} exhibits bands at 1250, 1280, 1320, 1420, 1610 and 1660 cm^{-1} , but when adsorbed on V–Sb–O catalysts additional absorptions occur (1250, 1280, 1320, 1370, 1420–1440, 1540, 1610, 1640 and 1670 cm^{-1}). Correlations for the changes of the sets of bands at 1250, 1320, 1420, 1620 and 1670 cm^{-1} and at 1280, 1370, 1440, 1540 and 1640 cm^{-1} have been observed during adsorption–desorption cycles of acrylic acid which indicate that two surface complexes of acrylic acid are formed on V–Sb–O catalysts. The first set of absorption bands is the same as that observed on Sb_6O_{13} . This gives us the reason to assign the other set of bands to vibrations of a surface compound of type (III). It is possible that this compound formation involves acrylic acid adsorption on V^{4+} ions, which have been identified in these catalysts by ESR spectroscopy.

5.9.4 BENZOIC ACID

Like the saturated and unsaturated acids, benzoic acid adsorbed on oxide surfaces forms stable H-bonded complexes with the weak basic hydroxyl groups or surface oxygens. The vibration frequencies are little changed from those of the free acid. On the formation of bonds with surface OH^- groups, the latter are disturbed. Surface benzoates are easily formed by the interaction of benzoic acid with practically all oxides. The spectral identification of these compounds

is based on the simultaneous presence of absorption bands characteristic of the benzene ring vibrations and ν_s and ν_{as} of the carboxyl group. Like those of surface acrylates, the properties of the surface benzoates depend on both the qualitative and quantitative properties of the catalyst.

5.10 Deactivation catalysts due to carbonaceous depositions as a result of catalyst interactions with hydrocarbons and their derivatives

The potential of molecular spectroscopy methods in the study of catalyst deactivation and regeneration cannot be overestimated. This particular subject could indeed occupy a separate chapter.

Besides the direct influence of the ‘poisons’ and impurities contained in a reaction mixture, the properties of a catalyst can be modified by a change in phase composition, both in the bulk solid and over the surface zone, by a redistribution of the cations in different valence and coordination states leading to deactivation, the formation of stable surface species which block the active centers of the catalyst surface, by the state of oxidation/reduction of the active surface centers due to influence of the reaction mixture, or by transformation (with time) of reaction intermediates into nonactive species. There is no possibility of us describing in detail all of these aspects here. Therefore, only some of the common problems of deactivation which are related to degradation of hydrocarbons on the surfaces of oxide catalysts (the main subject of this chapter) will be discussed below.

It has already been mentioned above that the formation of polycarbonium ions, observed by both IR and UV–Vis spectroscopic techniques on acid–base catalysts (Al_2O_3 and zeolites), can be the first stage of the hydrocarbon conversion into aromatic and polyaromatic compounds which can deactivate such catalysts (see, for example, Sections 5.1.2 and 5.2.2 [1155, 1560b, 1560c]).

When a supported metal catalyst is exposed at high temperature to a reaction mixture containing carbon monoxide or hydrocarbons, various forms of carbonaceous compounds, such as saturated oligomers, unsaturated oligomers, carboxylates or polyaromatic materials, are deposited on the catalyst surface. Some forms of these deposits can cause catalyst deactivation, whereas others assist and are indeed necessary for chemical reactions to proceed. Deactivation by carbonaceous deposits is a problem of serious magnitude for the petroleum industry in the conversion of coal and heavy feedstocks to clean fuels, in steam reforming, in the Fischer–Tropsch synthesis, and in many other important catalytic processes, as is evidenced by the fairly extensive published literature (for example, [1560d]).

More specifically, the concept of deactivation by carboxylate surface compounds (formed from the adsorption of practically all hydrocarbons and their derivatives, such as alcohols, aldehydes, acids and others) has been widely considered. This is based on the high thermostability (high temperature of decomposition) of these compounds *in vacuo* – higher than the reaction temperature. The participation of such surface compounds as intermediates in catalytic oxidation reactions will also be discussed in Chapter 6.

Other well-known mechanisms of deactivation are related to the formation of sulfur-containing compounds on the surfaces of catalysts. Again, the potentialities of spectroscopic methods are also very wide, i.e. from monitoring of the changes in electron density on metal cations due to the S-containing ligands, to detection of the formation of surface (or even bulk) sulfates leading to changes in catalyst activity.

Raman spectroscopy was the first technique to be used to study the final stages of the hydrocarbon deactivation process, i.e. the formation of carbon. In spite of the widely known fact that the different kinds of carbon can be successfully investigated by means of Raman spectroscopy [15], practically no applications to catalysis have appeared in the literature until very recently. Figure 5.44 shows distinguishable Raman spectra obtained from different kinds of carbon. Two bands characterize the wide spread of the different forms of carbon; ‘amorphous carbon’

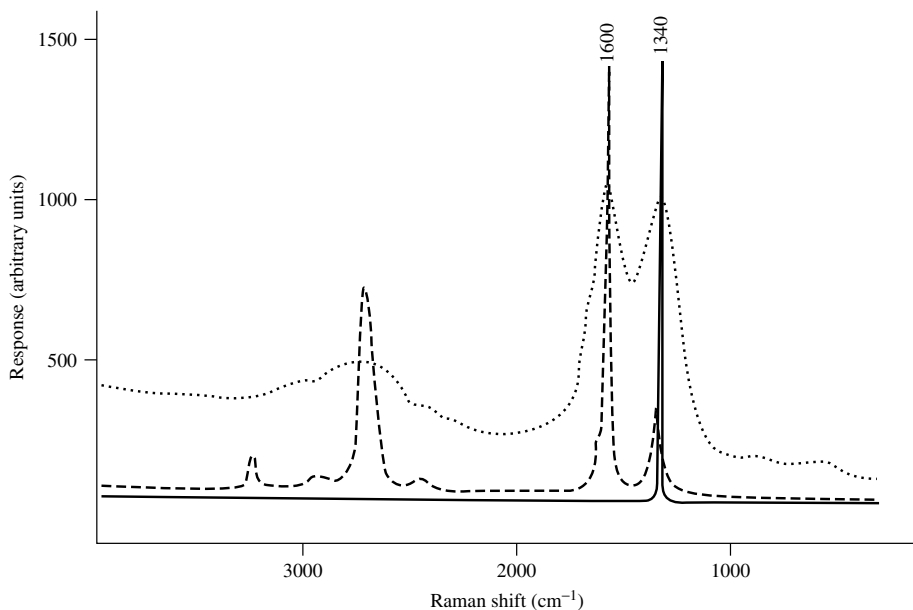


Figure 5.44. Raman spectra of different allotropic forms of carbon: (solid line) diamond; (dashed line) soft graphite; (dotted line) amorphous carbon.

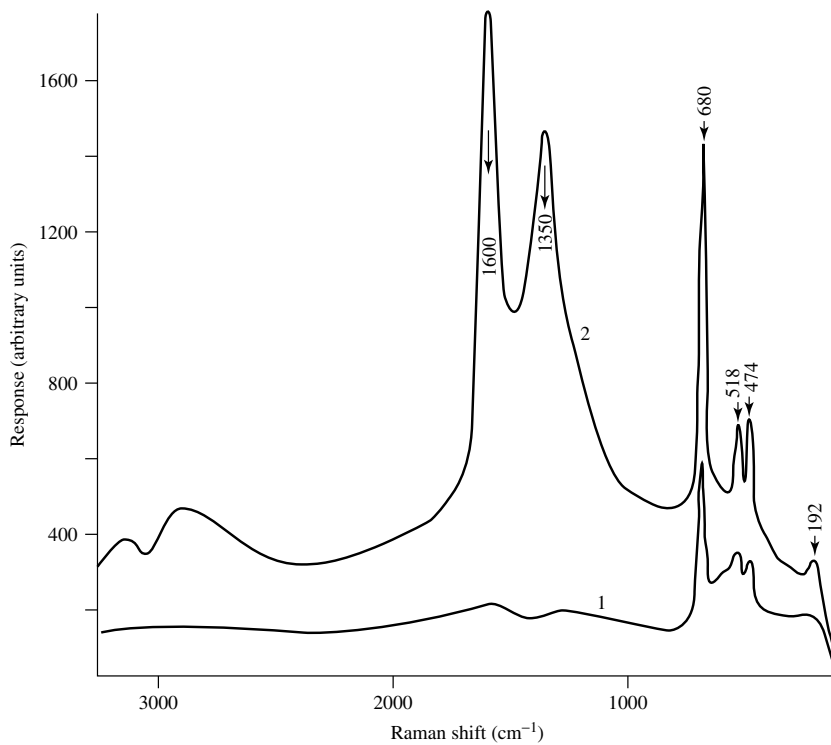


Figure 5.45. Raman spectra of (1) a $\text{Co}/\text{Al}_2\text{O}_3$ catalyst used in the Fisher–Tropsch reactor (1000 h), and (2) after oxidation by O_2 at 523 K.

and 'soft graphite' are characterized by 'D' and 'G' bands, respectively. Raman spectra of Co/Al₂O₃ catalysts after their long-time use in Fisher–Tropsch reactors display bands similar to those in the Raman spectrum of amorphous carbon (Figure 5.45). Regeneration of the catalysts removes these bands from the spectrum (Figure 5.45). In similar work on the methane conversion process, the Raman spectra of Ni/Al₂O₃ catalysts show that amorphous carbon is deposited into the catalyst, while some other regions of the catalyst also contain graphite-like carbon.

6 THE MECHANISMS OF HETEROGENEOUS CATALYTIC REACTIONS

The analysis of IR spectra provides information on the physico-chemical properties of surface complexes, adsorption forms of the substrate, and molecular changes that take place due to the adsorption. This information is important for elucidating the mechanisms of adsorption and catalysis. It should be noted, however, that many surface complexes are fairly stable. These complexes can either be the so-called 'dead-end' species, when they do not participate in catalytic reactions, or compounds which themselves modify the surface by the formation of new active sites or by changes in the properties of surface sites. The use of IR spectral data on surface complexes as evidence for mechanistic catalytic processes is unjustified if there is no proof that these complexes take part in the reaction (i.e. that they are reaction intermediates). Developments of molecular spectroscopy methods for investigation of adsorption and catalytic processes continues mainly in the direction of identifying such intermediates.

IR- and UV-Vis spectroscopies are widely used for investigations of gas- and liquid-phase reactions and for carrying out kinetic studies of such reactions. It can also be used to investigate the kinetics of surface reactions, to determine the reaction order for individual components and to evaluate the rate constants. With the aid of low- and high-temperature spectroscopic analysis it is possible to determine the activation energies of surface reactions. This type of information, in conjunction with results obtained by traditional kinetic studies, can contribute significantly to our understanding of the mechanisms of the processes.

As has already been noted [30], in order to establish the participation of surface compounds in a catalytic reaction, three levels can be separated. The first is a simple observation of the formation of the reaction intermediate. For this, two methods are commonly used to show that the surface complexes participate as intermediates in the catalytic reaction, i.e. (i) the combination of for example, IR spectroscopy and thermal desorption, with chromatographic or mass spectrometric analyses of the desorption products, can provide evidence that a reaction product is formed from a particular surface compound, and (ii) direct comparison of the rate constants or activation energies of surface complexes with the corresponding characteristics of the overall catalytic reaction. Recent years have seen considerable advances in the level of experimental facilities available. New methods have evolved and the sensitivity of traditional methods (Fourier-transform IR spectroscopy, etc.) has been considerably increased. Special IR cells and equipment have been created (allowing high-temperature and high-pressure studies) using the IR cell as a reactor so that the spectrum can be taken directly during a catalytic reaction. This has made possible the investigation of the reactions *in situ*. Following Davydov [30], Krylov and Matyshak [65] noted that 'in order to determine with certainty whether or not the surface complex is an intermediate

in a reaction, it is necessary to compare the rate of its formation and consumption with the rate of formation of the products, i.e. it is necessary to study the conversion kinetics of the surface compounds at the same time as we measure the rate of the catalytic reaction'. However, sometimes *in situ* measurements fail to give information on the reaction mechanism. This has also been commented upon by Busca [66]. Transformations of the intermediates cannot always be observed by means of spectroscopic methods. The latter is caused by the type of the reaction mechanism realized on the catalyst (e.g. character of the reagent activation and the nature of the limited stage) or by a limited transmission range or low intensities of bands.

At present, the methods of molecular spectroscopy (generally, UV–Vis, Raman or FTIR, in both transmission and diffuse reflectance modes) are widely used to study the mechanisms and kinetics of the transformations involved in heterogeneous catalytic reactions (see, for example, [21, 30, 169–173, 1561–1564]). A more unusual method for the detection of intermediates in heterogeneous catalytic reactions – their trapping on free centers of the support – should be noted as being available for supported systems. In such cases, the support plays the role of an active matrix for reactive species (see, for example, [713–717, 1565]).

As is well known, two main types of mechanisms are usually considered for heterogeneous catalytic reactions, namely the so-called Langmuir–Hinshelwood and Rideal-type (or Rideal–Eley-type) mechanisms. In the first case, the reaction is assumed to occur between adsorbed molecules on the catalyst, while in the second case the reactant molecules from the gas phase react with other adsorbed molecules. Obviously, in the case of complex reactions, several successive steps necessarily occur via one or other mechanism, thus giving rise to the complex reaction pathway. For example, in the case of selective oxidation reactions over metal oxide catalysts, the so-called Mars–van Krevelen or redox mechanism [1566] is widely accepted to occur. According to this mechanism, the oxidized surface of a catalyst oxidizes the reactant, while the catalyst is re-oxidized by O₂ from the gas phase in a separate step (Rideal-type mechanism). In this case, several successive steps or parallel steps give rise to the products.

Boreskov, Sokolovski and Davydov and their co-workers (see, for example, [30, 94, 311, 1567–1570] and references therein) have shown that catalytic oxidation reactions on solid catalysts proceed via two types of mechanism, i.e. a stepwise mechanism Rideal (Mars–van Krevelen) with an alternating oxidation–reduction of the catalyst surface by the reagents, or an associative (non-stepwise, concerted or ‘push–pull’)–Langmuir–Hinshelwood mechanism in which the reaction of oxygen with the catalyst and the formation of the reaction products take place simultaneously in the presence of both reagents. According to the Boreskov’s terminology, when the reaction rate in a pulse of reactant mixture differs from those associated with individual reactants, a concerted mechanism is present; in the opposite case, the mechanism is stepwise. The question about which type of reaction mechanism – concerted or stepwise – is present may be resolved by the use of pulse-flow equipment with chromatographic analysis of the reagents, for example, by a comparison of the degrees of conversion (yields of products) or by a comparison of the conversion rates for the separate components and the reaction mixture.

It has been established that even reactions of the same type, for example, an oxidation reaction, producing the same products, can proceed by different ways, depending on the experimental conditions. Detailed studies over a wide temperature range of the oxidation of hydrogen or carbon monoxide [94, 1567–1570], the water-gas shift (WGS) reaction [30, 94, 311] and the full oxidation of hydrocarbons [1571–1574] showed that there are two regions with different mechanisms, i.e. (i) a low-temperature region in which the process proceeds mainly according to the concerted mechanism, and (ii) a high-temperature region corresponding to a stepwise oxidation–reduction mechanism. The reaction pathway may be changed at different temperatures. At high temperatures, when the stepwise mechanism is realized, the steady-state rate of catalysis and the rates of the separate interactions of the reactants (hydrogen, carbon monoxide, hydrocarbons, etc.) with

oxygen were found to coincide, as expected for the redox reaction scheme. In the low-temperature region, a concerted mechanism of catalytic oxidation was found. The rate of catalysis in the latter case was considerably greater than the separately measured rates of oxidation and reduction on the steady-state catalyst, and the activation energies of the catalytic reactions were lower. However, it is clear that at the molecular level the mechanism can be understood only with the use of physical methods. Such understandings of the mechanisms give the possibility of deciding upon the heterogeneous catalytic process for the preferred product, e.g. to change the character of activation of the reacting molecules, or to change the strength of the bond between an intermediate and the surface (directions and rates of transformation of the intermediate species).

6.1 Reactions involving carbon monoxide

In studies on heterogeneous catalysis, much attention has been paid to reactions involving carbon monoxide. As has been shown earlier, IR spectroscopy can be used to obtain important information on the nature of adsorption of this simple molecule. The interactions of metal oxides, containing coordinately unsaturated metal ions, oxygen ions and OH groups, with carbon monoxide can produce different types of complexes (see Chapter 2).

Carbonyl-like surface compounds correspond to a reversible form of carbon monoxide adsorption. The strength of the bond between the carbon monoxide molecule and the surface site depends on the valence and coordinate state of the adsorption center and, for transition-metal oxides, reflects the participation of d-shells in the binding of CO.

The reaction of CO with oxygen atoms on metal oxide surfaces can lead to the formation of carbonate–carboxylate compounds. The strength of bonding of these compounds to the surface depends on the strength of the M–O bond within the oxide surface.

Hydroxyl groups on the surface of metal oxides react with CO to yield surface formates. The strength of bonding of these surface formates depends on the strength of bonding of the participating surface hydroxyl groups.

Surface carbonate–carboxylate species, and the majority of formate derivatives, decompose to yield CO₂, i.e. they are irreversible forms of adsorption of carbon monoxide. Below, we shall consider the results of spectroscopic investigations of reaction mechanisms involving CO. By using different examples, the roles of the surface compounds detected by spectroscopic methods can be analyzed.

6.1.1 THE OXIDATION OF CARBON MONOXIDE

There is no necessity to examine here the data concerning the mechanism of CO oxidation in detail. This has been investigated for many years and practically all of the problems have been discussed in the text of Bielanski and Haber [82], plus the aim of this present chapter is to analyze the role of surface intermediates revealed by spectral methods. However, it should be noted that recently the interest in studying the oxidation of CO on oxide surfaces has diminished because of the previous success that has been achieved. It is clear that the methods of molecular spectroscopy play a significant role in the solution of such problems. The largest amount of information about the role of surface compounds in CO oxidation has been obtained in the studies by A. A. Davydov *et al.* [30]. Investigating the rates of transformations of surface species by means of IR spectroscopy, and comparing these with those of the yield of CO₂, has shown that (i) the carbonate–carboxylate compounds are intermediate surface complexes, and (ii) there are both low- and high-temperature regions, where the reactions proceed mainly via concerted or stepwise redox mechanisms, respectively [1567–1570].

An investigation of the catalytic activity, for example, of chromium oxide in the oxidation reaction [1567] shows that at all pressures employed and at temperatures below 573 K the rate

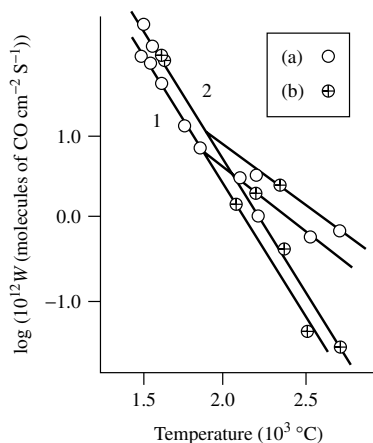


Figure 6.1. Arrhenius plots for (a) the rate of catalysis, and (b) the rate of reduction of the stationary catalyst: (1) 6 mm Hg; (2) 12 mm Hg.

of catalysis is higher than the rate of reduction of the stationary catalyst. The reaction activation energy under these conditions is significantly less than that of the reduction. At ca. 573 K, the Arrhenius relationship for the reaction rate shows a characteristic bend (Figure 6.1), while at higher temperatures the activation energies for the catalysis and for the reduction coincide. IR spectroscopic studies allowed the determination of the nature of the mechanisms and of the separate reaction steps proceeding on the surfaces of numerous oxides.

The results of infrared spectroscopic studies of the adsorption of oxygen, carbon monoxide, and carbon dioxide, and mixtures of carbon monoxide with oxygen, on the oxidized and reduced surfaces of chromium oxide at different temperatures [1575] indicate that at temperatures between 473 and 700 K during the reaction between the catalyst and the CO + O₂ mixture a dissociative chemisorption of oxygen takes place, leading to the appearance of surface metal oxide (MO) groups which differ in their reactivities. The dissociative chemisorption of oxygen readily occurs on reduced surfaces, even at temperatures below the reaction temperature. This shows the adsorption of oxygen is not the limiting stage, a fact that has also been confirmed by kinetic measurements. Hence, the rate of the oxidation reaction of carbon monoxide is independent of the pressure of oxygen [1576]. Adsorbed oxygen species of different reactivities interact with CO to yield various carbonate compounds that are relatively strongly bound to the surface. The effect of oxygen from the gas phase on the rate of decomposition of these carbonates, revealed by Davydov *et al.* [1575], showed that such carbonates, in spite of their strong thermal stabilities, can be intermediates in the CO oxidation reaction even at low temperatures.

For a great number of ‘complete-oxidation’ catalysts, IR spectroscopic studies have revealed the formation of surface species of the carbonate–formate–carboxylate type during the interaction of the reagent to be oxidized with the catalyst itself [30]. These species are formed even at low temperatures and can be quite stable on the catalyst surfaces under vacuum or an inert atmosphere. However, these surface-oxidized species are rapidly decomposed under the influence of oxygen, producing CO₂ (see, for example, for carbonates, Figure 6.2).

The rates of decomposition of surface carbonates and the catalytic oxidation of carbon monoxide have been measured under identical conditions for several systems [1567–1569]. The rates were found to be close, which confirms the participation of the surface species as intermediates in the catalytic reaction (see, for example, for ZnO Figure 6.3 and Table 6.1). It has also been shown that decomposition of the carbonates proceeds because oxidation (by oxygen) of the metal

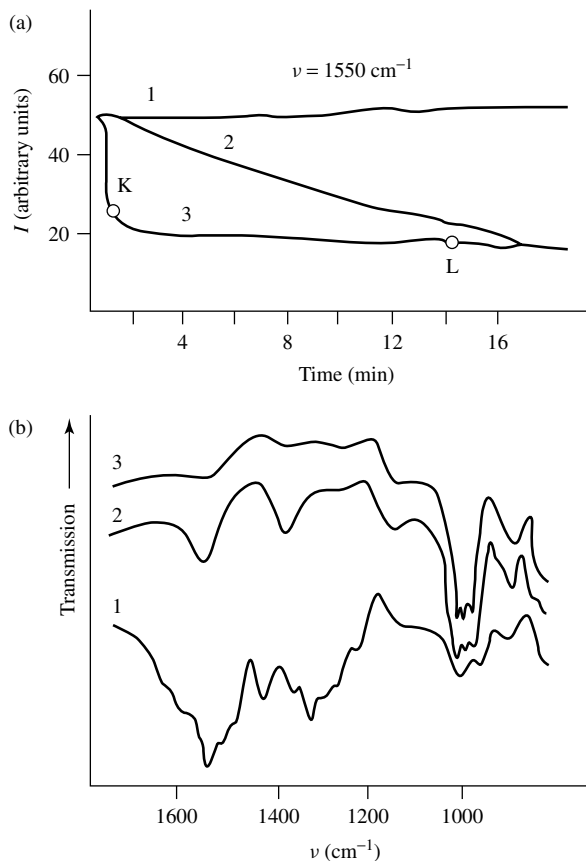


Figure 6.2. Desorption of surface compounds from chromium oxide at 423 K. (a) Desorption kinetics of the surface carbonate characterized by a band at 1550 cm^{-1} : (1) on admission of carbon monoxide; (2) *in vacuo*; (3) on admission of oxygen. (b) Infrared spectra of surface carbonates: (1) initial spectrum following reaction with carbon monoxide at 423 K; (2) spectrum at the K point; (3) spectrum at the L point.

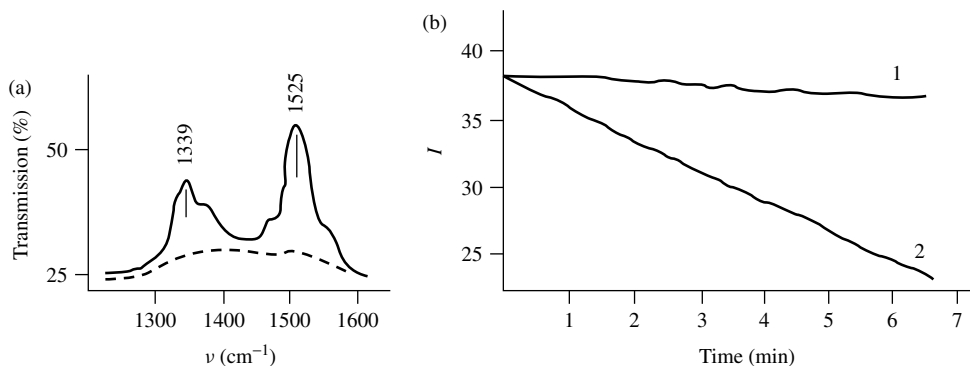
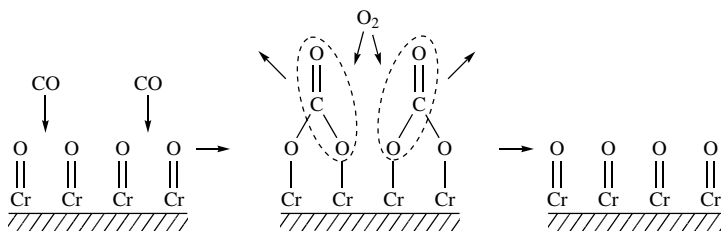


Figure 6.3. (a) Infrared spectrum of carbon monoxide adsorbed at 423 K on ZnO (the dashed trace represents the background spectrum); (b) decomposition of surface carbonates (1) *in vacuo*, and (2) and in oxygen (I is the intensity, in arbitrary units, of the signal at 1335 cm^{-1}).

Table 6.1. Comparison of the rates of CO oxidation and conversion of surface intermediates $[\text{CO}_3]$ and $[\text{O}_2^-]$ on various zinc oxide samples.

Sample	T (K)	W (molecules of O_2 cm^{-2} s^{-1})	$[\text{CO}_3]$ ($0.5 \times \text{cm}^{-2}$ s^{-1})	$[\text{O}_2^-]$ (cm^{-2} s^{-1})
ZnO (I)	423	0.5×10^{10}	0.7×10^{10}	—
ZnO (II)	373	1.2×10^9	—	1.6×10^9
ZnO (III)	373	0.7×10^9	0.8×10^9	0.5×10^9

ions is reduced as a result of the formation of carbonates on the catalyst surfaces. A mechanism for the process has been proposed, with its salient feature being the concerted catalyst oxidation and decomposition of carbonate species at low temperatures:

**Scheme 6.1**

At high temperatures, the decomposition of carboxylate surface species can be quite fast, even in the absence of oxygen in the gas phase.

These results show that the concerted mechanism of oxidation of carbon monoxide involves the formation of surface compounds of the carbonate–carboxylate type, followed by the decomposition of these compounds by molecular oxygen.

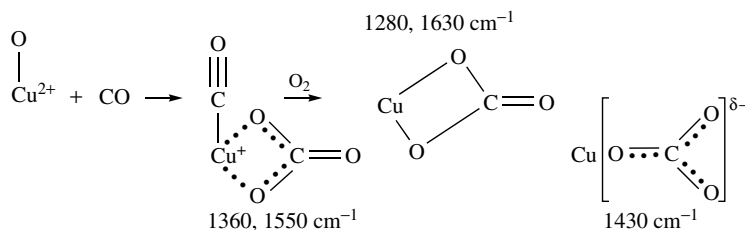
A comparison of IR spectroscopic and catalytic results showed that the transition of the concerted mechanism into a stepwise mechanism at higher temperatures is due to a sharp decrease in the concentration of the surface intermediate structures on the surfaces of the catalysts. At temperatures above 573 K, the surfaces of the catalysts are almost free of carbonate structures. In the same temperature range, changes occur in the temperature-dependence of the reaction rate. The oxidation of carbon monoxide involves, in this case, oxygen from the catalyst surface without the direct participation of oxygen in the gas phase.

The study of CO oxidation on ZnO by means of spectroscopic methods (IR and ESR) [1568] exposed the nature of the action of oxygen on the increases in the decomposition rates of the carbonates. It has been established that this proceeds because of a concerted process of oxidation and reduction of the type shown in Scheme 6.1. It was shown by means of ESR that the decomposition of carbonates and oxidation of the surface occurs through O_2^- ions, the rate of decomposition of which is similar to that of carbonate decomposition, as well as to the reaction rate (Table 6.1) – the so-called conjunction mechanism [30].

The transition of the concerted mechanism to the stepwise mechanism, and the nature of the latter, in the case of ZnO are similar to those obtained for Cr_2O_3 . By independent studies, it has been established that the irreversible adsorption of CO at room temperature (carbonates) causes the surface to become unsaturated with respect to the adsorption of oxygen [1576, 1577].

The above conclusions were drawn from the results obtained when the reaction proceeded under static conditions. Later detailed investigations of this reaction *in situ* have been made by using a flow reactor-cell [1578]. For Cr_2O_3 , the results obtained were fully analogous to those obtained

under static conditions and supported the conclusion that the carbonates are intermediates in this reaction. The decomposition rates of the surface carbonates, measured by means of spectroscopic methods, and the rates of product formation (CO_2) were the same. These rates were also the same during CO oxidation over CuO [1579]. These data confirm Gardner's assumption, made on the basis of calorimetric measurements [1577], that carbonates are intermediates in the low-temperature oxidation of CO on CuO. However, no direct effect of oxygen on the stabilities of surface carbonates has been observed on CuO, unlike the cases of chromium and zinc oxides. In the relevant spectral region, the appearance of carbonates at high temperatures with the production of CO_2 was observed. It should be noted that in O_2 (under dynamic as well as static conditions) changes are observed in the spectra of the carbonates: the formation of the 'usual' carbonates (due to interaction of CO with CuO), in addition to 'new' carbonates, was seen (under flow conditions), or rearrangements (under static conditions), characterized by the bands at 1430, 1280 and 1630 cm^{-1} could be observed. These processes can be represented as follows, from consideration of the data of Courtois and Techner [1580]:



Scheme 6.2

In the presence of excess oxygen, the carbonyl complexes are oxidized, and the possibility arises of the carbonates not competing with the carbonyls for coordination on the copper ions, i.e. 'pre-oxidation' of the carbonates by oxygen takes place. The appearance of new carbonates could also be due to the fact that other forms of surface oxygen participate in the reaction with an increase in reaction temperature.

The role of carbonyl-like complexes is not discussed in detail here because it has been discussed in detail earlier and it follows from the scheme that their formation represents an initial stage of the complexing of CO – intermediate to the formation of surface carbonates [30]. Carbonyls can also be intermediates in the transformation of CO to CO_2 on supported metals [1581].

The fact that the reaction of CO oxidation proceeds via the two above-examined mechanisms has been established for practically all transition-metal oxides [94, 1582]. This gives the expectation that the detailed steps established for a number of oxides by means of spectroscopic techniques may be common to other systems. Thus, the formation of carbonates are observed on the surfaces of the majority of oxides during interaction with CO and is accompanied by reduction of the oxides. In the following stage of the interaction with oxygen, the surface is re-oxidized and CO_2 is released. As has been shown in Chapter 2 (Section 2.3.2), the stabilities of the surface carbonates on different oxides depend on the energies of the M–O surface bonds and decrease in parallel with the latter. For numerous oxides, the temperatures of transformation from a concerted to a stepwise mechanism can be explained by the stabilities of the surface carbonates; these decrease for oxides with low M–O bond strengths.

On most transition-metal oxides, hydrogen oxidation occurs via a stepwise mechanism in the middle temperature region [82, 94]. Infrared investigation of the separate stages of the low-temperature mechanism of H_2 oxidation on ZnO [1583] showed that the stage for production of

water from the surface hydroxyl groups, resulting from the dissociative adsorption of hydrogen on the oxidized surface of ZnO, proceeds easily. Considering the results from hydrogen adsorption over ZnO [1584], it seems to be reasonable to suppose that the formation of Zn–H–Zn or (giving bands at 3475 and 3400 cm^{-1} species $\text{ZnO}-\text{H}\cdots\text{O}^{2-}$), accompanied by a change in the electrical conductivity, constitutes a stage in the formation of active intermediates. Moreover, the formation of these compounds and the change in the conductivity perhaps assist the electron transfer to the oxygen atom obtained from the gas phase during the reoxidation process.

6.1.2 THE WATER-GAS SHIFT REACTION

The interest in this reaction has grown significantly in recent years because of the increasing requirements for the production of hydrogen. A considerable increase in the number of studies concerning this problem has occurred in comparison with those published in the 1980s (see, for example, [1585–1591]).

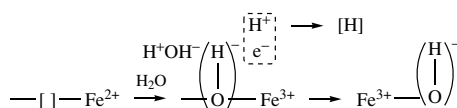
Usually, this reaction proceeds on different catalysts at different temperatures (low-, high- and middle-temperature conversions). It is clear, that the low-temperature conversion is more interesting [30, 311, 802, 1585, 1592, 1593]. The methods of vibration spectroscopy are very useful in investigating the mechanisms of the reactions, as well as the nature of the active components (together with UV–Vis spectroscopy [30, 802]), and the reasons for the reaction proceeding at different temperatures. Decision on these questions indicate the differences in such types of catalysts and the creation of new low- and middle-temperature-type catalysts that can function via different mechanisms, in different temperature ranges. Thus, in the case of iron- and iron–chromium oxide (industrially used catalysts), a stepwise mechanism involving a separate interaction between CO and the oxygen of the catalyst to produce CO_2 , and an oxidation of the surface by water vapor with the formation of hydrogen [1592], has been shown by kinetic investigations. The fact that CO conversion on such catalysts proceeds via the stepwise mechanism has been proven by comparison of the rates of both the oxidation and reduction stages. In the steady state, these rates were equal to that of the water-gas shift reaction.

In the cases of MgO, Cr_2O_3 , CuCr_2O_4 and a solid solution of copper in magnesium oxide [311, 1593], the rates of reduction are significantly lower than the reaction rate, and the formation of hydrogen does not occur directly as a result of the interaction with water. Another mechanism, ‘stepwise’, is realized on these catalysts. The results obtained suggest that on iron–chromium oxides the conversion is mediated by an alternating oxidation and reduction of the surface, as proposed by Kul’kova and Temkin [1592]. On other catalysts, the reaction proceeds according to a concerted mechanism, involving a complex including both reacting molecules.

Detailed investigations by IR spectroscopy of the interactions of surfaces of such catalysts with molecules of CO and H_2O , and their mixtures, revealed the different character of the interaction of these molecules with different groups of catalysts and established the nature of the separate stages of these mechanisms [311, 1594, 1595].

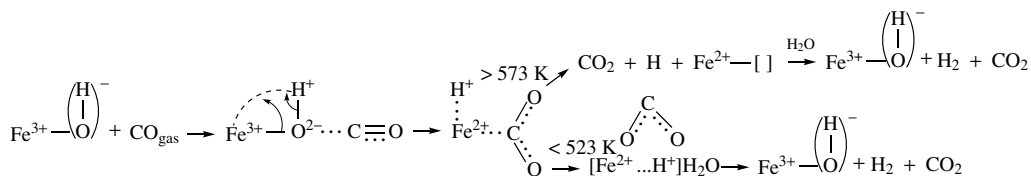
High-temperature catalysts

On interaction with water, the oxidation of the steady-state surfaces of iron- and iron–chromium oxide catalysts leads to the formation of OH groups and to a change in the oxidation state of the Fe according to the following scheme [1594]:



Scheme 6.3

The change in transmission of the sample upon interaction with water reflected this change. When the interaction occurs between the reduced catalyst surface and water, the transformation of Fe^{2+} to Fe^{3+} makes possible the hydrogen separation as shown in Scheme 6.3. The interaction with carbon monoxide leads to the reduction of the catalyst surface through the interaction with surface oxygen. The interaction of CO with the iron–chromium catalyst may be represented by the following scheme:



Scheme 6.4

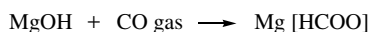
It follows from this scheme that the process of decomposition of oxidized complexes of CO (carboxylate type) may occur at high temperature ($> 573 \text{ K}$) and leads to separation of both H_2 and CO_2 . Under these conditions, the stepwise mechanism is realized.

Middle-temperature catalysts

Catalysts like MgO , ZnO and Cr_2O_3 are typical examples of middle-temperature catalysts and are mostly investigated by spectral methods, sometimes *in situ*, as in the studies of Ueno *et al.* (ZnO and MgO) [1596] and Davydov *et al.* (MgO and Cr_2O_3) [311]. An interesting feature has been revealed during investigations of the reaction mechanisms on such catalysts. It was found that in such cases a concerted mechanism occurs [311], unlike, for example, with the Fe–Cr catalyst where the reaction occurs by a stepwise mechanism. The nature of the concerted mechanism has been established by means of IR spectroscopy [311, 1594, 1595], taking into consideration earlier data obtained and reviewed by Tamaru [21], who showed that formates are intermediates in the reaction over MgO and ZnO . In the majority of IR spectroscopic studies of the water-gas shift reaction, the formation of formate groups, in addition to other carbonyl-like groups of various types, has been observed on the surfaces of the catalysts.

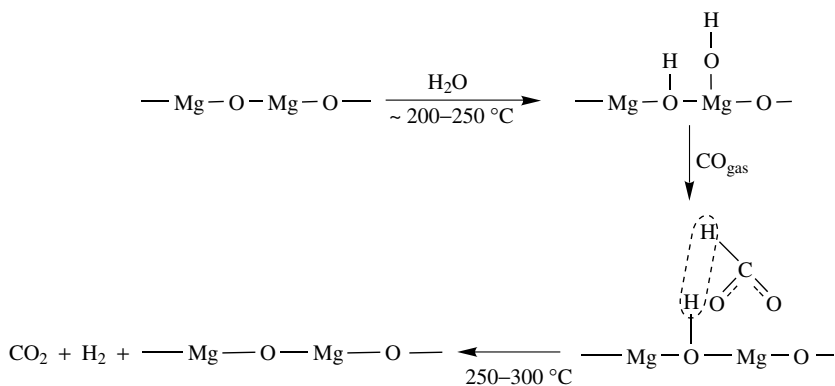
MgO

Following Tamaru [21], Davydov *et al.* [311] have shown that in the shift reaction over MgO at 523 K and above, water is adsorbed via dissociation, with the formation of two types of hydroxyl groups, characterized by IR bands at 3620 and 3760 cm^{-1} . The reaction of CO with the MgO surface containing hydroxyl groups takes place only at temperatures above 373 K, resulting in the formation of formate complexes. During the course of the reaction the intensity of the absorption bands due to surface hydroxyl groups and the concentration of CO in the gas phase decrease. This indicates that the following reaction takes place:



Scheme 6.5

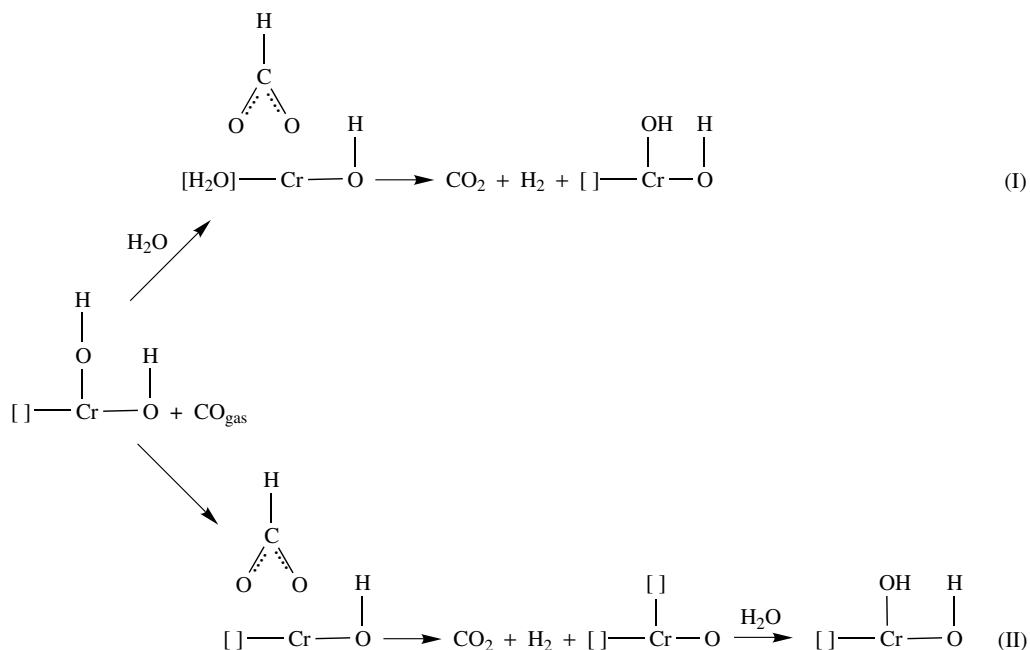
Two types of formates, characterized by maxima at 1340 and 1390 ($\nu_s\text{COO}^-$), 1620 and 1585 ($\nu_{as}\text{COO}^-$) and 2760 and 2840 (νCH) cm^{-1} are detected on the catalyst surface, in accordance with the indicated two types of surface hydroxyl groups. Davydov *et al.* [311] have specified that the formation of formates on MgO occurs from gaseous carbon monoxide reacting with surface hydroxyl groups. This reaction at appropriate temperatures indicates that formates are intermediates in the shift reaction. This has been confirmed [21, 1596] by direct IR measurements of the decomposition rates of formate compounds (limiting step of the reaction) on MgO and by the fact that these rates were equal to that of the shift reaction. Later [1595], this mechanism was confirmed for both types of formates. No adsorption of CO molecules on magnesium cations has been observed in the case of the hydroxylated surface of MgO. The reaction of CO_{gas} with the OH group of the surface MgO takes place only at elevated temperatures (ca. 473 K) with the formation while formates, while the decomposition of such formates with the evolution of CO_2 begins at 573 K without any acceleration in the presence of water vapor. The overall shift reaction over MgO can be described as follows:



Scheme 6.6

Cr_2O_3

Two types of OD groups are formed in the reaction of D_2O with the chromium oxide surface [311, 1594]. The OD groups are characterized by IR bands at 2670 and 2720 cm^{-1} due to OD stretching vibrations. If the degree of reduction corresponds to steady-state conditions, the adsorption of CO on a surface treated with H_2O or D_2O at 473 K and higher proceeds with the formation of two types of formate complexes, characterized by absorption bands at 1360, 1390, 1565 and 1600 cm^{-1} (νCO vibrations) and at 2890 and 2975 cm^{-1} (νCH vibrations). The intensities of the absorption bands due to OH or OD groups decrease simultaneously. The formation of formate complexes on Cr_2O_3 once again seems to take place via the reaction of surface OH groups with gaseous carbon monoxide and the reaction proceeds only at elevated temperatures. Spontaneous decomposition of the formate complexes in the presence of CO begins at 623 K (path II, Scheme 6.7), whereas in the presence of water the decomposition occurs even at 373 K and yields CO_2 (path I). A decrease in the decomposition temperature of the formate complexes is due to their reaction with H_2O . The introduction of the water molecules into the coordination sphere of the chromium atom seems to be possible on coordinatively unsaturated chromium ions. When the reaction is carried out in the presence of an excess of water vapor, a complex is apparently formed which includes both formate ions and coordinated water molecules:


Scheme 6.7

In this process, the conversion of the formate complex into CO_2 and H_2 proceeds mainly through interaction with adsorbed water molecule via path (I). Thus, for chromium oxide there is a more highly organized mechanism than is the case for MgO , with the dissociation of the water molecule and the decomposition of the formate complex occurring in a single stage. The cleavage of the bonds in the formate complex is compensated by the formation of new Cr-OH bonds. Apparently, for this reason the rate of the shift reaction over chromium oxide is faster than on magnesium oxide. When the reaction proceeds via path (I) in the presence of Cr_2O_3 , the formation of the formate complex, which requires higher temperatures (473 K and above), can be the most difficult stage. At low partial pressures of water vapor and high temperatures, the catalytic reaction may proceed via pathway (II), as in the case of MgO .

ZnO

On this oxide at 500 K, the rate of decomposition of the surface formates is equal to the rate of evolution of H_2O and CO into the gas phase on the hydrogenation of the CO_2 [21].

Low-temperature catalysts

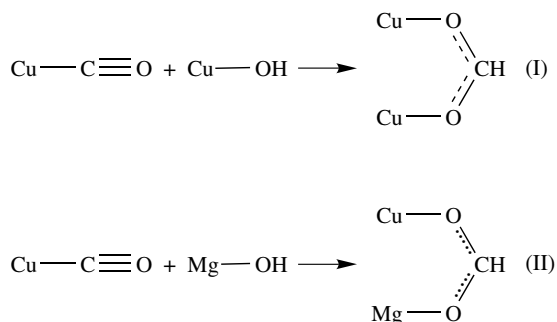
Earlier [30, 311, 1594, 1595], it was established that those oxide systems on which carbonyl-like compounds are easily formed are low-temperature catalysts. Here, the formation of carbonyl-like compounds (with a loosened CO bond as compared with that in the gas phase) appears to represent an intermediate stage on the path to formate formation via the mechanism established by Davydov *et al.* [30, 311, 1594, 1595]. Copper-containing catalysts, including CuO-MgO and CuCr_2O_4 on which, as has been shown by Davydov *et al.* [311, 1594, 1595], the reaction does not proceed via the stepwise mechanism, are such active low-temperature catalysts. The detailed scheme of

this reaction mechanism has been revealed by means of infrared spectroscopic studies [30, 311, 1594 1595].

CuO–MgO

When carbon monoxide interacts at 293 K with the surface of CuO–MgO (20 wt % Cu) [311, 1594, 1595] at the degree of adsorption that can give rise to the steady-state reaction, two types of carbonyl compounds are formed, characterized by maxima at 2110 and 2140 cm^{-1} . During the simultaneous adsorption of CO and H₂O, these maxima are shifted to 2090 and 2125 cm^{-1} , respectively (Figure 6.4, spectra 2). A decrease in the frequencies of the νCO vibrations of the surface carbonyls can be explained by the donor effect of the water molecule, adsorbed on copper ions, or by the hydrogen-bonding in H₂O molecules to an oxygen ion which is in the vicinity of a copper ion.

Since water is adsorbed on the surface of CuO–MgO as hydroxyl groups bound to both copper and magnesium atoms [1595], the reaction with adsorbed CO can result in the formation of two types of formate complexes, with one type being stabilized on two copper cations (I) and the other bound to both copper and magnesium ions (II):



Scheme 6.8

These reactions have been detected via the simultaneous decrease of the intensities of copper carbonyl complexes and the increase of those of formates [311, 1595].

During the reaction at 293 K between a CO + H₂O mixture and the surface of CuO–MgO, infrared bands due to formate species appear at 1400 cm^{-1} ($\nu_s\text{COO}^-$), 1540 cm^{-1} ($\nu_{as}\text{COO}^-$) (Figure 6.4), 2870 cm^{-1} (νCH) and 2050 cm^{-1} (νCD when the mixture of CO and D₂O is used) (Figure 6.4 spectra 3). Since formate complexes giving bands at the same spectral positions are not observed over the CuO–MgO surface which is free of copper-bound hydroxyl groups, these ions may be considered to be due to formate complexes of type I. At 373–423 K, these formate complexes decompose. A decrease in intensities of the 1400 and 1540 cm^{-1} bands make it possible to identify the 1350 and 1600 cm^{-1} bands (Figure 6.4, spectra 3), characteristic of the second formate complex. This is formed at 293 K during the reaction of copper carbonyl with the surface hydroxyl groups held by magnesium ions (type II), and this formate decomposes at 473 K. The difference in the decomposition temperatures of the two types of formate which are produced is due to the low activity of isolated ions and the high activity of copper ion pairs or larger associates in the CO shift reaction [802].

Measurements of the decomposition rates of formates on CuO–MgO at 523 K, and comparison of the rates with those for MgO alone [1595], show that for the solid solution the decomposition

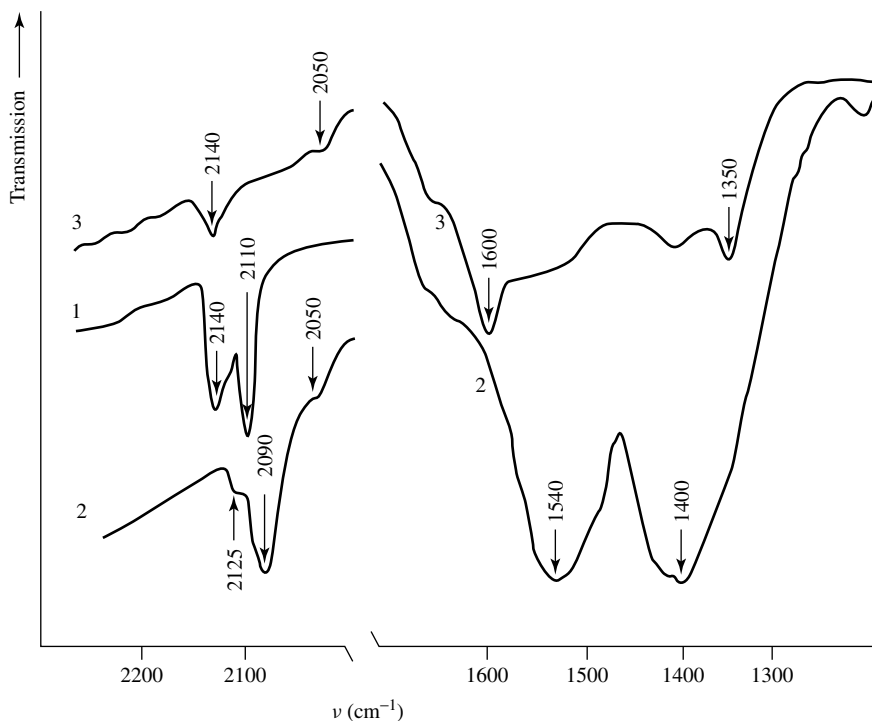


Figure 6.4. Infrared spectra of CO and CO + D₂O mixtures adsorbed on CuO–MgO: (1) CO (10 mm Hg), at 293 K; (2) CO (10 mmHg) plus D₂O 10 mmHg at 293 K; (3) mixture at 423 K.

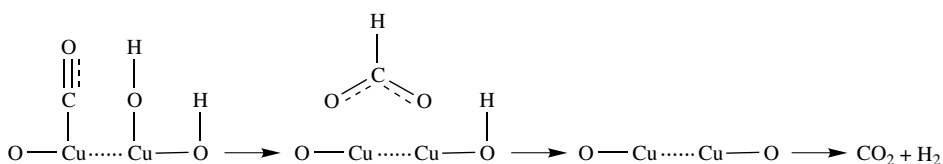
rate of the formates is faster than for MgO alone by approximately three orders of magnitude. This is in agreement with data obtained from catalytic measurements which indicated that the rate of the water-gas shift reaction over CuO–MgO is higher than that of MgO by three to four orders of magnitude. Hence, the shift reaction over a CuO–MgO catalyst proceeds via formate complexes which are produced through the reaction of adsorbed CO on copper ions and water molecules in the form of carbonyl complexes and hydroxyl groups, respectively. The fact that formate complexes are readily converted into CO₂ and H₂ (their decomposition begins at 372 K) ensures a high conversion rate of CO on a CuO–MgO catalyst.

CuCr₂O₄

In contrast to chromium oxide, but similar to CuO–MgO, the adsorption of carbon monoxide on copper chromite at 293 K results in the formation of carbonyl complexes involving Cu⁺ ions (νCO at 2140 cm^{-1}) [311]. In the presence of water, a shift of this band has been observed up to 2120 cm^{-1} , in addition to the appearance of bands with maxima at 1380 and 1560 cm^{-1} which are characteristic of formate complexes. With time, the intensities of the νCO bands in the carbonyl complex diminish, and simultaneously the intensities of the bands due to the formate complex increase. The decomposition of the formates takes place at 423 K.

Hence, on copper chromite and on CuO–MgO there is an activation, not only of the water molecules but also of carbon monoxide, which is not the case for MgO or Cr₂O₃. The presence of surface copper carbonyls with a weakened C–O bond and hydroxyl groups held by copper ions ensures the formation of copper formate complexes even at room temperature. Their

decomposition into CO_2 and H_2 proceeds more readily than on chromium and magnesium oxides. The mechanism of the water-gas shift reaction on copper-containing catalysts can be formulated as follows:



Scheme 6.9

On high-active CuO-MgO and $\text{Cu Cr}_2 \text{O}_4$ catalysts, the reaction proceeds via the Langmuir-Hinshelwood mechanism involving adsorption complexes including both reacting molecules. When considering such mechanism of the water-gas shift reaction, one can identify the following stages: activation of CO and H_2O molecules, their reaction leading to the formation of an intermediate compound, and its subsequent decomposition to form the final products. One should bear in mind the basic difference of this mechanism from the stepwise mechanism on iron-chromium catalysts. In the latter case, the bonds in the molecules become rearranged separately during the reaction so that each stage leads to the formation of one of the reaction products. In this process, the valency of the surface cations changes. In the case of $\text{Cu Cr}_2 \text{O}_4$ and CuO-MgO catalysts, such rearrangements of bonds cannot take place separately. Both of the reacting molecules give the activated complex, and in this complex the redistribution of the electron density and extensive rearrangement, result in the formation of the final reaction products.

On chromium and magnesium oxides, as a result of the reaction of the surface OH groups with gaseous CO , relatively stable formate complexes are also formed at high temperatures. These complexes decompose at a noticeable rate, yielding CO_2 and H_2 at 523–573 K. On chromium oxide catalysts, owing to the high coordinative unsaturation of surface Cr^{3+} cations, an energetically more favorable decomposition of the formate complexes becomes possible through their reaction with water (concerted mechanism). As a result, the rate of decomposition increases in comparison with the reaction on MgO (but not in comparison with that on CuO-MgO catalysts).

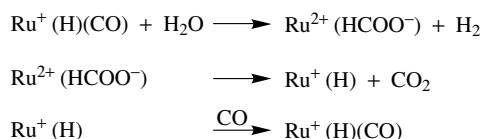
On highly active copper-containing catalysts, owing to the capability of copper ions to adsorb water and carbon monoxide, the latter as carbonyl complexes with loosened C-O bonds, unstable copper formates are formed even at room temperature. Their decomposition into CO_2 and H_2 at a noticeable reaction rate takes place at 373–423 K. Therefore, high reaction rates of the carbon monoxide shift reaction over copper-containing catalysts can be achieved by lowering the activation barrier for both the formation and decomposition of the formate complexes. These reaction rates are due to two peculiar features of copper ions – the ability of Cu^+ to produce carbonyl complexes with weakened C-O bonds, which lowers the activation barrier for the formation of formates in comparison with MgO and Cr_2O_3 catalysts, and the low stabilities of the surface formate complexes containing copper cations. Differences in the nature of the cations (copper, unlike magnesium) have a decisive effect on the formation and stability of the bond between the intermediate compound (formate) and the catalyst surface and, consequently, on the catalytic activity in the water-gas shift reaction. The main difference between low- and high-temperature catalysts is the ability of the first to activate carbon monoxide by loosening of the C-O bond.

Other catalysts

Yakerson and co-workers [1597] have supported the above-represented mechanism, and following Davydov *et al.* [311, 1594, 1595] indicated that copper carbonyls can also participate in the

formation of formates on Cu–ZnO and Cu–ZnO–Al₂O₃ catalysts in the WGS reaction. The same conclusion was drawn later [1598–1600] for similar catalysts. The nature of the active component in such a catalyst appears to be especially interesting. In fact, surface copper carbonyls are needed in order for the reaction to proceed. Such carbonyls require a loosened CO bond in respect with that in gaseous CO. No doubt, the CO molecule is adsorbed on the copper. However, the degree of copper oxidation has been discussed for a long time. Infrared absorption studies of the CO probe molecule adsorbed on such catalysts [479], together with experiments specifically carried out *in situ* DRES showed that Cu⁺ (the band at around 17000 cm⁻¹) and not Cu⁰ sites are needed to reach the greatest activity and selectivity for this reaction [802].

A similar mechanism has been discussed for this reaction on Ru/NaY at 473–573 K, but the observed first-order kinetics with respect to P_{H₂O} exclude the participation of tightly bound OH groups in the reaction [1601]. An *in situ* study of the UV spectra allowed the valence state of the Ru to be determined: the result obtained led to the following reaction mechanism:



Scheme 6.10

Thus, the presence on the catalyst of easily but only partially reduced cations (which do not achieve the metallic state) during the reaction and which are also able to form carbonyl-like compounds with loosening of the CO bond is a distinguishing characteristic of low-temperature catalysts. Cations of Cu, Ag, Au, Rh and Ru in low oxidation states may form such complexes and be easily reduced to intermediate degrees of oxidation which allow us to recommend these cations as being active components for such catalysts.

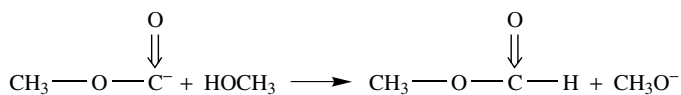
An FTIR study of the WGS reaction over Cu/ZnO and Cu/TiO₂ showed, however, that CO is adsorbed on metallic copper particles dispersed on two types of sites, i.e. the normal terrace sites and interfacial sites, and confirmed the role of copper carbonyl complexes in the formation of formates as intermediates in the WGS reaction for these catalysts also [1591].

Carbon monoxide and water co-adsorption experiments on gold-supported ZnO and TiO₂ [1591] showed the dissociative adsorption of water on both catalysts. Due to the different acidities of the supports, the mobile protons (H atoms) are produced on Au/ZnO, while on Au/TiO₂ only immobile OH groups are formed. Unfortunately, the rates of transformation of the surface species have not been measured in these studies.

6.1.3 CARBONIZATION AND HYDROFORMYLATION

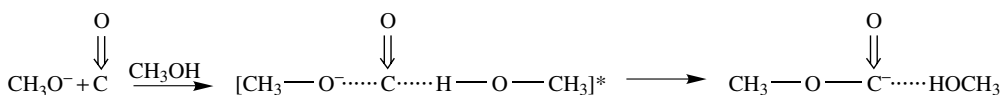
The reaction of CO with methanol in the presence of methoxyls of both alkali and alkaline-earth metals was discovered more than 150 years ago [1602], and there are many patents on this type of process. New data on carbonization and hydroformylation have been presented in a recently published review [1603]. Let us now briefly examine several studies involving spectroscopic investigations of these processes.

The formation of methyl formate during the reaction between methanol and CO in the presence of strong bases is examined as an example of this type of reaction, which includes a nucleophilic attack of the CO molecules by the base with the formation of a carbanion as an intermediate. The formed carbanion is unstable and easily accepts a proton:



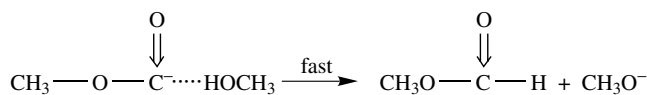
Scheme 6.11

It is probable that in the intermediate state the negative charge on the carbon atom of CO is insufficiently high for H^+ to be accepted by the carbanion. The methanol molecule, which according to the kinetic equation, participates in the rate-limiting stage, possibly only solvates, forming a carbanion by a hydrogen-bond to the originated unshared pair of the sp^2 orbital, thus stabilizing the carbanion and lowering the energy of the intermediate state of the reaction:



Scheme 6.12

The carbanion splits off a proton from CH_3OH in the following stage:



Scheme 6.13

It is not to be expected that the Na^+ ion, which polarizes the CO molecule and relieves the attack of CO by CH_3O^- , participates in the reaction of methanol hydroformylation. It has been shown that the methanol molecule adds to methoxyls to form methylcarbonate groups, $\text{CH}_3\text{O}[\text{COO}]^-$ [1604]. The formation of anionic compounds including CH_3O^- as well as the activation of CO on cations has already been illustrated above. So the reaction proceeding through the schemes proposed (6.11–6.13) is quite reasonable.

Hydrocarbons also undergo carbonization and hydroformylation. This was first demonstrated in the case of basic oxides such as BeO, MgO and ZnO. As was shown, olefins and aromatic hydrocarbons easily form carbanions on the surface (Section 5.2). Some studies pointed out the possibility of the carboxylation of such hydrocarbons (for example, toluene on Al_2O_3 or C_3H_6 on MgO). Since paraffins can be activated with formation of anions (Section 5.4), the formation of the carbonylated hydrocarbons from them in the presence of activated CO can take place. As shown in Figure 6.5, propane is already easily carbonized on MgO at room temperature. Most probably, the carbanion, C_3H_7^- , adds the CO group to form a carbonyl-containing surface compound. The appearance of the band at $1680\text{--}1700\text{ cm}^{-1}$ confirm this fact.

It is clear that surface carbonyl compounds play a significant role in this reaction as well as in the character of the hydrocarbon activation. Support for this comes from the type of catalysts, which as a rule, are noble metals supported on oxides, which easily form different carbonyls. For example, the active surface species and the reaction mechanism for the hydroformylation of ethene in the gas phase at 443 K as a $\text{C}_2\text{H}_4/\text{CO}/\text{H}_2$ (1:1:1) mixture over Co/SiO_2 , promoted with various noble metals, has been studied by using an *in situ* diffuse reflectance FTIR spectroscopic approach. The promoted Co/SiO_2 showed strong absorption bands of linear and bridged CO species and acyl species under the reaction conditions, thus suggesting that oxygenates were

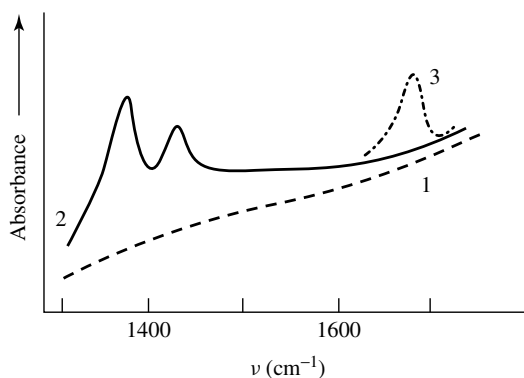
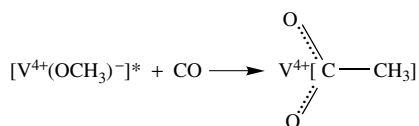


Figure 6.5. IR spectra of propane adsorbed (2) at 293 K on MgO dehydroxylated at 973 K, and (3) with CO pre-adsorbed at room temperature (trace (1) represents the background spectrum).

formed by CO insertion into the surface acyl species. The time-sequence in the changes of the IR bands during the reaction of pre-adsorbed CO with ethene/H₂ showed that linear CO species play a major role in this CO insertion. Although the Co/SiO₂ derived from Co²⁺ acetate was almost inactive in this reaction, promotion with Ir, Rh, Pt, Re, Ru or Pd compounds strikingly enhanced its activity and oxygenation selectivity [1605]. Supported metal carbonyls are used as carbonylating agents [1606]. The intermediate compounds of ethene hydroformylation are HRh(CO)_x in the case of supported Rh-carbonyl complexes and RhY zeolites.

Carbonization of methane has been observed during the photochemical radiation of a CH₄ + CO mixture in the presence of V/η-Al₂O₃, which occurs according to the following scheme [1607]:



Scheme 6.14

Ethene and CO interact [1608] at low pressures on a reduced Phillips catalyst to yield CO/C₂H₄ mixed complexes involving the most exposed type of Cr(II) cations (A type) (see Table 3.10). The Cr centers responsible for ethene polymerization form the most stable mixed complexes. At high pressure (≥ 40 torr) Cr_A(CO)C₂H₄ mixed complexes react with a second ethene molecule to yield a metallocyclohexanone species. After reaction, polymerization is prevented and Cr_A may be re-established in this way.

6.1.4 THE SYNTHESIS AND DECOMPOSITION OF ALCOHOLS

The synthesis of methanol and other lower alcohols from carbon monoxide or carbon dioxide and hydrogen occurs by different pathways and leads to different distribution of products over Zn–Cr or copper-based catalysts (Cu/ZnO, Cu/ZnO/Al₂O₃) and those containing metals of group VIII [1609, 1610]. As a model system for study of these reactions, zinc oxide is also often used. We will examine the spectroscopic data of the mechanism of alcohol synthesis/decomposition on Zn-containing catalysts.

Alcohols syntheses, as well as their decompositions, occur through a number of stages at equilibrium, and the same intermediates should be formed upon the interaction of either the reaction mixture or the reaction product with the catalyst surface. This is why, in order to establish an intermediate in alcohol syntheses over ZnO and Zn–Cr–K–O (the high-temperature alcohol synthesis catalyst which gives a good yield of higher alcohols) [1611], the decomposition of methanol, ethanol and isobutanol has been studied by infrared spectroscopy. Such a study showed that the interaction of methanol with the reduced catalyst surface produces a weakly bound form of the alcohol (hydrogen-bonded or coordinatively bound) and formaldehyde, as shown by the appearance in the spectrum of absorption bands at 2810 cm^{-1} , with a shoulder at $2760\text{--}2790\text{ cm}^{-1}$, and at 2930 cm^{-1} , with a shoulder at $2870\text{--}2890\text{ cm}^{-1}$ ($\nu_s\text{CH}_3$ and $\nu_{as}\text{CH}_3$), which are removed after vacuum treatment at $373\text{--}473\text{ K}$. In addition to the bands associated with the weakly bound alcohol, an intense band at $1070\text{--}1080\text{ cm}^{-1}$ has also been detected. On the basis of data on the interaction of methanol with chromium oxide and other oxide systems, this band has been assigned to surface methoxy groups. The νCH bands at $2860\text{--}2870$ and $2910\text{--}2940\text{ cm}^{-1}$, and the $\nu\text{C}\text{--}\text{O}$ bond at 1070 cm^{-1} , corresponding to the methoxy groups, can be observed only after removing the weakly bound alcohol (at 473 K).

Besides methoxy species on the oxidized surface, the formation of formates is observed even at room temperature, i.e. at this temperature methanol is already completely converted to alcoholates and formates. It has been established that the same types of surface compounds are also observed after adsorption of other alcohols (ethanol, isopropanol and isobutanol, with the formation of isopropyl, isobutyl and ethoxy groups). Furthermore, after adsorption of all of these alcohols (except methanol), the formation of carboxylates has been observed, together with formate species. Similar data were obtained on ZnO [1468] for the adsorption and conversion of methanol. In the case of methanol decomposition on silica-supported Cu, the mechanism has been investigated by means of infrared spectroscopy and TPD. Infrared spectra have revealed the following surface species: methanol, methoxy groups, formaldehyde, methylene bis(oxy) and formate groups [1623].

The HREELS method showed that the methanol decomposition reaction over ZrO_2 depends on the crystallographic orientation of the surface. On the (100) surface, methoxides are decomposed near 630 K to produce CO and CH_4 . In contrast, on the (110) surface the primary methoxide decomposition pathway is oxidation to produce CH_2O . This difference in activity can be related to the local atomic structures of the two surfaces [1613].

In the synthesis of alcohols on ZnO, an IR spectroscopic investigation of the $\text{H}_2 + \text{CO}$ interaction at room temperature showed that the centers adsorbing hydrogen and CO are formed of a triplet of exposed zinc ions and at least one reactive oxygen ion. These active groups of ions are mutually interacting and are grouped to form a two-dimensional array that is similar to a partly reconstructed (001) face [1584]. Since a surface zinc ion covalently bound to a hydrogen atom has a sufficient positive charge and a sufficiently low coordination it can polarize strongly one and/or two CO molecules. The second scheme, characterized by a Zn–H group closely interacting with two equivalent or nearly equivalent nearby zinc ions, is more strongly favored. Later, a more detailed scheme was proposed [1612].

When the dynamics of the adsorption and hydrogenation of CO on an active ZrO_2 catalyst was studied by the FTIR technique, four different types of coordinatively unsaturated surface sites were revealed. Carbon monoxide adsorption over ZrO_2 leads to the formation of various types of CO adsorption species having different activities towards hydrogen. These species also played a significant role in the hydrogenation of CO to form methane and methyl alcohol on this catalyst [1613].

The formation of carbonyl complexes, especially those involving a loosening of the $\text{C}=\text{O}$ bond is needed in order for the reactions of CO hydrogenation and formation of surface methoxyls from carbonyls to take place. Over zinc–chromium catalysts, no formation of such carbonyls is

observed. They are detected only over ZnO–ZnCr₂O₄ upon reduction (the band at 2100 cm⁻¹ corresponding to ν CO in a Zn^{δ+}-CO complex). As has been shown by separate experiments, a stronger reducibility is characteristic of the Zn–Cr–K–O catalyst [193, 1614]. This leads to the formation of carbonyl complexes with greater degrees of loosening of the bonds, which probably assists the hydrogenation of carbonyl to methoxyl. If a catalytic system is more readily reducible, the synthesis of alcohols proceeds more easily.

According to IRS studies [1598–1600, 1615–1619], the characteristic feature of catalysts for this reaction is the presence on their surfaces of reduced centers which activate the CO molecules via the loosening of the CO bond, similar to that obtained in the case of the water-gas shift reaction. For example, in methanol synthesis the Cu–ZnO and Cu–Zn–Al₂O₃ systems are the most generally used. Numerous data show that the synthesis reaction occurs with the participation of carbonyls, which are more easily hydrogenated (probably due to the loosening of the C≡O bond), with the formation of formate species and/or methoxyls. These surface species are observed during both the synthesis and decomposition of alcohols on all of the catalysts used.

The state of the active component in such catalysts has been discussed before (Chapters 2 and 3). It is clear that in the case of Cu-containing catalysts, the degree of oxidation of the reduced copper is still under discussion. Some authors believe that Cu⁺ ions are the active component, whereas others conclude that the active component is highly dispersed Cu⁰. As has been shown in Chapter 3, when copper in such catalysts is in a state closer to Cu⁺ than to Cu⁰ (Cu^{δ+}) the effective charge of such a copper ion is lowered. This is perhaps the main characteristic of the alcohol synthesis catalysts. Carbonyl complexes formed with the participation of such copper ions undergo hydrogenation to alcohols. In contrast, in the case of hydrocarbon synthesis occurring on the metal particles CO dissociation takes place with the formation of M–C fragments, which then are hydrogenated and polymerized to produce hydrocarbons. The latter process depends on the type of metal involved.

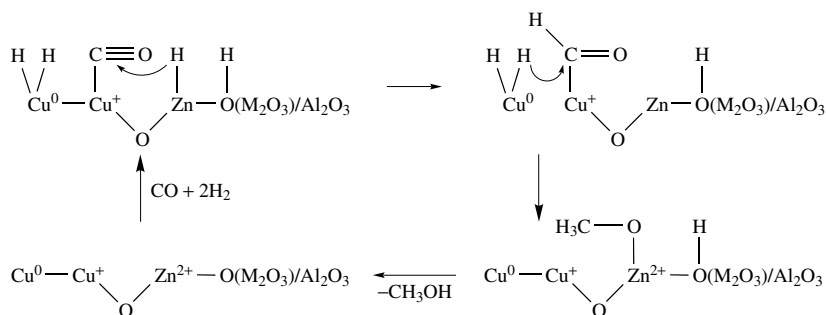
Numerous studies of the modification of alcohol-synthesis catalysts show that the change in the ability of the active component to be reduced is the main result of the modifier action. Small amounts of cobalt affect Zn–Cr catalysts through inhibition of their abilities to activate hydrogen dissociatively. In the case of Cu-containing catalysts, cobalt ions do not modify the properties of the surface copper species. In this case, the methanol synthesis is inhibited by cobalt, again through inhibition of the hydrogen dissociation on the spinel phase that would represent the first step in hydrogen activation [1622]. In a number of works it has been suggested that the alcohol-synthesis reaction proceeds with the participation of CO₂ [1621]. As has been shown above, due to the WGS reaction CO₂ is easily formed in the reaction mixture together with CO. The proposed schemes are also insignificantly changed if such an assumption is accepted, because, especially over metals, CO₂ is easily dissociated into CO and oxygen.

Spectro-kinetic measurements are widely used in investigations of the synthesis reactions of alcohols (especially methanol). Different surface compounds, such as formates [1586, 1596–1600, 1615–1619], carbonates [1586, 1598, 1600, 1616, 1618], methoxy [1596, 1599, 1615] and formyl groups [1589, 1599, 1617, 1619], have been revealed. Infrared spectroscopic measurements on Cu/ZnO and Cu/ZnO/Al₂O₃ catalyst surfaces have revealed the presence of formates, carbonates, methoxy groups and formyl groups (HCO), as well as adsorbed carbonyl species. Adsorbed CH₂O has also been detected [1598]. Many of these investigations propose the series of transformation for these compounds given in Scheme 6.15.



Scheme 6.15

The main stages of the hydrogenation can be represented by the following scheme:



Scheme 6.16

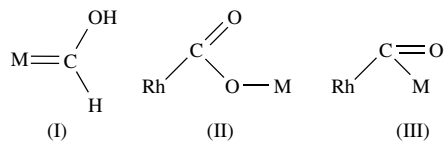
According to Liu *et al.* [1620], the rate-limiting step is formyl formation, as follows from the appearance of an adsorption band due to HCO in the infrared spectrum immediately after the passage of a pulse through the $H_2 + CO$ mixture.

The synthesis of hydrocarbons (HCs) is another important catalytic reaction proceeding on oxide and metallic catalysts. According to the common point of view, the formation of hydrocarbons on metal catalysts proceeds through the hydrogenation of carbon from dissociatively adsorbed CO molecules. IRS (see, for example, [1624] can demonstratively show this.

The formation of branched carbon chain products is a characteristic of CO hydrogenation over 'difficult-to-reduce' oxide catalysts, a well-known process termed 'iso-synthesis' [1625]. However, linear hydrocarbons such as linear butenes are also formed over oxide catalysts [1626].

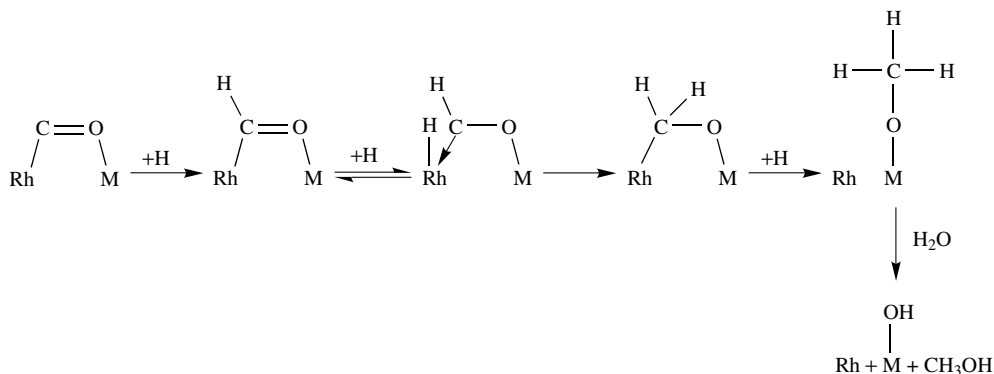
Partial reduction of CeO_2 leads to strong adsorption of CO. The amount of the strongly adsorbed CO increases with an increase in the degree of the reduction, and according to XPS measurements [1627] Ce^{3+} ions are formed which are active component of the CO activation and the following hydrogenation reaction. Adsorption of CO on the partially reduced CeO_2 does not change the concentration of Ce^{3+} .

In HC synthesis from $CO + H_2$ mixtures over Fe-Cr-O catalysts, during the pathway to steady-state conditions the catalyst surfaces are significantly changed, i.e. namely the catalyst is reduced, and metal iron clusters are formed on the surface [1628]. These clusters activate the CO-derived carbonyl species which are similar to those obtained on the metal iron. Accordingly, the mechanism of the hydrocarbon synthesis is analogous to that suggested in the case of a metal iron [1628], which includes the stage of CO bond dissociation following hydrogenation of carbon on the surface, and the formation of hydrocarbon chains on the surface. In spite of numerous experimental data [see, for example, [1629-1637]], a detailed examination of the mechanism of hydrocarbon synthesis over metals is not discussed here because oxides only are discussed in this present book. It should be noted, however, that the formation of an intermediate carbene-type compound (I) and also carbon monoxide bound at the metal/support boundary (compounds II and III) has been observed [1631]:



Scheme 6.17

These compounds are hydrogenated according to the scheme [1638]:



Scheme 6.18

The same pathway for the hydrogenation of CO_2 has been suggested [1639] in the case of lanthanide-ion promoted $\text{Rh}/\text{Al}_2\text{O}_3$ catalysts. When CO hydrogenation over Rh/ZrO_2 was investigated *in situ* using FTIR spectroscopy, with different catalyst parameters (including the reduction temperature, reaction temperature, total pressure and H_2/CO ratio), formates, carbonates and carbonyls on the Rh surface and hydrocarbons were detected. The relationship between the formates and carbonates as surface intermediates in the formation of oxygenates, particularly ethanol, was also discussed [1640].

6.2 Reactions with the participation of hydrocarbons

6.2.1 COMPLETE OXIDATION OF HYDROCARBONS AND THEIR DERIVATIVES

As was shown in Chapter 5, hydrocarbons (saturated, unsaturated, aromatic, etc.), alcohols, ketones, aldehydes and acids on the surfaces of all oxides can easily form surface compounds with a carboxyl group ($\text{R}-\text{COO}^-$). These compounds were first observed in spectroscopic studies beginning in the 1960s. For most oxides, such a reaction occurs through the interaction with surface oxygen. As a result, the temperatures of formation of such compounds depend on the strengths of the surface metal–oxygen bonds, decreasing when that strength decreases. As a rule, these compounds are quite strongly bound, especially on such catalysts as Al_2O_3 , ZnO , TiO_2 and MgO . This is why there were different points of view on the role of these compounds in catalytic reactions. Some authors believed that they are the ‘dead-end’ compounds in catalytic reactions, whereas others have proposed that they are active intermediates. However, no direct evidence for the participation of these surface complexes as intermediates was found until the 1970s. The situation changed when the great importance of the second component of the reaction mixture, namely O_2 (gas), on the oxidation of the above-mentioned compounds was revealed [30, 1148, 1149, 1241, 1280, 1281, 1283, 1569, 1571–1574, 1642], similar to that observed in the case of carbonate decompositions (for reactions of CO oxidation, see Section 6.1.1 above). This was a major discovery. Davydov and co-workers showed that the decomposition of surface carboxylates in the presence of oxygen occurs at significantly lower temperature than without oxygen, i.e. in the temperature region where catalytic reactions proceed. This showed directly that such surface compounds (carboxylates) participate in catalytic reactions, at least in catalytic oxidations, as intermediates. The fact that carboxylates are intermediates in reactions for the full oxidation

of hydrocarbons having different lengths and structures, such as paraffins [1571–1573, 1642], olefins (alkenes) [1573, 1574, 1642], alkynes [1573, 1574, 1642] and aryls [1332, 1334], as well as alcohols [1191, 1452–1454, 1468, 1643, 1644], ketones [1643, 1644], aldehydes [1505] and acids [1645], has been proved by comparison of the decomposition rates of these compounds with those of the formation of reaction products. From the early studies, and in spite of static conditions, these measurements have been made essentially *in situ*, because they were realized at the temperatures of the catalytic reactions and in the presence of the reaction mixtures. Later, the reaction-intermediate character of these compounds was supported by measurements of the reaction rates under dynamic conditions [1642–1644].

The data obtained as a result of these spectroscopic investigations allowed construction of detailed schemes for the mechanisms of full oxidation for the above types of compounds. Similar to CO oxidation, this mechanism depends significantly on the temperature and is different in low- and high-temperature regions (Figure 6.6).

In the literature [1571–1574], more detailed information about the nature of the various reaction stages, obtained using IR spectroscopy, has been reported. Reactions involved in the complete oxidation of hydrocarbons can proceed via two types of mechanism, i.e. (i) a stepwise mechanism with alternating oxidation and reduction of the catalyst surface by the reagents, and (ii) a concerted mechanism, according to which the reaction of oxygen with the catalyst and the formation of the reaction product take place simultaneously. To elucidate the oxidation mechanism of hydrocarbons (as for CO), the rates of the catalytic reactions between hydrocarbons and oxygen are compared with the rates of interaction of the separate components (oxygen and hydrocarbons) on the stationary catalyst (Figure 6.6).

A comparison of the IR spectroscopic data with thermal desorption results shows that the irreversible forms of adsorbed hydrocarbons, surface formates and carboxylate compounds, on numerous oxides, are decomposed to produce the products of complete oxidation – CO₂ and H₂O [1149]. A comparison of the decomposition rates of the surface compounds with those of

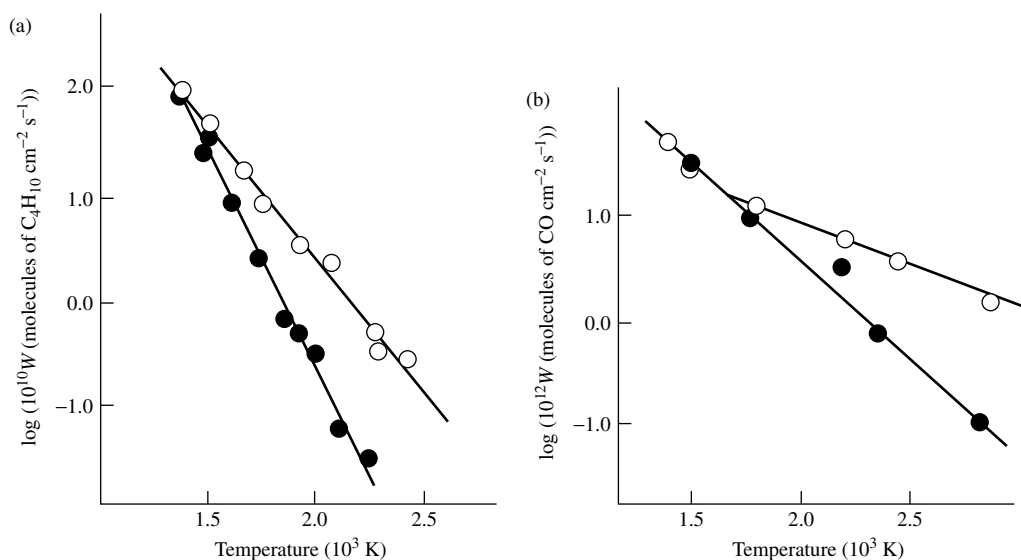
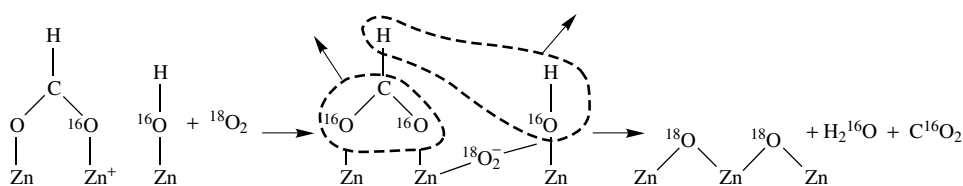


Figure 6.6. Temperature dependences of the rates of catalysis (O) and reduction (●) for (a) *n*-butane oxidation on cuprous oxide ($P_{C_4H_{10}} = 0.02$ torr; $P_{O_2} = 0.3$ torr), and (b) CO oxidation on chromium oxide ($P_{CO} = 0.28$ torr; $P_{O_2} = 0.14$ torr).

the oxidations of alkenes, alkanes and alkynes on CuO and Cu₂O [1571–1574], including *in situ* experiments [1642], confirms that surface formates and carboxylates are intermediate compounds in the complete oxidation of these hydrocarbons. It has also been shown that the decomposition of carboxylates and formates proceeds by the oxidation (involving oxygen) of the reduced metal ions produced on the formation of carbonates on the catalyst surface. A mechanism of the process has been proposed, with its salient feature being the simultaneous catalyst oxidation and decomposition of carboxylate and formate species at low temperatures. At high temperatures, the decomposition of the surface species can be quite fast, even in the absence of oxygen in the gas phase (like for CO oxidation – see Section 6.1). As for low temperatures, the formates are stable and their decomposition occurs only with the participation of oxygen from the gas phase. A more detailed mechanistic study of the decomposition of surface-oxidized species (carboxylates and formates) has been carried out with the aid of the oxygen isotope, ¹⁸O, in the oxidation of butane on zinc oxide. This made possible the determination of the role of molecular oxygen in this process [1646]. The reaction products were found to include surface oxygen, while oxygen from the gas phase provided the role of an oxidizing agent of the reduced surface sites:



Scheme 6.19

In the oxidation of hydrocarbons, a successive fragmentation of the hydrocarbon chain occurs up to the stage of formation of surface formate species. The principles of decomposition of the latter are similar to those for surface carbonates, i.e. at low temperatures the decomposition is accelerated by molecular oxygen, while at high temperatures their spontaneous and rather fast decomposition, accompanied by the evolution of CO₂ and water, takes place.

The participation of strongly bound surface oxidized species as intermediates in complete oxidation reactions suggests an explanation for the effects of the differences in reaction mixtures and the alternating admission of reductants and oxidants onto the catalysts. Detailed investigations of the mechanism of complete oxidation of many hydrocarbons of different composition have shown that at low temperatures the catalytic oxidation rate is close to the rate of their decomposition in the presence of O₂ (Table 6.2), that is, the concerted mechanism is accomplished at these temperatures. On achieving the temperature of the thermal decomposition of the surface oxidized species, the rate of formation of the products in the catalytic reaction (involving the participation of both reactants) and the rate of the interaction of the oxidized substance with the catalyst are the same, which indicates the stepwise reaction mechanism (Figure 6.6). In intermediate situations, both concerted and stepwise mechanisms contribute to the total rate of the catalytic reaction.

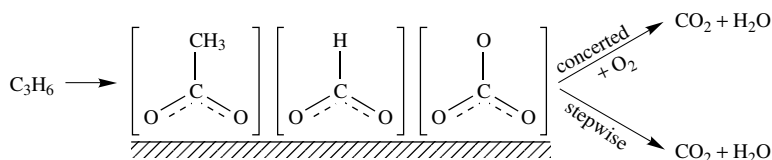
Thus, when complete oxidation occurs through oxidized formate–carboxylate intermediates the stepwise and concerted mechanisms reflect two paths of decomposition of the surface species, i.e. under the action of molecular oxygen and thermal decomposition. In the former case, a peculiar conjugation of catalyst oxidation–reduction takes place, which makes facile the mutual electron transfer and decomposition of the surface species. This mechanism has been called *the mechanism of conjugated transfer* or *the conjugated mechanism* [1570]. The transition of one mechanism into another is determined by the thermal stabilities of the surface species, which, in turn, depend on the energy of binding of the oxygen abstracted from the catalysts during

Table 6.2. Rates of CO₂ formation on cuprous oxide as a function of the feeding reaction mixture and individual reagents onto the steady-state catalyst ($T = 473$ K; $P_{O_2} = 0.3$ torr; $P_R = 0.05$ torr).

Reagent	W (molecules of CO ₂ cm ⁻² s ⁻¹ ($\times 10^{10}$))	
	Catalytic values	IRS values
C ₂ H ₆ + O ₂	3.5	~2
O ₂	3.3	—
C ₂ H ₆	0.3	—
C ₄ H ₁₀ + O ₂	3.2	~2
O ₂	3.8	—
C ₄ H ₁₀	0.4	—
C ₆ H ₁₄ + O ₂	3.4	~2
O ₂	2.9	—
C ₆ H ₁₄	0.5	—

the course of decomposition. The lower the strength of oxygen binding, then the lower is the temperature of the mutual transition of the mechanisms.

The general scheme of the mechanism of the complete oxidation reaction, including both types of concerted mechanisms and the interpretation of the regularities observed, is as follows:

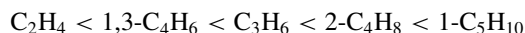


Scheme 6.20

Gorokhovatskii and Kuznetsov [1647] reached a conclusion about the role of formate and carboxylate complexes in the complete oxidation of propene over chromium oxide by a comparison of the activation energies of the decomposition of surface-formate–carboxylate intermediates with those obtained for similar reactions. Later, this was also demonstrated for oxidation propene on CoO–MgO and Bi–Mo–Mg–O catalysts [1648].

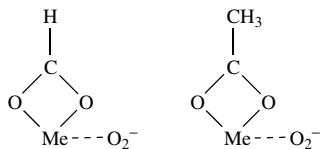
The adsorption of oxygen from the gas phase before the stage of the oxidation of adsorbed olefin has been confirmed [1649]. These results indicate separately the reality of the phenomenon of the influence of oxygen on the thermal stabilities of the adsorbed complexes.

As revealed by Anshits *et al.* [1571] on the basis of their reactivity behavior in forming such olefin–oxygen complexes, olefins appear to be sequenced as follows:



Later, the interactions between oxygen and propene adsorbed on Co₃O₄, NiO, Fe₂O₃, CuO, Cr₂O₃, V₂O₅, TiO₂ and MoO₃ was studied by Ono *et al.* [1650]. It was established that over Co₃O₄ the C₃H₆–oxygen surface complex is formed even at 195 K. The amount of oxygen needed to form this complex is similar to that required for Co₃O₄ with pre-adsorbed C₂H₄. Infrared spectroscopic studies clearly confirm these results. In fact, Co₃O₄ has the weakest bound oxygen, and both ethene and propene when adsorbed on this oxide from the same types of

complexes, i.e. carboxylates and formates. The following adsorption of oxygen involves the cations of these complexes:



Scheme 6.21

In the case of CuO, NiO or Fe₂O₃, the interaction of O₂ with C₃H₆ occurs at 273 K, whereas on Cr₂O₃, V₂O₅, TiO₂ and MoO₃ oxygen does not interact with propene under the same conditions. The reactivity of oxides in the oxidation of adsorbed C₃H₆ is changed in the sequence in a similar way to that of the catalytic oxidation of C₃H₆ on the corresponding oxides. This is in good agreement with data from infrared studies, which indicate that the temperatures of the formation and decomposition of carbonate–formate complexes depend on the binding energies of the surface oxygens and fall when these energies decrease. On the other hand, it is known that the catalytic activities in the reactions of complete hydrocarbon oxidations also correlate with the energies of the surface oxygen bonds and increase when the latter decrease [94].

After the interaction of O₂ with propene adsorbed on ZnO at 343 K, both OH groups and π -allylic complexes are formed on the ZnO surface, conforming the data of Kugler and Kokes [1651]. At higher temperatures, surface complexes of another unknown type are formed and lead to the formation of surface formate- and acetate-like ions, as noted above. This shows that gaseous oxygen participates in the formation of carboxylate complexes.

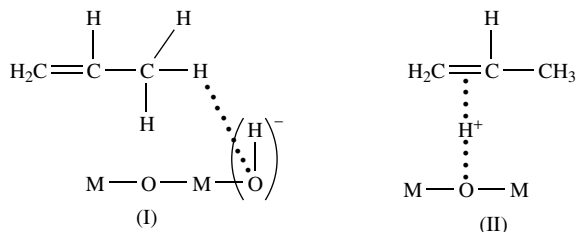
The formation of carboxylate and formate structures has also been shown on catalytic combustion catalysts such as chromites [66, 1652, 1653]. However, their role in catalytic reactions was not noted by the authors although in the case of adsorption of alkyl aromatic compounds Busca *et al.* [1654] observed the formation of benzoates and noted that carboxylate species produce CO₂ and demethylated hydrocarbons (toluene from xylenes and benzene from toluene). On the basis of a comparison of the infrared spectra obtained upon toluene oxidation over vanadia–titania with those observed over the combustion catalysts Fe₂O₃ [1654], MgCr₂O₄ [1652] and CuO [1157], Busca and co-workers believe that the benzoate structures existing in these systems are responsible for the formation of the complete oxidation products. Support for this comes from the extremely high activities of the latter materials as toluene combustion catalysts.

6.2.2 SELECTIVE TRANSFORMATIONS OF ALKENES

In the case of selective transformation reactions of hydrocarbons, short of complete oxidation, the pathways depend on the character of the hydrocarbon activation, which is specific for each type of reaction.

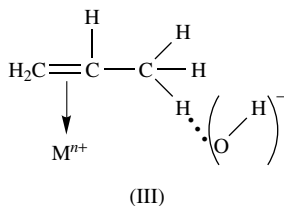
Isomerization

This reaction belongs to the simplest catalytic reaction type, i.e. A \rightarrow B, where A and B are compounds of similar chemical nature. As it has been shown in Section 5.1, alkenes can yield various types of surface compounds in their reactions with the surfaces of oxide catalysts. Hydrogen-bonded surface compounds are formed with the participation of surface hydroxyl groups. Two basically different types of interactions have been identified:



Scheme 6.22

IR spectroscopic investigations have enabled distinctions between surface hydroxyl groups according to the type of reactions they undergo with alkenes. Basic hydroxyl groups do not form complexes which are stable at room or elevated temperatures. This makes it possible to estimate the alkene–surface bond (complex type I) energy as ca. $4\text{--}10\text{ kJ mol}^{-1}$. The presence on the oxide surface of energetically more advantageous centers (for example, coordinatively unsaturated cations which stabilize alkenes in the form of a π -complex) can, given favorable geometric parameters, result in further stabilization of the alkene involving participation of the basic hydroxyl groups according to the following scheme:

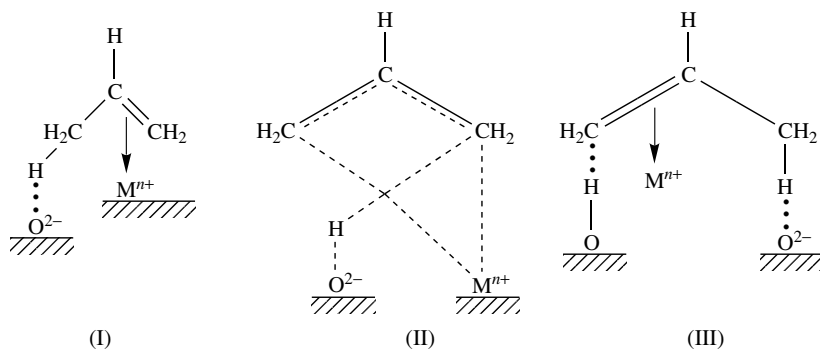


Scheme 6.23

In hydrocarbons, an H–D exchange with surface hydroxyl groups involving hydrogen-bonded complexes is possible. This is especially likely in an exchange involving a complex of type III, since during the coordination of the alkene via the double bond the mobility of the proton in the CH_3 group increases [30, 1655]. The possibility of the isomerization of the double bond via such cyclic complexes is in accordance with an associative, concerted mechanism and has been considered in numerous investigations.

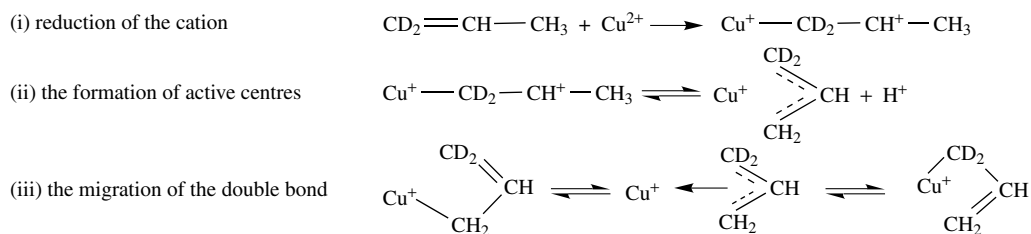
With the participation of acid–base pairs, the formation of allyl–surface compounds is possible on some catalysts. It would be (sufficiently) simple to present the isomerization reaction of alkenes as involving π - and π -allyl surface compounds [473, 1087]. In the general case, the isomerization of the double bonds in alkenes can be ensured by intra- and intermolecular hydrogen transfer according to both coordination and noncoordination (stepwise) mechanisms.

The formation of *cis*-2-isomers (the absence of basic differences in the formation of alkene complexes of different structures makes it possible to consider the isomerization mechanism by using propene complexes as an example) during the isomerization of the double bond can proceed in general via the formation of the complex (I), and for complex (II) for intramolecular isomerization (for example, through an intermediate state), and complex III for intermolecular hydrogen transfer according to the coordination mechanism where the transfer requires the presence, next to the paired center, of a hydroxyl group with a sufficiently mobile proton:


Scheme 6.24

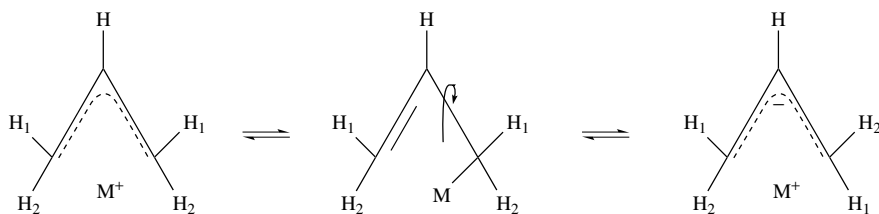
A study of the isomerization of butene-1 and *cis*-butene on ZnO, Al₂O₃ and Cr₂O₃ by IRS and kinetic measurements showed that the mechanism of this reaction includes the intermediate formation of *syn*- and *anti*- π -allyls and their interconversion through the dynamic σ - π -equilibrium [1258, 1259, 1656].

Upon the interaction of butene-1, 3,3-dimethylbutene-1, and deuteropropene over Cu²⁺ Y zeolite it has been demonstrated that the active sites are formed during the reduction of the Cu²⁺ ions with alkenes, while the reduction process is a reaction of the first-order [1657]. On the basis of the redistribution of deuterium in propene, both associative and dissociative mechanisms of the isomerization have been examined. The reaction proceeds through three stages as follows:


Scheme 6.25

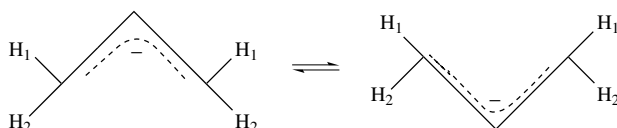
The primarily intramolecular character of olefin isomerization, in particular for CD₂=CH-CH on chromium catalysts, has been supported by Haller and Johns [1658]. According to this, the analysis of the intensities corresponding to the 1₀₁ → 2₀₂ rotation transitions used to calculate the molar compositions of the deuteropropenes showed that intramolecular isomerization on amorphous chromia occurs through an allylic carbanion. On microcrystalline chromia, the energy of the formation of an intermediate is about 5–6 kcal mol⁻¹ less than that of the allylic carbanion and represents, probably, covalently bound σ - or π -allyls.

Isomerization via an allyl anion does not involve coordination. For alkenes with a longer carbon chain than propene this should result in the predominant formation of the thermodynamically favorable *trans*-2-isomer. The transfer of substitutes from a *cis*- or a *trans*-position can proceed in two ways. First, this can result from an equilibrium between allyls bound in the π - and σ -forms:



Scheme 6.26

Secondly, the transfer can take place because of bending of the carbon skeleton [1659]:



Scheme 6.27

The majority of non-transition-metal allyl derivatives investigated so far exist in the π -allyl form under ordinary conditions, or transfer into this form from the σ -allyl form when heated [1660, 1661]. Because of this, a *cis-trans* isomerization according to scheme (6.26) is more probable and the equilibrium is shifted in the direction of the π -allyl formation.

IR and UV-Vis spectroscopic investigations have shown that the stability of the unsubstituted allyl anion, for example on Al_2O_3 [473], is high (up to 473 K *in vacuo*). This may indicate that the limiting stage in the isomerization through allyl anions is their protonation with the surface hydroxyl groups. However, in this analysis no account is paid to the possible effect of weakly adsorbed or gas-phase hydrocarbon molecules on the desorption rate from allyl anions. The hydrocarbon molecules can be better proton donors than basic hydroxyl groups and thus facilitate the desorption of allyl anions in the form of isomerized alkenes.

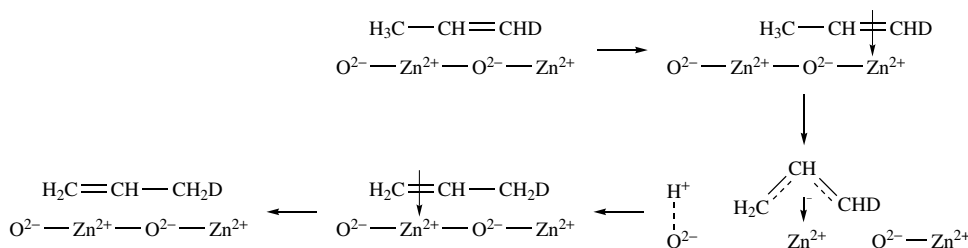
In general, if there are no OH groups near a paired ion center, $\text{M}^{n+}\text{O}^{2-}$, the hydrogen transfer to alkene can proceed only intramolecularly via a coordination or noncoordination mechanism through the intermediate complexes I or allyl (compound (III)), respectively (Scheme 6.24). This transfer is determined by two factors, i.e. (i) the rate of dissociation of the C-H bond in the alkene, and (ii) the rate of protonation of the allyl anion which is formed [1661]. The relationship between these rates, which is determined by $\Delta\text{p}K_a$, the nucleophilic surface center and the related acid center (OH group), determines the path of a hydrogen transfer.

If the OH group is near the double adsorption center, the probability of intermolecular proton transfer according to both the noncoordination and coordination paths increases with increasing $\Delta\text{p}K_a$ of the competing OH group on the catalyst surface. In this case, the acid is linked to the O^{2-} center. The noncoordination pathway is ensured by the formation of the intermediate allyl anion, while the coordination pathway involves the formation of complex (I).

According to Rosynek and Hightower [1662], 1-butene isomerization and butene-deuterium exchange on alumina occur on two different types of sites, denoted as 'I' and 'E' sites, respectively. In addition, two other types of sites can be important in catalytic reactions at moderate temperature because of their quite strong bonding to butene. At least a part of the stronger-bound butene is attached to the α -sites, as described by Peri [1663]. The Lewis acid sites, on which the olefin π -complexes are formed, and also the acid-base pairs which give rise to the π -allylic complexes discussed above, seem to be such centers [473, 1087].

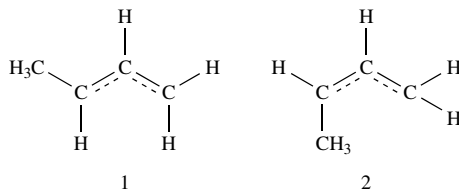
An upper limit for the concentration of the E-sites established from CO₂ poisoning experiments was $3-8 \times 10^{12}$ sites cm⁻², and the estimated number of α -sites lies in the same range [1662, 1663]. Thus, Larson and Hall [1664] showed that the number of sites active in the equilibrium of CH₄ and CD₄ over alumina was 4×10^{12} sites cm⁻².

Thus, the isomerization of deuteropropenes on zinc oxide (on the surface of ZnO, olefins easily form both π - and π -allyl anions at room temperature) results in the formation of an equilibrium mixture of CH₂D-CH=CH₂, CH₃-CH=CHD and CH₃-CD=CH₂ [1665]. A band corresponding to the formation of the OH group and five bands corresponding to the formation of the symmetrical π -allyl species are observed in the IR spectrum. This indicates that the isomerization proceeds via a dissociative cleavage of a C-H bond. The intermediate (π -allyl) exists in the anionic form (C₃H₃)⁻. The first stage of the reaction is evidently the formation of the π -complex (Scheme 6.27a).



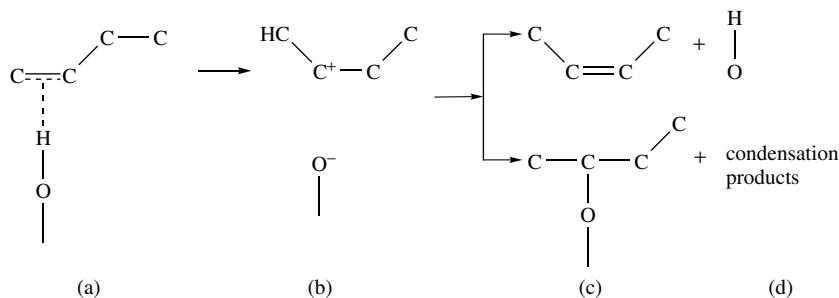
Scheme 6.27a

In the isomerization of but-1-ene to but-2-ene on ZnO, the bands observed in the IR spectra corresponding to the π -complexes of but-1-ene, *cis*-butene and *trans*-butenes, as well as the π -allyl complexes, were observed in the IR spectra [1656]. Two possible methyl- π -allyls:



may be the precursors of *trans*- and *cis*-butene. However, only complex 2 was detected on the surface. The most intense absorption bands in the spectra of π -complexes are those of the *cis*-butene π -complex, although a greater amount of *trans*-butene is formed in the equilibrium gas mixture. Consequently, form 1 exists only as a short-lived precursor in the reaction $2 \rightleftharpoons 1 \rightleftharpoons \text{trans-butene}$. Under catalytic conditions, the intensity of the signal due to π -C₄H₈⁻ (1) diminishes slowly, while that of the signal of π -*cis*- and π -*trans*-C₄H₇⁻ increase slowly. At the same time, complex 2 is initially formed at a rate close to the overall rate of isomerization, which remains constant. Hence, one may conclude that the π -allyl is a true intermediate.

On surfaces with acidic properties, alkenes can interact with both Brønsted and Lewis acid sites, as has been shown above (Chapter 5). In the first case, depending on the properties of the protic sites, interaction ends at the stage of the hydrogen-bond formation (complex type a), or proton transfer to the alkene molecule with carbonium ion formation type b is observed (Scheme 6.27b) (the evidence for such complexes is given above in Section 5.1).



Scheme 6.27b

Both of these pathways lead to the reactions of oligomerization and isomerization. The formation of a π -complex with acidic OH groups was supported in the study of the isomerization of but-1-ene to *cis*-butene on HY zeolites and other acid silicates at 250–473 K [1666]. The obtained correlation between the reaction rate and the number of acidic OH groups supported the fact that the conversion of complex type a into complex type b is the rate-limiting stage. In a kinetic study, it was observed that the formation of saturated complexes c and d is accompanied by a decrease in the rate of isomerization. Evidently, species c and d are 'dead-end' compounds which deactivate the catalyst. As follows from analysis of the corresponding data presented above in Section 5.1.2, at a temperature of 273 K and above the carbenium ions are also observable in the case of zeolites. No doubt, these carbenium ions are involved in isomerization via a carbocationic mechanism [454, 735]. A band at 1510 cm^{-1} ($\nu_{\text{as}}\text{CCC}$ in allyl carbocations formed with the participation of bridged OH groups) was observed in the IR spectra after the isomerization of hex-1-ene to hex-2-ene and the subsequent *cis*–*trans* isomerization on H-ZSM-5 zeolite at 473 K. At the same time, the spectrum of the OH groups was also changed. On this basis, Bezoukhanova *et al.* [1667] concluded that the reaction proceeds via the formation of an intermediate carbonium ion (a reaction of the $a \rightarrow b$ type). Isomerization reactions can proceed on Lewis acid sites of such catalysts according to the above schemes all the more if the Lewis acid sites of zeolites which also react are involved as ion pairs. The schemes presented for the mechanism based on spectral data are in good agreement with kinetic and other experimental data [1668, 1669].

Hydrogenation

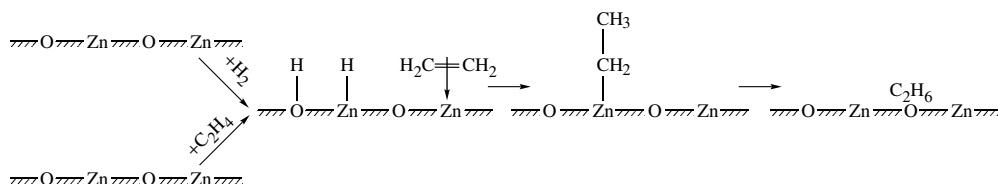
The character of hydrogen activation and bonding on the surfaces of catalysts plays the main role in the hydrogenation of unsaturated hydrocarbons on both oxides and metals [1670–1675]. Depending on the system in question, different forms of adsorption, including those which are active sites in dehydrogenation processes on the metal surface, can be formed. *In situ* Fourier-transform infrared studies of ethene surface-reaction kinetics have been made [1673–1675]. This and other olefins easily form π -, σ - and di- σ -complexes on metals, including ethylidene ($\text{CH}=\text{CH}_2$) from ethene, and half-hydrogenated compounds (C_2H_5) and saturated hydrocarbons due to their interaction with activated hydrogen [1676]. The literature shows that π -complexes are suitable surface species for catalyzing hydrogenation reaction, in cases of their co-adsorption on neighboring or on the same sites to adsorbed hydrogen.

Kokes and Dent were among the first to use a combination of *in situ* spectroscopic and kinetic measurements to study the mechanism of olefin hydrogenation on ZnO [550, 1257, 1276, 1665]. They unambiguously demonstrated the participation of the π -complexes of C_3H_6 , C_2H_4 and C_4H_8 in the interactions with hydrogen atoms of the H_2 molecule. On the one hand, hydrogen adsorption on ZnO easily proceeds in a reversible form with the formation of $\text{Zn}-\text{H}$ ($\nu_{\text{Zn}-\text{H}}$, 1710 cm^{-1})

and OH (OH, 3510 cm^{-1}) bonds; on the other hand, a slow irreversible adsorption takes place, involving diffusion of the hydrogen into the bulk of the catalyst. The latter adsorption form is probably characterized by the absorption bands in the region of vibrations of the Zn–H–Zn bridge bonds ($800\text{--}1200\text{ cm}^{-1}$), as revealed in other studies [374, 1225].

The formation of ethene π -complexes involving Zn^{2+} ions [1163] leads to the appearance of the bands at 1438 , 1451 and 1600 cm^{-1} . The data obtained by Kokes and Dent [1665] on the changes of the absorption bands characteristic of the π -complex upon adsorption on ZnO pretreated by hydrogen, and hence containing Zn–H and OH bonds, show that such absorption bands, (as well as those from the Zn–H bond) both decrease together, due to the formation of the half-hydrated surface compound (C_2H_5), which in turn transforms into ethane, involving at this stage reactions with the OH groups (3510 cm^{-1}).

When C_2H_4 is replaced by C_2D_4 , the initial rate of the disappearance of the C_2H_5 absorption bands is close to the stationary rate of hydrogenation, i.e. the step corresponding to this process is rate-limiting in the reaction. The proposed mechanism can be represented as follows:

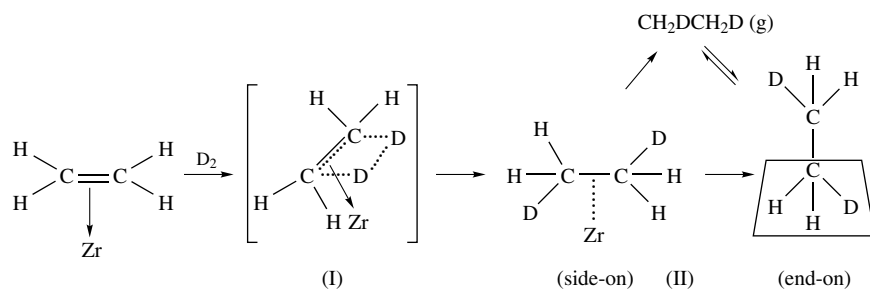


Scheme 6.28

Other olefins undergo hydrogenation probably via the same mechanism. However, the only deuterium-containing products of C_3H_6 , C_4H_8 and C_4H_6 were $\text{C}_3\text{H}_6\text{D}_2$, $\text{C}_4\text{H}_8\text{D}_2$ and $\text{C}_4\text{H}_6\text{D}_2$, respectively. This shows that hydrogen participates in the reaction in a molecular form rather than in an atomic form as in the hydrogenation of ethene: this difference can be attributed to the weaker chemisorption of the ethene on zinc oxide as compared with propene, butene and butadiene. Therefore, the latter are adsorbed as π -allyl complexes [1677, 1678] and hydrogenation probably proceeds with a participation of these hydrocarbons and molecularly adsorbed hydrogen.

Tanaka *et al.* [1679] studied the mechanism of the hydrogenation of butadiene-1,3 on ZnO by using isotopic substitution. The data obtained again allowed the conclusion that hydrogenation on ZnO is connected with heterolytic dissociation of the H_2 molecule. A mechanism was proposed involving the formation of the intermediate π -allylic structure. Upon the adsorption of cyclopentene on ZnO, the π -bonded forms are mainly formed, whereas the adsorption of cyclobutene is accompanied by an opening of the ring [1680].

The IR spectra of hydrogen adsorbed on ZrO_2 at $273\text{--}373\text{ K}$ also shows a heterolytic dissociation of H_2 with the formation of Zr–H and OH groups [1681]. However, hydrogen bound in this way does not react with ethene from the gas phase but the latter is simply replaced by it, i.e. the intensity of the Zr–H band decreases, and bands of $\pi\text{-C}_2\text{H}_4$ (1446 cm^{-1}) and of the tightly bound C_2H_4 complex (1338 cm^{-1}) are found. However, the hydrogenation of C_2H_4 is also detectable even at 173 K , when the heterolytic dissociation of H_2 is inconceivable. Under these conditions the adsorbed ethene interacts with D_2 from the gas phase by the following mechanism [1233]:



Scheme 6.29

In this reaction, complex (I) is an intermediate, while complex (II) is a side product.

An IR spectroscopic study of ethene hydrogenation on Cu/ZnO showed that under reaction conditions Cu^0 is at the origin of the H_2 activation and that Cu^0 and ZnO are both able to activate ethene bound as a weakly π -bound species [1225]. The scheme of ethene hydrogenation proposed by these authors includes the interaction of adsorbed ethene π -complexes and Zn–H groups.

The assignment of the observed IR bands of the adsorbed ethene π -complex formed on Cu^0 (1550 cm^{-1} to νCC , 1290 cm^{-1} to scissors CH_2 , and 920 cm^{-1} to wagging CH_2) has been made on the basis of data on ethene adsorption over various metals [1682, 1683]. In spite of disagreements with all other literature reports concerning spectral manifestations of ethene π -complexes with Cu^+ ions as noted above (Section 5.1.3), these authors assigned the 1550 cm^{-1} band to νCC in complexes with Cu^0 , although it is known that such complexes are characterized by the band below 1500 cm^{-1} .

According to IR and UV–Vis studies of the hydrogenation of benzene adsorbed on Y-type zeolites containing various low contents of platinum [1684], the hydrogenation reaction proceeds on the metal: hydrogen is dissociated on Pt and benzene which is weakly adsorbed on the support can migrate to the metallic phase for hydrogenation.

Oligomerization, polymerization and cracking

The molecular spectroscopy studies of the oligomerization reaction which takes place over the surfaces of different types of catalysts have already been described in detail in Chapter 5 and is not analyzed further here. All the more so, as in spite of many efforts spectro-kinetic data concerning the stages occurring over such surfaces are practically absent in the case of these reactions. Probably, cracking reactions occur via surface species similar to those analyzed above for oligomerization reactions. This is in complete agreement with an *ab initio* quantum-chemical investigation of the elementary steps of the catalytic cracking of isobutane [1685] which showed that the adsorbed carbenium and carbonium ions represent the low-energy transition state of the corresponding elementary reactions.

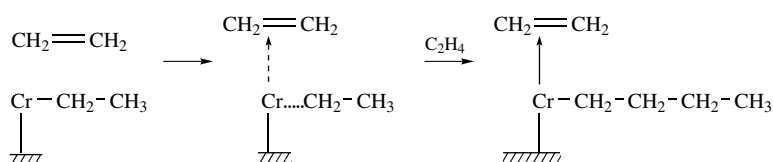
Polymerization of ethene

For the polymerization of ethene and other olefins, *chromium-containing systems* are well known as catalysts for such reactions. Views concerning the mechanism of ethene homopolymerization on a Cr/SiO₂ catalyst (Phillips-type catalysts) and the nature of the active component (the state of oxidation of chromium) remain in conflict despite the commercial significance of this reaction and the corresponding amount of related research which has been reported.

The silica-supported chromium used to catalyze the polymerization of ethene is usually activated by high-temperature oxidation followed by reduction using ethene (in industry) or CO (in

the laboratory). The oxidation state of the resulting active Cr sites has remained contentious since the development of these catalysts in the early 1950s. The main question discussed is the role of the surface chromium ions in different (Cr(II) and Cr(III)) oxidation states. According to Rebenstorff and Larsson [1686], both of these oxidation states are involved in the active sites. Myers and Lunsford [1687] supported this point of view in experiments using the catalysts prepared from Cr(II) and Cr(III) salts. Zielinski *et al.* [1688] noted that the treatment conditions are very important in the activation of the catalyst. Thus, only the Cr(III) species were observed on a catalyst activated by high-temperature ultra-high evacuation, whereas both Cr(II) and Cr(III) appeared on the catalyst activated by CO reduction. They identified the Cr active species as Cr(III) by using IR spectroscopic data of adsorbed CO and obtained a value for the ethene polymerization activation energy of $12.1 \text{ kcal mol}^{-1}$. The Cr(III) active sites were characterized by the CO bands at 2228, 2214 and 2202 cm^{-1} . These authors believed that the Cr(II), relatively inactive at room temperature because of its higher activation energy (18 kcal mol^{-1}), becomes increasingly active with increasing temperature. Such Cr species are characterized in the IR spectra by the broad band between 2200 and 2170 cm^{-1} [1689].

The mechanism of ethene polymerization on Cr/SiO₂ catalysts has been the subject of discussion in many research papers [1690–1699]. Hogan [1693] proposed the following scheme for polymer growth:



Scheme 6.30

In this scheme, a methyl group terminates each polymer chain. However, this provided no explanation for the origin of the additional hydrogen atom required per chain. The views of different authors concerning the initial hydrogen atom are various. Thus, McDaniel and co-workers [1692] suggested the possibility of β -elimination of hydrogen from the chain, whereas other workers [1694, 1698] have proposed that silanols may be the sources of the initial hydrogen atom. The latter viewpoint is in contradiction with the data of McDaniel and Welch [1695], who have argued that the polymerization proceeds rapidly even when silanol groups have been removed.

Another initiation mechanism has been proposed by Krauss and Hums [1690] and summarized by McDaniel and co-workers [1692]. According to this mechanism, two ethene molecules interact on a single Cr site to form an allylic species. This is in agreement with the available IR and NMR spectroscopic evidence, according to which each polymer chain contains a vinyl group on one end and a methyl group on the other [1692, 1693]. Similar views have been offered in other papers [1689, 1692]. Rebenstorff and Larsson [1686] proposed a two-chromium-atom active site with a Cr-CH₂-R-CH₂-Cr structure. The latter is supported by IR studies [1234, 1689], the authors of which attributed the weak broad absorption band at ca. 2750 cm^{-1} to the νCH mode of a carbene group interacting with the adsorption center. The carbene, according to this hypothesis, is formed by the migration of hydrogen from a CH₂ group to a surface oxygen atom. The catalytic cycle is completed by a shift of a proton from the new hydroxyl group back to its host carbon atom, thereby eliminating 'hydrogen-scrambling'. However, McDaniel and co-workers [1692] concluded that no hydrogen shift occurs during the propagation reaction.

Since Ghiotti *et al.* [1689] did not obtain any IR spectral evidence for the presence of vinyl or methyl groups in the polymer, they proposed that terminal groups are not presented in the polymer

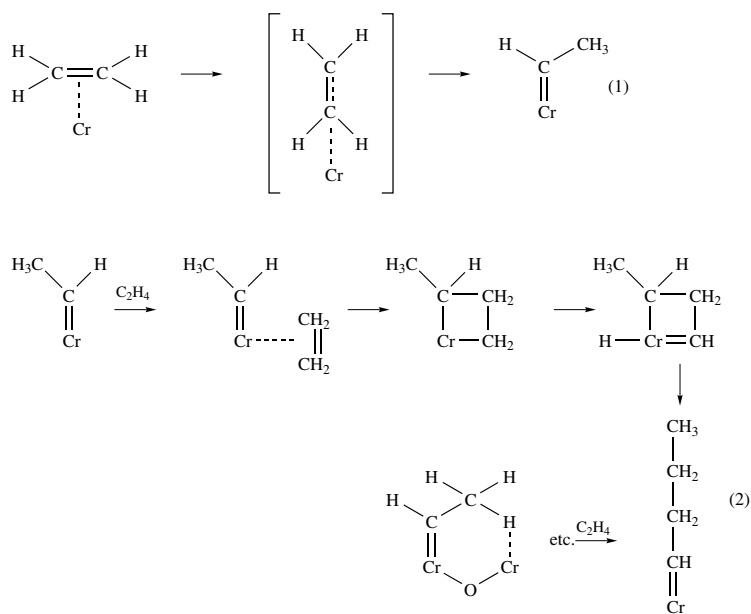
chains, i.e. that the chains form cyclic structures. Such a cyclic structure was also proposed by Rebenstorff and Larsson [1691] and later supported by Zielinski and Dalla Lana [1699]. Vikulov *et al.* [1700] showed that polymerization of ethene was proceeded by a rapid initial adsorption of the monomer.

Using CO adsorption at low temperature, Rebenstorff [1697] suggested that the binuclear site was the only active one for ethene polymerization at low temperatures, but in these studies there was no direct observation of adsorption complexes giving rise to polymerization or kinetic data on the transformation of the complexes.

Zielinski and Dalla Lana [1699], using fast-scanning FTIR spectral measurements, examined the reaction during the earliest seconds of polymerization. They showed that ethene adsorbs reversibly in a molecular form, probably as a π -complex, and also dissociatively, with the formation of an intermediate in the form of paired carbene structures linked to two chromium active sites. However, they obtained no spectral evidence for this intermediate. Vikulov *et al.* [1700] and other authors [1234, 1699, 1701, 1702] observed only π -adsorbed ethene on Cr^{2+} centers at the beginning of the reaction.

The adsorption and polymerization of ethene have been investigated on the basis of the kinetics of transformations of surface compounds by means of the analysis of absorption bands characterizing the polymer: 1446 cm^{-1} ($\delta=\text{CH}_2$, presumably in adsorbed ethene), 1472 cm^{-1} (δCH_2 in polyethene, plus a component from adsorbed ethene), 2850 cm^{-1} ($\nu_s\text{CH}_2$ in polyethene) and 2920 cm^{-1} ($\nu_{as}\text{CH}_2$ in polyethene) [1699]. The authors associated an induction period for the reaction with the dissociation of ethene. They suggested that the formation of carbenes as active centers for the polymerization of ethene resulted from ethene dissociation.

Later, under dynamic conditions Kantcheva *et al.* [1701] observed an absorption band at about 3016 cm^{-1} , which was assigned to νCH groups. This band appeared with an induction period and then disappeared simultaneously with an increase in the intensities of the absorption bands characteristic of the polymer (2927 and 2855 cm^{-1}). The data obtained allowed a relatively valid scheme of ethene polymerization to be formulated:



Scheme 6.31

According to this scheme, ethylidene species, characterized by an absorption at 3016 cm^{-1} ($\nu\text{CH=}$), are formed as a result of initial interaction (stage 1). Support for this comes from the experiments of Al-Mashta *et al.* [1197, 1199] who studied ethene polymerization on sulfated anatase and observed the surface species characterized by the bands at 3010 ($\nu\text{CH=}$) and 2965 ($\nu_{\text{as}}\text{CH}_3$) cm^{-1} assigned to the ethylidene groups. The ethylidene species formed participate in the following reaction, according to stage 2, as has been proposed earlier by Al-Mashta *et al.* [1199], and a metallocyclic compound is formed. On the basis of an observed irregular oscillation of the 3016 cm^{-1} band intensity, Kantcheva *et al.* [1701] suggested that the $\text{Cr}=\text{C}$ bond is restored after ethene insertion. However, the NMR spectroscopic measurements of McDaniel and co-workers [1692] did not support this mechanism. Moreover, it should be taken into consideration that the band in this region is also characteristic of π -complexes of ethene (see Section 5.1.3). The number of sites presumably active in polymerization is about 1/40 of the number of chromium ions to which ethylene is π -adsorbed. Davydov [1702] showed that Cr^{2+} ions in $\text{Cr}/\text{Al}_2\text{O}_3$ catalyst are more active in ethene polymerization than Cr^{3+} ions since coordinate two C_2H_4 molecules as π -complexes. The latter are quickly converted to dimers, while the π -complex of olefins with Cr^{3+} ions has only one coordination vacancy, and so it is stable and converts to the polymer very slowly.

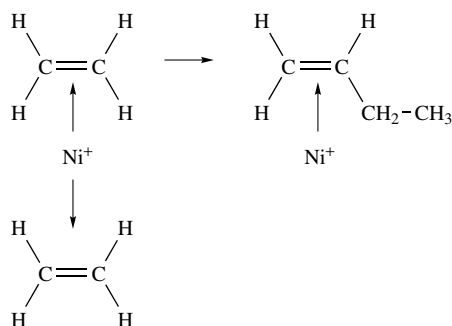
Nickel-containing systems, e.g. materials such as nickel oxide and nickel salts supported on silica and/or alumina, have been used as catalysts for the dimerization or oligomerization of olefins [1703–1705]. The activities and selectivities of these catalysts may be affected by strong adsorption of the products and by isomerization and copolymerization of olefins into branched products [1706, 1707]. Espinoza *et al.* [1708] showed that at low Ni concentrations the higher activity per Ni site for ethylene oligomerization can be achieved by a selective exchange of nickel with sites of higher acid strengths on silica–alumina. Chauvin and co-workers [1705, 1709] described a system of nickel oxide supported on γ -alumina modified with sulfate ions as very active for propene oligomerization. Ethylene oligomerization over nickel-exchanged zeolite (NiNaY) have also been investigated by Ng and Creaser [1710] and Heveling *et al.* [1710, 1711]. For the majority of catalysts described in the literature, the conversion of ethylene is observed to decrease rapidly with reaction time from deactivation of the catalysts, and the steady state was not generally reached [1708, 1710, 1712]. However, Cai *et al.* [1713] showed that this system has good catalytic properties towards ethylene dimerization.

Ethylene oligomerization was also studied by using Ni(II) sulfated alumina catalysts. This catalyst exhibited very good oligomerization activity with no apparent deactivation in the slurry reactor at temperature at or below 523 K and near atmospheric pressure. With a reaction temperature in the range tested at (523 K), 100 % conversion of ethylene with selectivities of 89 % and 11 % for 1-butene and 1-hexene production, respectively, were achieved [1714].

As for the nature of the active component of this type of catalyst, there are different points of view in the literature at present. Yashima *et al.* [1715] concluded that the active site is zero-valence nickel, highly dispersed on the zeolite. Other studies have shown the formation of Ni^+ species from well-dispersed Ni^{2+} ions on the surface of alumina [1704] or on zeolites [1716, 1717] by photoradiation under a hydrogen atmosphere, or even by contact with olefin. These authors also suggested that the Ni^+ species are the active sites for the olefin dimerization reaction. Nevertheless, all researchers have observed that Ni^{2+} can be reduced by H_2 and CO , by vacuum, or by contacting with olefins. Cai *et al.* [1713] observed an induction period for ethylene oligomerization over a $\text{NiSO}_4/\text{Al}_2\text{O}_3$ catalyst calcined in an oxygen atmosphere, but no induction period with the catalyst heated under vacuum. This appears to support the argument that the Ni^+ species is the active center since the induction period could result from the reduction of Ni^{2+} to Ni^+ during the initial period of the reaction. Based on ESR and FTIR spectroscopic experiments, they proposed that the Ni(I) species, in conjunction with the strong acid centers of the support,

are the active sites for ethylene dimerization. Other authors [1718] have suggested that the high coordinatively unsaturated Ni^{2+} ions are the active components in this reaction; however, they did not support their suggestion by direct observation (or other persuasive arguments).

It is of interest that several years ago the question arose of the nature of the active component of nickel-containing zeolite catalysts in olefin dimerizations. It was shown that the Ni^+ ions are the active centers for this reaction [1716]. Investigations of ethene dimerization and the nature of the active sites by CO adsorption using FTIR spectroscopy and reported by Davydov *et al.* [1719] inferred that the Ni^+ ions are active centers for ethene oligomerization because the samples investigated had the highest activity only after reduction treatment. The formation of active centers, in the authors' opinion, is associated with the presence of isolated Ni^{2+} ions which are selectively reduced to Ni^+ ions with the participation of Brønsted acid sites. The latter appear on the surface due to the presence of SO_4^{2-} ions. By means of co-adsorption and the consecutive adsorption of CO and ethene on Ni^+ ions, it has been established that dimerization proceeds in the coordination sphere of Ni^+ ions via the following mechanism [1720]:



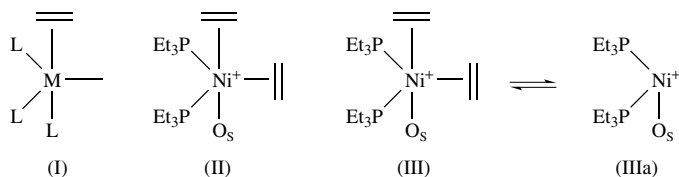
Scheme 6.32

namely, the Ni^+ ions allow the interaction of two ethene molecules according to the rules of orbital symmetry. These data are in good agreement with the results obtained earlier by EPR spectroscopy for various Ni-containing systems [862]. EPR spectroscopy showed that the monomeric paramagnetic Ni^+ species, dispersed in X-type zeolites or on SiO_2 , could reversibly bind a ligand (L), such as CO, C_2H_4 and C_3H_6 , to give rise to various $\text{Ni}(\text{L})_n^+$ species, depending on the pressure. Under low pressure (< 40 torr), tetrahedral $\text{Ni}(\text{L})^+$ and square planar $\text{Ni}(\text{L})_2^+$ entities were obtained. At higher pressures, Ni^+ with a trigonal bipyramid structure formed $\text{Ni}(\text{L})_3^+$ and $\text{Ni}(\text{L})_4^+$ complexes [862]. This stereochemistry implies in each case a given number of surface oxide ions, O_s^{2-} , acting as ligands. The 17- and 19-electron Ni^+ complexes easily undergo mono-substitution in their coordination spheres, while addition reactions were observed for the 17-electron complexes. At room temperature, the supported Ni^+ ions were active and selective for ethene and propene dimerization. After pretreatment at 973 K, the silica-supported catalysts showed trimerization, along with dimerization. Via poisoning experiments, it has been shown that two olefin molecules bound to each Ni^+ favors dimerization.

Che and co-workers [862] reported that one, two or four ligands (of triethylphosphine) are selectively introduced into the coordination sphere of silica-supported Ni^+ ions. It was shown that the five-coordinated species, $\text{Ni}^+ \text{L}_4(\text{O}_s)$, was inactive in C_2H_4 dimerization, while the square planar $\text{Ni}^+ \text{L}_2(\text{O}_s)_2$ and unsaturated $\text{Ni}^+ \text{L}(\text{O}_s)_2$ species were active, stable and selective at 313 K.

For saturated Ni^+ species, a d_z ground state is generally observed, giving a five-coordinate complex of D_{3h} symmetry. On the other hand, the adsorption of butadiene onto metallic cations has

been described in terms of π -bound complexes (Scheme 6.33, I) [1766–1768] with the butadiene ligand in the meridional position of the five-coordinate species. Che *et al.* [862] proposed structure (II) (Scheme 6.33) for the complexes resulting from the adsorption of butadiene onto diphosphine species. These authors have shown that two olefin molecules are bound to each Ni^+ ion when dimerization takes place, and also proposed that this species resulted from the equilibrium between the two following species (III and IIIa):



Scheme 6.33

It has been established by means of IR spectroscopy that the interaction of ethene with reduced *vanadium-containing catalysts* (for instance, $\text{V}_2\text{O}_5/\text{Al}_2\text{O}_3$ (10 mol% V_2O_5) [1050, 1167], containing mainly V^{3+} ions on the surface) leads to polymerization. This process is probably due to coordination of two ethene molecules by a single V^{3+} ion. The availability of two coordination sites in V^{3+} ions was established by the adsorption of NO and CO molecules (see Chapter 3) which formed dinitrosyl or dicarbonyl complexes, respectively. Such catalysts, unlike oxidized catalysts, do not contain Brønsted acid sites. Unlike ethene, propene is not polymerized on the surface of such a catalyst, perhaps because of steric obstacles to coordination of the second molecule of propene on the same V^{3+} ion. In this case, π -complexes of propene are formed with both V^{3+} and V^{4+} ions. The complex $\text{V}^{3+}-\text{C}_3\text{H}_6$ has an absorption band at 1615 (1555 cm^{-1} for C_3D_6) in the $\nu\text{C}=\text{C}$ stretching region. The V^{5+} ions do not coordinate ethene and propene molecules. There is no polymerization or oligomerization on the oxidized surface of this catalyst, in spite of the presence of Brønsted acid sites. The latter are responsible for the interaction of ethene and propene with the surface of this catalyst. Adsorption leads to the formation of ethoxy and 2-propoxy surface species, respectively, as a result of proton transfer to the ethene (propene) molecule. In the case of propene, the surface complexes show absorption bands at 1095 cm^{-1} (δCH) and isotopic shifts characteristic of such bands for C_3D_6 adsorption [1050, 1167].

Recently, catalysts for ethene polymerization based on reduced $\text{V}_2\text{O}_5/\text{Al}_2\text{O}_3$ and $\text{V}_2\text{O}_5/\text{SiO}_2$ systems, an active component of which more probably, is V^{3+} (as has been suggested by Davydov [1050]), have been widely developed. It was shown that the polymerization reactivity of reduced $\text{V}_2\text{O}_5/\text{Al}_2\text{O}_3$ was higher than that of the $\text{MoO}_3/\text{Al}_2\text{O}_3$ [1721, 1722].

The oligomerization of olefins on *molybdenum-containing systems*, in particular, on alumina–molybdenum (8 atom % Mo), has been widely investigated. It has been established that the oligomerization (in structure and length) on such a type of catalyst significantly depends on the degree of reduction of the catalyst [1723]. Thus, $\text{C}_{12}-\text{C}_{16}$ oligomers, the main part of which are *tert*-butyl groups, are formed on an oxidized surface during ethene oligomerization. Taking into consideration the presence of Brønsted acid sites in significant concentration in such a type of catalyst, it seems more probable that the oligomerization occurs on these centers via a carbanionic mechanism (see Section 5.1). It is known that such centers easily isomerize hydrocarbons.

On a slightly reduced (0.25 electron per Mo^{6+} average value of reduction degree related to one molybdenum ion) surface, an oligomer of the type $\text{C}_{10}\text{H}_{20}$ is formed, similar to that produced during the oligomerization of isopentene in 80 % H_2SO_4 , with the isopentyl species being the main structural fragment. Since protic acid sites are still present in the catalyst after such reduction, and hydrocarbons interacting with the surface produce surface carbenes, it is believed that the

reaction can proceed either on protic acid sites or by participation of paired centers involving carbenes and protons. When the degree of reduction is more than 0.5 e/Mo, the formation of hydrides is observed. These participate in polymerization via alkyl formation.

The formation of stable carbenes on the interaction of hydrocarbons with reduced (especially photoreduced (in CO) Mo-supported catalysts) has been established by means of IR and UV-Vis spectroscopic studies [1724–1728]. Surface carbene species of the Mo=CH₂ and Mo=CH-CH₃ types, which appear due to the interaction of methylcyclopropane with coordinatively unsaturated Mo⁴⁺ ions, are characterized by a charge-transfer absorption band at 450–460 nm in the UV-Vis spectrum. In the IR spectrum, Mo=CH₂ species exhibit bands at 3080 and 2945 cm⁻¹ (ν_s and ν_{as} of the =CH₂ group), while for Mo=CH-CH₃ complexes four bands at 2985, 2910, 2890 and 2850 cm⁻¹ were found in the C-H stretching region. Similar structures, together with olefinic π -complexes with Mo⁴⁺, have also been detected on the interaction of propene, ethene (C₂H₄ and C₂D₄) or 1,3,5-cycloheptatriene with such catalysts. The spectral characteristics of the carbenes formed on the interaction of different hydrocarbons with photoreduced silica-molybdena catalysts have been reported by Vikulov *et al.* [1728]. These carbenes are found to be thermostable *in vacuo* up to 650–700 K, oxygen resistant at 293 K and to react with water vapor at about 400 K to produce CH₄ in the case of Mo=CH₂.

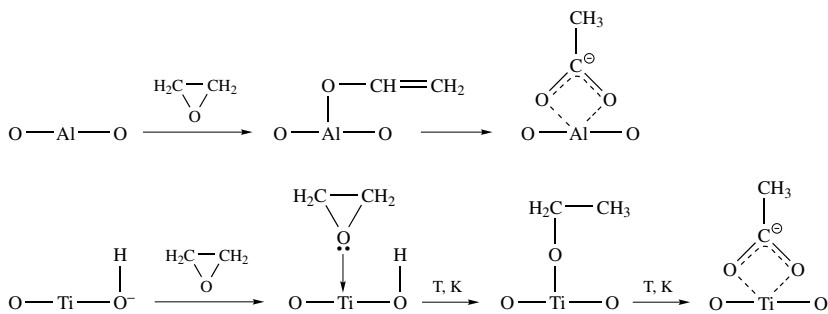
Polymerization of ethene oxide

Earlier [1729, 1730] the method of infrared spectroscopy has been used to study the mechanism of ethene oxide (EO) polymerization on the surfaces of aluminosilicate catalysts. Ethene oxide was weakly adsorbed on the surface of silica, and reacted chemically only with the surface of aluminosilica gel. The adsorption bands at 1620 and 1735 cm⁻¹ obtained in the spectra of the reaction products were attributed to the vibrations of the CH=CH₂ and C=O groups. The presence of a band at 3720 cm⁻¹, characteristic of the vibration of the C-H group, along with another band at 1735 cm⁻¹ from C=O, led to the conclusion that there is an aldehyde group at the end of the chain in the polymerization product. No spectrum of ethene oxide itself adsorbed on the surface of an aluminosilica gel could be observed. The interaction with a surface hydroxyl group takes place, whereby the ring opens with the formation of compounds of the type-O-CH₂-CH₂-OH on the surface. The presence of acid surface centers is essential for the polymerization. Ammonia pre-adsorption on the surface of an aluminosilica gel leads to the loss of catalytic activity of the catalyst.

The necessity for the presence of strong acid centers for EO polymerization has been shown by Naccache *et al.* [1729] and also that if the dehydration degree of the oxide surface is lowered then so is the catalytic activity of the aluminosilicate. It was proposed that the surface hydroxyl groups participate in the opening of the EO ring. In contrast to earlier studies [1730], it has been reported that unscreened metal cations on the surface are active polymerization centers. However, no direct data were obtained in this work to show the participation of such surface centers in the reaction. These questions, as well as that of the influence of these centers on the character of the initial activation of the monomer, are important considerations.

For this purpose [1731], catalysts such as SiO₂, Al₂O₃ and TiO₂ have been studied, with their different acceptor abilities of cations and mobility of protons in the hydroxyl groups. It was shown that the presence of surface hydroxyl groups on SiO₂ does not initiate the polymerization, and that EO forms only the H-bonded complexes (absorption bands at 3080, 3060, 3040 and 3350 cm⁻¹); at higher temperatures only a thermal degradation of EO to acetaldehyde is observed. The polymerization of EO does take place on Al₂O₃. By using alumina with variable degrees of dehydroxylation it was shown that the polymerization of EO proceeds on LASSs. Surface carboxylic groups are formed as a side reaction. Using TiO₂, which has weaker LASSs, showed that the opening of C-O-C ring takes place due to presence of strong LASSs; On weak LASSs, the

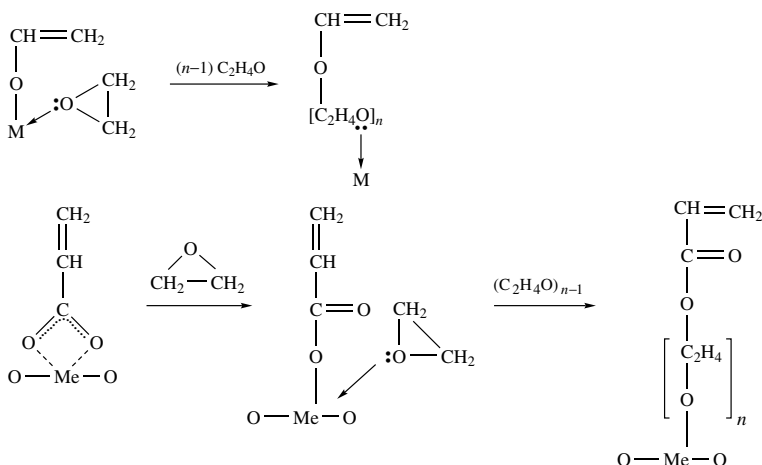
molecular form of adsorbed EO (absorption bands at 1270, 3025 and 3100 cm^{-1}) is stabilized as complexes of the following types:



Scheme 6.34

In addition, carboxylates are also formed.

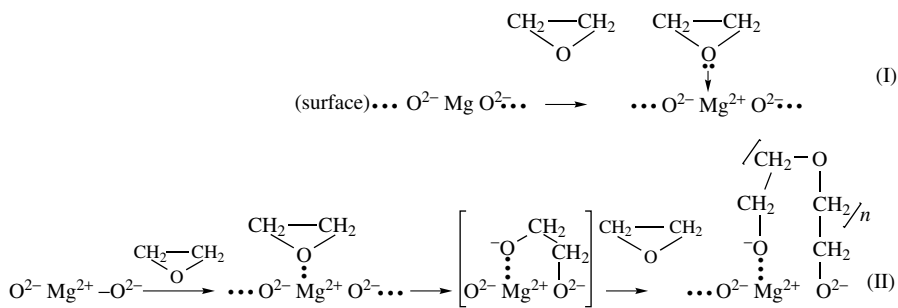
The mechanism of incorporation of a monomer molecule in a polymeric chain involving both alcoholates and carboxylates has been established [1732]:



Scheme 6.35

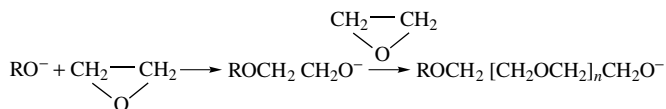
As has been shown by variations in the alcoholate groups (methoxy-, ethoxy- and iso-propoxylates) on the surface, and by measurements of the rates of polymerization, such incorporation proceeds at the M–O bond without participation of the C=C bonds.

In the early 1980s only one infrared study [1733] appeared in the literature concerning the interaction between ethene oxide and basic solids $[\text{MgO}$ and $\text{Mg}(\text{OH})_2$]. In this case, the polymerization proceeds probably via anionic intermediates. A radical mechanism for the polymerization of ethene oxide on reactive silica and oxygen-treated reactive silica has also been investigated by means of IR spectroscopy [1734]. Later, Platero and Zecchina [1735] and Loiko and Davydov [1731] published the results of infrared investigations of ethene oxide polymerization on MgO and MgO (CaO), respectively, where it has been shown that the monomer is coordinated at the surface magnesium ions:



Scheme 6.36

and that ethene oxide is inserted via an anionic mechanism:



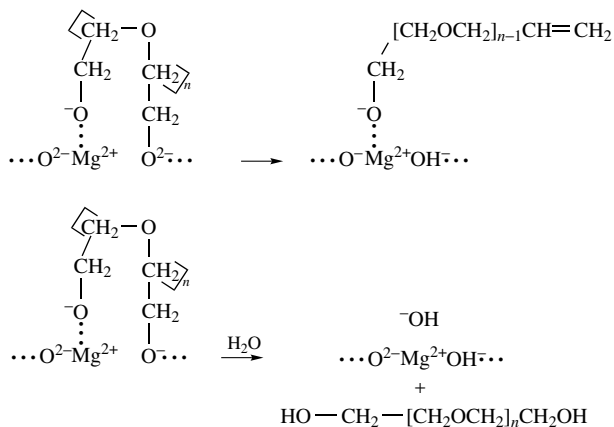
Scheme 6.37

Together with these processes, the formation of carboxylates has been revealed:



Scheme 6.38

Moreover, in the case of basic oxides and the presence of water the, following reactions can take place [1735]:



Scheme 6.39

Metathesis

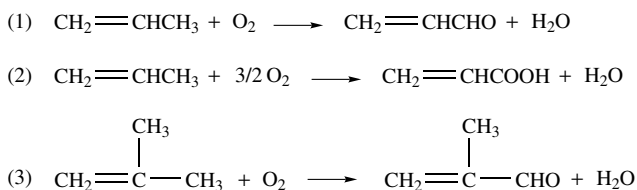
The metathesis of alkenes is a more complex type of reaction than those examined above. However, it is not difficult to observe and detect intermediate complexes in such cases, because the mechanism of this reaction is relatively simple. It is known that all of the reactants in this process belong to the same class of alkenes. This means that the intermediates should also be of the same type. Carbenes can be such intermediate complexes, as revealed in the case of the different photo-reduced Mo-containing catalysts examined above, for the metathesis reaction [1724–1728]. In fact, intermediate carbene complexes have been detected in the propene metathesis reaction. The data of (Vikulov *et al.* [1725, 1726] show that the fast transformation of Mo:CHCH₃ to Mo:CH₂ in the presence of excess gaseous ethene is accompanied by evolution propene into the gas phase. It should be noted that the possibility of the appearance of carbenes occurs in general metathesis processes and not just in photochemical reduction reactions.

6.2.3 PARTIAL OXIDATION

Alkenes

The recent appearance of several reviews of this much-investigated subject [66, 82, 1570, 1736–1739] has made it a lot easier to write this part of the book.

The partial oxidation of olefins, e.g. propylene to acrolein, and acrolein to acrylic acid or acrylonitrile, as well as the oxidative dehydrogenation of butene to butadiene, followed by oxidation to methacrolein, plays an important role in the chemical industry for organic synthesis. These reactions occur via a stepwise mechanism, as has been determined for several catalysts [94, 1570, 1740–1742]:



Scheme 6.40

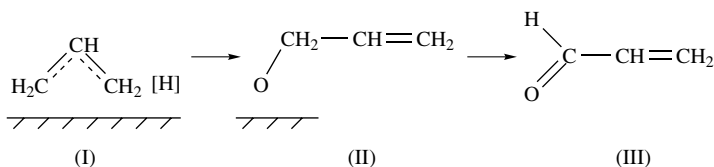
It should be noted that although fairly simple species are responsible for full oxidation, the intermediate structures during partial oxidation are more complicated. For their formation, specific sites with certain parameters should be present.

The oxidation of propene to acrolein

The methods of molecular spectroscopy have been used for a long time to investigate this important industrial reaction in order to establish the detailed mechanism. However, in spite of this, such information in the literature is ambiguous and sometimes even incorrect. First of all, no catalysts have 100 % selectivity for this reaction and this causes the presence of different types of surface species leading to different products. This makes very difficult the interpretation of the quite complicated spectra obtained as a result of such interactions, as well as the detection of surface species and active intermediates. Moreover, before spectral investigations were applied it was shown on the basis of isotopic data for Cu₂O [1736, 1737, 1743, 1744] and Bi–Mo oxide [1745] catalysts that the symmetrical allyl species is an intermediate in this reaction. Because of this,

numerous spectroscopic experiments were devoted to looking for such species. This led to incorrect identification of the surface species in many older articles leading to mechanistic schemes in the literature based only on hypothetical species. Since these schemes are still described, even in recent reviews, we believe that it is necessary to look at these results once more, despite the fact that in previous monograph [30] it was noted that some of the results were incorrect. This first relates to the spectral identification of allyl species on the surface of Bi–Mo catalysts [64, 1739]. It seems that to this day there are no reliable IRS data on the formation of such compounds on this catalyst. On the basis of data obtained in the 1970s and 1980s, authors continue to say that the absorption at 1510 cm^{-1} (unfortunately only one) observed in the spectra of propene adsorbed on $\text{Bi}_2\text{O}_3\text{--MgO}$ or Bi–Mo–Mg catalysts characterizes the $\nu_{\text{as}}\text{CCC}$ of the allyl species [64, 1739]. It should be noted, however, that no one has ever observed such an absorption band for pure bismuth molybdate (without MgO). In addition, absorption in this region is characteristic for the spectra of MgO obtained after interaction with the products of oxidation of different molecules, for example CO_2 [646]. Clearly, the presence of MgO in the catalyst makes the catalyst nonselective (unfortunately data about selectivity are not provided in published articles from these authors) and also, as MgO is a strongly basic oxide, this can give very different conversions of olefins in comparison with Bi–Mo–O. All of this was not considered by Matyshak and Krylov [64, 1739]. Data obtained in other studies of C_3H_6 conversion on pure bismuth molybdate [1278] or Bi–Mo–O/ SiO_2 [1506] supported the conclusion that the formation of stable surface species (associated with the absorption at 1510 cm^{-1}) is caused by the presence of MgO in the catalyst. For Bi–Mo–O catalysts without MgO, different authors observed the spectra which did not include the 1510 cm^{-1} absorption. The formation of the reaction product, acrolein, occurred at high interaction temperatures for C_3H_6 with such a catalyst [1278, 1506]. Through application of the high-sensitivity FTIR Spectroscopic method [1278], a weakly bound surface species were observed with an activated C–H bond (see Chapter 5). The latter complex is converted into acrolein on raising the temperature. This led to the conclusion [1278] that there is no need to activate the C=C bond for the conversion of C_3H_6 into acrolein – it is necessary instead to activate an allylic methyl C–H bond, which results in acrolein being formed immediately after the breakage of the C–H bond in the $\text{C}_2\text{H}_5\text{C-H}\dots\text{O}^{2-}$ complex. It is interesting that the same results were obtained on the other highly selective catalysts for the oxidation of propene to acrolein – Ti–Sb–O [1746] and Fe–Sb–O [246]. It should be noted that the results obtained do not contradict an allyl mechanism of oxidation of C_3H_6 to $\text{C}_3\text{H}_4\text{O}$ and only show that the rupture of the C–H bond is the limiting stage in the formation of the allyl species and so, in partial oxidation of C_3H_6 [246, 1746]. The above data show that whether allyls are observed or not on the surfaces of catalysts under reaction conditions is dependent on the rate-determining step of the reaction.

Spectroscopically, allyls have been observed just for a limited number of oxide systems (see Chapter 5), among which only Cu_2O and Ga–Mo–O catalysts are quite selective ($\sim 70\%$). It has been shown [30, 1148–1151] that surface π -allyl compounds are converted to acrolein. A principal scheme for such a reaction could be as follows [30, 1149]:



Scheme 6.41

The formation of allyls may occur on the cations or ionic pairs side-on or vertically, with the participation of its π - (π -allyl) or σ - (σ -allyl) orbital, respectively. Kondo *et al.* [1747], by means of microwave analysis of the products of propene–deuterium exchange, showed that for Bi_2O_3 – MoO_3 catalysts the σ -allyl predominates at low temperatures. However, studies of Sachtler and de Boer with ^{14}C -labeled propene generalized in [82] and also Adams and Jennings [1743, 1744] with deuterated propenes and C_4 – C_8 olefins demonstrated that the symmetric side-on allyls are intermediates in the selective oxidation reaction of olefins. Because of this evidence, a dynamic equilibrium between σ - and π -allyls (this existence of which was assumed by Kondo *et al.* [1747]) seems to exist and is described as a *dynamic allyl*. A significant role of the acid–base properties of oxide catalysts in the reaction of propene partial oxidation was repeatedly noted in the literature (see, for example, [1570, 1742, 1750, 1751]). It confirms the participation of the ionic pairs in the formation of allyls due to heterolytic dissociation (Chapter 5). It should be noted that a point of view exists that the reaction of partial oxidation proceeds via an allylic radical [1752, 1753].

An investigation of the oxidation reaction mechanism for propene on catalysts leading to partial oxidation (gallium-molybdenum and copper-containing oxide catalysts [1149, 1281]) has shown that the allyl complex (I) Scheme 6.41 is converted into compound II (Figure 6.7) and that this reaction leads to the subsequent transformation of the alkene into acrolein. As can be seen from Figure 6.7, within the limits of experimental error the initial decomposition rates of the allyl complex and for the formation of a σ -compound are comparable. It has been shown [1150, 1256] that the possibility of an allyl attaching itself to oxygen on the catalyst surface is determined by its state of charge. In order for an allyl to be changed into the acrolein-like surface compound II, it is necessary for the allyl on the catalyst surface to be ‘carbonium cation’ in nature [1150, 1256].

The study of the IR and TD spectra of propene and allylbromide adsorbed over ZnO and Cu_2O [1149, 1150] showed that the direction of propene oxidation depends on the charge on the allyl species. An allyl anion formed over ZnO upon propene adsorption is not converted to the product of partial oxidation. In the presence of oxygen, electron transfer from an allyl anion to oxygen with the formation of an O_2^- ion was observed [1748], similar to that seen for MgO [1251, 1252, 1749] and oxidation of allyls to formates and carboxylates takes place.

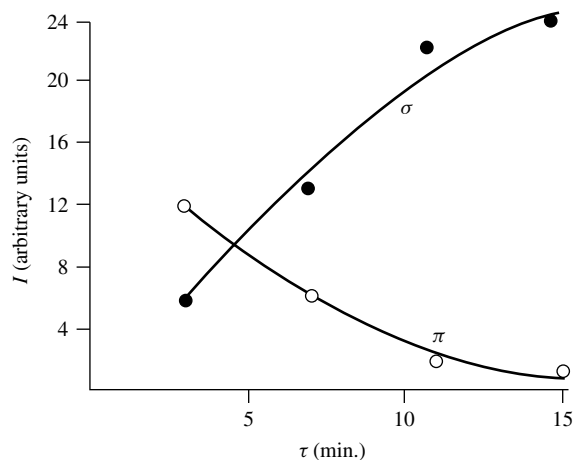
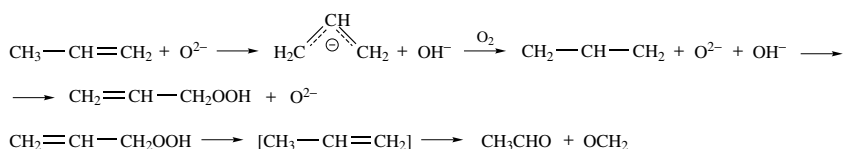


Figure 6.7. Changes with time of the integral intensities (I) of (O) the 1400 cm^{-1} ($\nu_{\text{as}}^{\text{CCC}}$) band for a π -allyl on a Ga–Mo oxide catalyst at 293 K and (●) the 1100 cm^{-1} ($\nu_{\text{C-O}}$ in compounds of type II) absorption band.

The formation of formate and carboxylate structures on ZnO seems to occur via a mechanism similar to that obtained in the case of MgO through intermolecular electron transfer between the carbanion formed upon dissociative heterolytic adsorption and gaseous oxygen. The radical formed can be either dimerized to benzene [1150] without participation of the gas phase oxygen or oxidized to surface formates and carboxylates, probably even through a peroxide intermediate. Formates and carboxylates are then converted to the full oxidation products (CO_2 and H_2O).

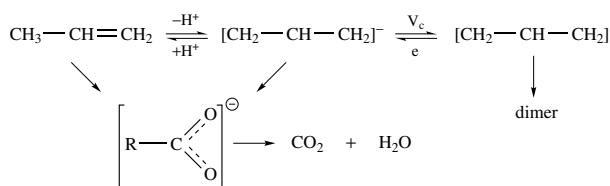
Using the interaction of propene with oxygen on a ZnO surface at 303 K, Kugler and Kokes [1748] showed, using IR spectroscopy, that in the presence of propene adsorbed as a π -allyl, the absorption of oxygen increases, and that a number of new absorption bands belonging to an 'X-species' appears in the IR spectrum. By spectral investigation of the adsorption of a number of compounds which could be formed during the reaction (acrolein, allyl, propene, isopropene, crotonaldehyde, propionic acid, acetic acid and acetaldehyde) it has been established that only the spectrum obtained in the case of acrolein coincides with that of the 'X-species'. This fact supports a proposition that the oxidation of propene proceeds through the interaction of adsorbed π -allyl with O_2^- , with the formation of a $\text{Zn-O-O-CH}_2\text{-CH=CH}_2$ peroxide compound which then decomposes over the ZnO surface producing water and adsorbed acrolein. The formation of propene peroxide compounds on ZnO upon oxidation, with oxygen, may proceed according to the scheme proposed by Garrone *et al.* [1749]:



Scheme 6.42

However, the data obtained [1150] indicated that such peroxide compounds decompose with the formation of formates and acetates, i.e. lead to the formation of the full oxidation products. The reaction of propene with oxygen on the surface of ZnO does not lead to the formation of acrolein. The reason is that the allyl complex of a 'carbanion' type formed on ZnO is incapable of converting directly to acrolein. An attempt was made to prove that the cationic form of the allyl fragment can be obtained on ZnO and also to follow its conversion into a product of selective oxidation. Indeed, an analysis of the IR spectra and the thermal desorption data of allyl bromide, which has a tendency to dissociate into C_3H_5^+ and Br^- , confirmed the formation of surface allyl complexes of a 'carbocation' nature. The spectral characteristics of these were similar to those of the allyl formed on copper-containing catalysts, plus the possibility of its conversion to acrolein.

As can be seen from Figure 6.8, the thermal desorption of allyl bromide on the ZnO surface is accompanied by the evolution to acrolein (curve 2). On the basis of these data, the following scheme has been proposed for propene conversion on ZnO:



Scheme 6.43

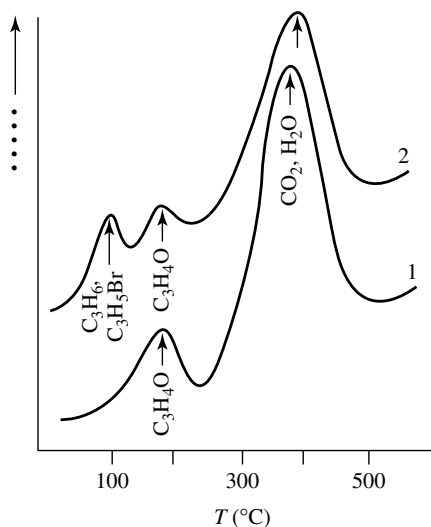
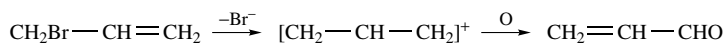


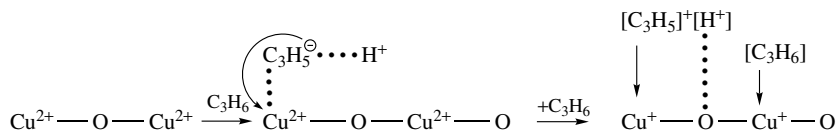
Figure 6.8. Thermal desorption traces for (1) acrolein and (2) allyl bromide desorbing from the oxidized surface of ZnO.

No acrolein is formed in the course of these reactions. To convert propene into acrolein, an electron transfer from the allyl radical is required, with the formation of a carbocation which then reacts with the oxygen ion on the catalyst surface. On ZnO, as on an **n**-type semiconductor with a high concentration of carriers, such transfer is hindered, and therefore dimerization is the main reaction path. The difficulty of charge transfer in the surface allyl can be avoided if propene is replaced by allyl bromide, which directly forms a carbocation. In this case, the following reaction path leads to the formation of acrolein:



Scheme 6.44

If a **p**-type semiconductor, e.g. CuO, is used as a catalyst for the oxidation of the allyl, an allyl cation is formed more readily and the direct conversion of propene to acrolein takes place. ESR and IR spectroscopy have been employed in investigations of the reaction of propene with model copper-containing catalysts [1253]. It was established that during the formation of allyl on the oxidized catalyst surface (containing only Cu^{2+} ions) a transfer of electrons from an allyl fragment took place. The transfer was not only to the copper-ion-stabilized allyl but also to the neighboring ion, according to the scheme:



Scheme 6.45

In this way it was shown that the presence of the ion pair $\text{Cu}^{2+}-\text{O}-\text{Cu}^{2+}$ is required for the formation of an allyl fragment ('carbocation') capable of undergoing conversion into acrolein.

As can be seen from the reaction scheme, the electron transfer to the neighboring Cu^{2+} ion requires a reaction between adjacent copper ions ($\text{Cu}^{2+}-\text{O}-\text{Cu}^{2+}$). In the case of an isolated Cu^{2+} ion, the transfer of the second electron could be hindered because of the spatial separation of the Cu^{2+} ions, and the formation of the 'carbocation form' of π -allyl will be unlikely. The transfer of one of the electrons to an isolated Cu^{2+} ion, which stabilizes an allyl species, is equivalent to the formation of an allyl radical. This form could be responsible for the formation of dimers [1235, 1570]. Consequently, we could expect changes in the reaction course of propene conversion on copper-containing catalysts.

An ESR spectroscopic investigation of the adsorption of propene on zeolites containing isolated copper ions has indeed shown that the transfer of electrons from allyl to Cu^{2+} ions does not occur, but in contrast to the result for CuY-A zeolites, the polymerization of propene takes place (Figure 6.9, spectra 2). Thus, it was possible to accomplish the process of propene conversion on different types of surface sites in the case of copper-containing systems.

Based on an analysis of spectral data on adsorbed propene species, a relationship between the nature of the olefin adsorption centers (of oxide catalysts), adsorbed during pre-catalysis, and the direction of propene conversion was already established in the 1980s. For the majority of oxide catalysts, in the oxidation of propene the C-H bond rupture is the rate-limiting step. It is therefore probable that the reaction with the alkene in the pre-catalysis stage will stop when a π -complex or H-bonded complex with participation of nucleophilic oxygen of the surface and CH_3 group of olefin are formed. Subsequently, an increase in temperature may result in a rapid transformation of the these complexes which form into reaction products via the cleavage of the

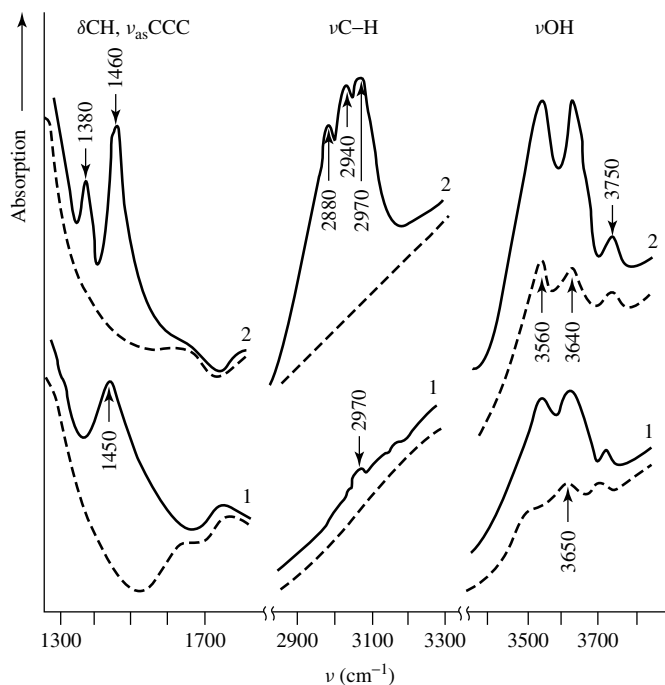


Figure 6.9. Infrared spectra of propene adsorbed on (1) CuY-A and (2) CuY-I zeolites at 293 K, after desorption at 373 K.

C–H bond. Obviously, this explains why the number of systems is limited for which the formation of stable allyl complexes can be generated. For some oxide systems, a direct transformation of the surface π - and H-bonded complexes into the corresponding aldehydes has been established [30, 1150]. For CuO–MgO in the case of which the presence of weakly bonded oxygen, unusual for the catalysts of partial oxidation, has been detected, the π -complexes are decomposed with increasing temperature through destruction of the double bond and the formation of oxidized compounds of the formate and carboxylate types [1241].

A comparison of the data obtained for different systems shows that the properties of the oxygen of the catalyst surface largely determine the nature of the alkene chemisorption, including the reaction of the surface π -complexes. Thus, for oxides of transition metals with weakly bound oxygen on their surfaces, a predominantly destructive oxidation of alkenes takes place, resulting in the formation of carboxylates and formates.

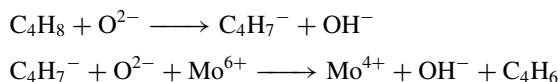
For systems with strongly bound oxygen, the primary stages of complex formation with alkenes have been established and a relationship found between the adsorption forms and directions of the subsequent reactions. An importance of the properties of surface oxygen in propane conversion can be seen, for example, from a comparison of the spectroscopic data obtained for solid solutions of CoO–MgO and NiO–MgO [1242] and for such solid solutions containing molybdenum ions [1216]. For the solid solutions without molybdenum ions, the reaction, $C_3H_6 + O_2$, results in alkene destruction and the formation of formate and carboxylate complexes, even at room temperature. On catalysts containing molybdenum ions, destructive oxidation was inhibited. On the surface of the latter catalysts, the alkene is stabilized only as a π -complex (573 K), at temperatures up to those required for the catalytic oxidation. Above 573 K, it produces acrylate and aldehyde-like surface compounds.

Thus, the reaction starts with the activation of propene on the cation (π -complex) which is then attacked by nucleophiles (O^{2-}). This stage also includes a hydrogen abstraction (on ionic pairs) with the formation of the allyl anion. The next stage is an electron transfer from the allyl anion to the cation; the latter is thus reduced. Due to the nucleophilic attack by the lattice oxygen, the oxidized product is formed and desorbed as acrolein. Oxygen vacancies are thereby left on the surface, which are replenished by oxygen from the gas phase with reoxidation of the cations. Obviously, this scheme represents a stepwise mechanism which is common in the case of the partial oxidation of olefins [82, 1737]. There is only one study in which it has been proposed that the propene oxidation proceeds via a concerted mechanism [1754]. In this case, the spectral data obtained showed that acrolein is not formed upon interaction of the oxidized catalyst (MoO_3/SiO_2) with propene.

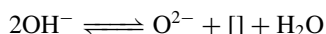
Generally, the conversion of propene to acrolein does not require the activation of the double bond in the alkene; the activation of the C–H bond in the CH_3 group is more important. For some oxide catalysts, e.g. Sb_6O_{13} [244], and for highly selective Fe–Sb–O catalysts [246], as well as for Bi–Mo catalyst the reaction of propene–oxygen mixtures results in the formation of a weakly bound propene complex on the catalyst surface. This complex is stabilized by oxygen on the surface of catalyst by a hydrogen-bond involving the hydrogen atom in the CH_3 group. In principle, this complex can be converted to acrolein by breaking the latter C–H bond. Unfortunately, no quantitative data have yet been obtained for the conversion of such compounds because of the low concentration of these compounds on the catalyst surface. Structural forms of this type are undoubtedly of interest in determining reaction intermediates produced during partial oxidation. It should be noted that the formation of carboxylates or formates on the surface of high selective catalysts (Bi–Mo; Fe–Sb; Ti–Sb; Sb_6O_{13}) was not observed spectroscopically. This may indicate that the formation of the irreversible form which has been detected by thermal desorption [1755] is connected to the conversion of the reaction products.

Butene oxidation

A very important recently discovered reaction of partial oxidation is butane oxidative dehydrogenation to butene and then to the products of greater oxidation. For this, V–P–oxide systems are the most active catalysts. While not examining here the first stage of the reaction (oxidative dehydrogenation of alkanes to alkenes, which was analyzed in Section 5.4), it should be noted that the data on conversion and selectivity indicate the following reaction sequence: but-1-ene \rightarrow butadiene \rightarrow furan [82]. According to Bielanski and Haber [82], the reaction starts by an α -hydrogen abstraction and the formation of a π -allyl complex, which then loses the second hydrogen atom and is desorbed as butadiene:

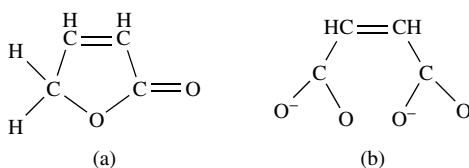


Two OH^- groups recombine and are desorbed as water and leave a vacancy on the catalyst surface:



The oxidation of *n*-butane and *n*-butenes over V–P–O catalysts has been investigated by IR spectroscopy [1227, 1229, 1231, 1503, 1758–1763]. Only two types of reversible butene complexes (probably π -complexes) are formed on the surfaces at reaction temperatures up to 520 K. Further temperature increases gives rise to the formation of compounds such as cyclic anhydrides (adsorptions at 1780 and 1850 cm^{-1} are observed). An investigation of furan and 2,5-dihydrofuran adsorptions showed that the bands at 1715 and 1620 cm^{-1} , which also appear at higher temperatures, seem to be due to an intermediate species in the oxidation of butadiene to maleic anhydride: an unsaturated lactone (or maleic acid [1229]) or an adsorbed form of furan (or carboxylate species [1227, 1231, 1760–1763]) respectively. Such an assignment is confirmed by similar spectra obtained after butadiene adsorption on V–P–O, V_2O_5 – TiO_2 [1764] and MoO_3 – TiO_2 [1491], showing that on all of the listed catalysts there are particular sites able to insert an oxygen atom into the 1,4-position of butadiene, giving rise to furan-like cyclic compounds. Unfortunately, there are not yet convincing data concerning the formation of allylic compounds over catalysts involving butene in selective oxidation.

In the oxidation of but-1-ene on V_2O_5 – $\text{P}_2\text{O}_5/\text{Al}_2\text{O}_3$ at 373–423 K (i.e. below the stationary reaction temperature) adsorbed 1- C_4H_8 (two π -complexes), 1,3- C_4H_6 , furan, maleic anhydride and 2(5*H*)-furanone were detected by IR spectroscopy. Butadiene forms complexes of two types: π -complexes (1,2 and 1,4) and a σ -complex. Furan is adsorbed at the C(2) atom, and 2(5*H*)-furanone forms the following complex (a), whereas maleic anhydride is adsorbed in both physisorbed and chemisorbed forms, and in the last case as the stable complex (b):



Scheme 6.46

Among all complexes observed, only the 2(5*H*)-furanone (a) is active under the catalysis conditions [1231].

The oxidation of propene to acetone

This reaction was first studied 1968 and is now known as *oxydehydrogenation*. The reaction proceeds in the temperature range of 373–473 K. The $\text{SnO}_2\text{-MoO}_3$ and $\text{TiO}_2\text{-MoO}_3$ and $\text{SnO}_2\text{-V}_2\text{O}_5$ systems are found to be the best catalysts for this reaction. In the case, for example, of an $\text{SnO}_2\text{-MoO}_3$ catalyst with an Sn/Mo ratio of 9:1, the selectivity to propene conversion to acetone is 90 %. As has been reviewed in [82], the participation of surface OH groups in the propene transformation to acetone has been shown by using isotopic labeling because extremely rapid H–D exchange between propene and D_2O takes place. Moreover, experiments with H_2^{18}O proved that the oxygen atom in the acetone that is produced comes from water. Kinetic studies showed that isopropanol is an intermediate in this reaction.

The first infrared spectroscopic study of this reaction on an $\text{SnO}_2\text{-MoO}_3$ catalyst, which included separate studies of both acidic and redox centers of the catalyst and the interaction of these centers with the reaction mixtures, involving mixtures including isotopically labeled molecules, was made by Davydov and co-workers [748, 1168, 1765]. The bi-functional action of such a catalyst was demonstrated. The formation of isopropoxide surface species was observed upon propene interaction with protic acid sites (acidic functions), and then the isopropoxides were transformed into acetone by oxidative dehydrogenation (redox functions) [1765].

In the reaction of a tin–molybdenum oxide catalyst with a mixture including propene, an isopropoxide surface compound is formed on the surface of the catalyst, even at room temperature. The reaction occurs via a transfer of a proton to the alkene molecule with the formation of an isopropoxide complex in a similar way to that formed upon the adsorption of isopropyl alcohol. The determining role of the mobile surface protons in the formation of compounds of the isopropoxide type was shown by investigations of catalysts with Brønsted acid centers blocked by sodium ions. No compounds of the isopropoxide type were observed for such catalysts [748, 1168].

As can be seen from data presented in Figure 6.10, compounds of the isopropoxide type (spectrum 1), after being heated at 423 K (spectrum 2), have been almost completely converted

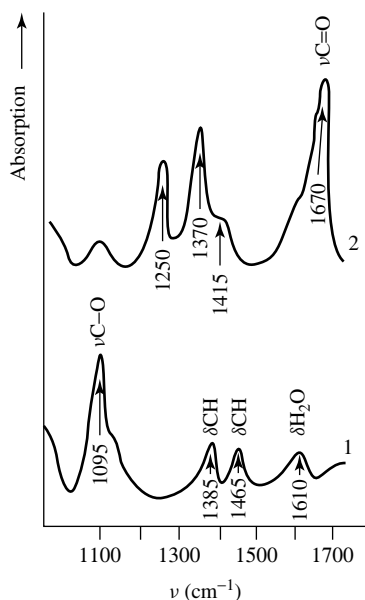
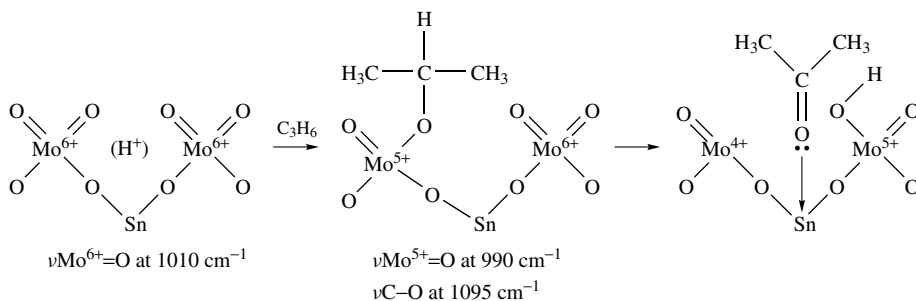


Figure 6.10. Infrared spectra of propene adsorbed on a hydrated surface of a Sn–Mo-oxide-type catalyst at (1) 293 K and (2) 423 K.

into acetone. Spectrum 2, recorded after the C_3H_6 has reacted with the hydrated surface of a tin–molybdenum catalyst, coincides completely with the spectrum of acetone absorbed at 293 K on the same catalyst [748, 1168].

The rate of decrease in the concentrations of isopropoxide compounds and the rate of increase in the concentration of acetone produced were compared [748]. The comparison was based on measurements of the absorbency values of the most characteristic absorption bands of these compounds ($\nu C-O$ at 1095 cm^{-1} and $\nu C=O$ at 1670 cm^{-1}). The results shows that the formation of acetone is due solely to the reaction of isopropoxide compounds. On an alkali-treated catalyst, no acetone was detected, which also indicates that it is produced from isopropoxide compounds.

The conversion of propene to acetone according to Davydov *et al.* [30, 748] shows that water participates in this reaction:



Scheme 6.47

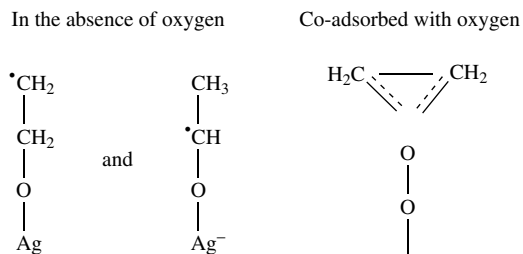
Its participation involves the hydration of the catalyst surface and the generation of mobile protons. Oxygen reoxidizes the catalyst surface after the evolution of the reaction product – acetone. Hence, the catalysts for the conversion of propene to acetone are typically bi-functional catalysts which combine acidic and redox properties. From the analysis given above, it follows that the composition of these catalysts should include cations of the transition elements in their highest oxidation states (e.g. V^{5+} and Mo^{6+}).

The limiting stage of this reaction is the separation of H atoms from isopropylates [748]. On an oxidized catalyst containing V and Mo, at low temperature propene can undergo partial oxidation to acetone, but not to acrolein [215, 219, 221, 1050, 1167, 1168, 1186, 1483]. Spectral studies [1739, 1765] of this reaction detected the surface isopropoxides. As reported by Matyshak and Krylov [1739], oxidative transformations of olefins on Sn–V–O catalysts take place via a reaction pathway which is similar to that described by Davydov and Shepotko [1483]. The only difference is the presence of molecularly adsorbed isopropyl alcohol (in addition to propoxide). However, there is no proof of the formation of these species in [1739].

The oxidation of ethene

It is generally accepted that ethene is not adsorbed on reduced metallic silver [1766, 1767], but its adsorption was observed after pre-adsorption of oxygen [759, 1203, 1768] or chlorine [1769], i.e. such a reaction takes place on an oxidized surface only. Davydov and co-workers [30, 759, 1211, 1203] and Force and Bell [1770] demonstrated by IR spectroscopy that ethene absorbs as a π -complex on an oxidized silver catalyst surface. The related coordination of ethene with Ag^+ ions was reported earlier [759, 1771] and examined above in detail in Chapter 5. However, the kind

of oxygen participating in the oxidation of π -complexes to ethene oxide has yet to be established. The data allow the proposal of the following structure for adsorbed ethene oxide [1770]:



Scheme 6.48

In infrared studies of ethene interaction with oxidized Ag/SiO₂ [1772], an absorption band at 870 cm⁻¹ has been interpreted as the O–O vibration in the organic peroxide species CH₂–CH–O–O–Ag. The infrared spectrum obtained after heating of the sample up to 383 K is identical to that obtained in the case of the adsorption of ethene oxide on a reduced silver surface. Support for the above assignment of the 870 cm⁻¹ band comes from the data obtained when using an equilibrated ¹⁶O₂ + ¹⁶O¹⁸O + ¹⁸O₂ mixture, when three bands are observed at 870, 859 and 848 cm⁻¹ [1773]. In the case of a nonequilibrated ¹⁶O₂ + ¹⁸O₂ mixture, only two bands are observed at 870 and 848 cm⁻¹, proving that the two oxygen atoms in the adsorbed peroxide species originate from the same gaseous oxygen molecule. Above 433 K, dissociation of molecular oxygen takes place at the surface.

Later, the interaction of C₂H₄ with a Ag (110) face, precovered with adsorbed oxygen, was studied by Back *et al.* [1774]. Adsorption of ethene was found to be promoted by the presence of monoatomic oxygen. No significant shift of the ν CH or δ C–H vibrations were observed, indicating that there was no significant rehybridization.

Diffuse reflectance Fourier-transform infrared spectroscopy and the transient response method have simultaneously been applied to elucidate the structure of the surface compounds formed on a silver surface during ethene oxidation and acetaldehyde formation. In both reactions, at temperatures from 353 to 453 K, the adsorbed compounds showed very similar character in their nature and reactivity: they produced acetic acid and a small amount of ethyl alcohol when exposed to H₂, but decomposed into CO₂ and H₂O if exposed to O₂ [1775].

Oxidative dehydrogenation

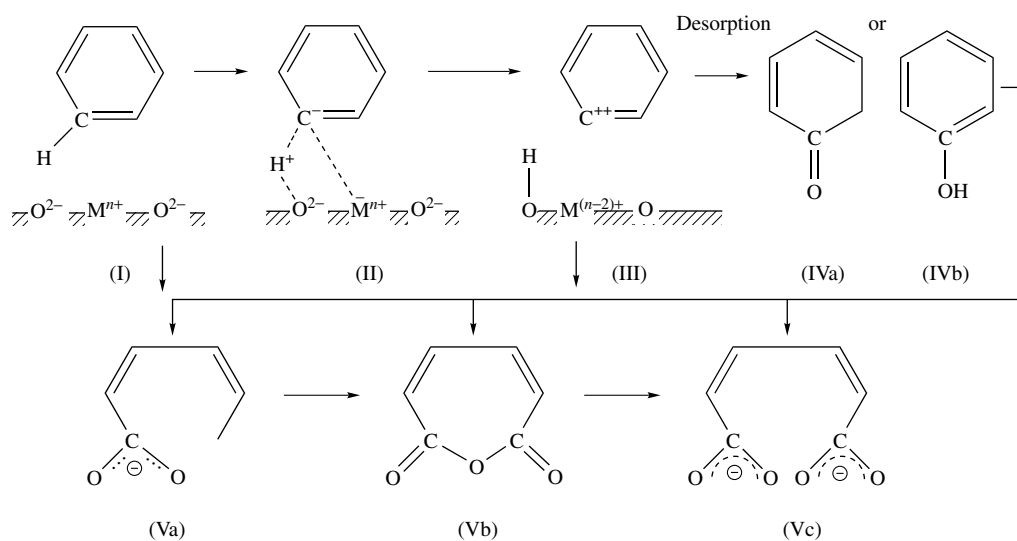
Oxidative dehydrogenation reactions of olefins proceed most probably through the participation of their π -complexes, since these are the only complexes to have observed on typical catalysts for olefin dehydrogenations, such as Ni–P–O and Ga–La–Sb–O [1778a]: It should be pointed out that the π -complexes formed are bound by an additional bond to surface oxygen via a hydrogen bond of the CH₂ or CH₃ groups.

The oxidation of aryls

For the partial oxidation of aryls, spectral investigations of the transformation of such compounds on oxide surfaces (or of spectro-kinetic studies of the interactions of surface compounds) confirming the structure of intermediates are rare in the literature, even though IRS and UV–vis studies started as early as the 1960s. Odrin *et al.* [1779] performed a series of studies concerning the

mechanism of naphthalene oxidation over vanadium-containing catalysts. However, they found vibrations of carboxyl groups only. Based on the high stabilities of such surface species (the temperature of removal of these compounds exceeds that of the oxidation process), these vibrations have been assigned to structures that deactivated the catalyst. The role of the oxygen component of the reaction mixture has not been taken into consideration. The influence of oxygen on the thermal stabilities of such surface compounds was established later and has already been described above in Section 6.2.1. Sachtler *et al.* reported later the data on toluene oxidation [1780]; they detected the formation of a surface compound of the type BzCOO^- which is responsible, in their opinion, for initiating the partial oxidation reaction. Later, Niwa *et al.* [1781] made the first study by *in situ* diffuse reflectance spectroscopy of the ammoxidation of methylaryls over vanadia–alumina.

We will examine the data on the participation of aryl complexes (see Section 5.2) in the oxidation. The oxidation of benzene, except for the formation of phenol or quinone (see below), proceeds via ring opening. Possible schemes for benzene transformations on the majority of oxides can be represented as follows:



Scheme 6.49

Compounds of type (V) can then be oxidized to simple surface carboxylates and formates depending on the amount of oxygen and magnitude of the bonding energy on the surfaces of the catalysts. No doubt, the compound (Vc) leads to the formation of the products of full oxidation. Heterolytic dissociation of benzene and the formation of the surface compounds (I)–(III) are reasonable assumptions taking into account the data on olefin transformations analyzed above, and also some additional results concerning benzene transformations obtained by Davydenko *et al.* [1334]. Compounds (Va) and (Vc) gave practically the same spectral patterns. This makes identification of their common or separate presences impossible. At the same time, the compound (Vb) has also been detected (see Chapter 5).

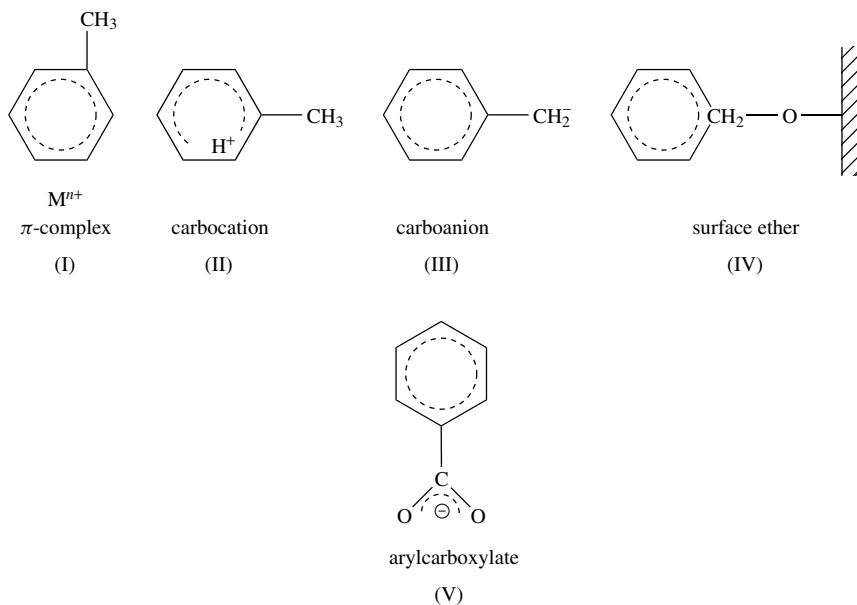
It has been established that V–oxide catalysts and ZSM zeolites are highly selective catalysts for the transformation of benzene to phenol [1782–1784]. The idea concerning the possible participation of contaminant iron ions in the partial oxidation of benzene to phenol on ZSM

zeolites has been confirmed [1784]. An FTIR spectroscopic study of these zeolites involving adsorbed NO molecules [1785] showed that the states such as $\text{Fe}^{2+}-\text{O}-\text{Fe}^{3+}$, $\text{Fe}^{3+}-\text{O}-\text{Fe}^{3+}$ or $\text{Fe}^{2+}-\text{O}-\text{Fe}^{2+}$ occur in the ZSM-type zeolites, similar to those established for FeY-type zeolites [30, 491]. According to these studies, there are no unusual states of iron ions in Fe-ZSM zeolites as with FeY zeolites and it is more probable that the oxidation state pairs like $\text{Fe}^{2+}-\text{O}-\text{Fe}^{3+}$, $\text{Fe}^{3+}-\text{O}-\text{Fe}^{3+}$ or $\text{Fe}^{2+}-\text{O}-\text{Fe}^{2+}$ are active in the oxidation reaction. Even given a small content of iron in a zeolite, the presence of such groupings is highly possible because iron ions cluster strongly together. It is clear that such states are dominated at the low concentration of iron ions since the formation of the oxide phase is excluded, and after using up the bridged oxygen, they can be easily oxidized by N_2O . At the same time, the oxidation of these states by oxygen meets some difficulties because isolation of these pairs.

Based on the information given above, the scheme for the reaction pathway becomes clear. According to this, the catalysts achieve two functions: (i) they oxidize benzene by oxygen from one of the bridges and/or by oxygen from a V-containing phase [1784], and (ii) they protonate the product formed due to the high mobile protons present in such catalysts. Hence, both types of highly selective catalysts for benzene partial oxidation to phenol are bifunctional. The first function is oxidative while the second is acidic.

Vanadia-based catalysts can also be used for other oxidation processes [66, 82], for example, for the gas-phase selective oxidation of *para*-xylene to phthalic anhydride, the gas-phase ammoxidation of toluene to aromatic nitriles, and the gas-phase oxidation of *para*-xylene to carboxylic acids. The gas-phase selective oxidation of *ortho*-xylene to phthalic anhydride over $\text{V}_2\text{O}_5-\text{TiO}_2$ -based catalysts leads to the main products of maleic anhydride and carbon dioxide and to the minor byproducts, i.e. *ortho*-tolualdehyde, *ortho*-toluic acid, phthalide, benzoic acid, toluene, benzene and citraconic anhydride.

As was shown above, the character of activation of alkylaromatic compounds depends on the type of active centers present on the surfaces. In the case of toluene, for example, the following surface compounds have been identified on the oxide surface (Chapter 5) [1157]:



Scheme 6.50

At present, it is not easy to exactly establish the kinds of surface compounds that are intermediates because of the absence of spectro-kinetic measurements. However, a common use of IRS and TDS data demonstrated that compounds of the type (V) lead to aryl acids and/or aldehydes. Probably, a conjugation of $C\equiv O$ bonds with a benzene ring, like that between the $C=C$ bond and the carboxylic group in the case of acrylates, makes the $Bz-C$ bond stronger. The latter inhibits the separation of CO_2 into the gas phase, as usually observed during the conversion of carboxylates during full oxidation of hydrocarbons (see Section 6.2.1). Davydov and Budneva [1304] even established that the conversion of compounds of type (V), formed during the interaction between ortho-xylene and $V/Ti-O$ catalysts to form products of partial oxidation, is accelerated in the presence of oxygen. This means that the formation of the products in this case occurs via a concerted mechanism [1786], in contrast to the fact that partial oxidation of hydrocarbons usually proceeds in stages.

The initial activation of alkylaromatic compounds on oxidized surfaces of vanadia-containing catalysts is due to the presence of BAS, the strength of which is more than in the case of zeolites [460]. This process leads to the formation of carbocations stabilized on surface oxygen (Section 5.12). Dehydrogenation of such compounds leads to the formation of aldehyde-like compounds. This is clear directly from the spectra (Figure 6.11), since under vacuum these compounds are easy transformed to species containing the $C=O$ bond. The presence of a proton perturbing the aromatic nature of the ring leads to the easy oxidation of the cationic species which are formed to give aldehydes, with the appropriate bands in the 1700 cm^{-1} region ($\nu C=O$) becoming detectable.

Under a reducing atmosphere, the catalyst is changed. This fact, as known (see Section 2.4.1), in the case of bifunctional catalysts, leads to the loss of protic acidity and changes the character

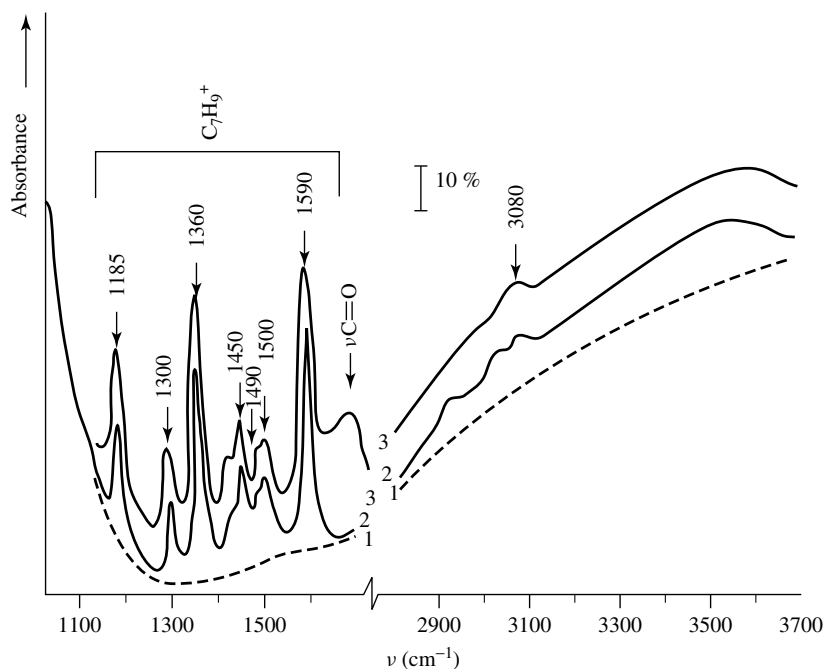


Figure 6.11. IR spectra of toluene adsorbed on V_2O_5/Al_2O_3 and on V_2O_5 : (1) background spectra of the oxidized V_2O_5/Al_2O_3 ; (2) toluene (6 torr) at 300 K; (3) subsequent desorption at 300 K.

of toluene activation. As has been shown for V_2O_5/Al_2O_3 [1157] and V/Sb catalysts [1303], benzyl species are formed. There is no disagreement between these data and other published results [1787, 1788], as have been suggested by Busca [66]. The latter conclusion is the result of a misunderstanding of the processes taking place in this case, since the possibility of the reaction proceeding via two different pathways (transfer and abstraction of the proton) in the case of such catalysts was not taken into account. Such a possibility has clearly been shown for propene oxidation to acetone (proton transfer to propene) and to acrolein (proton abstraction from propene). These two processes take place on the same catalysts containing the metal (Mo, V, Sb etc.) in high oxidation states (≥ 4). Contribution of each of these processes is determined by the reaction temperature and degree of reduction of the catalyst. Thus, on the oxidized catalysts at low temperatures mainly acetone is formed. Taking into account that the Bi-Mo catalyst for partial oxidation of propene to acrolein is slightly reduced in the steady state and its proton-donor properties are lowered, acetone formation is inhibited.

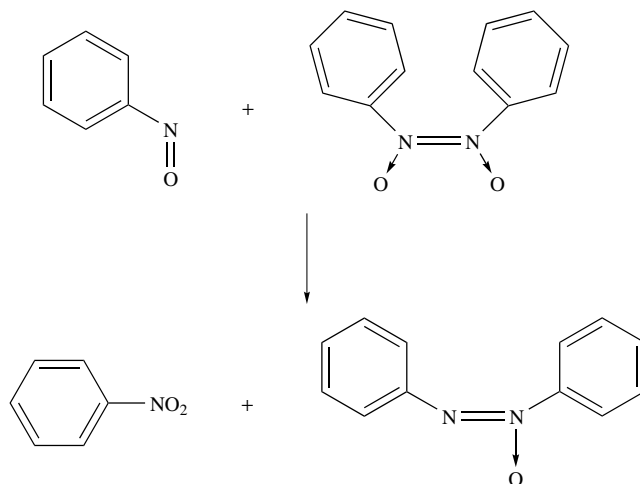
The spectral identification of the benzyl species, including the adsorption of isotopically substituted molecules, has also been carried out [1157, 1303]. Based on the appearance of a new hydroxyl group on V/ Al_2O_3 , and also on data verifying that the benzyl species appears more easily in the case of an ammoniated surface of the V/Sb/O catalyst, the process of heterolytic dissociation of toluene with the formation of H^+ and benzyl anions has been deduced (Section 5.2). The formation of more basic N^{3-} or NH_2^- and NH^{2-} groups on the amination of the surface promotes such heterolytic rupture. Busca's opinion about the rupture of H^- from the hydrocarbons [66] has not been approved and is based only on a general analysis of the acidic properties of supported V-containing catalysts. All the more, it is not clear, in the light of such a suggestion, regarding the rupture of the H^- ion from the CH_3 group, as to which benzyl group has to be formed – $BzCH_2^+$? Such a group would react with oxygen immediately and produce a benzyl surface compound such as $Bz-CH_2-O-$, although the authors did not detect this. Why was this so? It is also impossible to agree with Busca's suggestion [66] that the basic centers are not important for C–H bond activation on catalysts of such a type. Of course, V_2O_5 itself has weak basic centers [646], but vanadia-supported systems, the basic properties of which are well known [1157, 1192, 1193], are used as catalysts for oxidation reactions. Moreover, it is known that in a reduced state the carrier is activated and its basic properties are exhibited, even given a significant content of the active component.

Unlike Busca [66], we have proposed a scheme for toluene oxidation to aldehydes based on various studies [1157, 1249, 1277, 1303, 1325, 1193] and postulated that the heterolytic dissociation of toluene to H^+ and $BzCH_2^-$ (Section 5.2.4), a scheme similar to that suggested for the oxidation of propene to acrolein, seems to be more reasonable [212, 214, 215, 1167, 1186, 1303]. The latter suggests two-electron transfers to the clustered cations of V^{4+} with formation of a benzyl cation, followed by the combination of that cation to oxygen. Such a complex probably produces an arylaldehyde.

The processes of proton transfer to aromatic molecules and of proton abstraction have different natures, proceed on different centers, and lead to different products. It should be taken into account that in the case of proton transfer a carbocation is formed and its following oxidation proceeds more probable, with the opening of the ring and the formation of the certain oxidation products, whereas in proton abstraction, benzyl species are formed and may be converted to aromatic aldehydes under favorable conditions (the possibility of two-electron transfer to the catalyst). Either of these processes may take place over V-supported catalysts – which is prevalent depends on the degree of oxidation/reduction of the catalyst (the temperature of the oxidation process).

Recently published data [1789, 1790] on the selective oxidation of nitrobenzene and the deoxygenation of nitrobenzene on oxide catalysts have established the role of lattice oxygen atoms in

the oxidation of nitrosobenzene to nitrobenzene. These experiments used isotopically labeled oxides and $^{18}\text{O}_2$ as oxidants. Based on these results, the Mars and van Krevelen mechanism (oxidation by lattice oxygen atoms) is the main reaction mechanism if the most active catalyst, i.e. $\gamma\text{-Mn}_3\text{O}_4$, is used, whereas on $\alpha\text{-Fe}_2\text{O}_3$ and $\gamma\text{-Al}_2\text{O}_3$ the Langmuir–Hinshelwood mechanism (disproportionation of nitrobenzene) prevails:



Scheme 6.51

Among other types of surface compounds of aryls, the cation-radical adsorption forms should be noted. Their formation has been observed more often on alumina–silica catalysts (amorphous or crystalline) by means of ESR [1791] and DRES [17, 46–49, 1792, 1793] spectroscopies. A number of different experiments have been carried out in this area. Some of these were initiated by Academician A. N. Terenin and performed by E. N. Kotov and co-workers [17, 1792, 1793]. Other data have been analyzed in a comprehensive review [46]. This appearance of the cation radical M^+ and the molecular ion MH^+ (the bands at 430 and 260 nm, respectively) is considered to result from the primary interaction of an aniline molecule (M) with active surface sites, while the protonated cation radical $\text{M}^+ - \text{MH}^+$ (560 nm) and cation radical $\text{M} - \text{M}^+$ (820 nm) of benzidine are considered to be formed due to secondary processes, with the participation of M , MH^+ and M^+ occurring on the surface of the alumina–silica gel. The formation of molecular ions of type MH^+ is well established. These are formed on BAS as a result of proton transfer to form $\text{H}_3\text{N}^+ - \text{Bz}$. According to Vymovkov and Kotov [1793], the $\text{Si}^+ - \text{O}_{3/2}$ centers which are formed, together with centers of the types $\text{Al} - \text{O}_{3/2}$ and $\text{Al} - \text{O}_{4/2}$, play the role of specific electron-acceptor centers on the surface of the gel. Through interaction with such centers, an electron is donated by the aniline molecule. The latter is then converted to the cation radical M^+ , which migrates to the closest $\text{Al} - \text{O}_{4/2}$ center and is stabilized there.

Oxidative dehydrogenation

The conversion of ethylbenzene to styrene is a well-known example of oxidative dehydrogenation and has great industrial importance. This reaction probably proceeds through the participation of the aryl's π -complexes since only complexes of this type have been observed on the typical catalysts which are used [see, for example, 1794, 1795]. It should be pointed out that the π -complexes formed are bound by an additional bond to the surface oxygen via the $\text{O} \dots \text{H}$ bond of the CH_2 or CH_3 groups of the alkylaryl [1794].

The oxidation of alkanes

The selective conversion of alkanes to partial oxidation products has received much attention by researchers due to the necessity of obtaining the valuable hydrocarbons from such cheap gaseous feedstocks. These processes, which have been intensively developed in recent years, include: (i) methane oxidative dimerization, (ii) oxidative dehydrogenation of C₂–C₄ alkanes, and (iii) methane oxidation to methanol or formaldehyde. Significant progress has been made in understanding these processes. The data obtained from different spectral methods have made important contributions to our understanding of the questions concerning the mechanisms of these processes.

It is clear that the processes of alkanes conversions are determined by the activation of the C–H bond, which depends in turn on the nature of the surface active sites (see, for example, [1796]).

The partial oxidation of methane has been achieved with high selectivity by the direct high-pressure gas-phase oxidation of natural gas to methanol and other oxygenates [1797]. Direct catalytic oxidation at atmospheric pressure does not provide high selectivity or yields, but a majority of carbon oxides are formed as a result of the 'deep' oxidation of formaldehyde (CH₄ → HCOH → CO_x). The rate constant for the HCHO oxidation to CO derived from the data of this study is 50–1000 times higher than that for methane conversion [1797]. As for catalytic conversion of methane, that takes place at much lower temperature than the gas-phase oxidation. The silica-supported molybdenum oxide and vanadium oxide are more selective catalysts for the partial oxidation of CH₄ to formaldehyde [1798]. The reactivity for methane conversion appears to be essentially related to the presence of dispersed isolated surface metal oxide species, with the surface vanadium oxide species being more reactive than the molybdenum oxide species. The higher reactivity of the surface vanadium oxide sites may be related to the different nature of the interaction of the oxides with oxygen. Silica-supported vanadium oxide catalysts, despite their higher activities, show lower yields of HCHO than those obtained from silica-supported molybdenum oxide. The results indicate that the activity depends on the MoO₃ content. A major issue in the partial oxidation reaction over oxide catalysts is the role of the lattice oxygen. The ¹⁸O₂ isotopic technique has been used to study the mechanism of oxygen incorporation into CH₄. The results confirmed that the selective oxidation proceeds via the Mars–van Krevelen mechanism in which the lattice oxygen is incorporated into the methane molecule while the oxygen consumed is restored by dioxygen from the gas phase [1799–1802].

It has been reported that different heteropolyoxometalates are selective catalysts in methane partial oxidation [1803]. In this case, the reaction is inhibited by proton–cation exchange. Studies of ethane and isobutane conversions on heteropolyoxometalates showed that the mechanism of such processes is related to the elemental composition in the vicinity of the anion of the catalyst and the acidic strength of the solid acid [1804]. In C–H bond scission, the catalyst plays an important role. Both the selectivities and yields of these processes depend on the strength of the terminal oxygen–anionic metal bond.

In situ FTIR spectroscopic studies showed the generation of a peroxide species (an absorption band at 895 cm⁻¹, which shifted to 849 cm⁻¹ when ¹⁶O₂ was replaced by ¹⁸O₂, and three absorption bands observed at 895, 870 and 849 cm⁻¹ if the adsorbed mixture was ¹⁶O₂ + ¹⁸O₂) which appears on contact of an H₂–O₂ gas mixture or of N₂O with Fe–Al–P–O catalysts at ≥ 573 K [1805]. It was revealed that this species reacts with CH₄. The results showed that the intensity of the band at 890 cm⁻¹ decreased significantly when the temperature was raised to 473 K and new bands at 3668, 2396, 2870 and 1050 cm⁻¹ appeared. The adsorption at 3668 cm⁻¹ can be assigned to the newly formed OH group due to the reaction of CH₄ with iron peroxide species. The bands at 2936 and 2870 cm⁻¹ had been assigned to the ν^{as} and ν^s modes of CH₃ groups, and the band at 1050 cm⁻¹ to the νC–O mode of a methoxy species [1806].

Dehydrogenation or oxidative dehydrogenation are important reactions in the conversions of paraffins. Dehydrogenation, for example, of propane takes place on the same La–Ga–Sb oxide catalysts, probably by a mechanism involving heterolytic rupture of the C–H bond with formation of the anionic species $(C_3H_7)^{\delta-}$ (Section 5.4) which can convert to propene, by hydride (H^-) separation. The V–Mg–O system is a good catalyst for propane dehydrogenation, too. The mechanisms of propane and butane oxidative dehydrogenations on this catalyst have been investigated [1807, 1808]. The important role of the oxygen species (most likely, monatomic dissociated oxygen) in the breaking of a C–H bond to form an adsorbed alkyl species has been shown. Oxidative dehydrogenation of propane can occur via two alternative mechanisms, with the first via hydride ion abstraction and carbenium ion formation, which the second is related to the redox properties of the catalyst [1808].

These examples, along with the data presented in Section 5.4, illustrate the important role of the initial activation on the surface with the formation of different surface compounds. We will examine the role of such surface compounds in methane transformations.

The role of surface species in the direction of methane conversion

The behavior of metal–methyl groups forming on some oxides (Section 5.4) depends on the catalyst and temperature. Thus, in the case of MgO (Figure 6.12, spectrum 2), after increasing the interaction temperature to 973 K (spectrum 2a), the concentration of these groups strongly decreases, probably due to their conversion into the reaction products (simultaneous increase of the $\nu=C-H$ band at 3085 cm^{-1} indicates the separation of ethene), and also as a result of their oxidation to form formates and then the reaction products (CO, CO_2 and H_2O). The conversion of metal–methyl groups also observed over alumina probably occurs mainly in this way. The proportion of the latter process is less if the oxide has been dehydrated before interaction with methane at a higher temperature.

It has been shown in direct experiments of methane conversion [1809], in which specially synthesized metal–methyl groups on the oxide surfaces have been used, that if weakly bound reactive oxygen is absent on the oxide surface, then oxidative coupling is the main product. In the presence of such weakly bound reactive oxygens on the surfaces metal–methyl groups are oxidized to full oxidation products. In the case of hydrocarbons with longer chains, such metal–alkyl groups are unstable and easily split off hydrogen, thus leading to the products of dehydrogenation (olefins).

For a number of oxide catalysts, for example SiO_2 [1810], supported molybdenum oxide systems [1811], or Fe_2O_3 (Figure 6.13, spectrum 1), the formation of methoxy groups upon interaction of methane has been observed by infrared spectroscopy. According to the spectral data (Figure 6.13), these groups are converted to formates with increasing temperature. That means that they take the role of intermediates in the full oxidation process.

A very interesting possibility for the formation of acrylic acid by direct catalytic oxidation of propane has not been revealed so far at temperatures up to 693 K [1812]. It was proved by IR studies that the reduced heteropolymolybdophosphoric acids are catalysts for this reaction and it was shown that both the acidic character and the highly reduced state of the $H_3PMO_{12}O_{40}$ catalyst play substantial roles in the course of propane oxidation with molecular oxygen. The authors propose the co-operation of proton and electron transfers in the reduced HPA catalyst provides acidity for the activation of molecular oxygen and subsequently of propane: molecular dioxygen first reacts with two protons and two electrons to form one molecule of water.

The most successful oxidation of lower alkanes has been the selective oxidation of *n*-butane to maleic anhydride; this has been successfully demonstrated and commercialized using the crystalline V–P–O catalysts [1813]. It should be noted, however, that the character of the initial activation has not been established. Immediately after the introduction of the reaction mixture on

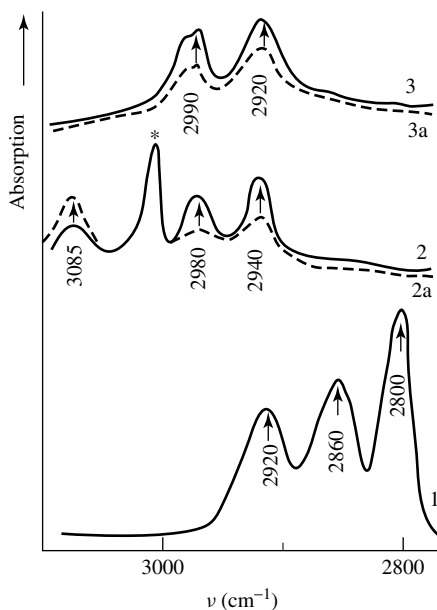


Figure 6.12. Infrared spectra in the region of the CH stretching vibrations of (1) CH_3OH adsorbed on MgO at 273 K, followed by desorption at 473 K, and adsorbed species: (2) CH_4 at 773 K and (2a). 973 K; $(\text{CH}_3)_2\text{SnCl}_2$ adsorbed on MgO , dehydroxylated at (3) $(\text{CH}_3)_2\text{SnCl}_2$ adsorbed on MgO , dehydroxylated at 973 K; (3a) the spectrum of $(\text{CH}_3)_2\text{SnCl}_2$ itself (* represents the absorption band corresponding to CH_4 (gas) due to incomplete compensation of the gas phase).

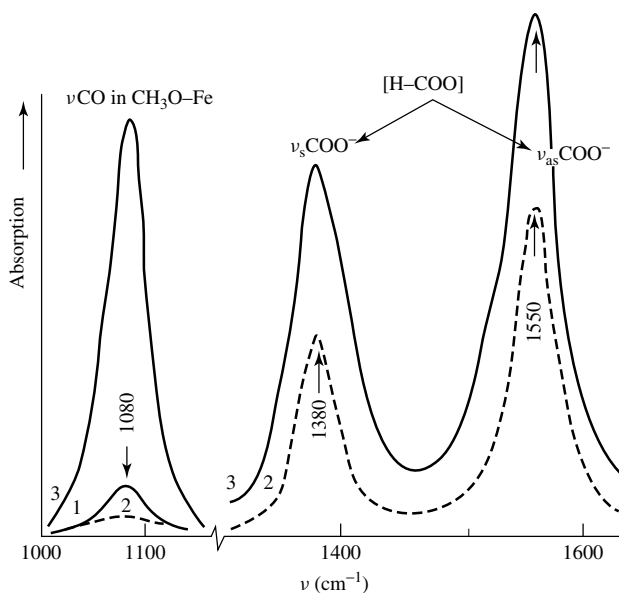


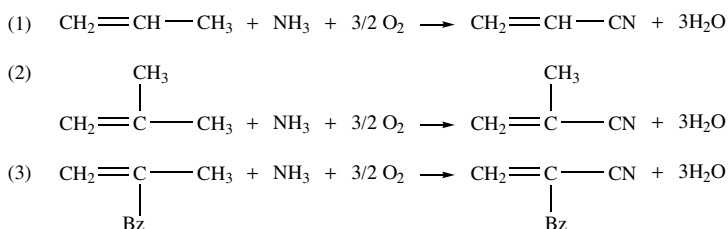
Figure 6.13. Infrared spectra of Fe_2O_3 oxidized at 723 K after interaction (1) with CH_4 at 423 K and (2) 573 K, and (3) with CH_3OH at 273 K, followed by desorption at 373 K.

to the catalyst, bands at 1710 and 1780 cm^{-1} appeared in the spectrum. No doubt, this points to the formation of a compound containing the C=O bond [1814].

It has been established that the selectively stable oxidative dehydrogenation of butane to butene can take place on heteropolyoxoanion catalysts [1815]. The solid-state rearrangement of the Wells–Dawson $\text{K}_6\text{P}_2\text{W}_{18}\text{O}_{63}\cdot 10\text{H}_2\text{O}$ catalyst to a stable Keggin-type heteropolyanion phase leads to the selective oxidation of isobutane to isobutene. There are also schemes for the conversion of C_4 paraffins to maleic anhydride, which as a rule include a stage of initial dehydrogenation of the paraffin with the formation of the olefin.

6.2.4 AMMOXIDATION OF HYDROCARBONS AND THEIR DERIVATIVES

The most important commercial allylic oxidation process is ammoxidation of propylene. Mixed metal molybdates and antimonates are the most active catalysts for ammoxidation of olefins. Such catalysts (i) possess optimum M–O bond strength, (ii) isolated active sites, (iii) have a solid-state redox couple consisting of a multivalence element in close structural proximity to the active site of dissociatively chemisorbed gaseous oxygen, (iv) promote oxygen ion transport, (v) stabilize oxygen deficient structures, and (vi) maintain the active sites in a highly oxidized state [1736, 1737]. Active sites are involved in the rate-determining allylic hydrogen abstraction, ammonia activation, and O or NH insertion into the allylic group:



Scheme 6.52

The main steps are olefin and ammonia chemisorption, rate-determining α -hydrogen abstraction, oxygen and NH insertion. One of the components of the catalyst has to be unsaturated, in order to have a vacant orbital for chemisorption and to promote an electron transfer from the π -cloud of the olefin to the metal.

As was shown above, π -complexes and complexes with an activated $\text{C}\cdots\text{H}\cdots\text{O}^{2-}$ bond, as detected on Bi–Mo–O and Fe–Sb–O catalysts, can play the role of the initially activated molecule of propene. In the limiting stage, these complexes are transformed to allyls which, due to the transfer of electrons to the catalyst's cation, are easily converted to allyl cations. The latter, in turn, react with basic centers (O^{2-}) producing acrolein or with more basic (NH_x^-) groups giving nitriles. Formation of the basic groups, NH_x^- (NH_2^- , NH^{2-} , and even N^{3-}) [459, 1303, 1820] derived from the interaction of the catalyst with ammonia, have been detected by means of infrared spectroscopy on the surfaces of some transition-metal oxides. In the case of molybdenum and vanadium oxides, which are the components of selective catalysts, even the $\text{N}^{\delta-}$ group is formed on the surface. It is clear that the addition of an allyl cation to such centers will lead to the formation of the nitrile.

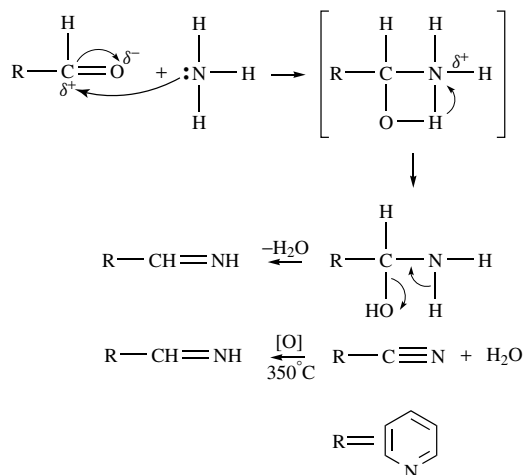
Ammoxidation of a number of compounds, such as hydrocarbons, aldehydes and alcohols, occurs in reactant mixtures containing ammonia. It is now well established that all ammoxidation catalysts are affected by the strong influence of ammonia [197, 459, 1303, 1376, 1816–1818, 1820]. The latter, when it interacts with the catalysts, modifies their surfaces, by protonation or dehydration, with the formation of coordinated NH_3 , NH_2^- , NH^{2-} and N^{2-} . These fragments

can be bound to both surface cations and anions. The $M-NH_2^{\delta-}$ or $NH^{\delta-}$ species, mentioned above (Chapter 3), can be directly identified on the surfaces of practically all oxides, whereas the presence of $M^{n+}-N^{\delta-}$ groups are identified, as a rule, by using the adsorption of CO, which forms isocyanate (NCO) groups (by interaction with such a fragment). The NCO group has a characteristic infrared spectrum with a high extinction coefficient of the absorption band [459].

Due to its strong electron-donor properties, the ammonia molecule is able to compete with oxygen ligands from the coordination sphere of the cation. This especially applies to the cases of V^{5+} and Mo^{6+} cations. Ammonia is coordinated by high-charged V^{5+} or Mo^{6+} cations producing a donor-acceptor complex with strong V-N (or V-Mo) bonds. The formation of the coordination bonds leads to a strong weakening of the N-H bonds in the coordinated ammonia molecule, and hence promotes both the interaction of $H^{\delta+}$ with oxygen anions in the coordination sphere of vanadium (or molybdenum) and the formation of new strong nucleophilic centers of the types $NH_2^{\delta-}$ and $NH^{\delta-}$, or even $N^{\delta-}$ [459].

An especially intensive formation of the dehydrogenated forms of adsorbed ammonia has been observed on the surface of the catalysts used for the selective ammoxidation of aromatic compounds (on V-Sb-Bi-O [1303]) and propane (on Ga-La-Sb [1376]). Perhaps the high reactivity of Ga-Sb-O and Ga-La-Sb in propane ammoxidation (the yield of acrylonitrile reaches 60.9 % on catalysts [1820] of this type – the highest selectivity yet formed) is due to the strong basicity of these systems (Table 6.3).

One of the possible mechanisms of hydrocarbon ammoxidation on the catalysts used for partial oxidation involves the addition of ammonia to the product of partial oxidation (e.g. an aldehyde) [1819]:



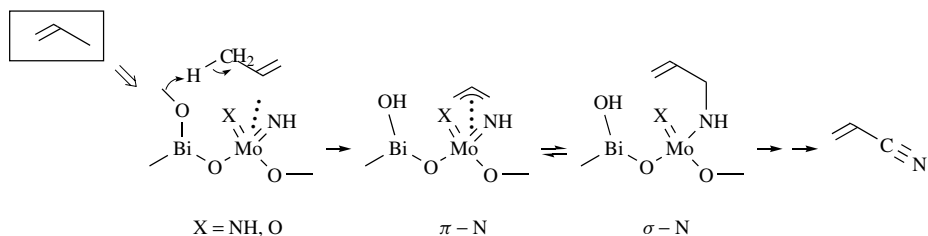
Scheme 6.53

Table 6.3. Best indexes of propane ammoxidation on multi-component gallium-antimony catalysts.

Catalyst system	Ratio of additives to C_3H_8		X (%) ^a	$S_{C_3H_3N}$ (%)	Yield (%)	
	$C_3H_6:C_3H_8$	$CH_3Br:C_3$			C_3H_3N	Total nitrile
Ga-Sb-Ni/P-La-O	0.13	–	75.5	53.3	41.0	70.0
Ga-Sb-Ni/P-Mo-O	–	0.004	85.4	50.3	43.0	60.0
Ga-Sb-Ni/P-W-O	0.13	0.000 14	90.0	58.2	52.3	65.2

^a X, conversion of C_3 . Feed (vol %): C_3 , 5; NH_3 , 6; air, 89 ($t = 550^\circ\text{C}$).

This scheme is probably correct because aldehydes have been separated as reaction intermediates on a number of such catalysts. However, besides the above scheme, direct participation of ammonia with dehydrated fragments in the reaction is also known. For example, in the case of Bi–Mo–O catalysts, which are the most selective ones for this reaction, the following scheme has been presented [1737]:



Scheme 6.54

Ammoxidation of paraffins

The question as to how the propane ammoxidation products are formed on complex oxide catalysts has been examined by Sokolouskii *et al.* [1820], based on a gallium–antimony system. These authors compared the ammoxidation of propane and considered propylene as a probable intermediate product; they elucidated the steady-state oxidation products while varying the ammonia concentration in the reaction mixture. Studies of the selectivity as a function of conversion have revealed a distinctive consecutive reaction mechanism. The initial selectivity towards acrylonitrile was ca. 100 %. When the conversion was increased, the selectivity towards acrylonitrile dropped, while that towards the products of ‘deep’ oxidation was increased. The comparison of propane and propylene ammoxidation on gallium–antimony oxide catalysts provides evidence for the formation of similar reaction products in both reactions (Table 6.4); i.e. acrylonitrile, carbon oxides and minor amounts of both acetonitrile and hydrocyanic acid. With propylene ammoxidation, small amounts of acrolein were also detected. The rate of propylene conversion was higher than that of propane by 1.5 orders of magnitude. This fact shows that the unsaturated nitrile is formed on the gallium–antimony catalysts via the sequence, propane–propylene–acrylonitrile (see Scheme 6.55 below). However, the above data do not allow the exclusion of the possibility of acrylonitrile formation from propane without propylene desorption from the surface, i.e. that propylene can be formed as an intermediate which, without desorption, is quickly converted to an allyl and subsequently, an aldehyde and a nitrile. Kinetically, this route can be described as a direct nitrile formation from propane.

The reaction scheme of propane ammoxidation via propylene formation was also proposed for bismuth–vanadomolybdate catalysts [1821]. However, for V–Sb–O-based systems the kinetics of the direct acrylonitrile synthesis from propane indicate that acrylonitrile is formed either directly from propane or through propylene formation (the latter pathway seems to dominate) [1822, 1823].

For gallium–antimony catalysts doped with nickel and phosphorous, the selectivity dependence on conversion was studied at various starting ammonia concentrations (0–2 %). The data obtained indicate that acrolein is formed at low ammonia concentrations. When the ammonia concentration increases, the selectivity towards acrolein drops while that towards acrylonitrile increases. At 2 % ammonia concentration, acrolein is completely converted to acrylonitrile.

The large difference between the propane and propylene conversion rates (see Table 6.4) shows that propane dehydrogenation to propylene proceeds much slower than the conversions that follow. As a result, the steady-state concentration of propylene itself should be very low. This

Table 6.4. Comparison of propane and propene ammoxidation on gallium–antimony–oxide catalysts.

Catalyst	S_{sp} (m ² g ⁻¹)	T (°C)	τ (S)	X (%) ^a	Selectivity (%)				
					C ₃ H ₃ N	C ₃ H ₄ O	C ₂ H ₃ N	HCN	CO + CO ₂
Ga ₁ Sb ₄₉ O ₁₂₄	75	480	18.5	10.2	42.6	–	11.6	4.0	41.8
			550	18.5	28.3	35.3	–	5.0	8.0
Ga ₁ Sb ₉ O ₂₄	83	450	7.9	6.4	68.3	–	1.2	–	30.5
			22.0	15.0	50.0	–	–	–	50.0
		450	11.0	74.3	78.7	0.4	1.0	1.5	18.4
			20.0	83.5	60.0	–	0.5	5.3	34.2
			42.0	92.0	56.0	–	0.4	3.0	40.6
Ga ₁ Sb _{4.5} O _{12.75}	80	450	12.0	24.0	27.5	–	–	6.0	66.5
			4.0	52.5	61.2	0.5	2.1	4.0	32.8
		450	6.0	45.7	35.7	2.6	1.7	5.2	54.8

^a X, conversion.

apparently gives rise to only a small amount of propylene among the reaction products on the gallium–antimony systems.

If the reaction proceeds through a positively charged or radical hydrocarbon residue, then C–H bond dissociation should occur at the central carbon atoms (secondary and tertiary atoms of propane and isobutane, correspondingly). In this case, the hydrocarbon residues are the most stable and the rate of isobutane conversion should exceed that of propane. The data cited above speak for the opposite situation. Thus, the intermediate is probably a carbanion. Since the primary carbanions are more stable, the CH₃–CH₂–CH₂[–] structure (I) is likely to be the intermediate in propane conversion. Similarly, CH₃–CH(CH₃)–CH₂[–] (II) is the most probable intermediate of the isobutane conversion. The latter structure is less stable than the first one. A higher stability of structure (I) compared to structure (II) explains the higher conversion rate of propane compared to isobutane.

The results obtained correlate with the IR spectroscopic data on propane interaction with the Ca–Sb oxide catalyst surface. Absorption bands at 2860, 2930 and 2960 cm⁻¹, typical for adsorbed propane, were detected upon propane adsorption on Ga–Sb–La (1:3:1) catalysts [1376] (Section 5.4; Figure 5.33). In this case, the ratio between the 2960 ($\nu_{as}CH_3$) and 2940 ($\nu_{as}CH_2$) cm⁻¹ intensities and, respectively, the relative contents of methyl and methylene fragments in the adsorbed propane, change essentially in favor of the latter (Figure 5.33). If the alkyl residues formed upon propane activation were of the radical or cationic types, the C–H bond should have dissociated through the methylene fragment. If this is the case, the ratio of the intensities from the methylene and methyl groups should change in the opposite way. Taking into account the carbanionic nature of the fragments formed, it has been suggested that propane dissociation involves the basic sites on the Ga–Sb oxide catalysts.

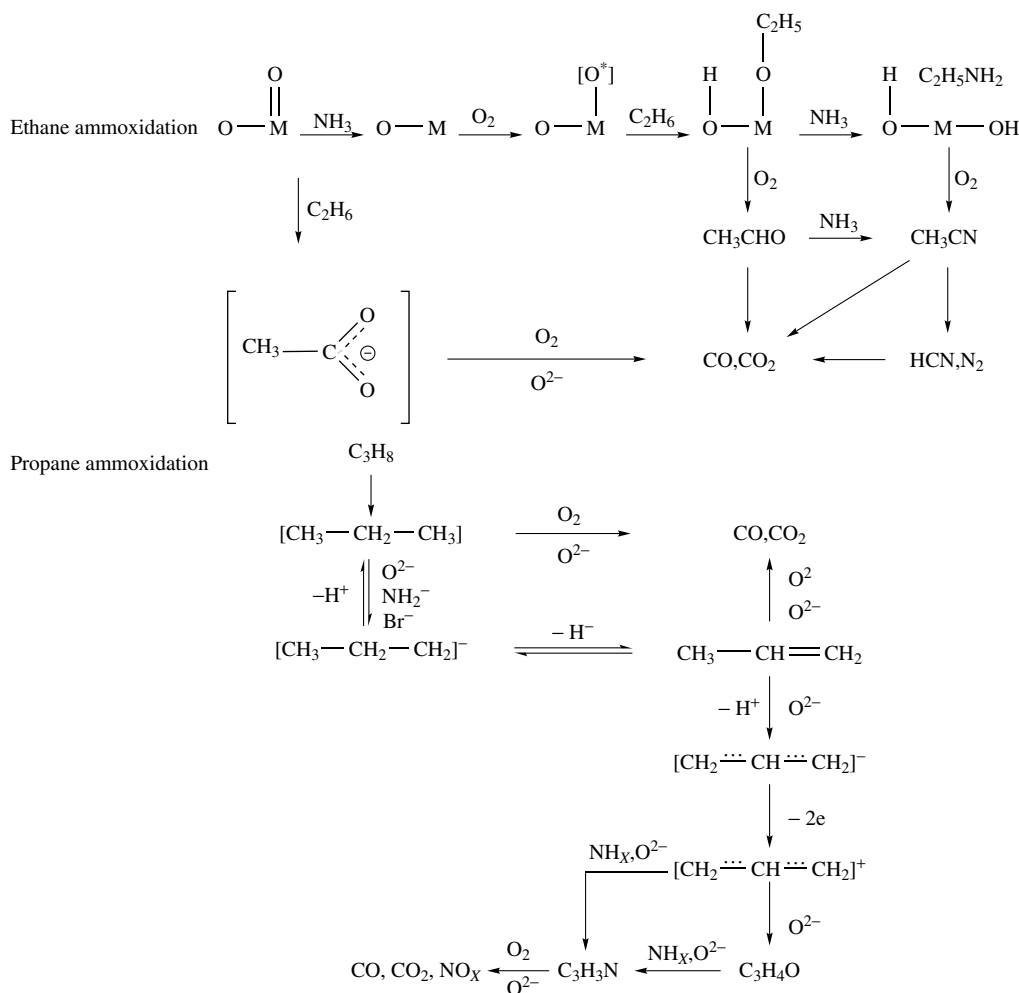
It might seem that the results obtained for the ammoxidation of propane over catalysts containing V–Sb–O, which are acidic systems, are in contradiction with the conception of a catalyst based on the presence of surface basic centers. However, it should be noted that this contradiction is only apparent since in the case of vanadium-containing catalysts such as V–Sb–Bi–O [1303], V_xO_y/Al₂O₃, V_xO_y/TiO₂, and V_xO_y/SiO₂ [459], the strong formation of dehydrogenated

forms of ammonia is observed due to the interaction between ammonia and the surfaces of such catalysts. This implies that the surfaces of the catalysts are enriched with strong basic centers.

The above discussions are in good agreement with the experimental data reported by Centi *et al.* [1818], which show that in the initial few moments of the process the selectivity towards acrylonitrile on freshly prepared V-Sb-O catalysts is very small and that 'deep oxidation' predominantly occurs. With time, the basic sites of the type NH_x^- are probably consolidated, and the selectivity towards acrylonitrile increases.

On an ammoniated surface of a Ga-La-Sb-O catalyst the dissociation of propene with the formation of C_3H_7^- ions has been observed even at room temperature. The latter, as is well known, are easily dehydrogenated, with the formation of propene, which is then converted on the catalyst predominantly to aldehyde; this, in turn, is transformed on the ammoniated surface to amine or imine due to the substitution of oxygen by the N-containing group.

A study of the ethane ammoxidation mechanism on scandium and chromic molybdates permits the suggestion of the following scheme for ethane conversion:



Scheme 6.55

The reaction mixture containing ammonia acts as a strong reducing agent, and creates on the catalyst surface specific reduced coordinatively unsaturated molybdenum ions. These ions interact with molecular oxygen, resulting in the formation of active oxygen species which possess higher reactivity than the lattice oxygen and thus can cleave the C–H bond of ethane, with the formation of neutral or positively charged alkyl groups. Dehydrogenation next produces an olefin, which then converts further. The comparative data on ethane and ethene ammoxidation indicate that ethene is unlikely to be the intermediate of ethane ammoxidation.

The aldehyde pathway is an alternative route. The alkyl species can react with an oxygen ion, thus giving the surface alcoholate, $-\text{O}-\text{C}_2\text{H}_5$, which can then transform to an aldehyde. Infrared spectra [1376] confirm the probability of such a pathway by showing that the aldehyde formed can be quickly converted to acetonitrile.

Cyclohexane ammoxidation

FTIR spectroscopy has been used to study cyclohexane adsorption on a similar type of catalyst at 290–673 K [1377, 1435]. Figure 6.14(a) shows the FTIR traces of C_6H_{12} and C_6D_{12} adsorbed on a Ti–Sb–O catalyst. Along with a slightly perturbed complex of cyclohexane, a complex with a strong C–H (C–D) shift towards low frequencies has been found, thus indicating a strong

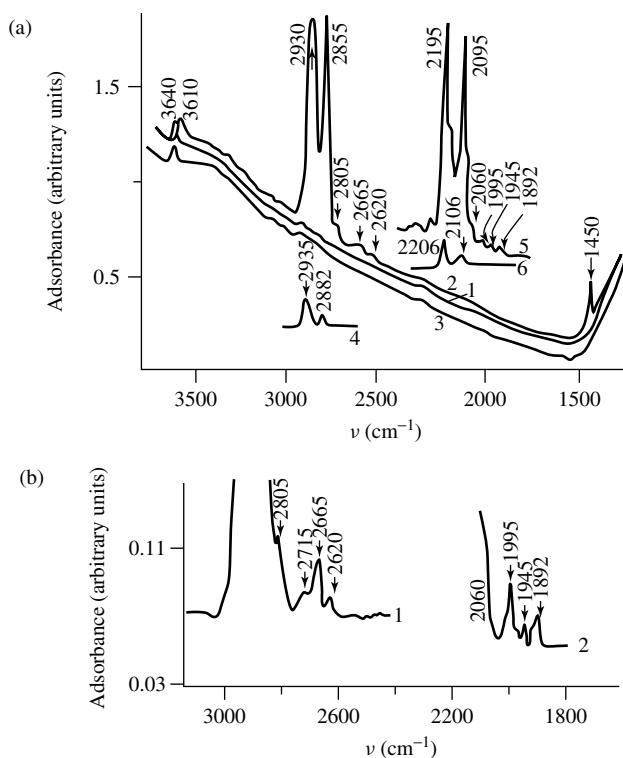


Figure 6.14. IR spectra of cyclohexane adsorption on a Ti–Sb–O catalyst. (a) Adsorption of C_6H_{12} and C_6D_{12} (10 torr) at 298 K: (1) initial sample; (2) C_6H_{12} adsorption; (3) evacuation, at 298 K for 20 min; (4) C_6H_{12} in the gas phase; (5) C_6D_{12} adsorption; (6) C_6D_{12} in the gas phase. (b) Low frequencies in the spectra of adsorbed C_6H_{12} and C_6D_{12} : (1) C_6H_{12} adsorption, at 10 torr and 298 K; (2) C_6D_{12} adsorption, at 10 torr and 298 K.

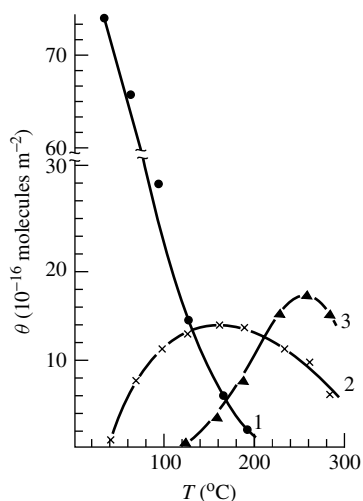


Figure 6.15. Concentrations of surface compounds (θ) as a function of reaction temperature: (1) SC_{II} ; (2) SC_{IV} ; (3) SC_V (0.05 g; $V = 15 \text{ cm}^3 \text{ min}^{-1}$; composition of original mixture (vol%) – C_3H_4O (0.25), O_2 (0.5), with the remainder He.

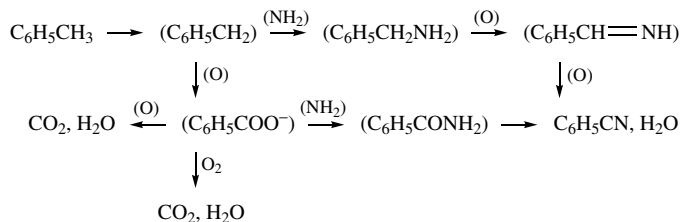
perturbation (a strong weakening) of a C–H bond in cyclohexane (Figure 6.15(b)). This complex can participate in the selective oxidation of cyclohexane [1377, 1435]. According to Sokolovskii *et al.* [1820], adiponitrile is formed from adsorbed cyclohexane. To elucidate the mechanism of adiponitrile formation, the Ti–Sb–O catalyst was pre-treated with helium and then exposed to ammonia and oxygen pulses, followed by cyclohexane pulses. Adiponitrile was also formed in this case, thus showing the participation of certain forms of adsorbed ammonia in this process. These may be either coordinatively bound ammonia, or partially dehydrogenated NH_2^- and NH^{2-} , absorption bands of which appeared in the spectra of Ti–Sb–O pellets heated at 573 K in the oxygen and ammonia mixture.

Taking into account the unlikelihood that a very active oxygen species, different from the surface oxygen of the catalyst, is remaining on the surface for a long time between pulses, it is possible to conclude that oxygen of the catalyst surface participates in the adiponitrile formation. Infrared spectroscopic studies of adiponitrile adsorption, simultaneous adiponitrile and NH_3 , or adiponitrile and NH_3 , plus O_2 , adsorption on the Ti–Sb–O catalyst (during cyclohexane ammoxidation in the IR cell) have shown that adiponitrile is polymerized in the presence of NH_3 [1377, 1435]. This could be a reason for the declining activity of the catalyst during the process [1824].

Toluene ammoxidation

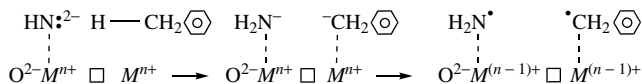
Murakami and co-workers [1781] have proposed that the reaction mechanism of toluene ammoxidation on V_2O_5 includes three steps, i.e. (i) oxidative adsorption of toluene, accompanied by abstraction of hydrogen atoms from the side chain, (ii) interaction between the adsorbed species and ammonia, and (iii) re-oxidation of the catalyst by oxygen. Based on infrared spectroscopic data, the adsorption of toluene seems to lead to the formation of a surface benzoate ion, $C_6H_5COO^-$, which then produces benzonitrile by reaction with ammonium ions [1781]. This mechanism was later accepted for the ammoxidation of xylenes over supported vanadium pentoxide [1781]. The similarity is characteristic for such toluene conversion on the catalysts

and can be described by the following scheme in which the species in parentheses denote adsorbed states:



Scheme 6.56

The mechanism of toluene conversion (oxidation and ammoxidation) has been studied on a V–Ti–O catalyst by Busca *et al.* [66, 1825] and also by Azimov and co-workers [1303] for a similar (V–Sb–O) catalyst. The results of these studies are confirmed in general. Unfortunately, the idea suggested by Azimov *et al.* [1303] has not been completely understood by Busca [66]. As has been shown above (Section 5.1) a carbenium ion is formed from the toluene molecules over oxidized surfaces, but this is not involved in the reaction of ammoxidation. This ion is an intermediate of the other reactions of toluene conversion, probably alkylation or partial oxidation with the opening of the ring. It also can participate in the formation of the products of full oxidation. These reactions have not been studied in detail by Azimov *et al.* [1303]. The reaction of ammoxidation proceeds on a partly reduced surface of the catalyst (treated by the ammonia–oxygen mixture), on which new strong basic centers of the type $\text{NH}_x^{\delta-}$ appear while the BASs disappear. Over such a type of catalyst, the activation of toluene is due to another mechanism. No carbenium ions are formed but instead the formation of benzyl species was observed. The benzyl species is directly converted to nitrile:

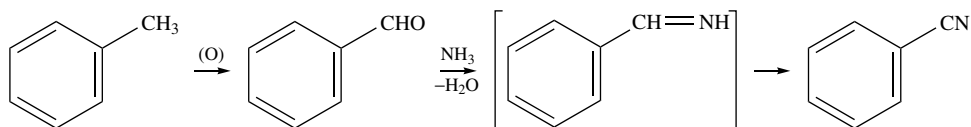


Scheme 6.57

It is not possible to agree with Busca's idea about hydrogen abstraction in the form of H^- or H^\bullet , as was suggested [66], since there is no evidence in the literature that during the adsorption of benzene derivatives M–H bonds are formed on the surface, while new hydroxyl groups do appear due to aryl adsorption (see, for example, the well-known spectrum of toluene adsorbed on ZnO [1277] and also Section 5.2). The example given by Busca [66] for such a suggestion is not a good one, because the allylbenzene molecule has a C=C bond in the side chain. In Section 5.2, it was shown that those molecules which have a C=C bond react more strongly with acidic centers of the oxidized surface due to protonation of this C=C bond (the formation of carbenium ions!). The latter are strongly held by the surface and are easily transformed to the oxidation products at room temperature. The heterolytic rupture of the C–H bond over MgO is accompanied by a stabilization of the anion formed on the weak acceptor center (Mg^{2+}), and as a result this anion is not converted in practice. Because of the data listed above, the conception of heterolytic dissociation of the C–H bond via the mechanism of proton abstraction on basic centers seems to be the more correct one.

Martin *et al.* [1826] noted the possible participation of ammonium ions in the toluene ammoxidation reaction [1827]. Such a point of view is not new [1781]; however, it is based only on the observation of ammonium ions by means of infrared spectroscopy and changes in their spectra after interaction with toluene. No other evidence for the participation of ammonium ions in the ammoxidation process has been obtained.

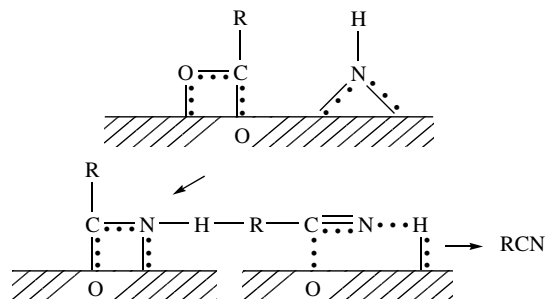
Based on the fact that they did not observe benzoic acid or amide as byproducts and observed the formation of benzaldehyde, Kulkarni *et al.* [1827] believe that benzonitrile is formed from toluene, and that benzyl alcohol is produced via the formation of benzaldehyde and the corresponding imine:



Scheme 6.58

In the case of nonzeolite mixed-oxide catalysts, the presence of benzoic acid, CO_2 and the benzoate ion as intermediates has been established, as was discussed above. In the case of (SAPO) catalysts, BASs (and LASs), due to the substitution of silicon in place of phosphorous, mild basic centers and oxygen vacancies are probably the active centers. As for (VSAPO), catalysts tetrahedral VO_4^- acidic centers and oxygen vacancies are the active centers. Ammoxidation of toluene over Cu-Na-ZSM-5 has been discussed in terms of the stability of a Cu(II)NH_3 (toluene) complex [1827].

The isobutanol ammoxidation reaction to isobutyronitrile has been studied on ZnO [197]. According to these authors, isobutanol ammoxidation to isobutyronitrile (the C-N bond formation) on ZnO takes place most likely due to the interaction of surface isobutyrate and carboxylates with imino compounds:

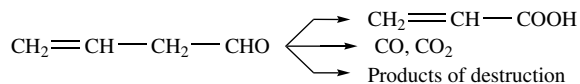


Scheme 6.59

6.3 Transformations of aldehydes and ketones

6.3.1 OXIDATION OF ACROLEIN

The catalytic transformations of acrolein on oxide catalysts yields acrylic acid, carbon oxides and the products of destructive oxidation:



Scheme 6.60

The first stage of the catalytic process is the chemisorption of reactants on the catalyst surface, as has been shown above in Section 5.7.2. The structure of the chemisorbed molecules, amounts of adsorbed species, and the binding energies of both the reactants and reaction products predetermine the direction and the rate of the catalytic reaction. We showed above that acrolein may be adsorbed on the surfaces of oxide catalysts by different mechanisms, with the formation of σ - ($\text{CH}_2-\text{CH}-\text{CH}=\text{O}:\text{M}^{n+}$) and π -complexes

$\text{H}_2\text{C}=\overset{\downarrow}{\text{C}}\text{H}-\text{CH}=\text{O}$ (complexes I and II, respectively) and hydrogen-bonded moieties (complex III), or that carbonyl-bonded acrolein is formed via dissociative adsorption $\text{CH}_2=\text{CH}-\overset{\text{O}}{\parallel}{\text{C}}-\text{O}-\text{M}$, (complex IV), as well as oxidized fragments

such as surface acrylates ($\text{CH}_2=\text{CH}-\text{COO}^-$, complex V), carboxylates (CH_3COO^- , complex VI), 2-formylacetates ($^- \text{OOC}-\text{CH}_2-\text{CHO}$, complex VII) and malonates ($^- \text{OOC}-\text{CH}_2-\text{COO}^-$, complex VIII) see Section 5.8.2. The probability of the formation of a particular surface complex is governed by the nature of the adsorption center and by the experimental conditions of adsorption (temperature, concentration of adsorbed species, etc.). Hydrogen-bonded acrolein species (complex III) are held unusually weakly and can be destroyed at room temperature via acrolein desorption. Complex III seems to take no part in the catalytic oxidation.

The σ -complex is the generally found form from acrolein interaction with oxide catalysts containing poly-charged coordinatively unsaturated cations on the surfaces. Indeed, the σ -complex is formed upon acrolein adsorption at room temperature on a majority of the catalysts discussed above (exceptions include MgO , $\text{K}_3\text{PMo}_{12}\text{O}_{40}$, and Cu , Cr and Zn oxides). The coordinatively bonded σ -complexes of acrolein may be either desorbed into the gas phase in the molecular form or oxidized by oxygen of the catalyst with the formation of additionally oxidized surface species, depending upon the strength of the complex bond to the surface and on the reactivity of surface oxygen.

Earlier [1505, 1507], Davydov *et al.* have shown that the formation of the coordinatively bonded σ -complex of acrolein is accompanied by polarization of the C-H bond. If nucleophilic oxygen is present at the surface, a heterolytic scission of this bond takes place, yielding the $(\text{CH}_2-\text{CH}-\text{C}-\text{O})^-$ fragment with a formal charge, q , of -1 . This fragment is a powerful electron donor and is capable of reducing the catalyst via transfer of electrons from the carbonyl group with the ultimate formation of the electrophilic species, $(\text{CH}_2-\text{CH}-\text{C}-\text{O})^+$. Calculations show that the positive charge is almost completely localized on the carbon atom of the carbonyl group ($q = +0.8$). This results in a high activity of this entity with respect to nucleophilic attack by the oxygen atom of the catalyst, yielding complex IV. The conversion of the carbonyl-bonded complex (IV) into a symmetric acrylate (V) is energetically favorable and proceeds readily. Due to the presence of weakly bonded reactive oxygens on the catalysts for 'deep' oxidation (CuO , ZnO and Cr_2O_3), the conversion rate of complex I into V and then into complex VI is high. This fact accounts for the formation of oxidized surface complexes of acrolein (complexes V and VI), even upon adsorption at room temperature.

The reactivity of acrylates is determined by their bond strengths to the surface and by the activities of the surface oxygens. Since the surface bond of the acrylate has an ionic character (a salt-like surface compound), the strength of the bond is essentially governed by the acid-base properties of the center responsible for the stabilization of complex V. It has been shown [1522] that the acrylates, formed upon adsorption of acrylic acid on Mo- and V-containing catalysts

(V–Mo–Si–O, MoO₃/SiO₂, V₂O₅ and V₂O₄), are decomposed at 473 K with evolution of acrylic acid to the gas phase. Surface acrylates on MgO remain virtually unchanged up to 673 K, but are destroyed at higher temperatures with the formation of surface acetate and carboxylate species, which are desorbed at $T > 773$ K in the form of products of ‘deep’ oxidation.

It should be noted that if acrolein is adsorbed on MgO, then the mechanism of surface acrylates formation is likely to be different from that on oxide catalysts. In this case, a dissociative adsorption of acrolein with the formation of oxidized surface compounds, including acrylates, takes place even at room temperature, despite the presence of the very strongly bonded oxygen of MgO and the absence of the acrolein σ -complex. Most likely, the rupture of a C–H bond attached to the carbonyl group of acrolein upon interaction with MgO occurs via the attack of a hydrogen atom on a sub-surface oxygen atom, as allowed by the symmetry rules [1505].

Unlike MgO, for copper oxide, a typical catalyst of ‘deep’ oxidation, an increase of the temperature up to 373 K results in strong oxidation of the surface acrylates to carbonates and carboxylates (complex VI). The latter are decomposed at $T > 473$ K, with evolution of carbon oxides into the gas phase. The low temperature required for the oxidation of surface acrylates is caused by the existence of weakly bonded oxygen in the CuO.

According to various authors [1505, 1507, 1511], carbonyl-bonded acrolein (complex IV) is assumed to be an intermediate in the process of formation of acrylic acid, although no direct evidence has been provided for the relationship between: (i) the rates of formation and consumption of this complex, and (ii) the rate of formation of the acid until the study [1829] has been published.

Adsorption of acrolein on low-coordinated cations preferentially proceeds with the formation of π -complexes (complex II). There are no available experimental data on the reactivity of π -complexes of acrolein. On the basis of the results of quantum-chemical analysis of acrolein interaction with MgO [1518], which indicates the weakening of the C=C and C=O bonds in acrolein upon π -complex formation, one may expect that the strongly bonded π -complexes of acrolein are intermediates for the formation of products of ‘deep’ and destructive oxidation.

Activation of a molecule occurs upon acrolein adsorption on the surfaces of metals [1510, 1512, 1828a], as a result of dative and donor–acceptor interactions. The energy of dative interaction increases with a decrease in the electronegativities of the metals. Thus, a strong adsorption results through dative interaction of the d-orbitals of a metal with the antibonding π^* -orbital of acrolein, leading to the rupture of a C–C bond with formation of acyl structures and surface carbonyls. As a result, no selective products of acrolein oxidation are found with metal catalysts.

In the case of acrolein interaction with MgO and Al₂O₃, a formylacetate complex has been detected, in addition to surface acrylates [1505, 1512, 1516]. The former is oxidized into a malonate species at high temperatures. Taking into account the fact that the products of destructive oxidation are mainly formed during acrolein oxidation on MgO, one may anticipate that they are produced via the intermediate formyl acetate and malonate complexes.

In addition to acrolein oxidation reactions, polymerization may proceed on the surfaces of oxide catalysts. As shown by XPS [1828b], for instance, a decrease in the temperature of acrolein adsorption on CoMoO₄ and MoO₃ resulted in the disappearance of the peak characteristic for the species containing a C=C bond (287.6 eV), and in the appearance of a new line (285.3 eV) attributed to ‘partial structures’ with saturated C–C bonds. The authors explained these results of acrolein polymerization via cleavage of the double bond. The formation of acrolein polymers has also been observed by IR spectroscopy [1506, 1508, 1520].

Thus, the main factors governing the mechanism of acrolein complex formation on the surfaces of oxide catalysts, and of the pathways of further transformations of the surface complexes to reaction products, are the nature of the adsorption centers and the reactivities of the oxygen species on the catalyst surfaces.

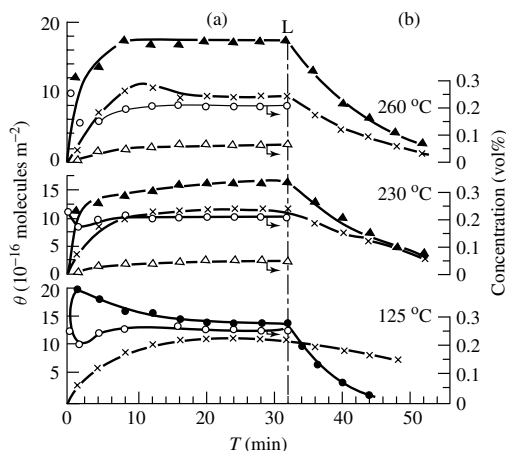
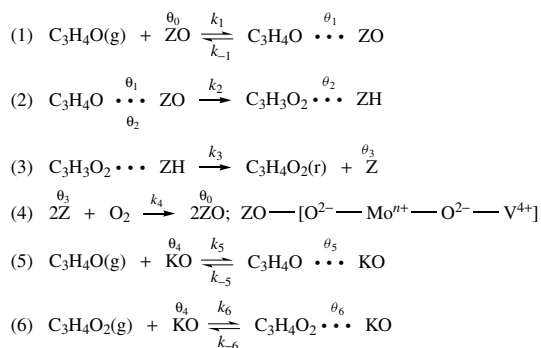


Figure 6.16. Concentrations of surface compounds (θ) and gaseous components (C_3H_4O and $C_3H_4O_2$) as a function of time with (a) passage of the reaction mixture through the reactor, and (b) passage of helium to (1–3)-concentrations of SC_{II} , SC_{IV} , and SC_V , respectively, (4 and 5) concentrations of C_3H_4O and $C_3H_4O_2$, respectively: ●, 1; ×, 2; ▲, 3; ○, 4; △, 5.

Under the conditions of acrolein partial oxidation to acrylic acid on V–Mo–Si–O catalysts [1829], infrared spectroscopy has been used to study the kinetics of the surface compound conversion process. Figure 6.15 shows the coverage (θ) of the catalyst with surface complexes as a function of the reaction temperature. At low temperatures (370 K), all that is observed on the surface is a coordinatively bonded acrolein (species II). As the temperature is raised, the concentration of species II drops off sharply, along with the appearance of the acrylate (IV). The concentration of such the acrylate is changed within the 370–670 K temperature interval, passing through a maximum at 450–480 K. Kinetic curves for species II, IV and V, along with those of acrolein and acrylic acid in the gas phase, are shown in Figure 6.16. The values of acrolein conversion (X), selectivities with respect to acrylic acid and carbon oxides (S), stationary concentrations of the surface compounds (SC – molecules m^{-2}) and rates of accumulation of acrylic acid and carbon oxides under the conditions of reaction (W_{acc}), plus the rates of decomposition of the surface compounds (W_{acc}) are listed in Table 6.5. Starting from Scheme 6.60, the kinetic model of acrolein oxidation to acrylic acid is described by the following set of stages:



Scheme 6.61

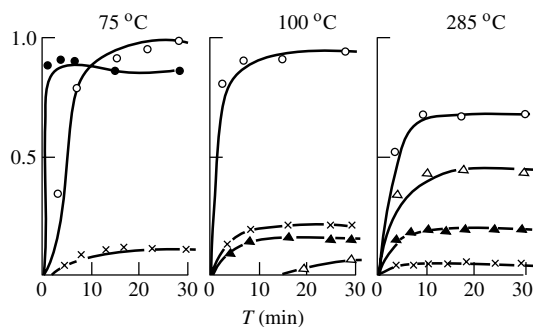


Figure 6.17. Comparison of calculated (continuous curves) and experimental (symbols) values of the relative concentrations of surface compounds and gaseous components as a function of time. Notation same as in Figure 6.16.

Table 6.5. Comparison of rates of catalysis with rates of breakdown of surface compounds of acrolein on V–Mo–Si–O catalysts (0.05 g; $S = 142 \text{ m}^2 \text{ g}^{-1}$; $V = 15 \text{ cm}^3 \text{ min}^{-1}$); composition of original mixture (vol%) – $\text{C}_3\text{H}_4\text{O}(0.25)$, $\text{O}_2(0.5)$, with the remainder He.

T (°C)	X (%)	S (%)		$\theta_{\text{sta}} (\times 10^{-16})$			$W_{\text{acc}} (\times 10^{-14})$		$W_{\text{dec}} (\times 10^{-14})$		
		$\text{C}_3\text{H}_4\text{O}_2$	$\text{CO} + \text{CO}_2$	SC_{II}	SC_{IV}	SC_{V}	$\text{C}_3\text{H}_4\text{O}_2$	$\text{CO} + \text{CO}_2$	SC_{II}	SC_{IV}	SC_{V}
125	1.8	100.0	–	14.6	11.3	Trace	0.4	–	4.5	0.5	–
190	6.4	97.0	3.0	2.0	13.0	8.0	1.1	0.03	–	0.6	0.3
230	12.0	97.0	3.0	Trace	11.0	16.0	2.7	0.08	–	1.0	1.4
260	21.0	96.0	4.0	–	8.0	17.3	4.7	0.20	–	1.2	2.2
285	30.0	96.0	4.0	–	5.0	14.0	7.2	0.30	–	0.5	5.2

The following values were found for the rate constant of the various stages:

$$\begin{aligned}
 k_1 &= 23 \text{ s}^{-1} \text{ atm}^{-1} \\
 k_{-1} &= 1.8 \times 10^2 \exp(-10\,000/RT) \text{ s}^{-1} \\
 k_2 &= 4.5 \times 10^6 \exp(-19\,000/RT) \text{ s}^{-1} \\
 k_3 &= 2.1 \times 10^3 \exp(-13\,000/RT) \text{ s}^{-1} \\
 k_4 &= 1.8 \times 10^{-14} \exp(-8000/RT) \text{ m}^2 \text{ molecules s atm} \\
 k_5 &= 46 \text{ s}^{-1} \text{ atm}^{-1} \\
 k_{-5} &= 2.5 \times 10^3 \exp(-2000/RT) \text{ s}^{-1} \\
 k_6 &= 3.7 \times 10^{-1} \exp(-2000/RT) \text{ s}^{-1} \text{ atm}^{-1} \\
 k_{-6} &= 8.9 \times 10^{-3} \exp(-10\,000/RT) \text{ s}^{-1}
 \end{aligned}$$

The calculated and experimental changes in the concentrations of the surface complexes and gaseous components of the reaction mixture are shown in Figure 6.17. The deviations of the calculated concentrations from the experimental values are all within 30 %. Thus, a nonstationary kinetic model has been successfully proposed for the reaction on the basis of spectroscopic kinetic studies that give a satisfactory description of the basic relationships in the oxidation of acrolein on V–Mo–O catalysts and describe the ‘time-dependent-wise’ changes in the concentrations of surface compounds and the gaseous components of the reaction mixture.

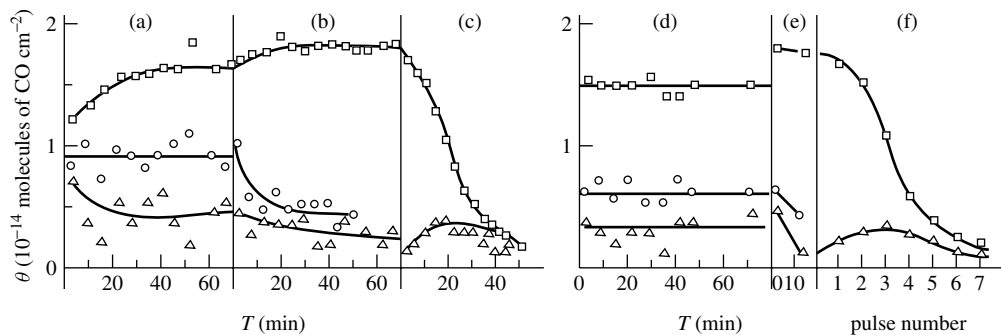
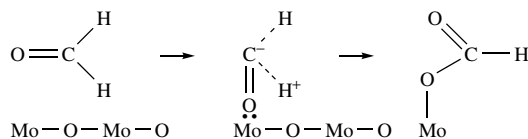


Figure 6.18. Changes in the structure of the coating of a CuO surface by acetate (\square), isopropylate (\circ), and formate (\triangle) during successive sample treatment: (a, d) with the reaction mixture; (b, e) with He; (c, f) with O_2 : (a–c) $T = 408$ K; (d–f), $T = 433$ K.

6.3.2 OXIDATION OF FORMALDEHYDE

Based on data analyzed above (Section 5.7.1), it is clear that the oxidation of formaldehyde to formic acid occurs via the formation of surface formates, and the direction of the transformation depends on the properties of these formates, which in their turn depend on the nature of the surface cations and also on the properties of the surface oxygen involved in the stabilization of formaldehyde. In the case of transition-metal oxides where oxygen is strongly bound, surface formates are transformed to the acid, as a rule, through the covalently bound complex with surface oxygen [1452, 1463, 1830]:



Scheme 6.62

As for oxides, where surface oxygen is weakly bound and depending on the type of oxide formates are converted to CO plus H_2O or to CO_2 plus H_2 , as has been analyzed in detail for the decomposition of formic acid (Section 5.8.1).

6.3.3 TRANSFORMATION OF ACETONE

Numerous studies have been devoted to the transformation of acetone during its adsorption on oxides [1831–1833, 1838, 1839] and acid catalysts [1529, 1834–1837] using IR techniques. For a long time, organic cations have been proposed as active intermediates in reactions catalyzed by the hydroxyls of strong solid acids. The general rules of proton transfer in hydrogen-bonded ‘neutral’ and ‘ion-paired’ acid–base complexes, $AH + B \rightleftharpoons A^- \cdots HB^+$, have been formulated. In this equilibrium, the chemical and geometric structures of the interacting molecules, as well as the physico-chemical properties of the environment, play important roles. According to this assumption, based on the studies of molecular interactions in solutions, the *interacting* complexes of simple aldehydes and ketones with bridged hydroxyls ($AlOHSi$) of strongly acidic zeolites should have predominantly an ‘ion-paired’ character. However, later published data cause serious

doubt on such proton transfer. By using FTIR and NMR spectroscopies, along with quantum-chemical calculations, a preferable formation of 'neutral' hydrogen-bound complexes of acetone on the surfaces of H-zeolites has been shown at room temperature.

6.3.4 HYDROGENATION OF ALDEHYDES AND KETONES

It is clear that complexes similar to those indicated above can also participate in the hydrogenation of aldehydes and ketones on metal catalysts. The reactivities of isolated C=C bonds on metals are always higher than those of C=O bonds, a difference which is related to the strengths of the adsorption bonds [1840]. Substitution (by methyl groups, phenyl groups, etc.) decreases the possibility of adsorption through this bond, and thus, the reactivity in hydrogenation. As an example of the use of infrared spectroscopy to study such reactions, the work of Bocuzzi *et al.* [1841] may be chosen. According to this paper, on mildly reduced samples at room temperature deuterioacetone is mainly adsorbed in a molecular 'end-on' form; on heating, minor amounts of CO are formed, indicating that in this case adsorption is only molecular. Upon heating, the abstraction of deuterium atoms and a breaking of C-C bonds take place. In the IR spectra, the deuteration reaction at room temperature produces bands assigned to the modes of perdeuterioisopropyl alcohol. However, even after very long contact times, a large amount of nonreacted deuterioacetone remained in the cell. For strongly reduced samples an almost complete loss of IR transmission occurs with the growth of strong bands in the OD stretching region after interaction with acetone-d₆, i.e. under these conditions deuterioacetone much more easily loses deuterium atoms. After a long contact time, the broad band at 1580 cm⁻¹, related to the formation of an unsaturated diketone, is observed in the spectrum. The interaction with D₂ also produces perdeuterioisopropyl alcohol, and deuterioacetone remains in the cell or is chemisorbed by the surface. Such a difference in the dehydrogenating and hydrogenating activity of samples with different degrees of reduction is due to the changes in the surface states of the metal particles [1841].

6.4 Transformations of alcohols

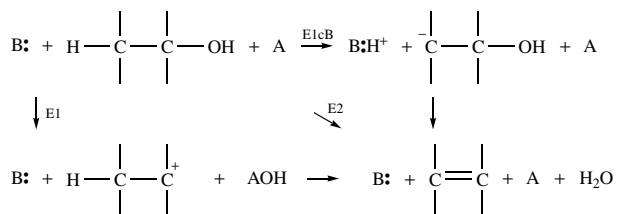
Many studies of alcohol conversion have been carried out, often involving the use of IR spectroscopy. Surface compounds of alcohols on oxide systems can be classified either as alcohols bound via a hydrogen-bond to the surface OH groups and surface oxygen (the spectral characteristics of these alcohols differ insignificantly from those in the gas phase, and are weakly bound to the surface), alcohols bound via a coordination bond, and different coordinated alkoxides formed by various mechanisms [30] (Section 5.6). There are two main pathways for alcohol transformations, i.e. (i) dehydration with the formation of alkene and water, and (ii) dehydrogenation with the formation of aldehyde and hydrogen. Dehydration is favored on acidic sites and dehydrogenation on basic centers [1842, 1843]. The following sequence of selectivity in dehydration catalysts can be shown: WO₃ < SiO₂ < Al₂O₃ < TiO₂ < Cr₂O₃ < FeO < ZnO < MgO < CaO [79]. In the case of dehydrogenation, this sequence occurs in the opposite direction. For metal oxides, dehydration increases with the covalent character of the M-O bond of the catalyst, whereas dehydrogenation is enhanced by increasing the ionic character [79]. The H-forms of zeolites and HPAs are highly active catalysts for dehydration. In the case of HPAs, the reaction proceeds on the surface as well as in the bulk of the solid. Each proton in the solid HPA can participate in the reaction because of the 'pseudo-liquid' nature of the dehydration.

6.4.1 DEHYDRATION OF ALCOHOLS

This is a typical acid-catalyzed reaction which proceeds over Lewis or Brønsted acid sites and has been examined on the basis of data obtained for the first member of the series, i.e. methanol,

because of its simplicity and the range of data obtained. Acid catalysts, such as alumina, silica–alumina and zeolites, produce dimethyl ether.

In general, the catalytic dehydration of alcohols may proceed via the following types of mechanisms [79]:



Scheme 6.63

where A and B are acid and basic centers, respectively; A can be either an LAS or BAS type. In the case of the E1cB mechanism, a carbanion is formed by the participation of strongly basic surface centers. If the E1 mechanism holds, the carbenium ion can be produced with the intermediacy of the oxonium ion [79].

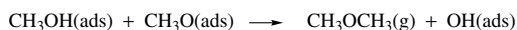
The surface alcoholates formed on most oxide and zeolite catalysts can be readily identified by their IR spectra (e.g. according to $\nu\text{C}-\text{O}$, which increases in comparison with that for the alcohol in the gas phase. Both linear and bridged methoxy groups have been detected by IR spectroscopy in all studies devoted to the decomposition of methanol on oxides, for example, on Cr_2O_3 [1191, 1453, 1454, 1471, 1482, 1843, 1844], ZnO [1468, 1845], $\alpha\text{-Fe}_2\text{O}_3$ [202, 1481], TiO_2 [1461], CuO [1469, 1846, 1847], ThO_2 [1846], MoO_3 [1452, 1463, 1464], Mo/SiO_2 [1848], $\text{Fe}-\text{Mo}-\text{O}$ [393, 1470], V/SnO_2 [1483], $\text{Cr}-\text{Mo}-\text{O}$ [1462, 1482] and $\text{Zn}-\text{Cr}-\text{K}-\text{O}$ [1466].

Al_2O_3

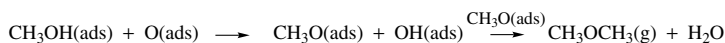
The study of alcohol adsorption and conversion on Al_2O_3 and modified catalysts, e.g. on Al_2O_3 treated by NaOH or HCl , using both isotopically labeled molecules and isotopic-exchanged surface oxygen or hydroxyl groups (^{18}O and OD , respectively), together with chromatographic analysis of the reaction products [1086, 1843], showed already in the 1970s that the surface alkoxides are key compounds in alcohol dehydration on Al_2O_3 . The mechanism of alcohol conversion has been examined in detail in many previous studies for different alcohols adsorbed on numerous oxide systems and have been summarized, for example, by Tanabe [79].

A recent *in situ* study of methanol conversion, with a periodic modulation of the free stream of methanol with a 1 s resolution [1849], showed that two mechanisms of methanol dehydration are possible, namely:

- (1) Dissociative mechanism involving surface methoxyls

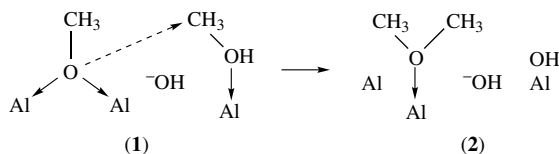


- (2) Associative mechanism with participation of molecularly bound methanol



Scheme 6.64

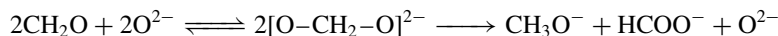
The data on the adsorption form of methanol on alumina have been examined in Section 5.7.1. On the basis of these data, and also from information about the participation of molecular-bound alcohol in the reaction, Busca proposed a very reasonable mechanism for methanol dehydration to dimethyl ether over alumina:



Scheme 6.65

Four different methanol adsorbed species were observed [66], with the more strongly bound one being a bridging methoxide obtained by the activated dissociation of adsorbed species (structure 1) coordinated to tetrahedral aluminum ions through the oxygen lone pair. The second undissociated form is coordinatively bound to $\text{Al}_{\text{cuo}}^{3+}$. Another form which is obtained is H-bonded to surface oxide anions. The identification of these undissociated forms of methanol was made on the basis of the analysis of Fermi resonance features in the spectra [1850]. This mechanism is consistent with that proposed by Knozinger [1851] and also agrees with the pathway presented by Schiffrino and Merrill [1849], except that in the latter case a second pathway represented the reaction between two methoxygroups. Support for this type of mechanism comes from studies of methanol/ CO_2 co-adsorption on alumina, which showed that the adsorbed methoxygroups act as nucleophilic species, according to the reaction [1852], $\text{CH}_3\text{O}^- + \text{CO}_2 \rightarrow \text{CH}_3\text{-O-COO}^-$.

The formation of nucleophilic CH_3O^- species to replace pre-adsorbed coordinated ammonia over Cr_2O_3 has also been shown [1482]. Surface methoxyls at temperatures of 473 K and above are transformed to formates that are intermediates in the methanol decomposition [1086, 1447]. In the latter study [1086], a pathway for carboxylate formation through the interaction of alkoxides with surface hydroxyl groups has been suggested. An interesting way for the formation of formate-like structure on alumina via a formaldehyde stage has also been proposed [1487]. Formaldehyde reversibly adsorbed on alumina as dioxymethylene, $[\text{O-CH}_2\text{-O}]^{2-}$, species which undergo a Cannizzaro-type disproportionation, producing methoxy groups and formate species:



Transformations of other alcohols on oxides, e.g. isobutyl alcohol on Al_2O_3 [1853] and isopropyl alcohol on ThO_2 [1846], occur due to the same mechanism, involving surface alkoxides. According to measurements of the rates of evolution of the gaseous products, the kinetics of the decompositions of both linear and bridge alcoholates correlate with those of the dehydration of *tert*-butyl and isopropyl alcohols.

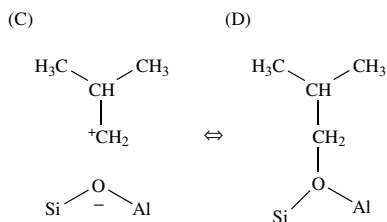
An *in situ* diffuse IR spectroscopic study, made together with kinetic measurements [1853], carried out for a series of alcohols on Al_2O_3 , confirmed the viewpoint that alkoxides are intermediates in the alcohol dehydration reaction.

Zeolites

In the case of Brønsted acid sites of zeolites, the carbocationic mechanism of methanol dehydration takes place [1177, 1181, 1854] (Section 5.7.1). Protonation of the alcohol molecule favors the subsequent nucleophilic substitution. Alcohol adsorption on HZSM-5 [1445, 1855] zeolites

occurs with the participation of acid hydroxyl groups, as detected by the disappearance from the IR spectra of the bands which belong to such groups. The results of exchange studies of both isopropyl and *tert*-butyl alcohols with D₂O indicate that the alcohol molecules are dehydrated with the formation of carbonium ions before desorption.

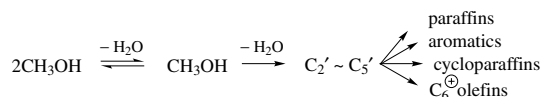
The following short-lived carbonium ion (C):



Scheme 6.66

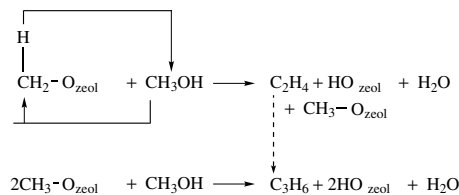
according to NMR data [1484, 1856], seems to be an intermediate in the dehydration of *tert*-butyl alcohol, whereas the alkoxide (D) is an intermediate in isobutyl alcohol dehydration.

Dehydration of alcohols over zeolite catalysts is a well known ‘methanol-to-gasoline’ (MTG) process:



Scheme 6.67

The most difficult stage of the MTG reaction is the formation of the first C–C bond. It is well established that olefins are intermediates which are easily converted to aryls. At present, several types of mechanisms have been suggested for this reaction; carbene, oxonium-ion and carbonium-ion mechanisms are popular [79]. As shown in Section 5.7.1, based on the data of IR and UV spectroscopies, the last mechanism seems to be more probable. These data are in good agreement with the results obtained by Gorte and co-workers [1445, 1857], who showed that alcohols are dehydrated to form carbenium-ion-like intermediates prior to being desorbed as olefin products. Support for the formation of carbenium ions in zeolites comes from NMR data [1858], although other viewpoints also exist. Thus, Novakova *et al.* [1441] proposed that the formation of the first C–C bond on zeolites takes place due to the reaction of the gaseous methanol with very reactive surface C₁-species:

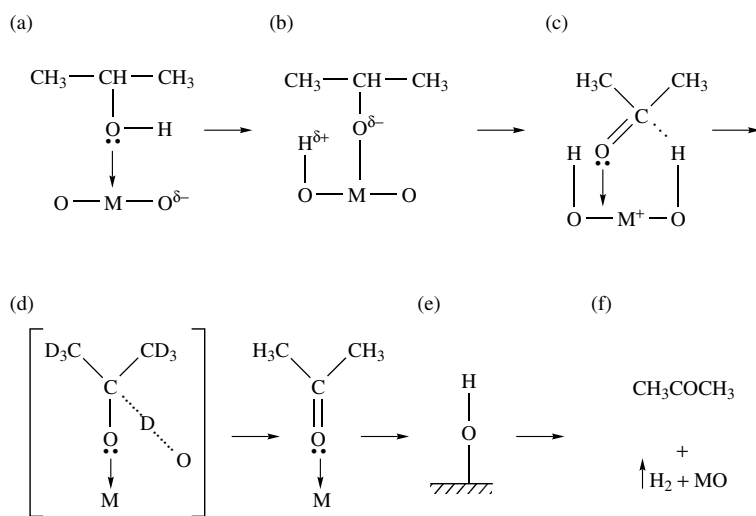


Scheme 6.68

The reaction of dimethyl ether (DME) formed from methanol with methoxyls, and yielding propene, was described by Ceckiewicz [1443]; an interaction between DME or methanol and methyl carbonium ions, formed from methoxyls, was suggested by Ono and Mori [1444].

6.4.2 DEHYDROGENATION OF ALCOHOLS

This type of conversion on oxide surfaces no doubt proceeds with the participation of alkoxide structures; the presence of strong basic (nucleophilic) centers are essential for the reaction to occur via this pathway. According to Efremov and Davydov [1190], isopropanol conversion on Sn–Mo oxide catalyst occurs only if the weakly bound alcohol does not block the neighboring centers (probably O^{2-}):

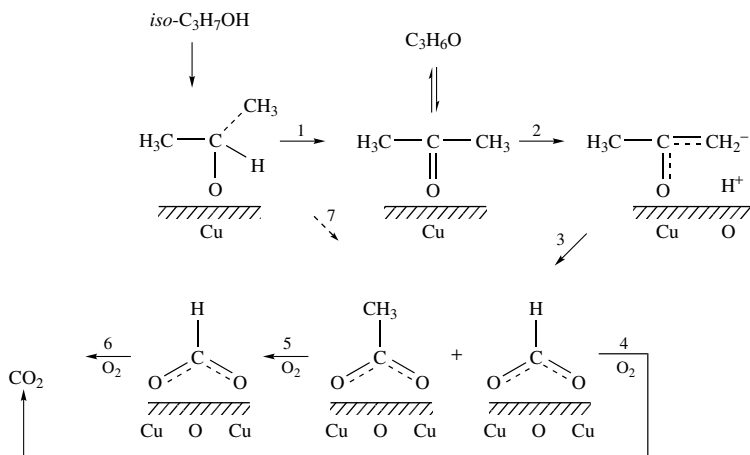


Scheme 6.69

Using isotopically substituted molecules, it has been proved directly [748] that the rupture of the C–H bond occurs in the limiting stage of this reaction. The formation of the intermediate (d) has been observed when the breaking of this bond was slowed down by using deuterio-substituted adsorbates because the C–D bond is stronger than the C–H one. Later, the results of these investigations were confirmed on Sn–V-catalysts.

A scheme for the dehydrogenation of cyclohexanol to cyclohexanone with intermediate formation of alcoholates on Cu^{1+} and Cu^0 centers stabilized in the oxide matrix ($Cu-Zn-Al_2O_3$ and Cu/MgO catalysts) has been suggested, on the basis of IRS data, by Fridman and Davydov [1859].

Over CuO , methoxy groups are already formed during the dissociative adsorption of methanol at low temperatures and by room temperature methanol has been oxidized to formates [810, 1469]. At 420 K, methoxy groups are no longer detectable over the CuO surface, the formate species are decomposed and only carbonate species can be found. Using isopropyl alcohol as a reagent [1473–1475], it has been shown that the formation of destructive oxidation products on the surface proceeds via the oxidation of the reaction product, acetone, which is decomposed through an intermediate enolate-type species:



Scheme 6.70

The rates of transformation of acetate and formate compounds coincide with the rates of formation of the full oxidation products (Figure 6.18), i.e. these compounds are intermediates in this reaction [1473, 1474]. Thus, the data examined above allow the conclusion that formate and carboxylate species formed from surface ethers are intermediates in the full oxidation of different alcohols on CuO. The rate of decomposition of acetates is significantly increased in the presence of gaseous oxygen. Similar conclusions have been made for alcohols on other full oxidation catalysts, such as Cr₂O₃ [1453, 1454, 1471, 1482], Fe₂O₃ [1481] and ZnO [1468], and partial oxidation catalysts like TiO₂ [1461], MoO₃ [1452, 1463], Fe–Mo–O [393], Cr–Mo–O [1462, 1482], V–Sn–O [1483] and MoO₃/SiO₂ [1848] on the basis of comparisons of IRS and TPD data. Support for this comes from other authors [66,1860], according to which similar groups are formed upon the adsorption of alcohols over Co₃O₄ and MgCr₂O₄ [1861, which show very poor selectivity with respect to formaldehyde production. The formation of these compounds can also occur due to formaldehyde oxidation [1452, 1463, 1487]. On the catalysts for selective oxidation, for example, TiO₂, MoO₃, V₂O₅, Fe–Mo–O, Cr–Mo–O, V–Sn–O, MoO₃/SiO₂ and MoO₃/TiO₂, the formation of formaldehyde comes from surface alkoxides; however, the aldehydes formed over these catalysts are not converted to formates and carboxylates in the temperature region of the reaction. On the surface of partial oxidation catalysts, aldehyde is adsorbed only in its molecular form [393, 1452, 1499, 1463]. The formation of surface alkoxides on partial oxidation catalysts involves protic acidic sites [393, 1462, 1463, 1470]. Spectral data and directions of the transformation of alkoxides on a number of different oxides are shown in Table 5.29.

On V₂O₅/TiO₂ [66], Sn–Mo–O and Sn–W–O [1862], methanol is oxidized to methylformate whereas on V₂O₅ and V₂O₅/SiO₂ it is converted to formaldehyde. A spectroscopic study of methylformate formation showed that the methanol adsorption gives rise to methoxy groups that begin to be oxidized at temperatures above 400 K. Formaldehyde is adsorbed on such catalysts as dioxymethylene species which react with methanol at relatively low temperatures, producing dimethoxymethane.

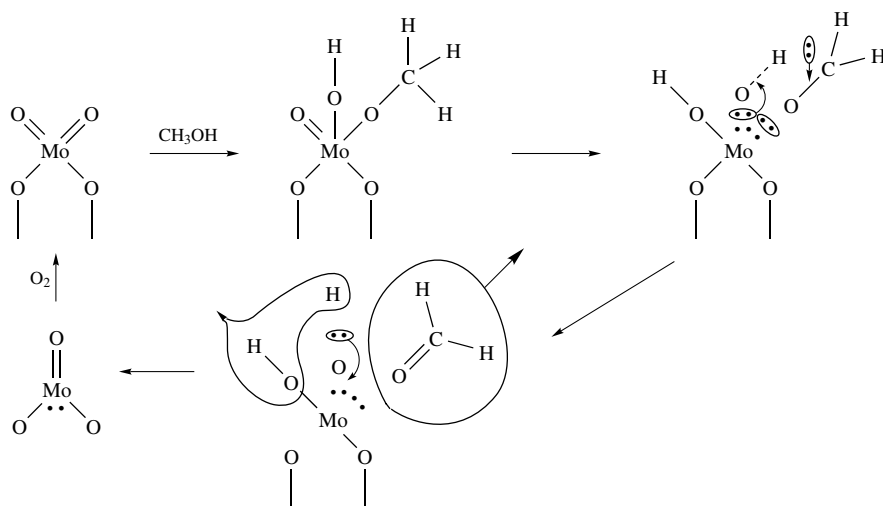
It should be noted that the structural sensitivities for the selective oxidation of methanol have been shown for different crystallographic faces of MoO₃ [1863] and V₂O₅ [1864] with established morphologies. In fact, Ohuchi *et al.* [1865] have shown that on the (010) face only physical adsorption of methanol takes place without any chemical transformations. At the same time, on the surface perpendicular to the (010) face, methoxy groups are formed as a result of

the interaction between methanol and surface OH groups at room temperature. If the temperature increases, the methoxy groups begin to react with the formation of both formaldehyde and water, which are rapidly desorbed with reduction of the MoO_3 surface [1864]. The presence of such CH_3O^- groups at the surface of MoO_3 has been detected by IR spectroscopy [1863]. It has recently been reported that the monoclinic β -face of MoO_3 exhibits a higher catalytic activity in the partial oxidation of alcohol when compared with the α -face. This is not surprising taking into consideration the fact that different surface structures are formed on different faces.

6.4.3 METHANOL OXIDATION TO FORMALDEHYDE

Oxide catalysts

This is an industrially important reaction, and many studies have been devoted to it. To convert methanol selectively, two types of catalysts are now used, i.e. Fe–Mo–O or Cr–Mo–O and Ag-supported oxides. The mechanism of the reaction has been represented by a scheme of methanol transformation on Mo-containing catalysts based on spectral observation of the surface methoxyls on MoO_3 [30, 1452, 1463, 1464, 1866]:



Scheme 6.71

FTIR and DRFT-IR spectroscopic studies of the reaction on Fe–Mo–O [393, 1470] and Cr–Mo–O [1462, 1482] catalysts, which had not been investigated earlier because of their small specific areas ($\sim 1 \text{ m}^2 \text{ g}^{-1}$), provided new information about the role of BASs in the transformation of the alcohol molecule to formaldehyde, about the mechanism of methoxyl formation, their dehydration by surface oxygen, and also about the roles of the separate components of the catalysts in this reaction [393, 1462, 1482]. The interaction of methanol with the surface of Cr–Mo–O [1462, 1482] and Fe–Mo–O [393, 1470] already leads to the evolution of water at 298 K, together with the formation of alkoxide structures, as proved by the appearance of a 1620 cm^{-1} absorption band from $\delta\text{H}_2\text{O}$ in the IR spectrum during the adsorption of the alcohol and by an analysis of the desorption products formed at room temperature. In the absence of the reaction products, such an observation suggests the formation of alkoxides via esterification involving the proton acid centers (H^+) of the surface and the hydroxyl group of the alcohol.

The presence of proton centers as the centers of stabilization of the structures responsible for the partial oxidation determines the efficiency of the catalytic action. Since the Brønsted acidity of molybdenum-containing catalysts is associated with the presence of Mo ions, one can expect that those samples having a small excess of molybdenum oxide will be the most effective [393]. On the other hand, the reduced catalyst lacks acid centers and shows a lower selectivity than the oxidized one.

The strengths of the acid centers and their nature has a noticeable effect on the selectivities of the catalysts. Since protonation occurs quite easily (even for adsorption of alcohol on Cr–Mo–O without heating, with a slight shift of the desorption equilibrium at 298 K on Fe–Mo–O), the BASs should not be strong. Strong BASs promote the transformation of CH_2O to HCOOH and then to CO , thus decreasing the yield of the end product. The surface proton centers of highly acidic catalysts should be of moderate strength for high selectivity.

Thus, the variations in the number and strength of the proton centers lead to a gradual increase or decrease in the selectivity of the catalysts, indicating the possibility of control of the process by regulation of the active surface centers. The approach is analogous to that applied in the homogeneous oxidation of alcohols, that is, by correspondingly selecting ligands via the introduction of additives it is possible to obtain more selective catalysts. We have succeeded in finding a correlation between the oxidation of alcohols catalyzed in homogeneous reactions. The acid medium and the mobile protons of the acid surface react in a similar way with the reactants in the formation of the intermediate alkoxide structures. So, by changing the acid properties it is possible to control the direction of the process in both types of reactions.

Ag-containing catalysts

Moreover, a supported silver catalyst is one of a few examples when the application of spectral methods allows an increase in the selectivity of the catalyst in industrial processes when using the modifiers which stabilize silver ions in the Ag^{1+} oxidation state [1867]. Silver is a unique catalyst for the partial oxidation of methanol and ethylene. The nearest analogues – copper and gold – are also able to oxidize methanol, but their catalytic properties are much less effective. Because of the difficulties in studying high-temperature methanol oxidation, the mechanism of methanol oxidation and the nature of the active sites on such catalysts are still under discussion. As a rule, the active sites of silver catalysts are considered to be different forms of oxygen adsorbed on the silver. From studies of these forms of adsorbed oxygen, most researchers believe that they determine the alternative directions of the transformation, such as dehydrogenation, partial or deep oxidation.

First, we will discuss the differences in electronic characteristics between silver and its isoelectronic neighbors, gold and copper. Silver participation in the oxidizing processes and its catalytic characteristics are associated with electronic transitions and the formation of different ionic states. The formation of silver surface ions as a result of oxygen adsorption is the first and necessary stage of the process. Without oxygen, the formaldehyde synthesis does not occur. Silver is the only transition metal that has only one stable ionic state, i.e. the cation Ag^+ . Higher silver oxides (Ag_2O and Ag_2O_3) are formed only in the presence of strong oxidizers and are thermally unstable. Gold and copper also show stable oxidation states (+1) but they are fairly easy to transform to highly charged Cu^{2+} and Au^{3+} ionic states. The single-charged cation M^+ seems to be an active state of silver and its analogues in partial oxidation. The transition to a higher-charged state probably causes a decline in selective oxidation, catalysis ‘deep’ oxidation, and decomposition of the products. The amount of M^+ states on oxidized silver is larger than with copper and gold and this may account for the better catalytic properties of silver.

In real catalytic systems, the effective ionic charge may differ notably from the formal degree of oxidation, a fact that greatly affects the catalytic properties of metals. Hence, assuming Ag^+

to be in an active state, it is necessary to investigate the change of this state in different catalytic systems.

The support of a metal catalyst is one of the most important agents affecting the metal electronic states. As it is the main method for studying the electronic states of silver, DRES was selected as a direct technique for evaluating the surface and sub-surface layers [898]. Investigations of the Ag/SiO_2 and $\text{Ag}/\text{Al}_2\text{O}_3$ systems enabled the determination of the influence of the particle size, degree of clustering and state of oxidation by using the UV–Vis spectra of silver. To interpret such spectra, samples have to be chosen which contain only one or two (as a maximum) states of silver on the surface of the support. Independent methods of studying these states such as electron microscopy, small-angle neutron scattering, adsorption of oxygen and hydrogen, XRD and ESR spectroscopy (Table 3.6) have been used to interpret the DRES spectra. It is clear that supports such as Al_2O_3 and aluminosilicate, which are more selective in this reaction, stabilize silver preferably in the ionic-state (type) Ag^+ (more details can be found in Section 3.5).

As was shown in Section 3.5 and in Figure 3.26, the Ag^+ supported alumina silicate has the highest νCO and the largest effective charge. This is explained by the minimal electron-donor influence on Ag^+ of the surface oxygen ions (O^-) from the support crystal lattice.

Testing of the silver catalysts on the different supports used in methanol oxidation showed that silver supported on natural (pumice) and synthetic (D-53) aluminosilicates exhibits the highest efficiency (Figure 6.20). The formaldehyde yield on these samples reached a maximum value at 1–3 wt% Ag, which conforms to an approximately monomolecular metal coverage of the support surface. In this case, the average size of the silver particles increases to 300–500 nm and more, but this exerts only a little, if any, effect on the catalyst activity. Such an effect is explained by the external diffusion mechanism involved in the methanol oxidation process. At high temperatures (773–973 K) the sizes and form of the silver particles have little or no effect on the catalytic properties of the silver. In contrast, on a MgO support the efficiency of the silver catalyst is very low. Only at high silver concentrations, during the formation of a metal film on the support surface, does the selectivity of Ag/MgO increase to 40–60%. On Al_2O_3 , silver has an intermediate efficiency.

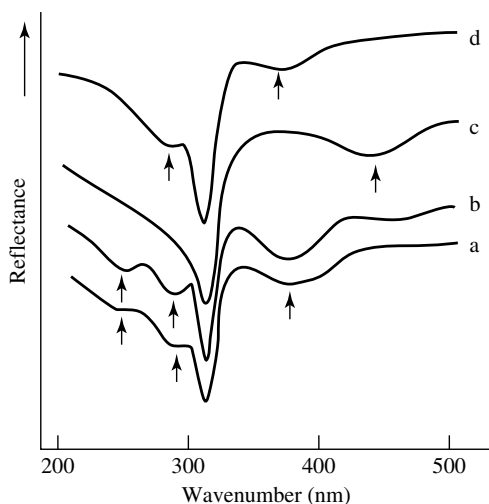


Figure 6.19. DRE spectra of Ag modified by (a) CeO_2 , (b) ZrO_2 , and (c) Cs_2O ; spectrum (d) represents silver.

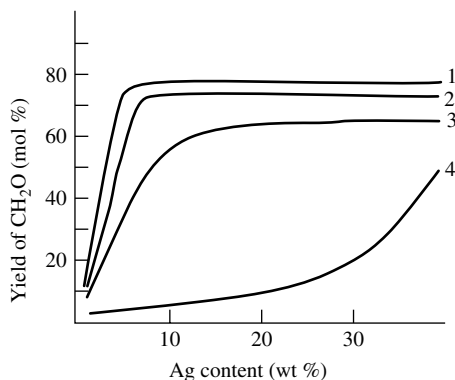


Figure 6.20. Formaldehyde yield as a function of silver content in various catalyst systems: (1) Ag/aluminasilicate; (2) Ag/pumice; (3) Ag/ α -Al₂O₃; (4) Ag/MgO.

On comparing the spectral and catalytic data one may deduce that the active state of silver is Ag¹⁺ cations with a maximum effective charge. This is also confirmed by the spectroscopic data for the other noble metals, which are the electronic and catalytic analogues of silver and have the dⁿs¹ configuration of the valence electronic shell (Chapter 3, Section 3.5, Figure 3.27). As seen in Figure 3.27, in this series of noble metals the silver cations have the most effective charge, correlating well with the catalytic properties of silver. The resistance to donation of the d-shell of silver explains, in particular, its unusually weak capability of adsorbing the nonoxidizing adsorbates, i.e. carbon monoxide, methanol, ethylene, etc.

Of course, the IR spectroscopic data obtained for the model samples may not be directly relevant to 'real' catalysts. In the industrial synthesis of formaldehyde, supported catalysts with low surface areas are used. The major part of silver in these catalysts is in the form of large metal aggregates, and a support can have little influence on the electronic properties of these aggregates.

However, investigations carried out by Noskova *et al.* [887] showed that in industrial catalysts the support is not completely covered with a metallic film even at high silver concentrations, but instead contains highly dispersed silver ions and clusters which strongly interact with the support. Here, the amount of silver in one of these states is high, i.e. the electronic states of these dispersed particles are directly influenced by the support. Such particles take part in the catalytic process, along with the larger aggregates of metal.

This conclusion is confirmed by catalytic investigations of samples of an industrial catalyst with 40 wt% Ag/pumice and 35 wt% Ag/aluminasilicate treated in nitric acid [898]. According to DRES (Figure 6.21), electron microscopy and low-angle X-ray scattering data, the initial samples contain silver in the form of pieces of metal film of about 5000 nm thick (absorption band at 310 nm), ions of Ag⁺ (240–250 nm) and Agⁿ⁺ clusters (280 and 370–390 nm). The data from hydrogen chemisorption showed that the portion of the charged states of silver on aluminasilicate is about 50 %, and on pumice about 30 %. Nitric acid completely dissolves the metallic silver shell, leaving only silver ions, isolated atoms and some 6–10 wt% of charged clusters strongly interacting with the support. However, the initial catalytic activity of the treated samples differs slightly from that of the initial samples. In other words, the yield of formaldehyde decreases only by 2–3 % (Figure 6.22), and it is only after 4–5 h that the activity of the samples drastically falls as a result of intensive carbonization of the exposed surface of the support. This proves that the highly dispersed ionic states of silver are important and active participants in the catalytic process as well as the metal film and large particles. This also corroborates the above-mentioned conclusion that the size and form of the silver particles do not influence the catalytic properties

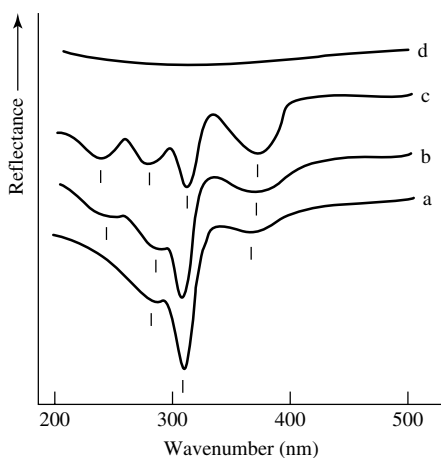


Figure 6.21. DRE spectra of industrial catalyst samples: (a) 30 wt% Ag/aluminasilicate (initial); (b) 30 wt% Ag/alumina silicate, treated with O_2 at 773 K; (c) 6 wt% Ag/alumina silicate boiled with HNO_3 for 2 h; (d) Ag_2O .

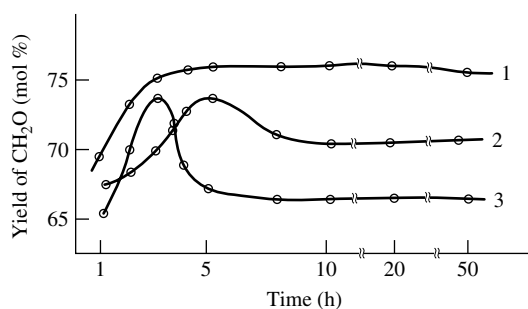


Figure 6.22. Formaldehyde yield as a function of silver content in various catalyst systems: (1) 38 % Ag/pumice; (2) 14 % Ag/pumice; (3) 6 % Ag/pumice.

of silver. The Ag^+ cations seem to be active sites in the catalytic oxidation of methanol on both the supported catalyst and the surface of metallic films or crystals.

Modifying additives of metal oxides are important factors impacting on the surface state of silver. The spectra of Ag/Al_2O_3 modified by Ce and Zr oxides exhibit more intense bands at 240, 280 and 370 nm corresponding to different ionic states of silver (Figure 6.19). In the spectrum of the sample modified by Cs_2O , all of these bands are absent, but a signal at 420 nm is detected (plasma resonance absorption of large silver clusters). Obviously, additions of cerium and zirconium oxides stabilize the oxidized state of silver and raise its degree of dispersion. Cesium oxide, on the other hand, favors the reduction of Ag^+ and hence an aggregation of the metal into large particles. Investigation of these samples by the methods of electron microscopy, FTIR spectroscopy of adsorbed CO, and H_2 adsorption, verifies this conclusion (Section 3.5). The various observed effects are associated with an electronic donor–acceptor interaction of silver atoms and ions with the M^{n+} and $O^{\delta-}$ ions of the oxide modifiers. Oxygen ions of the Cs_2O basic oxide have a high electronic density, so the effective charge of silver falls drastically at the expense of the electron-releasing $O^{\delta-}-Ag^{\delta+}$ effect. Highly charged Zr^{4+} and Ce^{4+} ions, in contrast, retard

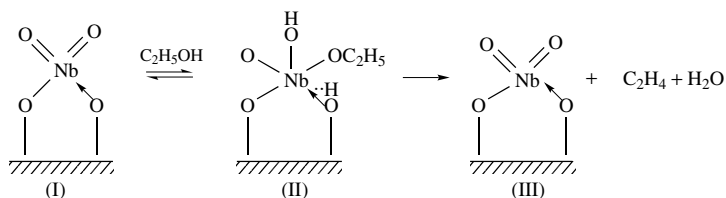
Table 6.6. Spectroscopic and catalytic characteristics of 15 wt% Ag/support (methanol oxidation at 923 k).

Catalyst	νCO in Ag^+-CO (cm^{-1})	Yield of formaldehyde (mol%)	Selectivity (mol%)
Ag/aluminosilicate	2195	74.6	89.6
Ag/ Al_2O_3	2175	70.2	82.7
Ag/MgO	—	24.7	38.2
Ag– $\text{ZrO}_2/\text{Al}_2\text{O}_3$	2190	75.4	86.2
Ag– $\text{CeO}_2/\text{Al}_2\text{O}_3$	2190	73.2	85.1
Ag– $\text{La}_2\text{O}_3/\text{Al}_2\text{O}_3$	2165	60.0	78.2
Ag– $\text{Cs}_2\text{O}/\text{Al}_2\text{O}_3$	2162	68.4	80.3

the surface diffusion of silver particles and favor their oxidation because of a strengthening of the strong metal–support interaction.

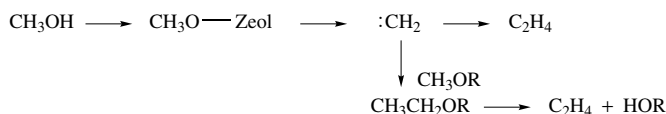
IRS measurements of the CO adsorption confirm that the additions of zirconium or cerium oxides into the catalyst stabilize the oxidized states of silver [899]. On the other hand, additions of La, Rb and Cs oxides hamper the oxidation of silver and reduce the effective charge of the Ag^+ cations (reflected in a low-frequency shift of νCO , see Figure 3.28). By comparing spectral data and the results of catalytic investigations of modified samples of silver (Table 6.6), it has become evident that zirconium and cerium oxides are the promoters of choice for silver, whereas La, Rb and Cs oxides decrease its activity. In the latter case, the promoters intensify the methanol dehydrogenation (the yield of hydrogen increases). Catalytic tests of modified pumice (without any silver support) showed that the addition of each of the above modifiers increases the yield of formaldehyde (see Table 6.6). Here, the intrinsic promotion properties of the modifiers are effective during methanol oxidation but not during methanol dehydrogenation (the yield of hydrogen falls). Additions of La, Ce and Zr oxides increase the degree of dispersion of supported silver by 2 to 3 times but, as has been discussed above, this does not influence the catalytic process. In studies by Pestryakov *et al.* [1868], involving formaldehyde synthesis in a commercial reactor, it was determined that the modifiers increase the surface acidity of the support and the rate of carbonization on the catalyst surface. However, for short times on-stream the influence of these factors is negligible. Therefore, it is reasonable to assume that the positive influence of zirconium and cerium oxides, and the negative effect of La, Rb and Cs oxides is probably explained by their indirect influence on the electronic and redox properties of silver rather than on the intrinsic catalytic properties of the additives. Other factors can also contribute to this.

The dependence of the selectivity of ethanol dehydrogenation on the size of oxide clusters has also been established [1869]. The adsorbed species (I) are too stable under vacuum to be dehydrogenated and are dehydrated at much higher temperatures than 573 K to (II), and then to (III):

**Scheme 6.72**

On the other hand, in the presence of in the gas phase, the dehydrogenation of the latter was found to proceed at a much lower temperature (423 K) with 100 % selectivity [1869].

The first C–C bond is the most problematical and, according to Chang and co-workers [1870, 1871] proceeds via an intermediate formation of carbenes:

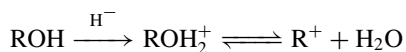


Scheme 6.73

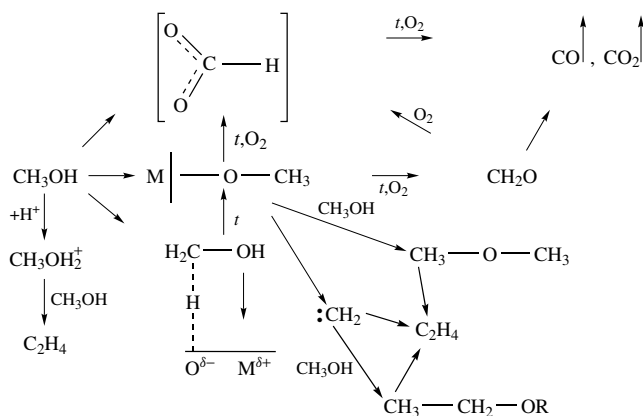
The fact that there are no problems when ethanol or other alcohols with longer hydrocarbon chains are converted into hydrocarbon shows that the formation of the C–C bond is the limiting stage in methanol conversion.

As was observed by various authors [1177, 1181, 1183] by means of IR and UV–Vis spectroscopies, methanol on ZSM and HY zeolites easily interacts at 473–513 K with oligomeric alkyl, allyl and polyenyl cations, and thus the alkylation of hydrocarbons probably proceeds mainly through such carbocations.

Mechanistic schemes proposed on the basis of IR and UV–Vis spectroscopic data have been mainly confirmed by NMR spectroscopic data [1872, 1873]. Such work also confirmed the formation of oxonium ions upon the interaction of methanol or dimethyl ether with the $\text{CH}_3 + \text{RH}$ surface groups. Thus, an NMR spectroscopic study of the dehydration of allyl alcohol on the HZSM-5 zeolite [1837] enabled the detection of the intermediate oxonium and carbonium compounds and to establish the sequence of the transformations as follows:

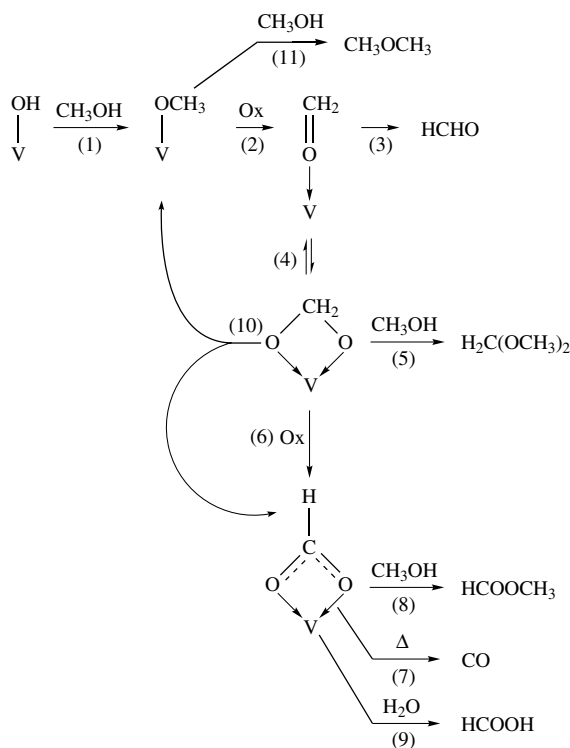


As opposed to the cationic pathway, the radical mechanism for methanol conversion to hydrocarbons on various zeolites has been investigated by ESR spectroscopy [1874]. Generalized mechanisms for heterogeneously catalyzed conversion of methanol have been presented by Davydov [30]:



Scheme 6.74

and Busca [66]:



Scheme 6.75

6.5 Transformations of nitrogen-containing compounds

6.5.1 DECOMPOSITION OF NITRIC OXIDE

Although several different reaction mechanisms have been put forward for NO decomposition on oxide surfaces, the main issue over how these mechanisms differ is whether or not a redox mechanism is involved. There has also been discussion about the nature of the reaction intermediates and the active sites involved in the catalytic reaction. Still in the earliest studies of the NO interaction with CuO/Al₂O₃ [481] and CuO/SiO₂ [1888], Cr₂O₃ [594], Fe₂O₃ [595] and Fe₂O₃/Al₂O₃ [30, 481] as well as in the above cases, it was shown that the NO decomposition proceeds only on the reduced Cu¹⁺ or Cr²⁺ centers, and Fe²⁺ which are probably formed on oxidized surface due to the formation and decomposition of nitrate–nitrite species. The NO complexes responsible for decomposition are characterized by the weakening (in comparison with NO in the gas phase) of the NO bonds. It is important that the above results have been confirmed by both spectroscopic and catalytic investigation of CuCr₂O₄ [830]. As has already been mentioned above (Section 2.3.5), NO decomposition on Cr₂O₃ occurs through the formation of NO⁻ species, whereas on Fe₂O₃ as well as on Cu-containing systems, it is due to the formation of the Fe²⁺–NO complex with a weakened bond (1805 cm⁻¹) or Cu¹⁺–NO (–1740 cm⁻¹).

CuY

Among all of the NO decomposition catalysts studied by spectroscopic methods, the copper-containing systems have a specific future since they are able to decompose NO under oxidative

conditions. Due to detailed investigations of the reaction mechanisms, at the end of the 1970s the catalysts (CuY-A zeolites and CuO–MgO) for this reaction had already been discovered and even used in laboratory catalytic reactors [1875]. On the basis of the detailed spectroscopic investigation of NO interaction with different Cu-containing catalysts, it was shown that the Cu–Y-zeolites have different distributions of copper ions influencing the character of the NO activation (Section 3.1 and [30, 326, 481, 520–22, 1884, 1878, 1879]). The main principle of this catalytic process has been formulated as a necessity for the presence of reduced Cu^+ centers on the surfaces of the catalysts. The appearance of such centers on Cu-containing catalysts under oxidation conditions is stipulated by either a desorption of oxygen from the Cu–O–Cu bridges or reduction of copper ions due to formation of nitrites/nitrates at the interaction with NO.

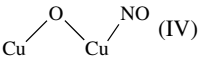
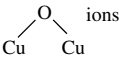
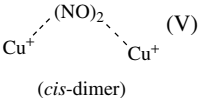
In the early 1990s, Iwamoto *et al.* [1876, 1896] and Held *et al.* [1877] independently reported the selective catalytic decomposition and reduction of NO_x by hydrocarbons in excess oxygen and developed a catalyst on the basis of Cu-ZSM zeolites, which has been used in industry. We will examine these systems in more detail.

The conditions under which copper is inserted into a zeolite, the amount of copper added, and the treatment of the sample have a strong effect on the state of copper in a zeolite skeleton (Section 3.1). In CuY-I zeolites prepared by ion-exchange under conditions excluding hydrolysis of the exchanging salt, the Cu^{2+} cations are stabilized as isolated or weakly associated ions, coordinated either exclusively to the oxygen ions of the zeolite skeleton (S_I) or to both the skeleton oxygen and the hydroxyl groups or H_2O molecules. At low copper contents (up to 2 %), the Cu^{2+} ions are found mainly at S_I sites, which offer a high level of coordination saturation (octahedral surroundings). Increasing the copper content in dehydrated CuY zeolites produces coordinatively unsaturated Cu^{2+} ions in S_I , S_{II} , and other sites (isolated or weakly associated). CuY–A zeolites also contain strongly associated $\text{Cu}^{2+}\text{–O–Cu}^{2+}$ species.

A study of the adsorption of NO on CuY zeolites [1878, 1879] revealed complexes of NO with copper cations in different states (Section 3.1 and Table 6.7). The formation of oxidized NO complexes (i.e. the reduction of Cu^{2+} ions) is observed in CuY-I zeolites only on heating the zeolite in NO at 573 K and is accompanied by the appearance of weak infrared absorption bands corresponding to the NO complexes on reduced Cu centers. In CuY-A zeolites treated in an oxidative atmosphere, in addition to the complexes I and II, the adsorption of NO on strongly associated copper ions (complex IV) and the formation of oxidized structures of the nitrate type have been revealed. The latter structures are formed due to the oxidation of NO by oxygen from strong associates.

The interaction of NO with an oxidized CuY-A at 293 K produces oxidized NO complexes of the nitrate type (as obtained on $\text{CuO}/\text{Al}_2\text{O}_3$ [481]), which were already directly observed in

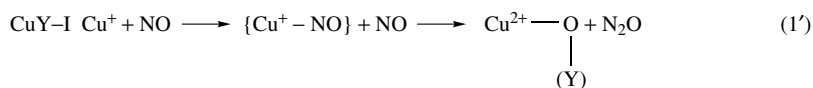
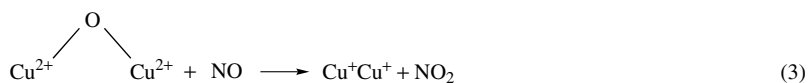
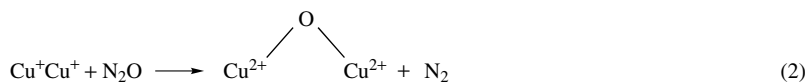
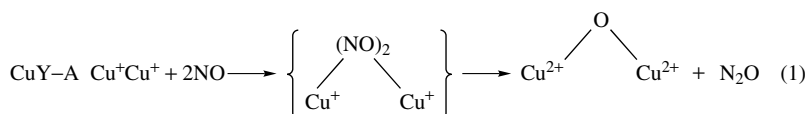
Table 6.7. Complexes of NO with the copper cations in Cu- zeolites.

Zeolite	νNO (cm^{-1})	Complex	State of the adsorption center
CuY-I	1920	$\text{Cu}^{(2-\delta)+}\text{NO}^{\delta+}$ (I)	Isolated Cu^{2+} ions
	1950	$(\text{Cu}^{2+} \dots \text{Cu})^{(2-\delta)+}\text{NO}^{\delta+}$ (II)	Weakly associated $\text{Cu}^{2+} \dots \text{Cu}^{2+}$ ions
	1740	Cu^+NO (III)	Strongly associated Cu^+ ions
	1900	 (IV)	 ions
CuY-A	1835 } 1795 }	 (V) (<i>cis</i> -dimer)	Paired $\text{Cu}^+ \text{Cu}^+$ centers, formed by the reduction of strongly associated Cu^{2+} ions

1975 by Lokhov and Davydov [481, 1878, 1879, 1884] and which should be accompanied by the reduction of some of the Cu^{2+} ions, i.e. leads to the reduction of the centers needed for the decomposition of NO. Later it was shown for numerous oxides, though even in 1996 Sadykov *et al.* [1880] presented the formation of nitrate structures and their effect on NO decomposition as a new occurrence, and explained the effects obtained on the basis of the concept suggested by other workers [481, 1878], but without both direct experimental proofs and citation of all relevant data [481, 1878, 1879].

The activation energy (E_a) for the decomposition of NO on a CuY-I zeolite, measured by Davydov [806], is 84 kJ mol^{-1} , and the kinetic order of the reaction is close to 1, whereas for CuY-A zeolites $E_a = 42\text{--}46.2 \text{ kJ mol}^{-1}$ and the order of the reaction is close to 2. The lower activation energy of the NO decomposition on strong associates can be due to (i) the possibility of a reaction through dimeric structures, and/or (ii) a greater activity of the oxygen in strong associates. The higher E_a value of the weak associates can be caused by a greater stability of the intermediate complex III (as compared with the complex V) in the decomposition of NO and/or by the difficulty of regenerating the reduced Cu^+ centers.

By comparison of both IRS and kinetic data [806], Davydov suggested the following scheme for the NO decomposition on CuY zeolites:



Scheme 6.76

The stages of the formation of nitrites and nitrates leading to the appearance of the Cu^{1+} and $\text{Cu}^{1+}\text{Cu}^{1+}$ centers are not shown in this scheme.

CuZSM

Keeping in mind that the 'new' Cu zeolite systems (Cu-ZSM-5) have been developed for the NO decomposition reaction, it is interesting to compare the earlier and newer data. The attractiveness of direct NO_x decomposition into N_2 and O_2 over a catalyst ($2 \text{ NO} \rightarrow \text{N}_2 + \text{O}_2$) without the use

of a reducing agent, led to an FTIR study [1881] of the surface interactions between NO and Cu-exchanged zeolites in order to determine in detail the role of 'over-exchanged' Cu-ZSM-5, and of Cu ions in different zeolite matrices such as Y systems and mordenite. A catalytic performance of Cu in a zeolite matrix for NO decomposition was linked to the $\text{Cu}^+ \rightleftharpoons \text{Cu}^{2+}$ redox cycle which was essential for the formation of the $\text{ON}-\text{Cu}^{2+}-\text{NO}_2^-$ complex and depended on the relative stability of the Cu(I) and Cu(II) species. The redox chemistry of Cu sites in 'over-exchanged' ZSM-5 catalysts has been well matched to the NO decomposition mechanism. In other zeolite matrices, Cu^{2+} was too stable, e.g. CuM-57. This permitted high oxidation rates, but regeneration of Cu(I) sites became difficult and so the reaction ceased after the first cycle. In other cases, Cu(I) was stable, e.g. CuUHSY-165, and the oxidation to Cu^{2+} via the cited reaction scheme was unfavorable [1881]. The main role of the $\text{Cu}^+/\text{Cu}^{2+}$ transition has been noted in numerous studies. Thus, Aylor *et al.* [1882] investigated the interactions of NO with Cu-ZSM-5 systems by means of IR spectroscopy. Because of the reduction by CO, copper is predominantly present as Cu^+ cations. Room-temperature exposure of the reduced catalyst to NO results in the immediate appearance of Cu^+ (NO) and Cu^+ (NO)₂. With time, these species disappear and are replaced by Cu^{2+} (NO) and Cu^{2+} (O⁻)(NO). Evidence for the formation of Cu^{2+} (NO₂⁻) and Cu^{2+} (NO₃⁻) and of adsorbed N₂O and N₂O₃ was also observed. Similar species are observed upon room-temperature exposure of 'auto-reduced' and pre-oxidized Cu-ZSM-5 catalysts. Above 573 K, the catalyst is active for NO decomposition to N₂ and N₂O. Infrared spectra taken under reaction conditions show the weak peaks for Cu^+ (NO), Cu^{2+} (O⁻)(NO) and Cu^{2+} (NO₃⁻). With increasing temperature, the intensities of the peaks for Cu^+ (NO) and Cu^{2+} (O⁻)(NO) decrease, but the proportion of the former species increases relative to the latter. Based on this evidence and data on the rates reported in the literature, a mechanism was proposed for the decomposition of NO. The first step in this mechanism is the formation of N₂O via a decomposition of Cu^+ (NO)₂; N₂ is then formed via the reaction of N₂O with Cu^+ sites. Oxygen (O₂) formation is envisioned to proceed via the release of oxygen atoms from Cu^{2+} O⁻ and the subsequent reaction of oxygen atoms with additional Cu^{2+} O⁻ to produce Cu^{2+} O₂⁻.

The variation of the fraction of Cu^+ with temperature, deduced from the proposed mechanism, is in qualitative agreement with recent X-Ray Absorption Near Edge Spectroscopy (XANES) observations. There is good agreement between these data and those obtained by Grunert and Shpiro using ESR spectroscopy [1883]. These authors showed that the external surfaces of the as-prepared zeolites are highly enriched in copper oxide species. The latter, however, become well dispersed due to pretreatment. In exchanged zeolites, as has been shown by different physical methods, copper becomes dispersed in the zeolite channels, in the form of both isolated, fivefold coordinate ions and small clusters containing 'extra-lattice' oxygen. These conceptions are very close to those developed in [1878, 1879]. In particular, this state of copper is an active component of the reaction. Thus, the most likely intermediate in the NO decomposition is a dinitrosyl species formed by the co-adsorption of two NO molecules on a single site. Such adsorption in pairs on coordinatively unsaturated ions is characteristic of NO adsorption. This is due to the stabilization derived from the mutual interaction of the unpaired electrons on each NO unit. *Gem*-dinitrosyls probably occur as nonionized surface species. It is clear from the previous discussion that the regeneration of active centers is the key problem for these systems. So, numbers of recent studies have been devoted to this question. We will shortly examine the more interesting results of these studies.

As has been pointed out above, the activity of the Cu-ZSM-5 zeolite was first reported by Iwamoto *et al.* [1896]. These authors used a ZSM-5 zeolite with a Si/Al ratio of 50. Studies of these catalysts have grown like an avalanche recently (see, for example, [1897-1899] and references therein). The reactant gas was a mixture of 4 % NO in He. They obtained 64 % conversion of NO to N₂ under steady-state conditions at a temperature of 773 K.

Motivated by the unique catalytic activity of Cu/ZSM-5 in the decomposition of NO to N₂ and O₂, the redox chemistry of Cu in ZSM-5 zeolites has been studied by using FTIR, TPR, EPR and EXAFS [1900, 1901]. Isolated ions, Cu²⁺, oxo-cations, [Cu–O–Cu]²⁺ and oxide particles have all been identified. Their relative abundance depends on the overall Cu loading, the pH value during ion-exchange, and the gas atmosphere. Oxo-cations are only detected at a level of Cu exchange that exceeds 40 %; their concentration is higher in high-pH preparations which favor hydrolysis. Oxo-cations are reduced by the CO and NO molecules at room temperature; they act as the catalytic sites for the disproportionation of NO into N₂O + NO₂. Particles of CuO are detected; at elevated temperatures under a He atmosphere they are converted to Cu₂O. In addition, Cu⁺ has been detected by FTIR spectroscopy using CO or NO as a probe. Flowing H₂ reduces the Cu²⁺ ions – the first detectable product is Cu⁺ because Cu⁰ is thermodynamically unstable in the presence of Cu²⁺. After all of the Cu²⁺ is used up, Cu⁰ is detected. In CO, only oxide particles and oxo-cations are reduced, but in the presence of CO they react with Cu⁰ to form Cu⁺ ions. Zeolite protons oxidize Cu⁰ to Cu⁺; this process is accelerated by the molecules of CO which form the stable Cu⁺–CO complex. Protons also react with CuO to give Cu²⁺ and H₂O.

Cu/ZSM-5 zeolites have been studied primarily with a viewpoint of an active component for the reaction. *In-situ* photoluminescence, EPR, EXAFS, FTIR and UV–Vis spectroscopic studies of the Cu⁺/ZSM-5 catalyst formed in this way indicated that most of the Cu⁺ ions in the ZSM-5 zeolite exist as isolated Cu⁺ monomer species, which plays a significant role in this reaction [1895]. This point of view is widely held [1883].

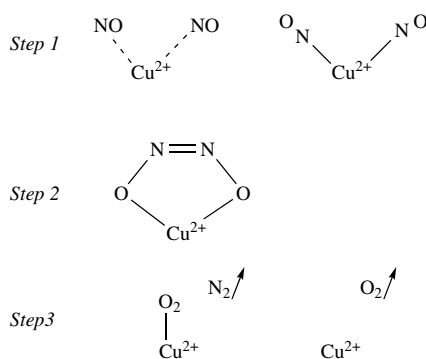
In ZSM-5 there are two types of isolated Cu²⁺ ions, i.e. one in the four-coordinated square-planar configuration and the other in a five-coordinated configuration [1902]. The occurrence of the four-coordinated species increases with increasing Cu loading while the five-coordinated species are predominant at low loadings. There is a patent which claims that the Cu²⁺ ions in the square-planar configuration are the active sites in the selective reduction of NO [1903]. Three different copper zeolite systems, i.e. Cu-ZSM-5, Cu-UHSY and Cu-mordenite have been prepared with variable (from low up to in excess of exchange levels) copper loadings. The surface chemistry of these systems has been studied by using the IR spectra of adsorbed NO. Most of the copper in Cu-ZSM-5 was in the form of Cu⁺. The Cu(II) species were predominant in the Cu-mordenite. For Cu-UHSY, the number of Cu⁺ species increased as the level of copper loading increased. The catalytic activity in NO decomposition appeared to depend on a Cu(I) redox cycle which resulted in the formation of an ON–Cu²⁺–NO₂[–] complex. This complex was previously postulated as a critical intermediate in the reaction. Both oxidation and regeneration of the Cu(I) sites in Cu-ZSM-5 occur readily. In Cu-UHSY, oxidation was low, suggesting that Cu(I) species were more stable. The Cu(II) was the prominent copper species in Cu-mordenite, and regeneration of the Cu(I) sites was difficult. Stability, oxidation and regeneration of Cu(I) sites are factors which play a major role in NO decomposition. In ‘over-exchanged’ Cu-ZSM-5, the Cu(I) sites were more stable, and the rate of oxidation was high. Furthermore, a large number of reduced sites was readily regenerated from Cu(II), thus making it the most effective catalyst for the decomposition of NO.[1881].

Kharas *et al.* [1909] concluded that the copper chemistry has a central importance, and the Brønsted acidity of the zeolite plays no role in the SCR of NO. Their model suggests that the exchanging species are not the Cu²⁺ cations, as formerly assumed, but rather [CuOH]⁺ and its related oligomers. The working catalyst exhibits a dynamic Cu²⁺ → Cu⁺ conversion under catalytic conditions, while Cu⁺ can be the predominant oxidation state under reaction conditions.

Iwamoto *et al.* [1910] have proposed two different pathways: one involving the direct decomposition of NO to N₂ and O₂ and the other involving the formation of N₂O and its subsequent decomposition to the elements. However, these authors observed the formation of N₂O only at

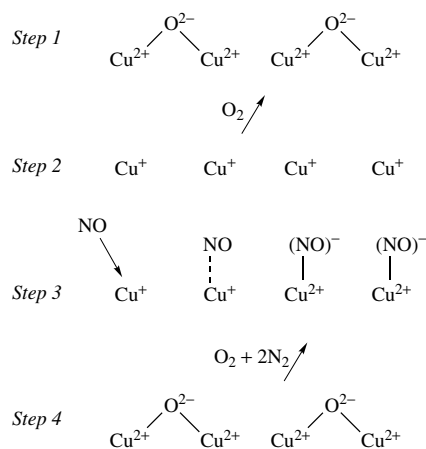
temperatures below 673 K. It has already been mentioned that at these temperatures the adsorbed oxygen poisons the catalyst. Their results may be reinterpreted in the light of the dinitrosyl intermediate. The N atoms are successfully paired to form the nitrous oxide, which has a linear structure (NNO), but the catalyst is unable to release the second atom of oxygen (which is strongly adsorbed) unless the reaction temperature is increased. In this way, the N_2O molecule is desorbed and a dissociated oxygen atom remains on the surface, so poisoning the catalyst. Thus, N_2O is an undesirable side, not an intermediate, product in NO decomposition.

Simultaneously with oxygen desorption, Li and Hall [1911] observed that the Cu^{2+} species were spontaneously reduced to Cu^+ . Iwamoto *et al.* [1910] proposed a cyclical mechanism that accounts for these observations and Hall and co-workers [1911, 1912] have elaborated on this mechanism. Li and Hall [1911] hypothesized that the reduced copper species is the one that is active for NO decomposition, and they proposed a redox mechanism which ends with an O^{2-} bridge spanned between two adjacent Cu_2^+ sites:



Scheme 6.78

Shelef [1913] proposed a nonredox mechanism in which the cupric ions adsorb *gem*-dinitrosyls and are the active sites:



Scheme 6.79

In this mechanism, two NO molecules are adsorbed on a single Cu^{2+} site. He presented convincing evidence that the negatively charged adsorbed nitrosyls would be thermodynamically unstable at elevated temperatures and questioned their existence at all. On the other hand, he has stated that the nitrosonium (NO^+) ion is favored and is far more likely to be adsorbed or formed on Cu^{2+} (d^9) than on Cu^+ (d^{10}). The former copper ion is a better electron acceptor. Shelef's proposal is plausible as NO would be stabilized by donating its unpaired electron to the copper ion to form the nitrosonium ion. Later, however, Shelef [1913] suggested that the adsorbed *gem*-dinitrosyls are neutral surface species chemisorbed through their lone-pairs. To justify the role of Cu^{2+} rather than Cu^+ , he suggested that the isolated cupric ions which are found in ZSM-5 are resistant to the reduction and stated that the desorption of oxygen upon heating from these ions has been shown not to be associated with their reduction, i.e. that adsorption on these ions occurs simply because they are coordinatively unsaturated.

According to Shelef, the difference between the two mechanisms of NO decomposition over Cu-ZSM-5 is as follows. If the isolated copper ion in the high Si/Al structure can be spontaneously reduced by heating in a highly oxidizing atmosphere (NO , O_2 or NO_2) to the Cu^+ state, a redox mechanism is plausible, and if not, the pairing of the nitrogens is not dependent on the change in oxidation state of the metal. In fact, Cu^+ is a diamagnetic d^{10} species with no means of accommodating the unpaired electron that resides in the antibonding orbital of the NO molecules. Valyon and Hall [1912] have used this consideration to motivate their proposition that NO is adsorbed on this species as a negative ion and forms a fairly strong bond while oxidizing copper to Cu^{2+} in the process. However, the pairing of an unpaired electron of the NO molecule with an electron from the copper ion, may be an impediment to the interaction of the nitrogen atoms of two NO molecules which is needed for the formation of dinitrogen. Therefore, one would expect this species to carry only a slight charge.

Based on electron paramagnetic resonance hyperfine structure data from NO adsorbed on Cu^+ , Chao and Lunsford [632] reported that the unpaired electron of NO spends 20 % of its time on the Cu^+ . This adsorption on CuY zeolite is unique when compared with NO adsorption on MgO, ZnO or NaY.

Infrared evidence has been presented that the nitrosyls are not formed on Cu^{2+} sites, and that they oxidize the catalyst [1912]. When NO is adsorbed on Cu^+ , the νNO value is lower than that of the gas phase, suggesting that back-bonding has put more electron density into the antibonding orbitals, thus further weakening the NO bond. However, a formal charge was assigned to any adsorbed species. They went on to suggest that the extra electron density present in the $\text{Cu}^{(1+\delta)+}-\text{NO}^{\delta-}$ species, the formation of which has been shown by a number of authors [806, 1878, 1879], allows the addition of a second NO molecule to form the dinitrosyl species.

Centi and Perathoner [1914] commented that due to the higher ionic radius, Cu^+ ions isolated at room temperature are located in more open positions in the hexagonal or pentagonal rings facing the ZSM-5 channel in comparison to Cu^{2+} ions. At room temperature, the mobility of copper ions is limited so that it is reasonable to expect that dinitrosyl species are formed on Cu^+ and not on Cu^{2+} , but this is due to steric hindrance of the facing lattice oxygen and not for electronic reasons. It is expected from orbital overlap and electrostatic repulsion considerations that the coordination of a second NO molecule is easier on a $(\text{Cu}^{2+})^{\delta-}-\text{NO}^{\delta+}$ species than on a $\text{Cu}^{(1+\delta)+}-\text{NO}^{\delta-}$ complex. An analogous mechanism has been proposed by Spoto *et al.* [1915].

In summary, it seems most likely that Cu^+ is the active species, and that $(\text{NO})_2$ is the reaction intermediate which is decomposed to different products depending on the reaction conditions. For example, at low temperatures all of the oxygen remains on the surface and nitrogen is liberated, while at higher temperatures N_2O is desorbed and molecular oxygen exists on the surface. It is

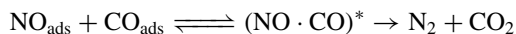
only at temperatures above 673 K that the entire complex is desorbed as molecular oxygen and nitrogen. Thus, the conclusion seems to be that the uniqueness of Cu-ZSM-5 lies in two areas: its ability to stabilize adsorbed nitrosyl complexes (unlike, for instance, CuY) and the self-reduction of the copper species at temperatures that are low enough still for the nitrosyl complexes to form, without the formation of metallic copper.

6.5.2 THE REDUCTION OF NITROGEN OXIDES

It is clear from the previous examination that for NO decomposition the presence of reduced surface centers is necessary, so the presence of a reducer in such case should be very profitable. Interest in the NO + reducer (CO, NH₃, hydrocarbons, etc.) reaction has grown significantly recently because of environmental concerns. There is no doubt that the problem of nitrogen-containing gases is closely linked to the problem of their decomposition. This is true for situations both with and without oxygen mediums. Of course, a reducing agent increases the rate of the reaction significantly and leads to this reaction proceeding. That is why the complete understanding of the reaction mechanism cannot be reached without examining the decomposition of the nitrogen-containing gases in the same system. This is clear, as well as the fact that all of these reactions, independently of reduction, have many similarities. Only the reactions proceeding over oxides are examined in this section.

NO+CO mixtures

At present, there is much data in the literature on the catalytic reduction of NO by CO over transition-metal oxides. A study of the reaction mechanism by the direct method, based on a comparison of the rate of the catalyst reduction-oxidation with that of a catalytic reaction on a steady-state surface, led to the conclusion that, in the case of bulk Fe₂O₃ [595] and supported Fe₂O₃ or CuO [30, 481, 1884], the reaction proceeds via a step-wise mechanism. This is a usual redox mechanism, including three stages, i.e. (i) reduction of the catalyst surface by the reductive reagent, (ii) desorption of the oxidized product, and (iii) re-oxidation of the surface by the nitrogen oxide. The last stage, according to Shelef *et al.* [1885], is the limiting one. However, Alkhazov and Gasan-zade [1886], studying the reaction by the impulse method, concluded that on both chromium and nickel oxides the associative mechanism occurs. The same mechanism has been proposed by Panajotov *et al.* [1887] for the CuCo₂O₄ spinel at low reaction temperatures:



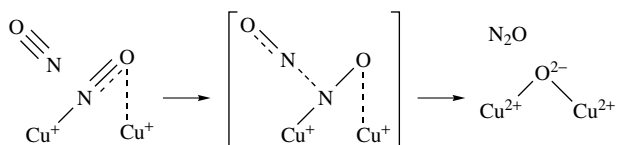
The intermediate complex involving both molecules (NO.CO)*, according to these authors, is characterized by bands in the 1330–1350 cm⁻¹ region and at 1420 cm⁻¹. At higher temperatures (above 473 K) the redox mechanism operates place. Because the rates of the NO + CO reaction and NO adsorption increased with an increased degree of reduction of the catalysts on Fe₂O₃ [595], CuO [481, 1884, 1888], Cr₂O₃ [1886] and SnO₂ [1889], it is possible to suggest that the reduced surface sites are the catalytic active centers. In the case of Fe₂O₃, this suggestion has been confirmed by data from different independent methods such as conductivity, IRS [595] and γ -resonance spectroscopy [30].

Taking into account the data about the character of the CO/NO interaction with oxides, it is not difficult to draw a scheme for the stepwise mechanism of the reaction – the reduction of the catalysts due to the formation and decomposition of carbonates and subsequent oxidation of the reduced centers with NO. However, it is more difficult to draw the scheme for the mixed CO/NO complexes (for example isocyanates) and their participation in the reaction as the intermediates.

London and Bell [1888], examining IRS and kinetic data obtained on CuO/SiO₂, proposed a mechanism including nine elementary steps. The main points of such a mechanism are (i) NO

dissociates upon adsorption, with the formation of $\text{Cu}^+ \text{NCO}^-$ isocyanate complexes (the band at 2200 cm^{-1}) under reaction conditions at 473 K confirming this, (ii) N_2O is an intermediate, and (iii) CO keeps the catalyst surface at a certain degree of reduction and also competes for the sites needed for NO dissociation. These authors believe that centers of different types, such as Cu^0 , Cu^+ and Cu^{2+} , exist on the surface, and that the $\text{Cu}^0 \text{NO}$ complex (1880 cm^{-1}) is responsible for the NO dissociation.

Davydov and co-workers [30, 481, 1884], unlike London and Bell [1888], supposed that over $\text{CuO}/\text{Al}_2\text{O}_3$ NO decomposition, as well as the $\text{NO} + \text{CO}$ reaction, occur through the participation of both the $\text{Cu}^+ - \text{NO}$ surface complex (1780 cm^{-1}) and NO molecules from the gas phase:

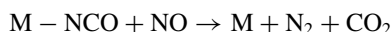
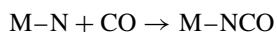


Scheme 6.77

A more detailed scheme was shown in [30]. The N_2O_2 activated complex decomposes in the low-temperature region yielding N_2O and oxidizes the Cu^+ ions with the formation of $\text{Cu}^{2+} - \text{O} - \text{Cu}^{2+}$ species. At high temperatures, an evolution of nitrogen due to the above mechanism is observed owing to the increase in the rate of N_2O decomposition.

It should be pointed out that the role of the isocyanate complexes, which have been the main subject of several studies, is quiet exaggerated. The suggestion of several authors that isocyanate complexes can be the intermediates in this reaction is doubtful, especially in relation to the isocyanate complexes being characterized by νCO at 2240 and $2260\text{--}2270 \text{ cm}^{-1}$ for alumina-supported catalysts, and at 2300 cm^{-1} for silica-supported catalysts, since it has been shown that these complexes are formed through the participation of $\text{Al}_{\text{cuo}}^{3+}$, $\text{Al}_{\text{cut}}^{3+}$ and SiO_2 , respectively. Clearly, surface compounds stabilized on the support cannot be the intermediates. It is doubtful that in the case of such a simple reaction, which includes the NO dissociation as a separate stage, the isocyanate complex can be an intermediate. More probably, the formation of isocyanate complexes is due to the interaction of CO with the dissociated NO fragments.

Solymosi and co-workers, by studying the interaction of NO with CO over SnO_2 (pure and as Cr_2O_3 admixtures) [1889, 1890] and Cr_2O_3 (bulk and supported) [1891, 1892] by different physico-chemical methods, found that the reaction proceeds via a redox mechanism. They suggested that ions of Sn^{2+} in SnO_2 , Cr^{3+} in $\text{SnO}_2 + \text{Cr}_2\text{O}_3$ and Cr^{2+} in Cr_2O_3 are catalytic active centers, on which the NO dissociation takes place. However, these authors believe that the reaction can also occur through the isocyanate complex:



A study of the kinetics of the NO decomposition on $\text{Cr}_2\text{O}_3/\text{SiO}_2$, with a simultaneous registration of the infrared spectra [1893], has found that the catalyst surface under reaction conditions is predominantly covered by some chemisorbed form of NO. The bands at 1735 and 1846 cm^{-1} (weak) corresponding to this species have been assigned to dinitrosyl complexes. The adsorption of NO on CeO_2 , $\text{CeO}_2\text{--Al}_2\text{O}_3$ and Al_2O_3 and its activities in these reactions were studied by using FTIR and ESR spectroscopy and TPR techniques [1894]. The NO adsorption produced nitrite and hyponitrite ($\text{N}_2\text{O}_2^{2-}$) ions. On pure ceria at temperatures $\geq 295 \text{ K}$, the hyponitrite ions

were decomposed to N_2O and O_2^{2-} ions and nitrate ions were reduced to NO by CO at 600 K. The higher ability of pure CeO_2 , in comparison with its supported form, to reduce NO at low temperatures is related to its capability of forming associated oxygen vacancy sites (the sites for hyponitrite ion formation), which are more difficult to generate when ceria is well dispersed on the alumina substrate. Surface nitrate ions, formed on both ceria and alumina, decomposed to give NO_2 and O_2 at temperatures > 700 K.

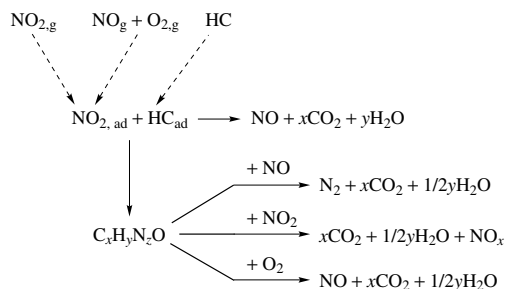
Thus, from the analysis of the data on the interaction between NO and CO on oxide catalysts it follows that (i) at a relatively low temperature (373–595 K), the reduction of NO occurs through the stage of the formation of the N_2O intermediate species, (ii) in the majority of cases the mechanism of the $\text{NO} + \text{CO}$ reaction is redox in nature, and (iii) the reduced sites of the catalyst surface are the active centers for chemisorption and activation of NO. Several authors, who observed in the infrared spectra the absorption bands of surface isocyanate complexes, suggest that NO dissociation takes place, and an atomic nitrogen participates in the reaction. However, such a conclusion is not clear, since the reaction $[\ast-\text{NO}] + \text{CO} \rightarrow [\ast-\text{N}] + \text{CO}_2$ seems to be a source for the production of N_{ads} species needed to form the NCO complex [1893].

Reduction by hydrocarbons

The selective catalytic reduction of NO in the presence of hydrocarbons, i.e. $a \text{NO} + \text{C}_b \text{H}_c \rightarrow b\text{CO}_2 + (a/2) \text{N}_2 + (c/2)\text{H}_2\text{O}$, (where $a = 2b + c/2$), is of interest not only with a view to eliminating vehicle emission, but also due to the possibility of substituting hydrocarbons for ammonia as a reducing agent for NO_x abatement in stationary sources. Oxygen promotes the conversion of both NO and hydrocarbons in the presence of transition metals supported either on zeolites or nonzeolites. The maximum NO conversion is observed at an oxygen concentration of about 2 %.

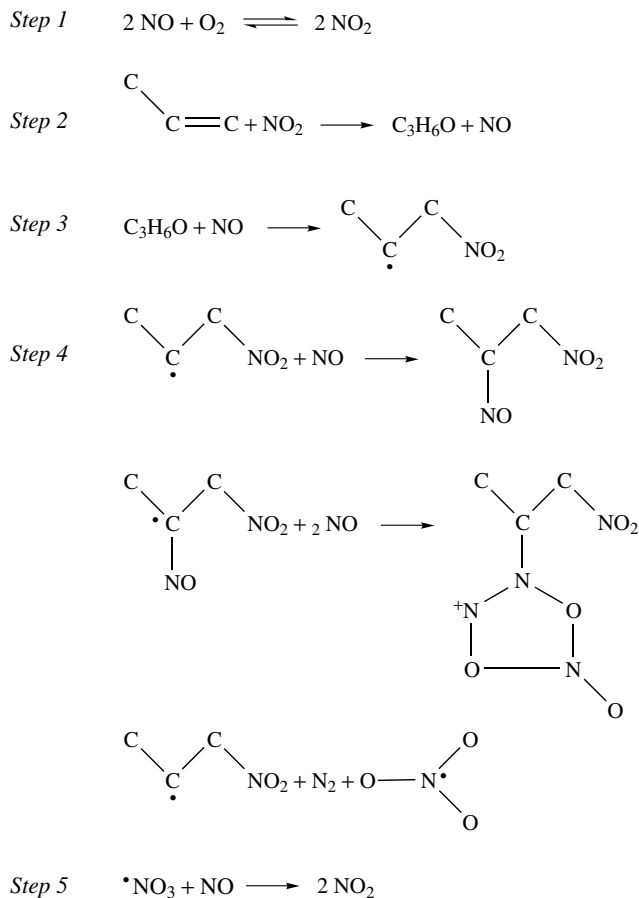
In general, the activity of hydrocarbons in the NO decomposition increases in the following order: *i*-paraffins < aromatics < *n*-paraffins < olefins \approx alcohols \approx ketones [1916–1919]. Petunchi *et al.* [1920] and Smits and Iwasawa [1921] summarized the possible reaction mechanisms that have been advanced. (It should be noted that no mention was made in any of the schemes about how nitrogen pairing occurs.) First, NO decomposition occurs, producing nitrogen and oxygen, with the hydrocarbon regenerating the active sites by removing surface oxygen; by this mechanism, the formation of N_2O over Pt is explained. Secondly, the carbonaceous residue or coke deposited on the catalyst reduces nitric oxide (or possibly nitrogen dioxide). Thirdly, partial oxidation products from the hydrocarbon form reaction intermediates which lead to the selective reduction of NO. Finally, nitric oxide is oxidized to nitrogen dioxide which reacts preferentially with the hydrocarbon reducing agent; this leads to the formation of nitrogen.

Jewell *et al.* [1922] have summarized the various proposals in the following scheme:



Scheme 6.80

Based on the involvement of nitrogen oxides in two mechanisms presented in the literature, the reaction pathway involving propylene has been proposed as follows [1921]:



Scheme 6.81

As shown in the new mechanism, NO is rapidly oxidized to NO_x , which attacks propylene to form $\text{C}_3\text{H}_6\text{O}$ in the rate-determining step; this species, in turn, attacks NO to form a 1-nitro-2-propyl radical, which initiates a radical chain mechanism leading to NO disproportionation into N_2 and NO_2 .

One of the pathways of hydrocarbon participation in the reaction can be through the formation of stable intermediate carboxylate-type species. Such intermediates are much more reactive towards NO than the hydrocarbon itself [1922]. It should be pointed out that such carboxylate compounds can play the role of the storage for hydrocarbons, i.e. to accumulate on the catalyst surface during the run under a reducing atmosphere and be spent in the atmosphere 'reach' with oxygen via the mechanisms proposed, for example in Section 6.2.1.

To elucidate the mechanism of catalytic purification of exhaust gases containing O_2 , NO, CO and hydrocarbons, the state of copper ions in the working Cu-ZSM-5 catalyst at high temperatures was monitored by *in situ* experiments. The equilibrium state of copper oxidation in the catalyst

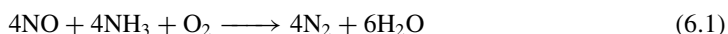
depends both on the temperature and composition of the gas mixture. At 773 K in a mixture containing NO and propene or ethanol with excess of O₂, virtually of all the copper ions were in the Cu²⁺ state. At 473–523 K in the same gas mixtures, a partial reduction of the Cu²⁺ was observed [1904]. The species detected at low temperatures are not representative of those detected at high temperatures when the catalyst is active. The oxidized nitrogen-containing species have been observed on copper (the band at 2580 cm⁻¹) under reaction conditions (673 K). In contrast, at low temperatures, when the catalyst is less active, coke and Cu⁺–CO predominated [1905].

With a NO/propylene/O₂ mixture the added NO was rapidly oxidized by oxygen to NO₂. Organic nitro (1558 cm⁻¹) and nitrito (1658 cm⁻¹) compounds, and also isocyanate (2266 and 2241 cm⁻¹) species were formed on the surface during reaction at 373 K with, in addition, carboxylate, nitrate, etc. If the temperature was raised to 423 or 473 K [1906], the band from the nitro compounds rapidly decreased in parallel with the formation of N₂ in the gas phase. *In situ* FTIR spectroscopic experiments using isotopes were carried out to study the adsorbed species during selective catalytic reduction (SCR) of NO_x by ethylene on Cu-ZSM-5. No oxygen-containing species were observed, and no reaction proceeded in the presence of gaseous O₂. In the presence of adsorbed NO₂ (or a more oxidized NO_x) species, gaseous ethene and NO, the organic nitrite or nitrate species appeared immediately, giving a band at 1670 cm⁻¹. This was accompanied by N₂ and N₂O evolution along with the gradual formation of the carbonyl species. Thus an SCR occurs even at room temperature via a reaction which does not involve O₂, except for NO₂ formation. At 473 K, no nitrogen-containing species were observed, and both N₂ and CO evolved very rapidly, together with a steep increase in the intensities of the IR bands of carboxylates, whereas the bands due to CO₂ and carbonyl species increased more slowly [1907].

For the reaction mixture of NO + C₂H₄ converted on V₂O₅/ZrO₂ [1908], only carboxylate species were observed at higher temperatures, although at lower temperatures the nitrate species were formed. No bands due to a complex of NO + C₂H₄ were observed, and it was proposed that (i) ethene is oxidized by the catalysts to form the carbon dioxide via the carbonyl and carboxylate species, and (ii) nitric oxide re-oxidizes the catalyst to form nitrogen. Quantitative analysis of the V=O band in the region of 1100–900 cm⁻¹ by band-shape analysis indicated that only the species in the top layer of the catalyst interacts with the adsorbed species.

6.5.3 REACTIONS OF NO_x AND NH₃ MIXTURES

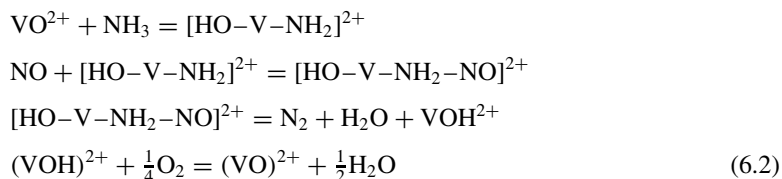
It is well known the vanadium-containing systems are widely used catalysts in the NO plus NH₃ reaction. Different viewpoints exist concerning the mechanism of the interaction of NO with NH₃ in the presence of oxygen on such catalysts:



It is believed that two kinds of adsorbed species (NO₂ and NH₄⁺) participate in this reaction on both V₂O₅ and V₂O₅/Al₂O₃ [427]. Probably one of the stages of this reaction, namely the NO oxidation to NO₂, can easily occur at room temperature even before desorption. Based on the results of IR and ESR spectroscopic studies, and also on kinetic and isotopic adsorption (¹⁵N) measurements, the following mechanism of the reaction has been suggested [422, 423]: (i) NH₃ is adsorbed as NH₄⁺ (ads) with participation of V⁵⁺=O groups; (ii) NO from the gas phase reacts with NH₄⁺ (ads) according to the Eley–Rideal mechanism to form N₂, H₂O and V–OH groups; (iii) V⁴⁺–OH groups are re-oxidized into V⁵⁺=O by gaseous oxygen. It was found that the V⁵⁺=O groups are the sites responsible for the catalytic activity of both bulk and supported vanadia. Similar results were obtained by Jansson *et al.* [428], with the use of labeled NH₃ and O₂ on V₂O₅, V₂O₅/TiO₂, V₂O₅/Al₂O₃/SiO₂ and V₂O₅/Al₂O₃. A dual-site mechanism

of the $\text{NO} + \text{NH}_3$ reaction in the presence of oxygen has been proposed with the participation of two neighboring $\text{V}^{5+}=\text{O}$ groups as active sites. As follows from the data of EXAFS and IR spectroscopy, and also data on the activity of V_2O_5 , both mono- and polycrystals with different morphologies [1924], $\text{V}-\text{OH}$, and not $\text{V}=\text{O}$, groups participate in the reaction. Thermal desorption and Auger spectroscopy studies [1925] imply that the reaction occurs via the Langmuir–Hinshelwood mechanism through the spillover of adsorbed NO species from the carrier onto reduced vanadium centers on which ammonia is adsorbed. The forms of NH_3 and NO adsorption on vanadium-containing catalysts have been studied previously [212–215, 427, 1031, 1926].

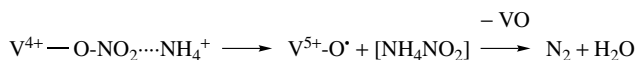
As a result of IR spectroscopic studies of the adsorption of NO , NO_2 and NH_3 on $\text{V}_2\text{O}_5/\text{TiO}_2$ at different temperatures, the following mechanism has been suggested [1927]:



Unfortunately, it is impossible to choose a preferential scheme of the reaction shown in Equation (6.1) because data on the kinetics of transformations of surface compounds and also data obtained *in situ* are practically absent in the literature. Moreover, the majority of studies were performed on oxidized samples.

The study of the form of adsorption of NH_3 and NO and the subsequent interactions of NO_{ads} with NH_3 , and $\text{NH}_{3(\text{ads})}$ with NO , on vanadium-containing catalysts with different degrees of reduction [1928] show that on particularly reduced surfaces a simultaneous coordination of both of the molecules NO (dinitrosyl) and NH_3 occurs on the ions (cations) of vanadium which is in a strong exchange interaction. It was found that both reacting molecules (NO and NH_3) form a common complex with the possibility of electron exchange via the vanadium cations making possible the interaction of these molecules according the Langmuir–Hinshelwood mechanism. It should be mentioned that this activation of molecules is facilitated by the specific state of the catalyst containing clusters of vanadium-oxide formations, which are easily reduced to V^{4+} and re-oxidized to V^{5+} . The role of gas-phase oxygen also becomes evident in this connection. This probably provides a specific (V^{4+}) degree of oxidation of the vanadium cations, as a better oxidant than NO , and does not allow them to be ‘over-reduced’ to V^{3+} .

The following scheme, based on infrared data, has been suggested by Kantcheva *et al.* [1929]:



Scheme 6.82

The nitrate species coordinated to V^{4+} react with an ammonium ion located in the immediate vicinity. Nitrate species are decomposed with the liberation of a nitrite ion and a $\text{V}-\text{O}^\bullet$ radical, and the nitrite species then couple with NH_4^+ ions to produce nitrogen and water.

Results reported by Bushev *et al.* [1930] show that the majority of surface species formed during NO_2 adsorption on anatase cannot react with ammonia; monodentate nitrates are located at the Lewis acid sites and block them for ammonia adsorption. The nitro–nitrito species, formed at higher temperatures are, on the contrary, replaced by ammonia. The only sites on anatase

where co-adsorption of NO_2 and NH_3 occurs, are the surface hydroxyl groups. However, in this case NH_4^+ is coupled by NO_3^- , producing NH_4NO_3 -like species that are decomposed to N_2O upon heating.

The results obtained on Fe-ZSM-5 [1931] suggest that the rate-determining step in the reaction is the formation of adsorbed NO_2 *o*-nitrate species, which then form N_2 through rapid reaction with adsorbed ammonia.

Ammonium ions were not formed on ammonia adsorption over the catalysts belonging to the CuO-TiO_2 and $\text{MgO-Fe}_2\text{O}_3$ systems [1932]. In all such cases, ammonia is molecularly coordinated over Lewis acid sites. A reaction pathway from ammonia to NO via amide-imide-nitroxyl species was proposed.

On Cu-ZSM-5 in the presence of O_2 , the Cu^{2+}/NO species, formed at ambient temperatures during NO adsorption, were converted to nitrate via N_2O_3 and N_2O_4 [1933]. These results indicated that surface nitrates are important intermediates in the SCR process since they are thermally stable and resistant to interaction with CO_2 , N_2 and O_2 , and are only slightly affected by H_2O and NO . *In situ* IR measurements, using $^{18}\text{O}_2$ and ^{15}NO , showed the presence of NO_3^- species acting as intermediates for the formation of N_x at 573 K [1934]. An infrared mechanistic study [1935] showed that NO_x ($x = 2$ or 3) was formed upon NO adsorption, and this was obviously enhanced over cerium- or lanthanum-exchanged mordenite. These NO_x species reacted with ammonia over cerium-exchanged mordenite, leading to the achievement of redox properties.

Ammonia can be adsorbed as coordinated NH_3 and ammonium ions, which both have comparable thermostability. In the presence of gas-phase O_2 , the following compounds can be observed in increasing order of thermodynamic stability [1936]: linear nitrites, bridged nitrites, monodentate nitrates, bridged nitrates and bidentate nitrates. The formation of these species is strongly enhanced in the presence of O_2 , and probably proceeds by NO oxidation, i.e. nitrosylic compounds are unstable in an O_2 -containing atmosphere. No ammonia oxidation is observed on alumina-supported manganese oxide catalysts if oxygen is absent. The interaction with NO is very weak, although strongly bound oxidized species can also be formed in the presence of oxygen, resulting in NO_2 , nitrito and nitrate groups [1937]. These species are decomposed, giving back the NO gas. Based on the IR spectra of NH_3 - NO co-adsorption, it has been suggested that the Mn^{3+} species can bind both one NO and one NH_3 molecule. In the absence of oxygen, the reaction between NO and NH_3 was observed in the infrared cell in the temperature range 300–423 K, whereas in the presence of oxygen, the reaction already tended to completion at 325 K, provided that ammonia is pre-adsorbed relative to NO . Oxygen plays several roles, i.e. (i) it oxidizes the catalyst, favoring NO adsorption, (ii) it permits hydrogen abstraction from adsorbed ammonia, thereby activating it for reaction with NO , and (iii) it can oxidize gas-phase NO to NO_2 .

The $\text{SO}_4^{2-}/\text{TiO}_2$ system, which behaves as a super-acid, exhibits a considerable activity, exceeding that of $\text{V}_2\text{O}_5/\text{TiO}_2$ at temperatures above 673 K, and reaches a peak activity at 773–798 K. TGA, XPS and IR analyses of the catalyst indicated that the SO_4^{2-} ions were formed on TiO_2 , and the structure of the TiO_2 surface sulfate under the SCR reaction conditions was bridged bidentate, i.e. $\text{Ti}_2\text{SO}_3(\text{OH})$ [1938]. The reaction proceeds via the Eley-Rideal mechanism, on Brønsted acid sites of the $\text{SO}_4^{2-}/\text{TiO}_2$ surface.

REFERENCES

1. Griffiths, P. R. (1974), *Chemical Infrared Fourier Transform Spectroscopy*, Wiley, New York.
2. Schrader, B. (1995), *Infrared and Raman Spectroscopy: Methods and Applications*, VCH, Weinheim.
3. Grasselli, J. G. and Bulkin, B. J. (1991), *Analytical Raman Spectroscopy*, Wiley, New York.
4. Volkenshtein, M. V., Gribov, L. A., Elyashevich, M. V. and Stepanov, B. A. (1972), *Molecular Vibrations*, Nauka, Moscow.
5. Gilson, T. and Hendra, P. J. (1970), *Laser Raman Spectroscopy*, Wiley, New York.
6. Harris, D. C. and Bertolucci, M. D. (1978), *Symmetry and Spectroscopy. An Introduction to Vibrational and Electronic Spectroscopy*, Oxford University Press, Oxford, UK.
- 7a. Cotton, F. A. and Wilkinson, G. (1988), *Advanced Inorganic Chemistry*, 5th Edn, Wiley, New York.
- 7b. Cotton, F. A. and Wilkinson, G. (1971), *Chemical Applications of Group Theory*, Wiley, New York.
8. Rao, C. N. R. (1970), *Ultraviolet and Visible Spectroscopy: Chemical Applications*, Butterworths, London.
- 9a. Kortum, G. (1969), *Reflectance Spectroscopy: Principles, Methods and Applications*, Springer-Verlag, Berlin.
- 9b. Wendland, W. W. and Hecht, H. G. (1966), *Reflectance Spectroscopy*, Wiley-Interscience, New York.
10. Herzberg, G. (1966), *Electronic Spectra of Polyatomic Molecules*, Van Nostrand Reinhold, New York.
11. Herzberg, G. (1956), *Vibrational Spectra of Diatomic Molecules*, Van Nostrand Reinhold, New York.
12. Herzberg, G. (1962), *Infrared and Raman Spectra of Polyatomic Molecules*, Van Nostrand Reinhold, Princeton, NJ.
13. Bellamy, L. J. (1975), *The Infrared Spectra of Complex Molecules*, Chapman & Hall, London.
14. Sverdlov, L. M., Kovner, M. A. and Krainov, E. P. (1970), *Kolebatel'ny spektry mnogoatomnykh molekul (Vibrational Spectra of Polyatomic Molecules)*, Nauka, Moscow (Wiley, New York, 1974).
- 15a. Nakamoto, K. (1985), *IR and Raman Spectra of Inorganic and Coordination Complexes*, Wiley, New York.
- 15b. Nakamoto, K. (1997), *IR and Raman Spectra of Inorganic and Coordination Complexes, Part A: Theory and Applications in Inorganic Chemistry*, 5th Edn, Wiley, New York.
16. Wilson, E. B., Decius, J. C. and Cross, P. C. (1958), *Molecular Vibrations*, McGraw-Hill, New York.
17. Terenin, A. N. (1975), *Selected Works: Spectroscopy of Adsorbed Molecules and Surface Compounds*, Vol. 3, Nauka, Leningrad.
18. Little, L. H. (1966), *Infrared Spectra of Adsorbed Molecules*, Academic Press, London.
19. Kiselev, A. V. and Lygin, V. I. (1972), *Infrared Spectra of Surface Compounds*, Nauka, Moscow (Wiley, New York, 1975).
20. Hair, M. L. (1967), *Infrared Spectroscopy in Surface Chemistry*, Marcel Dekker, New York.
21. Tamaru, K. (1978), *Dynamic Heterogeneous Catalysis*, Academic Press, London.
22. Ward, J. W. (1976), 'Analysis of the surface and reactivity of zeolites with IR spectroscopy', in *Zeolite Chemistry and Catalysis*, Rabo, J. A. (Ed.), American Chemical Society, Monograph 7, Washington, DC, pp. 118–287.
23. Kung, H. H. (1989), *Transition Metal Oxides: Surface Chemistry and Catalysis*, Elsevier, New York.
24. Bell, A. T. and Hair, M. L. (Eds) (1980), *Vibrational Spectroscopies for Adsorbed Species*, American Chemical Society, Symposium Series 137, Washington, DC.
25. Delgass, W. H., Haller, G. L., Kellerman, R. and Lunsford, J. H. (1979), *Spectroscopy in Heterogeneous Catalysis*, Academic Press, New York.
26. Willis, R. F. (Ed.) (1980), *Vibrational Spectroscopy of Adsorbates*, Springer-Verlag, Berlin.
27. Morterra, C. and Magnassa, G. (1996), 'A case study: surface chemistry and surface structure of catalytic aluminas, as studied by vibrational spectroscopy of adsorbed species', *Catal. Today*, **27**, 497–532.
28. Ertl, G. and Kupers, J. (1985), *Low Energy Electrons in Surface Chemistry*, VCH, Weinheim.
29. Ibach, H. and Mills, D. L. (1982), *Electron Energy Loss Spectroscopy and Surface Vibrations*, Academic Press, New York.

- 30a. Davydov, A. A. (1984), *IR Spectroscopy in the Surface Chemistry of Oxides* (in Russian), Nauka, Novosibirsk.
- 30b. Davydov, A. A. (1990), *Infrared Spectroscopy of Adsorbed Species on the Surface of Transition Metal Oxides*, Wiley, Chichester, UK.
31. Fierro, J. L. G. (1990), *Spectroscopic Characterisation of Heterogeneous Catalysts, Part A: Methods of Surface Analysis, Part B: Chemisorption of Probe-Molecules*, Elsevier, Amsterdam.
32. Yates, J. T. and Madey, T. E. (Eds) (1992), *Vibrational Spectroscopy of Molecules on Surfaces*, Plenum Press, New York.
33. Imelik, B. and Vadrine, J. C. (Eds) (1994), *Catalysts Characterization. Physical Techniques for Solid Materials*, Plenum Press, New York.
34. Pemble, M. E. (1997), 'Vibrational spectroscopy from surfaces', in *Surface Analysis – The Principal Techniques*, Vickerman, J. C. (Ed.), Wiley, Chichester, UK, pp. 267–311.
- 34a. Ertl, G., Knozinger, H. and Weitkamp, J. (Eds) *Handbook of Heterogeneous Catalysis*, v. 2 Wiley-VCH, Weinheim.
- 35a. Niemantsverdriet, J. W. (1995), *Spectroscopy in Catalysis*, VCH, Weinheim.
- 35b. Grinberg, A. A. (1966), *Coordination Chemistry (Koordinatsionnaya Khimiya)*, (in Russian), Chemistry, Moscow.
- 35c. Wilkinson, G. (1987), in *Comprehensive Coordination Chemistry*, Gillard, R. D. and McCleverty, J. E. (Eds.); Pergamon Press, Oxford.
- 35d. Jorgensen, G. K. (1963), *Inorganic Complexes*, Academic Press, New York.
- 35e. Jorgensen, G. K. (1962), *Absorption Spectra and Chemical Bond in Complexes*, Pergamon, Elmsford.
- 35f. Che, M. and Bonneviot, L. (1988), 'Role of oxide surface in coordination chemistry of transition metal ions in catalytic systems', *Pure Appl. Chem.*, **60**, 1369–1378.
- 35g. Che, M., Bonneviot, L., Louis, C. and Kermarec, M. (1985), 'Coordination chemistry involving oxide catalysts', *Mater. Chem. Phys.*, **13**, 201–220.
- 35h. Dyrek, K. and Che, M. (1997), 'EPR as a tool to investigate the transition metal chemistry on oxide surfaces', *Chem. Rev.*, 305–331.
- 35i. Morrison, S. (1977), *Chemical Physics of Solid Surfaces*. Plenum Press, New York.
- 35j. Terenin, A. N. (1900), 'Optical investigation of activated adsorption', *Russ. J. Phys. Chem.*, **14**, 1362–1371.
36. Hollins, P. (1992), 'The influence of surface defects on the infrared spectra of adsorbed species', *Surf. Sci. Rep.*, **16**, 51–94.
37. Pritchard, J., Gatterick, T. and Gupta, R. K. (1976), 'Infrared spectroscopy of chemisorbed carbon monoxide on copper', in Anderson, R. B. and Dawson, P. T. (Eds), *Experimental Methods in Catalytic Research*, Academic Press, New York, pp. 281–297.
38. Yates, J. T., Jr (1985), 'Studies of weakly adsorbed and transient surface species by infrared spectroscopy at low temperatures', in *Catalyst Characterization by Surface Science and Solid State Chemistry*, Deviney, M. L. and Gland, J. L. (Eds), American Chemical Society, Washington, DC, pp. 315–347.
39. Lercher, J. A., Gruendling, C. and Eder-Mirth, G. (1996), 'Infrared studies of the surface acidity of oxides and zeolites using adsorbed probe molecules', *Catal. Today*, **27**, 353–376.
40. Hendra, P. J. and Fleischmann, M. (1978), 'Raman spectroscopy at surfaces', in Kay, E. and Bacus, P. S. (Eds), *Topics in Surface Chemistry*, Plenum Press, New York, pp. 373–402.
41. Morrow, B. A. (1980), 'Raman spectroscopic studies of surface species', in Bell, A. T. and Hair, M. L. (Eds), *Vibrational Spectroscopies for Adsorbed Species*, ACS Symposium Series 137, American Chemical Society, Washington, DC, pp. 119–140.
42. Shchekochikhin, Yu. M. and Davydov, A. A. (1983), *Methodologies of IR Studies in the Physicochemistry of Semiconductor Surfaces*, No. 5014-83, VINITI, Moscow, 110 pp.
43. Ballico, M. J. and Jones, T. P. (1995), 'Novel experimental technique for measuring high-temperature spectral emissivities', *Appl. Spectrosc.*, **49**, 335–341.
44. Busca, G. (1996), 'The use of vibrational spectroscopies in studies of heterogeneous catalysis by metal oxides: an introduction', *Catal. Today*, **27**, 323–352.
45. Eischens, R. P. and Pliskin, W. A. (1958), 'Infrared spectra of adsorbed molecules', *Adv. Catal.*, **10**, 1–56.
46. Leftin, H. P. and Hobson, M. S. (1963), 'Application of spectrophotometry to the study of the catalytic systems', *Adv. Catal.*, **14**, 115–201.
47. *Uspekhi Fotoniki* (1974) (in Russian), **4**, LGU, Leningrad, Vilesov, V. I. (Ed).
48. *Uspekhi Fotoniki* (1975) (in Russian), **5**, LGU, Leningrad, Vilesov, V. I. (Ed).
49. *Uspekhi Fotoniki* (1987), 'IR spectroscopy and the investigation of surfaces' (in Russian), **9**, LGU, Leningrad, Akopyam M. E. (Ed).
50. Morterra, C. and Low, M. J. D. (1973), 'Reactive silica. Novel aspects of the chemistry of silica surfaces', *Ann. N. Y. Acad. Sci.*, **220**, 245–340.
51. Peri, J. B. (1984), 'Infrared spectroscopy in catalytic research', in Anderson, J. R. and Boudart, M. (Eds), *Catalysis Science and Technology*, Vol. 5, Springer-Verlag, Berlin, pp. 171–221.
52. Lavalley, J. C. (1996), 'Infrared spectrometric studies of the surface basicity of metal oxides and zeolites using adsorbed probe molecules', *Catal. Today*, **27**, 377–401.

53. Knozinger, H. and Ratnasamy, C. (1978), 'Catalytic aluminas: surface models and characterization of surface sites', *Catal. Rev. Sci. Eng.*, **17**, 31–70.
54. Boehm, H. P. and Knozinger, H. (1976), 'Nature and estimation of functional groups on solid surfaces', *Adv. Catal.*, **25**, 43–207.
55. Sheppard, N. and Nguyen, T. T. (1978), 'The vibrational spectra of carbon monoxide chemisorbed on the surfaces of metal catalysts – a suggested scheme of interpretation of infrared and Raman spectra', in Clark, R. J. H. and Hester, R. E. (Eds), *Advances in Infrared and Raman Spectroscopies*, Vol. 5, Heyden, London, pp. 67–148.
56. Zecchina, A., Coluccia, S. and Morterra, C. (1985), 'Infrared spectra of molecules adsorbed on oxide surfaces', *Appl. Spectrosc. Rev.*, **21**, 259–310.
57. Kung, M. C. and Kung, H. H. (1985), 'IR studies of NH₃, Pyridine, CO and NO adsorbed on transition metal oxides', *Catal. Rev. Sci. Eng.*, **27**, 425–460.
58. Zecchina, A. (1985), 'Analogies between the chemistry of alkaline earth oxides and the chemistry of organometallic compounds', *Mater. Chem. Phys.*, **13**, 379–392.
59. Che, M., Oliver, C. and Bonnevot, L. (1988), 'Classification of the various types of coordination chemistry occurring with oxides in catalytic systems', in *Catalyst: Theory to Practice. Proceedings of the 9th International Congress on Catalysis*, Calgary, Canada, 1988, Phillips, M.J. and Ternan, M., (Eds.), The Chemical Institute of Canada, Ottawa, Ontario, 1988, pp. 1750–1757.
60. Zecchina, A. and Arean, C. (1993), 'Structure and reactivity of surface species obtained by interaction of organometallic compounds with oxidic surfaces: IR studies', *Catal. Rev. Sci. Eng.*, **35**, 261–317.
61. Klier, K. (1980), 'Investigations of adsorption centers, molecules, surface complexes and interactions among catalyst components by diffuse reflectance spectroscopy', in Bell, A. T. and Hair, M. L. (Eds), *Vibrational Spectroscopies for Adsorbed Species*, American Chemical Society, Symposium Series, 137, Washington, DC, pp. 141–162.
- 62a. Sheppard, N. (1988), 'Vibrational spectroscopic studies of the structure of species derived from the chemisorption of hydrocarbons on metal single-crystal surfaces', *Annu. Rev. Phys. Chem.*, **39**, 589–644.
- 62b. Sheppard, N. and De la Cruz, C. (1996), 'Vibrational spectra of hydrocarbons adsorbed on metals. Part I: Introductory principles, ethylene and the higher acrylic alkenes', *Adv. Catal.*, **41**, 1–111.
63. Chuang, S. S. C., Brundage, M. A., Balakos, M. W. and Srinivas, G. (1995), 'Transient *in situ* infrared methods for investigation of adsorbates in catalysis', *Appl. Spectrosc.*, **49**, 1151–1163.
64. Matushak, V. A. and Krylov, O. V. (1996), '*In situ* IR spectroscopy of intermediates in heterogeneous oxidative catalysis', *Catal. Today*, **25**, 1–88.
- 65a. Krylov, O. V. and Matyshak, V. A. (1994), 'Intermediates and mechanism of heterogeneous catalytic reactions. The simplest reactions of hydrocarbons, alcohols, and acids', *Usp. Khim.* (in Russian); *Russ. Chem. Rev.* (English translation), **63**, 559–574.
- 65b. Krylov, O. V. and Matyshak, V. A. (1995), 'Reactions involving hydrogen and the monoxides of carbon and nitrogen', *Russ. Chem. Rev.* (English translation), **64**, 61–86.
- 65c. Krylov, O. V. and Matyshak, V. A. (1995), 'Oxidation reactions involving molecular oxygen and sulfur', *Russ. Chem. Rev.* (English translation), **64**, 167–186.
66. Busca, G. (1996), 'Infrared studies of the reactive adsorption of organic molecules over metal oxides and of the mechanisms of their heterogeneously catalyzed oxidation', *Catal. Today*, **27**, 457–496.
67. Pauling, L. (1960), *Nature of the Chemical Bond*, Cornell University Press, Ithaca, New York.
68. Shriver, D. F., Atkins, P. W. and Langford, A. (1990), *Statement of the Principles of Inorganic Chemistry*, Oxford University Press, Oxford, UK.
69. Basolo, F. and Pearson, P. (1967), *Mechanisms of Inorganic Reactions. A Study of Metal Complexes in Solution*, 2nd Edn, Wiley, New York.
70. Nefedov, V. I. (1984), *X-Ray Electron Spectroscopy of Chemical Compounds* (in Russian), Chemistry, Moscow.
71. Trietiakov, J. D. (1974), *Chemistry of Non-Stoichiometric Oxides* (in Russian), MGU, Moscow.
72. Catlow, C. A. (1981), in Surenson, O. T. (Ed.), *Nonstoichiometric Oxides*, Academic Press, New York.
73. Breck, D. W. (1974), *Zeolite Molecular Sieves*, Wiley, New York.
74. Minachev, Kh. M. and Isakov, Ya. I. (1976), *Metal-Containing Zeolites* (in Russian), Nauka, Moscow.
75. Okuhara, T., Mizuno, N. and Misono, M. (1996), 'Catalytic chemistry of heteropoly compounds', *Adv. Catal.*, **41**, 113–252.
76. Rabo, J. A. (1981), 'Unifying principles in zeolite chemistry and catalysis', *Catal. Rev. Sci. Eng.*, **23**, 293–313.
77. Deviney, M. L. and Gland, J. L. (Eds) (1989), *Catalyst Characterization: Surface Science and Solid State Chemistry*, Surface Chemistry and Catalysis Series, Elsevier, Amsterdam.
78. Henrich, V. E. and Cox, P. A. (1993), *The Surface Science of Metal Oxides*, Cambridge University Press, Cambridge, UK.
79. Tanabe, K. (1989), *New Solid Acids and Bases and their Catalytic Properties*, Kodansha, Tokyo; Elsevier, Amsterdam.

80. Tanabe, K. (1983), 'Solid acid and base catalysts', in Anderson, J. R. and Boudart, M. (Eds), *Catalysis Science and Technology*, Vol. 2, Springer-Verlag, Berlin, pp. 231–265.
81. Tanabe, K. (1970), *Solid Acid and Bases*, Kodansha, Tokyo; Academic Press, New York.
82. Bielanski, A. and Haber, J. (1991), *Oxygen in Catalysis*, Marcel Dekker, New York.
83. Okihara, T., Mizuno, N. and Misono, M. (1994), 'Catalytic chemistry of heteropoly compounds', *Adv. Catal.*, **41**, 113–252.
84. Kozhevnikov, I. V. (1995), 'Heteropoly acids and related compounds as catalysts for fine chemical synthesis', *Catal. Rev. Sci. Eng.*, **37**, 311–352.
85. Morrison, S. R. (1977), *The Chemical Physics of Solid Surfaces*, Plenum Press, New York.
86. Kiselev, V. F. and Krylov, O. V. (1978), *Adsorption Processes on the Surfaces of Semiconductors and Dielectrics* (in Russian), Nauka, Moscow.
87. Shopov, D. and Andreev, A. (1979), *Chemical Bonding in Adsorption and Catalysis I. Metals* (in Russian), BAN, Sofia.
88. Shopov, D. and Andreev, A. (1979), *Chemical Bonding in Adsorption and Catalysis II. Oxides* (in Russian), BAN, Sofia.
89. Krylov, O. V. and Kiselev, V. F. (1981), *Adsorption and Catalysis on Transition Metals and their Oxides* (in Russian), Khimia, Moscow.
90. Somorjai, G. A. (1981), *Chemistry in Two Dimensions: Surfaces*, Cornell University Press, Ithaca, New York.
91. Bonnelle, J. P., Delmon, B. and Derouane, E. (1982), *Surface Properties and Catalysis by Non-Metals*, D. Reidel Publishing Company, Lancaster, PA.
92. Grasselli, R. K. and Brazdil, J. F. (Eds) (1985), *Solid State Chemistry in Catalysis*, American Chemical Society, Washington, DC.
93. Rochester, C. H. (1970), *Acidity Functions*, Academic Press, New York.
94. Borekov, G. K. (1986), *Heterogeneous Catalysis* (in Russian), Nauka, Moscow.
95. White, M. G. (1990), *Heterogeneous Catalysis*, Prentice Hall, NJ.
96. Moffat, J. B. (1990), *Theoretical Aspects of Heterogeneous Catalysis*, Van Nostrand Reinhold, New York.
97. Gates, B. (1992), *Catalytic Chemistry*, Wiley, New York.
98. Wells, A. F. (1984), *Structural Inorganic Chemistry*, Clarendon Press, Oxford, UK.
99. Ormont, B. F. (1950), *Structures of Inorganic Substances*, Gostekhizdat, Moscow–Leningrad.
100. Porai-Koshitz, M. A. and Atovmian, L. O. (1974), *Crystalchemistry and Stereochemistry of Coordination Compounds of Molybdenum* (in Russian), Nauka, Moscow.
101. Nyquist, R. A. and Kagel, R. O. (1971), *Infrared Spectra of Inorganic Compounds, 3800–3845 cm⁻¹*, Academic Press, New York.
102. Sadler, A. (1976), *Catalog of IR Spectra of Inorganic Compounds*, Vols 1 and 2, Aldrich.
103. Yurchenko, E. N., Kustova, G. N. and Batsanov, S. S. (1981), *Vibrational Spectra of Inorganic Compounds*, Nauka, Novosibirsk.
104. Wachs, I. E. (1992), *Characterization of Catalytic Materials*, Butterworth-Heinemann, Greenwich, C. T.
105. Wachs, I. E. (1996), 'Raman and IR studies of surface metal oxide species on oxide supports: Supported metal oxide catalysts', *Catal. Today*, **27**, 434–455.
106. Davydov, A. A. and Goncharova, O. I. (1993), 'Use of infrared spectroscopy in studies of catalysts based on molybdenum heteropolycompounds supported on oxides', *Usp. Chim.* (in Russian); *Russ. Chem. Rev.* (English translation), **62**, 105–120.
- 107a. Flanigen, E. M., Katami, H. and Szymanski, H. A. (1976), 'Structure and properties of zeolites' *Adv. Chem. Ser.*, **101**, 201–235.
- 107b. Flanigen, E. M., Patton, R. L. and Wilson, S. T. (1988), 'Structural, synthetic and physicochemical concepts in aluminophosphate-based molecular sieves', *Study Surf. Sci. Catal.*, **37**, 13–14.
108. Gai-Boyes, P. L. (1992), 'Defects in oxide catalysts. Fundamental studies of catalysis in action', *Catal. Rev. Sci. Eng.*, **34**, 1–54.
109. Ozin, G. A. (1977), 'Very small metallic and bimetallic clusters: The metal cluster–metal surface analogy in catalysis and adsorption processes', *Catal. Rev. Sci. Eng.*, **16**, 191–289.
110. Moskovitz, M. and Ozin, G. A. (Eds) (1976), *Cryochemistry*, Wiley, New York.
111. Yermakov, Yu. I., Kuznetsov, B. N. and Zakharov, V. A. (1981), *Catalysis by Supported Complexes*, Elsevier, Amsterdam.
112. Collmann, J. P., Hegedus, L. S., Norton, J. R. and Finke, K. G. (1987), *Principles and Applications of Organotransition Metal Chemistry*, University Science Books, Mill Valley, CA.
113. Iwasawa, Y. (Ed.) (1986), *Tailored Metal Catalysts*, D Reidel Publishing Company, Dordrecht, The Netherlands.
114. Karge, H. G., Niessen, W. and Bludau, H. (1996), 'In-situ FTIR measurements of diffusion in coking zeolite catalysts', *Appl. Catal., A: Gen.*, **146**, 339–349.
115. Speight, J. G. (1994), 'Application of spectroscopic techniques to the structural analysis of coal', *Appl. Spectrosc. Rev.*, **29**, 117–169.
116. Cotton, F. A. (1971), *Chemical Applications of Group Theory*, Wiley, New York.

117. Garbowski, E. and Praliand, H. (1994), 'Electronic spectroscopy', in Imelik, B. and Vadrine, J. C. (Eds), *Catalysts Characterization. Physical Techniques for Solid Materials*, Plenum Press, New York, pp. 61–90.
118. Shchekochikhin, Yu. M. and Davydov, A. A. (1983), *Interpretation of Surface Compounds Spectra on the Basis of Theoretical Calculations of Vibrational Spectra*, No. 5013-83, VINITI, Moscow, 106 pp.
119. Bell, A. T. (1992), 'Infrared spectroscopy of high-area catalytic surfaces', in Yates, J. T. and Madey, T. E. (Eds), *Vibrational Spectroscopy of Molecules on Surfaces*, Plenum Press, New York, pp. 105–134.
120. Fierro, J. L. G. (1990), 'Chemisorption of probe molecules', in Fierro, J. L. G. (Ed.), *Spectroscopic Characterisation of Heterogeneous Catalysts. Part B: Chemisorption of Probe Molecules*, Elsevier, Amsterdam, pp. B1–B66.
121. Hair, M. L. (1980), 'Transmission infrared spectroscopy for high surface area oxides', in Bell, A. T. and Hair, M. L. (Eds), *Vibrational Spectroscopies for Adsorbed Species*, American Chemical Society, Symposium Series 137, Washington, DC, pp. 1–12.
122. Fierro, J. L. G. (1990), 'Surface spectroscopic techniques', in Fierro, J. L. G. (Ed.), *Spectroscopic Characterisation of Heterogeneous Catalysts. Part A: Methods of Surface Analysis*, Elsevier, Amsterdam, pp. A1–A78.
123. Fierro, J. L. G. (1990), 'Infrared spectroscopy', in Fierro, J. L. G. (Ed.), *Spectroscopic Characterisation of Heterogeneous Catalysts. Part B: Chemisorption of Probe-Molecules*, Elsevier, Amsterdam, pp. B67–B144.
- 124a. Kazansky, V. B., Borovkov, V. Yu. and Kustov, L. M. (1984), 'IR diffuse reflectance study of oxide catalysts. Use of molecular hydrogen adsorption as a test for surface active sites', in *Proceedings of the 8th International Congress on Catalysis* Berlin, 1984, Verlag Chemie, Weinheim, Germany, Vol. III, pp. 3–14.
- 124b. Borovkov, V. Yu. and Kazansky, V. B. (1985), 'Comparison of the band intensities from the IR-diffuse scattering and transmission spectra in the study of adsorption on finely divided oxide catalysts', *Zh. Fiz. Khim.* (in Russian), **59**, 333–335.
125. Coudurier, G. and Lefebvre, F. (1994), 'Infrared spectroscopy', in Imelik, B. and Vadrine, J. C. (Eds), *Catalysts Characterization. Physical Techniques for Solid Materials*, Plenum Press, New York, pp. 11–60.
126. Smith, A. L. (1970), *Applied Infrared Spectroscopy: Fundamentals, Techniques and Analytical Problem-Solving*, Wiley-Interscience, New York.
127. Bell, A. T. (1980), 'Applications of Fourier transform infrared reflection spectroscopy to studies of adsorbed species', in Bell, A. T. and Hair, M. L. (Eds), *Vibrational Spectroscopies for Adsorbed Species*, American Chemical Society, Symposium Series 137, Washington, DC, pp. 13–36.
- 128a. Tarasevich, Yu. S., Davydov, A. A. and Shchekochikhin, Yu. M. (1975), 'Cells for researching of *in situ* infrared spectra', *Zh. Prikl. Spektrosk.* (in Russian); *J. Appl. Spectrosc.* (English translation), **22**, 1136–1138.
- 128b. Shchekochikhin, Yu. M., Davydov, A. A., Akulich, N. A. and Tarasevich, Yu. S. (1969), 'Low temperature vacuum cell with silicon window for investigations of the infrared spectra of solids and adsorbed molecules', *Zh. Prikl. Spektrosk.* (in Russian); *J. Appl. Spectrosc.* (English translation), **10**, 880–882.
- 128c. Basu, P., Ballinger, T. H. and Yates, J. T., Jr (1988), 'Wide temperature range IR spectroscopy cell for studies of adsorption and desorption on high-area solids', *Res. Sci. Instrum.*, **59**, 1321–1327.
- 128d. Yates, J. T., Jr (1998), *Experimental Innovations in Surface Science*, Springer, New York.
129. Shchekochikhin, Yu. M. and Davydov, A. A. (1975), 'IR spectroscopic study of surface species under conditions of chemical reaction', *Kinet. Katal.* (in Russian); *Kinet. Catal.* (English translation), **16**, 997–1001.
130. Richards, P. L. and Tobin, R. G. (1992), 'Infrared spectroscopy of adsorbates on metals: Direct absorption and emission', in Yates, J. T. and Madey, T. E. (Eds), *Vibrational Spectroscopy of Molecules on Surfaces*, Plenum Press, New York, pp. 417–464.
131. Greenler, R. G. (1969), 'Reflection method for obtaining the IR spectrum of a thin layer on a metal surface', *J. Chem. Phys.*, **50**, 1963–1968.
132. Yates, J. T. Jr., Greenler, R. G., Ratajczykowa, I. and King, D. (1973), 'Reflection-absorption infrared spectrum of α -CO chemisorbed on polycrystalline tungsten', *Surf. Sci.*, **36**, 739–755.
133. Pritchard, J. and Sims, M. L. (1970), 'Infrared reflection spectra of adsorbed CO on copper', *Trans. Faraday Soc.*, **66**, 427–433.
134. Hayden, B. E. (1992), 'Reflection absorption infrared spectroscopy', in Yates, J. T. and Madey, T. E. (Eds), *Vibrational Spectroscopy of Molecules on Surfaces*, Plenum Press, New York, pp. 267–344.
135. Hollins, P. and Prichard, J. (1980), 'Intermolecular interactions and the infrared reflection-absorption spectra of chemisorbed carbon monoxide on copper', in Bell, A. T. and Hair, M. L. (Eds), *Vibrational Spectroscopies for Adsorbed Species*, American Chemical Society, Symposium Series 137, Washington, DC, pp. 51–74.
136. Harrick, N. J. (1967), *Internal Reflection Spectroscopy*, Wiley-Interscience, New York.
137. Richardson, N. V. and Sheppard, N. (1992), 'Normal modes at surfaces', in Yates, J. T. and Madey, T. E. (Eds), *Vibrational Spectroscopy of Molecules on Surfaces*, Plenum Press, New York, pp. 1–48.
138. Blank, R. E. and Wakenfield, Th. (1979), 'Double-beam photoacoustic spectrometer for use in the ultraviolet, visible and near-infrared spectral regions', *Anal. Chem.*, **51**, 50–54.
139. Ferraro, J. R. and Nakamoto, K. (1994), *Introductory Raman Spectroscopy*, Academic Press, San Diego CA.

140. Cardiner, D. J. and Graves, P. R. (1989), *Practical Raman Spectroscopy*, Springer-Verlag, Berlin.
141. Garbovskii, E. and Coudurier, G. (1994), 'Raman spectroscopy', in Emilic, B. and Vadrine, J. (Eds), *Catalysis Characterization. Physical Techniques for Solid Materials*, Plenum Press, New York, pp. 45–60.
142. Morrow, B. A. (1980), 'Raman spectroscopy studies of surface species', in Bell, A. T. and Hair, M. L. (Eds), *Vibrational Spectroscopies for Adsorbed Species*, American Chemical Society, Symposium Series 137, Washington, DC, pp. 119–140.
143. Morrow, B. A. (1990), 'Surface groups on oxides', in Fierro, J. L. G. (Ed.), *Spectroscopic Characterisation of Heterogeneous Catalysts. Part A: Methods of Surface Analysis*, Elsevier, Amsterdam, pp. A161–A224.
144. Angell, S. M. (1982), 'Resonance Raman and photoselective spectroscopy of transition-metal complexes', in Ferraro, J. R. and Basile, L. J. (Eds), *Fourier Transform Infrared Spectroscopy*, Academic Press, New York, pp. 1–36.
145. Stencel, J. M. (1990), *Raman Spectroscopy for Catalysis*, Van Nostrand Reinhold, New York.
146. Campion, A. (1992), 'Raman spectroscopy', in Yates, J. T. and Madey, T. E. (Eds), *Vibrational Spectroscopy of Molecules on Surfaces*, Plenum Press, New York, pp. 345–416.
147. Pockrand, I. (1984), *Surface Enhanced Raman Vibrational Studies at Solid/Gas Interfaces*, Springer, Berlin.
148. Chang, R. K. and Furtak, T. E. (Eds) (1982), *Surface Enhanced Raman Scattering*, Plenum Press, New York.
149. Avery, N. R. (1992), 'Electron energy loss spectroscopy', in Yates, J. T. and Madey, T. E. (Eds), *Vibrational Spectroscopy of Molecules on Surfaces*, Plenum Press, New York, pp. 223–266.
150. Ibach, H. (Ed.) (1977), *Electron Spectroscopy for Surface Analysis*, Springer-Verlag, Berlin.
151. Ibach, H. (1991), *Electron Energy Loss Spectrometers*, Springer-Verlag, Berlin.
152. Baro, A. M. (1990), 'Electron vibrational spectroscopy', in Fierro, J. L. C. (Ed.), *Spectroscopic Characterization of Heterogeneous Catalysts. Part A: Methods of Surface Analysis*, Elsevier, Amsterdam, pp. B145–B199.
153. Dubois, L. H. and Somorjai, G. A. (1980), 'The application of high resolution electron energy loss spectroscopy to the characterization of adsorbed molecules on rhodium single crystal surfaces', in Bell, A. T. and Hair, M. L. (Eds), *Vibrational Spectroscopies for Adsorbed Species*, American Chemical Society, Symposium Series 137, Washington, DC, pp. 163–190.
154. Thiel, P. A. and Weinberg, W. H. (1980), 'An electron energy loss spectroscopy investigation of the adsorption of nitric oxide, carbon monoxide and hydrogen on the basal plane of ruthenium', in Bell, A. T. and Hair, M. L. (Eds), *Vibrational Spectroscopies for Adsorbed Species*, American Chemical Society, Symposium Series 137, Washington, DC, pp. 191–216.
155. Gadzuk, J. W. (1992), 'Excitation mechanisms in vibrational spectroscopy of molecules on surfaces', in Yates, J. T. and Madey, T. E. (Eds), *Vibrational Spectroscopy of Molecules on Surfaces*, Plenum Press, New York, pp. 49–104.
156. Wolfram, T. (Ed.) (1978), *Inelastic Electron Tunneling Spectroscopy*, Springer-Verlag, Berlin.
157. Hansma, P. K. (Ed.) (1982), *Tunneling Spectroscopy: Capabilities, Applications and New Techniques*, Plenum Press, New York.
158. Kirtley, J. (1980), 'Inelastic electron tunneling spectroscopy', in Bell, A. T. and Hair, M. L. (Eds), *Vibrational Spectroscopies for Adsorbed Species*, American Chemical Society, Symposium Series 137, Washington, DC, pp. 217–246.
159. Hansma, P. K. (1992), 'Inelastic electron tunneling spectroscopy', in Yates, J. T. and Madey, T. E. (Eds), *Vibrational Spectroscopy of Molecules on Surfaces*, Plenum Press, New York, pp. 135–182.
160. Bates, J. B. (1979), 'Infrared emission spectroscopy', in Ferraro, J. R., and Basile, L. J. (Eds), *Fourier Transform Infrared Spectroscopy*, Vol. 1, Academic Press, New York, pp. 99–142.
161. Taub, H. (1980), 'Neutron scattering spectroscopy of adsorbed molecules', in Bell, A. T. and Hair, M. L. (Eds), *Vibrational Spectroscopies for Adsorbed Species*, American Chemical Society, Symposium Series 137, Washington, DC, pp. 247–280.
162. Cavanagh, R. R., Rush, J. J. and Kelley, R. D. (1992), 'Incoherent inelastic neutron scattering: Vibrational spectroscopy of adsorbed molecules on surfaces', in Yates, J. T. and Madey, T. E. (Eds), *Vibrational Spectroscopy of Molecules on Surfaces*, Plenum Press, New York, pp. 183–222.
163. Jobic, H. (1994), 'Applications of neutron scattering to catalysis', in Imelik, B. and Vadrine, J. C. (Eds), *Catalysis Characterization. Physical Techniques for Solid Materials*, Plenum Press, New York, pp. 347–376.
164. Fedyk, J. D. and Dignam, M. J. (1980), 'Investigation of carbon monoxide on nickel (100) by infrared ellipsometric spectroscopy', in Bell, A. T. and Hair, M. L. (Eds), *Vibrational Spectroscopies for Adsorbed Species*, American Chemical Society, Symposium Series 137, Washington, DC, pp. 75–98.
165. Dignam, M. J. and Fedyk, J. D. (1978), 'Infrared ellipsometric spectroscopy of adsorbed species', *Appl. Spectrosc. Rev.*, **14**, 249–285.
166. Bell, A. T., Alexander, R. W. and Ward, C. A. (1980), 'Surface electromagnetic wave spectroscopy', in Bell, A. T. and Hair, M. L. (Eds), *Vibrational Spectroscopies for Adsorbed Species*, American Chemical Society, Symposium Series 137, Washington, DC, pp. 99–118.

- 167a. Shafranovski, P. A., Sinev, M. Yu., Zhizhin, G. N. and Shub, B. R. (1988), 'SEW spectroscopy in heterogeneous catalysis. I. Interaction of methane with oxide systems', *Kinet. Katal.* (in Russian); *Kinet. Catal.* (English translation), **29**, 1721–1728.
- 167b. Shafranovski, P. A., Sinev, M. Yu., Zhizhin, G. N. and Shub, B. R. (1989), 'SEW spectroscopy in heterogeneous catalysis. II. Interaction of methane, hydrogen and water with alumina films', *Kinet. Katal.* (in Russian); *Kinet. Catal.* (English translation), **30**, pp. 1–7.
168. Zhizhin, G. N., Sinev, M. Yu., Shafranovski, P. A. and Shub, B. R. (1988), 'Study of the methane adsorption on Al_2O_3 and CaO by IR SEW spectroscopy', *Kinet. Katal.* (in Russian); *Kinet. Catal.* (English translation); **29**, pp. 663–668.
169. Highfield, J. G., Ruterrana, P., Thamp, K. R. and Graetzel, M. (1989), 'Catalyst characterization and *in situ* FTIR studies of carbon dioxide methanation over ruthenium supported on titania', in Morterra, C., Zecchina, A. and Costa, G. (Eds), *Structure and Reactivity of Surfaces*, Elsevier, Amsterdam, pp. 469–479.
170. Balakos, M. W., Chuang, S. C., Srinivas, G. and Brundage, M. A. (1995), 'Infrared study of the dynamic of adsorbed species during CO hydrogenation', *J. Catal.*, **157**, 51–65.
171. Lapinski, M. P. and Ekerdt, J. G. (1992), '*In situ* Fourier transform infrared study of ethylene surface reaction kinetics on alumina-supported nickel', *J. Phys. Chem.*, **96**, 5069–5077.
172. Popova, G. Ya., Davydov, A. A., Andrushkevich, T. V. and Budneva, A. A. (1987), 'IR-spectroscopic studies of surface acrolein and acrylic acid compounds in conditions of catalytic oxidation of acrolein on a V–Mo–Si–O catalyst', *React. Kinet. Catal. Lett.*, **33**, 293–298.
173. Quinn, C. M. (Ed.) (1992), Identification of Intermediate Species in Catalytic Reactions, *Catalysis Today*, Volume 12.
174. Solomennikov, A. A. and Davydov, A. A. (1981), 'Methodical problems of the application of IRS methods for determining the kinetic parameters of the reaction stages on the surfaces of catalysts', *React. Kinet. Catal. Lett.*, **18**, 39–44.
175. Solomennikov, A. A. and Davydov, A. A. (1983), 'IR-spectroscopic study of the influence of the electron state on the properties of supported platinum in the $\text{O}_{\text{ads}} + \text{CO}$ reaction', *Kinet. Katal.* (in Russian); *Kinet. Catal.* (English translation), **24**, 650–656.
176. Marshneva, V. I., Dubkov, K. A., Mokrinskii, V. V., Paukshtis, E. A. and Davydov, A. A. (1990), 'Study of the heats of adsorption of reactants in the Claus process in a series of oxide catalysts', *Kinet. Katal.* (in Russian), **31**, 1199–1205; *Kinet. Catal.* (English translation), **31**, 1051–1057.
177. Maradudin, A. (1969), *Elementary Excitations in Solids*, Plenum Press, New York.
- 178a. Davydov, A. A., Shchekochikhin, Yu. M., Keier, N. P. and Zeif, A. P. (1969), 'IR spectra of oxygen adsorbed on MnO_2 , Fe_2O_3 and Cr_2O_3 ', *Kinet. Katal.* (in Russian), **10**, 1125–1132.
- 178b. Davydov, A. A., Kuznetsova, A. S. and Shchekochikhin, Yu. M. (1973), 'Manifestation of surface vibrations in infrared spectra of polycrystalline semiconductor oxides', *Russ. J. Phys. Chem.*, **47**, 2499–2503 (English Translation).
179. Davydov, A. A., Rubens, N. A. and Shchekochikhin, Yu. M. (1976), 'Investigation of the properties of chromium oxide surface with IR spectroscopy', *Adsorptsiya Adsorbenty* (in Russian), **4**, 81–86.
180. Filimonov, V. N. (1963), 'Investigation of oxygen interaction with NiO , Fe_2O_3 and Cr_2O_3 with IR absorption spectra in the infrared region', *Kinet. Katal.* (in Russian); *Kinet. Catal.* (English translation), **4**, 367–372.
181. Zecchina, A., Coluccia, E., Guglielminotti, E. and Ghiotti, G. (1971), 'An infrared study of the surface properties of α -chromia. II. Oxygen chemisorption', *J. Phys. Chem.*, **75**, 2783–2790.
182. Davydov, A. A., Shchekochikhin, Yu. M. and Keier, N. P. (1972), 'Oxygen state on chromium oxide surface', *Kinet. Katal.* (in Russian); *Kinet. Catal.* (English translation), **13**, 1088–1090.
183. Carrott, P. J. M. and Sheppard, N. (1983), 'IR-study of the adsorption of $^{16}\text{O}_2$, $^{16}\text{O}-^{18}\text{O}$ and $^{18}\text{O}_2$ on Cr_2O_3 ', *J. Chem. Soc., Faraday Trans. 1*, **79**, 2425–2437.
184. Davydov, A. A. (1991), 'Infrared spectroscopic study of O_2^- on the surface of Cr_2O_3 : the effect of surface pretreatment', *J. Chem. Soc., Faraday Trans. 1*, **87**, 913–915.
185. Hadziivanov, K., Klissurski, D. and Davydov, A. A. (1988), 'Influence of the surface structure of metal oxides on their adsorption properties', *Annu. L'Universite Sofia Kliment Ohridski*, **75**, 64–75.
186. Klissurski, D., Hadziivanov, K. and Davydov, A. A. (1988), 'Infrared study of the nature and localization of some forms of oxygen adsorbed on the α -chromia surface', *J. Catal.*, **111**, 421–424.
187. Kostov, I. (1973), *Mineralogy*, Nauka i Izkustvo, Sofia.
- 188a. Hadziivanov, K., Davydov, A. A. and Klissurski, D. (1988), 'IR spectroscopic study of the nature of active centers on the surface of anatase', *Kinet. Katal.* (in Russian); *Kinet. Catal.* (English translation), **29**, 161–167.
- 188b. Hadziivanov, K. I. and Klissurski, D. G. (1996), 'Surface chemistry of titania (anatase) and titania-supported catalysts', *Chem. Soc. Rev.*, 61–69.
189. Barraclough, C. C., Lewis, J. and Nyholm, R. S. (1959), 'Stretching frequencies of metal–oxygen double bonds', *J. Chem. Soc.*, 3552–3560.
190. Rubens, N. A. and Davydov, A. A. (1976), 'Spectral analysis of copper chromite surface', *Teor. Eksp. Khim.* (in Russian); *Theor. Exp. Chem.* (English translation), **12**, 391–397.

191. Shepotko, M. L. and Davydov, A. A. (1990), 'The steady state of copper cations at $\text{CuCr}_2\text{O}_4/\text{Al}_2\text{O}_3$ by means of IR spectra of adsorbed CO', *Teor. Eksp. Khim.* (in Russian); *Theor. Exp. Chem.* (English translation), **26**, 633–636.
192. Rubens, N. A., Davydov, A. A., Kravtsov, A. V., Usheva, N. A. and Smolyaninov, S. I. (1976), 'IR spectroscopic study of the chemisorption of water and carbon monoxide on the surface of an iron–chromium oxide catalyst for the water-gas shift reaction', *Kinet. Katal.* (in Russian); *Kinet. Catal.* (English translation), **17**, 465–471.
193. Itina, G. V., Davydov, A. A. and Kurina, L. N. (1990), 'IR spectroscopic study of the surface properties of the zinc–chromium catalysts', *Zh. Fiz. Khim.* (in Russian); *Russ. J. Phys. Chem.* (English translation), **64**, 1122–1125.
194. Davydov, A. A., Komarova, M. P., Anufrienko, V. F. and Maksimov, N. G. (1973), 'Study of oxygen adsorption onto reduced titanium dioxide with IR spectroscopy and ESR methods', *Kinet. Katal.* (in Russian); *Kinet. Catal.* (English translation), **14**, 1519–1523.
195. Bocuzzi, F., Borello, E., Chiorino, A. and Zecchina, A. (1979), 'IR detection of surface microscopic modes of microcrystalline ZnO', *Chem. Phys. Lett.*, **61**, 617–619.
196. Marshneva, V. I. and Davydov, A. A. (1980), 'The investigation of the mechanism of hydrogen oxidation on zinc oxide', *Kinet. Katal.* (in Russian); *Kinet. Catal.* (English translation), **21**, 706–713.
- 197a. Maketov, A. K., Davydov, A. A. and Suvorov, B. V. (1993), 'The mechanism of isobutanol ammonolysis to isobutyronitrile on zinc oxide', *Zh. Fiz. Khim.* (in Russian); *Russ. J. Phys. Chem.* (English translation), **67**, 717–721.
- 197b. Maketov, A. K., Davydov, A. A. and Suvorov, B. V. (1987), 'The study of the ammoxidation mechanism of isobutanol on ZnO by IR-spectroscopy.1. Isobutanol adsorption', *Bull. Kazakhstan Acad. Sci.*, **246**, 51–56.
- 197c. Maketov, A. K., Davydov, A. A. and Suvorov, B. V. (1988), 'The study of the ammoxidation mechanism of isobutanol on ZnO by IR-spectroscopy.4. Isobutyronitril adsorption', *Vestnik Kazakhstan Acad. Sci.*, 29–32.
- 197d. Maketov, A. K., Davydov, A. A. and Suvorov, B. V. (1989), 'The study of the ammoxidation mechanism of isobutanol on ZnO by IR-spectroscopy.2. Ammonia adsorption', *Bull. Kazakhstan Acad. Sci.*, **253**, 40–46.
- 197e. Maketov, A. K., Davydov, A. A. and Suvorov, B. V. (1989), 'The study of the ammoxidation mechanism of isobutanol on ZnO by IR-spectroscopy.3. Isobutyric aldehyde and acid adsorption', *Bull. Kazakhstan Acad. Sci.*, **253**, 46–50.
- 197g. Maketov, A. K., Davydov, A. A. and Suvorov, B. V. (1989), 'The study of the ammoxidation mechanism of isobutanol on ZnO by IR-spectroscopy.5. Consecutive adsorption of isobutanol and ammonia', *Bull. Kazakhstan Acad. Sci.*, **254**, 53–59.
- 197h. Maketov, A. K., Davydov, A. A. and Suvorov, B. V. (1989), 'The study of the ammoxidation mechanism of isobutanol on ZnO by IR-spectroscopy.6. Consecutive adsorption of isobutyric aldehyde and acid with ammonia', *Bull. Kazakhstan Acad. Sci.*, **254**, 63–67.
198. Griffiths, D. W. L., Hallam, H. E. and Thomas, W. J. (1970), 'IR study of adsorption and oxidation of NH_3 on ferric oxide', *J. Catal.*, **17**, 18–23.
199. Davydov, A. A. and Shechekochikhin, Yu. M. (1971), 'About an interpretation of the molecular form of adsorbed oxygen on Fe_2O_3 ', *Kinet. Katal.* (in Russian); *Kinet. Catal.* (English translation), **12**, 808–812.
200. Rochester, C. H. and Topham, S. A. (1979), 'IR spectroscopic studies of the adsorption of probe molecules onto the surface of haematite', *J. Chem. Soc., Faraday Trans. 1*, **75**, 1259–1267.
201. Rochester, C. H. and Topham, S. A. (1979), 'IR spectroscopic studies of the adsorption of probe molecules onto the surface of goethite', *J. Chem. Soc., Faraday Trans. 1*, **75**, 872–882.
202. Busca, G. and Lorenzelli, V. (1980), 'Infrared study of methanol, formaldehyde and formic acid adsorbed on hematite', *J. Catal.*, **66**, 155–161.
203. Al-Mashta, F., Sheppard, N., Lorenzelli, V. and Busca, G. (1982), 'IR study of the adsorption on oxygen-covered $\alpha\text{-Fe}_2\text{O}_3$: Bands due to adsorbed oxygen and their modification by co-adsorbed hydrogen and water', *J. Chem. Soc., Faraday Trans. 1*, **78**, 979–989.
204. Lorenzelli, V., Busca, G. and Al-Mashta, F. (1982), 'Infrared studies of the diatomic molecules O_2 , N_2 , NO and H_2 adsorbed on Fe_2O_3 ', *J. Mol. Struct.*, **80**, 181–186.
205. Lorenzelli, V., Busca, G., Al-Mashta, F. and Sheppard, N. (1981), 'IR evidence for the formation of oxidized species from N_2 adsorbed on $\alpha\text{-Fe}_2\text{O}_3$ surfaces', *J. Catal.*, **72**, 38–91.
206. Lorenzelli, V. and Busca, G. (1985), 'Infrared studies of the surface of $\alpha\text{-Fe}_2\text{O}_3$ ', *Mater. Chem. Phys.*, **13**, 261–281.
207. Shepot'ko, M. L. and Davydov, A. A. (1991), 'Nature of the surface sites on $\alpha\text{-Fe}_2\text{O}_3$ ', *Zh. Prikl. Spektrosk.* (in Russian); *J. Appl. Spectrosc.* (English translation), **54**, 480–485.
208. Davydov, A. A. and Shepot'ko, M. L. (1992), 'IR spectra of NH_3 , CO and NO , adsorbed on $\alpha\text{-Fe}_2\text{O}_3$ and nature of the sites on the surface', *Zh. Prikl. Spektrosk.* (in Russian); *J. Appl. Spectrosc.* (English translation), **56**, 487–490.
209. Davydov, A. A., Chuang, K. T. and Sanger, A. (1998), 'The mechanism of oxidation by ferric oxide and hydroxide surfaces', *J. Phys. Chem., B*, **102**, pp. 4745–52.

210. Gundrizer, T. A. and Davydov, A. A. (1975), 'Infrared spectra of oxygen adsorbed on SnO_2 ', *React. Kinet. Catal. Lett.*, **3**, 67–70.
211. Davydov, A. A. (1992), 'IR spectroscopic study of oxygen state and its reactivity on the surface of SnO_2 ', *Zh. Prikl. Spektrosk.* (in Russian); *J. Appl. Spectrosc.* (English translation), **56**, 597–605.
212. Davydov, A. A. and Budneva, A. A. (1983), 'Investigation of surface centres in vanadium-containing catalysts with IR spectra of adsorbed ammonia', *Teor. Eksp. Khim.* (in Russian); *Theor. Exp. Chem.* (English translation), **19**, 240–244.
213. Davydov, A. A. (1993), 'Investigation of the state of transition metal cations on catalyst surfaces by means of IR spectroscopy of adsorbed probe molecules. IX. Vanadium ions on the surface of vanadium-containing catalysts', *Kinet. Katal.* (in Russian); *Kinet. Catal.* (English translation), **34**, 333–340.
214. Davydov, A. A. (1993), 'IR spectra of ammonia adsorbed on $\text{V}_2\text{O}_5/\text{Al}_2\text{O}_3$. Influence of the reduction degree on adsorption of ammonia', *Kinet. Katal.* (in Russian); *Kinet. Catal.* (English translation), **34**, 894–899.
215. Davydov, A. A. (1993), 'A study of vanadium-oxide compositions on supports by optical spectroscopy', *Kinet. Katal.* (in Russian); *Kinet. Catal.* (English translation), **34**, 1056–1067.
216. Davydov, A. A. and Shepot'ko, M. L. (1990), 'Study of surface properties of vanadium solid solutions in SnO_2 by IR spectroscopy', *Teor. Eksp. Khim.* (in Russian); *Theor. Exp. Chem.* (English translation), **26**, 505–509.
217. Busca, G., Centi, G., Marchetti, L. and Trifiro, F. (1986), 'Chemical and spectroscopic study of the nature of a vanadium oxide monolayer supported on high-surface-area TiO_2 anatase', *Langmuir*, **2**, 568–576.
218. Busca, G. (1986), 'FTIR study of the surface chemistry of the anatase-supported vanadium oxide monolayer catalysts', *Langmuir*, **2**, 577–586.
219. Davydov, A. A. (1982), 'Infrared spectroscopic studies of the surface properties of tin–molybdenum catalysts', *React. Kinet. Catal. Lett.*, **19**, 377–382.
220. Kasumov, F. B., Efreimov, A. A., Davydov, A. A., Adzhomov, K. Yu. and Alhazov, T. G. (1982), 'Investigation of acid centres of the oxidized Sn–Mo catalyst by IR spectroscopy', *Kinet. Katal.* (in Russian); *Kinet. Catal.* (English translation), **23**, 700–706.
221. Davydov, A. A. and Goncharova, O. I. (1984), 'Infrared spectroscopic study of the acidic properties of the surfaces of molybdenum–aluminum oxide catalysts', *Kinet. Katal.* (in Russian); *Kinet. Catal.* (English translation), **25**, 905–912.
222. Bocuzzi, F., Coluccia, S., Ghiotti, G., Morterra, C., and Zecchina, A. (1978), 'Infrared study of surface modes on silica', *J. Phys. Chem.*, **82**, 1298–1303.
223. Morrow, B. A. and Cody, I. A. (1976), 'IR studies of reactions on oxide surface. 5. Lewis acid sites on dehydroxylated silica', *J. Phys. Chem.*, **80**, 1995–1998.
224. Morrow, B. A. and Cody, I. A. (1976), 'IR studies of reactions on oxide surfaces. 6. Active sites on dehydroxylated silica for the chemisorption of ammonia and water', *J. Phys. Chem.*, **80**, 1998–2004.
225. Low, M. J. D. (1981), 'Penta- and hexacoordinated silicon sites on silica surfaces', *J. Phys. Chem.*, **85**, 3543–3545.
226. Iler, R. K. (1979), *The Chemistry of Silica*, Wiley, New York.
227. Knozinger, H., Krietenbrink, H., Muller, H. D. and Schultz, M. (1976), 'Cooperative effects in surface chemical and heterogeneously catalysed reactions on metal oxides', in *Proceedings of the 6th International Congress on Catalysis, London, 1976*, Bond, G. C., Wells, P. B. and Tompkins, F. S. (Eds.), The Royal Society of Chemistry, London, 1977, Vol. 1, pp. 183–194.
228. Lavalley, J. C. and Benaissa, M. (1984), 'IR spectroscopic evidence for surface vibrational modes formed upon dehydroxylation of alumina', *J. Chem. Soc., Chem. Commun.*, 908–909.
229. Marchese, L., Bordiga, S., Coluccia, S., Martra, G. and Zecchina, A. (1993), 'Structure of the surface sites of $\delta\text{-Al}_2\text{O}_3$ as determined by high-resolution transmission electron microscopy, computer modeling and IR spectroscopy of adsorbed CO', *J. Chem. Soc., Faraday Trans. 1*, **89**, 3483–3489.
230. Morterra, C., Bolis, V. and Magnacca, G. (1994), 'IR spectroscopic and microcalorimetric characterization of Lewis acid sites on (transition-phase) Al_2O_3 using adsorbed CO', *Langmuir*, **10**, 1812–1824.
231. Zecchina, A., Loohouse, A. and Stone, F. S. (1975), 'Reflectance spectra of surface states of MgO and CaO', *J. Chem. Soc., Faraday Trans. 1*, **71**, 1476–1490.
232. Garrone, E., Zecchina, A. and Stone, F. S. (1980), 'An experimental and theoretical evaluation of surface states in MgO and other alkaline earth oxides', *Phil. Mag.*, **42**, 680–703.
233. Colluccia, S., Bocuzzi, A., Ghiotti, G. and Morterra, C. (1982), 'Infrared study of hydrogen adsorption on MgO, CaO and SrO', *J. Chem. Soc., Faraday Trans. 1*, **78**, 2111–2119.
234. Coluccia, S., Deane, M. and Tench, A. (1978), 'Photoluminescent spectra of surface states in alkaline earth oxides', *J. Chem. Soc., Faraday Trans. 1*, **71**, 1476–1490.
235. Coluccia, S. and Tench, A. J. (1980), 'Spectroscopic studies of H_2 adsorption on highly dispersed MgO', in *New Horizons in Catalysis, Proceedings of the 7th International Congress on Catalysis, Tokyo, June 30–July 4, 1980*, Seiyama, T. and Tanabe, K. (Eds.) *Studies in Surface Science and Catalysis*, v.7, Kodansha, Tokyo, Elsevier, Amsterdam, 1980, pp. 1154–1163.

236. Coluccia, S., Deane, M. and Tench, A. (1976), 'Photoluminescent spectra of surface states in alkaline earth oxides', in *Proceedings of the 6th International Congress on Catalysis, London, 1976*, Bond, G.C., Wells, P.B. and Tompkins, F.S. (Eds.), The Royal Society of Chemistry, London, 1977, pp. 171–178.
237. Coluccia, S., Tench, A. J. and Segall, R. L. (1979), 'Surface structure and surface states in magnesium oxide powders', *J. Chem. Soc., Faraday Trans. 1*, **75**, 1769–1776.
238. Che, M. and Tench, A. J. (1982), 'Characterization and reactivity of mononuclear oxygen species on oxide surfaces', *Adv. Catal.*, **31**, 77–133.
239. Che, M. and Tench, A. J. (1983), 'Characterization and reactivity of molecular oxygen species on oxide surfaces', *Adv. Catal.*, **32**, 1–147.
240. Anpo, M., Yamada, Y., Doi, T., Matsuura, I., Coluccia, S., Zecchina, A. and Che, M. (1989), 'Photoluminescence, photo-induced reactivities and catalytic properties of Na- and Li-doped MgO', in Morterra, C., Zecchina, A. and Cista, C. (Eds.), *Structure and Reactivity of Surfaces*, Elsevier, Amsterdam, pp. 1–10.
241. Anpo, M., Sunamoto, M., Doi, T. and Matsuura, I. (1988), 'Oxidative coupling of methane over ultrafine crystalline magnesium oxide doped with lithium. Role of lower coordinative surface sites produced by lithium-doping', *Chem. Lett.*, 701–704.
242. Chiong, T. T., Isupova, L. A. and Davydov, A. A. (1989), 'Investigation of the state of active centres on the surface of Co(II) and Co(III) oxides by means of IR spectroscopy of the CO probe molecule', *Russ. Chem. Bull. SO AN SSSR* (in Russian), **3**, 26–29.
243. Chiong, T. T. and Davydov, A. A. (1989), 'IR spectra of carbon oxide adsorbed on cobalt oxide', *Zh. Fiz. Khim.* (in Russian); *Russian J. Phys. Chem.* (English translation), **63**, 271–273.
244. Gordymova, T. A., Davydov, A. A. and Efremov, A. A. (1983), 'Ammonia and propylene complex formation on antimony oxide', *React. Kinet. Catal. Lett.*, **22**, 143–146.
245. Davydov, A. A. (1993), 'Study of hydrocarbon adsorption on oxide catalysts by means of IR spectroscopy. XVIII. The nature and properties of the surface of a titanium-antimony oxide catalyst and the mechanism of transformation of propylene to acrolein', *Kinet. Katal.* (in Russian); *Kinet. Catal.* (English translation), **34**, 699–702.
246. Davydov, A. A. and Gordymova, T. A. (1993), 'The investigation of the adsorption of ammonia and propene on the surface of an Fe-Sb-oxide catalyst by means of IR spectroscopy', *Zh. Fiz. Khim.* (in Russian); *Russ. J. Phys. Chem.* (English translation), **63**, 271–273.
247. Lunsford, J. H. (1973), 'Electron spin resonance of adsorbed species of oxygen', *Catal. Rev.*, **8**, 135–157.
248. Che, M., Dyrek, K., Kermarec, M. and Tench, A. J. (1984), 'Characterization of oxygen species adsorbed on oxide surfaces by infrared spectroscopy', *Rev. Chim. Min.*, **21**, 669–691.
249. Blunt, F. J., Hendra, P. J. and Mackenzie, J. R. (1969), 'The laser Raman spectra of salts containing the anions O_2^- and O_2^{2-} ', *J. Chem. Soc., Chem. Commun.*, 278–279.
250. Long, C. A. and Ewing, G. E. (1971), 'Infrared spectrum of bound state oxygen dimers in the gas phase', *Chem. Phys. Lett.*, **9**, 225–231.
251. Jones, R. D., Summerville, D. A. and Basolo, F. (1979), 'Synthetic oxygen carriers related to biological systems', *Chem. Rev.*, **79**, 139–179.
252. Cains, B. R. and Pimentel, G. C. (1963), 'Infrared spectra of solid α - and β -oxygen', *J. Chem. Phys.*, **43**, 3432–3438.
253. Evans, J. C. (1969), 'The peroxide-ion fundamental frequency', *J. Chem. Soc., Chem. Commun.*, 682–683.
254. Bates, J. B., Broecker, M. H. and Boyd, G. E. (1972), 'Raman spectra of molten alkali metal carbonates. Raman spectra of O_2^- and O_3^- ions in alkali metal superoxides and ozonides', *Chem. Phys. Lett.*, **16**, 391–395.
255. Graghton, J. A. and Lippincott, E. R. (1964), 'Vibrational frequency and dissociation energy of the superoxide ion', *J. Phys. Chem.*, **40**, 1779–1782.
256. Shamir, J., Binenboym, J. and Claasen, H. H. (1964), 'The vibrational frequency of the O_2^+ cation', *J. Am. Chem. Soc.*, **90**, 6223–6224.
257. Edwards, A. J., Falconer, W. E., Griffiths, J. E., Sunder, W. A. and Vasile, M. J. (1974), 'Synthesis and properties of dioxygenyl fluorometalate salts', *J. Chem. Soc., Dalton Trans.*, 1129–1133.
258. Urban, M. W., Nakamoto, K. and Basolo, F. (1982), 'IR spectra of molecular oxygen adducts of (tetraphenylporphyrinato) manganese(II) in argon matrices', *Inorg. Chem.*, **21**, 3406–3408.
259. McIntosh, D. and Ozin, G. A. (1977), 'Metal atom chemistry and surface chemistry. I. Dioxygen silver, $Ag^+ O_2^-$ and tetraoxygen silver $Ag^+ O_4^-$. Reactive intermediates in the silver atom-dioxygen systems. Relevance to surface chemistry', *Inorg. Chem.*, **16**, 59–71.
260. Andrews, L. (1971), 'Matrix reactions of cesium and rubidium atoms with oxygen molecules', *J. Chem. Phys.*, **54**, 4935–4943.
261. Hatzenbuehler, D. A. and Andrews, L. (1972), 'Raman and IR spectra of LiO_2^- in oxygen matrices', *J. Chem. Phys.*, **56**, 3398–3403.
262. Andrews, L., Hwang, J. T. and Trindle, C. (1973), 'Matrix reactions of Ce atoms with oxygen molecules. Infrared spectrum and vibrational analysis of $Cs^+ O_2^-$. IR observations of $Cs^+ O_2^{2-}$, Cs^+ and $Cs^+ O_4^+$. Theoretical structure elucidation of $M^+ O_4^-$ ', *J. Phys. Chem.*, **77**, 1065–1073.

263. Andrews, L. (1969), 'IR spectra and bonding in the sodium superoxide and sodium pentoxide molecules', *J. Phys. Chem.*, **73**, 3922–3928.
264. Metcalfe, A. and Ude Shankar, S. (1980), 'Interaction of oxygen with evaporated silicon films. An IR study', *J. Chem. Soc., Faraday Trans. 1*, **76**, 630–636.
265. Gland, J. L., Sexton, B. A. and Fisher, G. B. (1980), 'Oxygen interactions with the Pt (111) surface', *Surf. Sci.*, **95**, 587–602.
266. Sexton, B. A. and Madix, R. J. (1980), 'Vibrational spectra of molecular and atomic oxygen on Ag(110)', *Chem. Phys. Lett.*, **76**, 294–297.
267. Backx, C., deGroot, P. P. M. and Biloen, P. (1981), 'Adsorption of oxygen on Ag (110) studied by high resolution EELS and TPD', *Surf. Sci.*, **104**, 300–317.
268. Howe, R. F., Liddy, J. P. and Metcalfe, A. (1972), 'Infrared spectroscopic studies of oxygen adsorbed on evaporated germanium films', *J. Chem. Soc., Faraday Trans. 1*, **68**, 1595–1600.
269. Harrison, P. G. and Thornton, E. W. (1978), 'Tin oxide surface. Part 4. IR study of the adsorption of O₂ and CO + O₂ mixtures on tin(IV) oxide and the adsorption of CO₂ on NH₃⁻ pretreated SnO₂', *J. Chem. Soc., Faraday Trans. 1*, **74**, 2597–2603.
270. Zecchina, A., Coluccia, S., Cerruti, L. and Borello, E. (1971), 'An IR study of the surface properties of α -cromia', *J. Phys. Chem.*, **75**, 2783–2788.
- 271a. Tsyganenko, A. A., Rodionova, T. A. and Filimonov, V. N. (1979), 'Infrared studies of low temperature adsorption of oxygen on NiO surfaces', *React. Kinet. Catal. Lett.*, **11**, 113–116.
- 271b. Tsyganenko, A. A. and Filimonov, V. N. (1980), 'IR-spectroscopic evidence for the surface complexes of singlet oxygen', *Spectrosc. Lett.*, **13**, 583–592.
272. Lumnov, A. I., Miheikin, I. D., Chuvylkin, N. D., Zhidomirov, G. M. and Kazanskii, V. B. (1976), 'Model scheme for calculation of the electron structures of molecules coordinated with ions of transition elements, and the Ti⁴⁺ O₂⁻ system', *Kinet. Katal.* (in Russian); *Kinet. Catal.* (English translation), **17**, 802–805.
273. Anufrienko, V. F., Maksimov, N. G., Schastnev, P. V., Gundrizer, T. A. and Tarasova, D. V. (1973), 'EPR spectra of O₂⁻ system', *Kinet. Katal.* (in Russian); *Kinet. Catal.* (English translation), **14**, 372–375.
274. Topchieva, K. V., Spiridonov, S. E. and Loginov, A. Yu. (1986), 'Paramagnetic CO-species adsorbed on the surfaces of Sc, Y and La oxides', *J. Chem. Soc., Chem. Commun.*, 636–637.
275. Topchieva, K. V., Spiridonov, S. E. and Loginov, A. Yu. (1986), 'Elementary surface reactions involving radicals. III. Formation and reactivity of paramagnetic dimeric forms of CO adsorption on oxides of the rare-earth elements', *Zh. Fiz. Khim.* (in Russian); *Russ. J. Phys. Chem.* (English translation), **60**, 239–242.
276. Li, C., Domen, K., Maruya, K. I. and Onishi, T. (1989), 'Dioxygen adsorption on well-outgassed and partially reduced CeO₂ studied by FTIR', *J. Am. Chem. Soc.*, **111**, 7683–7687.
277. Nakamura, M., Fujita, S. I. and Takezawa, N. (1992), 'The state of adsorbed oxygen species formed in the decomposition of N₂O on CaO', *Catal. Lett.*, **14**, 315–320.
278. Li, C., Domen, K., Maruya, K. I. and Onishi, T. (1988), 'IR spectra of dioxygen species formed on CeO₂ at room temperature', *J. Chem. Soc., Chem. Commun.*, 1541–1543.
279. Haller, K., Lunsford, J. H. and Laane, J. (1996), 'Temperature dependence of the Raman Spectra of barium peroxide', *J. Phys. Chem.*, **100**, 551–555.
280. Giamello, E., Sojka, Z., Che, M. and Zecchina, A. (1986), 'Spectroscopic study of superoxide species formed by low temperature adsorption of oxygen onto CoO–MgO solid solution: an example of synthetic heterogeneous oxygen carriers', *J. Phys. Chem.*, **90**, 6084–6091.
281. Davydov, A. A. (1979), 'Molecular uncharged forms of adsorbed oxygen', *Kinet. Katal.* (in Russian); *Kinet. Catal.* (English translation), **20**, 1506–1511.
282. Forster, H. and Schuldt, M. (1977), 'IR active fundamentals of D₂, N₂ and O₂ in zeolite matrices', *J. Chem. Phys.*, **66**, 5237–5238.
283. Iwamoto, M., Yoda, Y., Yamazoe, N. and Seiyama, T. (1978), 'Study of metal oxide catalysts by TPD. 4. Oxygen adsorption on various metal oxides', *J. Phys. Chem.*, **82**, 2564–2570.
284. Davydov, A. A. (1977), 'State of titanium dioxide surface according to IR data', *Adsorptsiya Adsorbentny* (in Russian), **5**, 83–89.
285. Sokolovskii, V. D., Borekov, G. M., Anufrienko, V. F. and Davydov, A. A. (1972), 'Reaction-capable forms of adsorbed oxygen in low-temperature isotopic exchange of oxygen on oxide catalysts, *Proceedings of the Symposium 'Adsorbed Oxygen' in catalysis Preprint 11, Institute of Catalysis, Novosibirsk, SB AN USSR, 1972.*
286. Sokolovski, V. D., Borekov, G. K., Osipova, Z. G. and Davydov, A. A. (1973), 'Reactive power of molecular forms of oxygen adsorbed on titania dioxide surfaces', *Teor. Eksp. Khim.* (in Russian); *Theor. Exp. Chem.* (English translation); **9**, 540–544.
- 287a. Bulanin, K. M., Lavalley, J.-C. and Tsyganenko, A. A. (1997), 'Infrared study of ozone adsorption on CaO', *J. Phys. Chem., B*, **101**, 2917–2922.
- 287b. Bulanin, K. M., Lavalley, J.-C. and Tsyganenko, A. A. (1995), 'Infrared study of ozone adsorption on TiO₂', *J. Phys. Chem., B*, **99**, 10294–10300.
- 287c. Bulanin, K. M., Lavalley, J.-C. and Tsyganenko, A. A. (1995), 'Infrared study of adsorbed ozone', *Coll. Surf., A*, **101**, 153–157.

288. Vavilov, V. S. (1963), *Action of Radiation on Semiconductors*, (in Russian), Fizmatgiz, Moscow.
289. Grade, M. and Hirschler, W. (1979), 'Identification of the gaseous molecules zinc sulfide (g) and zinc telluride (g), cadmium telluride (g) and mercury (II) selenide (g) in equilibrium with the solid phase', *Ber. Bunsenges. Phys. Chem.*, **83**, 1269–1272.
290. Finster, J. and Lorenz, P. (1979), 'Quantitative ESCA surface analysis applied to catalysts: investigation of concentration gradients', *Surf. Interface. Anal.*, 179–184.
291. Boccuzzi, F., Ghiotti, G. and Chiorino, A. (1987), 'A metal–semiconductor interaction: effect of H₂ chemisorption on the IR transparency of Cu/ZnO', *Surf. Sci.*, **183**, L285–L289.
292. Boccuzzi, F., Chiorino, A., Chiotti, G., Francesco, P., Strukul, G. and Tessari, R. (1990), 'Pt/ZnO catalysts: spectroscopic and catalytic evidences of ligand effects as a consequence of PtZn alloying', *J. Catal.*, **126**, 381–387.
293. Guglieminotti, E. and Boccuzzi, F. (1989), 'An infrared study of CO adsorbed on a Ru/ZnO catalyst', In *Proceedings of European Conference on Structure and Reactivity of Surfaces*, Trieste, 1988 Elsevier, Amsterdam, pp. 437–446.
294. Guglieminotti, E., Boccuzzi, F., Ghiotti, G. and Chiorino, A. (1987), 'Infrared evidence of metal–semiconductor interactions in an Ru/ZnO system', *Surf. Sci.*, **190**, 331–338.
295. Hong, C.-T., Yeh, C.-T. and Yu, F.-H. (1989), 'Effect of reduction and oxidation treatments on Pd/ZnO catalysts', *Appl. Catal.*, **48**, 385–396.
296. Boccuzzi, F., Chiorino, A., Ghiotti, G. and Guglieminotti, E. (1989), 'Metal/n-ZnO interactions: effect of the surrounding atmosphere on IR transparency', *Langmuir*, **5**, 66–70.
297. Peri, J. B. (1965), 'IR and gravimetric study of the surface hydration of γ -alumina. A model for the surface of γ -Alumina. IR study of adsorption of ammonia on dry γ -alumina', *J. Phys. Chem.*, **69**, 220–221.
298. Paukshtis, E. A. (1992). *Infrared Spectroscopy of Heterogeneous Acid–Base Catalysis* (in Russian), Nauka, Novosibirsk.
299. Tsyganenko, A. A., Mardilovich, P. P., Lysenko, G. N. and Trohimets, A. I. (1987), 'Hydroxyl cover and electron acceptor sites on the alumina surface', in: 'IR spectroscopy and the investigation of surfaces', *Usp. Fotoniki* (in Russian), **9**, 28–68.
300. Tsyganenko, A. A., Homenya, A. V. and Filimonov, V. N. (1976), 'IR spectroscopic study of the proton-donating ability of hydroxyl groups of oxide surfaces', in: *Adsorptsiya Adsorbenty*, **4**, 86–91.
301. Rodionova, T. A., Tsyganenko, A. A. and Filimonov, V. N. (1982), 'The investigation of a low temperature adsorption of CO on metal oxides by means of IR spectroscopy', *Adsorptsiya Adsorbenty* (in Russian), **10**, 33–42.
302. Primet, M., Pichat, P. and Mathieu, M. V. (1971), 'IR study of the surface of titanium dioxides I. Hydroxyl groups', *J. Phys. Chem.*, **75**, 1216–1220.
303. Primet, M., Pichat, P. and Mathieu, M. V. (1971), 'IR study of the surface of titanium dioxides II. Acidic and basic properties', *J. Phys. Chem.*, **75**, 1221–1226.
304. Busca, G., Saussey, H., Saur, O., Lavalley, J.-C. and Lorenzelli, V. (1985), 'FT-IR characterisation of the surface acidity of different TiO₂ anatase preparations', *Appl. Catal.*, **14**, 245–260.
- 305a. Suda, Y. and Marimoto, T. (1987), 'Molecularly adsorbed water on the bare surface of titania (rutile)', *Langmuir*, **3**, 766–795.
- 305b. Suda, Y., Marimoto, T. and Nagao, M. (1987), 'Adsorption of alcohols on titania dioxide', *Langmuir*, **3**, 99–105.
306. Parfitt, G. D. (1976), 'The surface of titanium dioxide' in Gadenhead, D. A. and Danielli, J. F. (Eds), *Progress in Surface and Membrane Science*, Vol. 11: Academic Press, New York, pp. 181–226.
- 307a. Jones, P. and Hockey, J. A. (1971), 'Infrared studies of rutile surfaces', *Trans. Faraday Soc.*, **67**, 2669–2678.
- 307b. Jones, P. and Hockey, J. A. (1971), 'Infrared studies of rutile surfaces. 2. Hydroxylation, hydration and structure of rutile surfaces', *Trans. Faraday Soc.*, **67**, 2679–2685.
- 307c. Jones, P. and Hockey, J. A. (1972), 'Infrared studies of rutile surfaces. 3. Adsorption of water and dehydroxylation of rutile', *Trans. Faraday Soc.*, **68**, 907–1001.
308. Atherton, K., Newbold, G. and Hockey, J. A. (1971), 'IR spectroscopic studies of zinc oxide surfaces', *Discuss. Faraday Soc.*, **52**, 33–43.
309. Morterra, C. (1988), 'IR-spectroscopic study of anatase properties. 6. Surface hydration and strong Lewis acidity of pure and sulfate-doped preparations', *J. Chem. Soc. Faraday. Trans. 1*, **84**, 1617–1637.
310. Tsyganenko, A. A. and Filimonov, V. N. (1974), 'Influence of crystalline structure of oxides on IR spectra of surface OH groups', *Usp. Fotoniki* (in Russian), **4**, 51–74.
311. Davydov, A. A., Borekov, G. K., Yurieva, T. M. and Rubene, N. A. (1977), 'Associative mechanisms of the water-gas shift reaction of CO', *Dokl. AN SSSR* (in Russian); *Proc. AN USSR*, (English translation), **236**, 1402–1405.
- 312a. Coluccia, S., Lavagnino, S. and Marchese, L. (1988), 'The hydroxylated surface of MgO powders and the formation of surface sites', *Mater. Chem. Phys.*, **18**, 445–464.
- 312b. Coluccia, S., Lavagnino, S. and Marchese, L. (1987), 'Adsorption and dissociation of ammonia on the hydroxylated surface of MgO powders', *J. Chem. Soc., Faraday Trans. 1*, **83**, 477–486.

313. Anderson, P. J., Horlock, R. F. and Oliver, J. F. (1965), 'Interaction of water with a magnesium oxide surface', *Trans. Faraday Soc.*, **61**, 2754–2762.
314. Wakabayashi, F., Fujino, T., Kondo, J. N., Domen, K. and Hirose, C. (1995), 'FT-IR studies of interactions between zeolite hydroxyl groups and small molecules. 2 Adsorption of O₂, H₂ and rare gases on H-mordenite at low temperature', *J. Chem. Phys.*, **99**, 14805–14812.
315. Busca, G. and Rossi, P. F. (1983), 'FT-IR spectroscopic and calorimetric characterization of the adsorbed forms of water on α -Fe₂O₃ obtained by thermal decomposition of α -FeOOH', *Mater. Chem. Phys.*, **9**, 561–570.
316. Busca, G. and Lorenzelli, V. (1980), 'IR characterization of surface hydroxyl groups on haematite', *React. Kinet. Catal. Lett.*, **15**, 273–278.
317. Morimoto, T., Nagao, M. and Tokuda, F. (1969), 'The relation between the amounts of chemisorbed and physisorbed water on metal oxides', *J. Phys. Chem.*, **73**, 243–248.
318. Ivlieva, R. R., Zubkov, S. A., Borovkov, V. Yu. and Kazansky, V. B. (1991), 'Diffuse reflectance IR spectroscopy study of the surface of yttrium, erbium and holmium oxides. I Surface hydroxyls', *Kinet. Katal.* (in Russian); *Kinet. Catal.* (English translation), **32**, 368–372.
319. Tsyganenko, A. A. and Filimonov, V. N. (1973), 'Infrared spectra of surface hydroxyl groups and crystalline structures of oxides', *J. Mol. Struct.*, **19**, 579–589.
320. Tsyganenko, A. A. (1993), 'Structure and properties of hydroxylated surfaces of oxides', *React. Kinet. Catal. Lett.*, **50**, 33–38.
- 321a. Zecchina, A., Bordiga, S., Spoto, G., Marchese, L., Petrini, G., Leofani, G. and Padovan, M. (1992), 'Silicalite characterization. 1. Structure, adsorptive capacity and IR spectroscopy of the framework and hydroxyl modes', *J. Phys. Chem.*, **96**, 4985–4991.
- 321b. Zecchina, A., Bordiga, S., Spoto, G., Marchese, L., Petrini, G., Leofani, G. and Padovan, M. (1992), 'Silicalite characterization. 2. IR spectroscopy of the interaction of CO with internal and external hydroxyl groups', *J. Phys. Chem.*, **96**, 4991–4997.
322. Smirnov, E. P. and Tsyganenko, A. A. (1977), 'CNDO study of the properties of the OH groups', *React. Kinet. Catal. Lett.*, **7**, 425–429.
323. Chuiko, A. A. and Gorlov, Yu. U. (1990), *Silica Surface Chemistry. Surface Structure. Active Centers. Sorption Mechanisms* (in Russian), Naukova Dumka, Kiev.
324. Chuiko, A. A. (1993), 'Problems of silica surface chemistry', *React. Kinet. Catal. Lett.*, **50**, 1–13.
325. Zhuravlev, L. T. (1993), 'Characterization of an amorphous silica surface', *React. Kinet. Catal. Lett.*, **50**, 15–25.
326. Burneau, A., Barres, O., Gallas, J. P. and Lavalley, J. C. (1990), 'Comparative study of the surface hydroxyl groups of fumed and precipitated silicas. 2. Characterization by IR spectroscopy of the interactions with water', *Langmuir*, **6**, 1364–1367.
327. Zhdanov, R. S., Kosheleva, L. S. and Titova, T. I. (1987), 'IR study of hydroxylated silica', *Langmuir*, **3**, 960–967.
328. Chukin, G. D. and Apretova, A. I. (1989), 'IR spectra of silica gels and aerosils structure', *Zh. Prikl. Spektrosk.* (in Russian); *Russ. J. Appl. Chem.* (English translation), **50**, 639–646.
329. Smirnov, K. S. (1993), 'Vibrational spectrum of the geminal hydroxyl groups on the silica surface. A molecular dynamics study', *Vibrational Spectrosc.*, **4**, 255–259.
330. Zecchina, A., Bordiga, S., Spoto, G., Scrano, D., Petrini, G., Leofanti, G., Padovan, M. and Arean, C. O. (1992), 'Low-temperature Fourier-transform infrared investigation of the interaction of CO with nanosized ZSM-5 and silicalite', *J. Chem. Soc., Faraday Trans. 1*, **88**, 2959–2969.
331. Woolery, G. L., Alemany, L. B., Dessan, R. M. and Chester, A. W. (1986), 'Spectroscopic evidence for the presence of internal silanols in highly siliceous ZSM-5', *Zeolites*, **6**, 14–16.
332. Kustov, L. M., Kazansky, V. B., Beran, S., Kubelkova, L. and Jiru, P. (1987), 'Adsorption of carbon monoxide on ZSM-5 zeolites. IR Spectroscopy study and quantum chemical calculations', *J. Phys. Chem.*, **91**, 5247–5252.
333. Datka, J., Boxcar, M. and Rymarowicz, K. (1988), 'Heterogeneity of OH groups in Na-HZSM zeolite studies by IR spectroscopy', *J. Catal.*, **114**, 368–371.
334. Zholobenko, V. L., Kustov, L. M., Borovkov, V. Yu. and Kazansky, V. B. (1988), 'A new type of acidic hydroxyl groups in ZSM-5 zeolite and in mordenite according to diffuse reflectance IR spectroscopy', *Zeolites*, **8**, 175–178.
- 335a. Van Santen, R. A. (1995), 'Concepts in theoretical heterogeneous catalytic reactivity', *Catal. Rev. Sci. Eng.*, **37**, 557–698.
- 335b. Van Santen, R. A. (1994), 'Concepts in theoretical heterogeneous catalytic reactivity', *Stud. Surf. Sci. Catal.*, **85**, 273–294.
336. Jobic, H. (1991), 'Observation of the fundamental bending vibrations of hydroxyl groups in HNaY zeolite by neutron inelastic scattering', *J. Catal.*, **131**, 289–293.
337. Jacobs, W. P. J. H., Jobic, H., Van Woplut, J. H. M. C. and Van Santen, R. A. (1992), 'Fourier transform infrared and inelastic neutron scattering study of HY zeolites', *Zeolites*, **12**, 315–319.

338. Kustov, L. M., Borovkov, V. Yu. and Kazansky, V. B. (1982), 'Spectra of hydroxyl groups in zeolites in the near-IR region', *J. Catal.*, **72**, 149–159.
339. Saur, J. (1989), 'Acidic sites in heterogeneous catalysts: Structure, properties and activity', *J. Mol. Catal.*, **54**, 312–323.
340. Dwyer, J. (1988), 'A critical evaluations of the concepts of Brønsted acidity related to zeolites', *Stud. Surf. Sci. Catal.*, **37**, 333–354.
341. Jacobs, P. A. and von Ballmoos, R. (1982), 'Framework hydroxyl groups of H-ZSM-5 zeolites', *J. Phys. Chem.*, **86**, 3050–3052.
342. Topsøe, N. Y., Pedersen, K. and Derouane, E. G. (1981), 'IR and TPD study of the acidic properties of ZSM-5 type zeolites', *J. Catal.*, **70**, 41–52.
343. Loeffler, E., Lohse, U., Peuker, Ch., Oehlmann, G., Kustov, L. M., Zholobenko, V. L. and Kazansky, V. B. (1990), 'Study of different states of nonframework aluminium in hydrothermally dealuminated HZSM-5 zeolites using diffuse reflectance IR spectroscopy', *Zeolites*, **10**, 266–271.
344. Bordiga, S., Arean, C. O., Platara, E. E., Zecchina, A. and Lamberti, C. (1992), 'Low-temperature CO adsorption on NaZSM-5 zeolites on FT-IR investigation', *J. Catal.*, **137**, 179–185.
345. Uytterhoeven, J. B., Christner, L. G. and Hall, W. K. (1965), 'Studies of the hydrogen held by solids. VIII. The decationated zeolites', *J. Phys. Chem.*, **69**, 2117–2126.
346. Jacobs, P. A., Mortier, J. W. and Uytterhoeven, J. B. (1978), 'Properties of zeolites in relation to electronegativity: acidity, carbogenic activity and strength of interaction in transition metal complexes', *J. Inorg. Nucl. Chem.*, **40**, 1919–1923.
347. Jacobs, P. A. and Mortier, J. W. (1982), 'An attempt to rationalize the stretching frequencies of lattice hydroxyl groups in hydrogen-zeolites', *Zeolites*, **2**, 226–230.
348. Orlova, L. B. and Davydov, A. A. (1990), 'The investigation of the hydroxyl cover of faujasite by means of IR spectroscopy', *Zh. Prikl. Spektrosk.* (in Russian); *Russ. J. Appl. Spectrosc.* (English translation), **53**, 104–110.
349. Chukin, G. D., Kulikov, A. S. and Sergienko, S. A. (1984), 'Nature of Lewis acidity in H-zeolites', *React. Kinet. Catal. Lett.*, 287–291.
350. Chukin, G. D. and Khusid, B. L. (1989), 'Structure of the outer surface of zeolite crystals', *Kinet. Katal.* (in Russian); *Kinet. Catal.* (English translation), **30**, 1260–1271.
351. Chukin, G. D., Khusid, B. L., Konoval'chikov, L. D. and Nefedov, B. K. (1988), 'Structure of the outer surface of crystals of high silica zeolites', *Kinet. Katal.* (in Russian); *Kinet. Catal.* (English translation), **29**, 1012–1016.
352. Chukin, G. D., Khusid, B. L., Lupina, M. I., Zhdan, P. A. and Nefedov, B. K. (1987), 'Acid centers and catalytic activity of high-silica zeolites', *Kinet. Katal.* (in Russian); *Kinet. Catal.* (English translation), **28**, 1211–1216.
353. Brunner, G. O. (1987), 'Reaction of HZSM-5 with water as studied by IR spectroscopy', *Zeolites*, **7**, 10–15.
354. Jentys, A., Warecka, G., Derewinski, M. and Lercher, J. A. (1989), 'Adsorption of water on ZSM-5 zeolites', *J. Phys. Chem.*, **93**, 4837–4843.
355. Davydov, A. A., 'Diffuse reflectance IR spectroscopy study of the surface hydroxyls on transition metal oxides' (unpublished data).
356. Librovich, N. B., Sakun, V. P. and Sokolov, N. D. (1981), *The Hydrogen Bond* (in Russian), Nauka, Moscow, 174 pp.
357. Tsyganenko, A. A., Smirnov, K. S., Rzhetskii, A. M. and Mardilovich, P. P. (1990), 'IR spectroscopic evidence for the structural OH groups of spinel alumina modifications', *Mater. Chem. Phys.*, **26**, 35–46.
358. Kawakashi, H. and Yoshida, S. (1984), 'Theoretical approach to the basicity of alkaline-earth metal oxide catalysts', *J. Chem. Soc., Faraday Trans. 2*, **80**, 921–932.
359. Pelmenchchikov, A. G., Mikheikin, I. D., Zhidomirov, G. M. and Zamaraev, K. I. (1981), 'Cluster scheme of the quantum-chemical calculation of the surface structures by the MINDO/3 method', *Kinet. Katal.* (in Russian); *Kinet. Catal.* (English translation), **22**, 1427–1430.
360. Baumgarten, E., Hollenberg, D. and Hoffkens, H. (1982), 'Untersuchungen zur reaktivitat von aluminiumoxiden, sowie gemischten silicium-bzw. Bor-Aluminiumoxiden bei reactionen von hexen-1', *Z. Phys. Chem.*, **129**, 239–254.
361. Mardilovich, P. P. and Trohimets, A. I. (1981), 'Regions of manifestations of stretching vibrations of unper-turbed and H-bounded OH(OD) groups of the alumina', *Zh. Prikl. Spektrosk.* (in Russian); *Russ. J. Appl. Spectrosc.* (English translation), **35**, 1029–1033.
362. Busca, G., Lorenzelli, V., Ramis, G. and Willey, R. J. (1993), 'Surface sites on the spinel-type and corundum-type metal oxide powders', *Langmuir*, **9**, 1492–1499.
363. Busca, G., Lorenzelli, V., Escrivano, V. S. and Guidetti, R. (1991), 'FT-IR study of the surface properties of the spinels NiAl₂O₄ in relation to those of the transition aluminas', *J. Catal.*, **131**, 167–177.
364. Della Gatta, G., Fubini, B., Ghiotti, G. and Morterra, C. (1976), 'Chemisorption of CO on various transition aluminas', *J. Catal.*, **43**, 90–98.
365. Trohimets, A. I., Mardilovich, P. P. and Lysenko, G. N. (1979), 'IR spectra of hydroxyl cover on γ -Al₂O₃', *Zh. Prikl. Spektrosk.* (in Russian); *Russ. J. Appl. Spectrosc.* (English translation), **30**, 873–877.

366. Trohimets, A. I., Mardilovich, P. P., Buslov, D. K. and Lysenko, G. N. (1979), 'IR spectra of hydroxyl cover on γ -Al₂O₃', *Zh. Prikl. Spektrosk.* (in Russian); *Russ. J. Appl. Spectrosc.* (English translation), **31**, 270–274.
367. Trohimets, A. I., Mardilovich, P. P. and Buslov, D. K. (1980), 'IR spectra of hydroxyl cover on χ -Al₂O₃', *Zh. Prikl. Spektrosk.* (in Russian); *J. Appl. Spectrosc.* (English translation), **33**, 298–301.
368. Chukin, G. D. (1976), 'The surface structure of the γ -alumina', *Zh. Strukt. Khim.* (in Russian); *J. Struct. Chem.* (English translation), **17**, 122–128.
369. Chukin, G. D. and Seleznev, Yu. L. (1989), 'Mechanism of thermal decomposition of boehamite and a model of aluminum oxide structure', *Kinet. Katal.* (in Russian); *Kinet. Catal.* (English translation), **30**, 69–77.
370. Morterra, C., Chiorino, A. and Borello, E. (1984), 'An IR-spectroscopic characterization of α -FeOOH (goethite)', *Mater. Chem. Phys.*, **10**, 199–215.
371. Parfitt, R. L., Russell, J. D. and Farmer, V. C. (1976), 'Confirmation of the surface structures of goethite (α -FeOOH) and phosphated goethite by IR spectroscopy', *J. Chem. Soc., Faraday Trans. 1*, **72**, 1082–1087.
372. McCafferty, E. and Zettmoyer, A. C. (1971), 'Adsorption of water vapor on α -Fe₂O₃', *Discuss. Faraday Soc.*, **52**, 239–254.
373. Marimoto, T., Yanai, H. and Nagao, M. (1976), 'IR spectra of ammonia adsorbed on zinc oxide', *J. Phys. Chem.*, **80**, 471–475.
- 374a. Boccuzzi, F., Borello, E., Zecchina, A., Bossi, A. and Camia, M. (1978), 'Infrared study of Zn surface properties. I. H₂ and D₂ chemisorption at room temperature', *J. Catal.*, **51**, 150–159.
- 374b. Boccuzzi, F., Borello, E., Zecchina, A., Bossi, A. and Camia, M. (1978), 'Infrared study of Zn surface properties. II. H₂-CO interaction at room temperature', *J. Catal.*, **51**, 160–169.
375. Zettelmoyer, A. C. and McCafferty, E. (1973), 'Water on oxide surfaces', *Croat. Chem. Acta*, **45**, 173–185.
376. Morterra, C., Chiotti, G., Garrone, E. and Fiscaro, E. (1980), 'Spectroscopic study of anatase properties. Part 3. Surface acidity', *J. Chem. Soc., Faraday Trans. 1*, **76**, 2102–2113.
377. Griffiths, D. M. and Rochester, C. H. (1977), 'IR study of the adsorption of water on the surface of rutile', *J. Chem. Soc., Faraday Trans. 1*, **73**, 1510–1529.
378. Tanaka, K. and White, J. M. (1982), 'Characterisation of species adsorbed on oxidized and reduced anatase', *J. Phys. Chem.*, **86**, 4708–4714.
379. Bensitel, M., Moravek, V., Lamotte, J., Saur, O. and Lavalley, J. C. (1987), 'Infrared study of alcohols adsorption on zirconium oxides: reactivity of alkoxy species towards CO₂', *Spectrochim. Acta, Part A*, **43**, 1487–1491.
380. Jackson, N. B. and Ekerdt, J. G. (1986), 'Methanol synthesis mechanism over zirconium dioxide', *J. Catal.*, **101**, 90–102.
381. Onishi, T., Abe, H., Maruya, K. and Domen, K. (1986), 'Surface species formed from the reaction of H₂-CO over ZrO₂ as studied by infrared spectroscopy', *J. Chem. Soc., Chem. Commun.*, 103–104.
382. He, M. Y. and Ekerdt, J. G. (1984), 'IR studies of the adsorption of synthesis gas on zirconium dioxide', *J. Catal.*, **87**, 381–388.
383. Tanabe, K. (1985), 'Surface and catalytic properties of ZrO₂', *Mater. Chem. Phys.*, **13**, 347–364.
- 384a. Bensitel, M., Saur, O. and Lavalley, J. C. (1987), 'Acidity of zirconium oxide and sulfated ZrO₂ samples', *Mater. Chem. Phys.*, **17**, 249–258.
- 384b. Bensitel, M., Saur, O., Lavalley, J. C. and Morrow, B. A. (1988), 'An IR study of sulfated zirconia', *Mater. Chem. Phys.*, **19**, 147–156.
385. Ghiotti, G., Boccuzzi, F. and Scala, R. (1985), 'IR study of ZnO surface properties: CO adsorption and CO/D₂ interaction at 77 K', *J. Catal.*, **92**, 79–97.
386. Dent, A. L. and Kokes, R. J. (1970), 'The nature of adsorbed propene on zinc oxide. I. Formation of π -allyl species', *J. Am. Chem. Soc.*, **92**, 6709–6723.
387. Tsyganenko, A. A., Lamotte, J., Saussey, J. and Lavalley, J. C. (1989), 'Bending vibrational of OH groups resulting from H₂ dissociation on ZnO', *J. Chem. Soc., Faraday Trans. 1*, **85**, 2397–2423.
388. Piero Del, G., Trifiro, G. and Vaccari, A. (1984), 'Non-stoichiometric Zn-Cr spinel as the active phase in the catalytic synthesis of methanol', *J. Chem. Soc., Chem. Commun.*, 656–659.
- 389a. Davydov, A. A. (1993), 'Protic acidity of transition element oxides', *Zh. Fiz. Khim.* (in Russian); *Russ. J. Phys. Chem.* (English translation), **67**, 1709–1714.
- 389b. Davydov, A. A. (1982), 'Infrared spectroscopic studies of surface properties of Sn-Mo-O catalyst', *React. Kinet. Catal. Lett.*, **19**, 377–382.
390. Valyon, J., Schneider, R. L. and Hall, W. K. (1984), 'Site selective chemisorption of sulfided molybdena-alumina catalysts', *J. Catal.*, **85**, 277–283.
- 391a. Budneva, A. A. and Davydov, A. A. (1979), 'Infrared spectroscopic studies of the acidity of chromium molybdate catalysts', *React. Kinet. Catal. Lett.*, **11**, 133–137.
- 391b. Davydov, A. A., Budneva, A. A. and Sokolovski, V. D. (1981), 'IR study of hydrocarbons adsorption. IX. Adsorption forms of ammonia, propane and ethane on the oxidative ammonolysis catalysts', *Kinet. Katal.* (in Russian), **22**, 213–221.

392. Erenburg, E. M., Andrushkevich, T. V., Popova, G. Ya. and Davydov, A. A. (1979), 'Influence of water vapor on propylene oxidation on V/Mo catalyst', *React. Kinet. Catal. Lett.*, **12**, 5–11.
393. Davydov, A. A. and Shepotko, M. L. (1990), 'IR investigation of the nature of the surface sites and methanol adsorption on Fe–Mo–O catalysts', *Teor. Eksp. Khim.* (in Russian); *Theor. Exp. Chem.* (English translation), **26**, 474–480.
394. Saled, S. L., McVicker, G. B., Murrell, L. L., Sherman, L. G., Dispenziere, N. C., Hsu, S. L., Jr and Waldman, D. (1988), 'Comparison of the acidities of $\text{WO}_3/\text{Al}_2\text{O}_3$ and ultrastable faujasite catalysts', *J. Catal.*, **111**, 286–295.
395. Goncharova, O. I., Davydov, A. A. and Yurieva, T. M. (1984), 'IR spectroscopic manifestation of poly-molybdenum compounds on the surface of a molybdenum–aluminum oxide catalyst', *Kinet. Katal.* (in Russian); *Kinet. Catal.* (English translation), **25**, 152–158.
396. Goncharova, O. I., Davydov, A. A., Yurieva, T. M. and Shokhireva, T. Kh. (1983), 'IR spectroscopic study of silicon–molybdenum oxide catalysts', *Kinet. Katal.* (in Russian); *Kinet. Catal.* (English translation), **24**, 683–687.
397. Davydov, A. A. and Goncharova, O. I. (1993), 'Application of IR spectroscopy for investigation of heteropolymers supported on oxides', *Usp. Khim.* (in Russian); *Russ. Chem. Rev.* (English translation), **62**, 22–38.
398. Borovkov, V. Yu., Alexeev, A. A. and Kazansky, V. B. (1983), 'On the nature of strong acidic Brønsted sites on amorphous silica–aluminas', *J. Catal.*, **80**, 462–464.
399. Benedict, W. S. and Plyer, E. K. (1957), 'Vibration–rotation bands, molecular dimensions and harmonic frequencies of NH_3 and deuterated ammonia', *Can. J. Phys.*, **35**, 1235–1241.
400. Corset, J., Guilletmet, J. and Lascombe, J. (1966), 'Spectres infrarouges de l'ammmoniac a l'etat liquide et solution dans le tetrachlorure de carbone, a differents tans de deuterium', *Bull. Soc. Chim. Fr.*, 1231–1235.
401. Cannon, C. G. (1958), 'The infrared spectrum of NH_3 in carbon tetrachloride', *Spectrochim. Acta*, **10**, 425–429.
402. Reding, F. R. (1951), 'The vibrational spectra of molecules and complex ions in crystals V. Ammonia and deuterio-ammonia', *J. Chem. Phys.*, **79**, 594–601.
403. Goubeau, J. (1958), 'Das Schwingungs spectrum von $\text{BF}_3 \cdot \text{NH}_3$ ', *Z. Phys. Chem.*, **14**, 61–64.
404. Goubeau, J. and Ricker, E. (1961), 'Borinhydrasin und sein pyrolyseprodukte', *Anorg. Allgem. Chem.*, **310**, 123–142.
405. Paterson, E. (1961), 'Interaction of boron trifluoride with hydrazine', *Can. J. Chem.*, **39**, 986–994.
406. Grinberg, A. A. and Varshavsky, Yu. S. (1966), 'Frequencies of deformational vibrations of coordinated ammonia and their relationship with properties of transition metal ammoniates', in Korshunov, A. V. (Ed.), *Application of Molecular Spectroscopy in Chemistry* (in Russian), Nauka, Moscow, pp. 104–107.
407. Kozerenko, S. P. and Polishykh, S. A. (1975), 'Titanium tetrafluoride ammine', *Koord. Khim.*, **1**, 1643–1645 (in Russian).
408. Nakanishi, K. (1962), *Infrared Absorption Spectroscopy*, Holden Day, Inc., San Francisco, CA; Nankodo Company Ltd, Tokyo, 210 pp.
409. Wauner, E. L. and Hornig, D. F. (1950), 'The vibrational spectra of molecules and complex ions in crystals. III. Ammonium chloride and deuterioammonium chloride', *J. Chem. Phys.*, **18**, 296–304.
410. Treffer, M. and Wilkinson, G. R. (1969), 'Motion of ammonium ions in non-cubic crystal sites', *Discuss. Faraday Soc.*, **48**, 108–115.
411. Novak, A., Porter, J. and Bouclier, P. (1965), 'Infrared spectra of Li, Na, and K amides', *C.R. Seances Acad. Sci.*, **261**, 455–457.
412. Tsyganenko, A. A., Pozdnyakov, L. V. and Filimonov, V. N. (1975), 'Ammonia adsorption on metal oxide surfaces: an IR study', *Usp. Fotoniki.*, **5**, 150–177 (in Russian).
413. Dixit, L. and Rao, P. T. S. R. (1996), 'Spectroscopy in the measurements of acidic–basic properties of solids', *Appl. Spectrosc. Rev.*, **31**, 369–472.
414. Parry, E. P. (1963), 'An infrared study of pyridine adsorbed on acidic solids. Characterization of surface acidity', *J. Catal.*, **2**, 371–379.
415. Taagelpera, M., Henderson, W. G., Brownlee, R. T. C., Beauchamp, J. L., Holtz, D. and Taft, R. W. (1972), 'Gas phase basicities and pyridine substituent effects', *J. Am. Chem. Soc.*, **94**, 1369–1374.
416. Jensen, W. B. (1980), *The Lewis Acid–Base Concepts. An Overview*, Wiley, New York.
417. Stair, P. C. (1972), 'The concept of Lewis acids and bases applied to surfaces', *J. Am. Chem. Soc.*, **104**, 4044–4052.
418. Paukshtis, E. A. and Yurchenko, E. N. (1983), 'Study of the acid–base properties of heterogeneous catalysts by IR spectroscopy', *Usp. Khim.* (in Russian); *Russ. Chem. Rev.* (English translation), **52**, 426–454.
419. Coluccia, S., Garrone, E. and Borello, E. (1983), 'Infrared spectroscopic study of molecular and dissociative adsorption of NH_3 on MgO, CaO and SrO', *J. Chem. Soc., Faraday Trans. 1*, **79**, 607–613.
420. Svatos, G. F., Sweeny, D. M., Mizushima, S., Curran, S. and Quageano, J. V. (1957), 'Infrared absorption spectra of inorganic coordination complexes. XII. The characteristic NH_3 deformation vibrations of solid inorganic complexes', *J. Am. Chem. Soc.*, **79**, 3313–3315.

- 421a. Belokopytov, Yu. V., Kuznetsov, V. A., Kholyvenko, K. M. and Gerei, S. V. (1976), 'An IR study of the surface properties of metal oxides. 1. The interaction of ammonia with the surface Cr_2O_3 ', *J. Catal.*, **44**, 1–4.
- 421b. Belokopytov, Yu. V., Kuznetsov, V. A., Kholyvenko, K. M. and Gerei, S. V. (1979), 'An IR study of the surface properties of metal oxides. 2. The interaction of NH_3 with the surfaces of Fe_2O_3 , ZnO , MoO_3 and V_2O_5 ', *J. Catal.*, **60**, 1–7.
422. Inomata, M., Miyamoto, A. and Murakami, Y. (1980), 'Mechanism of the reaction of NO and NH_3 on vanadium oxide catalyst in the presence of oxygen under dilute gas conditions', *J. Catal.*, **62**, 140–148.
423. Miyamoto, A., Kobayashi, K., Inomata, M. and Murakami, Y. (1982), 'Nitrogen-15 tracer investigation of the mechanism of the reaction of NO with NH_3 on vanadium oxide catalyst', *J. Phys. Chem.*, **86**, 2945–2950.
424. Kline, C. H. and Turkevich, J. (1944), 'The vibrational spectrum of pyridine and the thermodynamic properties of pyridine vapours', *J. Chem. Phys.*, **12**, 300–309.
425. Davydov, A. A. and Shchekochikhin, Yu. M. (1969), 'Study of electron-accepting centers of aluminosilicate catalysts with IR spectroscopy', *Kinet. Katal.* (in Russian); *Kinet. Catal.* (English translation), **10**, 647–653.
426. Davydov, A. A. and Gordymova, T. A. (1992), 'Analysis of spectral manifestations of ammonia ions and their correlation with the proton donor ability of oxide systems', *Zh. Prikl. Spektrosk.* **56**, 587–590 (in Russian).
- 427a. Tagaki, M., Kawai, T., Soma, M. and Tamaru, K. (1976), 'Mechanism of catalytic reactivity between NO and NH_3 on V_2O_5 in the presence of oxygen', *J. Phys. Chem.*, **80**, 430–431.
- 427b. Takagi, M., Kawai, T., Soma, M., Onishi, T. and Tamaru, K. (1977), 'The mechanism of the reaction between NO_x and NH_3 on V_2O_5 in the presence of oxygen', *J. Catal.*, **50**, 441–446.
- 428a. Janssen, F., van den Kerkof Bosch, H. and Ross, J. (1987), 'Mechanism of the reaction of NO, NH_3 and O_2 over vanadia catalysts. 1. The role of O_2 studies by way of isotopic transients under dilute conditions', *J. Phys. Chem.*, **91**, 5921–5927.
- 428b. Janssen, F., van den Kerkof Bosch, H. and Ross, J. (1987), 'Mechanism of the reaction of NO, NH_3 and O_2 over vanadia catalysts. 2. Isotopic transients studies with oxygen-18 and nitrogen-15', *J. Phys. Chem.*, **91**, 6633–6638.
429. Bars, J. Le., Vedrin, J. C., Aurox, A., Trautmann, S. and Baerns, M. (1994), 'Microcalorimetric and infrared studies of the acid–base properties of $\text{V}_2\text{O}_5/\gamma\text{-Al}_2\text{O}_3$ catalysts', *Appl. Catal., A: Gen.*, **119**, 341–354.
430. Brec, R., Novak, A. and Rouxel, J. (1967), 'Infrared spectra of lithium, sodium and potassium amidoaluminate', *Bull. Soc. Chim. Fr.*, 2432–2435.
431. Kharitonov, Yu. Ya. and Sarukhanov, M. A. (1977), *Chemistry of Metal Complexes with Hydroxylamine* (in Russian), Nauka, Moscow.
432. Gordymova, T. A. and Davydov, A. A. (1983), 'Spectral manifestation of ammonia adsorption forms on $\gamma\text{-Al}_2\text{O}_3$ ', *Zh. Prikl. Spektrosk.* (in Russian); *J. Appl. Spectrosc.* (English translation), **39**, 621–627.
433. Tench, A. J. and Giles, D. (1972), 'IR study of the adsorption of NH_3 on MgO ', *J. Chem. Soc., Faraday Trans. 1*, **68**, 193–196.
434. Take, J., Yeda, T. and Yoneda, Y. (1978), 'An IR study of acid sites on silica–alumina catalysts poisoned with sodium hydroxide', *Bull. Chem. Soc. Jpn.*, **51**, 1581–1584.
- 435a. Stolz, H. and Knozinger, H. (1971), 'Adsorption properties of alumina. III. An IR investigation of the adsorption of pyridine', *Kolloid-Z. Z. Polym.*, **243**, 71–78.
- 435b. Stolz, H. and Knozinger, H. (1971), 'Adsorption properties of alumina. IV. An IR investigation of the adsorption of pyridine', *Kolloid-Z. Z. Polym.*, **243**, 243–254.
436. Morterra, C., Chiorino, A., Ghiotti, G. and Garrone, E. (1979), 'Surface acidity of η -alumina. I. Pyridine chemisorption at room temperature', *J. Chem. Soc., Faraday Trans. 1*, **75**, 271–288.
437. Ghosh, A. K. and Curthoys, G. (1983), 'Acidity of dealuminated mordenites studied by IR spectroscopy', *J. Chem. Soc., Faraday Trans. 1*, **74**, 805–813.
438. Wilmshurst, J. K. (1960), 'Sensitive frequencies. V. The sensitive amine frequencies and electronegativities of complexes of transition metal ion radicals', *Can. J. Chem.*, **38**, 467–475.
439. Van Tongelen, M. (1966), 'Determination of the nature of catalyst acid sites by infrared spectroscopy', *J. Catal.*, **5**, 535–549.
- 440a. Lysenko, G. N. and Trokhimets, A. I. (1984), 'IR spectroscopic study of pyridine interaction with $\eta\text{-Al}_2\text{O}_3$ surface', *Zh. Prikl. Spektrosk.* (in Russian); *J. Appl. Spectrosc.* (English translation), **40**, 84–88.
- 440b. Lysenko, G. N. and Trokhimets, A. I. (1982), 'IR spectroscopic study of the pyridine species adsorbed on $\theta\text{-Al}_2\text{O}_3$ ', *Zh. Prikl. Spektrosk.* (in Russian); *J. Appl. Spectrosc.* (English translation), **34**, 49–54.
- 441a. Lysenko, G. N., Mardilovich, P. P. and Trokhimets, A. I. (1986), 'Inhomogeneity of strong Lewis acid centers on Al_2O_3 surface', *React. Kinet. Catal. Lett.*, **31**, 377–381.
- 441b. Lysenko, G. N., Mardilovich, P. P. and Trokhimets, A. I. (1985), 'Influence of the dehydroxylation degree of $\eta\text{-Al}_2\text{O}_3$ on the interaction of pyridine with its surface on the basis of IR spectroscopy', *Zh. Prikl. Spektrosk.* (in Russian); *J. Appl. Spectrosc.* (English translation), **43**, 110–114.
- 442a. Hadjiivanov, K., Sauer, O., Lamotte, J. and Lavalley, J. C. (1994), 'FT-IR spectroscopic study of NH_3 and CO adsorption and coadsorption on TiO_2 (anatase)', *Z. Phys. Chem.*, **187**, 281–300.

- 442b. Hadjiivanov, K. (1998), 'FTIR study of CO and NH₃ co-adsorption on TiO₂ (rutile)', *Appl. Surf. Sci.*, **135**, 331–338.
443. Burwell, R. L., Jr, Haller, G. L., Taylor, K. C. and Reed, J. F. (1969), 'Chemosorptive and catalytic behavior of chromia', *Adv. Catal.*, **20**, 1–96.
444. Parfitt, G. D., Ramsbotham, J. and Rochester, C. H. (1971), 'An infrared study of pyridine adsorption on rutile surfaces', *Trans. Faraday Soc.*, **67**, 1500–1506.
445. Sohn, J. R., Ryu, S. G., Park, M. Y. and Pae, Y. P. (1992), 'Preparation and characterization of chromium oxide supported on zirconia', *Bull. Korean Chem. Soc.*, **13**, 605–612.
446. Zecchina, A., Guglieminotti, E., Cerruti, L. and Coluccia, S. (1972), 'An IR study of surface properties of α -chromia. IV. Pyridine and heavy water adsorption on oxygen-covered surfaces', *J. Phys. Chem.*, **76**, 571–577.
447. Busca, G. and Lorenzelli, V. (1981), 'IR study of characterization and reactivity of pyridine on hematite', *Mater. Chem.*, **6**, 175–185.
448. Massoth, F. E. (1977), 'Characterization of molybdena catalysts', *Adv. Catal. Related Subjects*, **27**, 265–310.
449. Kiviat, F. E. and Petrakis, L. (1973), 'Surface acidity of transition metal modified aluminas. IR and NMR investigations of adsorbed pyridine', *J. Phys. Chem.*, **77**, 1232–1238.
450. Franse, T., Van der Meer, O. and Mars, P. (1976), 'Surface structure and catalytic activity of a reduced molybdenum oxide–alumina catalyst. I. The adsorption of pyridine in relation with molybdenum valence', *J. Phys. Chem.*, **80**, 2103–2110.
451. Komaya, T. and Misono, M. (1983), 'Activity patterns of molybdophosphoric acid (H₃PMoO₁₂O₄₀) and its alkali salts for oxidation reactions', *Chem. Lett.*, 1177–1180.
452. Martin, C., Martin, I. and Rives, V. (1992), 'An FT-IR study of the adsorption of pyridine, formic acid and acetic acid on magnesia and molybdena–magnesia', *J. Mol. Catal.*, **73**, 51–63.
453. Maksimov, N. G., Ismailov, E. G., Anufrienko, V. F. and Davydov, A. A. (1975), 'Study of the adsorption of O₂, CO, C₃H₆ and NH₃ molecules on molybdena–magnesia catalysts by the ESR method', *Teor. Eksp. Khim.* (in Russian); *Theor. Exp. Chem.* (English translation), **11**, 260–265.
454. Jacobs, P. (1977), *Carbonogenic Activity of Zeolites*, Elsevier, Amsterdam.
455. Zaki, M. I. and Knozinger, H. (1987), 'CO – a low temperature IR probe for the characterization of hydroxyl group properties on metal oxide surfaces', *Mater. Chem. Phys.*, **17**, 201–215.
456. Davydov, A. A. (1983), 'Study of the mechanism of propene conversion to acetone by infrared spectroscopy. Bifunctionality of the catalyst', in Davydov, A. A. (Ed.), *Proceedings of the 7th Soviet–Japan Symposium on Catalysis*, Irkutsk 1–7 July 1983, Institute of Catalysis, Novosibirsk, pp. 178–184.
457. Kasumov, F. B. and Davydov, A. A. (1991), 'Klaus reaction. II. H₂S adsorption centres on the surface of an Sn–Mo oxide catalyst on the basis of infrared spectroscopy data', *Kinet. Catal.* (in Russian); *Kinet. Catal.* (English translation), **32**, 1193–1195.
458. Kim, E. Kh., Zhdanova, K. P., Timashkova, B. V., Alekseeva, N. V., Batasheva, L. P. and Schmidt, F. K. (1983), 'Influence of the heterogeneity of molybdenum compounds on the acidity of molybdena–alumina catalysts', *React. Kinet. Catal. Lett.*, **22**, 325–329.
459. Davydov, A. A. (1993), 'Dissociative adsorption, in the atomic nitrogen mode, on the surfaces of vanadium-containing catalysts from adsorbed NH₃ and NO', *Zh. Fiz. Khim.* (in Russian); *Russ. J. Phys. Chem.* (English translation), **67**, 127–130.
460. Budneva, A. A., Paukshtis, E. A. and Davydov, A. A. (1986), 'IR spectroscopic studies of strength and concentration of acid centres on V₂O₅/Al₂O₃ catalysts', *React. Kinet. Catal. Lett.*, **34**, 63–67.
- 461a. Cook, D. (1961), 'Vibrational spectra of pyridinium salts', *Can. J. Chem.*, **39**, 2009–2014.
- 461b. Angell, C. L. and Sheffer, P. C. (1966), 'Carbon monoxide adsorption on zeolites', *J. Phys. Chem.* **70**, 1413–1421.
- 461c. Bobrov, N. N., Borekov, G. K., Davydov, A. A. and Ione, K. G. (1975), 'Influence of the state of nickel cations on catalytic properties of NiY zeolites. I. Catalytic properties of NiY zeolites in CO oxidation', *Izv. Akad. Nauk. SSSR Ser. Khim.*, (in Russian), 24–29.
- 461d. Arean, C. A., Tsyganenko, A. A., Platero, E. E., Carrone, E. and Zecchina, A. (1998), 'Two coordination modes of CO in zeolites: A temperature-dependent equilibrium', *Angew. Chem. Int. Ed.*, **37**, 3161–3163.
462. Mashenko, A. I., Kon, M. Ya., Shvets, V. A. and Kazanskii, V. B. (1972), 'Study of CO and NH₃ adsorption onto V₂O₅ on silica gel with EPR and IR spectroscopy', *Teor. Eksp. Khim.* (in Russian); *Theor. Exp. Chem.* (English translation), **8**, 801–806.
463. Gay, R. R., Nodine, M. H., Henrich, V. E., Zieger, H. J. and Solomon, E. I. (1980), 'Photoelectron study of the interaction of CO with ZnO', *J. Am. Chem. Soc.*, **102**, 6752–6761.
464. Sayers, M. J., McClellan, M. A. and Gay, R. R. (1980), 'Angle resolved photoemission investigation of the bonding geometry of CO to ZnO (1010)', *Chem. Phys. Lett.*, **75**, 575–578.
465. Ovsyannikova, I. A., Davydov, A. A. and Tunina, O. V. (1987), 'Study of the CO adsorption on nickel by X-ray absorption and IR spectroscopic methods', *Zh. Fiz. Khim.* (in Russian); *Russ. J. Phys. Chem.* (English translation), **60**, 957–960.

466. Denisenko, L. A., Tsyganenko, A. A. and Filimonov, V. N. (1984), 'Infrared study of the interaction between adsorbed molecules in the CO/ZnO system', *React. Kinet. Catal. Lett.*, **25**, 23–26.
- 467a. Rebenstorf, B. and Larsson, R. (1979), 'IR studies of coordinatively unsaturated surface compounds on silica gel. I. CO complexes of Mn(II), Fe(II) and Co(II)', *Z. Anorg. Allgem. Chem.*, **453**, 127–138.
- 467b. Rebenstorf, B. and Larsson, R. (1979), 'IR studies of coordinatively unsaturated surface compounds on silica gel. II. CO complexes of Ni(II)', *Z. Anorg. Allgem. Chem.*, **453**, 139–152.
- 467c. Rebenstorf, B. and Larsson, R. (1979), 'IR studies of coordinatively unsaturated surface compounds on silica gel. III. Adsorption of CO on main group metal ions', **454**, 139–152.
468. Beyer, H. K. and Jacobs, P. A. (1979), 'Evidence for the nature of true Lewis sites in faujasite-type zeolites', *J. Phys. Chem.*, **83**, 1174–1177.
469. Dutka, J. (1981), 'Y-zeolites studies by IR spectroscopy. Adsorption of benzene and toluene', *J. Chem. Soc., Faraday Trans. 1*, **77**, 511–517.
470. Kazansky, V. B. (1984), 'The study of the Brønsted and Lewis acidity of decationized and dealuminated zeolites by IR diffuse reflection spectroscopy and quantum chemistry', *Studies Surf. Sci. Catal.*, **18**, 61–75.
471. Kazansky, V. B. (1987), 'On the nature of Lewis acid sites in high-silica zeolites and mechanism of their dehydroxylation', *Catal. Today*, **3**, 367–372.
472. Borode, R., Sayari, A., Adnot, A. and Kaliaguine, S. (1990), 'Characterization of acidity in ZSM-5 zeolites: an X-ray photoelectron and IR spectroscopy study', *J. Phys. Chem.*, **94**, 5989–5994.
- 473a. Gordymova, A. A. and Davydov, A. A. (1979), 'IR spectroscopic study of hydrocarbon adsorption on oxide surfaces. V. Sites for propylene adsorption on γ -alumina. Nature of the weak-bonded mode of propylene', *Kinet. Katal.* (in Russian); *Kinet. Catal.* (English translation), **20**, 727–732.
- 473b. Gordymova, A. A. and Davydov, A. A. (1979), 'IR spectroscopic study of hydrocarbon adsorption on oxide surfaces. VI. Allylic species on alumina and isomerization mechanism', *Kinet. Katal.* (in Russian); *Kinet. Catal.* (English translation), **20**, 733–740.
474. Guglielminotti, E., Coluccia, S., Garrone, E., Cerruti, L. and Zecchina, A. (1979), 'IR study of CO adsorption on magnesium oxide', *J. Chem. Soc., Faraday Trans. 1*, **75**, 96–105.
475. Garrone, E., Zecchina, A. and Stone, F. S. (1988), 'CO adsorption on MgO and CaO', *J. Chem. Soc., Faraday Trans. 1*, **84**, 2843–2854.
476. Zecchina, A., Coluccia, S., Spoto, G., Scrano, D. and Marchese, L. (1990), 'Revising MgO–CO surface chemistry: an IR investigation', *J. Chem. Soc., Faraday Trans. 1*, **86**, 703–709.
477. Babaeva, M. A., Bystrov, D. S., Kovalgin, A. Yu. and Tsyganenko, A. A. (1990), 'CO interaction with the surface of thermally activated CaO and MgO', *J. Catal.*, **123**, 396–416.
478. Babaeva, M. A., Bystrov, D. S. and Tsyganenko, A. A. (1987), 'The interaction of CO with the surfaces of thermal activated oxides of calcium and magnesium', *Usp. Fotoniki*, **9**, 69–96 (in Russian).
479. Davydov, A. A. (1985), 'Study of the state of transition-metal cations on catalyst surfaces by the IR spectroscopy of adsorbed probe molecules (CO, NO). VI. State of copper in CuO. Influence of supports on the state of copper', *Kinet. Katal.* (in Russian); *Kinet. Catal.* (English translation), **26**, 157–167.
480. Davydov, A. A. and Budneva, A. A. (1983), 'Infrared spectra of CO and NO adsorbed on CuO', *React. Kinet. Catal. Lett.*, **25**, 121–124.
481. Musil, Z., Lokhov, Yu. A. and Davydov, A. A. (1979), 'An IR-spectroscopic study of the adsorption of NO and CO on CuO/Al₂O₃', *Kinet. Katal.* (in Russian); *Kinet. Catal.* (English translation), **20**, 256–259.
482. Harrison, P. G. and Thornton, E. W. (1978), 'Tin oxide surfaces. Part 9. IR study of the adsorption of CO, NO and CO + NO mixtures on tin(IV) oxide gels containing ion-exchanged Cr³⁺, Mn²⁺, Fe³⁺, Co²⁺, Ni²⁺ and Cu²⁺', *J. Chem. Soc., Faraday Trans. 1*, **74**, 2703–2713.
483. Rebenstorf, B. (1977), 'Preparation and reactions of a coordinatively unsaturated surface compound of Co(II) on silica gel', *Acta Chem. Scand., Ser. A*, **31**, 208–221.
484. Scarano, D., Spoto, G., Bordiga, S., Coluccia, S. and Zecchina, A. (1992), 'CO adsorption at 77 K on CoO–MgO and NiO–MgO solid solutions: A Fourier transform infrared study', *J. Chem. Soc., Faraday Trans. 1*, **88**, 291–296.
485. Zecchina, A., Scarano, D., Bordiga, S., Ricchiardi, G., Spoto, G. and Geobaldo, F. (1996), 'IR studies of CO and NO adsorbed on well characterized oxide single microcrystals', *Catal. Today*, **27**, 403–435.
486. Rebenstorf, B. and Larsson, R. (1981), 'IR studies of coordinatively unsaturated surface compounds on silica gel. VI. Carbonyl complexes of Cr(II) and Cr(III)', *Z. Anorg. Allgem. Chem.*, **478**, 119–138.
487. Bordiga, S., Lambertini, C., Geobaldo, F., Zecchina, A., Palomino, G. T. and Arean, C. O. (1995), 'FTIR study of CO adsorbed at 77 K on H-mordenite and alkali-metal-exchanged mordenites', *Langmuir*, **11**, 527–533.
488. Budneva, A. A., Pankrat'ev, Yu. D. and Davydov, A. A. (1991), 'Acceptor properties of the Al³⁺ ions in oxide catalysts containing aluminium', *Zh. Fiz. Khim.* (in Russian); *Russ. J. Phys. Chem.* (English translation), **65**, 35–37.
489. Morterra, C., Mognacca, G. and Del Favero, N. (1993), 'IR study of CO adsorption at 77 K on α -Al₂O₃', *Langmuir*, **9**, 642–645.

490. Borovkov, V. Yu., Typaev, A. P., Mal'tseva, N. V., Zubkov, S. A., Kazanskii, V. B. (1988), 'Influence of the preparation of γ -Al₂O₃ on the nature of active centers and catalytic properties in hydrocarbon conversions', *Kinet. Katal.* (in Russian); *Kinet. Catal.* (English translation), **29**, 494–497.
491. Davydov, A. A. and Shepotko, M. L. (1991), 'IR spectroscopic study of complexation of iron cations with NO or CO in oxide matrixes', *Koord. Khim.* (in Russian); *Coord. Chem.* (English translation), **17**, 1505–1509.
492. Guglielminotti, E. (1994), 'Spectroscopic characterization of the Fe/ZrO₂ system. I. CO adsorption', *J. Phys. Chem.*, **98**, 4884–4891.
- 493a. Zecchina, A., Garrone, E., Giotti, G. and Coluccia, E. (1975), 'On the chemistry of silica supported chromium ions. I. Characterization of samples', *J. Phys. Chem.*, **79**, 966–972;
- 493b. Zecchina, A., Garrone, E., Giotti, G. and Coluccia, E. (1975), 'On the chemistry of silica supported chromium ions. II. One-ligand complexes. Adsorption of CO, CO₂ and pyridine', *J. Phys. Chem.*, **79**, 972–978.
494. Eley, E., Rochester, C. and Scurrill, M. (1973), 'The polymerization of ethylene on chromium oxide catalysts. III. An infrared study of the adsorption of CO on active catalysts', *J. Catal.*, **29**, 20–30.
- 495a. Kawakami, H. and Yoshida, S. (1985), 'Quantum-chemical studies of alumina. 1. Brønsted acidity and basicity', *J. Chem. Soc., Faraday Trans. 2*, **81**, 1117–1127.
- 495b. Kawakami, H. and Yoshida, S. (1985), 'Quantum-chemical studies of alumina. 2. Lewis acidity', *J. Chem. Soc., Faraday Trans. 2*, **81**, 1129–1137.
496. Hadjiivanov, K. I. (1998), 'FT-IR spectroscopic study of NH₃ and CO adsorption and coadsorption on TiO₂ (rutile)', *Appl. Surf. Sci.*, **135**, pp. 331–338.
497. Hadjiivanov, K. I., Sauer, O., Lamotte, J. and Lavalley, J. C. (1994), 'FT-IR Spectroscopic study of NH₃ and CO adsorption and coadsorption on TiO₂ (anatase)', *Z. Phys. Chem.*, **187**, 281–300.
498. Smart, R. S. T. C., Slager, T. L., Little, L. H. and Greenler, R. G. (1973), 'Carbon monoxide adsorption on magnesium oxide', *J. Phys. Chem.*, **77**, 1019–1023.
499. Zecchina, A. and Stone, F. S. (1974), 'Reflectance spectra of CO chemisorbed on MgO and evidence for the formation of cyclic adsorbed species', *J. Chem. Soc., Chem. Commun.*, 582–584.
500. Morris, R. M., Kaba, R. A., Groshens, T. G., Klabunde, K. J., Baltisberger, R. J., Woosley, N. F. and Stenberg, V. I. (1980), 'Paramagnetic CO on MgO', *J. Am. Chem. Soc.*, **102**, 3419–3424.
501. Marchese, L., Coluccia, S., Martra, G., Giamello, E. and Zecchina, A. (1991), 'Novel dimeric species produced by CO interaction with surface F-type centers on magnesium doped magnesia: an IR study', *Mater. Chem. Phys.*, **29**, 437–445.
502. Coluccia, S., Baricco, M., Marchese, L., Martra, G. and Zecchina, A. (1993), 'Surface morphology and reactivity towards CO on MgO particles: FTIR and HATEM studies', *Spectrochim. Acta, Part A*, **49**, 1289–1298.
503. Tashiro, T., Ito, J., Sim, R.-B., Mijazawa, K., Hamada, E., Toi, K., Kobayashi, H. and Ito, T. (1995), 'Adsorption of CO on an MgO surface. Characterization of adsorbed species', *J. Phys. Chem.*, **99**, 6115–6122.
504. Kafafi, Z. H., Hauge, R. H., Billups, W. E. and Margreave, J. L. (1983), 'Carbon dioxide activation by lithium metal. I. Infrared spectra of Li⁺C₂O₄ and Li₂²⁺CO₂²⁻ in inert-gas matrices', *J. Am. Chem. Soc.*, **105**, 3886–3893.
505. Kafafi, Z. H., Hauge, R. H., Billups, W. E. and Margreave, J. L. (1983), 'Carbon dioxide activation by lithium metal. 2. Infrared spectra of M⁺CO₂⁻ and M₂²⁺CO₂²⁻ in argon and nitrogen matrices', *J. Inorg. Chem.*, **23**, 177–183.
506. Coluccia, S., Garrone, E., Guglielminotti, E. and Zecchina, A. (1981), 'IR study of CO adsorption on Ca and Sr oxides', *J. Chem. Soc., Faraday Trans. 1*, **77**, 1063–1073.
507. Shvets, V. A., Kuznetsov, A. V., Fenin, V. A. and Kazansky, V. B. (1985), 'On the nature of luminescence centres on MgO surfaces', *J. Chem. Soc., Faraday Trans. 1*, **81**, 2913–2919.
508. Zecchina, A., Scrano, D., Marchese, L., Coluccia, S. and Giamello, E. (1988), 'Defect centres on Mg-doped MgO surfaces', *Surf. Sci.*, **194**, 531–534.
509. Zecchina, A. and Stone, F. S. (1978), 'Reflectance spectra of CO adsorbed on alkaline earth oxides', *J. Chem. Soc., Faraday Trans. 1*, **74**, 2278–2292.
510. Babaeva, M. A. and Tsyganenko, A. A. (1987), 'Infrared spectroscopic evidence for the formation of carbonyl CO₂²⁻ ions in CO interaction with basic oxide surface', *React. Kinet. Catal. Lett.*, **34**, 9–14.
511. Lamotte, J., Lavalley, J. C., Lorenzelli, V. and Freund, E. (1985), 'IR spectroscopic study of the adsorption of H₂ and CO on tightly dehydroxylated thoria', *J. Chem. Soc., Faraday Trans. 1*, **81**, 215–221.
512. Loginov, A. Yu., Vydrin, S. N. and Bobolev, A. V. (1986), 'Forms of adsorbed CO and the structure of the surface layer of copper-containing rare-earth oxide catalysts', *Kinet. Katal.*, **28**, 1163–1169 (in Russian).
513. Ivleva, R. R., Zubkov, S. A., Borovkov, V. Yu. and Kazanskii, V. B. (1991), 'Diffuse reflectance IR spectroscopy study of the surface of Y, Er and Ho oxide. II. Carbon monoxide adsorption', *Kinet. Katal.* (in Russian); *Kinet. Catal.* (English translation), **32**, 417–422.

514. Davydov, A. A., Rubene, N. A. and Budneva, A. A. (1978), 'Study of the adsorption species of CO on the solid solution of CuO–MgO by the IR spectroscopy method', *Kinet. Katal.* (in Russian); *Kinet. Catal.* (English translation), **19**, 969–975.
- 515a. Zecchina, A., Spoto, G., Borello, E. and Giamello, E. (1984), 'Spectroscopic study of the CO adsorption on CoO–MgO solid solutions. 1. Sample characterization and CO adsorption on extended faces', *J. Phys. Chem.*, **88**, 2875–2881.
- 515b. Zecchina, A., Spoto, G., Borello, E. and Giamello, E. (1984), 'Spectroscopic study of the CO adsorption on CoO–MgO solid solutions. 2. CO adsorption on isolated cobalt ions located on edges and steps', *J. Phys. Chem.*, **88**, 2582–2591.
516. Tsyganenko, A. A., Denisenko, L. A., Zverev, S. M. and Filimonov, V. N. (1985), 'Infrared study of lateral interactions between carbon monoxide molecules adsorbed on oxide catalysts', *J. Catal.*, **94**, 10–15.
517. Tsyganenko, A. A., Denisenko, L. A. and Zverev, S. M. (1987), 'Spectral images of lateral interactions between molecules adsorbed on oxide surfaces', *Usp. Fotoniki.*, **9**, 96–125 (in Russian).
518. Woodruff, D. P., Hayden, B. E., Prince, K. and Bradshaw, A. M. (1982), 'Dipole coupling and chemical shifts in IRAS of CO adsorbed on Cu (110)', *Surf. Sci.*, **123**, 397–412.
519. Coluccia, S. (1989), 'Surface characterization of ionic microcrystalline systems by optical spectroscopies, in Morterra, C., Zecchina, A. and Costa, G. (Eds), *Structure and Reactivity of Surfaces*, Elsevier, Amsterdam, pp. 289–306.
520. Lokhov, Yu. A. and Davydov, A. A. (1979), 'Study of the state of transition metal cations on the surface of catalysts by IR spectroscopy of adsorbed test molecules (CO, NO). II. Reduced sites on the surface of copper-containing catalysts', *Kinet. Katal.* (in Russian); *Kinet. Catal.* (English translation), **20**, 1498–1505.
521. Lokhov, Yu. A. and Davydov, A. A. (1979), 'Study of the state of transition metal cations on the catalyst surfaces by IR spectroscopy of adsorbed probe molecules (CO, NO). I. Cu²⁺ ions on the surface of copper-containing catalysts', *Kinet. Katal.* (in Russian); *Kinet. Catal.* (English translation), **20**, 1235–1241.
522. Lokhov, Yu. A., Morozov, L. N., Davydov, A. A. and Kostrov, V. V. (1980), 'Study of the state of transition metal cations on the catalyst surfaces by IR spectroscopy of adsorbed probe molecules (CO, NO). III. Copper–alumina catalysts (CuO/Al₂O₃)', *Kinet. Katal.* (in Russian); *Kinet. Catal.* (English translation), **21**, 1295–1298.
523. Davydov, A. A. and Shepotko, M. L. (1990), 'Study of the copper cations state in CuCr₂O₄/Al₂O₃ catalysts by IR spectra of adsorbed carbon monoxide', *Teor. Eksp. Khim.* (in Russian); *Theor. Exp. Chem.* (English translation), **25**, 633–636.
524. Tikhov, S. F., Sadykov, V. A., Kryukova, G. N., Paukshtis, E. A., Popovskii, V. V., Starostina, T. G. (1992), 'Microstructural and spectroscopic investigations of the supported copper-alumina oxide system: nature of aging in oxidizing reaction media', *J. Catal.*, **134**, 506–524.
- 525a. Zecchina, A., Spoto, G., Coluccia, S. and Guglieminotti, E. (1984), 'Spectroscopic study of the adsorption of carbon monoxide on solid solutions of nickel oxide and magnesium oxide. 1. Standard samples', *J. Chem. Soc., Faraday Trans. 1*, **80**, 1875–1889.
- 525b. Zecchina, A., Spoto, G., Coluccia, S. and Guglieminotti, E. (1984), 'Spectroscopic study of the adsorption of carbon monoxide on solid solutions of nickel oxide and magnesium oxide. 2. Sample pretreated with hydrogen', *J. Chem. Soc., Faraday Trans. 1*, **80**, 1891–1901.
526. Anufrienko, V. F., Maksimov, M. G., Shinkarenko, V. G., Davydov, A. A., Lokhov, Yu. A., Bobrov, N. N. and Ione, K. G. (1977), 'The investigation of the state of cations in zeolites by spectroscopic techniques', in Boreksov, G. K. and Minachev, Kh. M. (Eds), *Application of Zeolites in Catalysis*, Akademiai Kiado, Budapest, pp. 109–152.
527. Rao, K. M., Scarano, D., Spoto, G. and Zecchina, A. (1988), 'CO adsorption on cobalt particles supported on MgO: an IR investigation', *Surf. Sci.*, **204**, 319–330.
528. Morterra, C., Aschieri, R., Bolis, V. and Borello, E. (1989), 'Adsorbate–adsorbate interactions at the surface of polycrystalline monoclinic zirconia, in Morterra, C., Zecchina, A. and Costa, G. (Eds), *Structure and Reactivity of Surfaces*, Elsevier, Amsterdam, pp. 703–712.
529. Morterra, C., Cerrato, G., Bolis, V., Lamberti, C., Ferroni, L. and Montanaro, A. (1995), 'Surface characterization of yttria-stabilized tetragonal ZrO₂. 2. Adsorption of CO', *J. Chem. Soc., Faraday Trans. 1*, **91**, 113–123.
530. Eischens, R. P., Francis, S. A. and Pliskin, W. A. (1956), 'The effect of surface coverage on the spectra of chemisorbed CO', *J. Phys. Chem.*, **60**, 194–201.
531. Sheppard, N. and Yates, D. J. (1956), 'Changes in the infrared spectra of molecules due to physical adsorption', *Proc. R. Soc. London, A*, **238**, 69–89.
532. Chang, C. C., Dixon, L. T. and Kokes, R. J. (1973), 'The nature of molecular hydrogen adsorbed on zinc oxide', *J. Phys. Chem.*, **77**, 2634–2639.
533. Maslov, S. Yu., Denisenko, L. A., Tsyganenko, A. A. and Filimonov, V. N. (1982), 'Infrared spectroscopic studies of dihydrogen adsorbed on oxide surfaces', *React. Kinet. Catal. Lett.*, **20**, 273–276.
534. Borovkov, V. Yu., Muzyka, I. S. and Kazanskii, V. B. (1982), 'The study of the adsorption of molecular and dissociative hydrogen on γ - and η -alumina at the temperature interval between 80–300 K by means of DRIR spectroscopy', *Dokl. AN SSSR* (in Russian); *Proc. AN USSR* (English translation), **265**, 109–113.

535. Zubkov, S. A., Borovkov, V. Yu. and Kazanskii, V. B. (1986), 'IR study of the low temperature adsorption and activation of D₂ on γ - and η -alumina', *Dokl. AN SSSR* (in Russian); *Proc. AN USSR* (English translation), **287**, 900–903.
536. Kazanskii, V. B., Borovkov, V. Yu. and Kustov, L. M. (1984), 'IR diffuse reflectance study of oxide catalysts. Use of molecular hydrogen adsorption as a test for surface active sites', in *Proceedings of the 8th International Congress on Catalysis*, Berlin, 1984, Verlag Chemie, Weinheim, Germany, Vol. III, pp. 3–14.
537. Zubkov, S. A., Borovkov, V. Yu. and Kazanskii, V. B. (1985), 'The study of the active sites for H₂ adsorption on Y₂O₃ by means of DRIR', *Dokl. AN SSSR* (in Russian); *Proc. AN USSR* (English translation), **285**, 382–385.
538. Folman, M. and Kozirovski, M. (1972), 'Induced infrared absorption in H₂, D₂ and HD adsorbed on higher surface area NaCl and CsI', *J. Colloid Interface Sci.*, **38**, 51–57.
539. Garrone, E., Kazansky, V. B., Kustov, L. M., Sauer, J., Senchenya, I. N. and Ugliengo, P. (1992), 'Spectroscopic and *ab initio* study of the interaction of molecular H₂ with the isolated silica hydroxyls and related systems', *J. Phys. Chem.*, **96**, 1040–1065.
540. Smudde, G. H., Slager, T. L., Coe, C. G., Macdougall, J. E. and Weigel, S. J. (1995), 'DRIFTS and Raman spectroscopy investigation of N₂ and O₂ adsorption on zeolites at ambient temperatures', *Appl. Spectrosc.*, **49**, 1747–1755.
541. Kustov, L. M., Alekseev, A. A., Borovkov, V. Yu. and Kazanskii, V. B. (1981), 'A study of the low temperature adsorption of molecular hydrogen on oxides by diffuse scattering IR spectroscopy', *Dokl. AN SSSR* (in Russian); *Proc. AN USSR* (English translation), **261**, 1374–1377.
542. Denisenko, L. A., Tsyganenko, A. A. and Filimonov, V. N. (1983), 'IR studies of low-temperature adsorption of H₂ on ZnO', *React. Kinet. Catal. Lett.*, **22**, 265–270.
543. Kustov, L. M., Borovkov, V. Yu. and Kazansky, V. B. (1984), 'Study of ethylene oligomerization on Brønsted and Lewis acidic sites of zeolites using diffuse reflectance IR spectroscopy', in Jacobs, P. A., Jaeger, N. I., Jiru, P., Kazanskii, V. B., and Schulz-Ekloff, G. (Eds), *Structure and Reactivity of Modified Zeolites*, Elsevier, Amsterdam, pp. 241–247.
544. Kustov, L. M., Kazansky, V. B. and Khodakov, A. Yu. (1994), 'Adsorption and polarization of molecular hydrogen and light paraffins on cationic forms of zeolites: IR-spectroscopic study', *Zeolite Sci. (Recent Progress and Discussions Studies in Surface Science and Catalysis)*, **98**, 217–218.
545. Sigl, M., Weitkamp, J. and Knozinger, H. (1997), 'Characterization of the acid properties of [Al]-, [Ga]- and [Fe]-HZSM-5 by low-temperature FTIR spectroscopy of adsorbed dihydrogen and ethylbenzene disproportionation', *Catal. Lett.*, **45**, 27–33.
546. Kustov, L. M., Bordiga, S. and Garrone, E. (1994), 'Comparative IR studies of low temperature H₂ and CO adsorption on Na-zeolites', *J. Chem. Soc., Faraday Trans. I*, **90**, 3367–3375.
547. Tonkov, M. V. (1970), *Spectroscopy of Interacting Molecules*, LGU, Leningrad.
548. Ito, T., Sekino, T., Mariai, N. and Tokuda, T. (1981), 'Hydrogen adsorption on magnesium oxide powders', *J. Chem. Soc., Faraday Trans. I*, **77**, 2181–2192.
549. Ito, T., Murakami, T. and Tokuda, T. (1983), 'Isotopic study of hydrogen adsorption on magnesium oxide powders', *J. Chem. Soc., Faraday Trans. I*, **79**, 913–924.
- 550a. Dent, A. L. and Kokes, R. J. (1969), 'Hydrogenation of C₂H₄ by ZnO I. Role of slow hydrogen chemisorption', *J. Phys. Chem.*, **73**, 3772–3780.
- 550b. Hussain, G. and Sheppard, N. (1990), 'A Fourier-transform spectral-ratioed reinvestigation of the infrared spectra from H₂ and D₂ adsorbed on ZnO at room temperature and 160°C', *J. Chem. Soc. Faraday Trans.*, **86**, 1615–1617.
551. Busca, G., Vaccari, A., Ceriotti, A., Lorinzelli, V. (1987), 'Heterolytic dissociation of H₂ on a high temperature methanol synthesis catalyst', *J. Catal.*, **108**, 491–494.
552. Davydov, A. A., Itina, G. V. and Kurina, L. M. (1991), 'Study of the adsorption of hydrogen on an oxide Zn–Cr–K alcohol-synthesis catalyst by thermal desorption and infrared spectroscopy', *Zh. Fiz. Khim.* (in Russian); *Russ. J. Phys. Chem.* (English translation), **65**, 389–392.
553. Jacob, K. H., Knozinger, E. and Benfer, S. (1994), 'Chemisorption of H₂ and H₂–O₂ on polymorphic zirconia', *J. Chem. Soc., Faraday Trans. I*, **90**, 2969–2975.
554. Trunschke, A., Hoang, D. L. and Lieske, H. (1995), 'In situ FTIR studies of high-temperature adsorption of hydrogen on zirconia', *J. Chem. Soc., Faraday Trans. I*, **91**, 4441–4444.
555. Zemlyanov, D. Yu., Smirnov, M. Yu. and Gorodetskii, V. V. (1997), 'HREELS characterization of hydrogen adsorption states on the Pt (100)-(hex) and (1 × 1) surfaces', *Catal. Lett.*, **43**, 181–187.
556. Ho, W., DiNardo, N. J. and Plummer, E. W. (1980), 'Angle resolved and variable-impact energy electron excitation spectroscopy of molecules adsorbed on surfaces', *Vac. Sci. Technol.*, **17**, 134–152.
- 557a. Busca, G. (1990), 'IR spectra of hydrogen adsorbed on solids', *J. Mol. Struct.*, **218**, 363–368.
- 557b. Busca, G. (1989), 'FT-IR spectroscopic study of the adsorption of hydrogen on chromia and on some metal chromates', *J. Catal.*, **120**, 303–313.
558. Baro, A. M. and Erley, W. (1981), 'The chemisorption of hydrogen on a (110) iron crystal studied by vibrational spectroscopy (EELS)', *Surf. Sci.*, **112**, L759–L764.

559. Karisson, P. A., Martensson, A. S., Andersson, S. and Nordlander, P. (1986), 'Vibrational motion of hydrogen atoms chemisorbed on Ni (100)', *Surf. Sci.*, **175**, L759–L766.
560. Martensson, A. S., Nyberg, C. and Andersson, S. (1988), 'Adsorption of H₂ on a stepped nickel surface', *Surf. Sci.*, **205**, 12–24.
- 561a. Richter, L. J., Gurney, B. A. and Ho, W. (1987), 'The influence of adsorbate–adsorbate interactions on the surface structure: The coadsorption of carbon monoxide and hydrogen on Rh (100)', *J. Chem. Phys.*, **86**, 477–485.
- 561b. Richter, L. J., Gurney, B. A., Sethna, J. P. and Ho, W. (1988), 'EELS of H adsorbed on Rh (100): Interpretation of overtone spectra as two-phonon bound states', *Phys. Rev. B*, **38**, 10403–10405.
562. Nyberg, C. and Tengstal, C. G. (1983), 'Vibrational interaction between hydrogen atoms adsorbed on Pd (100)', *Phys. Rev. Lett.*, **50**, 1680–1685.
563. Conrad, H., Scala, R., Stenzel, W. and Unwin, R. (1984), 'Adsorption of hydrogen and oxygen on Ru (001)', *J. Chem. Phys.*, **81**, 6371–6378.
564. Shi, H. and Jacobi, K. (1994), 'Hydrogen vibrations on the Ru (001) surface revisited', *Surf. Sci.*, **313**, 289–298.
565. Mate, C. M. and Somorjai, G. A. (1986), 'Delocalized quantum nature of hydrogen adsorbed on the Rh (111) crystal surface', *Phys. Rev. B*, **34**, 7417–7420.
566. Chakarov, D. V. and Marinova, T. S. (1988), 'Interaction of H₂ with Ir (111) and Ir (110) surfaces', *Surf. Sci.*, **204**, 147–160.
567. Conrad, H., Kordesch, M. E., Scala, R. and Stenzel, W. (1986), 'Surface resonances on Pd (111)/hydrogen observed with HREELS', *J. Electron Spectrosc. Rel. Phenom.*, **38**, 289–298.
568. Richter, L. J. and Ho, W. (1987), 'Vibrational spectroscopy of hydrogen on Pt (111): Evidence for universally soft parallel modes', *Phys. Rev. B*, **36**, 9797–9800.
569. Baro, A. M., Ibach, H. and Bruchman, H. D. (1979), 'Vibrational modes of hydrogen adsorbed on Pt (111): Adsorption site and excitation mechanism', *Surf. Sci.*, **88**, 384–398.
570. Reutt, J. E., Chabal, Y. J. and Christman, S. B. (1987), 'Hydrogen phonon spectra on transition metal surfaces: IR reflection–absorption investigations of Mo (100), W (100) and Pt (111)', *Electron Spectrosc. Rel. Phenom.*, **44**, 325–332.
571. Lee, G. and Plummer, E. W. (1995), 'Interaction of hydrogen with the Ag (111) surface', *Phys. Rev. B*, **51**, 7250–7261.
572. Richter, L. J., Germer, T. A. and Ho, W. (1988), 'Carbon monoxide adsorption-induced site changes: bridging hydrogen from CO and hydrogen on Rh (100)', *Surf. Sci.*, **195**, L182–L192.
573. McCash, E. M., Parker, S. F., Pritchard, J. and Chesters, M. A. (1989), 'The adsorption of atomic hydrogen on Cu (111) investigated by reflection–adsorption IR spectroscopy, electron energy loss spectroscopy and low energy diffraction', *Surf. Sci.*, **215**, 363–377.
574. Woods, J. P., Kuami, A. D., Erskine, J. L. and Wettle, F. W. (1987), 'Vibrational properties of β_1 -hydrogen and β_1 -D on W (001): EELS measurements and lattice dynamical calculations', *Phys. Rev. B*, **36**, 5848–5860.
575. Chabal, Y. J., Christman, S. B., Arrecis, J. J., Prybyla, J. A. and Estrup, P. J. (1987), 'Hydrogen-induced reconstruction on W (100) and Mo (100) by surface IR spectroscopy', *J. Electron Spectrosc. Rel. Phenom.*, **44**, 17–26.
576. Zubkov, S. A., Gagarin, S. G., Borovkov, V. Yu. and Kazansky, V. B. (1984), 'IR study of N₂ adsorbed on alumina', *Chem. Phys. Lett.*, **107**, 337–341.
577. Ravi, A., King, D. A. and Sheppard, N. (1968), 'Infrared spectra of nitrogen adsorbed on iridium', *Trans. Faraday Soc.*, **64**, 3358–3360.
578. Roev, L. M. (1972), 'Study of diatomic molecules adsorption over transition metals and their oxides by means of infrared spectroscopy and molecular orbitals methods', *D.Sc. Thesis* (in Russian), Kiev Institute of Physical Chemistry, Ukraine Academy of Science.
579. Roev, L. M., Batychko, S. V. and Rusov, M. T. (1970), 'IR spectroscopic investigation of the adsorption of nitrogen on nickel', *Kinet. Katal.* (in Russian); *Kinet. Catal.* (English translation), **12**, 1072–1074.
580. Borod'ko, Yu. G., Ivleva, I. N., Kachapina, L. M., Shilova, A. K. and Shilov, A. E. (1971), 'Reduction of nitrogen to hydrazine in a binuclear complex of iron', *J. Chem. Soc., Chem. Commun.*, 1185–1186.
581. Borod'ko, Yu. G. (1973), 'Spectroscopic investigation of molecular nitrogen complexes', *D.Sc. Thesis* (in Russian), Kurnakov Institute of General Chemistry, Chernogolovka.
582. Fouad, N. E., Knozinger, H., Ismail, H. M. and Zaki, M. I. (1991), 'Chromia on silica and alumina catalysts: chromia dispersion as determined by nitrogen adsorption measurements', *Z. Phys. Chem.*, **173**, 201–215.
583. Vedenev, V. I., Gurvich, L. V., Kondrat'ev, V. N. and Medvedev, V. A. (1962), *Energiya Dissotsiatsii Khimicheskikh Svyazey* (in Russian); (*The Dissociation Energy of Chemical Bonds*), Nauka, Moscow.
584. Weast, R. C. (Ed.) (1989), *Handbook of Chemistry and Physics*, 75th Edn. CRC Press, Boca Raton, FL.
585. Deng, F., Du, Y. R., Ye, C. H., Wang, J. Z., Ding, T. T. and Li, H. X. (1995), 'Acid sites and hydration behavior of dealuminated zeolite HZSM-5: A high-resolution solid state NMR study', *J. Phys. Chem.*, **99**, 15208–15214.

586. Smith, L., Cheethan, A. K., Morris, R. E., Marchese, L., Thomas, J. M. and Wright, P. A. (1996), 'On the nature of water bound to a solid acid catalyst', *Science*, **271**, 799–802.
587. Sauer, J. (1996), 'Probing catalysts with water', *Science*, **271**, 774–775.
588. Marchese, L., Chen, J. S., Thomas, J. M., Coluccia, S. and Zecchina, A. (1994), 'Brønsted, Lewis and redox centers on CoAPO-18 catalysts. 1. Vibrational modes of adsorbed water', *J. Phys. Chem.*, **98**, 13350–13356.
589. Borello, E., Della Gata, G., Fubini, B., Morterra, C. and Venturello, G. (1974), 'Surface rehydration of variously dehydrated Eta-alumina', *J. Catal.*, **35**, 1–10.
590. Coluccia, S., Marchese, L., Lavagnino, S. and Anpo, M. (1987), 'Hydroxyls on the surfaces of MgO powders', *Spectrochim. Acta, Part A*, **43**, 1573–1576.
591. Kittaka, S., Sasaki, T., Fukuhara, N. and Kato, H. (1993), 'Fourier-transform infrared spectroscopy of H₂O molecules on the Cr₂O₃ surface', *Surf. Sci.*, **282**, 255–261.
592. Munuera, G., Moreno, F. and Prieto, J. A. (1972), 'TPD of water adsorbed on anatase surface', *Z. Phys. Chem. (Leipzig)*, **78**, 113–117.
- 593a. Pozdnyakov, D. V. and Filimonov, V. N. (1973), 'Study of chemisorption of nitrogen oxide and dioxide on metal oxides with IR spectrometry', *Kinet. Katal.* (in Russian); *Kinet. Catal.* (English translation), **14**, 760–766.
- 593b. Laane, J. and Olsen, J. R. (1986), 'Characterization of nitrogen oxides by vibrational spectroscopies, in *Progress in Inorganic Chemistry*, Lippard, S. J. (Ed.), v.27, pp. 465–513.
- 593c. Hadjiivanov, K. I. (2000), 'Identification of neutral and charged N_xO_y surface species by IR spectroscopy', *Catal. Rev.-Sci. Eng.*, **42**, 71–144.
594. Davydov, A. A., Lokhov, Yu. A. and Shchekochikhin, Yu. M. (1978), 'Study of nitrogen oxide interaction with a Cr₂O₃ surface with IR spectroscopy', *Kinet. Katal.* (in Russian); *Kinet. Catal.* (English translation), **19**, 673–680.
595. Glazneva, G. V., Davydov, A. A., Sazonova, I. S. and Shchekochikhin, Yu. M. (1978), 'IR study of interaction between nitrogen oxide and carbon monoxide on Fe₂O₃', *Kinet. Katal.* (in Russian); *Kinet. Catal.* (English translation), **19**, 997–1003.
596. Tsyganenko, A. A., Rodionova, T. A., Babaeva, M. A., Denisenko, L. A. and Filimonov, V. N. (1984), 'Study of the low-temperature adsorption of CO, NO and SO₂ on oxide surfaces by the infrared spectroscopy method', in Vozdvizenski, V. F. (Ed.) *Optical Spectra in Adsorption and Catalysis*, Institute of Organic Catalysis and Electrochemistry KAS Alma-Ata, Kazakhstan, pp. 123–139.
597. Roev, L. M. and Alekseev, A. V. (1966), 'IR spectra of nitrogen oxide molecules adsorbed on a series of transition metal oxides', in Filimonov, V. N., and Vilesov, V. I. (Eds.) *Elementary Photoprocesses in Molecules*, Nauka, Moscow, 346–359.
598. Andrews, L. S. and Pimentel, G. C. (1966), 'Infrared spectrum, structure and bonding of lithium nitroxide, LiON', *J. Chem. Phys.*, **44**, 2361–2371.
599. Tevault, D. E. and Andrews, L. (1973), 'Matrix infrared spectrum and evidence for photoisomerism of Li⁺(ON)⁻. Infrared spectrum of Li⁺(ON)²⁻ Li⁺', *J. Phys. Chem.*, **77**, 1640–1645.
600. Tevault, D. E. and Andrews, L. (1973), 'Matrix reactions of sodium, potassium, rubidium and cerium atoms with nitric oxide. Infrared spectra of the M⁺(NO)⁻ species', *J. Phys. Chem.*, **77**, 1646–1649.
601. Connelly, N. J. (1972), 'Recent developments in transition metal nitrosyl chemistry', *Inorg. Chim. Acta*, **6**, 47–89.
602. Primet, M., Che, M., Naccache, C., Mathieu, M. and Imelik, B. (1970), 'Etude par RPE et spectrometric infrarouge de l'adsorption de NO par le bioxyde de titane', *J. Chim. Phys., Physicochim. Biol.*, **67**, 1629–1635.
603. Niwa, M., Minami, T., Kodama, H., Hatorri, T. and Murakami, Y. (1978), 'Adsorption of nitric oxide on tin oxide', *J. Catal.*, **53**, 198–207.
604. Terenin, A. and Roev, L. (1959), 'Infrared spectra of adsorbed NO of transition metals, their salts and oxides', *Spectrochim. Acta*, **7**, 946–957.
605. Batychko, S. V., Rusov, M. T. and Roev, L. M. (1970), 'IR spectroscopic study of the nitric oxide adsorption on nickel', *Dokl. AN SSSR* (in Russian); *Proc. AN USSR* (English translation), **191**, 1309–1313.
606. Davydov, A. A. 'Influence of the magnesia basicity on the electronic state of Ni²⁺ ions in NiO–MgO solid solutions. IR spectra of adsorbed NO', (in preparation).
607. Serebryakova, N. V. and Sokolova, N. P. (1981), 'Study of the interaction of NO and NO₂ with rhenium surfaces by means of infrared spectroscopy', *Zh. Fiz. Khim.* (in Russian); *Russ. J. Phys. Chem.* (English translation), **51**, 652–655.
608. Serebryakova, N. V., Sokolova, N. P. and Spitsin, V. I. (1982), 'Chemisorption of CO and nitrogen oxides on highly dispersed technetium', *Dokl. AN SSSR* (in Russian); *Proc. AN USSR* (English translation), **262**, 1189–1192.
609. Peri, J. B. (1974), 'IR study of NO and CO adsorbed on Cr/Al₂O₃', *J. Phys. Chem.*, **78**, 588–594.
610. Chen, N. and Yang, R. T. (1995), 'Activation of nitric oxide by heteropoly compounds: surfaces of nitric oxide linkages in tungstophosphoric acid with Keggin units', *J. Catal.*, **157**, 76–86.

611. Yang, R. T. and Chen, N. (1994), 'A new approach to designation of NO using sorbent/catalyst without reducing gas: use of heteropoly compounds', *Ind. Eng. Chem. Res.*, **33**, 825–839.
612. Chen, N. and Yang, R. T. (1994), 'Spectroscopic determination of oxidation and coordination states of Mo cations in the reduced Mo/Al₂O₃ catalyst', *J. Catal.*, **146**, 306–309.
613. Portela, L., Grange, P. and Delmon, B. (1995), 'The adsorption of nitric oxide on supported Co–Mo hydrodesulfurization catalysts: A review', *Catal. Rev. Sci. Eng.*, **37**, 699–731.
614. Kazuaka, A. and Howe, R. F. (1980), 'Interaction of NO with supported chromium, molybdenum and tungsten catalysts', *J. Catal.*, **63**, 447–455.
615. Rosen, R. P., Segawa, K.-I., Millman, W. S. and Hall, W. K. (1984), 'Mo[CH₃CN]₄(NO)₂(BF₄)₂] as a model for NO on reduced MoO₃/Al₂O₃ catalysts', *J. Catal.*, **90**, 368–370.
616. Peri, J. B. (1982), 'Computerized infrared studies of Mo/Al₂O₃ and Mo/SiO₂ catalysts', *J. Phys. Chem.*, **86**, 1615–1622.
617. Millman, W. S. and Hall, W. K. (1979), 'Identification of catalytically active sites on reduced molybdena–alumina catalysts', *J. Phys. Chem.*, **83**, 427–428.
618. Naccache, C. and Ben Taarit, Y. (1973), 'Nature of NO and NO₂ adsorbed on chromium and nickel exchanged zeolites. ESR and IRS study', *J. Chem. Soc., Faraday Trans. 1*, **69**, 1475–1486.
619. Topsoe, N. and Topsoe, H. (1982), 'Adsorption studies of hydrodesulfurization catalysts. I. Adsorption study of NO adsorption on alumina-supported cobalt, molybdenum and cobalt–molybdenum catalysts in their calcined state', *J. Catal.*, **75**, 354–374.
620. Yuen, S., Chen, Y., Kubsh, J. E., Dumesic, J. A., Topsoe, N. and Topsoe, H. (1982), 'Metal oxide–support interactions in silica-supported iron oxide catalysts probed by NO adsorption', *J. Phys. Chem.*, **86**, 3022–3032.
621. Tanabe, K., Ikeda, H., Iizuka, T. and Hattori, H. (1979), 'Effect of supports on the acidity of molybdenum and iron catalysts for the reduction of NO with H₂', *React. Kinet. Catal. Lett.*, **11**, 149–154.
622. Kugler, E., Kokes, R. J. and Gruder, J. W. (1975), 'IR study of NO adsorbed on silica-supported chromia', *J. Catal.*, **36**, 142–151.
623. Kugler, E. L., Kadet, A. B. and Gruder, J. W. (1976), 'The nature of NO adsorption on chromia', *J. Catal.*, **41**, 72–81.
- 624a. Zecchina, A., Garrone, E., Morterra, C. and Coluccia, S. (1975), 'On the chemistry of silica-supported chromium ions; III. Two-ligand complexes. NO adsorption', *J. Phys. Chem.*, **79**, 978–983.
- 624b. Zecchina, A., Garrone, E., Morterra, C. and Coluccia, S. (1975), 'On the chemistry of silica-supported chromium ions; IV. Three-ligand complexes. Interaction of pyridine, ammonia, carbon monoxide and water with preadsorbed NO', *J. Phys. Chem.*, **79**, 984–988.
625. Murrell, J. N., Kettle, S. F. A. and Tedder, J. M. (1965), *Valence Theory*, Wiley, London.
626. Glushko, V. P. (Ed.) (1978), *Thermodynamic Properties of Individual Substances*, Nauka, Moscow.
- 627a. Attina, M., Cacace, F. and Yanez, M. (1987), 'Electrophilic aromatic nitration in the gas phase', *J. Am. Chem. Soc.*, **109**, 5092–5097.
- 627b. Titov, A. I. (1963), 'The free radical mechanism of nitration', *Tetrahedron*, **19**, 557–580.
628. Malysheva, L. V., Paukshtis, E. A. and Ione, K. G. (1995), 'Nitration of aromatics by nitrogen oxides on zeolite catalysts: comparison of reactions in the gas phase and solutions', *Catal. Rev. Sci. Eng.*, **37**, 179–226.
629. Goupil, J. M., Hemidy, J. F. and Cornet, D. (1982), 'Adsorption of NO₂ on modified Y zeolites', *Zeolites*, **2**, 47–50.
630. Nogin, A. V., Alekseev, A. V. and Filimonov, V. N. (1976), 'Investigation of adsorption of nitrogen oxides on the zeolites NaA, NaX and NaY by means of IR spectroscopy', *Zh. Fiz. Khim.* (in Russian); *Russ. J. Phys. Chem.* (English translation), **50**, 183–186.
631. Pietrzak, T. M. and Wood, D. E. (1970), 'EPR study of the hindered motion of NO₂ and CO₂ adsorbed in synthetic zeolites', *J. Phys. Chem.*, **53**, 2454–2459.
- 632a. Chao, C. C. and Lunsford, J. H. (1971), 'IR studies of the disproportionation reaction of NO on Y-type zeolites', *J. Am. Chem. Soc.*, **93**, 71–77.
- 632b. Chao, C. C. and Lunsford, J. H. (1971), 'Adsorption of NO on Y-type zeolites. A low-temperature infrared study', *J. Am. Chem. Soc.*, **93**, 6794–6800.
633. Imazuli, M., Kubota, S. and Isobe, T. (1971), 'An ESR study of NO adsorbed on silica gel surfaces', *Bull. Chem. Soc. Jpn.*, **44**, 3227–3229.
634. Ramis, G., Busca, G., Bregany, F. and Forzatti, F. (1990), 'FTIR study of the adsorption and coadsorption of NO, NO₂ and NH₃ on TiO₂ anatase', *Appl. Catal.*, **64**, 243–257.
635. Ramis, G., Busca, G., Lorenzelli, V. and Forzatti, F. (1990), 'FT-IR study of the adsorption and co-adsorption of NO, NO₂ and NH₃ on V/TiO₂ and the mechanism of selective reduction', *Appl. Catal.*, **64**, 259–278.
- 636a. Dines, T. J., Rochester, C. H. and Ward, A. M. (1991), 'IR and Raman study of the adsorption of NH₃, pyridine, NO and NO₂ on anatase', *J. Chem. Soc., Faraday Trans. 1*, **87**, 643–651.
- 636b. Dines, T. J., Rochester, C. H. and Ward, A. M. (1991), 'IR study of the reaction between nitrogen oxides and NH₃ on titania-supported vanadia catalysts', *J. Chem. Soc., Faraday Trans. 1*, **87**, 1473–1477.

637. Hadjiivanov, K. I., Klissurski, D. G. and Bushev, V. Ph. (1995), 'IR spectroscopic study of NO₂ adsorption on chromia', *J. Chem. Soc., Faraday Trans. 1*, **91**, 149–153.
638. Kancheva, M. M., Bushev, V. Ph. and Hadjiivanov, K. I. (1992), 'Nitrogen dioxide adsorption on deuterioxytated titania (anatase)', *J. Chem. Soc., Faraday Trans. 1*, **88**, 3087–3089.
- 639a. Hadjiivanov, K. I., Bushev, V. Ph., Kantcheva, M. M. and Klissurski, D. G. (1994), 'IR spectroscopy study of the species arising during NO₂ adsorption on TiO₂ (anatase)', *Langmuir*, **10**, 464–471.
- 639b. Bushev, V. Ph., Hadjiivanov, K. I., Kantcheva, M. M. and Klissurski, D. G. (1991), 'An IR Spectroscopic Study of NO + NH₃ Interaction on TiO₂ (anatase)', *Z. Phys. Chem.*, **173**, 217–225.
640. Jones, L. H., Swanson, B. I. and Agnew, S. F. (1985), 'IR studies of autoionization of thin films of dinitrogen tetroxide', *J. Chem. Phys.*, **82**, 4389–4390.
641. Takagi-Kawai, M., Soma, M., Onishi, T. and Tamaru, K. (1980), 'The adsorption and the reaction of NH₃ and NO_x on supported V₂O₅ catalyst. Effect of supported materials', *Can. J. Chem.*, **58**, 2132–2137.
642. Bertsch, J. and Habgood, H. W. (1963), 'An infrared spectroscopic study of the adsorption of water and carbon dioxide by the Linde molecular sieve X', *J. Phys. Chem.*, **67**, 1621–1628.
643. Ward, J. W. and Habgood, H. W. (1966), 'The infrared spectra of CO₂ adsorbed on zeolite X', *J. Phys. Chem.*, **70**, 1178–1182.
- 644a. Angell, C. L. (1966), 'Carbon dioxide adsorbed on Linde X and Y zeolites', *J. Phys. Chem.*, **70**, 2420–2431.
- 644b. Angell, C. L. and Sheffer, P. C. (1966), 'Carbon monoxide adsorption on zeolites', *J. Phys. Chem.*, **70**, 1413–1421.
- 645a. Peri, J. B. (1965), 'Nature of active sites and of adsorbed hydrocarbons in the polymerization of butene on silica-alumina', in *Proceedings of the 3rd International Congress on Catalysis, Amsterdam, 1964*, North-Holland, Amsterdam, 1965, pp. 1100–1112.
- 645b. Peri, J. B. (1966), 'IR study of the reaction of HCl with the surface of γ -Al₂O₃ and its effect on the surface acid sites', *J. Phys. Chem.*, **70**, 1482–1509.
- 645c. Peri, J. B. (1966), 'IR study of OH and NH₂ groups on the surface of a dry silica aerogel', *J. Phys. Chem.*, **70**, 2937–2945.
- 645d. Peri, J. B. (1966), 'IR study of the adsorption of CO₂, HCl and other molecules on 'acid' sites on dry silica-alumina and γ -alumina', *J. Phys. Chem.*, **70**, 3168–3179.
646. Davydov, A. A., Shepotko, M. L. and Budneva, A. A. (1994), 'IR-spectroscopic methods for studying the basic centers of the surfaces of oxides. Analysis of IR spectra of the adsorbed probe molecule CO₂ as a method for studying basic centres at the surfaces of oxides', *Kinet. Katal.* (in Russian); *Kinet. Catal.* (English translation), **35**, 299–306.
647. Fink, P. (1967), 'Emige beobachtungen uber die bildung von oberflachen-carboxylat structuren auf γ -Al₂O₃', *Z. Chem.*, **7**, 284–285.
648. Davydov, A. A., Schekochikhin, Yu. M. and Keier, N. P. (1969), 'IR-study of the mechanism of CO oxidation on Cr₂O₃', *Kinet. Katal.* (in Russian); *Kinet. Catal.* (English translation), **10**, 1337–1344.
649. Morterra, C., Coluccia, S., Ghiotti, G. and Zecchina, A. (1977), 'Infrared spectroscopic characterization of α -Al₂O₃ surface properties. Carbon dioxide adsorption', *Z. Phys. Chem. (Leipzig)*, **104**, 275–290.
650. Morterra, C., Emanuel, C., Cerrato, G. and Magnacca, G. (1992), 'IR study of some surfaces properties of boemite (γ -AlO₂H)', *J. Chem. Soc., Faraday Trans. 1*, **88**, 339–348.
651. Busca, G. and Lorinzelli, V. (1982), 'IR spectroscopic identification of species arising from reactive adsorption of carbon oxides on metal oxide surfaces', *Mater. Chem.*, **7**, 89–126.
- 652a. Deo, A. V., Dalla Lana, I. G. and Habgood, H. W. (1971), 'IR studies of the adsorption and surface reactions of H₂S and SO₂ on some aluminas and zeolites', *J. Catal.*, **21**, 270–276.
- 652b. Fiedorow, R., Dalla Lana, I. G. and Wanke, S. E. (1978), 'Adsorption of sulfur dioxide on heat treated γ -aluminas at room temperature', *J. Phys. Chem.*, **82**, 2474–2476.
- 653a. Forster, H. and Schuldt, M. J. (1975), 'IR spectroscopic study of the adsorption of H₂S on zeolites NaA and NaCaA', *Colloid. Interface. Sci.*, **52**, 380–385.
- 653b. Forster, H. and Schuldt, M. J. (1975), 'Infrarot-Bandenform adsorbierter molekule in hohbraumen von zeolithen des typs A', *Spectrochim. Acta, Part A*, **31**, 685–688.
654. Lechert, H. and Henning, H. J. (1971), 'Das verhalten der protonen- und der ²³Na-resonanz in zeolithen vom faujasit typ in abhangigkeit von der belegung mit schwefelwasserstoff', *Z. Phys. Chem. (Leipzig)*, **76**, 319–327.
655. Karge, H. G. and Rasko, J. (1978), 'Hydrogen sulfide adsorption on faujasite-type zeolites with systematically varied Si–Al ratios', *J. Colloid. Interface. Sci.*, **64**, 522–534.
656. Karge, H. G., Tower, R. W., Dudzik, Z. and George, Z. M. (1980), 'Claus reaction. Influence of electron-donor and related properties of activated alumina catalyst', in *New Horizons in Catalysis, Proceedings of the 7th International Congress on Catalysis, Tokyo, June 30–July 4, 1980*, Seiyama, T. and Tanabe, K. (Eds) *Studies in Surface Science and Catalysis*, v.7, Kodansha, Tokyo, Elsevier, Amsterdam, 1980, pp. 643–654.
657. Karge, H. G., Zhang, Y., Trevizan de Suarez, S. and Ziolk, M. (1984), 'Studies on the modified Claus reaction over alkaline faujasites by simultaneous infrared, kinetics and ESR measurements', in Jacobs, P. A., Jaeger, N. I., Jiru, P., Kazanskii, V. B., and Schulz-Ekloff, G. (Eds), *Structure and Reactivity of Modified Zeolites*, Elsevier, Amsterdam, pp. 49–59.

658. Tugioka, M., Nakayama, T., Uemichi, Y. and Kanazuka, T. (1990), 'Promotive effect of H₂S for hydrocarbon conversions over Na zeolites', *React. Kinet. Catal. Lett.*, **41**, 345–349.
659. Ziolk, M., Kujawa, J., Sauer, O. and Lavalley, G. C. (1995), 'Influences of H₂S adsorption on catalytic properties of metal oxides', *J. Mol. Catal., A*, **97**, 49–56.
660. Karge, H. G., Ziolk, M. and Lanieski, M. (1987), 'UV–Vis and infrared spectroscopic study of hydrogen sulfide adsorption on faujasite-type zeolites', *Zeolites*, **7**, 197–205.
661. Karge, H. G. (1992), 'Investigations of Claus catalysts and related phenomena on alumina and zeolites', in Viswana, B. and Pillai, C. N. (Eds), *Recent Developments in Catalysis. Theory and Practice*, Editions Technip, Paris, pp. 1–12.
662. Karge, H. G., Laniecki, M. and Ziolk, M. (1988), 'UV–Visible spectroscopic investigations of the modified Claus reaction on NaX zeolite catalysts', *J. Catal.*, **109**, 252–262.
663. Karge, H. G., Laniecki, M. and Ziolk, M. (1986), 'Combined UV and IR spectroscopic studies on the adsorption of SO₂ onto faujasite-type zeolites', in Murakami, Y., Iijima, A. and Ward, J. W. (Eds), *Proceedings of the 7th International Zeolite Conference. New Developments in Zeolite Science and Technology*, Tokyo, August 17–22, 1986, Elsevier, Amsterdam; Kodansha, Tokyo, pp. 617–622.
664. Khulbe, K. C., Mann, R. S. and Manoojian, A. (1985), 'An electron spin resonance study of SO₂ and H₂S over Na-Y zeolite', *Zeolites*, **5**, 2–3.
665. Davydov, A. A. and Dalla Lana, I. G., 'Chemistry, mechanism and kinetics of heterogeneous catalytic sulfur recovery from hydrogen sulfide' *Russ. Chem. Rev.*, (2003) in press.
666. Davydov, A. A., Shepotko, M. L. and Dalla Lana, I. G., 'The mechanism of reaction between H₂S and SO₂ on alumina', *Appl. Cat.* (2003) in press.
667. Slager, T. L. and Amberg, C. H. (1972), 'IR investigation of H₂S adsorption and decomposition on alumina and alumina supported molybdenum sulfide', *Can. J. Chem.*, **50**, 3416–3423.
668. Karge, H. G. and Dalla Lana, I. G. (1984), 'Infrared study of SO₂ adsorption on a Claus catalyst by selective poisoning of sites', *J. Phys. Chem.*, **88**, 1538–1543.
669. Lansford, J. H., Zingery, L. W. and Rosynek, M. P. (1975), 'Exposed aluminum ions as active sites on γ -alumina', *J. Catal.*, **38**, 179–188.
670. Deane, A. M., Griffiths, D. L., Lewis, I. A., Winter, J. A. and Tench, A. J. (1975), 'IR study of the interaction of H₂S and H₂O with MgO surface', *J. Chem. Soc., Faraday Trans. 1*, **71**, 1005–1012.
671. Lavalley, J. C., Travert, J., Laroche, D. and Saur, O. R. (1977), 'IR spectroscopic study of species formed by the adsorption of H₂S and some thiols on alumina', *Acad. Sci. (Paris), Ser. C*, **285**, 385–392.
672. Lavalley, J. C., Travert, J., Chevrean, T., Lamotte, J. and Saur, O. (1979), 'Infrared study of coadsorption of H₂S and CO₂ on alumina', *J. Chem. Soc., Chem. Commun.*, 146–152.
673. Lavalley, J.-C., Saad, M. A. B., Tripp, C. P. and Morrow, B. A. (1986), 'Comment on the adsorption of H₂S on alumina', *J. Phys. Chem.*, **90**, 980–985.
674. Lavalley, J. C., Lamotte, J., Saur, O., Saad, M. A. B., Tripp, C. and Morrow, B. A. (1985), 'Surface adsorbed species: infrared studies of SO₂ and H₂S adsorbed on oxides', *Proc. Soc. Photo-Opt. Instrum. Eng.*, **553**, 486–491.
675. Lavalley, J. C., Janin, A. and Preud'homme, J. (1981), 'SO₂ adsorption of hydroxylated alumina', *React. Kinet. Catal. Lett.*, **18**, 85–88.
676. Saur, O., Chevrean, T., Lamotte, J., Travert, J. and Lavalley, J.-C. (1981), 'Comparative adsorption of H₂S, CH₃SH and (CH₃)₂S on alumina', *J. Chem. Soc., Faraday Trans. 1*, **77**, 427–437.
677. Saad, M. A. B., Saur, O., Wang, Y., Tripp, C. P., Morrow, B. A. and Lavalley, J. C. (1995), 'Effect of sodium on the adsorption of SO₂ on Al₂O₃ and on its reaction with H₂S', *J. Phys. Chem.*, **99**, 4620–4625.
678. Datta, A. and Cavell, R. G. (1985), 'Claus catalysts. 2. An FTIR study of the adsorption of H₂S on the alumina catalysts', *J. Phys. Chem.*, **89**, 450–456.
679. Saussey, H., Lavalley, J. C., Ziolk, M. and Kujiawa, J. (1987), 'Activity of alumina impregnated with NaOH in the oxidation of hydrogen sulfide', in *Proceedings of the 6th International Symposium on Heterogeneous Catalysis*, Sofia, pp. 462–467.
680. Okamoto, Y., Hara, M. O., Maetzava, A., Imanaka, T. and Teranishi, S. (1986), 'H₂S adsorption on Al₂O₃ and MoO₃/Al₂O₃', *J. Phys. Chem.*, **90**, 2396–2407.
681. Desyov, I. V., Paukshtis, E. A. and Mashkina, A. V. (1990), 'Infrared spectroscopic studies of H₂S adsorption on γ -Al₂O₃', *React. Kinet. Catal. Lett.*, **41**, 85–88, 161–165.
682. Schoonheydt, R. A. and Lunsford, J. H. (1972), 'Infrared spectroscopic investigation of the adsorption and reactions of SO₂ on MgO', *J. Catal.*, **26**, 261–271.
683. Kasumov, F. B. (1992), 'The Claus reaction. V. Investigation of the reaction of H₂S and SO₂ with γ -Al₂O₃', *Kinet. Katal.* (in Russian); *Kinet. Catal.* (English translation), **33**, 374–380.
- 684a. Blyholder, G. and Bowen, D. O. (1962), 'IR spectra of sulphur compounds adsorbed on silica supported nickel', *J. Phys. Chem.*, **66**, 1288–1291.
- 684b. Blyholder, G. and Richardson, E. A. (1962), 'IR and volumetric data on the adsorption of NH₃, H₂O and other gases on activated iron(III) oxide', *J. Phys. Chem.*, **66**, 2597–2602.

685. Kasumov, F. B., Davydov, A. A. and Kerimov, I. Ya. (1991), 'Claus reaction. 1. Study of the H₂S interaction with a tin–molybdenum oxide catalyst by means of infrared spectroscopy', *Kinet. Katal.* (in Russian); *Kinet. Catal.* (English translation), **32**, 1187–1192.
686. Kasumov, F. B., Davydov, A. A. and Kerimov, I. Ya. (1991), 'Claus Reaction. 3. Study of the SO₂ interaction with a tin–molybdenum oxide catalyst surface by means of infrared spectroscopy', *Kinet. Katal.* (in Russian); *Kinet. Catal.* (English translation), **32**, 1425–1429.
687. Davydov, A. A. and Shepotko, M. L. (2003), 'Claus reaction. VI. Mechanism on Sn–Mo–O catalyst', *Kinet. Katal.* (in Russian) 44.
688. Beck, D. D., White, J. M. and Ratcliffe, C. T. (1986), 'Catalytic reduction of CO with hydrogen sulfide. 2. Adsorption of H₂O and H₂S on anatase and rutile', *J. Phys. Chem.*, **90**, 3123–3131.
689. Davydov, A. A. and Shepotko, M. L. (2003), 'Claus reaction. VIII. TiO₂ (anatase)', *Kinet. Katal.* (in Russian) (in preparation).
690. Dobrynkin, N. M., Davydov, A. A., Batygina, M. V. and Budneva, A. A. (1998), 'IR spectroscopic study interaction between H₂S and O₂ on V₂O₅/Al₂O₃ catalyst', *Zh. Fiz. Khim.* (in Russian); *Russ. J. Phys. Chem.* (English translation), **78**, 1027–1030.
691. Davydov, A. A. and Shepotko, M. L. 'Claus reaction. IX. V₂O₅/TiO₂' (in preparation).
692. Dudzik, Z. and George, Z. M. (1980), 'Electron donor properties of Claus catalysts. I. Influence of NaOH on the catalytic activity of silica gel', *J. Catal.*, **63**, 72–82.
- 693a. Steijns, M., Koopman, P., Nienwenhuijze, B. and Mars, P. (1976), 'The mechanism of catalytic oxidation of H₂S. II. The kinetics and mechanism of H₂S oxidation catalyzed by sulfur', *J. Catal.*, **42**, 87–95.
- 693b. Steijns, M., Koopman, P., Nienwenhuijze, B. and Mars, P. (1976), 'The mechanism of catalytic oxidation of H₂S. III. The ESR study of sulfur catalyzed oxidation of H₂S', *J. Catal.*, **42**, 96–102.
694. Ismailov, E. G., Shvets, V. A. and Kazanskii, V. B. (1987), 'Interaction of H₂S with the surface of the oxides, TiO₂, SnO₂ and ZnO', *Zh. Fiz. Khim.* (in Russian); *Russ. J. Phys. Chem.* (English translation), **61**, 1288–1292.
- 695a. Kolosov, A. K., Shvets, V. A., Chuvylkin, N. D. and Kazanskii, V. B. (1977), 'EPR study of S₂⁻ species on the surface of MoO₃/SiO₂ and MoO₃/Al₂O₃ catalysts', *J. Catal.*, **47**, 190–196.
- 695b. Kolosov, A. K., Shvets, V. A., Chuvylkin, N. D. and Kazanskii, V. B. (1978), 'ESR study of S₃⁻ anion radicals on the surface of supported MoO₃/MgO, WO₃/MgO and CrO₃/MgO catalysts', *J. Catal.*, **55**, 394–401.
696. Gur'yanova, E. N., Isaeva, E. S., Shifrina, R. R., Moshchenok, S. V., Chernoplekova, V. A. and Terent'ev, V. A. (1981), 'Coordination properties of SO₂', *Zh. Obshch. Khim.* (in Russian); *Russ. J. Gen. Chem.* (English translation), **51**, 1639–1644.
697. Ryan, R. R., Kubas, G. H. J., Moody, D. C. and Eller, P. G. (1981), 'Structure and bonding of transition metal–sulfur dioxide complexes', **46**, 47–100 (Berlin), *Struct. Bonding*.
698. Grundnes, J. and Christian, S. D. (1967), 'Solvent effects on strong charge-transfer complexes. I. Trimethylamine and sulfur dioxide in gas and in heptane', *J. Am. Chem. Soc.*, **90**, 2239–2245.
699. Sakaki, S., Sato, H., Imai, Y., Morokuma, K. and Ohkubo, K. (1985), 'Comparison of electronic structure, stereochemistry and coordinate bonds between Ni(0)–SO₂ complexes and non-metal SO₂ complexes. An MO study', *Inorg. Chem.*, **24**, 4538–4544.
700. Sass, C. S. and Ault, B. S. (1984), 'Matrix isolation infrared spectroscopic study of sulfur dioxide–amine complexes', *J. Phys. Chem.*, **88**, 432–440.
701. Laniecki, M., Ziolk, M. and Karge, G. (1987), 'Effect of water on the formation of HSO₃⁻ ions upon SO₂ adsorption onto faujasite-type zeolites', *J. Phys. Chem.*, **91**, 4–6.
702. Babaeva, M. A., Tsyganenko, A. A. and Filimonov, V. N. (1984), 'IR spectra of adsorbed SO₂', *Kinet. Katal.* (in Russian); *Kinet. Catal.* (English translation), **25**, 921–927.
- 703a. Goodsel, A. J., Low, M. J. D. and Takezawa, N. (1972), 'Reaction of gaseous pollutants with solids. II. IR study of sorption of SO₂ on MgO', *Environ. Sci. Technol.*, **6**, 268–273.
- 703b. Goodsel, A. J., Low, M. J. D. and Takezawa, N. (1971), 'IR study of the sorption of SO₂', *Environ. Sci. Technol.*, **5**, 1191–1195.
704. Kaneko, K. and Matsumoto, A. (1989), 'Role of surface defects in the chemisorption of NO and SO₂ on variable size crystalline α-FeOOH', *J. Phys. Chem.*, **93**, 8090–8095.
705. Shor, A. M., Dubkov, K. A., Rubaylo, A. I., Pavlenko, N. I., Sharonova, O. M. and Anshits, A. G. (1992), 'IR spectroscopic study of H₂O influence on SO₂ adsorption on TiO₂ surface', *J. Mol. Struct.*, **267**, 335–338.
706. Chang, C. C. (1978), 'Infrared studies of SO₂ on γ-Al₂O₃', *J. Catal.*, **53**, 374–381.
707. Datta, A., Cavell, R. G., Tower, R. W. and George, Z. M. (1985), 'Claus catalysts I. Adsorption of SO₂ on the alumina catalyst studied by FTIR and EPR spectroscopy', *J. Phys. Chem.*, **89**, 443–449.
708. Nam, S.-W. and Gavalas, G. R. (1989), 'Adsorption and oxidative adsorption of sulfur dioxide on γ-alumina', *Appl. Catal. A Gen.*, **55**, 193–213.
709. Berben, P. H., Kappers, M. J. and Geus, J. W. (1988), 'An FT-IR study of adsorption of sulfur dioxide on alpha- and gamma-alumina', *Mikrochim. Acta.*, **11**, 15–18.

710. Dalla Lana, I. G., Karge, H. G. and George, Z. M. (1993), 'Dissociative adsorption of sulfur dioxide on γ -alumina investigated by TPD and mass spectrometry', *J. Phys. Chem.*, **97**, 8005–8011.
711. Karge, H. G., Dalla Lana, I. G. and Trevizan de Suarez, S. (1984), 'On the mechanism of the catalytic reaction of H_2S with SO_2 over gamma-alumina', in *Proceedings of the 8th International Congress on Catalysis, Berlin 1984*, Verlag Chemie, Weinheim, Germany, 1984, 453–463.
712. Gutsze, A., George, Z., Dalla Lana, I. G. and Karge, H. G. (1988), 'Generation and reactivity of SO_2^- anion radicals on an alumina catalyst', in *Catalyst: Theory to Practice. Proceedings of the 9th International Congress on Catalysis*, Calgary, Canada, 1988, Phillips, M. J. and Ternan, M., (Eds.), The Chemical Institute of Canada, Ottawa, Ontario, 1988, 1791–1797.
713. Davydov, A. A. (1991), 'IR spectroscopic study of the synthesis of isocyanate complexes from NO and CO on catalysts containing transition metals', *Zh. Prikl. Spektrosk.* (in Russian); *J. Appl. Spectrosc.* (English translation), **54**, 458–463.
714. Alikina, G. M., Davydov, A. A., Sazonova, I. S. and Popovskii, V. V. (1985), 'IR spectroscopic studies of surface compounds in the reduction of NO by CO on supported Pt, Pd and Rh catalysts', *React. Kinet. Catal. Lett.*, **27**, 279–282.
715. Alikina, G. M., Davydov, A. A., Sazonova, I. S. and Popovskii, V. V. (1986), 'Influence of the composition of the reaction mixture $\text{NO} + \text{CO} + \text{O}_2$ on the catalytic properties and surface states of supported noble metals. I. $\text{Pt}/\gamma\text{-Al}_2\text{O}_3$ ', *Kinet. Katal.* (in Russian); *Kinet. Catal.* (English translation), **27**, 875–883.
716. Alikina, G. M., Davydov, A. A., Sazonova, I. S. and Popovskii, V. V. (1987), 'Influence of composition of the reaction mixture $\text{NO} + \text{CO} + \text{O}_2$ on the catalytic properties and surface states of supported noble metals. II. $\text{Pd}/\gamma\text{-Al}_2\text{O}_3$ ', *Kinet. Katal.* (in Russian); *Kinet. Catal.* (English translation), **28**, 418–426.
717. Alikina, G. M., Davydov, A. A., Sazonova, I. S. and Popovskii, V. V. (1987), 'Influence of composition of the reaction mixture $\text{NO} + \text{CO} + \text{O}_2$ on the catalytic properties and surface states of supported noble metals. III. $\text{Rh}/\gamma\text{-Al}_2\text{O}_3$. Comparison of results from studies of platinum, palladium and rhodium catalysts', *Kinet. Katal.* (in Russian); *Kinet. Catal.* (English translation), **28**, 655–664.
718. Solymosi, F., Volgyesi, L. and Rasko, J. (1980), 'The effects of different supports on the formation and reactivity of surface isocyanate on Pd, Ir, Ru and Rh', *Z. Phys. Chem. (Leipzig)*, **120**, 79–87.
719. Solymosi, F., Volgyesi, L. and Sarkani, J. (1978), 'The effect of the support on the formation and stability of surface isocyanate on platinum', *J. Catal.*, **54**, 336–344.
720. Lorimer, D. and Bell, A. (1979), 'Reduction of NO by CO over a silica supported platinum catalyst: IR and kinetic studies', *J. Catal.*, **59**, 223–238.
721. Solymosi, F. and Bansagi, T. (1979), 'IR spectroscopic study of the adsorption of isocyanic acid', *J. Phys. Chem.*, **83**, 552–553.
722. Maki, A. and Decius, J. C. (1959), 'Vibrational spectrum of cyanate ion in various alkali halide lattices', *J. Chem. Phys.*, **31**, 772–776.
723. Davydov, A. A. and Bell, A. (1977), 'An IR study of NO and CO adsorption on a silica-supported Ru catalyst', *J. Catal.*, **49**, 345–355.
724. Dalla Betta, R. A. and Shelef, M. (1976), 'Isocyanates from the reaction of NO and CO on supported noble-metal catalysts', *J. Mol. Catal.*, **1**, 431–434.
725. Unland, M. (1973), 'Isocyanate intermediates in the reaction of $\text{NO} + \text{CO}$ over a $\text{Pt}/\text{Al}_2\text{O}_3$ catalyst', *J. Phys. Chem.*, **77**, 1952–1956.
726. Arai, H. and Tominaga, H. (1976), 'An IR study of nitric oxide and carbon monoxide adsorbed on rhodium–alumina catalyst', *J. Catal.*, **43**, 131–142.
727. Solymosi, F. and Sarkany, J. (1979), 'An infrared study of the surface interaction between NO and CO on a $\text{Rh}/\text{Al}_2\text{O}_3$ catalyst', *Appl. Surf. Sci.*, **3**, 68–82.
728. Matyshak, V. A., Gazarov, R. A., Panchshnyi, V. I. and Kadushin, A. A. (1988), 'Influence of O_2 on the interaction of CO and NO over supported Pt, Rh and Pt–Rh catalysts', *Kinet. Katal.* (in Russian); *Kinet. Catal.* (English translation), **29**, 1389–1392.
729. Rasko, J. and Solymosi, F. (1984), 'NO + CO interaction and NCO formation on PdY zeolites studied by IR spectroscopy', *J. Chem. Soc., Faraday Trans. 1*, **80**, 1841–1845.
730. Rasko, J. and Solymosi, F. (1981), 'IR spectroscopic study of the formation and stability of intermediate species on some unsupported noble metals', *J. Catal.*, **71**, 219–222.
731. Corte, R. J., Schmidt, L. D. and Sexton, B. A. (1981), 'The electron energy loss spectrum of isocyanic acid on the Pt (111) surface', *J. Catal.*, **67**, 387–391.
- 732a. Solymosi, F. and Rasko, J. (1977), 'An infrared spectroscopic study of the formation of isocyanates on $\text{Ru}/\text{Al}_2\text{O}_3$ ', *J. Catal.*, **49**, 240–243.
- 732b. Solymosi, F. and Rasko, J. (1980), 'An IR study on the formation of isocyanate in the $\text{NO} + \text{CO}$ reaction on supported Ir catalyst', *J. Catal.*, **63**, 217–225.
- 732c. Solymosi, F. and Rasko, J. (1980), 'An infrared study of CO and NO adsorption on alumina-supported iridium catalyst', *J. Catal.*, **62**, 253–263.
- 732d. Solymosi, F. and Rasko, J. (1977), 'Formation of isocyanate surface complexes on $\text{Pt}/\text{Al}_2\text{O}_3$ catalysts', *J. Catal.*, **46**, 297–307.

733. Grill, C. M. and Gonzalez, R. D. (1980), 'Infrared study of the adsorption of CO and NO on silica-supported Pd and Pt-Pd', *J. Phys. Chem.*, **84**, 873–882.
734. Hyde, E. A., Rudham, R. and Rochester, C. N. (1984), 'Infrared study of the interaction between NO and CO on Rh/Al₂O₃ catalysts', *J. Chem. Soc., Faraday Trans. 1*, **80**, 531–547.
735. Olah, G. A., Prokash, G. K. S. and Somer, J. (1985), *Superacids*, Wiley, New York.
736. Barthomeuf, D. (1991), 'Intrinsic Lewis acid strengths for main group elements', *Studies Surf. Sci. Catal.*, **65**, 157–174.
737. Luo, Y. R. and Benson, S. W. (1991), 'Intrinsic Lewis acid strengths for main-group elements. A new electronegative scale', *Inorg. Chem.*, **30**, 1676–1677.
738. Umansky, B. S. and Hall, W. K. (1990), 'The spectrophotometric study of the acidity of some solid acids', *J. Catal.*, **124**, 97–108.
739. Kazansky, V. B. (1977), 'New data on the nature of the transition state in heterogeneous acid catalysis', *Kinet. Katal.* (in Russian); *Kinet. Catal.* (English translation), **18**, 966–981.
740. Kazansky, V. B., Gritscov, A. M., Andreev, V. M. and Zhidomirov, G. M. (1978), 'A spectroscopic study of proton transfer in heterogeneous acidic catalysis', *J. Mol. Catal.*, **4**, 135–151.
741. Fejes, P., Forster, H., Kiricsi, I. and Seebode, J. (1982), 'Frequencies, anharmonicities and dissociation energies of OH groups in H-mordenite', *React. Kinet. Catal. Lett.*, **20**, 241–247.
742. Rouxhet, R. G. and Sempels, R. E. (1974), 'Hydrogen bond strengths and acidities of hydroxyl groups on silica-alumina surfaces and in molecules in solution', *J. Chem. Soc., Faraday Trans. 1*, **70**, 2021–2032.
743. Iogansen, A. V. (1971), 'Fermi resonance and structure of the $\nu(\text{A-H})$ bands in complexes with hydrogen bonds I. Expected picture', *Opt. Spektrosk.*, **3**, 328–331.
744. Odinokov, S. E., Mashkovsky, A. A., Glazunov, V. P., Iogansen, A. V. and Rassadin, B. V. (1976), 'Spectral manifestations of intermolecular and interionic hydrogen bonding in adducts of various acids with pyridine', *Spectrochim. Acta, Part A*, **32**, 1355–1363.
- 745a. Hair, M. and Hertl, W. (1970), 'Acidity of surface hydroxyl groups', *J. Phys. Chem.*, **74**, 91–94.
- 745b. Arnett, E. M. 'Problems of modern physical chemistry', *M. Mir.*, 1967.
- 745c. Paukshtis, E. A., Karakchiev, L. G. and Kotsarenko, N. S. (1979), 'IR-spectroscopic investigation of the formation of strong hydrogen bonds and mechanism of proton transfer during the adsorption of bases on the surface of zeolite HNaY', *Kinet. Katal.*, **20**, 198–201.
- 745d. Paukshtis, E. A., Karakchiev, L. G. and Kotsarenko, N. S. (1979), 'The effect of basicity of adsorbed molecules and the proton-donor capacity of the hydroxyl groups of catalyst surface on the formation of a hydrogen bond', *Kinet. Katal.*, **20**, 202–206.
746. Morterra, C., Cerrato, G., Emanuel, C. and Bolis, V. (1993), 'On the surface acidity of some sulfate-doped ZrO₂ catalysts', *J. Catal.*, **142**, 349–367.
747. Goncharova, O. I., Paukshtis, E. A., Yur'eva, T. M. and Yurchenko, E. N. (1986), 'Acid properties of applied HPCs of molybdenum by the method of IR spectroscopy', *Kinet. Katal.* (in Russian); *Kinet. Catal.* (English translation), **27**, 463–469.
748. Davydov, A. A. and Efremov, A. A. (1983), 'Study of hydrocarbons adsorption on oxide catalysts by IR spectroscopy. XIV. Interaction of propene with Sn-Mo oxide catalyst', *Kinet. Katal.* (in Russian); *Kinet. Catal.* (English translation), **24**, 1434–1441.
749. Hughes, T. R. and White, H. M. (1967), 'A study of the surface structure of decationized Y-zeolite by quantitative infrared spectroscopy', *J. Phys. Chem.*, **71**, 2192–2201.
750. Miyamoto, A., Yamazaki, Y., Inomata, M. and Murakami, Y. (1978), 'Determination of the number of V⁵⁺=O species on the surface of a V₂O₅ catalyst', *Chem. Lett.*, 1355–1358.
751. Makarova, M. A., Zholobenko, V. L., Al-Ghefailli, P. K., Thompson, N. E. and Dwyer, J. (1994), 'Brønsted acid sites in zeolites. FTIR study of molecular hydrogen as a probe for acidity testing', *J. Chem. Soc., Faraday Trans. 1*, **90**, 1047–1054.
752. Seanor, D. A. and Amberg, C. H. (1965), 'Infrared band intensities of adsorbed carbon monoxide', *J. Chem. Phys.*, **42**, 2967–2978.
753. Soltanov, R. I., Paukshtis, E. A. and Yurchenko, E. N. (1982), 'IR spectroscopic study of thermodynamic parameters of carbon monoxide interaction with the surfaces of certain oxide catalysts', *Kinet. Katal.* (in Russian); *Kinet. Catal.* (English translation), **23**, 164–170.
754. De Jong Gens, K. P. and Jorjasse, J. W. (1980), 'An IR spectroscopic study of the adsorption of carbon monoxide on silica-supported particles', *J. Appl. Surf. Sci.*, **7**, 273–287.
755. Davydov, A., Efremov, A. A. and Pankrat'ev, Yu. D. (1993), 'Heats of formation and thermodynamic characteristics of surface carbonyl complexes', *Zh. Fiz. Khim.* (in Russian); *Russ. J. Phys. Chem.* (English translation), **67**, 994–997.
756. Pel'menshikov, A. G. and Zhidomirov, G. M. (1983), Quantum-chemical study of the Lewis acid centers of oxide catalysts taking into account structural non-rigidity of the surface', in Davydov, A. A. (Ed.), *Proceedings of the 7th Soviet-Japanese Catalysis Seminar*, Irkutsk, June 1983, Institute of Catalysis Novosibirsk, pp. 52–56.
757. Davydov, A. A. (1992), 'Donor-acceptor properties of the cations of oxide surfaces', *Zh. Fiz. Khim.* (in Russian); *Russ. J. Phys. Chem.* (English translation), **66**, 3270–3275.

758. Bolis, V., Fubini, B., Garone, E., Giamello, E. and Morterra, C. (1989), A comparison between the Lewis acidity of non-d metal cations in Y-zeolites and on ionic surfaces', in Morterra, C., Zecchina, A. and Costa, G. (Eds), *Structure and Reactivity of Surfaces*, Elsevier, Amsterdam, pp. 159–166.
759. Efremov, A. A., Pankratiev, Yu. D., Davydov, A. A. and Boreskov, G. K. (1982), 'Heats of formation of π -complexes of ethylene, propylene and carbonyl complexes with Ti, Co, Ni, Zn, Ag and Cu cations on oxide catalysts', *React. Kinet. Catal. Lett.*, **20**, 87–91.
760. Auroux, A. and Gervasini, A. (1990), 'Microcalorimetric study of the acidity and basicity of metal oxide surfaces', *J. Phys. Chem.*, **94**, 6371–6379.
761. Barthomeuf, D. (1996), 'Basic zeolites: characterization and uses in adsorption and catalysis', *Catal. Rev. Sci. Eng.*, **38**, 521–570.
762. Barthomeuf, D. (1985), 'Importance of the acid strength in heterogeneous catalysis', in Imelik, B. (Ed.), *Catalysis by Acids and Bases*, Elsevier, Amsterdam, pp. 75–90.
- 763a. Barthomeuf, D. (1987), 'Zeolite acidity dependence of structure and chemical environment. Correlation with catalysis', *Mater. Chem. Phys.*, **17**, 49–71.
- 763b. Barthomeuf, D. (1988), 'Basicity and basic catalytic properties of zeolites', **18**, 553–575.
764. Scokart, P. O. and Rouxhet, P. G. (1980), 'Characterization of basicity of oxides through the IR study of pyrrole adsorption', *J. Chem. Soc., Faraday Trans. 1*, **76**, 1476–1489.
765. Rossi, P. F., Busca, G., Lorenzelli, V., Lion, M., and Lavalley, J. C. (1988), 'Characterisation of the surface basicity of oxides by means of microcalorimetry and FTIR spectroscopy of adsorbed hexafluoroisopropanol', *J. Catal.*, **109**, 378–386.
766. Binet, C., Jadi, A., Lamotte, J. and Lavalley, J. C. (1996), 'Use of pyrrole as an IR spectroscopic molecular probe in a surface basicity study of metal oxides', *J. Chem. Soc., Faraday Trans. 1*, **92**, 123–129.
767. Huang, M. and Kaliaguine, S. (1992), 'Zeolite basicity characterized by pyrrole chemisorption: an infrared study', *J. Chem. Soc., Faraday Trans. 1*, **88**, 751–758.
768. Davydov, A. A., Sokolovskii, V. D., Budneva, A. A., Rajput, A. M. and Buevskaya, O. V. (1990), Investigation of surface basic sites for catalysts of oxidative dimerisation of methane', in Viswanathan, B. and Pillai, C. N. (Eds), *Recent Developments in Catalysis Theory and Practice*, Technip Paris, pp. 431–440.
769. Paukshtis, E. A., Kotsarenko, N. S. and Karakchiev, L. G. (1979), 'Use of chloroform to study the proton-acceptor properties', *React. Kinet. Catal. Lett.*, **12**, 315–319.
770. Gordymova, A. A. and Davydov, A. A. (1983), 'Infrared spectra of chloroform adsorbed on γ -Al₂O₃ and identification of basic surface sites in oxides', *React. Kinet. Catal. Lett.*, **23**, 233–238.
771. Uvarova, E. B., Kustov, L. M. and Kazansky, V. B. (1995), 'Basicity of zeolites: IR-spectroscopic study using adsorbed molecular probes', in Beyer, H. K., Karge, H. G., Kiriesi, I. and Nagy, J. B. (Eds), *Catalysis by Microporous Materials*, Vol. 94, Elsevier, Amsterdam, pp. 254–261.
772. Davydov, A. A. (1995), 'Basic sites on the surface of oxide catalysts responsible for oxidative methane coupling', *Chem. Eng. Technol.*, **18**, 7–11.
773. Chen, L., Lin, Z., Xu, Z., Zang, T. and Liang, D. (1995), 'Interaction of methane with surfaces of silica, aluminas and HZSM-5 zeolite. A comparative FT-IR study', *Catal. Lett.*, **35**, 245–258.
774. Davydov, A. A. and Budneva, A. A. (1995), 'Study of hydrocarbons adsorption on oxide catalysts by IR spectroscopy. XX. Diffuse-reflectance spectra of paraffins adsorbed on simple oxides', *Kinet. Katal.* (in Russian); *Kinet. Catal.* (English translation), **36**, 781–786.
775. Muzyka, I. S., Zubkov, V. Yu., Borovkov, V. Yu. and Kazanskii, V. B. (1985), 'Study of methane adsorption over η -Al₂O₃ by means of diffuse reflectance IR-spectroscopy', *Dokl. AN SSSR* (in Russian); *Proc. AN USSR* (English translation), **284**, 391–394.
776. Zubkov, S. A., Borovkov, V. Yu. and Kazanskii, V. B. (1986), 'IR-spectroscopic study of low-temperature adsorption and deuterium (hydrogen) activation on γ - and η -Al₂O₃', *Dokl. AN SSSR* (in Russian); *Proc. AN USSR* (English translation), **287**, 900–903.
777. Omata, K., Aoki, A. and Fujimoto, K. (1990), 'Oxidative coupling of methane over CaO–MgO mixed oxide', *Catal. Lett.*, **4**, 241–244.
778. Philipp, R., Omata, K., Aoki, A. and Fujimoto, K. (1992), 'On the active site of MgO/CaO mixed oxide for oxidative coupling of methane', *J. Catal.*, **134**, 422–433.
779. Sinev, M. Yu., Filkova, D. T., Bychkov, V. Yu., Krylov, O. V. (1991), 'Basicity of oxide catalysts for oxidative condensation of methane', *Kinet. Katal.* (in Russian); *Kinet. Catal.* (English translation), **32**, 157–165.
780. Dunski, H., Jozwiak, W. K. and Sugier, P. A. (1994), 'Dehydroxylation of the surface of MgO by TPD', *J. Catal.*, **146**, 166–172.
781. Xu, Y., Yu, Lin, Cai, C., Huang, J. and Guo, X. (1995), 'A study of the oxidative coupling of methane over SrO–La₂O₃/CaO catalysts by using CO₂ as a probe', *Catal. Lett.*, **35**, 215–223.
782. Kaßner, R. and Baerns, M. (1996), 'Comparative characterization of basicity and acidity of metal oxide catalysts for the oxidative coupling of methane by a different method', *Appl. Catal. A: Gen.*, **139**, 107–115.
783. Davydov, A. A., Shepot'ko, M. L. and Budneva, A. A. (1995), 'Basic sites on oxide surfaces: their effect on catalytic methane coupling', *Catal. Today*, **24**, 225–230.

784. Pfau, A. and Schierbaum, K. D. (1990), 'The electron structure of stoichiometric and reduced CeO₂ surfaces: An XPS, UPS and HREELS study', *Surf. Sci.*, **323**, 1–2.
785. Henderson, B. and Wertz, J. E. (1977), *Defects in the Alkaline Earth Oxides*, Taylor & Francis, London.
- 786a. Hughes, A. E. and Henderson, B. (1972), in Crawford, P. and Slifkin, L. M. (Eds), *Defects in Crystalline Solids*, Plenum Press, New York.
- 786b. Spoto, G., Bordiga, S., Garrone, E., Ghiotti, G. and Zecchina, A. (1992), 'Cr(II) and Cr(III) ions grafted at internal nests of a pentasilic (silicalite): characterization and formation of polycarbonylic, polynitrosylic and mixed species by interaction with CO and NO', *J. Mol. Catal.*, **74**, 175–184.
787. Kuznetsov, A. V. and Shvets, V. A. (1990), 'The investigation of the interaction of CO with surface F_s⁺ and F_s⁰ sites of MgO by means of EPR, UV–Vis spectroscopy and luminescence', *Zh. Fiz. Khim.* (in Russian); *Russ. J. Phys. Chem.* (English translation), **64**, 717–723.
788. Che, M. and Giamello, E. (1994), 'Electron paramagnetic resonance: principles and applications to catalysis', in Imelik, B. and Vedrin, J. C. (Eds), *Catalyst Characterization. Physical Techniques for Solid Materials*, Plenum Press, New York, pp. 131–179.
789. Vymorokov, Yu. B. and Kotov, E. I. (1975), 'Spectral manifestations of the formation of cation radicals of benzidine in the adsorption of aniline on aluminasilica gel', *Kinet. Katal.* (in Russian); *Kinet. Catal.* (English translation), **16**, 491–496.
790. Meijers, S. and Ponec, V. (1996), 'An FTIR spectroscopic study of the selective oxidation of nitrobenzene by metal oxides', *J. Catal.*, **160**, 1–9.
791. Radtsig, V. A. and Bobyshev, A. A. (1986), 'Twofold coordinated Si and Ge atoms and "hydrogen". Paramagnetic centers in amorphous SiO₂ and GeO₂', *Phys. stat. solidi, b*, **133**, 621–627.
792. Bobyshev, A. A. and Radtsig, V. A. (1987), 'Silanone groups on the surface of mechanically activated silicon dioxide', *Kinet. Katal.* (in Russian); *Kinet. Catal.* (English translation), **29**, 638–647.
793. Berestetckaya, I. V. and Butyagin, P. Yu. (1981), 'Mechanicochemical activation of a magnesium oxide surface', *Dokl. AN SSSR* (in Russian); *Proc. AN USSR* (English translation), **260**, 361–366.
794. Davydov, A. A. and Shepot'ko, M. L. (1993), 'IR study of the changes in the properties of metal oxide surfaces during mechanical activation', *Proceedings In Come 93 v.1*, p. 137–141 1st International Conference on mechanochemistry, March 23–26, 1993, Košice-Slovakia Preprint B16, Vol. 1, 137–140.
795. Shepot'ko, M. L. and Davydov, A. A. (1997), 'IR spectroscopic study of the changes in the properties of the chromia surface upon mechanical activation', *Russian Journal of Physical Chemistry* (in Russian); *Kinet. Catal.* (English translation), **71**, 875–879.
- 796a. Mestl, G., Herzog, B., Schlogl, R. and Knozinger, H. (1995), 'Mechanically activated MoO₃. 1. Particle size, crystallinity, and morphology', *Langmuir*, **11**, 3027–3034.
- 796b. Mestl, G., Herzog, B., Schlogl, R. and Knozinger, H. (1995), 'Mechanically activated MoO₃. 2. Characterization of defect structures', *Langmuir*, **11**, 3035–3041.
- 796c. Mestl, G., Herzog, B., Schlogl, R. and Knozinger, H. (1995), 'Mechanically activated MoO₃. 3. Characterization by vibrational spectroscopy', *Langmuir*, **11**, 3795–3804.
797. Isupova, L. A., Aleksandrov, V. Yu., Popovskii, V. V., Balashov, V. A., Davydov, A. A., Budneva, A. A., and Kryukova, N. N. (1986), 'Effect of mechanical activation on the catalytic physical and chemical properties of copper oxide', *React. Kinet. Catal. Lett.*, **31**, 195–202.
798. Shvets, V. A. (1986), 'Application of electron paramagnetic resonance and ultraviolet spectroscopy to the study of coordination-unsaturated transition metal ions on the surfaces of catalysts', *Usp. Khim.* (in Russian); *Russ. Chem. Rev.* (English translation), **55**, 427–449.
799. Ballhausen, C. J. (1962), *Introduction to Ligand Field Theory*, McGraw-Hill, New York.
800. Bersuker, I. B. and Ablov, A. V. (1979), *Chemical Bonding in Complex Compounds* (in Russian), Khimiya, Leningrad.
801. Bobrov, N. N., Davydov, A. A., Maksimov, N. G., Ione, K. G. and Anufrienko, V. F. (1975), 'Peculiarities of the interaction of CO with copper cations in zeolites according to the data of the ESR and IR spectra', *Izv. AN SSSR, Ser. Khim.; Russ. Chem. Bull.* (English translation), 748–753.
802. Boretkov, G. K., Yurieva, T. M., Chigrina, V. A. and Davydov, A. A. (1978), 'Nature of the catalytic active sites of the copper containing catalysts for the WGS reaction', *Kinet. Katal.* (in Russian); *Kinet. Catal.* (English translation), **19**, 969–978.
803. Hartway, B. I. (1973), 'The evidence for "out of the plane" bonding in axial complexes of the copper(II) ion', *Struct. Bond.*, **14**, 49–67.
804. Huang, Y. Y. (1973), 'IR study of copper(I) carbonyls in Y zeolites', *J. Am. Chem. Soc.*, **95**, 6636–6640.
805. Naccashe, C. and Ben Taarit, C. (1971), 'Oxidizing and acidic properties of copper-exchanged Y zeolites', *J. Catal.*, **22**, 171–181.
- 806a. Davydov, A. A. (1991), 'Decomposition of NO on copper-containing catalysts', *Russ. J. Phys. Chem.*, **65**, 269–272.
- 806b. Davydov, A. A. (1978), 'IR study of the interaction of NO with CuY zeolites', *React. Kinet. Catal. Lett.*, **8**, 47–52.
807. Lokhov, Yu. A. and Davydov, A. A. (1980), 'Study of the state of transition-metal cations on the surfaces of adsorbed test molecules (CO, NO) V. Influence of the state of adsorption sites on the frequency of

- the stretching vibration of adsorbed carbon monoxide', *Kinet. Katal.* (in Russian); *Kinet. Catal.* (English translation), **21**, 1523–1529.
808. Jong, K. P., Geus, J. W. and Joziassse, J. (1980), 'An IR spectroscopic study of the adsorption of CO on silica-supported copper oxide', *J. Catal.*, **65**, 437–441.
809. Amara, M., Bettahar, M., Gengembre, L. and Olivier, D. (1987), 'Preparation, spectroscopic characterization and stability of silica supported copper(I) species', *Appl. Catal.*, **35**, 153–168.
810. Busca, G. (1987), 'FTIR study of the surface of copper oxide', *J. Mol. Catal.*, **43**, 225–237.
- 811a. Howard, J. and Nicol, J. M. (1988), 'FTIR studies of copper-containing Y-zeolites: Location of copper(I) carbonyl complexes', *Zeolites*, **8**, 42–150.
- 811b. Howard, J. and Nicol, J. M. (1989), 'FTIR studies of copper-containing Y zeolites', *J. Chem. Soc., Faraday Trans. 1*, **85**, 1233–1244.
812. Kohler, M. A., Cant, N. W., Wainwright, M. S. and Trimm, D. L. (1989), 'IR spectroscopic studies of carbon monoxide adsorbed on a series of silica supported copper catalysts in different oxidation states', *J. Catal.*, **117**, 188–201.
813. Vogt, F., Achkar, I., Wendland, K.-P., Hobert, H. and Meier, M. (1990), 'FTIR spectroscopic examination of the interaction of CO with Cu²⁺ ions in zeolites', *Z. Chem.*, **30**, 112–121.
814. Fu, Y., Tian, Y. and Lin, P. (1991), 'A low temperature IR spectroscopy study of selective adsorption of NO and CO on CuO/Al₂O₃', *J. Catal.*, **132**, 85–91.
815. Millar, G. J., Rochester, C. H. and Waugh, K. C. (1991), 'IR study of CO adsorption on reduced and oxidized silica supported catalysts', *J. Chem. Soc., Faraday Trans. 1*, **87**, 1467–1472.
816. Kantcheva, M., Hadjiivanov, K. I., Davydov, A. A. and Budneva, A. A. (1992), 'Low temperature CO adsorption on Cu²⁺/TiO₂ catalysts', *Appl. Surf. Sci.*, **55**, 49–55.
817. Davydov, A. A. (1994), 'Study of the state of copper in Cu/SiO₂ according to infrared spectra of adsorbed CO', *Zh. Fiz. Khim.* (in Russian); *Russ. J. Phys. Chem.* (English translation), **68**, 2045–2048.
818. Shepotko, M. L., Davydov, A. A. and Budneva, A. A. (1994), 'Investigation of the state of transition metal cations on the surfaces of catalysts using IR spectroscopy of adsorbed test molecules (CO and NO). X. Identification of the state of copper on the surface of Cu/SiO₂', *Kinet. Katal.* (in Russian); *Kinet. Catal.* (English translation), **35**, 612–615.
819. Padley, M. B., Rochester, C. H., Hutchings, G. J. and King, F. (1994), 'FTIR spectroscopic studies of thiophene, SO₂ and CO adsorbed on Cu/Al₂O₃ catalysts', *J. Catal.*, **148**, 438–452.
820. Padley, M. B., Rochester, C. H., Hutchings, G. J. and King, F. (1994), 'FTIR spectroscopic study of the effects of sulfur poison of CO adsorption on Cu/SiO₂ catalysts', *J. Chem. Soc., Faraday Trans. 1*, **90**, 203–206.
821. Itho, Y., Nishiyama, S., Tsuruya, K. and Masai, M. (1994), 'Redox behavior and mobility of copper ions in NaZSM-5 zeolites during oxidation', *J. Phys. Chem.*, **98**, 960–967.
822. Pieplu, T., Pognant, F., Vallet, A., Saussey, J. and Lavalley, J. C. (1995), 'Oxidation state of copper during the reduction of NO_x with propene on H-Cu-ZSM-5 in excess oxygen', *Studies Surf. Sci. Catal.*, **96**, 619–625.
823. Hadjiivanov, K. I., Klissurski, D., Ramis, G. and Busca, G. (1996), 'FTIR study of NO_x adsorption on a CuZSM-5 DeNO_x catalyst', *Appl. Catal., B*, **7**, 251–264.
824. Waqif, M., Lakhdar, M., Saur, O. and Lavalley, J. C. (1994), 'FTIR study of the influence of sulfate species on the adsorption of NO, CO and NH₃ on CuO/Al₂O₃ catalysts', *J. Chem. Soc., Faraday Trans. 1*, **90**, 2815–2820.
825. Chen, H. W., White, J. M. and Ekerdt, J. G. (1986), 'Electronic effect of supported copper catalysts', *J. Catal.*, **99**, 293–303.
826. Hadjiivanov, K. I., Klissurski, D., Kantcheva, M. and Davydov, A. A. (1991), 'State and localization of cobalt, nickel and copper ions adsorbed on titania (anatase)', *J. Chem. Soc., Faraday Trans. 1*, **87**, 907–911.
827. Marion, M. C., Garbowski, E. and Primet, M. (1990), 'Physicochemical properties of copper oxide loaded alumina in methane combustion', *J. Chem. Soc., Faraday Trans. 1*, **86**, 3027–3035.
828. Hierl, R., Knozinger, H. and Urbach, H. P. (1981), 'Surface properties and reduction behavior of calcined CuO/Al₂O₃ and CuO-NiO/Al₂O₃ catalysts', *J. Catal.*, **69**, 475–486.
829. Solomatin, G., Sobolevskii, V. S., Lafer, L. I. and Yakerson, V. I. (1979), 'IR spectra of catalysts and adsorbed molecules 26. State of water in the surface of copper-containing catalysts in the reaction of low-temperature carbon monoxide conversion', *Izv. Acad. Nauk. SSSR, Ser. Khim.* (in Russian); *Russ. Chem. Bull.* (English translation), 2437–2443.
830. Tarasov, A., Osmanov, Shvets, V. A. and Kazanskii, V. B. (1990), 'IR spectroscopic study of the adsorbed CO and NO states of Cu-Cr/Al₂O₃ catalyst surfaces and mechanism of reduction of NO by CO', *Kinet. Katal.* (in Russian); *Kinet. Catal.* (English translation), **31**, 645–649.
831. London, J. W. and Bell, A. T. (1973), 'IR spectra of CO, CO₂, NO, NO₂, N₂O and N₂ adsorbed on copper oxide', *J. Catal.*, **31**, 32–40.
832. Aubke, F. and Wang, C. (1994), 'Stabilization of unusual cations by very weakly basic fluoro anions', *Coord. Chem. Rev.*, **137**, 483–487.
833. Bruce, M. I. (1972), 'Complexes containing metal-carbon σ -bonds', *Organomet. Chem.*, **2**, 320–364.

- 834a. Huang, K. H. (1991), 'Transition metal bonding functions and their applications in catalytic absorptions and reactions. Part 1. Theoretical model', *J. Mol. Catal.*, **64**, 53–84.
- 834b. Huang, K. H. (1991), 'Transition metal bonding functions and their applications and reactions. Part 2. Micromechanism of CO chemisorption and a new concept of σ - π coordination', *J. Mol. Catal.*, **64**, 85–101.
- 834c. Huang, K. H. (1991), 'Transition metal bonding functions and their applications and reactions. Part 3. Effect of metal valence band and periodic trend of CO σ - π bonding functions of transition metals', *J. Mol. Catal.*, **64**, 103–117.
- 834d. Huang, K. H. (1991), 'Transition metal bonding functions and their applications and reactions. Part 4. Characterization of CO adsorption-bonding. IR spectra, surface species, population and adsorption heats', *J. Mol. Catal.*, **64**, 119–132.
835. Zecchina, A., Spoto, G. and Scarano, D. (1987), 'Infrared spectra of species adsorbed on dispersed systems', in King, D. A., Richardson, N. V., and Holloway, S. (Eds.), *Vibrations at Surfaces*, 1985, Elsevier, Amsterdam.
836. Boccuzzi, F., Chiotti, G. and Chiorino, A. (1985), 'CO adsorption on small particles of copper dispersed on microcrystalline ZnO', *Surf. Sci.*, **156**, 933–942.
837. Chiotti, G., Boccuzzi, F. and Chiorino, A. (1985), 'Surface characterization of copper/zinc oxide catalysts: IR with UV study of CO chemisorption', *Studies Surf. Sci. Catal.*, **21**, 235–46.
838. Zecchina, A. A., Bordiga, S., Salvalaggio, M., Spoto, G., Scarano, D. and Lamberti, C. (1998), 'Formation of nonplanar Cu^I(CO)₃ tricarbonyls on Cu^I-ZSM-5: An FTIR study at 80 K', *J. Catal.*, **173**, 540–542.
839. Hierl, R., Knozinger, H. and Urbach, H.-P. (1981), 'Surface properties and reduction behavior of calcined CuO/Al₂O₃ and CuO-NiO/Al₂O₃ catalysts', *J. Catal.*, **69**, 475–486.
840. Klier, K. (1984), 'Structure and function of real catalysts', *Appl. Surf. Sci.*, **19**, 267–97.
841. Davydov, A. A., Prudnikova, O. Yu. and Yur'eva, T. M. (1989), 'Investigation of the state of transition metal cations on the surfaces of catalysts using IR spectroscopy of adsorbed test molecules (CO and NO). VII. Copper-zinc-aluminum catalyst', *Kinet. Katal.* (in Russian); *Kinet. Catal.* (English translation), **30**, 477–480.
842. Anufrienko, V. F., Yur'eva, T. M., Hadzieva, F. S., Minyukova, T. P. and Burylin, C. Yu (1985), 'Spectroscopic studies of the state of Cu²⁺ ions in Cu-Zn-Al oxide catalysts', *React. Kinet. Catal. Lett.*, **27**, 201–205.
843. Boccuzzi, F., Chiotti, G. and Chiorino, A. (1985), 'Surface reactions of CO on metal-semiconductor systems: Cu/ZnO', *Surf. Sci.*, **162**, 361–374.
844. Hadjiivanov, K. I., Kantcheva, M. and Klissurski, D. (1996), 'IR study of CO adsorption on Cu-ZSM-5 and CuO/SiO₂ catalysts: σ and π components of the Cu⁺-CO bond', *J. Chem. Soc., Faraday Trans. 1*, **92**, 4595–4600.
845. Zecchina, A., Bordiga, S., Salvalaggio, M., Spoto, G., Scorrano, D. and Lamberti, C. (1998), 'Formation of nonplanar Cu^{I+} (CO)₃ tricarbonyls on Cu^{I+}-ZSM-5: An FTIR study at 80 K', *J. Catal.*, **173**, 540–542.
846. Boccuzzi, F., Chiorino, A., Martra, G., Gargano, M., Ravasio, N. and Carrozzini, B. (1997), 'Preparation, characterization, and activity of Cu/TiO₂ catalysts. I. Influence of the preparation method on the dispersion of copper in Cu/TiO₂', *J. Catal.*, **165**, 129–139.
847. Fridman, V. Z. and Davydov, A. A. (1993), 'Surface properties of the Ni-Cu-Cr oxide catalyst for dehydrogenative hydrolysis of amines', *Izv. Acad. Nauk. SSSR, Ser. Khim.* (in Russian); *Russ. Chem. Bull.* (English translation), **42**, 288–291.
848. Bianchi, D., Chafik, T., Khalfallah, M. and Teichner, S. J. (1994), 'Intermediate species on zirconia-supported methanol aerogel catalysts. III. Adsorption of carbon monoxide on copper-containing solids', *Appl. Catal. A: Gen.*, **112**, 57–73.
849. Giotti, G., Boccuzzi, F. and Chiorino, A. (1985), 'Spectroscopic evidence for a new surface carbonyl species on a Cu/ZnO catalyst', *J. Chem. Soc., Chem. Commun.*, 1012–1014.
850. Boksha, O. I. and Grum-Gruzimailo, S. V. (1972), *Investigation of Optical Spectra of Crystals with the Ions of Iron group metals at Room and Lower temperatures* (in Russian), Nauka, Moscow.
851. Garbowski, E., Kadratoff, Y., Mathieu, M. V. and Imelik, B. (1972), 'Etude par spectrometric ultraviolette de zeolithes de type faujasite content des ions Ni²⁺', *J. Chim. Phys., Phys. Chim. Biol.*, **69**, 1386–1389.
852. Klier, K. and Ralek, M. (1968), 'Spectra of synthetic zeolites containing transition metal ions. II. Ni²⁺ ions in type A Linde molecular sieves', *J. Phys. Chem. Solids*, **29**, 951–959.
853. Reley, P. E. and Seff, K. (1972), 'Three-coordinate Co(II). The crystal structure of fully dehydrated, partially-Co(II)-exchanged zeolite A', *J. Chem. Soc., Chem. Commun.*, 1287–1288.
854. Yamagida, R. Y., Vance, T. B. and Seff, K. (1973), 'Three- and five-coordinate manganese(II) in zeolite A', *J. Chem. Soc., Chem. Commun.*, 382–383.
855. Bobrov, N. N., Boreskov, G. K., Davydov, A. A. and Ione, K. G. (1975), 'Influence of the state of nickel cations on catalytic properties of NiY zeolites. I. Catalytic properties of NiY zeolites in CO oxidation', *Izv. Acad. Nauk. SSSR, Ser. Khim.* (in Russian); *Russ. Chem. Bull.* (English translation), 24–29.
856. Galezot, P. and Imelik, B. (1973), 'Location of nickel ions in Y zeolites. I. Influence of thermal and exchange level on nickel positions', *J. Phys. Chem.*, **77**, 652–656.

857. Ione, K. G., Bobrov, N. N. and Davydov, A. A. (1975), 'Catalytic activity of nickel compounds of different dispersivity', *Kinet. Katal.* (in Russian); *Kinet. Catal.* (English translation), **16**, 1234–1240.
858. Martin, G. A., Primet, M. and Dalmon, J. A. (1978), 'Reactions of CO and CO₂ on Ni/SiO₂ above 373 K as studied by infrared spectroscopic and magnetic methods', *J. Catal.*, **53**, 321–330.
859. Peri, J. B. (1984), 'IR studies of Ni held at low concentrations on alumina supports', *J. Catal.*, **86**, 84–94.
- 860a. Orlova, L. B., Lokhov, Yu. A., Ione, K. G. and Davydov, A. A. (1979), 'Use of IR spectra of adsorbed CO to investigate the state of nickel in zeolites', *Izv. Acad. Nauk. SSSR, Ser. Khim.* (in Russian); *Russ. Chem. Bull.* (English translation), 1937–1941.
- 860b. Ione, K. G., Romannikov, V. N., Davydov, A. A. and Orlova, L. B. (1979), 'Peculiarity of the catalytic action of nickel in zeolites of type Y in hydrogenation reactions', *J. Catal.*, **57**, 126–135.
- 861a. Grabovski, E., Mathieu, M. V. and Primet, M. (1977), 'Study by UV spectrometry of the reduction of Ni(II) ions in different zeolites', *Chem. Phys. Lett.*, **49**, 247–250.
- 861b. Grabovski, E., Mathieu, M. V. and Primet, M. (1977), 'Formation of nickel(I) ions by hydrogen reduction of nickel(II) zeolites, Molecular Sieves', *ACS Symp. Ser.*, **40**, 281–289.
- 862a. Bonneviot, L., Olivier, D. and Che, M. (1983), 'Dimerization of olefins with nickel-surface complexes in X-type zeolites or on silica', *J. Mol. Catal.*, **21**, 415–430.
- 862b. Bonneviot, L., Legende, O., Kermarec, M., Olivier, D. and Che, M. (1990), 'Characterization by UV–Vis–NIR reflectance spectroscopy of the exchange sites of nickel on silica', *J. Colloid Interface Sci.*, **134**, 534–547.
- 862c. Kermarec, M., Oliver, D., Richard, M. and Che, M. (1982), 'Electron paramagnetic resonance and IR studies of the genesis and reactivity toward carbon monoxide of Ni⁺ ions in a NiCa-X zeolite', *J. Phys. Chem.*, **86**, 2818–2827.
- 862d. Cai, F. X., Lepetit, C., Kermarec, M., Oliver, D. and Che, M. (1987), 'Dimerization of ethylene into 1-butene over supported tailor-made nickel catalysts', *J. Mol. Catal.*, **43**, 93–116.
863. Kubelkova, L., Novakova, J., Jaeger, N. I. and Schulz-Ekloff, G. (1987), 'Characterization of nickel species at Ni/γ-Al₂O₃ and Ni/faujasite catalysts by carbon monoxide adsorption', *Appl Catal A:General*, **95**, 87–101.
864. Davydov, A. A. and Coville, N. (1995), 'States of cobalt and iron in catalysts supported on TiO₂ from data of diffuse reflectance IR spectra of adsorbed carbon monoxide', *Izv. Acad. Nauk. SSSR, Ser. Khim.* (in Russian); *Russ. Chem. Bull.* (English translation), **44**, 1866–1871.
865. Lapidus, A. L., Krylova, A. Yu., Kazanskii, V. B., Borovkov, V. Y., Zaitsev, A. V., Kozlova, G. V., Zuka, A., Ratkouski, I. and Yangalkova, M. (1991), 'Spectroscopic study of alkali promoted aluminocobalt catalysts for hydrocarbons synthesis from CO', *Izv. Acad. Nauk. SSSR, Ser. Khim.* (in Russian); *Russ. Chem. Bull.* (English translation), 2444–2449.
866. Prudnikova, O. and Davydov, A. A. (1987), 'Investigation of the state of transition metal cations on the surface of catalysts using IR spectroscopy of adsorbed test molecules (CO and NO). XI. Copper–cobalt–aluminum catalyst', *Kinet. Katal.* (in Russian); *Kinet. Catal.* (English translation), **30**, 477–480.
867. Sato, K., Inoue, Y., Kojima, I., Miyazaki, E., and Yasumori, I. (1984), 'IR and X-ray photoelectron spectroscopy studies of CO adsorbed on silica supported cobalt catalysts', *J. Chem. Soc., Faraday Trans. 1*, **80**, 841–850.
868. Amsorge, J. and Forster, H. (1981), 'Transient IR spectroscopic investigation of surface carbonyl forms on a supported cobalt catalyst', *J. Catal.*, **68**, 182–185.
869. Zecchina, A., Sporto, G., Garrone, E. and Bossi, A. (1984) 'III. CO adsorption on aggregates of Co²⁺', *J. Phys. Chem.*, **88**, 2587–2591.
870. Ishchenko, O. B., Alekseeva, I. V., Zhdanova, K. P. and Schmidt, F. K. (1991), 'The mechanism of the interaction of CO with cobalt zeolite catalysts', *Zh. Fiz. Khim.* (in Russian); *Russ. J. Phys. Chem.* (English translation), **65**, 1200–1208.
871. Rao, K. M., Scarano, D., Sporto, G. and Zecchina, A. (1988), 'CO adsorption on Co particles supported on MgO: an IR investigation', *Surf. Sci.*, **204**, 319–330.
- 872a. Scorano, D., Zecchina, A., Sporto, G. and Geobaldo, V. (1995), 'CoO–ZnO solid solution as a model to investigate the CO–cation interaction: an FTIR and HRTEM study', *J. Chem. Soc., Faraday Trans. 1*, **91**, 4445–4450.
- 872b. Riva, R., Miessner, H., Del Piero, C., Reours, B. and Roy, M. (1998), 'Dispersion and reducibility of Co/SiO₂ and Co/TiO₂', in Parmaliano, A., Sanfilippo, D., Frusteri, F., Vaccari, A., Arena, F. (Eds), *Natural Gas Conversion. V, Studies Surf. Sci. Catal.*, **119**, pp. 203–208.
- 872c. Ledford, J. S., Houalla, M., Proctor, A. and Hercules, D. M. (1989), 'Influence of lanthanum on the surface structure and CO hydrogenation activity of supported cobalt catalysts', *J. Phys. Chem.*, **93**, 6770–77.
- 872d. Matsuzaki, T., Takeuchi, K., Hanaoka, T., Arakawa, H. and Sugi, Y. (1996), 'Hydrogenation of carbon monoxide over highly dispersed cobalt catalysts derived from cobalt(II) acetate', *Catal. Today*, **28**, 251–259.
- 872e. Kazansky, V. B., Zaitsev, A. V., Borovkov, V. Yu. and Lapidus, A. L. (1988), 'Infrared diffuse reflectance study of alkali promoted iron/alumina and cobalt/alumina Fischer–Tropsch catalysts prepared by decomposition of carbonyls', *Appl. Catal.*, **40**, 17–25.

- 872f. Fridriksen, G. R., Blekkan, E. A., Schanke, D. and Holmen, A. (1993), 'CO hydrogenation on supported cobalt catalysts studied by *in situ* FTIR-spectroscopy', *Ber. Bunsenges. Phys. Chem.*, **97**, 308–312.
- 872g. Sato, K., Inoue, Y., Kojima, I., Miyazaki, E. and Yasumori, I. (1984), 'Infrared and X-ray photoelectron spectroscopy studies of carbon monoxide adsorbed on silica-supported cobalt catalysts', *J. Chem. Soc., Faraday Trans. 1*, **80**, 841–850.
- 872h. Ducreux, O., Lynch, J., Rebours, R., Roy, M. and Chaumette, P. (1998), 'In situ characterization of cobalt-based Fischer–Tropsch catalysts: a new approach to the active phase', in Parmaliano, A., Sanfilippo, D., Frusteri, F., Vaccari, A., Arena, F. (Eds), *Natural Gas Conversion. V, Studies Surf. Sci. Catal.*, **119**, 125–130.
- 872i. Dees, M. J., Shido, T., Iwasawa, Y. and Ponec, V. (1990), 'Infrared studies of CO adsorbed on supported Pt–Co catalysts', *J. Catal.*, **124**, 530–540.
- 872j. Gopalakrishnan, R. and Viawanathan, B. (1984), 'Temperature-programmed desorption and infrared studies on the activation of carbon monoxide on cobalt surfaces', *J. Colloid Interface Sci.*, **102**, 370–378.
- 872k. Anderson, K. G. and Ekerdt, J. G. (1989), 'Hydrocarbon surface fragments over Co/SiO₂: an FTIR study', *J. Catal.*, **116**, 556–567.
- 872l. Xiao, F.-S., Fukuoka, A. and Ichikawa, M. (1992), 'Mechanism of formation of oxygenated compounds from CO + H₂ reaction over SiO₂-supported Ru–Co bimetallic carbonyl clusters-derived catalysts', *J. Catal.*, **138**, 206–222.
- 872m. Fredriksen, G. R., Blekkan, E. A., Schanke, D. and Holmen, A. (1995), 'CO hydrogenation over cobalt catalysts: FTIR and gravimetric studies', *Chem. Eng. Technol.*, **18**, 125–131.
- 872n. Heal, M. J., Leisegang, E. C. and Torrington, R. G. (1978), 'Infrared studies of carbon monoxide and hydrogen adsorbed on silica-supported iron and cobalt catalysts', *J. Catal.*, **51**, 314–325.
873. Jermyn, J. W., Johnson, T. J., Vansant, E. F. and Lunsford, J. H. (1973), 'Study of iron–nitrosil complexes formed in zeolites', *J. Phys. Chem.*, **77**, 2964–2969.
- 874a. Davydov, A. A. and Shepotko, M. L. (1991), 'IR spectroscopic study of iron cation complexation with NO and CO in an oxide matrix', *Koord. Khim.*, **17**, 1505–1509 (in Russian).
- 874b. Lox, E. S., Marin, G. B., De Grave, E. and Bussiere, P. (1988), 'Characterization of a promoted precipitated iron catalyst for Fischer–Tropsch synthesis', *Appl. Catal.*, **40**, 197–218.
- 874c. King, D. L. and Peri, J. B. (1983), 'An infrared study of nitric oxide chemisorption on alumina-supported iron and alkalinized iron Fischer–Tropsch catalysts', *J. Catal.*, **79**, 164–175.
- 874d. Banerjee, D. and Chakrabarty, D. K. (1992), 'Supported iron, cobalt and iron–cobalt bimetallic catalysts for Fischer–Tropsch synthesis: catalyst preparation and characterization', *Indian J. Tech.*, **30**, 81–84.
- 874e. Jorgensen, N. and Rochester, C. H. (1986), 'An infrared study of carbon monoxide adsorption on promoted and unpromoted iron', *Appl. Catal.*, **25**, 69–76.
- 874f. Jonston, C., Jorgensen, N. and Rochester, C. H. (1988), 'Volumetric and infrared studies of carbon monoxide adsorption on silica-supported iron catalysts characterized by thermogravimetric analysis and X-ray diffraction', *J. Chem. Soc., Faraday Trans. 1*, **84**, 309–319.
- 874g. Freund, C. M., Queeney, K. T. and Chen, D. A. (1999), 'Structure and reactivity of thin-film oxides and metals', *Appl. Surf. Sci.*, **142**, 99–105.
- 874h. Rao, K. R. P., Huggins, F. E., Huffman, G. P., Gormley, R. J., O'Brien, R. J. and Davies, B. H. (1996), 'Mössbauer study of iron Fischer–Tropsch catalysts during activation and synthesis hydrocarbons. Energy and fuels'. **10**, 546–551.
875. Texier, J., Hastrelter, J. J. and Hall, J. L. (1983), 'Spectroscopic configuration of the tetrahedral geometry of Ag(H₂O)₄⁺', *J. Phys. Chem.*, **78**, 4690–4693.
876. Hormes, J. and Happel, G. (1983), 'Inner shell excitation of matrix isolated silver', *J. Phys. Chem.*, **78**, 1758–1762.
877. Srdanov, V. I. and Pesic, D. S. (1981), 'Analysis of the E–X and C–X band system isotopically enriched Ag₂', *J. Mol. Spectrosc.*, **90**, 27–32.
878. Steinbruchel, Ch. and Gruen, D. M. (1981), 'Interactions of photoinduced diffusion and clustering of matrix isolated metal atoms', *Surf. Sci.*, **106**, 160–164.
879. Ozin, G. A. and Huber, H. (1978), 'Cryophotoclustering techniques for synthesizing very small naked silver clusters Ag_n of known size (where n = 2 – 5). The molecular metal cluster–bulk metal particle interface', *Inorg. Chem.*, **17**, 155–163.
880. Sahyun, M. R. V. (1980), 'Growth and properties of metal clusters', in *Proceedings of the 32nd Meeting of the Society of Chemical Physics*, Villeurbanne, September 24–28, 1979, Bourdon, J. (Ed.), Amsterdam, Elsevier, pp. 379–386.
881. Mitchell, S. A. Kenney-Wallace, G. A. and Ozin, G. A. (1983), 'Disilver: spectroscopy and photoproperties in rare-gas matrixes', *J. Am. Chem. Soc.*, **103**, 6030–6035.
882. Kreibig, U. (1978), 'Anomalous frequency and temperature dependence of the optical absorption of small gold particles', *Z. Phys.*, **31**, 39–44.
883. Fornasiero, D. and Griesser, F. (1987), 'Analysis of the vibrational absorption and SERS excitation spectra of silver sols', *J. Phys. Chem.*, **87**, 3213–3217.
884. Petrov, Yu. I. (1986), *Clusters and Small Particles* (in Russian), Nauka, Moscow.

885. Schoonheydt, R. A., Hall, M. B. and Lunsford, J. H. (1983), 'Silver clusters in zeolites: Fenske–Hall self-consistent field MO calculation', *Inorg. Chem.*, **22**, 3834–3839.
886. Pestryakov, A. N. and Davydov, A. A. (1994), 'Active sites of silver catalysts of methanol oxidation', *Kinet. Katal.* (in Russian); *Kinet. Catal.* (English translation), **35**, 279–281.
887. Noskova, S. P., Davydov, A. A., Pestryakov, A. N., Goldenberg, G. I. and Popova, T. K. (1988), 'Physico-chemical study of silver catalysts for oxidative methanol dehydrogenation', *Zh. Prikl. Spektrosk.* (in Russian); *J. Appl. Spectrosc.* (English translation), **61**, 2051–2056.
888. Pestryakov, A. N., Davydov, A. A. and Kurina, L. N. (1986), 'The Study of a silver catalyst by means of diffuse reflection electronic spectroscopy', *Zh. Prikl. Spektrosk.* (in Russian); *J. Appl. Spectrosc.* (English translation), **60**, 2081–2083.
889. Bogdanchikova, N. E., Anufrienko, V. F. and Davydov, A. A. (1989), 'State of silver in supported quartz glass catalysts from the data of diffuse reflection electronic spectroscopy', *Izv. Khim. Soc., SOAN SSSR*, 144–149.
890. Kharlamov, G. V., Ivankin, I. A., Bogdanchikova, N. E., Anufrienko, V. F. and Davydov, A. A. (1990), 'Spectroscopic study of the silver state in CaO', *React. Kinet. Catal. Lett.*, **41**, 47–51.
891. Bogdanchikova, N. E., Dulin, M. N., Davydov, A. A. and Anufrienko, V. F. (1990), 'Diffuse reflectance electronic spectroscopic study of the state of silver clusters on SiO₂', *React. Kinet. Catal. Lett.*, **41**, 73–8.
892. Pestryakov, A. N., Davydov, A. A. and Kurina, L. N. (1988), 'Influence of supports of different nature on the change of electronic states of supported silver', *Zh. Fiz. Khim.* (in Russian); *Russ. J. Phys. Chem.* (English translation), **62**, 1813–1816.
893. Bogdanchikova, N. A., Anufrienko, V. F., Davydov, A. A., Finn, L. P., Zaikovskii, V. I., Kolomichuk, V. N., Moroz, E. M. and Boldyreva, N. N. (1988), 'States of silver supported on different types of SiO₂', *Kinet. Katal.* (in Russian); *Kinet. Catal.* (English translation), **29**, 914–922.
894. Pestryakov, A. N. and Davydov, A. A. (1995), 'Study of states of supported silver by the method of diffuse reflectance, electronic spectroscopy', *J. Electron Spectrosc. Rel. Phenom.*, **74**, 195–199.
895. Vorobiov, V. N., Korontsevich, A. Yu. and Rasikov, K. H. (1984), 'The formation of active centers in Ag/SiO₂ catalysts', *Zh. Fiz. Khim.* (in Russian); *Russ. J. Phys. Chem.* (English translation), **58**, 2980–2983.
896. Tarasov, A. L., Shvets, V. A. and Kazanskii, V. B. (1988), 'Optical spectroscopy study of the effect of the state of Ag in Ag/Al₂O₃ catalysts on the reaction of oxidation of CO', *Kinet. Katal.* (in Russian); *Kinet. Catal.* (English translation) **29**, 1189–1195.
897. Pestryakov, A. N., Davydov, A. A. and Kurina, L. N. (1988), 'Some regularities in the spectral manifestations of surface carbonyls for noble metals', *Poverhmost*, **2**, 143–145 (in Russian).
898. Pestryakov, A. N. and Davydov, A. A. (1994), 'Active electronic states of silver catalysts for methanol selective oxidation', *Appl. Cat.*, **120**, 7–15.
899. Pestryakov, A. N., Davydov, A. A. and Kurina, L. N. (1987), 'Effect of modifying additives on the electronic state and dispersion of supported silver', *Zh. Fiz. Khim.* (in Russian); *Russ. J. Phys. Chem.* (English translation), **61**, 2381–2385.
900. Bateman, J. E. and Chesters, M. A. (1989), 'A transmission FTIR study of the adsorption of CO and cyclohexane on evaporated silver films', in Morterra, C., Zecchina, A. and Costa, G. (Eds), *Structure and Reactivity of Surfaces*, Elsevier, Amsterdam, pp. 75–83.
901. Arai, M., Mitsui, M., Ozaki, J. I. and Nishiyama, Y. (1994), 'Dispersion and optical absorption of Au and Ag particles supported on an amorphous SiO₂ substrate', *J. Colloid Interface Sci.*, **168**, 473–477.
902. Pestryakov, A. N., Davydov, A. A. and Tsyrlunikov, P. G. (1996), *Role of electronic states of silver and copper catalysts in the partial or total oxidation of alcohols and hydrocarbons*, American Chemical Society 211th National Meeting, New Orleans, LA, ACS Division of Petrol Chemistry, Preprint 41.
903. Pestryakov, A. N. and Davydov, A. A. (1996), 'The influence of modifying additions of La and Ce oxides on the electronic states of surface atoms and ions of supported copper', *Appl. Surf. Sci.*, **108**, 479–487.
904. Naccache, C. C., Primet, M. and Mathieu, M. V. (1973), 'Study of hydrogen and carbon monoxide interactions with palladium zeolite by ESR and IR spectroscopy, in *Advances in Chem Series 121 American Chemical Society* Washington, DC, pp. 226–280.
905. Ben Taarit, Y., Vedrine, J. C., Dutel, F. and Naccache, C. C. (1978), 'EPR investigation of the structure and reactivity of Pd(I) species generated in synthetic mordenite-type zeolites', *J. Magn. Reson.*, **31**, 251–257
906. Che, M., Dutel, J. F., Callezot, P. and Primet, M. (1976), 'A study of the chemisorption of nitric oxide on PdY zeolite. Evidence for a room temperature oxidative dissolution of Pd crystallites', *J. Phys. Chem.*, **80**: 2371–2381.
907. Maksimov, N. G. and Lkhov, Yu. A. (1980), 'ESR study of carbon monoxide interaction with PdY zeolite', *Kinet. Katal.* (in Russian); *Kinet. Catal.* (English translation), **21**, 1340–1342.
908. Lkhov, Yu. A. and Davydov, A. A. (1980), 'Study of the state of transition metal cations on the surface of catalysts by the method of IR spectroscopy of adsorbed probe molecules (CO, NO). IV. Adsorption of carbon monoxide on palladium-containing catalysts', *Kinet. Katal.* (in Russian); *Kinet. Catal.* (English translation), **21**, 1515–1522.
909. Lkhov, Yu. A. and Davydov, A. A. (1980), 'The study of the state of cations of transition metals on the surface of catalysts by means of IR spectroscopy of adsorbed molecule-probes', in *Proceedings of*

- the V Soviet–Japan Seminar on Catalysis*, Tashkent, Uzbekistan, FAN Oct. 29–Nov. 1, 1979, Tashkent, pp. 203–206.
910. Davydov, A. A. and Shepot'ko, M. L. (1987), 'Study of characteristic features of the state of palladium cations in PdY zeolites according to IR spectra of adsorbed NO', *Zh. Prikl. Spektrosk.* (in Russian); *J. Appl. Spectrosc.* (English translation), **49**, 815–820.
 911. Garbowski, E., Primet, M. and Mathieu, M. V. (1978), 'Mise en evidence par spectrometrie ultraviolette d'une interaction NO–CO avec des ions Pd(II)', *J. Chim. Phys. Chim. Biol.*, **75**, 329–332.
 912. Enermark, J. H. and Feltham, R. D. (1974), 'Principles of structure, bonding and reactivity for metal nitrosyl complexes', *Coord. Chem. Rev.*, **13**, 339–406.
 913. Nefedov, V. N., Sinitsin, N. N., Salin', Ya. V. and Bayer, L. (1975), 'Determination of nitrosyl group charge in complexes by ESCA', *Koord. Khim.* (in Russian); *Russ. J. Coord. Chem.* (English translation), **1**: 1618–1624.
 914. Bozon-Verduraz, F., Omar, A., Escard, J. and Pontviannet, B. (1978), 'Chemical state and reactivity of supported palladium. I. Characterization by XPS and UV–Vis spectroscopy', *J. Catal.*, **53**, 126–134.
 915. Tardy, M. and Bozon-Verduraz, F. (1975), 'Notes des membres et correspondants et notes presentees on transmises par leurs soins', *C.R. Acad. Sci. (Paris)*, **280**, 317–324.
 - 916a. Savel'eva, G. A., Sass, A. S., Vozdvozhenskaya, V. F., Tungatarova, S. A. and Popova, N. M. (1988), 'CO adsorption and its interactions with oxygen on Pd, Co and Pd–Co/Al₂O₃ catalysts', *Zh. Fiz. Khim.* (in Russian); *Russ. J. Phys. Chem.* (English translation), **62**, 1021–1025.
 - 916b. Savel'eva, G. A., Sass, A. S., Speranskaya, G. V. and Shvets, V. A. (1988), 'Interaction of carbon monoxide with oxygen in adsorption layers on Pd, Ce and Pd–Ce catalysts supported on γ -Al₂O₃', *Kinet. Katal.* (in Russian); *Kinet. Catal.* (English translation), **29**, 866–871.
 917. Filimonov, I. N., Ikonnikov, I. A. and Loginov, A. Yu. (1994), 'EPR investigation of paramagnetic species on palladium-promoted yttria and lanthana', *J. Chem. Soc., Faraday Trans. 1*, **90**, 219–226.
 918. Espeel, P. H., Peuter, G., Tielen, M. C. and Jacobs, P. A. (1994), 'Mechanism of the Wacker oxidation of alkenes over Cu–Pd-exchanged Y zeolites', *J. Phys. Chem.*, **98**, 11588–11596.
 919. Kovalenko, N. A., Borovkov, V. Y., Petkevich, T. S. and Egiazarov, Y. G. (1995), 'Study of the state of palladium on the surface of carriers based on titanium dioxide by diffuse-reflectance IR spectroscopy', *Kinet. Katal.* (in Russian); *Kinet. Catal.* (English translation), **36**, 688–693.
 920. Palazov, A., Chang, C. C. and Kokes, R. J. (1975), 'The infrared spectrum of carbon monoxide on reduced and oxidized palladium', *J. Catal.*, **36**, 338–350.
 - 921a. Davydov, A. A. and Bell, A. T. (1977), 'An infrared study of the adsorption of CO and NO adsorption on a silica-supported Ru catalyst', *J. Catal.*, **49**, 332–344.
 - 921b. Davydov, A. A. and Bell, A. T. (1977), 'Infrared study of the reaction between NO and CO and NO and H₂ on a silica-supported Ru catalyst', *J. Catal.*, **49**, 345–355.
 922. Dalla Betta, R. A. (1975), 'Carbon monoxide adsorption on supported ruthenium', *J. Phys. Chem.*, **79**, 2519–2531.
 923. Kobayashi, M. and Shirosaki, T. (1974), 'The EPR study of CO adsorbed ruthenium–silica catalysts', *J. Catal.*, **32**, 254–260.
 924. Anderson, J. R. and Howe, R. F. (1977), 'Generation of a supported iridium catalyst of extremely high dispersion', *Nature (London)*, **268**, 129–130.
 925. Dubois, L. H. and Somorjai, G. A. (1980), 'The chemisorption of CO and CO₂ on Rh(III) from studies by HREELS', *Surf. Sci.*, **91**, 514–532.
 926. Jizuka, T. and Lunsford, J. H. (1980), 'The reduction of nitric oxide by carbon monoxide over rhodium–Y zeolites', *J. Mol. Catal.*, **8**, 391–400.
 927. Yang, A. C. and Garland, C. W. (1957), 'Infrared studies of carbon monoxide chemisorbed on rhodium', *J. Phys. Chem.*, **61**, 1504–1512.
 928. Primet, M. (1978), 'Infrared study of CO chemisorption on zeolite and alumina supported rhodium', *J. Chem. Soc., Faraday Trans. 1*, **74**, 2570–2580.
 929. Yates, D. J. C., Murrell, L. L. and Prestrige, E. B. (1979), 'Ultradispersed rhodium rafts: their existence and topology', *J. Catal.*, **57**, 41–63.
 930. Yao, H. C. and Shelef, M. (1980), 'Characterization of Rh oxide on η -Al₂O₃', in *New Horizons in Catalysis, Proceedings of the 7th International Congress on Catalysis, Tokyo, June 30–July 4, 1980*, Seiyama, T. and Tanabe, K. (Eds.) *Studies in Surface Science and Catalysis*, v.7, Kodansha, Tokyo, Elsevier, Amsterdam, 1980.
 931. Niwa, N. and Lansford, J. H. (1982), 'The catalytic reaction of CO and H₂O over supported rhodium', *J. Catal.*, **75**, 302–313.
 932. Rice, C. A., Worley, S. D. and Gurtis, C. W. (1981), 'The oxidation state of dispersed Rh on Al₂O₃', *J. Chem. Phys.*, **74**, 6487–6497.
 933. Basu, P., Panayotov, D. and Yates, J. T. (1987), 'Spectroscopic evidence for the involvement of OH groups in the formation of Rh¹⁺(CO)₂ on metal oxide supports', *J. Phys. Chem.*, **91**, 3133–3136.
 934. Gutschik, D. and Miessner, H. (1984), 'IR spectroscopic investigation of the adsorption of CO on Rh supported on the basic carriers MgO on ZnO', *React. Kinet. Catal. Lett.*, **26**, 387–390.

935. Van't Blik, H. F. J., Van Zon, J. B. A. D., Miizinga, T., Vis, J. C., Koningsberger, D. C. and Prins, R. (1985), 'Structure of rhodium in an ultradispersed Rh/Al₂O₃ catalyst as studied by EXAFS and other techniques', *J. Am. Chem. Soc.*, **107**, 3139–3147.
936. Solimosi, F. and Pasztor, M. (1985), 'An infrared study of the influence of CO chemisorption on the topology of supported rhodium', *J. Phys. Chem.*, **89**, 4789–4793.
937. Yao, H. C. and Rothschild, W. G. (1978), 'Infrared spectra of chemisorbed CO on Rh/ γ -Al₂O₃: site distributions and molecular mobility', *J. Chem. Phys.*, **68**, 4774–4780.
938. Solomennikov, A. A. and Lokhov, Yu. A., Davydov, A. A. and Ryndin, Yu. A. (1979), 'Frequency of the stretching vibrations of adsorbed carbon monoxide as an indicator of the electronic state of a supported platinum surface', *Kinet. Katal.* (in Russian); *Kinet. Catal.* (English Translation), **20**, 714–720.
- 939a. Liang, J. and Wang, H. P. (1985), 'FT-IR study of nitric oxide chemisorbed on Rh/Al₂O₃', *J. Phys. Chem.*, **89**, 5840–5847.
- 939b. Highfield, J. G., Ruterana, P., Thamp, K. R. and Graetzel, M. (1989), 'Catalyst characterization and *in situ* FTIR studies of carbon dioxide methanation over ruthenium supported on titania', in Morterra, C., Zecchina, A. and Costa, G. (Eds), *Structure and Reactivity of Surfaces*, Elsevier, Amsterdam, pp. 469–479.
- 939c. Prairie, M. R., Renken, A., Highfield, J. G., Thampi, K. R. and Gratzel, M. (1991), 'A Fourier transform infrared spectroscopic study of CO₂ methanation on supported ruthenium', *J. Catal.*, **129**, 130–144.
- 939d. (i) Solymosi, F., Pasztor, M. and Rakhely, G. (1988), 'Infrared studies of the effects of promoters on CO-induced structural changes in Rh', *J. Catal.*, **110**, 413–415. (ii) Solymosi, F. and Rasko, J. (1989), 'An infrared study of the influence of CO adsorption on the topology of supported ruthenium', *J. Catal.*, **111**, 107–119.
- 939e. Odriozola, J. A., Carrizosa, I. and Alvero, R. (1989), 'Adsorption and dissociation of CO₂ on lanthanide ion promoted Rh/Al₂O₃ catalysts', in Morterra, C., Zecchina, A. and Costa, G. (Eds), *Structure and Reactivity of Surfaces*, Elsevier, Amsterdam, pp. 713–721.
- 939f. Catania, M. G., Parmigiani, F. and Ragaini, V. (1989), 'A Study of ruthenium catalysts on oxide supports', *Surf. Sci.*, **211–212**, 1097–1105.
- 939g. Chudek, J. A., McQuire, M. W., McQuire, G. W. and Rochester, C. H. (1994), 'In situ FTIR study of Co–H₂ reactions over Rh/TiO₂ catalysts at high pressure and temperature', *J. Chem. Soc., Faraday Trans. 1*, **90**, 3699–3709.
- 939h. Chudek, J. A., McQuire, M. W., McQuire, G. W. and Rochester, C. H. (1992), 'Comparative FT-IR and MAS NMR spectroscopic studies of Rh/SiO₂ catalysts exposed to CO/H₂ at high temperature and pressure', *J. Catal.*, **135**, 358–366.
- 939i. Guerra, G. R. (1969), 'Infrared spectroscopic studies of CO adsorption by metals. The effect of other gases in adsorption', *J. Colloid Interface Sci.*, **29**, 229–234.
- 939j. (i) Brown, M. F. and Gonzalez, R. D. (1976), 'An infrared study of the interaction between adsorbed CO and adsorbed NO on supported Ru and supported Pt', *J. Catal.*, **44**, 477–482. (iii) Brown, M. F. and Gonzalez, R. D. (1977), 'An infrared study of the adsorption of CO and NO on supported Ru–Pt bimetallic clusters', *J. Catal.*, **45**, 292–301.
- 939k. (i) Fujimoto, K., Kameyama, M. and Kunugi, T. (1980), 'Hydrogenation of adsorbed carbon monoxide on supported platinum group metals', *J. Catal.*, **61**, 7–14. (ii) Kuznetsov, V. L. and Bell, A. T. (1980), 'An infrared study of alumina- and silica-supported ruthenium cluster carbonyls', *J. Catal.*, **65**, 374–389.
- 939l. Pfnur, H., Menzel, D., Hoffmann, F. M., Ortega, A. and Bradshaw, A. M. (1980), 'High resolution vibrational spectroscopy of the CO on Ru (001): The importance of lateral interactions', *Surf. Sci.*, **93**, 431–452.
- 939m. (i) Guglielminotti, E., Bocuzzi, F., Ghiotti, G. and Chiorino, A. (1987), 'Infrared evidence of metal–simiconductor interactions in Ru/ZnO systems', *Surf. Sci.* **189–190**, 331–338. (ii) Guglielminotti, E. and Bocuzzi, F. (1989), 'An infrared study of CO adsorbed on a Ru/ZnO catalyst', in Morterra, C., Zecchina, A. and Costa, G. (Eds), *Structure and Reactivity of Surfaces*, Elsevier, Amsterdam, pp. 437–446. (iii) Guglielminotti, E. (1986), 'Influence of the support and of the preparation on the surface structure of the Ru/MgO system', *Langmuir*, **2**, 812–820.
- 939n. (i) Hoffman, F. M., Weisel, M. D. and Peden, C. H. F. (1991), 'In-situ FT-IRAS study of the CO oxidation reaction over Ru (001) II. Coadsorption of carbon monoxide and oxygen', *Surf. Sci.*, **253**, 59–71. (ii) Peden, C. H., Goodman, D. W., Hoffman, F. M. and Weisel, M. D. (1992), 'I. Evidence for an Eley-Rideal mechanism at high pressures', *Surface Science of Catalysis*, **253**, 44–58. (iii) Hoffman, F. M. and Paul, J. (1987), 'FT-IRAS study of the vibrational properties of CO adsorbed on Cu/Ru (001). I. The structural and electronic properties of Cu', *J. Chem. Phys.*, **86**, 2990–2996. (iv) Hoffman, F. M. and Paul, J. (1987), 'FT-IRAS study of the vibrational properties of CO adsorbed on Cu/Ru (001). II. The dispersion of copper', *J. Chem. Phys.*, **87**, 1857–1865.
- 939o. Mizushima, T., Tohji, K., Udagawa, Y. and Ueno, A. (1990), 'EXAFS and IRS study of the CO-adsorption-induced morphology change in Ru catalysts', *J. Am. Chem. Soc.*, **112**, 7887–7893.
- 939p. Liu, R., Tesche, B. and Knozinger, H. (1991), 'Characterization of RuCu/SiO₂ catalysts by infrared spectroscopy of adsorbed carbon monoxide', *J. Catal.*, **129**, 402–413.
- 939q. Rasband, P. B. and Hecker, W. C. (1993), 'Catalyst characterization using quantitative FTIR: CO on supported Rh', *J. Catal.*, **139**, 551–560.

- 939r. Schwank, J., Parravano, G. and Gruber, H. L. (1980), 'An infrared study of CO adsorption on magnesia-supported ruthenium, gold and bimetallic ruthenium-gold clusters', *J. Catal.*, **61**, 19–28.
- 939s. Cant, N. W. and Bell, A. T. (1982), 'Studies of carbon monoxide hydrogenation over ruthenium using transient response techniques', *J. Catal.*, **73**, 257–271.
- 939t. Kellner, C. S. and Bell, A. T. (1981), 'Infrared studies of carbon monoxide hydrogenation over alumina supported ruthenium', *J. Catal.*, **71**, 296–307.
- 939u. Winslow, P. and Bell, A. T. (1984), 'Application of transient response techniques for quantitative determination of adsorbed carbon monoxide and carbon present on the surface of a ruthenium catalyst during Fischer-Tropsch synthesis', *J. Catal.*, **86**, 158–172.
- 939v. (i) Zecchina, A. and Guegliminotti, E. (1982), 'Surface characterization of the $\text{Ru}_3(\text{CO})_{12}/\text{Al}_2\text{O}_3$ system. I. Interaction with the hydroxylated surface', *J. Catal.*, **74**, 225–239. (ii) Guegliminotti, E. and Zecchina, A. (1982), 'Surface characterization of the $\text{Ru}_3(\text{CO})_{12}/\text{Al}_2\text{O}_3$ systems. II. Structure and reactivity of the surface carbonylic complexes', *J. Catal.* **74**, 240–251.
- 939w. (i) McQuire, M. W. and Rochester, C. H. (1993), 'In situ FTIR study of CO/H_2 reactions over Ru/SiO_2 at high temperature and pressure', *J. Catal.*, **141**, 355–367. (ii) McQuire, M. W. and Rochester, C. H. (1995), 'FTIR study of CO/H_2 reactions over Ru/TiO_2 and $\text{Ru}-\text{Rh}/\text{TiO}_2$ catalysts at high temperature and pressure', *J. Catal.*, **157**, 396–402. (iii) McQuire, M. W., McQuire, G. W. and Rochester, C. H. (1992), 'In situ FTIR study of CO/H_2 reactions over $\text{Rh}/\text{Al}_2\text{O}_3$ catalysts at high temperature and pressure', *J. Chem. Soc., Faraday Trans. 1*, **88**, 1203–1209. (iv) McQuire, M. W. and Rochester, C. H. (1991), 'FTIR study of Rh/TiO_2 catalysts exposed to CO/H_2 mixtures at high temperature and pressure', *J. Chem. Soc., Faraday. Trans. 1*, **87**, 1921–1928.
- 939x. Wang, H. P. and Yates, J. T., Jr (1984), 'Spectroscopic study of the interaction of chemisorbed surface species: the reaction $\text{Rh}^{1+}(\text{CO})_2 + \text{CO} \rightarrow \text{Rh}^{1+}(\text{CO})_3$ ', *J. Catal.*, **89**, 79–92.
- 939y. Yokomizo, G. H., Louis, C. and Bell, A. T. (1989), 'An infrared study of CO adsorption on reduced and oxidized Ru/SiO_2 ', *J. Catal.*, **120**, 1–14.
- 939z. Hadjiivanov, K., Lavalley, J. C., Lamotte, J., Mauge, F., Saint-Just, J. and Che, M. (1998), 'FTIR study of CO interaction with Ru/TiO_2 catalysts', *J. Catal.*, **176**, 415–425.
- 939aa. De la Cruz, C. and Sheppard, N. (1990), 'A review of CO bond-stretching wavenumbers for CO ligands in metal coordination compounds or clusters with emphasis on the less common types of metal/CO bonding patterns, and of the relationship between CO and the internuclear distance, $r(\text{CO})$ ', *J. Molec. Structure*, **224**, 141–161.
940. Primet, M., Basset, J. M., Garbowski, E. and Mathieu, M. V. (1975), 'Influence of metal particle size on the chemisorption properties of supported platinum; analogy with cluster compounds', *J. Am. Chem. Soc.*, **97**, 3655–3659.
941. Solomennikov, A. A. and Davydov, A. A. (1984), 'Influence of the oxidative treatment on the electron state of surface atoms of supported platinum', *Kinet. Katal.* (in Russian); *Kinet. Catal.* (English translation), **25**, 403–407.
942. Primet, M., Basset, J. M., Matieu, M. V. and Prettre, M. (1973), 'IR study of CO adsorbed on $\text{Pt}/\text{Al}_2\text{O}_3$. A method for determining metal-adsorbate interaction', *J. Catal.*, **29**, 213–223.
943. Stoop, E., Toolenaar, F. J. C. M. and Ponec, V. (1982), 'Geometric and ligand effects in the IR spectra of adsorbed CO', *J. Catal.*, **73**, 50–56.
944. Mojet, B. L., Kappers, M. J., Miller, J. T. and Koningsberger, D. C. (1996), 'Metal-support interaction in supported platinum catalysts: zeolites and amorphous supports', in Hightower, J. W., Deglass, W. N., Iglesia, E. and Bell, A. T. (Eds) in *Proceedings of the 11th International Congress on Catalysis, Studies Surf. Sci. Catal.*, **101**, 1165–1174.
945. Blyholder, G. J. (1975), 'CNDO model of CO chemisorbed on nickel', *J. Phys. Chem.*, **79**, 756–774.
946. Messmer, R. P., Knudson, S. K., Johanson, K. H., Diamond, J. B. and Yang, C. Y. (1976), 'MO studies of transition and noble-metal clusters by the self-consistent field- $X\alpha$ scattered-wave method', *Phys. Rev. B*, **13**, 1396–1425.
947. Kuznetsov, B. N., Ovsyannikova, I. A., Ryndin, Yu. A., Erenburg, S. B., Gilvarg, A. B. and Ermakov, Yu. I. (1978), 'Catalysts obtained by the reaction of transition metal organometallic compounds with the surface of supports. Study of the properties of silicon dioxide supported tungsten-nickel catalysts', *Kinet. Katal.* (in Russian); *Kinet. Catal.* (English translation), **19**, 749–756.
948. Della Betta, R. A. and Boudart, M. (1973), 'Well-dispersed platinum on Y zeolite: Preparation and catalytic activity', in Hightower, J. (Ed.) *Proceedings of the 5th International Congress on Catalysis*, Miami Beach, 1972, FL, North Holland, Amsterdam Vol. 2, 1329–1337.
949. Anderson, J. R. (1975), *Structure of Metallic Catalysts*, Academic Press, New York.
950. Primet, M. (1984), 'Electronic transfer and ligand effects in the infrared spectra of adsorbed carbon monoxide', *J. Catal.*, **88**, 273–282.
951. Palazov, A. (1973), 'Benzene adsorption and its interaction with CO on alumina-supported platinum – an IRS study', *J. Catal.*, **30**, 13–20.
952. Queau, R. and Poilblanc, R. (1972), 'Interaction between Lewis bases chemisorbed on transition metal surface – IR spectroscopic studies', *J. Catal.*, **27**, 200–206.

953. Queau, R., Labroue, D. and Poilblanc, R. (1981), 'Interactions of chlorine and bromine with chemisorbed carbon monoxide on evaporated Pt, Rh and Ir films', *J. Catal.*, **69**, 249–256.
954. Hammaker, R. M., Francis, S. A. and Eischens, R. P. (1965), 'IR study of intermolecular interactions for carbon monoxide chemisorbed on platinum', *Spectrochim. Acta, Part A*, **21**, 1295–1299.
- 955a. Toolenaar, F. J. C. M., Stoop, F. and Ponec, V. (1983), 'Electronic and geometric effect of alloying. An infrared spectroscopic investigation of the adsorption of carbon monoxide on platinum–copper alloys', *J. Catal.*, **82**, 1–12.
- 955b. Toolenaar, F. J. C. M., Stoop, F. and Ponec, V. (1983), 'Effect of particles size in the adsorption of carbon monoxide on iridium: an infrared investigation', *J. Catal.*, **82**, 35–44.
956. Oranskaya, O. M. and Semenskaya, I. V. (1987), 'Application of isotope dilution of carbon monoxide in the study of aluminoplatinum catalysts by means of infrared spectroscopy', *Usp. Fotoniki*, **9**, 136–148 (in Russian).
957. Hendricks, H. A. C. M., Des Bouvrie, C. and Ponec, V. (1988), 'On the electronic competition effect upon CO adsorption on metals', *J. Catal.*, **109**, 120–125.
958. Shigeishi, R. A. and King, D. A. (1976), 'Characterization of CO on Pt(III): the reflection–absorption IR spectroscopy method', *Surf. Sci.*, **58**, 379–396.
959. Marchese, L., Boccuti, M. R., Colccia, S., Lavagnino, S., Zecchina, A., Bonnevot, L. and Che, M. (1989), 'The Pt/Al₂O₃ system: Infrared studies', in Morterra, C., Zecchina, A. and Costa, G. (Eds), *Structure and Reactivity of surfaces*, Elsevier, Amsterdam, pp. 653–663.
960. Primet, M., Foulilloux, P. and Imelik, B. (1979), 'Propene–vanadium(V) oxide interaction studied by infrared emission spectroscopy', *Surf. Sci.*, **85**, 457–470.
961. Gallezot, P., Datka, J., Massardier, J., Primet, M. and Imelik, B. (1977), 'Universal catalytic behavior of very small platinum particles encaged in Y zeolites', in *Proceedings of the 6th International Congress on Catalysis, London, 1976*, Bond, G. C., Wells, P. B. and Tompkins, F. S. (Eds.), The Royal Society of Chemistry, London, 1977, pp. 696–703.
962. Mojet, B. L., Kappers, M. J., Miller, J. T. and Koningsberger, D. C. (1996), 'Metal–support interaction in supported platinum catalysts: zeolites and amorphous supports', in Hightower, J. W., Deglass, W. N., Iglesia, E. and Bell, A. T. (Eds), in *Proceedings of the 11th International Congress on Catalysis, Studies Surf. Sci. Catal.*, **101**, 1165–1174.
- 963a. Stakheev, A. Yu., Shpiro, E. S., Tkachenko, O. P., Jaeger, N. I. and Schulz-Ekloff, G. (1997), 'Evidence for monatomic platinum species in H-ZSM-5 from FTIR spectroscopy of chemisorbed CO', *J. Catal.*, **169**, 382–388.
- 963b. Stakheev, A. Yu., Shpiro, E. S., Tkachenko, O. P., Jaeger, N. I. and Schulz-Ekloff, G. (1995), 'Electronic state and location of Pt metal clusters in KL zeolites. An FTIR study of CO chemisorption', *Catal. Lett.*, **32**, 147–158.
964. Sachtler, W. M. H. and Stakheev, A. Yu. (1992), 'Electron deficient palladium clusters and bifunctional sites and zeolites', *Catal. Today*, **12**, 283–295.
965. Shpiro, E. S., Tuleuova, G. J., Zaikovskiy, V. I., Tkachenko, O. P. and Minachev, Kh. M. (1989), 'The state of transition metals and their distribution', *Kinet. Katal.* (in Russian); *Kinet Catal.* (English translation), **30**, 939–943.
966. Zholobenko, V. L., Lei, G.-D., Carvill, B. T., Lenner, B. A. and Sachtler, W. M. H. (1994), 'Identification of isolated Pt atoms in H-mordenite', *J. Chem. Soc., Faraday Trans. I*, **90**, 233–238.
967. Bischoff, H., Jaeger, N. I., Schulz-Ekloff, G. and Kubelkova, L. (1993), 'Interaction of CO with platinum species in zeolites: evidence for platinum carbonyls in partially reduced zeolite PtNaX', *J. Mol. Catal.*, **80**, 95–104.
- 968a. Stakheev, A. Y., Jaeger, N. I., Shpiro, E. S., Tkachenko, O. P., and Schulz-Ekloff, G. (1995), 'Electronic state and location of Pt metal clusters in KL zeolites', *Catal. Lett.*, **32**, 147–158.
- 968b. Stakheev, A. Y., Jaeger, N. I., Rarge, H. G. and Weitkamp, J. (Eds) (1994), 'FTIR evidence of Pt carbonyls formation from Pt metal clusters in KL zeolites', *Proceedings of the 10th International Zeolite Conference*, Garmisch-Partenkirchen, Germany, July 17–22, 1994, *Studies Surf. Sci. Catal.*, **98**, 108–109.
- 968c. Chuang, K. T., Davydov, A. A., Sanger, A. R. and Zang, M. (1997), 'Effect of fluorination of alumina support on activity of Pt for the complete oxidation of benzene', *Catal. Lett.*, **49**, 155–161.
969. Tauster, S. J., Funk, S. C. and Garten, R. L. (1978), 'Strong metal support interactions. Group 8 noble metals supported on TiO₂', *J. Am. Chem. Soc.*, **100**, 170–175.
970. Den Otter, G. J. and Dautzenberg, F. M. (1978), 'Metal support interaction in Pt/Al₂O₃ catalysts', *J. Catal.*, **53**, 116–125.
971. Lamber, R. and Romanowski, W. (1987), 'Dispersion changes of Pt supported on silica glass during thermal treatment in oxygen and hydrogen atmospheres', *J. Catal.*, **105**, 213–226.
972. Lamber, R., Jaeger, N. and Schulz-Ekloff, G. (1990), 'Metal–support interaction in the Pd/SiO₂ system: influence of the support pretreatment', *J. Catal.*, **123**, 285–297.
973. Adamiec, J., Wanke, S. E., Tesche, B. and Klengler, U. (1982), 'Metal–support interaction in the platinum/magnesia system', *Stud. Surf. Sci. Catal.*, **11**, 7784–7789.

974. Hippe, C., Lamber, R., Schultz-Ekloff, G. and Schubert, U. (1997), 'Influence of the strong metal-support interaction on CO chemisorption at a Pt/SiO₂ catalyst', *Catal. Lett.*, **43**, 195–199.
975. Hadjiivanov, K., Sant-Just, J., Che, M., Tatibouet, J. M., Lamotte, J. and Lavalley, J. C. (1994), 'Preparation and characterization of multiple ion-exchanged Pt/TiO₂', *J. Chem. Soc., Faraday Trans. 1*, **90**, 2277–2281.
976. Dilara, P. A. and Vohs, J. M. (1995), 'Interaction of CO with Pt supported on ZrO₂ (100): evidence for CO adsorbed at the Pt-ZrO₂ interface', *J. Phys. Chem.*, **99**, 17259–17264.
977. Giotti, G., Boccuzzi, F. and Chiorino, A. (1985), 'Spectroscopic evidence for a new surface carbonyl species on a Cu/ZnO catalyst', *J. Chem. Soc., Chem. Commun.*, 1012–1014.
978. Dalmon, J. A., Primet, M., Martin, G. A. and Imelik, B. (1975), 'Magnetic and IR study of CO chemisorption on silica supported nickel-copper alloys', *Surf. Sci.*, **59**, 95–105.
979. Ponec, V. (1977), 'Catalysts by supported and unsupported metals and alloys', *Int. J. Quantum. Chem. Suppl.*, **2**, 12–17.
980. Slinkin, A. A. (1981), 'Current problems in the field of catalysis of alloys', *Kinet. Katal.* (in Russian); *Kinet. Catal.* (English translation), **22**, 71–85.
981. Burch, R. (1982), 'Importance of electronic ligand effects in metal alloy catalysts', *Acc. Chem. Res.*, **15**, 24–31.
982. Kharson, M. S., Slinkin, A. A., Fedorovskaya, E. A., Pimenov, V. G. and Kiperman, S. L. (1984), 'Cluster and ligand effects in CO adsorption on high dispersity supported Ni-Cu alloys', *React. Kinet. Catal. Lett.*, **24**, 389–393.
983. Nadirov, N. K., Vozdvizhenskii, V. F., Kondratkova, N. I. and Fatkulina, A. A. (1985), 'Influence of Zr, Ge, B and Co additives on the activity of Pt/Al₂O₃ catalysts for dehydrocyclization', *React. Kinet. Catal. Lett.*, **25**, 191–194.
984. Drozdov, V. A., Tsyrl'nikov, P. G., Popovskii, V. V., Davydov, A. A. and Moroz, E. M. (1986), 'Effect of additions of cerium, lanthanum and zirconium on the state of platinum and the activity of aluminoplatinum catalysts for the complete oxidation of hydrocarbons', *Kinet. Katal.* (in Russian); *Kinet. Catal.* (English translation), **27**, 162–166.
985. Drozdov, V. A., Tsyrl'nikov, P. G., Popovskii, V. V., Pankrat'ev, Yu. D., Davydov, A. A. and Moroz, E. M. (1985), 'Increase in the thermal stability of aluminoplatinum catalysts for complete oxidation from the introduction of cerium, lanthanum and zirconium additives', *Kinet. Katal.* (in Russian); *Kinet. Catal.* (English translation), **27**, 721–725.
- 986a. Kogan, S. B., Moroz, A. M., Oranskaya, O. M., Semenskaya, I. V., Gorodetskaya, I. V. and Bursean, N. R. (1983), 'Study of the platinum-alumina catalysts modified by alkali metals by means of the IRS and ESR methods', *Zh. Prikl. Khim.* (in Russian); *Russ. J. Appl. Chem.* (English translation), **56**, 1975–1977.
- 986b. Kogan, S. B., Moroz, A. M., Oranskaya, O. M., Semenskaya, I. V., Tysovskii, G. I. and Bursean, N. R. (1983), 'Study of the platinum-alumina catalysts modified by three group cations by means of the IRS and ESR methods', *Zh. Prikl. Khim.* (in Russian); *Russ. J. Appl. Chem.* (English translation), **56**, 1884–1886.
- 986c. Chuang, K. T., Davydov, A. A., Sanger, A. R. and Zang, M. (1997), 'Effect of fluorination of alumina support on activity of Pt for the complete oxidation of benzene', *Catal. Lett.*, **49**, 155–161.
987. Drozdov, V. A., Tsyrl'nikov, P. G., Pstryakov, A. N., Davydov, A. A., and Popovskii, V. V. (1988), 'Study of catalyst activity in the extensive oxidation of butane and the state of platinum in lanthanum- and cerium-modified Pt/Al₂O₃ catalysts', *Kinet. Katal.* (in Russian); *Kinet. Catal.* (English translation), **29**, 484–488.
988. Meriaudeau, P., Thangaraj, A. and Naccache, C. (1996), 'Platinum/indium bimetallic in silicate: preparation, characterization and use in the vinylcyclohexene transformation', in *11th International Congress on Catalysis-40th Anniversary. Proceedings of the 11th ICC, Baltimore, MD, USA, June 30-July 1996*, Hightower, J. W., Delgass, W. N., Iglesia, E. and Bell, A. T., *Studies in Surface Science and Catalysis*, v.101, Elsevier, Amsterdam, 1996, 1313–1320.
989. Zaitsev, A. V., Tyupaev, A. P., Borovkov, V. Yu., Timofeeva, E. A., Isagulyants, G. V. and Kazansky, V. B. (1986), 'Catalytic and physico-chemical properties of aluminoplatinum catalysts promoted by In and Ga', *Izv. Acad. Nauk. SSSR, Ser. Khim.* (in Russian); *Russ. Chem. Bull.* (English translation), 759–765.
990. Zaitsev, A. V., Tsapkina, M. V., Savel'ev, M. M., Borovkov, V. Yu., Lapidus, A. L. and Kazanskii, V. B. (1986), 'Influence of the alkali promotor nature on properties of iron carbonyl catalysts', *Izv. Acad. Nauk. SSSR, Ser. Khim.* (in Russian); *Russ. Chem. Bull.* (English translation), 1483–1487.
991. Kochetkova, E. I. and Sokolova, N. P. (1986), 'Study of chemisorption of carbon monoxide on the adsorbents RhCu/SiO₂, RhAg/SiO₂ and PdAu/SiO₂', *Zh. Fiz. Khim.* (in Russian); *Russ. J. Phys. Chem.* (English translation), **60**, 475–478.
992. Bulgakova, R. A. and Sokolova, M. P. (1986), 'Infrared spectra of carbon monoxide chemisorbed on Pt-Ni/Al₂O₃', *Zh. Fiz. Khim.* (in Russian); *Russ. J. Phys. Chem.* (English translation), **60**, 1914–1917.
993. Kochetkova, E. I. and Sokolova, N. P. (1986), 'State of the surfaces of Rh, Pd and Cu/SiO₂ adsorbents and the according infrared spectra of chemisorbed CO', *Zh. Fiz. Khim.* (in Russian); *Russ. J. Phys. Chem.* (English translation), **60**, 2893–2897.

994. Fransén, T., Van der Meer, O. and Mars, P. (1976), 'Interaction of the surface structure and activity of molybdenum oxide containing catalysts. I. An IR study of the surface structure of Mo-Al catalysts', *J. Catal.*, **42**, 79–86.
995. Lapez, A. A., Gill, F. J., Galleja, J. M. and Fernandes, V. J. (1981), 'Raman spectra of Mo/Al₂O₃', *J. Raman Spectrosc.*, **11**, 454–458.
996. Wang, L. and Hall, W. K. (1982), 'The preparation and genesis of Mo-Al and related catalyst systems', *J. Catal.*, **77**, 232–241.
997. Jeziorowski, H. and Knozinger, H. (1979), 'Raman and ultraviolet spectroscopic characterization of molybdenum on alumina catalysts', *J. Phys. Chem.*, **83**, 1166–1173.
998. Knozinger, H. and Jeziorowski, H. (1978), 'Raman spectra of molybdenum oxide supported on the surface of alumina', *J. Phys. Chem.*, **82**, 2002–2004.
- 999a. Giordano, N., Bart, J. C. J., Vaghi, A., Castellan, A. and Mattinatti, O. (1975), 'A surface spectroscopic study of molybdenum-alumina catalysts using X-ray, photoelectron, ion-scattering and Raman spectroscopies. 1. Solid state properties of oxidized catalysts', *J. Catal.*, **36**, 81–92.
- 999b. Giordano, N., Bart, J. C. J., Vaghi, A., Castellan, A. and Mattinatti, O. (1975), 'A surface spectroscopic study of molybdenum-alumina catalysts using X-ray, photoelectron, ion-scattering and Raman spectroscopies. 2. Solid state properties of reduced catalysts', *J. Catal.*, **37**, 204–214.
- 999c. Giordano, N., Bart, J. C. J., Vaghi, A., Castellan, A. and Mattinatti, O. (1975), 'A surface spectroscopic study of molybdenum-alumina catalysts using X-ray, photoelectron, ion-scattering and Raman spectroscopies. 4. Nature of sites for oxyhydrogenation of propylene to acetone', *J. Catal.*, **38**, 11–18.
1000. Ripan, R. and Cheteanu, I. (1972), *Inorganic Chemistry* (in Russian), Mir, Moscow.
1001. Parks, G. A. (1965), 'Isoelectronic points of solid oxide', *Chem. Rev.*, **65**, 177–195.
1002. Asmolov, G. N. and Krylov, O. V. (1970), 'Molybdenum-oxide catalysts, applied on γ -Al₂O₃ and magnesium oxide, studied by DRS', *Kinet. Katal.* (in Russian); *Kinet. Catal.* (English translation), **11**, 1028–1033.
1003. Edmonds, T. and Mitchell, P. C. H. (1980), 'XPS of some MoO₃/Al₂O₃ catalysts and the distribution of molybdenum in catalyst extrudates following drying and calcining', *J. Catal.*, **64**, 491–493.
1004. Medema, J., Van Stam, C., Beer De, V. H. J., Konings, A. J. A. and Koningsberger, D. S. (1978), 'Raman spectroscopic study of Co-Mo/ γ -Al₂O₃ catalysts', *J. Catal.*, **53**, 386–400.
- 1005a. Che, M., Figueras, F., Forissier, M., McAteer, J., Peppin, M., Paptifaix, J. L. and Praliand, H. (1977), 'Influence of the symmetry of the molybdenum ion on the selectivity for propylene oxidation', in *Proceedings of the 6th International Congress on Catalysis, London, 1976*, Bond, G.C., Wells, P.B. and Tompkins, F.S. (Eds.), The Royal Society of Chemistry, London, 1977, Vol. 1, 261–270.
- 1005b. Priliand, H. and Forissier, M. (1978), 'Valence state and coordination number of molybdenum supported on SiO₂ or MgO during the oxidation of propene', *React. Kinet. Catal. Lett.*, **8**, 451–457.
1006. Zingg, D. S., Makovsky, L. I., Tischer, R. E. and Brown, F. R. (1980), 'A surface spectroscopic study of a molybdenum-titania catalyst using X-ray, photoelectron, ion-scattering and Raman spectroscopies', *J. Phys. Chem.*, **84**, 2898–2906.
1007. Loktev, M. I. and Slinkin, A. A. (1980), 'Structure and physico-chemical characteristics of Al-Co-Mo hydrotreating catalysts', in *Kinetics and Catalysis, Advances in Science and Technology*, VINITI, Moscow.
1008. Goncharova, O. I., Boreskov, G. K., Yurieva, T. M., Yurchenko, E. N. and Boldyreva, N. N. (1981), 'Active state of molybdenum in molybdenum-alumina catalysts for propylene oxidation', *React. Kinet. Catal. Lett.*, **16**, 349–353.
1009. Startsev, A. N., Kuznetsov, B. N., Mamaeva, E. K., Budneva, A. A., Davydov, A. A. and Ermakov, Yu. I. (1977), 'Synthesis and properties of molybdenum surface complexes prepared by the interaction of [Mo(OC₂H₅)₅]₂ with SiO₂', in Kuznetsov, V.N. and Ermakov, Yu. I. (Eds), *Catalysts Containing Supported Complexes* (in Russian), Institute of Catalysis, Novosibirsk, pp. 59–62.
1010. Maksimov, N. G., Anufrienko, V. F., Yurieva, T. M., Shokhireva, T. Kh. and Chumachenko, N. N. (1980), 'ESR studies of the state of molybdenum in silica-molybdenum oxide catalysts', *React. Kinet. Catal. Lett.*, **14**, 93–97.
1011. Marov, I. N. and Kostromina, N. A. (1979), *ESR and NMR in the Chemistry of Coordination Compounds* (in Russian), Nauka, Moscow.
1012. Louis, C. and Che, M. (1992), 'EPR and diffuse reflectance studies of the physico-chemical phenomena occurring during the preparation of Mo/SiO₂ catalysts by the grafting method', *J. Catal.*, **135**, 156–172.
1013. Castellan, A., Bart, J. C. J., Vaghi, A. and Giordano, N. (1976), 'Structure and catalytic activity of the MoO₃-SiO₂ system. I. Solid state properties', *J. Catal.*, **42**, 162–172.
1014. Gerasimov, S. F. and Filimonov, V. N. (1981), 'Infrared spectra of the photosorption products of hydrogen and carbon monoxide on Al₂O₃ and SiO₂ containing transition metal ions', *Kinet. Katal.* (in Russian); *Kinet. Catal.* (English translation), **22**, 469–473.
1015. Ramis, G., Busca, G. and Lorenzelli, V. (1987), 'FT-IR study of the reactivity of molybdenum oxide supported on titania', *Appl. Catal.*, **32**, 305–313.
1016. Alkhozov, T. G., Adzhomov, K. Yu. and Khanmamedova, A. K. (1982), 'Catalytic oxidation of propene', *Usp. Khim* (in Russian); *Russ. Chem. Rev.* (English translation), **51**, 950–968.

1017. Vanhove, D., Op, S. R., Fernandes, A. and Blanchard, M. (1979), 'Catalytic oxidation of 1-butene and butadiene. Study of MoO₃-TiO₂ catalysts', *J. Catal.*, **57**, 253-263.
1018. Goroshenko, Ya. G. (1970), *Khimiya Titana (The Chemistry of Titanium)* (in Russian), Naukova Dumka, Kiev.
1019. Kravets, G. A., Shokhireva, T. Kh., Anufrienko, V. F. and Yurieva, T. M. (1982), 'Studies of molybdenum in molybdena-titania catalysts', *React. Kinet. Catal. Lett.*, **19**, 95-99.
1020. Hu, H., Wachs, I. and Bare, S. R. (1995), 'Surface structure of supported molybdenum oxide catalysts: characterization by Raman and Mo L₃-edge XANES', *J. Phys. Chem.*, **99**, 1087-1091.
1021. Zaki, M. L., Vielhaber, B. and Knozinger, H. (1986), 'Low temperature CO adsorption and state of molybdenum supported on alumina, titania, ceria and zirconia. An IR spectroscopic investigation', *J. Phys. Chem.*, **90**, 3176-3183.
1022. Valyon, J. and Hall, W. K. (1983), 'The chemisorption of oxygen and nitric oxide on reduced and sulfided molybdena-alumina catalysts', *J. Catal.*, **84**, 216-228.
1023. Gao, X. and Xin, Q. (1994), 'Spectroscopic determination of oxidation and coordination states of Mo cations in the reduced Mo/Al₂O₃ catalyst', *J. Catal.*, **146**, 306-309.
1024. Maksimov, N. G., Ismailov, E. G., Anufrienko, V. F. and Davydov, A. A. (1975), 'Investigation of adsorption of O₂, CO, C₃H₆ and NH₃ molecules on molybdenum-magnesium oxide catalysts using the EPR method', *Teor. Eksp. Khim.* (in Russian); *Theor. Exp. Chem.* (English translation), **11**, 260-265.
1025. Delgado, E., Fuentes, G. A., Herman, G. A., Kunzmann, C. and Knozinger, H. (1984), 'State characterization on reduced and on sulfided Mo/Al₂O₃ catalysts by adsorption of probe molecules', *Bull. Soc. Chim. Belg.*, **83**, 735-742.
1026. Yan, Y., Xin, Q., Jiang, S. and Guo, X. X. (1991), 'IR studies of CO and/or NO adsorption on reduced W/Al₂O₃ catalysts', *J. Catal.*, **131**, 234-242.
1027. Bond, G. C., Zurita, J. P., Flamerz, S. (1986), 'Structure and reactivity of titania-supported oxides. 1. Vanadium oxide on titania in the sub- and super-monolayer regions', *Appl. Catal.*, **22**, 361-370.
1028. Miyata, H., Nakagawa, Y., Ono, T. and Kubokawa, Y. (1983), 'IR study of NH₃ and pyridine adsorbed on V-Ti oxide', *Chem. Lett.*, 1141-1144.
1029. Christiani, C., Forzatti, P. and Busca, G. (1989), 'On the surface structure of V-Ti catalyst: combined laser-Raman and FTIR investigation', *J. Catal.*, **116**, 586-589.
1030. Busca, G., Centi, G., Marchetti, L. and Trifiro, F. (1986), 'Chemical and spectroscopic study of the nature of a vanadium oxide monolayer supported on a high-surface-area TiO₂ anatase', *Langmuir*, **2**, 568-577.
- 1031a. Busca, G. (1986), 'FT-IR study of the surface chemistry of anatase-supported vanadium-oxide monolayer catalysts', *Langmuir*, **2**, 577-582.
- 1031b. Busca, G. (1988), 'On the mechanism nature of V-supported on different carriers. An FT-IR study', *Mater. Chem. Phys.*, **19**, 157-165.
- 1031c. Busca, G., Centi, G., Marchetti, L. and Trifiro, F. (1986), 'Chemical and spectroscopic study of the nature of a vanadium oxide monolayer supported on a high-surface-area TiO₂ anatase', *Langmuir*, **2**, 568-577.
1032. Nag, N. R. and Massoth, F. E. (1990), 'ESCA and gravimetric reduction studies on V/Al₂O₃ and V/SiO₂ catalysts', *J. Catal.*, **124**, 127-132.
1033. Kang, Z. C. and Bao, Q. X. (1986), 'A study of the interaction of V₂O₅/TiO₂(anatase) by high resolution electron microscopy (HREM)', *Appl. Catal.*, **26**, 251-263.
1034. Went, G. T., Oyama, S. T. and Bell, A. T. (1990), 'Laser Raman spectroscopy of supported vanadium oxide catalysts', *J. Phys. Chem.*, **94**, 4240-4246.
1035. Pope, M. T. and Dale, B. W. (1968), 'Isopoly-vanadates, niobates and tantalates', *Q. Rev. Chem. Soc.*, **22**, 527-563.
1036. Busca, G., Marchetti, L., Centi, G. and Trifiro, F. (1985), 'Surface characterization of a grafted V-Ti-dioxide catalyst', *J. Chem. Soc., Faraday Trans. 1*, **81**, 1003-1014.
- 1037a. Kozlowski, R., Pettifer, R. F. and Thomas, J. M. (1983), 'X-ray absorption fine structure investigation of V₂O₅-TiO₂ catalysts. 1. The titania support', *J. Phys. Chem.*, **87**, 5172-5176.
- 1037b. Kozlowski, R., Pettifer, R. F. and Thomas, J. M. (1983), 'X-ray absorption fine structure investigation of V₂O₅-TiO₂ catalysts. 2. The vanadium oxide active phase', *J. Phys. Chem.*, **87**, 5176-5181.
1038. Haber, J., Kozlowska, A. and Kozlowski, R. (1986), 'The structure and redox properties of vanadium oxide surface compounds', *J. Catal.*, **102**, 52-63.
1039. Martin, C. and Rives, V. (1987), 'V₂O₅/TiO₂ oxidation catalysts. 1. Preparation and characterization by XRD and IR spectroscopies', *React. Kinet. Catal. Lett.*, **33**, 381-386.
- 1040a. Roozeboom, F., Medema, J. and Gellings, P. J. (1978), 'Vanadium oxide monolayer catalysts. 2. A laser-Raman spectroscopic study of the acidic vanadium/γ-alumina catalyst', *Z. Phys. Chem.*, **111**, 215-224.
- 1040b. Roozeboom, F., Medema, J. and Gellings, P. J. (1980), 'Vanadium oxide catalysts. 3. A Raman spectroscopic and TPR study of monolayer and crystal type vanadia on various supports', *J. Phys. Chem.*, **84**, 2783-2791.
1041. Busca, G., Centi, G., Marchetti, L. and Trifiro, F. (1986), 'Chemical and spectroscopic study of the nature of a vanadium oxide monolayer supported on a high-surface-area TiO₂ anatase', *Langmuir*, **2**, 568-577.

1042. Ishida, S., Imamura, S., Ren, F., Tatematsu, Y. and Fujimura, Y. (1992), 'Ethene polymerization on Lewis acid sites of a reduced V_2O_5/Al_2O_3 catalyst', *React. Kinet. Catal. Lett.*, **46**, 199–207.
1043. Hausinger, G., Schmelz, H. and Knozinger, H. (1988), 'Effect of the method of preparation on the properties of titania supported vanadia catalysts', *Appl. Catal.*, **39**, 267–283.
1044. Kantcheva, M., Hadjiivanov, K. and Klissurski, D. (1992), 'An IR spectroscopy study of the state and localization of vanadium oxo species adsorbed on TiO_2 (anatase)', *J. Catal.*, **134**, 299–310.
1045. Kantcheva, M., Davydov, A. A. and Hadjiivanov, K. (1993), 'Spectroscopic study of the nature of vanadium oxo-species adsorbed on anatase', *J. Mol. Catal.*, **81**, L25–L30.
1046. Busca, G. and Lavalley, J. C. (1986), 'Use of overtone bands to monitor the state of the catalysts active phases during infrared studies of adsorption and catalytic reactions', *Spectrochim. Acta, Part A*, **42**, 443–449.
- 1047a. Hanke, W., Bienert, R. and Yerschkewitz, H. G. (1975), 'Untersuchungen an katalytisch aktive oberflächenverbindungen I Herstellung und untersuchung von Vanadineoxide-phasen auf SiO_2 ', *Z. Anorg. Allgem. Chem.*, **414**, 109–129.
- 1047b. Hanke, W., Bienert, R. and Yerschkewitz, H. G. (1978), 'Zur existenz unterschiedlicher V(V)–oxid–oberflächenphasen auf SiO_2 und ihre katalytischen eigenschatten', *Z. Anorg. Allgem. Chem.*, **438**, 176–194.
1048. Davydov, A. A., Budneva, A. A. and Maksimov, N. G. (1982), 'Effect of the state of vanadium cations on the IR spectra of adsorbed carbon monoxide', *React. Kinet. Catal. Lett.*, **20**, 93–98.
1049. Alekseev, A. V. and Gerasimov, S. F. (1987), 'Photostimulated reactions on the surfaces of simple and modified oxide sorbents', *Usp. Fotoniki*, **9**, 149–189 (in Russian).
1050. Davydov, A. A. (1990), 'Study of the adsorption of hydrocarbons on oxide catalysts by means of infrared spectroscopy. XVI. Interaction of C_3H_6 and C_2H_4 with V_2O_5/Al_2O_3 ', *Kinet. Katal.* (in Russian); *Kinet. Catal.* (English translation), **31**, 652–658.
1051. Kim, D. S. and Wachs, I. E. (1993), 'Surface chemistry of supported chromium oxide catalysts', *J. Catal.*, **142**, 166–171.
1052. Schneider, H., Maciejewski, M., Kohler, K., Wokaun, A. and Baiker, A. (1995), 'Chromia supported on titania VI. Properties of different chromium oxide phases in the catalytic reduction of NO by NH_3 studied by *in situ* diffuse reflectance FTIR spectroscopy', *J. Catal.*, **157**, 312–320.
1053. Indovina, V., Cimino, A., Rossi, S., Ferraris, G., Ghiotti, G. and Chiorino, A. (1992), 'Nature of the active site for propene hydrogenation on CrO_3/ZrO_2 catalysts', *J. Mol. Catal.*, **75**, 305–319.
1054. Sohn, J. R. and Ryu, S. G. (1993), 'Surface characterization of a chromium oxide–zirconia catalyst', *Langmuir*, **9**, 126–131.
1055. Hardcastle, F. D. and Wachs, I. (1988), 'Raman spectroscopy of chromium oxide supported on Al_2O_3 , TiO_2 and SiO_2 : a comparative study', *J. Mol. Catal.*, **46**, 173–186.
1056. Conway, S. J., Falconer, J. W., Rochester, C. H. and Downs, G. W. (1989), 'Chromia/silica–titania cogel catalysts for ethene polymerization', *J. Chem. Soc., Faraday Trans. 1*, **85**, 1841–1851.
1057. Kim, D. S., Tatibouet, J. M. and Wachs, I. E. (1992), 'Surface structure and reactivity of CrO_3/SiO_2 catalysts', *J. Catal.*, **136**, 209–221.
1058. Fouad, N. F., Knozinger, H., Zaki, M. I. and Mansour, S. A. A. (1991), 'Chromia on silica and alumina catalysts. A thermoanalytical and spectroscopic investigation of thermal genesis of the catalysts', *Z. Phys. Chem.*, **171**, 75–96.
1059. Szabo, Z. G., Kamaras, K., Szabeni, Sz. and Ruff, I. (1978), 'Investigation of chromate salts by diffuse reflectance spectroscopy', *Spectrochim. Acta, Part A*, **34**, 607–612.
1060. Knozinger, H., Zaki, M. I. and Mansour, S. A. A. (1991), 'Chromia on silica and alumina catalysts. A thermoanalytical and spectroscopic investigation of thermal genesis of the catalysts', *Z. Phys. Chem.*, **171**, 75–796.
1061. Sohn, J. R., Ryu, S., Park, M. Y. and Pae, Y. (1992), 'Preparation and characterization of chromium oxide supported on zirconia', *Bull. Korean Chem. Soc.*, **13**, 605–612.
1062. Conway, S. J., Falconer, W. J. and Rochester, C. H. (1989), 'Chromia/silica–titania cogel catalysts for ethene polymerization. Infrared study of nitric oxide adsorption', *J. Chem. Soc., Faraday Trans. 1*, **85**, 79–90.
- 1063a. Pershin, A. N., Shelimov, B. N. and Kazanskii, V. B. (1980), 'Study of the interaction of Mo^{4+} ions with nitrogen oxides on the surface of silica gel', *Kinet. Katal.* (in Russian); *Kinet. Catal.* (English translation), **21**, 753–759.
- 1063b. Shelimov, B. N., Pershin, A. N. and Kazanskii, V. B. (1980), 'Selective photoreduction of molybdenum ions on silica', *J. Catal.*, **64**, 426–436.
- 1063c. Pershin, A. N., Shelimov, B. N. and Kazanskii, V. B. (1980), 'Low temperature photoreduction—a new approach to the preparation of low coordinated ions of transition metals on the surfaces of oxide catalysts, in *New Horizons in Catalysis, Proceedings of the 7th International Congress on Catalysis, Tokyo, June 30–July 4, 1980*, Seiyama, T. and Tanabe, K. (Eds.) *Studies in Surface Science and Catalysis*, v.7, Kodansha, Tokyo, Elsevier, Amsterdam, 1980, Paper B39, pp. 1210–1219.
1064. Vuurman, M. and Wachs, I. E. (1992), '*In situ* Raman spectroscopy of alumina-supported metal oxide catalysts', *J. Phys. Chem.*, **96**, 5008–5016.

1065. Franklin, D., Hardcastle, D. and Wachs, I. E. (1988), 'Raman spectroscopy of chromium oxide supported on Al_2O_3 , TiO_2 , and SiO_2 : a comparative study', *J. Mol. Catal.*, **46**, 173–186.
- 1066a. Rebenstorf, B. (1988), 'An IR study of the polymerization mechanism of the Philips catalyst', *J. Mol. Catal.*, **45**, 263–274.
- 1066b. Rebenstorf, B. (1989), 'On the catalytic activity of mononuclear and dinuclear chromium(II) – a surface species on silica gel', *Acta Chem. Scand.*, **43**, 413–416.
- 1066c. Rebenstorf, B. (1990), 'Modified chromium/silica gel catalysts: impregnation of the silica gel with titanylacetate and comparison with chromium on SiO_2 and TiO_2 ', *J. Chem. Soc., Faraday Trans. 1*, **86**, 2783–2788.
1067. Haukka, S. and Saastamoinen, A. (1992), 'Determination of chromium and titanium in silica-based catalysts by ultraviolet/visible spectrophotometry', *Analyst*, **117**, 1381–1384.
1068. Fubini, B., Ghiotti, G., Stradella, L., Garrone, E. and Mortera, C. (1980), 'The chemistry of silica-supported Cr ions: a characterization of the reduced and oxidized forms of chromia/silica catalysts by calorimetry and ultraviolet–visible spectroscopy', *J. Catal.*, **66**, 200–213.
- 1069a. Vuurman, M. A., Stufkens, D. J., Oskam, A. and Wachs, I. E. (1992), 'Structural determination of surface rhenium oxide on various oxide supports (Al_2O_3 , ZrO_2 , TiO_2 and SiO_2)', *J. Mol. Catal.*, **76**, 263–285.
- 1069b. Scheithauer, M., Knozinger, H. and Vannice, M. A. (1998), 'Raman spectra of La_2O_3 dispersed on $\gamma\text{-Al}_2\text{O}_3$ ', *J. Catal.*, **178**, 701–705.
- 1069c. Mar, S. Y., Chen, C. S., Huang, Y. S. and Tiong, K. K. (1995), 'Characterization of RuO_2 thin films by Raman spectroscopy', *Appl. Surf. Sci.*, **90**, 497–504.
- 1069d. Graham, G. W., Potter, T. J. and Weber, W. H. (1989), 'Formation of platinum oxide during the thermal oxidation of noble-metal alloys', *J. Vac. Sci. Technol.*, **7**, 1694–1696.
- 1069e. Tolia, A. A., Smiley, R. J., Deglass, W. N., Takoudis, C. G. and Weaver, M. J. (1994) 'Surface oxidation of rhodium at ambient pressures as probed by surface-enhanced Raman and X-ray photoelectron spectroscopy', *J. Catal.*, **150**, 56–70.
- 1069f. Zuo, J. and Xu, C. (1996), 'Raman spectra of nanophase Cr_2O_3 ', *J. Raman Spectrosc.*, **26**, 921–923.
- 1069g. Gotic, M., Popovic, I., Music, S., Tukovic, A. and Furic, K. (1997), 'Raman investigation of nanosized TiO_2 ', *J. Raman Spectrosc.*, **28**, 555–558.
- 1070a. Davydov, A. A. and Goncharova, O. I. (1989) 'Use of the compensation method to study the IR spectra of Mo-containing systems deposited on oxide carriers', *Zh. Prikl. Spektrosk.* (in Russian); *J. Appl. Spectrosc.* (English translation), **50**, 76–80.
- 1070b. Banerjee, D. and Chakraborty, D. K. (1992) 'Supported iron, cobalt and iron–cobalt bimetallic catalysts for Fischer–Tropsch synthesis: Catalyst preparation and characterization', *Indian J. Technol.*, **30**, 81–84.
1071. Mikhilchenko, V. G., Davydov, A. A., Budneva, A. A., Kuznetsov, B. N. and Sokolovskii, V. D. (1975), 'The role of σ - and π -allyl complexes in the oxidation of propylene to acrolein', *React. Kinet. Catal. Lett.*, **2**, 163–170.
1072. Oliferenko, O. V., Davydov, A. A. and Pak, V. N. (1990), 'Structure, thermal transformations of molybdenum-containing silica gel and peculiarities of its interaction with methanol according to infrared spectroscopic data', *Zh. Prikl. Spektrosk.* (in Russian); *J. Appl. Spectrosc.* (English translation), **63**, 2505–2509.
1073. Basset, J. M. and Choplin, A. (1983), 'Organometallic chemistry on surfaces. Reactivity of metal–carbonyl compounds on metal oxides', *J. Mol. Catal.*, **21**, 95–103.
1074. Lamb, H. H., Gates, B. C. and Knozinger, H. (1988), 'Surface organometallic chemistry: a new approach to heterogeneous catalysis?', *Angew. Chem., Int. Ed. Engl.*, **27**, 1127–1132.
1075. Evans, J. (1988), 'Catalysis by supported organometallic complexes', in Basset, J. M., Gates, B. C., Candy, J. P. (Eds), *Surface Organometallic Chemistry: Molecular Approaches to Surface Catalysis*, Kluwer Academic Publishers, Dordrecht, The Netherlands, pp. 47–65.
1076. Kuznetsov, B. N. and Kovalchuk, V. I. (1995), 'Carbonyl clusters of transition metals on oxide supports as heterogeneous catalysts for hydrocarbon synthesis', in *Proceedings of the 1st Russian Cluster Chemistry Conference*, St Petersburg, 1994, *Kinet. Catal.* (in Russian); *Kinet. Catal.* (English translation), **36**, 353–361.
1077. Ichikawa, M. and Shikakura, K. (1980), 'Characterization of surface supported Rh, Pt and Ir carbonyl clusters and their catalytic behaviors in the syntheses of methanol and ethanol from CO and H_2 ', in *New Horizons in Catalysis, Proceedings of the 7th International Congress on Catalysis, Tokyo, June 30–July 4, 1980*, Seiyama, T. and Tanabe, K. (Eds.) *Studies in Surface Science and Catalysis*, v.7, Kodansha, Tokyo, Elsevier, Amsterdam, 1980, pp. 925–939.
1078. Guglielminotti, E., Zecchina, A., Boccuzzi, F. and Borello, E. (1980), 'Growth and properties of metal clusters', in Bourdon, J. (Ed.) *Proceedings of the 32nd International Meeting of the Societe de Chimie Physique*, Villerbanc, September 24–28, 1979 Elsevier, Amsterdam, pp. 165–210.
1079. Rundin, Yu. A., Gorodova, L. V., Tyunina, O. V., Davydov, A. A. and Yermakov, Yu. I. (1984) 'IR spectroscopic studies of $\text{Ru}_3(\text{CO})_{12}$ interactions with dispersed metallic palladium supported on SiO_2 ', *React. Kinet. Catal. Lett.*, **26**, 79–84.
1080. Rundin, Yu. A., Gorodova, L. V., Kozlov, M. A., Kochubei, D. I. and Davydov, A. A. (1984), 'Preparation of bimetallic catalysts by interaction of carbonyl clusters with a supported metal surface', in

- Proceedings of the 1st Italian–Soviet Seminar on Catalytic Applications to the Energy Problem*, Messina, Italy, Vol. 1, 165–190.
1081. Matyshak, V. A., Kadushin, A. A. and Edreva-Kardzhieva, R. M. (1983), 'Effect of temperature of the support pretreatment on activation of $\text{Mo}(\text{CO})_6/\text{Al}_2\text{O}_3$ catalysts for C_3H_6 methathesis', *Kinet. Katal.* (in Russian); *Kinet. Catal.* (English translation), **24**, 1255–1258.
1082. Ivashenko, V. L., Sayapin, E. V., Davydov, A. A. and Egorova, G. M. (1986), 'Metal-complex heterogeneous catalysts for purification of waste gases from nitric acid production', *Z. Prikl. Khim.* (in Russian); *Russ. J. Appl. Chem.* (English translation), **61**, 431–434.
1083. Filicheva, O. D., Davydov, A. A., Belikhmaer, Ya. A. and Ivashenko, V. L. (1992), 'Study of the diffuse reflectance electron spectroscopy of cobalt tetrasulphatophthalocyanine supported on $\gamma\text{-Al}_2\text{O}_3$ ', *Zh. Fiz. Khim.* (in Russian); *Russ. J. Phys. Chem.* (English translation), **66**, 3276–3280.
1084. Filicheva, O. D., Belikhmaer, Ya. A., Davydov, A. A. and Ivashenko, V. L. (1993), 'Formation of an active component of the tetrasulphatophthalocyanine catalyst fixed on $\gamma\text{-Al}_2\text{O}_3$ ', *Zh. Fiz. Khim.* (in Russian); *Russ. J. Phys. Chem.* (English translation), **67**, 1987–1990.
1085. Spoto, G., Zecchina, A., Bordiga, S., Scrano, D. and Coluccia, S. (1993), 'Interaction of chromocene with MgO and reactivity of the adsorbed species towards CO: an IR study', *Spectrochim. Acta, Part A*, **49**, 1235–1245.
1086. Shekochkhin, Yu. M. and Davydov, A. A. (1976), 'Study of reactions on Al_2O_3 by means of IR spectroscopy', (in Russian), *Adsorptsiya Adsorbenty*, **4**, 75–80.
1087. Gordymova, T. A. and Davydov, A. A. (1979) 'Spectroscopic investigation of propylene complexes on the surface of γ -aluminum oxide and mechanisms of isomerization', *Dokl. AN SSSR* (in Russian); *Proc. AN USSR* (English translation), **245**, 635–639.
1088. Davydov, A. A. and Shekochihin, Yu. M. (1969), 'IR spectra of ND_3 adsorbed on Al_2O_3 ', *Kinet. Katal.* (in Russian); *Kinet. Catal.* (English translation), **10**, 163–171.
1089. Engelhardt, J., Onyestyak, K. and Hall, W. K. (1995), 'Induced catalytic activity of fluorided alumina in the reactions of isobutane', *J. Catal.*, **157**, 721–729.
1090. Komarov, V. S. and Sinilo, M. F. (1986), 'IR-spectroscopic investigation of the acid properties of the surface of zirconium oxide modified by sulfate ions', *Kinet. Katal.* (in Russian); *Kinet. Catal.* (English translation), **29**, 701–705.
1091. Hadzhiivanov, K. I. and Davydov, A. A. (1986), 'IR spectroscopic study of the surface of TiO_2 anatase modified with sulfuric acid', *Kinet. Katal.* (in Russian); *Kinet. Catal.* (English translation), **29**, 398–402.
1092. Zundel, G. (1969), 'Hydration structure and intermolecular interaction in polyelectrolytes', *Angew. Chem.*, **8**, 499–511.
1093. Morrow, B. A., McFarlane, R. A., Lion, M. and Lavalley, J. C. (1987), 'An infrared study of sulfated silica', *J. Catal.*, **107**, 232–239.
1094. Saur, O., Bensitel, M., Saad, A. B. M., Lavalley, J. C., Tripp, C. P. and Morrow, B. A. (1986), 'The structure and stability of sulfated alumina and titania', *J. Catal.*, **99**, 104–110.
1095. Corma, A., Fornes, V., Juan-Rajadell, M. I. and Lopez Nieto, J. M. (1994), 'Influence of preparation conditions on the structure and catalytic properties of $\text{SO}_4^{2-}/\text{ZrO}_2$ superacid catalysts', *Appl. Catal., A: Gen.*, **116**, 151–163.
1096. Hadzhiivanov, K. I., Klissurski, D. G. and Davydov, A. A. (1989), 'Study of phosphate-modified TiO_2 (anatase)', *J. Catal.*, **116**, 498–505.
1097. Burylin, S. Yu., Davydov, A. A., Rachkovskaya, L. N., Budneva, A. A., Frolova, I. I. and Anufrienko, V. F. (1992), 'Infrared spectroscopic study of the nature and properties of the surface of divinyl-carbonized aluminum oxide', *Zh. Prikl. Spektrosk.* (in Russian); *J. Appl. Spectrosc.* (English translation), **57**, 239–245.
- 1098a. Atkinson, R. J., Parfitt, R. L. and Smart, R. S. C. (1974), 'IR study of phosphate adsorption on goethite', *J. Chem. Soc., Faraday Trans. 1*, **70**, 1472–1479.
- 1098b. Atkinson, R. J., Parfitt, R. L. and Smart, R. S. C. (1977), 'IR spectra from binuclear bridging complexes of sulfate adsorbed on goethite', *J. Chem. Soc., Faraday Trans. 1*, **73**, 796–802.
- 1098c. Atkinson, R. J., Parfitt, R. L. and Smart, R. S. C. (1977), 'Adsorption of hydrous oxide. I. Oxalate and benzoate on goethite', *J. Soil Sci.*, **28**, 29–41.
- 1098d. Atkinson, R. J., Parfitt, R. L. and Smart, R. S. C. (1977), 'Adsorption of hydrous oxide. II. Mechanism of various ions', *J. Soil Sci.*, **28**, 41–62.
1099. Signoretto, M., Pinna, F., Strukul, G., Chies, P., Cerrato, G., Di Ciero, S. and Morterra, C. (1997), 'Platinum-promoted and unpromoted sulfated zirconia catalysts prepared by a one-step aerogel procedure. 2. Catalytic activity in the isomerization of *n*-butane', *J. Catal.*, **167**, 522–532.
1100. Morterra, C., Cerrato, G., Pinna, F. and Signoretto, M. (1995), 'Crystal phase, spectral features, and catalytic activity of sulfate-doped zirconia systems', *J. Catal.*, **157**, 109–123.
1101. Arata, K. (1996), 'Preparation of superacids by metal oxides for reactions of butanes and pentanes', *Appl. Catal., A: Gen.*, **146**, 3–32.
1102. Przystajko, W., Fiedorow, R. and Dalla Lana, I. G. (1985), 'Surface properties of sulphate-containing aluminas', *Appl. Catal.*, **15**, 265–275.

1103. Wagif, M., Bachelier, J., Saur, O. and Lavalley, J. C. (1992), 'Acidic properties and stability of sulfate-promoted metal oxides', *J. Mol. Catal.*, **72**, 127–138.
1104. Ramis, G., Busca, G., Lorenzelli, V., Rossi, P., Bensitel, M., Saur, O. and Lavalley, J. C. (1992), Olefin oligomerization on supported phosphoric acid: an FT-IR study of the active sites, in *New Frontiers in Catalysis. Proceedings of the 10th International Congress on Catalysis, Budapest, Hungary, 19–24 July, 1992*, Gucci, L., Solimosi, F. and Tetenyi, P. (Eds.) *Studies in Surface Science and Catalysis*, v.75, Elsevier, Amsterdam, 1992, pp. 1874–1881.
1105. Flanigen, E. M. (1986), 'Adsorption properties of molecular zeolites', in Murakami, Y., Iijima, A., and Ward, J.M. (Eds.) *Proceedings of the 8th International Conference on Zeolites*, Tokyo, August 17–22, 1986 Kodasha Tokyo pp. 2–18.
1106. Sohn, J. R., Jang, H. J. and Kim, H. W. (1990), 'Catalytic activities and acid properties of NiO–ZrO₂ catalysts modified with acids', *Korean J. Chem. Eng.*, **7**, 7–12.
1107. Kibbi, C. L. and Hall, W. K. (1985), 'Surface properties of calcium phosphates', in Graselli, R. K. and Brazdil, J. F. (Eds.) *Solid State Chemistry of Catalysts*, ACS Symp Series 279, American Chemical Society, Washington, DC, pp. 663–729.
1108. Lange, F., Hadjiivanov, K., Schmelz, H. and Knozinger, H. (1992), 'Low temperature infrared study of carbon monoxide adsorption on sulfated titania', *Catal. Lett.*, **16**, 97–107.
1109. Mennour, A., Ecolivet, C., Cornet, D., Hemidy, J. F. and Lavalley, J. C. (1989), 'Characterization by transmission and reflectance vibrational spectroscopy of phosphated alumina', in Morterra, C., Zecchina, A. and Costa, G. (Eds.) *Structure and Reactivity of Surfaces*, Elsevier, Amsterdam, pp. 25–30.
1110. White, R. L., Sikabwe, E. C., Coelho, M. A. and Resasco, D. E. (1995), 'Potential role of pentacoordinated sulfur in the acid site structure of sulfated zirconia', *J. Catal.*, **157**, 755–758.
1111. Hattori, H., Takahashi, O., Takagi, M. and Tanabe, K. (1981), 'Solid super acids: preparation and their catalytic activities for reaction on alkanes', *J. Catal.*, **68**, 132–143.
1112. Tanabe, K. (1985), 'Surface and catalytic properties of ZrO₂', *Mater. Chem. Phys.*, **13**, 347–364.
1113. Srinivasan, R., Keogh, A. and Davis, B. H. (1996), 'Sulfated zirconia catalysts: are Brønsted acid sites the source of the activity?', *Catal. Lett.*, **36**, 51–57.
1114. Morterra, C., Cerrato, G., Emanuel, C. and Bolis, V. (1993), 'On the surface acidity of some sulfate-doped ZrO₂ catalysts', *J. Catal.*, **142**, 349–367.
1115. Spielbauer, D., Mekhemer, G. A. H., Bosch, E. and Knozinger, H. (1996), '*n*-butane isomerization on sulfated zirconia. Deactivation and regeneration as studied by Raman, UV–VIS diffuse reflectance and ESR spectroscopy', *Catal. Lett.*, **36**, 59–68.
1116. Nascimento, P., Akrapoulou, C., Oszagyan, M., Coudurier, G., Travers, C., Joly, J. F. and Vedrine, J. C. (1992), 'ZrO₂–SO₄²⁻ catalysts. Nature and stability of acid sites responsible for *n*-butane isomerization, in *New Frontiers in Catalysis. Proceedings of the 10th International Congress on Catalysis, Budapest, Hungary, 19–24 July, 1992*, Gucci, L., Solimosi, F. and Tetenyi, P. (Eds.) *Studies in Surface Science and Catalysis*, v.75, Elsevier, Amsterdam, 1992, pp. 1185–1197.
1117. Ramis, G., Busca, G. and Lorenzelli, V. (1989), 'Surface acidity of solid acids and superacids: an FT-IR study of the behavior of titania doped with phosphoric, sulphuric, tungstic and molybdic acids', in Morterra, C., Zecchina, A. and Costa, G. (Eds.) *Structure and Reactivity of Surfaces*, Elsevier, Amsterdam, pp. 777–786.
1118. Mennour, A., Ecolivet, C., Cornet, D., Hemidy, J. F. and Lavalley, J. C. (1988), 'Characterization by transmission and reflectance vibrational spectroscopy of phosphated alumina', *Mater. Chem. Phys.*, **19**, 301–313.
1119. Jin, T., Yamaguchi, T. and Tanabe, K. (1986), 'Mechanism of acidity generation on sulfur promoted metal oxide', *J. Phys. Chem.*, **90**, 4794–4796.
1120. Yamaguchi, T., Jin, T., Ishida, T. and Tanabe, K. (1987), 'Spectral identification of acid sites of sulfur-promoted solid super acid and construction of its structure on silica support', *Mater. Chem. Phys.*, **17**, 3–19.
1121. Yamaguchi, T. (1990), 'Recent progress in solid superacid', *Appl. Catal.*, **61**, 1–25.
1122. Tanabe, K., Hattori, H. and Yamaguchi, T. (1990), 'Surface properties of solid super acids', *Crit. Rev. Surf. Chem.*, **1**, 1–40.
1123. Morterra, C., Pinna, F., and Cerrato, G. (1994), 'The Brønsted acidity of a dehydrated and rehydrated (inactive) superacid sulphate-doped ZrO₂ system', *J. Phys. Chem.*, **98**, 12373–12381.
1124. Kustov, L. M., Kazansky, V. B., Figueras, F. and Tichit, D. (1994), 'Investigation of the acidic properties of ZrO₂ modified by SO₄²⁻ anions', *J. Catal.*, **150**, 143–149.
1125. Sayed, M. B. (1987), 'Origin of boron mobility over boron-impregnated ZSM-5', *J. Chem. Soc., Faraday Trans. 1*, **83**, 1751–1763.
1126. Delmastro, A., Gozzelino, G., Mazza, D. and Vallino, M. (1992), 'Characterization of microporous amorphous alumina–boria', *J. Chem. Soc., Faraday Trans. 1*, **88**, 2065–2070.
1127. Ramirez, J. *et al.* (1995), 'Effect of boron addition on the activity and selectivity of hydrotreating CoMo/Al₂O₃ catalysts', *Appl. Catal., A: Gen.*, **132**, 317–334.
1128. Engels, S., Herold, E., Lausch, H., Mayr, H., Meiners, H. W. and Wilde, M. (1993), 'Boron—an acidity and texture modifier for alumina supported catalysts', in *New Frontiers in Catalysis. Proceedings of the*

- 10th International Congress on Catalysis, Budapest, Hungary, 19–24 July, 1992, Guzzi, L., Solimosi, F. and Tetenyi, P. (Eds.) *Studies in Surface Science and Catalysis*, v.75, Elsevier, Amsterdam, 1992, pp. 871–878.
1129. Xu, W.-Q., Suib, S. L. and Young, C.-L. O. (1993), 'Studies of acidic sites on borates by temperature-programmed desorption (TPD) of NH_3 , C_2H_4 and C_4H_8 ', *J. Catal.*, **144**, 285–295.
1130. Delmastro, A., Gozzelino, G., Mazza, D., Vallino, M., Busca, G. and Lorenzelli, V. (1992), 'Characterization of microporous amorphous alumina-boria', *J. Chem. Soc., Faraday Trans. 1*, **88**, 2065–2070.
1131. Segawa, K., Kim, D. S., Kurusu, Y. and Wachs, I. E. (1980), Surface design of supported molybdena catalysts, in *New Horizons in Catalysis, Proceedings of the 7th International Congress on Catalysis, Tokyo, June 30–July 4, 1980*, Seiyama, T. and Tanabe, K. (Eds.) *Studies in Surface Science and Catalysis*, v.7, Kodansha, Tokyo, Elsevier, Amsterdam, 1980, pp. 1960–1967.
1132. Laperches, J. P. and Tarte, P. (1966), 'Spectres d'absorption infrarouge de borates de terres rares', *Spectrochim. Acta, Part A*, **22**, 1201–1210.
1133. Broadhead, P. and Newman, G. D. (1972), 'OH groups and hydrogen bonding in some boron–oxygen compounds', *Spectrochim. Acta, Part A*, **28**, 1915–1923.
1134. Denning, J. H. and Ross, S. D. (1972), 'The vibrational spectra and structures of some rare-earth borates', *Spectrochim. Acta, Part A*, **28**, 1775–1788.
- 1135a. Ross, S. D. (1972), 'The vibrational spectra of some minerals containing tetrahedrally coordinated boron', *Spectrochim. Acta, Part A*, **28**, 1555–1561.
- 1135b. Davydov, A. A. (unpublished data).
1136. Akimoto, M., Tsuchida, Y. and Echigoya, E. (1980), 'Regulation of oxidative activity of Mo^{6+} ions in different 12 HPAs (Mo)', *Chem. Lett.*, 1205–1208.
1137. Goncharova, O. I. Yurieva, T. M. and Davydov, A. A. (1986), 'Influence of the nature of the support on the composition and structure of molybdenum supported heteropolycompounds', *Kinet. Katal.* (in Russian); *Kinet. Catal.* (English translation), **27**, 942–949.
- 1138a. Kazanskii, L. P. (1975), 'Molecular and electronic structure of HP complexes. I. Correlation between electronic transitions of heterogeneous polyanions and the reduction half-wave potentials', *Izv. Acad. Nauk. SSSR, Ser. Khim.* (in Russian); *Russ. Chem. Bull.* (English translation), 497–502.
- 1138b. Kazanskii, L. P. (1975), 'Molecular and electronic structure of HP complexes. II. IR and Raman spectra of crystalline heterogeneous polyacids and their aqueous solutions', *Izv. Acad. Nauk. SSSR, Ser. Khim.* (in Russian); *Russ. Chem. Bull.* (English translation), 502–510.
1139. Yurchenko, E. N. (1986), *Molecular Spectroscopy in the Chemistry of Coordination Compounds and Catalysts* (in Russian), Nauka, Novosibirsk.
1140. Tsigdinas, G. A. (1978), 'Heteropoly compounds of molybdenum and tungsten', in *Topics in Current Chemistry*, Vol. 76, Springer-Verlag, Berlin, pp. 1–17.
1141. Kazanskii, L. P., Torchenkova, E. A. and Spitsyn, V. I. (1974), 'Structural principles in the chemistry of HPCs', *Usp. Khim.* (in Russian); *Russ. Chem. Rev.* (English translation), **43**, 1137–1159.
1142. Okuhara, T., Kasai, A., Hayakama, N., Yoneda, Y., Misono, M., and Sakata, K. (1983), 'Catalysis by HPC. 6. The role of the bulk acid sites in catalytic reactions over $\text{Na}_x\text{H}_{3x}\text{PW}_{12}\text{O}_{40}$ ', *J. Catal.*, **83**, 121–130.
1143. Misono, M., Sakata, K., Yoneda, Y. and Lece, W. Y. (1980), Acid-redox bifunctional properties of HPC in *New Horizons in Catalysis, Proceedings of the 7th International Congress on Catalysis, Tokyo, June 30–July 4, 1980*, Seiyama, T. and Tanabe, K. (Eds.) *Studies in Surface Science and Catalysis*, v.7, Kodansha, Tokyo, Elsevier, Amsterdam, 1980.
1144. Yur'eva, T. M., Shohireva, T. Kh., Goncharova, O. I. and Boreskov, G. K. (1985), 'Phase composition and catalytic properties of molybdenum-containing oxide catalysts', *Kinet. Katal.* (in Russian); *Kinet. Catal.* (English translation), **26**, 1439–1445.
1145. Davydov, A. A., Kuznetsova, T. G. and Andrushkevich, T. V. (1986), 'IR spectra of individual compounds formed in V–Mo–O systems under catalytic oxidation of acrolein', *React. Kinet. Catal. Lett.*, **30**, 173–178.
1146. Rushala, F., Shiryaev, P. A., Kutyrev, M. Yu., Kushnarev, M. Ya. and Shashkin, D. P. (1981), 'Effect of phosphorus ions on the structure and catalytic properties of nickel and cobalt molybdates', *Kinet. Katal.* (in Russian); *Kinet. Catal.* (English translation), **22**, 1307–1312.
1147. Oganowska, W., Hanuza, J., Jezowska-Trzebiatowska, B. and Wrzysla, J. (1975), 'Physico-chemical properties and structure of MgMoO_4 – MoO_3 catalyst', *J. Catal.*, **39**, 161–172.
1148. Mikhailchenko, V. G., Sokolovskii, V. D., Filippova, A. A. and Davydov, A. A. (1973), 'Formation of products of complete and partial oxidation of adsorbed propylene', *Kinet. Katal.* (in Russian); *Kinet. Catal.* (English translation), **14**, 1253–1259.
1149. Davydov, A. A., Mikhailchenko, V. C., Sokolovskii, V. D. and Boreskov, G. K. (1978), 'Surface complexes of propylene and their role in catalytic oxidation', *J. Catal.*, **55**, 299–313.
1150. Davydov, A. A., Efremov, A. A., Mikhailchenko, V. C. and Sokolovskii, V. D. (1979), 'The surface compounds and the routes of formation of the reaction products in the interaction of propylene with zinc oxide', *J. Catal.*, **58**, 1–7.
- 1151a. Davydov, A. A. (1985), 'The nature of surface sites of the oxide and their role in the formation of olefin complexes', *Mater. Chem. Phys.*, **13**, 243–260.

- 1151b. Davydov, A. A. (1992), 'Donor-acceptor properties of the cations of oxide surface', *Kinet. Katal.* (in Russian); *Kinet. Catal.* (English translation), **66**, 3270-3275.
1152. Liengme, B. V. and Hall, W. K. (1966), 'Studies of hydrogen held by solids. Part 2. Interaction of simple olefins and pyridine with decationated zeolites', *Trans. Faraday Soc.*, **62**, 3229-3236.
- 1153a. Onida, B., Allian, M. and Carrone, E. (1997), 'IR study of the adsorption of unsaturated hydrocarbons on highly outgassed silica. Spectroscopic and thermodynamic results', *Langmuir*, **13**, 5107-5112.
- 1153b. Natal-Santiago, M. A., de Pablo, J. J. and Dumesic, J. A. (1997), 'Microcalorimetric, FTIR and DFT studies of the adsorption of isobutene on silica', *Catal. Lett.*, **47**, 119-128.
- 1154a. Datka, J. (1980), 'Transformations of but-1-ene molecules adsorbed in NaHY zeolites studied by infrared spectroscopy', *J. Chem. Soc., Faraday Trans. 1*, **76**, 2437-2447.
- 1154b. Datka, J. (1980), 'IR spectroscopy studies of butene adsorption', *J. Chem. Soc., Faraday Trans. 1*, **76**, 705-710.
- 1154c. Kondo, J. N., Liqun, S., Wakabayashi, F. and Domen, K. (1997), 'IR study of adsorption and reaction of 1-butene on H-ZSM-5', *Catal. Lett.*, **47**, 129-133.
- 1155a. Gordymova, T. A. and Davydov, A. A. (1979), Spectroscopic investigation of propylene complexes on catalysts and mechanisms of isomerization', in *Heterogeneous Catalysis, Proceedings of the 4th International Symposium of the Bulgarian Academy of Sciences, Varna Sofia, 1979, BAS Part 1*, pp. 157-162.
- 1155b. Gordymova, T. A. and Davydov, A. A. (1980), Investigation of propylene transformations on Al₂O₃ and type Y zeolites by means of IR spectroscopy', in *Vozdvizenskii, V. F. (Ed.) Abstracts of the 6th All Union Workshop on the Use of Optical Spectroscopy in Adsorption and Catalysis* (in Russian), Institute of Organic Catalysis and Electrochemistry, Alma-Ata, Kazakhstan, pp. 91-92.
- 1156a. Busca, G., Lorenzelli, V., Ramis, G., Saussey, J. and Lavalley, J. C. (1992), 'FT-IR spectra of ethylene molecularly adsorbed on metal oxides', *J. Mol. Struct.*, **267**, 315-329.
- 1156b. Busca, G., Marchetti, L., Zerlia, T., Girelli, A., Sorlino, M. and Lorenzelli, V. (1984), Spectroscopic studies of the adsorption of unsaturated hydrocarbons and of their reaction with surface oxygen species on metal oxides', in *Proceedings of the 8th International Congress on Catalysis, Berlin 1984*, Verlag Chemie, Weinheim, Germany, 1984, III299-III310.
- 1156c. Busca, G., Lorenzelli, V., Ramis, G. and Escibano Sanchez, V. (1991), 'Chemistry of olefins at metal oxide surfaces: a tool for surface science investigations of oxide catalysts', *Mater. Chem. Phys.*, **22**, 175-189.
1157. Davydov, A. A. (1988), 'Nature of surface sites of oxides and their role in the formation of toluene complexes', *Mater. Chem. Phys.*, **19**, 97-112.
1158. Spoto, G. and Bordiga, S. (1994), 'IR study of ethene and propene oligomerization on H-ZSM-5. Hydrogen-bonded precursor formation, initiation, mechanisms and structure of the entrapped oligomers', *J. Chem. Soc., Faraday Trans. 1*, **90**, 2827-2833.
1159. Gussoni, M. (1986), 'Infrared intensities: a new tool in chemistry', *J. Mol. Struct.*, **141**, 63-71.
1160. Duncan, J. L., McKean, D. C. and Mallison, P. D. (1973), 'IR crystal spectra of ethylene, ethylene-d₄, and ethylene-d₂ and the general harmonic force field of ethylene', *J. Mol. Spectrosc.*, **45**, 221-235.
1161. Knippers, W., Van Helwoort, K., Stolte, S. and Reuss, G. (1985), 'Raman overtone spectroscopy of ethylene', *J. Chem. Phys.*, **89**, 1-10.
1162. Panchenko, Yu. N. (1975), 'Vibrational spectrum of 1,3-butadiene-2,3-d₂', *Spectrochim. Acta, Part A*, **31**, 1201-1205.
1163. Efremov, A. A. and Davydov, A. A. (1980), 'Investigation of hydrocarbon adsorption on oxide catalysts by means of IR spectroscopy. VIII. Modes of adsorption and sites of propylene and ethylene stabilization on ZnO', *Kinet. Katal.* (in Russian); *Kinet. Catal.* (English translation), **21**, 488-493.
1164. Eberly, P. E. (1967), 'High temperature IR studies of olefins adsorbed on faujasites', *J. Phys. Chem.*, **71**, 1717-1721.
1165. Novakova, J., Kubelkova, L., Dolejek, Z. and Jiru, P. (1979), 'Different activities of H-ZSM-5 and HNaY zeolites in the interaction with ethylene. Effect of water vapor', *Collect. Czech. Chem. Commun.*, **44**, 3341-3356.
1166. Kazanskii, V. B. (1987), 'Modern conceptions regarding the mechanism of heterogeneous acid catalysts', *Kinet. Katal.* (in Russian); *Kinet. Catal.* (English translation), **28**, 47-63.
1167. Davydov, A. A. and Budneva, A. A. (1982), 'Interaction of propylene with a V₂O₅/Al₂O₃ catalyst', *React. Kinet. Catal. Lett.*, **20**, 107-112.
1168. Davydov, A. A., Efremov, A. A., Kasumov, F. B. and Adzhamov, K. Yu. (1981), 'Role of acid centers of Sn/Mo oxide catalysts in propylene conversion to acetone', *React. Kinet. Catal. Lett.*, **18**, 29-32.
1169. Vedrin, J. C., Dejaife, P., Garbovski, E. D. and Derouane, E. G. (1980), 'Aromatic formation from methanol and light olefins conversions on H-ZSM-5 zeolite: mechanism and intermediate species', in Imelik, B., Naccache, C., Bentaazit, Y., Vedziué, T. C., Gouzduéri, G., and Pzaliaud, H. (Eds), *Proceedings of International Symposium on Catalysis by Zeolites*, Ecully Lyon, September 9-11, 1980 Elsevier, Amsterdam, pp. 29-35.
1170. Garbovski, E. D. and Praliand, H. (1979), 'UV spectroscopy study of the interaction of olefins with acid centers in heterogeneous catalysts', *J. Chim. Phys. Chim. Biol.*, **76**, 687-695.

1171. Coudurier, G., Dekamp, T. and Praliand, H. (1982), 'Comparison of copper and cobalt exchanged zeolites by UV-Vis and IR spectroscopies', *J. Chem. Soc., Faraday Trans. 1*, **78**, 2661-2678.
1172. Fejes, P., Forster, H., Kiricsi, I. and Seebode, J. (1984), 'Carbocation formation in zeolites. UV-Vis and NIR spectroscopic investigations on H-mordenite', in Jacobs, P. A. Taeger, N. I. Tiru, P., Kazanskii, V. B. and Schulz-Ekloff, J. (Eds), *Proceedings of International Conference of Structure and Reactivity of Modified Zeolites*, Pzaque, 1984 Elsevier, Amsterdam, pp. 91-100.
1173. Forster, H. and Seebode, J. (1985), 'Spectroscopic and kinetic studies of cyclopropane isomerization over mordenites of different acidity', in *Proceedings of International Symposium on Zeolite Catalysts*, Siofok, Hungary, Budapest pp. 413-419.
1174. Deno, N. K. (1963), 'Carboanions', in Cohen, S. G., (Ed), *Progress in Physical Organic Chemistry*, Wiley, New York, pp. 393-451.
1175. Bolis, V., Vedin, J. C., Van de Berg, J. P., Wolthuizen, J. P. and Derouane, E. G. (1980), 'Adsorption and activation of ethene by zeolite H-ZSM-5', *J. Chem. Soc., Faraday Trans. 1*, **76**, 1606-1613.
- 1176a. Haber, J., Komorek, J. and Romotowski, T. (1985), Formation of deposits from aromatics on HNaY zeolite', in *Proceedings of International Symposium on Zeolite Catalysts*, Siofok, Hungary, Budapest pp. 671-678.
- 1176b. Dzwigai, S., Haber, J. and Romotowski, T. (1984), 'Initiating effect of C_2^+ olefins and alcohols on the transformations of methanol on crystalline and amorphous aluminosilicates', *Zeolites*, **4**, 147-153.
1177. Demidov, A. V., Davydov, A. A. and Kurina, L. N. (1986), Mechanism of the formation of surface aromatic complexes from methanol and propene over zeolites, in *Trudy IV. Vsesoyuznoi Konferentsii po Mekhanizmu Kataliticheskikh Reaktsii* (in Russian) (*Abstracts of Papers presented to the 4th All-Union Conference on the Mechanisms of Catalytic Reactions*), Moscow, Vol. 1, pp. 295-299.
1178. Kontnik-Mattechka, B., Gorska, M., Eysymantt, J. and Salek, A. (1982), 'Infrared study of methanol, deuterated methanol and ethene on the surface of ZSM-5 type zeolite', *J. Mol. Struct.*, **80**, 199-215.
1179. Grosh, A. K. and Kydd, R. A. (1986), 'Fourier-transform infrared spectral study of propene reactions on acidic zeolites', *J. Catal.*, **100**, 185-191.
1180. Leichert, H., Dimitrov, C., Bezuhanova, C. and Nenova, V. (1983), 'Infrared spectral characteristics of the interaction of olefins with H-ZSM-5 zeolite', *J. Catal.*, **80**, 457-463.
1181. Demidov, A. V. and Davydov, A. A. (1994), 'Spectroscopic evidence for the formation of carbenium ions on H-ZSM-5 zeolites', *Mater. Chem. Phys.*, **39**, 13-20.
- 1182a. Demidov, A. V., Davydov, A. A. and Kurina, L. N. (1989), 'Alkenyl carbenium ions on HTsVK zeolites', *Izv. Acad. Nauk. SSSR, Ser. Khim.* (in Russian); *Russ. Chem. Bull.* (English translation), **6**, 1229-1233.
- 1182b. Demidov, A. V., Davydov, A. A. and Kurina, L. N. (1987), 'Study of hydrocarbons adsorption by means of IR spectroscopy. XV. Alkenyl carbenium ions formed on HTsVK zeolites', *Kinet. Katal.* (in Russian); *Kinet. Catal.* (English translation), **28**, 1278-1279.
1183. Demidov, A. A., Kazantseva, T. A. and Davydov, A. A. (1990), 'The formation of surface aromatic complexes from olefins and methanol on high-silica zeolites', *Zh. Fiz. Khim.* (in Russian); *Russ. J. Phys. Chem.* (English translation), **64**, 259-262.
1184. Sorensen, T. S. (1965), 'The preparation and reactions of a homologous series of aliphatic polyenylic cations', *J. Am. Chem. Soc.*, **87**, 5075-5081.
1185. Medin, A. S., Borovkov, V. Yu. and Kazanskii, V. B. (1986), 'About the mechanism of oligomerization and aromatization of lower olefins on ZSM type zeolites', in *Trudy IV. Vsesoyuznoi Konferentsii po Mekhanizmam Kataliticheskikh Reaktsii* (in Russian) (*Abstracts of Papers presented to the 4th All-Union Conference on the Mechanisms of Catalytic Reactions*) Moscow, Vol. 1, pp. 275-281.
1186. Davydov, A. A. (1981), 'Nature of the adsorption centers of oxide catalysts and the direction of propylene conversion', *React. Kinet. Catal. Lett.*, **18**, 25-28.
- 1187a. Sanchez Escribano, E., Busca, G. and Lorenzelli, V. (1990), 'FT-IR spectroscopic studies of the reactivity of vanadia-titania catalysts towards olefins. I. Propene', *J. Phys. Chem.*, **94**, 8939-8944.
- 1187b. Sanchez Escribano, E., Busca, G. and Lorenzelli, V. (1990), 'FT-IR spectroscopic studies of the reactivity of vanadia-titania catalysts towards olefins. II. Ethene', *J. Phys. Chem.*, **94**, 8945-8950.
- 1187c. Sanchez Escribano, E., Busca, G. and Lorenzelli, V. (1990), 'FT-IR spectroscopic studies of the reactivity of vanadia-titania catalysts towards olefins. III. *n*-Butenes and iso-butene', *J. Phys. Chem.*, **95**, 5541-5547.
1188. Ono, T., Mukai, T., Miyata, H., Ohno, T. and Hatayama, F. (1989), 'Selectivities and intermediates in the oxidation of butene on vanadium oxides on titania', *J. Appl. Catal.*, **49**, 273-285.
1189. Miyata, H., Kohno, M., Ono, T., Ohno, T. and Hatayama, F. (1989), 'Structure of vanadium oxides on ZrO_2 and the oxidation of butene', *J. Chem. Soc., Faraday Trans. 1*, **85**, 3663-3373.
1190. Efremov, A. A. and Davydov, A. A. (1982), 'IR-spectroscopic studies of adsorption and conversion of isopropyl alcohol on a Sn/Mo oxide catalyst', *React. Kinet. Catal. Lett.*, **18**, 363-366.
1191. Davydov, A. A., Shchekochikhin, V. M., Zaitsev, P. M. and Keier, N. P. (1971), 'Reactivity of oxygen species absorbed on chromia', *Kinet. Katal.* (in Russian); *Kinet. Catal.* (English translation), **12**, 698-703.
1192. Davydov, A. A., Budneva, A. A. and Paukshtis, E. A. (1991), 'IR spectroscopic study of hydrocarbon adsorption on oxide catalysts. 17. Formation of butenyl carbonium ion on the surface of the acid catalyst V_2O_5/Al_2O_3 ', *Kinet. Katal.* (in Russian); *Kinet. Catal.* (English translation), **32**, 404-409.

1193. Davydov, A. A., Budneva, A. A. and Paukshtis, E. A. (1989), 'Formation of aromatic carbonium ions on V_2O_5/Al_2O_3 ', *React. Kinet. Catal. Lett.*, **39**, 419–424.
1194. Ledo, B., Rives, V., Sanchez-Escribano, V. and Busca, G. (1993), 'An FT-IR assessment of iso- C_4H_8 reactivity with V_2O_5/TiO_2 catalysts', *Catal. Lett.*, **18**, 329–335.
1195. Busca, G., Ramis, G. and Lorenzelli, V. (1989), 'Adsorption and oligomerization of isobutene on oxide catalyst surfaces', *J. Chem. Soc., Faraday Trans. 1*, **85**, 137–143.
1196. Sanchez-Escribano, V., Busca, G. and Lorenzelli, V. (1991), 'FTIR studies of the reactivity of vanadia–titania catalysts toward olefins', *J. Phys. Chem.*, **95**, 5541–5547.
1197. Al-Mashta, F., Davanzo, C. U. and Sheppard, N. (1983), 'Room temperature polymerization of ethylene on a TiO_2 (anatase) surface; infrared spectroscopic evidence for an alkylidene- Ti^{4+} polymer end-group and for a hydrogen-bonding type of interaction of CH bonds of the polymer chain with the oxide surface', *J. Chem. Soc. Chem. Commun.*, 1258–1259.
1198. Davydov, A. A. (unpublished data).
1199. Al-Mashta, F., Sheppard, N. and Davanzo, C. U. (1985), 'An infrared spectroscopic study of the initial species formed on the polymerization of alkenes on an anatase, TiO_2 , catalyst with surface sulfate', *Mater. Chem. Phys.*, **13**, 315–329.
1200. Aleksanyan, V. G. (1978), Vibrational spectra of π -complexes, in Aleksanyan, V. G. (Ed.), in *Proceedings of the 18th Congress on Spectroscopy*, Part 1, Nauka, Moscow, p. 235.
1201. Carter, J. L., Yates, D. J. C., Lucchesi, P. J., Elliott, J. J. and Kevorkian, V. (1966), 'The adsorption of ethylene on a series of faujasite zeolites studied by infrared spectroscopy and calorimetry', *J. Phys. Chem.*, **70**, 1126–1132.
- 1202a. Efremov, A. A., Lokhov, Yu. A. and Davydov, A. A. (1981), 'IR Spectroscopic Study of hydrocarbon adsorption on oxide catalysts. 10. Modes of adsorption and nature of the adsorption sites for ethylene and propylene on the reduced copper-containing catalysts', *Kinet. Katal.* (in Russian); *Kinet. Catal.* (English translation), **22**, 702–709.
- 1202b. Efremov, A. A., Lokhov, Yu. A. and Davydov, A. A. (1981), 'Spectroscopic study of hydrocarbon adsorption on oxide catalysts. 12. Spectral manifestation of olefin π -complexes', *Kinet. Katal.* (in Russian); *Kinet. Catal.* (English translation), **22**, 1240–1246.
1203. Davydov, A. A. and Efremov, A. A. (1980), Spectral manifestation of olefinic adsorption complexes', in *Proceedings of the 6th All Union Workshop on the Use of Optical Spectroscopy in Adsorption and Catalysis* (in Russian), Alma-Ata Kazakhstan, Institute of Organic Catalysis and Electrochemistry KAS pp. 84–99.
1204. Beran, S. (1984), 'Quantum chemical study of the influence of the zeolite electrostatic field on the physical characteristics of ethylene', *React. Kinet. Catal. Lett.*, **24**, 385–390.
1205. Huang, Y.-Y. (1980), 'Ethylene complexes in copper(I) and silver(I) Y zeolites', *J. Catal.*, **61**, 461–476.
1206. Zakhariyeva, O., Forster, H. and Tuzneva, M. (1994), 'Normal coordinate analysis of deuterio propenes in the free and zeolite-adsorbed state', *Spectrochim. Acta, Part A*, **50**, 19–28.
1207. Zakhariyeva-Pencheva, O. and Forster, H. (1991), 'Normal coordinate analysis of molecules adsorbed on zeolite surfaces. III. *Cis*- and *trans*-but-2-ene in the gas phase and adsorbed in zeolites A', *Vibrational Spectrosc.*, **2**, 227–238.
1208. Zakhariyeva-Pencheva, O. and Forster, H. (1992), 'Quantum chemical studies on the sorption states of hydrocarbons in zeolites. SCC- X_{α} calculations on propene adsorbed to calcium. Part 3. *Cis*- and *trans*-but-2-ene in the gas phase and adsorbed in zeolites A', *J. Mol. Struct.*, **258**, 209–214.
1209. Kirichi, I., Tasi, G. and Fejes, P. (1989), 'Adsorption of propene in zeolites possessing sites of different adsorption energies', *J. Mol. Catal.*, **51**, 341–348.
1210. Efremov, A. A. and Davydov, A. A. (1980), 'Infrared spectra of π -complexes of propylene and ethylene on TiO_2 ', *React. Kinet. Catal. Lett.*, **15**, 327–331.
1211. Efremov, A. A., Pankratiev, Yu. D. and Davydov, A. A. (1982), Energies of olefins complexation on the surface of oxide catalysts', in Borekov, G. K. (Ed.), *Heterogeneous Catalysis* (in Russian), Nauka, Novosibirsk, pp. 102–105.
1212. Davydov, A. A. (unpublished data).
1213. Bash, H. (1972), 'Electronic structure of the silver (1+) ethylene complexes', *J. Chem. Phys.*, **56**, 441–450.
1214. McIntosh, D. and Ozin, G. A. (1976), 'Direct synthesis using copper vapor: infrared and ultraviolet–visible spectra and molecular orbitals: investigation of monoethylene gold(0), $(C_2H_4)_nAu$ ', *J. Organomet. Chem.*, **121**, 127–136.
- 1215a. Huber, H., McIntosh, D. and Ozin, G. A. (1976), 'Direct synthesis using copper vapor: a route to novel binary ethylene complexes of zerovalent copper, $(C_2H_4)_nCu$ (where $n = 1, 2$ or 3)', *J. Organomet. Chem.*, **112**, C50–C54.
- 1215b. Huber, H., Ozin, G. A. and Power, W. J. (1976), 'Modeling catalytic reactions with transition metal atoms. 1. Synthesis and characterization of reactive intermediates in the nickel–ethylene system, $(C_2H_4)_nNi$ (where $n = 1, 2$ or 3) in low-temperature matrices', *J. Am. Chem. Soc.*, **98**, 6508–6511.
- 1215c. Ozin, G. A., Huber, H. and McIntosh, D. (1977), 'Cryochemical studies of zerovalent copper–ethylene complexes $(C_2H_4)_nCu$ and $(C_2H_4)_mCu_2$ (where $n = 1, 2, 3$ or 4 , $m = 4$ or 6) and their use in forming

- copper clusters. Localized bonding models for ethylene chemisorption onto bulk copper', *Inorg. Chem.*, **16**, 3070–3072.
1216. Grabowski, R., Efremov, A. A., Davydov, A. A. and Haber, E. (1981), 'Investigation of hydrocarbon adsorption on oxide catalysts by means of IR spectroscopy. XI. Modes of adsorption and sites of propylene and ethylene stabilization on NiO–MgO–MoO₃ and CoO–MgO–MoO₃', *Kinet. Katal.* (in Russian); *Kinet. Catal.* (English translation), **22**, 1014–1018.
1217. Soma, Y. (1976), 'Low-temperature infrared spectra of ethylene adsorbed on alumina-supported platinum and palladium', *J. Chem. Soc., Chem. Commun.*, 1004–1005.
1218. Busca, G., Zerlia, T., Lorenzelli, V. and Girelly, A. (1984), 'Fourier transform-infrared study of the adsorption of unsaturated and aromatic hydrocarbons on the surface of α -Fe₂O₃', *J. Catal.*, **88**, 125–131.
1219. Busca, G., Lorenzelli, V., Ramis, G. and Sanchez Escribano, V. (1991), 'Chemistry of olefins at metal oxide surfaces: a tool for surface science investigation of oxide catalysts', *Mater. Chem. Phys.*, **29**, 175–189.
1220. Bandy, B. J., Chester, M. A., James, D. I., McDougall, G. S., Pemble, M. E. and Sheppard, N. (1986), 'EELS spectroscopy of adsorbed ethylene', *Philos. Trans. R. Soc. London, A*, **318**, 141–161.
1221. Backman, A. L. and Masel, R. I. (1990), 'Ethylene adsorption and decomposition on Pt (210): chemistry of the π -bond', *J. Phys. Chem.*, **94**, 5300–5311.
1222. Albert, M. R. and Yates, J. T., Jr (1987), *The Surface Scientist's Guide to Organometallic Chemistry*, American Chemical Society, Washington, DC.
1223. Powell, D. B., Scott, J. G. V. and Sheppard, N. (1985), 'IR and Raman spectra of the ν C=C stretching frequencies of some silver–olefin and platinum–olefin complexes', *Spectrochim. Acta, Part A*, **28**, 327–335.
1224. Bigorgne, M. (1978), 'Complexes ethyleniques de platine(II), cuivre(I) et fer(O)', *J. Organomet. Chem.*, **160**, 345–349.
1225. Chiotti, G., Bocuzzi, F., Chiorino, A. (1989), An IR study of ethylene hydrogenation at room temperature on a Cu/ZnO catalyst', in Morterra, C., Zecchina, A. and Costa, G. (Eds), *Structure and Reactivity of Surfaces*, Elsevier, Amsterdam, pp. 415–421.
1226. Burfield, D. R. (1978), 'Interaction of VCl₄ with α -olefins', *J. Organomet. Chem.*, **150**, 321–344.
1227. Rozhkova, E. V., Gerei, S. V. and Gorokhovatsky, Ya. B. (1973), 'Investigation of the chemisorption of butenes on CuO and Cu₂O catalysts by IR spectroscopy', *J. Catal.*, **29**, 1–7.
1228. Busca, G. and Centi, G. (1989), 'Surface dynamics of adsorbed species on heterogeneous oxidation catalysts: evidence from the oxidation of C₄ and C₅ alkanes on vanadyl pyrophosphate', *J. Am. Chem. Soc.*, **111**, 46–58.
- 1229a. Wenig, R. W. and Schrader, G. L. (1986), 'In situ FTIR study of *n*-butane selective oxidation to maleic anhydride on V–P–O catalysts', *J. Phys. Chem.*, **90**, 6480–6488.
- 1229b. Wenig, R. W. and Schrader, G. L. (1987), 'In situ FTIR study of 1-butene and 1,3-butadiene selective oxidation to maleic anhydride on V–P–O catalysts', *J. Phys. Chem.*, **91**, 1911–1918.
- 1229c. Wenig, R. W. and Schrader, G. L. (1987), 'In situ FTIR study of crotyl alcohol, maleic acid, crotonic aldehyde and maleic aldehyde oxidation on a V–P–O industrial catalyst', *J. Phys. Chem.*, **91**, 5674–5680.
- 1230a. Puttock, S. Y. and Rochester, C. H. (1986), 'IR study of water and Py adsorption on the surface of anhydrous vanadyl pyrophosphate', *J. Chem. Soc., Faraday Trans. 1*, **82**, 2773–2779.
- 1230b. Puttock, S. Y. and Rochester, C. H. (1986), 'IR study of the adsorption of CO, CO₂, acetic acid and acetic anhydride on the surface of anhydrous vanadyl pyrophosphate', *J. Chem. Soc., Faraday Trans. 1*, **82**, 3013–3018.
1231. Ramstetter, A. and Baerns, M. (1988), 'Infrared spectroscopic investigation of the adsorption states of 1-butene, 1,3-butadiene, furan, 2,5-H-furanone, and maleic anhydride on alumina-supported V₂O₅-P₂O₅ catalyst', *J. Catal.*, **109**, 303–313.
1232. Zhang-Lin, Y., Forissier, M., Sneed, R. P., Vedrin, J. C. and Volta, J. C. (1994), 'Mechanism of *n*-butane oxidation to maleic anhydride on a VPO catalyst', *J. Catal.*, **145**, 256–267.
1233. Kondo, J., Domen, K. and Onishi, T. (1993), 'A mechanism of ethene hydrogenation over ZrO₂ studied by infrared spectroscopy', *Res. Chem. Intermediates*, **19**, 521–551.
1234. Ghiotti, G., Garrone, E., Coluccia, S., Morterra, C. and Zecchina, A. (1979), 'Evidence for alkylidene configuration of polymethylene chains on a Phillips catalyst', *J. Chem. Soc., Chem. Commun.*, 1032–1033.
1235. Morterra, C., Cerrato, G., Emanuel, C. and Bolis, V. (1993), 'On the surface acidity of some sulfate-doped ZrO₂ catalysts', *J. Catal.*, **142**, 349–367.
1236. Burch, R. and Hayes, M. J. (1995), 'C–H bond activation in hydrocarbon oxidation on solid catalysts', *J. Mol. Catal., A*, **100**, 13–34.
1237. Lansford, J. H. (1990), 'The catalytic conversion of methane to higher hydrocarbons', *Catal. Today*, **6**, 235–251.
1238. Sokolovskii, V. D. (1986), 'Reaction mechanism and principles of choosing catalysts for selective oxidation of C–H bonds', *React. Kinet. Catal. Lett.*, **32**, 159–163.
1239. Choudhary, V. R. and Rane, V. H. (1991), 'Acidity/basicity of rare-earth oxides and their catalytic activity in oxidative coupling of methane to C₂-hydrocarbons', *J. Catal.*, **130**, 441–457.

1240. Otsuka, K., Murakami, Y., Wada, Y., Said, A. A. and Morikawa, A. (1990), 'Oxidative coupling of methane, ethene and propene with sodium peroxide at low temperatures', *J. Catal.*, **121**, 122–128.
- 1241a. Davydov, A. A. and Budneva, A. A. (1974), 'Investigation of hydrocarbon adsorption on oxide catalysts by means of IR spectroscopy. I. Adsorption of propylene on solid CuO–MgO solutions', *Kinet. Katal.* (in Russian); *Kinet. Catal.* (English translation), **15**, 1557–1562.
- 1241b. Davydov, A. A. and Budneva, A. A. (1975), 'Investigation of hydrocarbon adsorption on oxide catalysts by means of IR spectroscopy. II. Interaction of propylene with CuO and CuO–MgO at high temperatures', *Kinet. Katal.* (in Russian); *Kinet. Catal.* (English translation), **16**, 480–485.
1242. Kadushin, A. A. (1975), 'Surface complexes of olefins with oxygen on oxide catalysts', in Krylov, O. V. (Ed.), *Problems of Kinetics and Catalysis* (in Russian), Vol. 16, Nauka, Moscow, pp. 67–78.
1243. Kelks, G. W. and Zuolong, Yu. (1984), 'The detection of surface intermediates formed during the selective oxidation of propylene', in *Proceedings of the 8th International Congress on Catalysis*, Berlin, in *Proceedings of the 8th International Congress on Catalysis, Berlin 1984*, Verlag Chemie, Weinheim, Germany, 1984.
1244. Corberan, V. C. and Tejuca, L. G. (1989), 'A comparative study of propene adsorption on total and partial oxidation catalysts', *J. Colloid Interface Sci.*, **192**, 270–275.
1245. Mikhail'chenko, V. G., Davydov, A. A., Bydneva, A. A., Kuznetsov, B. N. and Sokolovskii, V. D. (1975), 'The role of σ - and π -allyl complexes in the oxidation of propylene to acrolein', *React. Kinet. Catal. Lett.*, **2**, 163–170.
1246. Haber, J. (1987), 'The concept of structure–sensitivity in catalysis by oxides', in Morterra, C., Zecchina, A. and Costa, G. (Eds), *Structure and Reactivity of Surfaces*, Elsevier, Amsterdam, pp. 447–467.
1247. Ai, M. (1980), 'Effect of metal-oxide combination on the catalytic action in vapor phase oxidation', in *New Horizons in Catalysis, Proceedings of the 7th International Congress on Catalysis, Tokyo, June 30–July 4, 1980*, Seiyama, T. and Tanabe, K. (Eds) *Studies in Surface Science and Catalysis*, v.7, Kodansha, Tokyo, Elsevier, Amsterdam, 1980, Tokyo, pp. 1060–1073.
- 1248a. Grasselli, R. K. (1987), 'Factors affecting selectivity and activity of oxidation catalysts', *React. Kinet. Catal. Lett.*, **35**, 327–335.
- 1248b. Grasselli, R. J. (1985), 'Selective oxidation and ammoxidation catalysis', in Grasselli, R. K. and Bradzil, F. J. (Eds), *Solid State Chemistry in Catalysis*, American Chemical Society, Washington, DC, pp. 182–210.
1249. Gordymova, T. A., Budneva, A. A. and Davydov, A. A. (1982), 'IR spectra of toluene adsorbed on γ -Al₂O₃', *React. Kinet. Catal. Lett.*, **20**, 113–117.
1250. Dent, A. L. and Kokes, R. J. (1970), 'Formation of π -allyl complexes by adsorption of propylene on zinc oxide', *J. Am. Chem. Soc.*, **92**, 1092–1097.
1251. Garrone, E., Zecchina, A. and Stone, F. (1980), 'Anionic intermediates in surface processing leading to O₂⁻ formation on magnesium', *J. Catal.*, **62**, 396–401.
1252. Garrone, E. and Stone, F. S. (1984), 'The behaviour of MgO as a Brønsted base in chemisorption and surface processes', in *Proceedings of the 8th International Congress on Catalysis*, Berlin, III441–III448.
1253. Efremov, A. A. and Davydov, A. A. (1983), 'Investigation of hydrocarbon adsorption on oxide catalysts by means of IR spectroscopy. XIII. Modes of adsorption and sites of propylene and ethylene stabilization on the oxidized surface of copper-containing catalysts', *Kinet. Katal.* (in Russian); *Kinet. Catal.* (English translation), **24**, 1180–1186.
1254. Nguyen, T. T. and Sheppard, N. (1978), 'Raman spectra of molecules adsorbed on heavy metal oxides. Propylene on ZnO: the anionic nature of adsorbed allyl species', *J. Chem. Soc., Chem. Commun.*, 868–871.
1255. Ismailov, E. G., Anufrienko, V. F., Maksimov, N. G. and Sokolovskii, V. D. (1975), 'Formation of allyl radicals in the adsorption of propylene on zinc oxide', *React. Kinet. Catal. Lett.*, **3**, 301–306.
1256. Davydov, A. A., Efremov, A. A. and Borekov, G. K. (1980), 'Effect of the charge state of surface allyl complexes on the course and transformation of their reactions,' in *Proceedings of the 5th Soviet–French Workshop on Catalysis*, Villeneuve D'Ascq, Lille, March 24–28 1980, Villeneuve D'Aseq, Preprint.
1257. Kokes, R. J. (1973), 'The nature of active sites', in Basolo, F. and Burwell, R. L., Jr (Eds), *Catalysis Progress in Research*, Plenum Press, New York, pp. 75–93.
1258. Dent, A. L. and Kokes, R. J. (1971), 'Butene isomerization over zinc oxide', *J. Phys. Chem.*, **75**, 487–491.
1259. Chang, C. C., Conner, W. C. and Kokes, R. J. (1973), 'Butene isomerization over zinc oxide and chromia', *J. Phys. Chem.*, **77**, 1957–1964.
1260. Baird, M. J. and Lunsford, J. H. (1972), 'Catalytic sites for the isomerization of butene over magnesium oxide', *J. Catal.*, **26**, 440–451.
1261. Hayes, N. W., Grunert, W., Huttchings, G. J., Joyner, R. W. and Shapiro, E. S. (1994), 'Formation, storage and reactivity of nitrile species during the lean NO_x reaction over Cu-HZSM-5 catalysts', *J. Chem. Soc., Chem. Commun.*, 531–533.
1262. Sokolovskii, V. D., Aliev, S. M., Buyevskaya, O. V. and Davydov, A. A. (1989), 'Type of hydrocarbon activation and nature of active sites of base catalysts in methane oxidative dehydrodimerization', *Catal. Today*, **4**, 293–300.
- 1263a. Cram, D. J. (1967), *Principles of Carbanion Chemistry*, Mir, Moscow.
- 1263b. Cram, D. J. (1965), *Fundamentals of Carbanion Chemistry*, Academic Press, New York.

1264. Lanfer, E. J. (1957), 'Structure of allylic anions', *J. Am. Chem. Soc.*, **79**, 5578–5584.
1265. Sourisseau, C. and Pasquier, B. (1975), 'Spectres de vibration et structures de composés allyliques du sodium, du lithium et du magnésium. Application à l'étude de l'allyllithium et du chlorure d'allylmagnésium en solution', *Spectrochim. Acta, Part A*, **31**, 287–292.
1266. Yurchenko, E. N., Kozhevina, L. I. and Smirnov, V. I. (1975), 'Analysis of kinematics of vibrations in some π -allylpalladium chloride derivatives', *Zh. Prikl. Spektrosk.* (in Russian); *J. Appl. Spectrosc.* (English translation), **23**, 475–478.
1267. Sourisseau, C. and Pasquier, B. (1973), 'Spectres de vibration du chlorure et bromure de π -allylpalladium, $(C_3H_5PdCl)_2$, $(C_3H_5PdBr)_2$ et du $(C_3D_5PdCl)_2$. Effect isotopique sur les vibrations métalallite', *Can. J. Spectrosc.*, 92–95.
1268. Rybinskaya, M. I. (1975), ' π -Complexes of monoolefins, in Nesmeyanov, A. N. (Ed.), *Methods of Organoelement Chemistry*, Nauka, Moscow, pp. 217–262.
- 1269a. Stone, F. S. and Zecchina, A. (1977), 'Diffuse reflectance spectroscopy applied to the adsorption and interaction of gases on MgO', in *Proceedings of the 6th International Congress on Catalysis*, London, in *Proceedings of the 6th International Congress on Catalysis, London, 1976*, Bond, G.C., Wells, P.B. and Tompkins, F.S. (Eds.), The Royal Society of Chemistry, London, 1977, pp. 162–167.
- 1269b. Stone, F. S. and Zecchina, A. (1981), 'Discussion', in *New Horizons in Catalysis, Proceedings of the 7th International Congress on Catalysis, Tokyo, June 30–July 4, 1980*, Seiyama, T. and Tanabe, K. (Eds.) *Studies in Surface Science and Catalysis*, v.7, Kodansha, Tokyo, Elsevier, Amsterdam, 1980, pp. 1163–1165.
1270. Bohme, D. K., Lee-Ruff, E. and Young, L. B. (1972), 'Acidity order of selected Brønsted acids in the gas phase at 300 K', *J. Am. Chem. Soc.*, **94**, 5153–5159.
1271. Chang, C. C. and Kokes, R. J. (1973), 'The nature of molecular nitrogen adsorbed over zinc oxide', *J. Phys. Chem.*, **77**, 2640–2645.
1272. Chang, C. C. and Kokes, R. J. (1971), 'Chemisorption of molecular hydrogen by zinc oxide', *J. Am. Chem. Soc.*, **93**, 7107–7112.
1273. Dent, A. L. and Kokes, R. J. (1970), 'The nature of adsorbed propylene on zinc oxide. II. Reaction of π -allyl species', *J. Am. Chem. Soc.*, **92**, 6718–6725.
- 1274a. Chang, C. C. and Kokes, R. J. (1970), 'Intermediates in allene–acetylene isomerization over zinc oxide', *J. Am. Chem. Soc.*, **92**, 7517–7527.
- 1274b. Chang, C. C. and Kokes, R. J. (1973), 'An Infrared study of isomerization of acetylenes over zinc oxide', *J. Catal.*, **28**, 92–103.
1275. Little, L. H., Sheppard, N. and Yates, D. J. C. (1960), 'Infrared spectra of chemisorbed molecules. 1. Acetylene and ethylene on silica supported metals', *Proc. R. Soc. London, A*, **259**, 242–256.
1276. Dent, A. L. and Kokes, R. J. (1971), 'Adsorption and hydrogenation of ethylene and propylene by zinc oxide as studied by conventional and infrared spectroscopic techniques', *J. Phys. Chem.*, **75**, 487–492.
1277. Chang, C. C. and Kokes, R. J. (1975), 'Base catalyzed adsorption of toluene by zinc oxide', *J. Catal.*, **38**, 491–497.
1278. Davydov, A. A. (1994), 'IR spectroscopic study of adsorption of hydrocarbons on oxide catalysts. 19. Propylene adsorption on a Bi–Mo oxide catalyst and the nature of surface sites', *Kinet. Katal.* (in Russian); *Kinet. Catal.* (English translation), **35**, 608–611.
1279. Kondo, J., Domen, K., Moruya, K. and Onishi, T. (1990), IR-study of ethene hydrogenation over ZrO₂ 'Part II. Ethane adsorption', *J. Chem. Soc., Faraday Trans. 1*, **86**, 3665–3669.
1280. Davydov, A. A. and Efremov, A. A. (1979), 'Investigation of hydrocarbon adsorption on oxide catalysts by means of IR spectroscopy. 7. Adsorption of allyl bromide on CuO–MgO', *Kinet. Katal.* (in Russian); *Kinet. Catal.* (English translation), **20**, 1242–1248.
1281. Efremov, A. A., Tichy, J. and Davydov, A. A. (1974), 'Investigation of hydrocarbon adsorption on oxide catalysts by means of IR spectroscopy. 4. Adsorption of propylene and allyl bromide on a Ga/Mo catalyst', *Kinet. Katal.* (in Russian); *Kinet. Catal.* (English translation), **20**, 154–160.
1282. Shchekochikhin, Yu. M. and Davydov, A. A. (1976), 'Investigation of reactions on Al₂O₃ surfaces by means of IR spectroscopy', *Adsorptsiya Adsorbenty* (in Russian), **4**, 75–80.
1283. Budneva, A. A., Davydov, A. A. and Mikhal'chenko, V. G. (1975), 'Investigation of hydrocarbon adsorption on the surfaces of oxide catalysts by means of IR spectroscopy. III. Propylene adsorption on chromia', *Kinet. Katal.* (in Russian); *Kinet. Catal.* (English translation), **16**, 486–490.
- 1284a. Kuznetsov, V. A., Gerei, S. V., Gorokhovskii, Ya. B. and Rozhkova, E. V. (1977), 'Interaction of hydrocarbons with the surfaces of oxide catalysts. I. IR spectroscopic study of hydrocarbon interaction with chromia', *Kinet. Katal.* (in Russian); *Kinet. Catal.* (English translation), **18**, 418–423.
- 1284b. Kuznetsov, V. A., Gerei, S. V., Govokhovskii, Ya. B. and Rozhkova, E. V. (1977), 'Interaction of hydrocarbons with the surfaces of oxide catalysts. II. IR spectroscopic study of olefin interaction with NiO and Fe₂O₃', *Kinet. Katal.* (in Russian); *Kinet. Catal.* (English translation), **18**, 424–428.
1285. Efremov, A. A., Pankratiev, Yu. D. and Davydov, A. A. (1982), 'Formation energies of HCOO⁻ type complexes from ethylene on Cr₂O₃', *React. Kinet. Catal. Lett.*, **21**, 137–140.

1286. Davydov, A. A. (1997), 'Study of hydrocarbons adsorption on oxide catalysts by means of IR-spectroscopy. 21. The mechanism of full propane oxidation over ZrO_2 ', *Kinet. Katal.* (in Russian); *Kinet. Catal.* (English translation), **38**, 836–842.
1287. Topchieva, K. V., Kubasov, A. A. and Ratov, A. N. (1969), 'IR spectroscopic study in the molecular interaction between cyclic hydrocarbon and zeolite-HY', *Dokl. AN SSSR* (in Russian); *Proc. AN USSR* (English translation), **184**, 379–384.
1288. Scokart, P. O. and Rouxhet, P. G. (1982), 'Comparison of the acid–base properties of various oxides and chemically treated oxides', *J. Colloid Interface Sci.*, **86**, 96–97.
1289. Karge, H. G. (1973), 'Formation of carbonium ions on zeolite surfaces', *Surf. Sci.*, **40**, 157–168.
- 1290a. Busca, G., Zerlia, T., Lorenzelli, V. and Girelli, A. (1984), 'A Fourier-transform infrared study of the adsorption of unsaturated and aromatic hydrocarbons on the surface of α - Fe_2O_3 . II. Benzene', *J. Catal.*, **88**, 131–136.
- 1290b. Busca, G., Zerlia, T., Lorenzelli, V. and Girelli, A. (1985), 'A Fourier-transform infrared study of the adsorption of unsaturated and aromatic hydrocarbons on the surface of α - Fe_2O_3 . III. Toluene, ethylbenzene and styrene', *React. Kinet. Catal. Lett.* **27**, 429–432.
1291. Addiego, W. P., Estrada, C. A., Goodman, D. W., Rosynek, M. P. and Windham, R. G. (1994), 'An infrared study of the dehydrogenation of ethylbenzene to styrene over iron-based catalysts', *J. Catal.*, **146**, 407–413.
1292. Rossi, P. F. and Busca, G. (1984), 'Microcalorimetric and FT-IR spectroscopic study of benzene adsorption on α - Fe_2O_3 and γ - Al_2O_3 ', *J. Therm. Anal.*, **29**, 745–753.
1293. Davydov, A. A. and Shepot'ko, M. L. (1990), 'Nature of the centers on the surfaces of oxide catalysts and the forms of adsorbed toluene', *Teor. Eksp. Khim.* (in Russian); *Theor. Exp. Chem.* (English translation), **26**, 710–715.
1294. Primet, M., Garbowski, E., Mathieu, M. and Imelik, B. (1989), 'Spectroscopic studies of benzene hydrogenation on platinum-loaded zeolites. I. Benzene adsorption on supports', *J. Chem. Soc., Faraday Trans. 1*, **76**, 1942–1950.
- 1295a. Perkampus, H.-H. and Baumgarten, A. (1964), 'IR-spectra of carbonium ions in acidic solutions', *Ber. Bunsenges. Phys. Chem.*, **68**, 70–76.
- 1295b. Perkampus, H.-H. (1966), in Gold, V. (Ed.), *Advances in Physical Organic Chemistry*, Academic Press, New York.
- 1295c. Perkampus, H.-H. (1965), *Progress in Physical Organic Chemistry*, Wiley, New York.
1296. Olah, G. A., Pittman, C. U., Waak, R. and Doran, M. (1966), 'The electronic spectra of carbonium ions in strongly acidic solutions', *J. Am. Chem. Soc.*, **88**, 1488–1495.
1297. Koptiyug, V. A. (1983), *Arenonium Ions: Structure and Reactivity* (in Russian), Nauka, Novosibirsk.
1298. Weston, R. E., Tsukamoto, A. and Lichtin, N. N. (1966), 'IR spectra and vibrational frequency assignment of triphenylcarbinol, methyl chloride, triphenylmethyl fluoroborate and the ^{13}C and d_5 analogs', *Spectrochim. Acta. Part A*, **22**, 433–453.
1299. Sharp, D. W. A. and Sheppard, N. (1957), 'Complex fluorides. Part 8. The preparation and properties of salts of the triphenylmethyl cation: the IR spectrum and configuration of the ion', *J. Chem. Soc.*, 674–682.
1300. Whiffen, D. H. (1956), 'Vibrational frequencies and thermodynamic properties of fluoro-, chloro-, bromo- and iodobenzene', *J. Chem. Soc.*, 1350–1359.
1301. Buckles, R. E., Erickson, R. E., Snyder, J. D. and Person, W. B. (1960), 'The formation of the trianisyl methylcarbonium ion by the interaction of tetraanisylethylene with electron acceptors', *J. Am. Chem. Soc.*, **82**, 2444–2451.
1302. Kiricsi, I., Flego, C. and Bellussi, G. (1995), 'Influence of isobutane on the formation of carbenium ions from 1-butene over La–beta–zeolite', *Appl. Catal. A: Gen.*, **126**, 401–410.
- 1303a. Azimov, A. B., Davydov, A. A., Vislovskii, V. P., Mamedov, E. G. and Rizaev, R. G. (1991), 'IR spectroscopic study of the interaction components of reaction mixtures for oxidative ammonolysis of toluene on V–Bi–Sb oxide catalysts. I. Adsorption and conversion of toluene, ammonia, benzonitrile and benzilamine on oxidized surfaces', *Kinet. Katal.* (in Russian); *Kinet. Catal.* (English translation), **32**, 109–117.
- 1303b. Azimov, A. B., Davydov, A. A., Vislovskii, V. P., Mamedov, E. G. and Rizaev, R. G. (1991), 'IR spectroscopic study of the interaction components of reaction mixtures for oxidative ammonolysis of toluene on V– β –Sb oxide catalysts. II. Adsorption and transformation of toluene on a surface treated with ammonia', *Kinet. Katal.* (in Russian); *Kinet. Catal.* (English translation), **32**, 118–124.
1304. Davydov, A. A. and Budneva, A. A. (1992), 'Infrared spectroscopic investigation of the forms of adsorption of *o*-xylene on vanadium compound catalysts', *Zh. Fiz. Khim.* (in Russian); *Russ. J. Phys. Chem.* (English translation), **66**, 2693–2697.
1305. Demidov, A. A., Davydov, A. A. and Kurina, L. N. (1989), 'Alkyl aromatic carbenium ions on H-ZSM', *Izv. Acad. Nauk. SSSR, Ser. Khim.* (in Russian); *Russ. Chem. Bull.* (English translation), 1486–1490.
1306. Angell, C. L. and Howell, M. V. (1968), 'IR spectroscopic investigations of zeolites and adsorbed molecules. III. Aromatic hydrocarbons', *J. Colloid Interface Sci.*, **28**, 279–287.
1307. De Mallmann, A. and Barthomeuf, D. (1986), 'New developments in zeolite science and technology', *Studies Surf. Sci. Catal.*, **28**, 28–39.

1308. De Mallmann, A. and Barthomeuf, D. (1988), 'Change in benzene adsorption with acido-basicity of (Cs, Na)X zeolites studied by infrared spectroscopy', *Zeolites*, **8**, 292–301.
1309. De Mallmann, A. and Barthomeuf, D. (1986), 'Changes with dealumination of the state of benzene adsorbed on faujasites', *J. Chem. Soc., Chem. Commun.*, 476–481.
1310. De Mallmann, A., Dzwigaj, S. and Barthomeuf, D. (1989), 'Zeolites: Facts, figures, future', *Studies Surf. Sci. Catal.*, **49B**, 935–944.
1311. Coughlan, B. and Keane, M. A. (1990), 'Adsorption of benzene on a range of activated Y zeolites', *J. Chem. Soc., Faraday Trans. 1*, **86**, 3961–3966.
1312. Su, B. L., Manoli, J. M., Potvin, C. and Barthomeuf, D. (1993), 'Adsorption of benzene on a KL zeolites', *J. Chem. Soc., Faraday Trans. 1*, **89**, 857–862.
1313. Dzwigaj, S., De Mallmann, A. and Barthomeuf, D. (1990), 'Adsorption of benzene and ethylbenzene on the acidic and basic sites on β -zeolites', *J. Chem. Soc., Faraday Trans. 1*, **86**, 431–437.
1314. Su, B. L. and Barthomeuf, D. (1995), 'Adsorption sites for benzene in KL zeolites: an infrared study of molecular recognition', *Zeolites*, **15**, 470–474.
1315. Su, B. L. and Barthomeuf, D. (1995), 'Comparison of acid–base properties of FAU, EMT, LTL and MOR (Na forms) in benzene adsorption and alkylation of aniline with methanol', *Appl. Catal. A: Gen.*, **24**, 81–96.
1316. Su, B. L. and Barthomeuf, D. (1995), 'Adsorption sites for benzene in KL zeolites: an infrared study of molecular recognition', *Zeolites*, **15**, 470–474.
1317. Wijekoon, W. M., Koenig, E. W. and Hetherington, W. M. (1993), 'Coherent anti-Stokes Raman scattering spectroscopy with guided waves, applied to the adsorption of benzene on the planar (0001) surface of ZnO', *J. Phys. Chem.*, **97**, 1065–1069.
1318. Ignatovich, M., Ogenko, V. and Chuiko, A. (1995), 'Spectral study of the donor–acceptor complexes of aromatic molecules adsorbed on zeolites', *Studies Surf. Sci. Catal.*, **99**, 614–619.
1319. Eremenko, A. M., Ogenko, V. and Chuiko, A. (1995), 'Electron-transfer complex formation and oxidation of naphthalene in zeolites', *Studies Surf. Sci. Catal.*, **99**, 606–611.
1320. Freeman, J. J. and Unland, M. L. (1978), 'Laser Raman study of benzene adsorption on alkali metal X or Y zeolites', *J. Catal.*, **54**, 183–196.
1321. Asmolov, G. N. and Krylov, O. V. (1978), 'Electron donor–acceptor interaction of aromatic hydrocarbon molecules with γ -Al₂O₃ surfaces. I. Investigation of adsorption of individual compounds by means of diffuse reflection spectra', *Kinet. Katal.* (in Russian); *Kinet. Catal.* (English translation), **19**, 1004–1009.
1322. Ananin, V. N. and Trokhimits, A. I. (1983), 'Mass-spectrometric studies of thermal desorption of benzene from γ -Al₂O₃', *React. Kinet. Catal. Lett.*, **23**, 239–247.
1323. Talybova, Z. A., Davydov, A. A., Lisovskii, A. E. and Alkhozov, T. G. (1984), 'The interaction of ethylbenzene with oxygen and sulphur dioxide on the surface of alumina', *Zh. Fiz. Khim.* (in Russian); *Russ. J. Phys. Chem.* (English translation), **58**, 453–457.
1324. Haaland, D. M. (1981), 'FTIR studies of the adsorption of benzene on alumina and alumina-supported platinum', *Surf. Sci.*, **102**, 405–423.
1325. Nguyen, T. T. and Sheppard, N. (1981), 'The adsorption of allylbenzene on zinc oxide: an infrared spectroscopic study', *J. Catal.*, **67**, 402–409.
1326. Nguyen, T. T., Lavalley, J. C., Saussey, J. and Sheppard, N. (1980), 'IR and Raman spectroscopic study of some aromatic acetylenic compounds adsorbed on ZnO', *J. Catal.*, **61**, 503–514.
1327. Nguyen, T. T. (1980), 'Raman and IR spectra of ethylbenzene adsorbed on ZnO', *J. Catal.*, **61**, 515–518.
1328. Miyata, H. (1995), 'FTIR studies of the interaction of aromatic hydrocarbons with vanadium oxide layered on ZrO₂ and TiO₂', *J. Chem. Soc., Faraday Trans. 1*, **91**, 3505–3517.
1329. Kuiper, A. E., Medema, J. and van Barhoven, J. (1973), 'IR and Raman spectra of benzaldehyde adsorbed on alumina', *J. Catal.*, **29**, 40–48.
1330. Kuiper, A. E., Deflin, M., Cornier, G., Baverez, M. and Bastick, J. (1973), 'Etude par spectrometrie infrarouge des produits de chimisorption du toluene sur l'alumine', *C. R. Seances Acad. Sci., C*, **276**, 623–626.
1331. Deflin, M., Eltantawy, J. M. and Baverez, M. (1978), 'Alumina–organic interaction: oxidation of aromatic compounds on an alumina surface', *J. Catal.*, **54**, 345–347.
1332. Davydenko, I. V., Davydov, A. A., Pyatnitskii, Yu. I., Belokopytov, Yu. V. and Agazade, A. G. (1990), 'Investigation of the transformations of chlorobenzene at the surface of a vanadium oxide catalyst by IR spectroscopic and thermal desorption methods', *Teor. Eksp. Khim.* (in Russian); *Theor. Exp. Chem.* (English translation), **26**, 468–473.
1333. Ohtani, H., Van Hove, M. A. and Somorjai, G. A. (1988), 'Molecular structure of benzene coadsorbed with CO on Pd (111): a dynamic low-energy electron diffraction analysis', *J. Phys. Chem.*, **92**, 3974–3980.
1334. Davydenko, I. V., Davydov, A. A., Pyatnitskii, Yu. I., Belokopytov, Yu. V. and Agazade, A. G. (1991), 'The forms of the adsorption of benzene and its chloro-derivatives on the surface of a vanadium oxide catalyst', *Zh. Fiz. Khim.* (in Russian); *Russ. J. Phys. Chem.* (English translation), **65**, 164–169.
1335. Davydov, A. A. (1993), 'IR-spectroscopic studies of interactions between chlorobenzenes and the CuO surface', *Zh. Fiz. Khim.* (in Russian); *Russ. J. Phys. Chem.* (English translation), **67**, 2447–2451.

1336. Davydov, A. A., Knyazeva, E. M. and Shepot'ko, M. L. (1988), 'The study of phenol adsorption on the surface of some oxide catalysts by means of IR-spectroscopy', *Zh. Prikl. Spektrosk.* (in Russian); *J. Appl. Spectrosc.* (English translation), **49**, 86–92.
1337. Bordiga, S., Ricchiardi, G., Spoto, G., Scrano, D., Carnelli, L., Zecchina, A. and Otero Arean, C. (1993), 'Acetylene, methylacetylene and ethylacetylene polymerization on H-ZSM5: a spectroscopic study', *J. Chem. Soc., Faraday Trans. 1*, **89**, 1843–1855.
1338. Zecchina, A., Bordiga, S., Spoto, G., Scarano, D., Petrini, G., Leofanti, G., Padovan, M. and Otero Arean, C. (1992), 'Low temperature FTIR investigation of the interaction of CO with nanosized ZSM-5 and silicalite', *J. Chem. Soc., Faraday Trans. 1*, **88**, 2959–2969.
1339. Pereira, C., Kokotailo, G. T. and Gorte, R. J. (1991), 'Acetylene polymerization in an H-ZSM-5 zeolite', *J. Phys. Chem.*, **95**, 705–709.
1340. Qin, G., Zheng, L., Xie, Y. and Wu, C. (1985), 'On the framework OH of H-ZSM-5 zeolites', *J. Catal.*, **95**, 609–612.
1341. Cox, S. D. and Stucky, G. D. (1991), 'Polymerization of methylacetylene in hydrogen zeolites', *J. Phys. Chem.*, **95**, 710–720.
1342. Dutta, P. K. and Puri, M. (1988), 'Formation of *trans*-polyacetylene on transition metal zeolites. A resonance Raman study', *J. Catal.*, **111**, 453–456.
- 1343a. Tam, N. T., Cooney, R. P. and Curthoys, G. (1976), 'Vibrational spectra of molecules on zeolites. I. Acetylene on A-type zeolites', *J. Chem. Soc., Faraday Trans. 1*, **72**, 2577–2591.
- 1343b. Tam, N. T., Cooney, R. P. and Curthoys, G. (1976), 'Vibrational spectra of molecules on zeolites. II. Acetylene and dimethylacetylene on X-type zeolites', *J. Chem. Soc., Faraday Trans. 1*, **72**, 2592–2597.
- 1343c. Tam, N. T., Cooney, R. P. and Curthoys, G. (1976), 'Vibrational spectra of molecules on zeolites. III. Raman spectra of pyrazine on zeolites X', *J. Chem. Soc., Faraday Trans. 1*, **72**, 2598–2604.
1344. Heaviside, J., Hendra, P. J., Tsai, P. and Cooney, R. P. (1978), 'Adsorption and polymerization of acetylene on oxide surfaces. A Raman study', *J. Chem. Soc., Faraday Trans. 1*, **74**, 2542–2549.
- 1345a. Nakajima, T., Sonoda, T., Mijata, H. and Kubokawa, Y. (1982), 'IR studies of oxidation of alkenes adsorbed on ZnO', *J. Chem. Soc., Faraday Trans. 1*, **78**, 555–565.
- 1345b. Nakajima, T., Sonoda, T., Mijata, H. and Kubokawa, Y. (1985), 'IR study of intermediates in propylene oxidation on ZnO using [¹⁸O₂] oxygen and dinitrogen oxide', *Chem. Lett.*, 95–99.
- 1346a. Yates, D. J. C. and Lucchesi, P. J. (1961), 'IR spectra of acetylene and acetylene derivatives adsorbed on alumina and silica', *J. Chem. Phys.*, **35**, 243–255.
- 1346b. Yates, D. J. C. and Lucchesi, P. J. (1963), 'The coexistence of the independent sites of alumina as shown by the IR spectra of chemisorbed acetylene and ethylene', *J. Phys. Chem.*, **67**, 1197–1208.
1347. Saussey, J., Lamotte, J., Lavalley, J. C. and Sheppard, N. (1975), 'IR study of the nature of some strongly adsorbed species given by 1-butyne, 2-butyne and 1,2-butadiene on alumina. Isomerization effect', *J. Chem. Phys.*, **71**, 818–828.
1348. Saussey, J., Lavalley, J. C. and Sheppard, N. (1977), 'Infrared spectroscopic study of the adsorption of acetylenic hydrocarbons on zinc oxide', *J. Chem. Phys.*, **74**, 329–338.
1349. Saussey, J. and Lavalley, J. C. (1978), 'Infrared study of adsorption sites of 1-butyne on zinc oxide by selective poisoning of surface', *J. Chem. Phys.*, **75**, 505–507.
1350. Hussain, G. and Sheppard, N. (1992), 'Infrared investigation of the surface species obtained by chemisorption of acetylene (ethyne)C₂H₂ and C₂D₂ on high-area zinc oxide', *J. Chem. Soc., Faraday Trans. 1*, **88**, 2927–2930.
1351. Rives-Arnau, V. and Sheppard, N. (1980), 'Raman spectroscopic study of the polymerization of acetylene on titanium dioxide (rutile)', *J. Chem. Soc., Faraday Trans. 1*, **76**, 394–412.
1352. Dissanayake, D. H., Lunsford, J. H. and Rosynek, M. P. (1994), 'Site differentiation in homolytic vs. heterolytic activation of methane over Ba/MgO catalysts', *J. Catal.*, **146**, 613–615.
1353. Gallo, R. and Lazzeri, V. (1996), 'Selective functionalization of alkanes by hydride transfer', *Appl. Catal., A: Gen.*, **146**, 87–106.
1354. Chen, L., Lin, L., Xin, Q., Ying, P., Cheng, M., Xu, Z. and Zhang, T. (1995), 'FT-IR evidence for the participation of protonic sites in the heterolytic cleavage of the C–H bond of methane over NZSM-5 zeolites', *React. Kinet. Catal. Lett.*, **56**, 267–272.
1355. Datka, J. (1980), 'Interaction of OH groups in NaHY zeolites with physically adsorbed alkanes', *J. Chem. Soc., Faraday Trans. 1*, **76**, 705–710.
1356. Li, C. and Xin, Q. (1992), 'FTIR spectroscopic investigation of methane adsorption on CeO₂', *J. Phys. Chem.*, **96**, 7714–7718.
1357. Li, C., Yan, W. and Xin, Q. (1994), 'Interaction of methane with surface alumina studied by FTIR spectroscopy', *Catal. Lett.*, **24**, 249–256.
1358. Anderson, J. R. and Tsai, P. (1985), 'Oxidation of methane over H-ZSM and other catalysts', *Appl. Catal.*, **19**, 141–152.
1359. Han, S., Martenak, D. J., Palermo, R. E., Pearson, J. A. and Walsh, D. E. (1994), 'Direct partial oxidation of methane over ZSM-5 catalysts: metal effects on higher hydrocarbon formation', *J. Catal.*, **148**, 134–137.

1360. Iglesia, E. and Baumgartner, J. E. (1993), 'Hydrogen transfer and activation of light alkanes on HZSM-5 modified by metal cations', *Prepr., Am. Chem. Soc., Div. Petrochem.*, 746–750.
1361. Chen, L., Liwi, L., Xu, Z., Zhang, T. and Liang, D. (1995), 'Interaction of methane with surfaces of silica, aluminas and HZSM-5 zeolite. A comparative FT-IR study', *Catal. Lett.*, **35**, 245–258.
1362. Davydov, A. A. (unpublished data).
1363. Olah, G. A. and Schlosserberg, R. H. (1968), 'Chemistry of super acids. 1. Hydrogen exchange and polycondensation of methane and alkanes in $\text{FSO}_3\text{H-SbF}_5$ ('magic acid') solution. Protonation of alkanes and the inter-diacid of CH_5^+ and related Hg ions. The chemical reactivity of 'paraffins' in ionic solution reaction', *J. Am. Chem. Soc.*, **90**, 2726–2734.
1364. Chen, L., Lin, L., Xin, Q., Ying, P., Cheng, M., Xu, Z. and Zhang, T. (1995), 'FT-IR evidence for the participation of protonic sites in the heterolytic cleavage of C–H bonds of methane over HZSM-5 zeolite', *React. Kinet. Catal. Lett.*, **56**, 267–272.
1365. Periana, R., Taube, D. J., Evitt, E. R., Liffler, D. G., Wentreck, P. R., Voss, G. and Masuda, T. (1993), 'A mercury-catalysed higher-yield system for the oxidation of methane to methanol.', *Science*, **259**, 340–343.
1366. Spielbauer, D., Mekhemer, G. A. H., Bosch, E. and Knozinger, H. (1996), '*N*-butane isomerisation on sulfated zirconia. Deactivation and regeneration as studied by Raman, UV–vis diffuse reflectance and ESR spectroscopy', *Catal. Lett.*, **36**, 59–68.
1367. Ivanova, I. I., Derouane, E. G. and Blom, N. (1995), 'A controlled atmosphere ^{13}C MAS (magic angle spinning) NMR study of the initial stages of propane activation over HZSM-5', *Studies Surf. Sci. Catal.*, **94**, 419–426.
1368. Cohen de Lara, E. and Delaval, Y. (1974), 'IR spectra of methane adsorbed on NaA, CaA and NaX zeolites', *J. Phys. Chem.*, **78**, 2180–2181.
1369. Cohen de Lara, E., Delaval, Y. and Trakiris, J. (1976), 'Spectre infrarouge du methane adsorbe par les zeolithes NaA, CaNaA and NaX. Technique et resultants experimentaux', *J. Chim. Phys. (France)*, **73**, 387–391.
1370. Cohen de Lara, E. and Seloudoux, R. (1983), 'Study of the temperature dependance of the mobility of methane adsorbed on NaA zeolite using IR spectroscopy', *J. Chem. Soc., Faraday Trans. 1*, **79**, 2271–2276.
1371. Yamazaki, Y., Watanuki, J., Ozawa, S. and Ogino, Y. (1988), 'Infrared spectra of methane adsorbed by ion-exchanged ZSM-5 zeolites', *Langmuir*, **4**, 433–438.
1372. Mudrakovskii, I. L., Shepelev, S. S., Mastikhin, V. M., Zamaraev, K. I., Paukshtis, E. A. and Boreskov, G. K. (1984), 'Methane adsorption on high silica zeolites', *Kinet. Katal.* (in Russian); *Kinet. Catal.* (English translation), **25**, 766–770.
1373. Huber, S. and Knozinger, H. (1995), 'FTIR studies of CH_4 adsorption on sodium and cesium-containing Y zeolites', *Chem. Phys. Lett.*, **244**, 111–117.
1374. Yamazaki, T., Watanuki, J., Ozawa, S. and Ogino, Y. (1988), 'Infrared spectra of methane adsorbed by ion-exchanged ZSM-5 zeolites', *Langmuir*, **4**, 433–438.
1375. Khodakov, A. Yu., Kustov, L. M., Kazansky, V. B. and Williams, C. (1993), 'IR spectroscopic study of the interaction of cations in zeolites with simple molecular probes. Part 3 Adsorption and polarization of methane and ethane on cationic forms of high-silica zeolites', *J. Chem. Soc., Faraday Trans. 1*, **89**, 1393–1395.
1376. Davydov, A. A., Budneva, A. A. S. and Sokolovskii, V. D. (1981), 'IR study of hydrocarbons adsorption. IX. Adsorption forms of ammonia, propane, and ethane on the oxidative ammonolysis catalysts', *Kinet. Katal.* (in Russian); *Kinet. Catal.* (English translation), **22**, 213–221.
1377. Ovsitser, O. Yu., Davydov, A. A., Osipova, Z. G. and Sokolovskii, V. D. (1989), 'FT-IR spectroscopic study of cyclohexane adsorption on Ti–Sb–O-catalysts', *React. Kinet. Catal. Lett.*, **40**, 307–312.
1378. Li, C. and Xin, O. (1992), 'Direct observation of chemisorbed methane on cerium(IV) oxide by FTIR spectroscopy', *J. Chem. Soc., Chem. Commun.*, 782–783.
1379. Parmaliano, A., Sokolovskii, V. D., Miceli, D., Arena, F. and Giordano, N. (1993), in Oyama Tand, Hightower, J. W. (Eds.) *Catalytic Selective Oxidation*, American Chemical Society, Symp. Series 253, 23–30 Washington, DC.
1380. Davydov, A. A. (unpublished data).
1381. Vikulov, K. A., Marta, G., Caluccia, S., Miceli, D., Arena, F., Parmaliano, A. and Paukshtis, E. (1996), 'FTIR spectroscopic investigation of the active sites on different types of silica catalysts for methane partial oxidation to formaldehyde', *Catal. Lett.*, **37**, 235–239.
1382. Davydova, L. P., Popovskii, V. V., Bulgakov, N. N., Davydov, A. A., Kazakova, A. A. and Dobrynkin, N. M. (1988), 'Study of methane and ethane interactions with the surfaces of oxide catalysts', *Kinet. Katal.* (in Russian); *Kinet. Catal.* (English translation), **29**, 1162–1168.
1383. McCee, K. C., Driessen, M. D. and Grassian, V. H. (1995), 'Ethyl chloride decomposition on oxide-supported platinum catalysts', *J. Catal.*, **157**, 730–739.
1384. Ballinger, T. H. and Yates, J. T., Jr (1992), 'Interaction and catalytic decomposition of 1,1,1-trichloroethane on high surface area alumina. An infrared spectroscopic study', *J. Phys. Chem.*, **96**, 1417–1423.

1385. Beebe, T. P., Jr Crowell, J. E. and Yates, J. T., Jr (1988), 'The reaction of chloromethane on alumina: An infrared study', *J. Phys. Chem.*, **92**, 1296–1301.
- 1386a. Dai, Q., Robinson, G. N. and Freedman, A. (1997), 'Reactions of halomethanes with γ -alumina surfaces. 1. An infrared spectroscopic study', *J. Phys. Chem.*, **101**, 4940–4946.
- 1386b. Dai, Q., Robinson, G. N. and Freedman, A. (1997), 'Reactions of halomethanes with γ -alumina surfaces. 2. X-ray photoelectron and temperature-programmed reaction spectroscopic studies', *J. Phys. Chem.*, **101**, 4947–4953.
1387. Fan, J. and Yates, J. T., Jr (1994), 'Infrared study of the oxidation of hexafluoropropene on TiO_2 ', *J. Phys. Chem.*, **98**, 10621–10627.
1388. Finocchio, E., Busca, G., Lorenzelli, V. and Willey, R. J. (1995), 'The activation of hydrocarbon C–H bonds over transition metal oxide catalysts: an FTIR study of hydrocarbon catalytic combustion over MgCr_2O_4 ', *J. Catal.*, **151**, 204–215.
1389. Davydov, A. A., Budneva, A. A., Aliev, S. M. and Sokolovskii, V. D. (1988), 'IR-spectra of methane adsorbed on MgO ', *React. Kinet. Catal. Lett.*, **36**, 491–495.
1390. Zhanpeisov, N. U., Pel'menshikov, A. G. and Zhidomirov, G. M. (1991), 'Cluster quantum chemical study of interaction of molecules with a magnesium oxide surface. I. Dissociative chemisorption of hydrogen and methane molecules', *Kinet. Catal.* (in Russian); *Kinet. Catal.* (English translation), **31**, 491–496.
- 1391a. Zhizhin, G. N., Sinev, M. Yu., Shafranovskii, P. A. and Shub, B. R. (1988), 'Study of methane chemisorption over Al_2O_3 and CaO by the IR EWS method', *Kinet. Catal.* (in Russian); *Kinet. Catal.* (English translation), **29**, 663–668.
- 1391b. Firsov, E. I., Sinev, M. Yu. and Shfranovsky, P. A. (1990), 'IR-Raman and SEW spectrokinetic study of the surface stages of heterogeneous catalytic reactions: oxygen, water and methane interaction with the surface of Al_2O_3 , BaO and CaO thin films', *J. Electron Spectrosc. Related Phenom.*, **54–55**, 489–500.
- 1391c. Firsov, E. I., Sinev, M. Yu. and Shfranovsky, P. A. (1988), 'EWS in heterogeneous catalysis. I. Methane interaction with oxide systems', *Kinet. Catal.* (in Russian); *Kinet. Catal.* (English translation), **29**, 1721–1729.
1392. Utaama, M., Hattori, H. and Tanabe, K. (1978), 'Exchange reaction of methane with deuterium over solid base catalysts', *J. Catal.*, **53**, 237–242.
1393. Mink, J. and Gellai, B. (1974), 'Force constant calculations for dimethylmercury', *J. Organomet. Chem.*, **66**, 338–347.
1394. McKean, D. C., McQuillan, G. P., Torto, I. and Morrison, A. R. (1986), 'IR spectra, methyl group structure and internal rotation in some methylmetal compounds', *J. Mol. Struct.*, **141**, 457–464.
1395. Sokolovskii, V. D., Aliev, S. M., Buevskaya, O. V. and Davydov, A. A. (1989), 'Type of hydrocarbon activation and nature of active sites of basic catalysts in methane oxidative dehydrodimerization', *Catal. Today*, **4**, 293–300.
1396. Vikulov, K. A., Elev, I. V., Shelimov, B. N. and Kazansky, V. B. (1989), 'IR and UV–vis spectroscopic studies of stable $\text{Mo}=\text{CH}_2$ carbene complexes over photoreduced silica–molybdena catalysts with chemisorbed cyclopropane, and their role in olefin metathesis reactions', *J. Mol. Catal.*, **55**, 126–145.
1397. Wang, Y., Otsuka, K. and Ebatani, K. (1995), 'In situ FTIR study on the active oxygen species for the conversion of methane to methanol', *Catal. Lett.*, **35**, 259–263.
1398. Beebe, T. R., Crowell, J. E. and Yates, J. T. (1988), 'Reaction of methylchloride with alumina surfaces: a study of the methoxy surface species by transmission IR spectroscopy', *J. Phys. Chem.*, **92**, 1296–1301.
1399. Ueda, W., Suzuki, Y., Lee, W. and Imaoka, S. (1996), 'Catalytic oxidation of propane to acrylic acid with molecular oxygen activated over reduced heteropolymolybdates', *Studies Surf. Sci. Catal.*, **101**, 1065–1074.
1400. Hodnett, B. K. (1985), 'Vanadium–phosphorus oxide catalysts for the selective oxidation of C_4 hydrocarbons to maleic anhydride', *Catal. Rev. Sci. Eng.*, **27**, 373–424.
1401. Centi, G., Trifiro, F., Busca, G., Ebner, J. R. and Cleaves, J. T. (1988), 'Selective oxidation pathways at the vanadyl pyrophosphate surface in light paraffin conversion', in *Catalyst: Theory to Practice. Proceedings of the 9th International Congress on Catalysis*, Calgary, Canada, 1988, Phillips, M.J. and Ternan, M., (Eds.), The Chemical Institute of Canada, Ottawa, Ontario, 1988, pp. 1538–1544.
1402. Cavani, F., Comuzzi, C., Dolcetti, G., Etienne, E., Finke, R. G., Selli, G., Trifiro, F. and Trovarelli, A. (1996), 'Oxidative dehydrogenation of isobutane to isobutene: Dawson-type heteropolyoxo anions as stable and selective heterogeneous catalysts', *J. Catal.*, **160**, 317–321.
- 1403a. Comuzzi, C., Dolosetti, G., Trovarelli, A., Cavani, F. and Trifiro, F. (1996), 'The solid-state rearrangement of the Wells–Dawson $\text{K}_6\text{P}_2\text{W}_{18}\text{O}_{63} \cdot 10\text{H}_2\text{O}$ to a stable Keggin-type heteropolyanion phase: a catalyst for the selective oxidation of isobutane to isobutene', *Catal. Lett.*, **36**, 75–79.
- 1403b. Deshmukh, S., Davydov, A. A., Borovkov, V. Yu., Kovalchuk, V. I. and d'Itry, J. I. (1999), 'Interaction of CF_3CFCl_2 with oxides: an in situ FTIR study', in *Proceedings of the 16th North American Society Meeting*, Boston, MA, June 1999.
- 1403c. Davydov, A. A., 'Interaction of CF_3CFCl_2 with oxides: an in situ FTIR study' (unpublished data).
- 1403d. Davydov, A. A., 'Interaction of CF_3CFCl_2 with oxides: a Raman study' (unpublished data).
- 1403e. Fox, M. A. and Whitesell, J. K. (1994), *Organic Chemistry*, Jones and Bartlett, New York.

- 1403f. Dai, Q., Robinson, G. N. and Freedman, A. (1977), 'Reaction of halomethanes with γ -alumina surfaces. I. An infrared spectroscopic study', *J. Phys. Chem.*, **101**, 4940–4946.
- 1403g. Fan, J. and Yates, J. T. (1994), 'Infrared study of hexafluoropropene adsorption on TiO_2 ', *J. Phys. Chem.*, **98**, 10621–10627.
- 1404a. Evans, J. and Lo, G. (1965), 'Raman and IR studies of acetonitrile complexed with zinc chloride', *Spectrochim. Acta, Part A*, **21**, 1033–1038.
- 1404b. Evans, J. and Bernstein, E. (1955), 'Intensity in the Raman effect. IV. Raman intensity, some rules and frequency assignments for CH_3CN , CD_3CN , CH_2Cl_2 and CD_2CCl_2 ', *Can. J. Chem.*, **33**, 1746–1753.
1405. Knozinger, H. and Krietenbirk, H. (1975), 'IR spectroscopic study of the adsorption of nitriles on aluminium oxide', *J. Chem. Soc., Faraday Trans. 1*, **71**, 2421–2430.
1406. Scokart, P., Declerc, F., Sempels, R. and Rouxhet, P. (1977), 'Evolution of acidic properties of silica–alumina gels as a function of chemical composition: the infrared approach', *J. Chem. Soc., Faraday Trans. 1*, **73**, 359–367.
1407. Tvaruzkova, Z., Habersberger, K. and Jiru, P. (1991), 'Adsorption of acetonitrile as a tool for the characterization of acid/base properties of zeolite catalysts', *React. Kinet. Catal. Lett.*, **44**, 361–365.
1408. Tvaruzkova, Z., Tupa, M., Jiru, P., Nastro, A., Giordano, G. and Trifiro, F. (1989), 'Role of surface complexes on titanium silicate in the ammoxidation of cyclohexanone', *Studies Surf. Sci. Catal.*, **46**, 281–289.
1409. Krietenbrink, H. and Knozinger, H. (1976), 'IR spektroskopische untersuchung der adsorption von blausaure, acetamid und acetonitril an aluminiumoxide', *Z. Phys. Chem. (Leipzig)*, **102**, 43–56.
1410. Yim, S.-G., Son, D. H. and Kim, K. (1993), 'Fourier-transform infrared spectroscopic study of acetonitrile adsorbed on silica-supported nickel and nickel oxide', *J. Chem. Soc., Faraday Trans. 1*, **89**, 837–843.
1411. Curthoys, G., Davydov, V. Y., Kiselev, A. V. and Kuznetsov, B. V. (1974), 'Hydrogen bonding in adsorption on silica', *J. Colloid Interface Sci.*, **48**, 58–72.
1412. Friend, C. M., Muettterties, E. L. and Gland, J. L. (1981), 'Vibrational studies of CH_3CN and CH_3NC adsorbed on Ni (111) and Ni (III)–C surfaces', *J. Phys. Chem.*, **85**, 3256–3262.
1413. Kishi, K. and Ikeda, S. (1981), 'Adsorption of acetonitrile on evaporated nickel and palladium films studied by X-ray photoelectron spectroscopy', *Surf. Sci.*, **107**, 405–416.
1414. Kishi, K., Okino, Y. and Fujimoto, Y. (1986), 'XPS studies of the adsorption of CH_3CN and $\text{C}_6\text{H}_5\text{CN}$ on the Ni (111) surface', *Surf. Sci.*, **176**, 23–31.
1415. Friend, C. M. and Serafin, J. G. (1988), 'Bonding and reactivity of acetonitrile on W (100)–(5 \times 1)C', *J. Chem. Phys.*, **88**, 4037–4045.
1416. Stevens, P. A., Madix, R. J. and Stohr, H. (1989), 'The bonding of acetonitrile and CH_2CN on Ag (110) detected by near-edge X-ray absorption fine structure: evidence for π -donor bonding and azimuthal ordering', *J. Chem. Phys.*, **91**, 4338–4345.
1417. Solomun, T., Christmann, K. and Baumgartel, H. (1989), 'Interaction of acetonitrile and benzonitrile with the gold (100) surface', *J. Phys. Chem.*, **93**, 7199–7208.
1418. Angell, C. L. and Howell, M. V. (1969), 'IR spectroscopic investigation of zeolites and adsorbed molecules. IV. Acetonitrile', *J. Phys. Chem.*, **73**, 2551–2554.
1419. Tretyakov, E. N. and Filimonov, V. N. (1973), 'Comparison of the electron-acceptor capability of aprotic acid centers of metal oxides by an IR spectroscopic method', *Kinet. Katal.* (in Russian); *Kinet. Catal.* (English translation), **14**, 803–805.
1420. Paukshtis, E. A., Shinkarenko, V. G. and Karakchiev, L. G. (1976), 'Spectroscopic study of acceptor properties of the surfaces of catalysts', *Kinet. Katal.* (in Russian); *Kinet. Catal.* (English translation), **17**, 1029–1036.
1421. Medin, A. S., Borovkov, V. Yu. and Kazanskii, V. B. (1988), 'Possibility of transformations of alkoxy groups in HZSM-5 zeolites', *Kinet. Katal.* (in Russian); *Kinet. Catal.* (English translation), **29**, 1518–1525.
1422. Medin, A. S., Borovkov, V. Yu., Kazanskii, V. B., Pelmenshchikov, A. G. and Zhidomirov, G. M. (1990), 'On the unusual mechanism of Lewis acidity manifestation in HZSM-5 zeolites', *Zeolites*, **10**, 668–673.
1423. Hagiwara, K., Yamazaki, T. and Ozawa, S. (1995), 'An infrared spectroscopic study on the adsorption of acetonitrile from solution onto several oxide surfaces at high pressure', *J. Colloid Interface Sci.*, **170**, 421–435.
1424. Paukshtis, E. A., Soltanov, R. I. and Yurchenko, E. N. (1983), 'Strength of aprotic acidic centers estimated from the IR spectra of adsorbed acetonitrile', *React. Kinet. Catal. Lett.*, **23**, 339–343.
1425. Szakyi, J. (1996), 'FTIR investigation of the co-adsorption of acetonitrile and CO on Cu-ZSM-5', *J. Chem. Soc., Faraday Trans. 1*, **92**, 5165–5177.
1426. Juchnovski, I., Dimitrova, J., Binev, I. and Kaneti, J. (1978), 'IR spectra and structure of carbanions. 13. A study of the species generated from acetonitrile, acetonitrile- d_3 and ^{15}N ', *Tetrahedron*, **34**, 779–783.
1427. Binet, C., Jadi, A. and Lavalley, J. C. (1992), 'Etude par spectroscopie infrarouge de l'adsorption de l'acetonitrile sur oxyde de cerium; influence de l'etat de reduction de l'oxyde', *J. Chim. Phys. Phys. Chim. Biol.*, **89**, 31–38.
1428. Corset, J. (1980), in Buncel, E. and Durst, T. (Eds), *Comprehensive Carbanion Chemistry*, Elsevier, Amsterdam.

1429. Barton, D. and Ollis, D. (1979), in Sutherland, I. (Ed.), *Comprehensive Organic Chemistry. The Synthesis and Reactions of Organic Compounds*, Vol. 2, Pergamon Press, Oxford, UK, pp. 542–565.
1430. Knozinger, H., Krietenbrink, H., Muller, H. D. and Schulz, W. (1976), 'Cooperative effects in surface chemical and heterogeneously catalysed reactions on metal oxides', in *Proceedings of the 6th International Congress on Catalysis, London, 1976*, Bond, G.C., Wells, P.B. and Tompkins, F.S. (Eds.), The Royal Society of Chemistry, London, 1977, pp. 183–194.
1431. Koubowetz, F., Latzel, J. and Noller, H. (1980), 'Adsorption of acetonitrile on magnesia; an IR and TPD study', *J. Colloid Interface Sci.*, **74**, 322–330.
1432. Lavalley, J. C. and Gain, C. R. (1979), 'Etude infrarouge de l'adsorption de l'acetonitrile sur l'oxyde de zinc', *C.R. Acad. Sci. (Paris)*, c, **288**, 177–180.
1433. Lorenzelli, V., Busca, G. and Sheppard, N. (1980), 'IR study of the surface reactivity of haematite', *J. Catal.*, **66**, 28–35.
1434. Aboulayt, A., Binet, C. and Lavalley, J. C. (1995), 'IR Study of acetonitrile adsorption on hydroxylated zirconium dioxide: mechanism of acetonitrile hydrolysis', *J. Chem. Soc., Faraday Trans. 1*, **91**, 2913–2921.
1435. Ovsitser, O. Yu., Davydov, A. A., Osipova, Z. G. and Sokolovskii, V. D. (1989), 'IR spectroscopic studies of adiponitrile and ammonia adsorption over Ti–Sb–O catalysts', *React. Kinet. Catal. Lett.*, **38**, 125–130.
1436. Beres, A., Konya, Z., Hannus, I., Molnar, A. and Kiricsi, I. (1996), 'Interconversion of unsaturated C₄ nitriles under basic conditions II. Catalytic and FTIR study over basic zeolite', *Appl. Catal., A: Gen.*, **146**, 331–339.
1437. Konya, Z., Hannus, I., Molnar, A. and Kiricsi, I. (1996), 'Interconversion of unsaturated C₄ nitriles under basic conditions. I. An IR–UV–Vis spectroscopic study in the presence of butyllithium', *Appl. Catal., A: Gen.*, **146**, 323–330.
1438. Davydov, A. A. (unpublished data).
1439. Moser, W. R., Chiang, C-C and Thompson, R. W. (1989), 'Infrared diffuse reflectance study of the silicon-rich H-ZSM-5 catalysis for ethanol conversion', *J. Catal.*, **115**, 532–541.
1440. Derouane, E. G., Nagy, J. B., Dejajfve, P., Van Hooff, J. H. C., Spekman, B. P., Vedrine, J. C. and Naccache, C. (1978), 'Elucidation of the mechanism of conversion of methanol and ethanol to hydrocarbons on a new type of synthetic zeolite', *J. Catal.*, **53**, 40–48.
1441. Novakova, J., Kubelkova, L. and Dolejsek, Z. (1987), 'Primary reaction steps in the methanol-to-olefin transformation on zeolites', *J. Catal.*, **108**, 208–215.
1442. Kubelkova, L., Novakova, J. and Jiru, P. (1984), 'Reaction of small amounts of methanol on HZSM-5, HY and modified Y zeolites', in Jacobs, P. Jaeger, N. I., Jiru, P., Kazansky, V. B., and Schulz-Ekloff, G. (Eds), *Structure and Reactivity of Modified Zeolites*, Elsevier, Amsterdam, pp. 217–222.
1443. Ceckiewicz, S. (1982), 'Sorption and desorption of methanol on decaionated forms of zeolites', *J. Colloid Interface Sci.*, **90**, 183–190.
1444. Ono, I. and Mori, I. (1981), 'Mechanism of methanol conversion into hydrocarbons over ZSM-5 zeolite', *J. Chem. Soc., Faraday Trans. 1*, **77**, 2209–2215.
1445. Aronson, M. T., Gorte, R. J. and Farneth, W. E. (1987), 'An infrared spectroscopy study of simple alcohols adsorbed on HZSM-5', *J. Catal.*, **105**, 455–460.
1446. Sidorov, A. N. (1956), 'Adsorption on porous glass by IR absorption spectra', *Zh. Fiz. Khim.* (in Russian); *Russ. J. Phys. Chem.* (English translation), **30**, 995–999.
1447. Greenler, R. G. (1962), 'IR study of the adsorption of methanol and ethanol on aluminum oxide', *J. Chem. Phys.*, **37**, 2094–2100.
1448. Uvarov, A. V. (1962), 'Application of IR spectroscopy to the study of the investigation of adsorbed water and ethanol vapors with surface hydroxyls of Al₂O₃', *Zh. Fiz. Khim.* (in Russian); *Russ. J. Phys. Chem.* (English translation), **36**, 1346–1351.
1449. Kiselev, A. V. and Uvarov, A. V. (1967), 'Infrared spectra and ESR of aluminum, silicon and titanium oxides of adsorbed substances', *Surf. Sci.*, **6**, 399–418.
1450. Borezkov, G. K., Shchekochikhin, Yu. M., Makarov, A. D. and Filimonov, V. N. (1964), 'Study by IR absorption spectra of the structure of surface compounds formed when ethanol is adsorbed on γ -Al₂O₃', *Dokl. AN SSSR* (in Russian); *Proc. AN USSR* (English translation), **156**, 901–906.
1451. Efremov, A. A. and Davydov, A. A. (1981), 'IR spectroscopic studies of adsorption and conversion of isopropyl alcohol on Sn/Mo oxide catalyst', *React. Kinet. Catal. Lett.*, **18**, 363–366.
1452. Kurina, L. N., Gerasimova, V. N., Davydov, A. A. and Sudakova, N. N. (1981), 'Interaction of the participants in the oxidation of methanol with the oxides of Ti, Mo and Fe', *Teor. Eksp. Khim.* (in Russian); *Theor. Exp. Chem.* (English translation), **15**, 713–718.
1453. Osipova, N. A., Davydov, A. A., Kurina, L. N. and Loiko, V. E. (1985), 'Study of the adsorption of alcohols on chromium oxide by IR spectroscopy', *Zh. Fiz. Khim.* (in Russian); *Russ. J. Phys. Chem.* (English translation), **59**, 1479–1483.
1454. Osipova, N. A., Davydov, A. A. and Kurina, L. N. (1985), 'Formation of the products of full and partial oxidation from different forms of methanol adsorbed on chromia', *Zh. Fiz. Khim.* (in Russian); *Russ. J. Phys. Chem.* (English translation), **59**, 1484–1486.

1455. Abe, H., Maruya, K., Domen, K. and Onishi, T. (1984), 'The IR spectroscopic study of the mechanism of methanol formation from CO and H₂ over zirconia', *Chem. Lett.*, 18757–18758.
1456. Busca, G., Rossi, P. F., Lorenzelli, V., Banaissa, M., Travert, J. and Lavalley, J. C. (1985), 'Microcalorimetric and Fourier transform spectroscopic studies of methanol adsorption on Al₂O₃', *J. Phys. Chem.*, **89**, 5433–5439.
1457. Edwards, J. F. and Schrader, G. L. (1985), 'Methanol, formaldehyde and formic acid adsorption on methanol synthesis catalysts', *J. Phys. Chem.*, **89**, 782–788.
1458. Kondo, J., Sakata, Y., Maruya, K., Tamaru, K. and Onishi, T. (1987), 'IR studies of methanol adsorbed on magnesium oxide', *Appl. Surf. Sci.*, **28**, 475–478.
1459. Chesters, M. A. and McCash, E. M. (1987), 'The adsorption and reaction of methanol on oxidized Cu (111) studied by FT reflection-absorption IR spectroscopy', *Spectrochim. Acta, Part A*, **43**, 1625–1630.
1460. Rodrigues, J. A. and Campbell, C. T. (1988), 'A quantum chemical study of the chemisorption of ammonia, pyridine, formaldehyde, formate and methoxy on ZnO (0001)', *Surf. Sci.*, **194**, 475–504.
1461. Davydov, A. A. and Shepotko, M. L. (1988), 'Adsorption forms of methanol on anatase and directions of their transformation', *Teor. Eksp. Khim.* (in Russian); *Theor. Exp. Chem.* (English translation), **24**, 707–712.
1462. Osipova, N. A., Davydov, A. A. and Kurina, L. N. (1988), 'Adsorption forms and conversion of alcohols on a chromium–molybdenum oxide catalyst', *Zh. Fiz. Khim.* (in Russian); *Russ. J. Phys. Chem.* (English translation), **62**, 1296–1302.
1463. Osipova, N. A., Davydov, A. A., Kurina, L. N. and Gerasimova, V. N. (1988), 'Investigation of surface compounds of methanol on molybdenum oxide by the infrared spectroscopic and thermal desorption methods', *Zh. Fiz. Khim.* (in Russian); *Russ. J. Phys. Chem.* (English translation), **62**, 2205–2207.
1464. Groff, R. P. and Manogue, W. H. (1983), 'An IR study of formate formation and reactivity on MoO₃ surface', *J. Catal.*, **79**, 462–465.
1465. Davydov, A. A., Knyazeva, E. M. and Shepotko, M. L. (1988), 'IR spectroscopic study of adsorption of phenol on the surface of a series of oxide catalysts', *Zh. Prikl. Spektrosk.* (in Russian); *J. Appl. Spectrosc.* (English translation), **49**, 86–92.
1466. Itina, G. V., Demidov, A. V., Davydov, A. A. and Kurina, L. N. (1989), 'Adsorption of alcohols on the surface of Zn–Cr–K catalysts for alcohol synthesis from CO and H₂', *Zh. Fiz. Khim.* (in Russian); *Russ. J. Phys. Chem.* (English translation), **63**, 140–145.
1467. Busca, G. (1989), 'On the mechanism of methanol oxidation over vanadia-based catalysts: an FTIR study of the adsorption of methanol, formaldehyde and formic acid on vanadia and nanadia silica', *J. Mol. Catal.*, **50**, 241–248.
1468. Davydov, A. A. and Shepotko, M. L. (1989), 'Effect of oxygen on the infrared spectra of methanol adsorbed on ZnO', *Zh. Fiz. Khim.* (in Russian); *Russ. J. Phys. Chem.* (English translation), **63**, 764–765.
1469. Davydov, A. A. (1990), 'Infrared spectroscopic investigation of the nature of surface centers and methanol adsorption forms on cupric oxide', *Zh. Fiz. Khim.* (in Russian); *Russ. J. Phys. Chem.* (English translation), **64**, 2795–2799.
1470. Davydov, A. A. and Shepotko, M. L. (1990), 'IR spectroscopic investigation of the nature of surface centers and of adsorption of methanol on the iron–molybdenum oxide catalyst', *Teor. Eksp. Khim.* (in Russian); *Theor. Exp. Chem.* (English translation), **26**, 474–480.
1471. Osipova, N. A., Davydov, A. A. and Kurina, L. N. (1991), 'Study of forms of adsorption for methanol on chromium oxide and their role in complete and selective oxidation of alcohols', *Zh. Prikl. Spektrosk.* (in Russian); *J. Appl. Spectrosc.* (English translation), **54**, 474–479.
1472. Shepotko, M. L. and Davydov, A. A. (1991), 'Adsorption forms of ethanol on anatase and directions of their transformation', *Teor. Eksp. Khim.* (in Russian); *Theor. Exp. Chem.* (English translation), **27**, 232–237.
1473. Dobrynkin, N. M., Davydov, A. A. and Popovskii, V. V. (1989), Spectrokinetic study of the mechanism of complete oxidation of propanol-2 on copper oxide', in *Proceedings of the 9th International Symposium on Catalysis*, Madras, 1988, Reprint OR22.
1474. Dobrynkin, N. M., Davydov, A. A., Budneva, A. A., Popovskii, V. V., Rogov, V. A. and Serebryakov, V. F. (1992), 'IR spectroscopic study of the mechanism of deep oxidation of 2-propanol on cupric oxide under catalytic reaction conditions', *Kinet. Katal.* (in Russian); *Kinet. Catal.* (English translation), **33**, 133–141.
1475. Rogov, V. A., Davydov, A. A., Serebryakov, V. F. and Dobrynkin, N. M. (1992), 'TPD and IR spectroscopic studies of adsorption of alcohols on a copper oxide surface', *Kinet. Katal.* (in Russian); *Kinet. Catal.* (English translation), **33**, 157–162.
1476. Lahousse, C., Mauge, F., Bachelier, J. and Lavalley, J. C. (1995), 'Acidic and basic properties of titania–alumina mixed oxides active sites for propane-2-ol dehydration', *J. Chem. Soc., Faraday Trans. 1*, **91**, 2907–2916.
1477. Rossi, P. F., Busca, G., Lorenzelli, V. and Sauer, V. (1987), 'Microcalorimetric and FT-IR spectroscopic study of the adsorption of isopropyl alcohol and hexafluoropropyl alcohol adsorption on TiO₂', *Langmuir*, **3**, 52–58.
1478. Busca, G., Elmi, A. S. and Forzatti, P. (1987), 'Mechanism of selective methanol oxidation over vanadium oxide–titanium oxide catalysts: An FTIR and flow-reactor study', *J. Phys. Chem.*, **91**, 5263–5269.

1479. Mijata, H., Hata, K., Nakajima, J. (1980), 'IR studies of the oxidation of 2-propanol on ZnO', *Bull. Chem. Soc. Jpn.*, **53**, 2401–2402.
1480. Aramendia, M. A., Borau, V., Jimenez, C., Marinas, J. M., Porras, A. and Urbano, E. J. (1996), 'Magnesium oxide as basic catalysts for organic process. Study of the dehydrogenation–dehydration of 2-propanol', *J. Catal.*, **161**, 829–838.
1481. Shepotko, M. L. and Davydov, A. A. (1992), 'Infrared spectroscopic and thermal desorption investigation of transformations of methanol adsorbed on Fe₂O₃', *Zh. Fiz. Khim.* (in Russian); *Russ. J. Phys. Chem.* (English translation), **66**, 2486–2492.
1482. Osipova, N. A., Davydov, A. A. and Kurina, L. N. (1991), 'Influence of the nature of surface centers on the adsorption forms of methanol on Cr₂O₃ and Cr–Mo–O catalysts', *Kinet. Katal.* (in Russian); *Kinet. Catal.* (English translation), **32**, 486–490.
1483. Davydov, A. A. and Shepotko, M. L. (1990), 'Study of the surface properties of a solid solution of vanadium in SnO₂ by means of IR spectroscopy', *Teor. Eksp. Khim.* (in Russian); *Theor. Exp. Chem.* (English translation), **26**, 505–509.
1484. Zamaraev, K. I. and Thomas, J. M. (1996), 'Structural and mechanistic aspects of the dehydration of isomeric butyl alcohols over porous aluminosilicate acid catalysts', *Adv. Catal.*, **41**, 335–358.
1485. Busca, G. (1982), 'IR study of isopropanol adsorption on haematite', *React. Kinet. Catal. Lett.*, **20**, 373–376.
1486. Diaz, C. D. C., Locatelli, S. and Gonzo, E. E. (1992), 'Acetaldehyde adsorption on HZSM-5 studied by IRS', *Zeolites*, **12**, 851–855.
1487. Busca, G., Lamotte, J., Lavalley, J. C. and Lorenzelli, V. (1987), 'FT-IR study of the adsorption and transformation of formaldehyde on oxide surfaces', *J. Am. Chem. Soc.*, **109**, 5197–5202.
1488. Hill, W. and Ohlmann, G. (1989), 'FT-IR study of the adsorption and of reactions of acetaldehyde on dispersed silica', *J. Chem. Soc., Faraday Trans. 1*, **85**, 691–711.
1489. Allian, M., Berelle, E., Ugliengo, P., Spano, G. and Garone, E. (1995), 'Infrared spectroscopic study of the adsorption of carbonyl compounds on severely outgassed silica: spectroscopic and thermodynamic results', *Langmuir*, **11**, 4811–4817.
1490. Yates, J. T., Jr and Cavanagh, R. R. (1982), 'Search for chemisorbed HCO: The interaction of formaldehyde, glyoxal and aromatic hydrogen + CO with Rh', *J. Catal.*, **74**, 97–109.
1491. Ramis, G., Busca, G. and Lorenzelli, V. (1987), 'FT-IR study of the reactivity of molybdenum oxide supported on titania', *Appl. Catal.*, **32**, 305–313.
1492. Wang, G. W. and Hattori, H. J. (1984), 'Reaction of adsorbed CO with H₂ on MgO', *J. Chem. Soc., Faraday Trans. 1*, **80**, 1039–1047.
1493. Edwards, J. F. and Schrader, G. L. (1985), 'Methanol, formaldehyde and formic acid adsorption on methanol synthesis catalysts', *J. Phys. Chem.*, **89**, 782–787.
1494. Lavalley, J. C., Lamotte, J., Busca, G. and Lorenzelli, V. (1985), 'FTIR evidence of the formation of dioxymethylene species from formaldehyde adsorption on anatase and thoria', *J. Chem. Soc., Chem. Commun.*, 1006–1007.
1495. Trillo, J. M., Munuera, G. and Criado, J. M. (1972), 'Catalytic decomposition of formaldehyde on metal oxides', *Catal. Rev. Sci. Eng.*, **7**, 51–76.
1496. Vukulov, K. A., Colussia, S. and Marta, G. (1993), 'FTIR spectroscopic studies on the adsorption of ketene on silica', *J. Chem. Soc., Faraday Trans. 1*, **89**, 1121–1125.
1497. Young, R. P. and Sheppard, N. (1967), 'IR spectroscopic studies of the adsorption and catalysis. Part 2. Aliphatic aldehydes and ketones adsorbed on silica', *Trans. Faraday Soc.*, **63**, pp. 2291–2300.
1498. Busca, G. (1989), 'On the mechanism of methanol oxidation over vanadia-based catalysts: an FTIR study of the adsorption of methanol, formaldehyde and formic acid on vanadia and vanadia–silica', *J. Mol. Catal.*, **50**, 241–256.
1499. Osipova, N. A., Davydov, A. A. and Kurina, L. N. (1988), 'Adsorption of formaldehyde on oxide catalysts', *Zh. Fiz. Khim.* (in Russian); *Russ. J. Phys. Chem.* (English translation), **62**, 1587–1591.
1500. Arakawa, H., Fukushima, T., Ichikawa, M., Takeuchi, K., Tatsuzaki, T. and Susi, Y. (1985), 'High pressure *in situ* FT-IR study of carbon monoxide and hydrogen on Rh/SiO₂ catalyst', *Chem. Lett.*, 23–26.
1501. Young, R. P. (1969), 'IR spectroscopic studies of adsorption and catalysis. 3. Carboxylic acids and their derivatives adsorbed on silica', *Can. J. Chem.*, **47**, 2237–2247.
- 1502a. Fukushima, T., Arakawa, H. and Ichikawa, M. (1985), 'High pressure IR spectroscopic evidence of acetyl and acetate species directly formed in CO–H₂ conditions on SiO₂-supported Rh and Rh–Mn catalysts', *J. Chem. Soc., Chem. Commun.*, 729–731.
- 1502b. Fukushima, T., Arakawa, H. and Ichikawa, M. (1985), 'In situ high pressure FTIR studies on the surface species formed in CO hydrogenation on SiO₂ supported Rh–Fe–catalysts', *J. Phys. Chem.*, **89**, 4440–4443.
1503. Busca, G. and Centi, G. (1989), 'Surface dynamics of adsorbed species on heterogeneous oxidation catalysts: evidence from the oxidation of C₄ and C₅ alkanes on vanadyl pyrophosphate', *J. Am. Chem. Soc.*, **111**, 46–54.
1504. Brogan, M. S., Cairns, J. A. and Rochester, C. H. (1995), 'IRS study of butane and propane adsorption on Pt/CeO₂–Al₂O₃ catalysts', *J. Chem. Soc., Faraday Trans. 1*, **91**, 733–742.

1505. Popova, G. Ya., Davydov, A. A., Andrushkevich, T. V. and Zakharov, I. I. (1994), 'Surface complexes of acrolein on oxide catalysts', *Kinet. Katal.* (in Russian); *Kinet. Catal.* (English translation), **36**, 125–136.
1506. Kubelkova, L. and Trifiro, F. (1972), 'Study of the propylene-d₆ and acrolein interaction with silica gel by IR spectroscopy', *J. Catal.*, **26**, 242–246.
1507. Popova, G. Ya., Davydov, A. A., Zakharov, I. I. and Andrushkevich, T. V. (1982), 'Investigation of the interaction between acrolein and the surface of a V–Mo–Si oxide catalyst by means of IR spectroscopy and thermodesorption', *Kinet. Katal.* (in Russian); *Kinet. Catal.* (English translation), **23**, 692–699.
1508. Trifiro, F., Kubelkova, L. and Pasquon, F. (1970), 'Adsorption of propylene and acrolein on a Bi–Mo–Si oxide catalyst', *J. Catal.*, **19**, 121–126.
1509. Rubezhov, A. Z. (1988), 'Dibenzylideneacetone complex of transition metals', *Usp. Khim.* (in Russian); *Russ. Chem. Rev.* (English translation), **57**, 2078–2090.
1510. Barteau, M. A., Bowker, M. and Madix, R. J. (1980), 'Acid–base reactions on solid surfaces: the reactions of HCOOH, H₂CO and HCOOCH₃ with oxygen on Ag (110)', *Surf. Sci.*, **94**, 303–322.
1511. Serwicka, E. M., Black, J. B. and Goodenough, J. B. (1987), 'Acrolein oxidation over 12-molybdophosphates. III. Reaction mechanism', *J. Catal.*, **106**, 23–37.
1512. Anderson, J. R. and Rochester, C. H. (1989), 'IR study of the adsorption of acetone, acrolein, ethanoic acid and propene–nitric oxide mixture on Rh/Al₂O₃ catalysts', *J. Chem. Soc., Faraday Trans. 1*, **85**, 1117–1128.
1513. Morozova, O. S., Rozentuller, B. V., Kutuyev, M. Y., Kadushin, A. A., Krylov, O. V. (1978), 'IR spectroscopic study of the surface complexes formed from unsaturated aldehydes and acids on cobalt molybdate', *Izv. Acad. Nauk. SSSR, Ser. Khim.* (in Russian); *Russ. Chem. Bull.* (English translation), **3**, 541–546.
1514. Popova, G. Ya., Davydov, A. A. and Andrushkevich, T. V. (1990), 'Infrared spectroscopic studies of the adsorbed forms of acrolein and acrylic acid on Sb₆O₁₃ and V–Sb–O catalysts', *React. Kinet. Catal. Lett.*, **41**, 33–38.
1515. Tichy, J. and Davydov, A. A. (1976), 'Interaction of acrolein with vanadium–molybdenum oxide catalyst surfaces', *Collect. Czech. Chem. Commun.*, **41**, 834–838.
1516. Niva, M., Tanaka, Y. and Murakama, Y. (1982), 'IR study of the adsorption of acrolein on MgO', *J. Colloid Interface Sci.*, **89**, 571–573.
1517. Sokolov, V. A., Kadushin, A. A. and Krylov, O. V. (1967), 'Adsorption of acrolein and ethyl alcohol on MgO, studied by IR spectroscopy', *Kinet. Katal.* (in Russian); *Kinet. Catal.* (English translation), **8**, 848–854.
- 1518a. Orlov, A. N., Kolchin, I. K. and Lygin, V. I. (1972), 'Adsorption of propylene on a tin–molybdenum catalyst studied by the IR spectroscopic method', *Kinet. Katal.* (in Russian); *Kinet. Catal.* (English translation), **13**, 807–813.
- 1518b. Orlov, A. N., Kolchin, I. K. and Lygin, V. I. (1973), 'Use of quantum-chemical calculations for the interpretation of IR spectra of adsorbed complexes', *Kinet. Katal.* (in Russian); *Kinet. Catal.* (English translation), **14**, 1228–1235.
- 1519a. Harrison, P. G. and Maundens, B. (1985), 'Tin oxide surfaces. 15. IR study of the adsorption of propene on SnO₂, SnO₂/SiO₂ and SnO₂–Pd oxide', *J. Chem. Soc., Faraday Trans. 1*, **81**, 1329–1343.
- 1519b. Harrison, P. G. and Maundens, B. (1985), 'Tin oxide surfaces. 16. IR study of the adsorption of formic acid, acrylic acid and acrolein on tin(IV) oxide, tin(IV) oxide–silica and tin(IV) oxide–palladium oxide', *J. Chem. Soc., Faraday Trans. 1*, **81**, 1343–1355.
1520. Grabovski, R., Haber, J. and Sloczynski, J. (1979), 'IR spectroscopic studies of the interaction of propylene and acrolein with CoMoO₄ catalyst', *React. Kinet. Catal. Lett.*, **12**, 119–124.
1521. Eischens, R. P. (1964), 'Infrared spectroscopy and catalysis research', *Science*, **146**, 486–498.
1522. Davydov, A. A., Popova, G. Ya. and Andrushkevich, T. V. (1984), 'Investigation of adsorption of acrylic acid on certain oxide catalysts by means of IR spectroscopy', *Kinet. Katal.* (in Russian); *Kinet. Catal.* (English translation), **25**, 1175–1180.
1523. Jovel, I. and Shimanskaya, M. V. (1979), 'Catalytic oxidation of furan on a Mo–Ti–O catalyst: an IR and TPD study', *React. Kinet. Catal. Lett.*, **12**, 171–175.
1524. Rivasseau, J., Canesson, P. and Blandchard, M. (1980), 'Catalytic oxidation of furan on Mo–Ti–O catalysts. IR and TDS study', *J. Phys. Chem.*, **84**, 2791–2795.
1525. Davydov, A. A. (1993), 'IR spectroscopic study of maleic anhydride adsorption over V₂O₅/Al₂O₃ and CuO', *Zh. Fiz. Khim.* (in Russian); *Russ. J. Phys. Chem.* (English translation), **67**, 2477–2479.
1526. Miyata, H., Wakamiya, M. and Kubokawa, Y. (1974), 'Infrared studies of the interaction of oxygen with 2-propanol and acetone adsorbed on MgO and NiO', *J. Catal.*, **32**, 117–123.
- 1527a. Griffiths, D. M. and Rochester, C. H. (1977), 'IR study of the adsorption of hexafluoroacetone', *J. Chem. Soc., Faraday Trans. 1*, **73**, 1980–1987.
- 1527b. Griffiths, D. M. and Rochester, C. H. (1977), 'IR study of the adsorption of water on the surface of rutile', *J. Chem. Soc., Faraday Trans. 1*, **73**, 1510–1529.
- 1527c. Griffiths, D. M. and Rochester, C. H. (1978), 'Infrared study of the adsorption of acetone on rutile', *J. Chem. Soc., Faraday Trans. 1*, **74**, 403–417.
1528. Martin, C., Martin, I. and Rives, V. (1994), 'A FTIR study of surface nucleophilicity of TiO₂ and MoO₃/TiO₂ doped with alkaline cations', *J. Catal.*, **145**, 239–242.

1529. Efremov, A. A. and Davydov, A. A. (1981), 'IR spectroscopic studies of acetone adsorption on an Sn/Mo oxide catalyst', *React. Kinet. Catal. Lett.*, **18**, 353–356.
1530. Busca, G. and Lorenzelli, V. (1982), 'IR spectroscopic study of the reactivity of acetone and hexachloroacetone adsorbed on hematite', *J. Chem. Soc., Faraday Trans. 1*, **78**, 2911–2919.
- 1531a. Hirota, K., Kuwata, K. and Nakai, Y. (1958), 'Infrared study of the adsorption of formic acid on copper, nickel and zinc', *Bull. Chem. Soc. Jpn.*, **31**, 861–866.
- 1531b. Hirota, K., Kuwata, K. and Nakai, Y. (1958), 'On the state of formic acid adsorbed on dehydrated silica', *Bull. Chem. Soc. Jpn.*, **31**, 780–786.
- 1531c. Hirota, K., Kuwata, K. and Nakai, Y. (1959), 'Studies on the state of formic acid adsorbed on silica and alumina by a combined method of NMR and IR adsorption', *Bull. Chem. Soc. Jpn.*, **32**, 1261–1267.
- 1531d. Hirota, K., Kuwata, K. and Nakai, Y. (1961), 'Catalytic decomposition of formic acid', in *Proceedings of the 2nd International Congress on Catalysis*, Paris, Technip, Paris, pp. 809–815.
1532. Eischens, R. P. and Pliskin, W. A. (1961), IR studies of the chemisorption and decomposition of formic acid', in *Proceedings of the 2nd International Congress on Catalysis*, Paris, Technip, Paris, pp. 789–793.
1533. Munuera, G. (1970), 'A study of the mechanism of the formic acid dehydration on titania', *J. Catal.*, **18**, 19–31.
- 1534a. Noto, Y., Fukuda, K., Onishi, T. and Tamaru, K. (1967), 'Mechanism and selectivity of decomposition of formic acid on metal oxides. Dynamic study of chemisorbed particles during the reaction', *Trans. Faraday Soc.*, **63**, 2300–2312.
- 1534b. Noto, Y., Fukuda, K., Onishi, T. and Tamaru, K. (1970), 'Dynamic technique to elucidate the reaction intermediates on surfaces catalysed water-gas shifts reaction', *Trans. Faraday Soc.*, **66**, 756–767.
1535. Tamaru, K. and Onishi, T. (1975), 'Dynamic investigation of the mechanism of catalytic reactions as related by spectroscopic techniques', *Appl. Spectrosc. Rev.*, **9**, 133–141.
1536. Davydov, A. A., Budneva, A. A. and Yur'eva, T. M. (1974), Study of the surface compounds in the water-gas shift reaction on solid solutions of CuO–MgO by the IR spectroscopy method', *All-Union Conference on the Mechanisms of Heterogeneous Catalytic Reactions* (in Russian), Moscow, September 3–9, 1974, Preprint 39.
1537. Davydov, A. A. (1993), 'Spectrokinetics study of the formates decomposition on Cr₂O₃', *Zh. Prikl. Spektrosk.* (in Russian); *J. Appl. Spectrosc.* (English translation), **58**, 456–459.
1538. Takezawa, N. (1971), 'IR reflectance spectra of adsorbed species on opaque metal oxides', *J. Chem. Soc., Chem. Commun.*, 1451–1453.
1539. Davydov, A. A. (1993), 'Spectral parameters and thermal stability of surface formate compounds', *Zh. Fiz. Khim.* (in Russian); *Russ. J. Phys. Chem.* (English translation), **67**, 1085–1089.
1540. Grigor'ev, A. I. (1971), *Kolebatel'nye Spectry v Neorganicheskoi Khimii (Vibrational Spectra in Inorganic Chemistry)*, Nauka, Moscow, 116p.
1541. Spinner, E. (1975), 'The effect of disc pressing on the IR-spectrum of potassium formate. Two modifications of HCO₂K and DCO₂K', *Spectrochim. Acta, Part A*, **31**, 1545–1548.
- 1542a. Hayden, B. E., Prince, K., Woodruff, D. P. and Bradshaw, A. M. (1983), 'IRAS study of formic acid and surface formate adsorbed on Cu (110)', *Surf. Sci.*, **133**, 589–603.
- 1542b. Hayden, B. E., Prince, K., Woodruff, D. P. and Bradshaw, A. M. (1983), 'Infrared active combination band in a surface formate species', *Phys. Rev. Lett.*, **51**, 475–477.
1543. Ito, K. and Bernstein, H. J. (1956), 'The vibrational spectra of the formate, acetate and oxalate ions', *Can. J. Chem.*, **34**, 170–175.
1544. Deacon, G. B. and Phillips, R. J. (1980), 'Relationships between the carbon–oxygen stretching frequencies of carboxylato complexes and the type of carboxylate coordination', *Coord. Chem. Rev.*, **33**, 227–241.
- 1545a. Millar, G. J., Rochester, C. H. and Waugh, K. C. (1991), 'Infrared spectroscopy of the adsorption of formic acid on silica-supported copper and oxidized copper catalyst', *J. Chem. Soc., Faraday Trans. 1*, **87**, 1491–1498.
- 1545b. Millar, G. J., Rochester, C. H. and Waugh, K. C. (1994), 'In situ FT-IR investigation of formic acid adsorption on reduced and reoxidized copper catalysts', *Appl. Spectrosc.*, **48**, 827–839.
1546. Li, C., Kazunare, D. and Ken-ichi, M. (1990), 'Spectroscopic investigation of adsorbed species derived from the adsorption and decomposition of formic acid, methanol and formaldehyde on cerium oxide', *J. Catal.*, **125**, 445–449.
1547. Millar, G. J., Rochester, C. H. and Waugh, K. C. (1995), 'An FTIR study of the adsorption of formic acid and formaldehyde on potassium promoted Cu/SiO₂ catalysts', *J. Catal.*, **155**, 52–61.
1548. Millar, G. J., Rochester, C. H. and Waugh, K. C. (1992), 'Evidence for the adsorption of molecules at special sites located at copper/zinc oxide interfaces: Part I. A Fourier-transform infrared study of formic acid and formaldehyde adsorption on reduced and oxidized Cu/ZnO/SiO₂ catalysts', *J. Chem. Soc., Faraday Trans. 1*, **88**, 1033–1045.
1549. Pertric, W. T. (1991), 'An HREELS investigation of the adsorption and reaction of formic acid on the (0001) surface of ZnO', *Surf. Sci.*, **245**, 315–323.
1550. Truong, C. M., Wu, M. C. and Goodman, D. W. (1992), 'Adsorption and reaction of formic acid on NiO (100) films', *J. Chem. Phys.*, **97**, 9447–9453.

1551. Bandara, A., Kubota, J. and Hirose, C. (1996), 'Adsorption and reaction of formic acid on (2 × 2) NiO (111)/Ni (111) surface. 2. IRAS study under catalytic steady-state conditions', *J. Phys. Chem.*, **100**, 14962–14971.
1552. Xu, C. and Goodman, D. W. (1996), 'Structure sensitivity of oxide surfaces: the adsorption and reaction of carbon monoxide and formic acid on NiO (100) and NiO (111)', *Catal. Today*, **28**, 297–305.
1553. Yamamoto, H., Watanabe, B. and Hirose, Ch. (1997), 'Adsorption and decomposition of formic acid on MgO (001) surfaces as investigated by TPD and sum-frequency generation spectroscopy: recurrence induced defect sites', *J. Chem. Phys.*, **106**, 4734–4747.
1554. Popova, G. Ya., Budneva, A. A. and Andrushkevich, T. V. (1997), 'Identification of adsorption forms by IR spectroscopy for formaldehyde and formic acid on K₃PMo₁₂O₄₀', *React. Kinet. Catal. Lett.*, **61**, 35–42.
1555. Kiselev, A. V. and Uvarov, A. V. (1967), 'Infrared spectra and ESR studies of aluminum, silicon and titanium oxides and of adsorbed substances', *Surf. Sci.*, **6**, 399–404.
- 1556a. Hasegawa, H. and Low, M. J. D. (1969), 'Infrared study of adsorption *in situ* at the liquid–solid interface. II. Adsorption of stearic acid on ZnO', *J. Colloid Interface Sci.*, **29**, 593–597.
- 1556b. Hasegawa, H. and Low, M. J. D. (1970), 'Infrared study of adsorption *in situ* at the liquid-solid interface. III. Adsorption of stearic acid on silica and alumina and decanoic acid on magnesia', *J. Colloid Interface Sci.*, **30**, 378–384.
1557. Imanaka, T., Tanemoto, T. and Teranishi, S. (1973), Catalytic conversion of acetic acid on metal oxides', in *Proceedings of the 5th International Congress on Catalysis, Palm Beach, Fl 1972*, Hightower, J. (Ed.), North-Holland, Amsterdam, 1973, pp. 163–168.
1558. Tompkins, H. G. and Allara, D. L. (1974), 'The study of the gas–solid interaction of acetic acid with a cuprous oxide surface using reflection–absorption spectroscopy', *J. Colloid Interface Sci.*, **49**, 410–417.
1559. Hill, W. and Ohlmann, G. (1989), 'FT-IR study of the adsorption and reactions on dispersed silica', *J. Chem. Soc., Faraday Trans. 1*, **85**, 691–697.
- 1560a. Neagle, W. and Rochester, C. (1989), 'Infrared study of the adsorption of ethanoic acid and trifluoroethanoic acid on BaSO₄', *J. Chem. Soc., Faraday Trans. 1*, **85**, 429–439.
- 1560b. Demidov, A. V., Davydov, A. A. and Kurina, L. N. (1985), 'IR spectroscopic investigation of the interaction of methanol and propene with HNaY zeolite', *Zh. Fiz. Khim.* (in Russian); *Russ. J. Phys. Chem.* (English translation), **59**, 2364–2366.
- 1560c. Karge, H. G., Laniecki, M., Ziolk, M., Onyestyak, G., Kiss, A., Kleinschmit, P. and Siray, M. (1989), 'UV–Visible spectroscopic investigations and related studies on coke formation over industrial H-ZSM-5-based catalysts', in Jacobs, P. A. and Van Santen, R. A. (Eds.) *Proceedings of the 8th International Conference on Zeolites*, Amsterdam, July 10–14 1989, Elsevier, Amsterdam, pp. 1–11.
- 1560d. Galuszka, J., Sano, T. and Sawicki, J. A. (1992), 'Study of carbonaceous deposits on Fischer–Tropsch oxide-supported iron catalysts', *J. Catal.*, **136**, 96–109.
1561. Onishi, T. (1993), 'IR spectroscopic studies on surface reactions', in Richardson, J. T. (Eds), *Fundamental of Applied Catalysis*, Plenum Press, New York, 237–258.
1562. Tamaru, K. (1997), 'In situ surface dynamics in heterogeneous catalysis', *Appl. Catal., A: Gen.*, **151**, 167–177.
1563. Burch, R. (1991), 'In situ methods in catalysis', *Catal. Today*, **9**, 1–227.
1564. McKelvy, M. L., Britt, T. R., Davis, B. L. (1996), 'Infrared spectroscopy', *Anal. Chem.*, **68**, 93R–106R (and references therein).
1565. Davydov, A. A. (1991), 'IR spectroscopic detection of the spillover of carbon–oxygen species in the course of interaction of propene with V₂O₅/Al₂O₃', *Zh. Fiz. Khim.* (in Russian); *Russ. J. Phys. Chem.* (English translation), **65**, 1803–1810.
1566. Satterfield, C. N. (1991), *Heterogeneous Catalysis in Industrial Practice*, 2nd Edn, McGraw-Hill, New York.
1567. Sokolovskii, V. D., Borekov, G. K., Davydov, A. A., Anshits, A. G. and Shchekochikhin, Yu. M. (1974), 'Nature of the associative mechanism and factors causing the mechanisms of transformation of CO oxidation over chromia oxide', *Dokl. AN SSSR* (in Russian); *Proc. AN USSR* (English translation), **214**, 1361–1364.
1568. Sokolovskii, V. D., Borekov, G. K., Davydov, A. A., Gundrizer, T. A., Anufrienko, V. F., Ismailov, E. A., Budneva, A. A. and Maksimov, N. G. (1974), 'Conjunction of the processes of catalyst oxidation–reduction as a cause of the highly effective mechanism for CO oxidation over zinc oxide', *Dokl. AN SSSR* (in Russian); *Proc. AN USSR* (English translation), **216**, 599–602.
1569. Sokolovskii, V. D., Borekov, G. K., Davydov, A. A., Anshits, A. G., Anufrienko, V. F. and Gundrizer, T. A. (1974), Nature of the associative mechanism and transformation of the mechanisms in the oxidation reaction of CO and hydrocarbons oxidation over several oxide catalysts', *All-Union Conference on the Mechanisms of Heterogeneous Catalytic Reactions* (in Russian), Moscow, September 3–9, 1974, Preprint 100.
1570. Sokolovskii, V. D. (1990), 'Principles of oxidative catalysis on solid oxides', *Catal. Rev. Sci. Eng.*, **32**, 1–49.
1571. Anshits, A. G., Sokolovskii, V. D., Borekov, G. K. and Davydov, A. A. (1973), 'Relative reactivity and mechanism of complete oxidation of *n*-alkanes on CuO', *Dokl. AN SSSR* (in Russian); *Proc. AN USSR* (English translation), **213**, 607–610.

1572. Anshits, A. G., Sokolovskii, V. D., Borekov, G. K., Davydov, A. A., Budneva, A. A., Avdeev, V. I. and Zakharov, I. I. (1975), 'Relative reactivity and mechanism of complete oxidation of hydrocarbons on oxide catalysts', *Kinet. Katal.* (in Russian); *Kinet. Catal.* (English translation), **16**, 92–102.
1573. Anshits, A. G., Sokolovskii, V. D., Borekov, G. K. and Davydov, A. A. (1977), 'Relative reactivity of aliphatic hydrocarbons in the complete oxidation reaction on copper oxide catalysts', *4th Japan–Soviet Seminar on New Approaches to Catalysis*, 26–28 September, 1977 Tokyo, Japan, Preprints, 4.1–4.22.
1574. Anshits, A. G., Sokolovskii, V. D., Borekov, G. K. and Davydov, A. A. (1978), 'Relative reactivity and mechanism of complete oxidation of hydrocarbons on oxide catalysts. III. Oxidation of *n*-alkenes and *n*-alkynes on cuprous oxide', *Kinet. Katal.* (in Russian); *Kinet. Catal.* (English translation), **19**, 366–371.
1575. Davydov, A. A., Shchekochikhin, Yu. M. and Keier, N. P. (1969), 'Infrared spectroscopic investigation of the oxidation mechanism of carbon monoxide on chromium oxide', *Kinet. Katal.* (in Russian); *Kinet. Catal.* (English translation), **10**, 1341–1349.
1576. Winter, E. (1958), 'The reactivity of oxide surfaces', *Adv. Catal. Related Subj.*, **10**, 196–239.
1577. Stone, F. S. (1962), 'Chemisorption and catalysis on metallic oxides', *Adv. Catal.*, **13**, 1–54.
1578. Davydov, A. A., Budneva, A. A., Sokolovsky, V. D. (1992), 'Carbonate-like intermediates in the oxidation reactions of CO on Cr₂O₃', *Kinet. Katal.* (in Russian); *Kinet. Catal.* (English translation), **33**, 635–669.
1579. Davydov, A. A., Budneva, A. A. and Sokolovskii, V. D. (1989), 'IR spectroscopic study of the mechanism of oxidation of CO on copper oxides', *Kinet. Katal.* (in Russian); *Kinet. Catal.* (English translation), **30**, 1407–1413.
1580. Courtois, M and Teichner, S. J. (1962), 'Infrared study of CO, O₂ and CO₂ gases and their interaction products, chemically adsorbed on nickel oxide', *J. Catal.*, **1**, 121–135.
- 1581a. Choi, K. I. and Vannice, M. A. (1991), 'CO oxidation over Pd and Cu catalysts. III. Reduced Al₂O₃-supported Pd', *J. Catal.*, **131**, 1–21.
- 1581b. Choi, K. I. and Vannice, M. A. (1991), 'CO oxidation over Pd and Cu catalysts. IV. Prereduced Al₂O₃-supported copper', **131**, 22–35.
- 1581c. Choi, K. I. and Vannice, M. A. (1991), 'CO oxidation over Pd and Cu catalysts. V. Al₂O₃-supported bimetallic Pd–Cu particles', **131**, 36–50.
- 1582a. Borekov, G. K. and Marshneva, V. I. (1973), 'Mechanism of carbon monoxide oxidation on oxides of period IV transition metals', *Dokl. AN SSSR* (in Russian); *Proc. AN USSR* (English translation), **213**, 112–115.
- 1582b. Borekov, G. K. Marshneva, V. I. and Sokolovski, V. D. (1971), 'Mechanism of carbon monoxide oxidation on metal oxides', *Dokl. AN SSSR* (in Russian); *Proc. AN USSR* (English translation), **199**, 1091–1093.
1583. Marshneva, V. I. and Davydov, A. A. (1979), 'Mechanism of hydrogen oxidation on zinc oxide', *Kinet. Katal.* (in Russian); *Kinet. Catal.* (English translation), **21**, 706–713.
1584. Boccuzzi, F, Garrone, E, Zecchina, A, Bossi, A and Camia, M (1978), 'Infrared study of ZnO surface properties. II. H₂–CO interaction at room temperature', *J. Catal.*, **51**, 160–168.
1585. Lund, C. R., Kubsh, J. E. and Dumesic, J. A. (1985), 'Water-gas shift over magnetite-based catalysts. Nature of active sites for adsorption and catalysis', in Grasselli, R. K. and Brazdil, J. F. (Eds), *Solid State Chemistry in Catalysis*, American Chemical Society, Washington, DC, pp. 313–338.
1586. Edwards, J. P. and Schrader, G. L. (1985), 'In situ Fourier transform infrared study of methanol sythesis on mixed oxide catalysts', *J. Catal.*, **94**, 175–186.
- 1587a. Van Herwijnen, T. and de Jong, W. A. (1980), 'Kinetics and mechanism of the CO shift on Cu/ZnO. I. Kinetics of the forward and reverse CO shift reactions', *J. Catal.*, **63**, 83–93.
- 1587b. Van Herwijnen, T., Guzaliski, R. T. and de Jong, W. A. (1980), 'Kinetics and mechanism of the CO shift on Cu/ZnO. II. Kinetics of the decomposition of formic acid', *J. Catal.*, **63**, 94–101.
1588. Hadden, R. A., Vandervell, H. D., Waugh, K. C. and Webb, G. (1988), Kinetics and mechanism of the reverse shift reaction on unsupported copper, in *Catalyst: Theory to Practice. Proceedings of the 9th International Congress on Catalysis*, Calgary, Canada, 1988, Phillips, M. J. and Ternan, M., (Eds.), The Chemical Institute of Canada, Ottawa, Ontario, 1988, pp. 1835–1839.
- 1589a. Andreeva, D. and Giovanni, R. (1996), 'The low temperature water-gas shift reaction on Au/α-Fe₂O₃ catalysts', *Appl. Catal.*, **134**, 275–283.
- 1589b. Andreeva, D., Idakiev, V., Tabakova, T. and Andreev, A. (1996), 'Low temperature water-gas shift reaction over Au/α-Fe₂O₃', *J. Catal.*, **158**, 354–355.
1590. Ovesen, C. V., Clausen, B. S., Askgaard, T., Hammershi, B. S., Steffonsen, G., Chorkendorff, I., Noskov, J. K., Rasmussen, P. B., Stollze, P. and Taylor, P. (1996), 'A microkinetic analysis of the water-gas shift reaction under industrial conditions', *J. Catal.*, **158**, 170–180.
- 1591a. Boccuzzi, F. and Chiorino, A. (1996), 'FTIR study of carbon monoxide oxidation and [isotope] scrambling at room temperature over copper supported on ZnO and TiO₂', *J. Phys. Chem.*, **100**, 3617–3624.
- 1591b. Boccuzzi, F. and Tsubota, S. (1996), 'FTIR study of carbon monoxide oxidation and [isotope] scrambling at room temperature over gold supported on ZnO and TiO₂', *J. Phys. Chem.*, **100**, 3625–3631.
1592. Kul'kova, N. V. and Temkin, M. I. (1949), 'Kinetics of the reaction of the conversion of CO by water vapor', *Zh. Fiz. Khim.* (in Russian); *Russ. J. Phys. Chem.* (English translation), **23**, 695–713.

1593. Boreskov, G. K., Yurieva, T. M. and Sergeeva, A. S. (1970), 'Mechanism of carbon monoxide conversion on an iron–chromium catalyst', *Kinet. Katal.* (in Russian); *Kinet. Catal.* (English translation), **11**, 1476–1479.
1594. Davydov, A. A., Pubene, N. A. and Yurieva, T. M. (1978), 'The study of the mechanism of the water-gas shift reaction by means of IR spectroscopy', *Kinet. Katal.* (in Russian); *Kinet. Catal.* (English translation), **2**, 94–102.
- 1595a. Davydov, A. A., Budneva, A. A. and Yurieva, T. M. (1974), 'An investigation of surface compounds in carbon monoxide conversion on solid solutions of CuO–MgO by the infrared spectroscopic method', *All-Union Conference on the Mechanisms of Heterogeneous Catalytic Reactions* (in Russian), Moscow September 3–9, 1974, Preprint 39.
- 1595b. Davydov, A. A., Rubene, N. A. and Budneva, A. A. (1978), 'The study of CO adsorption on the surface of CuO–MgO solid solutions by means IR-spectroscopy', *Kinet. Katal.*, **19**, 969–978.
1596. Ueno, A., Onishi, T. and Tamaru, K. (1970), 'Dynamic technique to elucidate the reaction of intermediates on a catalyst's surface', *Trans. Faraday Soc.*, **66**, 756–763.
- 1597a. Salomatin, G. I., Gelman, V. I., Sobolevskii, V. S., Golosman, E. Z. and Yakerson, V. I. (1982), in Boreskov, G. K. (Ed) *Proceedings of the 3rd All-Union Conference on the Mechanisms of Catalytic Reactions* (in Russian), Nauka, Novosibirsk, pp. 222–227.
- 1597b. Salomatin, G. I., Sobolevskii, V. S. and Yakerson, V. I. (1986), in *Proceedings of the 4th All-Union Conference on the Mechanisms of Catalytic Reactions* (in Russian), Vol. 1, Nauka Moscow, pp. 318–324.
1598. Kiennemann, A., Idriss, H., Hindermann, J. P., Lavalley, J. C., Vallet, A., Chaumette, P. and Courty, Ph. (1989), 'Methanol synthesis on Cu/ZnAl₂O₄ and Cu/ZnO–Al₂O₃ catalysts. Influence of CO pretreatment on the formation and concentration of formate species', *Appl. Catal.*, **59**, 165–184.
1599. Chauvin, C., Saussey, J., Lavalley, J. C., Idriss, H., Hindermann, J. P., Kiennemann, A., Chaumette, P. and Courty, P. (1990), 'Combined infrared spectroscopy, chemical trapping, and thermoprogrammed desorption studies of methanol adsorption and decomposition on ZnAl₂O₄ and CuAl₂O₄ catalysts', *J. Catal.*, **121**, 56–69.
1600. Arakawa, H. and Sayama, K. (1992), 'Methanol synthesis from CO₂ and H₂ over a supported copper–zinc oxide catalyst. Significant influence of the support on methanol formation', *New Frontiers in Catalysis, Studies Surf. Sci. Catal.*, **75C**, 2777–2780.
1601. Verdonck, J., Schoonheydt, R. A. and Jacobs, P. A. (1980), New ruthenium complex stabilized in faujasite-type zeolites. An active water-gas shift catalyst, in *New Horizons in Catalysis, Proceedings of the 7th International Congress on Catalysis, Tokyo, June 30–July 4, 1980*, Seiyama, T. and Tanabe, K. (Eds.) *Studies in Surface Science and Catalysis*, v.7, Kodansha, Tokyo, Elsevier, Amsterdam, 1980.
1602. Eidus, Ya. T. and Puzitskii, K. V. (1964), 'Hydride ion transfer under acidic catalysis conditions during the carboxylation reaction with CO', *Usp. Khim.* (in Russian); *Russ. Chem. Rev.* (English translation), **33**, 991–1016.
1603. Beller, M., Cornils, B., Frohning, C. D. and Kohlpaintner, C. W. (1995), 'Progress in hydroformylation and carbonylation', *J. Mol. Catal., A: Gen.*, **104**, 17–85.
1604. Tsyganenko, A. A. and Trusov, E. A. (1985), 'Study of the interaction of carbon dioxide with methoxy groups of the oxide surfaces by means infrared spectroscopy', *Zh. Fiz. Khim.* (in Russian); *Russ. J. Phys. Chem.* (English translation), **59**, 2602–2603.
1605. Takeuchi, K., Ogasawa, S. (1995), 'In situ diffuse reflectance FT-IR spectroscopic studies of noble metal promoted Co/SiO₂ for selective vapor phase hydroformylation', *Studies Surf. Sci. Catal.*, **92**, 269–274.
1606. Li, Z., Zang, J., Liu, D. (1995), 'Hydroformylation of 1-heptene catalyzed homogeneously and heterogeneously by Ru₃(CO)₁₂ catalyst', *J. Fuel. Chem. Technol.*, **23**, 219–224.
1607. Gerasimov, S. F. and Filimonov, V. N. (1985), 'Photoinduced reactions of H₂ + CO and CH₄ + CO mixtures on η-Al₂O₃ and V/η-Al₂O₃', *React. Kinet. Catal. Lett.*, **29**, 387–393.
1608. Ghiotti, G., Garrone, E. and Zecchina, A. (1991), 'An infrared study of CO/C₂H₄ coadsorption and reaction on silica-supported Cr(II) ions', *J. Mol. Catal.*, **65**, 73–83.
1609. Klier, K. (1982), 'Methanol synthesis', *Adv. Catal.*, **31**, 243–313.
1610. Vedage, G. A., Himelfarb, P. B., Simmons, G. W. and Klier, K. (1985), 'Alkali-promoted copper–zinc oxide catalysts for low alcohol synthesis', in Grasselli, R. K. and Brazdil, J. F. (Eds), *Solid State Chemistry in Catalysis*, ACS Symposium Series 279, American Chemical Society, Washington, DC, pp. 295–311.
1611. Itina, G. V., Demidov, A. V., Davydov, A. A. and Kurina, L. N. (1989), 'Adsorption of alcohols on the surface of Zn–Cr–K catalyst of their synthesis from CO and H₂', *Zh. Fiz. Khim.* (in Russian); *Russ. J. Phys. Chem.* (English translation), **63**, 140–145.
1612. Manoon, S. C., Yamashita, H. and Anpo, M. (1994), *Proceedings of the International Symposium on Acid–Base Catalysis II Symposium (Sapporo, Japan, 1993)*, *Studies Surf. Sci. Catal.*, **90**, 479–484.
1613. Dilara, P. A. and Vohs, J. M. (1994), 'Structure sensitivity in the reaction of methanol on ZrO₂', *Surf. Sci.*, **321**, 8–18.
1614. Itina, G. V., Davydov, A. A., Osipova, N. A. and Kurina, L. N. (1991), 'Promoting effect of potassium on catalytic and surface properties and phase composition', *React. Kinet. Catal. Lett.*, **45**, 243–250.

1615. Baiker, A., Kilo, M., Maciejewski, M., Menzi, S. and Wokaun, A. (1993), 'Hydrogenation of CO₂ over copper silver and gold/zirconia catalyst: comparative study of catalyst properties and reaction pathways', in *New Frontiers in Catalysis. Proceedings of the 10th International Congress on Catalysis, Budapest, Hungary, 19–24 July, 1992*, Gucci, L., Solimosi, F. and Tetenyi, P. (Eds.) *Studies in Surface Science and Catalysis*, v.75, Elsevier, Amsterdam, 1992, 1257–1267.
1616. Neophytides, S. G., Marchi, A. J. and Froment, G. F. (1992), 'Methanol synthesis by means of diffuse reflectance infrared Fourier transform and temperature-programmed reaction spectroscopy', *Appl. Catal.*, **86**, 45–64.
1617. Amenomiya, J. and Tagawa, T. (1984), 'Infrared study of methanol synthesis from CO₂+H₂ on supported copper-zinc oxide catalysts', in *Proceedings of the 8th International Congress on Catalysis, Berlin 1984*, Verlag Chemie, Weinheim, Germany, 1984, Vol. 2, pp. 557–562.
1618. Millar, G. J., Rochester, C. H., Bailey, S. and Waugh, K. C. (1992), 'A combined temperature-programmed reaction spectroscopy and FTIR spectroscopy study of CO₂-H₂ and CO-CO₂-H₂ interactions with model ZnO/SiO₂, Cu/SiO₂ and Cu/ZnO/SiO₂ methanol-synthesis catalysts', *J. Chem. Soc., Faraday Trans., I*, **88**, 2085–2093.
1619. Millar, G. J., Rochester, C. H., Bailey, S. and Waugh, K. C. (1993), 'A combined temperature-programmed reaction spectroscopy and FTIR spectroscopy study of CO₂, CO and H₂ interactions with model ZnO/SiO₂, Cu/SiO₂ and Cu/ZnO/SiO₂ methanol-synthesis catalysts', *J. Chem. Soc., Faraday Trans., I*, **89**, 1109–1115.
- 1620a. Liu, D., Zhu, Q. and Li, J. (1988), 'Mechanistic studies on methanol synthesis over copper-based catalysts', in *Catalyst: Theory to Practice. Proceedings of the 9th International Congress on Catalysis*, Calgary, Canada, 1988, Phillips, M. J. and Ternan, M., (Eds.), The Chemical Institute of Canada, Ottawa, Ontario, 1988, Vol. 2, pp. 577–584.
- 1620b. Liu, D., Zhu, Q. and Li, J. (1987), 'Fundamental research on synthesis of fuel-grade methanol from carbon monoxide/hydrogen over copper-based catalysts', *Studies Surf. Sci. Catal.*, **24**, 647–652.
1621. Rozovski, A. Ya. (1989), 'Kinetics of catalytic reactions involving strongly (irreversibly) chemisorbed species', *Kinet. Katal.* (in Russian); *Kinet. Catal.* (English translation), **30**, 533–547.
1622. Busca, G., Pattuelli, M. E., Trifiro, F. and Vaccari, A. (1989), 'Effect of cobalt on the surface properties of Zn-Cr and Cu-Zn-Cr methanol synthesis catalysts', in Morterra, C., Zecchina, A. and Costa, G. (Eds), *Structure and Reactivity of Surfaces*, Elsevier, Amsterdam, pp. 239–248.
1623. Clarke, D. B., Lee, D. K., Sandoval, M. J. and Bell, A. T. (1994), 'Infrared studies of the mechanism of methanol decomposition on Cu/SiO₂', *J. Catal.*, **150**, 81–93.
1624. Davydov, A. A., Tunina, O. V. and Kravtsov, A. V. (1983), 'Infrared spectroscopic study of the hydrogenation of carbon monoxide on a platinum/alumina catalyst', *Zh. Fiz. Khim.* (in Russian); *Russ. J. Phys. Chem.* (English translation), **57**, 2089–2091.
1625. Pichler, H. and Ziesecke, K. H. (1949), 'High-pressure hydrogenation of CO to predominantly iso-paraffinic hydrocarbon compounds (iso-synthesis). (I), (II) mixed catalysts and conversion of Me₂O', *Brennst. Chem.*, **30**, 13–22.
1626. Maruya, K., Maehasti, T., Haraoka, T., Narui, S., Asakawa, Y., Domen, K. and Onishi, T. (1988), 'The carbon monoxide hydrogen reaction over zirconium dioxide to selectively form isobutene', *Bull. Chem. Soc. Jpn.*, **61**, 667–671.
1627. Arai, T., Maruya, K.-I., Domen, K. and Onidhi, T. (1993), 'Strongly adsorbed species to form linear hydrocarbons over partially reduced CeO₂', *J. Catal.*, **141**, 533–539.
- 1628a. Rubene, N. A., Davydov, A. A., Kravtsov, A. V., Usheva, N. V. and Smolyaninov, S. I. (1976), 'IR spectroscopic study of the chemisorption of H₂O and CO on the surface of Fe-Cr conversion catalyst', *Kinet. Katal.* (in Russian); *Kinet. Catal.* (English translation), **17**, 465–471.
- 1628b. Rubene, N. A., Davydov, A. A., Kravtsov, A. V., Usheva, N. V. and Smolyaninov, S. I. (1976), 'Study of surface reactions occurring at the interaction of carbon oxide and water with Fe-Cu-oxide catalysts by means of infrared spectroscopy', in *Problems of Kinetics and Catalysis* (In Russian), Institute of Chemical Technology, Ivanovo, Vol. 3, pp. 64–70.
1629. Chiang, P., Liu, W., Wang, H. and Huang, S. (1984), 'Kinetics and reaction mechanisms in the hydrogenation of CO adsorbed species over metal catalysts', in *Proceedings of the 8th International Congress on Catalysis, Berlin 1984*, Verlag Chemie, Weinheim, Germany, 1984, Vol. 3, pp. 197–205.
1630. Naito, S., Yoshioka, H., Orita, H. and Tamaru, K. (1984), 'The nature of active sites for oxygenated compound formation from the CO-H₂ reaction under mild conditions', in *Proceedings of the 8th International Congress on Catalysis, Berlin 1984*, Verlag Chemie, Weinheim, Germany, 1984, Vol. 3, pp. 207–218.
1631. Sato, B. K., Inoue, Y., Kojima, I., Miyazaki, E. and Yasumori, I. (1984), 'Infrared and X-ray photoelectron spectroscopy studies of carbon monoxide adsorbed on silica-supported cobalt catalysts', *J. Chem. Soc., Faraday Trans. I*, **80**, 841–850.
1632. Highfield, J. G., Ruterana, P., Thampi, K. R. and Graetzel, M. (1989), 'Catalyst characterization and *in situ* FTIR studies of carbon dioxide methanation over ruthenium supported on titania', in Morterra, C., Zecchina, A. and Costa, G. (Eds), *Structure and Reactivity of Surfaces*, Elsevier, Amsterdam, pp. 469–479.
1633. Ma, B., Li, C., Liu, S. and Lu, Y. (1992), 'IR evidence for the formation of tilted CO on alumina-supported nickel catalyst', *Chem. Phys. Lett.*, **196**, 433–436.

1634. Fredriksen, G. R., Blekkan, E. A., Schanke, D. and Holmen, A. (1993), 'CO hydrogenation on supported cobalt catalysts studied by *in situ* FTIR spectroscopy', *Ber. Bunsenges. Phys. Chem.*, **97**, 308–312.
1635. McQuire, M. W. and Rochester, C. H. (1995), 'FTIR study of CO/H₂ reactions over Ru/TiO₂ and Ru-Rh/TiO₂ catalysts at high temperature and pressure', *J. Catal.*, **157**, 396–402.
1636. Balakos, M. W., Chuang, S. S. C., Srinivas, G. and Brundage, M. (1995), 'Infrared study of the dynamics of adsorbed species during CO hydrogenation', *J. Catal.*, **157**, 51–65.
1637. Fredriksen, G. R., Blekkan, E. A., Schanke, D. and Holmen, A. (1995), 'CO hydrogenation over supported cobalt catalysts: FTIR and gravimetric studies', *Chem. Eng. Technol.*, **18**, 125–131.
1638. Guglieminotti, E., Giamello, E., Pinnat, F., Strukul, G., Martinengo, S. and Zanderighi, L. (1994), 'Elementary steps in CO hydrogenation on Rh catalysts supported on ZrO₂ and Mo/ZrO₂', *J. Catal.*, **146**, 422–436.
1639. Odrizola, J. A., Carrizosa, I. and Alvero, R. (1989), 'Adsorption and dissociation of CO₂ on lanthanide ion promoted Rh/Al₂O₃ catalysts', in Morterra, C., Zecchina, A. and Costa, G. (Eds), *Structure and Reactivity of Surfaces*, Elsevier, Amsterdam, pp. 713–721.
1640. Anderson, J. A. and Khader, M. M. (1996), 'A high pressure, high temperature infrared study of CO hydrogenation over Rh/ZrO₂', *J. Mol. Catal., A: Gen.*, **105**, 175–183.
1641. Boellaard, E. (1994), *Ph. D. Thesis*, University of Utrecht, Utrecht, The Netherlands.
1642. Davydov, A. A. (1996), 'IR study of high-temperature interactions of alkanes, alkenes and alkynes C1-C4 with copper oxides', *Zh. Fiz. Khim.* (in Russian); *Russ. J. Phys. Chem.* (English translation), **70**, 1254–1259.
1643. Dobrynkin, N. M., Davydov, A. A., Budneva, A. A., Popovskii, V. V., Rogov, V. A. and Serebryakov, V. F. (1992), 'Infrared spectroscopic study of the mechanism of propanol-2 deep oxidation on copper oxide under conditions of catalytic reaction', *Kinet. Katal.* (in Russian); *Kinet. Catal.* (English translation), **33**, 133–141.
1644. Dobrynkin, N. M., Davydov, A. A. and Popovskii, V. V. (1988), 'Spectrokinetic study of the mechanism of complete oxidation of propanol-2 on copper oxide', in *Proceedings of the 9th International Symposium on Catalysis*, Madras, 1988, Madras, reprint OR-22.
1645. Davydov, A. A. (1993), 'Spectrokinetic study of formate decomposition over Cr₂O₃', *Zh. Prikl. Spektrosk.* (in Russian); *J. Appl. Spectrosc.* (English translation), **58**, 456–459.
1646. Anshits, A. G., Sokolovskii, V. D., Boretkov, G. K. and Boronin, A. I. (1977), 'Participation of molecular oxygen in the formation of complete oxidation products via a concerted mechanism', *React. Kinet. Catal. Lett.*, **7**, 115–120.
1647. Gorokhovatskii, Ya. B. and Kuznetsov, B. A. (1977), 'Surface carboxylates as intermediate forms in the complete oxidation reaction of olefins', *Dokl. AN SSSR* (in Russian); *Proc. AN USSR* (English translation), **232**, 375–378.
1648. Kadushin, A. A., Kutyreva, N. A., Matyshak, V. A. and Morozova, O. S. (1980), 'IR spectroscopic study of the reaction kinetics of surface compounds under conditions of the catalytic oxidation of propylene', *Kinet. Katal.* (in Russian); *Kinet. Catal.* (English translation), **22**, 233–239.
1649. Kubokawa, Y., Ono, T., Tomino, T. and Yano, N. (1970), 'Oxidation of propylene adsorbed on oxide catalysts', *Bull. Chem. Soc. Jpn*, **43**, 291–299.
1650. Ono, T., Tomino, T. and Kubokawa, T. (1973), 'Interaction of oxygen with propylene adsorbed on metal oxide catalysts', *J. Catal.*, **31**, 167–172.
1651. Kugler, B. L. and Kokes, R. J. (1974), 'Intermediates in the oxidation of propylene over zinc oxide', *J. Catal.*, **32**, 170–173.
1652. Finocchio, E., Busca, G., Lorenzelli, V. and Willey, R. Y. (1994), 'The activation of hydrocarbon C–H bonds over transition metal oxide catalysts: an FTIR study of hydrocarbon catalytic combustion over MgCr₂O₄', *J. Catal.*, **151**, 204–215.
1653. Finocchio, E., Busca, G., Lorenzelli, V. and Willey, R. Y. (1994), 'FTIR studies of the selective oxidation and combustion of light hydrocarbons on metal oxide surfaces. Propane and propene oxidation on MgCr₂O₄', *J. Chem. Soc., Faraday Trans. 1*, **90**, 3347–3356.
- 1654a. Busca, G., Zerlia, T., Lorenzelli, V. and Girelli, A. (1984), 'FT-IR study of the adsorption of unsaturated and aromatic hydrocarbons on the surface of α -ferric oxide. I. Ethylene', *J. Catal.*, **88**, 125–130.
- 1654b. Busca, G., Zerlia, T., Lorenzelli, V. and Girelli, A. (1984), 'FT-IR study of the adsorption of unsaturated and aromatic hydrocarbons on the surface of α -ferric oxide. II. Benzene', *J. Catal.*, **88**, 131–136.
- 1654c. Busca, G., Zerlia, T., Lorenzelli, V. and Girelli, A. (1985), 'FT-IR study of the adsorption of unsaturated and aromatic hydrocarbons on the surface of α -ferric oxide. III. Toluene, ethylbenzene and styrene', *React. Kinet. Catal. Lett.*, **27**, 429–432.
1655. Krylov, O. V., Kislyuk, M. U., Shub, B. R. (1972), 'Rate constants of elementary heterogeneous catalytic reactions', *Kinet. Katal.* (in Russian); *Kinet. Catal.* (English translation), **13**, 598–610.
1656. Chang, C. C., Konner, W. C. and Kokes, R. J. (1973), 'Butene isomerization over zinc oxide and chromia', *J. Phys. Chem.*, **77**, 1957–1964.
1657. Johns, C. S. and Leach, H. F. (1977), 'Determination of the active site and mechanism for alkene isomerization in Cu-exchanged Y-type zeolite', *J. Chem. Soc., Faraday Trans. 1*, **73**, 1595–1604.

1658. Haller, G. L. and Johns, C. S. (1992), 'The mechanism of olefin isomerization on different forms of chromia investigated by microwave spectroscopy', in *New Frontiers in Catalysis. Proceedings of the 10th International Congress on Catalysis, Budapest, Hungary, 19–24 July, 1992*, Guzzi, L., Solimosi, F. and Tetenyi, P. (Eds.) *Studies in Surface Science and Catalysis*, v.75, Elsevier, Amsterdam, 1992, pp. 965–978.
1659. Kritskaya, I. I. (1975), 'Metal allylic derivatives and some related compounds', in *Methods of Elementorganic Chemistry*, Vol. 2, Nauka, Moscow, pp. 734–908.
1660. Turner, J. D. M., Paul, S. O., Reid, F. and Hendra, P. J. (1976), 'Laser-Raman study of the isomerization of olefins over alumina', *J. Chem. Soc., Faraday Trans. 1*, **12**, 2829–2835.
1661. Cram, D. J. (1965), *Fundamentals of Carbanions Chemistry*, Academic Press, New York, 1965, 251 pp.
1662. Rosynek, M. P. and Hightower, J. W. (1973), 'Site concentration on gamma alumina by poisoning techniques', in *Proceedings of the 5th International Congress on Catalysis, Palm Beach, FL 1972*, Hightower, J. (Ed), North-Holland, Amsterdam, 1973, Vol. 2, pp. 851–865.
1663. Peri, J. B. (1966), 'IR study of adsorption of CO₂, HCl and other molecules on acid sites on dry silica-alumina and γ -alumina', *J. Phys. Chem.*, **70**, 3168–3179.
1664. Larson, J. G. and Haul, W. K. (1965), 'Studies of the hydrogen held by solids. VII. The exchange of the hydroxyl groups of alumina and silica-alumina catalysts with deuterated methane', *J. Phys. Chem.*, **69**, 3080–3089.
1665. Kokes, R. G. and Dent, A. L. (1972), 'Hydrogenation and isomerization over ZnO', *Adv. Catal.*, **22**, 1–50.
1666. Paukshtis, E. A., Malysheva, A. V., Kotsarenko, N. S. and Karachiev, L. B. (1980), 'Kinetics and IR spectroscopic study of the mechanism of 1-butene isomerization on acidic catalysts', *Kinet. Katal.* (in Russian); *Kinet. Catal.* (English translation), **21**, 455–463.
1667. Bezoukhanova, A., Lechert, H., Tabanska, G. and Meyer, A. (1989), 'IR study of the *cis-trans* isomerization of olefines on HZSM-zeolites', *React. Kinet. Catal. Lett.*, **40**, 209–214.
1668. Lombardo, E. A., Conner, W. C., Jr, Madon, R. J., Hall, K. W., Kharlamov, V. V. and Minachev, Kh. M. (1978), 'Tracer studies of acid-base catalyzed reactions. XIII. The isomerisation of *n*-butenes over zinc oxide and alumina', *J. Catal.*, **53**, 135–149.
1669. Lemberon, J. L., Perot, G. and Guisnet, M. (1980), 'Mechanism of the isomerization of butenes on titanium dioxide', *New Horizons in Catalysis, Studies Surf. Sci. Catal.*, **7**, 993–1005.
1670. Sassen, N. R. M., den Hartog, A. J. and Jongerius, F. (1989), 'Adsorption and reactions of ethyne: effect of modifiers and formation of bimetallics', *Faraday Discuss. Chem. Soc.*, **87**, 311–320.
1671. Trunchke, A. and Knozinger, H. (1993), 'Generation of alkyl fragments on rhodium/silica and vanadium oxide-promoted rhodium/silica', *Catal. Lett.*, **17**, 295–302.
1672. Jackson, S. D. and Casey, N. J. (1993), 'Hydrogenation of propyne. Identification by IRS of surface species during propyne hydrogenation', *React. Kinet. Catal. Lett.*, **49**, 231–234.
1673. Campione, T. J. and Ekerdt, J. G. (1986), 'Fourier transform infrared study of butene adsorption and reaction on a silica-supported nickel catalyst', *J. Catal.*, **102**, 64–79.
1674. Anderson, K. G. and Ekerdt, J. G. (1989), 'Hydrocarbon surface fragments over Co/SiO₂: an FTIR study', *J. Catal.*, **116**, 556–567.
1675. Lapinski, M. P. and Ekerdt, J. G. (1992), 'In situ Fourier transform infrared study of ethylene surface reaction kinetics on alumina-supported nickel', *J. Phys. Chem.*, **96**, 5069–5077.
- 1676a. Sheppard, N. and De la Cruz, C. (1996), 'Vibrational spectra of hydrocarbons adsorbed on metals. Part I. Introductory principles, ethylene, and the higher acyclic alkenes', *Adv. Catal.*, **41**, 1–111.
- 1676b. Sheppard, N. (1988), 'Vibrational spectroscopic studies of the structure of species derived from the chemisorption of hydrocarbons on metal single-crystal surfaces', *Ann. Rev. Phys. Chem.*, **39**, 589–644.
1677. Naito, S., Shimizu, H. and Hagiwara, E. (1971), 'Behavior of chemisorbed hydrogen under reaction conditions and the mechanism of the H/D exchange reaction over ZnO', *Trans. Faraday Soc.*, **67**, 1519–1597.
1678. Ueno, A., Yamamoto, T. and Onishi, T. (1969), 'Behavior of chemisorbed species under reaction conditions and the mechanism of the water-gas shift reaction on zinc oxide and magnesium oxide', *Bull. Chem. Soc. Jpn.*, **42**, 3040–3048.
1679. Tanaka, K., Aomura, K., Okuhara, T. and Miyahara, K. (1981), 'Orientation in the addition of HD molecules to buta-1,3-diene over a ZnO catalyst. A method of judging heterolytic and homolytic dissociation of hydrogen in the catalyst', *J. Chem. Soc., Faraday Trans. 1*, **77**, 1697–1706.
1680. Oyskan, S. and Dent, A. L. (1978), 'An infrared study of isomerization of cyclo-olefins over zinc oxide', *J. Catal.*, **52**, 32–44.
1681. Kondo, J., Domen, K., Maruya and Onishi, T. (1992), 'Infrared studies of ethene hydrogenation over ZrO₂. 3. Reaction mechanism', *J. Chem. Soc., Faraday Trans. 1*, **88**, 2095–2099.
1682. Ghiotti, G., Boccuzzi, F. and Chiorino, A. (1986), 'The operation of the "metal-surface selection rule" on the vibrational spectra of species adsorbed on supported copper particles', *Surf. Sci.*, **178**, 553–564.
1683. Stuve, E. M. and Madix, R. G. (1985), 'Use of the $\pi-\sigma$ parameter for characterization of rehybridization upon adsorption on metal surfaces', *J. Phys. Chem.*, **89**, 3183–3185.
- 1684a. Primet, M., Garbowski, E., Mathieu, M. V. and Imelik, B. (1980), 'Spectroscopic studies of benzene hydrogenation on platinum-loaded zeolites. Part I. Benzene adsorption on supports', *J. Chem. Soc., Faraday Trans. 1*, **76**, 1942–1952.

- 1684b. Primet, M., Garbowski, E., Mathieu, M. V. and Imelik, B. (1980), 'Spectroscopic studies of benzene hydrogenation on platinum-loaded zeolites. Part 2. Hydrogenation of adsorbed species', *J. Chem. Soc., Faraday Trans. 1*, **76**, 1953–1961.
1685. Kazansky, V. B., Frash, M. V. and Santen, R. A. (1996), 'Quantum-chemical study of isobutane cracking on zeolites', *Appl. Catal., A: Gen.*, **146**, 225–247.
1686. Rebenstorf, B. and Larsson, R. (1983), 'Polymerization of ethylene by chromium surface compounds on silica gel', *J. Catal.*, **84**, 240–242.
- 1687a. Myers, D. L. and Lunsford, J. H. (1985), 'Silica-supported chromium catalysts for ethylene polymerization', *J. Catal.*, **92**, 260–271.
- 1687b. Myers, D. L. and Lunsford, J. H. (1986), 'Silica-supported chromium catalysts for ethylene polymerization: the active oxidation state of chromium', *J. Catal.*, **99**, 140–148.
- 1687c. Lansford, J. H., Fu, S.-L. and Myers, D. L. (1988), 'Ethylene polymerization over a highly dispersed form of Cr(III) on silica', *J. Catal.*, **111**, 231–234.
1688. Zielinski, P. A., Szymura, J. A. and Dalla Lana, I. G. (1992), 'Identification of Cr oxidation states active in ethylene polymerization on Cr/SiO₂ at room temperature', *Catal. Lett.*, **13**, 331–339.
1689. Ghiotti, G., Garrone, E. and Zecchina, A. (1988), 'IR investigation of polymerization centers of the Phillips catalyst', *J. Mol. Catal.*, **46**, 61–77.
1690. Krauss, H. L. and Hums, E. (1979), 'Oberflächenverbindung von Übergangsmetallen. XXII. Die Umsetzung von Oberflächen-chrom(II) auf Silicagel mit Olefinen bei höherer Temperatur. Zum Mechanismus von Aufbau-, Abbau-methathese- und Isomerisierungs-Reaktionen an koordinativ ungesättigten Oberflächen Metallionen', *Z. Naturforsch., B, Anorg. Chem. Org. Chem.*, **34b**, 1628–1636.
1691. Rebenstorf, B. and Larsson, R. (1981), 'Why do homogeneous analogs of Phillips (CrO₃/SiO₂) and Union Carbide (Chromocene/SiO₂) polyethylene catalysts fail? Some answers from IR investigations', *J. Mol. Catal.*, **11**, 247–255.
- 1692a. McDaniel, M. P. (1985), 'Supported chromium catalysts for ethylene polymerization', *Adv. Catal.*, **33**, 47–98.
- 1692b. McDaniel, M. P., Leigh, C. H. and Sharry, S. M. (1989), 'Ethylene polymerization catalysts from supported organotransition metal complexes. III. Support interactions', *J. Catal.*, **120**, 170–181.
1693. Hogan, J. P. (1983), 'Ethylene alpha-olefin copolymers made in the gas phase', in *Applied Industrial Catalysis*, Academic Press, New York, Chapter 6, pp. 371–450.
1694. Groeneveld, C., Wittgen, P. P. M. M., Swinnen, H. P. M., Wernsen, A. and Schuit, C. A. (1983), 'Hydrogenation of olefins and polymerization of ethene over chromium oxide/silica catalysts. V. *In situ* infrared measurements and investigation of the polymer', *J. Catal.*, **83**, 346–361.
1695. McDaniel, M. P. and Welch, M. B. (1983), 'The activation of the Phillips polymerization catalyst. I. Influence of the hydroxyl population', *J. Catal.*, **82**, 98–109.
- 1696a. Rebenstorf, B. (1984), 'New chromium-on-silica-gel catalysts with very high activity for the polymerization of ethylene', *Z. Anorg. Allgem. Chem.*, **513**, 103–113.
- 1696b. Rebenstorf, B. (1988), 'An IR study of the polymerization mechanism of the Phillips catalyst', *J. Mol. Catal.*, **45**, 263–274.
- 1697a. Rebenstorf, B. (1989), 'On the active sites of the Phillips catalyst for ethylene polymerization', *J. Catal.*, **117**, 71–77.
- 1697b. Rebenstorf, B. (1989), 'On the catalytic activity of mononuclear and dinuclear chromium (II)–A surface species on silica gel', *Acta Chem. Scand.*, **43**, 413–416.
1698. Jozwiak, W. K., Dalla Lana, I. G. and Fiedorow, R. (1990), 'On the role of surface hydroxyls during the Cr/SiO₂-catalyzed polymerization', *J. Catal.*, **121**, 183–195.
1699. Zielinski, P. and Dalla Lana, I. G. (1992), 'An IR spectroscopic view of the initiation of ethylene polymerization on Cr/SiO₂ catalysts', *J. Catal.*, **137**, 368–376.
1700. Vikulov, K., Spoto, G., Coluccia, S. and Zecchina, A. (1992), 'FTIR investigation of ethylene coordination and polymerization on reduced chromium/silica catalysts', *Catal. Lett.*, **16**, 117–121.
1701. Kantcheva, M., Dalla Lana, I. G. and Szymura, J. A. (1995), 'FTIR spectroscopic investigation of the initiation of ethylene polymerization on Cr/silica', *J. Catal.*, **154**, 329–334.
1702. Davydov, A. A. (unpublished data).
1703. Matsuda, T., Miura, H., Sugiyama, K., Ohno, N., Keino, S. and Kaise, A. (1979), 'Selectivity of ethylene dimerization over supported nickel oxide catalysts', *J. Chem. Soc., Faraday Trans. 1*, **6**, 1513–1519.
1704. Bonneviot, L., Che, M., Dyrek, K., Schollner, R. and Wendt, G. (1986), 'An EPR study of the formation of Ni⁺ ions by photoreduction in hydrogen of Ni/Al₂O₃ catalysts', *J. Phys. Chem.*, **90**, 2379–2384.
1705. Chauvin, Y., Commerc, D. C., Hugues, F. and Thivolle-Cazat, E. (1988), 'Nickel-based heterogeneous catalysts for olefin oligomerization. Support and anion effect', *J. Appl. Catal.*, **42**, 205–216.
1706. Aljarallah, A. M., Anabtawi, J. A., Siddiqui, M. A. B., Aitani, A. M. and Alsadoun, A. W. (1992), 'Ethylene dimerization and oligomerization to butene-1 and linear α -olefins', *Catal. Today*, **14**, 1–124.
1707. Skupinska (1991), 'Oligomerization of α -olefins to higher oligomers', *Chem. Rev.*, **91**, 613–648.

- 1708a. Espinosa, R. L., Korf, C. J., Nicolaidis, C. P. and Snel, R. (1987), 'Catalytic oligomerization of ethene over nickel-exchanged amorphous silica-alumina. I. Effect of the reaction conditions and modelling of the reaction', *Appl. Catal.*, **29**, 175–184.
- 1708b. Espinosa, R. L., Nicolaidis, C. P., Korf, C. J. and Snel, R. (1987), 'Catalytic oligomerization of ethene over nickel-exchanged amorphous silica-alumina. II. Effect of the acid strength of the support', *Appl. Catal.*, **31**, 259–266.
- 1708c. Espinosa, R. L., Snel, R., Korf, C. G. and Nicolaidis, C. P. (1987), 'Catalytic oligomerization of ethene over nickel-exchanged amorphous silica-alumina. III. Effect of the nickel concentration', *Appl. Catal.*, **29**, 295–303.
1709. Chauvin, Y. (1990), *French Patent*, 2641477.
1710. Ng, F. T. T. and Creaser, D. C. (1992), 'Ethylene dimerization over modified nickel exchanged Y-zeolites', *Progr. Catal.*, Studies in Surface Science and Catalysis, **73**, 123–129.
1711. Heveling, J., Nicolaidis, C. P. and Scurrell, M. S. (1991), 'Identification of novel catalysts and conditions for the highly efficient and stable heterogeneous oligomerization of ethylene', *J. Chem. Soc., Chem. Commun.*, 126–127.
1712. Goledzinowski, M. and Briss, V. I. (1993), 'Oligomerization of low-molecular-weight olefines in ambient temperature-molten salts', *Ind. Eng. Chem. Res.*, **32**, 1795–1801.
1713. Cai, T., Cao, D., Song, Z. and Li, L. (1993), 'Catalytic behavior of NiSO₄/γ-Al₂O₃ for ethene dimerization', *Appl. Catal.*, A: Gen., **95**, L1–L8.
1714. Davydov, A. A., Kantcheva, M. and Shepotko, M. L. (unpublished data).
1715. Yashima, T., Ushida, Y., Ebisawa, M. and Hara, N. (1975), 'Polymerization of ethylene over transition metal exchanged Y zeolites', *J. Catal.*, **36**, 320–326.
1716. Bonneviot, L., Oliver, D. and Che, M. (1983), 'Dimerization of olefins with nickel-surface complexes in X-type zeolites or on silica', *J. Mol. Catal.*, **21**, 415–430.
1717. Elev, I. V., Shelimov, B. N. and Kazansky, V. B. (1984), 'The role of Ni⁺ ions in the activity of NiCaY zeolite catalysts for ethylene dimerization', *J. Catal.*, **89**, 470–477.
1718. Wendt, G., Findter, J., Schollner, R. and Siegel, H. (1980), 'Studies on nickel oxide mixed catalysts. II. Catalytic properties of nickel oxide (NiO)/silicon dioxide catalysts', *Z. Anorg. Allgem. Chem.*, **467**, 51–60.
1719. Davydov, A. A., Kantcheva, M. and Chepotko, M. L., (2002) 'FTIR spectroscopic study of the nature of active sites on an alumina-supported nickel sulfate catalyst and the role of these sites in the catalytic dimerization of ethene' *Catal. Lett.*, **83**, 97–108.
1720. Davydov, A. A. and Dalla Lana, I. G., 'Effect of the nature and properties of the silicalite and Ni/silicalite surface centers on ethene polymerization according to IR spectroscopy data' (unpublished data).
1721. Ishida, S., Imamura, S., Ren, F., Tatematsu, Y. and Fujimura, Y. (1992), 'Ethylene polymerization on Lewis acid sites of a reduced V₂O₅/Al₂O₃ catalyst', *React. Kinet. Catal. Lett.*, **46**, 199–207.
1722. Ishida, S., Ren, F., Imamura, S. and Fujimura, Y. (1992), 'Kinetics of C₂H₄ polymerization on reduced V₂O₅/Al₂O₃ catalyst', *React. Kinet. Catal. Lett.*, **46**, 215–223.
- 1723a. Antshits, A., Vereshchagin, S. V., Korniets, E. D., Kholopova, G. D. and Hall, W. K. (1988), 'Oligomerization of olefins on an alumina-molybdenum catalyst. 1. Formation of branched and linear surface oligomers based on data from H¹ NMR spectra and chromatographic-mass spectral analysis', *Kinet. Katal.* (in Russian); *Kinet. Catal.* (English translation), **29**, 626–637.
- 1723b. Antshits, A., Vereshchagin, S. V., Maksimov, N. G. and Hall, W. K. (1990), 'Oligomerization of olefins on an alumina-molybdenum catalyst. 2. Structure and pathways of formation of ethylene polymers with low degrees of catalyst surface reduction by hydrogen', *Kinet. Katal.* (in Russian); *Kinet. Catal.* (English translation), **31**, 636–644.
1724. Elev, I. V., Shelimov, B. N. and Kazansky, V. B. (1989), 'First IR spectroscopic observation of the stable Mo=CH₂ carbene complex on the surface of an active catalyst for olefin metathesis: photo-reduced silica-molybdena with chemisorbed cyclopropane', *Catal. Lett.*, **2**, 121–124.
1725. Vikulov, K. A., Elev, I. V., Shelimov, B. N. and Kazansky, V. B. (1989), 'IR and UV-VIS spectroscopic studies of the stable Mo=CH₂ carbene complexes over photo-reduced silica-molybdena catalysts with chemisorbed cyclopropane, and their role in olefin metathesis', *J. Mol. Catal.*, **55**, 126–145.
1726. Vikulov, K. A., Shelimov, B. N. and Kazansky, V. B. (1991), 'IR and UV-VIS spectroscopic studies of the surface Mo=CH₂ and Mo=CH-CH₂ carbene complexes produced by methylcyclopropane chemisorption over photoreduced silica-molybdena catalysts', *J. Mol. Catal.*, **65**, 393–402.
1727. Vikulov, K. A., Shelimov, B. N. and Kazansky, V. B. (1992), 'Determination of the Mo=C bond energy in Mo=CH₂ carbene complexes on the surface of photoreduced silica-molybdena catalysts based on calorimetric measurements', *J. Mol. Catal.*, **72**, 1–11.
1728. Vikulov, K. A., Shelimov, B. N. and Kazansky, V. B. (1992), 'Formation of Mo=CH₂ carbene complexes on a photoreduced silica-molybdena catalyst treated with 1,3,5-cycloheptatriene', *J. Mol. Catal.*, **72**, 117–125.
1729. Naccache, C., Bandiera, I., Wicker, G. and Imelik, B. (1965), 'Polymerization of ethylene oxide on SiO₂-Al₂O₃ catalysts', in Proceedings of the 2nd International Congress on Catalysis, Paris, 1960, Technip, Paris, Vol. 2, pp. 1113–1121.

1730. Krylov, O. V., Kushnerev, M. I., Markova, Z. A. and Fokina, E. A. (1965), 'Mechanism of the heterogeneous catalytic polymerization of ethylene oxide', in Proceedings of the 2nd International Congress on Catalysis, Paris, 1960, Technip, Paris, Vol. 2, pp. 1122–1134.
1731. Loiko, V. E. and Davydov, A. A. (1987), 'IR spectroscopic study of the adsorption and transformation of ethene oxide on some metal oxides', *Zh. Prikl. Spektrosk.* (in Russian); *J. Appl. Spectrosc.* (English translation), **47**, 231–237.
1732. Loiko, V. E. and Davydov, A. A. (1988), 'Monomer incorporation mechanism in ethene oxide polymerization on a metal oxide', *Zh. Prikl. Spektrosk.* (in Russian); *J. Appl. Spectrosc.* (English translation), **49**, 60–64.
1733. Markova, Z. A. (1962), 'Application of infrared spectroscopy to a study of the catalytic polymerization of ethylene oxide', *Kinet. Katal.* (in Russian); *Kinet. Catal.* (English translation), **55**, 366–369.
1734. Sotani, N. (1982), 'Adsorption of ethylene oxide on Cab-o-Sil silica, reactive silica, and oxygen-treated reactive silica', *Bull. Chem. Soc. Jpn.*, **55**, 1992–1998.
1735. Platero, E. E. and Zecchina, A. (1987), 'IR-spectroscopic investigation of ethylene oxide adsorption and polymerization on MgO', *J. Catal.*, **104**, 299–306.
1736. Gates, B. C., Kartzler, J. R. and Shuit, C. A. (1979), *Chemistry of Catalytic Processes*, McGraw-Hill New York.
1737. Grasselli, R. K. (1985), 'Selective oxidation and ammoxidation catalysis', in Grasselli, R. K. and Brazdill, J. E. (Eds) *Solid State Chemistry in Catalysis*, ACS Symposium Series 279, American Chemical Society, Washington, DC, pp. 182–210.
1738. Cavani, F. and Trifiro, F. (1990), 'Selective oxidation of light alkanes: interaction between the catalyst and the gas phase on different classes of catalytic materials', *Catal. Today*, **51**, 561–580.
1739. Matyshak, V. A. and Krylov, O. V. (1996), 'In situ IR spectroscopy of intermediates in heterogeneous oxidative catalysis', *Catal. Today*, **25**, 1–88.
1740. Margolis, L. Ya. (1977), *Oxidation of Hydrocarbons on Heterogeneous Catalysts*, Khimia, Moscow.
1741. German, J. E. (1969), *Catalytic Conversion of Hydrocarbons*, Academic Press, London.
1742. Golodets, G. I. (1982), 'Heterogeneous Catalytic Reactions Involving Molecular Oxygen', *Studies Surf. Sci. Catal.*, **15**. Elsevier, Amsterdam.
1743. Adams, C. R. and Jennings, T. J. (1963), 'Investigation of the mechanism of catalytic oxidation of propylene to acrolein and acrylonitrile', *J. Catal.*, **2**, 63–68.
1744. Adams, C. R. and Jennings, T. J. (1964), 'Mechanism studies of the catalytic oxidation of propylene', *J. Catal.*, **3**, 549–558.
1745. Imachi, M., Kuczkowski, R. L., Groves, J. T. and Cant, N. W. (1983), 'The mechanism of propylene oxidation to acrolein over bismuth molybdate, copper oxide and rhodium catalysts', *J. Catal.*, **82**, 355–364.
1746. Davydov, A. A. (1993), 'Study of hydrocarbon adsorption on oxide catalysts by IR spectroscopy. 18. Nature and properties of the surface of Ti–Sb oxide catalyst and the mechanism of propene conversion to acrolein', *Kinet. Katal.* (in Russian); *Kinet. Catal.* (English translation), **34**, 699–702.
1747. Kondo, T., Saito, S. and Tamaru, K. (1974), 'A new method to identify the reaction intermediates of hydrogen transfer or exchange of propene by means of microwave spectroscopy', *J. Am. Chem. Soc.*, **96**, 6857–6864.
1748. Kugler, B. L. and Kokes, R. J. (1974), 'Intermediates in the oxidation of propylene over zinc oxide', *J. Catal.*, **32**, 170–173.
1749. Garrone, E., Giamello, E., Coluccia, S., Spoto, G. and Zecchina, A. (1988), Mechanism of oxidation of hydrocarbons over basic oxides: comparison between pure and Co⁺⁺ doped MgO', in *Catalyst: Theory to Practice. Proceedings of the 9th International Congress on Catalysis*, Calgary, Canada, 1988, Phillips, M. J. and Ternan, M., (Eds.), The Chemical Institute of Canada, Ottawa, Ontario, 1988. pp. 1577–1584.
1750. Desikan, A. N., Zhang, W. and Oyama, S. T. (1995), 'The effect of acid–base properties of supported molybdenum oxide in propylene oxidation', *J. Catal.*, **157**, 740–748.
1751. Ai, M. (1980), Effect of metal-oxide combination on the catalytic action in vapor-phase oxidation', in *New Horizons in Catalysis. Proceedings of the 7th International Congress on Catalysis, Tokyo, June 30–July 4, 1980*, Seiyama, T. and Tanabe, K. (Eds.) *Studies in Surface Science and Catalysis*, v.7, Kodansha, Tokyo, Elsevier, Amsterdam, 1980, pp. 1060–1073.
1752. Sojka, Z. (1995), 'Molecular aspects of catalytic reactivity. Application of EPR spectroscopy to studies of the mechanism of heterogeneous catalytic reactions', *Catal. Rev. Sci. Eng.*, **37**, 461–512.
1753. Garibyan, T. A. and Margilis, L. Ya. (1989–1990) 'Heterogeneous–homogeneous mechanism of catalytic oxidation', *Catal. Rev. Sci. Eng.*, **31**, 355–384.
1754. Efremov, A. A., Khandros, L. E., Davydov, A. A. and Boreskov, G. K. (1979), 'Associative mechanism of the partial oxidation of propylene on MoO₃/SiO₂', *Kinet. Katal.* (in Russian); *Kinet. Catal.* (English translation), **20**, 1215–1219.
1755. Veniaminov, S. A. (1977), 'Study of the mechanism of olefin oxidation over molybdenum- and antimony-based catalysts', in Sokolovski, V. D. (Eds), *Mechanism and Kinetics of Catalytic Processes*, Institute of Catalysis SB RAS, Novosibirsk, pp. 107–132.

1756. Howe, R. F. and Minning, H. (1988), Propene oxidation over molybdenum zeolite catalysts', in *Catalyst: Theory to Practice. Proceedings of the 9th International Congress on Catalysis*, Calgary, Canada, 1988, Phillips, M. J. and Ternan, M., (Eds.), The Chemical Institute of Canada, Ottawa, Ontario, 1988, Vol. 4, 1585–1608.
1757. Haber, J. (1985), Partial oxidation of propylene on Sn–Sb–O and Sn–Sb–FeO, in Grasselli, R. K. and Brazdil, J. S. (Eds), *Solid State Chemistry in Catalysis*, ACS Symposium Series 279, American Chemical Society, Washington, DC, pp. 363–378.
1758. Puttoch, S. J. and Rochester, C. H. (1986), 'IR study of the adsorption of but-1-ene, buta-1,3-diene, furan and maleic anhydride on the surface of anhydrous vanadyl pyrophosphate', *J. Chem. Soc., Faraday Trans. 1*, **82**, 3033–3039.
1759. Ramis, G., Busca, G. and Lorenzelli, V. (1994), 'Spectroscopic characterization of magnesium vanadate catalysts. 2. FTIR study of the surface properties of pure and mixed-phase powders', *J. Chem. Soc., Faraday Trans. 1*, **90**, 1293–1299.
1760. Gerei, S. V., Rozhkova, E. V. and Gorokhovatsky, Ya. B. (1973), 'Propylene and oxygen chemisorption on cupric oxide and cuprous oxide catalysts', *J. Catal.*, **28**, 341–350.
1761. Rozhkova, E. V., Gerei, S. V. and Gorokhovatsky, Ya. B. (1977), 'IR spectroscopic study of ammonia adsorption on a vanadium–phosphorus catalyst', *Kinet. Katal.* (in Russian); *Kinet. Catal.* (English translation), **15**, 694–699.
1762. Busca, G., Centi, G. and Trifiro, F. (1987), 'Proceedings of the 4th International Symposium, Autwerp, September 1987', in Delmon, B. and Froment, G. F. (Eds), *Catalyst Deactivation*, Elsevier, Amsterdam, pp. 427–431.
1763. Do, N. T. and Baerns, M. (1988), 'Effect of support material on the adsorption structures of furan and maleic anhydride on the surface of V₂O₅/P₂O₅ catalysts. II. Results of *in situ* IRS studies', *Appl. Catal.*, **45**, 9–26.
1764. Ramis, G., Busca, G. and Lorenzelli, V. (1989), 'On the mechanism of the selective oxidation of C₄ linear hydrocarbons to maleic anhydride: an FT-IR study of the adsorption and oxidation of 1,3-butadiene on vanadia-titania', *J. Mol. Catal.*, **55**, 1–11.
1765. Davydov, A. A. (1983), Study of the mechanism of propene conversion to acetone by infrared spectroscopy. Bifunctionality of the catalyst, in Davydov, A. A. (Ed.), *Proceedings of the 7th Soviet–Japan Symposium on Catalysis*, Irkutsk, June 1983, Institute of Catalysis, pp. 178–184.
1766. Marcinkowsky, A. E. and Bertly, J. M. (1973), 'Ethylene adsorption on oxygenated silver: evidence for two types of chemisorbed oxygen', *J. Catal.*, **29**, 494–499.
1767. Flank, W. H. and Beachell, H. C. (1967), 'The geometric factor in ethylene oxidation over gold–silver alloy catalysts', *J. Catal.*, **8**, 316–325.
1768. Hayward, D. O. and Trapnell, B. M. W. (1964), *Chemisorption*, Butterworths, London.
1769. Meisenheimer, R. G. and Wilson, J. N. (1962), 'Interaction of oxygen and of ethylene dichloride with a silver surface', *J. Catal.*, **1**, 151–155.
1770. Force, E. L. and Bell, A. T. (1975), 'Infrared spectra of adsorbed species present during the oxidation of ethylene over silver', *J. Catal.*, **38**, 440–460.
1771. Carter, J. L., Yates, D. Y. C., Luchessi, P. J., Elliott, V. V. and Kevorkian, V. (1966), 'Adsorption of ethylene on a series of near-faujasite zeolites studied by IRS and calorimetry', *J. Phys. Chem.*, **20**, 1126–1131.
1772. Gerei, S. V., Kholyavenko, K. M. and Rubanik, M. Ya. (1965), 'IR-spectra of oxygen adsorbed on Ag/SiO₂', *Ukr. Khim. Z.*, **31**, 449–455.
1773. Kilty, P. A., Rol, N. C. and Sachtler, W. M. H. (1973), in *Proceedings of the 5th International Congress on Catalysis, Palm Beach, Fl 1972*, Hightower, J. (Ed), North-Holland, Amsterdam, 1973, Vol. 2, pp. 929–943.
1774. Backx, C., Griif, C. P. M. and Biloen, P. (1980), 'Adsorption of oxygen and ethylene on a silver single crystal surface studied by ELS and TPD', *Appl. Surf. Sci.*, **6**, 256–263.
1775. Kanno, T. and Kobayashi, M. (1984), 'Dynamic behavior of the adsorbed compounds in the oxidation of ethylene and acetaldehyde over a silver catalyst', in *Proceedings of the 8th International Congress on Catalysis, Berlin 1984*, Verlag Chemie, Weinheim, Germany, 1984, Vol. 3, pp. 277–287.
1776. Higashijima, M. and Masunaga, T., Kojima, Y., Watanabe, E., and Wada, K. (1994), 'New hetero-bimetallic Pd–Cu catalyst for Wacker reaction', in *Proceedings of the 2nd 'Advanced Catalytic Science and Technology' Conference, Studies Surf. Sci. Catal.*, **92**, 319–322.
1777. Stobbe-Kreemans, A. W., Dielis, R. B. MacKee, M. and Scholten, J. J. F. (1995), 'Heteropolyanions as redox components in heterogeneous Wacker oxidation catalysts', *J. Catal.*, **154**, 175–186.
1778. Stobbe-Kreemans, A. W., Van der Lans, M., MacKee, M. and Scholten, J. J. F. (1995), 'Palladium salts of heteropolyacids as catalysts in the Wacker oxidation of 1-butene', *J. Catal.*, **154**, 187–193.
- 1779a. Odrin, V. M., Kachkurova, I. Ya., Roev, L. M. and Korneichuk, G. P. (1965), 'Study of the interaction of a vanadium pentoxide catalyst with naphthalene–air mixtures by the method of infrared spectroscopy', *Proceed. AN SSSR*, **163**, 410–415.

- 1779b. Odrin, V. M., Korneichuk, G. P. and Roev, L. M. (1968), 'Study of the reaction of a vanadium oxide catalyst with naphthalene and its oxidation products', *Kinet. Katal.* (in Russian); *Kinet. Catal.* (English translation), **9**, 810–815.
1780. Sachtler, W. M., Dorgelo, G. J. H., Fahrenfort, J. and Voorhoeve, R. J. H. (1971), Correlation between catalytic and thermodynamic parameters of transition metal oxides, in Hightower, J. W. (Ed.), *Reports of the 4th International Congress on Catalysis*, Moscow (1968), *Catal. Soc.* **2**, 604–627.
- 1781a. Niwa, M., Ando, H. and Murakami, Y. (1977), 'Reaction mechanism of ammoxidation of toluene. II. Identification of reaction intermediates adsorbed on V_2O_5/Al_2O_3 by infrared spectroscopy', *J. Catal.*, **49**, 92–96.
- 1781b. Niwa, M., Ando, H. and Murakami, Y. (1981), 'Ammoxidation of xylenes on a V_2O_5/Al_2O_3 catalyst', *J. Catal.*, **70**, 1–13.
- 1781c. Murakami, Y., Niwa, M., Hattori, T., Ogawa, S., Igushi, I. and Ando, H. (1977), 'Kinetic studies of reaction steps by pulse and flow techniques', *J. Catal.*, **49**, 83–91.
1782. Suzuki, K., Nakashiro, K. and Ono, Y. (1988), 'Reaction mechanism of ammoxidation of toluene. I. Kinetic studies of reaction steps by pulse and flow techniques', *Chem. Lett.*, 953–955.
1783. Ivamoto, M., Matsukami, K. and Millini, R. (1983), 'Diffuse reflection IR and photoluminescence spectra of surface vanadyl groups. Direct evidence for change of bond strength and electronic structure of metal–oxygen bonds upon a supporting oxide', *J. Am. Chem. Soc.*, **105**, 3719–3720.
- 1784a. Panov, G. I., Sheveleva, G. A., Kharitonov, A. S., Romannikov, V. N. and Vostrikova, L. A. (1992), 'Oxidation of benzene to phenol by nitrous oxide over Fe-ZSM-5 zeolites', *Appl. Catal., A: Gen.*, **82**, 31–36.
- 1784b. Panov, G. I., Kharitonov, A. S. and Sobolev, V. I. (1993), 'Oxidative hydroxylation using di-nitrogen monoxide: a possible route for organic synthesis over zeolites. A review', *Appl. Catal. A: Gen.*, **98**, 1–20.
- 1784c. Kharitonov, A. S., Sheveleva, G. A., Panov, G. I., Sobolev, V. I., Paukshtis, E. A. and Romannikov, V. N. (1993), 'Ferrisilicate analogs of ZSM-5 zeolite as catalysts for one-step oxidation of benzene to phenol', *Appl. Catal. A: Gen.*, **98**, 33–44.
1785. Davydov, A. A. (unpublished data).
1786. Yabrov, A. A. and Ivanov, A. A. (1980), 'Mechanism of partial oxidation of *o*-xylene on V_2O_5/TiO_2 ', *React. Kinet. Catal. Lett.*, **14**, 347–351.
1787. Miyata, H., Mukai, T., Ono, T., Ohno, T. and Hatayama, F. (1988), 'FT-IR investigation of intermediates in the oxidation of toluene on vanadia/titania', *J. Chem. Soc., Faraday Trans. 1*, **84**, 2465–2476.
1788. Hatayama, F., Ohno, T., Yoshida, T., Ono, t. and Miyata, H. (1991), 'FTIR investigation of the structure of vanadium oxides on zirconia and oxidation of toluene on it', *React. Kinet. Catal. Lett.*, **44**, 451–456.
1789. Grootendorst, E. J., Verbeek, Y. and Ponec, V. (1995), 'The role of the Mars and van Krevelen mechanism in the selective oxidation of nitrosobenzene and the deoxygenation of nitrobenzene on oxidic catalysts', *J. Catal.*, **157**, 706–712.
1790. Meijers, S. and Ponec, V. (1996), 'An FTIR spectroscopic study of the selective oxidation of nitrosobenzene to nitrobenzene by metal oxides', *J. Catal.* **160**, 1–9.
1791. Slinkin, A. A. and Kucherov, A. V. (1985), 'Radical processes in the adsorption of olefins on zeolites', *Usp. Khim.*, (in Russian); *Russ. Chem. Rev.* (English translation), **54**, 39–53.
1792. Vymorokov Yu., B. and Kotov, E. I. (1975), 'Spectral manifestations of the formation of cation radicals of benzidine in the adsorption of aniline on aluminosilica gel', *Kinet. Katal.* (in Russian); *Kinet. Catal.* (English translation), **16**, 491–496.
1793. Vymorokov, Yu. B., Zhdanov, S. P., Kotov., E. I. and Smirnova, L. G. (1973), 'Spectral manifestations of the formation of cation radicals of bezidine on zeolites?' in *Russ. J. Appl. Spectr.*, **19**, 483–489.
1794. Talybova, Z., Davydov, A. A., Lisovskii, A. and Alkhozov, T. G. (1984), 'Study of the interaction of ethylbenzene with oxygen and sulphur dioxide on the surface of alumina', *Kinet. Katal.* (in Russian); *Kinet. Catal.* (English translation), **58**, 453–457.
1795. Addiego, W. P., Cesar, A., Estrada, D., Goodman, D. W. and Rosinek, M. P. (1994), 'An infrared study of the dehydrogenation of ethylbenzene to styrene over iron-based catalysts', *J. Catal.*, **146**, 407–414.
1796. Burch, R. and Hayes, M. J. (1995), 'A review of C–H bond activation in saturated hydrocarbon oxidation on solid catalysts', *J. Mol. Catal. A: Gen.*, **100**, 13–33.
1797. Arutyunov, V. S., Basevich, V. Ya. and Vedenev, V. I. (1996), 'Direct high-pressure gas-phase oxidation of natural gas to methanol and other oxygenates', *Chemical Rev.*, **65**, 197–224. *Usp. Khim.* (in Russian); *Russ. Chem. Rev.* (English translation), **65**, 197–224.
1798. Faraldos, M., Banares, M. A., Anderson, J. A., Hu, H., Wachs, I. E. and Fierro, J. L. G. (1996) 'Comparison of silica-supported MoO_3 and V_2O_5 catalysts in the selective partial oxidation of methane', *J. Catal.*, **160**, 214–221.
1799. Banares, M. A., Guerrero-Ruiz, A., Rodriguez-Ramos, I. and Fierro, J. (1993), 'Partial oxidation of methane on silica supported vanadium and molybdenum oxide catalysts', in Gucci, L., Solymosi, F. and Tetenyi, P. (Eds), *New Frontiers in Catalysis*, Elsevier, Amsterdam, pp. 1131–1140.
1800. Koranne, M. J., Goodwin, J. G. and Marcelin, G. J. (1993), 'Oxygen involvement in the partial oxidation of methane on supported and unsupported V_2O_5 ', *J. Catal.*, **148**, 378–383.

1801. Mauti, R. and Milms, C. A. (1993), 'Partial oxidation of methane to formaldehyde over vanadia catalysts. Reaction mechanism', *Catal. Lett.*, **21**, 201–208.
1802. Karthereuser, B., Hodnett, B. K., Zanthoff, H. and Baerns, M. (1993), 'Transient experiments on the selective oxidation of methane to formaldehyde over vanadia/silica studies in the temporal analysis of a products reactor', *Catal. Lett.*, **21**, 209–213.
1803. Ahmed, S. H., Kasztelan, S. and Moffat, J. B. (1989), 'The oxidation of methane on silica supported heteropoly oxometalates', *Faraday Discuss. Chem. Soc.*, **87**, 23–32.
1804. Moffat, J. B. (1996), 'Conversion of C₂–C₅ alkanes on heteropoly oxometalates', *Appl. Catal., A: Gen.*, **146**, 65–86.
1805. Wang, Y., Otsuka, K. and Ebatani, K. (1995), 'In situ FTIR study on the active oxygen species for the conversion of methane to methanol', *Catal. Lett.*, **35**, 259–263.
1806. Beebe, T. R., Crovelli, J. E. and Yates, J. T. (1988), 'Reaction of methyl chloride with alumina surfaces: study of the methoxy surface species by transition infrared spectroscopy', *J. Phys. Chem.*, **92**, 1296–1301.
1807. Kung, H. H. (1989), 'Transition metal oxides: Surface chemistry and catalysis', *Studies Surf. Sci. Catal.*, **45**.
1808. Pantazidis, A. and Mirodatos, C. (1996), 'Mechanistic approach of the oxidative dehydrogenation of propane over VMgO catalysts by *in situ* spectroscopic and kinetics techniques', *Studies Surf. Sci. Catal.*, **101**, 1029–1031.
1809. Sokolovskii, V. D., Osipova, Z. G., Plyasova, L. M., Davydov, A. A. and Budneva, A. A. (1993), 'Acid–base properties and direction of oxidative transformations of methane on magnesium–phosphorus catalysts', *Appl. Catal., A: Gen.*, **101**, 15–23.
1810. Morterra, C. and Low, M. J. D. (1973), 'Reactive silica. Novel aspects of the chemistry of silica surfaces', *Ann. N.Y. Acad. Sci.*, **220**, 245–340.
1811. Liu, H.-F., Lin, R.-S., Liew, K. Y., Johnson, R. E. and Lunsford, J. H. (1984), 'Partial oxidation of methane by nitrous oxide over molybdenum on silica', *J. Am. Chem. Soc.*, **106**, 4117–4121.
1812. Ueda, W., Suzuki, Y., Lee, W. and Imaoka, S. (1996), 'Catalytic oxidation of propane to acrylic acid with molecular oxygen activated over reduced heteropolymolybdates', *Studies Surf. Sci. Catal.*, **101**, 1065–1074.
1813. Hodnett, B. K. (1985), 'Vanadium–phosphorus oxide catalysts for the selective oxidation of C₄ hydrocarbons to maleic anhydride', *Catal. Rev. Sci. Eng.*, **27**, 373–424.
1814. Centi, G., Trifiro, F., Busca, G., Ebner, J. R. and Cleaves, J. T. (1988), 'Selective oxidation pathways at the vanadyl pyrophosphate surface in light paraffin conversion', in *Catalyst: Theory to Practice. Proceedings of the 9th International Congress on Catalysis*, Calgary, Canada, 1988, Phillips, M. J. and Ternan, M., (Eds.), The Chemical Institute of Canada, Ottawa, Ontario, 1988, Vol. 4, pp. 1538–1544.
1815. Cavani, F., Comuzzi, C., Dolcetti, G., Etienne, E., Finke, R. G., Sella, G., Trifiro, F. and Trovarelli, A. (1996), 'Oxidative dehydrogenation of isobutane to isobutene: Dawson-type heteropolyoxoanions as stable and selective heterogeneous catalysts', *J. Catal.*, **160**, 317–321.
1816. Anderson, A., Anderson, S. L. T., Centi, G., Graselley, R. K., Sanati, M. and Trifiro, F. (1994), 'Surface characterization and reactivity in ammoxidation reactions of vanadium antimonate catalysts', *Appl. Catal., A: Gen.*, **113**, 43–57.
1817. Albonetti, S., Blanchard, G., Burattin, P., Cassidy, T. J., Masetti, S. and Trifiro, F. (1997), 'Mechanism of ammoxidation of propane on a Sb/V/O system', *Catal. Lett.*, **45**, 119–123.
1818. Centi, G., Marchi, F. and Perathoner, S. (1997), 'Effect of ammonia chemisorption on the surface reactivity of V–Sb–oxide catalysts for propane ammoxidation', *Appl. Catal., A: Gen.*, **149**, 225–244.
1819. Kulkarni, S. J., Rao, R. R., Subrahmanyam, M., Rao, A. V. R., Sarkany, A. and Guzzi, L. (1996), 'Oxidation and ammoxidation of toluene and benzyl alcohol over silicoaluminophosphate and metal–silicoaluminophosphate catalysts', *Appl. Catal., A: Gen.*, **139**, 59–74.
1820. Sokolovskii, V. D., Davydov, A. A. and Ovsitser, O. Yu. (1995), 'Mechanism of selective paraffin ammoxidation', *Catal. Rev. Sci. Eng.*, **37**, 425–459.
- 1821a. Kim, Y.-Ch., Ueda, W. and Moro-oka, Y. (1990), in Centi, G. and Trifiro, F. (Eds), *New Developments in Selective Oxidation*, *Studies Surf. Sci. Catal.*, **55**, 491.
- 1821b. Centi, G., Grasselli, R. K., Patane, E. and Trifiro, F. (1990), in Centi, G. and Trifiro, F. (Eds), 'New Developments in Selective Oxidation', *Studies Surf. Sci. Catal.*, **55**, 515.
1822. Centi, G., Grasselli, R. K. and Trifiro, F. (1992), 'Propane ammoxidation to ferrylonitrile. An overview', *Catal. Today.*, **13**, 661–666.
1823. Centi, G., Foresti, E. and Guarnieri, F. (1994), in Corberan, V. C. and Vic Bellon, S. (Eds), *New Developments in Selective Oxidation*, *Studies Surf. Sci. Catal.*, **82**, 281.
1824. Ovsitser, O. Yu., Osipova, Z. G. and Sokolovskii, V. D. (1989), 'Pulse studies of cyclohexane oxidative ammonolysis to adiponitrile over titanium–antimony–oxygen catalysts', *React. Kinet. Catal. Lett.*, **38**, 91–96.
1825. Busca, G., Cavani, F. and Trifiro, F. (1987), 'Oxidation and ammoxidation of toluene over vanadium–titanium oxide catalysts: A Fourier transform infrared and flow reactor study', *J. Catal.*, **106**, 471–482.
1826. Martin, A., Zang, Y., Zanthoff, H. W., Meisel, M. and Baerns, M. (1996), 'The ammonium ions during toluene ammoxidation on α -(NH₄)₂(VO)₃(P₂O₇)₂ used as catalysts', *Appl. Catal., A: Gen.*, **139**, L11–L16.

1827. Kulkarni, S. J., Rao, R. R., Subrahmanyam, M., Zakumbaevama, L., Rao, A. V., Sarkany, A. and Guzzi, L. (1996), 'Oxidation and amoxidation of toluene and benzyl alcohol over silicoaluminophosphate catalysts', *Appl. Catal.*, **139**, 59–74.
1828. Zakumbaeva, G. D. (1978) *Vzaimodeistvie Organicheskikh Soedinenii s Poverhnost'yu Metallov VIII Gruppy (Interactions of Organic Compounds with the Surfaces of VIII Group Metals)*, Alma-Ata Kazakhstan, Nauka.
1829. Popova, G. Ya., Andrushkevich, T. V., Meshcheryakov, V. D. and Davydov, A. A. (1990), 'Kinetics of conversion of surface compounds under conditions of the acrolein oxidation reaction on vanadia-molybdena-silica catalyts', *Kinet. Katal.* (in Russian); *Kinet. Catal.* (English translation), **31**, 408–414.
- 1830a. Cheng, W.-H. (1996), 'Methanol and formaldehyde oxidation study over molybdenum oxide', *J. Catal.*, **158**, 477–485.
- 1830b. Anderson, J. A. and Rochester, C. H. (1989), 'Infrared study of the adsorption of acetone, acrolein, ethanoic acid and propene on a rhodium/alumina catalyst', *J. Chem. Soc., Faraday Trans. 1*, **85**, 1117–1128.
1831. Anderson, J. A. and Rochester, C. H. (1989), 'Infrared study of the adsorption of ethanoic acid, acrylic acid, acetone, acrolein and propene-nitric oxide mixtures on a rhodium/silica catalyst', *J. Chem. Soc., Faraday Trans. 1*, **85**, 1129–1138.
1832. Lercher, J. A. (1982), 'Acid-base properties of $\text{Al}_2\text{O}_3/\text{MgO}$ oxides. I. Infrared study of adsorption of acetone', *Z. Phys. Chem. (Leipzig)*, **129**, 209–218.
1833. Hanson, B. E., Wieserman, L. F., Wagner, G. W. and Kaufman, R. A. (1987), 'Identification of acetone enolate on γ -alumina: implications for the oligomerization and polymerization of adsorbed acetone', *Langmuir*, **3**, 549–555.
1834. Kubelkova, L. and Novakova, J. (1991), 'TPD and conversion of acetone and diethylketone preadsorbed on HZSM', *Zeolites*, **11**, 822–826.
1835. Kubelkova, L., Cejka, J. and Novakova, J. (1991), 'Surface reactivity of ZSM-5 zeolites in interaction with ketones at ambient temperature (an FTIR study)', *Zeolites*, **11**, 48–53.
- 1836a. Xu, T., Munson, E. J. and Haw, J. (1994), 'Toward a systematic chemistry of organic reactions in zeolites. *In situ* NMR studies of ketones', *J. Am. Chem. Soc.*, **116**, 1962–1972.
- 1836b. Biaglow, A. I., Gorte, R. J., Kokotailo, G. T. and White, D. (1994), 'A ^{13}C NMR study of the condensation chemistry of acetone and acetaldehyde adsorbed at the Brønsted acid sites in H-ZSM-5', *J. Catal.*, **151**, 373–384.
1837. Biaglow, A. I., Gorte, R. J. and White, D. (1993), 'Evidence for the allyl and secondary cation intermediates on adsorption of allyl alcohol on H-ZSM-5 zeolite', *J. Chem. Soc., Chem. Commun.*, 1164–1166.
1838. Bell, V. A. and Gold, H. S. (1983), 'Carbon-13 nuclear magnetic studies of the Aldol condensation products of acetone on an activated alumina catalyst', *J. Catal.*, **79**, 286–290.
1839. Griffiths, D. M. and Roch, C. H. (1978), 'IR-spectroscopic study of the adsorption of acetone on rutile', *J. Chem. Soc., Faraday Trans. 1*, **74**, 403–409.
1840. Ponec, V. (1997), 'Forty years in catalysis: what have we learned?', *Appl. Catal., A: Gen.*, **149**, 27–48.
1841. Boccuzzi, F., Ghiotti, G. and Chiorino, A. (1993), 'Adsorption and deuteration of acetone- d_6 on Pt/ZnO catalysts: an IR study of the effects of sample pretreatment', *J. Mol. Catal.*, **81**, 373–386.
1842. Yashima, T., Suzuki, H. and Hara, N. (1974), 'Decomposition of 2-propanol over alkali cation exchanged zeolites', *J. Catal.*, **33**, 486–492.
1843. Shchekochikhin, Yu. M. and Davydov, A. A. (1976), 'Study of the reactions on the surface of Al_2O_3 by means of IR-spectroscopy', *Adsorptsiya Adsorbenty* (in Russian), **4**, 75–80.
1844. Yamashita, K., Naito, S. and Tamaru, K. (1985), 'The behavior of surface formate ions as reaction intermediates in the decomposition of methanol over Cr_2O_3 ', *J. Catal.*, **94**, 353–359.
1845. Roberts, D. L. and Griffin, G. L. (1985), 'Combined infrared and programmed desorption study of methanol decomposition on ZnO', *J. Catal.*, **95**, 617–620.
1846. Lamotte, J., Moravec, V., Benzitel, M. and Lavalley, G. C. (1988), 'FT-IR study of the structure and reactivity of methoxy species on torium and ceria', *React. Kinet. Catal. Lett.*, **36**, 113–117.
1847. Rogov, V. A., Davydov, A. A., Serebryakov, V. F. and Dobrynkin, N. M. (1992), 'Study of the alcohols adsorption on the surface of CuO by means of TPD and IRS methods', *Kinet. Katal.* (in Russian); *Kinet. Catal.* (English translation), **33**, 157–162.
1848. Oliferenko, V. V., Davydov, A. A. and Pak, V. N. (1990), 'Structure, thermal transformations of Mo-containing silicagel and its interaction with methanol according to infrared spectroscopic data', *Zh. Prikl. Khim.* (in Russian); *J. Appl. Chem.* (English translation), **63**, 2505–2509.
1849. Schiffino, R. S. and Merrill, R. P. (1993), 'A mechanistic study of the methanol dehydration reaction on γ -alumina catalyst', *J. Phys. Chem.*, **97**, 6425–6435.
1850. Derouault, J., Le Calve, J. and Forel, M. (1972), 'Discussion des vibrations de valence $\nu(\text{CH}_3)$ et $\nu(\text{CD}_3)$ des groupes OCH_3 et OCD_3 . Influence de la formation d'une liaison de coordination entre l'oxygene et les halogenures d'aluminium ou le trifluorure de bore', *Spectrochim. Acta, Part A*, **28**, 359–371.
1851. Knozinger, H. (1968), 'Dehydratisierung von alkoholen an aluminiumoxid', *Angew. Chem.*, **7**, 778–792.
1852. Lamotte, J., Saur, O., Lavalley, J. C., Busca, G., Rossi, P. F. and Lorenzelli, V. (1986), *J. Chem. Soc., Faraday Trans. 1*, **82**, 3019–3026.

1853. Hattori, T., Shirai, K., Niwa, M. and Murakami, N. (1981), 'Quantitative interpretation of DRIR spectra over whole concentration range', *Bull. Chem. Soc. Jpn.*, **54**, 1964–1967.
1854. Demidov, A. V., Davydov, A. A. and Kurina, L. N. (1985), 'Study of the interaction of methanol and propene with HY-zeolite by means of IRS', *Zh. Fiz. Khim.* (in Russian); *Russ. J. Phys. Chem.* (English translation), **59**, 2364–2366.
1855. Mozer, W. R., Chiang, C. C. and Thompson, R. W. (1989), 'Infrared diffuse reflectance study of the silicon-rich H-ZSM-5 catalysts of ethanol conversion', *J. Catal.*, **115**, 532–541.
1856. Stepanov, A. G. and Zamaraev, K. I. (1993), 'Carbon-13 solid state NMR evidence for the existence of the isobutyl-carbenium ion in the alcohol dehydration reaction on H-ZSM-5 zeolite catalyst', *Catal. Lett.*, **19**, 153–158.
1857. Grady, M. C. and Gorte, R. J. (1985), 'Adsorption of 2-propanol and propene on H-ZSM-5: evidence for stable carbenium ion formation', *J. Phys. Chem.*, **89**, 1305–1308.
1858. Zardkoohi, M., Haw, J. F. and Lunsford, J. H. (1987), 'Solid-state NMR evidence for the formation of a carbocation from propene in acidic zeolite-Y', *J. Am. Chem. Soc.*, **109**, 5278–5280.
1859. Fridman, V. Z. and Davydov, A. A. (1999), 'New data about the well-known dehydrogenation reaction of cyclohexanol on copper-containing catalysts', in Herkes, F. E. (Ed.), *Catalysis of Organic Reactions*, Marcel Dekker, New York, pp. 495–506.
1860. Busca, G., Guidetti, R. and Lorenzelli, V. (1990), 'FTIR study of the surface properties of cobalt oxides', *J. Chem. Soc., Faraday Trans. 1*, **86**, 989–994.
1861. Arve, A. A., Miliades, G. and Vickerman, J. C. (1980), 'The oxidation of methanol over chromium containing spinel ($\text{MgAl}_{2-x}\text{Cr}_x\text{O}_4$) and corundum ($\alpha\text{-Al}_{2-x}\text{Cr}_x\text{O}_3$) solid solutions', *J. Catal.*, **62**, 202–210.
1862. Alkhozov, T. G. and Margolis, L. Ya. (1988), *Highly Selective Catalysts of Hydrocarbons Oxidation* (in Russian), Khimiya, Moscow.
1863. Groff, R. P. (1984), 'An infrared study of methanol and ammonia adsorbed on molybdenum trioxide', *J. Catal.*, **86**, 215–218.
1864. Haber, J. (1989), 'The concept of structure–sensitivity in catalysis by oxides', in Morterra, C., Zecchina, A. and Costa, G. (Eds.), *Structure and Reactivity of Surfaces*, Elsevier, Amsterdam, pp. 447–467.
1865. Ohuchi, F., Firment, L. E., Chowdhry, U. and Feretti, A. (1984), *J. Vac. Sci. Technol. A*, **2**, 1022.
1866. Cheng, W.-H., Chowdhry, U., Ferretti, A., Firment, L. E., Groff, R. P., Machiels, C. J., McCarron, E. M., Ohuchi, F., Staley, R. H. and Sleight, A. W. (1985), 'Methanol oxidation over molybdate catalysts', in Grasselli, R. K. and Brazdil, J. F. (Eds) *Solid State Chemistry in Catalysis*, American Chemical Society, Washington, DC, pp. 165–181.
- 1867a. Davydov, A. A. (1988), 'Method for production of formaldehyde', *Russian Patent*, 4 294 226.
- 1867b. Pestryakov, A. N., Belousova, V. N. and Roznina, M. I. (1993), 'Surface acidity and degree of coking on modified silver catalysts', *Zh. Prikl. Khim.* (in Russian); *J. Appl. Chem.* (English translation), **66**, 1148–1154.
1868. Pestryakov, A. N., Roznina, M. I. and Belousova, V. N. (1993), 'Promotion of silver catalysts for selective oxidation of methanol', *Zh. Prikl. Khim.* (in Russian); *J. Appl. Chem.* (English translation), **66**, 2285–2291.
1869. Nishimura, M., Asakura, K. and Iwasawa, Ya. (1988), 'Self-assisted dehydrogenation of ethanol on inorganic oxide-attached Nb-monomer catalysts', in *Catalyst: Theory to Practice. Proceedings of the 9th International Congress on Catalysis*, Calgary, Canada, 1988, Phillips, M. J. and Ternan, M., (Eds.), The Chemical Institute of Canada, Ottawa, Ontario, 1988, pp. 1842–1849.
1870. Chang, C. D. and Silvestry, A. J. (1977), 'The conversion of methanol and other oxygen-compounds to hydrocarbons over zeolite catalysts', *J. Catal.*, **47**, 249–259.
1871. Chang, C. D., Hellring and Pearson, J. A. (1989), 'On the extent and role of free radicals in methanol conversion to hydrocarbons over HZSM-5', *J. Catal.*, **115**, 282–285.
1872. Mole, T. and Whiteside, J. (1982), 'Conversion of methanol to ethylene over ZSM-5 zeolite in the presence of deuterated water', *J. Catal.*, **75**, 284–290.
1873. Olah, G. A., Doggweiler, H., Felberg, J. D., Frohlich, S. (1984), 'Ylide chemistry. I. Bifunctional acid–base-catalysed conversion of heterosubstituted methanes into ethylene and hydrocarbon derivatives. The onium mechanism of the C1→C2 conversion', *J. Am. Chem. Soc.*, **106**, 2143–2149.
1874. Clarke, J. K. A., Darcy, R., Hegarty, B. F., Donoghue, E., Amir-Ebrahimi, V. and Rooney, J. J. (1986), 'Free radicals in dimethyl ether on H-ZSM-5 zeolites. A novel dimension of heterogeneous catalysis', *J. Chem. Soc., Chem Commun.*, 425–426.
1875. Davydov, A. A. and Yur'eva, T. M. (1979), 'Development of catalysts for NO decomposition in the presence of oxygen', *Scientific Report on Soviet–American Collaboration on Catalysis*, Topic 5.
1876. Iwamoto, M., Yahiro, H., Yu, Y., Shundo, S. and Mizuno, N. (1990), 'Influence of sulphur dioxide on catalytic removal of nitric oxide over copper ion exchanged ZSM-5 zeolite', *Shokubai*, **32**, 430–437.
1877. Held, W., Konig, A., Richter, T. and Puppe, L. (1990), *Catalytic NO_x Reduction in Net Oxidizing Exhaust Gas*, SAE Technican Paper, Ser. 900-496.
1878. Lokhov, Yu. A. and Davydov, A. A. (1975), 'Infrared study of the adsorption and reactions of nitric oxide on CuY zeolites', *React. Kinet. Catal. Lett.*, **3**, 39–46.

1879. Davydov, A. A. and Lokhov, Yu. A. (1978), 'Infrared study of the interaction of nitric oxide with CuY zeolites', *React. Kinet. Catal. Lett.*, **8**, 47–52.
1880. Sadykov, V. A., Baron, S. L., Matyshak, V. A., Alikina, G. M., Bunina, R. V., Rozovskii, A. Ya., Lunin, V. V., Lunina, E. V., Kharlamov, A. N., Ivanova, A. S. and Veniaminov, S. A. (1996), 'The role of surface nitrite and nitrate complexes in NO_x selective catalytic reduction by hydrocarbons under excess oxygen', *Catal. Lett.*, **37**, 157–162.
1881. Cheung, T., Bhargava, S. K., Hobday, M. and Fogger, K. (1996), 'Adsorption of NO on Cu exchanged zeolites, an FTIR study: Effects of Cu levels, NO pressure and catalyst pretreatment', *J. Catal.*, **158**, 301–310.
1882. Aylor, A. W., Larsen, S. C., Reimer, J. A. and Bell, A. T. (1995), 'An infrared study of NO decomposition over Cu-ZSM-5', *J. Catal.*, **157**, 592–602.
1883. Grunert, W., Haynes, N. W., Joyner, R. W., Shpiro, E. S., Siddique, M. R. H. and Baeva, G. N. (1994), 'Structure, chemistry and activity of Cu-ZSM-5 catalysts for the selective reduction of NO_x in the presence of oxygen', *J. Phys. Chem.*, **98**, 10846–10852.
1884. Lokhov, Yu. A., Musil, Z. and Davydov, A. A. (1978), 'Study of the mechanism of NO decomposition and NO reduction by CO over CuO/Al₂O₃ by means of IR spectroscopy', in *Proceedings of the All-Union Conference on the Mechanism of Catalytic Reactions*, Moscow, 1978, Nauka, Moscow, Vol. 1, pp. 305–312.
1885. Shelef, M., Otto, K. and Gandhi, H. (1968), 'The oxidation of CO by O₂ and by NO on supported chromium oxide and other metal oxide catalysts', *J. Catal.*, **12**, 361–370.
1886. Alkhozov, T. G. and Gasan-zade, G. Z. (1981), 'Catalytic reduction of NO by CO over transition metal oxides', *Kinet. Katal.* (in Russian); *Kinet. Catal.* (English translation), **18**, 103–119.
1887. Panajotov, D., Matyshak, V., Sklyarov, A., Vlasenko, A. and Mehandjiev, D. (1989), 'Interaction between NO and CO on the surface of CuCo₂O₄ spinel', *Appl. Catal.*, **24**, 37–52.
1888. London, J. W. and Bell, A. T. (1973), 'A simultaneous infrared and kinetic study of the reaction of nitric oxide by carbon monoxide over copper oxide', *J. Catal.*, **31**, 96–109.
1889. Solymosi, F. and Kiss, J. (1976), 'Adsorption and reduction of NO on tin(IV) oxide catalysts', *J. Catal.*, **41**, 202–211.
1890. Solymosi, F. and Kiss, J. (1974), 'Removal of NO_x pollutant by catalytic combustion reactions', in *Proceedings of the 15th International Symposium on Combustion*, Tokyo, Kodansha, Tokyo, pp. 1233–1242.
1891. Rasko, F. and Solymosi, F. (1980), 'Infrared spectroscopic study of isocyanate formation in the reaction of NO and CO over Cr₂O₃/Al₂O₃ and Cr₂O₃/SiO₂', *J. Chem. Soc., Faraday Trans. 1*, **76**, 2383–2395.
1892. Solymosi, F. and Rasko, J. (1980), 'Infrared studies on the formation of the isocyanate surface species over unsupported chromia', *J. Catal.*, **65**, 235–237.
1893. Shih, S. S., Shihabi, D. S. and Squires, R. G. (1977), 'A simultaneous infrared and kinetic study of the reduction of nitric oxide by carbon monoxide over a chromia-silica catalyst', in *Proceedings of the 6th International Congress on Catalysis, London, 1976*, Bond, G. C., Wells, P. B. and Tompkins, F. S. (Eds.), The Royal Society of Chemistry, London, 1977, Vol. 2, pp. 978–987.
1894. Cataluna, R., Arcoya, A. (1995), 'Catalysis and Automotive Pollution Control III. Proceedings of the Third International Symposium (CaPoC 3) Brussels, Belgium, April 20–22, 1994 Eds: Frennet, A. and Bastin, J.-M. Effect of CeO₂ dispersion on alumina on its reactivity for CO and NO conversion', *Studies Surf. Sci. Catal.*, **96**, 215–227.
1895. Yamashita, H., Matsuona, M., Suji, K. T., Shioya, Y., Giamello, E., Che, M. and Aupo, M. (1994), 'In situ investigation on the interaction of NO and CO with Cu⁺/ZSM-5 catalyst', *Proceedings of the 2nd Tokyo 'Advanced Catalytic Science and Technology' Conference* (Tokyo, 1994), *Studies Surf. Sci. Catal.*, **92**, 227–232.
1896. Iwamoto, M., Furukawa, H., Mine, Y., Uemura, F., Mikuriya, S. and Kagawa, S. (1986), 'Copper(II) ion-exchanged ZSM-5 zeolites as highly active catalysts for direct and continuous decomposition of nitrogen monoxide', *J. Chem. Soc. Chem. Commun.*, 1272–1273.
1897. Armor, J. N. (1995), 'Catalytic reduction of nitrogen oxides with methane in the presence of excess oxygen', *Catal. Today*, **26**, 147–158.
1898. Walker, A. P. (1995), 'Mechanistic studies of the selective reduction of NO_x over Cu/ZSM-5 and related systems', *Catal. Today*, **26**, 107–128.
1899. Bethke, K. A., Kung, M. C., Yang, B., Shah, M., Alt, D., Li, C. and Kung, H. H. (1995), 'Metal oxide catalysts for lean NO_x reduction', *Catal. Today*, **26**, 169–183.
1900. Beutel, T., Sarkany, J., Lei, G. D., Yan, J. Y. and Sachtler, W. M. H. (1996), 'Redox chemistry of Cu/ZSM-5', *J. Phys. Chem.*, **100**, 845–851.
1901. Adelman, B. J., Beutel, T., Lei, G.-D. and Sachtler, W. M. H. (1996), 'Mechanistic cause of hydrocarbon specificity over Cu/ZSM-5 catalysts in the selective catalytic reduction of NO_x', *J. Catal.*, **158**, 327–335.
1902. Shelef, M. (1992), 'On the mechanism of nitric oxide decomposition over Cu-ZSM-5', *Catal. Lett.*, **15**, 305–310.
1903. Takeshima, S. (1991), US Patent, 5 017 538; *Chem. Abstr.*
1904. Kucherov, A. V., Gerlok, G. L. and Shelef, M. (1996), 'State of copper in a working, low-concentration CuH-ZSM-5 catalyst for exhaust gas purification: *in situ* ESR monitoring', *Catal. Today*, **27**, 79–84.

1905. Bell, V. A., Feeley, J. S., Deeba, M. and Farrauto, R. J. (1994), 'In situ high temperature FTIR studies of NO_x reduction with propylene over Cu/HZSM catalysts', *Catal. Lett.*, **29**, 15–26.
1906. Yasude, H., Miyamoto, T. and Misono, M. (1995), 'IR study of catalytic reduction of NO_x by propene in the presence of O₂ over CeZSM-5 zeolite', in *Proceedings of the 207th ACS National Meeting* (San Diego, CA), ACS Symposium Series 587, American Chemical Society, Washington, DC, pp. 110–122.
1907. Tabata, T., Ohtsuka, H. (1995), 'IR investigation of selective reduction of NO by ethene on Cu-ZSM-5', *Bull. Chem. Soc. Jpn.*, **68**, 1905–1914.
1908. Ohno, T., Hatayma, F., Toda, Y., Konishi, S. and Miyata, H. (1994), 'Fourier transform infrared study of the reduction of nitric oxide by ethylene over V₂O₅ layered on ZrO₂', *Appl. Catal., B: Environ.*, **5**, 89–101.
1909. Kharas, K. C. C., Robota, H. J. and Liu, D. J. (1995), 'Structure–function properties in Cu/ZSM-5 decomposition and NO SCR catalysts', *Catal. Today*, **26**, 129–145.
1910. Iwamoto, M., Yokoo, S., Sakai, K. and Kagawa, S. (1981), 'Catalytic decomposition of nitric oxide over copper(II)-exchanged Y-type zeolites', *J. Chem. Soc., Faraday Trans. 1*, **77**, 1629–1638.
1911. Li, Y. and Hall, W. K. (1991), 'Catalytic decomposition of nitric oxide over Cu-zeolites', *J. Catal.*, **129**, 202–215.
1912. Valyon, J. and Hall, W. K. (1993), 'Studies of the surface species formed from NO on copper zeolites', *J. Phys. Chem.*, **97**, 1204–1212.
1913. Shelef, M. (1995), 'Selective catalytic reduction of NO_x with N-free reductants', *Chem. Rev.*, **95**, 209–225.
1914. Centi, G. and Perathoner, S. (1995), 'Role and importance of oxidized nitrogen oxides adsorbed species on the mechanism and dynamics of the reaction over copper-based catalysts', *Appl. Catal. A: Gen.*, **132**, 179–259.
1915. Spoto, G., Bordiga, S., Scrano, D. and Zecchina, A. (1992), 'Well-defined copper nitrosyls (Cu^I(NO), Cu^I(NO)₂ and Cu^{II}(NO)_x (x = O⁻ and/or NO₂⁻) complexes in CuI-ZSM-5 prepared by the interaction of H-ZSM-5 with gaseous cuprous chloride', *Catal. Lett.*, **13**, 39–44.
1916. Burch, R. and Millington, P. J. (1995), 'Selective reduction of nitrogen oxides by hydrocarbons under lean-burn conditions using supported platinum group metal catalysts', *Catal. Today*, **26**, 185–206.
1917. Iwamoto, S., Shimizu, S. and Inui, S. (1994), in Weitkamp, J., Karge, H., Pfeifer, H. and Holderich, W. (Eds), 'Zeolites and Related Microporous Materials: State of the Art, Studies Surf. Sci. Catal.', **84**, 1523–1530.
1918. Kim, M. H., Nam, I.-S. and Kim, Y. G. (1995), 'Selective catalytic reduction of nitrogen oxide by hydrocarbons over mordenite-type zeolite catalysts', *Appl. Catal., B: Environ.*, **6**, 297–310.
1919. Miyadera, T. (1993), 'Alumina-supported silver catalysts for the selective reduction of nitric oxide with propene and oxygen-containing organic compounds', *Appl. Catal., B: Environ.*, **2**, 199–205.
1920. Petunchi, J. O., Sill, G. and Hall, W. K. (1993), 'Study of the selective reduction of nitric oxides by hydrocarbons', *Appl. Catal. B: Environ.*, **2**, 303–321.
1921. Smits, R. H. H. and Iwasawa, Y. (1995), 'Reaction mechanisms for the reduction of nitric oxide by hydrocarbons on Cu-ZSM-5 and related catalysts', *Appl. Catal., B: Environ.*, **6**, L201–L207.
1922. Jewell, L., Sokolovskii, V. D., Coville, N. J., Glasser, D. and Hildebrandt, D. (1996), 'A catalytic trap for low-temperature complete NO reduction in oxygen-rich media', *J. Chem. Soc., Chem. Commun.*, 2081–2082.
1923. Davydov, A. A. (1993), 'Atomic form of nitrogen from adsorbed NO and NH₃ on the surface of vanadium-containing catalysts', *Zh. Fiz. Khim.* (in Russian); *Russ. J. Phys. Chem.* (English translation), **67**, 127–130.
1924. Gasior, M., Haber, J., Machej, R., and Czeppe, T. (1988), 'Mechanism of the reaction of NO + NH₃ on V₂O₅ catalysts', *J. Mol. Catal.*, **43**, 359–369.
1925. Odriozola, J. A., Heinemann, H., Somorjai, G. A., Garsia de la Banda, L., and Pereira, P. (1989), 'AES and TDS study of the adsorption of NH₃ and NO on V₂O₅ and TiO₂: mechanistic implications', *J. Catal.*, **119**, 71–82.
1926. Rajadhyaksha, R. A. and Knozinger, H. (1989), 'Ammonia adsorption on vanadia supported on a titania-silica catalyst. An infrared spectroscopic investigation', *Appl. Catal.*, **51**, 81–92.
1927. Ramis, G., Busca, G., Bregani, F. and Forzatti, P. (1990), 'An FTIR-study of the adsorption and coadsorption of nitric oxide, nitrogen dioxide and ammonia on vanadia-titania and the mechanism of selective catalytic reduction', *Appl. Catal.*, **64**, 259–278.
1928. Davydov, A. A. (1994), 'Mechanism of interaction of NO with NH₃ on vanadium-containing catalysts based on IR spectroscopic data', *Izv. Acad. Nauk. SSSR, Ser. Khim.* (in Russian); *Russ. Chem. Bull.* (English translation), **43**, 214–218.
1929. Kantcheva, M., Bushev, V. and Klissurski, D. (1994), 'Study of the NO₂-NH₃ interaction on a titania (ANATASE) supported vanadia catalyst', *J. Catal.*, **145**, 96–106.
1930. Bushev, V., Hadjiivanov, K., Kantcheva, M. and Klissurski, D. (1991), 'An IR spectroscopic study of NO₂-NH₃ interaction on TiO₂ (anatase)', *Z. Phys. Chem. (Leipzig)*, **173**, 217–223.
1931. Komatsu, T., Uddin, M. A. and Yashima, T. (1995), 'IR spectroscopic studies on the reduction of nitric oxide with ammonia over MFI-ferrisilicate', *Studies Surf. Sci. Catal.*, **97**, 437–441.
1932. Ramis, G., Yi, Li, Busca, G., Turco, M., Kotur, E. and Willey, R. J. (1995), 'Adsorption, activation and oxidation of ammonia over SCR catalysts', *J. Catal.*, **157**, 523–535.

1933. Hadjiivanov, K. I., Klisurski, D., Ramis, G., Busca, G., (1996), 'Fourier transform IR study of NO_x adsorption on a CuZSM-5 de-NO_x catalyst', *Appl. Catal. B: Environ.*, **7**, 251–267.
1934. Komatsu, T., Ogawa, T. and Yashima, T. (1995), 'Nitrate species on Cu-ZSM-5 catalyst as an intermediate for the reduction of nitric oxide with ammonia', *J. Phys. Chem.*, **99**, 13053–13055.
1935. Ito, E., Mergler, Y. J., Nieuwenhuys, B., and Galis, H. (1995), 'NO_x reduction with ammonia over cerium-exchanged mordenite in the presence of O₂. An IR mechanistic study', *Studies Surf. Sci. Catal.*, **98**, 146–147.
1936. Kijlstra, W. S., Brands, D. S., Poels, E. K. and Blik, A. (1997), 'Mechanism of the selective catalytic reduction of NO by NH₃ over MnO_x/Al₂O₃. I. Adsorption and desorption of the single reaction components', *J. Catal.*, **171**, 208–218.
1937. Kapteijn, F., Singoredjo, L., Vandriël, M., Andreini, A., Moulijn, J. A., Ramis, G. and Busca, G. (1994), 'Alumina-supported manganese oxide catalysts. 2. Surface characterization and adsorption of ammonia and nitric oxide', *J. Catal.*, **150**, 105–116.
1938. Chen, J. P. and Yang, R. T. (1993), 'Selective catalytic reduction of NO with NH₃ on SO₄²⁻/TiO₂ superacid catalyst', *J. Catal.*, **139**, 277–288.
1939. Meijers, S. and Ponec, V. (1996), 'An FTIR spectroscopic study of the selective oxidation of nitrosobenzene to nitrobenzene by metal oxides', *J. Catal.*, **160**, 1–9.

INDEX

Note: Page numbers in *italics* refer to figures; those in **bold type** refer to tables.

- Absorption bands
adsorbed ammonia, 81
aryl halides, 378
assignment, 309
band widening, 36
benzene, 367
carbenium ions, 317, 361
carbon dioxide, 134
carbon monoxide, 96
chlorofluorocarbons, 409
chromium oxide systems, 33, 34, 270
copper carbonyls, 201
and copper content, 188
ethene, **330, 332**
formates, **448, 450**
heteropoly compounds, 297, 302, **303, 305**
hydroxyl groups, **58–59, 63**
intensities, 34
iron oxide systems, 37–38
manganese dioxide, 39
Ni-Y zeolites, 207
nitric oxide, **126**
nitrogen, **120**
oxide systems, **32**
palladium carbonyls, 229
platinum catalysts, **240**
surface isocyanate complexes, **157, 159**
vanadium catalysts, 260, 268
- Absorption coefficients, **168**
- Acetaldehyde
from ethene oxide, 496
oligomerization, 431
polymerization, 431
- Acetaldehyde adsorption, 430–435
on vanadium systems, 435
on zeolites, 430
- Acetamide, 415
- Acetate ion, 453
- Acetates–carboxylates, 453
- Acetic acid, complexation, 453
- Acetone, 256, 321, 423, 431
desorption, 445
dissociation, 444
from propene, 507
transformation, 531–532
- Acetone complexation, 442–445
absorption frequencies, **444**
on alumina, 443
on oxides, 442–445
on titanium dioxide, 445
on zeolites, 442
- Acetonitrile, 84, 411–415, 520
cation complexes, 413–414
hydrogen bonding, 412–413
ion pair complexes, 414–415
IR frequencies, **414**
IR spectra, *412, 413*
polymerization, 415
silicon dioxide, 412–413
zeolites, 413
- Acetylene, 138, 174, 348
adsorption, 381, 385
polymerization, 382
as probe, 385
spectral data, **384**
- Acetylide, 386, 388
- Acid-base pairs
alumina, 101
hydrogen adsorption, 117, 118
- Acidic protons, 291
- Acidic surface properties, 161–171
- Acidity, measurement, 164
- Acrolein, 321, 351, 435–439, 520
absorption bands, **437**
catalysis rates, **530**
hydroxyl groups, 436

- Acrolein (*continued*)
with metal cations, 436–438
molecular orbitals, 435
oxidation, 526–531
on oxides, 439
polymerization, 528
production, 499–505
surface complexes, **438**
with surface oxygen, 438–439
thermal desorption, 503
- Acrylates, 321, 354, 438–439, 455, 527
- Acrylic acid, 406
adsorption, 527, 529
complexation, 453–455
IR characteristics, **454**
thermodesorption, 453
- Acrylonitrile, 520, 522
- Active centers, numbers of, 169, **177**
- Active sites, 28–31
- Adipodinitrile, 415
- Adiponitrile, 524
- Adsorbate–adsorbent systems, 10
- Adsorption capacity, and pH, 254
- Adsorption centers, 29
cations, 200
- Adsorption sites
charge states, 271
and stretching frequencies, 271–275
- Aerogels, 60
- Aerosil
hydrogen bonding, 431
proton affinity, 164
spectra, 152
- Aerosillogel, 413
- Aerosols, silica, 60
- Ag/CaO systems, 225
- AgX zeolite, 330
- Air pollution, 146
- Al–O vibration mode, 41
- Al–O–Al bonds, 67
- Alcoholates, 341, 400, 401, 421–425,
533
- Alcohols
chemisorption energies, 419
complexation, 416–430
copper-containing catalysts, 477
dehydration, 532–536
dehydrogenation, 536–538
halogenated, 427
hydrogenation, 477
on oxides, 421–427
saturated, 416–427
silver catalysts, 539–542
synthesis and decomposition, 475–479
transformation, 532–545
zeolites, 416–420
on zinc oxide, 476
- Aldehydes and ketones
complexation, 430–445
hydrogenation, 532
transformations, 526–531
- Aldol condensation, 430
- Alkali earth metal oxides, surface properties, 41–43
- Alkali halides, hydrogen adsorption, 114
- Alkanes
oxidation, 480
partial oxidation, 515–518
- Alkanes adsorption
dissociative forms, 399–407
effects on OH groups, **390**
HNaY zeolites, 390
IR spectra, 397, 403
two-center, 396
zirconium dioxide, 404
- Alkanes complexation, 389–407
interactions with cations, 392–395
interactions with OH groups, 389–392, 399
- Alkenes
at Brønsted acid sites, 487
at Lewis acid sites, 487
and cation-anion pairs, 342–350
coordination, 336
deuterated, 489
fragmentation, 354
hydrogen bonding, 484
hydrogenation, 488–490
interactions with cations, 327–350
isomerization, 483–488
metal oxide systems, 319–327
metathesis, 499
nickel-containing systems, 493–495
oligomerization and polymerization, 490–498
oxidation, 480
partial oxidation, 499–509
 π -complexes, 324, 488
selective transformations, 483–499
- Alkenes complexation, 310–355
with OH groups, 310–313
with surface oxygen, 351–355
- Alkenoxides, 351–353
- Alkoxides
bonding, 319
formation, 315, 401, 538, 539
interactions, 535
surface, 421
- Alkoxy compounds, 313–327, 402, 417, 422, 425
- Alkylaromatic compounds, 511, 512
absorption frequencies, **371**

- Alkynes
aromatic, 388
IR spectra, 387
oxidation, 480
- Alkynes complexation, 381–388
aluminum oxide, 385–386
silicon dioxide, 381
titanium dioxide, 387–388
zeolites, 381–382
zinc oxide, 386
- Allyl anions, 485–486
- Allyl bromide, 501
thermal desorption, 503
- Allyl carbocations, 315
- Allyl cations, 518
- Allyl fragments, 314, 315, 347
- Allyl halides, 351
- Allyl radicals, 321
- Allylbenzene, 373, 374, 375
IR frequencies, **374**
- Allylcyanide, 415
- Allylic cations, 392
- Allylic complexes, 342–348
aluminum oxide, 344–345
Bi-Mo catalysts, 499–500
copper-containing systems, 346–348
energy diagram, 348
magnesium oxide, 345–346
zinc oxide, 343–344
- α -centers, 138
- α -sites, 487
- Alumina
ammonia and pyridine adsorption, 78–80,
86–87
boron-containing compounds, 292
carbon monoxide adsorption,
101–102
chromium catalysts, 269
defect sites, 101
fluorinated, 251
hydrated, 41
Lewis acid sites, 86–87
model surface, 65, 66
surface dehydration, 86
- Alumina-palladium catalysts, 235
- Aluminosilicates, 291
fluorination, 285
zeolites, 63
- Aluminum
coordination number, 65
four-coordinated, 65
- Aluminum ions
coordination, 87
in zeolites, 185
- Aluminum oxide
carbon dioxide adsorption, 175
hydrogen adsorption, 116
hydrogen sulfide adsorption, 142
hydroxyl groups, 65–68, 66
proton-donating centers, 92
spectra, 38
sulfur dioxide adsorption, 150, 151
surface isocyanates, 158
surface properties, 40–41
unsaturated cations, 169
water adsorption, 122
- Aluminum oxifluoride, 409
- Aluminum sulfate, 290
- Aluminum-alkyl compounds, 404
- Amides, 83
vibrational frequencies, **83**
- Amines, 84, 147, 325
- Ammonia
coordinated, 78
deformation vibrations, 85
dehydrogenation, 518, 522
desorption, 190
dissociation, 69
heat of adsorption, 85, 170
ionization potential, 170
pre-dissociation states, 88
as probe, 142
spectral characteristics, **79, 81, 82**
- Ammonia adsorption, 78–84
alkenes, 320, 325–326
chromium oxide, 88–90
copper oxides, 86
Cu zeolites, 183–184, 189, 193
hydroxyl groups, 80–84
IR spectra, 267
magnesium oxide, 87
molybdenum oxide, 91–92
NiY zeolites, 208
on platinum, 246
schemes, 87
spectra, 40, 285, 286
titanium dioxide, 49, 88
vanadium catalysts, 91–92, 165, 260, 262,
264–266
zinc oxide, 87–88
- Ammonia centers, Lewis acids, 284
- Ammonia complexes, oxidised, 86
- Ammonia (pyridinium) ions, 78
- Ammoniates, 189
- Ammonium paramolybdate, 252, 256,
307
- Ammonium vanadate, 259
- Amoxidation reactions, 518–526

- Anatase, 48
 ethene π -complexes, 331
 Lewis acid sites, 260
 nitrogen dioxide reactions, 133
 sulfate modified, 287
 surface, 72, 104
 surface forms, **104**
- Anatase-molybdenum oxide solid solution, 256
- Angle deformations, 10
- Anharmonicity constant, 10
 OH bonds, 162
- Aniline, 367
- Anions, coordination environments, 171
- Anthracene, 368
- Antimonates, 75, 94, 518
- Antimony hexafluoride, 30
- Antimony oxide, 44
 acrylic acid adsorption, 455
 ammonia adsorption, 91
 propene adsorption, 505
 surface, 428
- Apparent absorbance, 5
- Aprotic sites
 carbon dioxide adsorption, 138
 complex formation, 173
- Aragonite structures, 292
- Aromatic compounds
 chemisorption, 369
 on ferric oxide, 370
 ionic pair interactions, 373–376
 IR spectra, 357, 361
 and oxide systems, 368–373
 oxidised complexes, 376–377
 ring opening, 379, 381
 side chains, 365
 surface oxygen complexation, 376–378
 vanadium systems, 358–362, 364, 375
 and zeolites, 366–368
- Aromatic structures
 formation, 314
 ring vibration, 367, 381
- Arrhenius plots, 462, 462
- Aryl compounds
 complexation with oxygen, 376–377
 oxidised complexes, 376–377
 partial oxidation, 509–514
- Aryl compounds and aryl halides, complexation, 355–381
- Aryl halide complexes, 378–381
 cation interactions, 378–379
 copper-containing systems, 379–380
 IR spectra, 379, 380
 oxygen interactions, 379–381
 vanadium systems, 378–379
- Arylaldehydes, 513
- Aryloxides, 362
- Asymmetric deformation, ammonia, 85
- Attenuated total reflection spectroscopy, 11, 17–18
- B–O bond, 292
- Back-bonding, 337, 551
- Band splitting, copper, 182
- Barium oxide
 carbon monoxide adsorption, 105
 oxygen absorption, 52–53
 Raman spectra, 53
 surface properties, 41
- Barium peroxide, 53
- Barium sulfate, 453
- Bases, protonated, 80
- Basic surfaces, properties, 171–177
- Basicity, ammonia and pyridine, 78
- Bending vibrations, ammonia, 85
- Benzaldehyde, 375, 439–440, 526
- Benzamide ion, 416
- Benzene
 amine derivatives, 367
 hydrogenation, 490
 ionization, 178
 IR spectra, 356, 356
 oxidation, 510–511
 ring opening, 376, 510
- Benzene adsorption
 on alumina, 369
 on haematite, **371**
 on oxides, 348, 368
 on palladium, 234
 on platinum systems, 246
 on vanadium systems, 360
 and water, 370
 on zeolites, 367
- Benzenium ions, 360
- Benzidine, 514
- Benzoate ions, 372, 376–377, 439, 483
- Benzoic acid, 377, 455–456, 511
- Benzonitrile, 84, 415–416, 524
- Benzyl compounds, 372, 375, 513, 525
- Benzylacetophenone, 443
- Benzylimine, 416
- Bi-Mo oxide catalysts, 499–500
- Bicarbonate structures, 136
- Bimolecular initiation, 392
- Binary oxides, 86, 425
- Binuclear bridging complexes, 287
- Biphenyl, 368
- Bismuth molybdate, 500
- Bismuth oxide, hydrogen sulfide adsorption, 145
- Bismuth vanadomolybdate catalysts, 520

- Bisulfite complexes, 150, 153
- Bisulfite ion, 149
- Boemite, 67
- Bond dissociation energy, OH bonds, 162
- Bond multiplicity, 34
- Bond stability, 274
- Bond stretching, 10
- Bond synergy, 201
- Borates, 292
- Boron oxide, 292
- Boron-modified systems, metal oxides, 291–294
- Boron-oxygen surface compounds, 292
- Boron/titanium dioxide IR spectra, 293
- Bragg reflection, 23
- Branched oligomers, 314
- 4-Bromoacetophenone, 443
- Brønsted acid sites
 - alcohols, 539
 - alkenes, 319
 - ammonia and pyridine adsorption, 92–95
 - methane adsorption, 390
 - oligomerization, 314
 - properties, 166
 - sulfate-modified systems, 290, 291
 - vanadium catalysts, 263, 267, 268
 - water adsorption, 122
- Brønsted acids, 30
 - criteria, 78
 - hydroxyl groups, 63, 75, 122
 - strengths, 165
- Brønsted bases
 - magnesium oxide, 348–350
 - zinc oxide, 350
- Brukite, 71
- Bulk adsorbents, IR absorbance, 31
- Butadiene
 - adsorption, 318, 323, 325–326, 494
 - hydrogen bonding, 313
 - hydrogenation, 489
 - ionic structures, 325
 - spectra, 318, 324, 325
- Butane, 406
 - dehydrogenation, 506, 518
 - oxidation, 480, 481
 - zirconia interactions, 391
- tert*-Butanol, 535
- 1-Butanol, on zeolites, 419
- Butenes, 138, 375
 - chemisorption, 350
 - complexes, 506
 - isomerization, 485, 486, 487, 493
 - oxidation, 506
 - π -complexes, 341
 - vanadium catalysts, 322
 - on ZnO, 344
- tert*-Butyl acetylene, 386
- But1-yne, 386
- C–H bonds
 - activation, 389, 395–407, 500, 515
 - dissociation, 342, 400, 486, 505
 - loosening, 395–399
 - polarization, 396, 527
- CaA zeolites, 140
 - methane adsorption, 392
- Cabosils, 60
- CaCo-Y zeolites, 218
- Calcite structures, 292
- Calcium molybdate, IR spectra, 307, 307
- Calcium oxide
 - carbon dioxide adsorption, 175
 - carbon monoxide adsorption, 105, **107**
 - hydrogen adsorption, 117
 - hydrogen sulfide adsorption, 142
 - sulfur dioxide adsorption, 150
 - surface properties, 41
- Calcium phosphates, 290
- CaNa-A zeolites, 393
- CaNa-X zeolites, 218
- Cannizzaro reactions, 420, 434, 534
- Carbanions, 342, 473–474
- Carbene complexes, 406, 478, 491, 496
- Carbenium ions, 165, 313–327, 342
 - alcohols, 416, 420
 - alkenyl, 315, 318, 319, 324, 391
 - alkylaromatic, 358–366
 - alkynes, 382–385
 - allyl, 316, 317
 - aromatic compounds, 377
 - formation, 323
 - frequencies, **363**
 - methanol, 535
 - methyl allyl, 318
 - polyenyl, 317, 325
 - toluene adsorption, 525
 - unsaturated, 314
- Carbocationic complexes
 - alcohols, 420, 534
 - alkylaromatic compounds, 512
 - allyl, 488, 502
 - transformations, 382
- Carbon, Raman spectra, 457
- Carbon dioxide
 - absorption bands, 134
 - cation interactions, 134
 - chemisorption, 133, 137
 - dissociation, 477

- Carbon dioxide (*continued*)
 formation rates, **482**
 heat of adsorption, 177
 hydrogenation, 479
 interaction energies, 177
 poisoning experiments, 487
 as probe, 174
 and sulfur compounds, 142
 surface compounds, **138**
- Carbon dioxide adsorption, 133–139
 aluminum oxide, 175
 calcium oxide, 175
 interaction with oxygen, 134–136
 magnesium oxide, 175
 oxides, 137–139
 strontium oxide, 177
 zeolites, 137
- Carbon isotopes, 242, 246
- Carbon monoxide
 activation, 472
 adsorption sites, 271
 and allyl anions, 350
 binding energy, 275
 in carbonyl complexes, **220**
 chemisorption, 204, 231
 conjugated cyclic compounds, 106
 dimers, 106, 207
 electron donor properties, 272
 extinction coefficient, 105
 heat of adsorption, 95, 171
 hydrogenation, 476
 interaction with cations, 95–97
 ‘islands’, 242
 molecular orbitals, 95, 96
 polymers, 106
 as probe, 48, 95, 142, 167, 217
 re-adsorption, 204
 σ complexes, 96
 stretching vibrations, **216**, 246, **272**
 thermodesorption, 250
- Carbon monoxide adsorption, 95–114
 alumina, 41, 101–102
 barium oxide, 105
 calcium oxide, 105, **107**
 carbonate formation, 105
 cerium oxide, 478
 chemical shift, 109
 chromium oxide, 103, 114
 cobalt oxide, 112–113, 218, 219
 copper chromate, 111
 copper oxides, 111–112
 coverage and spectral data, **109**
 Cu zeolites, 186, 190, 195, *196*
 Fe zeolites, 222
 ferric oxide, 102
 and hydrogen adsorption, 115
 magnesium oxide, 105–109, **108**
 molybdenum systems, 114, 257
 Ni zeolites, 211
 nickel oxide clusters, *216*
 oxides, 100–101, **258–259**
 palladium, 233, 248
 platinum systems, *240*, **240**, 245–247, *249*
 rare earth metal oxides, 109
 silver cations, 225
 solid solution spectra, *206*
 spectral features, **99–100**, **258–259**
 strontium oxide, 105
 sulfate-modified systems, 290
 titanium dioxide, 103–105
 tungsten oxide, 114
 vanadium catalysts, 114, 260, 263
 zinc chromates, 110
 zinc oxide, 96, 109–110
 zirconium dioxide, 113, 476
- Carbon monoxide IR spectra, 98
 cobalt systems, *113*
 copper-containing systems, *196*, **198**, *471*
 Fe zeolites, 223
 nickel-containing systems, *211*, *214*
 palladium compounds, 228, 229, *230*
 platinum distribution, *241*
 silver compounds, 226, 227
 on solid solutions, *206*
 supported platinum, 238–248
 vanadium catalysts, 264, 268
 on zinc oxide, *463*
- Carbon monoxide oxidation, 461–466
 chromium oxide catalysts, 461–462
 high temperature, 464
 rates, **464**
- Carbon monoxide reactions, 461–479
 carbonization and hydroformylation, 473–475
- Carbon monoxide-ammonia co-adsorption, 105
- Carbon-carbon stretching frequencies
 butenes, **344**
 π -complexes, **333**, **334**
- Carbon-halogen bonds, 352
- Carbon-oxygen bond, 96
- Carbonaceous deposits, 456
- Carbonate formation, 105, 110
- Carbonate groups, on surfaces, 34, 175
- Carbonate structures, 135, 138, 418
- Carbonate-carboxylate compounds, 461, 462
 correlation, **135**
 Ni zeolites, 212
 types, *135*
 vibration frequencies, 134

- Carbonates
 - adsorbed, 174
 - Cu zeolites, 196
 - intermediates, 462, 465
 - spectral features, **175**
- Carbonium ions, 322, 324, 488
- Carbonyl complexes
 - cations, 95–97, 100
 - copper systems, 465
 - iron, 102
 - palladium, 158
 - spectral properties, **169**
 - zinc-containing systems, 110, 476
- Carbonyl ligands, 282
- Carbonyls
 - formation, 402
 - four-electron donor, 207
- Carboxylates
 - alkanes, 402
 - alkenes, 353–355
 - butene oxidation, 341
 - decomposition, 464, 479
 - formation temperatures, 353
 - as intermediates, 479–480, 483, 505, 527
- Carboxylic acids, 445, 453
 - as probes, 173
- Catalysis rates, and temperature, 480
- Catalyst deactivation, 456–458
- Catalysts
 - bi-functional, 92
 - industrial, 541
- Catalytic cracking, isobutane, 490
- Cation exchange, zeolites, 64, 366, 442
- Cation states, 181
- Cation-oxygen bonds, 31
- Cationic modification, 308
- Cations
 - complexing capacity, 166
 - neutralizing, 234
- Cell reactors, 13, 14, 16
 - for electron spectroscopy, 5
 - high-temperature, 14
 - for IR spectroscopy, 12
 - schematics, 17
- Cerium oxide
 - adsorbed oxygen, 52
 - CFC's, 410, 411
 - silver stabilization, 226, 542
- Cesium iodide disks, 31
- Cesium oxide, 226, 542
- Charge delocalization, 317
- Charge transfers, 2
 - sulfur dioxide, 148
- Charge-transfer bands
 - Cu zeolites, 190–195
 - Ni zeolites, 210
- Chemical shift, 242, 394
- Chloride ions, site blocking, 105
- Chloroalkyls, 173
- Chloroaromatics, 173
- Chlorobenzenes, 378–381
- Chlorofluorocarbons
 - aluminum oxide systems, 409
 - cerium oxide, 410, 411
 - chemisorbed species, **409**
 - chromium oxide, 409
 - complexation, 407–411
 - Raman spectra, 410, 411
 - silicon dioxide, 410, 411
 - titanium dioxide systems, 408
 - vibration frequencies, **408**
- Chloroform, as probe, 173, 174
- Chromate ion, 36
- Chromatography, desorption products, 309, 325
- Chromites, 483
- Chromium ions
 - alkene complexes, 352
 - clustering, 269
 - coordination by hydroxyl groups, 123
 - coordinatively unsaturated, 35
 - electron positivity, 35
 - four-coordinated, 36
 - oxidation potential, 36
 - oxidation state, 491
 - photoreduction, 270
 - and pyridine, 90
 - unsaturated, 103
- Chromium nitrosyls, 270
- Chromium oxide
 - ammonia adsorption, 88–90
 - carbon monoxide adsorption, 103, 114
 - chloride modification, 285
 - desorption spectra, 463
 - ethene adsorption, 354
 - IR spectra, 33, 47
 - Nitric oxide adsorption, 126–128
 - oxygen adsorption, 45–48
 - oxygen state at surface, 34
 - reduction at surfaces, 48
 - supported, 269
 - water adsorption, 122–123
- Chromium oxide systems, vibrations, 33–37
- Chromium ³⁺ states, on chromium oxide face, 34
- Chromium-CO complexes, 273
- Chromium-containing systems, 269–271
 - olefin polymerization, 490–491
- Chromium-oxygen bond, 35

- Chromium-oxygen systems, coordination states, 35, 89
- Chromocene, 284
- Citraconic anhydride, 511
- Claus process, 146
- CN stretching frequency, 412
- CNDO method, 329
- Co/Al₂O₃ catalyst, Raman spectra, 457
- Co/TiO₂ systems, 219
- Cobalt
- hexaaqua complexes, 217
 - interactions with hydrocarbons, 218
 - metallic, 219
 - see also* Palladium-cobalt systems
- Cobalt aluminate, 219
- Cobalt carbonyls, 219
- Cobalt ions
- coordination, 217
 - reduction, 112, 219
 - stabilization, 53
 - titania-supported, 219
- Cobalt oxide
- binding energy, 482
 - carbon monoxide adsorption, 112–113, 219
 - Raman spectroscopy, 279, 280
 - surface properties, 43
- Cobalt oxide-magnesium oxide
- adsorbed oxygen surface, 53
 - solid solutions, 53, 112, 219, 505
- Cobalt oxide-zinc oxide systems, 219
- Cobalt-boron-titania catalysts, 294
- Cobalt-containing systems, 217–220
- oxides, 218–220
 - zeolites, 217–218
- Combination bands, 10
- CoNa-X zeolites, 218
- Conjugated cyclic compounds, carbon monoxide, 106
- Conjugated mechanism, 481
- Conjunction mechanism, 464
- Coordination number, metal atoms, 34, 35
- Coordination states
- chromium-oxygen systems, 35
 - ligands, 35
- Coordinative saturation values, surface cations, 34
- Coordinatively unsaturated ions, 181
- Copper
- absorption spectra, 203
 - coordination states, 111
 - hydrated complexes, 188, 189
 - metallic, 203
 - zero-valent, 203
 - see also* Cu
- Copper acetate, 455
- Copper carbonyl complexes
- absorption bands, 201, 203, 204
 - ESR, 186
 - oxide surfaces, 201
 - π -bonding, 274
 - WGS reaction, 470, 471, 472–473
- Copper chromate, carbon monoxide adsorption, 111
- Copper chromite, 111
- water-gas shift reaction, 471–472
- Copper content, and absorption band, 188
- Copper dimers, 200
- bridged, 194
- Copper hydrates
- charge transfer band, 191
 - splitting parameter, 188
- Copper ions
- charge transfers, 190–195
 - clusters, 197
 - coordination state, 194–195
 - d–d transitions, 187–190
 - electronic states, 182
 - exchange interactions, 185
 - magnetic interactions, 185–187
 - paramagnetic interactions, 185
 - redox mechanisms, 550
 - reduction, 185, 202, 549
 - states and transformations, 184
 - types, 184, 189
 - weak adducts, 195
 - weak associates, 189
- Copper oxide
- acrolein production, 499
 - ammonia adsorption, 86
 - carbon monoxide adsorption, 111–112
 - nitric oxide adsorption, 128
 - surface properties, 43, 531
- Copper oxide-magnesium oxide system, 192, 194, 217
- Copper oxide-silica fixation, 202
- Copper phenolate, 381
- Copper-containing systems
- allylic complexes, 346–348
 - cation states, 182–207
 - oxides, 200–207
 - zeolites, 182–201
- Copper-magnesium oxide catalysts, 188
- Copper-nitric oxide complex, 200
- Copper-palladium systems, 237
- Copper-zinc oxide catalysts, 201
- Corundum
- crystallization, 65
 - decomposition, 67
 - surface planes, 35
- Covalent bonds, Cu–O, 194

- Crotonaldehyde, 430, 435
Crotononitrile, 415
Crystal fields, copper ions, 182
Crystal structures, identification of, 27
Crystallographic phases, 32
Crystallographic shear, 179
Crystobalite, 61, 62
Cu zeolites
 carbon monoxide adsorption, 186, 190, 195
 charge-transfer bands, 190–195
 infrared spectra, 195–200
 nitric oxide adsorption, 198
Cu-mordenite, 549
Cu-O covalent bond, 194
Cu-ZSM-5 zeolites, 207
Cu/TiO₂ catalysts, 206
Cu/Zn/Al oxide solid solutions, 204
Cu/ZnO systems, 204, 205
 boundary species, 248
Cu/ZnO–Al₂O₃ systems, 205
Cumene, 355, 368
CuNaY zeolites, electron spectra, 188
CuO-MgO systems, 205
CuO/ZnO/ZrO₂ catalysts, 207
CuO/ZrO₂ catalysts, 207
Cutoff frequencies, 31, 36
CuY zeolites, 183
 ESR spectra, 186
CuY-A zeolites, 187, 192, 195, 200
CuY-I zeolites, 187
 charge transfer spectra, 191, 192
 dehydration, 191, 192
 electronic spectra, 187, 193
CuZSM zeolites, 547–552
Cyclic anhydrides, 322
Cyclic structures, haematite, 70–71, 70
Cyclization, 314
1,3,5-Cycloheptatriene, 496
Cyclohexane, 395, 398, 399, 404
 ammoxidation, 523–524
 IR spectra, 523
Cyclohexanol, dehydrogenation, 536
Cyclohexanone, 431
Cyclohexene, 355
2-Cyclohexen-1-one, 431
Cyclopentadienyl chromium, 284
Cyclopentanone, 431
Cyclopentene, 489
Cyclopropane, 315, 392, 406

d–d transitions
 copper ions, 187–190
 nickel ions, 210
Dative bonding, 271
Deconvolution procedure, 165
Dehydroxylation, 77, 94
 Lewis acidity, 88
Delocalized electrons, 328
Delocalized protons, 75
Desorption, stepwise, 309
Deuteration
 pyridine, 93
 reagents, 315
 silica, 40
Deuterium adsorption, on zeolites, 116
Deuteroacetylene, 386–387
Deuteroalkenes, 334
Deuteroethene, 169
Deuteropropene, 169, 485, 487
Dewar-Chat-Duncanson model, 327, 430, 436
Diammoniates, 190
Dibenzene-chromium, 370
Dicarbonyl complexes, 100, 103, 495
Dichloromaleic anhydride, 442
Dienes, 316, 318
Diffuse reflectance electron spectroscopy
 boron-modified systems, 292, 293
 cobalt catalysts, 281
 copper-containing systems, 203
 silver-containing systems, 223–225, 541
 zeolites, 181
Diffuse reflectance infrared spectroscopy, 18
 hydrogen and nitrogen adsorption, 114
 nitrogen adsorption, 119
Diffuse reflectance spectroscopy, 5, 12
 basic surfaces, 172
Diffuse reflectance UV spectroscopy, allylic
 complexes, 349
Diffuse reflectance UV-Vis spectroscopy, 260, 263
Diffuse scattering spectra, vanadium oxides, 76
2,5-Dihydrofuran, 506
Dilution media, infrared transmission spectra, 11
Dimethoxymethane, 537
Dimethyl acetylene, 385
Dimethyl ether, 419, 534, 544
1,3-Dimethylnaphthalene, 356, 364, 366
Dinitrosyl complexes, 548
Dinitrosyl groups, 126, 127, 128, 257, 262, 269,
 495, 548, 549, 551
Dioxygen compounds, 38
Dioxymethylene, 431, 434, 537
 absorption frequencies, **432**
1,1-Diphenylethene, 358
Dipole charges, 5, 22
Dipole–dipole interactions, 185, 247
Dispersed oxide catalysts, vibrational spectra, 31
Dispersion, in samples, 34
Disproportionation reactions, 420, 434, 514, 534

- Donor capacity, 169
Donor-acceptor interactions, metal carbonyls, 282
Double-center adsorption, 173
Dynamic allyls, 501
Dynamic shift, 242
- E-sites, 486–487
Electromagnetic spectrum, 2
Electron acceptor capacity, 170
Electron concentration, semiconductors, 55
Electron delocalization, 332
Electron donation, 178
Electron energy loss spectroscopy, 5, 21–22
Electron paramagnetic resonance data, 551
Electron paramagnetic resonance spectroscopy, 179
Electron positivity, chromium ions, 36
Electron proton resonance spectroscopy, 48
Electron spin resonance spectroscopy
 adsorbed oxygen, 44
 basic surfaces, 172
 carbonyl complexes, 96
 cation-exchanged zeolites, 271
 copper ion parameters, **184**
 hydrogen sulfide adsorption, 145
 molybdenum systems, 253, 254, 256
 palladium zeolites, 232
 sulfur dioxide, 150, 155
 vanadium catalysts, 268
 Y-zeolite spectrum, 183
Electron transfers, 4
Electron-adsorbate interactions, 21–22
Electronic factor, 250, 335
Electronic resonance, 21
Electronic spectroscopy, 1–5
Emission spectroscopy, infrared, 14–15
Energy levels, 2, 8
Enolates, 426, 443, 445, 536
Equilibrium distance, O–O bond, 48
Erbium oxide, 73
Esterification reactions, 362, 422
Esters, 147
Ethane, ammoxidation, 522–523
Ethane adsorption
 Cr–Mo catalysts, 398–399
 dissociative, 404
 zirconium dioxide, 396
Ethanol
 adsorption, 319, 476
 on alumina, 422
 conversion to hydrocarbons, 544–545
 dehydrogenation, 543
 on zeolites, 419
- Ethene, 169
 carbon-carbon stretching, 311, 335
 copper systems, 337
 dimerization, 493, 494
 dissociation, 492
 formation, 405
 heat of adsorption, 330
 hydroformylation, 474–475
 hydrogenation, 490
 IR frequencies, **333, 338**
 IR spectra, 331
 low-temperature interactions, 339
 molecular orbitals, 327
 nickel-containing systems, 494
 oligomerization, 493, 494
 oxidation, 508–509, 556
 π -complexes, 489, 490, 492, 508
 polarization, 328
 polymerization, 342, 490–496
 protonation, 165
 substituted, 386
 surface-reaction kinetics, 488–489
 symmetry, 337
 total intensities, **312**
 transition metals, 332
 vanadium-containing systems, 495
 wavenumbers, **312**
Ethene adsorption
 on platinum, 246
 on silver, 509
Ethene oxide
 aluminosilicate systems, 496
 and basic oxides, 497–498
 on oxides, 497
 polymerization, 496–498
 radical mechanism, 497
 on silver systems, 509
Ethene-hydroxyl complexes, 311
Ethene-metal complexes, 337
Ethers, 352, 417, 425
Ethoxy groups, 401, 422, 495
Ethyl acetylene, 381
Ethyl chloride, 401
Ethylbenzene, 370, 377
 oxidative dehydrogenation, 514
Ethylene *see* Ethene
Ethylidene complexes, 341–342, 493
Ethylnylbenzene, 373
Exchange interactions, copper ions, 185, 187, 198
Exciton absorption processes, 42
Experimental conditions, choice of, 310
Experimental principles, 6–7
Extended Hückel method, 333

- Extended X-ray absorption fine structure spectroscopy, 257
- Extinction coefficients
ammonia, 165
carbon monoxide, 105
copper ions, 187
- Factor group analysis, 27
- Faujasite, 149, 328, 368
structure, 30
- Fe-Y zeolites, 220
- Fe/Sb oxide systems, 44
- Fermi level, 228
- Fermi resonance, 411, 447, 534
- Ferric ion, coordination states, 90
- Ferric oxide
alkene π -complexes, 337
ammonia and pyridine adsorption, 90–91
carbon monoxide adsorption, 102
disordered face, 91
heat treatment, 70
hydrogen sulfide adsorption, 145
hydroxyl groups, 69–71
IR spectra, 38
oxygen adsorption, 52
spectra, 517
sulfate modification, 287
surface properties, 37–38
water adsorption, 122
- Fischer-Tropsch synthesis, 458
- Flow reactor cells, 464
- Fluorine and chlorine-modified systems, 285–286
- Fluorobenzene, 362
- Foliated pie method, 49
- Formaldehyde, 256, 399, 420, 425
absorption frequencies, **432**
on cerium oxide, 434
chemisorption, 433
complexation, 430–435
industrial production, 541
oxidation, 515, 531, 537
on oxides, 431–435
polymerization, 433
on vanadium systems, 434–435
yield, 541, 542
- Formate ions, 431, 433, 446
- Formate-carboxylate surface compounds, 446, 448
- Formates
absorption frequencies, 353, 400, **448, 450**
activation energies, 448
in alcohols complexation, 418, 426, 476
in alkane complexation, 392
in alkene complexation, 352
in alkyne complexation, 387
formation mechanisms, 448
as intermediates, 481
IR spectra, 449
in propene oxidation, 502
thermal stability, 448
WGS reaction, 467–469
zinc-containing systems, 110
- Formic acid, 531
complexation, 445–452
copper-containing systems, 450–452
dehydration, 445
hydrogen bonding, 446, 449
IR band assignments, **451**
IR spectra, 447
physisorption, 446
vanadium systems, 452
- Formyl formation, 478
- Formylacetates, 439, 527, 528
- Fourier transform IR spectroscopy, 11, 15
alkanes, 390
carbon monoxide, 100
cerium oxide, 52
metal oxide systems, 281
platinum clusters, 251
- Fundamental vibrations, 27
- Furan, 322, 440, 506
2(5H)-Furanone, 506
- Gallium sulfate, 290
- Gallium-containing systems, 519
- Gallium-molybdenum catalysts, 501
gamma spectroscopy, 220
- Geometric effect, 243
- Geometric factor, 242, 247
- Glass, porous, 114
- Goethite, 69, 70, 122
modification, 287
- Gold, optical absorption spectra, 228
- Grain size effects, 281
- Graphite, 458
- Grinding, defect formation, 179
- Group characteristic, 10
- H-H vibrations, 115
- Haematite, 69, 70
crystal structure, 70
pyridine adsorption, 90
water adsorption, 122
- Hafnium oxide, 290
- Halogen atoms, donor ability, 407
- Halogen exchange reactions, 409
- Halomethanes, 402
- Hammett method, 161
- Hard acids and bases, 77

- Harmonic frequency, OH bond, 162
Harmonic vibrations, Raman effect, 20
Harrick Collector, 18
Heterogeneous catalytic reactions, 459–558
Heterometallic groups, 251
Heteropoly acids
 acidic properties, 300–303
 acrylic acid formation, 406
 ammonia and pyridine adsorption, 300
 effect of concentration, 301–302
 effect of support type, 302
 FTIR, 281
 IR spectra, 255, 304, 306
 Lewis acid centers, 303
 pre-treatment, 302
 proton affinity, 166, 302
 proton replacement, 302–303
 strengths, 164, 166
 supported, 68
 thermal stability, 303–308
Heteropoly compounds, 30, 95, 128, 256, 294–303
 alumina-supported, 298
 effects of supports, 295–300
 IR spectra, 296, 297, 299, 301
 structure, 295
Heteropolyanions, 295
Heteropolyoxoanions, 407
Heteropolyoxometalates, 515
Hex-1-ene, adsorption, 314
Hexaammoniates, 208
Hexachloroacetone, 443
Hexafluoroacetone, 444
Hexafluoropropane-2,2-diol, 444
Hexafluoropropene, 409
Hexamethylbenzene, 360, 364
n-Hexane, aromatization, 251
1-Hexene, production, 493
High temperature treatment, 43
 molybdenum systems, 95
High-resolution electron energy loss spectroscopy,
 29
 hydrogen adsorption, 118
Highest-occupied molecular orbital, 160, 430, 436,
 438
HM zeolites, 311
HNaY zeolites, 149
Holmium oxide, 73
HY zeolites, 140, 149, 311, 355, 368, 417
Hydride transfer, 389, 392
Hydrides, 118, 496
 linear, 116
Hydroamino complexes, 195
Hydrocarbon oxidation, 29, 479–483
 thermal desorption, 480
Hydrocarbons
 activation temperatures, 402
 alkylation, 544
 ammoxidation, 518–526
 carbonization, 474
 chain fragmentation, 481
 demethylation, 483
 hydroxyl groups, 484
 partial oxidation, 499–518
 reactions involving, 479–526
 saturated, 315
 synthesis, 478–479
Hydrocyanic acid, 520
Hydrofluorocarbons, 407
Hydrogen
 activation, 488
 dissociation, 69, 350, 477
 dissociative adsorption, 117
 liquid and solid phases, 117
 oxidation, 465
 as probe, 114, 115
 production, 466
Hydrogen adsorption, 114–119
 acid-base pairs, 117, 118
 aluminum oxide, 116
 bridged structures, 118
 calcium oxide, 117
 and carbon monoxide adsorption, 115
 dissociative, 348
 magnesium oxide, 117
 mode frequencies, **118**
 platinum, 118, 119
 silanol groups, 115
 spectral characteristics, **115**
 spectral features, **117**
 strontium oxide, 117
 zinc oxide, 117
 zirconium dioxide, 116
Hydrogen atoms, in INSS, 23
Hydrogen bonding
 acetonitrile, 412–413
 aerosil, 431
 alkanes, 395–399
 alkenes, 311, 351, 483
 alkynes, 381–382
 ammonia, 78, 80, 260
 aryl compounds, 376
 aryls, 355–358, 376
 Brønsted acids, 92
 butadiene, 313
 formic acid, 446, 449
 haematite, 70
 halogenated hydrocarbons, 407
 hydrogen sulfide, 139, 144

- methanol, 426
 - nitrogen dioxide, 132
 - nitrogen dioxide dimers, 132
 - propene π -complexes, 336
 - pyridine, 84
 - silanols, 60, 62, 64
 - sulfate-modified systems, 289
 - titanium systems, 288
 - unsaturated hydrocarbons, 337
 - vanadium and molybdenum systems, 75
 - water, 120
- Hydrogen chloride, 138
- Hydrogen molecules
- adsorption, 115
 - dissociation, 116
- Hydrogen reduction, spectra, 40
- Hydrogen sulfide
- absorption forms, **144**
 - adsorption, 139–145
 - co-adsorption, 142
 - deformation vibration, 144
 - dissociative adsorption, 140, 142
 - heat of adsorption, **144**
 - interaction with water, 142
 - oxide system interactions, 145
 - spectra, 143
 - spectral bands, **141**
 - stretching vibration, 144
 - surface compounds, 142
- Hydrogen sulfide adsorption
- aluminum oxide, 142
 - calcium oxide, 142
 - magnesium oxide, 142
 - oxides, 141–145
 - silicon dioxide, 139–140
 - titanium dioxide, 142
 - vanadium oxides, 145
 - zeolites, 139–140
- Hydrogen-scrambling, 491
- Hydrosulfide ion, 140
- Hydroxo complexes, 208
- Hydroxoamino complexes, 193
- Hydroxonium ions, 121, 417
- Hydroxyl groups
- absorption bands, **58–59, 63**
 - acrolein, 436
 - alcohols, 421
 - alkanes, 392
 - aluminum oxide, 65–68, 66, 67
 - ammonia adsorption, 80–84
 - aromatic compounds, 369
 - bending vibrations, 61
 - bridge type, 92, 122
 - Brønsted acids, 122
 - on chromium oxide, 122–123
 - cluster models, 66
 - and crystalline structure, 57
 - CuO-MgO systems, 470
 - ferric oxide, 69–71
 - hydrocarbons, 484
 - and hydrogen adsorption, 115
 - interactions with alkanes, 389–392
 - IR spectra, 418
 - magnesium oxide, 68–69
 - molybdenum oxide, 75–77
 - rare earth metal oxides, 73, 74
 - spinel, 74–75
 - stretching frequencies, 57, 60
 - sulfate modification, 287
 - titanium dioxide, 72–73
 - toluene, 356
 - vanadium oxides, 75–77
 - zeolites, 63–65
 - zinc oxide, 73–74
 - zirconium dioxide, 73
 - see also* Surface hydroxyl groups
- Hydroxyl stability, alkenes, 313
- Hydroxylation, solid, 120
- Hyponitrite ions, 553
- HZSM zeolites, 64, 115, 121, 132, 139
- alcohols, 417
 - aldehydes, 430
 - alkanes, 390–391
 - alkenes, 311, 315, 317
 - alkynes, 381, 382
 - aromatic compounds, 365
 - copper in, 207
 - methane, 390, 394
 - methanol, 418
 - platinum, 250
- I-sites, 486
- Imines, 526
- Imino compounds, 526
- Impact scattering, 22
- In situ* measurements, 24–25
- Inclusions, defects, 178
- Indicators, 161
- spectroscopic peaks, **162**
- Indium
- ligand effect, 243
 - and platinum, 251
- Inelastic electron tunnelling spectroscopy, 22
- Inelastic neutron scattering spectroscopy, 5, 23
- Inelastic scatter, 19, 22
- Infrared cells, as reactors, 459
- Infrared diffuse scattering spectroscopy, hydroxyl groups, 64

- Infrared ellipsometric spectroscopy, 23
Infrared frequencies, oxygen bonds, 47
Infrared spectra
 adsorbed oxygen, 17
 oxidized catalysts, 40
Infrared spectroscopy, 5, 11–18
 emission, 14–15
 experimental installation, 24
 molybdenum systems, 256
 optical materials for, **13**
 reflection, 15–18
 transmission, 11–14
Inorganic compounds, on active surfaces, 277–308
Integral absorbance, **168**
Integration spheres, 18
Intermetallic compounds, 248
Intermolecular interaction, 275
Internal reflection spectroscopy, 17–18
Iodobenzene, 362
Ion exchange conditions, copper ions, 183
Ion exchange salts, hydrolysis, 194
Ionic pair interactions, aromatic compounds,
 373–376
Iridium
 isocyanate complexes, 161
 nitrogen adsorption, 119
 SO₂ complexes, 148
Iron
 clusters, 478
 nitrogen adsorption, 119
 see also Fe, Ferric
Iron carbonyl, 102
Iron containing systems, 220–223
 in benzene oxidation, 511
 oxides, 223
 types of sites, **222**
 zeolites, 220–222
Iron peroxide, 406
Iso-synthesis, 478
Isobutane
 adsorption, 396
 catalytic cracking, 490
 IR spectra, 391, 397
Isobutanol
 adsorption, 476, 535
 ammoxidation, 526
Isobutene, 322
Isobutyronitrile, 526
Isocyanate, as probe, 161
Isocyanate complexes *see* Surface isocyanate
 complexes
Isocyanates
 extinction coefficient, 519
 molecular orbitals, 160
Isopentene, 495
Isopolyanions, 295
Isopolymolybdates, 252
Isopropanol
 adsorption, 319, 423, 425, 476, 534, 536
 as intermediate, 507
Isopropoxy compounds, 321, 423, 507–508
Isopropyl alcohol *see* Isopropanol
Isopropylbenzene, 356
Isotopic effects, band shifts, 34, 318, 335
Isotopic exchange, 8, 315
Jahn-Teller effect, 182
Keggin structure, 30, 166, 303, 304, 438, 518
Ketones, 147, 170, 443
Kirchoff law, 15
KL zeolite, 251
Kramer–Kronig equation, 15
KRS crystal, 18
Ksonotolite, 62
Kubelka-Munk function, 5, 18, 187
KX zeolites, 137
Lactones, 506
Lambert-Beer law, 4, 11, 14, 15, 25
Langmuir-Hinshelwood mechanism, 460, 514, 557
Lanthanide ions, 479, 558
Lanthanum oxide, 175, 226, 235, 279
Laser development, for Raman spectroscopy, 20
Lattice absorption limit, 31
Lattice defects, 27, 178
Lattice modes, overtones, 43
Lewis acid sites, 85, 166–171
 absorbance coefficients, **168**
 anatase, 260
 benzonitrile, 416
 concentration, 171
 heteropoly acids, 303
 oligomerization, 314
 properties, **171**
 sulfate-modified systems, 291
 vanadium catalysts, 264
Lewis acids, 30, 40
 adsorbed pyridine, 84, 93
 on alumina surfaces, 67, 102, 402
 centers, 78
 chromium oxides, 90
 classification, **77**
 hydrogen sulfide adsorption, 142
Lewis acids and bases, classification, **77**
Lewis bases, on rutile, 72
Ligand effect, 243
Ligand-metal bonds, degree of covalence, 191

- Ligands
 coordination state, 35
 coordinative, 195
- Linear defects, 178
- Linear oligomers, 314
- Linkam Scientific Instruments, 20
- LiX zeolites, 137, 430
- Low-temperature measurements, 114
- Lowest-unoccupied molecular orbital, 148, 438
- Luminescence, emission, 42
- Madelung energy, 41, 42, 172
- Magic angle spinning, 392
- Magnesia, incorporation of molybdenum, 92
- Magnesium acrylate, 439
- Magnesium methyrate, 404
- Magnesium molybdate, 92
- Magnesium oxide
 ammonia adsorption, 87
 as Brønsted base, 348–350
 carbon dioxide adsorption, 175
 carbon monoxide adsorption, 105–109, **108**
 defect sites, 108
 desorption spectra, 69
 hydrogen adsorption, 117
 hydrogen sulfide adsorption, 142
 hydroxyl groups, 68–69
 solid solutions, 109
 spectra, 42
 surface plane, 43, 68
 surface properties, 41
 water adsorption, 122
- Magnesium sulfate, 290
- Magnetic interactions, copper ions, 185–187
- Maleates, 440–442
- Maleic acid, 440
- Maleic anhydride, 322, 341, 406, 440–442
 absorption frequencies, **441**
 in butene oxidation, 506
- Malonates, 439, 528
- Manganese, ligand effect, 243
- Manganese dioxide, surface properties, 39
- Manganese hydroxides, 39
- Mars-van Krevelen mechanism, 460, 514, 515
- Mass spectroscopy, desorption products, 309
- Matrix-isolated techniques, 201
- Mechanical activation, 179
- Mesityl oxide, 443
- Mesitylene, 360, 364
- Metal carbonyls, 95, 274, 282–284
- Metal clusters, 181
- Metal dispersion, 228
- Metal nitrosyls, 282–284
- Metal oxide crystallites, 278
- Metal oxides
 boron-modified systems, 291–294
 dehydrated, 278
 interactions with acids and bases, 284–294
 modifiers, 281
 monolayers, 278, 281
 sulfate modification, 286–290
- Metal peroxides, 52
- Metal reflectors, 17
- Metal sulfides, 139
- Metal-CO complexes
 adsorption sites, 272–275
 molecular orbitals, 273
 stability, 272
- Metal-dioxygen interactions, 45
- Metal-methyl groups, 516
- Metal-oxygen bonds, vibrations, 32–44
- Metal-oxygen double bonds, 31
- Metal-support interaction, 223
 platinum, 248
- Metalloacyclic compounds, 493
- Metals
 NO adsorption, 125
 sorption capacity, 247
- Methacrylonitrile, 415
- Methane
 carbonization, 475
 coupling catalysts, 177
 dissociation, 404, 405
 heat of adsorption, 394
 interactions with OH groups, 389–392
 NMR spectroscopy, 394
 oxidation, 400, 516–518
 oxidative dimerization, 515
 spectral characteristics, **389**
 vibration frequencies, 389
- Methane activation, 392
- Methane adsorption, 43
 alumina, 398, 402
 aluminum oxide, 392
 Brønsted acid sites, 390
 CaA zeolites, 392
 calcium oxide, 396
 chromium oxide, 400
 CsY zeolites, 395
 DRIR spectra, 400
 ferric oxide, 400
 IR spectra, 398
 IR spectral data, **393**
 magnesium oxide, 398, 404
 NaA zeolites, 392
 NaX zeolites, 392
 NaY zeolites, 395
 silicon dioxide, 390, 399

- Methanol
adsorbed forms, **424**
chromium oxide, 423
conversion to hydrocarbons, 544–546
decomposition, 533
dehydration, 533
dehydrogenation, 543
desorption, 417
on ferric oxide, 427
hydroformylation, 474
and hydroxyl groups, 422
IR spectra, 418, 517
IR spectral data, **427**
oxidation, 256, 434, 538–545
radical reactions, 544
synthesis, 450, 475–477
on titanium dioxide, 423
on zeolites, 419
- Methanol to gasoline reactions, 535
- Methoxides, 401, 427
- Methoxy groups, 404, 417, 423, 425, 431, 476, 516, 534
- Methoxylation, silica, 40
- Methoxyls, 418, 419, 420, 422
- Methyl acetylene, 350, 381, 386, 387
- Methyl ethyl ketone, 322
- Methyl formate, 473, 537
- Methyl groups, 521
IR spectra, 405
- 2-Methyl propane *see* Isobutane
- 2-Methyl-2-propanol, on zeolites, 419
- Methylallyl compounds, 345
- Methylaryls, ammoxidation, 510
- Methylates, 401
- Methylbenzenium ion, 360
- Methylcyclopropane, 496
- Methylene groups, 375, 521
- Microcalorimetry, 122
- Microgravimetric measurements, 201
- MINDO/3 method, 66
- Mirror reflection *see* Reflection-absorption IR spectroscopy
- Mobile protons, 288, 301
- Model catalytic systems, 31, 294
- Molar absorption coefficient, 4
- Molecular orbitals
carbon monoxide, 96
dioxygen molecule, 45
ethene bonding, 327
isocyanates, 160
metal-CO complexes, 273
N–H, 85
Nitric oxide, 124
nitrogen dioxide, 128, 131
sulfur dioxide, 147
- Molecular radical-ion adsorption, 44
- Molecular spectroscopy, used for analysis, 309
- Molecules
diatomic, 8
‘fingerprints’, 27
polarizability, 19
- Molybdates, 75, 94, 252–253, 518
modified, 305–308
- Molybdenum
organometallic compounds, 282
see also Heteropoly acids; Heteropoly compounds
- Molybdenum carbonyls, 283–284
- Molybdenum compounds, thermal stability, 303–308
- Molybdenum ions
Brønsted acidity, 539
coordination, 253, 254, 256
reduction temperature, 305
- Molybdenum oxide
ammonia and pyridine adsorption, 91–92
carbon monoxide adsorption, 114
DRES spectra, 179
hydroxyl groups, 75–77
IR spectra, 307
stability, 303–305
surface properties, 39
- Molybdenum systems, 94
- Molybdenum tartrate, 255
- Molybdenum-aluminum oxide catalysts, 252–253
Raman spectra, 279
- Molybdenum-containing systems, 252–257
- Molybdenum-oxygen bonds, 295
- Molybdenum-silicon oxide systems, 253–255
products, 254
- Molybdenum-titanium oxide catalysts, 255–257
- Monoammoniates, 190
- Monovanadate groups, 259
- Mordenite, 100, 117, 150, 174, 251, 548, 558
- Mössbauer spectroscopy, 220, 271
- Multilayer coating, 151
- NaA zeolites, 54, 140
methane adsorption, 392, 393
- Naphthalene, 368, 510
- Naphthylamine, 368
- Natural gas, 515
- NaX zeolites, 116, 137, 140, 149, 392
- NaY zeolites, 115, 140, 149
- Nephelauxetic series, 191
- Neutron scattering, methane adsorption, 393–394

- Ni zeolites
 electronic spectra, 207–211
 infrared spectra, 211–215
Ni-Cu-Cr oxide catalysts, 207
Ni-Y zeolites
 absorption bands, 207
 electronic spectra, 208
Nickel
 emission spectra, 241
 hexaaqua complexes, 208
 metallic, 214, 217
 SO₂ complexes, 148
 supported, 241
 titania-supported, 217
 see also Ni
Nickel allyl, 282
Nickel ammoniate, 208
Nickel carbonyls, 215, 283
Nickel ions
 in alkene polymerization, 494
 clusters, 208
 coordination, 209, 210, 217
 oxygen bridges, 212
Nickel oxide
 adsorbed oxygen, 54
 clusters, 217
 oxygen chemisorption, 56
 surface properties, 44
Nickel oxide–magnesium oxide solid solutions,
 217, 505
Nickel-containing systems, 207–217
 oxides, 215–217
 zeolites, 207–215
NiO/NiY, 212
Niobia, 269
Nitrate ions, 132, 554
Nitrates, 123, 128, 132, 133
Nitric oxide
 absorption bands, **126**
 activation energy, 547
 adsorption, 123–130
 and ammonia, 556
 decomposition, 127, 545–552, 553
 dimers, 126, 128, 200
 molecular orbitals, 124
 and oxygen adsorption, 127
 as probe, 217
 spectral characteristics, **129**
 spectral features, **125, 127**
 surface treatment, 86
Nitric oxide adsorption
 chromium oxide, 127–128
 copper oxides, 128, 545
 Cu zeolites, 198, 545–547
 Fe oxides, 223
 Fe-Y zeolites, 220
 Ni zeolites, 213
 palladium zeolites, 231–235
 ruthenium, 126
 spectral characteristics, **127, 198**
 vanadium catalysts, 262, 268, 556–557
Nitric oxide IR spectra
 Cu zeolites, 201
 Fe zeolites, 221
 Ni zeolites, 213, 215
 Pd zeolites, 232, 233
 vanadium catalysts, 262, 262, 268
Nitric oxide-copper complexes, **546**
Nitric oxide-metal complexes, 125
Nitric oxide-propene-oxygen mixtures, 556
Nitrides, 119
Nitriles, 84, 147, 518
Nitriles complexation, 411–416
Nitrite ion, 132, 553
Nitrites, 123, 128
p-Nitroaniline, 367
Nitrobenzene, 179, 367, 513
Nitrogen
 absorption bands, **120**
 heat of adsorption, 119
 as probe, 114
Nitrogen adsorption, 119–120
 iron, 119
 Raman spectra, 119
 spectra, **120**
Nitrogen dioxide
 dimerization, 130, 132
 free radical species, 132
 molecular orbitals, 131
Nitrogen dioxide adsorption, 130–133
 Pd zeolites, 232
 titanium dioxide, 133, 557
 zeolites, 132
Nitrogen oxide *see* Nitric oxide
Nitrogen oxides
 and ammonia, 556–558
 reduction, 552–556
 reduction by hydrocarbons, 554–556
 selective catalytic reduction, 554, 556
 stretching vibrations, **124, 125**
Nitrogen-containing systems, transformations,
 545–558
Nitronium ion, 130, 133
Nitrosobenzene, 514
Nitrosonium ion, 123, 128, 551
Nitrosyls, 551
 chromium, 270
 iron, 160

- Nitrosyls (*continued*)
 Mössbauer spectroscopy, 220
 stability, 275
- Nitrous oxide, 200, 269, 554
 formation, 548
- NiY zeolites
 ammonia adsorption, 208
 dehydrated, 208–209
 electronic spectra, 209
- NiY-A zeolites, 211, 212
 dehydration, 208
- NiY-I zeolites, 209
- NO + CO mixtures, 552–554
- NO + hydrocarbons reactions, 554–556
- NO bonding, classification, **125**
- NO stretching vibrations, 130
- Noble metals
 carbonyl complexes, 227
 hydroformylation, 474
- Non-crystalline phases, 28
- Nuclear magnetic resonance spectroscopy
 methane, 394
 mordenite, 166
 propane, 392
- Nucleophilic attack, 44
- Nucleophilic substitution, 438
- O-O bond, equilibrium distance, 49
- O-O vibrations, 45, 48
- OH groups *see* Hydroxyl groups
- OH stretching vibration, 57, 311
 haematite, 71
- Olefin complexes, on oxide surfaces, 331
- Olefin-oxygen complexes, 482
- Olefins, 168
 adsorption centers, 504
 aluminum systems, 355
 bending modes, 311
 heat of adsorption, 331
 isomerization, 485
 molybdenum-containing systems, 495
 partial oxidation, 499–509
 vanadium–phosphorus systems, 341
- Oligomerization, 314, 322, 345
 acetaldehyde, 431
 alkynes, 388
 nickel ions in, 216
- Oligomers
 formation, 314, 315, 317, 326
 neutral, 384
- Optical density, 4
- Optical materials, for infrared spectroscopy, **13**
- Optical spectroscopy, cation-exchanged zeolites, 271
- Organic acids, complexation, 445–456
- Organic molecules, surface complexes, 309–458
- Organometallic complexes, 281–282
 supported, 277
- Orthoborates, 292
- Orthophosphoric acid, 305
- Oscillator
 anharmonic, 10
 harmonic, 8
- Oxalates, 287
- Oxidant molecules, 181
- Oxidation, catalytic, 194
- Oxide conductivity, 55–56
- Oxide ions, low coordination, 42
- Oxide particle size, 11
- Oxide surface centers, solid structures, 27–28
- Oxide surfaces, spectra, 31–76
- Oxide systems
 absorption bands, **32**
 surface properties, 43–44
- Oxide-hydroxyl-hydrate systems, 77
- Oxides
 carbon monoxide adsorption, 100–101
 supported, 20
- Oxidized catalysts, infrared spectra, 40
- Oxo-cations, 549
- Oxoanions, polymeric, 295
- Oxonium ions, 419, 533, 544
- Oxygen
 dissociative chemisorption, 462
 and hydrocarbon oxidation, 481
 isotopic exchange, 54–55
 isotopic mixtures, 46, 48
 molecular forms, 44–56, 481
 non-lattice, 209
 reactive, 354
 reactivity, 197
 uncharged species, 54–55
- Oxygen adsorption
 carbonate formation, 462
 chromium oxide, 45–48
 cobalt oxide-magnesium oxide, 53
 ferric oxide, 52
 interactions with carbon dioxide, 134–136
 low temperature, 54
 model, 49
 nickel oxide, 54
 tin dioxide, 50–52
 titanium dioxide, 48–50
- Oxygen bonds
 infrared frequencies, 47
 vibrational frequencies, **46**
- Oxygen ions, adsorbed on cations, 34

- Oxygen molecules
 dissociation, 48
 inactivity, 54
- Oxygen spectra
 on tin dioxide, 50, 51
 on titanium dioxide, 49
- Oxygen states, on oxide surfaces, 44
- Oxygen-cation bonds, 34, 233
- Oxygenates, 474
- Oxymethyl groups, 405
- Ozone *see* Trioxygen molecule
- P-Mo-anhydride, 304
- Palladium
 carbonyl complexes, 158, 228, 228–231, 233
 clusters, 231
 (CO)(NO) complexes, 234
 metallic, 231, 234
 oxides systems, 235–237
 re-oxidation, 234
 see also Pd
- Palladium catalysts, spectroscopic characteristics, **236**
- Palladium ions, 228
 coordination, 232
 reduction, 237
- Palladium nitrosyls, 234
- Palladium oxide, 237
- Palladium zeolites
 carbon monoxide adsorption, 232
 nitric oxide adsorption, 231–235
- Palladium-cobalt systems, 235
- Palladium-containing systems, 228–237
 oxides, 235–237
 zeolites, 228–235
- Paraffins, 174
 activation, 400
 ammoxidation, 520–523
 dehydrogenation, 406
- Paramagnetic ions, ESR, 185
- Paramagnetic oxides, 44
- Paramagnetic sites, 172
- Paramagnetic species, sulfur dioxide adsorption, 150
- Partial oxidation, olefins, 499–509
- Particle sizes, decreasing, 179
- Pd-Y zeolites, 228
- Pd/Al₂O₃, 235
- Pd/MgO catalysts, 235
- Pd/SiO₂ catalysts, 235
- Penta-ammoniates, 183, 189–190
- Pentadienes, 326
 IR spectra, 326
- Peroxide intermediates, 502
- Peroxide species, 406, 515
- Peroxide systems, 52
- Phase states, IR spectroscopy in, 111
- Phase transitions, chromium oxide systems, 33
- Phenol, 427–430, 510
 absorption frequencies, **429**
 acidity, 163
 IR spectra, 379
- Phenolate complexes, 381, 428, 430
- Phenols, as probes, 173
- Phenylallyl anions, 373
- p*-Phenylenediamine, 367
- Phenylpropynes, 373
- Phenyl-1-propynes, 388
- Phillips-type catalysts, 490
- Phosphates, 287, 290
 protic acid sites, 166
- Phosphomolybdic acid, 166
- Phosphorus, as modifier, 305–306
- Phosphotungstic acid, 128
- Photoacoustic spectroscopy, 18–19
- Photoemission spectroscopy, 274
- Photoionization, zinc oxide, 204
- Photoluminescence, defect induced, 178
- Photoluminescence spectroscopy, 172
- Photoradiation, 493
- Photothermic effect, 18
- Phthalic anhydride, 511
- Phthalide, 511
- Phthalocyanine complexes, 284
- Physisorption, 311, 341
 methanol, 419
- π -acceptors, 171
- π -allylic complexes, 342
- π -allyls
 band intensities, 501
 propene adsorption, 502
- π -bonds, 271, 274
 borates, 292
 polarization, 367
- π -complexes, 166
 acrolein, 436
 alkenes, 327, 487
 see also specific alkenes
 alkynes, 385
 aryl compounds, 356, 366–373
 benzene, 368
 binding energies, 336
 carbon–carbon stretching frequencies, **333**
 with cations, 328–341
 heat of adsorption, 332
 on oxides, 331–341
 stability, 334

- π -complexes (*continued*)
 - toluene, 359, 362
 - on zeolites, 328–331, 366–368
- π^* -orbitals, NO, 123–125
- pK_a , X-H molecules, **349**
- Planar defects, 178
- Plasma resonance absorption, 224
- Platinum
 - boundary complexes, 248
 - boundary species, 248, 248
 - cation states, 248–252
 - deposition, 239
 - dicarbonyls, 251
 - dispersivity, 239–241, **239**, 246
 - electron density, 241, 246
 - electronic states, 245, 246
 - heat treatment, 235, **239**
 - hydrogen adsorption, 119
 - isocyanate complexes, 161
 - lateral interactions, 241–242
 - metal-support interaction, 248
 - metallic, 235–243
 - molecular orbitals, 245
 - particle sizes, 239, 241, 244
 - promoters, 251
 - re-oxidation, 251
 - SO₂ complexes, 148
 - stabilization centers, 245, 246
 - supported, 242, 243–247, 246, 251
 - surface inhomogeneity, 242
 - see also* Pt
- Platinum carbonyls, 239, 244
 - stretching vibrations, 244
- Platinum distribution, carbon monoxide IR spectra, 241
- Platinum films, 248
- Platinum ions, oxidation state, 248
- Platinum silicides, 247
- Platinum-cobalt systems, promoters, **243**
- Platinum-containing systems, 235–249
- Point defects, 178
- Poisoning effects, 142
- Polarizable molecules, 77
- Polarization, paraffins, 174
- Poly-oxides, 304
- Polyacetylenes, 388
- Polycarbonium ions, 456
- Polycarbonyl complexes, 100
- Polycyclic aromatics, 392
- Polyenes, 317
- Polyenyl cations, 392
 - stability, 317
- Polyethene, 492
- Polymerization
 - acetylene, 382
 - cationic, 324
 - ethene, 342, 490–496
 - ethene oxide, 496–498
- Polymolybdates, 253
- Polyolefins, 417
- Polyoxymethylene, 431, 434
 - absorption frequencies, **432**
- Polysorption, water, 121
- Polyvanadates, 259
- Potassium bromide disks, 31
- Potential energy functions, 9, 11
- Precise catalysts, 277
- Preserved center of gravity, 182
- Probes
 - for adsorption centers, 181
 - ammonia, 78
 - for basic sites, 173
 - criteria for, 78
 - protonated, 68
 - pyridine, 78
- Promoted metallic systems, 251
- Promotional additives, 235
- Propane
 - adsorption, 395, 401
 - ammoxidation, 519, **519**
 - dehydrogenation, 516
 - IR spectra, 401, 521
 - nuclear magnetic resonance spectroscopy, 392
- 1-Propanol, on zeolites, 419
- 2-Propanol, on zeolites, 419
- Propargyl ions, 350
- Propargylic anion, 386, 388
- Propene, 169
 - adsorption, 262, 319
 - on alumina, 344–345
 - ammoxidation, 518, **521**
 - copper oxide systems, 503
 - deuterated, 343, 344, 350, 501
 - dimers, 504
 - dissociation, 522
 - dissociative adsorption, 343, 345, 347
 - heat of adsorption, 321, 344, 347
 - interaction with zeolites, 315
 - IR frequencies, **333**, **339**
 - IR spectra, 320, 340, 346, 351, 353, 475, 504, 507
 - magnesium oxide systems, 500
 - metathesis, 499
 - oligomerization, 493
 - oxidation, 256, 482, 483, 513
 - oxydehydrogenation, 507–508
 - partial oxidation, 351, 499–505

- π -complexes, 331, 336, 495, 500, 505
 - polymerization, 504
 - protonation, 165, 359
 - spectra, 316
 - zinc oxide systems, 502
- Propene adsorption, on alumina, 101
- Propene peroxides, 502
- Propene-hydroxyl complexes, 311
- 2-Propoxy group, 495
- 2-Propylate complexes, 319, 320
- Propylene *see* Propene
- Protic acid sites, 92, 162–166
 - etherification, 425
 - modified transition metal oxides, 285, 288
 - strength determination, 163
 - vanadium catalysts, 263, 425
- Protic centers
 - concentration of, 68, 323
 - oligomer formation, 322
 - strength, **163**
- Proton affinity values, 162, 163, 164, 166
- Proton transfer
 - alcohols, 419
 - ammonia, 80
 - conjugate bases, 419
- Protonic acid centers, 145
- Protons, mobile, 92, 93
- Pt/Si alloys, 247
- PtIn sites, 251
- Pyrazine, 385
- Pyridinates, 183, 190
- Pyridine
 - and chromium ions, 90
 - complex formation, 167
 - desorption, 84
 - deuteration, 93
 - heat of adsorption, 167, 413
 - as probe, 93
 - ring vibration, 84
 - spectra, 93
 - spectral ranges, 79
- Pyridine adsorption, 75, 78–80, 84
 - alumina, 41
 - Cu zeolites, 190
 - on platinum, 246, 251
 - rutile, 88
 - zeolites, 183
- Pyridine-SO₂ complexes, 151
- Pyridinium ions, 84, 93, 286
- Pyrrole, 173
- Quantitative measurements, 25
- Quartz, bulk phase, 61
- Quartz cells, 13
- Quinine, 510
- R-phase compounds, 74
- Raman anti-Stokes scattering, 19
- Raman effect, energy-level transitions, 20
- Raman spectra
 - barium oxide, 53
 - cobalt oxide, 280
 - Mo/Al₂O₃ catalysts, 279
 - nitrogen adsorption, 119
- Raman spectroscopy, 5, 19–21
 - advantages and disadvantages, 21
 - Al-Mo catalysts, 252
 - aromatic compounds, 368
 - CFC's, 409
 - cobalt oxide, 279
 - hydroxyl groups, 77
 - molybdenum systems, 257
 - supported catalysts, 278
- Raman Stokes scattering, 19, 20
- Rare earth metal oxides, 52
 - carbon monoxide adsorption, 109
 - copper catalysts, 206
 - DRIR spectroscopy, 64
 - hydroxyl groups, 73, 74
- Rayleigh effect, 19, 20
- Reaction intermediates, surface complexes, 459–460
- Reaction kinetics, IRS in, 25
- Redox catalysts, 165
- Redox mechanism, 460
- Redox systems, 29
- References, 559–641
- Reflectance ellipsometry, 23
- Reflection spectroscopy, infrared, 15–18
- Reflection-absorption IR spectroscopy, 17
- Resonance interactions, vibrational dipoles, 109, 242
- Resonance Raman spectroscopy, 21, 388
- Reverse transfer bonding, 271
- Rhenium oxide, 278
- Rhenium-containing systems, 237–238
- Rhodium
 - isocyanate complexes, 161
 - SO₂ complexes, 148
- Rhodium carbonyls, 237–238, 475
- Rhodium-containing systems, 237–238, 479
- Rideal mechanism, 460
- Rock salt
 - coordination number, 42
 - structure, 68, 339
- Rocking vibrations, ammonia, 85
- Rubidium oxide, 226

- Ruthenium, Nitric oxide adsorption, 126
Ruthenium carbonyls, 283
Ruthenium oxide, 280
Ruthenium-containing systems, 237–238, 473
Ruthenium-palladium systems, 283
Rutile
 carbon monoxide adsorption, 103
 crystalline structure, 28, 73
 hydroxyl groups, 72–73
 low-temperature formation, 256
 pyridine adsorption, 88

Samarium oxide, 175
Sample amorphization, 179
Sample holders, 15
Sample mold, 12
Sample preparation, 12, 38
Sapphire, in cells, 13
Scattering
 multiple, 5, 17
 reduction of, 11
Scissors deformation mode, 122, 144
Selective oxidation reactions, 460
Selenates, 287
Semiconductors
 n-type, 37, 55
 p-type, 56, 503
Sensitivity, ultraviolet and visible spectroscopy, 5
Si-Mo system, 254
 σ bonds, 271
 metal carbonyls, 95
 σ -allylic complexes, 342, 501
 σ -donation, pyridine, 84
 σ -donors, 167, 170
 σ - π bonds, 44
Silane diol, 61
Silanol, 382
 modes, 40
Silanol absorptions, 385, 412
Silanol groups, 60–61
 bending vibration, 61
 ethene polymerization, 491
 hydrogen adsorption, 115
 hydrogen bonding, 413
Silanone groups, 179
Silica
 outgassing, 40
 pyrogenic, 60
 structure, 62
Silica gels, 60
Silica-alumina catalysts, 29
Silica-based zeolites, CO adsorption, 97–100
Silicalites, 97, 395
Silicon dioxide
 hydrogen sulfide adsorption, 139–140
 hydroxyl groups, 60–63
 modified, 277
 surface properties, 39–41
 water adsorption, 121
Silicon windows, 13
Siloxane bridges, 40, 400
Siloxane groups, 60
Silver
 charge transfer, 224
 clusters, 224, 225
 DRE spectra, 540
 electronic characteristics, 539
 ions, 225, 226
 see also Ag
Silver fluoroborate, 331
Silver-containing systems, 223–228
 additives, 542, 542–543
 DRE spectra, 542
 effects of nitric acid, 541
 ethene adsorption, 330–331
 spectra, 225
 spectral characteristics, **543**
 supports, 540–541
Silylacetates, 431
Singleton frequencies, 247
Sodalite, 218
Soft acids and bases, 77, 119
Solid structures, oxide surface centers, 27–28
Solvation effects, 78, 323, 378, 474
Spatial defects, 178
Spectra, oxide surfaces, 31–76
Spectra-Tech Collector, 18
Spectro-kinetic measurements, 477
Spectroscopic methods, 1–25
 characteristics, **3**
 experimental principles, 6–7
Spectroscopy, *see also* specific types, e.g.
 Electronic, Vibrational etc.
Spin–spin interactions, 394
Spinels, 36
 hydrocarbons on, 402
 hydroxyl groups, 74–75
 NO-CO systems, 552
 transition aluminas, 64
Splitting parameter, copper hydrates, 188
Static shift, 242
Stearic acid, 453
Steric effects, 364, 367, 393, 495
Stishovite, 40
Stoichiometric surfaces, chromium oxide, 35
Stretching frequencies, and adsorption sites,
 271–275

- Stretching vibrations, vanadium and molybdenum oxide, 39
- Strong associates
Cu zeolites, 192–194
Fe zeolites, 221
paramagnetic ions, 185
- Strong metal-support interaction, 247–248
- Strontium oxide
carbon dioxide adsorption, 177
carbon monoxide adsorption, 105
hydrogen adsorption, 117
surface properties, 41
- Structural looseness, 170
- Styrene, 365, 366, 370, 372
IR spectra, 366
- Succinates, 440
- Sulfate ion, 145, 558
- Sulfate modification, metal oxide systems, 286–291
- Sulfates, 155
- Sulfide ion, 140
- Sulfite ion, 145
- Sulfites, 150, 151, 153
- Sulfones, 148
- Sulfonyl group, 148
- Sulfur, elemental, 145
- Sulfur compounds
catalyst deactivation, 456
spectral features, **146–147**
- Sulfur dioxide
acceptor properties, 147
amphoteric nature, 155
bond-stretching vibrations, 146
charge transfer, 148
chemisorption, 151
complex formation, 151
dissociation, 153
heat of adsorption, **144**
molecular orbitals, 147
radicals, 150, 153
spectra, 152
spectral bands, **141**
surface process schemes, 154
surface-adsorbed species, **156**
- Sulfur dioxide adsorption, 146–157
aluminum oxide, 150, 151
calcium oxide, 150
donor-acceptor complexes, 151
oxides, 150–157
spectra, 152
spectral characteristics, **153**
titanium dioxide, 150
zeolites, 149–150
- Sulfur radicals, 140
- Sulfur-containing compounds, spectral data, **288**
- Super-acids, 30, 287, 289, 391, 558
- Superoxides, 52
- Support structure, and surface isocyanate complexes, 160
- Supported oxides, surface properties, 39
- Surface active sites, reagent interactions, 281
- Surface cation-oxygen bonds, 39, 44
- Surface cations, coordinative saturation values, 34
- Surface centers, 29
- Surface chemistry, *in situ* studies, 20
- Surface compound concentrations, and time, 529, 530, 531
- Surface coverage effects, 231
- Surface defects, 29, 177–179
aluminum oxide, 41
- Surface diffusion, 32, 44
- Surface electromagnetic wave spectroscopy, 23–24
coordinate systems and fields, 24
methane adsorption, 404
- Surface hydroxyl groups, 31, 56–77
chromium oxide, 34
- Surface impurities, 31–32
titanium dioxide, 48
vanadium and molybdenum systems, 39
- Surface interaction energy, 49
- Surface isocyanate complexes, 157–161
absorption bands, **157, 159**
copper, 553
spectra, 158, 159
stabilization, 158
and supports, 160
- Surface modification, reagent interaction, 277
- Surface organometallic chemistry, 277
- Surface oxygen, basicity, 396
- Surface reactions, 25
- Surface vibrations, 11
- Surface-enhanced Raman spectroscopy, 21, 281
- Surfaces, 28–29
structural flexibility, 170
vibrational modes, 31
- Symmetric deformation, ammonia, 85
- Symmetry groups, 10
- Synchronous radiation excitation, 241
- Temperature programmed desorption method, 55
- Tetraammoniates, 190
- Tetracyanoethene, 179
- Thermal stability, molybdenum compounds, 303–308
- Thermodesorption spectroscopy, 25
- Thiocarbonate compounds, 143
- Thiolate compounds, 142
- Ti/Sb oxide systems, 44

- Tin dioxide
adsorbed oxygen spectra, 50–52
defected sample, 51
- Tin oxide, spectra, 44
- Tin-containing catalysts, 507
- Tin–oxygen bonds, 51
- Titanium, coordination states, 104
- Titanium dioxide
ammonia adsorption, 88
boron-modified, 292
carbon monoxide adsorption, 103–105
chromium catalysts, 269
DRIFT spectra, 293
hydrogen sulfide adsorption, 142
hydroxyl groups, 71–73
IR spectra, 289, 293
nitrogen dioxide adsorption, 133
oxygen adsorption, 48–50
sulfate modified, 287
sulfur dioxide adsorption, 150
surface impurities, 48
surface properties, 37
surface vibrations, 37
vanadyl groups, 260
- Titanium hydroxide, 256
- Titanium ions, unsaturated, 105, 288
- Titanium–CO complexes, 273
- Titanium–molybdenum catalysts, 256
see also Molybdenum–titanium systems
- Titration methods, 172
- o*-Tolualdehyde, 511
- Toluene
ammoxidation, 524–526
dissociation, 373
frequency characteristics, **375**
IR spectra, 357, 358, 359, 377, 512
oxidation, 510, 513
spectral data, **360**
- Toluene adsorption, 348, 350, 356
on alumina, 377
copper-containing systems, 369, 377
frequencies, **375–376**
on oxides, 368
on titania, 370
two-centred, 369
on zinc oxide, 373
- o*-Toluic acid, 511
- Transition aluminas, 64, 65, 66
- Transition metals
acrolein complexation, 436
carbonates, 139
CO complexes, 273
local symmetry, 5
oxidation state, 5
- Transition temperatures, 32
- Transition-metal oxides, 64, 153, 157
Brønsted acid sites, 92
CO oxidation, 465
- Transitions
classification, 2
electronic, 1–2
- Transmission spectra, 4–5
- Transmission spectroscopy, infrared, 11–14
- Transmittance, defined, 4
- Treatment temperature, 32
- 1,1,1-Trichloroethane, 402
- ‘Triene’, 360, 362, 364
- Triethylamine–SO₂ complexes, 151
- Triethylphosphine, 494
- 1,1,1-Trifluoro-2-fluoro-2,2-dichloroethane, 407
- Trifluoroacetates, 409, 444
- Trifluoromethane, 174
- Trimethylamine, 413
- Trimethylamine–SO₂ complexes, 151
- 2,3,4-Trimethylpent-1-ene, 322
- Trioxygen molecule, adsorption, 55
- Triphenylcarbenium ions, 360, 362
- Triphenylcarbinol, 360, 362, 365
- Triphenylmethane, 358, 364
- Triphenylmethanol, 362
- Tungstates, 75, 94
- Tungsten oxide
ammonia and pyridine adsorption, 91
carbon monoxide adsorption, 114
- Turbid media, techniques for, 19
- Ultraviolet and visible spectroscopy, 2
acidic surface characterization, 161
sensitivity, 5
- Unsaturated atoms, at surfaces, 31
- Vacuum cells, 12, 14
- Vacuum conditions, ultra-high, 32
- Vacuum treatment
Ni zeolites, 212
Pd zeolites, 230
- Valence electrons per bond, 34
- van der Waals interactions, 282, 394
- Vanadates, 75, 94
- Vanadium carbonyls, **265**, 266, 322
- Vanadium catalysts
butene isomers, 322
iso-butene, 322
- Vanadium ions, coordination, 264, 268
- Vanadium oxide trichloride, 262
- Vanadium oxides
acid sites, 164, 165
alkenes, 321

- ammonia and pyridine adsorption, 91
- carbon monoxide adsorption, 114
- diffuse scattering spectra, 76
- dimers, 259
- hydrogen sulfide adsorption, 145
- hydroxyl groups, 75–77
 - polymeric, 268
 - surface properties, 39
- Vanadium-aluminum oxide compounds, 266–269
- Vanadium-containing systems, 257–269
- Vanadium-silicon oxide compounds, 263–266
- Vanadium-titanium oxide systems, 259–263
 - IR spectra, 261
 - reduction temperature, 265
- Vanadyl groups, 260, 266
- Vehicle emissions, 555
- Vibration, energy of, 8
- Vibrational dipoles, resonance interactions, 109, 242
- Vibrational frequencies, oxygen bonds, **46**
- Vibrational modes, 10, 22
 - at surfaces, 31
- Vibrational spectra, crystalline solids, 27
- Vibrational spectroscopy, 5–11
- Vibrations, metal-oxygen bonds, 32–44
- Vinyl group, 348, 350, 372
- Wacker reaction, 237
- Waste gas combustion, 284
- Water
 - in carbonyl complexes, 207
 - chemisorption, 89
 - dissociative adsorption, 72
 - dissociative chemisorption, 121
 - hydrogen bonding, 120
 - interaction with carbon dioxide, 137
 - interaction with hydrogen sulfide, 142
 - polysorption, 121
- Water adsorption, 120–123
 - Aluminum oxide, 122
 - chromium oxide, 122–123
 - Cu zeolites, 189
 - ferric oxide, 122
 - magnesium oxide, 122
 - silicon dioxide, 121
 - zeolites, 121–122
- Water molecules, dissociation, 56
- Water-gas shift reaction, 56, 447, 448, 460, 466–473
 - chromium oxide, 468–469
 - copper chromite, 471–472
 - CuO-MgO catalysts, 470–471
 - high-temperature catalysts, 466–467
 - iron and chromium catalysts, 466–467
 - low-temperature catalysts, 469–473
 - magnesium oxide catalysts, 467–468
 - middle-temperature catalysts, 467–469
 - other catalysts, 472–473
 - zinc oxide, 469, 473
- Weak associates
 - copper ions, 189, 192, 195, 197
 - paramagnetic ions, 185
- Wells-Dawson catalyst, 518
- Wotton Scientific, 20
- X-Ray Absorption Near Edge Spectroscopy, 548
- X-ray diffraction methods, 27
 - metal oxides, 278
 - molybdenum systems, 256
- X-ray photoelectron spectroscopy, 56
 - basic surfaces, 172
 - molybdenum systems, 253, 303
- Xerogels, 60
- Xylenes, 364, 368, 511, 512, 524
- Yttrium oxide, 73, 235
- Zeise's salt, 337
- Zeolites
 - carbon dioxide adsorption, 137
 - chemisorption, 137
 - copper-containing systems, 182–201
 - for diffuse reflectance electron spectroscopy, 181
 - hydrogen adsorption, 115
 - hydrogen sulfide adsorption, 139–140
 - hydroxyl groups, 63–65
 - infrared spectra, 98, 102
 - nitrogen dioxide adsorption, 132
 - pre-treatment, 231
 - properties, 29
 - scattering behavior, 181
 - Si/Al ratios, 63
 - silica-based, 97–100
 - sorption cavity, 119
 - strongly acidic, 75
 - sulfur dioxide adsorption, 149–150
 - supercages, 140
 - water adsorption, 121–122
 - see also* Faujasite; specific zeolites, eg Cu, Na zeolites
- Zinc chromates, carbon monoxide adsorption, 110
- Zinc formate, 446, 452
- Zinc hydride, 476
- Zinc ions, electron-acceptance, 109

Zinc oxide

- allylic complexes, 343–344
- ammonia adsorption, 87–88
- as Brønsted base, 350
- carbon monoxide adsorption, 96, 109–110
- energy levels, 204
- hydrogen adsorption, 117
- hydroxyl groups, 73–74
- oxygen desorption, 55–56
- photoionization, 204
- surface properties, 37

Zirconia, 29

- chromium catalysts, 269
- sulfated, 290

Zirconium dioxide

- carbon monoxide adsorption, 113
- hydrogen adsorption, 116
- hydroxyl groups, 73
- ion pairs, 404
- silver stabilization, 226, 544
- sulfate-modified, 290

Zirconium sulfate, 290

ZSM-5 zeolite *see* HZSM zeolites